2015-03-01

Shear Strength Prediction Methods for Grouted Masonry Shear Walls

Patrick Dillon
Brigham Young University - Provo

Shear Strength Prediction Methods for Grouted Masonry Shear Walls

Patrick B. Dillon

A dissertation submitted to the faculty of
Brigham Young University
in partial fulfillment of the requirements for the degree of

Doctor of Philosophy

Fernando S. Fonseca, Chair
Richard J. Balling
Paul W. Richards
G. Bruce Schaalje
Michael A. Scott

Department of Civil & Environmental Engineering

Brigham Young University

March 2015

ABSTRACT

Shear Strength Prediction Methods for Grouted
Masonry Shear Walls

Patrick B. Dillon
Department of Civil & Environmental Engineering, BYU
Doctor of Philosophy

The research in this dissertation is divided between three different approaches for predicting the shear strength of reinforcement masonry shear walls. Each approach provides increasing accuracy and precision in predicting the shear strength of masonry walls. The three approaches were developed or validated using data from 353 wall tests that have been conducted over the past half century. The data were collected, scrutinized, and synthesized using principles of meta-analysis.

Predictions made with current Masonry Standards Joint Committee (MSJC) shear strength equation are unconservative and show a higher degree of variation for partially-grouted walls. The first approach modifies the existing MSJC equation to account for the differences in nominal strength and uncertainty between fully- and partially-grouted walls. The second approach develops a new shear strength equation developed to perform equally well for both fully- and partially-grouted walls to replace and improve upon the current MSJC equation. The third approach develops a methodology for creating strut-and-tie models to analyze or design masonry shear walls. It was discovered that strut-and-tie modeling theory provides the best description of masonry shear wall strength and performance.

The masonry strength itself provides the greatest contribution to the overall shear capacity of the wall and can be represented as diagonal compression struts traveling from the top of the wall to the compression toe. The shear strength of masonry wall is inversely related to the shear span ratio of the wall. Axial load contributes to shear strength, but to a lesser degree than what has been previously believed. The prevailing theory about the contribution of horizontal shear reinforcement was shown to not be correct and the contribution is much smaller than was originally assumed by researchers. Horizontal shear reinforcement principally acts by resisting diagonal tensile forces in the masonry and by helping to redistribute stresses in a cracked masonry panel. Vertical reinforcement was shown to have an effect on shear strength by precluding overturning of the masonry panel and by providing vertical anchorages to the diagonal struts.

Keywords: masonry, full grouting, partial grouting, shear, strength prediction, linear regression

ACKNOWLEDGMENTS

Partial financial support for this research project was provided by research Grant 2012.003 and the Paul and Helen Lenchuk 2013-2014 Engineering Student Scholarship—both awarded by the National Concrete Masonry Association Education and Research Foundation. Additional support was provided by the Youd Family Fellowship, the Civil & Environmental Graduate Committee Scholarship, and the Ira A Fulton College of Engineering and Technology Scholarship. This financial support by the NCMA Education and Research Foundation, the BYU Civil Engineering Scholarship Society, and the Ira A Fulton College of Engineering and Technology is greatly appreciated.

Special mention should go out to those who have performed masonry shear wall tests over the past several decades. This study performed no experimental testing of it own and relied wholly on the raw experimental data that was produced by others. I wish to acknowledge the hours of work that each of them spent in their respective labs to build and test their masonry shear wall specimens. The current study could not have been performed without the individual labors and contributions to masonry knowledge made by these researchers.

I wish to thank my adviser Dr. Fonseca for his support, encouragement, and helpful feedback. Thank you for giving me the freedom to learn and explore new methods and approaches for solving the problems encountered in this study. I thank my committee members for their time and effort in providing me useful feedback on this dissertation and for all of the things I have learned from them in the classroom. This research would not have been possible without the foundational principals and critical thinking learned in their classes.

I also wish to thank our department secretaries Kim Glade, Jolene Johnson, and their student assistants for their help with completing the necessary paperwork, checking for formatting errors, helping me keep track of all of the many college and university requirements, and all the other ancillary duties which they perform. Their contributions are essential to the functionality of our department but frequently go unrecognized.

I want to thank my parents for helping me to see my potential and for cultivating my never-ending curiosity while growing up. I wish to thank my parents and my in-laws for their constant encouragement and support during these many years of study and work. I thank my grandmother Louise for her support, for donating the computer on which most of the analysis and writing was done, and for graciously covering the publication costs. It is with great affection that I thank my late grandfather, Marshall, for his ceaseless and sincere expressions of his pride in my accomplishments over the year. These expressions have inspired me to overcome my weaknesses and to reach my full potential.

I wish to thank my family for their constant support for me during these many years. Thank you to my sons Braxton and Carston for their unremitting love and understanding, notwithstanding their many sacrifices of my time and attention. Most importantly, I wish to express my heart-felt appreciation to my wife, Hillary, for her help, understanding, comfort, love, and personal sacrifices during my PhD program. All of this would not have been possible without her faithfully at my side.

TABLE OF CONTENTS

LIST OF TABLES

LIST OF FIGURES

A_c	area of confinement (internal vertical) reinforcement
A_t	area of flexural (external vertical) reinforcement
A_g	gross shear area of wall
A_h	area of bond beam reinforcement
A_j	area of joint reinforcement
A_{nv}	net shear area of wall
A_v	total area of (horizontal) shear reinforcement
c	cohesion of masonry unit/mortar joint interface
d_v	shear length of the wall
E_m	Elastic modulus of masonry
f'_b	compressive strength of masonry unit
f'_m	compressive strength of the concrete
f'_g	compressive strength of grout
f'_j	compressive strength of mortar
f'_m	compressive strength of the masonry
$f'_{m(\text{eff})}$	effective compressive strength of masonry
$f'_{m(gro)}$	predicted compressive strength of grouted prism
$f'_{m(ung)}$	predicted compressive strength of ungrouted prism
f_{yc}	tensile strength of confinement reinforcement
f_{yh}	tensile strength of bond beam reinforcement
f_{yj}	tensile strength of joint reinforcement
f_{yt}	tensile strength of flexural reinforcement
f_{yv}	tensile strength of reinforcement
f_y	yield strength of reinforcement
$\frac{h}{t}$	prisms aspect ratio
h_e	height from base to inflection point
h_g	geometric height of wall
k	mean prism strength correction factor
l_c	length of contact between masonry panel corner and external frame
l_w	length of masonry wall
M_u	ultimate moment demand
P	applied vertical axial load (force)
P_u	ultimate vertical load on the wall
s_c	horizontal spacing of confinement reinforcement
s_h	vertical spacing of bond beam reinforcement
s_j	vertical spacing of joint reinforcement
s_t	horizontal spacing of flexural reinforcement
s_v	vertical spacing of shear reinforcement
s_{gh}	horizontal grout spacing of partially grouted walls
s_{gv}	vertical grout spacing of partially grouted walls
t	thickness of masonry wall, equal to t_{sp}
t_s	shear thickness of wall, taken as the total face shell thickness for partially-grouted walls and as t_{sp} otherwise

t_{sp}	specified thickness of wall
V_n	nominal (predicted) shear capacity
V_{nm}	nominal shear strength provided by masonry
V_{np}	nominal shear strength provided by axial load
V_{ns}	nominal shear strength provided by reinforcement
V_u	ultimate shear demand
w	width of masonry prism in narrowest dimension
w_s	width of compressive strut
w_t	minimum of reinforcement diameter plus twice the clear cover and the wall thickness
α_s	strut inclination angle (measured from the vertical)
α_d	angle between the struts and the center line of the wall diagonal
β_i	strut inclination factor
β_n	node efficiency factor
β_s	strut efficiency factor
ϵ	strain in a member or element
ε	statistical model error
ϵ_{mu}	crushing strain of masonry
ϵ_{rup}	cracking strain of masonry
ϵ_s	tensile strain in the concrete in the direction of the tensile tie
γ_g	grouted shear wall factor
ν	ratio of net to gross masonry area
ϕ	resistance (or strength reduction) factor
φ	friction angle of masonry unit/mortar joint interface
σ_0	applied vertical axial load (stress)
σ_1	principal tensile stress
σ_2	principal compressive stress
τ	shear stress
τ_{max}	peak shear stress in wall
θ	angle between the panel diagonal and the bed joints

CHAPTER 1. INTRODUCTION

1.1 Background

Masonry is the most enduring building method used by mankind. Despite its lengthy period of use and widespread usage throughout the world, masonry remains today one of the least understood building media (Schneider, 1969). The lack of understanding of masonry can be attributed to—among other things—its heterogeneous composition, its anisotropic behavior, and negative stigma resulting from the poor seismic performance of unreinforced masonry during the first part of the twentieth century. The development of grouted, reinforced masonry during the past century has done much to dispel the poor perception of masonry, but it has also complicated its study by introducing new mechanisms and behaviors into the medium. Masonry research has accelerated in the past few decades due to the advent of numerical modeling procedures (e.g., finite element analysis), improved computational power, and advanced testing machines.

One of the relatively recent developments in reinforced masonry has been the practice of partial grouting. In partially-grouted masonry walls, only the cells containing reinforcement are grouted, leaving the remaining cells hollow. This practice saves on the construction costs for labor, materials, and weight, but introduces stress patterns that are different from those found in fully-grouted masonry walls. Significant research has been conducted on partially-grouted masonry walls to understand the effects that different design parameters have on stresses and behavior. Research has shown that partially-grouted masonry walls can be a practical lateral load-resisting system under seismic loading (Schultz et al., 1998).

One particularly important point of research in the past three decades has been to determine an accurate and safe equation to predict the lateral in-plane shear strength of partially-grouted masonry walls. The shear strength equation in the Masonry Standards Joint Committee (MSJC, 2013) code provisions currently applies to both fully- and partially-grouted masonry construction. The equation was developed using data primarily from fully-grouted masonry wall tests and does not

account for the different stress patterns that are present in partially-grouted masonry walls. Three recent projects (Elmapruk, 2010; Minaie, 2009; Nolph, 2010) were conducted under funding by the National Concrete Masonry Association (NCMA) and concluded that the MSJC shear equation over-predicted the shear strength for partially-grouted masonry walls. This is to say that the equation is unconservative and potentially life-threatening. To address this issue, the MSJC introduced the grouted wall factor γ_g into the 2013 code to compensate for this reduction in strength for partially-grouted masonry shear walls.

During the past half century, researchers throughout the world have conducted tests on hundreds of masonry shear wall specimens. The varied focus of each research study has generated a large pool of experimental data that covers a wide range of possible design parameters. A select few studies have compared and analyzed a notable portion of this data pool (Matsumura, 1987; Okamoto et al., 1987; Anderson and Priestley, 1992; Fattal, 1993). In other studies, researchers typically report their own experimental results and compare them to experimental results from a few other specimens with similar parameters to their own. To date, however, the full breadth of knowledge contained in this large pool of data has yet to be fully utilized.

There are numerous probabilistic tools that are available for analyzing experimental data. These tools become increasingly powerful as the sample size becomes large and can, in some cases, be used in lieu of performing additional specimen tests. By leveraging the large sample size of the pool of masonry shear wall data, certain conclusions can be made with more confidence than can be done with an individual research study.

1.2 Significance of Research

The most recent MSJC (2013) nominal shear strength equation is given by

$$V_n = \gamma_g \left[4.0 - 1.75 \frac{M_u}{V_u d_v} \right] A_{nv} \sqrt{f'_m} + 0.25 P_u + 0.5 \frac{A_v}{s} f_y l_w \tag{1.1}$$

where

γ_g = the partially-grouted modification factor,

M_u = the ultimate moment demand,

V_u = the ultimate shear demand,

P_u = the ultimate vertical load on the wall,

l_w = the shear length of the wall,

A_{nv} = the net shear area of the wall,

A_v = the area of (horizontal) shear reinforcement,

s = the vertical spacing of shear reinforcement,

f'_m = the compressive strength of the masonry,

f_y = the yield strength of the shear reinforcement, and

$\frac{M_u}{V_u l_w}$ = need not be greater than one.

The nominal shear strength V_n is subject to the upper constraint

$$V_n \leq \begin{cases} 6\gamma_g A_{nv}\sqrt{f'_m} & \text{for} \quad \dfrac{M_u}{V_u l_w} \leq 0.25 \\ 4\gamma_g A_{nv}\sqrt{f'_m} & \text{for} \quad \dfrac{M_u}{V_u l_w} \geq 1.0 \end{cases} \tag{1.2}$$

which is intended to prevent designers from using excessive amounts of reinforcement within the wall. In using Equation (1.2) the code permits designers to linearly interpolate for intermediate values of $\frac{M_u}{V_u l_w}$. The nominal shear strength is reduced by a shear resistance (or strength reduction) factor ϕ_v of 0.8 to obtain the design strength (MSJC, 2013).

In light of the recent studies (Elmapruk, 2010; Minaie, 2009; Nolph, 2010), the MSJC (2013) has introduced a modification factor into the shear equation for the most recent code edition. The current grouted wall factor γ_g is intended to account for the effects of partial grouting in masonry walls and is to be taken as 0.75 for partially-grouted cases and 1.0 for all other cases. Hollow, unreinforced masonry are governed under a different code equation and are not included in this discussion. The 0.75 factor was obtained by dividing 0.9 by 1.16 where 0.9 is the average over-prediction factor for partially-grouted masonry walls from Minaie (2009) and 1.16 is the average under-prediction factor for fully-grouted masonry walls from Davis (2008). The factor is applied to both the masonry and reinforcement components of the shear equation. Additionally, in the current approach the same shear strength reduction factor, ϕ_v is used for both fully and partially-grouted walls.

The MSJC (2013) has recognized that there is a research gap in the area of partially-grouted masonry shear walls than needs to be filled. The MSJC code commentary states that the grouted wall factor γ_g is "used to compensate for this reduced strength [in partially-grouted walls] until methods can be developed to more accurately predict the performance of these elements" MSJC (2013). It has admitted that the current method is meant as a temporary solution to bridge the gap in understanding until an accurate approach can be developed. This study will develop accurate approaches to fill this void and will further the overall knowledge of grouted masonry shear walls.

The principal pitfalls of the current grouted wall factor method are that it is based on the research of a select few researchers, that it is based on average values, and that part of the factor was developed from data for fully-grouted walls. The 0.9 over-prediction factor used in developing the grouted wall factor is based solely on the findings of Minaie (2009) at Drexel University. The research of Nolph (2010) and Elmapruk (2010) at Washington State University (WSU) yielded over-prediction factors 0.8 and 0.73 based on their respective experimental data. The data also suggest that the value of 0.9 obtained by Minaie may be too large, resulting in an grouted wall factor that is not small enough. To overcome experimental bias, data from many studies should be used—ideally from all compatible partially-grouted shear wall research available—to determine any modifications to the MSJC shear equation. Analysis of a greater number of specimens will increase the number of degrees of freedom in the statistical analysis, increase the statistical power of the results, and make the data set more representative of the whole population.

The 0.9 and 1.16 factors used in developing the grouted wall factor were based on expected (i.e., mean) values obtained from the research. The expected values represent a 50 percent chance of being exceeded and do not account for variability in the specimens or in the experiment. Furthermore, both mean values were from data sets with different variances, meaning that the two mean values cannot be effectively compared by simply dividing one by the other. The 1.16 value under-prediction factor could represent the fact that the MSJC shear equation was likely developed using some sort of tolerance level in predicting shear strength for fully-grouted masonry walls. Similarly, an equation for partially-grouted shear strength prediction should also contain some level of tolerance to account for variability in the materials and equations.

The vast majority of partially-grouted masonry shear wall research has examined a relatively small number of specimens when compared with the number of parameters being tested.

A few exceptions are the studies in Matsumura (1987), Johal and Anderson (1988), and Tomaževič et al. (1996) which each tested a relatively larger number of specimens. Small-sample testing has been conducted, understandably, because of the additional expense inherent in performing repeated specimen tests. Unfortunately, setting up experimental research programs in this way limits the number of degrees of freedom in the statistical analysis and makes the tests highly susceptible to experimental variability and error. Fattal (1993), Matsumura (1987), Nolph (2010), and Voon (2007) have each proposed other models for partially-grouted shear walls, but they are either too complex or were developed using too few observations to be adopted into a design standard. Masonry standards from other countries contain provisions for partially-grouted shear walls, but it is uncertain whether these equations are equally applicable to the construction practices used in the United States. In short, no practical model is available to use in the MSJC that can accurately predict the shear strength of partially-grouted shear walls with a known level of confidence.

Most researchers base their experimental designs on a relative approach by comparing the effects of different parameters on wall behavior. Only in a few select studies do researchers attempt to estimate absolute population values for masonry shear walls. Using the relative approach researchers are able to use their results to make conclusions on how their experimental parameters either positively or negatively affect wall performance. The two main issues observed in studies that use this approach are that their conclusions are only comparative in nature and that too few researchers include replicate specimens in their experimental design. The difficulty with many qualitative conclusions is that they provide little if any numerical representation of a parameter's effect on the behavior of a wall. For example, it has been observed by Yancey and Scribner (1989) and Ghanem et al. (1992) that decreasing the spacing of horizontal reinforcement improves the shear strength of a wall, but no study has definitively shown by what amount reinforcement spacing affects shear strength. The omission of replicate specimens from a research study limits the number of statistical degrees of freedom in the data analysis and provides no insight into the variation between similar specimens.

The statistical analyses for this study will be performed on a data set comprised of all compatible fully- and partially-grouted wall tests documented in the literature. Fully-grouted specimens are included in the analysis to provide a baseline against which the partially-grouted shear wall data can be effectively compared. Since the conglomeration of tests in the dataset includes

studies from many different regions, the dataset will be more representative of masonry walls across all regions than any single study could be. Furthermore, since the number of tests far outweighs the number of parameters being tested, this analysis has many more degrees of freedom and the results will more closely estimate those of the entire masonry shear wall population. In all, the three recommended approaches developed through this research will be more appropriate for inclusion in a widely-used masonry standard and will provide design engineers effective tools for use in designing masonry shear walls in the future.

1.3 Objective Scope

The motivation behind this research program is the inherent unconservative nature of the MSJC (2013) shear equation for partially-grouted masonry shear walls. The objective of this research program is to develop models for predicting the shear capacity of both fully- and partially-grouted masonry shear walls which are improvements over the current MSJC shear equation. During the course of this program, new insights and understanding of the behavior and performance of masonry shear walls will be gained by using statistical, meta-analysis, and strut-and-tie modeling tools which have not been used before in masonry shear wall research.

This project will focus on three approaches for developing improved masonry shear wall strength prediction models. The first approach will quantify and mitigate the errors in the current MSJC shear equation. The second approach will develop a new, updated, and more accurate shear equation to replace the one in the in the MSJC code. The third approach will develop a procedure for designers to following in creating strut-and-tie models for masonry shear walls.

The dataset used in the three approaches will be created solely from existing fully- and partially-grouted masonry shear wall specimen data found in the literature. The data will be formatted and synthesized to follow the same data reporting standards. The parameters used in constructing the strength prediction models will be limited to those collected and presented in the literature; no new specimen tests will be proposed for use with masonry.

1.4 Outline of Paper

This dissertation is divided into six parts—each of which in comprised of several chapters—references, and appendices. The following subsections offer a brief description of the contents of each part.

Part I

Part I provides a review of the foundational knowledge that will be the basis for aspects and phases of this study. Chapter 2 provides a primer for the current state of the art of masonry shears walls. Chapter 3 presents a primer and introduction into the theory of linear least-squares regression. Chapter 4 provides a detailed introduction into the principles of meta analysis.

Part II

Part II provides details into the process of data analysis used in assembling and analyzing the dataset for this study. Chapter 5 presents a literature review of the processes used by the original researchers to test the specimens analyzed in this study. Chapter 6 details how the dataset was assembled from the previous research studies and how the data were synthesized to overcome incompatibilities between the difference research studies. Chapter 7 finishes Part II with an overview of the completed dataset and its properties are shown and discussed in detail.

Part III

Part III details the first analysis approach developed in this study. Chapter 8 presents a literature review of previous studies which analyzed and suggested improvements to existing shear equations. Chapter 9 outlines the methodology for analyzing the MSJC (2013) equation developed from the analysis techniques used by previous researchers. Chapter 10 details the results of the analysis and Chapter 11 provides a discussion of the modified MSJC shear equation.

Part IV

Part IV details the second analysis approach developed in this study to create a new linear model for the prediction of masonry shear wall strength. Chapter 12 is a literature review of linear model building techniques typically employed by statisticians and continues with a review of the development of the current MSJC shear equation, its precursors, as well as other shear equations from around the world. Chapter 13 introduces the methodology that will be used in analyzing the previous shear models and in developing a new, improved shear model for masonry. Chapter 14 presents an investigation of the precursor models which led up to the current MSJC equation. Chapter 15 is the principal focus of Part IV and details the development of a proposed shear model to replace the current MSJC shear equation. Chapter 16 presents comparison and discussion of all of the shear prediction models using the extensive dataset constructed for this study.

Part V

Part V details the third and last approach which was the development of the strut-and-tie modeling procedures for masonry shear walls. Chapter 17 introduces and explains strut-and-tie modeling theory and provides a review of uses of the method for masonry from the literature. Chapter 18 continues with an outline of the methodology used in developing the strut-and-tie modeling procedures for masonry shear walls. Chapter 19 details the creation of strut-and-tie models for masonry and development of the modeling procedures for masonry. Chapter 20 presents a comparison of the performance of the practice with the existing and proposed shear equations and a discussion of the method's use in design practice.

Part VI

Part VI provides general discussion and conclusions for the entire research study. Chapter 22 discusses the performance of masonry shear walls as an assemblage and details the behavior leading to the two principal failure modes. Chapter 21 discusses how each design parameter influences the masonry shear capacity, performance, and failure mode. Chapter 23 presents the overall conclusions and recommendations from this study.

Part I

Foundational Knowledge

This part provides a review of the foundational knowledge that will be the basis for aspects and phases of this study. Chapter 2 provides a primer for the current state of the art of masonry shears walls. Chapter 3 presents a primer and introduction into the theory of linear least-squares regression. Chapter 4 provides a detailed introduction into the principles of meta analysis.

CHAPTER 2. PRIMER: MASONRY

2.1 Introduction

Masonry is the oldest documented construction material known to modernity. This should not be construed as meaning that masonry was the first building method used by mankind. The longevity of masonry as a building material has permitted ancient masonry structures to outlast other ancient structures built from other materials—particularly organic materials such as wood, thatching, and bone. Since men have historically built from materials that were readily available to their locale, it is conceivable that separated civilizations concurrently developed disparate construction media that best matched their respective surroundings, climate, and available resources.

Despite the long history of masonry usage, masonry remains today one of the least understood building materials due to its material properties and common perceptions. Masonry is a heterogeneous and anisotropic material, making the structural behavior of masonry more difficult to model, analyze, and explain than for other commonly-used construction materials like steel and reinforced concrete. The differences within the constituent materials and the manufacturing processes make the properties of masonry assemblages more variable than those of more homogeneous and isotropic materials. More recently, masonry has been affected by vacillations in public perception about its utility, economy, and overall safety resulting from the poor performance of unreinforced masonry structures in recent earthquakes.

2.2 History

2.2.1 Ancient

The first documented masonry structures were built in pre-historic times in the Mediterranean basin. In this rocky area with little timber for construction, these primitive structures were dome-shaped and constructed by stacking stones one upon another. The Mycenaeans would later

build beehive-shaped structures by developing and using the corbelling method of dome building. They found that by stacking flat stones such that each course protruded beyond the previous course in a balanced manner, a dome could be constructed without need for centering. Once both sides met at the top the horizontal constraint provided lateral stability to the completed dome. This method was made easier by using smaller, lighter blocks in the higher courses. Eventually, they would expand this technology to building half-domes and corbelled arches (Escrig, 2006; Fletcher, 1996).

The first use of clay masonry was developed in the Mesopotamian Plains and Nile River Valley. In these alluvial areas the scarcity of stone and timber compelled the inhabitants to search for other materials for use in construction. Mesopotamia was first to use unfired mud-bricks and the practice later spread to Egypt. The early Mesopotamian mud-brick buildings continued the earlier tradition of constructing either round or oval-shaped structures. Eventually rectangular structures with arched roofs and stone foundations took over as normal practice (Escrig, 2006; Fletcher, 1996).

The use of mud bricks facilitated the development and wide-spread use of the arch within the Fertile Crescent region. The bricks were light enough for a single workman to carry and could be easily formed or shaped into voussoirs for use in arches. Similar to the earlier domes of the region, the inhabitants developed new technology whereby an arch was constructed without the need for centering. Each arch was constructed from concentric, inclined rings. As each ring was constructed the voussoirs partially rested on the previously completed ring. The friction between the adjacent rings was sufficient to keep the partially-built ring standing until the key could be placed (Bagenal, 1980; Fletcher, 1996).

In Egypt, mud-brick masonry became the predominant form of construction, supplanting the flimsy, clay-covered reed and timber method for the primary structure. The Egyptian style was different from that of Mesopotamia in that the Egyptians continued to use flat, clay-covered reed roofs. Since the roof provided little lateral support to the brick walls the Egyptians tapered their walls from bottom to top for added stability. To preserve vertical surfaces on the interior of their structures they only battered the exterior faces of their walls. This practice was a distinction of Egyptian architecture that would influence the design of future structures (Fletcher, 1996).

Hewn stone first began to be used in Egypt during the Third Dynasty, in the twenty-seventh century BC. The first royal tombs were flat-roofed mastabas constructed from limestone hewn from nearby outcroppings. Though the interiors of the mastabas were solid, the common practice of battering the exterior faces continued. The grandeur of the royal tombs steadily increased with each pharaoh trying to out-do the accomplishments of the previous. Gradually, the mastabas grew in height and the battered walls became steeper. This practice continued such that the walls met at an apex and a pyramid was formed. Through the end of the dynasty, the pyramid became the design of choice for royal tombs (Fletcher, 1996).

The Egyptians incorporated several innovations into their pyramid construction practices. One of which was the use of bed joints that were inclined inward to provide lateral stability to the higher courses. They also used a thin lime-based mortar between the blocks as a lubricant to aid in positioning them. The Egyptians understood and built arches for other uses—particularly with mud-brick—but they chose to use large stone lintels or triangular arches in their monumental structures to span openings (Fletcher, 1996). Their use of these innovations gives the intimation that the Egyptians understood the principle of masonry arching.

Masonry arching enables most of the downward gravity load above an opening to be transferred diagonally, through the masonry, to the supports adjacent to the opening. If there is sufficient lateral restraint around the opening and adequate masonry height above the opening, then the masonry around and above the opening will behave more like a corbelled arch. In this case the lintel spanning the opening will not experience the full weight of all the masonry above it but will only have to support the weight of the triangular section of masonry immediately above it (Drysdale and Hamid, 2008).

During the New Kingdom, Egyptian focus shifted away from building pyramids and towards building smaller, more-elaborate tombs and temples. This change in scope led to new design challenges to overcome. The new designs did not provide the same amount of lateral stability as was inherent in the pyramids. Similarly, the new structures were to gradually contain more and more usable space. The new challenge was to find new stable ways of transferring all gravity loads downward. The Egyptians surmounted this by making another advance in masonry construction, the use of vertical stone columns. In building the temples, chapels, and other buildings during

this period they continued the practice of using stone lintels or triangular arches to span between columns (Fletcher, 1996).

While the Egyptians were using hewn stone for their monumental structures, the Mesopotamians devised another material that would work well for their larger structures. They discovered that by firing their mud bricks they became substantially stronger and weathered much better. Together with bitumen-based mortar they constructed several large edifices and ziggurats, using the fired brick in areas subject to higher stresses. Later, the Babylonians developed this technology further by creating glazed bricks, which they used in some of their most important buildings (Fletcher, 1996).

2.2.2 Classical

Through their trade empire, the seafaring Minoans came into contact with the Egyptian masonry technologies and architecture and spread this knowledge to the Mycenaeans in Greece. The Greeks continued the column, lintel, and triangular arch components of the Egyptian stonework and also incorporated the use of corbelled arches which they had previously developed. This knowledge blossomed into new architectural styles during the Classical and Hellenistic Greek periods. Additionally, the Greeks expanded the use of stone columns by gradually making them more slender and by using keys between column sections to align them and resist lateral shear forces (Fletcher, 1996). A further innovation, the discovery of pozzolanic cement, created a new, stronger mortar to be used in masonry construction (Hegemier et al., 2003; Malhotra and Mehta, 1996). Much of the Greek architecture and practice was adopted by the Romans at the outset of Roman rule.

The Romans had a large influence on the further development and spreading of masonry knowledge. They were skilled at incorporating existing technology from other cultures, innovating new ones, and spreading them throughout their broad reach. The vastness of the Roman Empire put them in contact with the masonry technologies of Mesopotamia, Egypt, and Greece (Fletcher, 1996). The first innovation of the Romans was to combine the arch technology from Mesopotamia with the stonework and concrete technology from Greece to form large stone arches. The Romans later improved the methods of making and using cement in construction (Malhotra and Mehta, 1996)

Through Roman masonry technology stone masonry walls became more slender, creating more usable space within the structure. The next step was to construct walls in an annular manner to form hollow towers. The cross-section of a tower is efficient because the material at the extremities of the structure work as a couple to resist lateral and overturning forces. The efficiency of the shape permitted the exterior walls to be relatively thinner compared to free-standing walls of comparable height. The Romans constructed many notable masonry walls, cities, and towers throughout Europe and the Near East during their rule (Drysdale and Hamid, 2008).

The Romans also made new developments in the use of the arch. Unlike previous civilizations the Romans used centering in constructing their arches and domes due to the larger scale and their use of concrete. Roman engineers understood that a semi-circular arch was not as efficient as a parabolic or catenary arch, but determined that the semi-circular shape was simplest to lay out and construct. Semi-circular arches use a single, constant radius with voussoirs that are all identically shaped. As Roman construction technology improved parabolic and catenary shapes were used, as is evident in some of their significant later projects. In the case of all arches, vaults, and domes, the horizontal component of the interior force causes outward thrust at the base that must be restrained. Romans discovered that by adjoining barrel vaults perpendicular to the edges of large domes or other vaults, the in-plane shear strength of the vault could be used to confine the outward thrust of the much larger dome or vault (Drysdale and Hamid, 2008).

Masonry was developed further by the Byzantines who used domes in a new architectural style. Unlike the Romans who settled with building domes over circular shaped spaces, the Byzantines discovered means to construct domes over octagonal- and—later—square-shaped spaces by combining portions of domes of different radii. By using pendentives they could direct the vertical forces of a large dome into the corners of the structure and the lateral forces were resisted by either half domes or barrel vaults. The Byzantines developed the dome further by using a catenary shape, which enabled them to construct thin-shell vaults and domes that were thinner and lighter (Bagenal, 1980).

European masonry took on a new form in the Medieval period with the advent of Gothic architecture. The first defining aspect was the acceptance of the ribbed domes originally invented by the Muslims. The Europeans took the concept of the ribbed dome and generalized it for use in vaults (Escrig, 2006). By using ribbed vaults, the ribs could be constructed initially and the other

portions of the vault could be constructed in sections. This decreased the quantity of centering that was needed in constructing the vaults. Another characteristic was the use of pointed arches, originally developed by the Byzantines, which decreased the amount of outward thrust at the base of the arch. The combination of ribbed vaults and pointed arches led to the creation of the Gothic vault, a characteristic feature of Gothic architecture (Bagenal, 1980).

The Gothic method of design was two dimensional. This enabled designers to more easily understand load paths and optimize the designs to bring the materials to the limit of their stress capacity. This understanding—coupled with the development of flying buttresses—enabled the Gothic builders to reach astounding heights with their structures. The height and use of ribbed vaults enabled Gothic structures to include many more windows than had previously been used in masonry structures. Up to that period, Gothic architecture was the most luminous method that had yet to be designed and built (Escrig, 2006).

2.2.3 Contemporary

The earliest appearance of modern reinforced masonry technology dates back to the early nineteenth century when iron hoops were placed in the mortar joints of two brick shafts in London. This construction technique was investigated further by several engineers throughout England. Another advance in masonry technology that occurred soon afterward was the discovery and use of portland cement as a cementitious agent in mortar. Both of these technologies were highly publicized in 1851 at the Great Exposition of London. The use of reinforced masonry did not spread to the United Stated and other nations until a century after its initial discovery in England (Schneider and Dickey, 1994).

The deficiencies of unreinforced masonry were highly publicized after the 1933 Long Beach earthquake in which 70 schools built of unreinforced masonry were completely destroyed. The State of California subsequently passed laws and new building codes that prohibited the use of unreinforced masonry (Commission, 2009; Hess, 1979). Over the next four decades, the vast majority of research on reinforced masonry was conducted within the State of California. The regulations based on the findings from these research programs were included in the Uniform Building Code (UBC) (Schneider and Dickey, 1994).

The understanding of reinforced masonry during the last half century has increased through the efforts of research institutions, both domestically and internationally. This research has been aided by more sophisticated testing and data collection systems, the advent of Finite Element Analysis, greater computational power, and the formation of research coalitions dedicated to the subject.

2.3 Properties

2.3.1 Materials

Masonry Units

Concrete and clay are the two principal materials used in making masonry units. Load-bearing clay masonry comes in two types, structural clay tile and hollow clay brick. The latter type is distinct from the more widely known solid clay bricks that are commonly used as veneers in many structures worldwide. The term is most frequently used for concrete masonry, particularly most recently, is concrete masonry unit. Standards for load-bearing structural clay tile, hollow clay brick, and concrete masonry unit are set forth in ASTM C34, ASTM C652, and ASTM C90, respectively.

Mortar

Multiple types of mortar are used throughout the literature. The most common type of mortar used by researchers is portland cement/lime-based mortar, which is also the most widely-used mortar today in the United States masonry industry. Two other types, masonry cement- and mortar cement-based mortars, are proprietary blends of portland cement, lime, and/or other materials that come premixed in bags from the manufacturer. Earlier masonry codes restricted these latter two mortars from use in seismic force-resisting masonry walls due to the uncertainty in their performance at the time. Research has been carried out to study the performance of these two mortars (Johal and Anderson, 1988) and they were found to perform equally as well as portland cement/lime-based mortars.

Some researchers (Meli et al., 1968; Meli and Salgado, 1969; Haach et al., 2010b) used only portland cement-based mortar without lime in their masonry specimens. This is the case in Latin America and some other countries where lime is not readily available or where it hasn't been traditionally used. Lime-less mortar has the advantage of having, in general, higher compressive strength than similarly proportioned mortars with lime include. Additionally, the absence of lime results in the mortar and concrete masonry having more similar Poisson's ratios, increasing material compatibility within masonry assemblages and decreasing assembly anisotropy.

In the United States, mortars are grouped into types based on their proportioning of lime and are designated as M, S, N, and O. Compressive strength and ductility are related to the mortar type, with the first type being the strongest and least ductile mortar and the last type being the weakest but most ductile. Increasing the proportion of lime within mortar decreases the compressive strength of the mortar but increases its ductility. The use of lime in mortar greatly increases the workability and longevity of wet mortar by increasing its ability to retain moisture. The ease of use helps to decrease errors in construction and reduce variability within masonry walls. Another benefit of using lime in mortar is the ability over time for cracks in the mortar to heal through autogenous healing.

Grout

Masonry grout is a mixture or portland cement concrete wherein the aggregate sizes are generally limited to sizes smaller than is typically allowed in normal concrete usage. Grout must have a high slump for it to flow down the masonry cores and fill the voids around the reinforcement. High-slump grout is made created through the use of plasticizers within the grout mix. Grout has several purposes within partially grouted masonry walls. The primary purpose is to transfer loads from the masonry to the reinforcement so that the two act as a unit. The grout also serves to cover and protect the reinforcement from corrosion, permits the full development of strength in the reinforcing bars at splices and hooks, and adds to the net shear area of the wall, increasing shear capacity.

Reinforcement

Reinforcement used in masonry walls is generally made from steel, though carbon fiber and other fibrous media are sometimes employed. While the study of other reinforcing materials in masonry is gaining traction around the world, the widespread use of these other materials is still years away. This study will focus solely on the two types of steel reinforcement used in masonry construction, deformed bars and welded wire.

The deformed bars used in masonry are the same as those used in reinforced concrete design and construction. Deformed bars come in sizes that vary from country to country; the sizes used for each specimen are reflected in Appendix A. Deformed bars are placed vertically within the cores of the masonry units and horizontally within bond beams and are grouted in place.

The second type of reinforcement used in masonry walls, welded wire reinforcement, consists of two parallel wires that are attached together in one of two ways. In ladder-type reinforcement, short bars that run perpendicular to the two wires are welded onto the wires at regular intervals. In truss-type reinforcement, a third continuous wire is bent into a zigzag shape and welded onto the other two bars at its corners. The purposes of the central wires in each type are to keep the two primary wires at a uniform distance apart, to keep the primary wires straight, and to provide some lateral anchorage to the wires when they are embedded within the wall.

Both truss- and ladder-type reinforcement are used primarily as horizontal reinforcement and are placed within the bed joints of the masonry. This reduces labor and materials by avoiding the use of special units and grouting necessary in forming bond beams. However, the limited size of the bed joints constrains the amount of welded wire reinforcement that can be included in the wall. A recent study by Haach et al. (2010b) has determined that welded wire reinforcement can be effectively used as vertical reinforcement within walls as well.

Reinforcement can be placed in masonry shear walls in two orthogonal directions, horizontally and vertically. In the case of shear walls the horizontal reinforcement is also called shear reinforcement because it is laid parallel to and is most effective in resisting the lateral in-plane shear forces. As wall panels develop diagonal shear cracks from increasing shear forces the shear reinforcement spans these cracks and provides means of resisting the lateral tensile forces from one side of the crack to the other. For this reason, the two terms are used interchangeably within the literature.

The vertical reinforcement is sometimes called the flexural reinforcement because it resists the tensile forces created by the overturning moment within the wall. This term can be somewhat of a misnomer because only the vertical reinforcement nearest the ends of the wall is truly effective in resisting the overturning moment forces within the wall (Ghanem et al., 1992, 1993). The vertical reinforcement in the interior of the wall panel is not very effective in resisting the in-plane moment force due to its proximity to the neutral axis. This reinforcement primarily provides vertical confinement to the masonry and acts in resisting any out-of-plane moment forces.

The MSJC code contains provisions for prescribed reinforcement for specially reinforced masonry shear walls. Among the prescriptions, the code requires that reinforcement be spaced no more than 48 inches (1220 mm) in both the vertical and horizontal directions.

2.3.2 Assemblages

Masonry units are assembled in several different ways. Methods include traditional mortared joints, so-called "dry stack" masonry, and thin-bedded joints. The remainder of this dissertation will refer exclusively to the traditional mortared joint method which is the most common technique used today. Since masonry assemblages are heterogeneous and anisotropic, the mechanical properties of the constituent materials cannot be directly equated to the strength of the whole assemblage. To understand this disparity in strengths, one must look at the complex internal reactions that occur within a masonry panel.

2.3.3 Joints

Joints are a major source of the anisotropy within masonry assemblages. Bed joints run horizontally and are generally continuous from one end of a panel to the other. Head joints run vertically and may or may not run continuously from the bottom to top of a masonry panel, depending on the bond pattern used in laying the wall.

Running bond, the most commonly used bond pattern, is defined in the MSJC code as a pattern in which the head joints of adjacent courses are offset by a distance of at least a fourth the length of a masonry unit. Stack bond is defined as a bond pattern in which the head joints of each consecutive course are aligned so that each head joint runs continuously from the bottom to top of

the wall. By these definitions, it is possible for a wall to be laid in neither running bond nor stack bond. In the MSJC code, walls not meeting the requirements for running bond are referred to as "not laid in running bond." The term stack bond is not used in the MSJC code; walls laid in stack bond are included in the group of walls not laid in running bond.

Bed joints are mortared in one of two ways, full bedding or face shell bedding. A fully bedded joint describes the case when the tops of both face shells and webs of the masonry units are mortared. A face shell-bedded joint describes when only the tops of the face shells of the masonry units are mortared. When face shell-bedded walls are partially grouted, the webs around the grouted columns are also grouted to prevent the grout from leaking into the adjacent cores. In partially grouted walls, the in-plane shear stresses transferred between masonry webs is insignificantly small, leading to the usage of face shell bedding in a majority of cases. In circumstances where full bedding would be necessary to provide adequate vertical bearing area within a partially grouted wall, a fully grouted wall would generally be more practical.

When mortar is placed on a masonry unit, some of the wet cement paste is wicked into the drier masonry unit by capillary action. Through this the bond between the mortar and masonry becomes significantly stronger than a comparable bond between mortar and a non-porous material. To achieve optimum bond strength between the mortar and masonry, the mortar and masonry units must be within an acceptable range of moisture content. If the masonry unit is too wet, the mortar will not wick into the masonry. If the masonry unit is too dry, then too much of the moisture in the mortar will be sucked out and the cement in the mortar will not have enough water to properly hydrate, forming a weak mortar joint. The standards for masonry and mortar moisture content are contained in ASTM C270 (2014).

2.3.4 Prisms

Compressive strength parameters are often measured by testing a series of masonry prisms. Masonry prisms are assemblages that are typically a half to a whole block long and multiple courses high. Half block-long prisms are the most common, but may not be truly representative of actual conditions in some cases since they do not contain any head joints. Prisms may be left hollow or be fully-grouted, though grouted specimens rarely contain any vertical reinforcement. Horizontal

confinement reinforcement is included in the bed joints in only a few unique cases to study the confining effect of ties on masonry splitting. One such case is shown by Mayes et al. (1976b).

Masonry prisms tested under vertical compression loading will demonstrate an ultimate net compression stress less than that of the masonry units or grout. The ultimate stress for the prism is generally greater than that of the mortar. This phenomenon is related to the three-dimensional stress states within the masonry prism. Masonry units, mortar, and grout each have a different Poisson's ratio. The masonry units have a Poisson's ratio less than that of the mortar or grout. This disparity in ratios results in each material expanding laterally at different rates as they are strained in the vertical direction. These differences in lateral expansion rates induce lateral strains in the materials because they are all jointly interconnected together.

Since the mortar has a higher Poisson's ratio than the masonry units, the mortar seeks to expand laterally more than the adjacent masonry units. This causes the mortar to be confined in the two lateral directions, placing it into compression in all three coordinate directions. This tri-dimensional compression state allows the mortar to resist greater compressive loads than it could in a typical uniaxial compression state. This correlates to research which has determined that masonry prism strength is not well influenced by deviations in mortar strength.

While the masonry units are confining the mortar, the mortar is inducing outward forces on the masonry units themselves. This is further compounded by the inclusion of grout within the masonry cells which induces further outward strains on the masonry. Masonry prisms typically fail by cracking and spalling of the face shells instigated by the lateral tension induced within it. The lateral tension results in prisms having lower compression strength than the masonry units alone.

For prism tests to be truly representative of actual conditions they should be at least two courses high because the top and bottom masonry surfaces are laterally confined by the platens of the testing machine. Prisms of three courses are more representative because the central course is laterally unconfined from its top to its bottom, but the results from two-course prism tests can be used by applying an adjustment factor. Taller prisms may be tested as well, but this is generally avoided because the added costs are considered to outweigh the benefits. The results from taller prisms are similarly adjusted to account for slenderness effects. Common failure modes in masonry prisms include the vertical split, conical break, shear break, semi-conical break, and combinations of these modes (ASTM C1314, 2014).

In lieu of testing masonry prisms, the MSJC permits assemblage compressive strength to be derived using the "Unit Strength Method." This method allows the strength to be interpolated from values in a table grouped by the masonry unit compressive strength and mortar type. This method is considered by many to be overly conservative.

2.3.5 Failure Modes

Partially grouted shear walls demonstrate two distinctive failure modes: a flexural mode and a shear mode. Both modes of failure can occur at the post-peak loading of a wall due to the indeterminate nature of reinforced masonry walls. This is referred to in the literature as a flexural/shear failure.

The flexural mode of failure is characterized by horizontal bed joint cracking in the bottom courses, yielding of the vertical reinforcement, and ultimately by toe crushing. Flexure failures have been observed to be more ductile in large part because the failure requires yielding of the reinforcement. The amount that the reinforcement yields before crushing commences in the masonry toe is dependent on the quantity of vertical reinforcement. For large areas of vertical reinforcement, the reinforcement may yield only slightly or not at all before the masonry begins to crush at the far end of the wall. For walls with small areas of reinforcement, toe crushing is delayed and the reinforcement will undergo large amounts of plastic yielding before toe crushing begins. In the extreme case of plastic yielding, a rocking failure will occur when tested cyclically.

A rocking failure occurs when a continuous flexural crack forms from one end of a wall to the opposite end, usually in one or more bed joints (Kasparik, 2009) This is precipitated by the lack of vertical confinement inherent in the small amount of vertical reinforcement. In this case the wall is split into two parts connected only by the vertical reinforcement. As the lateral load reverses repeatedly the wall rocks back and forth, causing the reinforcement to yield in tension and compression with each subsequent cycle. Ultimate failure occurs by gradual disintegration and trituration of the mortar joint from repeated loading and by fatigue fracture of the reinforcement. A rocking failure also results in a significant loss in lateral stiffness.

The shear mode of failure is characterized by cracking and disintegration of the interior wall panel. In some cases the failure can occur suddenly in a brittle manner, but much research has been conducted to determine means of increasing ductility in shear failures. Cracking occurs

predominately as diagonal cracks proliferate within the masonry panel. However, in cases of low vertical confinement walls may experience a sliding shear failure. A sliding shear failure occurs when a continuous horizontal crack forms from one end of the wall to the other. The upper wall segment slides along the bottom segment with aggregate-interlock friction and dowel action of the vertical reinforcement acting as the only lateral force resisting mechanisms (Sveinsson et al., 1985).

The first sign of shear failure under lateral loading occurs as a 45 degree diagonal crack starting and spreading from the center of the wall. The diagonal cracking load is dependent on the tensile strength of the masonry and of the orientation of stresses within the wall by the superposition of vertical axial stress. This can be observed by using Mohr's circle to represent the biaxial stress pattern within the wall (Mayes et al., 1976c). Axial load also increases the aggregate interlock force, increasing the mechanical bond resistance and prolonging the breaking of the chemical bonds in the cementitious material (Ghanem et al., 1992, 1993; Shing et al., 1990). Since the reinforcement is not engaged until the masonry cracks, it is not effective in increasing the cracking strength of the wall panel. Many researchers have confirmed that the diagonal cracking load is not influenced by the quantity of reinforcement (Matsumura, 1987; Schultz et al., 1998; Ghanem et al., 1992, 1993; Shing et al., 1989; Haach et al., 2010a).

Once initial diagonal cracking has taken place within the panel, the horizontal reinforcement begins resisting the lateral forces and helps to keep the crack from opening. Though not directly operative in resisting the lateral load, it has been shown that distributed vertical reinforcement is also effective in keeping the shear cracks from opening (Ghanem et al., 1992). By keeping the diagonal crack closed, the masonry along both sides of the crack are able to transfer shear stresses via crack friction, resulting in an increased lateral capacity beyond the diagonal cracking load. Without adequate confinement, the diagonal crack will open and the masonry will no longer provide resistance to the lateral load.

The load at which diagonal cracking first occurs is referred to as the cracking load. The horizontal cracking load is not discussed in the shear literature though it is discussed in the MSJC code when referring to flexural strength of walls. At loads beyond the diagonal cracking load the wall, strength is provided by the horizontal reinforcement and by crack friction. As the load

continues to increase additional cracks begin to form in other parts of the masonry panel. These additional cracks transfer the lateral load via the same mechanisms as the initial diagonal crack.

Shear failure initiates in one of two ways. A brittle shear failure occurs in walls that are heavily reinforced, in which reinforcement is concentrated into small areas, or which are subjected to large axial loads (Ghanem et al., 1992; Nolph, 2010). Brittle failure appears as a sudden crushing of the masonry between adjacent horizontal reinforcement. Ductile shear occurs in walls that are lightly reinforced with distributed reinforcement and subjected to axial load less than 5 percent of the compressive strength (Ghanem et al., 1992). Ductile failure initiates as yielding of the horizontal reinforcement and is followed by sliding along the cracked planes and ultimately by crushing of the masonry. While a ductile shear failure is more difficult to achieve, modern research has shown that the implementation of certain provisions can force masonry shear walls to behave in a ductile manner (Schultz et al., 1998).

2.3.6 Shear Span Ratio

The shear span ratio is a value that has a significant influence on the failure mode of masonry panels (Matsumura, 1987; Schultz, 1996a,b; Maleki, 2008) and is mentioned by nearly every author in the literature either directly or indirectly. The definition of the shear span ratio is the ratio of the height of the inflection point to the horizontal length of the wall panel. It is frequently represented in the code and literature by

$$\frac{M_u}{V_u l_w} \tag{2.1}$$

where

M_u = the ultimate moment demand at a particular height along the wall panel,
V_u = the ultimate shear demand at the same height along the wall panel, and
l_w = the length of the wall panel.

It is more representative to think of the shear span ratio as being represented by

$$\frac{M_u/V_u}{l_w} \equiv \frac{h_e}{l_w} \tag{2.2}$$

where M_u/V_u and h_e are the *effective wall height*—or the height of the inflection point.

In wall panels tested under cantilever-type loading, the effective height h_e and the geometric height h_g of the wall are the same. For wall panels tested with both their top and bottom edges fixed against rotation (i.e., fixed-fixed or reverse-curvature loading), the inflection point is located at the mid-height of the wall and the effective height is half the geometric height. This definition of shear span ratio permits the equations to be used with walls which have other boundary conditions or loadings (e.g., when the top surface is only partially restrained against rotation).

2.4 Engineering Uncertainty

2.4.1 Development of Strength Design Theory

Prior to the implementation of strength design, structures in the United States were designed using the working stress method, which employed the use of safety factors to account for the uncertainties in loads, resistance, and models used in structural analysis. Standard-writing committees developed and adjusted these factors over time based on their increasing experience with existing structures, perceptions regarding the accuracy of structural analysis methods, and engineering judgment. The intuition-based design method worked well in producing structures for which the probability of failure was judged to be acceptably low, but they presented difficulty to designers in quantifying performance levels, producing consistent reliability between all structures, and quantifying the likelihood of failure. These weaknesses were especially pronounced for non-routine design situations for which there was little experience or precedence (Ellingwood and Galambos, 1982; Ellingwood, 2000).

During the middle part of twentieth century, engineering professionals were spurred by natural and man-made failures and public scrutiny to find means of overcoming the shortcomings of the working stress method. The solution was to create new, probabilistic design procedures that took advantage of the observed stochastic regularities demonstrated by structural materials and

loads. The ACI 318 code first introduced ultimate strength design in 1963 based on ultimate limit states of loads and resistances, as opposed to working stress of the material (MacGregor, 1983). In 1969, a consortium of engineers assembled by the American Iron and Steel Institute (AISI) and the American Institute of Steel Construction (AISC) was charged with further developing this theory for steel structures. The system the consortium assembled was an amalgamation of structural analysis and reliability theory that became known as Load and Resistance Factor Design (LRFD) (Ellingwood and Galambos, 1982; Ellingwood, 2000). The LRFD system first appeared in the 1986 version of the AISC code.

The new advances in design theory enabled U.S. code writers to standardize the load requirements for structures that had previously varied between material standards. In 1979 the National Bureau of Standards assembled a team to develop a universal set of load factors for use in building design (MacGregor, 1983). The common load requirements were adopted into ANSI Standard A58.1 by ballot in 1982. With the exception of the seismic and wind provisions, these requirements—which are now published in ASCE 7 (2010)—have changed little since that time (Ellingwood, 2000).

2.4.2 LRFD Theory

The LRFD theory is based on the requirement that

$$\phi R_n \geq \sum_{k=1}^{j} \gamma_k Q_{km} \tag{2.3}$$

where

R_n = the nominal strength of the structure,
ϕ = the resistance (or strength reduction) factor less than unity,
Q_{km} = the mean load effect, and
γ_k = the corresponding load factor equal to or greater than unity.

The left side of equation 2.3 reflects the uncertainty in the resistance (or capacity) of the structure while the right side represents uncertainties in the loads acting on it (Ravindra and Galambos,

1994). Beginning with the publication of ANSI Standard A58.1 (1982), the responsibility for specifying factors for each side of the equation has been divided between material design standards and load standards. The left hand side of Equation 2.3 is the purview of respective material design codes while the right hand side is defined by ASCE 7 (2010) (Ellingwood, 2000).

Resistance factors reflect the variability inherent in the mechanical properties of the materials, of variations in dimensions (tolerances), and the uncertainties in the theory underlying the design definition of member strength. In other terms, the sources of variability come from uncertainties in the material strength or stiffness, in member fabrication, and in the underlying assumptions used in developing the models. It is assumed that the sources of variation are independent of each other (Ravindra and Galambos, 1994). The development of appropriated resistance factors may also consider qualitative measures, such as the risk to occupants if the member fails without warning, the importance of the member within the structure, and the familiarity of the designer with the LRFD method (MacGregor, 1983; Ellingwood et al., 1980). The latter two considerations are difficult to quantify objectively and do not appear to be accounted for in the resistance factors, though the importance of a member within a structural may be incorporated into the load factor portion (right side) of Equation (2.3) through the consideration of tributary areas and live load reduction factors. Bažant and Yu (2006) also noted that reduction factors frequently contain a covert component which accounts for variation resulting from formula error. This modeling-error variation is not apparent to designers and is difficult to separate from the variation of the materials themselves.

The probability of failure p_f is the probability that the load exceeds the resistance (or strength) of a member and is represented by

$$p_f = P\left[(R - Q) \leq 0\right] \tag{2.4}$$

where $R - Q$ is known as the safety margin (MacGregor, 1983). Assuming that R and Q are randomly distributed, the safety margin Y has an expected value of

$$E(Y) \equiv \mu_Y = \mu_R - \mu_Q = E(R) - E(Q) \tag{2.5}$$

and variance of

$$\text{var}(Y) \equiv \sigma_Y^2 = \sigma_R^2 + \sigma_Q^2 \tag{2.6}$$

where σ_R^2 is the variance of R and σ_Q^2 is the variance of Q. The reliability of a structural member is measured by the safety index β (MacGregor, 1983) which is given by

$$\beta = \frac{\mu_Y}{\sigma_Y} \tag{2.7}$$

Since the probability distributions for R and Q are unknown, the safety index only represents a relative measure of reliability (Ravindra and Galambos, 1994).

By setting β as a constant, the structural reliability of all similar structure types becomes fixed. Ravindra and Galambos (1994) show that by assuming β to be constant, Equation 2.7 can be rearranged to produce

$$\mu_R = \theta \mu_Q \tag{2.8}$$

where θ is the central safety factor which is given by

$$\theta = \exp\left(\beta \sqrt{\frac{\sigma_R^2}{\mu_R^2} + \frac{\sigma_Q^2}{\mu_Q^2}}\right) \tag{2.9}$$

Using a first order approximation for the square root term, Ravindra and Galambos (1994) are able to combine Equations 2.8 and 2.9 to produce

$$\exp\left(-\alpha\beta \frac{\sigma_R}{\mu_R}\right) \mu_R \geq \exp\left(\alpha\beta \frac{\sigma_Q}{\mu_Q}\right) \mu_Q \tag{2.10}$$

which is another representation of Equation 2.3. The coefficient α is a constant chosen to minimize the errors in the approximation. Using the above approach, the resistance factor ϕ is calculated by

$$\phi = \exp\left(-\alpha\beta\frac{\sigma_R}{\mu_R}\right)\frac{\mu_R}{R_n} \tag{2.11}$$

where R_n is the nominal resistance from the predictive model.

2.4.3 Uncertainty in Masonry Design

The development of LRFD design criteria has been well-documented for ASCE 7, structural steel, and reinforced concrete but review of the literature has failed to produce the probabilistic rationale for for choosing the current 0.80 shear reduction factor for masonry. Ellingwood et al. (1980) performed an analysis of strength prediction equations for several materials and determined that the mean ratio of experimental to predicted strength is typically between 0.98 and 1.05 amongst various materials but provided no information on the variation of reinforced masonry shear walls because most of the masonry information was not available at the time. Research into the field of reliability analysis suggests that a common practice is to use a lower-bounded 90 or 95 percent confidence interval (Ellingwood et al., 1980). The MSJC (2013) specifies the use of the fifth-percentile (i.e., 95 percent upper confidence interval) of the measured strength distribution for steel anchor bolts but is mute for masonry shear or any other situation.

A practice presented in the literature is to use confidence intervals to account for the variation in material strengths. The use of a confidence internal in this case is statistically incorrect because a confidence interval applies only to an estimated parameter (e.g., mean or variance) from the sample (i.e, dataset). A confidence interval cannot be used as the basis for predicting strength values for future structural elements. The proper tool to use in calculating reduction factors for structural materials is to use a tolerance interval (Vardeman, 1992).

Masonry material strength frequently shows relatively high variability compared to other building materials. Blume and Proulx (1968) suggested that a variation of about 10 percent between test and predicted strength could be attributed to the inherent variability of masonry construction. The temptation may be to artificially deflate the shear strength factor for masonry shear walls because of the variability in material strength and the severity of failure mode. However, the shear strength equations were developed assuming static and cyclic loading conditions (Tomaževič

et al., 1996), which is the worst-case scenario in terms of strength. Due to the nature and methodology of masonry shear wall testing, the calculated strength is lower due to the strength degradation that occurs with repeated loadings near the ultimate strength. In practice, the greatest load experienced by a masonry shear wall will typically be applied either dynamically or monotonically, but not both, meaning that the nominal masonry predicted strength is slightly conservative because the worst-case scenario is not a typically load seen by structures.

In the case of seismic loading, seismic events produce shear loads that are cyclic and dynamic. Abrams (1988), Paulson and Abrams (1990), Tomaževič and Velechovsky (1992), Tomaževič (2000), Tomaževič et al. (1996) , and Williams and Scrivener (1974) determined that the apparent shear strength of masonry walls increases under dynamic loading due to strain rate effects. During a seismic event, the wall undergoes both strength and stiffness degradation as load approaches the ultimate strength. Stiffness degradation in the wall causes the fundamental period of the structure to increase and the center of rigidity to move away from the wall toward the other, more rigid, walls. As the period of the structure lengthens the overall induced lateral forces on the structure tend to decrease. As the center of rigidity moves away from the wall, the lateral forces are transferred to other parallel walls, further decreasing the lateral load demand on the damaged wall. Even in the cases where the ultimate strength is exceeded, the masonry wall will continue to dissipate energy if the reinforcement is detailed properly. All of these properties create an inherent conservativeness in the equation for seismic events.

In the case of gravity loads, the loads are typically applied monotonically and quasi-statically to masonry assemblages. Dillon and Fonseca (2014a; see Appendix B) determined that masonry shear walls loaded monotonically demonstrate an ultimate strength 19 percent greater than when tested cyclically. The load reversals of below-peak cyclic loading, which cause graduate strength degradation in cyclic masonry shear wall specimens, are absent in monotonic-type loadings. Monotonic loading is a greater concern to designers because the failure is frequently sudden and provides little warning. The surplus shear strength for monotonic loading creates an additional margin of safety over the nominal structural strength. As a result, the shear strength reduction factor need not be unnecessarily high to account for the severity of the brittle shear failure mode because the nominal strength equation already accounts for it.

CHAPTER 3. PRIMER: STATISTICAL METHODS

3.1 Introduction

Least squares regression has been used by scientists and statisticians for over two centuries as a technique to an overdetermined system of equations of the form

$$\boldsymbol{X}\boldsymbol{\beta} = \boldsymbol{y} \tag{3.1}$$

where

$$\boldsymbol{X} \in \mathbb{R}^{(m\times n)} = \text{the matrix of predictor variables,} \tag{3.2}$$
$$\boldsymbol{\beta} \in \mathbb{R}^{(n\times 1)} = \text{the unknown vector of regression coefficients,} \tag{3.3}$$
$$\boldsymbol{y} \in \mathbb{R}^{(m\times 1)} = \text{the vector of response variables, and} \tag{3.4}$$
$$m > n. \tag{3.5}$$

Since few overdetermined systems are consistent, the above approximation typically has no solution. The equation can be transformed by introducing the error term $\boldsymbol{\varepsilon}$ which represents the variation in the response variable $\boldsymbol{y}$. This transformation produces the consistent equation

$$\boldsymbol{X}\boldsymbol{\beta} + \boldsymbol{\varepsilon} = \boldsymbol{y} \tag{3.6}$$

for which a unique solution can be determined using the method of least squares as long as the matrix $\boldsymbol{X}$ is full rank.

3.2 History

The discovery and proof of the method of least squares forms an integral part of the development of statistical theory. Prior to the twentieth century, the field of statistics had yet to be

treated as a distinct field of study and was considered to be an extension and tool of the fields of mathematics and science. The method of least squares first appeared in print in 1805 during a time when the principal focus of mathematicians and scientists was concentrated on problems of astronomical motions, geodesy, social sciences, meteorology, and medicine. The discovery and proof of the method of least squares occurred at the confluence of two previously disjointed paths of discovery, combination of observations and probabilistic inference. With the discovery and quick acceptance of the method by a wide-spread audience in the early nineteenth century, the full justification and understanding of the method would take another century to complete.

3.2.1 Beginning Roots in Mathematical Probability

Prior to the eighteenth century, topics of probability were limited in scope to games of chance. By the beginning of the eighteenth century mathematicians had developed means to determine a priori the probabilities for different combinations and permutations. Up to this point no one had taken the understanding of probability and applied it to quantify the uncertainties in other areas of study. The first work at determining probabilities a posteriori was performed by Jakob and Nicolaus Bernoulli (Stigler, 1986).

Jakob Bernoulli (1713) wrote what would later be deemed to be the first exposition on the mathematical theory of probability. His principal contribution to the field, *Ars Conjectandi*, was posthumously published by his nephew Nicolaus Bernoulli. In the fourth section, Jakob Bernoulli introduced his Law of Large Numbers, which postulated that as the number of observations increases the uncertainty decreases, and set forth to prove it. The basis of his work was a binomial situation in which the numbers of fertile cases r and sterile cases s were both integers. He wished to prove (shown here in modern notation) that

$$P\left(\left|\frac{X}{N-p}\right| \leq \varepsilon\right) > cP\left(\left|\frac{X}{N-p} - p\right| > \varepsilon\right) \tag{3.7}$$

where

X = the number of observed fertile cases out of a total of N observations,

p = the unknown proportion of fertile cases (r) to total cases ($r + s$),

ε = an arbitrarily small number, and

c = an arbitrarily large number (Stigler, 1986).

In his proof, Bernoulli showed that by increasing the number of observations N to a sufficiently large number the true proportion $p = r/(r + s)$ can be approximated within a limit of $\pm 1/(r + s)$ with a guaranteed chance exceeding $c/(c + 1)$ (Bernoulli, 1713; Stigler, 1986; Hald, 1998).

In qualitative terms, Jakob Bernoulli's work was considered a success. For the first time in history Bernoulli proved that uncertainty in measurements can be quantified and that this uncertainty can be made smaller by increasing the number of observations. In quantitative terms, his work was deemed impractical for the time. The solution to his example problem of estimating the correct proportion of fertile to sterile cases would require 25,550 observations. This prohibitively high requirement was created by the unnecessarily high level of certainty he required for his problem (1,000 to 1). This failure was soon overcome, in part, by the later contributions of his nephew, Nicolaus Bernoulli (Stigler, 1986).

In addition to publishing his uncle's work, Nicolaus Bernoulli—whose work of note is published in Montmort (1713)—built upon it by treating the same problem from the complementary perspective. Where Jakob approached the problem by finding the number of observations needed to meet an assumed population proportion, Nicolaus assumed that the number of observations was fixed and set forth to determine a bound for the population proportion. Nicolaus' reformulation to determine a posteriori the proportion of fertile cases in the population was more typical of the problems faced by scientists and mathematicians in his day. He demonstrated his formulation through an example in which he successfully determined an interval for the proportion of male to female births in London (Stigler, 1986).

Abraham de Moivre would later pick up where the Bernoullis left off in attempting to approximate the sum of symmetric binomial terms. His work culminated in 1733, after notably substantial effort, with determining an accurate curve to approximate the binomial terms. This was made possible only after discovering an approximation for large factorials,

$$\left(\frac{2n}{n}\right)\left(\frac{1}{2}\right)^{2n} \cong \frac{1}{\sqrt{\pi n}}, \tag{3.8}$$

which enabled him to transform his expression into exponential form. His curve became the first appearance of the normal distribution curve, though de Moivre showed no intimation of understanding of the probability distribution function or its relation to his curve. He compared his curve to the binomial distribution for $n = 100$ and concluded confidently that his approximation was "tolerably accurate" for such a relatively small value when compared with Jakob Bernoulli's interminable value (Moivre, 1733; Stigler, 1986; Hald, 1998).

3.2.2 Three Questions and the Formation of Observational Combinations

Prior to 1750, the sentiment among the erudite class on combining and averaging data was not very favorable. The first publication touching on the possible favorability of combining observations appeared in 1722, when part of Roger Cotes' work was posthumously published in *Opera Miscellanea* (Cotes, 1722). In his work, Cotes observed that for observations made under different conditions the most probably correct estimate is determined by taking the weighted mean (i.e., the center of gravity) of the data points (Hald, 1998). Cotes' rule, as it has been called, was the first appearance of the theory of errors (Stigler, 1986).

In lieu of Cotes' work, the feeling at the middle of the eighteenth century, particularly amongst mathematicians, was that errors in observations accumulated when the observations were combined together. Astronomers and navigators were a little more willing to average observational data, but the practice was generally limited to instances where the observations were made under similar conditions and where measurements were considered to have equivalent accuracy (Placket, 1958). When Thomas Simpson (1756) later published a letter applying Cotes' Rule to a discussion on errors of observations, he provided the following historical delineation of the intellectual environment of his time:

> "It is well known... that the method practiced by astronomers, in order to diminish the error arising from the imperfections of instruments, and of the organs of sense, by taking the Mean of several observations, has not been so generally received, but that some persons, of considerable note, have been of opinion, and even publickly [sic] maintained, that one single observation, taken with care, was as much to be relied on as the Mean of a great number." (Simpson, 1756)

During the eighteenth century, the three primary problems that presented particular difficulty to intellectuals were 1) to account for the apparent non-periodic inequality observed in the motions of Jupiter and Saturn (see Euler 1749), 2) to determine and mathematically model the motions of the moon (see Mayer 1750), and 3) to determine the shape and figure of the Earth (see Boscovich and Maire 1755). In each case, the problem was modeled mathematically subject to the scientific constraints understood at the time. The model was then compared to the observational data to determine the unknown variables in the equation. In all cases, the number of observations formed more equations than there were unknowns, leading to an overdetermined system of equations. At the time there was no known means of solving an overdetermined system of equations, nor was the intellectual climate of the mid-eighteenth century suitable for the discovery of one.

Leonhard Euler (1749) took up the challenge of accounting for the apparent nonperiodic motions of Jupiter and Saturn. His data set included 75 observations from multiple sources spanning 163 years from 1582 to 1745. His model contained eight unknown parameters, two of which he was able to derive with relative confidence. Euler tried to find and group sets of data with similar observational conditions in an attempt to annihilate terms in his equations. Using this method he was able to reduce his model to 21 equations. Unfortunately for Euler he was unable to find enough situations where different sets of equations produced the same results. Due to his background and training in mathematics, he could not bring himself to average observations together to further reduce the number of equations. Euler arrived at his conclusions by changing the unknown variable values such as to make the errors as small as possible, a rather tedious and laborious process (Stigler, 1986).

Tobias Mayer (1750) undertook the problem of determining the librations of the moon. Mayer's model reduced to three unknown variables which he attempted to find using 27 observations made between 1748 and 1749. He accomplished this by grouping his observations together into three groups and by using the mean of each group in the system of equations to solve for the three unknowns. For the first group, he selected the nine observations that produced the largest value for first parameter α. He did similarly for the second group with regards to the second parameter β. The remaining observations were formed into the final group. Mayer's method—as it would come to be called—was the first successful use of the mean to solve an overdetermined system of equations. Part of Mayer's innovation can be attributed to his willingness to combine

similar data resulting from his backgrounds as an astronomer and mapmaker and from his use of his own observational data (Stigler, 1986; Hald, 1998).

Roger Boscovich and Maire (1755) addressed the problem of determining the ellipticity of the Earth. Boscovich used five measures that he felt were most likely to be accurate. Since the equation to compute ellipticity contains only two unknowns, Boscovich solved his problem for each combination of observations, producing ten distinct solutions. When he first tried to average the ten pairs he judged the resulting mean to be too high. He then tried the same method again after dropping two of the pairs because of the closeness in latitude of two of the observations. This slightly decreased the mean computed-ellipticity and, seeing the disparity in solutions between pairs, Boscovich concluded against the Earth being ellipsoidal (Stigler, 1986; Eisenhart, 1961).

Simpson (1756) followed de Moivre's work on the binomial density function by looking at the errors in observations. In his treatment of celestial bodies Simpson chose to ignore the distribution of the observations and, assuming the mean to represent the actual position of the body, instead focused on the distribution of the errors of the observations. In his analysis, he hypothesized—albeit erroneously—that the error distribution was known and proportional to the symmetric triangle distribution. Using this formulation, he continued on to rebuff the opinion that a single good observation, "taken with care," is as reliable as the mean of multiple observations. The most innovative and important contribution of his 1756 analysis was in determining that the probability of the mean error of multiple observations does not exceed that of a single observation. In so doing, he not only proved his point but also produced the rough equivalent to that which we today refer to as a confidence interval (Stigler, 1986; Hald, 1998).

Unsatisfied by his previous conclusions about the ellipticity of the Earth, Boscovich (1760) published a subsequent reworking of his initial analysis using a new method of combining measurements. Boscovich proposed that correction factors be added to all of the observations subject to the conditions that the sum of all the corrections is zero and that the sum of the absolute values of the corrections is minimum. Using his new method he was able to find an oblateness ratio for the Earth similar to that initially proposed by Sir Isaac Newton. Given his new findings and his confidence in his new method, Boscovich abrogated his initial conclusions from five years before. Although he did very little in furthering the development of his method, he was the first to propose

a procedure of fitting a line through data by minimizing a function of the residuals (Stigler, 1986; Hald, 1998).

Johann Heinrich Lambert (1765) proposed a method similar to that of Boscovich for fitting a straight line through a set a data. Lambert divided his data set into two groups with the lowest values of the predictor variables in the first group and the highest predictor variables in the second group. He then determined the centers of gravity for both groups and fit a regression line through both points. He used his method in solving several problems, one of which was a study on barometric differences between 12 points in the French mountains and sea level. Another problem he undertook was the same that Boscovich solved, finding the ellipticity of the Earth. Using his method, Lambert determined an oblateness ratio only slightly higher than that of Boscovich (Hald, 1998).

3.2.3 Laplace on the Two Modes of Thought

Pierre Simon Laplace was the first to encounter and work on both probability theory and combining observations. His first workings were on probabilistic mathematics first published in 1774 and later he expanded to methods of combining observations. Laplace's first memoir on probability 1774 was a treatment on both the principle of inverse probability and on the choice of mean. In his consideration of causes and events, he was able to independently find the two axioms (provided here in modern notation)

$$\frac{P\left(A_i \left| E\right.\right)}{P\left(A_j \left| E\right.\right)} = \frac{P\left(E \left| A_i\right.\right)}{P\left(E \left| A_j\right.\right)} \tag{3.9}$$

and

$$P\left(A_i \left| E\right.\right) = \frac{P\left(E \left| A_i\right.\right)}{\sum_j P\left(E \left| A_j\right.\right)} \tag{3.10}$$

where E represents an event and A_i represents one of n different causes. Laplace's second axiom is equivalent to Bayes' theorem given the assumption that $P\left(A_i\right) = 1/n$, an assumption that was commonly made in Laplace's period (Stigler, 1986). Though Laplace did not provide a proof for

his axioms, Laplace effectively showed that probability theory can be equally used for a posteriori inference as well as for a priori deduction (Hald, 1998).

In his work to determine the mean that should be used for multiple data, Laplace's work was divided into two parts. The first objective was to determine the error curve $\phi(x)$. After the error curve was known, the second objective was to establish how the mean ought to be determined. His attempt at his first objective began by stated three assumptions which he felt the correct curve must have:

> "1 . . . it is equally probable that any observation varies from the true value to right as to the left [i.e., the curve is symmetric].
>
> "2 . . . the probability that the observation diverges from the true value by an infinite amount is evidently zero.
>
> "3 The total area under the curve should be equal to unity, since it is certain that any observation will fall [under the curve]." (Laplace 1774, translation by the author)

The fact that there are an infinite number of functions that meet these requirements was likely a daunting task for Laplace. He started by considering $\phi(x) \propto e^{-m|x|}$ and from there settled on

$$\phi(x) = \frac{m}{2} e^{-m|x|} \tag{3.11}$$

where $m/2$ is required such that $\int \phi(x)\, dx = 1$ (Stigler, 1986; Hald, 1998). This would later be known as the Laplace distribution function (or double exponential distribution). When he later started on his second objective of finding a mean, he chose the criterion to minimize the sum of the absolute value of the difference between the chosen mean and true value. Laplace soon discovered that his equation and criterion together generated a case where the arithmetic mean is not the optimum value for the chosen mean, except in the case where the scale parameter $m \to \infty$ (i.e., the uniform distribution). The difficulty of the problem coupled with his unfamiliarity with the concept of conditional probability led Laplace to make an error in his proof (Stigler, 1986; Hald, 1998).

Laplace held back his next publication on a new error curve until 1781. For his second attempt he ignored the assumption of an infinite range and derived the curve

$$\phi(x) = \frac{1}{2a}\log\left(\frac{a}{|x|} \;\middle|\; |x| \leq a\right). \tag{3.12}$$

Compared to the difficulty of his previous curve (Laplace, 1774), the new curve was even more difficult for him to unravel. Laplace determined that for the second curve, like his first, the arithmetic mean is not the optimum choice for the chosen mean except for the case where $a \to \infty$ (again the uniform distribution). For both curves he concluded that the posterior median is the best choice for the chosen mean. Despite the imperfections in his 1774 and 1781 memoirs, they are notable for containing the first examples of a two-parameter inverse probability model and being for an impetus for his future innovations (Stigler, 1986; Hald, 1998).

Laplace would postpone further work on probability to undertake the challenge of determining the ellipticity of the Earth, initially ignoring Boscovich's work (Laplace, 1786), but subsequently building off of Boscovich's method (Laplace, 1793, 1799). Like Boscovich, Laplace also felt that the most likely figure could be determined by applying two conditions, "1 that the sum of the errors be zero; 2 that the sum of the errors taken with the sign + be a minimum" (Laplace, 1793). Whereas Boscovich presented his method in a verbal and geometric representation, Laplace (1793) presented the method in analytical and algebraic forms. Laplace followed by showing that the method solved the given problem and further demonstrated its usefulness by solving the ellipticity problem two ways; one way using nine arc lengths (as Boscovich had done previous) and the other by using thirteen pendulum lengths from different latitudes.

Laplace revisited the ellipticity problem a third and final time in 1799 after observing that the structuring of the problem gave undue weight to the observations made at higher latitudes. Since determination of the length per degree of latitude was made using different arc lengths from one observation to another, Laplace felt that this would invariably affect the relative accuracy of each observation. To correct this, Laplace weighted each observation by the length of the measured arc (in degrees of latitude) and set forth to solve the problem, subject to the two conditions mentioned above, using seven arc measurements. He completed his analysis by providing an analytical proof that this was the correct solution to the stated problem.

The validation and publicity Laplace provided to Boscovich's method increased its propitiousness and employment within other fields, such as water flow (Prony, 1804), surveying (Puissant, 1807), and cometary data (Bowditch, 1809, 1815). The development and successful use of methods for combining data and solving overdetermined systems of equations had prepared the intellectual community for the development and acceptance of the method of least squares (Stigler, 1986).

3.2.4 Confluence of the Two Paths

Adrien Marie Legendre first came into contact with observational data in 1792 after joining the commission charged with determining the meridian quadrant length through Paris. One of his first memoirs 1798 gives the intimation that he was familiar with the methods of Mayer, Boscovich, and Laplace, but he had yet to discover the method of least squares. He discovered the method while writing his 1805 memoir *Nouvelles méthods pour la détermination des orbites des comètes* ("New methods for the determination of comet orbits") and promptly understood its potential.

Legendre began his 1805 memoir with an appendix entitled *Sur la méthod des moindres quarrés* ("On the method of least squares"). In describing his new method, Legendre stated that "there is nothing more general, more exact, or of easier application than . . . to minimize the sum of the squares of the errors." He further explains four points unique to his method:

> "If it were possible to satisfy all equations with all errors being zero [i.e., a consistent equation], one could equally obtain this result by [this method] . . . .
>
> "If after having determined all the unknowns. . . one judges the errors to be too large, then one needs only to drop the equations [i.e., observations] that produce the errors. . . and to determine the unknowns with the remaining equations . . . .
>
> "The method by which one finds the mean of different observations is a simple case of this method . . . .
>
> "These formulae are the same by which one finds the center of gravity of several equal masses." (Legendre 1805, translation by the author)

He finished his memoir with an example in which he re-solved the meridian quadrant problem using the method of least squares, finding a solution very similar to that of Laplace from the

commission's official report (Laplace, 1799). Despite Legendre's remarkable claims for the potential and power of his method—albeit that they were true—it was several years before true strength of the method of least squares was formally proved by others (Stigler, 1986; Hald, 1998).

Like his predecessors, Carl Friedrich Gauss (1809) also wrote on the celestial motions of planets. In his *Theora Motu Corporum Coelestium in Sectionibus Conicis Solum Ambientium* ("The Theory of the Motion of Heavenly Bodies Moving About the Sun in Conic Sections") Gauss (1809) presented a section on the combination of observations. Here, he presented a solution to an overdetermined system from a completely new perspective. He assumed that the errors between true and measured values to be distributed such that their probabilities could be determined using a curve $\phi_i(\varepsilon_i v)$. He next chose parameters to maximize $\Omega = \phi_1(\varepsilon_1)\,\phi_2(\varepsilon_2)\ldots\phi_n(\varepsilon_n)$ to find the most probable combination of values for the parameters. He then noted that this could be readily accomplished by finding the partial derivatives of Ω with respect to each of the parameters, setting the resulting equations to zero, and solving the new system of equations.

With a means in place of solving an overdetermined system of equations, Gauss used a bold assumption to fill in the last hole he needed, a distribution curve. Like Laplace 35 years earlier, he stated three necessary requirements for an error curve—that it be single-peaked, centered at zero, and that the tails go to zero—then asserted that the only curve that maximizes Ω is given by

$$\phi(x) = \frac{h}{\sqrt{\pi}} e^{-h^2 x^2} \tag{3.13}$$

where h is a positive constant. Statisticians would recognize this as the probability density function for the standard normal distribution for the case where $h = 1/\sqrt{2}$. He followed this assertion by showing how this error distribution could reduce to the method of least squares. Though his conclusion presented a logical departure from accepted reasoning, Gauss provided the stochastic argument for the method of least squares that was previously missing (Stigler, 1986).

By 1810, Laplace had again returned to the subject of probability and had published a new work (Laplace, 1810) on a new generalization of de Moivre's limit theorem. In it, Laplace stated that if the number of observation is large enough, then any mean or sum is approximately normally distributed. Today this is called the Central Limit Theorem. In the paper Laplace used his theorem to show how to deduce probabilities for cometary data being contained within a few

specified symmetric limits. Using this technique, Laplace then performed hypothesis testing to judge whether all comets had the same inclination.

After initially completing his 1810 memoir Laplace read Gauss' book and, despite the logical incongruence within it, could quickly see how his limit theorem coincided with linear estimation. In the same publication he wrote a supplement showing how Gauss' choice for the error curve $\phi(x)$ was a better approximation and used his limit theorem to prove it. Whereas Legendre presented the method of least squares and Gauss contributed a stochastic argument in favor of it, Laplace provided the crowning justification to their work.

Having used the central limit theorem to lend credence to the method of least squares, Laplace (1812) approached the problem from another angle in his *Théorie analytique des probabilités* ("Analytical theory of probabilities"). In it he did not make any assumptions about the error distribution and used the central limit theorem again to show that for an overdetermined system of equations solved using least squares, the error terms are approximately normally distributed and the total error is minimum. Laplace used an asymptotic method in his analysis such that his conclusions are valid for any specific probability density function for an error curve (Stigler, 1986).

Over a decade later, Gauss (1823) would continue where Laplace left off with the proof of the method of least squares. In his revised and logically correct exposition of the method, he provided a clear and simple proof of a theorem that states that the method of least squares provides estimates of the parameters that have minimum variance and that are unbiased. His theorem is known today as the Gauss-Markov theorem. Additionally, Gauss provided theorems and proofs for the unbiased estimate and variance of σ^2. Gauss showed, similar to Laplace, that these properties of the method of least squares are independent of the error distribution. With his final theorems in place, the method of least squares had received full justification as the superior means of combining observations and making probabilistically-based inference. Over the next century more was learned about the method as its use spread to other disciplines (Hald, 1998).

3.2.5 Evolution

After the introduction of the method of least squares by Legendre and the groundbreaking work performed by Gauss and Laplace, the world saw a sharp increase in the numbers of papers being written on statistical topics. The justification of the method was met with a fervid acceptance

in the intellectual nations of the time. As time progressed, others would critique, validate, and continue where Gauss and Laplace left off.

The first to follow was Siméon-Denis Poisson first in 1824 and again in 1829. In both papers Poisson (1824, 1829) continued the work of Laplace by improving on the proof of the central limit theorem and by rewriting it such that it would have more general applicability to a multitude of cases. He first showed that the theorem is applicable to identically distributed variables and then he generalized the results to variables with different distributions. Through his proofs he implicitly showed that the variance of the mean is related to the number of observations n (Hald, 1998).

Augustin-Louis Cauchy was the first to determine a method of using residuals for estimating the number of parameters to be estimated and how to estimate them. His method (1835) can be described as a generalization of the method of least squares, though the two are not the same. He began his method by first reparameterizing the model $y = \beta_1 x_1 + \beta_2 x_2 + \cdots + \varepsilon$ to find an estimator $\hat{y}_1$ as a function of β_1 and x_1 assuming that all other β values are zero. He then computed the residuals and if they are sufficiently small he stopped; otherwise, he continues by calculating an estimator $\hat{y}_2$ as a function of β_2 and x_2 following the same process. He repeated these steps until the residuals met a certain tolerance level or he reached $\hat{y}_m$, where m is the number of observations. After this point he back calculated the values of the estimates of the parameters β_i. Cauchy (1853a) later described how the least squares estimators could be obtained from this his $\hat{y}$ values (Hald, 1998).

Irénée-Jules Bienaymé looked at the confidence intervals of single parameters used by Gauss and Laplace and felt he could do better. In is paper on error probabilities, Bienaymé (1852) determined simultaneous confidence regions for the parameters by transforming certain combinations of the errors. His transformation corresponds to the χ^2 distribution. Using his transformation Beinaymé was able to produce confidence ellipses for multivariate situations. After having read the paper by Cauchy (1853a) the next year, Bienaymé (1853) noted—among other things—that Cauchy's method produced larger errors than the method of least squares and that to produce similar results using the method would require more steps. The ensuing dispute between Bienaymé and Cauchy about the validity of the method of least squares led Cauchy (1853b,c) to repeat Poisson's proof 1824; 1829 of the central limit theorem (Hald, 1998).

Robert Leslie Ellis (1844) proved the central limit theorem another way in his paper on the method of least squares. In his paper, Ellis criticized Laplace and Poisson for beginning their proofs with discrete variables and for having to take limits to reduce their proofs into equations applicable to continuous data. Ellis eliminated the need for this by starting his proof using the Fourier integral theorem and by so doing made the proof substantially simpler. Ellis' work was subsequently simplified by James W. L. Glaisher (1872) who replaced Fourier's double integral with Dirichlet's discontinuity factor (Hald, 1998). Deficiencies in the classical proofs of the central limits were slowly tackled one-by-one over the following decades by Chebyshev (1887), Markov (1900), Liapounov (1901), Mises (1919), Pólya (1920), and Lévy (1925).

Pafnuty Lvovich Chebyshev (1859, 1864, 1875) improved on Cauchy's methodology by presenting the first method whereby the parameters could be estimated with the method of least squares. Chebyshev accomplished this by first orthogonalizing the data matrix. By beginning this way he was able to compute the parameter estimates independently of each other, thereby reducing the number of arithmetic operations that needed to be performed. Using his method one is able to fit models of successively higher degrees to the data. The drawback of Chebyshev's method is that it uses continued fractions and recursion formulae, meaning that the addition of new terms required the recalculation of the previous parameters (Hald, 1998).

Jørgen Pedersen Gram was inspired by the work of Bienaymé and Chebyshev. Building off of their works, Gram (1879) presented a method similar to that of Chebyshev (1875) but that improved upon it by not requiring the recalculation of the previous parameters. Moreover, his proof of the method was similar but simpler than originally presented by Chebyshev. Gram's method of orthogonalization was later represented in simpler form by Ernhard Schmidt (1907). Today the method is known as Gram-Schmidt orthogonalization in their honor (Hald, 1998).

Francis Galton investigated the distributions of a great deal of social and anthropometric data and determined that they "normally" follow the "law of frequency error," and renamed the term the "Normal distribution." Due to his weakness in advanced mathematics, he invented ways of graphically fitting distribution curves to data, methods that are still used today. He did this initially (1875) by using distribution and frequency curves and later (1899) by replacing them with lines on normal probability paper, today know as a quantile-quantile plot. Some of his investigations

into non-normal data 1879 led him to discover the lognormal distribution and the geometric mean (Stigler, 1986; Hald, 1998).

In his attempt to understand hereditary behavior, Galton invented his quincunx, or bean counter, as a means of empirically observing the results that many independent disturbances had on data distribution. Using three versions of his apparatus Galton (1877, 1889b) was able to experimentally show that a mixture of normal distributions is itself normally distributed. Together with his sweet pea study Galton (1877) used his results to describe the reversion property, which says that the deviation of the progeny from the population mean is negatively proportional to that of the parents (Pearson, 1921; Stigler, 1986; Hald, 1998).

Galton (1889b) later developed this idea further with anthropometric data about the heights of men and women. He graphed his data onto a surface plot with height on the abscissa, midparent height on the ordinate, and frequency of observation on the applicate. By drawing contours on his plot he noticed that the contours were nearly elliptical and concentric. When smoothed, he observed that all of the ellipses were centered at the means of the two parameters and that the major and minor axes of each ellipse had the same slope, respectively. Following this and similar experiments, he began to relate the parameters of the progeny to those of the parents using a new term "regression." Galton (1889a) soon after completed a broader investigation into the regression of correlations for bivariate data. This study led him to discover the concept of correlation coefficients and he expounds their uses as a means of measuring how well one variable may be correlated with another (Pearson, 1921; Stigler, 1986; Hald, 1998).

3.2.6 Contemporary Developments

Karl Pearson followed Galton's investigation into fitting distribution functions to data. After two attempts at fitting data to binomial (Pearson, 1893) and normal (Pearson, 1894) distributions, Pearson (1895) introduced a four-parameter differential equation for representing probability densities. Pearson (1900) then turned to multivariate distributions and calculated a criterion for estimating the probability that a theoretical distribution fits an observed distribution. This criterion is known today as the χ^2 test. Pearson lists three tests that could be performed using the χ^2 distribution: goodness of fit, homogeneity of two samples, and independence within a contingency table.

Later, Pearson (1917) expanded the use of the χ^2 test to multivariate contingency tables (Hald, 1998, 2007).

William Sealy Gosset, more frequency known by his penname "Student," studied statistics under Pearson during a brief leave from his work at Guinness Brewery. Whereas most researchers previously studied the distributions of populations and large samples, Gosset focused his efforts on small-sample statistics. Aware that the classical probability interval became increasingly subject to error, Gosset 1908b; 1908a proposed a new confidence interval and correlation coefficient based upon new distributions for the sample mean and sample deviation. He proposed a new statistic z and determined the corresponding probability integral (Hald, 1998, 2007).

R. A. Fisher continued Galton's work on the correlation coefficient by solving the question of finding the distribution of the correlation coefficient. Fisher (1912) solved the problem using a yet-to-be-considered geometric approach, showing that the distribution is strongly dependent on the number of observations and the population correlation. The results of Fisher's work were subsequently misinterpreted and criticized by a group of Pearson's colleagues (Soper et al., 1917) who argued against—what they thought that Fisher had concluded—a uniform prior probability distribution for the correlation coefficient (Hald, 2007).

Understanding where Pearson's team was confused with his work, Fisher (1921) set out to clarify his earlier results and to shed further light on the problem. Using equivocatory language, he explained the differences between the maximum likelihood estimate and posterior mode. Using a transformation of the correlation coefficient he was able to show that it is approximately normally distributed. After having determined the distribution of the correlation coefficient, Fisher (1915) expanded his work to include partial and multiple correlation coefficients. Through his work he derived a new distribution for the multivariate coefficient of determination R^2, which is known today as the non-central χ^2 distribution (Hald, 2007).

As an ardent follower of Gosset, Fisher understood the importance of his work and in 1915 first filled in gaps in Gosset's proofs. He later (1925) generalized Gosset's ideas to testing regression coefficients and transformed Gosset's z statistic into a new t statistic. He similarly transformed Gosset's z-distribution to create the t-distribution, which is the form that is used today. Fisher recognized that the t-test involved two independent distributions, the standard normal distribution and the χ^2 distribution. Fisher (1925) showed that the t-test may be used to test the significance of the

difference between two means. His next goal was to find a way to perform the test for groups with disparate variances. Fisher (1928) solved this problem by using the ratio of the two variances and in doing so discovered the F distribution, as it is now named. Fisher showed the usefulness of the F distribution in performing analysis of variance (ANOVA) tests, testing multivariate correlation coefficients, testing correlation ratios, and testing goodness of fit for a regression formula (Hald, 2007).

In addition to his mathematical additions to the statistical sciences, Fisher also contributed many lexicographical additions to the field. In his *On the Mathematical Determinations of Theoretical Statistics*, Fisher (1922) defined and explained the concepts and terms associated with the frequency-based theory of statistics. He described three types of problems—those of specification, estimation, and distribution— and set forth the three criteria of estimation—consistency, efficiency, and sufficiency. Another notable change set forth by Fisher was the distinction in notation between sample and population values. Since Fisher published this paper in 1922, statisticians have described estimates and values using his notation (Hald, 2007).

3.2.7 Normal Ratio Distribution

The first attempt at describing the distribution of the ratio of two normally distributed variables was performed by Roy C. Geary (1930). Geary determined that if x and y are two normal variates with correlation r and means $\mu_x = \mu_y = 0$ and if

$$z = \frac{a + x}{b + y}, \tag{3.14}$$

then the transformation

$$t = \frac{bz - a}{\sqrt{\sigma_y^2 z^2 - 2r\sigma_x\sigma_y z + \sigma_x^2}} \tag{3.15}$$

has a standard normal distribution provided that $P\left(b + y < 0\right) \approx 0$. Geary considered the condition $b \geq 3\sigma_y$ to be sufficient to satisfy the latter constraint. Edgar C. Fieller began researching the comparison of normally distributed variables while working in Karl Pearson's group. In 1932, Fieller wrote a paper discussing the index (or ratio X/Y) of a bivariate normal distribution (x, y)

(Irwin and Rest, 1961), improving on the work performed previously by Geary by eliminating the assumption of zero means. Fieller determined the form of the probability distribution function for the ratio $W = X/Y$, given by

$$\begin{aligned}\psi(w) &= \frac{b(w)d(w)}{\sqrt{2\pi}\sigma_x\sigma_y a^3(w)}\left[\Phi\left(\frac{b(w)}{\sqrt{1-\rho^2}a(w)}\right)-\Phi\left(-\frac{b(w)}{\sqrt{1-\rho^2}a(w)}\right)\right] \\ &\quad + \frac{\sqrt{1-\rho^2}}{\pi\sigma_x\sigma_y a^2(w)}\exp\left(-\frac{c}{2\left(1-\rho^2\right)}\right)\end{aligned} \tag{3.16}$$

where

$$\begin{aligned}a(w) &= \left(\frac{w^2}{\sigma_x^2}-\frac{2\rho w}{\sigma_x\sigma_y}+\frac{1}{\sigma_y^2}\right)^{\frac{1}{2}}, \\ b(w) &= \frac{\mu_x w}{\sigma_x^2}-\frac{\rho\left(\mu_x+\mu_y w\right)}{\sigma_x\sigma_y}+\frac{\mu_y}{\sigma_y^2}, \\ c &= \frac{\mu_x^2}{\sigma_x^2}-\frac{2\rho\mu_x\mu_y}{\sigma_x\sigma_y}+\frac{\mu_y^2}{\sigma_y^2}, \\ d(w) &= \exp\left(\frac{b^2(w)-c\,a^2(w)}{2\left(1-\rho^2\right)a^2(w)}\right), \\ \phi(u) &= \frac{1}{\sqrt{2\pi}}e^{-\frac{1}{2}u^2}, \text{ and} \\ \Phi(v) &= \int_{-\infty}^{v}\phi(u)\,du\end{aligned}$$

(notation adapted from Hinkley 1969).

David V. Hinkley (1969) examined the distribution of the ratio of two normal random variates x/y and compared the theoretical results with the assumption that $P\left(b+y<0\right)\approx 0$. This assumption is valid for cases where $0<\sigma_y\ll\mu_y$ because as $\mu_y/\sigma_y\to\infty$ (or as $P\left(y>0\right)\to 1$) the cumulative distribution function $F(w)$ of W follows the limit

$$F(w)\to\Phi\left(\frac{\mu_y w-\mu_x}{\sigma_x\sigma_y a(w)}\right) \tag{3.17}$$

which Hinkley used to approximate $F(w)$. Hinkley compared the approximation $F^*(w)$ to the exact form $F(w)$ and determined that $f(w) > f^*(w)$ for all w. He observed that $F^*(w)$ is a good approximation of $F(w)$ over most of the range, though the bound become slacker in the tails. He suggested an improved approximation to $F(w)$ given by

$$F^{**}(w) = F^*(w) - \Phi\left(-\frac{\mu_y}{\sigma_y}\right). \tag{3.18}$$

He concluded that due to the simplicity of the approximations of $F(w)$, the Ratio distribution can be easily facilitated in future analyses.

3.2.8 Tolerance intervals

Samuel S. (Wilks, 1941) first addressed the problem of how to calculate a range of tolerances for samples from a mass-produced product or part. More specifically, he investigated the necessary sample size such that a specified portion of the population lie within two limits with at least some minimum probability. He initially determined an approximate solution for the non-parametric case where the distribution function is continuous but otherwise unknown to the analyst. For the non-parametric case, Wilks determined a solution by using truncated sample ranges and he set forth a means to calculate the minimum number of samples to take in determining the tolerance limits for a specified probability and proportion of the population. Abraham Wald (1943) later extended Wilk's first method to the bivariate and multivariate data for the non-parametric case.

Wilks (1941, 1942) also determined a solution for the parametric case assuming that the population follows the normal distribution. He determined that the portion of the population within the interval $x \pm ks$ is given by

$$p = \frac{1}{\sqrt{2\pi}} \int_{\bar{x}-ks}^{\bar{x}+ks} e^{-\frac{1}{2}(x-\mu)^2/\sigma^2}\, dx \tag{3.19}$$

where

$\hat{x}$ = the sample mean,

μ = the unknown population mean, and

σ^2 = the unknown population variance.

For the two-sided tolerance interval, he provides a solution for k such that

$$k = t_{p,n-1} s \sqrt{(n+1)/n} \tag{3.20}$$

where $t_{p,n-1}$ is the critical value for the t-distribution for which the probability is equal to p and n is the number of samples.

Wald (1943) and Wald and Wolfowitz (1946) examined the parametric case for problems where the population is normally distributed and where the population mean and variance are unknown. They presented an approximate solution for the problem such that it could be determined from tables for the normal and χ^2 distributions. They determined the the two-tailed tolerance interval for the normal distribution can be approximated by

$$\bar{x} \pm s\, z_p \sqrt{\frac{n-1}{\chi^2_{\{n-1,1-\alpha\}}}} \tag{3.21}$$

where

$$\begin{aligned}
z_p &= P(z \geq p), \\
z &= \text{the standard normal distribution}, \\
\chi^2_{\{n-1,1-\alpha\}} &= P\left(\chi^2_{n-1} \leq 1-\alpha\right), \text{ and} \\
\chi^2_{n-1} &= \text{the } \chi^2 \text{ distribution with } n-1 \text{ degrees of freedom.}
\end{aligned}$$

Krishnamoorthy and Mathew (2009) give the following solution for the one-sided tolerance interval, which they refer to as the "classical approach." Given a continuous random variable X with cumulative distribution function given by

$$F_x(u) = P(x \leq u) \tag{3.22}$$

and let $\boldsymbol{x} = (x_1, x_2, \ldots, x_n)$ be a vector of n random samples from $F_X(x)$. A one-sided tolerance interval of the form $(-\infty, U(\boldsymbol{x})]$ is required to satisfy the condition

$$P_{\boldsymbol{x}}\left\{P_x(\, x \leq X(\boldsymbol{x}) | \, \boldsymbol{x}) \geq p\right\} \;=\; 1 - \alpha \tag{3.23}$$

where

p = the proportion of the population included in the interval,
$1 - \alpha$ = the confidence level
$U(\boldsymbol{x})$ = the one-sided upper tolerance limit.

The exact-form solution for the condition shown in equation (3.23) is given by

$$\bar{x} + s\, t_{\{n-1,1-\alpha\}} \left(\frac{z_p}{s}\right) \tag{3.24}$$

where

$t_{\{n-1,1-\alpha\}} = P(t_{n-1} \leq 1 - \alpha)$,
t_{n-1} = the t distribution with $n - 1$ degrees of freedom,
z_p = $P(z \geq p)$, and
z = the standard normal distribution.

Hall and Sampson (1973) presented an approximate solution for deriving tolerance intervals for the ratio of two independent normal distributions. They set up the problem by letting X and Y be two independent, normally distributed variables for which the variances are unknown. Their assumption assumed that the coefficient of variations were small, on the order of 0.05 or less, which was necessary such that $P(X \leq 0) \approx 0$ and $P(X \leq 0) \approx 0$. Assuming that $U = \ln X$ and $V = \ln Y$, they determined an approximate solution for the upper limit L such that

$$L = t_1/t_2 \, \exp(k\, s_{u+v}) \tag{3.25}$$

where s_{u+v} is related to the standard deviation of $U+V$. The coefficients t_1 and t_2 are the geometric means of samples from the X and Y populations, respectively, such that

$$t_1 = \prod_{i=1}^{n} x_i^{1/n} \tag{3.26}$$

and

$$\tag{3.27}$$

$$t_2 = \prod_{i=1}^{m} y_i^{1/m} \tag{3.28}$$

where n is the sample size from the X population and m is the sample size from the Y population. The variable k is the solution to the condition

$$P(P\left(U/V \leq t_1/t_2 \exp\left(k\, s_{u+v}\right)\right) > p) = 1-\alpha \tag{3.29}$$

which is equivalent to

$$P\left(t_{\left\{f, z_p\sqrt{n'}\right\}} < k\sqrt{n'}\right) = 1-\alpha \tag{3.30}$$

where

$$n' = \frac{mn\left(\sigma_u^2+\sigma_v^2\right)}{m\sigma_u^2+n\sigma_v^2}, \text{ and}$$

$$f = \frac{\left(\sigma_u^2+\sigma_v^2\right)^2}{\frac{\sigma_u^4}{n-1}+\frac{\sigma_v^4}{m-1}}.$$

Zhang, Mathew, and Yang (2009) solved the problem of deriving tolerance intervals for ratios of two independent or dependent normally distributed variables by examining two cases for the ratio X/Y. In the first case, they base their solution on an approximation of the cumulative distribution function of (X,Y)—initially used by Hinkley (1969)—by assuming that $\mu_y > 0$ and that

the coefficient of variation σ_y/μ_y is small. The solution for the approximate case determined using the generalized pivotal quantity and Monte Carlo simulation. They also examined the solution for the exact cumulative distribution function of the Normal Distribution as provided by Hinkley (1969). For the exact case, the solution is also determined using the generalized pivotal quantity, which appears in integral form and must be evaluated using numerical integration. Further consideration of the problem of deriving tolerance limits for ratio distributions is outside of the scope of this dissertation.

3.3 Multivariate Least-Squares Regression Theory

The linear regression equation can be represented in the algebraic form

$$\boldsymbol{y} = \beta_0 \boldsymbol{j} + \beta_1 \boldsymbol{x}_1 + \cdots + \beta_k \boldsymbol{x}_k + \boldsymbol{\varepsilon} \tag{3.31}$$

or in the matrix notation

$$\boldsymbol{y} = \boldsymbol{X}\boldsymbol{\beta} + \boldsymbol{\varepsilon}, \tag{3.32}$$

where

$$\boldsymbol{X} = [\boldsymbol{j}, \boldsymbol{x}_1, \cdots, \boldsymbol{x}_k],$$

$$\boldsymbol{\beta} = \begin{bmatrix} \beta_0 \\ \beta_1 \\ \vdots \\ \beta_k \end{bmatrix},$$

y = an n-dimensional column vector of response variables known as the *response vector*,

$\boldsymbol{j}$ = an n-dimensional column vector of ones,

ε = an n-dimensional column vector of the errors known as the error vector,

$\boldsymbol{\beta}$ = a $(k+1)$-dimensional vector of regression coefficients know as the coefficient vector, and

n = the number of observations.

The data matrix $\boldsymbol{X}$ is an $n \times k+1$ matrix whose columns $\boldsymbol{x}_1, \cdots, \boldsymbol{x}_k$ are n-dimensional column vectors of predictor variables.

The expected value (or mean), variance, and covariance are denoted by $E(y)$, $\mathrm{var}(y)$, and $\mathrm{cov}(y_i, y_j)$, respectively. Assuming that y has a probability distribution function $f(y)$, the statistics are given by

$$\mu = E(y) = \int_{-\infty}^{\infty} y f\,(y)\; dy, \tag{3.33}$$

$$\begin{aligned} \sigma^2 &= E\,(y-\mu)^2 = E\,(y - E\,(y))^2 \\ &= \int_{-\infty}^{\infty} (y - E\,(y))^2\; f\,(y)\; dy, \end{aligned} \tag{3.34}$$

and

$$\begin{aligned} \sigma_{ij} \;=\; \mathrm{cov}\left(y_i, y_j\right) \;&=\; E\left[\left(y_i - \mu_i\right)\left(y_j - \mu_j\right)\right] \\ &=\; \int_{-\infty}^{\infty}\int_{-\infty}^{\infty} \left(y_i - \mu_i\right)\left(y_j - \mu_j\right)\; f\left(y_i, y_j\right)\; dy_i\, dy_j, \end{aligned} \tag{3.35}$$

respectively.

Since $\boldsymbol{\beta}$ and $\boldsymbol{\varepsilon}$ are unknown, the method of least squares finds the estimators $\hat{\boldsymbol{\beta}}$ and $\hat{\boldsymbol{\varepsilon}}$ which are called the least-squares estimator vector and the residual vector, respectively. They are defined as

$$\hat{\boldsymbol{\beta}} = \left(\boldsymbol{X}'\boldsymbol{X}\right)^{-1}\boldsymbol{X}'\boldsymbol{y} \tag{3.36}$$

and

$$\hat{\boldsymbol{\varepsilon}} = \boldsymbol{y} - \boldsymbol{X}\hat{\boldsymbol{\beta}}\,. \tag{3.37}$$

The Gauss-Markov theorem states that $\hat{\boldsymbol{\beta}}$ is the best, linear, unbiased estimator of β, with best meaning that $\hat{\boldsymbol{\beta}}$ has minimum variance among all possible linear unbiased estimators as long as $\mathrm{cov}(y) = \sigma^2\boldsymbol{I}$. This condition holds true independent of the distribution of $\boldsymbol{y}$ (i.e., normality is not

necessary to obtain the least-squares estimators). The estimated value of $E(\boldsymbol{y})$ predicted by using the least-squares estimator is given by

$$\hat{\boldsymbol{y}} = \boldsymbol{X}\hat{\boldsymbol{\beta}} = \boldsymbol{X}\left(\boldsymbol{X}'\boldsymbol{X}\right)^{-1}\boldsymbol{X}'\boldsymbol{y}\,. \tag{3.38}$$

Substituting this value into the definition of the residual vector produces the simpler definition

$$\hat{\boldsymbol{\varepsilon}} = \boldsymbol{y} - \hat{\boldsymbol{y}}\,. \tag{3.39}$$

The above definitions require that the matrix product $\boldsymbol{X}'\boldsymbol{X}$ be nonsingular or, in other words, that $\boldsymbol{X}$ is a full rank matrix and that $n > k + 1$. The former condition is met when $\text{rank}(\boldsymbol{X}) = k + 1$, with $k + 1$ being the number of columns of $\boldsymbol{X}$, meaning that all of the columns of $\boldsymbol{X}$ are mutually independent. The later condition is necessary for the definition of an overdetermined system of equations to hold.

The variance σ^2 of the population is also unknown but can be estimated by using the sample variance s^2. The estimate of the variance is unbiased as long as $\text{cov}(\boldsymbol{y}) = \sigma^2\boldsymbol{I}$. The estimate is given by:

$$E\left(\sigma^2\right) = s^2 = \frac{1}{n-k-1}\left(\boldsymbol{y} - \boldsymbol{X}\hat{\boldsymbol{\beta}}\right)'\left(\boldsymbol{y} - \boldsymbol{X}\hat{\boldsymbol{\beta}}\right)\,. \tag{3.40}$$

The coefficient of determination $R^2 \in [0, 1]$ is used to describe how well the regression surface fits the data points. R^2 is the quotient of the regression sum of squares (SSR) and the corrected total sum of squares (SST). The corrected total sum of squares is the sum of the regression sum of squares SSR and the sum of squares of the errors (SSE). These relationships are given by

$$SSE = \hat{\boldsymbol{\varepsilon}}'\hat{\boldsymbol{\varepsilon}} = \left(\boldsymbol{y} - \boldsymbol{X}\hat{\boldsymbol{\beta}}\right)'\left(\boldsymbol{y} - \boldsymbol{X}\hat{\boldsymbol{\beta}}\right) = \boldsymbol{y}'\left[\boldsymbol{I} - \boldsymbol{X}\left(\boldsymbol{X}'\boldsymbol{X}\right)^{-1}\boldsymbol{X}'\right]\boldsymbol{y}, \tag{3.41}$$

$$SSR = \left(\boldsymbol{X}_c\hat{\boldsymbol{\beta}}_1\right)'\left(\boldsymbol{X}_c\hat{\boldsymbol{\beta}}_1\right) = \boldsymbol{y}'\boldsymbol{X}\hat{\boldsymbol{\beta}} - n\bar{y}^2, \tag{3.42}$$

$$SST = SSR + SSE = \left(\boldsymbol{y} - \boldsymbol{j}\bar{y}\right)'\left(\boldsymbol{y} - \boldsymbol{j}\bar{y}\right)\,, \tag{3.43}$$

and

$$R^2 = \frac{SSR}{SST} = \frac{SSR}{SSR + SSE} = \frac{\boldsymbol{y}'\boldsymbol{X}\hat{\boldsymbol{\beta}} - n\bar{y}^2}{\boldsymbol{y}'\boldsymbol{y} - n\bar{y}^2}, \tag{3.44}$$

where

$\boldsymbol{I}$ = the identity matrix,
$\bar{y}$ = $\frac{1}{n}\boldsymbol{j}'\boldsymbol{y}$ is the mean of the response variables,
$\hat{\boldsymbol{\beta}}_1$ = $(\beta_1, \cdots, \beta_k)'$ is a partition of the $\hat{\boldsymbol{\beta}}$ vector excluding the $\hat{\beta}_0$ row, and
$\boldsymbol{X}_c$ = the data matrix in centered form.

The centered form of the data matrix is given by:

$$\boldsymbol{X}_c = \left(\boldsymbol{I} - \frac{1}{n}\boldsymbol{J}\right)\boldsymbol{X}_1, \tag{3.45}$$

where $\boldsymbol{X}_1 = [x_1, \cdots, x_k]$, and $\boldsymbol{J} = \boldsymbol{j}\boldsymbol{j}'$ is an $n \times n$ dimensional matrix of ones. Using these definitions, the partitioned vector of least-squares estimators can be equally expressed as

$$\hat{\boldsymbol{\beta}}_1 = \left(\boldsymbol{X}_c'\boldsymbol{X}_c\right)^{-1}\boldsymbol{X}_c'\prime y\,. \tag{3.46}$$

Since overly-complicated models naturally have a better fit to data than simpler models, the adjusted coefficient of determination R_a^2 is a metric for judging models by goodness of fit together and ease of-use. It is defined as:

$$R_a^2 = \frac{(n-1)\,R^2 - k}{n - k - 1}\,. \tag{3.47}$$

A complete linear model built using multivariate linear least-squares is subject to two "classical" assumptions (Rencher and Schaalje, 2008):

1. $E(\boldsymbol{\varepsilon}) = \boldsymbol{0}$ or $E(\boldsymbol{y}) = \boldsymbol{X}\boldsymbol{\beta}$
2. $\text{cov}(\boldsymbol{\varepsilon}) = \sigma^2\boldsymbol{I}$ or $\text{cov}(\boldsymbol{y}) = \sigma^2\boldsymbol{I}$

The notation of the latter assumption denotes two smaller assumptions: that the errors are homoscedastic (i.e., $\text{var}(\varepsilon_i) = \sigma^2$) and that the errors are uncorrelated (i.e., $\text{cov}(\varepsilon_i, \varepsilon_j) = 0$). Under the normality assumption, the errors $\boldsymbol{\varepsilon}$ are independent in addition to being uncorrelated. When all assumptions have been met, then the statistics $\hat{\boldsymbol{\beta}}$ and s^2 are jointly sufficient statistics to describe all of the information about $\boldsymbol{\beta}$ and σ^2 that can be extracted from the sample data (Rencher and Schaalje, 2008). One of the strengths of least-squares regression is that it will always produce the best estimators of $\boldsymbol{\beta}$ and $\boldsymbol{\varepsilon}$, regardless of the distributions of $\boldsymbol{X}$ or $\boldsymbol{\varepsilon}$. This strength can also be a detriment in the hands of an inexperienced analyst because the method will still produce values if one or more of the necessary assumptions are broken. When the classical assumptions are violated for a set of data, methods of data transformations and data weighting can be used to correct the violations within the data (Carroll and Ruppert, 1988).

CHAPTER 4. META-ANALYSIS INTRODUCTION AND METHODOLOGY

4.1 Introduction

Meta-analysis is a statistical tool used to pool the findings from multiple studies together to compute the summary effect and precision of a single or group of parameters (Borenstein and Hedges, 2009). The summary effect is the weighted average of the effect sizes from multiple studies for a single parameter and is analogous to the weighted mean of the individual effects from the individual studies. The effect size (not to be confused with size effect) is a term which describes the measure of the influence that a parameter has on a response variable.

The development of meta-analysis as a statistical tool initially took place in the 1980s and it was further refined during the 1990s. Its usage has become standard in the fields of medicine, education, psychology, criminology, business, and ecology. The perception within these areas of meta-analysis' usefulness has grown to the point that many government agencies now encourage or require researchers to conduct a meta-analysis of previous research data before they can begin new funded studies (Borenstein and Hedges, 2009) The use of meta-analysis (or any other advanced statistical method) in engineering materials testing and analysis is still in its infancy.

4.2 Benefits of Meta-Analysis

The advantage of determining the summary effects through meta-analysis is that it produces more precise and statistically powerful estimates of a parameter's effect because it is able to evaluate several studies as a whole as opposed to examining each study individually. Statistical power is the probability that a statistical test rejects a hypothesis that is false or identifies an effect which actually exists (Cohen, 1988). It can similarly be denoted by

$$P(\text{ reject } H_0 | H_0 \text{ is false}) = P\left(\hat{\beta}_i > 0 \,\middle|\, \beta_i > 0\right) \tag{4.1}$$

where

H_0 = the null hypothesis,

β_i = the true effect size of a parameter, and

$\hat{\beta}_i$ = the measured (or estimated) effect size of a parameter.

Meta-analyses increase statistical power by increasing the total number of specimens in the analysis, thereby decreasing the sampling variability associated with each condition's mean (Levin, 1998). This can be explained using the concept of confidence intervals. The width of a confidence interval becomes narrower as the sample size increases (assuming that the added data doesn't add significantly more variation to the dataset), increasing the precision and statical power of the analysis. The effect sizes determined from individual studies will generally be comparable to one another in that they measure and study the same phenomenon. The use of meta-analysis and summary effects gives researchers the added ability to understand the results of any one study in the context of all the other studies (Borenstein and Hedges, 2009).

Another benefit of meta-analysis is the increased "generalizability" of the conclusions due to test replication within the analysis. Many masonry shear wall test programs contain little or no replication within their experimental design, usually due to cost, space, or other constraints placed upon the researcher. The absence of replicates within tests provides no effective way to gauge whether some observed effects are due to random chance or whether they represent an effect which actually exists. One good example from the literature was Specimen 3 from Schultz (1996a) which displayed a significantly higher experimental strength than what might be expected by comparing plots of experimental strength versus various design variables. If two specimens of each type had be tested, it is probable that the replicate specimen would have shown a more characteristic strength and would have positively identified the specimen in question as an outlier. Even more important than internal replication (i.e., replicates tested by the same researcher at the same facility) are replications that are tested by other researchers in other facilities (so-called external replication). External replication is able to produce "generalizability" to the population if the conclusions between the two studies are in agreement with each other (Robinson and Levin, 1997).

4.3 Methodology

Meta-analysis is the foundation in the development of each of the three approaches performed in this study. In the first approach the effect size investigated is the relation between the actual and predict shear strengths using the current MSJC shear equation. In the second and third approaches multiple effect sizes are analyzed for several design parameters to investigate their effect on shear strength. The meta-analyses for the three approaches were carried out in four parts: 1) data compilation, 2) data scrutinization, 3) data synthesization, and 4) meta-regression. The first three analysis parts were common to the three approaches. Only the methodology in the meta-regression step varied between the three approaches.

First, it was necessary to systematically and thoroughly review the literature for data that could be used in developing these approaches. The earliest records of research on grouted masonry shear walls was found to have come from the late 1960s. The records were found from a variety of sources, including journal articles, conferences papers, technical reports, theses, and dissertations. In several cases the data from a series of shear wall tests were reported multiple times through various sources and in many cases the data was found in a single source. All of the specimen data were recorded in a spreadsheet.

Second, the data was scrutinized to identify and filter which specimens should be included within the analysis and which should not. The criteria to be used in scrutinizing the data were decided from the objectives and scope of the analysis and included factors such as grouting, failure mode, and completeness of data.

Third, it was necessary to synthesize the data such that the values and results would be compatible with each other since the data were collected from multiples sources, conducted by many different researchers using many different methods. The simplest synthesization that needed to be performed was to convert to a common system of units. Many other areas needing synthesization were identified during the data collections process. Since no previous methodology for synthesizing masonry shear wall data was available at the outset of this study, a methodology for standardizing the data needed to be developed for this study. The creation of the standardization method is detailed in Appendix C and its implementation is detailed in Section 6.4.

Lastly, the process of meta-regression performed withing this study varied between each of the three approaches analyzed in this paper. In all three approaches the response variable is the

experimental masonry wall shear strength for each specimen. In the first approach the parameter being investigated is the predicted shear strength using the MSJC (2013) equation and the summary effect is the ratio of the experimental shear strength to the predicted shear strength. In the second approach, the effects of multiple parameters are investigated where each parameter is a function of wall design variables and there are multiple summary effects, one for the relationship of each parameter to the experimental strength. In the third approach, the influence of several design procedures are investigated for their effect on the summary effect, which is the correlation of the design and experimental strengths.

Part II

Dataset Assembly

This part provides details into the process of data analysis used in assembling and analyzing the dataset for this study. Chapter 5 presents a literature review of the processes used by the original researchers to test the specimens analyzed in this study. Chapter 6 details how the dataset was assembled from the previous research studies and how the data were synthesized to overcome incompatibilities between the difference research studies. Chapter 7 finishes Part II with an overview of the completed dataset and its properties are shown and discussed in detail.

The completed dataset described in the part dataset contained 353 shear wall specimens, of which 171 were fully-grouted and 182 were partially grouted. This dataset represents the largest dataset of fully- and partially-grouted shear walls yet assembled for analysis. The specimens in the dataset were representative of a wide array of population parameter combinations and came from many studies distributed around the world. This dataset was the most comprehensive and representative of all masonry parameters typical used in structural design.

CHAPTER 5. LITERATURE REVIEW: EXPERIMENTAL TESTING

5.1 Early International Tests

5.1.1 Meli, Zeevaert Wolf, and Esteva

Meli, Wolf, and Esteva (1968) performed some of the first in-plane shear tests on partially-grouted masonry walls at La Universidad Nacional Autónoma de México. They tested 18 walls using either cantilever or diagonal compression testing procedures. Two of the walls were constructed using hollow clay bricks (HCBs) and the remainder were constructed using concrete masonry units (CMUs). All of the specimens were partially-grouted. This was likely chosen because partial grouting more closely resembles the construction of confined masonry walls which are extensively used in Mexico.

The purpose of their study was to develop methods for calculating flexural and shear strengths and the lateral stiffness of masonry walls. Their tests examined the influence of various vertical reinforcement ratios and vertical axial loadings on the behavior of walls subject to repeated shear loading. They subjected each wall to twelve cycles of alternating loads. The deformation amplitude was kept constant for all of the loading cycles of the same wall. They chose deformation amplitudes greater than those corresponding to the maximum shear strength. As such, the maximum shear strength was obtained on the first cycle.

Two types of loading were carried out in this research program. In the cantilever-type loading, equal and opposite lateral loads were applied to two diagonal corners of panel. The base was fixed against rotation and the top of the panel was permitted to rotate normal to the plane of the wall. In the diagonal compression-type loading, equal and opposite lateral loads were applied to two diagonal corners of the panel. Two equal and opposite vertical loads were also applied to the same corners as the lateral load and were oriented to resist the overturning moment generated by the lateral load couple. They observed that diagonal cracking is primarily concentrated in the

unreinforced panels of the walls. The presence of vertical load reduced the amount of cracking in the walls, but did not change the cracking pattern.

They compared the results to the equations developed by Esteva (1966) for confined masonry walls. They noted that the grouted cells do not provide as much lateral strength and stiffness as do the tie columns of a confined masonry wall. However, the effect of imposed vertical loads appeared to be the same between the two cases. They modified Esteva's earlier equation and proposed Equation (5.1) for use with partially-grouted walls.

$$V_n = \left(0.82\sqrt{f'_m} + 0.38 f_v\right) A_n \tag{5.1}$$

where

V_n = the predicted ultimate masonry shear strength (kg/cm^2),
f'_m = the compressions strength of masonry,
f_v = the vertical bearing stress (kg/cm^2), and
A_n = the net shear area of wall.

The walls tested under the cantilever loading failed in flexure and showed a more ductile behavior than those failing in shear.

Meli et al. observed that the addition of the first vertical load increased the shear capacity by a factor greater than what was in the existing shear strength equations for cantilever-type loading. In walls on which the second vertical loading was applied, no appreciable difference was found from the first loading scenario.

Meli et al. noted that the cracking strength of the walls appeared to be governed by diagonal tension in the wall panel, meaning that the cracking strength is independent of both the reinforcement ratio and the vertical axial load. In walls with no axial load the cracking strength was very close to the ultimate strength of the wall. In walls with axial load the strength continued to increase with drift after initial cracking.

Meli et al. noted that the amount of vertical reinforcement seemed to have no influence on the strength or stiffness degradation of the wall. They observed that the specimens with horizontal reinforcement were able to maintain strength and rigidity at slightly higher drift levels. Meli et

al. observed that no significant capacity was gained through the use of ties on the vertical reinforcement in the compression toe of the wall; however, they noted that it improved the behavior of the wall under repeated cyclic loads.

Meli et al. concluded that the presence of vertical axial load is decisive in improving behavior under repeated cyclic loads. They observed that the deterioration of the walls under the cantilever-type loading was marginally better than those under the diagonal compression-type loading.

5.1.2 Meli and Salgado

Meli and Salgado (1969) tested 46 reinforced masonry walls under two different loading conditions at La Universidad Nacional Autónoma de México. They tested 12 walls under lateral cyclic loading using hollow CMUs. The remaining 34 tests were performed under monotonic loading conditions using hollow CMUs, hollow clay bricks, or solid clay bricks. All but one of the walls constructed with hollow masonry units were partially-grouted. The specimens using solid clay bricks incorporated reinforcement cast into tie columns along the edges of the panel rather than bars running through the masonry. This would be classified as confined masonry today, for which much research has been performed outside of the United States.

The objective of their study was to observe the difference in behavior between walls of different materials, the influence of vertical axial load, and the quantity of interior reinforcement. The goal of their study was to propose methods to analyze and calculate the strength and stiffness of masonry walls. All of the walls contained only vertical reinforcement. In the majority of specimens the vertical reinforcement was limited only to the exterior cells. Five specimens included interior reinforcement evenly spaced along the length of the wall. The walls were all constructed with one reinforcing bar per cell. In walls with four bars in the extreme cells, the two extreme-most cells were grouted in each jamb.

Two loading methods were used for both the monotonic and cyclic load histories. In the cantilever-type loading, equal and opposite lateral loads were applied to two diagonal corners of the panel. The base was fixed against rotation and the top of the panel was permitted to rotate normal to the plane of the wall. In the diagonal compression-type loading, equal and opposite lateral loads were applied to two diagonal corners of the panel. Two equal and opposite vertical loads were

applied to the same corners as the lateral loads to resist the overturning moment generated by the lateral force couple. In the case of the cyclic loading, the vertical loads on the top corners were applied using rollers to reduce friction in the in-plane direction.

Meli and Salgado observed that increasing the amount of vertical reinforcement changed the failure mode from a flexural to diagonal tension. Within walls with less vertical reinforcement, flexural cracking of the bed joints dominated. Walls with higher amounts of interior reinforcement experienced diagonal cracking through the head and bed joints along the wall diagonal. They further observed that in these walls the quantity of vertical and horizontal reinforcement had a negligible effect on the diagonal cracking strength. However, they concluded that axial loading had a significant effect on the shear capacity of the wall. They observed that at values up to 20 percent of wall axial strength, the axial shear capacity increased by a factor of half the applied axial load. Lastly, they concluded that the ultimate shear strength of the wall is minimally affected by mortar quality, but that the cracking load is very sensitive to the mortar quality.

5.1.3 Williams and Scrivener

Williams (1971) and Williams and Scrivener (1974) tested 17 reinforced masonry walls under in-plane shear loading. The tests were performed primarily on fully-grouted masonry walls, but he also tested one partially-grouted wall constructed of clay brick. Williams referred to the partially-grouted walls as being "partially filled," hinting that the concept of partial grouting was still relatively new at that time.

The Williams and Scrivener study was divided into two phases. The first phase investigated the effects of cyclic loading on both hollow clay and hollow concrete masonry walls with varying levels of axial stress and included one partially-grouted specimen. The second phase investigated the material failure mechanisms and focused solely on fully-grouted clay specimens and included the experimental factors of variable axial loads, vertical reinforcement ratios, and aspect ratios. All of the wall specimens in both phases contained only vertical reinforcement.

The principle objective was to expand the understanding of masonry walls with post-elastic cyclic loading. Prior to his research, many of the masonry wall studies were performed with monotonically increasing loads to failure. Their tests were designed to study three responses: the ductility capacity, the stiffness degradation and load capacity deterioration characteristics, and the

ultimate load and failure mechanism. Williams and Scrivener observed that the partially-grouted wall attained 83 percent of the ultimate strength of the fully-grouted wall with comparable dimensions and reinforcement. They also observed that the partially-grouted wall exhibited greater stiffness degradation and load capacity deterioration.

5.2 UC-Berkeley Test Program on Masonry Piers

5.2.1 Mayes, Omote, and Clough

Mayes et al. (1976b,c) performed 17 tests on double-pier specimens consisting of eight identical pairs and a lone unreinforced specimen. Mayes et al. chose double-pier sections to simulate, as closely as possible, the end boundary conditions of the walls (piers) in actual structures. One pair of specimens was partially-grouted and all the remaining specimens were fully-grouted. Their tests were some of the first in the larger masonry test program on masonry piers undertaken at UC-Berkeley from 1975 to 1985. The remaining tests (Hidalgo et al., 1978; Chen et al., 1978; Hidalgo et al., 1979; Sveinsson et al., 1985) were all performed using fixed-end single masonry piers.

The purpose of their study was to investigate the effect of bearing stress, loading rate, quantity and distribution of reinforcement, and partial grouting on the strength and deformation properties of the masonry piers. Two cyclic loading conditions were used on each pair of walls. The first wall of each pair was tested under a pseudo-static loading and the second was tested under a dynamic loading. In all of the loading cases, the walls were tested with using gradually-increasing displacement amplitudes. The pseudo-static cases used a loading frequency of 0.2 Hz and the dynamic cases used a frequency of 3 Hz.

All of the panels were constructed from CMU blocks consisting of eight courses in running bond. The units contained reinforcement in the end cells only. The horizontal reinforcement distribution varied from specimen to specimen and was one of the variables under investigation in this project. The partially-grouted specimens contained only vertical reinforcement consisting of two #6 bars in each jamb. The ends of the piers were affixed to fully-grouted, reinforced masonry spandrels meant to simulate the effect of coupling beams on the piers. Their specimen layout is shown in Figure 5.1.

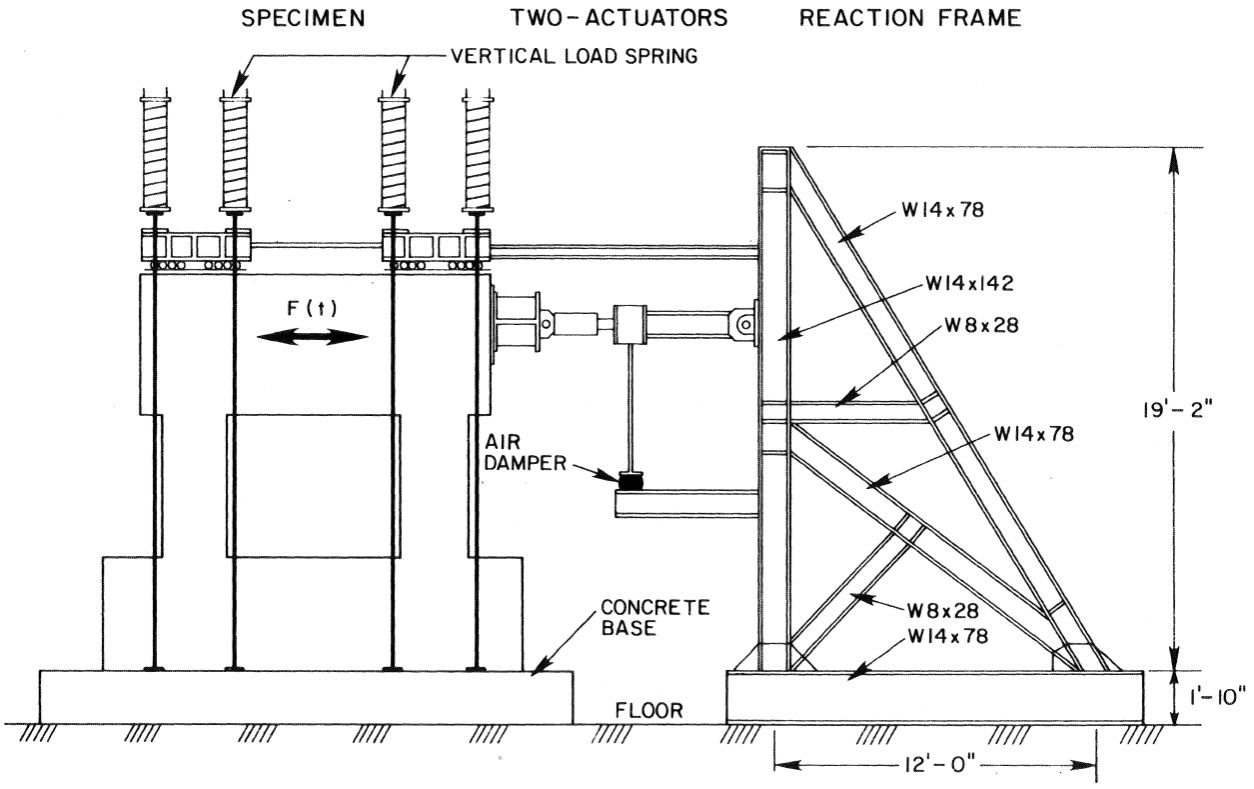

Figure 5.1: Masonry double-pier specimen from Mayes et al. (1976b)

Mayes et al. compared the fully- and partially-grouted wall test results for the same reinforcement and bearing load values. They observed that they both showed the same ultimate strength based on net area under the pseudo-static load. Under the dynamic loading the partially-grouted specimen showed an 80 percent decrease in net ultimate strength compared to the fully-grouted specimen. Mayes et al. observed that the partially-grouted piers displayed diagonal tension and vertical splitting failure modes. These failure modes were also observed in fully-grouted piers with large axial loadings. They noted that the effect of partial grouting on pier ductility was inconclusive. For the pseudo-static tests, the partially-grouted specimen's behavior was more elasto-plastic than that of the fully-grouted specimen. Under the dynamic loading, the initial stiffnesses and load degradations at higher deflections were similar for the two grouting types. However, the load capacity of the partially-grouted specimen plateaued before eventually falling off whereas that of the fully-grouted specimen continued to climb, peaked, and then fell.

Mayes et al. noted that the fully-grouted specimens collapsed at a lateral drift of 1.0 inch whereas the partially-grouted specimens collapsed at a drift of only 0.5 inches. The fully-grouted

walls with higher bearing load also collapsed at a drift of 0.5 inches. It this case the partially-grouted specimens exhibited the same failure mechanisms and ultimate drift as the fully-grouted walls with high bearing stress. Mayes et al. concluded that the partially-grouted specimens showed a tendency toward elasto-plastic behavior, but that the comparison between them and fully-grouted piers was inconclusive.

5.2.2 Hidalgo, Mayes, McNiven, and Clough

Hidalgo et al. (1978) tested fourteen full-scale masonry walls with a geometric aspect ratio of 2.0. Nine of the piers were constructed with hollow clay brick and the remaining five were constructed as double-wythe, grouted-core walls using solid clay bricks. Three of the hollow clay brick walls were partially-grouted and the remaining six were fully-grouted. Their tests were a part of the larger test program on masonry piers undertaken at UC-Berkeley. The three partially-grouted walls all contained a single #8 vertical bar in each end cell, but contained a different quantity of horizontal reinforcement, from none to three #5 bars. All of the other variables were constant between the tests.

Hidalgo et al. tested all of their walls using in-plane cyclic shear loading with increasing peak displacements. All of the walls were tested in the frame shown in Figure 5.2, in which the top and bottom of the walls remained parallel during the test. The frame subjected each wall to double-flexure bending, locating the inflection point at the mid-height of the wall, producing a shear span ratio of 1.0. All of the walls in each of the two test sets were subjected to the same applied axial load. He noted, though, that the boundary conditions were slightly flexible and that fixed-fixed boundary conditions were likely not achieved for small lateral displacements

All three of the partially-grouted specimens failed in shear due to the fixed-fixed loading condition. Hidalgo et al. observed that the partially-grouted specimens obtained a net ultimate shear stress 90 percent of that of the fully-grouted walls. They found that the deformational capacity of the partially-grouted walls was less than that of the fully-grouted walls at ultimate load. They, correspondingly, displayed less-ductile behavior than their fully-grouted counterparts.

Hidalgo et al. examined and compared the hysteresis plots for the two groups. They observed that stiffness degradation based on net area was similar between the two grouting types. They surmised that stiffness degradation is independent of the grouting type for the gradually in-

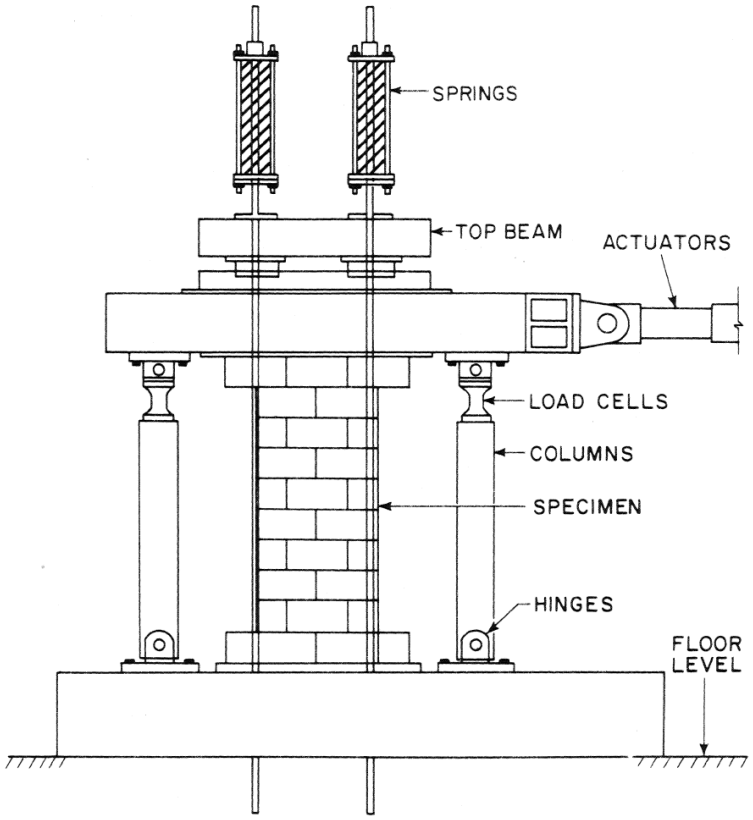

Figure 5.2: Masonry single-pier specimen from Hidalgo et al. (1978)

creasing cyclic load case. They used the hysteresis data to form displacement-EDT ratio graphs. Comparing the graphs, they saw similarities between the two grouting groups and concluded that energy dissipation is also independent of grouting type.

5.2.3 Chen, Hidalgo, Mayes, Clough, and McNiven

Chen et al. (1978) tested 31 masonry piers with an aspect ratio of 1.0. Eleven of the piers were constructed with hollow concrete masonry units, thirteen were constructed with hollow clay brick, and the remaining seven were constructed as double-wythe, grouted-core walls using solid clay bricks. Four of their concrete masonry piers and four of their hollow clay brick piers were partially-grouted and the remaining 23 piers were fully-grouted. Their study was the last in the masonry piers test program at UC-Berkeley to include partially-grouted specimens. The two subsequent tests in the series (Hidalgo et al., 1979; Sveinsson et al., 1985) tested only fully-grouted specimens.

Chen et al. tested all of their walls under in-plane loading using varying design parameters and a disparate test set-up from that of Hidalgo et al. (1978) explained above. Their test set-up produced a shear span ratio of 0.5 for their specimens. All of the specimens in each material group were tested under the same gross bearing stress—55 psi (0.38 MPa) for the concrete masonry group, 56 psi (0.39 MPa) for hollow clay brick group, and 42 psi (0.29 MPa) for the double-wythe, grouted-core group. The amount of vertical and horizontal reinforcement varied between the four partially-grouted specimens within each of the two material groups. The four combinations of reinforcement area were the same between the two groups. The test frame included a pinned column at both ends of the wall specimen that connected the top and bottom beams, as shown in Figure 5.3. The two columns were designed to keep the top and bottom beams parallel during the tests and impose fixed-end boundary constraints on the piers. Due to use of the pinned columns, additional compressive loads were developed in the piers by the downward displacement of the top beam as the top displaced laterally.

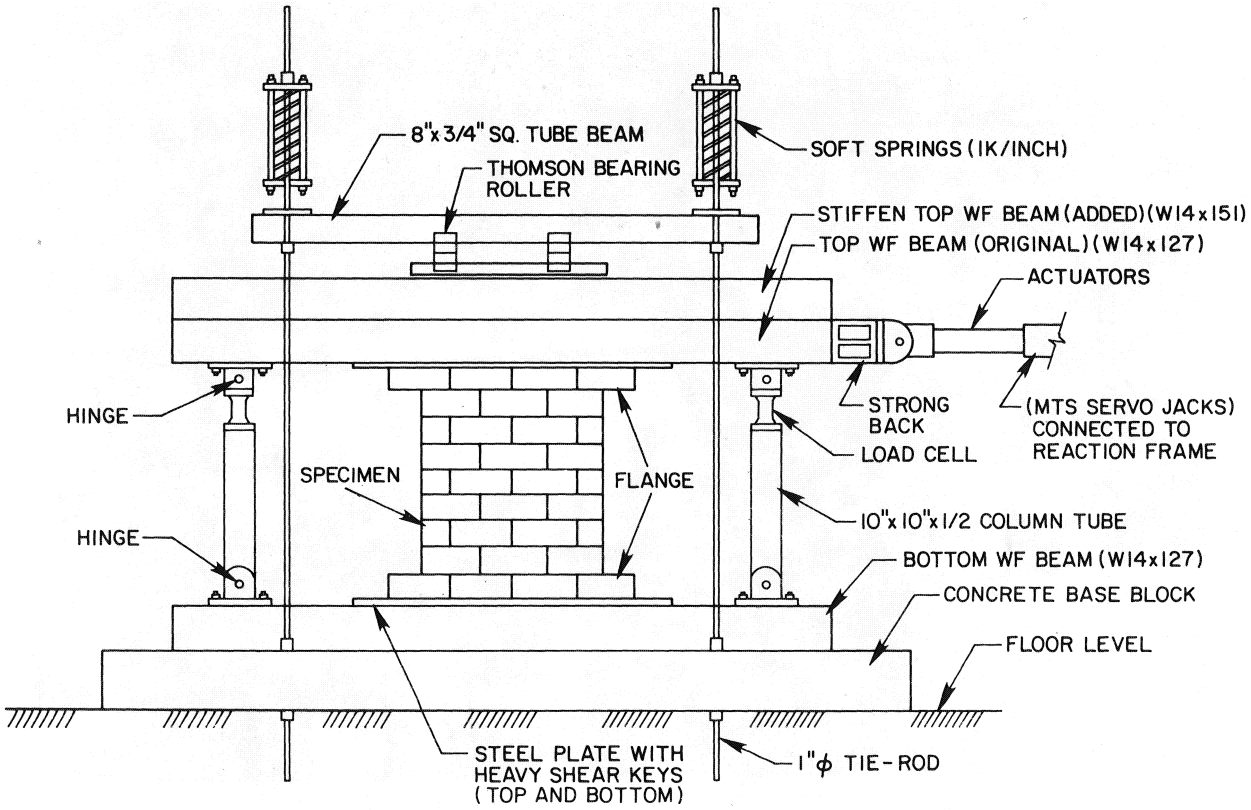

Figure 5.3: Masonry shear wall test setup from Chen et al. (1978)

Chen et al. observed that all of the piers showed a shear mode of failure; in some of the fully-grouted specimens this was accompanied by some flexural failure as well. Part of the reason for this was due to the additional compressive load on the piers at higher drift levels. The partially-grouted piers achieved a lower ultimate lateral load than that of the fully-grouted specimens. Chen et al. observed no significant difference between walls of each group for the two sizes of vertical reinforcement used. Since the walls all failed in the shear mode, the extra vertical reinforcement was redundant and did not affect the shear strength. Part of the reason for this redundancy was that the additional vertical compression stress counteracted part of the tensile forces that the reinforcement was intended to resist. This reduced the amount of vertical reinforcement required to force the wall into a shear mode of failure as opposed to a flexural mode.

Chen et al. observed that the net ultimate strength of the partially-grouted concrete masonry piers was 22 percent higher than that of the comparable fully-grouted piers. In the case of the hollow clay brick piers, the partially-grouted piers had a net ultimate stress 23 percent less than the corresponding fully-grouted piers. Chen et al. observed that the partially-grouted concrete masonry piers had better inelastic behavior based on net area than did the fully-grouted piers. In the case of the hollow clay brick piers, the fully-grouted piers showed better inelastic behavior. Within the concrete block and clay brick groups, the partially-grouted piers had a reduced deformation capacity with mean values of 82 percent and 62 percent, respectively, of the corresponding fully-grouted deformation capacity. Chen et al. did not examine how part of this may have been attributed to the additional compressive load on the fully-grouted walls at higher drift levels developed by the pinned columns. In all but two cases, the net bearing stress was greater for the partially-grouted piers than for the fully-grouted piers at their respective ultimate drifts, possible causing the partially-grouted walls to behave in a more brittle manner.

Chen et al. compared the hysteresis curves of the piers and observed no difference in stiffness degradation between the fully- and partially-grouted piers. The results for the energy dissipation characteristics of fully- and partially-grouted walls were inconclusive. In both cases the energy dissipation capacity increased with lateral drift due to increasing cracking and crack-interlock friction. Chen et al. commented on the effects of the axial offset caused by the frame columns. They noted that the problem would be resolved in future tests in the program. However,

the effects of partial grouting were not investigated further in any of the subsequent UC-Berkeley tests.

5.2.4 Hidalgo, Mayes, McNiven, and Clough

Hidalgo et al. (1979) tested eighteen full-scale masonry walls with a geometric aspect ratio of 0.5. Six of the piers were constructed with hollow clay brick, six were constructed with hollow concrete block, and the remaining six were constructed as double-wythe, grouted-core walls using solid clay bricks. All of the tested walls were were fully-grouted. Hidalgo et al. tested all of their walls using in-plane cyclic shear loading with increasing peak displacements. The frame subjected each wall to double-flexure bending, locating the inflection point at the mid-height of the wall, producing a shear span ratio of 0.25. All of the walls were tested using the same setup as Chen et al. (see Figure 5.3) and were subject to similar downward force induced by the hinged columns at either end of the specimen at higher lateral drifts. They observed, however, that in the case of walls with low aspect ratio, the axial force contribution from the hinged columns did not affect the failure mode of the specimens.

All of the twelve walls constructed with hollow brick or block contained three #7 bars, one in each end cell and one in the center of the wall. The quantity of horizontal reinforcement varied in each wall from none to four #6 bars in the concrete block walls and from non to five #7 bars in the clay brick walls. All of the other variables were kept constant between the tests.

Two of the concrete block specimens displayed a combined shear and sliding failure mechanism and the remaining four displayed typical shear failure characterized by diagonal cracking. Half of the six clay brick specimens displayed a combined flexural and sliding failure and the other half displayed a shear failure mechanism. Hidalgo et al. observed that there appeared to be a positive correlation between the amount of horizontal reinforcement and the ultimate strength. They observed that the shear deformation in the squat piers had a greater importance to the overall behavior of the specimens than for those with large aspect ratios.

5.2.5 Sveinsson, McNiven, and Sucuoglu

Sveinsson et al. (1985) conducted the final stage of the masonry shear wall research program at UC-Berkeley. They tested thirty piers, including twelve constructed with hollow concrete block, thirteen constructed with hollow clay brick, five constructed from two wythes of solid clay brick, with all of the walls being fully-grouted. They investigated the effect of horizontal reinforcement quantity, vertical reinforcement distribution, and the effect of wire truss bed-joint reinforcement. All walls had an aspect ratio of unity and a shear span ratio of 0.5. They used a test setup, shown in Figure 5.4, similar to that of Chen et al. (1978) with a modification such that the columns were replaced with actuators that were force-controlled. This modification enabled the specimens to be tested under double-curvature conditions while maintaining constant axial load for all lateral drifts.

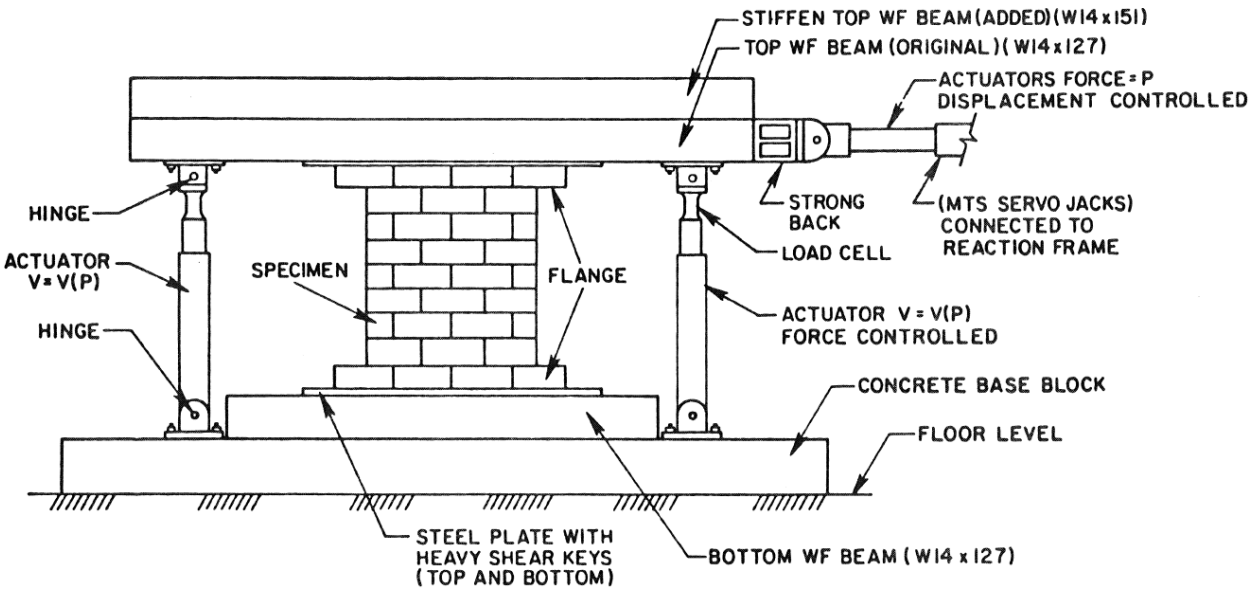

Figure 5.4: Masonry shear wall test setup from Sveinsson et al. (1985)

Sveinsson et al. observed a direct relationship between the failure mode of each specimen and its strength and inelastic response characteristics. Ductile shear failures were characterized by diagonal cracking which gradually spread throughout the wall panel with increasing horizontal load. This gradual spreading of shear cracks was made possible by the presence of horizontal reinforcement which enabled the tensile stresses to be transferred across the diagonal cracks. In

cases where there was not enough horizontal reinforcement to adequately transfer the tensile forces, the walls experienced a brittle shear failure.

They observed a combination of shear and sliding failure modes in walls with high horizontal reinforcement ratios. This failure mode was characterized by diagonal cracking, crushing of the compression toes, and sliding of the pier along the crushed bed joints. The presence of toe crushing in the combined shear/sliding failure model differed from that in the flexure failure mode in which the contribution of diagonal cracking is absent. Pure sliding failures were observed for walls with higher horizontal reinforcement ratios but with relatively small quantities of vertical reinforcement. For walls failing in the sliding mode, the cracking was generally limited to the bed joints at the tops and bottoms of the walls, leaving the rest of the panel undamaged.

Sveinsson et al. concluded that the horizontal reinforcement cannot be fully effective if it is not anchored around the vertical reinforcement in the end cells with a 180 degree hook or anchored with a plate welded to its end. Specimens in which the horizontal reinforcement was not well-anchored experienced a brittle failure immediately following the ultimate strength. They observed that the wire truss bed-joint reinforcement was not as effective in increasing the ultimate strength of the walls, but it improved the ductility of the walls. They observed that the equally distributed vertical reinforcement had a negligible effect on strength for the concrete masonry and it demonstrated inconsistent results for the clay brick specimens. They also observed no effect of the vertical reinforcement distribution on stiffness degradation. They concluded that uniform distribution of horizontal reinforcement improves wall ductility whereas uniformly spaced vertical reinforcement has no effect.

5.3 US-Japan Coordinated Program on Masonry Building Research

5.3.1 Matsumura

Matsumura (1985, 1987, 1988) amalgamated masonry shear wall research data from multiple researchers and studies performed in Japan. He performed a study on 80 reinforced masonry walls testing under in-plane shear loading to construct a model to compare the performance of fully- and partially-grouted shear walls. The parameters he investigated included shear reinforcement ratio, shear span ratio, axial stress, material strength, and grouting type. He generated a

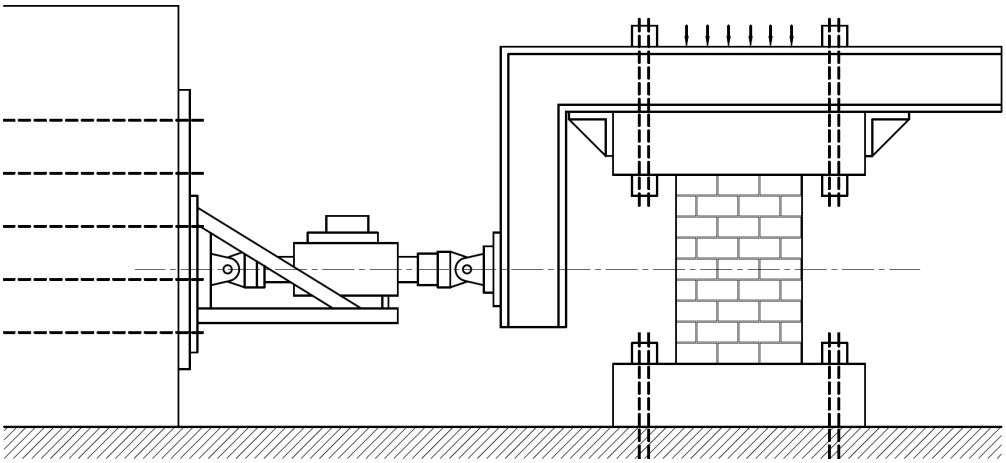

(a) Wall type loading

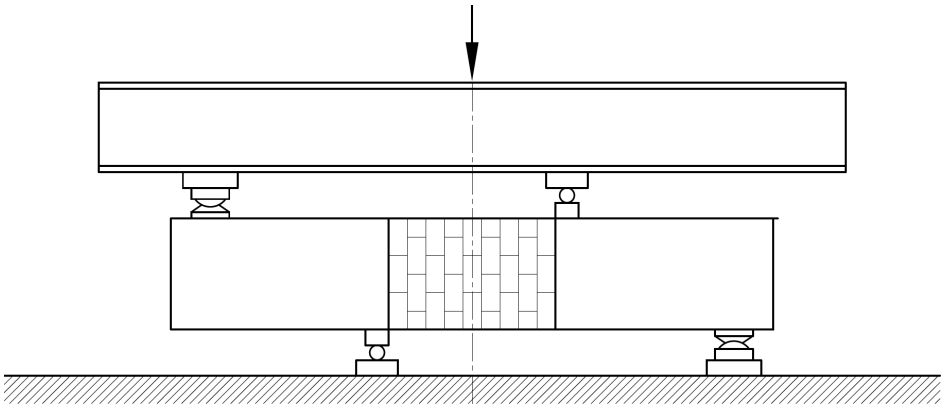

(b) Beam type loading

Figure 5.5: Test setups from Matsumura (1987)

dataset including 57 concrete masonry and 23 brick masonry walls where the majority of the specimens were full sized and the remaining were reduced scale. About two-thirds of the specimens he included were partially-grouted and the rest were fully-grouted.

Matsumura listed two loading methods used by the Japanese in performing their shear wall tests. In the first method, known as the "wall type loading," the base of the walls was fully fixed while the top of the wall was fixed to prevent rotation normal to the plane of the wall, as shown in Figure 5.5a. In the latter method, known as the "beam type loading," the walls were set in the test frame on one end (i.e., the bed joints were vertical) and subjected to vertical shearing loadings similar to those of a deep beam test, as shown in Figure 5.5b.

The wall type loading scenario used full-sized masonry walls with reinforced concrete beams above and below the masonry panel. The walls were loaded cyclically at the top of the wall. In most cases, four to five loading cycles were applied before the walls completely failed. During some of the wall type tests, a vertical actuator was used to apply a constant axial load to the top beam. The beam type loading was used mainly as a supplementary test. It used both full- and reduced-scale specimens, the majority of which were small. The test consisted of a single monotonic loading and unloading cycle to find the maximum shear resistances of each test.

Matsumura (1987) concluded that the ultimate shear strength is smaller for partially-grouted masonry walls than that for fully-grouted shear walls with the same geometry. This is expected because the Japanese only consider gross wall area in their calculations. He also observed that the lateral shear strength of reinforced masonry increases as the horizontal reinforcement ratio increases, with the rate of increase in shear strength decreasing with increasing reinforcement ratio. He further observed that shear strength is inversely proportional to the shear span ratio of the wall. Lastly, Matsumura concluded that the amount of reinforcement does not influence the shear cracking strength of the wall.

5.3.2 Okamoto, Yamazaki, Kaminosono, Teshigawara, and Hiraishi

Okamoto et al. (1987) performed a series of 35 masonry shear wall tests at the Building Research Institute of Japan, of which 25 were constructed using concrete blocks, 6 using clay bricks, and 3 using reinforced concrete. Two joint orientation were used: 23 masonry specimens were tested with lateral shear forces applied parallel to the bed joint and 9 specimens were oriented such that the lateral shear force was applied parallel to the head joints. The variables that were varied during the testing were the axial stress, the size and spacing of the shear reinforcement, the size of the flexural reinforcement, the shear span ratio, and the presence of spiral confining reinforcement in the wall toe.

The purpose of there tests was to investigate how the amount of shear reinforcement, axial stress, splices, compression toe confinement, and shear span ratio affected the shear and flexural behaviors of masonry walls and beams. All tests specimens were tested under double-curvature loading conditions using a test frame similar to that of Matsumura (1987) as shown in Figure 5.5a. The walls were testing using a cyclic loading pattern with incrementally increasing amplitudes.

Okamoto et al. (1987) observed that the maximum shear stress increased with increasing axial load, but the relationship is not linear. They also observed that increasing the amount of shear reinforcement increased the deformation capacity of walls and beams but did not increase the ultimate shear strength. They observed that the use of spiral reinforcement to confine the compression toe resulted in improved deformation capacity under large deformation amplitudes. The concluded that the ultimate shear strength increases with decreasing shear span ratio. They compared the performance of the beam specimens to the Architecture Institute of Japan (AIJ) design standard for reinforced concrete beams and concluded the equation to perform well for the beam specimens.

5.3.3 Shing, Schuller, Hoskere, Noland, Klamerus, and Spaeh

Shing et al. (1989, 1990) tested 22 masonry shear walls under in-plane cyclic loading at the University of Colorado-Boulder and was conducted as part of the U.S.-Japan Coordinated Program on Masonry Building Research. Their study included 16 concrete block specimens and 6 hollow clay brick specimens, all of which were constructed at fully scale and were fully grouted. The principal variables used in their study were the amounts of vertical and horizontal reinforcement and the amount of axial load applied to the walls. The walls within each material group were all constructed with the same dimensions and all walls were tested using reverse-curvature loading.

The walls were tested under drift histories patterned after those devloped by Porter (1987). Porter developed the TCCMAR phased-sequential displacement procedure in which drift cycles are organized into undulated sets, as shown in Figure 5.6. In each set, the drift amplitude of each succeeding cycle gradually increases up to a peak then gradually decreases to null. Each subsequent undulated set has a higher peak wave amplitude than the previous one. When the first major event (FME) occurs, the drift amplitude during the event is recorded for that specimen. The peak amplitude for each subsequent set is then determined as function of the drift at the FME. Schultz chose masonry cracking as the FME for his tests.

The principal objective of their study was to investigate the effects of the amount of reinforcement, the applied axial load, and the material on the limit-state capacities of masonry shear walls. The aim of the Shing et al. (1989, 1990) studies in the Coordinated Program on Masonry Building Research was to evaluate the validity of the UBC design formulae in reinforced masonry

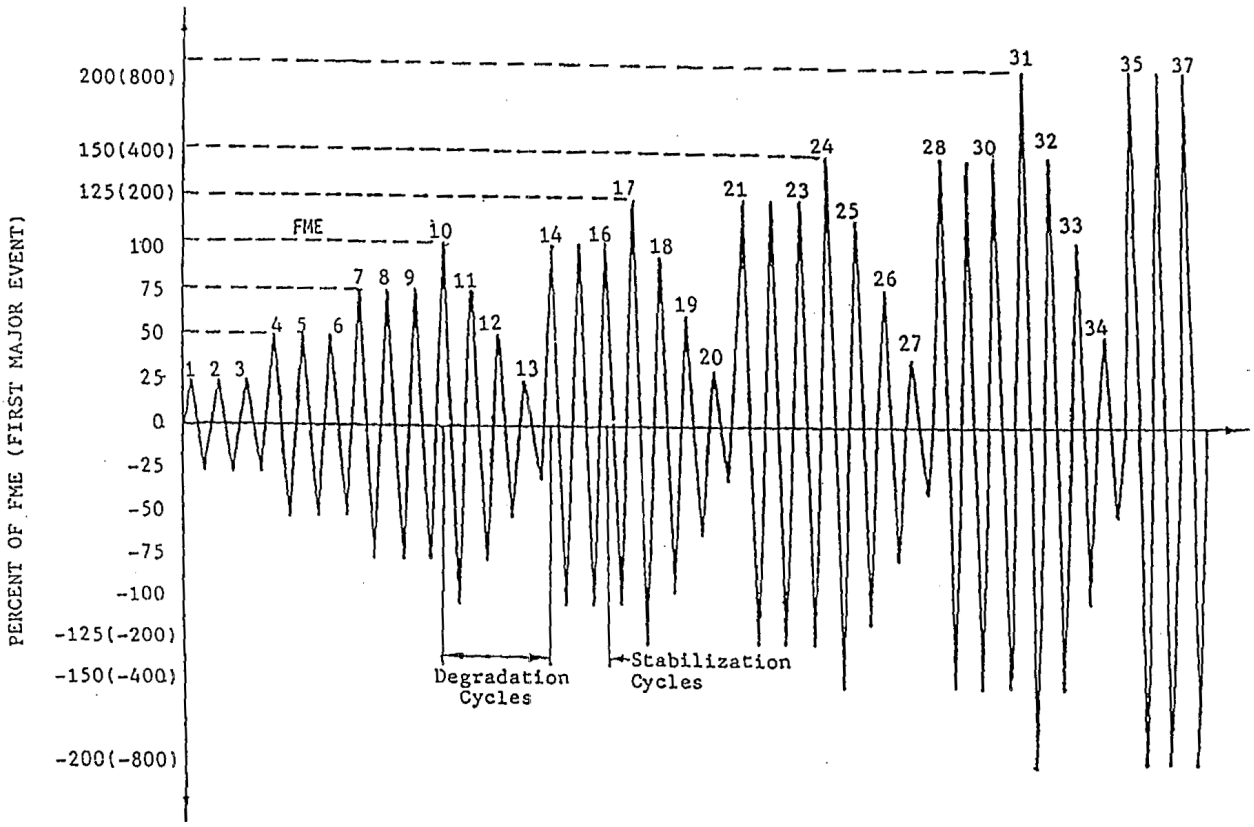

Figure 5.6: Phased-sequential displacement procedure (Porter, 1987)

shear wall strength. They evaluated formulae for both flexure and shear shear strength, determined that the existing UBC provision were overly simplistic, and proposed a new model for calculating shear strength.

Shing et al. (1989, 1990) observed four of the concrete masonry specimens and four of the clay masonry walls to be governed by flexural yeilding whereas the remaining 14 specimens were governed be diagonal shear cracking. The observed that the full grouting of the walls cause the diagonal cracks to propagate through the units rather than being confined to the joints. They observed that failure of the clay masonry walls was always initiated by spalling of the face shells from the grouted cores. They observed more brittle failures in the walls that failed in diagonal shear cracking and in those which failed with flexural toe crushing.

Shing et al. (1990) observed no correlation between the amount of reinforcement and the stress at the onset of diagonal cracking and concluded that they are unrelated. They observed that the contribution of the horizontal reinforcement given by $V_{ns} = A_v \rho_v f_y$ can overestimate the

contribution and proposed that the factor be reduced. They concluded that the amount of vertical reinforcement and the axial load have an influence on the shear strength by increasing the residual, post-cracking strength of the masonry.

5.4 Portland Cement Association

5.4.1 Johal and Anderson

Johal and Anderson (1988) undertook a series of 32 tests on masonry piers under in-plane cyclic loading. Their study included 16 tests on piers made from hollow concrete masonry units and 16 tests on piers constructed from hollow clay bricks. In each of the specimens, only the exterior jambs were reinforced and grouted; the remaining cells were all left ungrouted.

The purpose of their study was to evaluate the behavior of masonry piers using masonry cement mortar compared with piers using portland cement mortar. The test parameters that Johal and Anderson used in their experimental design were mortar type, cementitious material, cement brand, and masonry type. Other test parameters common to partially-grouted shear wall tests (e.g., aspect ratio, reinforcement ratio) were held constant from specimen to specimen. Two specimens were constructed and tested for each combination of test variables, giving 16 combinations and 32 total specimens. At least three masonry prisms were built and tested for each combination of test variables. The mean masonry compressive strength was provided for each of the 16 groups of masonry prisms.

Johal and Anderson applied shear loads using diagonal compression. Two compressive struts were used, one on each side of the wall, to control rotation of the top spandrel and to prevent in-plane axial load within the pier. Their test apparatus contained a hydraulic actuator and load cells located within each strut. Each pier was subjected to only shear and flexural loads with fixed-fixed end conditions. The loading scheme for the walls was load-controlled. A series of incrementally increasing cyclic loads were applied to opposite corners of the specimen for small deformations. As large deformations were observed for a given load level, the load was steadily increased until the ultimate load was reached. The test was stopped after the load capacity decreased.

All of the piers experienced a shear failure mode. In most cases, cracking started at the top of the piers and proliferated to the opposite corner of the pier. In a few cases, the cracking along

the entire diagonal occurred suddenly and simultaneously. In most cases, the cracks primarily ran through bed and head joints and cracking expanded into some masonry units as walls failed.

Johal and Anderson observed similar behaviors, cracking loads, and damage patterns for walls constructed with either portland cement- or masonry cement-based mortars. Their analysis showed that shear strength of partially-grouted masonry piers constructed with masonry cement-based mortars compared favorably with that of piers constructed with portland cement-based mortars. Additionally, they concluded than within the pier groups with similar mortar bases, the shear strength was only minimally influenced by using Type M or Type S mortar. They concluded that the restriction on use masonry cement in structural masonry walls in Seismic Zone Numbers 2, 3, and 4 should be eliminated from the Uniform Building Code.

5.5 National Institute of Standards and Technology

5.5.1 Yancey and Scribner

Yancey and Scribner (1989) performed the first study into the seismic performance of reinforced masonry walls at the Building and Fire Research Laboratory (BFRL), a division of the National Institute of Standards and Technology (NIST). They tested 13 walls at the NIST Tri-Dimensional Test Facility shown in Figure 5.7. All of the walls were constructed from eight-inch-nominal concrete masonry units and were 48 inches in length. Three of the walls did not experience a shear mode of failure due to their large aspect ratio of 2.17 and were subsequently not included in the report. The remaining ten walls had a aspect ratio of 1.17 (shear span ratio of 0.58 and consisted of seven courses, producing a height of 56 inches.

The purpose of their study was to determine how varying amounts and distributions of shear reinforcement affect the in-plane shear strength of partially-grouted masonry walls. All but one specimen were reinforced in the shear (i.e., horizontal) direction only; the remaining specimen was unreinforced. In eight of the ten specimens a bond beam was located at the mid-height (i.e., fourth course) of the wall. Four of the ten specimens contained joint reinforcement, one of which also contained a bond beam. Different sizes of reinforcement (#3, #4, or #5) were used in the bond beams while only 9-ga. ladder-type reinforcement was used for the bed joint reinforcement.

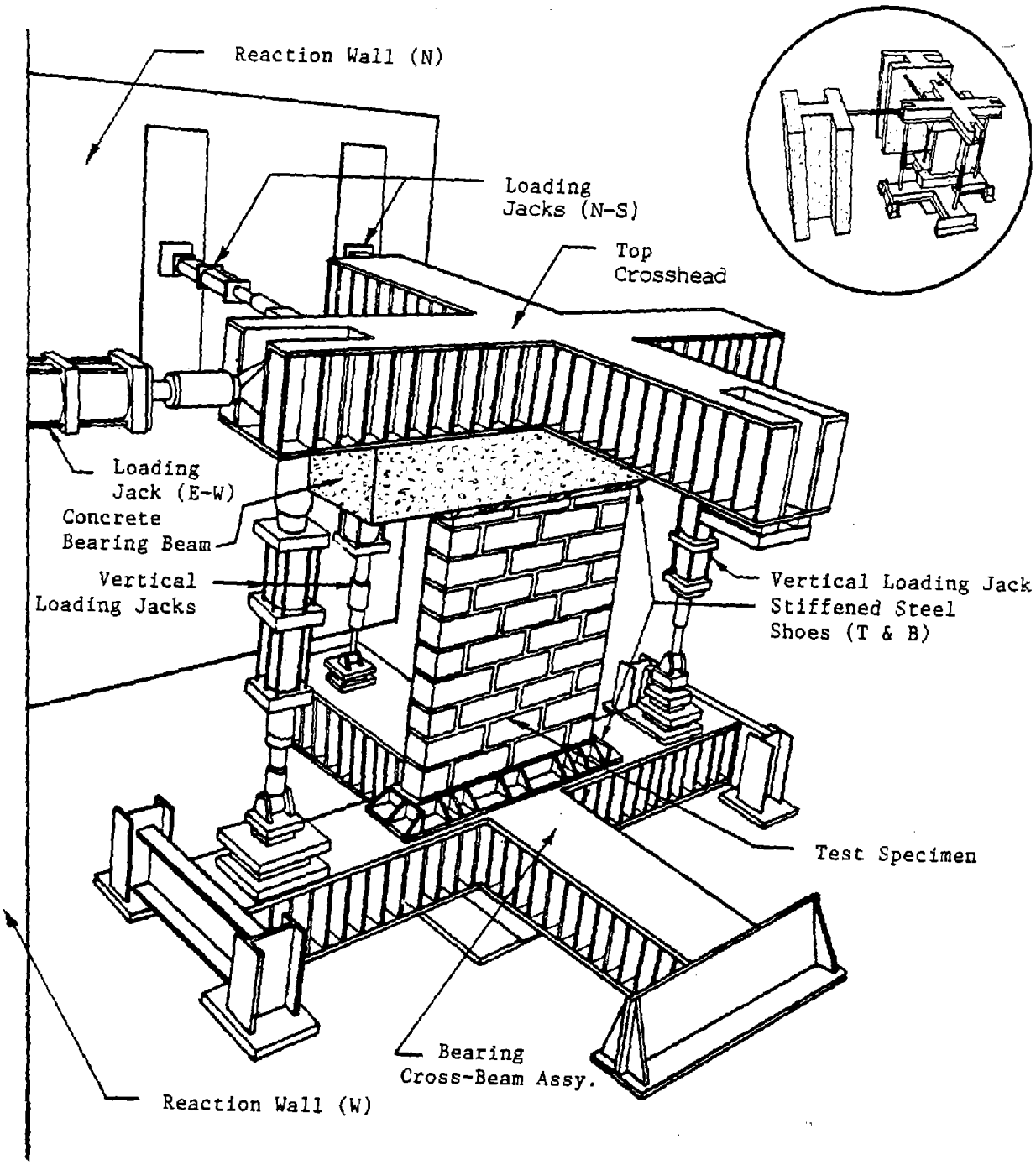

Figure 5.7: NIST Tri-Dimensional Test Facility (Yancey and Scribner, 1989)

Yancey and Scribner concluded that horizontal reinforcement was effective in increasing the ultimate shear strength of the walls. They observed that bed joint reinforcement placed in either every course and every-other-course is equally as effective as the other in increasing the in-place shear strength of the wall. They also compared the use of bed joint reinforcement with reinforced bond beams and observed that both were comparable in increasing the ultimate strength and deflection capacity of the walls. Their single specimen with both a reinforced bond beam and bed joint reinforcement exhibited a drift capacity twice that of the next best specimen. From the results from their tests, Yancey and Scribner concluded that ultimate shear strength increases with increasing horizontal reinforcement ratio. However, they observed that the relationship between the two factors is not linear.

5.5.2 Schultz

Schultz (1996a,b) tested six partially-grouted shear walls under in-plane shear loading. All six of his specimens were constructed from hollow concrete masonry units. He chose hollow concrete masonry units for his study because they have larger cells than other units of comparable size. The walls consisted of seven courses with a bond beam constructed within the middle (i.e., fourth) course. Only the exterior vertical cells were reinforced and grouted. The walls were tested under drift histories patterned after the TCCMAR phased-sequential displacement procedure devloped by Porter (1987).

The purpose of the study was to determine the influence of shear span ratio and shear reinforcement ratio on the behavior and shear strength of partially-grouted masonry walls. The walls were tested in the NIST Tri-Directional Testing Facility (see Figure 5.7). The walls were tested under in-plane cyclic loads and constant axial loading. The testing actuators in the facility were displacement controlled. This resulted in axial loads that varied slightly with the lateral drift of the wall due to vertical expansion of the wall from Poisson's effect. These variations were nowhere near as significant as were those that occurred during the tests of Chen et al. (1978).

Schultz observed that the initial cracks formed along the margins of the unreinforced masonry panel due to the stress concentrations between the grouted and ungrouted masonry. For all specimens except Wall No. 3, cracking was predominantly vertical and concentrated near the leading jamb. Eventually, this cracking proliferated through the joint between the horizontal and

vertical reinforcement, eroding the bond beam anchorage. The predominant cracking mode of Wall No. 3 was inclined cracking beginning at the mid-length of the top of the wall, and progressing toward the joint between the horizontal and vertical reinforcement. In this case, the cracking within the joint itself did not occur until later in the tests and had less of an effect on the bond beam anchorage than in the other tests.

In all of the tests, Schultz observed that the walls showed stable and gradual strength degradation. He noted that strength degradation occurred more rapidly with increasing shear span ratio. He observed that the force-displacement curves for the walls were nearly bi-linear and showed an obvious proportionality limit. He remarked that the reinforcement did not yield, yet the curves showed a behavior similar to that of a yielding system.

Schultz observed that increasing the shear span ratio has a negative effect on the ability of the wall to dissipate energy (toughness). The toughness of the wall is not affected by the horizontal reinforcement ratio. The deformation capacity, the drift at which strength falls to 75 percent of the ultimate strength, ranged from 0.33 percent to 1.0 percent for the walls. Schultz noted that these values are likely too low for high seismic-risk regions, but may be suitable for regions of lower risk.

Schultz used experimental data to compare the validity of four empirical formulas for predicting wall shear strength. The equation with the least amount of variability was that developed by Schultz's associate Fattal (1993) at NIST. Fattal's equation was a modification of the equation originally developed by Matsumura (1987) for partially-grouted masonry walls. Schultz determined that the mean ratio of measured-to-estimated shear strength using Fattal's formula was about 79 percent for all of his specimens.

Schultz observed that the shear span ratio of the walls had a distinct and inverse influence on the ultimate shear stress capacity of the walls. Similarly, horizontally reinforcement ratio was also shown to have small beneficial influence on the ultimate shear stress capacity of the walls.

5.5.3 Schultz, Hutchinson, and Cheok

Schultz et al. (1998) tested six reinforced masonry shear walls in the NIST Tri-Directional Testing Facility. Each specimen contained reinforcement and grouting only in the exterior vertical cells. Each wall was constructed of seven courses of hollow concrete masonry units using joint

reinforcement in each bed joint. They constructed three pairs of walls of different lengths to produce three distinct shear span ratios. They used the same dimensions as the six walls previously tested by Schultz (1996a,b). In the preceding study, each of Schultz's specimens was horizontally reinforced with a bond beam at mid-height.

The primary purpose of their study was to compare the behaviors of partially-grouted walls with joint reinforcement and bond beams. The reinforcement ladders placed in the joints were constructed from two different wire gages, with each wall within a pair receiving a different one. The first wall in each pair contained ladders with No. 9 Gage (0.148 in. diameter) wire and the latter contained ladders with No. 5 Gage (0.207 in. diameter) wire. This produced gross horizontal reinforcement ratios of 0.056 percent and 0.11 percent, respectively. The second parameter studied by Schultz:was the effect of shear span ratio on the behavior of partially-grouted masonry shear walls.

Schultz et al. tested their specimens using the TCCMAR phased-sequential displacement procedure explained previously. They selected the first instance of visible crack formation as the FME from which they determined the peak amplitudes for each subsequent wave of cycles. This was verified by identifying the first departure from a nearly linear force-displacement plot. They observed that the test data denoting the FME from each pair of wall tests were in relatively good agreement with each other. They observed that the lateral load at the FME was negatively correlated with the wall shear span ratio but was independent of shear reinforcement ratio.

Examination of the force-displacement envelops revealed that none of the walls failed suddenly. In all cases, the walls were able to demonstrate some level of plasticity before the load resistance steadily decreased with increasing displacement. They observed that the shear reinforcement ratio had an influential effect on walls being able to maintain peak load resistance with increasingly higher displacements. They concluded that wall shear span ratio appears to be negatively correlated with the ability of the wall to dissipate energy, but that horizontal reinforcement appeared to have no effect.

Schultz et al. concluded that partially-grouted masonry with bed joint reinforcement is a viable lateral load-resisting system for seismic design. They noted that horizontal reinforcement ratio had greater positive effect on ultimate shear strength in the slender walls (i.e. with higher shear span ratio). Overall, they concluded that wall performance using bed joint reinforcement

was improved over walls with a single bond beam at mid-height tested earlier (Schultz, 1996a,b). The walls showed stable hysteresis loops with increasing lateral drift and ample energy dissipation capacity.

5.6 Drexel University

5.6.1 Hamid, Chaderakeerthy, and Elnawawy

Hamid et al. (1992) built and tested 15 partially-grouted masonry prisms at Drexel University under eccentric, out-of-plane loading. The prisms were constructed of 1/3-scale hollow concrete masonry units. The bond wrench test method described in ASTM:C1072 (2014) was used to measure the flexural tensile strength of the units.

The purpose of Hamid's study was to determine the effect of grout spacing on flexural strength for bending normal to the bed joints. Five model walls of three courses were constructed using running bond. Each wall was grouted according to one of the five grouting conditions considered in this test. After curing, the walls were sawn into three symmetrical specimens for use in the bond wrench test.

His ungrouted specimens failed suddenly by debonding along the bed joint. His partially-grouted specimens failed by both mortar debonding along the bed joints and tension failure within the grouted cells. Since the faces of the cells were tapered for each block, the failures occurred where the grout area was minimum.

Hamid et al. calculated the tensile strength using ASTM:C1072 (2014). For the partially-grouted specimens, Hamid calculated in moment of inertia using the face shell bedding area, grouted area, and area of the webs adjacent to the grouted cells. He observed that the flexural tensile strength increases non-linearly with decreasing grout spacing. His tests also indicated that grouting is not effective for spacing greater than 32 inches on center.

Hamid et al. compared his values to those obtained in the ACI-ASCE (1988), which allows for linear interpolation between values for fully-grouted and ungrouted masonry. The factor of safety between the code values and the experimental value is not consistent since the experimental relationship is not linear. Hamid et al. proposed as an empirical method to predict the average

flexural tensile strength of partially-grouted walls given by

$$f_{t(pg)} = 4.4 f_{t(g)} s_{gh}^{-0.75} \tag{5.2}$$

where

$f_{t(pg)}$ = the flexural strength of partially-grouted masonry,
$f_{t(g)}$ = the flexural strength of grouted masonry, and
s_{gh} = the spacing of grouted cells.

Equation (5.2) is limited to spacings of 8 inches (i.e., fully-grouted) to 32 inches and cannot be used for ungrouted masonry or for grout spacings larger than 32 inches. In an attempt to find more universally applicable formulae, Hamid developed three more equations to be theoretically-based and he used his experimental data to validate his results. He proposed the following equations:

$$f_{t(pg)} = f_{t(ug)} \frac{S-8}{S+3.37} + f_{t(g)} \frac{11.37}{s_{gh}+3.37} \tag{5.3}$$

$$f_{t(pg)} = f_{t(ug)} \frac{S-8}{S+3.85} + f_{t(g)} \frac{11.85}{s_{gh}+3.85} \tag{5.4}$$

and

$$f_{t(pg)} = f_{t(ug)} \frac{S-8}{S+5.84} + f_{t(g)} \frac{13.84}{s_{gh}+5.84} \tag{5.5}$$

where $f_{t(ug)}$ is the flexural strength of ungrouted masonry. Equation (5.3) is to be used for 6-inch block, equation (5.4) for 8-inch block, and equation (5.5) for 12-inch block.

Hamid et al. designed Equations (5.3), (5.4), and (5.5) to cover the typical range of values of flexural tensile strength. Since the equations were validated solely on the data from this single experiment, it is uncertain whether they can be universally applied. Further experimentation would be necessary for verification and modification of the parameters. Similarly, the structure of the equations should be combined into a single equation and simplified for codification and use by designers.

5.6.2 Ghanem, Hamid, Essawy, Salama, and Elmagd

Ghanem et al. (1992) and Ghanem et al. (1993) tested 14 partially-grouted walls at Drexel University. All of the walls were constructed from 1/3-scale hollow concrete masonry units and tested under either monotonic or cyclic lateral loads. The walls were constructed with differing amounts of horizontal and vertical reinforcement and blocks of differing strengths and were tested under differing levels of vertical precompression load. The purpose of their study was to study the effects of three design parameters, horizontal and vertical reinforcement distribution and vertical axial load. In their study they used reduced-scale replicas of standard masonry constituent materials that were fabricated in-house.

Ghanem et al. observed that his walls with bars distributed throughout the wall performed better than the walls with bars concentrated in fewer areas. In all cases, the walls contained the same amount of reinforcement. They observed that due to the inclined cracking within the wall panel, the horizontal reinforcement bars at the top and bottom of the wall did not have adequate development length to fully activate their strength in resisting the shear forces. This lead Ghanem et al. to conclude only interior horizontal reinforcement is truly effective in resisting shear and in increasing wall ductility. They recommended that shear reinforcement be distributed throughout the interior of the wall panel and not concentrated at the top and bottom. They further noted that distributed vertical reinforcement is better at resisting shear and increasing ductility but that concentrating vertical reinforcement at the ends of the wall is most effective in resisting the flexural forces.

Ghanem et al. observed that the cracking load was the same for all walls with the same axial load, regardless of the amount of reinforcement in each wall. He concluded that the diagonal cracking load is independent of the amount of horizontal and vertical reinforcement. He explained that this is because the diagonal cracking load is dependent on the tensile strength of the masonry and of the orientation of stresses within the wall by the superposition of vertical axial stress. Increased axial force also increases the aggregate interlock force, increasing the shear strength of the masonry.

Ghanem et al. observed that ultimate shear capacity increased as axial load increased. They concluded that ultimate load is highly sensitive to the quantity of axial load applied to the wall. They further observed that increasing axial load increased the lateral stiffness of the wall

panels. Increasing the axial load also exhibited more brittle failure behavior with the post-peak load capacity falling more quickly. The walls with the lowest levels of axial load failed by toe crushing and yielding of the vertical reinforcement. The walls with the highest axial loads tended to fail in shear. They concluded that the ductility and failure behavior of the wall are both also sensitive to the axial load on the wall. They recommended that the axial load be less than 5 percent of the compressive strength of the wall to avoid brittle failure.

5.6.3 Minaie

Minaie (2009) tested eight full-scale masonry shear walls at Drexel University. The walls were tested under quasi-static, cyclic loading under displacement-controlled conditions. Four of the walls were fully-grouted and four were partially-grouted. Two of the fully-grouted walls were constructed of clay masonry and the other walls were constructed of concrete masonry. All of the walls had the same aspect ratio, reinforcement pattern, and displacement loading history. Minaie investigated and compared the effects of full and partial grouting, concrete and clay masonry, cantilever and fixed-fixed constraints, mortar type, and axial stress on masonry walls.

Minaie tested his wall specimens using the test setup shown in Figure 5.8. Within the partially-grouted group, he used either portland cement/lime-based mortar or masonry cement-based mortar and applied either a vertical axial load of 100 psi or zero based on net area. For walls with no axial loading, Minaie applied a moment load to the top of each wall to create a fixed-fixed boundary condition and move the inflection point to the middle of the wall. Within the fully-grouted subgroup, he used either concrete masonry units or clay masonry units bonded together with either portland cement-lime mortar or masonry cement mortar. All of the wall specimens had the same reinforcement design.

Minaie used 3D finite element models to model the in-plane and out-of-plane response of this specimens. He used shell elements to model the face shell, webs, and mortal joints of the masonry units, solid elements to model the grouted units, and beam elements to model the reinforcement. He used the Concrete Damaged Plasticity Model from Abaqus (see also Lubliner et al. 1989; Lee and Fenves 1998) to simulate the nonlinear response of the units, mortar, and grout. A key parameter in the finite element analysis of concrete members that governs the hysteretic plastic response is the dilation angle. Minaie varied the angle from 20 to 40 degrees and determined

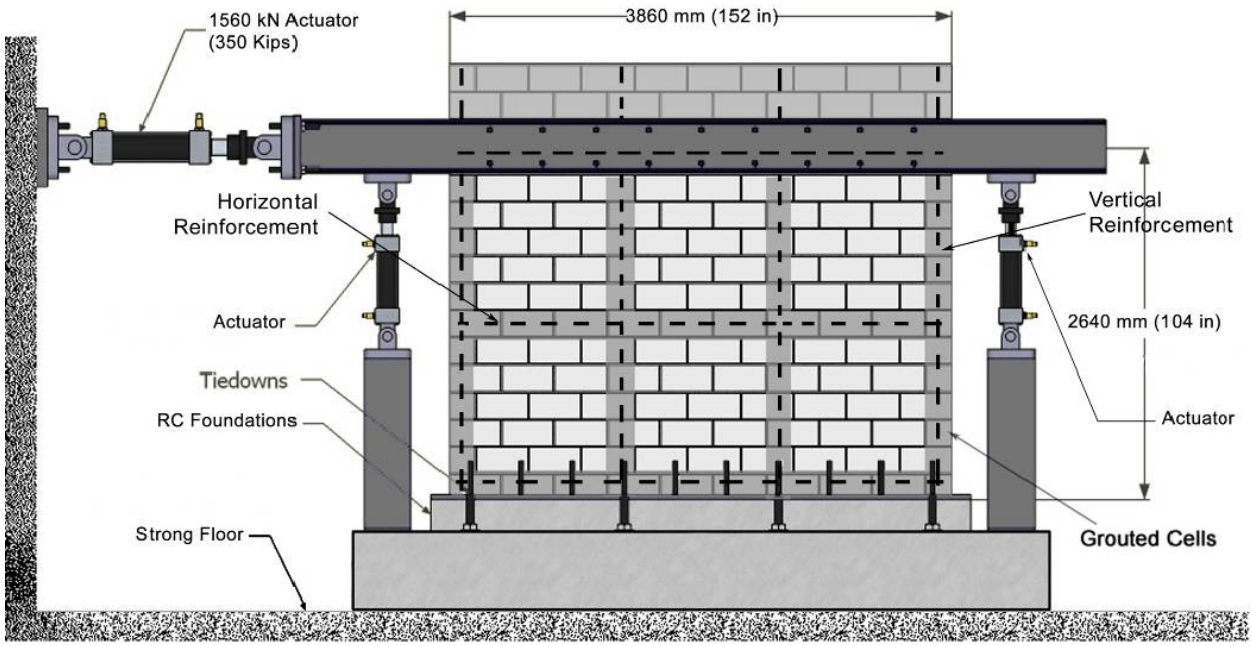

Figure 5.8: Test setup from Minaie (2009)

that the dilation angle has a significant effect on the shape of the hysteretic loops. He compared the simulated and experimental hysteretic responses and chose an angle of 38 degrees for use in his models. Minaie validated the results from his finite element models with those from his experimental tests.

The principle objective of Minaie was to establish the crucial behavioral mechanisms and seismic vulnerabilities of reinforced masonry shear walls. Most notably, Minaie sought to bridge the knowledge gap between partially-grouted and fully-grouted walls. He did this using both experimental and numerical methods. Using the test parameters from each wall, he used the MSJC shear equation to calculate the predicted shear strength for each of his test specimens and compared them to the experimental results. He then constructed finite element models for his specimens and compared the analytical strength, hysteretic plots, and behavior to those of the experiment.

Minaie determined that the MSJC strength design shear strength equations significantly over-predicts the capacity of partially-grouted walls (i.e., is un-conservative). He concluded that part of this is because the behavior of partially-grouted walls is more analogous to that of infilled frames. The equation becomes more unconservative for partially-grouted walls as the shear wall area increases, as the aspect ratio decreases below 1.0, and as the spacing of both the vertical and

horizontal reinforcement increases. Conversely, the equation becomes more conservative as the wall area decreases, as the aspect ratio increases, as the axial stress increases, and as the horizontal reinforcement ratio increases. Minaie concluded that the equation is sufficiently accurate for fully-grouted walls.

Minaie obtained conflicting results for the effect of mortar formulation on partially-grouted wall shear strength. His data showed that for partial grouting, the MSJC equation over-predicts the shear strength of walls with masonry cement-based mortar more than that of walls with portland cement/lime-based mortar. However, examination of this test determined that an f'_m value of 2,500 psi was used for the MSJC equation for both the PCL and MC walls. It is unlikely that the walls would have the same shear strength since the MC mortar had a lower compressive strength. This could have been verified through un-grouted prism tests, but no prisms test data (grouted or un-grouted) could be found in his report. He concluded that mortar formulation has a negligible effect on the strength of fully-grouted walls because the strength contribution from the grout is more significant than that from the mortar.

Minaie (2009) concluded that the finite element model combined with the concrete damage plasticity model is an appropriate analytical model to use in modeling the bi-directional performance, cracking pattern, and failure modes of both fully- and partially-grouted walls. He determined that the best results were obtained by using a dilation angle of 38 degrees and that the maximum value should be used for the damage variables at each strain level. Judging by the narrow scope of his research, further modeling would need to be performed on other test results to determine whether these parameters are widely applicable to masonry walls as a whole or whether they vary as functions of other variables.

5.7 Washington State University

5.7.1 Nolph

Nolph (2010) and Nolph and ElGawady (2012) tested six full-scale concrete masonry shear walls at Washington State University. The walls were all tested under displacement controlled, in-plane loading conditions using the test frame pictured in Figure 5.9. One of the walls was fully-grouted and the other five were partially-grouted. All of the walls had the same aspect ratio and

axial loading and had comparable vertical reinforcement ratios. Nolph investigated the effects of horizontal shear reinforcement ratio, grout horizontal spacing, and partial grouting on the performance of masonry shear walls.

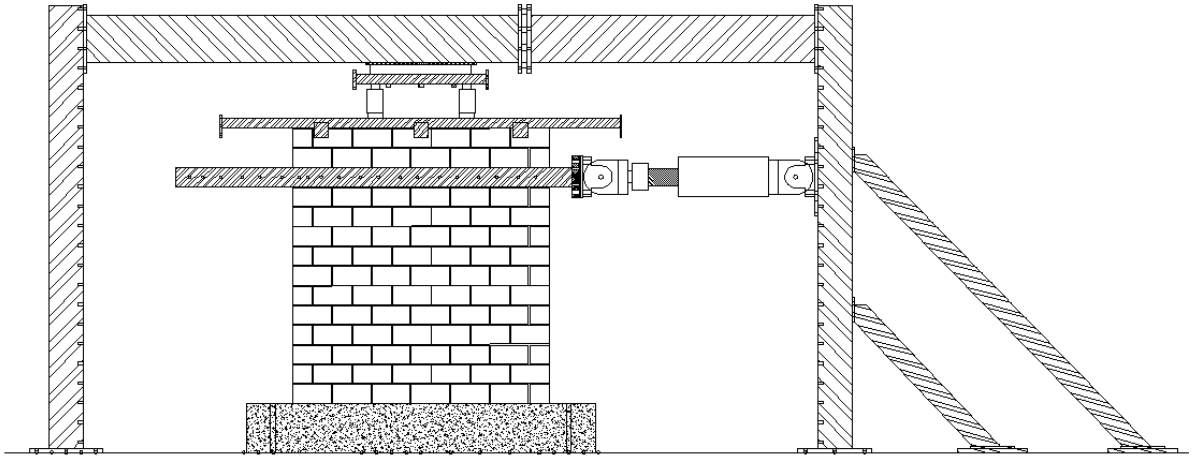

Figure 5.9: Test frame from Nolph (2010)

Nolph varied the horizontal reinforcement ratio, grout horizontal spacing, and grouting during his tests. The horizontal reinforcement ratios investigated were 0.085 percent, 0.120 percent, and 0.169 percent. The vertical reinforcement spacings he used were 24, 32, or 48 inches (610, 813, or 1220 mm). One fully-grouted wall was constructed using identical reinforcement parameters as the partially-grouted control specimen. All walls contained a bond beam at mid-height.

Nolph constructed strut-and-tie models to investigate the validity of the method's results with his experimental results. In each model, the grouted reinforcement cells act as tension ties and the ungrouted masonry act as compressions struts. ACI 318-08 states that for each strut, the strut angle α_s—the angle between the strut and the horizontal ties—must be between 25 and 65 degrees. In some of the specimens, the constraints allowed two or three alternative strut-and-tie models capable of modeling the walls. In such cases, Nolph analyzed all models and reported the detailed results of the most conservative model.

The principle objective of Nolph was to investigate whether the MSJC strength design equation for the shear strength of masonry walls is accurate for partially-grouted masonry walls. Using the test parameters from each wall, he used the MSJC equation to calculate the predicted

shear strength for each of his test specimens. He also investigated the applicability of shear strength equations from Fattal (1993) and the New Zealand Standard (Standard Association of New Zealand (NZS), 2004). A second objective was to analyze the effectiveness of strut-and-tie modeling in predicting the shear strength of partially-grouted masonry shear walls. After the tests were performed, he compared the results with the predicted values from the MSJC strength design equation, the other shear equations, and his strut-and-tie models.

Nolph determined that the MSJC equation over-predicted the shear strength of the partially-grouted wall with 48 in. (1220 mm) grout horizontal spacing and was adequate for grout horizontal spacings of 32 in. (813 mm) or less with horizontal reinforcement ratio of 0.085 percent. He observed that the Fattal (1993) equation was fairly accurate for only one specimen, was unconservative for four of the specimens, and was overly-conservative for the remaining specimen. He judged that the Fattal equation was better than the MSJC equation, but not sufficiently enough to replace it. The NZS equation produced results that were similar to those of the MSJC. He concluded that the strut-and-tie model was a good predictor of the partially-grouted walls, predicting values within -14 percent to +8 percent of measured peak shear strength.

Nolph observed that for grout horizontal spacing of 48 inches, (1220 mm) there is a threshold between 0.085 percent and 0.1 percent horizontal reinforcement ratios after which the effect on ultimate shear strength is negligible. He observed that walls with ratios greater than this threshold experienced failure of the masonry before yielding of the reinforcement. This is not ideal for design because failure initiates quickly as brittle shear cracking and crushing of the masonry units.

Nolph observed end shell splitting in two of his specimens and similar cracking patterns in the remaining specimens. This cracking pattern matches those characteristic of anchorage problems where the horizontal shear reinforcement are hooked around the vertical reinforcement. He notes that a 180-degree hook in a #5 reinforcing bar barely meets the clearance criteria inside of an 8-inch (200 mm) concrete masonry block. Nolph suggests that in this case the cover requirements may not be sufficient and that a limit on horizontal shear bar size should be considered.

Lastly, Nolph briefly comments on some evidence that during the tests, partially-grouted specimen plane sections did not necessarily remain plane, though not enough data were gathered to validate that claim. This claim is likely true because tests of deep beams exhibit this type of behavior. He notes that this behavior is more characteristic of masonry infill panels.

5.7.2 Elmapruk

Elmapruk (2010) tested six full-scale partially-grouted concrete masonry shear walls at Washington State University (WSU). All of the wall specimens had the same aspect ratio, vertical reinforcement ratio, and axial loading. Elmapruk investigated the effect of horizontal shear reinforcement ratio and the horizontal spacing of grouted flues on the performance of partially-grouted masonry shear walls using the test setup shown in Figure 5.10.

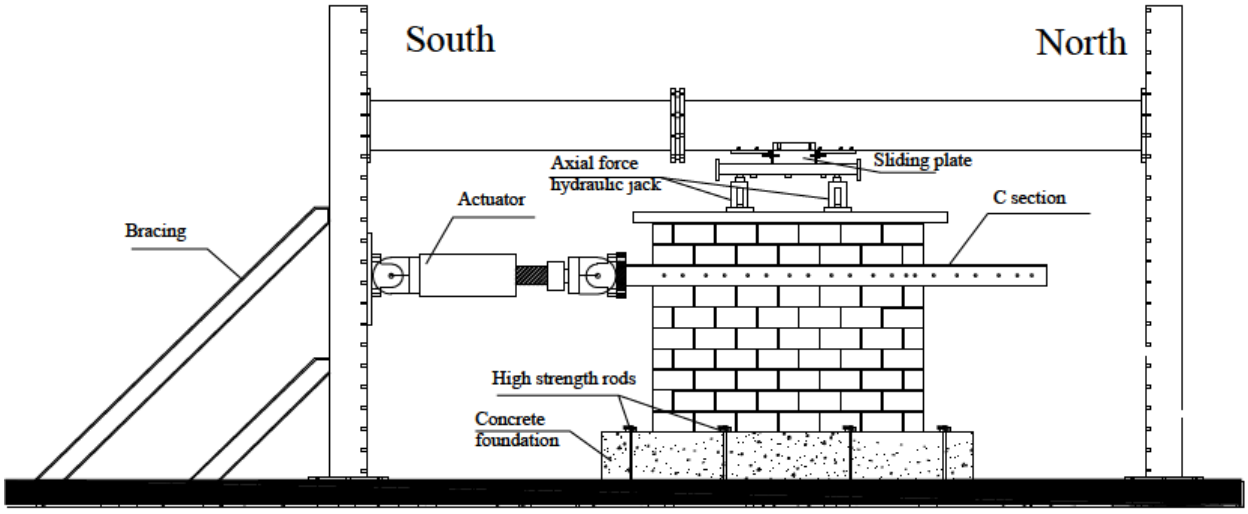

Figure 5.10: Test frame from Elmapruk (2010)

Elmapruk varied the horizontal reinforcement ratio and grout horizontal spacing during his tests. The horizontal reinforcement ratios investigated were 0.127, 0.180, and 0.254 percent. The vertical reinforcement spacing he used was 24, 32, or 48 inches (610, 813, or 1220 mm) and all walls contained a bond beam at mid-height. Elmapruk used two control specimens to validate the replicability of the tests. Elmapruk's tests were similar to those of his associate Nolph (2010) at WSU, except that his study used slightly shorter specimens.

Elmapruk constructed strut-and-tie models to investigate the validity of the method with his experimental results. Within each model, the grouted reinforcement cells act as tension ties and the ungrouted masonry act as compressions struts. ACI 318-08 states that for each strut, the strut angle ϕ—the angle between the strut and the horizontal ties—must be equal to or between 25 and 65 degrees. In for some of his specimens, this constraint permitted two alternative strut-

and-tie models capable of modeling the walls. In such cases, Elmapruk constructed and analyzed both models and compared their results to those from his tests to determine which model most accurately represented the real-life conditions.

The principle objective of Elmapruk was to investigate whether the MSJC (2013) strength design equation for the shear strength of masonry walls is accurate for partially-grouted masonry walls. Using the test parameters from each wall, he used the MSJC equation to calculate the predicted shear strength for each of his test specimens. Additionally, he calculated predicted shear strengths using the equation proposed by Nolph (2010). His second objective was to analyze the effectiveness of strut-and-tie modeling in predicting the shear strength of partially-grouted masonry shear walls. After the tests were performed, he compared the results with the predicted values from the MSJC strength design equation, the Nolph (2010) equation, and his strut-and-tie models.

Elmapruk observed that the MSJC equation significantly over-estimates the shear strength of partially-grouted masonry shear walls. He observed that Nolph's equation more accurately predicted the shear strength for his specimens within -7 to $+12$ percent of the measured peak shear strength. He also observed that strut-and-tie modeling was more effective, predicting values within ±20 percent. He provided no discussion as to why his analytical strut-and-tie models were more variable than Nolph's empirical equation. It is likely that Nolph's equation may have applied well to Elmapruk's experimental data because the test materials, construction, and test setup were similar.

Elmapruk proposed that there is a threshold for the horizontal reinforcement ratio at which any increase in reinforcement ratio yields no increase in shear strength. For higher reinforcement ratios, failure initiates in one of the compression struts rather than by yielding the reinforcement, as one would expect. It appears that he based this conclusion on his strut-and-tie model analysis since his experimental data only shows a linearly increasing regression for ρ_h versus V_n. It is possible he validated his conclusion through visual inspection of his specimen failure modes and through his research into the experiment work of Nolph (2010), though he did not explicitly state how his conclusions were founded. Nolph's tests did show decreasing shear strength for higher horizontal reinforcement ratios.

Elmapruk observed an inverse relationship between grout horizontal spacing and lateral shear strength. The specimens having grout spacing of 24 or 32 inches had the same peak net area

shear stress. This means that the increase in shear strength was caused by the increase in specimen net shear area, and that the geometry had negligible effect on the shear strength. The specimen having a grout spacing of 48 inches had a lower peak net area shear stress because failure initiated in the yielding of the reinforcement. Decreasing the grout horizontal spacing causes the initial failure mode to transition from yielding of the reinforcement to crushing of the masonry, increasing strength but decreasing ductility.

5.8 International Testing Programs

5.8.1 Tomaževič, Lutman, and Petković

Tomaževič et al. (1996) tested 16 pairs of half-scale partially-grouted hollow concrete masonry walls. The walls were constructed from seven courses with reinforcement in the exterior cells only and horizontal reinforcement placed in every bed joint. The geometry of the walls was designed for shear behavior, but the vertical reinforcement was designed for ductile flexure behavior. The purpose of the study performed by Tomaževič et al. was to compare the influence of the four different loading histories, of static versus dynamic loading, and of two different vertical stress levels on the behavior of partially-grouted walls. The study was designed with sixteen unique combinations of the tests parameters and each of the sixteen test conditions was replicated on two wall specimens, for a total of 32 specimens tested.

The walls were tested using four different loading types, one monotonic and three distinct displacement time histories, all of which were displacement-controlled. Tomaževič et al. used three cyclic time loading histories. The first cycle loading history (procedure B) consisted of cyclic lateral displacements grouped into three repeated amplitude cycles. The displacement amplitude increased with each subsequent group. In the second loading history (procedure C), the loading time history was based on that developed for TCCMAR by Porter (1987) described previously. The last loading history (procedure D) used the simulated seismic response of a three-story masonry building subjected to an earthquake time history during a previous experiment (Tomaževič and Velechovsky, 1992).

The static and dynamic monotonic tests were performed using loading rates of 0.033 and 80 mm/s, respectively. The static cyclic tests (types B, C, and D) were programmed based on a

frequency of 0.004 Hz, or a period of 250 sec. The dynamic cyclic tests were programmed based on a frequency of 1 Hz, or a period of 1 sec. This value was chosen because it corresponds to the natural period of vibration for a five- to six-story masonry structure in the nonlinear range of vibration.

They observed that the stepwise-increasing cyclic loading (procedure B) produced the best agreement with the calculated strength values for the walls. The TCCMAR and simulated seismic loadings (procedures C and D) produced good agreement with the calculated values whereas the monotonic loading (procedure A) produced a much larger disparity between measured and calculated results. They noted that this can be explained by the fact that the derivation of the strength equations was made using stepwise-increasing cyclic loading tests.

Tomaževič et al. concluded that the use of different lateral load histories and procedures can create significant differences in test results in partially-grouted masonry walls. They concluded that cyclic loading should be used to obtain the most reliable data about the degradation of strength and stiffness and about the energy dissipation capacity of masonry walls. They concluded that cyclic test procedures B and C were nearly equivalent. However, strain rate and precompression load must be taken into account to modify the test results.

5.8.2 Haider

Haider (2007) tested fifteen full-scale masonry shear walls at the Central University of Queensland in Australia. The testing program consisted of two sets of specimens. The first set of specimens included five pairs of partially-grouted masonry walls with each pair having a distinct distribution of vertical reinforcement and one unreinforced specimen. The second set of specimens included two more pairs of partially-grouted masonry walls with differing shear span ratios. All walls were constructed from hollow clay brick with portland cement/lime-based mortar. Each reinforced wall contained four N12 (12 mm diameter) steel bars which were grouted within their respective cores.

The purpose of the research was to increase the understanding of the structural behavior of wide-spaced reinforced masonry walls and to verify the prescriptive provided in the AS 3700 (2011). Haider defines wide-spaced reinforced masonry walls as partially-grouted walls in which

the reinforcement is in the vertical direction only. Haider refers to wide-spaced reinforced masonry walls with reinforcement only in the end cells as end-core reinforced masonry walls.

In his experimental design, Haider decided to test a single design parameter in his first set of specimens—reinforcement distribution. He then constructed a finite element model using micro-modeling techniques and used the experimental data to calibrate his model. The second set of specimens was constructed and tested to validate his model for specimens of different aspect ratios and precompression stresses. The model was then used to perform a sensitivity analysis of the other design parameters on the behavior of wide-spaced reinforced masonry walls.

Walls were tested using either reversed-monotonic or stepwise-increasing cyclic loading. The first wall in each of the first four pairs was tested using monotonic lateral loading. The data from the first wall was then used to determine the cyclic loading history for the other wall in the pair. Walls in the remaining groups were all tested using monotonic loading. All walls in the first test group were subjected to a constant vertical axial load of 0.50 MPa. The walls in the second test group were subjected to a vertical axial load of either 0.25 MPa or 0.04 MPa. The walls were fixed at their bases and their tops were permitted to rotate normal to the plane of the wall.

Haider observed that aspect ratio has a large effect on shear capacity of partially-grouted walls, but that precompression stress only has a marginal effect on shear capacity. Overall, he observed that geometric properties have a greater effect on the structural behavior than the variability in material properties. He that AS 3700 (2011) over-predicts shear capacity by 30 percent whereas the finite element model over-predicts strength by only 3.1 percent.

His analysis showed that shear stresses were concentrated in the diagonal region of the wall irrespective of the distribution of vertical reinforced cores in the wall for the wall with aspect ratio of 0.84. He further showed that partial grouting introduces discontinuities to the shear flow within the wall, but does not affect the diagonal failure planes. He found that for walls with smaller aspect ratios, cracks tend to propagate diagonally from the corners and included horizontal cracks between two of the intermediate reinforced cores.

Haider (2007) concluded that partially-grouted masonry walls are about 30 percent stronger and more ductile than unreinforced walls. He observed that reinforced cores at the ends of the wall prevent the wall from exhibiting a rocking-type failure mode. He further concluded that the FE algorithm using macro masonry material model, the damaged plasticity concrete model, and

the compression-disabled reinforcement bar model can be an effective numerical technique for modeling partially-grouted masonry walls.

5.8.3 Voon

Voon and Ingham (2006) and Voon (2007) tested ten reinforced masonry walls at the University of Auckland, New Zealand. Two of the walls were partially-grouted and the remaining walls were fully-grouted. Neither partially-grouted specimen contained shear reinforcement, but both contained different amounts of vertical reinforcement. Voon and Ingham used three axially loading conditions on the fully-grouted specimens (0, 0.25, and 0.50 MPa) but the partially-grouted specimens were not loaded axially. The purpose of the Voon and Ingham study was to investigate concrete masonry shear strength to assess the validity on the new shear equation in the Standard Association of New Zealand (NZS) (2004) code. All walls were tested using stepwise-increasing cyclic loading using the test setup shown in Figure 5.11.

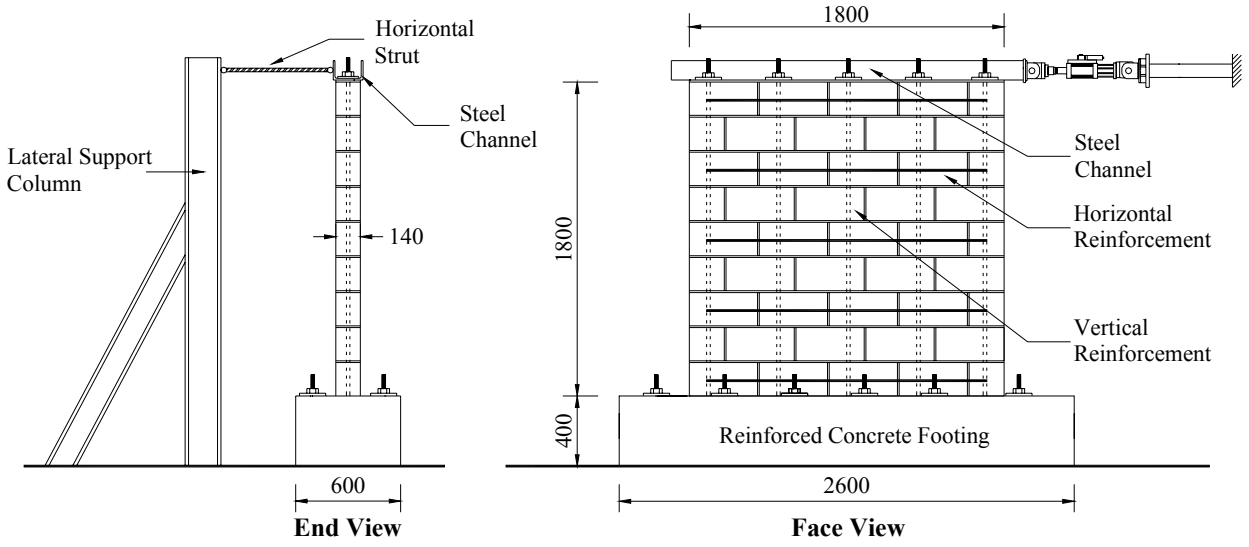

Figure 5.11: Test frame from Voon and Ingham (2006)

Voon and Ingham compared his experimental wall shear strengths to those predicted by Standard Association of New Zealand (NZS) (2004) and NEHRP (1997). He observed that the NEHRP (1997) equation did a better job predicting the experimental shear strengths than the 1990

Standard Association of New Zealand (NZS) equation. In one case, the NEHRP expression over-predicted the shear strength because it did not account for shear strength reduction in plastic hinge regions. In the two partially-grouted walls, both equations significantly under-estimated the shear strength. Part of the reason may stem from the New Zealander practice of only including the face shell areas in the shear area and neglecting the areas from the grouted cores.

5.8.4 Maleki

Maleki (2008) tested fourteen half-scale masonry shear specimens at McMaster University in Canada. Nine of the specimens were square wallettes tested using diagonal compression and five were tested under cantilever shear conditions. The nine wallettes were divided into three groups of three specimens each. The first group was fully-grouted, the second was partially-grouted, and the third was ungrouted. The two reinforced groups were contained reinforcement along their perimeters. The five cantilever walls were designed and constructed with differing aspect ratios and reinforcement patterns. For each wall the horizontal reinforcement ratio was maintained between 0.04 and 0.05 percent.

The objective of Maleki's study was to test the performance of partially-grouted masonry shear walls with reinforcement spacing greater than the limits imposed by the CSA S304.1 (2004). This was done with the intent to try to relieve some of the limitations imposed on partially-grouted masonry. He divided his research into three sections—the development of a finite element model for partially-grouted masonry, a study for validation of the model, and modification and use of the model for simulation.

Maleki observed that the partially-grouted square wallettes were able to maintain their integrity after diagonal cracking. Additionally, the partially-grouted wallettes also showed some post-cracking strength increase with peak strength slightly greater than the cracking strength. Failure initiated by crushing grouted masonry at the loaded corners. The fully-grouted and ungrouted wallettes also experienced diagonal cracking; however, the ungrouted specimens showed a shear-sliding failure mode whereas the grouted specimens all showed a stepped-pattern failure mode. Unlike the partially-grouted wallettes, the fully-grouted and ungrouted wallettes showed no post-cracking strength increase.

The first four walls experienced a shear mode of failure exhibited by an absence of yielding in the vertical reinforcement. The fifth wall experienced a combined shear-flexure mode of failure in which diagonal cracking and yielding of the vertical reinforcement were observed. Maleki compared the measured experimental strengths to those calculated using the Canadian masonry standard CSA S304.1 (2004) for each wall. He concluded that the CSA provisions agreed closely with the results of his tests. For the walls that failed in the shear mode, he determined that the calculated shear strength was less than the calculated flexural strength, confirming that shear was the appropriate mode of failure.

Maleki (2008) observed that the shear capacity is not significantly influenced by the spacing of the reinforcement. However, he observed that the shear capacity is very sensitive to the aspect ratio of the wall and that they are negatively correlated. He remarked that walls with higher aspect ratios experience greater moment forces at the base due to their greater height and moment arm. This causes flexural deformations and stresses to have a higher participation in behavior of the wall. He observed that the walls with lower aspect ratios exhibited greater initial stiffness.

5.8.5 Kasparik

Kasparik (2009) built and tested six reduced-scale masonry shear walls at McMaster University. Due to reinforcement anchorage problems in two specimens, Kasparik omitted the two tests from his analysis and discussion. The walls were all tested under simulated earthquake conditions corresponding to the 1940 El Centro earthquake N-S component. All of the walls were constructed of scaled concrete masonry units and had the same aspect ratio, axial loading, and loading procedure. Kasparik chose an shear span ratio of 1.9 to force his specimens to fail in flexure. For this reason, his specimens contained no horizontal shear reinforcement. Kasparik investigated the effects of vertical reinforcing pattern and ratio on the performance of partially-grouted shear walls failing in flexure.

Kasparik grouped his walls into three types according to vertical reinforcement ratio and distribution. The three reinforcement ratios used were 0.12 percent, 0.17 percent, and 0.20 percent. All three of these ratios are less than that permitted by the Canadian masonry standard CSA S304.1 (2004). All three groups contained reinforcement in the end cells and the second group also contained reinforcement in the center core since it had a lower spacing of vertical reinforcement.

Kasparik observed that, in general, the walls were all dominated by rocking-type behavior. This initiated with the formation of a continuous horizontal crack and subsequent separation of masonry along the bottom part of the wall. The horizontal cracks were located in a bed joint somewhere between the first and fourth course, depending on the wall. This was undoubtedly caused by the high shear span ratio of 1.9 used by Kasparik for his specimens. The initialization of this flexural mode of failure increased the energy dissipation capacity of the wall specimens such that the actuator capacity was not sufficient to induce failure in any of the specimens.

The average measured yield strengths for each of the three groups were 88, 102, and 67 percent of the calculated yield strength, respectively. He observed that stiffness degradation started at about 0.02 percent drift for all of the wall specimens. The initial stiffness of the walls ranged from 16 to 32 percent of the calculated stiffness for each wall. He observed that generally, the period linearly increased as the lateral drift increased. Lastly, the ductility factors for his wall specimens were based on an idealized bilinear curve. The ductility factors for the walls ranged from 1.9 to 2.6.

Kasparik (2009) made no conclusions for the general behavior of partially-grouted walls. Though not explicitly stated, the reason for this could be implicitly deduced from the fact that none of his specimens were tested to complete failure. He recommended that further research be conducted in which the walls are tested to failure and in which a greater number of design parameters are tested.

5.8.6 Haach, Vasconcelos, and Lourenço

Haach et al. (2010a) tested eight half-scale masonry walls at the University of Minho in Guimarães, Portugal. Seven of their specimens were partially-grouted and the remaining specimen was unreinforced. Their tests were unique from other partially-grouted masonry tests for two reasons. First, they used truss-type wire reinforcement for both horizontal and vertical reinforcement. Second, they used a custom portland cement-based mortar mix (with no lime) for both the mortar joints and grouting the reinforcement. This mortar mix was previously developed by Haach et al. (2007, 2010b). All tests were performed using lateral stepwise-increasing cyclic loading.

The purpose of their study was to test the use of truss-type wire reinforcement for both horizontal and vertical reinforcement. The parameters that Haach et al. tested were vertical and

horizontal reinforcement ratios, vertical axial load, and bond pattern using the test frame shown in Figure 5.12. The two bond patterns investigated were interrupted running bond—where a continuous vertical joint is located at each core containing vertical reinforcement—and standard running bond. Haach et al. constructed their specimens using three-core blocks with frogged ends. This allowed them to place the vertical reinforcement in either the center core of a block or between two adjacent blocks in the core formed by the two frogged ends. All horizontal reinforcement was laid in the bed joints of the walls.

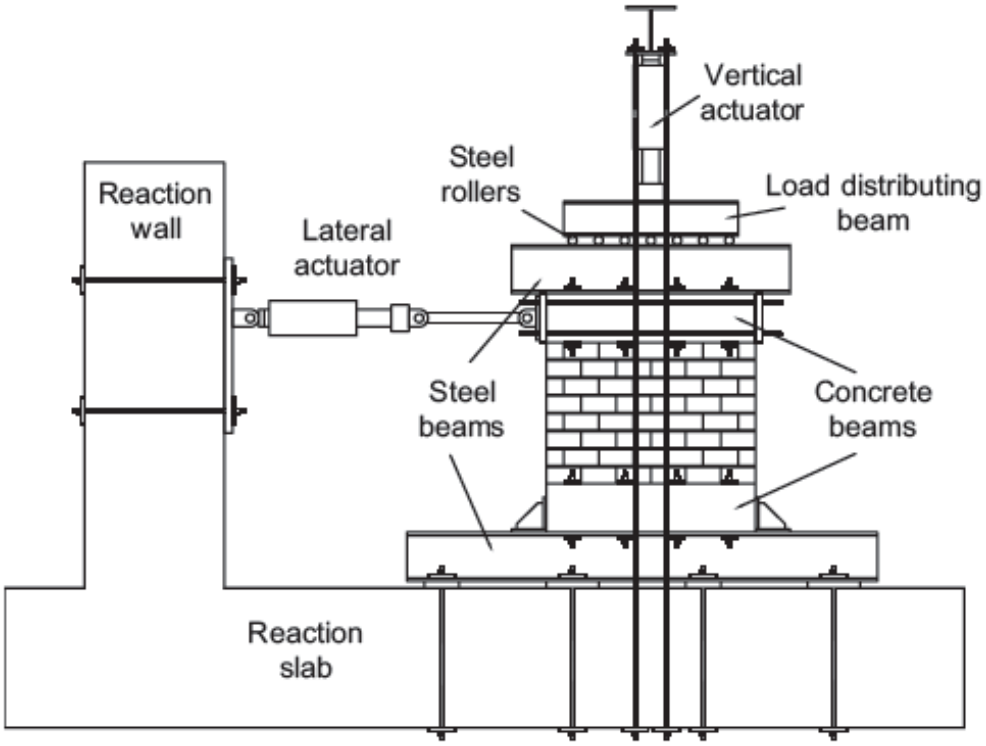

Figure 5.12: Test frame from Haach et al. (2010a)

Haach et al. observed that neither the vertical nor the horizontal reinforcement had any influence on the flexural cracking load. However, they concluded that diagonal cracking was clearly influenced by the vertical reinforcement. The inclusion of vertical reinforcement delayed the formation of diagonal cracks and lead to a 50 percent higher lateral load capacity than walls without vertical reinforcement. The vertical reinforcement also helped prevent the opening and propagation of horizontal flexural cracks throughout the wall panel.

Their tests further confirmed the findings of other researchers (Shing et al., 1989; Schultz et al., 1998) in that horizontal reinforcement has no influence on the lateral cracking load. Horizontal reinforcement is not effective with horizontal cracking patterns, meaning it has no influence in the cases of flexural or sliding-shear failures. They also observed that vertical axial load had the most significant effect on lateral cracking load.

Haach et al. observed that the walls in this program failed predominantly in the flexural mode. This was evident by the presence of toe crushing in the specimens and the low contribution of the horizontal reinforcement to the lateral strength of the walls. Comparison of the experimental and analytical lateral strengths of the walls also confirmed that the flexural mode governed. However, it should be noted that diagonal shear cracking was present in the wall panels, suggesting that a combined flexure-shear mode of failure may have taken place.

Haach et al. (2010a) concluded that in the case of their proposed reinforced masonry system, the bond pattern at the reinforced cores has no significant influence on the performance of the wall. They concluded that higher values of precompression lead to overall higher lateral strength but decrease the effectiveness of the reinforcement, leading to a more brittle failure. They concluded that the effectiveness of the horizontal reinforcement is linked to the presence of vertical reinforcement. They devised that vertical reinforcement delays the formation and propagation of horizontal flexural cracking, enabling the wall to develop diagonal cracking and to fail more in a shear mode than in a flexural mode.

They further remarked that that horizontal reinforcement ratio does not appear to influence the lateral strength, but this may have been due to toe crushing in the walls not permitting the walls to attain their full shear capacity. They concluded that horizontal reinforcement helps prevent the localization of cracks, enabling a more distributed spreading of cracks and stresses and larger non-linear lateral deformations.

CHAPTER 6. DATASET ASSEMBLY

6.1 Introduction

Meta-analysis requires that the constituent data are collected and scrutinized systematically and that they are synthesized together. Within the literature it appears that all studies reviewed have been systematic in their design and execution, though the methodologies used in testing the specimens and reporting the data have varied between studies. To synthesize the data is to objectively correct for variations in measurement and reporting methodologies and choose the criterion for weighting the individual specimens.

6.2 Data compilation

The first step in developing the three approaches for shear strength prediction was to compile data from the existing field of data. This step was conducted concurrently with the literature review. The end goal of this primary step was to collect sufficient quantitative and qualitative data about the behavior of masonry shear walls for use in developing the three approaches for this dissertation.

The purposes of the literature review were to understand how masonry properties affect shear behavior and to identify potential criteria to be used in building prediction models for masonry shear strength. The literature review was primarily focused on research conducted on the performance of masonry shear walls and reviewed the history of masonry shear wall research to understand how researchers have arrived at the current state of knowledge in masonry shear wall analysis and design and to understand which areas have yet to be examined. The process of reviewing the previous masonry shear wall research helped to clarify certain aspects of the code equation, to understand how it was developed, and to identify its limitations and ways that it can be improved.

The literature review covered other ancillary topics not directly related to masonry shear strength prediction to produce a broad knowledge base for this research program. A wide scope is necessary to identify potential effects of other properties on masonry shear wall behavior and performance not currently considered by the MSJC code equation. Broad knowledge of masonry principles was necessary for the creation of standardized data reporting procedures and correction factors for data synthesization.

Masonry shear wall research data were compiled from all available sources. As additional research was identified through the literature review of other sources, the data from the additional research were added to the growing collection of masonry shear wall data. Further research was identified from searches in databases of scholarly literature. These included academic journals, conference proceedings, theses, dissertations, and technical reports.

The data collected from each research study were gathered into a Microsoft Excel table. Each row of the table represented the single masonry shear wall specimen and the columns of the table represented the properties of the walls. The first approach developed herein only necessitated that those properties required for the MSJC shear equation be collected. The open-ended nature of the second and third approaches meant that the more wall properties that could be recorded, the deeper and more thorough of an analysis could be performed.

The data properties and experimental strength for each specimen were extracted from the respective research report. The data properties were primarily taken from tables listing the specimen details. Not all details were enumerated within the respective tables and the details missing from the tables were extracted from diagrams, data plots, and the text itself.

6.3 Data Scrutinization

The second step was to scrutinize the initial compilation of data to select which data were to be used in the analysis. There is no clearly defined way to determine which studies should and should not be included in a meta-analysis; the decision relies in part on the judgment of the researcher. Meta-analysis requires explicit mechanisms for deciding which studies to include and which ones to exclude. The mechanisms selected for filtering the data set were the attributes of grouting type, ultimate failure mode, sufficiency of data, and uniqueness. These attributes were

chosen so that the data set would best represent the population of masonry shear wall failures and to eliminate specimens that would cause foreseeable problems in the data analysis.

The first attribute examined was grouting type. Initially, this study was going to examine only those specimens that were partially-grouted. As the history behind the current MSJC equation was examined, it was apparent from the commentary to the 1997 NEHRP Provisions that there was little documentation about the rationale used in assembling the current equation from two previously proposed equations, Blondet et al. (1989) and Okamoto et al. (1987). The need to compare the equation for both fully- and partially-grouted cases was evident to truly quantify the difference, if any, between them.

Within this analysis, the fully-grouted walls and solid walls were treated together because for both types the net shear area is equal to the horizontal gross cross sectional area. Similarly, the partially-grouted and hollow (i.e., ungrouted) walls were treated together because for the two types the net shear area is not equal to the gross area nor the net area. For purpose of classification, solid and hollow wall definitions will follow that listed in the MSJC—that solid walls are made of units with net area at least 75 percent of the gross area. In the case of the partially-grouted and hollow walls, the net shear area was calculated using the recommendations in the MSJC, as outlined in Appendix C. The practice of segregating the fully- and partially-grouted specimens is in keeping with the conclusions made by Nolph (2010).

Further scrutinization revealed that many shear wall tests exhibited flexural failure modes. Masonry walls failing in flexure generally exhibit greater ductility than those failing in shear, but also fail at loads less than the shear capacity. For this reason those walls failing in flexure were excluded from the analysis because they would artificially decrease the mean experimental-to-predicted strength ratio, making the MSJC equation appear more unconservative. This practice is the same as that used in the previous data analyses of Blondet et al. (1989) and Anderson and Priestley (1992).

Relatively little has been written about the difference between sliding shear and diagonal shear failures. The principal difference between the two is that the former tends to occur in cases of low vertical axial load and the latter in cases of higher axial load. Due to the current gap in knowledge concerning this subject and the present lack of a separate equation for predicting

sliding shear capacity, this research will group both sliding and diagonal shear failures together as non-flexural failure types and will include both in the analysis.

Some tests did not provide enough data for complete analysis because the author omitted information required for predicting the shear strength. One common example is that many authors either did not test masonry prisms as part of their study or they did not report the masonry prisms strength. This was more common in older studies that took place before prism testing became standardized, but some more contemporary tests also neglected this important detail in their report. Among those papers missing masonry prism data, the vast majority included strengths of the constituent materials. Other examples of omitted information include missing prism height-to-thickness ratios, missing geometrical data, and missing failure modes.

It was decided that it would be better to estimate missing data (where possible) than to eliminate those specimens. The inclusion of a greater number of specimens increases the degrees of the freedom in the statistical analysis, increases the breadth of the parameters studied, and makes the sample more representative of the overall population. Since the equation consists of three components—masonry, axial, and reinforcement—an educated estimate affecting one portion of the equation would have only a limited effect on the overall accuracy of the whole equation for that given specimen. Furthermore, given the large variation that is present measuring masonry material strengths (Blume and Proulx, 1968), it was judged that estimated data determined using a regression model would likely not contain much more variation than the measured data. Those specimens with missing parameters that were deemed to be estimable were retained whereas that that were not were excluded from the analysis. Details of each of the parameter estimation procedures are outlined in Appendices C and D.

As the data set was expanded, several specimens were suspected of being duplicates of other specimens already included in the data set. This was more evident in cases where two reports including the same author(s) listed specimens with identical identifiers. In a few cases, articles or reports with difference authors reported the results from the same specimens. It was important to remove the duplicate specimens from the data set so that they would not exact undue influence on the analysis results and so that the specimens could be more accurately sub-grouped together to determine their respective weightings.

To identify duplicate reporting of specimens, tests from articles and reports were compared using specimen names, dimensions, and experimental shear values to identify and eliminate duplicates from the data set. In a few select cases, the reported results from a specimen were duplicated in more than one report, but there was a discrepancy between them. If the results were published in more than two reports, then the value that was most consistent between the papers was assumed to be the correct value. In the situation were the results were only published in two publications, then it was assumed that the more recent publication contained the correct values. This latter assumption was based on the thought that any error in earlier publications would have be recognized and corrected in the subsequent publication.

6.4 Data Synthesization

Meta-regression requires that disparate indices be converted to a common index before proceeding with the analysis (Borenstein and Hedges, 2009). Within the data set the principal indices that differed between specimens were the testing, measuring, and reporting methodologies used by the many researchers to report their findings. These differences between the data of difference research studies can be reduced by synthesizing the data based on standardized methodologies. This could be thought of as making the data to appear as though it had come from the same study.

Synthesization is an important step to minimize the variation in data between studies and, hence, the total variation within this analysis. The variation within individual studies is treated later in each analysis through the use of weighting. As no standardized methodology was available for reporting masonry shear wall data, it was necessary to formulate standard reporting procedures for use in this analysis. The development of these standardized procedures is detailed in Appendix C of this paper and Dillon and Fonseca (2014b).

With standards in place, the next step was to correct the data that did not conform to the standards. It was necessary to formulate a methodology for correcting non-conforming data to each new standard. Methodologies were needed for prism strength estimation, inflection height, net shear area, prism aspect ratio, shear reinforcement, loading patterns, loading rates, and experimental shear strength reporting.

6.4.1 Prism Geometry

The MSJC (2013) code equation bases the determination of f'_m on ASTM C1314, which sets a standardized prism aspect ratio of two. This choice of prism aspect ratio is different from that of other nations and is different from many American-tested specimens reported in the literature (Korany and Glanville, 2005). In assembling the data set used in this analysis, the standardized prism aspect ratio of five is used because research has shown that it better represents the compressive strength of the masonry in the field (Boult, 1979; Hegemier et al., 1978). Apart from the logical reasons, the use of a standard aspect ratio of five would lessen the quantity of specimens that would need to be corrected since five was the most commonly used ratio reported in the literature.

The prism aspect ratios were compared from four standards: ASTM C1314 (2014), CSA S304.1 (2004) Annex D, BS 5628-2 (2000) Appendix D, and AS 3700 (2011) Appendix C. Since the ASTM standard was the only one to use a standard aspect ratio other than five, the correction factors in ASTM were converted to the equivalent value assuming a standardized aspect ratio of five. All four of the standards permit linear interpolation of aspect ratios for non-integer values. The values for the four standards together with the average value are plotted in Figures 6.1a and 6.1b for ease of comparison.

A function was determined that correlated well with the mean of the four sets of correction factors. The true mean was only piecewise differentiable and three functions would be required to model it perfectly. It was decided that to use a continuously differentiable function with a good fit to model the mean factor would be more than sufficiently accurate. A smooth function is also likely to be more representative of the actual prism performance than a piecewise function.

First, the data were transformed such that the data point corresponding to an aspect ratio of 5.0 and a correction factor of 1.0 became the new coordinate origin. This was done by subtracting the aspect ratio from 5.0 and subtracting the respective correction factors from 1.0. The three data points away from the new origin were then transformed using the logarithmic function. The point at the origin was omitted because the logarithm of zero is undefined and the transformation would guarantee that the function would pass through this point. Linear regression was performed on the three transformed data points to find two regression coefficients. The regression model for the

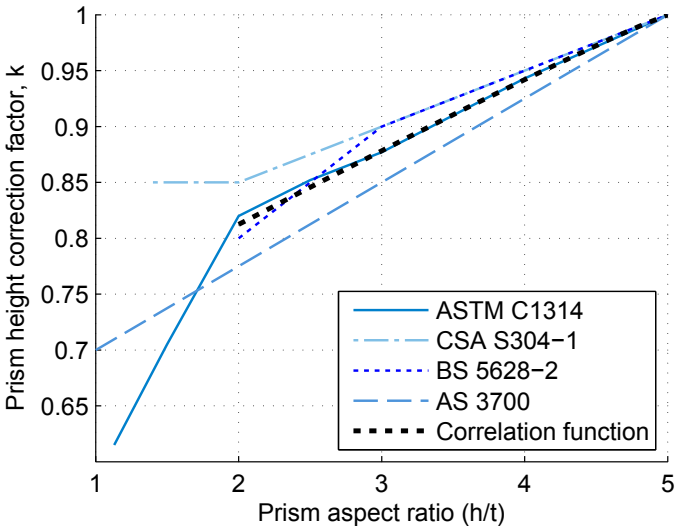

(a) Assuming a standard ratio of 5

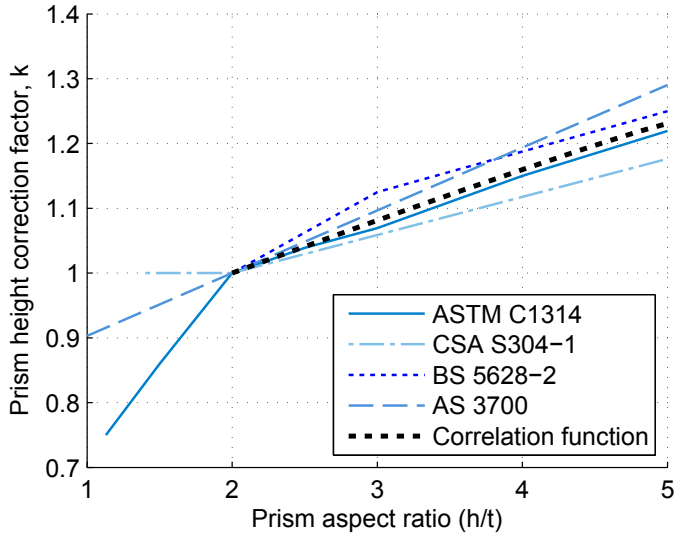

(b) Assuming a standard ratio of 2

Figure 6.1: Comparison of prism correction factors

mean prism strength correction factor k was untransformed to produce

$$k = 1 - 0.058\left(5 - \frac{h}{t}\right)^{1.07} \tag{6.1}$$

where $\frac{h}{t}$ is the aspect ratio of the prism.

Equation (6.1) deviates from the mean correction factor from the four codes by at most 0.3 percent, is within the precision of this analysis, and produces values closest to those specified in ASTM C1314 (2014). Other regression equations were examined, but Equation (6.1) had the highest correlation with the mean of the factors specified in the four codes.

6.4.2 Prism strength estimation

As reported in Appendix C, there were many studies in which the prism strength was not reported but included the strengths of the constituent materials. Currently, the underlying principles of masonry prism behavior are fairly well understood at a qualitative level but the high variability of prism data have made it difficult for researchers to formulate predictive equations for prism strength based in the strengths of the constituent materials. In order for these studies to be included within the analysis, equations were formulated to estimate prism strength from the constituent material strengths provided by the respective researchers.

The estimation of prim strength is likely to introduce measurement error into the analysis due to the high variability of masonry prism strengths. Including a greater number of specimens means that a larger domain of testing parameters would be included in the analysis. A larger domain of specimen parameters would make the results more representative of a larger portion of the masonry shear wall population. Since the results of this analysis are intended to cover the entire masonry shear wall population, it was judged more valuable to the analysis to analyze a greater number of specimens by including those with estimated f'_m values than to reduce possible measurement error by excluding them.

Masonry prism tests typically demonstrate high variability, with a coefficient of variation of 10 percent or lower considered to be good (Blume and Proulx, 1968; CSA S304.1, 2004). Much of this variability can be attributed to defects introduced during the assembly and handling of the prisms. The unknown measurement error introduced by estimating f'_m values for specimens is assumed to be less than that of prisms because constituent material tests typically have less variability. In fact, as better models are developed in the future to quantify the behavior of masonry assemblages it may become more accurate and economical to estimate f'_m from the constituent material properties than from testing masonry prisms.

Any measurement error in the f'_m value has a reduced impact on the error of the whole shear prediction equation. Part of this reduction comes from the use of the square root of the f'_m value. The root function has the effect of reducing any error from the term, especially at the higher values typically used for f'_m. The other part is due to the fact that the f'_m value is only used in the masonry component of the shear equation. The predicted shear strengths of the axial load and shear reinforcement components of the shear equation are unaffected by an error in the f'_m value.

Data Estimation

Two linear models were developed to predict the masonry prism strengths for ungrouted and grouted prisms, respectively. The details of how the models were developed is found in Appendix C. The selected prism strength prediction model for hollow masonry prisms is given by

$$f'_m = \nu^{0.636} f_b^{0.688} f_j^{0.317} \tag{6.2}$$

and the model for grouted masonry prisms is given by

$$f'_m = t^{-0.221} (1-\nu)^{0.0818} f_b^{-0.425} \left(f_j + f_b\right)^{1.01} \left(f_g + f_b\right)^{0.312} \tag{6.3}$$

where

ν = is the ratio of net to gross area,
f_b = the compressive strength of the brick or block,
f_j = the compressive strength of the mortar,
t = the thickness of the prism in the smallest dimension, and
f_g = the compressive strength of the grout.

The strength values from the data set used in this study were all converted to the equivalent aspect ratio of 2 as specified in ASTM C1314 (2014).

6.4.3 Shear Reinforcement Area

The MSJC (2013) code specifies the contribution of the shear reinforcement to the shear strength of the wall to be

$$V_{ns} \quad = \quad 0.5 \frac{A_v}{s} f_{yv} d_v \tag{6.4}$$

for all reinforced masonry shear walls. Equation (6.4) has the same form as that used for reinforced concrete but with a 0.5 factor added to the front. The NEHRP (1997) commentary noted that the 0.5 factor was an empirical factor added so that the equation would better fit the data. A detailed discussion of this equation and the 0.5 factor is provided by Anderson and Priestley (1992) and in Section 14.2 of this dissertation.

The A_v/s portion of the equation is exactly proportional to the shear reinforcement ratio in reinforced concrete walls where the reinforcement is equally spaced. In reinforced masonry, equal spacing of the shear reinforcement is not always possible because it must be spaced at intervals that are a multiple of the masonry unit height. Many experimental programs were designed such that predetermined shear reinforcement ratios were used for different specimens. The number of courses in the specimens was not always equally divisible by the number of reinforcement bars needed to achieve the desired reinforcement ratio. As a result, many specimens contained unequally spaced shear reinforcement.

During analysis of the specimens with unequal shear reinforcement spacing, the issue was which value to use for the spacing variable s in the shear equation. The spacing is proportional to the shear reinforcement ratio and is given by

$$\frac{A_v}{s} \quad \equiv \quad \frac{\sum A_v}{h} \quad = \quad \rho_v \, t \tag{6.5}$$

where ρ_v is the shear reinforcement ratio and t is the specified thickness of the wall. The equalities shown in Equation (6.5) are of particular benefit for case for when only the shear reinforcement ratio is reported.

6.4.4 Shear Length

Different masonry codes specify differing methods for calculating the effective shear length. Since the first approach presented herein was to compare and, as necessary, correct the existing MSJC masonry shear strength equation, it was necessary to use the shear length as defined by the MSJC code for the first approach. The MSJC defines shear length to be the entire length of the masonry shear area in the direction of shear. Since all researchers reported the lengths of their specimens in tabular or graphical format, there was no need to calculate or adjust shear length data for the first approach.

The second and third approaches were less constrained in nature. The shear lengths of the specimens were calculated using the other definitions and used in the second approach to determine which definition best fits the experimental data. The results of this simple study are presented in Appendix C.

6.4.5 Reported Shear Strength

In the literature, three different values have been used as the experimental shear strength of masonry walls. One value used has been the peak loads in each of the two directions (i.e., pushing and pulling), another has been the average of the peak load from each direction, and another has been the ultimate load in either direction. Wall strengths from monotonic testing have been taken as the ultimate load.

Unfortunately, many researchers reported only one of the three values though some researchers reported at least the last two values. In the latter case the peak load in the weaker direction can be calculated from the ultimate and average shear loads. In light of the different values reported, it was decided to use the average of the peak loads from the two directions for the shear strength (Dillon and Fonseca 2014b; Appendix C).

For specimens which only the ultimate shear strength was reported, the data needed to be adjusted to compensate for the exclusion of the peak strength in the weaker direction. A correction factor was calculated using the data from the specimens in which both the ultimate and the average peak shear strengths were reported. For each of these specimens, the ratio of the average peak strength to the ultimate strength was calculated. For visualization, the histogram of the ratios

of the average peak strength to the ultimate strength of the from the 176 specimens is shown in Figure 6.2. The correction factor used was 0.9. Specimens that were tested monotonically are described separately from the bidirectionally tested walls in the next section.

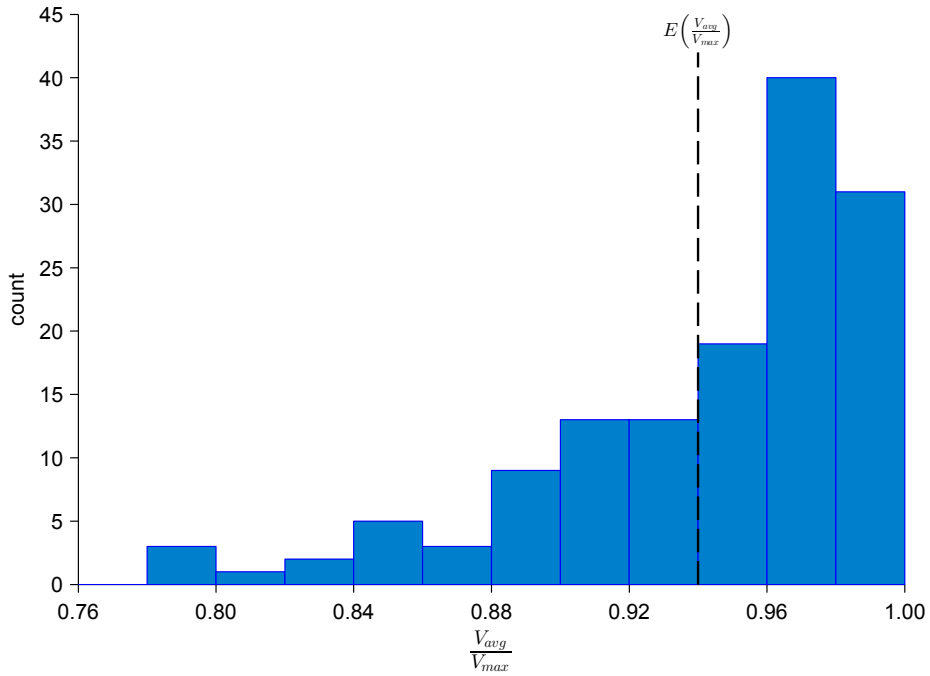

Figure 6.2: Histogram of average to ultimate strength ratios

6.4.6 Loading Pattern

Researchers have used different loading patterns for testing their masonry shear wall specimens, namely: monotonic, incrementally-increasing cyclic, sequential-phase displacement, and simulated seismic. Dillon and Fonseca (2014a) explained more in-depth these different loading patterns (see Appendix C) and showed that there is a non-significant difference in experimental strengths between walls tested using the different cyclic loading patterns. They determined that the monotonically tested walls exhibited an artificial increase in strength over walls tested with one of the periodic loading patterns and further determined this increase to be statistically significant.

The shear strengths from monotonic and reversed-monotonic tests were higher than those of cyclic tests because they did not experience cycles of strength degradation prior to their ultimate

strength. During cyclic tests, repeated opening and closing of existing cracks and the formation of new, more wide-spread cracking patterns occurred with increasing lateral amplitudes. As a cyclic specimen approaches its ultimate shear strength, the strength has been reduced by the more-widespread cracking and by repeated trituration of the aggregates along the shear cracks (Hidalgo et al., 1979; Yancey and Scribner, 1989).

The numerical difference between monotonic and cyclic loading patterns shown in Dillon and Fonseca (2014a) was determined through analysis on the data provided by Tomaževič et al. (1996). The Tomaževič et al. study was a well-designed experiment which included two replicates for each combination of variables. Other studies which used both monotonic and periodic loading patterns were conducted by Meli et al. (1968), Woodward and Rankin (1985), and Matsumura (1987). Unfortunately, these other three studies did not duplicate design variables between the specimens that were monotonically tested with those that were not and could not be used to determine a correction factor for monotonically tested specimens.

The data from Tomaževič et al. (1996) showed that monotonically tested specimens failed at notably higher loads than similar specimens tested cyclically, resulting in a mean ratio of cyclic-to-monotonic strengths of 0.81. The 95 percent confidence interval for this mean is bounded below by 0.72 and above by 0.91. This interval excludes unity by a fairly large margin, denoting that the difference is statistically significant. It should be noted that the specimens subjected to periodic loading and high confinement stress appeared to fail in a combined flexure/shear mode whereas the monotonically tested specimens appeared to fail predominantly in the flexural mode. The different modes of failure suggest that the value calculated herein may not perfectly reflect the relationship between the two loading patterns. Nevertheless, if the true value for a correction factor were different, it would most likely be lower because the strength of the monotonically tested specimens would have been higher if they had failed predominantly in the shear mode. Despite this potential source of error, the correction factor of 0.81 used in this analysis represents the best estimate for the relationship between monotonic and cyclic specimens given the limited data available.

6.4.7 Loading Rate

Masonry is subject to strain rate effects (Abrams, 1988; Paulson and Abrams, 1990; Tomaževič and Velechovsky, 1992; Tomaževič et al., 1996; Tomaževič, 2000; Williams and Scrivener,

1974). At higher rates of strain, the strength of the masonry increases proportional to the logarithm of the strain rate. Older studies did not specify which loading rate was used and were assumed to have been quasi-static because they pre-dated the wide-spread usage of electronic measuring and recording devices. In these tests the loads and displacements were read manually from dial gauges, eliminating the possibility of using dynamic load rates.

The majority of specimens included in the data set were tested using quasi-static strain rates while only a relatively small number were tested dynamically. Before the data could be analyzed, the experimental shear strengths of the dynamically tested specimens needed to be adjusted to the standardized static-equivalent strength. It was necessary to determine a correction factor for the specimens which were tested dynamically.

Within the data set there were only twelve pairs of specimens in which the only difference in variables was the loading rate under which the specimens were tested. These specimens were those tested by Williams (1971), Mayes et al. (1976b), and Tomaževič et al. (1996). An initial study of each of the three groups determined that only those from Tomaževič et al. showed a highly statistically-significant difference between the dynamic and static tests. The lack of statistical significance in the other data was attributed to the high variability of testing and recording procedures from the older studies.

The twelve pairs of specimens from the three studies were combined to determine a mean correction factor for the dynamically loaded specimens. The twelve dynamically tested specimens were tested at shear strain rates within a single order of magnitude, which was deemed to be sufficiently close for the results to be compatible. The three pairs of specimens from Tomaževič et al. (1996) were given double the weighting of the specimens because Tomaževič et al. replicated each test twice and reported the average of the two tests.

The combined, weighted mean analysis of the twelve pairs of specimens resulted in a reduction factor of 0.90 for the dynamically tested specimens in this data set. The statistical test produced a P-value of 0.15 for the case of strain rate effects in masonry shear walls, which is not quite significant by common statistical standards. However, it was determined that, in this case, the resulting factor was representative considering the small sample size and the fact that strain rate effects in masonry have been previously observed to exist.

6.4.8 Scaling

Many researchers employed small-scale specimens in their experimental studies. Analysis by Dillon and Fonseca (2014b) of the size effects in masonry concluded that the scales typically employed by researchers for masonry shear walls were not sufficient enough to produce any noticeable errors in resulting values of their analyses. They further noted that the studies would compensate for any size effects by testing scaled masonry prisms made from the same scaled materials.

The scaled masonry shear wall research used in this analysis was scaled to its equivalent full-scale prototype. The justification for this practice is found in Dillon and Fonseca (2014b) and in Appendix C. The geometric (i.e., units of length) and load parameters (i.e., units of force) for each specimen were scaled using the respective scale factor. The stress parameters for the constituent materials (i.e., units of force per area) were left unchanged. In most cases the scale factor provided by the researcher was only nominal. In each case a specific scale factor was calculated by examining the quotient of the scaled and prototype specimen geometries. The influence of scaling was irrelevant for the first approach because the ratio of experimental to predicted strengths was unit-less.

6.5 Meta-Regression

Meta-regression allows data from various research studies to be analyzed together. The benefits of meta-regression are that it allows researchers to gain the benefits of a larger pool of data, to compensate for errors from a single study, and to increase the statistical power of the analysis. The meta-regressions used in this analysis used weighted least squares regression techniques for analyzing the data set. The weight for each specimen was assigned according to which subgroup that specimen belonged and is detailed in Section 7.2.

CHAPTER 7. DATASET GROUPINGS AND PARAMETER DISTRIBUTIONS

7.1 Summary

The procedures of data collection, scrutinization, and synthesization employed in Chapter 6 produced a dataset consisting of 353 individual specimens. This is, by far, the largest dataset of grouted masonry shear wall specimens yet assembled for studying the behavior of shear forces in masonry walls. A summary of the various qualitative wall attributes for the dataset is provided in Table 7.1. The attribute that is the most evenly divided within the dataset is the type of grouting used, where partially grouted walls account for a little over half (51%) of the specimens in the dataset. The attribute that is the most divided within the dataset is the rate at which the walls were loaded. The vast majority of specimens (94%) were tested under quasi-static loading due to the extra expense and effort that is required for dynamically-loaded tests.

Most of the specimens (60%) were tested under fixed-fixed boundary conditions such that the walls were subjected to double-curvature. It may appear that this runs counter to the claim in Appendix C that cantilever testing is the most predominant mode of testing, but these two facts are not in disagreement. Cantilevered walls have a higher propensity for failing in flexure compared to walls of similar geometry tested under double-curvature conditions because the latter loading produces shear span ratios half of that for a cantilever loading. A disproportionately larger number of cantilever-tested walls were filtered out of the final dataset because they failed in the flexural mode.

7.2 Specimen Groupings

The specimens were grouped together with other specimen sharing common attributes so that the statistics of the group could be used to calculate weightings for the specimens within each group. Common delimiters used in dividing the groups were research study, material, and

Table 7.1: Summary of Specimen Attributes

Property	Attribute	Count
Grouting	Full	172
	Partial	181
Material	CMU	252
	Clay	101
Scale	Full	325
	Half	24
	Third	4
Shape	Cantilever	141
	Double-Curvature	212
Loading	Monotonic	47
	Cyclic	304
	Simulated Seismic	2
Rate	Quasi-static	331
	Dynamic	22
Failure	Shear	295
	Shear/Flexure	37
	Sliding	13
	Shear/Sliding	9
	Sliding/Flexure	1
	Shear/Sliding/Flexure	1

grouting. Each specimen was assigned a serial number for use in identifying the specimen. New identifiers were created for use in this analysis because there was little to no consistency between the identifiers used in the original studies. A unique identifier was also needed for the few cases where two researchers from two different studies assigned the same identifier to two different specimens.

Each identifier was constructed from a combination of ten letters and numbers. The first 4 digits were the year in which the specimen data were *first* published. The next 2 letters represent the country in which the test was performed. A summary of the tests and abbreviations for each country are given in Table 7.2. The next 2 letters represent the first two letters of the principal

researcher's surname. The last 2 numbers are a unique number assigned to each specimen from that particular study. The serial numbers are non-contiguous because they were assigned before specimens were filtered from the dataset during the scrutinization process.

Table 7.2: Summary of Specimens by Country

Country	Abbrev.	Count
Australia	AU	13
Canada	CA	4
Japan	JP	80
Mexico	MX	22
New Zealand	NZ	51
Portugal	PO	4
Slovenia	SL	16
United States	US	163

In forming the data group, the best effort was made to maintain similar attributes within each group. The data from Matsumura (1987) consisted of such a large number of specimens that the group was broken up further. Matsumura included data from several of his colleagues with his own data. Japanese and English versions of his colleagues' original research reports were found and used to as a basis to divide the data set. The remaining Matsumura data was divided based on the groupings already employed by Matsumura.

In a few cases, a lone specimen with a different attribute from the rest of the specimens in that study was grouped with the rest of the data despite the attribute difference. The smallest group that could be formed was with two specimens because at least two data values are necessary to compute the the second central moment (i.e., variance) of the group. The options for dealing with lone specimens was to either drop the specimen from the dataset or to add the specimen to a group from the same study. The latter option was judged to be most beneficial to the study. In no case was a specimen added to a group consisting of specimens from a different study. The specimen groupings are summarized in Table 7.3.

7.3 Distributions of Specimen Parameters

In this section, the quantitative attributes of the specimens are plotted as histograms for each of the two grouting types. The quantitative attributes make up the input parameters used in the shear prediction equations. Histograms were chosen because they facilitate easy visualization of the distribution of each of the parameters in a concise format.

7.3.1 Vertical Reinforcement

Vertical reinforcement serves two primary purposed within masonry shear walls subject to in-plane lateral loads. The first purpose of vertical reinforcement is to preclude flexural failure of the masonry by resisting the vertical tensile forces and reducing the opening and spreading of horizontal tensile cracks. Principles of mechanics show that the tensile stresses in the masonry shear walls are greatest along the ends of the wall, so the exterior vertical reinforcement (in the end cells of the wall) is most effective in resisting the flexural moment force. The interior vertical reinforcement is not as effective because it has a smaller moment arm and is not subjected to the same level of strain as the exterior reinforcement.

The second purpose of vertical reinforcement is to contribute to shear strength through vertical confinement and dowel action. As shear cracks appear in the masonry panel, the vertical confinement provided by the axial load and vertical reinforcement can help keep shear cracks closed, increasing the friction and shear transfer across the crack. Ghanem et al. (1992) concluded that only interior vertical reinforcement is effective in increasing the shear capacity. This is likely due to the fact that the exterior vertical reinforcement is principally engaged in resisting the overturning moment of the wall.

The exterior and interior vertical reinforcement are called by different names throughout the literature. Due to the different effects that the two types of vertical reinforcement have on masonry shear wall behavior, herein the author will refer to the exterior vertical reinforcement as *flexural reinforcement* and the interior vertical reinforcement as *confinement reinforcement*.

Table 7.3: Summary of Data Groupings

Group	Source	Specimen	Serial No.	Material	Grouting
1	Meli et al. 1968	Muro 309	1968-MX-ME-09	CMU	PG
		Muro 310	1968-MX-ME-10	CMU	PG
		Muro 311	1968-MX-ME-11	CMU	PG
		Muro 312	1968-MX-ME-12	CMU	PG
		Muro 313	1968-MX-ME-13	CMU	PG
		Muro 314	1968-MX-ME-14	CMU	PG
		Muro 315	1968-MX-ME-15	CMU	PG
		Muro 316	1968-MX-ME-16	CMU	PG
		Muro 317	1968-MX-ME-17	CMU	PG
		Muro 318	1968-MX-ME-18	CMU	PG
2	Meli and Salgado 1969	Muro 501	1969-MX-ME-11	CMU	PG
		Muro 504	1969-MX-ME-14	CMU	PG
		Muro 505	1969-MX-ME-15	CMU	PG
		Muro 506	1969-MX-ME-16	CMU	PG
		Muro 507	1969-MX-ME-17	CMU	PG
		Muro 508	1969-MX-ME-18	CMU	PG
		Muro 509	1969-MX-ME-19	CMU	PG
		Muro 510	1969-MX-ME-20	CMU	PG
		Muro 511	1969-MX-ME-21	CMU	PG
		Muro 514	1969-MX-ME-24	CMU	PG
		Muro 515	1969-MX-ME-25	CMU	FG
		Muro 519	1969-MX-ME-29	CMU	PG
3	Williams 1971 Williams and Scrivener 1974	Wall 1	1971-NZ-WI-01	Clay	FG
		Wall 2	1971-NZ-WI-02	Clay	FG
		Wall 3	1971-NZ-WI-03	Clay	FG
		Wall 4	1971-NZ-WI-04	Clay	PG
		Wall 5	1971-NZ-WI-05	Clay	FG
4	Williams 1971 Williams and Scrivener 1974	CB 1	1971-NZ-WI-06	CMU	FG
		CB 2	1971-NZ-WI-07	CMU	FG
		CB 3	1971-NZ-WI-08	CMU	FG
		CB 4	1971-NZ-WI-09	CMU	FG
5	Williams 1971 Williams and Scrivener 1974	A1	1971-NZ-WI-10	Clay	FG
		A2	1971-NZ-WI-11	Clay	FG
		B1	1971-NZ-WI-12	Clay	FG
		B2	1971-NZ-WI-13	Clay	FG
		B4	1971-NZ-WI-15	Clay	FG
		D1	1971-NZ-WI-16	Clay	FG
		D2	1971-NZ-WI-17	Clay	FG
	Williams 1971	Dyn 1	1971-NZ-WI-19	Clay	FG
		Dyn 2	1971-NZ-WI-20	Clay	FG
		Dyn B1	1971-NZ-WI-18	Clay	FG

Table 7.3: Summary of Data Groupings (Continued)

Group	Source	Specimen	Serial No.	Material	Grouting
6	Mayes et al. 1976a	HCBL-21-1	1976-US-MA-01	CMU	FG
		HCBL-21-2	1976-US-MA-02	CMU	FG
		HCBL-21-3	1976-US-MA-03	CMU	FG
		HCBL-21-4	1976-US-MA-04	CMU	FG
		HCBL-21-5	1976-US-MA-05	CMU	FG
		HCBL-21-6	1976-US-MA-06	CMU	FG
		HCBL-21-7	1976-US-MA-07	CMU	FG
		HCBL-21-8	1976-US-MA-08	CMU	FG
		HCBL-21-9	1976-US-MA-09	CMU	FG
		HCBL-21-10	1976-US-MA-10	CMU	FG
		HCBL-21-11	1976-US-MA-11	CMU	PG
		HCBL-21-12	1976-US-MA-12	CMU	PG
7	Priestley 1977	A1	1977-NZ-PR-05	CMU	FG
		A2	1977-NZ-PR-06	CMU	FG
		A3	1977-NZ-PR-07	CMU	FG
		A4	1977-NZ-PR-08	CMU	FG
		A5	1977-NZ-PR-09	CMU	FG
		A6	1977-NZ-PR-10	CMU	FG
8	Chen et al. 1978	HCBL-11-2	1978-US-CH-02	CMU	PG
		HCBL-11-3	1978-US-CH-03	CMU	FG
		HCBL-11-4	1978-US-CH-04	CMU	FG
		HCBL-11-5	1978-US-CH-05	CMU	PG
		HCBL-11-6	1978-US-CH-06	CMU	FG
		HCBL-11-7	1978-US-CH-07	CMU	FG
		HCBL-11-8	1978-US-CH-08	CMU	PG
		HCBL-11-9	1978-US-CH-09	CMU	FG
		HCBL-11-10	1978-US-CH-10	CMU	PG
		HCBL-11-11	1978-US-CH-11	CMU	FG
9	Chen et al. 1978	HCBR-11-3	1978-US-CH-14	Clay	FG
		HCBR-11-4	1978-US-CH-15	Clay	FG
		HCBR-11-5	1978-US-CH-16	Clay	PG
		HCBR-11-6	1978-US-CH-17	Clay	FG
		HCBR-11-7	1978-US-CH-18	Clay	FG
		HCBR-11-8	1978-US-CH-19	Clay	FG
		HCBR-11-9	1978-US-CH-20	Clay	PG
		HCBR-11-10	1978-US-CH-21	Clay	FG
		HCBR-11-11	1978-US-CH-22	Clay	PG
		HCBR-11-12	1978-US-CH-23	Clay	FG
		HCBR-11-13	1978-US-CH-24	Clay	FG

Table 7.3: Summary of Data Groupings (Continued)

Group	Source	Specimen	Serial No.	Material	Grouting
10	Hidalgo et al. 1978	HCBR-21-2	1978-US-HI-02	Clay	FG
		HCBR-21-3	1978-US-HI-03	Clay	PG
		HCBR-21-4	1978-US-HI-04	Clay	FG
		HCBR-21-5	1978-US-HI-05	Clay	PG
		HCBR-21-6	1978-US-HI-06	Clay	FG
		HCBR-21-7	1978-US-HI-07	Clay	PG
		HCBR-21-8	1978-US-HI-08	Clay	FG
		HCBR-21-9	1978-US-HI-09	Clay	FG
11	Hidalgo et al. 1979	HCBL-12-1	1979-US-HI-01	CMU	FG
		HCBL-12-2	1979-US-HI-02	CMU	FG
		HCBL-12-3	1979-US-HI-03	CMU	FG
		HCBL-12-4	1979-US-HI-04	CMU	FG
		HCBL-12-5	1979-US-HI-05	CMU	FG
		HCBL-12-6	1979-US-HI-06	CMU	FG
12	Hidalgo et al. 1979	HCBR-12-2	1979-US-HI-08	Clay	FG
		HCBR-12-3	1979-US-HI-09	Clay	FG
		HCBR-12-4	1979-US-HI-10	Clay	FG
13	Thurston and Hutchison 1982	Unit 2	1982-NZ-TH-01	CMU	PG
		Unit 3	1982-NZ-TH-02	CMU	FG
		Unit 4	1982-NZ-TH-03	CMU	PG
		Unit 5	1982-NZ-TH-04	CMU	PG
		Unit 6	1982-NZ-TH-05	CMU	FG
		Unit 7	1982-NZ-TH-06	CMU	FG
		Unit 9	1982-NZ-TH-08	CMU	FG
14	Matsumura and Igarashi 1983 Matsumura 1987	KW4-1	1983-JP-MA-01	CMU	FG
		KW3S-1	1983-JP-MA-03	CMU	FG
		KW2-1	1983-JP-MA-04	CMU	FG
15	Igarashi and Matsumura 1984 Matsumura 1987	CW5-2'-A2-1	1984-JP-IG-01	CMU	PG
		CW5-2'-A2-2	1984-JP-IG-02	CMU	PG
		CW4-2'-A2	1984-JP-IG-03	CMU	PG
		CW3-2'-A2	1984-JP-IG-04	CMU	PG
		CW2-2'-A2-1	1984-JP-IG-05	CMU	PG
		CW2-2'-A2-2	1984-JP-IG-06	CMU	PG
16	Fujisawa 1985 Okamoto et al. 1987 Kaminosono et al. 1988	WS1	1985-JP-FU-01	CMU	FG
		WS4	1985-JP-FU-03	CMU	FG
		WS7	1985-JP-FU-05	CMU	FG
17	Fujisawa 1985 Okamoto et al. 1987 Kaminosono et al. 1988	WSR1	1985-JP-FU-02	Clay	FG
		WSR4	1985-JP-FU-04	Clay	FG
		WSR7	1985-JP-FU-06	Clay	FG

Table 7.3: Summary of Data Groupings (Continued)

Group	Source	Specimen	Serial No.	Material	Grouting
18	Matsumura 1985 Matsumura 1987	WS2	1985-JP-MA-01	CMU	FG
		WS4	1985-JP-MA-02	CMU	FG
		WS5	1985-JP-MA-03	CMU	FG
		WS9	1985-JP-MA-05	CMU	FG
		WS10	1985-JP-MA-06	CMU	FG
19	Yamazaki et al. 1983 Okamoto et al. 1987 Isoishi et al. 1988	GS2	1985-JP-YA-05	CMU	FG
		GS3	1985-JP-YA-06	CMU	FG
		GS4	1985-JP-YA-07	CMU	FG
		GSR1	1985-JP-YA-08	CMU	FG
		GSR2	1985-JP-YA-09	CMU	FG
20	Sveinsson et al. 1985	HCBL-11-13	1985-US-SV-01	CMU	FG
		HCBL-11-15	1985-US-SV-02	CMU	FG
		HCBL-11-17	1985-US-SV-03	CMU	FG
		HCBL-11-18	1985-US-SV-04	CMU	FG
		HCBL-11-19	1985-US-SV-05	CMU	FG
		HCBL-11-20	1985-US-SV-06	CMU	FG
		HCBL-11-21	1985-US-SV-07	CMU	FG
		HCBL-11-22	1985-US-SV-08	CMU	FG
		HCBL-11-23	1985-US-SV-09	CMU	FG
		HCBL-11-24	1985-US-SV-10	CMU	FG
		HCBL-11-25	1985-US-SV-11	CMU	FG
		HCBL-11-26	1985-US-SV-12	CMU	FG
		HCBR-11-15	1985-US-SV-13	Clay	FG
21	Sveinsson et al. 1985	HCBR-11-17s	1985-US-SV-15	Clay	FG
		HCBR-11-19	1985-US-SV-16	Clay	FG
		HCBR-11-20	1985-US-SV-17	Clay	FG
		HCBR-11-21	1985-US-SV-18	Clay	FG
		HCBR-11-22	1985-US-SV-19	Clay	FG
		HCBR-11-23	1985-US-SV-20	Clay	FG
		HCBR-11-24	1985-US-SV-21	Clay	FG
		HCBR-11-25	1985-US-SV-22	Clay	FG
		HCBR-11-26	1985-US-SV-23	Clay	FG
		HCBR-11-27	1985-US-SV-24	Clay	FG
		HCBR-11-28	1985-US-SV-25	Clay	FG
		HCBR-11-30	1985-US-SV-26	Clay	FG
22	Igarashi et al. 1988 Matsumura 1987	WSR2-1	1986-JP-IG-01	Clay	FG
		WSR4-1	1986-JP-IG-02	Clay	FG
		WSR5-1	1986-JP-IG-03	Clay	FG
		WSR6-1	1986-JP-IG-04	Clay	FG
	Matsumura 1987	WS4	1986-JP-MA-53	Clay	PG
		WS4-B	1986-JP-MA-54	Clay	PG

Table 7.3: Summary of Data Groupings (Continued)

Group	Source	Specimen	Serial No.	Material	Grouting
23	Matsumura 1987	CW2-1-1	1986-JP-MA-15	CMU	PG
		CW2-1-2	1986-JP-MA-16	CMU	PG
		CW3-0-1	1986-JP-MA-17	CMU	PG
		CW3-0-2	1986-JP-MA-18	CMU	PG
		CW3-0-A2	1986-JP-MA-19	CMU	PG
		CW3-0'-A3	1986-JP-MA-20	CMU	PG
		CW3-0-A3	1986-JP-MA-21	CMU	PG
		CW3-1'	1986-JP-MA-22	CMU	PG
		CW3-1-1	1986-JP-MA-23	CMU	PG
		CW3-1-2	1986-JP-MA-24	CMU	PG
		CW3-1-A2	1986-JP-MA-25	CMU	PG
		CW3-1-A3	1986-JP-MA-26	CMU	PG
		CW3-1-A4	1986-JP-MA-27	CMU	PG
		CW3-2	1986-JP-MA-28	CMU	PG
		CW3-2-A2	1986-JP-MA-29	CMU	PG
		CW3-2-A3	1986-JP-MA-30	CMU	PG
		CW3-3	1986-JP-MA-31	CMU	PG
		CW3-3-A2	1986-JP-MA-32	CMU	PG
		CW3-3-A3	1986-JP-MA-33	CMU	PG
		CW3-4-A2	1986-JP-MA-34	CMU	PG
		CW4-1-1	1986-JP-MA-35	CMU	PG
		CW4-1-2	1986-JP-MA-36	CMU	PG
		CWB3-1	1986-JP-MA-37	CMU	PG
		CWB3-1'-A2	1986-JP-MA-38	CMU	PG
24	Matsumura 1987 Shigenobu et al. 1987	WS9-2	1986-JP-SH-01	CMU	FG
		WSB21	1986-JP-SH-02	CMU	FG
		WSB22	1986-JP-SH-03	CMU	FG
		WFB2	1986-JP-SH-04	CMU	FG
		WSB3	1986-JP-SH-05	CMU	FG
		WSB4	1986-JP-SH-06	CMU	FG
	Okamoto et al. 1987 Kaminosono et al. 1988	WSN1	1987-JP-OK-01	CMU	FG
		WSN2	1987-JP-OK-02	CMU	FG
25	Okamoto et al. 1987	WSB1	1987-JP-OK-10	CMU	FG
		WSB10	1987-JP-OK-11	CMU	FG
	Igarashi et al. 1988	WSR2-2	1988-JP-IG-05	Clay	FG
		WSR4-2	1988-JP-IG-06	Clay	FG
		WSR5-2	1988-JP-IG-07	Clay	FG
		WSR6-2	1988-JP-IG-08	Clay	FG
		WFR5	1988-JP-IG-09	Clay	FG

Table 7.3: Summary of Data Groupings (Continued)

Group	Source	Specimen	Serial No.	Material	Grouting
26	Tomaževič and Lutman 1988	CN-0	1988-SL-TO-01	CMU	PG
		CN-14	1988-SL-TO-02	CMU	PG
		CN-28	1988-SL-TO-03	CMU	PG
		CN-50	1988-SL-TO-04	CMU	PG
		CV-0	1988-SL-TO-05	CMU	PG
		DN-0	1988-SL-TO-09	CMU	PG
		DN-14	1988-SL-TO-10	CMU	PG
		DN-28	1988-SL-TO-11	CMU	PG
		DN-50	1988-SL-TO-12	CMU	PG
		DV-0	1988-SL-TO-13	CMU	PG
27	Johal and Anderson 1988	CM1	1988-US-JO-01	Clay	PG
		CM2	1988-US-JO-02	Clay	PG
		CM3	1988-US-JO-03	Clay	PG
		CM4	1988-US-JO-04	Clay	PG
		CM5	1988-US-JO-05	Clay	PG
		CM6	1988-US-JO-06	Clay	PG
		CP1	1988-US-JO-07	Clay	PG
		CP2	1988-US-JO-08	Clay	PG
		CS1	1988-US-JO-09	Clay	PG
		CS2	1988-US-JO-10	Clay	PG
		CS3	1988-US-JO-11	Clay	PG
		CS4	1988-US-JO-12	Clay	PG
		CS5	1988-US-JO-13	Clay	PG
		CS6	1988-US-JO-14	Clay	PG
		CP3	1988-US-JO-15	Clay	PG
		CP4	1988-US-JO-16	Clay	PG
28	Johal and Anderson 1988	DM1	1988-US-JO-17	CMU	PG
		DM2	1988-US-JO-18	CMU	PG
		DM3	1988-US-JO-19	CMU	PG
		DM4	1988-US-JO-20	CMU	PG
		DM5	1988-US-JO-21	CMU	PG
		DM6	1988-US-JO-22	CMU	PG
		DP1	1988-US-JO-23	CMU	PG
		DP2	1988-US-JO-24	CMU	PG
		DS1	1988-US-JO-25	CMU	PG
		DS2	1988-US-JO-26	CMU	PG
		DS3	1988-US-JO-27	CMU	PG
		DS4	1988-US-JO-28	CMU	PG
		DS5	1988-US-JO-29	CMU	PG
		DS6	1988-US-JO-30	CMU	PG
		DP3	1988-US-JO-31	CMU	PG
		DP4	1988-US-JO-32	CMU	PG

Table 7.3: Summary of Data Groupings (Continued)

Group	Source	Specimen	Serial No.	Material	Grouting
29	Shing et al. 1988 Shing et al. 1989 Shing et al. 1990	Wall 3	1988-US-SH-03	CMU	FG
		Wall 4	1988-US-SH-04	CMU	FG
		Wall 5	1988-US-SH-05	CMU	FG
		Wall 6	1988-US-SH-06	CMU	FG
		Wall 7	1988-US-SH-07	CMU	FG
		Wall 8	1988-US-SH-08	CMU	FG
		Wall 9	1988-US-SH-09	CMU	FG
		Wall 10	1988-US-SH-10	CMU	FG
		Wall 11	1988-US-SH-11	CMU	FG
		Wall 13	1988-US-SH-13	CMU	FG
		Wall 14	1988-US-SH-14	CMU	FG
		Wall 15	1988-US-SH-15	CMU	FG
		Wall 16	1988-US-SH-16	CMU	FG
30	Yancey and Scribner 1989	R2	1989-US-YA-02	CMU	PG
		R4	1989-US-YA-03	CMU	PG
		R5	1989-US-YA-04	CMU	PG
		R6	1989-US-YA-05	CMU	PG
		R7	1989-US-YA-06	CMU	PG
		R9	1989-US-YA-08	CMU	PG
		R10	1989-US-YA-09	CMU	PG
		R11	1989-US-YA-10	CMU	PG
31	Shing et al. 1990	Wall 21	1990-US-SH-21	Clay	FG
		Wall 22	1990-US-SH-22	Clay	FG
32	Matsumura and Igarashi 1991	CW322A2	1991-JP-MA-01	CMU	FG
		CW325A2	1991-JP-MA-02	CMU	FG
		CW332A2	1991-JP-MA-03	CMU	FG
		CW525A2	1991-JP-MA-04	CMU	FG
		CW532A2	1991-JP-MA-05	CMU	FG
		CW538A2	1991-JP-MA-06	CMU	FG
33	Ghanem et al. 1992	SWA	1992-US-GH-01	CMU	PG
		SWB	1992-US-GH-02	CMU	PG
	Ghanem et al. 1993	SWA-2	1993-US-GH-05	CMU	PG
		SWA-3	1993-US-GH-06	CMU	PG
34	Brunner 1996 Brunner and Shing 1996	Wall 1	1994-US-BR-01	Clay	FG
		Wall 2	1994-US-BR-02	Clay	FG
		Wall 3	1994-US-BR-03	Clay	FG

Table 7.3: Summary of Data Groupings (Continued)

Group	Source	Specimen	Serial No.	Material	Grouting
35	Brammer 1995 Ingham et al. 2001	Wall 1	1995-NZ-BR-01	CMU	FG
		Wall 2	1995-NZ-BR-02	CMU	PG
		Wall 3	1995-NZ-BR-03	CMU	FG
		Wall 4	1995-NZ-BR-04	CMU	FG
		Wall 6	1995-NZ-BR-06	CMU	PG
		Wall 7	1995-NZ-BR-07	CMU	PG
		Wall 8	1995-NZ-BR-08	CMU	PG
		Wall 10	1995-NZ-BR-10	CMU	PG
		Wall 11	1995-NZ-BR-11	CMU	PG
		Wall 12	1995-NZ-BR-12	CMU	PG
36	Tomaževič et al. 1996	V2-BS	1996-SL-TO-06	CMU	PG
		V2-BD	1996-SL-TO-08	CMU	PG
		V2-CS	1996-SL-TO-10	CMU	PG
		V2-CD	1996-SL-TO-12	CMU	PG
		V2-DS	1996-SL-TO-14	CMU	PG
		V2-DD	1996-SL-TO-16	CMU	PG
37	Schultz 1996a	Wall 3	1996-US-SH-02	CMU	PG
	Schultz et al. 1998	Wall 2	1998-US-SH-01	CMU	PG
		Wall 4	1998-US-SH-02	CMU	PG
		Wall 6	1998-US-SH-03	CMU	PG
		Wall 8	1998-US-SH-04	CMU	PG
		Wall 10	1998-US-SH-05	CMU	PG
		Wall 12	1998-US-SH-06	CMU	PG
38	Ohta et al. 2000	CAW10-1	2000-JP-OH-01	CMU	FG
		CAW10-2	2000-JP-OH-02	CMU	FG
		CAW03-1	2000-JP-OH-03	CMU	FG
		CAW03-2	2000-JP-OH-04	CMU	FG
39	Haider 2007 Dhanasekar 2011	WSRM 1	2007-AU-HA-01	Clay	PG
		WSRM 2	2007-AU-HA-02	Clay	PG
		WSRM 3	2007-AU-HA-03	Clay	PG
		WSRM 4	2007-AU-HA-04	Clay	PG
		WSRM 5	2007-AU-HA-05	Clay	PG
		WSRM 6	2007-AU-HA-06	Clay	PG
		WSRM 7	2007-AU-HA-07	Clay	PG
		WSRM 8	2007-AU-HA-08	Clay	PG
		ECRM 9	2007-AU-HA-09	Clay	PG
40	Haider 2007 Dhanasekar 2011	11	2007-AU-HA-11	Clay	PG
		12	2007-AU-HA-12	Clay	PG
		13	2007-AU-HA-13	Clay	PG
		14	2007-AU-HA-14	Clay	PG

Table 7.3: Summary of Data Groupings (Continued)

Group	Source	Specimen	Serial No.	Material	Grouting
41	Voon and Ingham 2006 Voon 2007	A1	2007-NZ-VO-01	CMU	FG
		A2	2007-NZ-VO-02	CMU	FG
		A4	2007-NZ-VO-04	CMU	FG
		A5	2007-NZ-VO-05	CMU	PG
		A6	2007-NZ-VO-06	CMU	PG
		A7	2007-NZ-VO-07	CMU	FG
		A8	2007-NZ-VO-08	CMU	FG
		A9	2007-NZ-VO-09	CMU	FG
		A10	2007-NZ-VO-10	CMU	FG
42	Haach et al. 2007 Haach et al. 2010a	N60-B1	2007-PO-HA-02	CMU	PG
		N60-B2	2007-PO-HA-03	CMU	PG
		N150-B1	2007-PO-HA-04	CMU	PG
		N150-B2	2007-PO-HA-05	CMU	PG
43	Maleki 2008	Wall 1	2008-CA-MA-01	CMU	PG
		Wall 2	2008-CA-MA-02	CMU	PG
		Wall 4	2008-CA-MA-04	CMU	PG
		Wall 5	2008-CA-MA-05	CMU	PG
44	Minaie 2009	PCL 1	2009-US-MI-01	CMU	PG
		MC 1	2009-US-MI-02	CMU	PG
		PCL 2	2009-US-MI-03	CMU	PG
		MC 2	2009-US-MI-04	CMU	PG
45	Minaie 2009	FPCL 2	2009-US-MI-07	Clay	FG
		FMC 2	2009-US-MI-08	Clay	FG
46	Elmapruk 2010	PG127-48	2010-US-EL-01	CMU	PG
		PG127-48i	2010-US-EL-02	CMU	PG
		PG180-48	2010-US-EL-03	CMU	PG
		PG254-48	2010-US-EL-04	CMU	PG
		PG127-32	2010-US-EL-05	CMU	PG
		PG127-24	2010-US-EL-06	CMU	PG
47	Nolph 2010	PG085-48	2010-US-NO-01	CMU	PG
		PG120-48	2010-US-NO-02	CMU	PG
		PG169-48	2010-US-NO-03	CMU	PG
		PG085-32	2010-US-NO-04	CMU	PG
		PG085-24	2010-US-NO-05	CMU	PG
		FG085-00	2010-US-NO-06	CMU	FG

Flexural Reinforcement

The distributions of the flexural reinforcement ratios ρ_f are shown in Figures 7.1 and 7.2. All but thirteen specimens between two grouting types contained flexural reinforcement in the end cells. Those specimens with little or no flexural reinforcement relied on high axial load, low shear span ratio, or a combination of both to prevent failure in the flexural mode. The distribution of flexural reinforcement ratios is a little more evenly distributed for the partially grouted walls. Since flexural reinforcement ratio is based on gross masonry area, the ratio of steel to masonry for the partially grouted walls is higher than what is shown by the ratio. Overall, the fully- and partially-grouted walls both have fairly similar distributions of flexural reinforcement ratios.

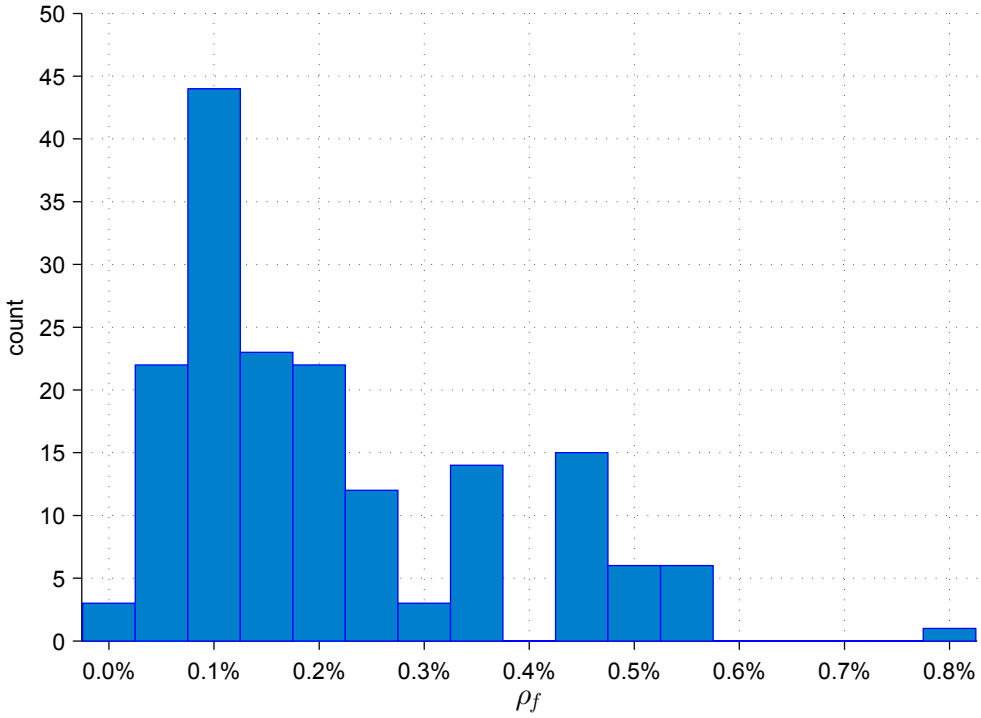

Figure 7.1: Distribution of flexural reinforcement in fully-grouted specimens

Confinement Reinforcement

The distribution of the confinement reinforcement ratios ρ_c are shown in Figures 7.3 and 7.4. The confinement reinforcement ratios are much more evenly distributed for the fully-grouted

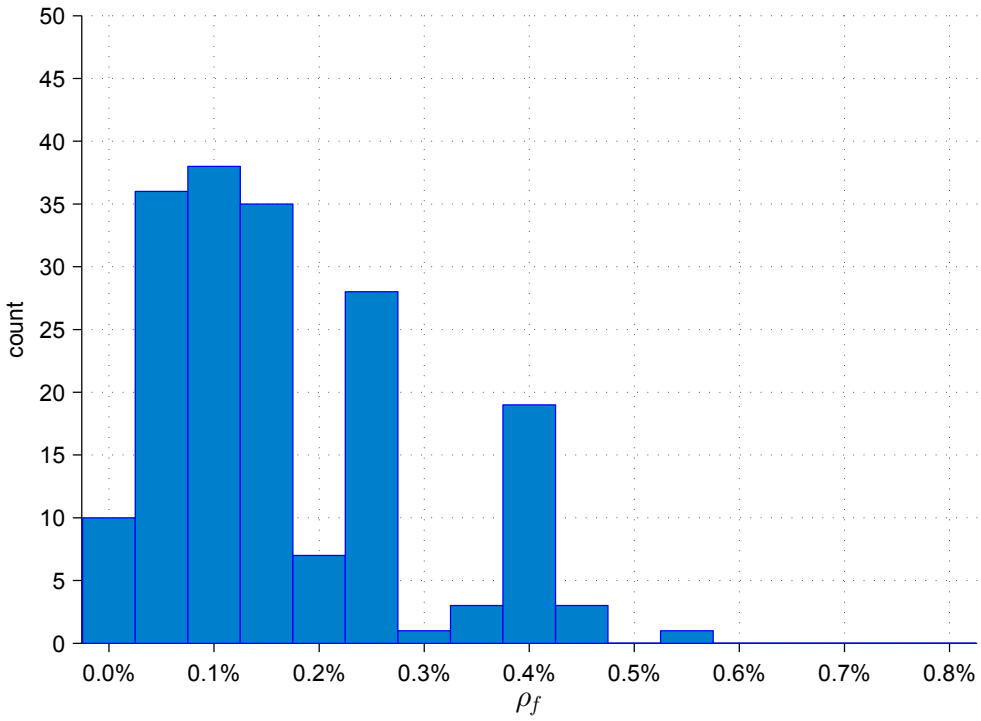

Figure 7.2: Distribution of flexural reinforcement in partially-grouted specimens

specimens than for the partially-grouted specimens. The partially-grouted specimens with no confinement reinforcement was considerably higher than those for fully-grouted specimens. This suggests that more research is needed in the area of partially-grouted walls with higher amounts of confinement reinforcement.

7.3.2 Shear Reinforcement

Shear reinforcement is placed horizontally in masonry shear walls to transfer shear forces across shear cracks and to control crack propagation. Horizontal reinforcement can be placed along the center line of the wall in grouted bond beams or can be placed near the faces of the wall within the mortared joints. The principal limitation of joint reinforcement is the size of the wires that can be placed within the masonry joints. There is inconsistency in the literature (Sveinsson et al., 1985; Yancey and Scribner, 1989; Schultz et al., 1998) concerning the contribution of joint reinforcement to ultimate shear strength, especially compared with the contribution of the bond

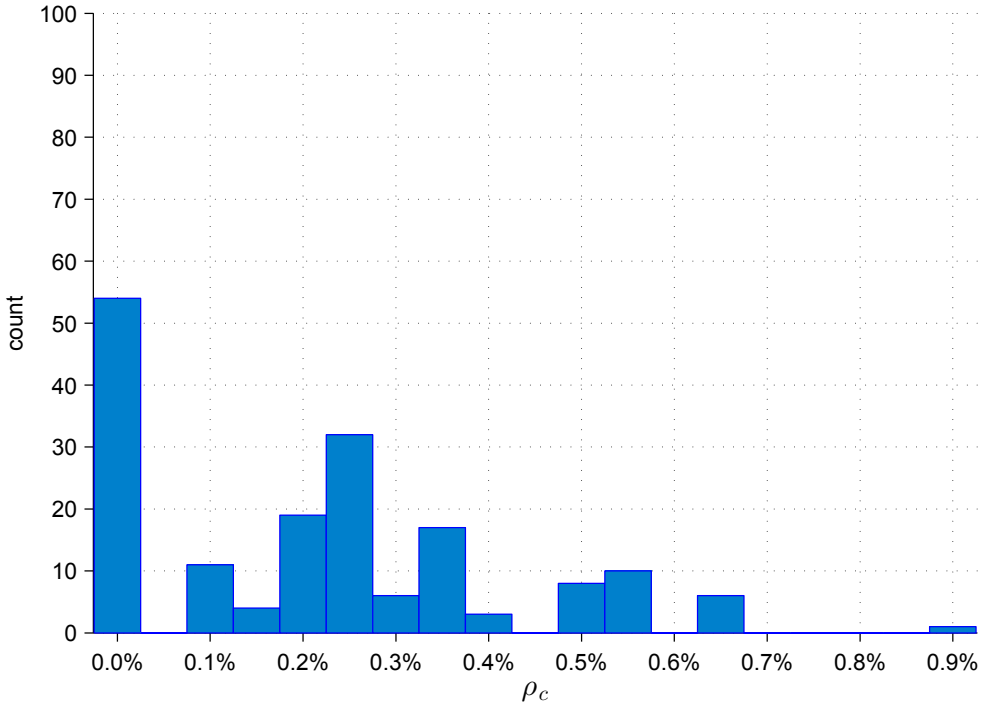

Figure 7.3: Distribution of confinement reinforcement in fully-grouted specimens

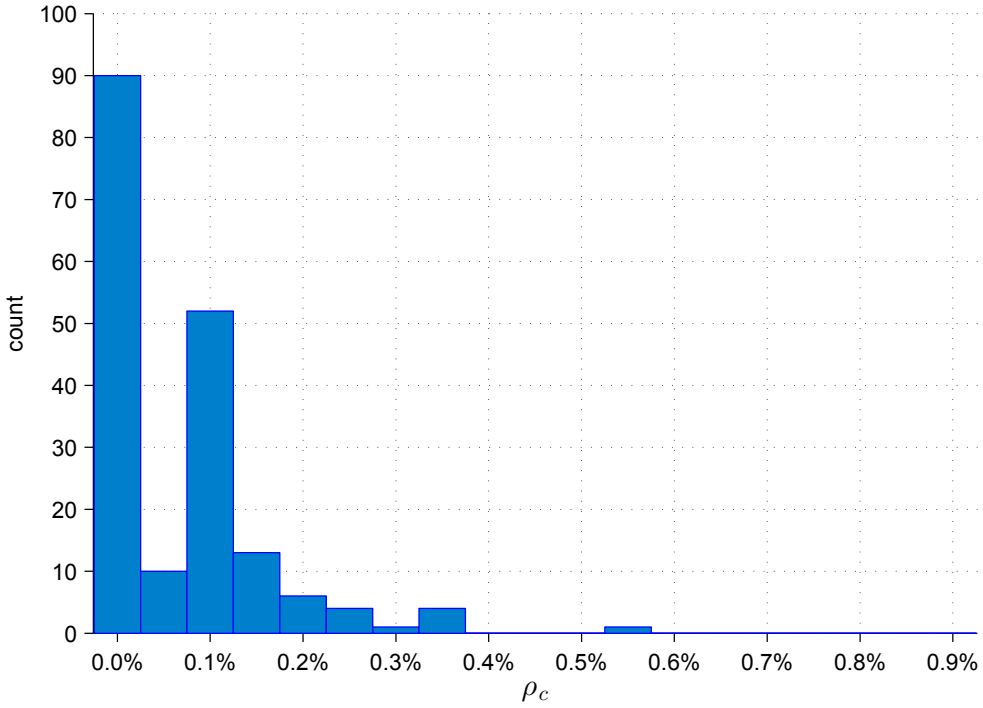

Figure 7.4: Distribution of confinement reinforcement in partially-grouted specimens

beam reinforcement. Since this question has yet to be settled, the two horizontal reinforcement types were investigated individually and combined.

Bond Beam Reinforcement

The distribution of the bond beam reinforcement ratios ρ_h are shown in Figures 7.5 and 7.6. The fully-grouted specimens showed a more uniform distribution of bond beam reinforcement ratios than did the partially-grouted specimens. The majority (62%) of all partially grouted specimens contained no bond beam. A likely reason for this is due to the added complexity in constructing a grouted bond beam in partially-grouted walls which must be cast without allowing the grout to flow into the empty cells below it. More research is needed to investigate the behavior of partially-grouted shear walls with bond beams.

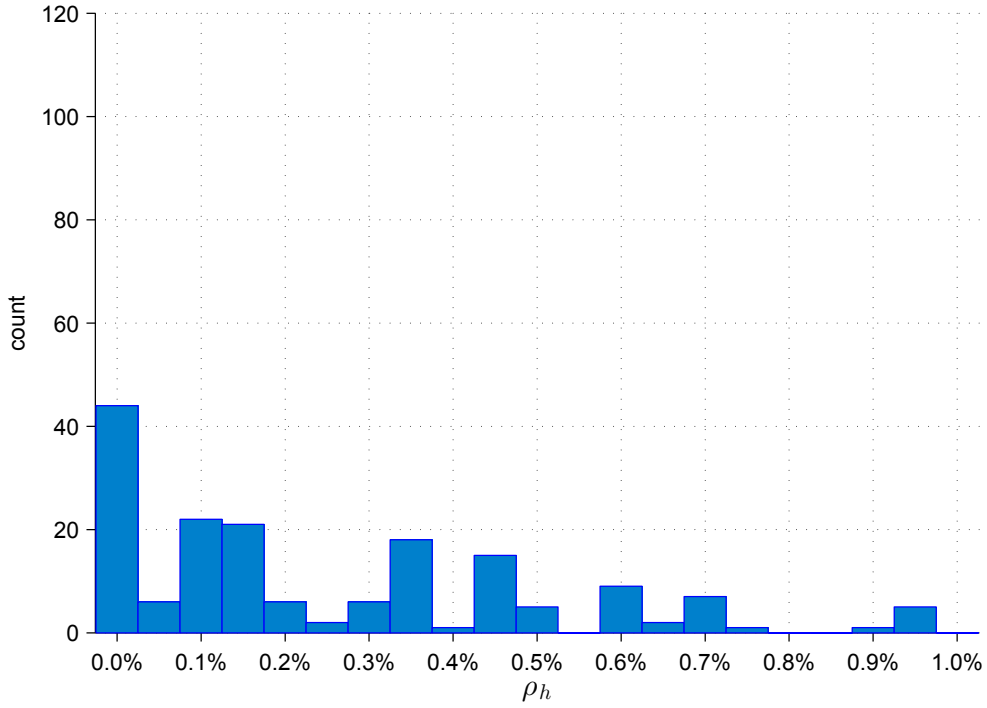

Figure 7.5: Distribution of bond beam reinforcement in fully-grouted specimens

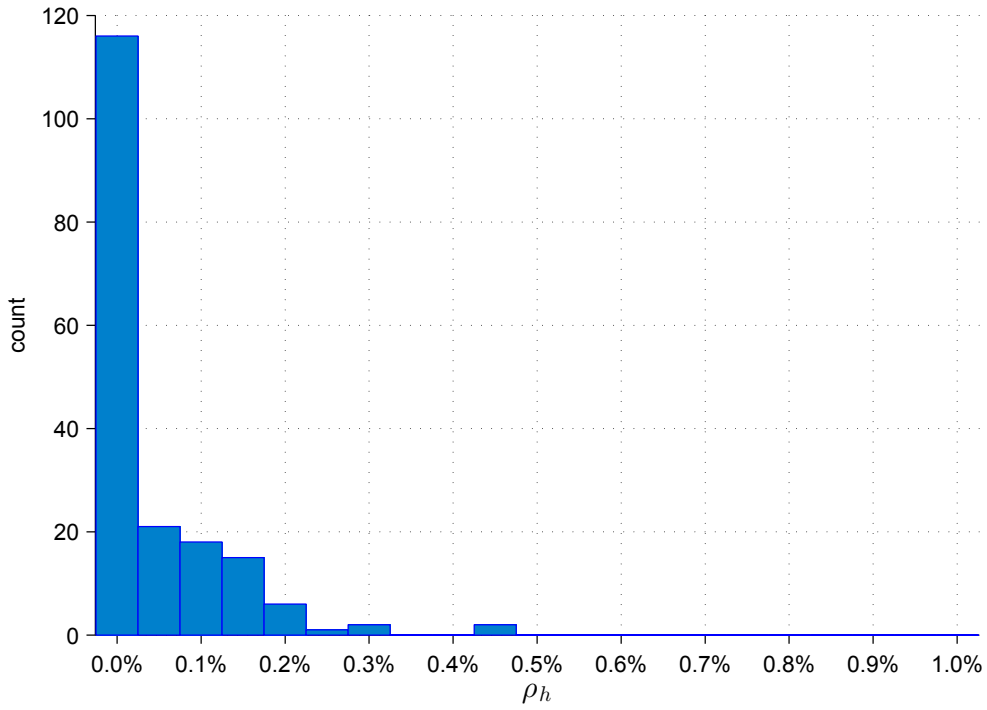

Figure 7.6: Distribution of bond beam reinforcement in partially-grouted specimens

Joint Reinforcement

The distribution of the joint reinforcement ratios ρ_j are shown in Figures 7.7 and 7.8. It is clear that there is a serious lack of research data available for masonry shear walls reinforced with joint reinforcement, particularly for fully-grouted walls. In total there were only 38 specimen (11%) which contained joint reinforcement. It is likely, due to the small number of specimens, that the analysis will not be able to find a statistically significant factor that explains the contribution of joint reinforcement. This is an area that requires additional testing.

All Horizontal Reinforcement

Since the number of specimens which included joint reinforcement was small, it may not be possible to study the effects of the two types of horizontal reinforcement separately and the combined values of both types of reinforcement may need to be used. The distribution of the combined horizontal reinforcement ratios ρ_v are shown in Figures 7.9 and 7.10. The distribution of horizontal reinforcement ratios are well dispersed for the fully-grouted specimens. The distribution

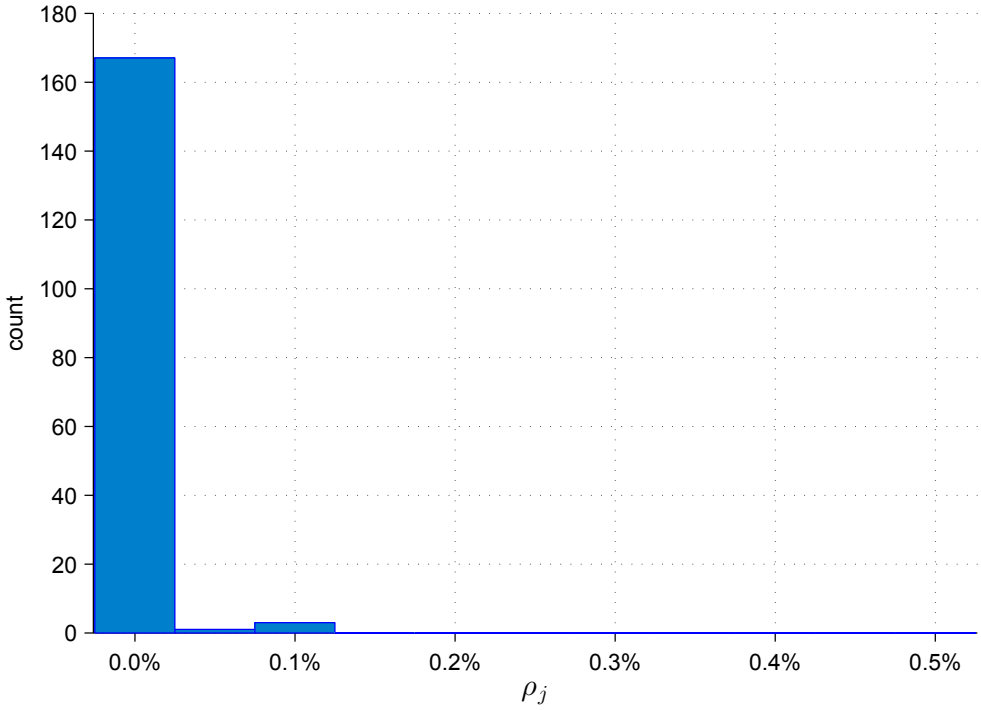

Figure 7.7: Distribution of joint reinforcement in fully-grouted specimens

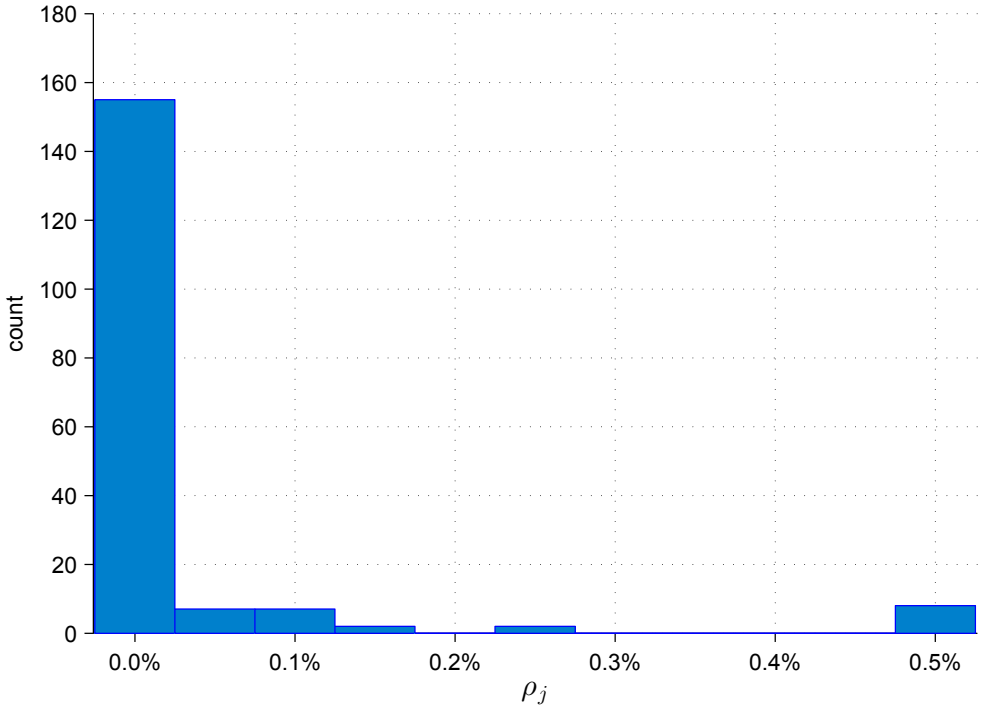

Figure 7.8: Distribution of joint reinforcement in partially-grouted specimens

of ratios for the partially-grouted specimens is improved over that shown in Figure 7.6 where the number of specimens without horizontal reinforcement has dropped from 116 (62%) specimens to 92 (49%) specimens. Since the horizontal reinforcement ratio is based on gross masonry area, the true ratios of steel to masonry area are proportionally higher than those shown.

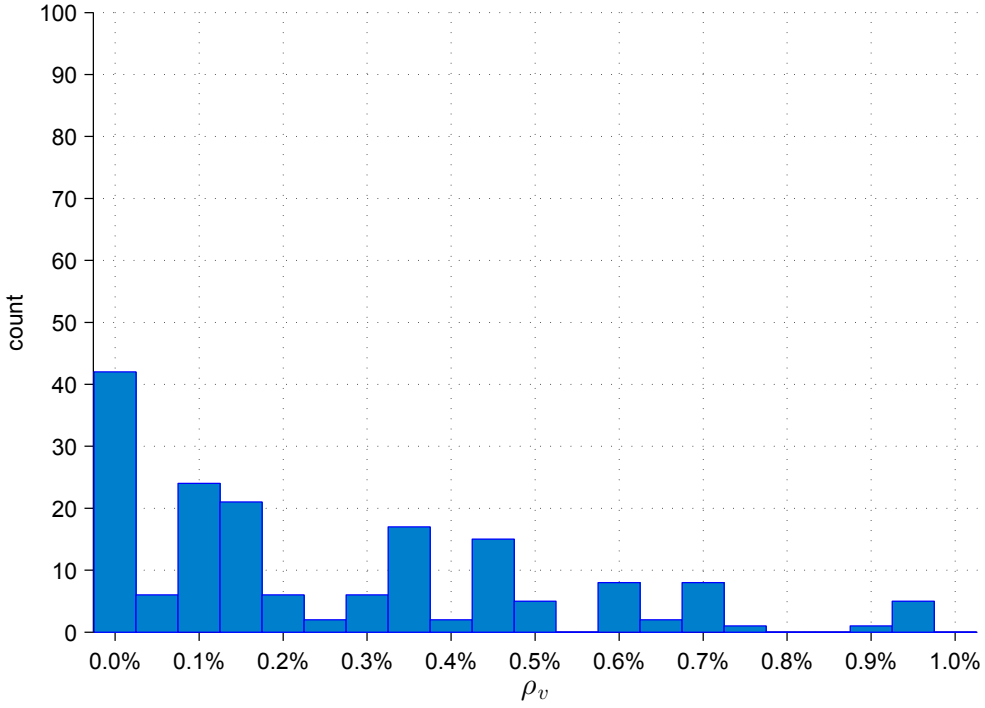

Figure 7.9: Distribution of horizontal reinforcement in fully-grouted specimens

7.3.3 Axial Load

The distributions of applied axial load stresses σ_0 are shown in Figures 7.11 and 7.12. These values for axial stress were computed using the net shear areas of the specimens. There is a higher proportion of fully-grouted specimens which included axial loading than partially-grouted specimens.

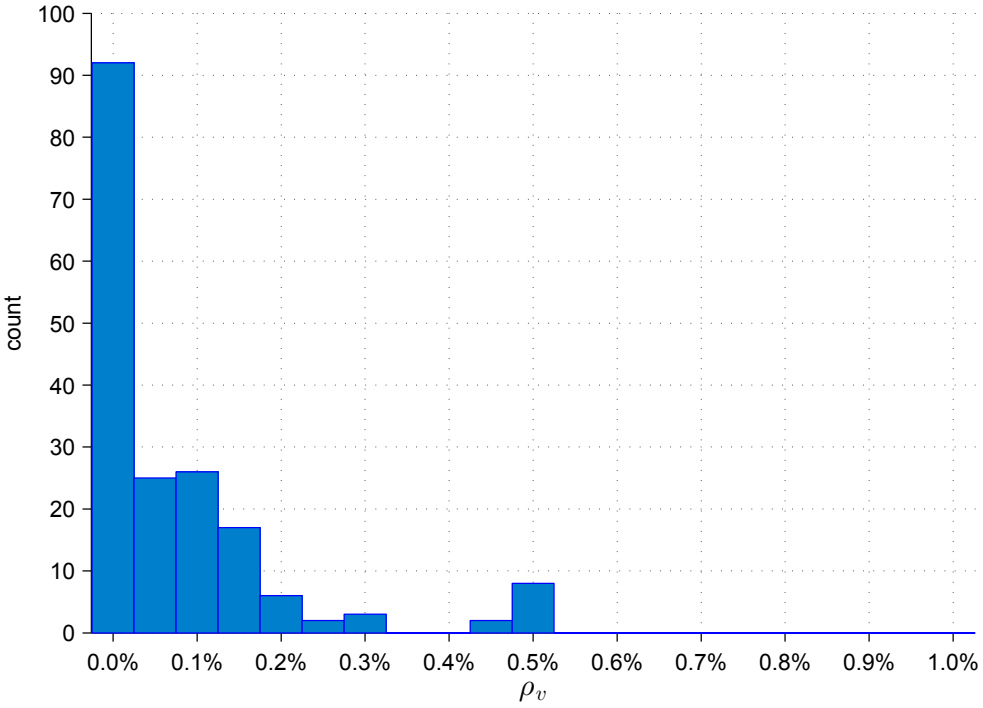

Figure 7.10: Distribution of horizontal reinforcement in partially-grouted specimens

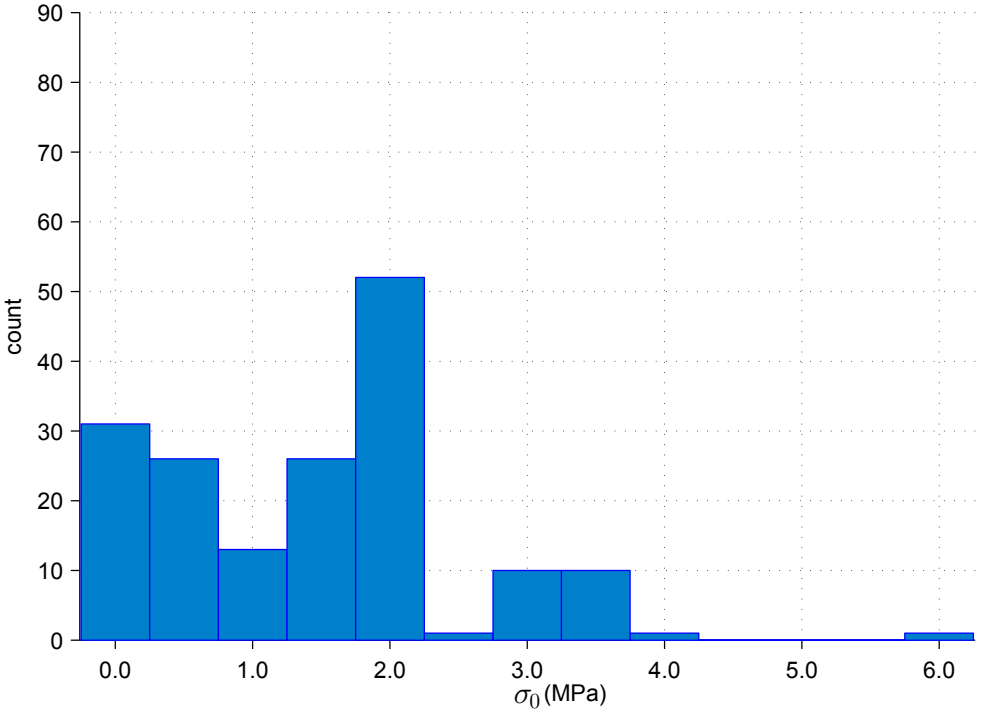

Figure 7.11: Distribution of applied axial loads on fully-grouted specimens

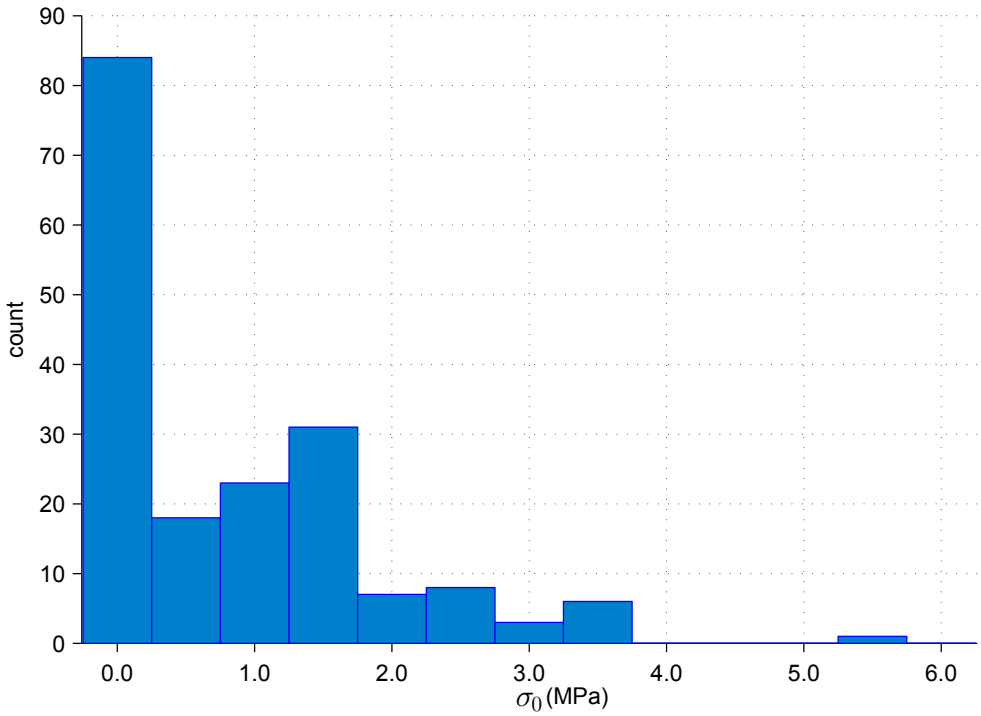

Figure 7.12: Distribution of applied axial loads on partially-grouted specimens

7.3.4 Masonry Strength

The distributions of masonry characteristic strengths f'_m are shown in Figures 7.13 and 7.14. These values were computed from grouted and ungrouted prism tests, respectively. The grouted prism strengths are less dispersed than the ungrouted strengths, likely due to stabilizing effect of grouting on the prism strength.

7.3.5 Geometric Properties

Aspect Ratio

The distributions of specimen aspect ratios are given in Figures 7.15 and 7.16. The overall distributions for the two types of grouting were fairly similar.

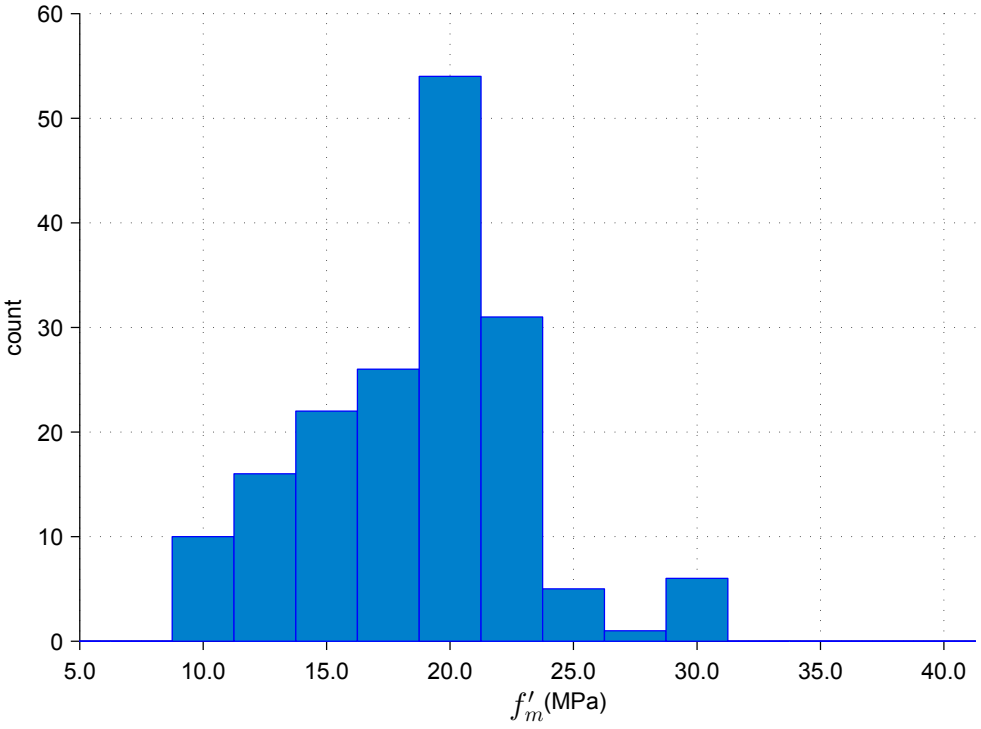

Figure 7.13: Distribution of masonry strengths for fully-grouted specimens

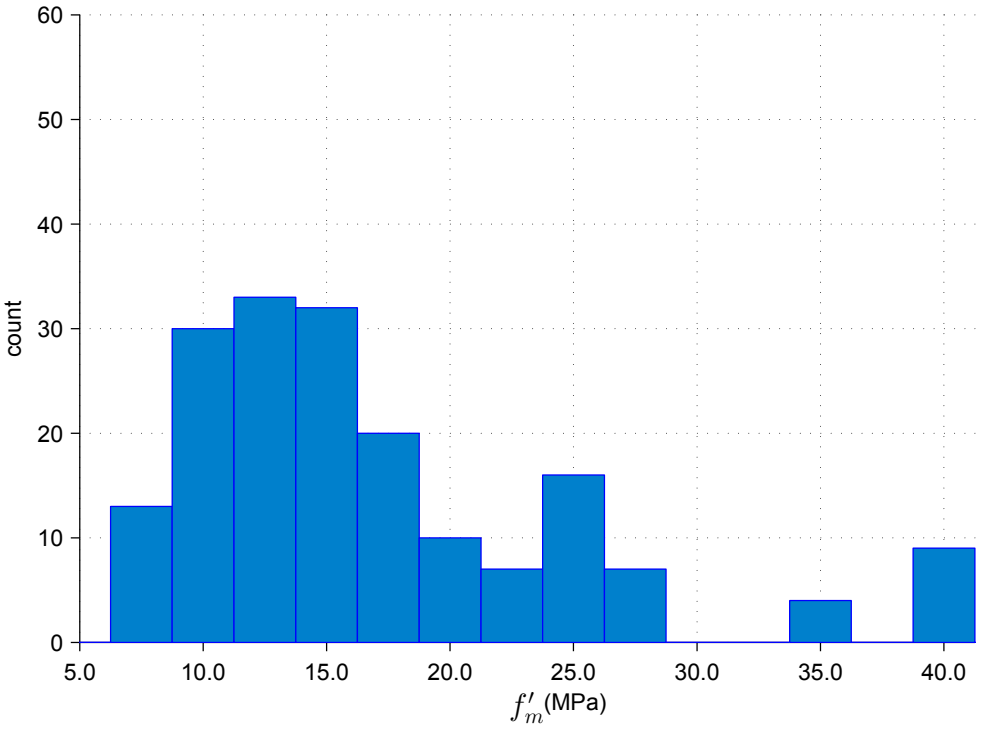

Figure 7.14: Distribution of masonry strengths for partially-grouted specimens

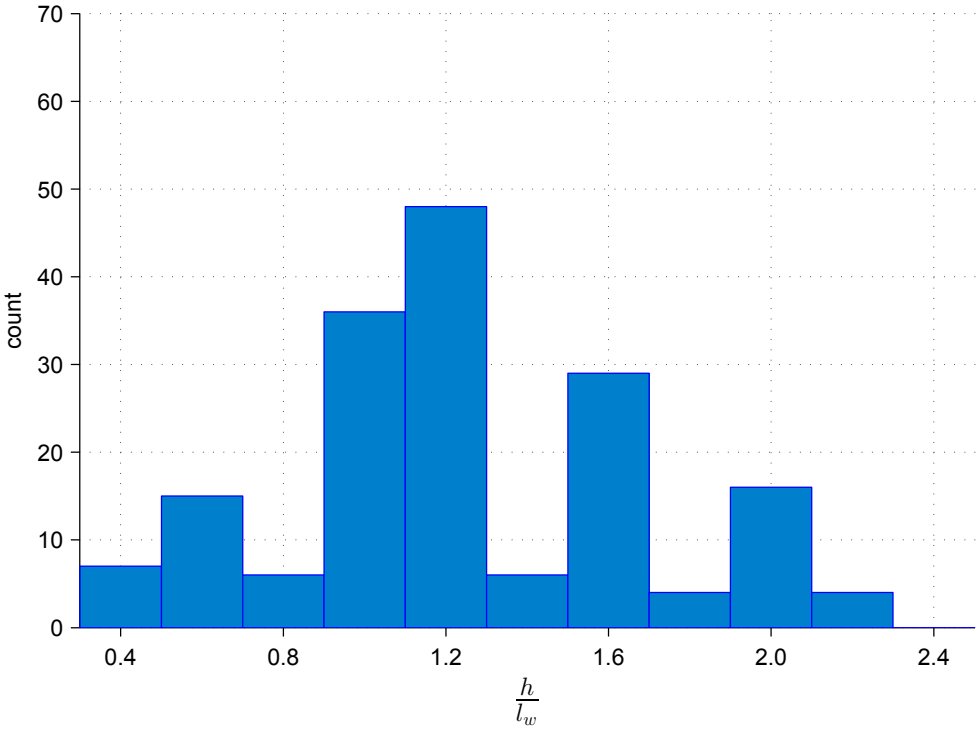

Figure 7.15: Distribution of aspect ratios for fully-grouted specimens

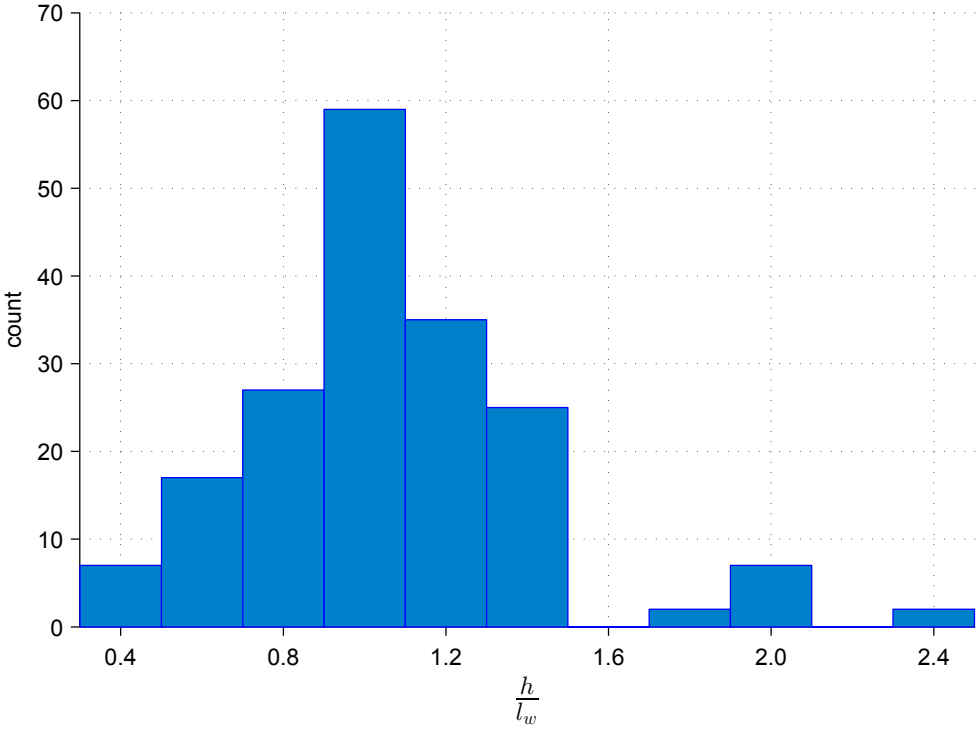

Figure 7.16: Distribution of aspect ratios for partially-grouted specimens

Spear Span Ratio

The distributions of specimen shear span ratios are given in Figures 7.17 and 7.18. The overall distributions for the two types of grouting were fairly similar. The majority of the shear span ratios are equal to or less than unity because that is typically the range in which shear walls fail in the shear mode. Figure 7.18 shows that there were three specimens with unusually high shear span ratios failing in shear. These specimens had sufficient flexural reinforcement and axial loading to prevent flexural failure.

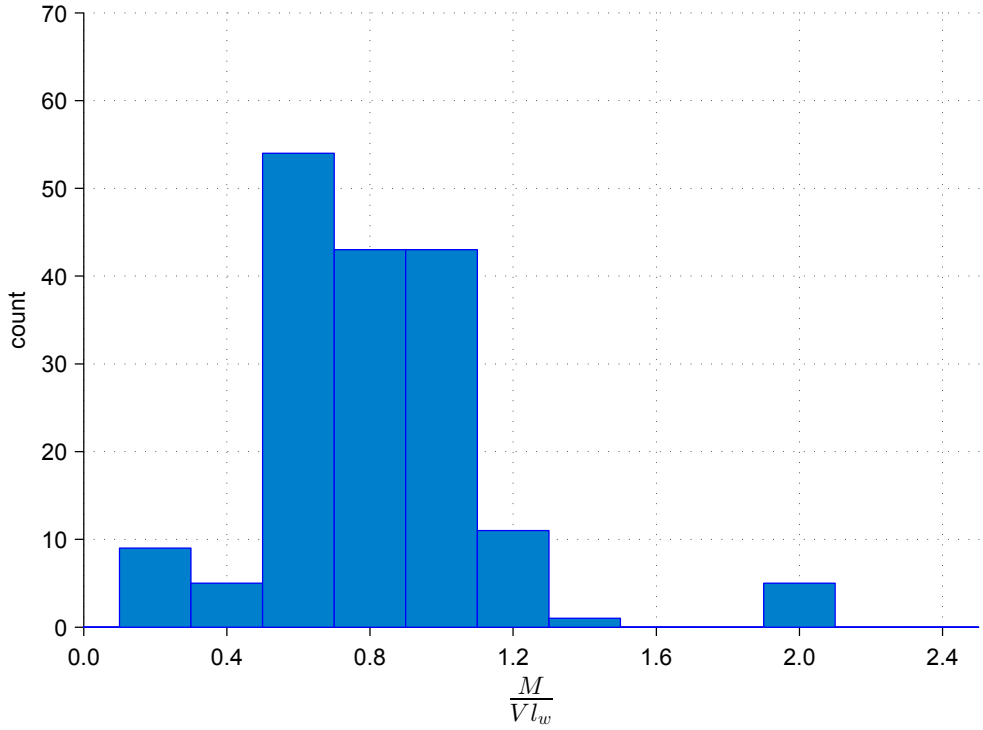

Figure 7.17: Distribution of shear span ratios for fully-grouted specimens

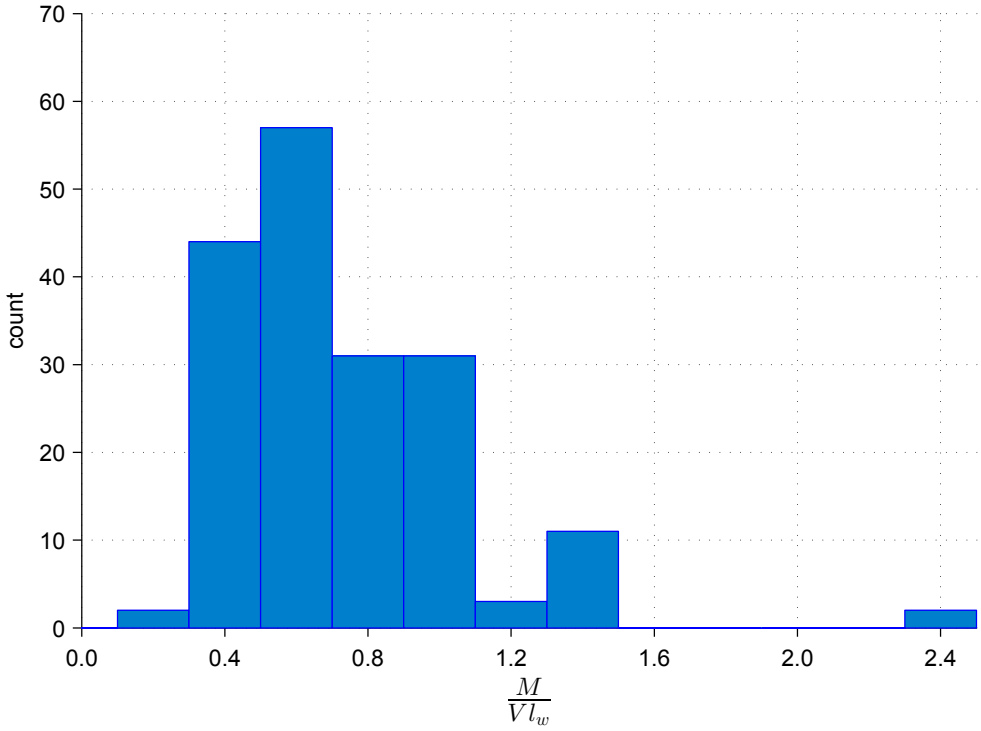

Figure 7.18: Distribution of shear span ratios for partially-grouted specimens

Part III

MSJC Shear Factor Modification

This part details the first analysis approach developed in this study. Chapter 8 presents a literature review of previous studies which analyzed and suggested improvements to existing shear equations. Chapter 9 outlines the methodology for analyzing the MSJC (2013) equation developed from the analysis techniques used by previous researchers. Chapter 10 details the results of the analysis and Chapter 11 provides a discussion of the modified MSJC shear equation.

This analysis was the first to validate the current MJSC grouted wall factor approach to account for the unconservative nature of the code equation. It was performed using the largest dataset of fully- and partially-grouted shear walls yet assembled for analysis. The analysis observed that there is a difference in both the mean and coefficients of variation between fully- and partially-grouted data. It was determined that the current grouted wall factor values in used in the MSJC code can be retained only if the resistance factor is lowered for partially-grouted data from 0.80 to 0.75.

CHAPTER 8. LITERATURE REVIEW: MODEL PERFORMANCE EVALUATION

8.1 Introduction

The purpose of this section is to validate or revise the grouted wall factor method currently in use in the MSJC (2013) code and represented by Figure 8.1. This will be done by determining and comparing the means and variances for both partially-grouted and fully-grouted walls. Probabilistic analysis will used to find the design factors to use such that the probabilities of failure for both grouting types are the same. The design factors that will be investigated in this analysis are the grouted wall factor γ_g and the shear resistance factor ϕ_v.

A probabilistic analysis is the most appropriate approach for determining the unconservative nature of the MSJC (2013) shear equation in the case of partially-grouted walls. For the analysis to be definitive, the sample must be representative of a large array of the different design combinations possible in actual construction. The number of walls necessary to effectively represent the functional range of each design parameter is outside the scope of any single research study. By amalgamating the existing data together into a single analysis, the scope of the analysis can be sufficiently large to represent the global population of masonry shear walls. The process of combining and analyzing data from many research studies is called meta-analysis.

8.2 Background

The most recent MSJC (2013) nominal shear strength equation is given by

$$\gamma_g V_n = \gamma_g \left[\left[4.0 - 1.75 \frac{M_u}{V_u l_w} \right] A_{nv} \sqrt{f'_m} + 0.25 P_u + 0.5 \frac{A_v}{s} f_{yv} l_w \right] \tag{8.1}$$

where $\frac{M_u}{V_u l_w}$ need not be greater than one. The nominal shear strength V_n is subject to the constraints

$$\gamma_g V_n \leq \begin{cases} 6\gamma_g A_{nv}\sqrt{f'_m} & \frac{M_u}{V_u l_w} \leq 0.25 \quad \text{for} \\ 4\gamma_g A_{nv}\sqrt{f'_m} & \frac{M_u}{V_u l_w} \geq 1.0 \quad \text{for} \end{cases} \tag{8.2}$$

for which the code permits designers to linearly interpolate for intermediate values of $\frac{M_u}{V_u l_w}$. The nominal shear strength is reduced by the resistance (or shear strength reduction) factor ϕ_v of 0.8.

The current grouting factor method assumes that the variances for fully- and partially-grouted walls are the same and that only the means differ, as idealized in Figure 8.1. The assumption that the distributions for fully- and partially-grouted wall are similar is denoted by the common shear resistance factor ϕ_v shared between the two types of grouting. The means of the two distributions are offset by the grouted wall factor γ_g, as shown in Figure 8.1. It is unknown whether the assumption of similar variances for both types of grouting is valid because a large-scale statistical analysis of both groups has yet to be performed.

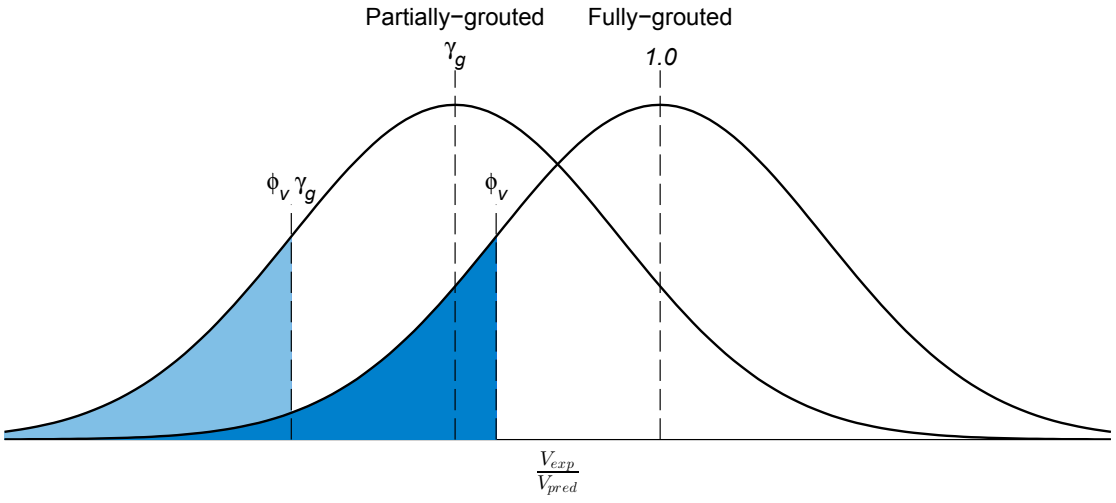

Figure 8.1: Distribution assumptions of current method

8.3 Previous Model Performance Evaluations

8.3.1 Ellingwood, Galambos, MacGregor, and Cornell

Ellingwood et al. (1980) conducted a statistical review of the loads and load combinations that are experienced by engineered structures over the course of their lifetime. The objective of their study was to develop load factors and combinations for to be used for structures of all material types incorporating the new LRFD methodology. Their recommendations were incorporated into the 1980 revision of the ANSI Standard A58.1 Standard. Stewardship of the specifications in the ANSI Standard A58.1 Standards was later shifted to ASCE 7 and they are currently published in ASCE-7 (ASCE 7, 2010).

As part of their research, they provided a methodology for the selection of resistance factors consistent with the load criteria developed in their research. This latter objective was performed by analyzing the ratios of experimental to predicted strengths for a large number of material specification groups. The ratio of experimental to predicted strength was used because civil engineering elements typically demonstrate a constant coefficient of variance, meaning that the variance increases with increasing element strength. Material specification groups were designated by both material type (steel, concrete, masonry, etc.), function (flexure, column, shear wall, etc.), characteristics (slender, inclusion of stirrups, stiffened flanges, presence of bracing, etc.), and limit state. While the principal scope of their material analyses was broad rather than deep, they included sufficient quantities of specimens in each material specification group to develop representative parameters for the development of their load factors.

Appendix D of Ellingwood et al. (1980) details their analysis of the masonry data and includes separate groupings for clay brick and concrete masonry elements. The distinction between masonry materials was necessary because the masonry design standards at that time were published separately for clay brick and concrete block. The standards for brick used in the analysis were published by BIA (1969) and those for concrete block were published by NCMA (1977). The member types analyzed were limited to walls subjected to various combinations of flexural and axial stresses. Their analysis resulted in the mean and coefficient of variation for the ratio of experimental to predicted strengths for each material specification group, as shown in Tables 8.1 and 8.2. The mean ratios of experimental to predicted strengths for masonry elements were typi-

cally in the range of 5.0 to 7.0, significantly higher than the typical range of 0.98 to 1.05 for most other material types. The coefficients of variation for the groups typically ranged from about 0.10 to about 0.20, which were only slightly larger than those for other structural materials. Though their analyses did not include masonry shear walls, their results showed the highly conservative nature of the primitive masonry strength prediction equations then employed.

Table 8.1: Brick Masonry in Compression Plus Bending (Adapted from Ellingwood et al. 1980)

Source	Description of Wall	n	$\bar{F}/F_n^*$	COV
BIA (1969)	$h/t = 20.5,\ e_2/t = 1/3,\ e_1/e_2 = -1$	12	4.94	0.073
	$h/t = 23,\ e_2/t = 0,\ e_1/e_2 = 0$	12	6.93	0.10
	$h/t = 23,\ e_2/t = 1/6,\ e_1/e_2 = 0$	12	46.96	0.12
	$h/t \leq 7,\ e_2/t = 1/6,\ e_1/e_2 = 1$	9	6.21	0.10
	$h/t \leq 7,\ e_2/t = 1/3,\ e_1/e_2 = 1$	9	5.87	0.14
	$h/t = 22,\ e_2/t = 1/6,\ e_1/e_2 = -1/2$	6	6.92	0.15
	$h/t = 10,\ e_2/t = 1/3,\ e_1/e_2 = -1$	10	4.60	0.11
	$h/t = 21,\ e_2/t = 1/3,\ e_1/e_2 = -1$	16	6.27	0.10
	$h/t = 23,\ e_2/t = 1/3,\ e_1/e_2 = -1$	15	6.02	0.16
	Flexure only, Single wythe, Type S, Inspected	15	3.89	0.26
Monk (1969)	$h/t = 20,\ e/t = 0$	15	9.88	0.12
	$h/t = 20,\ e/t = 1/6$	14	> 9	0.13
	Flexure only, Single wythe, Type S, Inspected	29	3.64	0.20
	Flexure only, Multi-wythe, Type S, Inspected	21	4.26	0.18
	Flexure only, Multi-wythe, Uninspected	6	6.25	0.25
Yokel et al. (1971)	2 ft × 8 ft-4 in brick — Pure compression	2	5.87	—
	2 ft × 8 ft-4 in brick — Pure compression	2	7.54	—
	2 ft × 8 ft-4 in brick — Pure compression	2	8.00	—
	2 ft × 8 ft-4 in brick — Pure compression	2	6.58	—
Fattal and Cattaneo (1976)	23” × 96” × 4”—Fixed ends	2	7.00	—
Simms (1965)	Story height, Pure compression	47	7.34	0.15
Astbury and West (1969)	Story height, Axial load, Type M, 9” wall	37	3.18	0.11
	Story height, Axial load, Type M	15	6.23	0.17
	Story height, Axial load, Type N	15	6.58	0.19
	Story height, $e/t = 1/8$, Type M	15	4.34	0.18
	Story height, $e/t = 1/8$, Type N	15	4.24	0.19
Curtin and Hendry (1969)	Story height, axial load, Type N	14	8.17	0.22

Table 8.2: Concrete Masonry in Compression Plus Bending (Adapted from Ellingwood et al. 1980)

Source	Description of Wall	n	$\bar{F}/F_n^*$	COV
Yokel et al. (1970)	8 in Unreinforced, Story height	12	4.28	0.17
	6 in Reinforced, Story height	9	5.62	0.13
Fattal and Cattaneo (1976)	6 in Unreinforced, h/t = 17	10	6.05	0.10
Fattal and Cattaneo (1977)	8 in Hollow block	2	4.50	—
	8 in Solid block	1	4.28	—
	4 in Block-block cavity	2	3.85	—
	8 in Hollow block	2	4.81	—
	8 in Hollow block	2	3.48	—
Hedstrom (1961)	8 in Block, 4 ft × 8 ft walls	7	6.4	—
Read and Clements (1972)	200 mm Hollow block, Story height, Type M	9	4.54	0.15
	100 mm Solid block, Story height, Type M	6	—	0.20
	100 mm Hollow block, Story height, Type M	9	—	0.15
	All data — f'_m assumed as 3000 psi	38	4.25	0.17

8.3.2 Davis

Davis (2008) performed a comparative analysis of masonry shear strength equations from several design standards from around the world. The dataset included 55 specimens collected from tests conducted by Shing et al. (1990); Matsumura (1987); Sveinsson et al. (1985); Voon and Ingham (2006). the analysis was limited to fully-grouted, reinforced masonry shear walls failing in shear. Davis found that the mean ratio of experimental to predicted strengths for the MSJC code equation was 1.16 with a coefficient of variation of 0.15. The study involved the performance of the shear equations considering six variables: masonry prisms strength f'_m, horizontal reinforcement contribution $\rho_h f_{yh}$, axial load σ_0, vertical reinforcement contribution $\rho_v f_y$, ductility factor μ, and shear span ratio h_e/l_w. The conclusion that the MSJC equation was the best predictor for four of the six variables studied and provided the best results overall.

8.3.3 Minaie

Minaie (2009) tested eight concrete masonry shear walls and compared the experimental strengths to the strengths predicted using the 2008 edition of the MSJC code. The tests contained both fully- and partially-grouted specimens. Minaie found that the MSJC shear equation was

highly unconservative for partially-grouted shear walls but appeared to be reasonable for fully-grouted walls. He concluded that the unconservative nature of the MSJC equation was due to it being developed exclusively from fully-grouted shear wall tests.

To further validate his findings, Minaie compared his and previous experimental results with several code shear strength equations. Minaie studied the results from 60 partially-grouted shear wall tests in addition to the four he tested in his own research. The specimens included in the analysis were collected from Ghanem et al. (1992, 1993), Schultz (1996a), Voon and Ingham (2006), Matsumura (1987, 1988), Chen et al. (1978), and Hidalgo et al. (1978). The partially-grouted wall data were organized into nine subsets and the mean and coefficient of variation were determined for the ratios of experimental to predicted strength of the specimens within each subset. The statistics calculated by Minaie for each partially-grouted subset are shown in Table 8.3. The analysis showed that the MSJC shear equation was unconservative for partially-grouted masonry shear walls. Minaie proposed four modifications to the MSJC shear equation: 1) to multiply the shear area by A_n/A_g, 2) define the net area as the face shell area, 3) limit l_w to the height of the wall, and 4) use the unreinforced masonry shear equation. Minaie concluded that the first option appeared to be the best modification to the code shear equation for partially-grouted walls.

Table 8.3: MSJC Equation Performance for Partially-Grouted Walls
(Adapted from Minaie 2009)

Subset	n	$\bar{V}/V_n^*$	COV
Minaie (2009)	4	0.44	0.10
Ghanem et al. (1992)	2	0.93	0.06
Ghanem et al. (1993)	2	0.89	0.08
Schultz (1996a)	6	0.64	0.05
Voon and Ingham (2006)	2	0.86	0.14
Matsumura (1987)	29	0.89	0.21
Matsumura (1988)	10	1.11	0.31
Chen et al. (1978)	6	1.14	0.10
Hidalgo et al. (1978)	3	0.93	0.13
Total	64	0.90	0.26

Minaie also studied the results from 43 fully-grouted shear wall specimens collected from Chen et al. (1978), Hidalgo et al. (1978, 1979), Sveinsson et al. (1985), Matsumura (1987, 1988), Okamoto et al. (1987), Shing et al. (1990), Brunner and Shing (1996), and Voon and Ingham (2006). The fully-grouted walls were organized into five subsets based on the institution where the data were produced. The mean and coefficient of variation were determined for the ratios of experimental to predicted strength of the specimens within each subset. The statistics calculated by Minaie for each fully-grouted subset are shown in Table 8.4. Minaie observed that the MSJC equation is conservative for fully-grouted masonry shear walls but that this conservatism decreased with increasing specimen size.

Table 8.4: MSJC Equation Performance for Fully-Grouted Walls
(Adapted from Minaie 2009)

Subset	n	$\bar{V}/V_n^*$	COV
Shing et al. (1990)	9	1.29	0.11
Voon and Ingham (2006)	6	1.00	0.11
Sveinsson et al. (1985) Chen et al. (1978) Hidalgo et al. (1978, 1979)	10	1.26	0.23
Matsumura (1987, 1988) Okamoto et al. (1987)	15	1.34	0.19
Brunner and Shing (1996)	3	1.59	0.16
Total	43	1.31	0.21

CHAPTER 9. METHODOLOGY: MSJC MODEL ANALYSIS

9.1 Introduction

The purpose of this analysis is to validate or revise the grouted wall factor method currently in use in the MSJC (2013) code. Before validation could be performed the mean and variance of the ratio of the experimental strengths to predicted strengths needed to be computed. The mean value is a measure of the accuracy of the predicted strengths compared to the experimental strength where a value of unity represents a situation where the predicted values correspond well (on average) with the experimental strengths. Values greater than unity represent a conservative case where the experimental values are higher (on average) than the predicted strength and values less than unity denote that the equation is unconservative. In the case of the MSJC shear equation the mean strength is represented by the grouted wall factor γ_g.

The variance is a statistic denoting the precision of the predicted strengths in representing the experimental strengths. Sources of variation come from the mechanical properties of the materials, variations in dimensions (tolerances), uncertainties in the theory underlying the design definition of member strength, construction practices, and formula error. The effect of each source of variance is unknown and cannot be distilled from the other sources of variation. The variance is used as the basis of the resistance (or strength reduction) factor that is multiplied by the nominal strength to obtain the design strength. Larger variances denote that a smaller resistance factor is needed to account for the increased uncertainty for that particular material and member type.

9.2 Data

The preliminary steps of data scrutinization and data synthesization produced a data set that was fit to be used in meta-regression. The specimens in the dataset were filtered to include only those which included the shear failure model. The complete data set was partitioned into

one group for the fully-grouted specimens (Group 1) and a second group for the partially-grouted specimens (Group 2) so that the statistics for each type of grouting could be computed individually and compared with the other group. More information about the data in the two groups is detailed in Chapter 7.

This analysis included only two variables, the experimental shear strength and the strength predicted from the full MSJC (2013) shear equation with the upper limit included. The aim of this study was to solve the over-determined, bivariate equation

$$\boldsymbol{v}_{exp} = \beta \boldsymbol{v}_{pred} + \boldsymbol{\varepsilon} \tag{9.1}$$

for the mean correlation β coefficient between the predicted shear strength $\boldsymbol{v}_{pred}$ and the experimental shear strength $\boldsymbol{v}_{exp}$. Equation (9.1) presents an issue in that the errors $\boldsymbol{\varepsilon}$ would be heteroscedastic because it has been observed that the variance increases with increasing $\boldsymbol{v}_{pred}$. This issue was overcome by transforming the equation to produce

$$\boldsymbol{v}_{exp} \oslash \boldsymbol{v}_{pred} = \beta + \boldsymbol{\varepsilon}^* \tag{9.2}$$

where $\boldsymbol{\varepsilon}^* = \boldsymbol{\varepsilon} \oslash \boldsymbol{v}_{pred}$ and $\oslash$ denotes element-wise division. The experimental shear strength was chosen for the numerator and the predicted strength for the denominator so that the resulting fraction would produce the reduction factor needed for the mean predicted strength to equal the experimental strength. This format is consistent with that used by Ellingwood et al. (1980) in their analysis of the nominal values of various material strength equations.

The consequence of using the quotient of experimental and predicted strengths is that the quotient has a normal ratio (or Gaussian quotient) distribution because it is the ratio of two hypothetically-normally distributed variables. The actual distribution for the predicted values is unknown because the values are the lesser of two calculated values from two separate equations (the base equation and upper limit equation), each with a different distribution. The distribution of the final MSJC predicted values were assumed to be normal because of the Central Limit Theorem and the large number of values. The complex mathematics involved in describing the normal ratio distribution are beyond the scope of this dissertation, so the data were fitted to the normal and log-

normal distributions to determine which distribution more closely matched the actual distribution of the data.

Hayya et al. (1975) found that for certain combinations of mean and variances, the normal ratio distribution can be approximated using a normal distribution. Since the variances of the experimental and predicted shear values was unknown, the validity of the Hayya et al. (1975) simplification could not be determined for these data. Monte Carlo analysis of several combinations of means and variances was performed to compare how the normal ratio distribution would compare with the normal and lognormal distributions. The results of the Monte Carlo analysis shown in Figures 9.1, 9.2, 9.3, and 9.4 revealed that values of Gaussian Ratio probability distribution function appears to fall somewhere between those of the normal and lognormal distribution functions. This finding suggests that either the normal or lognormal distribution would provide an appropriate approximation to the distribution of each data group.

The difference between the actual and approximated distributions should have minimal effect on the regression for three reasons. First, the range of the data in each of the two groups is relatively small (less than an order of magnitude). Second, the law of large numbers should have strong influence because the number of samples is relatively large in each data set. Lastly, weighted regression were used to give greater influence to those studies with a smaller coefficient of variation. In both data sets the specimens with greater weights were located near the center of each group of data, decreasing the influence of the data at the tails of the distributions.

Since two potential distributions were available to represent the two different groups being analyzed, it was possible that each of the two groups could be best approximated by a different distribution. In this case the question would arise of which distribution to assume when comparing the two data groups. This circumstance was complicated further by the introduction of weighting into the analysis, which could influence how the data fit the two distributions and potentially change which approximate distribution that the data group favored. These two analysis uncertainties were overcome by analyzing the two data groups twice. The first analysis assumed an a priori lognormal distribution for both groups of data and the second analysis assumed an a priori normal distribution for both groups. The results from the two analyses were compared to select which distribution to assume based on which distribution produced the overall smallest variances for both data groups.

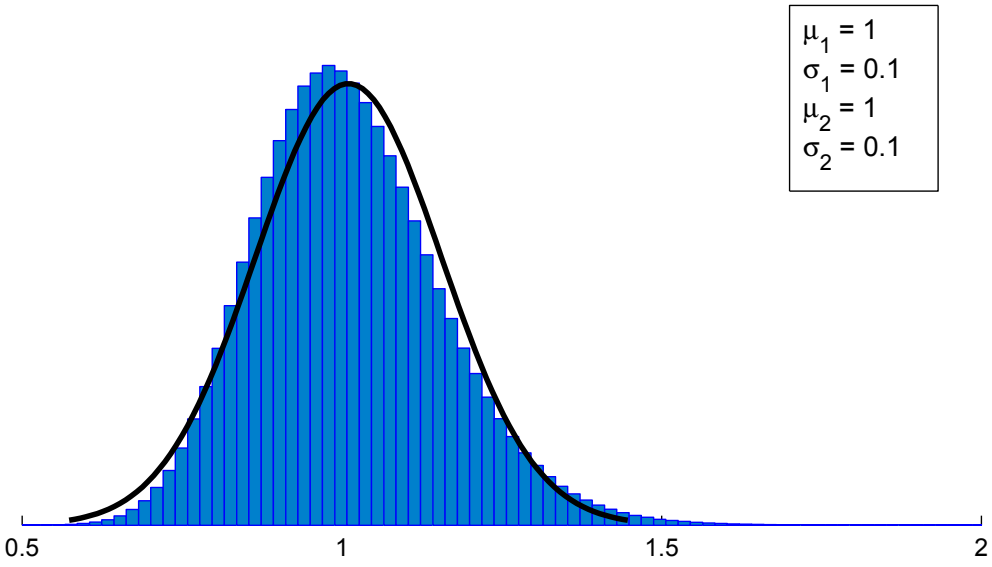

(a) normal distribution

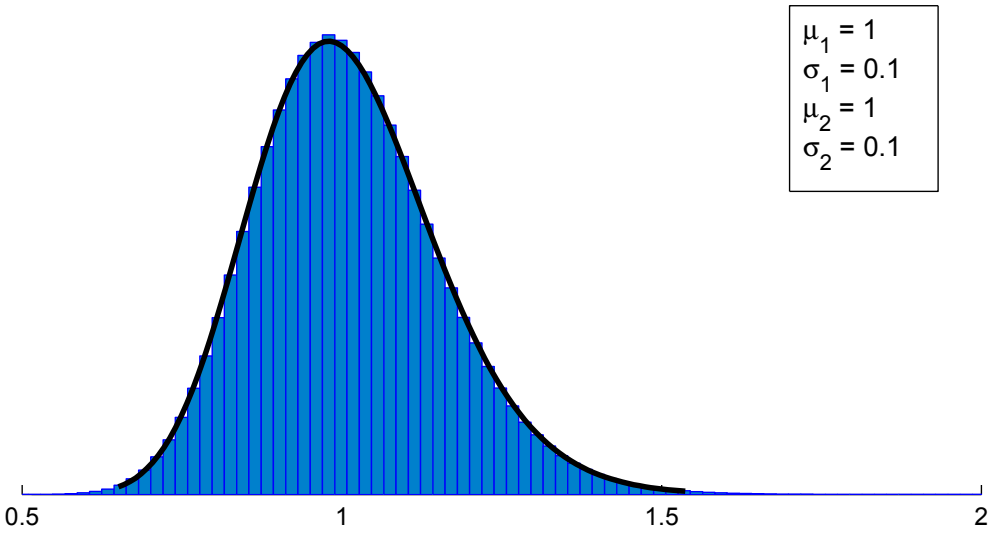

(b) lognormal distribution

Figure 9.1: Monte Carlo simulation for distributions with equal means and variances

9.2.1 Weighting Criteria

Least-squares regression assumes that the variance is the same for all data in the analysis. All of the data in the dataset came from a multitude of studies and each study demonstrated a different amount of variance between its specimens from other studies. This analysis overcame the

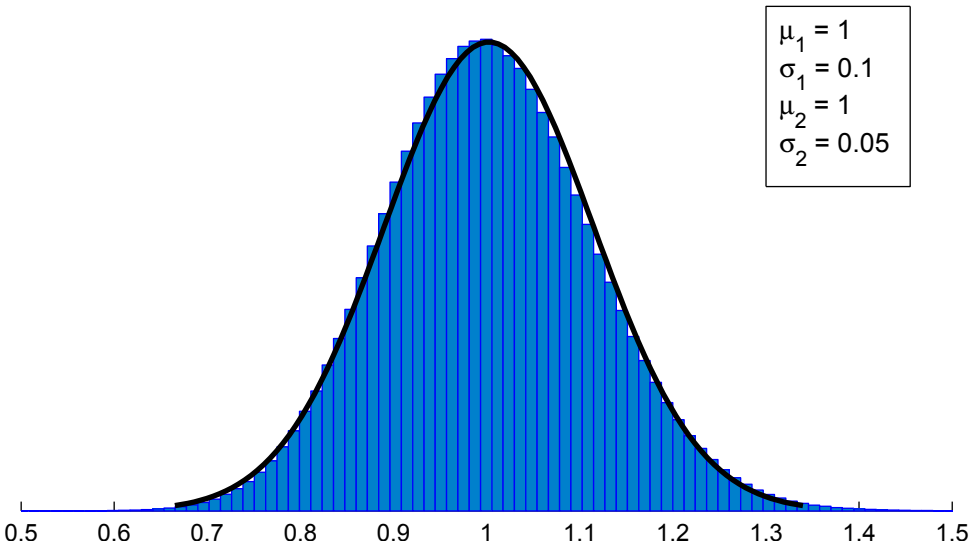

(a) normal distribution

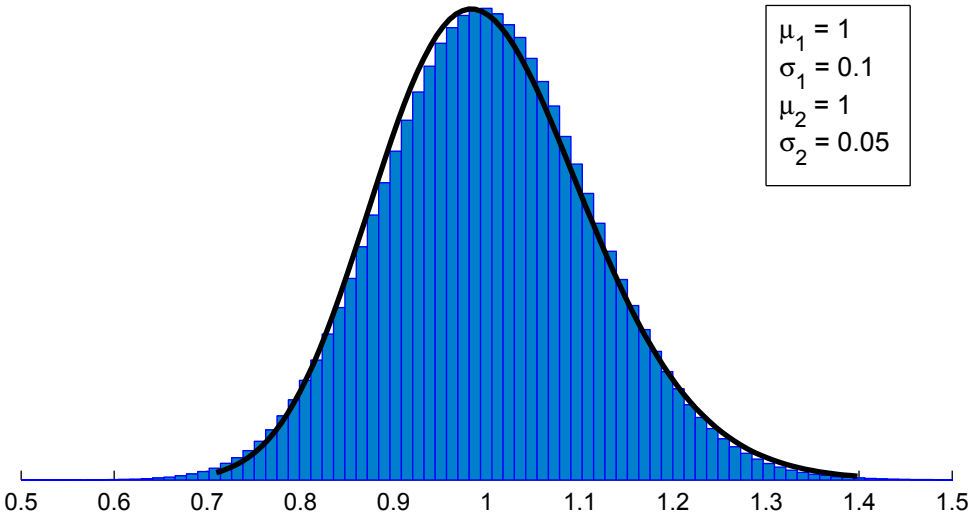

(b) lognormal distribution

Figure 9.2: Monte Carlo simulation for distributions with equal means and small σ^2

disparities in variance through the use of weighted least-squares regression. The specimens in the dataset were grouped together by the research study which originally performed the experimental tests. For studies which conducted a larger number of tests, the specimens in that group were further divided into groups with similar characteristics.

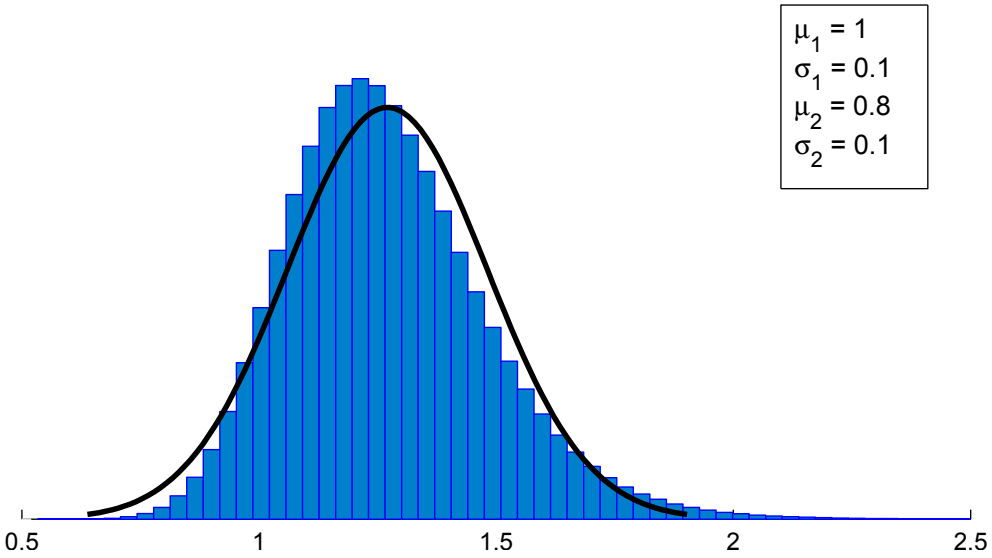

(a) normal distribution

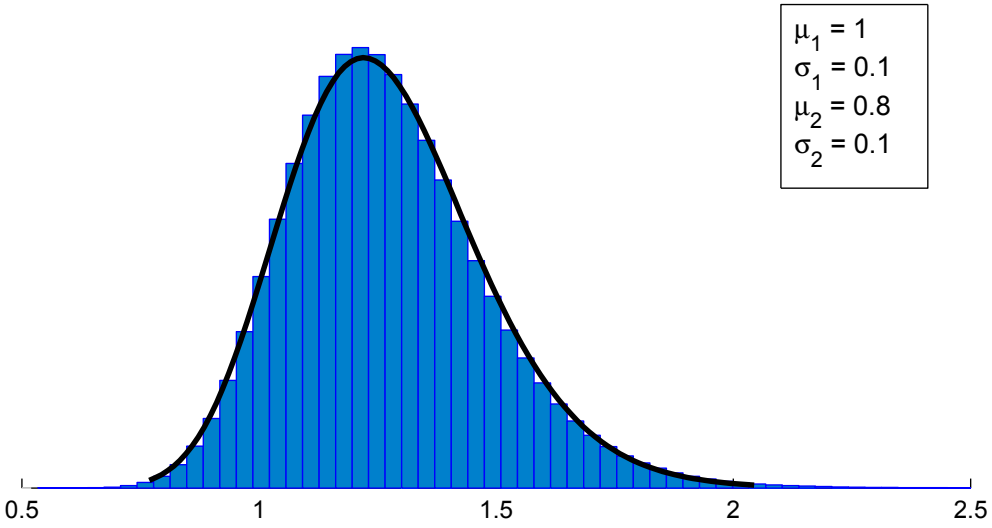

(b) lognormal distribution

Figure 9.3: Monte Carlo simulation for distributions with equal variance and small μ_2

The goal of the analysis is to determine a model which best estimates the true model—which is unknown. Without knowing the true model, it is not possible to calculate the residuals and variance of the data, but these statistics can be estimated by assuming that the given model is the true model. In performing each weighted analysis, it was assumed that the variance of the specimens was constant within each group because the specimens within each group were tested

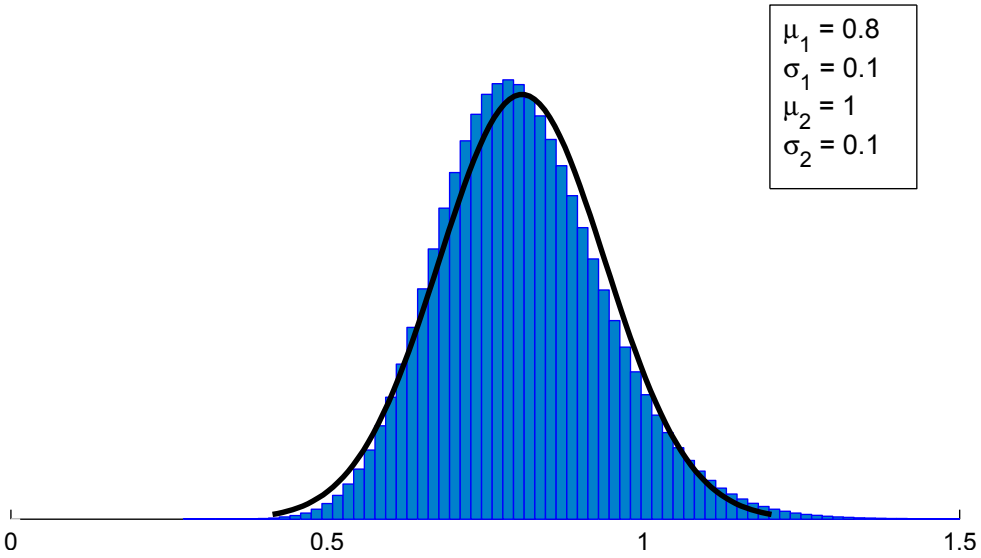

(a) normal distribution

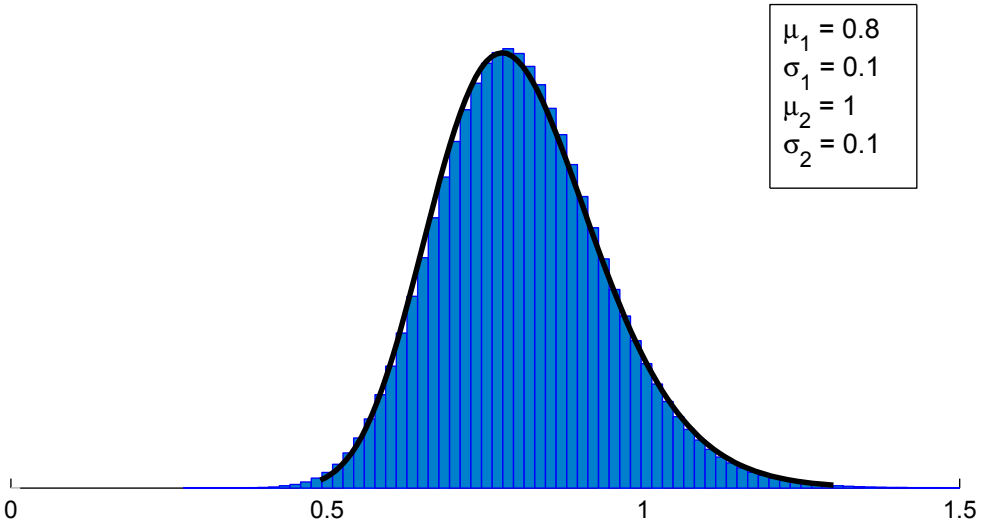

(b) lognormal distribution

Figure 9.4: Monte Carlo simulation for distributions with equal variance and small μ_1

by the same researchers using same test setup and similar materials. By making this assumption, the variance for the specimens for each group could be estimated directly from the residuals. The coefficient of variation for each group was calculated by dividing its standard deviation by the mean ratio of experimental to predicted strengths of its specimens.

The weighting chosen to use for each specimen in this analysis was the inverse of its group's coefficient of variation. This weighting scheme was chosen because it would give higher weights to those groups with lower coefficients of variation, and provide a robust weighting method that was guaranteed to converge (Carroll and Ruppert, 1988). It was felt that those groups with lower coefficients of variation more accurately followed the true model and should be given higher influence in determining the model's estimate. The weights for each group were not known initially and it was not possible to calculate both coefficient estimates and weights explicitly. It was necessary to use an iterative process to first calculate the coefficient value assuming equal weights for all specimens, from which the residuals and weights could then be determined. The calculated weights were then substituted back into the analysis and the process repeated until the coefficient and weight values converged.

9.3 Analysis

The statistics for the two data group were used to verify the current MSJC equation factors using two methods. The first method compared tolerance intervals for the two groups to determine the lower bound for the partially-grouted group that corresponded to the same level of confidence and population proportion as the fully-grouted group. The second method used LRFD theory to compute a resistance factor for the partially-grouted group based on the parameters from both groups. For this analysis the properties of the load equations employed in the formulation of the ASCE 7 (2010) load factors were not available so the analysis was performed using a comparative approach. Since the current MSJC (2013) equation was developed using fully-grouted data, it was assumed that the shear resistance factor was correct for fully-grouted walls. Using this assumption and the statistics calculated for the two data groups, the remaining properties for both groups could be determined.

9.3.1 Tolerance Interval Method

The tolerance interval is a useful statistic that is similar to the more frequently-used confidence interval. Despite the similarity, the tolerance interval is more appropriate for engineering predictions than the confidence interval because the confidence interval considers only the sam-

pling error while the tolerance interval considers both the sampling error and the variance of the population. In effect, a confidence interval can show how careful the researchers were in testing their shear wall specimens, but it gives no intimation about variance in the population of shear walls themselves. The tolerance interval is a more versatile tool than the confidence interval because its width considers both the sampling error and the variance of the population. Part of the increased power of the tolerance interval is because it requires one more input parameter than does the confidence interval. Both intervals require the analyst to specify the confidence level but the tolerance interval also requires the analyst to specify what proportion of the population should fall within the interval. The addition of this additional parameter enables the analyst to segregate the experimental variation from that of the materials and formula, which is a principal interest in engineering uncertainty analysis.

Tolerance intervals were selected to compute and compare grouted wall factors γ_g and resistance factors ϕ_v for each grouting type because they are better suited to accurately consider the variance of the masonry shear wall population. As the number of samples increases to infinity then the tolerance interval converges to the true population probability interval. Due to the large number of specimens in both groups, the values calculated by the tolerance intervals would be close to the actual values for resistance factor for each group.

The most appropriate values to use for the the confidence level and population proportion were unknown and were back-calculated using the data from the fully-grouted data. This practice was based on the assumption that the resistance factor for fully-grouted masonry was previously determined to account for the appropriate level of statistical risk. The calculated confidence level and population proportion from the fully-grouted data were then used to calculate the resistance factor for partially-grouted walls that assumes the same level of risk as that for fully-grouted walls. The difficulty with this method is that there were infinite combinations of confidence levels and population proportions that produce a tolerance interval of 0.8 for the fully-grouted data. This difficulty was rectified through the use of contour plots to compare infinite number of combinations for each group and to select which values to use.

9.3.2 LRFD Equation Method

The LRFD theory explained in Section 2.4.2 can be used to directly calculate resistance factors when the distributions and statistics for the load and resistance equations are known. Since the distributions and statics for the load equations were unknown, a similar approach to that above was used in which the data and statistics from the fully-grouted group were used to determine the unknown variables in Equation 2.11. The resistance factor for partially-grouted walls could then be determined using the variables determined using the fully-grouted data. In the case of shear, Equation 2.11 becomes

$$\begin{aligned}\phi &= \exp\left(-\alpha\beta\frac{\sigma_v}{\mu_v}\right)\frac{\overline{V_{exp}}}{\gamma_g V_n} \\ &= \exp\left(-\alpha\beta\frac{\sigma_v}{\mu_v}\right)\frac{\mu_v}{\gamma_g}\end{aligned}$$

where μ_v and σ_v are the mean and standard deviation for the ratio of experimental to predicted strength and the value for $\alpha\beta$ is unknown. (Ravindra and Galambos, 1994) cites the use of 0.55 as a good estimate for α, but this still leaves the value for β unknown. Similar to the previous approach, the value for $\alpha\beta$ was determined using the data from the fully-grouted data and then used to solve for the shear resistance factor ϕ_v for partially-grouted walls.

Equation 9.3 can be rearranged as

$$\alpha\beta = \ln\left(\frac{\mu_v}{\phi\gamma_g}\right)\frac{\mu_v}{\sigma_v} \tag{9.3}$$

to solve for the value of $\alpha\beta$ for masonry shear walls. Equation (9.3) was used to explicitly solve for the resistance factor for partially-grouted shear walls.

CHAPTER 10. ANALYSIS OF MSJC MODEL

10.1 Data Statistics

The unweighted data for solid and fully-grouted walls were plotted as the histogram shown in Figure 10.1. The data appeared fairly symmetric with an unusually large data bin at about 1.05. Two probability plots were generated for the normal and lognormal distributions, shown in Figure 10.2. Both the histograms and the probability plots revealed that the unweighted fully-grouted data were better fit by the normal distribution.

The unweighted data for partially-grouted walls were plotted as the histogram shown in Figure 10.3. The histogram shows a bimodal distribution with a slightly larger tail on the right side than on the left. Neither of the two fitted-distributions show a better fit to the unweighted partially-grouted data for the entire range of data. The two probability plots, shown in Figure 10.4, show that the distribution of the partially-grouted data falls somewhere between the normal and lognormal distributions.

There are at least two potential reasons that the fully-grouted data showed a more regular distribution than the partially-grouted data. First, the Monte Carlo simulations in the previous chapters showed that the ratio distribution becomes less normal as the mean of the denominator approaches zero. Since the mean of the partially-grouted data was lower than the mean of the fully-grouted it would tend to deviate more from the normal distribution than the fully-grouted data (Hayya et al., 1975). Second, the MSJC (2013) equation consists of two separate parts—the strength function and the limit function—each with a different distribution. Since both parts were originally formulated using fully-grouted experimental data, it is possible that the fits of the partially-grouted data to the two parts are so different that their two means have become distinguishable from each other in the histogram.

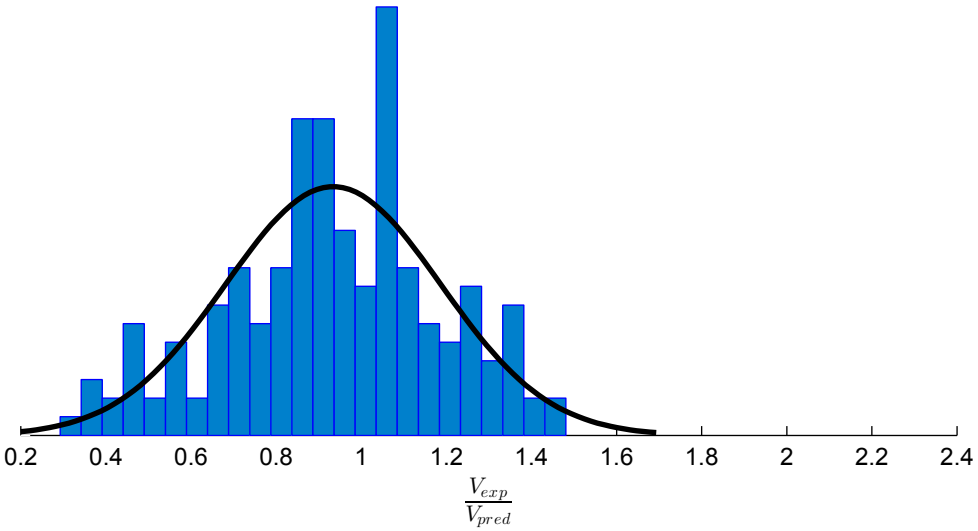

(a) With fitted normal distribution

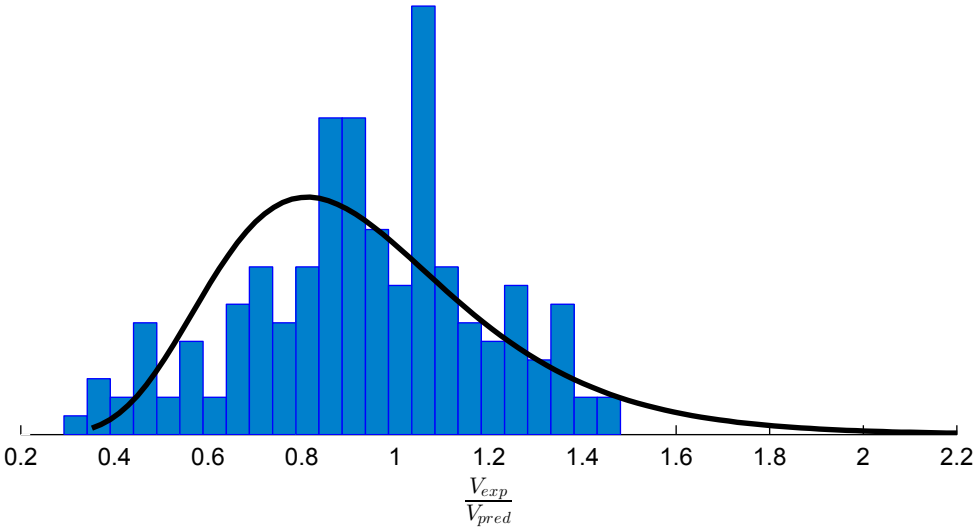

(b) With fitted lognormal distribution

Figure 10.1: Histogram of prediction efficacy for fully-grouted data

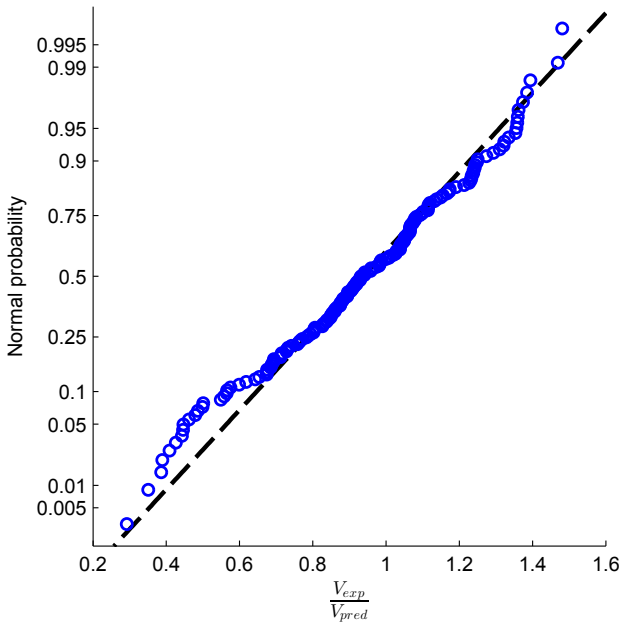

(a) Normal

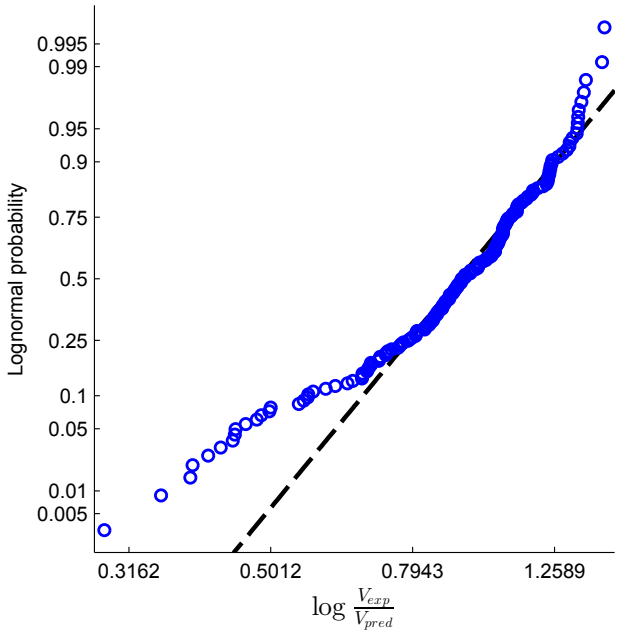

(b) Lognormal

Figure 10.2: Probability plots of prediction efficacy for fully-grouted data

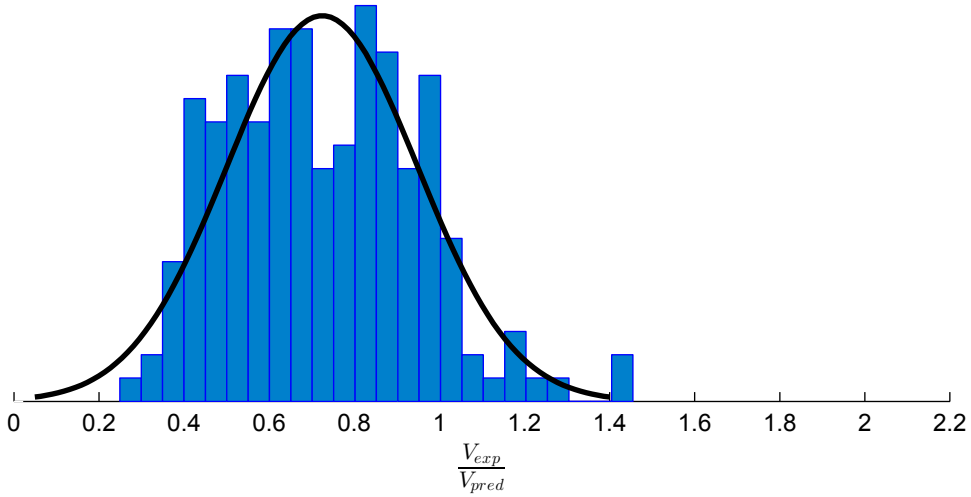

(a) With fitted normal distribution

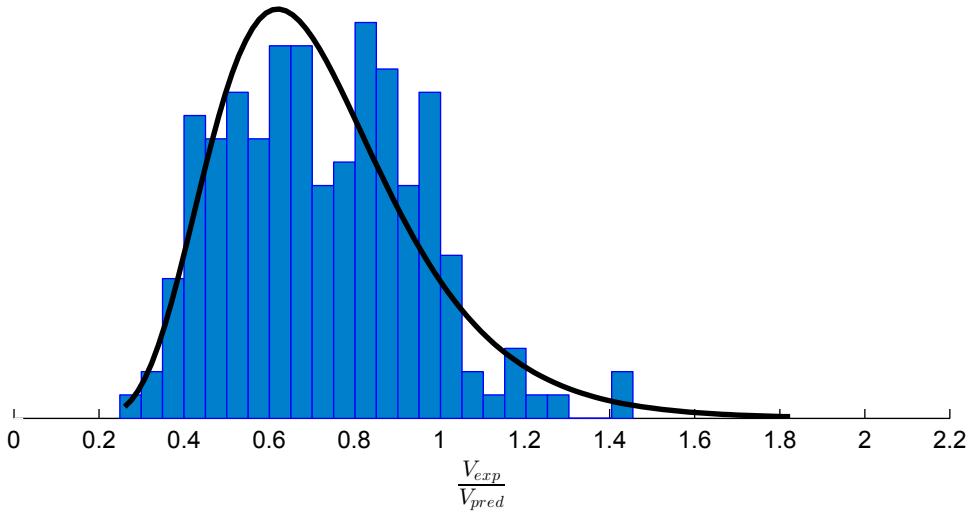

(b) With fitted lognormal distribution

Figure 10.3: Histogram of prediction efficacy for partially-grouted data

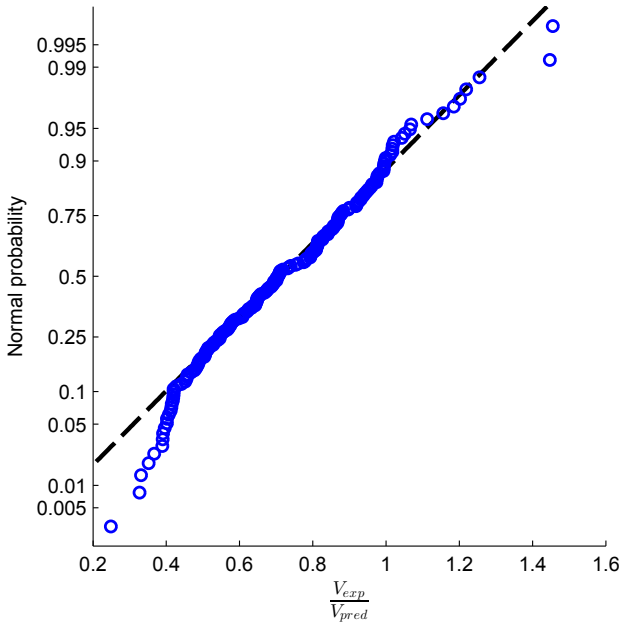

(a) Normal

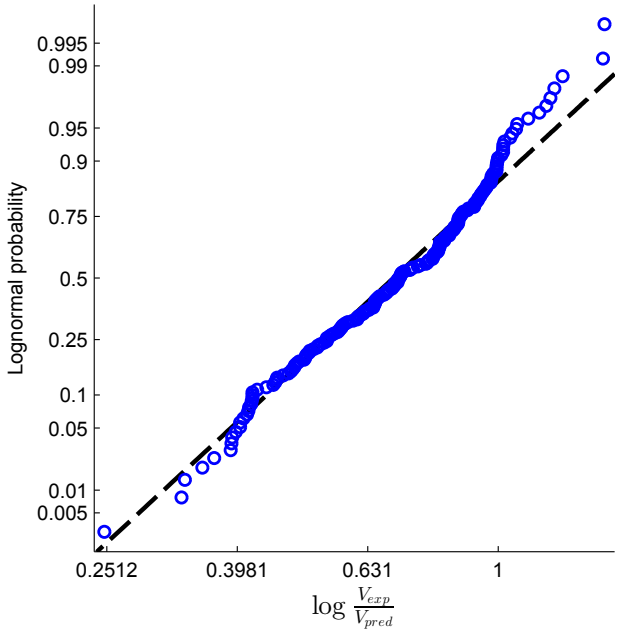

(b) Lognormal

Figure 10.4: Probability plots of prediction efficacy for the partially-grouted data

10.2 Weighted Data Analysis

10.2.1 Normal Distribution

The distribution parameters were first computed for the weighted data assuming an a priori normal distribution and are listed in Table 10.1. The value of the mean for the fully-grouted data was close to unity, suggesting that the MSJC code equation is fairly accurate for predicting the shear strength for fully-grouted masonry walls. The computed mean for fully-grouted walls was about 0.97, which is quite a bit lower than the value of 1.16 obtained by Davis (2008). Reasons for the difference are likely due to a higher number of specimens included in this analysis and the use of data weighting. The computed mean strength for partially-grouted walls was close to the 0.75 value chosen by the MSJC for the grouted wall factor γ_g. This value is also lower than the value of 0.90 calculated previously by Minaie (2009) but is between the 0.82 and 0.68 values determined by Nolph (2010) and Elmapruk (2010). The coefficient of variation for the partially-grouted data group is 21 percent higher than that of the fully-grouted data group.

Table 10.1: Data Parameter Estimates for the Normal Distribution

	Full	Partial
$\hat{\mu}$	0.9686	0.7322
$\hat{\sigma}^2$	0.05160	0.04976
mean	0.9686	0.7322
COV	0.2345	0.3047

Tolerance intervals were computed from the mean and variance of the data and their width was determined by the proportion of the population to be encompassed and the level of confidence desired. Values to use for the population proportion and confidence level are not specified for structural material reliability assessments. To overcome this uncertainty, the tolerance intervals for a broad range of confidence levels and population proportions were calculated and plotted as contour plots for both data groups, shown in Figure 10.5. The tolerance intervals show that the partially-grouted walls require an overall greater greater reduction in strength than fully-grouted

walls to maintain a similar failure probability. Both contour plots show that the lower bound is more sensitive to changes in the population proportion than to changes in the confidence level.

10.2.2 Lognormal Distribution

The calculated parameters for the two data groups assuming a lognormal distribution are given in Table 10.2. It should be noted that the parameters μ and σ^2 for the lognormal distribution are not the same as the mean and variance of the distribution, though they are functionally related. The means calculated for the lognormal case were negligibly higher than those calculated for the normal case (less that 0.5 percent difference between the two). The coefficients of variation between the two datasets were notably different by 22 percent, which is smaller than the difference between the two assuming a normal distribution. The reason for the decrease in the difference between the two datasets for the lognormal case is principally due to the greater increase in variance for the fully-grouted data (from 0.2345 to 0.2727, a 16 percent increase) compared to that for the partially-grouted data (from 0.3047 to 0.3457, a 13 percent increase).

Table 10.2: Data Parameter Estimates for the Lognormal Distribution

	Full	Partial
$\hat{\mu}$	-0.06395	-0.3639
$\hat{\sigma}^2$	0.07175	0.1129
mean	0.9723	0.7353
COV	0.2727	0.3457

Contour plots for tolerance intervals for the lognormal distribution are shown in Figure 10.6. The contours for both distributions show that the lognormal distribution produces lower population proportions and confidence levels than the normal distribution for similar lower bound values. This is due to the fact that the coefficients of variation for both data groups are larger for the lognormal distribution, which causes the lower bounds to be pushed out farther from the mean to compensate for the additional uncertainty. The notably higher variance of the partially-grouted group compared to the fully-grouted group shows the lack of fit between the partially-grouted data and the MSJC equation. The difference in variances would mean that the shear strength reduction

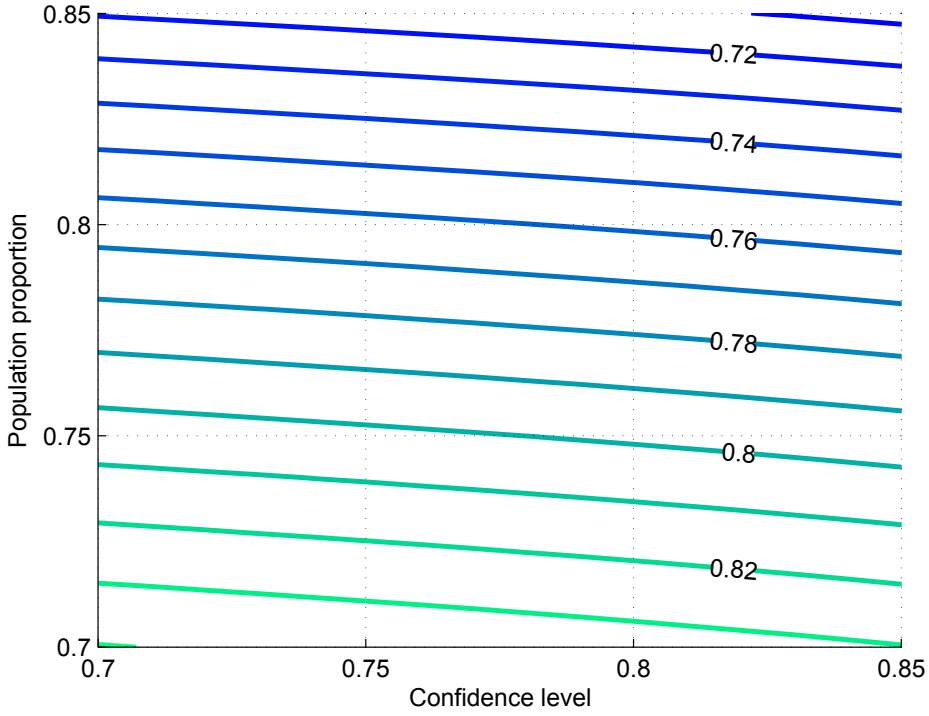

(a) Fully-grouted shear walls

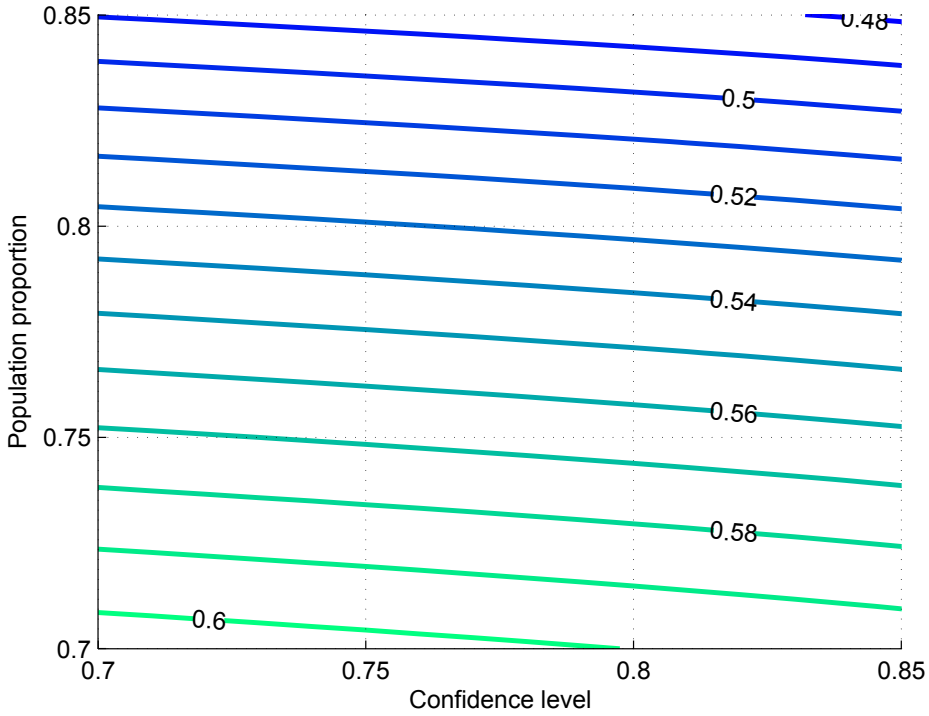

(b) Partiall-grouted shear walls

Figure 10.5: Contour plots of tolerance intervals assuming a normal distribution

factor for partially-grouted masonry walls should be less than that for fully-grouted walls because the data spread is larger. To calculate the reduction factor necessary for the partially-grouted data it will be necessary to use tolerance intervals.

The variances of both groups are noticeably smaller for the normal distribution. While this was expected for the fully-grouted group, the probability plots for the partially-grouted group suggested that the lognormal distribution might be a better fit the data. The comparison between the values in Tables 10.1 and reftab:logn indicates that both distributions results in similar means for both groups. From such a similarity it is reasonable to say that the current MSJC shear equation performs satisfactorily well for fully-grouted walls. It is difficult to judge from the histograms and probability plots how the weightings would affect the weighted distributions. The lower variance from the normal distribution produced tolerance intervals that were narrower for both groups than those from the lognormal distribution, as shown in Figure 10.6.

10.2.3 Summary

Analysis of the weighted data from both data groups showed that the normal distribution produced the better fit for both the fully- and partially-grouted data groups because it produced smaller coefficients of variation than did the lognormal distribution. Since the weighting factors were inversely proportional to the coefficient of variation, and not to the variance, it was initially suspected that the weighted data would favor the lognormal distribution because a characteristic of the distribution is that it has a constant coefficient of variation. Though the unweighted partially-grouted data showed a slightly better fit for the lognormal distribution, the fit to the normal distribution notably improved with the introduction of weighting. Both distributions resulted in nearly the same values for the means of each data group.

The data analysis shows that the MSJC equation is sufficiently accurate for fully-grouted walls but that it is very unconservative for partially-grouted walls. The precision of the MSJC shear equation is better for the fully-grouted walls than for the partially-grouted walls by 21 percent, meaning that the current assumption that the same resistance factor value can be used for both fully- and partially-grouted walls is not valid. It is necessary to calculate the total reduction that is necessary for calculated partially-grouted wall strength such that the probability of failure is the same as that for fully-grouted walls.

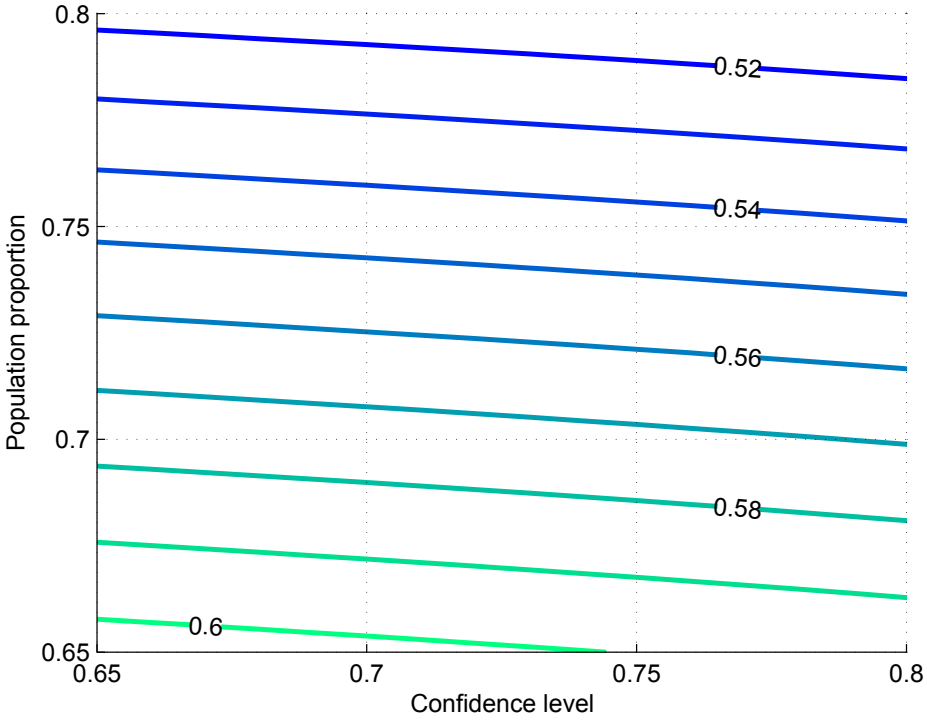

(a) Fully-grouted shear walls

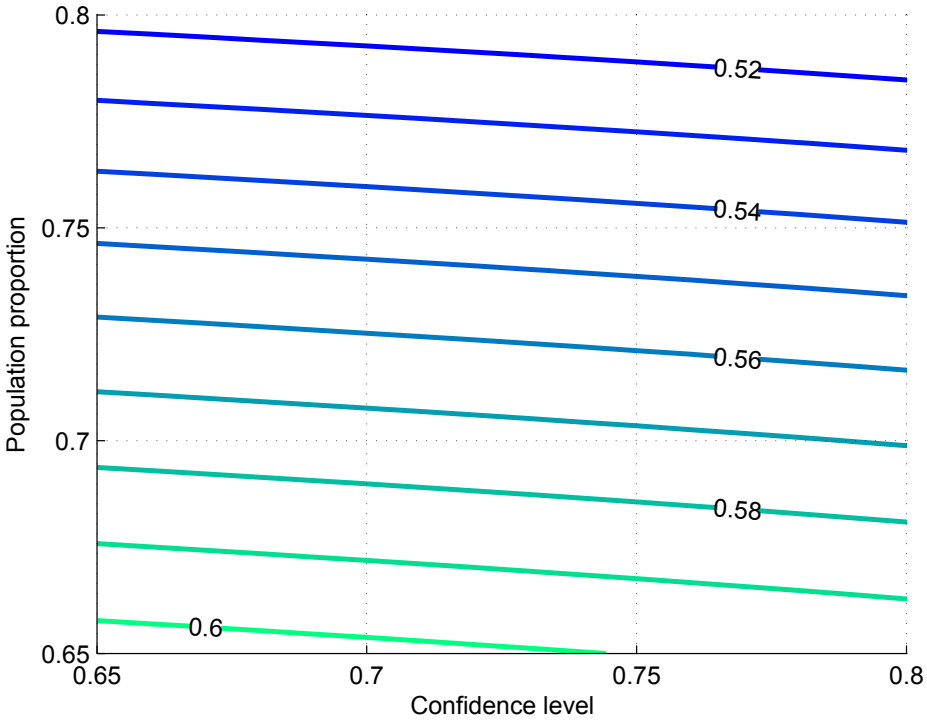

(b) Partially-grouted shear walls

Figure 10.6: Contour plots of tolerance intervals assuming a lognormal distribution

10.3 Tolerance Interval Method

The data parameters from the normal distribution were used to calculate the resistance factor for partially-grouted walls since it was shown to be the better fit for both data groups. The values of the population proportion and confidence level to use for the partially-grouted tolerance interval could not be explicitly determined from the fully-grouted data because there were one equation and two unknowns. One possible value could be calculated by assuming a value for either the population proportion or confidence level, calculating the other parameter using the fully-grouted data, then using both parameters to determine the lower-bound tolerance interval for the partially-grouted data. This method would need to be repeated over a range of both parameters to determine how the interval bound changed. A simpler method of performing this analysis is to superimpose the contour from the fully-grouted tolerance intervals corresponding to a value of 0.8 over the contour plot of the tolerance intervals for the partially-grouted data, as shown in Figure 10.7.

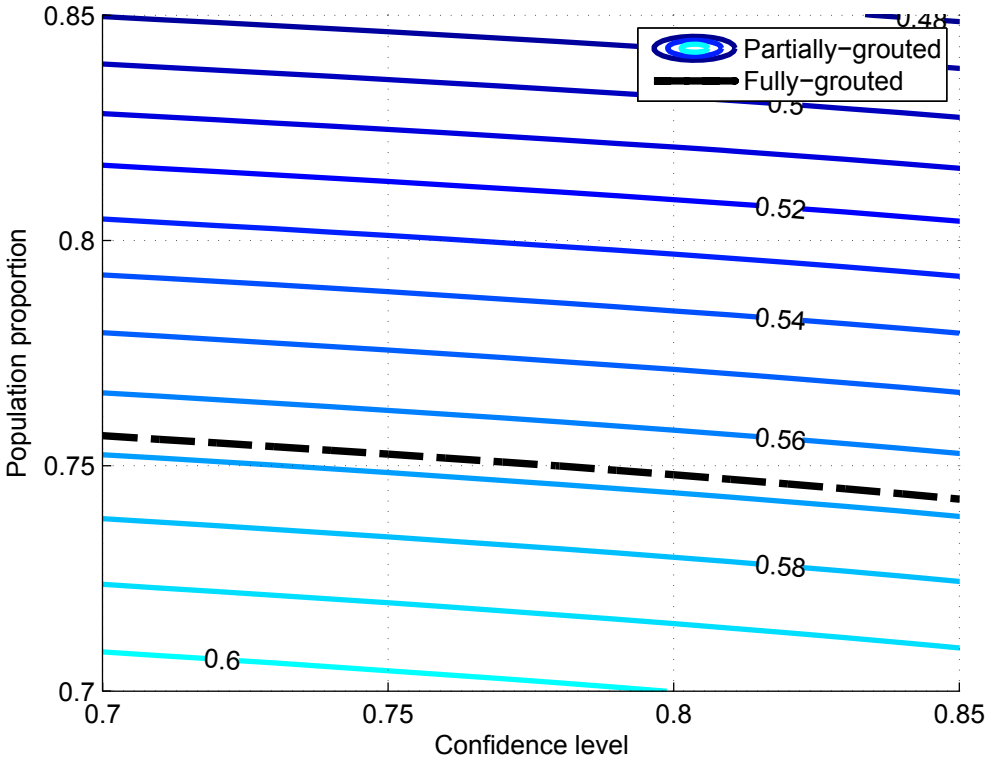

Figure 10.7: Fully-grouted bound on partially-grouted tolerance intervals for normal case

The contour from the fully-grouted tolerance interval lies parallel to the contours for the partially-grouted tolerance intervals, meaning that the relationship between partially-grouted and fully-grouted data reliability is constant for all values of population proportion and confidence levels. Predicted strengths for partially-grouted wall using the MSJC equation must be multiplied by a net factor of 0.567 to have the same probability of failure as fully-grouted walls. Since it has been shown that the current grouted wall factor of 0.75 accurately describes the nominal strength for partially-grouted walls, the resistance factor for partially-grouted walls should be reduced from 0.80 to 0.75. This resistance factor was obtained by dividing the lower tolerance bound of 0.567 by the grouted wall factor value of 0.75.

The simplicity of the solution method meant that the analysis could be repeated with the lognormal distribution parameters to compare the lower tolerance bound value with that determined above. The comparison of the contour lines from the lognormal cases shown Figure 10.8 produced a lower tolerance bound of 0.572, only slightly higher than that obtained for the normal case. This result suggests that the relationship between the failure probability for partially- and fully-grouted walls is not only independent of the population proportion or confidence interval, but that it is only slightly sensitive to the distribution fitted to the data.

10.4 LRFD Equation Method

The resistance factor for partially-grouted walls was determined using the LRFD approach from Galambos and Ravindra (1978) as explained in Sections 2.4.2 and 9.3.2. The value for the coefficient $\alpha\beta$ was determined by substituting the coefficient values for full-grouted walls into

$$\alpha\beta = \ln\left(\frac{\mu_V}{\phi_v \gamma_g}\right)\frac{1}{\frac{\sigma_V}{\mu_V}} \tag{10.1}$$

where

μ_V = 0.9686 (Table 10.1),
ϕ = 0.80 (MSJC, 2013),
γ_g = 1.0 (MSJC, 2013), and
$\frac{\sigma_V}{\mu_V}$ = 0.2345 (Table 10.1)

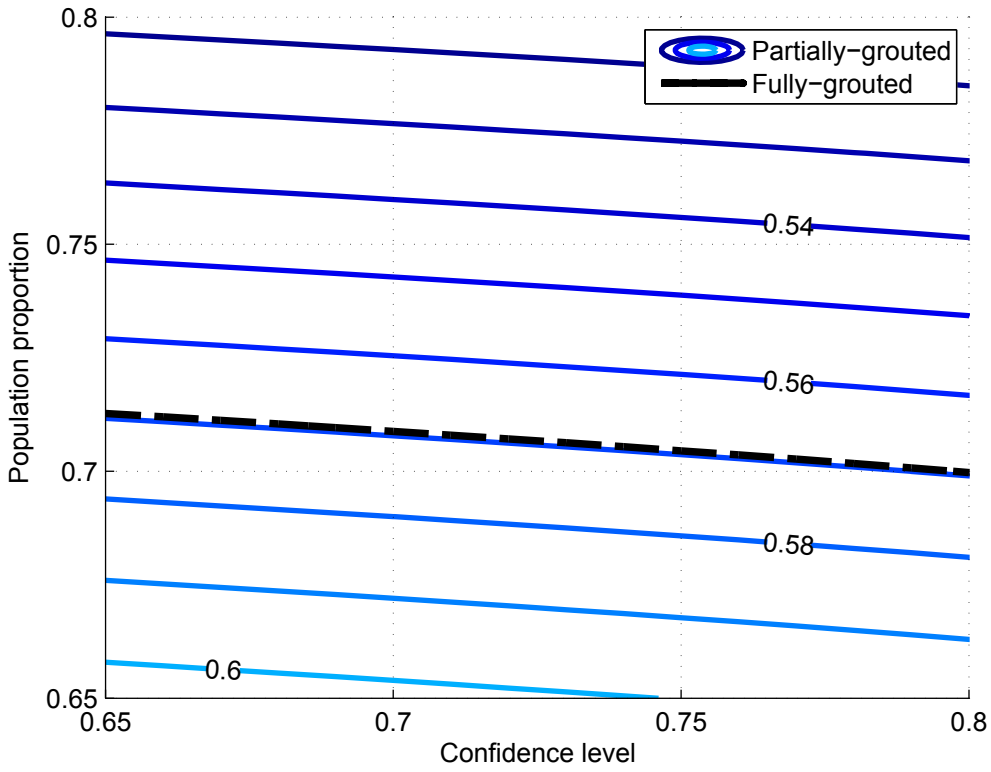

Figure 10.8: Fully-grouted bound on partially-grouted tolerance intervals for lognormal case

which results in the solution $\alpha\beta = 0.8155$. The resistance factor for partially-grouted masonry shear walls was determined using

$$\phi_v = \exp\left(-\alpha\beta \frac{\sigma_V}{\mu_V}\right) \frac{\mu_V}{\gamma_g} \tag{10.2}$$

where

$\alpha\beta = 0.8155$ (see above),
$\mu_V = 0.7322$ (Table 10.1),
$\gamma_g = 0.75$ (see Section 10.2.1), and
$\frac{\sigma_V}{\mu_V} = 0.3047$ (Table 10.1)

which results in the resistance factor $\phi_v = 0.7614$; this value would be simply rounded to 0.75.

CHAPTER 11. MSJC MODEL DISCUSSION AND RECOMMENDATIONS

11.1 Discussion

Both weighted data groups appear to more-closely follow the normal distribution than the lognormal. Though the lognormal distribution was a better fit to the partially-grouted data in the unweighted cases, the introduction of weighting created a better fit for the partially-grouted data to the normal distribution. Though it could be argued that it would be more conservative to use the values from the lognormal distribution, it is preferable to use the distribution that best fits the data. The tolerance interval is already conservative by nature because it accounts for both the experimental error and the variance of the material. Using the lognormal distribution would unnecessarily inflate the variance of both data groups such that they do not represent the variance of the data themselves.

The current analysis shows that the mean performance of current formula is approximately 0.97 for predicting the strengths of fully-grouted walls. This lies close to the typical range of 0.98 to 1.05 percent for most materials observed by Ellingwood et al. (1980) and is close enough to unity that no change to γ_g is warranted for fully-grouted walls. The mean for the partially-grouted data was 0.73, which is close enough to the value of 0.75 currently used for partially-grouted walls to warrant no change to γ_g for partially-grouted walls.

Plots of the probabilities of failure for both grouting types assuming the ultimate loading condition and using the current MSJC (2013) coefficient values are given in Figure 11.1. The current factors listed in the MSJC code result in a probability of failure that is 21 percent higher for partially-grouted masonry shear walls than for fully-grouted masonry shear walls. The increase in failure probability for partially-grouted walls is due to the greater variance for partially-grouted walls than for fully-grouted walls and needed to be accounted for in the design strength so that the probabilities of failure for the two grouting type are similar. The value of the resistance factor ϕ_v for partially-grouted masonry shear walls was determined to be 0.73 using tolerance intervals and 0.76

using LRFD theory. Both methods grave values that were in good agreement with each other and show that the resistance factor should be taken as 0.75 for partially-grouted shear walls (assuming that $\gamma_g = 0.75$). The total reduction in strength obtained from these factors is $\phi_v \gamma_g = 0.80$ for fully-grouted walls and $\phi_v \gamma_g = 0.567$ for partially-grouted walls.

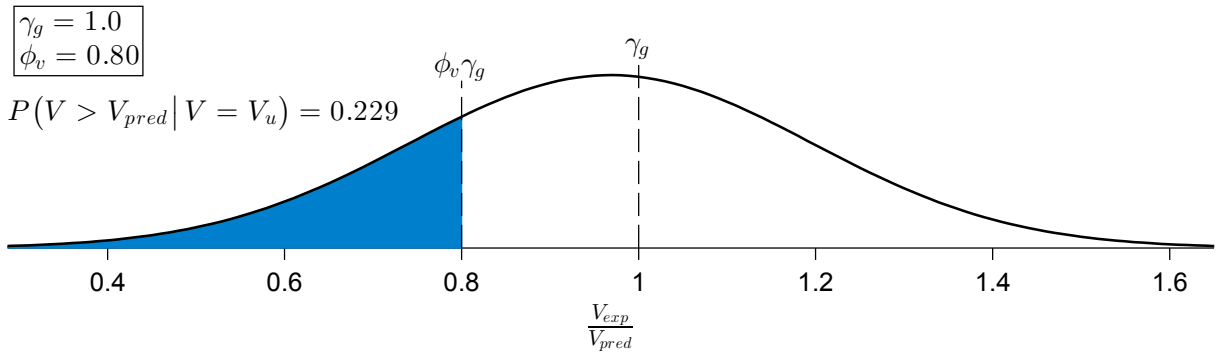

(a) Fully-grouted walls

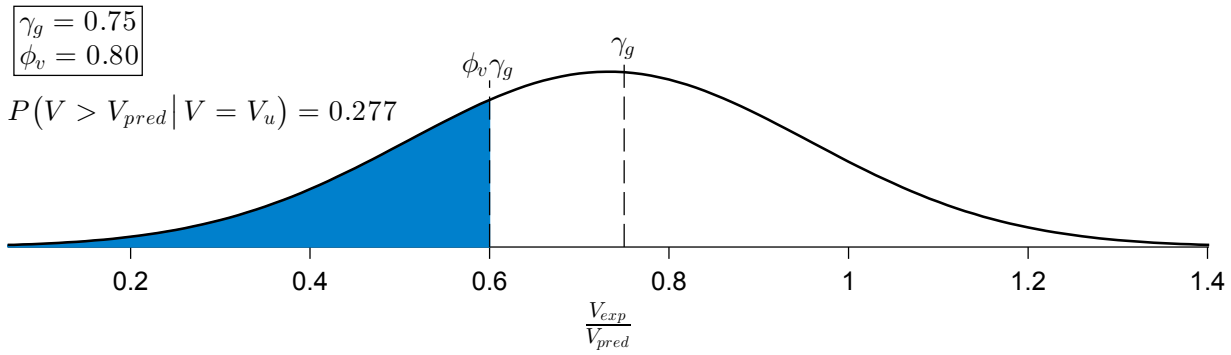

(b) Partially-grouted walls

Figure 11.1: Strengths and probabilities of failure for current MSJC coefficients

There are two possible methods to correct the discrepancy in failure probabilities for the two grouting types. Both methods involve adjusting one of the coefficients for partially-grouted masonry shear walls so that the predicted design strength accounts for the same amount of uncertainty as that for fully-grouted walls. The first method is to continue to use a single factor to account for the difference in both shear strength and uncertainty between the two shear wall types. The second method is to use the grouted wall factor to represent the difference in nominal strengths

and to use separate strength reduction factors to account for the difference in variation between the two grouting types.

11.1.1 Single Factor Method

In the method currently adopted by the MSJC (2013) code, the nominal shear strength formulae are multiplied by the grouted wall factor γ_g. The factor is taken as 1.0 for fully-grouted walls and 0.75 for partially-grouted walls, as explained in Section 1.2. Additionally, in the current approach the same shear strength reduction factor ϕ_v is used for both fully- and partially-grouted walls, which erroneously implies that the variance for fully-grouted and partially-grouted walls are the same and that only the means differ. It has been shown that this assumption is not valid and that difference strength reduction factors should be used for fully- and partially-grouted shear walls. It is anticipated that code writers may not be in favor of introducing a different resistance factor for partially-grouted walls, feeling that the grouted wall factor should be sufficient to account for the uncertainty as well.

A single factor is able to correctly represent the mean, variance, or a combination of the two statistics for partially-grouted walls, but not both. The continued use of a single factor in the MSJC code would require that the combination be given priority in the determination of the grouted wall factor. In order to maintain the same resistance factor for both types of grouting, the grouted wall factor would need to be taken as 0.70 for partially-grouted walls, which is obtained by dividing the total necessary strength reduction 0.567 by the resistance factor 0.80. The grouted wall factor of 0.70 for partially-grouted walls maintains approximately the same probability of failure as solid and fully-grouted walls, as shown in Figure 11.2. However, the nominal shear strength no longer represents the mean shear strength for partially-grouted walls, which is represented in Figure 11.2 by the shift of the γ_g line to the left. The weakness of this approach is that the factors γ_g and ϕ_v misrepresent the nominal strength and variance of the MSJC equation with regards to partially-grouted shear walls and produces a problem for those who attempt to perform reliability analyses.

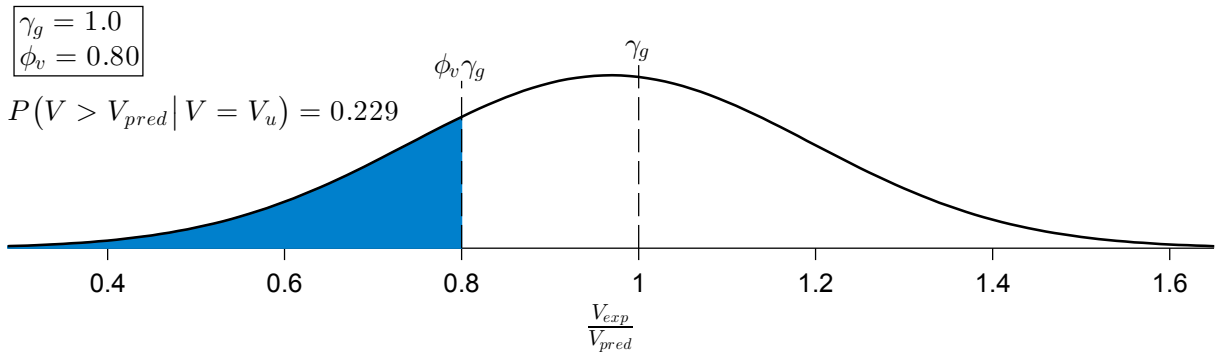

(a) Fully-grouted walls

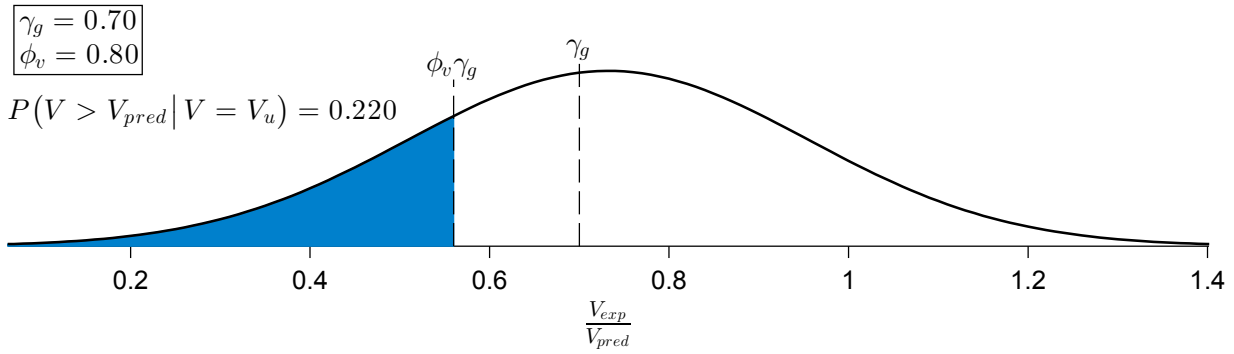

(b) Partially-grouted walls

Figure 11.2: Strengths and probabilities of failure for current approach

11.1.2 Improved Method

The improved method is similar to the current method in that it specifies a grouted wall factor be used with the nominal shear strength equation. The difference in the improved approach comes from the specification of two different shear strength reductions factor values: 0.80 for fully-grouted walls and 0.75 for partially-grouted walls. In this improved approach, the grouted wall factor accounts for the difference between the mean shear strengths of the two wall types, as would be expected. Two different strength reduction factors are specified for fully- and partially-grouted masonry which signifies to designers that there is also a difference in the variability of the two wall types.

The single concern for the improved method is that there is an additional resistance factor to be added to the masonry code and this could be viewed by code writers as making the code

unnecessarily complex. Such a concern should be dismissed because 1) the added complexity in the code from additional resistance factor is not only justified but necessitated due to the experimental evidence and 2) there are examples in other codes of resistance factors that are considerably more complex. For example, the ACI 318 (2011) resistance factor for flexure is a tri-linear function of the flexural reinforcement strain which requires linear interpolation to determine the value to use. The improved approach more accurately reflects the nature of the performance of partially-grouted shear walls. It is important for engineers to have an accurate representation of the properties of the materials, particularly for those performing reliability analyses. Reliability analysts typically assume that the code formulae represent the mean strength and infer the coefficient of variation from the reduction factor when the value is not provided (Bažant and Yu, 2006). To use the same strength reduction factor for all shear walls would be to imply that the coefficients of variation for the two grouting types are the same when, in fact, they are not.

The analysis determined that the grouted wall factor for partially-grouted masonry should be taken as 0.75 and the appropriate shear resistance factor for partially-grouted should be taken as 0.75. These two factors result in a probability distribution for the partially-grouted data that is similar in appearance to that for the fully-grouted walls, as shown in Figure 11.3. The figure shows the probability of failure for partially-grouted shear walls to be nearly the same as for fully-grouted walls—with a difference of only 2 percent.

By comparing the current factors in Figure 11.1 and the proposed factors shown in Figure 11.3, it can be seen that the improved approach more correctly represents both the mean and variance for partially and fully-grouted walls. The current single factor method is able to correctly represent the mean and variance for fully-grouted walls but not for partially-grouted walls. The inability of the current single factor method to represent both the mean and variance of partially-grouted walls is due to the significant difference in variances between fully- and partially-grouted walls. This limitation is surmounted in the improved approach by the introduction of a specific shear resistance factor for partially-grouted walls.

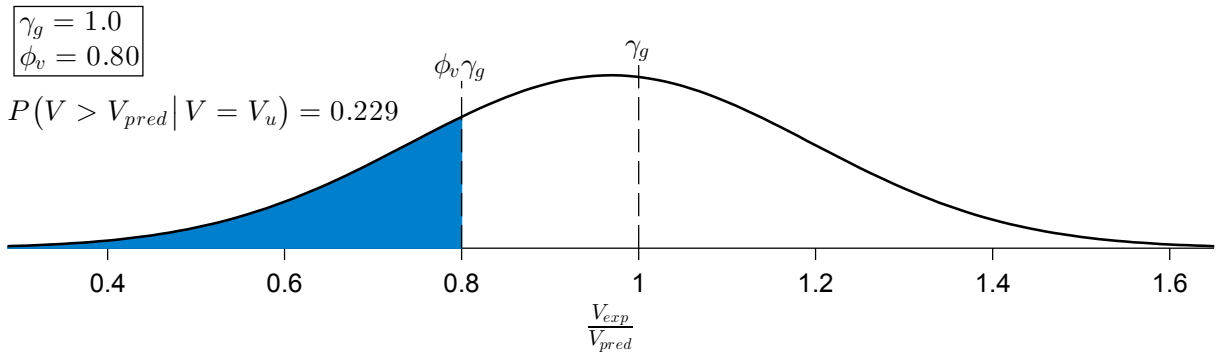

(a) Fully-grouted walls

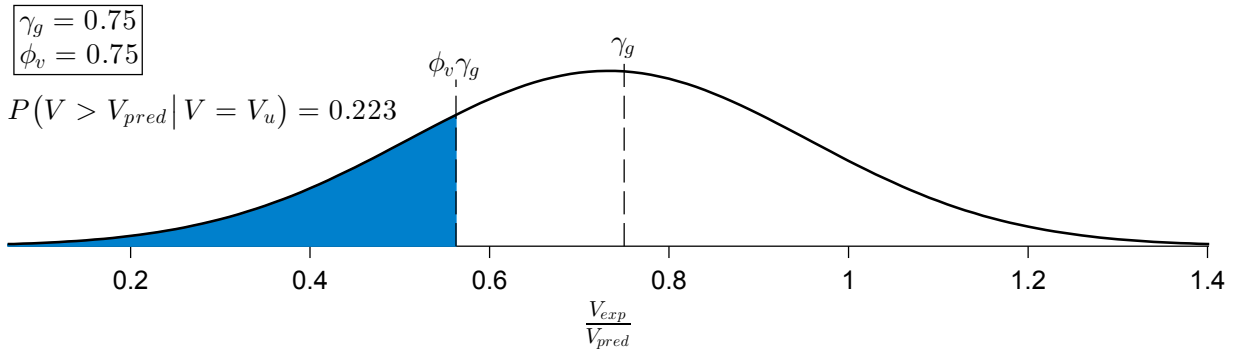

(b) Partially-grouted walls

Figure 11.3: Strengths and probabilities of failure for improved approach

11.2 Conclusions

The normal distribution was determined to be the best fit for both weighted data sets because it resulted in the lowest variance for both groups. This is likely because the MSJC equation was originally built assuming normal conditions. The calculated means for both groups are only slightly different for the normal and lognormal distributions.

The MSJC shear strength equation correlates well with the weighted mean of the experimental strengths for fully-grouted masonry shear walls. The grouted wall factor γ_g for fully-grouted shear walls should be taken as 1.0. The analysis presented herein confirmed earlier suspicions from researchers that the MSJC shear strength equation is unconservative for partially-grouted walls. The MSJC (2013) shear strength equation predicts strengths that are approximately

73 percent of the weighted mean of the experimental strengths for partially-grouted walls. The grouted wall factor for partially-grouted masonry should be taken as 0.75, as is currently is.

The MSJC shear strength equation correlates better with fully-grouted shear walls because the variance for partially-grouted shear walls is notably greater than that for fully-grouted and solid walls. The disparity in variances is likely because the MSJC shear strength equation was generated using fully-grouted and solid shear wall data. The shear resistance factor ϕ_v for partially-grouted masonry walls should be different from that for fully-grouted walls to represent the difference in variances, and should be taken as 0.75.

11.3 Recommendations

The findings for the improved approach above can be easily incorporated into the MSJC code and commentary. Recommended wording for revisions to the code and commentary are presented in Appendix H.

Part IV

Linear Regression Modeling

This part details the second analysis approach developed in this study to create a new linear model for the prediction of masonry shear wall strength. Chapter 12 is a literature review of linear model building techniques typically employed by statisticians and continues with a review of the development of the current MSJC shear equation, its precursors, as well as other shear equations from around the world. Chapter 13 introduces the methodology that will be used in analyzing the previous shear models and in developing a new, improved shear model for masonry. Chapter 14 presents an investigation of the precursor models which led up to the current MSJC equation. Chapter 15 is the principal focus of Part IV and details the development of a proposed shear model to replace the current MSJC shear equation. Chapter 16 presents comparison and discussion of all of the shear prediction models using the extensive dataset constructed for this study.

This analysis was the first to use multivariate least-squares regression to develop a model for predicting masonry shear strength. The proposed model was the first to be developed using both fully- and partially-grouted masonry data with the intention of being included in a masonry design standard. The proposed model was developed using the largest dataset of fully- and partially-grouted shear walls yet assembled for analysis. The goodness-of-fit statistics and scatter plots show that the proposed model has the best performance characteristics out of all the models yet developed for predicting masonry shear strength.

CHAPTER 12. LITERATURE REVIEW: LINEAR MODEL DEVELOPMENT

12.1 Previously Developed Models

12.1.1 Matsumura

Matsumura (1987) developed a shear strength model with the purpose of determined a numerical representation of the differences between fully- and partially-grouted walls and the effects of shear span ratio, axial load, and shear reinforcement. Matsumura used the results of 80 shear wall specimens, of which about two-thirds were partially-grouted and the remaining were fully-grouted. Matsumura built his shear equation in a piecewise manner by examining the influence of a single parameter, determining a mathematical representation of the parameter's influence, normalizing the experimental strength to include the parameter's influence, then using partial residual plots to examine the next parameter's influence. The process was repeated multiple times until all parameters were fully represented.

In analyzing his dataset, Matsumura observed that shear stress increased with increasing prism strength. In subsequent plots and analysis he divided the experimental shear stress values by the square root of the prism strength to eliminate the effects of prism strength on the visualization of other data with respect to strength. The square root of f'_m was chosen because the shear strength was not quite linearly correlated to the prism strength. By normalizing the shear strength he also stabilized the variance of the data, which tended to increase proportionally with wall shear strength and with prism strength.

Matsumura started his model building by adapting a model that he had previously developed for autoclaved cellular concrete members. He used the least squares method to determine the masonry strength coefficients for walls without reinforcement. With the intercept determined Matsumura then used scatter plots to visualize the relationships of the shear reinforcement on the increase in normalized shear strength of the walls. Within each plot he connected specimens from

the same group together to examine the trends in the shear strength versus the experimental shear strength. Matsumura noted that the effectiveness of shear reinforcement is larger in fully-grouted walls than in partially-grouted walls. He proposed that the shear reinforcement contribution to the shear strength of the wall is represented by

$$\Delta\tau_u = 0.18\gamma\delta\sqrt{\rho_h f_{yh} f'_m} \tag{12.1}$$

where

γ = 1.0 for clay masonry
= 0.6 for concrete masonry
δ = 1.0 for fixed-fixed (double bending) type loading
= 0.6 for cantilever (single bending) type loading
ρ_h = horizontal reinforcement ratio, and
f_{yh} = yield strength of horizontal reinforcement (MPa).

Matsumura next determined the influence of the aspect ratio on the strength of the walls. He did so by modifying his previous equation for autoclaved cellular concrete members to include the contribution of the shear reinforcement he had previously developed. Using the new representation for shear strength, including provisions for the influence of shear reinforcement, Matsumura re-normalized the shear strength to create a partial regression plot for the aspect ratio. He proposed that the masonry component of the shear strength is related to the equation

$$K_u K_p \left(\frac{0.38}{\frac{M}{Vd} + 0.35} + 0.012 \right) \tag{12.2}$$

where

K_u = 1.0 for fully-grouted masonry,

= 0.8 for partially-grouted brick masonry,

= 0.64 for partially-grouted concrete masonry,

K_p = $1.16\rho_t^{0.3}$, and

ρ_t = effective flexural reinforcement ratio.

Having determined models for all of his shear strength components, Matsumura's final equation is given by

$$V_u = \left[K_u K_p \left(\frac{0.38}{\frac{M}{Vd} + 0.35} + 0.012 \right) \sqrt{fm} + 0.18\gamma\delta\sqrt{\rho_h f_{yh} f'_m} + 0.2\sigma_0 \right] 10^3 bj \tag{12.3}$$

where

h = effective height of wall,

d = effective depth of wall,

j = 0.875 d,

f_m = fully-grouted compressive strength of masonry (MPa), and

σ_0 = axial load force gross wall area (MPa).

The principal concern with the Matsumura model is that it is considered by many to be too complex for use in a design standard (Schultz, 1994; Yancey and Scribner, 1989). Matsumura's process was slow and methodical and is practical for data from similar test series in which there is little inter-series variation, as was the case with the Japanese tests which used similar materials, construction practices, and test designs.

12.1.2 Architectural Institute of Japan

Okamoto, Yamazaki, Kaminosono, Teshigawara, and Hirashi (1987) compared their experimental results to the strengths predicted by the Architectural Institute of Japan (AIJ) Reinforced

Concrete Design Standards. They list no reference for the source of the equation and a review of the literature has revealed no information (at least in English) about the development of the AIJ equation. Okamoto et al. (1987) list the equation as being given by

$$\tau_{su} = \left[0.053 \rho_{te}^{0.23} \frac{f'_m + 180}{\dfrac{M}{Vl_w} + 0.12} + 2.7\sqrt{\sigma_{wh}\rho_{we}} + 0.1\sigma_{0e} \right] \frac{B_e j}{BD} \tag{12.4}$$

where

$\dfrac{M}{Vl_w}$ = shear span ratio,
d = effective depth of wall,
j = 0.875 d,
B = wall width,
B_e = equivalent wall width,
ρ_{te} = flexural reinforcement ratio,
ρ_{we} = shear reinforcement ratio,
σ_{wh} = yield strength of shear reinforcement, and
σ_{0e} = vertical axial stress.

12.1.3 Uniform Building Code

The 1988 edition of the Uniform Building Code contained an upper limit on masonry shear strength. The limit was a tri-linear function of the shear span ratio of the wall and consisted of two bounds, between which designers were allowed to linearly interpolate for intermediate values of M/Vl_w. The UBC upper limit equation is given by

$$V_n \leq \begin{cases} 0.50\sqrt{f'_m}A_e & \text{for} \quad \frac{M}{Vl_w} \leq 0.25 \\ 0.33\gamma_g\sqrt{f'_m}A_e & \text{for} \quad \frac{M}{Vl_w} \geq 1.0 \end{cases} \tag{12.5}$$

where A_e is the effective cross-sectional area of the wall.

12.1.4 Blondet, Mayes, Kelly, Villablanca, and Klinger

Blondet et al. (1989) analyzed data from U.S. studies to develop procedures for predicting the ultimate shear strength of fully-grouted masonry walls. Blondet et al. used the data from the UC-Berkeley tests (Mayes et al., 1976b; Chen et al., 1978; Hidalgo et al., 1978, 1979; Sveinsson et al., 1985) as the basis for developing their shear strength prediction formula for U.S. masonry. Blondet et al. assumed the ultimate shear strength of masonry to be dependent on the compressive strength of the masonry (i.e., prism strength) and the shear span ratio of the wall. They determined that the horizontal reinforcement ratio ρ_h also had a significant contribution to the ultimate shear strength while the axial load did not contribute remarkably to the strength.

Blondet et al. investigated two models for predicting the ultimate shear strength masonry walls. The first model was developed from the base equation

$$v_u = \left[\beta_0 - \beta_1 \frac{M}{Vd}\right] \sqrt{f'_m} \tag{12.6}$$

where the coefficients β_0 and β_1 vary depending on whether the wall is lightly reinforced ($\rho_h < 0.2\%$) or heavily reinforced ($\rho_h \geq 0.2\%$) in the horizontal direction. Through analysis, Blondet et al. developed the following expressions for concrete block

$$v_u = \begin{cases} \left(5.0 - 2.5\frac{M}{Vd}\right)\sqrt{f'_m} & \text{for} \quad \rho_h < 0.2\% \\ \left(6.0 - 3.0\frac{M}{Vd}\right)\sqrt{f'_m} & \text{for} \quad \rho_h \geq 0.2\% \end{cases} \tag{12.7}$$

and for hollow clay block

$$v_u = \begin{cases} \left(6.0 - 2.5\frac{M}{Vd}\right)\sqrt{f'_m} & \text{for} \quad \rho_h < 0.2\% \\ \left(7.0 - 3.0\frac{M}{Vd}\right)\sqrt{f'_m} & \text{for} \quad \rho_h \geq 0.2\% \end{cases} . \tag{12.8}$$

The second model was constructed from the assumption that the ultimate shear strength is equal to the sum of masonry and horizontal reinforcement components. In this case the masonry strength contribution is assumed to be equal to the masonry cracking shear strength. The masonry cracking shear stress v_{cr} is assumed to be functionally related to the principal tensile stress v_{cr0} as

given by

$$v_{cr} = \left[v_{cr0}^2 + (v_{cr0}\sigma_0/1.5)\right]^{\frac{1}{2}} \tag{12.9}$$

where σ_0 is the average applied axial compressive stress. The effect of axial load on the shear strength was determined to be unimportant in predicting shear strength; thus, axial load is not directly included as a parameter in the model, but it is considered in the calculation of the masonry cracking strength in Equation (12.9).

In the second model, the contribution of the horizontal shear reinforcement v_s is estimated as

$$v_s = \rho_h f_y \tag{12.10}$$

where f_y is the yield strength of the horizontal reinforcement. Blondet et al. assumed that only the horizontal reinforcement in the middle half of the wall was effective in resisting the shear force. Rather than determining a regression coefficient for the horizontal reinforcement component of the equation, they assumed the coefficient to be 0.5. In their final correlation of the equation with the experimental data, Blondet et al. used the equation

$$v_u = v_{cr} + \frac{1}{2}v_s \tag{12.11}$$

where v_{cr} is given by Equation (12.9) above. For cases where the axial load is null, Blondet et al. (1989) determined that the tensile cracking stress for grouted concrete block can be predicted by

$$v_{cr0} = \left(3.5 - 1.75\frac{M}{Vd}\right)\sqrt{f'_m} \tag{12.12}$$

and for grouted hollow clay brick by

$$v_{cr0} = \left(4.2 - 1.75\frac{M}{Vd}\right)\sqrt{f'_m}\,. \tag{12.13}$$

Equation (12.12) or (12.13) is substituted into Equation (12.9) to determine the masonry shear strength component.

Blondet et al. compared the values from the two models and determined that the two models generally correlated well with each other. The greatest similarity between the two models was for an axial stress value of about 100 psi. The observed model was found to be more conservative that the latter model, at least in part due to the discontinuity at $\rho_h = 0.2\%$ but also from the neglecting of the effects of axial load. They concluded that both models provided adequate correlation with the experimental measurements.

Blondet et al. did not describe the process they used in determining the coefficients for their models. Their process of reducing the problem to a set of bivariate data and his repeated use of the term "correlation" suggest that the coefficient values where either determined graphically or through the use of simple bivariate analysis. Their dataset contained a sufficient sample size that they could have used multivariate regression to determine more information from his data. Rather than assuming the shear reinforcement coefficient to be 0.5, multivariate regression would have revealed a superior estimate of the value and would have provided a means to test their hypothesis about what portion of the shear reinforcement contributed to the ultimate shear strength.

12.1.5 Shing, Schuller, and Hoskere

Shing et al. (1990) performed tests on 22 square masonry shear walls to examine the efficacy of different design formulae on predicting the flexural and shear strengths of masonry shear walls. The flexural strength prediction formula investigated was that contained in the 1988 Uniform Building Code. Those provisions were based on simple flexural theory—assuming that plane sections remain plane and that $\beta + 1 = 0.85$—identical to the provisions in the ACI 318-83 code for reinforced concrete. Shing et al. considered the shear strength prediction formula contained in the 1988 UBC in light of the masonry understanding at the time and concluded that the UBC specifications for masonry shear strength were overly simplistic because they did not account for factors such as axial load, vertical reinforcement, or aggregate interlock.

Shing et al. used the 1988 UBC shear equation for masonry as the basis for developing their shear equation. They adopted the general assumption, at that time, that the cracking strength of the masonry is proportional to the square root of the compressive strength, though they cite no references for the basis of this assumption. They plotted the normalized cracking shear stress against the axial stress and showed that there is a linear relationship between the cracking strength and

the axial load. After performing a similar analysis for vertical and horizontal reinforcement Shing et al. found that there is no apparent correlation between the cracking strength and the amount of vertical or horizontal reinforcement. They hypothesized that the horizontal reinforcement at the tops and bottoms of the walls do not contain sufficient anchorage to develop tensile resistance and proposed that the horizontal reinforcement component be given by

$$V_s = \left(\frac{l - 2d'}{s} - 1\right) A_h f_{yh} \tag{12.14}$$

where d' is the distance from the extreme vertical steel to the nearest end edge of the wall.

Shing et al. used a similar approach to that of Blondet et al. (1989) in that they assumed a relationship for the horizontal shear reinforcement contribution then calculated coefficient estimates for the masonry component of the equation. The two differed in that Shing et al. (1990) assumed that the axial load and vertical reinforcement also contributed to the masonry strength. Using a least-squares fit, Shing et al. found the average increase in normalized masonry strength for axial load to be about 0.0025 and for vertical reinforcement to be between 0.0014 and 0.0016. They proposed using the average value for both terms and proposed that the masonry component be calculated by

$$V_m = 0.083\left[0.0018\left(\rho_v + \sigma_0\right) + 2\right] A_g \sqrt{f'_m} \tag{12.15}$$

Using their equation, the predicted strength of masonry shear walls is given by the sum of Equations (12.14) and (12.15).

Shing et al. compared the predicted values from their new equation to those from the UBC equation and to their experimental results. In every case their equation produced conservative values that were substantially more accurate than those from the UBC equation. To further validate their new equation, Shing et al. considered the test results from Sveinsson et al. (1985). Shing et al. determined that the correlation of the new data with their new equation was good, but it did not closely capture the variation in shear strength in the Sveinsson et al. data due to inconsistencies in the data. They further noted that the UBC equation did not underpredict the shear strength for the Sveinsson data to the same large degree as it did for their own data. They explained that this was likely due to differences in testing procedures and in wall aspect ratios.

The Shing et al. equation was developed by reducing the data to two bivariate cases, one for normalized shear stress versus axial load and a second for normalized shear stress versus vertical reinforcement. The weakness of this approach is that it does not provide a mechanism for testing whether their assumed horizontal reinforcement contribution relationship is accurate. Even without analyzing the full model for the multivariate case, their assumption for the horizontal reinforcement contribution could have been examined through partial residual plots.

12.1.6 Fattal and Todd

Fattal and Todd (1991) performed a comparative study of four different equations and their ability to predict the ultimate shear stress in masonry shear walls. They studied experimental data for 62 fully-grouted, reinforced wall specimens from four different experimental studies. The four experimental studies included were Shing et al. (1988, 1990), Matsumura (1987), Okamoto et al. (1987), and Sveinsson et al. (1985). All experimental studies used cyclic, displacement-controlled loading histories characterized by increasing amplitudes until failure of the wall specimen was induced. All of the walls included by Fattal and Todd in their dataset failed in the shear mode.

Fattal and Todd compared previously-developed shear equations from four difference sources. The first equation was developed and reported by Shing et al. (1988, 1990) based on their tests conducted at the University of Colorado at Boulder. The second equation was developed and reported by Matsumura (1987) based on his other masonry shear wall tests conducted in Japan. The third equation was prescribed by the Architectural Institute of Japan (AIJ) and was examined by Okamoto et al. (1987) to test its validity for predicting masonry shear wall strength. The fourth equation was from the 1988 edition of the Uniform Building Code then in use to provide a lower bound for the shear capacity of masonry walls (NEHRP, 1997).

Fattal and Todd standardized the four equations to use the same notation and segmented each equation into the respective masonry, horizontal reinforcement, and axial load components. For equations which included the contribution of the vertical reinforcement, this contribution was grouped together with the masonry strength component. Each equation was used to predict the shear strength of all 62 of the test specimens to compare them with the experimental results. Actual, measured dimensions and material strengths were used in each equation. The experimental

strength considered for each specimen was the average of the peak ultimate strengths for both loading directions (i.e., push and pull).

Fattal and Todd found that the UBC equation is not adequate in predicting masonry shear strength. They determined that the performance of the AIJ equation is not as consistent as that for the Matsumura and Shing et al. equations and concluded that the AIJ equation gave too much weight to the contribution of the interior vertical reinforcement. They observed that the performance of the Shing et al. equation was good for only a limited range of variables because it had a tendency to over-predict the contribution of the horizontal shear reinforcement. They concluded that the Matsumura equation generally produced predicted values closest to the actual values, but it also displayed inconsistency due to the parametric form of the horizontal shear reinforcement. They proposed that the form of the horizontal reinforcement parameter in the Matsumura equation be adjusted and all the coefficient values be re-evaluated.

12.1.7 Anderson and Priestley

Anderson and Priestley (1992) assembled data from three primary sources: the University of California-Berkeley, the University of Colorado-Boulder, and the Building Research Institute of Japan. The Berkeley data was filtered down to those specimens tested by Sveinsson et al. (1985) because of uncertainty regarding the magnitude of the axial load at failure and the loading arrangement of the other tests. This uncertainty in the axial load magnitude was created by the tendency of the axial load to increase with higher levels of displacement induced by the loading arrangement. Anderson and Priestley felt that those tests from Mayes et al. (1976b) were unsuitable because double pier sections were tested and the shear strength values from these specimens represented the average from two piers. Anderson and Priestley included the data of twelve specimens from the Sveinsson et al. (1985) test.

Anderson and Priestley also included data from 16 of the 22 tests carried out by Shing et al. (1989) at the University of Colorado-Boulder. The Japanese tests were conducted by several researchers across Japan, particularly by Matsumura (1987) at Kanagawa University. Out of the extensive Japanese dataset, Anderson and Priestley selected 37 specimens to include in their analysis. They chose specimens which failed in the shear mode, including those specimens which also demonstrated characteristics of flexural or sliding failure.

Anderson and Priestley assume the shear strength is governed by the equation

$$V_u = V_m + V_v + V_p + V_s \tag{12.16}$$

where V_m is the masonry component, V_v is the vertical reinforcement component, V_p is the axial load component, and V_s is the horizontal reinforcement component. Each of the four components is given by

$$Vm = k_1 k_2 b_1 \sqrt{f'_m} l_w t \tag{12.17}$$

$$V_v = b_2 A_v f_{yv} \tag{12.18}$$

$$V_p = b_3 P \tag{12.19}$$

and

$$V_s = b_4 \frac{A_h}{s} f_{yh} l_w \tag{12.20}$$

where

k_1 = the aspect ratio coefficient,
k_2 = the ductility coefficient,
l_w = the length of the wall,
t = the thickness of the wall,
A_v = the area of vertical steel in the middle third of the wall,
f_{yv} = the yield strength of the vertical reinforcement,
A_h = the area of the horizontal reinforcement,
s = the vertical spacing of the horizontal reinforcement, and
f_{yh} = the yield strength of the horizontal reinforcement.

Anderson and Priestley determined the b parameters by fitting the above equation to the experimental data. They noted that the data were not sufficient to determine values for the k_1 and k_2 coefficients with any degree of confidence. They assumed k_1 to be unity for aspect ratios greater than one, which was the case for all of the wall specimens included within their analysis,

and assumed k_2 to also be unity. Their definition of aspect ratio was defined wholly on geometric dimensions and is not the same as the shear span ratio which is currently in use. Anderson and Priestley recommended that k_2 be equal to unity for a ductility factor up to 2 and that it should linearly decrease to zero at a ductility factor of 4.

Anderson and Priestley used a manual, iterative process to evaluate the fit of parameters to their dataset by varying the parameter values and comparing the calculated strength values to the experimental strength values. They initially chose parameters so as to minimize the sum of $(V_u - V_t)^2 / (V_u V_t)$ where V_t is the published shear strength. They determined that these values typically did not produce the minimum deviation of V_u/V_t from unity.

The optimum fit for the concrete block data, using their criterion, produced the four parameters

$$b_1 = 0.26, \qquad b_2 = 0.22, \qquad b_3 = 0.0, \qquad and \qquad b_4 = 0.54\,.$$

The values that minimized the deviation of the data about $V_u/V_t = 1$ are given by

$$b_1 = 0.24, \qquad b_2 = 0.25, \qquad b_3 = 0.0, \qquad and \qquad b_4 = 0.50\,.$$

They included these later values into Equation (12.16) to produce the concrete block shear strength equation given by

$$V_{ubl} = 0.24\sqrt{f'_m} l_w t + 0.25P + 0.50\frac{A_h}{s} f_{yh} d \tag{12.21}$$

Inspection of this equation reveals that at some point in their report they transposed the parameters b_2 and b_3 from how they were initially defined. Following the same procedure to find the parameters for the brick data produced the equation

$$V_{ubr} = 0.12\sqrt{f'_m} l_w t + 0.25P + 0.50\frac{A_h}{s} f_{yh} d \tag{12.22}$$

for the strength of brick shear walls.

The approach employed by Anderson and Priestley had the appearance of least squares regression because they sought to minimize the sum of the squares of the error—the difference between V_u and V_t. Their dividing of the square of the error by the product of the two terms appears to be an attempt to account for the otherwise heteroscedastic nature of the equation and data. The heteroscedasticity of the data come from the fact that the variance increases with increasing V_t. With limited explanation about the methodology used to calculate their coefficient values, it appears that they used an interative "guess-and-check" methodology to find their parameter coefficient values. The exact values could have been found explicitly using the multivariate least-squares regression approach given by Equation (3.36). However, to solve the equation explicitly, they would have needed to set up their problem in mathematically terms consistent with the assumptions of least-squares regression.

The goal of their analysis was to find the solution for the parameters in Equation (12.16) that best fit the data and minimized the error. To do so, one would consider the error ε from the vector equation

$$\boldsymbol{v}_t = \boldsymbol{v}_u + \boldsymbol{\varepsilon} \tag{12.23}$$

which is equivalent to

$$\boldsymbol{\varepsilon} = \boldsymbol{v}_t - \boldsymbol{v}_u \tag{12.24}$$

The explicit solution can be found by minimizing the sum of the errors

$$\begin{aligned} \boldsymbol{\varepsilon}'\boldsymbol{\varepsilon} &= (\boldsymbol{v}_t - \boldsymbol{v}_u)' (\boldsymbol{v}_t - \boldsymbol{v}_u) \\ &= \sum (v_t - v_u)_i^2 \end{aligned}$$

Instead, Anderson and Priestley (1992) assumed the error term was given by

$$\sum \frac{(v_t - v_u)_i^2}{(v_u v_t)_i} \tag{12.25}$$

and by so doing were actually finding the parameters that solved the equation

$$\frac{v_t}{\sqrt{v_u v_t}} = \frac{v_u}{\sqrt{v_u v_t}} + \varepsilon \tag{12.26}$$

or, in other terms,

$$\sqrt{\frac{v_t}{v_u}} = \sqrt{\frac{v_u}{v_t}} + \varepsilon \tag{12.27}$$

This transformation cannot be solved explicitly. Their choice of terms to minimize the fit to data produced the unintended consequence of finding solutions for a different equation from what they were trying to solve.

Anderson and Priestley noted that their error term did not produce the minimum variance for the difference between V_u/V_t and unity. To achieve this goal would have necessitated that they have chosen the error term as

$$\varepsilon = \frac{v_u}{v_t} - 1 \tag{12.28}$$

which is not equivalent to their initial choice in Equation (12.25) because

$$\left(\frac{v_u}{v_t} - 1\right)^2 = \frac{v_u^2}{v_t^2} - 2\frac{v_u}{v_t} + 1 \neq \frac{v_u}{v_t} + \frac{v_t}{v_u} - 2 = \frac{(v_t - v_u)^2}{v_u v_t} \tag{12.29}$$

This latter choice in error term is equivalent to determining the parameters for the equation

$$1 = \frac{v_u}{v_t} + \varepsilon \tag{12.30}$$

which is a reparameterization of the original model presented in Equation (12.16).

The reparameterized equation has the benefit of removing heteroscedasticity from the model by eliminating the correlation between the strength and the variance. This equation can also be solved explicitly using linear least-squares regression. However, the quotient $\frac{v_u}{v_t}$ has a normal ratio distribution and, depending on how the distribution differed from the normal distribution, could have conflicted with the normality assumption requirement of least squares regression. In

either case, the regression still would produces estimates of the parameters, but if the departure of the ratio distribution of the quotient $\frac{v_u}{v_t}$ from normality is too great, then the resulting coefficient estimates could not be guaranteed to have minimum variance. Additionally, the parameters and variance would not be jointly sufficient to fully describe the model, which would run counter to the purpose of the analysis. From a statistical standpoint, it would have been better for them to transform their data by dividing it by the shear area and/or masonry compressive strength, as was done by Matsumura (1987).

12.1.8 Fattal

Fattal (1993) performed a study of 72 tests on partially-grouted walls from three different studies. He selected 51 wall tests performed by Matsumura (1987), 11 tests performed by Chen et al. (1978), and 10 tests performed by Yancey and Scribner (1989). All of the walls Fattal chose to include in his analysis were tested with fixed-fixed boundary conditions, in which the top and bottom bed joints were kept parallel throughout the whole test. All of the walls were tested under displacement-controlled, cyclic-loading conditions where the drift amplitude was gradually increased until shear failure was observed. Fattal included both clay masonry and concrete masonry samples in his study.

Each test specimen had two shear failure strengths, one for each direction. Fattal used the average of the two shear strengths to represent the ultimate shear strength for each wall. Fattal further excluded wall specimens from his study that appeared to have failed in flexure. Each researcher performed masonry prism tests to determine the compressive strength of the masonry used in their respective wall specimens.

The purpose of the Fattal study was to examine the validity of the Matsumura equation for masonry shear wall strength to partially-grouted walls and, if necessary, make improvements to it. He took the test parameters from each wall specimen and put them into Matsumura's equation to find the predicted strength for each wall. Fattal then used linear regression to compare the predicted and measured strengths for each researcher and for the data as a whole. Additionally, Fattal investigated the effects of axial load, aspect ratio, horizontal reinforcement ratio, and compressive strength.

Fattal concluded that the Matsumura equation correlated well with the data set from his own study, but that the correlation varied when applied to data sets from other researchers. The equation showed poor correlation for walls without vertical reinforcement and could not be used at all for unreinforced walls. In all, the predicted strengths from the Matsumura equation varied from 23 to 180 percent of the measured strength, with less than half falling within ±20 percent. For most of the samples, the regression line for the scatter plot showed that the equation was unconservative in predicting shear strength. Fattal made improvements to the Matsumura equation, which is given by

$$\begin{aligned} v_n &= v_m + v_s + v_p \\ &= \left\{ k_u k_0 \left(\frac{0.5}{\left(\frac{h}{d}\right)+0.8} + 0.018 \right) \rho_v^{0.7} \sqrt{f'_{m(g)} f_{yv}} \right. \\ &\qquad +0.011 k_0 \gamma \delta f_{yh} \rho_h^{0.31} \\ &\qquad \left. +0.012 f'_m + 0.2\sigma_{0(g)} \right\} 0.875 t\, d_v \end{aligned} \tag{12.31}$$

where

v_n = predicted ultimate masonry shear strength (MPa),

k_0 = 1.0 for fully-grouted masonry,

= 0.6 for partially-grouted masonry,

k_u = 1.0 for fully-grouted masonry,

= 0.8 for partially-grouted brick masonry,

= 0.64 for partially-grouted concrete masonry,

k_p = $1.16\rho_{ve}^{0.3}$,

h = height of wall,

d_v = effect depth of wall,

$f'_{m(g)}$ = fully-grouted compressive strength of masonry (MPa),

$\sigma_{0(g)}$ = axial stress for gross wall area (MPa),

γ = 1.0 for fully-grouted masonry,

= 0.6 for partially-grouted masonry,

δ = 1.0 for fixed-fixed (double bending) type loading,

= 0.6 for cantilever (single bending) type loading,

ρ_h = horizontal reinforcement ratio,

f_{yh} = yield strength of horizontal reinforcement (MPa), and

ρ_{ve} = effective vertical reinforcement ratio.

His new equation predicted strengths from 43 to 146 percent of measured strength, with 68 percent of the specimens falling within the ±20 percent interval. Fattal labeled his equation as a "first step" and stated that it would need to be compared with future data sets in order to establish its validity.

12.1.9 TCCMaR

The Technical Coordinating Committee on Masonry Research (TCCMaR) considered the proposed equations from Matsumura (1987), the Architectural Institute of Japan (Okamoto et al., 1987), Blondet et al. (1989), Shing et al. (1990), and Anderson and Priestley (1992) in developing a new shear equation for predicting the ultimate shear strength of U.S. masonry. These equations were scrutinized in light of the research performed as part of the TCCMaR program. The equations were compared to the results of 62 masonry shear wall specimens from four experimental studies: Sveinsson et al. (1985), Matsumura (1987), Okamoto et al. (1987), and Shing et al. (1988). These appear to be the same 62 specimens considered by Fattal and Todd (see Section 12.1.6).

The TCCMaR members decided to use components from the Blondet et al. (1989) and Anderson and Priestley (1992) equations. The Blondet et al. (1989) form was used for the masonry strength component because the UC-Berkeley studies (Mayes et al., 1976b,c; Chen et al., 1978; Hidalgo et al., 1978, 1979; Sveinsson et al., 1985) concluded that the shear span ratio M/Vd was influential to the masonry shear strength and that it should be included in the equation. TCCMaR determined that there was little numerical difference between the two forms of the axial force component, so they chose the Anderson and Priestley (1992) form of $0.25P$. Both Blondet et al. (1989) and Anderson and Priestley (1992) used a coefficient of 0.5 for the horizontal reinforcement contribution. The final form of the TCCMaR equation for shear strength prediction is given for imperial units by

$$v_n = \left(4 - 1.75\frac{M}{Vd}\right)\sqrt{f'_m} + 0.5\rho_h f_{yh} + 0.25\sigma_0 \tag{12.32}$$

and for SI units by

$$v_n = 0.083\left(4 - 1.75\frac{M}{Vd}\right)\sqrt{f'_m} + 0.5\rho_h f_{yh} + 0.25\sigma_0 \tag{12.33}$$

The TCCMaR study investigated whether the vertical reinforcement contributed to the overall shear strength. Two values were considered for the vertical reinforcement contribution: $0.25\rho_v f_{yv}$ and $0.25\rho_{vi} f_{yv}$. The first value considered the ratio for all vertical reinforcement ρ_v and the second value considered the ratio for only the interior vertical reinforcement ρ_{vi} (neglecting the flexural reinforcement in the end cells). They determined that the correlation of the equation with the experimental data was not as good when either of their forms for the vertical reinforcement contribution was included in the equation.

The reason the vertical reinforcement was neglected was likely not because it wasn't influential, but because the original equation from Blondet et al. (1989) did not consider the contribution from vertical reinforcement. Depending on the method of analysis performed on the data from Anderson and Priestley (1992), the vertical reinforcement can have a statistically significant contribution to the shear strength; however, Anderson and Priestley (1992) likely did not find this contribution to be significant because of their analysis methods. In both cases, the coefficients they chose where likely not compatible with the inclusion of an additional parameter for vertical reinforcement, therefore adding in the vertical reinforcement contribution would artificially inflate the errors and make the correlation appear worse. If the equation parameter coefficients had been determined through multivariate regression, then the addition of a parameter for the vertical reinforcement could not have made the correlation worse. This is because the addition of an additional parameter to a linear regression can never make the correlation worse, it can only improve the correlation or have no effect (Rencher and Schaalje, 2008). The proper method to judge whether a parameter should be included is to build a model with the parameter included and to inspect whether the parameter's p-value is statistically significant.

12.2 Discussion

Equation (12.32) developed by the TCCMaR members is the basis for the current shear equation in the MSJC code. The MSJC equation differs only by specifying upper limits for the

predicted strength which were taken from the UBC and, recently, by incorporating a factor to account for the effect of partial grouting. The TCCMaR equation, and hence the MSJC equation, suffers from the same limitations as the other equations developed by Blondet et al. (1989), Shing et al. (1990), and Anderson and Priestley (1992). These equations are all promoted as being empirical equations developed from experimental research data. Though the equations were developed in light of the experimental data, only the masonry contribution portion of each equation can be classified as being empirical.

An empirical equation is one that is developed *solely* from observations or experimental data (OED, 2013). For each of the equations to be classified as being empirical, the coefficient for each parameter in the equation should have been determined through multivariate regression analysis based on the experimental observations (or data). In reality, many researchers determined the coefficients for all parameters but the masonry contribution based on assumptions made using logic, theory of mechanics, and engineering judgment without the influence of the experimental data. Unfortunately, no researchers attempted to validate their assumptions with the experimental data.

Anderson and Priestley (1992) differed from the other researchers in that they attempted to use optimization to implicitly estimate the coefficients for the entire model. Their approach was good but was unable to surmount two obstacles to produce the best estimates for their parameter coefficients (i.e., those with minimum variance). Since the coefficients for all of the parameter values are jointly distributed, one parameter value could not be changed without influencing the others. Using their manual, iterative process would have made it difficult to implicitly solve for the coefficient values because they would have changed with each iteration. Though the solution could have equally been found by using optimization techniques or multivariate least-squares regression, it appears that they may not have had familiarity with these tools. Second, the error models they used would have given disproportionately larger influence to some specimens than to others.

In summary, the current MSJC equation was developed based on the equations of previous researchers, each using a different approach and dataset. Though the equation showed a relatively good fit for a relatively small set of data from four studies, until now it has never been fully vetted against a larger, comprehensive dataset. Linear least squares regression produces unbiased coefficient estimates with minimum variance, but no researchers have used this approach in developing

their models. Many of the researchers showed some understanding of the principles of least squares fit and of bivariate regression, but it is not apparent that any of them understood that the tools that could determine the correlation between a bivariate pair of data might also be used for a multivariate case. This is unfortunate considering that this method had already been well-understood and employed for many decades prior to these studies.

CHAPTER 13. LINEAR MODELING METHODOLOGY

13.1 Introduction

This chapter explains the methodology undertaken in building and fitting models to the experimental data. The theoretical principles employed in fitting a linear model to data using least-squares regression are detailed in Chapter 3 and Appendix B. The first steps of this analysis are to refit the models of Blondet et al. (1989) and Anderson and Priestley (1992) and their respective datasets to determine what values they would have obtained had they used multivariate regression in their analysis. This will provide a means of examining the effectiveness of the parameters they chose and provide a starting point for the development of the parameters for the subsequent analysis. The results of these two analyses will be used to more accurately gauge the results of the subsequent analysis without the bias caused by their simplifying assumptions.

The second part of this analysis will be to develop different models and to compare how each of these models fits to the dataset. There are multiple parameters that can be developed from the different mechanical theories for masonry. Each of these parameters can be combined in multiple ways to produce different models. These models will be fitted and compared to determined which should be selected as the final model.

13.2 Analysis of Old Model

The current predictive model in the MSJC code was developed by TCCMaR members based on the models proposed by Blondet et al. (1989) and Anderson and Priestley (1992). A careful review of these models revealed that they were not developed using multivariate linear regression, but were developed using the methods and assumptions explained in Chapter 12. As these models have been around now for over two decades, members of the masonry community may be naturally biased against any proposed model that departs from what they have previously

developed. It was important to reanalyze their parameters and data to determined what coefficient values they would have obtained if they had used the same multivariate linear regression methods as those to be used in this dissertation. The results of this analysis provided an objective means to scrutinize their final models by comparing them with the new models developed in Chapter 14.

The data used in this analysis were taken directly from their respective reports and were separate from the dataset created for this study and detailed in Chapter 6. The dataset for the Blondet et al. model is given in Table 13.1 and was taken directly from Tables H-1 and H-2 in Blondet et al. (1989). The only difference from the original table is the addition of a column for the reinforcement yield strength f_y, which they stated as being $60,000$ psi. The dataset for the Anderson and Priestley model is given in Table 13.2 and was take directly from Table 1 in Anderson and Priestley (1992). Some of the variable notation was changed to avoid confusion with other variables in use herein and blank or unused columns and rows were omitted for sake of presentation. Blondet et al. (1989) and Anderson and Priestley (1992) had both previously narrowed their datasets down to those specimens which failed in one of the shear modes, so no further scrutiny of their published datasets was necessary. The dataset from Blondet et al. was given in imperial units and was not converted to SI units so that the masonry contribution coefficients calculated in this analysis could be directly compared to those that they determined.

Each of the models from Blondet et al. and Anderson and Priestley were first fitted to the respective datasets using the parameters and data as provided in the original reports. In the case of Blondet et al. (1989), the model parameters had units of stress because the data was normalized by the gross area of each specimen. The Anderson and Priestley (1992) model was analyzed using units of force. However, the two forms of error terms they used in their analysis were normalized by either the square root of the product of the experimental and calculated forces or by the experimental force. As noted earlier in Section 12.1.7, the first error term cannot be solved explicitly using least-squares linear regression and Anderson and Priestley discontinued the use of this term because models fitted with this scheme did not meet their optimization criterion. The Anderson and Priestley data was analyzed twice, once for their original model and a second time using their second error term.

The two models from Blondet et al. and Anderson and Priestley were compared to the final TCCMaR model (NEHRP, 1997) using the dataset from Fattal and Todd (1991). The Fattal

Table 13.1: Summary of Experimental Data (Adapted from Blondet et al. 1989)

Specimen	M/Vd	ρ_c (%)	ρ_h (%)	f'_m (psi)	f_y (psi)	v_{cr} (psi)	f_a (psi)	v_u (psi)
HCBL 21-1	1.00	0.92	0.00	2432	60000	144	67	135
HCBL 21-3	1.00	0.42	0.00	2256	60000	152	68	145
HCBL 21-5	1.00	0.92	0.00	2592	60000	114	-145	106
HCBL 21-7	1.00	0.92	0.24	2805	60000	226	-37	212
HCBL 21-9	1.00	0.00	0.00	2519	60000	164	292	154
HCBL 11-1	0.50	0.17	0.00	1330	60000	135	120	123
HCBL 11-3	0.50	0.17	0.00	1833	60000	134	69	127
HCBL 11-4	0.50	0.17	0.07	1833	60000	171	107	165
HCBL 11-5	0.50	0.43	0.29	1833	60000	226	144	199
HCBL 11-7	0.50	0.43	0.00	1905	60000	180	91	146
HCBL 11-9	0.50	0.43	0.15	1905	60000	155	114	146
HCBL 11-11	0.50	0.17	0.41	1330	60000	240	139	231
HCBL 11-13	0.50	0.17	0.29	1357	60000	223	273	283
HCBL 11-15	0.50	0.45	0.29	1357	60000	236	437	345
HCBL 11-17	0.50	0.45	0.39	2829	60000	241	400	357
HCBL 11-18	0.50	0.44	0.39	2829	60000	299	400	357
HCBL 11-19	0.50	0.45	0.39	2381	60000	270	252	330
HCBL 11-20	0.50	0.45	0.20	2381	60000	245	400	342
HCBL 11-21	0.50	0.45	0.20	2381	60000	220	400	324
HCBL 11-22	0.50	0.44	0.20	2381	60000	134	100	227
HCBL 11-23	0.50	0.45	0.10	2381	60000	222	400	278
HCBL 11-24	0.50	0.45	0.30	2381	60000	222	400	353
HCBL 11-25	0.50	0.45	0.20	2381	60000	244	252	385
HCBL 11-26	0.50	0.45	0.20	2381	60000	319	400	349
HCBL 12-1	0.25	0.30	0.00	2988	60000	200	85	310
HCBL 12-2	0.25	0.30	0.10	2988	60000	206	86	330
HCBL 12-3	0.25	0.30	0.20	2988	60000	215	83	398
HCBL 12-4	0.25	0.30	0.30	2988	60000	261	127	344
HCBL 12-5	0.25	0.30	0.40	2988	60000	226	106	361
HCBL 12-6	0.25	0.30	0.58	2988	60000	244	102	413
HCBR 21-1	1.00	0.00	0.00	4502	60000	267	580	244
HCBR 21-2	1.00	0.51	0.00	4502	60000	238	368	206
HCBR 21-4	1.00	0.51	0.11	4502	60000	308	415	273
HCBR 21-6	1.00	0.51	0.16	4502	60000	343	492	317
HCBR 21-8	1.00	0.51	0.21	4502	60000	346	485	321
HCBR 21-9	1.00	0.51	0.26	4502	60000	348	476	307

Table 13.1: Summary of Experimental Data (Continued)

Specimen	M/Vd	ρ_c (%)	ρ_h (%)	f'_m (psi)	f_y (psi)	v_{cr} (psi)	f_a (psi)	v_u (psi)
HCBR 11-1	0.50	0.00	0.00	2535	60000	278	328	255
HCBR 11-3	0.50	0.18	0.00	2535	60000	279	148	267
HCBR 11-4	0.50	0.18	0.08	2722	60000	353	323	337
HCBR 11-6	0.50	0.18	0.38	2722	60000	346	175	328
HCBR 11-7	0.50	0.18	0.38	2535	60000	280	241	267
HCBR 11-8	0.50	0.45	0.00	2866	60000	242	123	227
HCBR 11-10	0.50	0.45	0.15	2722	60000	296	153	287
HCBR 11-12	0.50	0.45	0.53	2535	60000	275	240	266
HCBR 11-13	0.50	0.45	0.53	2722	60000	329	312	320
HCBR 11-15	0.50	0.17	0.37	3781	60000	284	452	334
HCBR 11-17S	0.50	0.17	0.37	3781	60000	184	282	272
HCBR 11-19	0.50	0.45	0.20	2957	60000	216	400	267
HCBR 11-20	0.50	0.45	0.49	2957	60000	201	400	278
HCBR 11-21	0.50	0.45	0.20	2957	60000	256	400	341
HCBR 11-22	0.50	0.45	0.49	2957	60000	284	400	348
HCBR 11-23	0.50	0.44	0.20	2957	60000	214	400	295
HCBR 11-24	0.50	0.44	0.49	2957	60000	213	400	320
HCBR 11-25	0.50	0.45	0.20	2957	60000	283	400	316
HCBR 11-26	0.50	0.45	0.49	2957	60000	254	400	311
HCBR 11-27	0.50	0.45	0.25	2957	60000	240	400	327
HCBR 11-28	0.50	0.23	0.62	2957	60000	306	400	330
HCBR 11-30	0.50	0.45	0.10	4306	60000	391	400	391
HCBR 12-2	0.25	0.31	0.15	2838	60000	319	125	318
HCBR 12-3	0.25	0.31	0.30	2838	60000	351	150	368
HCBR 12-4	0.25	0.31	0.45	2838	60000	356	143	427
HCBR 12-5	0.25	0.31	0.60	2838	60000	394	154	389
HCBR 12-6	0.25	0.31	1.02	2838	60000	392	153	437

and Todd dataset was used so that there would be a common metric to analyze and compare the results from the three models. The columns from the Fattal and Todd dataset applicable to the three models are given in Table 13.3. The analysis was first performed to determine the goodness-of-fit statistics for each of the three models using the originally proposed coefficient values. The three models were also analyzed using multivariate linear regression to determine the coefficients with the smallest variance. The TCCMaR model was also analyzed with the addition of a parameter for the vertical reinforcement component to validate whether this parameter should have been removed from the final TCCMaR model.

Table 13.2: Summary of Experimental Data (Adapted from Anderson and Priestley 1992)

Specimen	V_t (kN)	f'_m (MPa)	l_w (mm)	t (mm)	A_c (mm^2)	d' (mm)	f_{yc} (MPa)	A_v (mm^2)	s_v (mm)	f_{yv} (MPa)	P (kN)
B-1	462	23.9	1219	194	0	76	765	198	284	407	445
J-24	506	22.3	1190	190	398	95	372	254	200	340	444
J-10	462	13.7	1190	190	398	95	330	254	200	350	288
J-19	441	22.3	1190	190	398	95	384	127	400	351	444
S-13	500	22.8	1829	143	855	102	448	127	400	462	287
S-14	467	22.8	1829	143	855	102	448	71	400	386	287
S-9	427	20.7	1829	143	594	102	441	71	400	386	287
S-11	409	22.1	1829	143	1164	102	496	127	400	462	0
S-2	403	20.0	1829	143	594	102	441	128	400	386	287
S-15	391	22.8	1829	143	855	102	448	127	400	462	180
S-1	367	20.0	1829	143	594	102	441	127	400	462	361
S-12	316	22.1	1829	143	594	102	441	127	400	462	180
S-10	203	22.1	1829	143	594	102	441	71	400	386	180
S-6	220	17.9	1829	143	594	102	441	71	400	386	0
S-8	216	20.7	1829	143	594	102	441	127	400	462	0
B-2	562	23.9	1219	194	0	76	465	198	284	407	713
B-3	430	12.2	1219	143	0	76	391	198	284	438	481
B-4	429	12.2	1219	143	508	76	410	198	284	438	481
B-10	424	13.9	1219	143	0	76	391	198	474	438	481
B-12	420	13.9	1219	143	0	76	391	198	474	438	481
B-6	411	13.9	1219	143	0	76	391	198	474	438	481
B-5	397	13.9	1219	143	0	76	391	198	284	438	303
B-7	390	13.9	1219	143	508	76	410	198	474	438	481
B-11	343	13.9	1219	143	0	76	391	198	474	438	300
B-9	334	13.9	1219	143	0	76	391	110	203	207	481
J-16	637	22.3	1190	190	398	95	372	254	200	340	444
J-29	616	33.3	1300	199	398	95	372	99	300	355	508
J-52	594	27.5	1190	190	398	95	348	127	200	359	444
J-33	592	22.9	1190	190	398	95	382	127	400	355	1331
J-54	587	31.4	1190	190	398	95	348	127	200	359	444
J-28	575	29.6	1300	190	398	95	372	99	300	355	508
J-135	560	24.6	1190	199	398	95	372	127	400	359	444
J-55	548	29.0	1190	190	398	95	348	127	200	359	444
J-32	544	22.9	1190	190	398	95	372	127	400	355	887
J-27	509	22.3	1190	190	398	95	372	127	200	340	444
J-53	507	26.5	1190	190	398	95	348	127	200	359	350
J-23	502	22.3	1190	190	398	95	372	127	200	340	444
J-50	495	26.2	1190	190	398	95	348	127	200	359	444
J-51	485	26.2	1190	190	398	95	348	127	200	359	444
J-21	448	22.3	1190	190	398	95	372	127	400	340	444

Table 13.2: Summary of Experimental Data (Continued)

Specimen	V_t (kN)	f'_m (MPa)	l_w (mm)	t (mm)	A_c (mm^2)	d' (mm)	f_{yc} (MPa)	A_v (mm^2)	s_v (mm)	f_{yv} (MPa)	P (kN)
J-20	445	22.9	1190	190	398	95	372	127	400	355	444
J-31	434	22.3	1190	190	398	95	384	127	400	351	444
J-22	430	22.3	1190	190	398	95	384	127	400	351	444
J-26	429	22.3	1190	190	398	95	384	127	400	351	444
J-15	419	17.4	1190	190	398	95	384	127	400	351	444
J-18	384	22.3	1190	190	398	95	384	127	400	34	444
J-9	386	13.7	1190	190	398	95	330	127	200	350	177
J-30	379	22.3	1190	190	398	95	384	0	400	0	444
J-8	361	21.6	1190	190	398	95	323	127	400	355	111
J-5	360	21.6	1190	190	398	95	323	127	400	355	111
J-7	358	21.6	1190	190	398	95	323	127	400	355	111
J-17	328	22.3	1190	190	398	95	372	0	400	0	444
J-25	307	18.0	790	190	199	95	372	127	400	355	294
S-16	536	17.2	1829	143	1164	102	496	127	400	462	487
S-3	456	20.7	1829	143	1164	102	496	71	400	386	487
S-7	431	20.7	1829	143	1164	102	496	71	400	386	180
S-5	385	17.9	1829	143	1164	102	496	71	400	386	180
S-4	354	17.9	1829	143	1164	102	496	71	400	386	0
J-1	357	22.9	1190	190	389	95	323	127	400	355	111
J-4	387	33.3	1300	199	398	95	323	199	150	355	127
J-2	379	21.6	1190	190	398	95	323	254	200	355	111
J-3	378	29.6	1300	199	398	95	323	199	150	355	127
J-6	373	21.6	1190	190	398	95	323	254	200	355	111
J-134	525	24.6	1190	190	398	95	323	127	400	355	111
B-8	273	13.9	1219	143	0	76	391	198	474	438	120

13.3 New Model Development

13.3.1 Formatting of Data

The dataset used in the second part of the analysis was constructed using the methodology detailed in Chapter 6. The results of this analysis are focused primarily on an audience of American masonry professionals, the masonry compressive strength as defined by ASTM C1314 was used for the f'_m values. Since the dataset values for the compressive strength used the standardized strength of prisms with aspect ratio of 5.0, the values from this field were divided by the correction factor 0.82 to obtain the equivalent strength for prisms with an aspect ratio of 2.0 as specified in

Table 13.3: Summary of Experimental Data (Adapted from Fattal and Todd 1991)

Specimen	f'_m (MPa)	f_{yh} (MPa)	f_{yv} (MPa)	ρ_h (%)	ρ_c (%)	σ_0 (MPa)	$\frac{M}{Vd}$	V_u (MPa)
3-S	20.87	385.84	496.08	0.122	0.687	1.88	1.0	1.74
4-S	17.91	385.84	498.08	0.122	0.887	0.	1.0	1.35
5-S	17.91	385.84	498.08	0.122	0.887	0.89	1.0	1.47
7-S	20.87	385.84	496.08	0.122	0.887	0.89	1.0	1.65
9-S	20.67	385.84	440.98	0.122	0.344	1.88	1.0	1.63
13-S	22.74	461.63	447.85	0.222	0.489	1.88	1.0	1.91
14-S	22.74	385.84	447.85	0.122	0.489	1.88	1.0	1.79
16-S	17.23	481.83	498.08	0.222	0.887	1.86	1.0	2.05
21-S	26.18	385.84	447.85	0.128	0.512	1.93	1.0	1.79
22-S	26.18	385.84	447.85	0.128	0.512	0.69	1.0	1.56
KW4-1-M	21.80	385.00	385.00	0.118	0.134	0.49	0.5	1.60
KW3-1-M	21.80	385.00	385.00	0.118	0.140	0.49	0.5	1.72
KW3S-1-M	21.80	385.00	385.00	0.118	0.140	0.49	0.5	1.87
KW2-1-M	21.80	385.00	385.00	0.118	0.155	0.49	0.5	1.61
WS2-M	22.30	385.00	385.00	0	0.111	1.98	0.5	1.70
WS4-M	22.30	385.00	385.00	0.187	0.111	1.98	0.5	1.89
WSS-M	22.30	385.00	385.00	0.334	0.111	1.98	0.5	2.28
WS9-M	22.30	385.00	385.00	0.334	0.111	1.98	0.5	2.29
WS10-M	22.30	385.00	385.00	0.888	0.111	1.98	0.5	2.93
WS9-2-M	29.00	385.00	385.00	0.334	0.111	1.98	0.5	2.59
WSB21-M	28.10	385.00	385.00	0.334	0.111	1.96	0.5	2.24
WSB22-M	27.40	385.00	385.00	0.400	0.111	1.98	0.5	2.63
WSB3-M	26.40	385.00	385.00	0.353	0.117	1.98	0.5	2.43
WSB4-M	31.40	385.00	385.00	0.334	0.111	1.98	0.5	2.59
WSR2-M	28.60	385.00	385.00	0	0.121	1.98	0.5	2.18
WSR4-M	28.80	385.00	385.00	0.167	0.121	1.96	0.5	1.95
WSRS-M	28.60	385.00	385.00	0.334	0.121	1.96	0.5	1.71
WSR6-M	28.80	385.00	385.00	0.888	0.121	1.98	0.5	2.04
WS1-O	17.91	354.44	371.18	0.167	0.292	0.	0.5	2.68
WS4-O	22.81	354.44	371.18	0.167	0.318	1.98	0.5	1.97
WS7-O	17.91	354.44	371.18	0.187	0.351	0.	0.5	2.04
WSN1-O	22.81	354.44	371.18	0.187	0.318	3.92	0.5	2.40
WSN2-O	22.81	354.44	371.18	0.167	0.318	5.87	0.5	2.61
WSR1-O	28.73	354.44	363.05	0.187	0.292	0.	0.5	3.12
WSR4-O	25.16	354.44	371.18	0.187	0.318	0.	0.5	2.32
WSR7-O	21.35	354.44	371.18	0.167	0.351	0.	0.5	2.04
WSRC-O	28.73	354.44	371.18	0.187	0.316	2.15	0.5	2.18
CB13-B	23.14	408.51	465.08	0.281	0	1.88	0.5	1.95

Table 13.3: Summary of Experimental Data (Continued)

Specimen	f'_m (MPa)	f_{yh} (MPa)	f_{yv} (MPa)	ρ_h (%)	ρ_c (%)	σ_0 (MPa)	$\frac{M}{Vd}$	V_u (MPa)
CB15-B	23.14	408.51	465.08	0.281	0	3.01	0.5	2.38
CB17-B	15.83	437.52	390.66	0.394	0	2.76	0.5	2.46
CB18-B	15.83	437.52	409.96	0.394	0.423	2.78	0.5	2.46
CB20-B	15.13	437.52	390.86	0.197	0	2.78	0.5	2.36
CB21-B	15.13	437.52	409.96	0.197	0.423	2.76	0.5	2.23
CB23-B	15.13	437.52	390.86	0.075	0	2.76	0.5	1.92
CB24-B	15.13	437.52	390.86	0.272	0	2.76	0.5	2.43
CB25-B	15.13	437.52	390.86	0.197	0	2.74	0.5	1.96
CB26-B	15.13	437.52	390.86	0.197	0	2.76	0.5	2.40
BR19-B	20.11	437.52	390.86	0.197	0	2.76	0.5	1.84
BR20-B	20.11	437.52	390.86	0.492	0	2.78	0.5	1.92
BR21-B	20.11	437.52	390.86	0.197	0.394	2.76	0.5	2.35
BR22-B	20.11	437.52	437.52	0.492	0.394	2.78	0.5	2.40
BR23-B	20.11	437.52	409.96	0.197	0.423	2.78	0.5	2.03
BR24-B	20.11	437.52	409.96	0.492	0.423	2.76	0.5	2.20
BR25-B	20.11	437.52	390.88	0.197	0	2.78	0.5	2.18
BR26-B	20.11	437.52	390.88	0.492	0	2.78	0.5	2.14
BR27-B	20.11	409.96	390.88	0.254	0	2.76	0.5	2.25
BR28-B	20.11	418.85	409.96	0.835	0	2.76	0.5	2.27
BR30-B	27.62	437.52	390.88	0.100	0	2.78	0.5	2.69
DBR8S-B	17.11	406.51	465.08	0.055	0	1.52	0.5	1.49
DBR9-B	17.11	465.08	465.08	0.277	0	2.29	0.5	1.63
DBR10-B	17.11	406.51	465.08	0.055	0	2.29	0.5	1.83
DBR12-B	17.11	398.24	465.08	0.059	0	2.29	0.5	1.88

ASTM C1314 (2014). The dataset and analysis were used with SI units to facilitate comparison of the results with other research.

13.3.2 Construction of Parameters Candidates

The first step of building and testing potential models to be analyzed through regression is to determine which parameters to use in constructing the models. This step is frequently not used or needed in common statistical analyses because they frequently use the experimental parameters directly in the model building process. This is not so in engineering empirical modeling because many of the experimental parameters do not directly influence the final value alone; rather, the pa-

rameters that influence the final value are often combinations of multiple parameters. Additionally, it is important in engineering formulae to maintain consistency amongst all of the parameters in the equation so that they can be related to some mechanical mechanism.

The potential parameters were constructed from combinations of the measured variables from each specimen using logic and the theory of mechanics. Parameters included in previous models were considered and new, previously unexamined parameters were also created and considered. The ease of testing different combinations of parameters coupled with the computing power available eliminated the constraint on how many parameters could be investigated in this analysis. A large number of variations for each parameter could be included and compared to determine which variation best described the masonry shear behavior. The large quantity and variety of specimens used in this analysis enabled the analysis to identify the parameter forms that best describes the wall behavior.

The various forms of each parameter form varied not only in which variables were included but also by which variable definition was considered. Several of the variables used to describe masonry shear walls are defined differently by many masonry standards around the world. Some variables with different definitions include shear length, shear area, height, aspect ratio, etc. One of the great powers of this analysis is the ability to build multiple parameters using each definition and to use the analysis to identify which definition best matches the experimental results.

The principal variations in the masonry strength contribution were given by differences in shear area definition and whether the masonry compressive strength or its root was used. All of the candidate variations for the masonry component are listed in Table 13.4. The influence of the axial load either acts independently of or in conjunction with the masonry compressive strength, as shown in Table 13.5. The rationale for the second parameter candidate is that the axial load acts by increasing friction across the cracks and that the crack friction coefficient is a function of the masonry compressive strength.

Each reinforcement parameter was constructed assuming that its strength contribution is a functions of its respective yield strength, spacing, and cross-sectional area at each location. Table 13.6 shows the contribution of the vertical reinforcement (neglecting the flexural reinforcement in the end cells) as a potential function of the full wall length, the flexural bar depth, or the distance between flexural bars. The contribution of the shear reinforcement was split between horizontal

bars embedded within bond beams and wire reinforcement embedded within the joints. These two terms were divided because it was felt that they might contribute differently because of the difference in placement and shape. Tables 13.7 and 13.8 show that the parameters for bond beam and joint reinforcement, respectively, are potentially functions of the height, various horizontal length definitions, or the smallest of the two dimensions.

Table 13.4: Parameter Candidates for the Masonry Component

Area Definition	Square root of prism strength	Prism strength
Gross area	$\sqrt{f'_m}\,A_g$	$f'_m\,A_g$
	$\sqrt{f'_m}\,A_g\,\dfrac{h_e}{l_w}$	$f'_m\,A_g\,\dfrac{h_e}{l_w}$
	$\sqrt{f'_m}\,A_g\,\min\left\{\begin{matrix}\dfrac{h_e}{l_w}\\ 1\end{matrix}\right.$	$f'_m\,A_g\,\min\left\{\begin{matrix}\dfrac{h_e}{l_w}\\ 1\end{matrix}\right.$
Bedded area	$\sqrt{f'_m}\,A_n$	$f'_m\,A_n$
	$\sqrt{f'_m}\,A_n\,\dfrac{h_e}{l_w}$	$f'_m\,A_n\,\dfrac{h_e}{l_w}$
	$\sqrt{f'_m}\,A_n\,\min\left\{\begin{matrix}\dfrac{h_e}{l_w}\\ 1\end{matrix}\right.$	$f'_m\,A_n\,\min\left\{\begin{matrix}\dfrac{h_e}{l_w}\\ 1\end{matrix}\right.$
Face Shell area	$\sqrt{f'_m}\,A_{fs}$	$f'_m\,A_{fs}$
	$\sqrt{f'_m}\,A_{fs}\,\dfrac{h_e}{l_w}$	$f'_m\,A_{fs}\,\dfrac{h_e}{l_w}$
	$\sqrt{f'_m}\,A_{fs}\,\min\left\{\begin{matrix}\dfrac{h_e}{l_w}\\ 1\end{matrix}\right.$	$f'_m\,A_{fs}\,\min\left\{\begin{matrix}\dfrac{h_e}{l_w}\\ 1\end{matrix}\right.$
Net Shear area	$\sqrt{f'_m}\,A_{nv}$	$f'_m\,A_{nv}$
	$\sqrt{f'_m}\,A_{nv}\,\dfrac{h_e}{l_w}$	$f'_m\,A_{nv}\,\dfrac{h_e}{l_w}$
	$\sqrt{f'_m}\,A_{nv}\,\min\left\{\begin{matrix}\dfrac{h_e}{l_w}\\ 1\end{matrix}\right.$	$f'_m\,A_{nv}\,\min\left\{\begin{matrix}\dfrac{h_e}{l_w}\\ 1\end{matrix}\right.$

Table 13.5: Parameter Candidates for Axial Component

Function	Parameter
Axial Load	P
Axial Strength and Load	$\sqrt{P\, f'_m\, A_g}$
	$\sqrt{P\, f'_m\, A_n}$
	$\sqrt{P\, f'_m\, A_{fs}}$
	$\sqrt{P\, f'_m\, A_{nv}}$

Table 13.6: Parameter Candidates for the Vertical Reinforcement Component

Length definition	Parameter
Full wall length	$\frac{A_c f_{vc}}{s_c}\, l_w$
Effective depth of flexural bars	$\frac{A_c f_{vc}}{s_c}\, d$
Distance between flexural bars	$\frac{A_c f_{vc}}{s_c}\, (2d - l_w)$

13.3.3 Treatment of Scedasticity

The MSJC shear strength equation, along with many other models intended for strength design methods, are presented in units of force because they are used with design loads, which are also in units of force. If a model with units of force was built and fitting using least-squares regression, then the model would demonstrate a heteroscedastic nature because the residuals would increase with increasing wall strength. This behavior is contrary to one of the assumptions of least squares regression which assumes that the variance is constant. There are many parameters which effect wall strength—such as geometry, size and distribution reinforcement, and axial load—and the specimens with the highest strength would have a disproportionately high influence (or leverage) on the results of the analysis. The heteroscedasticity within the model can be removed by transforming (i.e., normalizing) the data before performing the analysis.

Several researchers in the past have normalized their data by the shear area of each wall specimen. This approach was undertaken principally because allowable stress methods were pre-

Table 13.7: Parameter Candidates for the Horizontal Bar Reinforcement Component

Length definition	Parameter
Full wall length	$\frac{A_v f_{yv}}{s_v} l_w$
Effective depth of flexural bars	$\frac{A_v f_{yv}}{s_v} d$
Distance between flexural bars	$\frac{A_v f_{yv}}{s_v} (2d - l_w)$
Height of wall	$\frac{A_v f_{yv}}{s_v} h_g$
Height of inflectin point	$\frac{A_v f_{yv}}{s_v} h_e$
Smaller of h_g and l_w	$\frac{A_v f_{yv}}{s_v} \min \begin{Bmatrix} h_g \\ l_w \end{Bmatrix}$
Smaller of h_g and d	$\frac{A_v f_{yv}}{s_v} \min \begin{Bmatrix} h_g \\ d \end{Bmatrix}$
Smaller of h_g and $2d - l_w$	$\frac{A_v f_{yv}}{s_v} \min \begin{Bmatrix} h_g \\ 2d - l_w \end{Bmatrix}$

viously used in design and the design equations were in units of stress rather than force, as they are today. Dividing all parameters by the shear area of the wall helped to eliminate the influence of the wall size on the variance of the data. It still left the possibility of the variance being influenced by the strength of the materials, but this influence was minimized since most researchers used similar-strength materials for all of their specimens.

Several researchers have attempted to normalize their data by the experimentally measured shear strength—in effect they were trying to minimize the variance of the data around a unity ratio of experimental to theoretical strength. The ratio of the experimental to the theoretical strength is the quotient of two normally distributed variables and produces residuals with a right-skewed ratio distribution. The approach is simple but violates one of the assumptions of least-squares regression which assumes that the residuals are normally distributed. Using this normalization scheme may produce unbiased statistics, but they will not be sufficient to fully describe the nature of the data.

Table 13.8: Parameter Candidates for the Joint Wire Reinforcement Component

Length definition	Parameter
Full wall length	$\frac{A_j f_{vj}}{s_j} l_w$
Effective depth of flexural bars	$\frac{A_j f_{vj}}{s_j} d$
Distance between flexural bars	$\frac{A_j f_{vj}}{s_j} (2d - l_w)$
Height of wall	$\frac{A_j f_{vj}}{s_j} h_g$
Height of inflectin point	$\frac{A_j f_{vj}}{s_j} h_e$
Smaller of h_g and l_w	$\frac{A_j f_{vj}}{s_j} \min \left\{ \begin{array}{c} h_g \\ l_w \end{array} \right.$
Smaller of h_g and d	$\frac{A_j f_{vj}}{s_j} \min \left\{ \begin{array}{c} h_g \\ d \end{array} \right.$
Smaller of h_g and $2d - l_w$	$\frac{A_j f_{vj}}{s_j} \min \left\{ \begin{array}{c} h_g \\ 2d - l_w \end{array} \right.$

13.3.4 Weighting Criteria

Least-squares regression assumes that the variance is the same for all data in the analysis. All of the data in the dataset came from a multitude of studies and each study demonstrated a different amount of variance between its specimens and with those from other studies. This analysis overcame the disparities in variance through the use of weighted least-squares regression. The specimens in the dataset were grouped together by the research study which originally performed the experimental tests. For studies which conducted a larger number of tests, the specimens in that group were further divided into groups with similar characteristics.

The goal of the analysis is to determine a model which best estimates the true model—which is unknown. Without knowing the true model, it is not possible to calculate the residuals and variance of the data, but these statistics can be estimated by assuming that the given model is the true model. In performing each weighted analysis, it was assumed that the variance of the

specimens was constant within each group because the specimens within each group were tested by the same researchers using same test setup and similar materials. By making this assumption, the variance for the specimens for each group could be estimated directly from the residuals. The coefficient of variation for each group was calculated by dividing its standard deviation by the mean normalized experimental strength of its specimens.

The weighting chosen to use for each specimen in this analysis was the inverse of its group's coefficient of variance. This weighting scheme was chosen because it would 1) eliminate size effects, 2) give higher weights to those groups with lower coefficients of variation, and 3) provide a robust weighting method that was guaranteed to converge. It was felt that those groups with lower coefficients of variation more accurately followed the true model and should be given higher influence in determining the model's estimate.

The weights for each group were not known initially and it was not possible to calculate both coefficient estimates and weights explicitly. It was necessary to use an iterative process to first calculate coefficient estimates assuming equal weights for all specimens, from which the residuals and weights could then be determined. The calculated weights were then be substituted back into the analysis and the regression performed again to find improved estimates for the coefficients and weights. This process was repeated multiple times for each analysis until the coefficient estimates converged.

13.3.5 Selection of Model

Several criteria were used to determine which parameters to use in the final model. The first four models analyzed included all the parameter candidates normalized by each of the four shear area definitions. Each of these models were analyzed using stepwise regression to determine which parameters were best to include in subsequent model building. The two information criteria used in the stepwise regression analyses were the Akaike Information Criteria (AIC) and the Bayes Information Criteria (BIC). The models fitted using BIC identified which parameters were most influential in describing the data by narrowing the number of parameters down to the smallest number sufficient to describe the model. AIC was used because it tends to produce a larger number of parameters in the final model than does BIC (Chatterjee and Hadi, 2006), leaving more parameters which could be further investigated. This was important because the models were initially fitted

separately to the fully- and partially-grouted data and analysis using AIC had a higher chance of choosing parameters that were the same for the two grouting types.

Once the pool of parameter candidates was narrowed down to a smaller group, different model variations were analyzed using the whole dataset to determine the root mean square error and the R^2 value for each model. Additionally, the mean and variance for the residuals were calculated for each of the two grouting types. All of these statistics were calculated for each model using the weighting criteria detailed in Section 13.3.4. The goal of the analysis was to produce a model with the lowest values for the root mean square error and R^2 and to produce residual means and variances that were as close to equal as possible for the two grouting type subsets. Between the two sets of goals, the latter set was judged to be slightly more important than how well the model fit the data and some loss of fit was judged to be worth sacrificing to obtain it. If the means were equal between the fully- and partially-grouted subsets, then the model could be said to describe the nominal shear strength equally well for the two grouting types. If the variances were equal then it would eliminate the need to use separate resistance factors for the two grouting types.

The final criterion for consideration in constructing the final model was that it should be relatively simple and contain as few terms as possible. Since the final model was intended to be included in a design standard and to be used frequently by practicing engineers, acceptance of the model was prerequisite on being simple. The models developed by Matsumura (1987) was judged to be too complex for design work and were precluded in favor of the simpler models of Blondet et al. (1989) and Anderson and Priestley (1992). The goal of the proposed equation is to be simple enough for frequent use yet adequate enough to describe the shear behavior better than the current equation for both grouting types. It was intended that a more complex and accurate modeling procedure be developed in Part V of this dissertation.

13.3.6 Limit Criterion

The current MSJC (2013) shear model places an upper constraint on the shear strength values calculated from the model. This constraint is a function of the prism strength f'_m and the shear span ratio M/Vl_w of the wall and is a holdover from the 1988 edition of the UBC. The analysis was used to evaluate if the current constraint should be included with the new model or whether a new constraint should be proposed.

13.3.7 Comparison to Current Model

The analysis tools detailed in this section were used with the dataset to calculate the statistics for the current MSJC (2013) shear model. The model was analyzed once using the current coefficient values and again to determine was the best estimates of the coefficient would be if the model were kept in its current form. The purpose of this analysis was to provide a means to determine how much improvement the new model provides over the model currently in place.

CHAPTER 14. ANALYSIS OF OLD MODELS

14.1 Analysis of Blondet et al. Model

The model developed by Blondet et al. (1989) assumed that the shear strength contribution of the shear reinforcement was correlated to half of the reinforcement area. They then solved the resulting equation assuming that the axial stress was zero. It is uncertain how they determined the coefficient estimates that they provided since the data set did not contain any specimens with zero axial stress. Herein, two approaches were used to attempt to replicate their results by eliminating the contribution from the axial load from their experimental data: first, to ignore the contribution of the axial stress and second, to compensate for the contribution of the axial stress.

The first approach was accomplished by analyzing the dataset while ignoring the contribution of axial stress. This simplification reduced the analysis to a bivariate model given by

$$v_t - 0.5\rho_h f_y = \left(\beta_0 + \beta_1 \frac{M}{V\,d}\right)\sqrt{f'_m} \tag{14.1}$$

or similarly by

$$\frac{v_t - 0.5\rho_h f_y}{\sqrt{f'_m}} = \beta_0 + \beta_1 \frac{M}{V\,d} \tag{14.2}$$

where β_0 is the ordinate intercept and β_1 is the slope of the influence of the shear span ratio. Both forms of the equation were regressed using the original dataset to further understand the values they obtained. Equations (14.1) and (14.2) were first analyzed using the block and brick data separately to compare the results with those listed in their report. The two equations were subsequently analyzed for both material types. The calculated coefficient estimates from the six analyses, shown in Tables 14.1 and 14.2, were all notably different from those values provided by Blondet et al. (1989). The closest values were produced by solving Equation (14.1) and it appears

Table 14.1: Regression Models for Equation (14.1)

(a) Coefficient Estimates for Block Data

Parameter	Estimate	SE	tStat	pValue
$\sqrt{f'_m}$	6.0726	0.4691	12.945	2.4397e-13
$\frac{M}{Vd}\sqrt{f'_m}$	-3.28	0.80793	-4.0597	0.00035795
Number of observations: 30, Error degrees of freedom: 28				
Root Mean Squared Error: 52.5, R^2: 0.9465				

(b) Coefficient Estimates for Brick Data

Parameter	Estimate	SE	tStat	pValue
$\sqrt{f'_m}$	4.492	0.43917	10.228	1.8634e-11
$\frac{M}{Vd}\sqrt{f'_m}$	-0.94922	0.68157	-1.3927	0.17362
Number of observations: 33, Error degrees of freedom: 31				
Root Mean Squared Error: 55.8, R^2: 0.9447				

(c) Coefficient Estimates for Block and Brick Data

Parameter	Estimate	SE	tStat	pValue
$\sqrt{f'_m}$	5.1855	0.32927	15.748	3.6458e-23
$\frac{M}{Vd}\sqrt{f'_m}$	-1.9249	0.53118	-3.6238	0.00059291
Number of observations: 63, Error degrees of freedom: 61				
Root Mean Squared Error: 56, R^2: 0.94				

that Blondet et al. did not normalize the equation by the root of the prisms strength as shown in Equation (14.2) but performed their analysis using the form given by Equation (14.1).

The second approach was to compensate for the axial stress in the equation by subtracting it from the experimental strength. The masonry contribution is given by

$$v_{cr} = v_u - \frac{1}{2}v_s \tag{14.3}$$

which is related to the cracking strength v_{cr0} and axial stress σ_0 by

$$v_{cr}^2 = v_{cr0}^2 + \frac{v_{cr0}\,\sigma_0}{1.5} \tag{14.4}$$

Table 14.2: Regression Models for Equation (14.2)

(a) Coefficient Estimates for Block Data

Parameter	Estimate	SE	tStat	pValue
Intercept	5.7829	0.52553	11.004	1.1178e-11
$\frac{M}{Vd}$	-0.058777	0.018748	-3.1351	0.0040109
Number of observations: 30, Error degrees of freedom: 28				
Root Mean Squared Error: 1.21, R^2: 0.932				

(b) Coefficient Estimates for Brick Data

Parameter	Estimate	SE	tStat	pValue
Intercept	4.3614	0.38136	11.436	1.1838e-12
$\frac{M}{Vd}$	-0.012403	0.010417	-1.1907	0.24282
Number of observations: 33, Error degrees of freedom: 31				
Root Mean Squared Error: 1.03, R^2: 0.9407				

(c) Coefficient Estimates for Block and Brick Data

Parameter	Estimate	SE	tStat	pValue
Intercept	4.9146	0.31137	15.784	3.2658e-23
$\frac{M}{Vd}$	-0.027469	0.0094913	-2.8941	0.0052673
Number of observations: 63, Error degrees of freedom: 61				
Root Mean Squared Error: 1.15, R^2: 0.9305				

The cracking strength is also provided by the empirical equation

$$v_{cr0} = \left(\beta_0 + \beta_1 \frac{M}{V\,d}\right)\sqrt{f'_m} \tag{14.5}$$

The coefficients for Equation (14.3) can be determined by regression analysis using the cracking strength calculated from the experimental values using

$$v_{cr0} = \frac{1}{3}\sqrt{9\left(v_u - \frac{1}{2}v_s\right)^2 + f_a^2} - \frac{\sigma_0}{3} \tag{14.6}$$

Table 14.3: Regression Models for Equation (14.5)

(a) Coefficient Estimates for Block Data

Parameter	Estimate	SE	tStat	pValue
$\sqrt{f'_m}$	4.1447	0.51258	8.086	8.3628e-09
$\frac{M}{Vd}\sqrt{f'_m}$	-2.6783	0.88281	-3.0339	0.005165
Number of observations: 30, Error degrees of freedom: 28				
Root Mean Squared Error: 57.4, R^2: 0.8573				

(b) Coefficient Estimates for Brick Data

Parameter	Estimate	SE	tStat	pValue
$\sqrt{f'_m}$	3.0595	0.70334	4.3499	0.00013694
$\frac{M}{Vd}\sqrt{f'_m}$	-2.9759	1.0916	-2.7263	0.010441
Number of observations: 33, Error degrees of freedom: 31				
Root Mean Squared Error: 89.4, R^2: 0.4895				

(c) Coefficient Estimates for Block and Brick Data

Parameter	Estimate	SE	tStat	pValue
$\sqrt{f'_m}$	3.6676	0.47886	7.659	1.6998e-10
$\frac{M}{Vd}\sqrt{f'_m}$	-3.1807	0.7725	-4.1174	0.00011704
Number of observations: 63, Error degrees of freedom: 61				
Root Mean Squared Error: 81.5, R^2: 0.642				

which was used to by solve Equations (14.3) and (14.3) in terms of v_{cr0}. The results of this analysis, shown in Table 14.3, again display a distinct difference from the values they provided. In light of the information given in their report and the analyses performed using their data, it is not understood how the values of their coefficient estimates were obtained because their results cannot be replicated.

Another factor to analyze in the Blondet et al. analysis is whether their assumption that half the horizontal reinforcement contributed to the strength was a valid assumption. It is also important to understand how their assumption about the horizontal reinforcement affected the results of their analysis. This was done using multivariate regression on their dataset assuming the coefficient for the horizontal reinforcement was unknown. The multivariate regression also allowed the

opportunity to examine how the axial stress contributed to the shear strength. The analysis was performed twice for each material grouping, once including the contribution of the axial stress and once neglecting the axial stress contribution.

The results in Table 14.4, considering the axial load, show estimated coefficients that are notably different from those determined by Blondet et al. (1989). The estimate and pValue of the σ_0 parameter showed no appreciable or statistically significant contribution by the axial stress for the clay data and the value is effectively zero. The axial stress did have an impact on the strength of the block data and was also non-zero for the whole dataset. The contribution of the horizontal reinforcement was also notably smaller than Blondet et al. originally assumed, which gives the intimation that the horizontal reinforcement is not nearly as effective in increasing the total shear strength than what they had originally supposed.

The results in Table 14.5, neglecting the axial load, are similar to those in Table 14.4 and both are different from those determined by Blondet et al. (1989). Between the two tables, the analysis results were most similar for the clay data (Tables 14.4b and 14.5b) because the axial stress had little effect on the total strength. The coefficient estimates were higher for the block data without the axial stress because this latter model assumes that the masonry and reinforcement contribute more to the strength and that the axial stress does not contribute at all. This is the only case where the contribution of the horizontal reinforcement approaches the 0.5 value originally assumed by Blondet et al. (see Table 14.5a). All other analyses determined coefficients for the horizontal reinforcement that were significantly lower than what was hypothesized in the original analysis.

The latter analysis did not provide any additional insight into how Blondet et al. (1989) determined the coefficients for their model. The two most-common goodness-of-fit statistics, root mean square error (RMSE) and coefficient of determination R^2, were determined for the coefficients using the original dataset from Blondet et al. and included in Table 14.6. Blondet et al. (1989) determined coefficients for concrete block masonry and clay brick masonry shear walls separately, as shown in Tables 14.6a and 14.6b. The TCCMaR members selected coefficients for use with both concrete block and clay brick based on the conclusions of Blondet et al. (1989), which are given in Table 14.6c. Since the Gauss-Markov theorem states that multivariate least-squares regression produces unbiased estimators with the smallest variance (Markov, 1900), comparing the

Table 14.4: Regression Models for Blondet et al. Including Axial Stress

(a) Coefficient Estimates for Block Data

Parameter	Estimate	SE	tStat	pValue
$\sqrt{f'_m}$	5.5272	0.5578	9.9088	2.5649e-10
$\frac{M}{Vd}\sqrt{f'_m}$	-3.2278	0.72115	-4.4759	0.00013407
σ_0	0.2146	0.053241	4.0306	0.00043161
$\rho_h f_y$	0.37111	0.096343	3.852	0.00068695
Number of observations: 30, Error degrees of freedom: 26				
Root Mean Squared Error: 42.7, R^2: 0.9802				

(b) Coefficient Estimates for Brick Data

Parameter	Estimate	SE	tStat	pValue
$\sqrt{f'_m}$	6.5866	0.48111	13.69	3.4593e-14
$\frac{M}{Vd}\sqrt{f'_m}$	-2.7835	0.61914	-4.4958	0.00010273
σ_0	0.0058008	0.070312	0.082501	0.93482
$\rho_h f_y$	0.15726	0.053491	2.9399	0.0063845
Number of observations: 33, Error degrees of freedom: 29				
Root Mean Squared Error: 37.0, R^2: 0.9880				

(c) Coefficient Estimates for Block and Brick Data

Parameter	Estimate	SE	tStat	pValue
$\sqrt{f'_m}$	6.1282	0.37988	16.132	2.6677e-23
$\frac{M}{Vd}\sqrt{f'_m}$	-3.54	0.48325	-7.3254	7.6028e-10
σ_0	0.1611	0.04015	4.0125	0.00017169
$\rho_h f_y$	0.19942	0.051567	3.8671	0.00027718
Number of observations: 63, Error degrees of freedom: 59				
Root Mean Squared Error: 43.5, R^2: 0.9804				

goodness-of-fit statistics in Table 14.6 to those in Tables 14.4 and 14.5 shows that there are better coefficients to use in estimating masonry shear wall strength than those determined by Blondet et al.. This is further evidenced by the smaller RMSE values and larger R^2 values for the current analysis than those originally determined by Blondet et al. (compare Table 14.6). This conclusion follows for the TCCMaR equation as well since its coefficients were based on those determined by Blondet et al. (1989).

Table 14.5: Regression Models for Blondet et al. Excluding Axial Stress

(a) Coefficient Estimates for Block Data

Parameter	Estimate	SE	tStat	pValue
$\sqrt{f'_m}$	6.108	0.67405	9.0617	1.1252e-09
$\frac{M}{Vd}\sqrt{f'_m}$	-3.3074	0.90172	-3.6679	0.001058
$\rho_h f_y$	0.49147	0.11458	4.2895	0.000205
Number of observations: 30, Error degrees of freedom: 27				
Root Mean Squared Error: 53.5, R^2: 0.9679				

(b) Coefficient Estimates for Brick Data

Parameter	Estimate	SE	tStat	pValue
$\sqrt{f'_m}$	6.603	0.43038	15.342	9.6122e-16
$\frac{M}{Vd}\sqrt{f'_m}$	-2.7573	0.5224	-5.2781	1.0623e-05
$\rho_h f_y$	0.15785	0.052124	3.0284	0.0050178
Number of observations: 33, Error degrees of freedom: 30				
Root Mean Squared Error: 36.4, R^2: 0.9880				

(c) Coefficient Estimates for Block and Brick Data

Parameter	Estimate	SE	tStat	pValue
$\sqrt{f'_m}$	6.523	0.4105	15.89	3.5869e-23
$\frac{M}{Vd}\sqrt{f'_m}$	-3.017	0.52061	-5.7951	2.6947e-07
$\rho_h f_y$	0.24379	0.05635	4.3264	5.8238e-05
Number of observations: 63, Error degrees of freedom: 60				
Root Mean Squared Error: 48.7, R^2: 0.9750				

14.2 Analysis of Anderson and Priestley Equation

Anderson and Priestley (1992) used an optimization approach to determined the coefficient for a model which included four parameters: masonry, axial load, vertical reinforcement, and horizontal reinforcement. Their approach was to find the coefficients which minimized one of two error terms. After finding that the first error term did not produce results which matched their optimization criterion, they used a second error term. As noted in Section 12.1.7, this error term would produce estimates, but they likely were not the best estimates with the least variance. Their model and dataset were analyzed using multivariate regression to determine the optimum coeffi-

Table 14.6: Coefficients and Goodness-of-Fit Statistics for Original Models

(a) Block (Blondet et al., 1989)

Parameter	Coefficient
$\sqrt{f'_m}$	3.5
$\frac{M}{Vd}\sqrt{f'_m}$	-1.75
$\rho_h f_y$	0.5
RMSE: 106.4, R^2: 0.8729	

(b) Brick (Blondet et al., 1989)

Parameter	Coefficient
$\sqrt{f'_m}$	4.2
$\frac{M}{Vd}\sqrt{f'_m}$	-1.75
$\rho_h f_y$	0.5
RMSE: 73.85, R^2: 0.9504	

(c) Block and Brick (NEHRP, 1997)

Parameter	Coefficient
$\sqrt{f'_m}$	4.0
$\frac{M}{Vd}\sqrt{f'_m}$	-1.75
$\rho_h f_y$	0.5
RMSE: 80.33, R^2: 0.9298	

cients they might have obtained. Since their optimization method was not fully detailed, it would not be possible to reproduce their analysis. However, the root mean square error (RMSE) and coefficient of determination R^2 were determined for their coefficients using their original dataset are and included in Table 14.7.

The Anderson and Priestley (1992) model and dataset were analyzed using multivariate regression to determine the optimum coefficient estimates and to compare how their chosen coefficients compared with them. The dataset presented in Anderson and Priestley (1992) included only specimens constructed from concrete block masonry, so only the coefficients for concrete block can be effectively compared. However, since their coefficients for concrete block and clay brick were similar, the analysis for their concrete block data and model should produce similar conclusions

Table 14.7: Coefficients and Goodness-of-Fit Statistics
for Anderson and Priestley Model

(a) Units of Force (N)

Parameter	Coefficient
$\sqrt{f'_m}\,A_n$	0.24
P	0.25
$A_h\,f_y\,\frac{l_w}{s}$	0.50
RMSE: 8.927e+04, R^2: 0.9608	

(b) Units of Stress (MPa)

Parameter	Coefficient
$\sqrt{f'_m}$	0.24
σ_0	0.25
$\rho_h\,f_y\,\frac{h}{s}$	0.50
RMSE: 0.3613, R^2: 0.9678	

for their clay brick data as well. The dataset was analyzed twice, once including the contribution of the vertical reinforcement and once again neglecting the vertical reinforcement. Each analysis was conducted using both untransformed (units of force) and transformed (units of stress) data.

The results in Table 14.8 give the intimation that Anderson and Priestley may have been justified in neglecting the contribution of the vertical reinforcement to wall strength. The coefficient estimates for the vertical reinforcement are non-trivial, but both pValues are relatively large and suggest that the vertical reinforcement parameter does not affect the overall response and may be eliminated. The second analysis results in Table 14.9 show a negligible change in the goodness-of-fit statistics with the vertical reinforcement excluded from the analysis. In the case of the Anderson and Priestley (1992) dataset it can be reasonably concluded that the vertical reinforcement did not contribute to the overall wall shear strength.

The value of the coefficient estimate for the masonry parameter was determined to be approximately 0.24 for units of MPa (or 2.9 for units of psi). This value is identical to the value determined by Anderson and Priestley (1992). The analysis showed that Anderson and Priestley underestimated the contribution of the axial load and overestimated the contribution of the horizon-

Table 14.8: Regression Models for Anderson and Priestley Including Vertical Bars

(a) Units of Force (N)

Parameter	Estimate	SE	tStat	pValue
$\sqrt{f'_m}\,A_n$	0.23215	0.026721	8.688	2.9078e-12
P	0.35207	0.038074	9.2469	3.263e-13
$A_c\,f_y$	0.035946	0.065817	0.54615	0.58696
$A_h\,f_y\,\frac{l_w}{s}$	0.22188	0.060769	3.6511	0.00054362
Number of observations: 65, Error degrees of freedom: 61				
Root Mean Squared Error: 6.69e+04, R^2: 0.9773				

(b) Units of Stress (MPa)

Parameter	Estimate	SE	tStat	pValue
$\sqrt{f'_m}$	0.23734	0.025259	9.3961	1.8275e-13
σ_0	0.34505	0.03571	9.6626	6.5165e-14
$\rho_c\,f_y$	0.011702	0.067038	0.17456	0.862
$\rho_h\,f_y\,\frac{h}{s}$	0.25101	0.056399	4.4506	3.7059e-05
Number of observations: 65, Error degrees of freedom: 61				
Root Mean Squared Error: 0.282, R^2: 0.9798				

Table 14.9: Regression Models for Anderson and Priestley Excluding Vertical Bars

(a) Units of Force (N)

Parameter	Estimate	SE	tStat	pValue
$\sqrt{f'_m}\,A_n$	0.24259	0.018578	13.058	1.8774e-19
P	0.34564	0.036005	9.5999	7.0528e-14
$A_h\,f_y\,\frac{l_w}{s}$	0.21285	0.058148	3.6605	0.000522
Number of observations: 65, Error degrees of freedom: 62				
Root Mean Squared Error: 6.706e+04, R^2: 0.9772				

(b) Units of Stress (MPa)

Parameter	Estimate	SE	tStat	pValue
$\sqrt{f'_m}$	0.24042	0.017908	13.425	5.2297e-20
σ_0	0.34325	0.033918	10.12	9.3981e-15
$\rho_h\,f_y\,\frac{h}{s}$	0.24862	0.054281	4.5802	2.2943e-05
Number of observations: 65, Error degrees of freedom: 62				
Root Mean Squared Error: 0.2821, R^2: 0.9798				

tal reinforcement, as did Blondet et al. (1989). The coefficient estimate values for the horizontal reinforcement were close to those obtained above for the Blondet et al. dataset but the estimates for the axial load contribution differed considerably. The reason for the difference is likely due to the consideration of the shear span ratio in the Blondet et al. model and not in the Anderson and Priestley model. It appears that the coefficient for the axial load is sensitive to the inclusion of the spear span ratio in the model, more so than the horizontal reinforcement coefficient.

Comparing the goodness-of-fit statistics between the two models showed that the coefficients determined by Anderson and Priestley produced a model with approximately 30 percent higher error than the optimum values determined by multivariate least-squares regression. The Anderson and Priestley model produced a very high coefficient of determination, close to that of optimum model. The large disparity between the coefficient values for axial load and horizontal reinforcement between the original and new models in consideration of the relatively small difference in goodness-of-fit statistics suggests that the shear strength is not as sensitive to the axial load and horizontal reinforcement contributions.

The coefficient of determination R^2 values in Table 14.9 show that the fit of the model improves by normalizing the data by the shear area of the wall. As noted earlier in Section 13.3.3, a model with units of force would likely face issues with heteroscedasticity and would be better if transformed. The higher R^2 value for the force model compared to the stress model suggests that the force model experiences some increase in variance over the normalized model, likely due to some heteroscedasticity in the residuals.

14.3 Analysis of TCCMaR Equation

The TCCMaR equation was assembled from pieces of the Blondet et al. (1989) and Anderson and Priestley (1992) equations. Since the Blondet et al. and Anderson and Priestley models have been shown to produce less-than-optimum results, it follows that the TCCMaR model will similarly produce less-than-optimum results. The models from Blondet et al., Anderson and Priestley, and TCCMaR were compared using the dataset from Fattal and Todd (1991), which was the same dataset used by the TCCMaR members in comparing and choosing their model (NEHRP, 1997). The goodness-of-fit statistics in Table 14.10 were first calculated using the Fattal and Todd dataset to compare the performance of each equation. The model and coefficients of Anderson and

Priestley actually produced the best results of the three models. This is likely because they used an optimization methodology to determine their coefficients. The TCCMaR model was not the best model because the model was constructed by added parameters from the two previous models without attempting to redetermine the coefficients for their new, expanded model.

Table 14.10: Coefficients and Goodness-of-Fit Statistics for Original Models

(a) Blondet et al.

Parameter	Coefficient
$\sqrt{f'_m}$	0.33
$\frac{M}{Vd}\sqrt{f'_m}$	-0.15
$\rho_h f_{yh}$	0.50
RMSE: 0.6255, R^2: 0.9182	

(b) Anderson and Priestley

Parameter	Coefficient
$\sqrt{f'_m}$	0.24
σ_0	0.25
$\rho_h f_{yh}$	0.50
RMSE: 0.4859, R^2: 0.9506	

(c) TCCMaR (NEHRP)

Parameter	Coefficient
$\sqrt{f'_m}$	0.33
$\frac{M}{Vd}\sqrt{f'_m}$	-0.15
σ_0	0.25
$\rho_h f_{yh}$	0.50
RMSE: 0.5033, R^2: 0.9479	

It was shown in the two previous sections that the coefficients originally chosen by Blondet et al. and Anderson and Priestley for their respective models were not the optimum values. The optimum coefficients for these two models with the TCCMaR model were determined using multivariate least-squares regression on the Fattal and Todd (1991) dataset so that the results could be

compared with the original values and with each other. Additionally, the TCCMaR dataset was re-analyzed including the contribution of the vertical reinforcement to verify their original conclusion that it did not contribute to the strength. The results for these four models are reported in Table 14.11.

All three original models underestimated the contribution of the masonry and overestimated the contribution of the axial load and reinforcement to the overall strength of the wall. Only approximately 10 percent of the axial load contributes to the strength of the wall while the contribution of the horizontal reinforcement ranges from about 12 to 15 percent, depending on what other parameters are included in the model. Both values are significantly lower than the values developed based on the theoretical behavior and highlights the importance of validating engineering assumptions.

The results of the last model showed that the TCCMaR members were not completely justified in eliminating the contribution of the vertical reinforcement from the model. The pValue for the vertical reinforcement contribution is not quite statistically significant at the $\alpha = 0.05$ level but it is clearly significant at the $\alpha = 0.10$ level and its pValue is not much higher than that of the horizontal reinforcement. This suggests that variations in detailing or other reinforcement properties may be inflating the pValue and that the parameter should have remained in the model.

Part of the disparity in results between the current analysis and TCCMaR members is due to their methodology in evaluating their models. The TCCMaR members based their methodology on evaluating the ratios of experimental to to theoretical strengths. As noted earlier, the results of methodology will be affected by the lack of normality in these distributions. One of the other benefits to using multivariate regression modeling in this case is that the average of the predicted strength is equal to the average of the experimental strength. This cannot be said about the original models, which each have a predicted strength average less than the experimental strength.

Table 14.11: Comparison of Regression Results Using Fattal and Todd Dataset

(a) Blondet at el. Model

Parameter	Estimate	SE	tStat	pValue
$\sqrt{f'_m}$	0.51449	0.036754	13.998	2.0874e-20
$\frac{M}{Vd}\sqrt{f'_m}$	-0.16791	0.05236	-3.2068	0.0021688
$\rho_h\, f_{yh}$	0.1553	0.059297	2.6191	0.011189
Number of observations: 62, Error degrees of freedom: 59				
Root Mean Squared Error: 0.3408, R^2: 0.9757				

(b) Anderson and Priestley Model

Parameter	Estimate	SE	tStat	pValue
$\sqrt{f'_m}$	0.36789	0.020958	17.554	4.2566e-25
σ_0	0.11916	0.041662	2.8602	0.0058462
$\rho_h\, f_{yh}$	0.15109	0.060983	2.4776	0.016111
Number of observations: 62, Error degrees of freedom: 59				
Root Mean Squared Error: 0.3461, R^2: 0.9750				

(c) TCCMaR Model

Parameter	Estimate	SE	tStat	pValue
$\sqrt{f'_m}$	0.46759	0.03988	11.725	6.1609e-17
$\frac{M}{Vd}\sqrt{f'_m}$	-0.1465	0.050888	-2.8789	0.0055805
σ_0	0.099883	0.039871	2.5051	0.015071
$\rho_h\, f_{yh}$	0.11986	0.058547	2.0472	0.045173
Number of observations: 62, Error degrees of freedom: 58				
Root Mean Squared Error: 0.3265, R^2: 0.9781				

(d) TCCMaR Model with Vertical Reinforcment

Parameter	Estimate	SE	tStat	pValue
$\sqrt{f'_m}$	0.50707	0.044469	11.403	2.4629e-16
$\frac{M}{Vd}\sqrt{f'_m}$	-0.25707	0.077637	-3.3112	0.0016158
σ_0	0.10906	0.039366	2.7704	0.0075457
$\rho_c\, f_{yc}$	0.10275	0.055313	1.8576	0.068387
$\rho_h\, f_{yh}$	0.11689	0.05737	2.0375	0.046248
Number of observations: 62, Error degrees of freedom: 57				
Root Mean Squared Error: 0.3198, R^2: 0.9793				

CHAPTER 15. DEVELOPMENT OF AN IMPROVED LINEAR MODEL

15.1 Introduction

There are uncertainties in the model building process concerning which parameters and coefficients best represent the behavior of masonry shear walls. The models outlined in Chapter 12 each differed from each other in parameter choice and in overall form, providing no consensus between researchers as to what form the model should take nor as to which parameters should be included. The analysis in Chapter 14 of the models previously developed by Blondet et al. (1989), Anderson and Priestley (1992), and the TCCMaR (NEHRP, 1997) showed that those models did not contain the optimum values for the parameter coefficients. These models were developed with some parameters and coefficients chosen based on theoretical behavior and it was shown in Chapter 14 that the coefficients based on theory were far from representative of the actual effect on shear strength.

It was also shown in Chapter 14 that the models were underfitted because they all excluded the contribution of the vertical reinforcement to the wall shear strength, which was observed to contribute to the strength. Models that omit parameters that should be in the model (i.e., are underfitted) have parameters that are biased, meaning they do not represent the true values of the coefficients in the true model. In Part III of this dissertation, it was demonstrated that these models are insufficient for describing the behavior of partially-grouted walls. The reason for such insufficiency is that the previous three equations were all developed solely using fully-grouted shear wall data.

The non-consensus between researchers, the poor performance of parameters developed from theory, and the inability of researchers to adequately quantify the performance of partially-grouted shear walls have diminished the usefulness of previous methodologies or models in constructing a new model. This chapter details the development of a new linear model to describe the shear behavior equally well for both fully- and partially-grouted walls using multivariate lin-

ear regression, a method that has yet to be employed for this task. The new model was built and analyzed using the new, expanded dataset developed in Part II of this dissertation.

15.2 Parameter Selection

15.2.1 Automated Stepwise Regression

In light of the uncertainties and disagreements remaining from the previous research, it was judged best to start the model building process afresh by considering all potential combinations of parameters—including those previously dismissed by researchers—in constructing the new model. The Akaike Information Criteria (AIC) and the Bayes Information Criteria (BIC) were used in conjunction with stepwise linear regression to narrow the large pool of parameters to those that best described the experimental data. The use of stepwise regression was not intended to develop the final model, but rather to help in identifying the best parameter candidates for consideration in building the final model.

The results of the first series of stepwise regression are shown in Tables 15.1 and 15.2. From first inspection it is clear that the resulting models contained unnecessary duplications of terms and were overly-complex for consideration as the final model. By comparing the models for the fully- and partially-grouted dataset, there were some parameters which were common between the two models and some others that were unique. In the case of both the AIC and BIC analyses, the goodness of fit parameters were consistently better for the fully-grouted model than for the partially-grouted model. The larger number of $\sqrt{f'_m}$ terms than f'_m terms suggested that the previous conclusion that shear strength is related to the root of the compressive strength (Matsumura, 1987) may be valid and that the other term should be eliminated from future consideration. This will also maintain some harmony between masonry and reinforced concrete shear strength theory.

The elimination of the f'_m term from consideration in the second series of the stepwise regression analyses produced more similarity in terms between the fully- and partially-grouted models, as shown in Tables 15.3 and 15.4. However, there was still no consistency between models for the two grouting types nor between models analyzed using AIC versus BIC. The new models also contained multiple terms for each type of reinforcement, producing a model that is overly complex and likely not representative of the actual behavior. There appeared to be no identifiable

Table 15.1: First Stepwise Regression Using AIC

(a) Fully-Grouted Data

Parameter	Estimate	SE	tStat	pValue
$\sqrt{f'_m}\,\frac{M}{V\,l_w}$	0.08782	0.054206	1.6201	0.10716
$\sqrt{f'_m}\,\min\left(1.0,\,\frac{M}{V\,l_w}\right)$	-0.0863	0.029381	-2.9373	0.0037935
f'_m	0.055362	0.012692	4.3619	2.2866e-05
$f'_m\,\min\left(1.0,\,\frac{M}{V\,l_w}\right)$	-0.029528	0.0091294	-3.2344	0.0014778
σ_0	0.23824	0.025094	9.4942	2.8381e-17
$\frac{\rho_c\,f_{yc}}{s_c}\,l_w$	2.3119	0.50756	4.5551	1.0252e-05
$\frac{\rho_c\,f_{yc}}{s_c}\,l_r$	-2.3824	0.5797	-4.1097	6.2789e-05
$\frac{\rho_h\,f_{yh}}{s_h}\,h_g$	0.12711	0.021918	5.7991	3.3993e-08
$\frac{\rho_j\,f_{yj}}{s_j}\,h_g$	0.77413	0.28738	2.6938	0.0078085
Number of observations: 171, Error degrees of freedom: 162 Root Mean Squared Error: 0.3010, R^2: 0.9682 Mean: -0.0003469, Standard Deviation: 0.3092				

trend in whether there was a difference in the contribution of the horizontal and joint reinforcement. In the next iteration it was chosen to combine the horizontal and joint reinforcement into one term to help eliminate some of the duplication of parameters in the models.

The results from the third series of stepwise regression analyses shown in Tables 15.5 and 15.6. This latest series began to show some consolidation in the masonry and axial component terms and a notable decrease in the number of terms for each of the reinforcement components. The reinforcement terms still showed no intimation of agreement in the length term that should be included with the reinforcement strength term in the parameter. The use of the stepwise regression procedure in building models using term addition has provided the most benefit in narrowing the scope of parameters for inclusion in the masonry and axial parameters but some uncertainty remains in regards to which reinforcement terms should be used in the equation.

A new series of stepwise regression analyses were conducted in which the model was constructed using the interactions of input terms. Two types of terms were used in the analysis—strength terms and geometric terms—to investigate what parameters would be determined if the input terms were not limited to specific constructs. All four analysis results in Tables 15.7 and

Table 15.1: First Stepwise Regression Using AIC (Continued)

(b) Partially-Grouted Data

Parameter	Estimate	SE	tStat	pValue
$\sqrt{f'_m}$	0.47193	0.064838	7.2785	1.258e-11
$\sqrt{f'_m}\,\frac{M}{V\,l_w}$	-0.18431	0.11201	-1.6454	0.10177
$\sqrt{f'_m}\,\min\left(1.0,\,\frac{M}{V\,l_w}\right)$	-0.060819	0.042782	-1.4216	0.157
$\sqrt{f'_m}\,s_{gv}$	-0.00068802	0.00042961	-1.6015	0.11115
f'_m	-0.045165	0.013802	-3.2724	0.001296
$f'_m\,\frac{M}{V\,l_w}$	0.027814	0.019223	1.4469	0.14979
σ_0	0.22207	0.021897	10.142	3.9153e-19
$\sqrt{\sigma_0}\,\sqrt{f'_m}$	-0.080721	0.020891	-3.8639	0.00016255
$\frac{\rho_h\,f_{yh}}{s_h}\,\frac{M}{V}$	0.15642	0.097209	1.6092	0.10958
$\frac{\rho_h\,f_{yh}}{s_h}\,\frac{M}{V}$	0.83046	0.18217	4.5586	1.0259e-05
$\frac{\rho_h\,f_{yh}}{s_h}\,\min\left(h_g,\,l_r\right)$	-0.7528	0.19335	-3.8935	0.00014547
$\frac{\rho_j\,f_{yj}}{s_j}\,\frac{M}{V}$	-5.0931	1.4175	-3.5931	0.00043609
$\frac{\rho_j\,f_{yj}}{s_j}\,\min\left(h_g,\,l_r\right)$	3.0123	0.86818	3.4696	0.00067191
$\frac{\rho_h\,f_{yh}}{s_h}\,\frac{M}{V}$	0.81351	0.2368	3.4355	0.00074635
$\frac{\rho_h\,f_{yh}}{s_h}\,\min\left(h_g,\,l_w\right)$	67.506	46.683	1.446	0.15004
$\frac{\rho_h\,f_{yh}}{s_h}\,\min\left(h_g,\,d\right)$	-134.26	93.525	-1.4355	0.15301
$\frac{\rho_h\,f_{yh}}{s_h}\,\min\left(h_g,\,l_r\right)$	66.104	46.92	1.4089	0.16073
$\frac{\rho_j\,f_{yj}}{}\,l_w$	-1.172	0.48206	-2.4312	0.016107
$\frac{\rho_j\,f_{yj}}{}\,\frac{M}{V}$	-3.1999	0.93985	-3.4047	0.00082941
$\frac{\rho_j\,f_{yj}}{\min}\left(h_g,\,l_r\right)$	3.6531	1.1505	3.1753	0.001783
Number of observations: 181, Error degrees of freedom: 167				
Root Mean Square Error: 0.2025, R^2: 0.9584				
Mean: 0.002038, Standard Deviation: 0.2108				

15.8 identified the parameters $\sqrt{f'_m}$ and σ_0 as being highly statistically significant for both grouting types. This result is in agreement with the results of the previous analyses. The term $\sqrt{f'_m}\,\frac{M}{V\,l_w}$ has been included in the fully-grouted models but is absent from the partially-grouted models, suggesting that there may be some yet-unidentified term that is better suited for describing partially-grouted shear wall behavior. This may be partly to blame for the poor fit of the existing MSJC (2013) shear equation with partially-grouted walls.

Table 15.2: First Stepwise Regression Using BIC

(a) Fully-Grouted Data

Parameter	Estimate	SE	tStat	pValue
$\sqrt{f'_m}\,\frac{M}{V l_w}$	-0.064334	0.026195	-2.456	0.015099
f'_m	0.074242	0.0050531	14.692	1.1533e-31
$f'_m \min\left(1.0,\ \frac{M}{V l_w}\right)$	-0.036652	0.0080403	-4.5586	1.0062e-05
σ_0	0.23843	0.025218	9.4546	3.4712e-17
$\frac{\rho_c f_{yc}}{s_c} l_w$	2.2116	0.50626	4.3684	2.2193e-05
$\frac{\rho_c f_{yc}}{s_c} l_r$	-2.2593	0.57755	-3.9118	0.00013424
$\frac{\rho_h f_{yh}}{s_h} h_g$	0.1378	0.021005	6.5605	6.7918e-10
$\frac{\rho_j f_{yj}}{s_j} h_g$	0.81554	0.28766	2.8351	0.0051619
Number of observations: 171, Error degrees of freedom: 163 Root Mean Squared Error: 0.3034, R^2: 0.9676 Mean: 0.006828, Standard Deviation: 0.3108				

(b) Partially-Grouted Data

Parameter	Estimate	SE	tStat	pValue
$\sqrt{f'_m}$	0.0.26639	0.011889	22.407	2.6863e-53
$f'_m \min\left(1.0,\ \frac{M}{V l_w}\right)$	-0.030277	0.0029981	-10.099	3.4932e-19
σ_0	0.20393	0.017951	11.36	9.3238e-23
$\frac{\rho_h f_{yh}}{s_h} \frac{M}{V}$	1.1048	0.21322	5.1814	6.0177e-07
$\frac{\rho_h f_{yh}}{s_h} \min\left(h_g,\ l_w\right)$	0.66602	0.28349	2.3494	0.01992
$\frac{\rho_h f_{yh}}{s_h} \min\left(h_g,\ l_r\right)$	-1.5817	0.45385	-3.4852	0.00062164
Number of observations: 181, Error degrees of freedom: 175 Root Mean Square Error: 0.2219, R^2: 0.9501 Mean: 0.003093, Standard Deviation: 0.2257				

The interaction analyses also identified several partial terms in the models which have inconsistent units and are incomplete because they are missing either the strength or length component. Most of these terms are sporadic and appear in some but not all of the models. One exception is the term $\frac{\rho_h f_{yh}}{s_h}$ which occurs in all four models, though it is only statistically significant in the

Table 15.3: Second Stepwise Regression Using AIC

(a) Fully-Grouted Data

Parameter	Estimate	SE	tStat	pValue
$\sqrt{f'_m}$	0.29974	0.028552	10.498	5.4089e-20
$\sqrt{f'_m}\,\frac{M}{V\,l_w}$	-0.091233	0.033506	-2.7229	0.0071807
$\sqrt{f'_m}\,\min\left(1.0,\,\frac{M}{V\,l_w}\right)$	-0.10106	0.049855	-2.027	0.044299
σ_0	0.11808	0.075045	1.5735	0.11756
$\sqrt{\sigma_0\,f'_m}$	0.12636	0.062535	2.0207	0.04496
$\frac{\rho_c\,f_{yc}}{s_c}\,l_w$	4.7198	1.0741	4.3944	2.0016e-05
$\frac{\rho_c\,f_{yc}}{s_c}\,d$	-4.7765	1.1462	-4.1672	5.0064e-05
$\frac{\rho_h\,f_{yh}}{s_h}\,h_g$	0.11635	0.021564	5.3956	2.386e-07
$\frac{\rho_j\,f_{yj}}{s_j}\,h_g$	0.69926	0.27799	2.5154	0.012864
Number of observations: 171, Error degrees of freedom: 162				
Root Mean Squared Error: 0.06660, R^2: 0.9642				
Mean: 1.867e-16, Standard Deviation: 0.06950				

(b) Partially-Grouted Data

Parameter	Estimate	SE	tStat	pValue
$\sqrt{f'_m}$	0.29998	0.017461	17.181	3.0321e-39
$\sqrt{f'_m}\,\frac{M}{V\,l_w}$	-0.038234	0.024653	-1.5509	0.12276
$\sqrt{f'_m}\,\min\left(1.0,\,\frac{M}{V\,l_w}\right)$	-0.13458	0.040094	-3.3566	0.00096997
σ_0	0.19018	0.01954	9.7327	3.9736e-18
$\frac{\rho_h\,f_{yh}}{s_h}\,h_g$	-0.33495	0.17382	-1.927	0.055619
$\frac{\rho_h\,f_{yh}}{s_h}\,\frac{M}{V}$	1.36	0.27539	4.9386	1.8436e-06
$\frac{\rho_j\,f_{yj}}{s_j}\,\min\left(h_g,\,l_w\right)$	1.2995	0.48281	2.6915	0.0078105
$\frac{\rho_j\,f_{yj}}{s_j}\,\min\left(h_g,\,l_r\right)$	-2.1134	0.58629	-3.6047	0.00040851
Number of observations: 181, Error degrees of freedom: 173				
Root Mean Square Error: 0.05408, R^2: 0.9440				
Mean: 1.058e-16, Standard Deviation: 0.05631				

Table 15.4: Second Stepwise Regression Using BIC

(a) Fully-Grouted Data

Parameter	Estimate	SE	tStat	pValue
$\sqrt{f'_m}$	0.25026	0.023074	10.846	5.2906e-21
$\sqrt{f'_m}\,\frac{M}{V\,l_w}$	-0.13545	0.01963	-6.9002	1.0764e-10
$\sqrt{\sigma_0\,f'_m}$	0.23089	0.021486	10.746	9.9702e-21
$\frac{\rho_c\,f_{yc}}{s_c}\,l_w$	4.5542	1.1004	4.1387	5.5707e-05
$\frac{\rho_c\,f_{yc}}{s_c}\,d$	-4.6338	1.1722	-3.953	0.00011452
$\frac{\rho_h\,f_{yh}}{s_h}\,l_w$	0.12899	0.02455	5.2544	4.5643e-07
$\frac{\rho_j\,f_{yj}}{s_j}\,h_g$	0.76219	0.28093	2.7131	0.0073777
Number of observations: 171, Error degrees of freedom: 164 Root Mean Square Error: 0.06843, R^2: 0.9622 Mean: 4.602e-17, Standard Deviation: 0.07141				

(b) Partially-Grouted Data

Parameter	Estimate	SE	tStat	pValue
$\sqrt{f'_m}$	0.30109	0.016789	17.933	1.419e-41
$\sqrt{f'_m}\,\min\left(1.0,\,\frac{M}{V\,l_w}\right)$	-0.18106	0.023044	-7.857	3.7501e-13
σ_0	0.19181	0.019809	9.6833	4.8071e-18
$\frac{\rho_h\,f_{yh}}{s_h}\,\frac{M}{V}$	0.96402	0.22575	4.2704	3.187e-05
$\frac{\rho_h\,f_{yh}}{s_h}\,\min\left(h_g,\,l_r\right)$	-0.70473	0.20588	-3.423	0.00077041
Number of observations: 181, Error degrees of freedom: 176 Root Mean Squared Error: 0.05554, R^2: 0.9409 Mean: 1.472e-16, Standard Deviation: 0.05782				

BIC models. The sporadic nature and large number of inconsistent terms is likely due to variation in the individual datasets and not due to the actual behavior of the walls.

15.3 Manual Stepwise Regression

The results from the stepwise regression analyses showed that the parameters $\sqrt{f'_m}$ and σ_0 were common to both grouting types and that $\sqrt{f'_m}\,\frac{M}{V\,l_w}$ was consistently present in the fully-grouted models. Parameters for the different types of reinforcement contributions were also present

Table 15.5: Third Stepwise Regression Using AIC

(a) Fully-Grouted Data

Parameter	Estimate	SE	tStat	pValue
$\sqrt{f'_m}$	0.23407	0.03072	7.6194	1.9718e-12
$\sqrt{f'_m}\,\frac{M}{V\,l_w}$	-0.11002	0.028901	-3.8067	0.000199
σ_0	0.1157	0.074556	1.5519	0.12263
$\sqrt{\sigma_0\,f'_m}$	0.24988	0.087701	2.8493	0.0049479
$\sqrt{\sigma_0\,f'_m}\,\min\left(1.0,\,\frac{M}{V\,l_w}\right)$	-0.14255	0.077414	-1.8414	0.067375
$\frac{\rho_c\,f_{yc}}{s_c}\,l_w$	2.4481	0.50207	4.876	2.5534e-06
$\frac{\rho_c\,f_{yc}}{s_c}\,l_r$	-2.5371	0.5727	-4.4301	1.7211e-05
$\left(\frac{\rho_h\,f_{yh}}{s_h}+\frac{\rho_j\,f_{yj}}{s_j}\right)\,h_g$	0.11569	0.021932	5.2748	4.1768e-07
Number of observations: 171, Error degrees of freedom: 163				
Root Mean Squared Error: 0.06768, R^2: 0.9630				
Mean: 2.234e-16, Standard Deviation: 0.06932				

(b) Partially-Grouted Data

Parameter	Estimate	SE	tStat	pValue
$\sqrt{f'_m}$	0.29968	0.020671	14.498	1.089e-31
$\sqrt{f'_m}\,\frac{M}{V\,l_w}$	-0.039561	0.025279	-1.565	0.11942
$\sqrt{f'_m}\,\min\left(1.0,\,\frac{M}{V\,l_w}\right)$	-0.13252	0.044299	-2.9915	0.0031814
σ_0	0.20017	0.024608	8.1344	7.7275e-14
$\left(\frac{\rho_h\,f_{yh}}{s_h}+\frac{\rho_j\,f_{yj}}{s_j}\right)\,l_w$	1.4327	0.51518	2.781	0.0060201
$\left(\frac{\rho_h\,f_{yh}}{s_h}+\frac{\rho_j\,f_{yj}}{s_j}\right)\,l_r$	-1.7331	0.56375	-3.0743	0.0024527
$\left(\frac{\rho_h\,f_{yh}}{s_h}+\frac{\rho_j\,f_{yj}}{s_j}\right)\,h_g$	-0.50398	0.12654	-3.9828	0.00010016
$\left(\frac{\rho_h\,f_{yh}}{s_h}+\frac{\rho_j\,f_{yj}}{s_j}\right)\,\frac{M}{V}$	0.98556	0.2282	4.3189	2.6368e-05
Number of observations: 181, Error degrees of freedom: 173				
Root Mean Square Error: 0.05481, R^2: 0.9425				
Mean: 3.328e-17, Standard Deviation: 0.05607				

Table 15.6: Third Stepwise Regression Using BIC

(a) Fully-Grouted Data

Parameter	Estimate	SE	tStat	pValue
$\sqrt{f'_m}$	0.25232	0.023335	10.813	6.1351e-21
$\sqrt{f'_m}\,\frac{M}{V\,l_w}$	-0.13741	0.019878	-6.9125	9.9079e-11
$\sqrt{\sigma_0\,f'_m}$	0.23595	0.021644	10.902	3.4776e-21
$\frac{\rho_c\,f_{yc}}{s_c}\,l_w$	2.2138	0.51919	4.2639	3.372e-05
$\frac{\rho_c\,f_{yc}}{s_c}\,l_r$	-2.3001	0.59128	-3.89	0.00014515
$\left(\frac{\rho_h\,f_{yh}}{s_h}+\frac{\rho_j\,f_{yj}}{s_j}\right)\,d$	0.14342	0.026964	5.3189	3.356e-07
Number of observations: 171, Error degrees of freedom: 165				
Root Mean Square Error: 0.06954, R^2: 0.9610				
Mean: 2.724e-16, Standard Deviation: 0.07079				

(b) Partially-Grouted Data

Parameter	Estimate	SE	tStat	pValue
$\sqrt{f'_m}$	0.28489	0.016699	17.06	3.8058e-39
$\sqrt{f'_m}\,\frac{M}{V\,l_w}$	-0.15602	0.023081	-6.7594	1.9589e-10
σ_0	0.17899	0.024465	7.3162	8.6851e-12
$\left(\frac{\rho_h\,f_{yh}}{s_h}+\frac{\rho_j\,f_{yj}}{s_j}\right)\,h_g$	-0.21738	0.078282	-2.7769	0.0060834
$\left(\frac{\rho_h\,f_{yh}}{s_h}+\frac{\rho_j\,f_{yj}}{s_j}\right)\,\frac{M}{V}$	0.4868	0.12029	4.0469	7.7629e-05
Number of observations: 181, Error degrees of freedom: 176				
Root Mean Squared Error: 0.0568, R^2: 0.9382				
Mean: 1.385e-16, Standard Deviation: 0.05760				

in all of the models, but they appeared in different and varying forms. One weakness of the automated stepwise regression procedure is that it was unable to eliminate certain terms from consideration once a term within a class had been selected. For example, once the algorithm selected the parameter $\frac{\rho_j\,f_{yj}}{s_j}\,h_g$, there was nothing to prevent the algorithm from selecting $\frac{\rho_j\,f_{yj}}{s_j}\,\frac{M}{V}$ as well. This limitation was corrected by performing a manual stepwise regression analysis.

The data for the fully- and partially-grouted datasets were analyzed separately, as in the automated analyses, to identify the coefficients that best described the masonry shear behavior. Similar to the automated analyses, the $\sqrt{f'_m}$ and σ_0 parameters were both found to significantly

Table 15.7: Interaction Stepwise Regression Using AIC

(a) Fully-Grouted Data

Parameter	Estimate	SE	tStat	pValue
$\sqrt{f'_m}$	-0.06249	0.13258	-0.47136	0.63809
$\sqrt{f'_m}\,\frac{M}{V\,l_w}$	0.35894	0.13258	2.7072	0.0075998
$\sqrt{f'_m}\,\min\left(1.0,\,\frac{M}{V\,l_w}\right)$	-0.23799	0.082323	-2.8909	0.0044325
σ_0	-0.96667	0.27026	-3.5768	0.00047316
$\sqrt{\sigma_0}$	41976	17342	2.4204	0.016739
$\frac{\rho_c\,f_{yc}}{s_c}$	695.9	289.15	2.4067	0.017356
$\frac{\rho_h\,f_{yh}}{s_h}$	303.32	57.354	5.2887	4.4494e-07
$\frac{\rho_j\,f_{yj}}{s_j}$	-1607.4	1686.9	-0.95287	0.34224
d	0.00039815	0.00026948	1.4775	0.14171
h_g	-0.0013189	0.0004989	-2.6436	0.0091051
$\frac{M}{V}$	0.00010839	0.00062154	0.17439	0.8618
$\min\left(h_g,\,l_r\right)$	0.0011464	0.00027767	4.1288	6.1286e-05
$\sqrt{f'_m}\,h_g$	0.00048306	9.0234e-05	5.3534	3.3037e-07
$\sqrt{f'_m}\,\frac{M}{V}$	0.00070431	0.00020854	3.3773	0.00093991
$f'_m\,\frac{M}{V\,l_w}\,\min\left(1.0,\,\frac{M}{V\,l_w}\right)$	-0.045445	0.020282	-2.2407	0.026567
$\sqrt{f'_m}\,\frac{\rho_j\,f_{yj}}{s_j}\,\frac{M}{V\,l_w}$	884.7	614.25	1.4403	0.15194
$\sqrt{f'_m}\,d\,\frac{M}{V\,l_w}$	-0.0010647	0.00020189	-5.2736	4.7668e-07
$\sqrt{f'_m}\,\frac{\rho_c\,f_{yc}}{s_c}\,\min\left(1.0,\,\frac{M}{V\,l_w}\right)$	131.93	45.075	2.9269	0.0039759
$\sigma_0\,\sqrt{\sigma_0}$	12967	6151	2.1081	0.036743
$\sigma_0\,\frac{\rho_c\,f_{yc}}{s_c}$	-222.03	55.856	-3.9751	0.00011057
$\sigma_0\,\frac{\rho_h\,f_{yh}}{s_h}$	-59.431	32.691	-1.818	0.071135
$\sigma_0\,d$	0.00067381	8.9379e-05	7.5388	4.7374e-12
$\sigma_0\,h_g$	0.00019165	9.2693e-05	2.0675	0.040462
$\frac{\rho_c\,f_{yc}}{s_c}\,\min\left(1.0,\,\frac{M}{V\,l_w}\right)$	-0.4457	0.15491	-2.8771	0.00462
$d\,h_g$	-7.5202e-07	2.2934e-07	-3.2791	0.0013037
$d\,\frac{M}{V}$	4.5056e-07	1.9358e-07	2.3275	0.021321

Number of observations: 171, Error degrees of freedom: 145

Root Mean Square Error: 0.2268, R^2: 0.9819

Mean: -0.0003716, Standard Deviation: 0.06065

Table 15.7: Interaction Stepwise Regression Using AIC (Continued)

(b) Partially-grouted Data

Parameter	Estimate	SE	tStat	pValue
$\sqrt{f'_m}$	0.48831	0.04753	10.274	4.7267e-19
$\sqrt{f'_m}\,\frac{M}{V\,l_w}$	0.060872	0.26312	0.23135	0.81736
$\sqrt{f'_m}\,\min\left(1.0,\,\frac{M}{V\,l_w}\right)$	-0.52031	0.27697	-1.8785	0.06226
$\sqrt{f'_m}\,s_{gv}$	-0.00356	0.0026021	-1.3681	0.17334
σ_0	-0.64677	0.2022	-3.1987	0.0016867
$\sqrt{\sigma_0}$	2.2335e+05	43553	5.1282	8.9625e-07
$\frac{\rho_c\,f_{yc}}{s_c}$	407.93	83.157	4.9056	2.4131e-06
$\frac{\rho_h\,f_{yh}}{s_h}$	482.81	275.82	1.7505	0.082093
$\frac{\rho_j\,f_{yj}}{s_j}$	3551.7	1481.8	2.3969	0.017772
h_g	-0.00080878	0.00021571	-3.7495	0.00025304
$\min\left(1.0,\,\frac{M}{V\,l_w}\right)$	0.00024506	0.00057663	0.42499	0.67146
$\min\left(1.0,\,\frac{M}{V\,l_r}\right)$	0.0012101	0.0005877	2.0591	0.041228
$f'_m\,\frac{M}{V\,l_w}$	-0.17402	0.055446	-3.1385	0.0020474
$f'_m\,\min\left(1.0,\,\frac{M}{V\,l_w}\right)$	0.17394	0.055391	3.1402	0.0020365
$f'_m\,s_{gv}$	-0.00075926	0.00053229	-1.4264	0.15584
$\sqrt{f'_m}\,\frac{\rho_h\,f_{yh}}{s_h}$	-142.79	76.845	-1.8582	0.065116
$\sqrt{f'_m}\,\frac{\rho_j\,f_{yj}}{s_j}$	-852.41	375.12	-2.2723	0.024497
$\sqrt{f'_m}\,\min\left(1.0,\,\frac{M}{V\,l_r}\right)$	-0.0001922	4.253e-05	-4.5193	1.2556e-05

affect the overall shear strength for both walls. The $\sqrt{f'_m}\,\frac{M}{V\,l_w}$ parameter was also found to be highly correlated with the fully-grouted wall strength, but the correlation of the parameter with the partially-grouted data was marginal. The analysis showed that the partially-grouted was best modeled using the $\sqrt{f'_m}\,\frac{V\,s_{gh}}{M}$ parameter, as shown in Table 15.9b.

The best-fit parameters for the confinement and horizontal reinforcement were the same for both grouting-type models but differed slighting for the joint reinforcement parameter. In the fully-grouted model the best choice for the length term was the gross height of the wall h_g but in the partially-grouted model the best choice was to use the reinforced length l_r of the wall. The source of this disparity is uncertain, but it is likely due to distribution of joint-reinforced specimens

Table 15.7: Interaction Stepwise Regression Using AIC (Continued)

(c) Partially-grouted Data (Continued)

Parameter	Estimate	SE	tStat	pValue
$f'_m \, s_{gv} \, \frac{M}{V \, l_w}$	0.0012154	0.00049612	2.4497	0.015456
$\sqrt{f'_m} \, \sigma_0 \, \frac{M}{V \, l_w}$	0.15198	0.028266	5.3767	2.8717e-07
$\sqrt{f'_m} \, \frac{M}{V \, l_w} \, \frac{\rho_h \, f_{yh}}{s_h}$	174.13	67.394	2.5837	0.010736
$\sqrt{f'_m} \, \frac{M}{V \, l_w} \, h_g$	0.00015362	4.3093e-05	3.5649	0.00048953
$\sqrt{f'_m} \, \frac{M}{V \, l_w} \, \min\left(1.0, \, \frac{M}{V \, l_w}\right)$	0.00027195	0.00016566	1.6416	0.10279
$\sqrt{f'_m} \, \frac{M}{V \, l_w} \, \min\left(1.0, \, \frac{M}{V \, l_r}\right)$	-0.00034163	0.00015787	-2.164	0.032054
$\sqrt{f'_m} \, \sigma_0 \, s_{gv}$	0.0066949	0.0016579	4.0383	8.5895e-05
$\sqrt{f'_m \, \sigma_0} \, s_{gv}$	-932.68	331.6	-2.8127	0.0055754
$\sqrt{f'_m} \, s_{gv} \, \frac{\rho_h \, f_{yh}}{s_h}$	-8.4003	2.7209	-3.0873	0.0024092
$\sqrt{\sigma_0^3}$	-16435	5571.3	-2.9499	0.0036928
$\sqrt{\sigma_0} \, \frac{\rho_c \, f_{yc}}{s_c}$	-9.148e+07	1.7005e+07	-5.3796	2.8336e-07
$\sqrt{\sigma_0} \, h_g$	-104.01	20.427	-5.0917	1.0565e-06
$\sqrt{\sigma_0} \, \min\left(1.0, \, \frac{M}{V \, l_r}\right)$	29.754	13.998	2.1256	0.035186
$\frac{\rho_h \, f_{yh}}{s_h} \, \frac{\rho_j \, f_{yj}}{s_j}$	9.0776e+05	2.9446e+05	3.0828	0.0024439
Number of observations: 181, Error degrees of freedom: 149				
Root Mean Square Error: 0.1481, R^2: 0.9777				
Mean: 0.5.767e-05, Standard Deviation: 0.1633				

between the two groups. In practice, it would be desirable for the length term on both the horizontal and joint reinforcement to be the same since they are both oriented in the same direction.

15.4 Model Fitting

The findings from the previous analysis were used to further develop and fit a model to the data. It was apparent from the inconsistency between the parameter coefficients that there was some adjustment to the parameters that needed to be made before developing the final model. The adjustments were made one at a time to determine how they affected the goodness of fit for the model. The vast difference between the masonry contribution parameters for fully- and partially-grouted models showed that there was no feasible way to have a model that represented both grouting types equally well while maintaining the same coefficients for the masonry components.

Table 15.8: Interaction Stepwise Regression Using BIC

(a) Fully-Grouted Data

Parameter	Estimate	SE	tStat	pValue
$\sqrt{f'_m}$	0.42093	0.03222	13.064	4.695e-27
$\sqrt{f'_m}\ \min\left(1.0,\ \frac{M}{V\,l_w}\right)$	-0.29328	0.036778	-7.9743	2.6788e-13
σ_0	0.26322	0.035432	7.4289	6.0593e-12
$\frac{\rho_c\,f_{yc}}{s_c}$	-92	193.24	-0.4761	0.63465
$\frac{\rho_h\,f_{yh}}{s_h}$	-263.73	210.18	-1.2548	0.21138
$\frac{\rho_j\,f_{yj}}{s_j}$	1054.3	427.26	2.4676	0.014648
$\frac{M}{V}$	-0.00016841	6.0517e-05	-2.7829	0.0060325
$\sqrt{f'_m}\,\frac{\rho_h\,f_{yh}}{s_h}$	141.56	43.96	3.2201	0.0015505
$\sqrt{f'_m}\,\frac{\rho_c\,f_{yc}}{s_c}\ \min\left(1.0,\ \frac{M}{V\,l_w}\right)$	133.54	46.742	2.857	0.0048423
$\sigma_0\,\frac{\rho_h\,f_{yh}}{s_h}$	-104.97	35.335	-2.9708	0.0034255

Number of observations: 171, Error degrees of freedom: 161
Root Mean Square Error: 0.2997, R^2: 0.9684
Mean: -0.0002444, Standard Deviation: 0.3089

(b) Partially-grouted Data

Parameter	Estimate	SE	tStat	pValue
$\sqrt{f'_m}$	0.24961	0.015547	16.055	3.5734e-36
$\sqrt{f'_m}\,\frac{M}{V\,l_w}$	0.11816	0.035835	3.2973	0.0011834
$\sqrt{f'_m}\,s_{gv}$	-0.0011391	0.00043145	-2.6403	0.009037
σ_0	0.050756	0.046943	1.0812	0.2811
$\frac{\rho_h\,f_{yh}}{s_h}$	140.82	48.538	2.9013	0.0041961
$f'_m\,\frac{M}{V\,l_w}$	-0.042311	0.0057456	-7.3642	6.8338e-12
$\sqrt{f'_m}\,\sigma_0\,\frac{M}{V\,l_w}$	0.041599	0.012476	3.3342	0.0010453

Number of observations: 181, Error degrees of freedom: 174
Root Mean Squared Error: 0.2287, R^2: 0.9469
Mean: 0.006092, Standard Deviation: 0.2333

Table 15.9: Best-Fit Parameters from Manual Stepwise Regression

(a) Fully-Grouted Data

Parameter	Estimate	SE	tStat	pValue
$\sqrt{f'_m}$	0.070577	0.017641	4.0007	9.5165e-05
$\sqrt{f'_m}\,\frac{V\,l_w}{M}$	0.068849	0.0080365	8.567	7.2148e-15
σ_0	0.24724	0.028205	8.7659	2.1735e-15
$\frac{\rho_c\,f_{yc}}{s_c}\,l_w$	0.21597	0.033959	6.3598	1.906e-09
$\frac{\rho_h\,f_{yh}}{s_h}\,h_g$	0.17281	0.023179	7.4554	4.8106e-12
$\frac{\rho_j\,f_{yj}}{s_j}\,h_g$	0.82205	0.32639	2.5186	0.012734
Number of observations: 171, Error degrees of freedom: 165				
Root Mean Squared Error: 0.3473, R^2: 0.9576				
Mean: -0.007988, Standard Deviation: 0.3535				

(b) Partially-Grouted Data

Parameter	Estimate	SE	tStat	pValue
$\sqrt{f'_m}$	0.090355	0.009172	9.8512	1.7132e-18
$\sqrt{f'_m}\,\frac{V\,s_{gh}}{M}$	0.074162	0.0075839	9.7789	2.7212e-18
σ_0	0.17357	0.021497	8.0742	1.0554e-13
$\frac{\rho_c\,f_{yc}}{s_c}\,l_w$	0.14647	0.027386	5.3484	2.7474e-07
$\frac{\rho_h\,f_{yh}}{s_h}\,h_g$	0.084074	0.027878	3.0158	0.002945
$\frac{\rho_j\,f_{yj}}{s_j}\,h_g$	-0.014439	0.042003	-0.34376	0.73144
Number of observations: 168, Error degrees of freedom: 162				
Root Mean Squared Error: 0.3018, R^2: 0.9215				
Mean: 0.01274, Standard Deviation: 0.3018				

It was decided that since the masonry component contributed the most to the wall shear strength out of all the parameters, it would be best to use different coefficients for the masonry contribution parameters for fully- and partially-grouted walls while leaving the remaining parameters constant for both grouting types.

The two best model fitted to the dataset were produced using two different weighting schemes. The first model is given by

$$\begin{aligned} V_n &= V_m + V_p + V_c + V_s \\ &= \begin{cases} \left(1.8141 + 0.71402\dfrac{V\,l_w}{M}\right) A_{nv}\sqrt{f'_m} & \text{for fully-grouted} \\ \left(1.0337 + 1.0491\dfrac{V\,s_{gh}}{M}\right) A_{nv}\sqrt{f'_m} & \text{for partially-grouted} \end{cases} \\ &+ 0.14604P \\ &+ 0.12617\frac{A_c f_{yc}}{s_c} l_w \\ &+ 0.11366\left(\frac{A_h f_{yh}}{s_h} + \frac{A_j f_{yj}}{s_j}\right) h_g \end{aligned} \tag{15.1}$$

and was derived using the data weighting scheme described in Section 13.3.4. The second model is given by

$$\begin{aligned} V_n &= V_m + V_p + V_c + V_s \\ &= \begin{cases} \left(2.2451 + 0.70467\dfrac{V\,l_w}{M}\right) A_{nv}\sqrt{f'_m} & \text{for fully-grouted} \\ \left(0.99828 + 1.1490\dfrac{V\,s_{gh}}{M}\right) A_{nv}\sqrt{f'_m} & \text{for partially-grouted} \end{cases} \\ &+ 0.098459P \\ &+ 0.10751\frac{A_c f_{yc}}{s_c} l_w \\ &+ 0.11649\left(\frac{A_h f_{yh}}{s_h} + \frac{A_j f_{yj}}{s_j}\right) h_g \end{aligned} \tag{15.2}$$

and was derived using no weighting in the regression. In the latter model, it was observed from the coefficients of determination that the models consistently better fit the fully-grouted data than the partially-grouted data. The introduction of weighting in the analysis improved the fit of the model with the partially-grouted data and slightly diminished the fit with the fully-grouted data. This trade-off was justified because the end model would have closer coefficients of variation for the two grouting types (possibly eliminating the need to use two different resistance factors) and because the model produces a better fit than the current MSJC (2013) model. The standard deviation of the partially-grouted residuals was typically lower than that of the fully-grouted residuals, but since the

mean failure strength of the partially-grouted was also lower than the mean fully-grouted strength, the coefficient of variation was higher for the partially-grouted data.

The coefficients in the two models are too precise to use in a design because they would suggest that the numerical approximations made with the model are more accurate than they truly are. This was evident from the differences in coefficient values between the two models despite the fact that they were derived from the same dataset. The values in the models could not be simply rounded because the total model performance was more sensitive to some coefficient values than to other values and changing the values would affect the performance of the model for the two grouting types. Each adjustment to the model coefficients was compared against the recalculated goodness-of-fit parameters and the mean, standard deviation, and coefficient of variation of the residuals. The values in the weighted model were favored over the unweighted model because inspection of the residual plots showed it to be more homoscedastic that the unweighted model. After comparing numerous iterative adjustments to the model, the final model selected is given by

$$
\begin{aligned}
V_n &= V_m + V_p + V_s \\
&= \begin{cases} \left(1.8 + 0.7\dfrac{V\,l_w}{M}\right) A_{nv}\sqrt{f'_m} & \text{for fully-grouted} \\ \left(1.1 + 0.9\dfrac{V\,s_{gh}}{M}\right) A_{nv}\sqrt{f'_m} & \text{for partially-grouted} \end{cases} . \qquad (15.3) \\
&\quad + 0.15P \\
&\quad + 0.12\left[\frac{A_c f_{yc}}{s_c}\, l_w + \left(\frac{A_h f_{yh}}{s_h} + \frac{A_j f_{yj}}{s_j}\right) h_g\right]
\end{aligned}
$$

One assumption used in the building of the final model in Equation (15.3) what that the coefficients for all three reinforcement components should be the same. The assumption that the horizontal bar and wire joint reinforcement coefficients are equal was made previously. The assumption that the horizontal and vertical reinforcement contributions should have the same value was made because the coefficient estimates have been consistently close during many of the analyses. The theoretical belief that the horizontal reinforcement was directly involved in resisting the lateral shear force was previously invalidated by the analysis in Chapter 14. The new hypothesis is that the horizontal reinforcement works by keeping the diagonal cracks in the masonry closed and enabling the masonry to transfer stresses via strut action and crack friction, similar to the role of the vertical reinforcement. Since diagonal cracking typically forms at a 45 °angle, the horizontal

and vertical reinforcement are equally effective in restricting the diagonal cracks from opening and should have the same coefficient.

The coefficients in Equation (15.3) differed slightly from the optimal estimates shown in Equations (15.1) and (15.2), so the mean of the residuals was not equal to zero. Since the former two models were developed using both fully- and partially-grouted data, the residual means in these two models differed from zero, with the partially-grouted residual mean greater than zero (conservative) and the fully-grouted residual mean less than zero (unconservative). In the final equation, the coefficients for the fully- and partially-grouted components were able to be adjusted such that the model was slightly conservative for both grouting types.

In the final model, the coefficient of variation for the partially-grouted data was still approximately 20 percent higher than that for the fully-grouted data. In the former model employed by prior editions of the MSJC code prior to the introduction of the grouted wall factor, the difference in the coefficient of variation for the two grouting types was nearly twice that of the current model. The introduction of the grouted wall factor brought the coefficients of variance closer, but the model means differed greatly between the two grouting types. It appears that the variance for partially-grouted data is higher than that for fully-grouted data and that no model will produce comparable variances unless the coefficients are manipulated to artificially increase the variance of the model with respect to fully-grouted data.

15.5 Limit Function

The current MSJC (2013) shear strength limit was compared with the proposed model to determine if it would provide a good upper constraint for the model. The results of the comparison, displayed in Figure 15.1, show that the MSJC limit equation does not provide a useful upper bound for the model predictions. The data that is most affected by the limit equation are the specimens at the upper tier of the plot, which the model tends to under-predicts already and for which no constraint is necessary. The MSJC limit works fairly well for the current MSJC model because it tends to over-predict the strength for stronger walls, as shown in Figure 15.2.

A new limit was developed to use with the proposed shear model in equation (15.3) to better match the performance of the model and to better represent the behavior of the components of the shear wall. The limit function was developed using stress fields and the upper-bound theorem

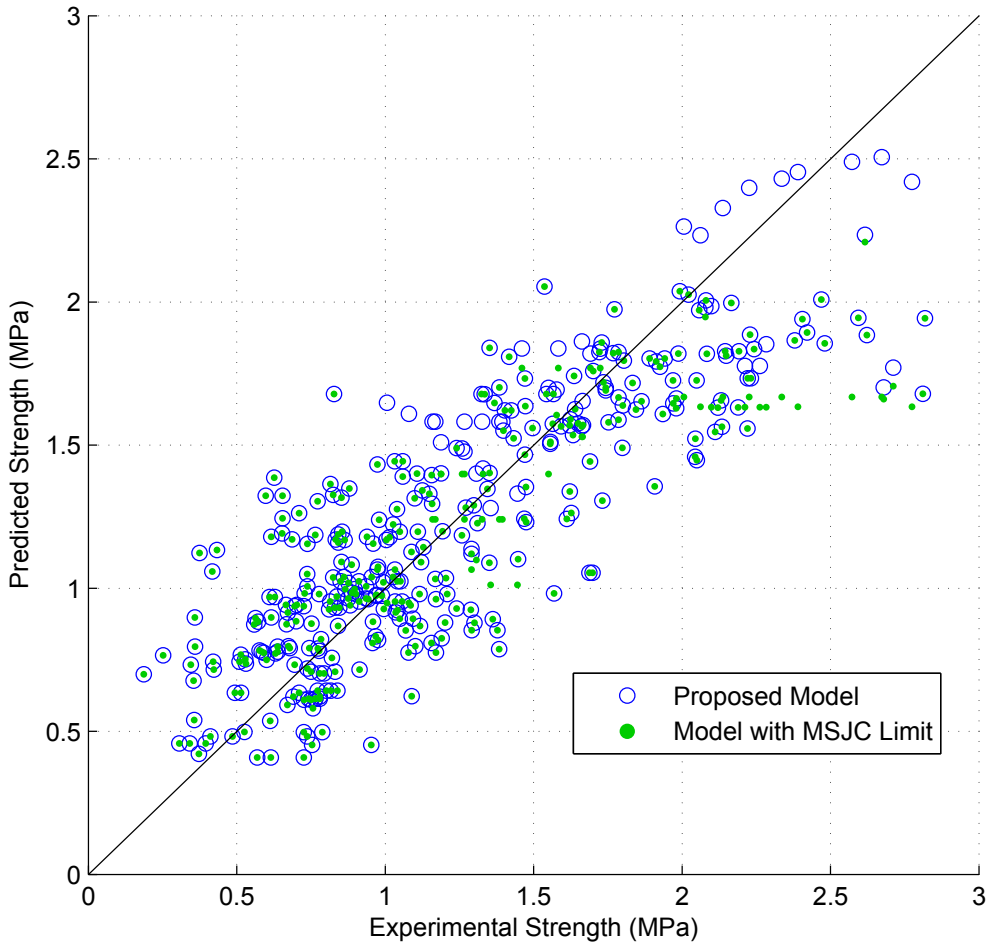

Figure 15.1: New model predictions with MSJC limit

from the theory of plasticity (Nielsen and Hoang, 2011) and is jointly based on the concepts of wall overturning from flexural theory and non-planar sections from the theory of plasticity. The limit assumes that the shear and axial forces become concentrated in the leading toe of wall, resulting in a compression block with length

$$a = \frac{A_f\, f_y + P + \dfrac{A_c\, f_{yc}}{s_c}\, l_w}{0.8\, f'_m\, t_s} \tag{15.4}$$

where t_s is the shear thickness of the wall and is taken as the gross thickness for fully-grouted walls and the total face shell thickness for partially-grouted walls. The total vertical force transferred through the block is equal to the sum of the axial load, flexural reinforcement yield strength, and yield strength of all the confinement reinforcement. The stress from the vertical force is assumed to

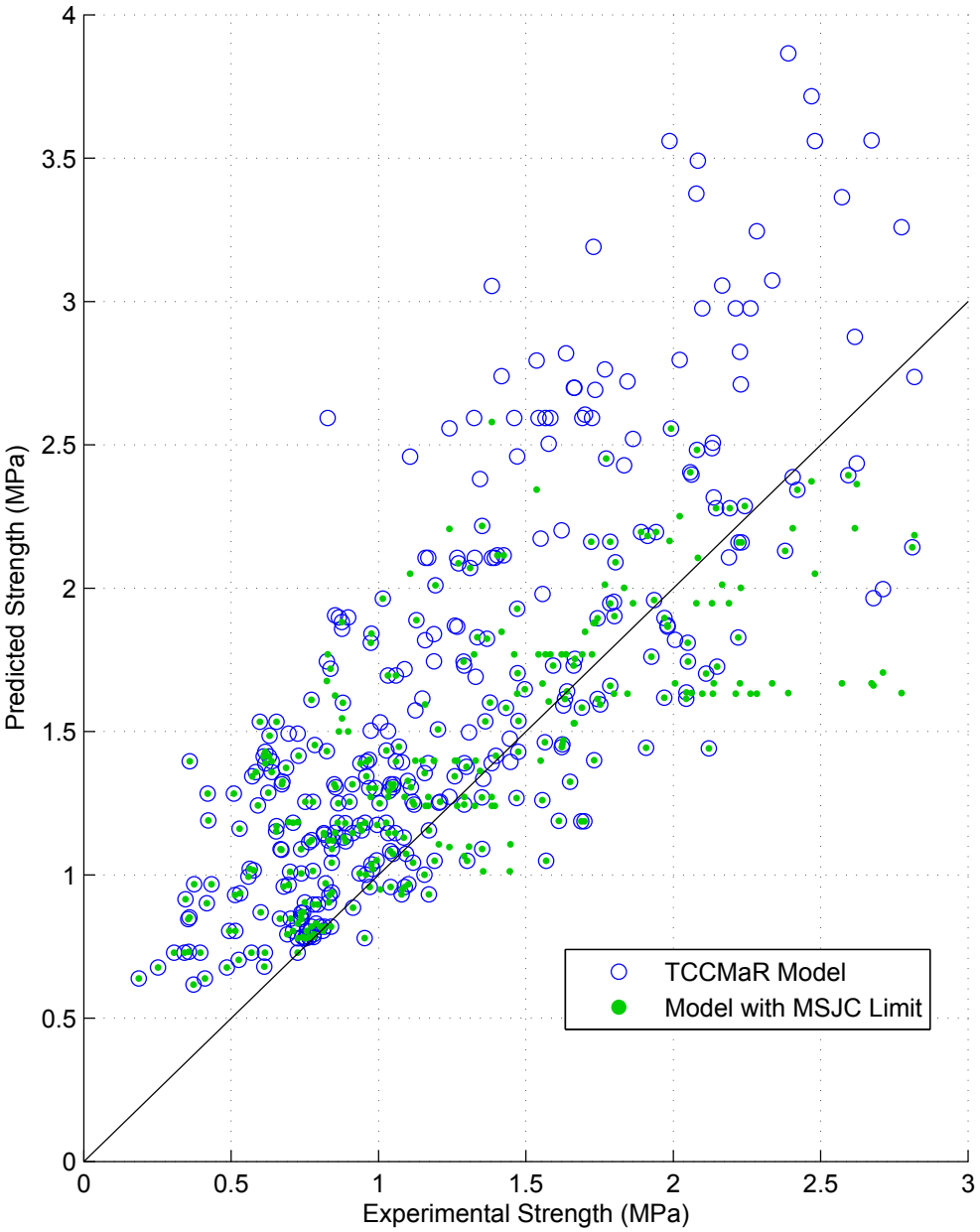

Figure 15.2: TCCMaR model predictions with MSJC limit

be uniformly distributed across the wall section at the height of the inflection point of the wall. In walls with cantilever loading conditions, the inflection point is at the top of the wall and the stress fields follow the path shown in figure 15.3a. Walls loaded in double-curvature have an inflection point located at the mid-height of the wall, producing the stress fields shown in figure 15.3b. The double-curvature case can be degenerated to two cantilevered sections, one on top of the other, by taking a slice through the mid-height of the wall, as shown in figure 15.4.

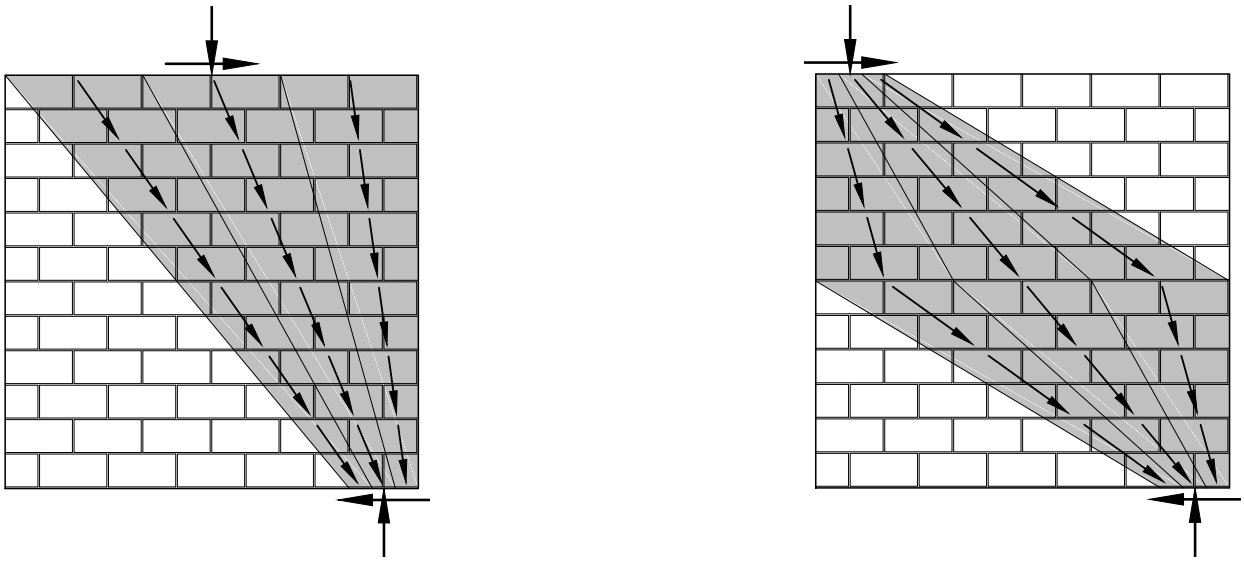

(a) Under cantilever loading (b) Under double-curvature loading

Figure 15.3: Stress fields in masonry shear walls

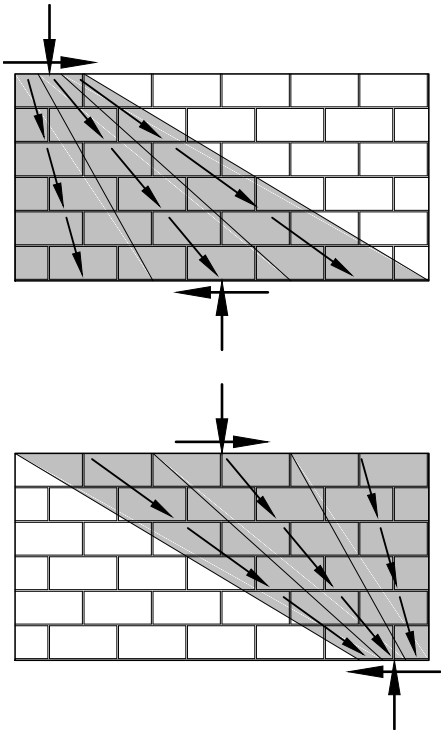

Figure 15.4: Degenerated case of stress fields in walls subject to double-curvature

The lateral offset between the resultant forces at the toe and inflection point of the wall generate a moment force which represents the upper bound of the ultimate shear strength of the

wall. The maximum shear force corresponding to this upper bound is given by

$$V_{n(max)} = \frac{0.8\, f'_m\, a\, t_n\, \dfrac{lw - a}{2} + A_f\, f_y \left(d - \dfrac{a}{2}\right)}{\dfrac{M_u}{V_u}} \tag{15.5}$$

which cannot be exceeded without causing the wall panel to begin to overturn. Equation (15.5) can be combined with equation (15.4) to produce a second potential form of the equation, which is given by

$$V_{n(max)} = \frac{\left(P + \dfrac{A_c\, f_{yc}}{s_c}\, l_w\right) \dfrac{l_w - a}{2} + A_f\, f_y \left(d - a + \dfrac{l_w}{2}\right)}{\dfrac{M_u}{V_u}}\,. \tag{15.6}$$

When the limit is exceeded the wall will begin to experience large, appreciable horizontal cracking due to the overturning of the wall panel. Should the wall reach this level of shear force without crushing the masonry, the vertical reinforcement will begin to strain harden and prevent the wall from overturning. The limit function assumes all of the confinement reinforcement to contribute in resisting the overturning force. This assumption is based on the redistribution of forces which occurs within the wall panel when cracks form in the wall panel. Once cracking has occurred within the wall panel, plane sections are interrupted and the paths of stresses are redistributed to minimize the strain energy within the panel. Further discussion of the topics of plasticity and stress fields is performed in-depth in part V of this dissertation.

The new limit function was compared with the predictions from the linear model to determine how the predicted values changed. Figure 15.5 shows that the proposed model with the new limit performs better overall, particularly for many of the lower- and higher-strength specimens. This behavior suggests that many of the specimens which appeared to fail in shear may have failed prematurely before reaching their ultimate shear capacity.

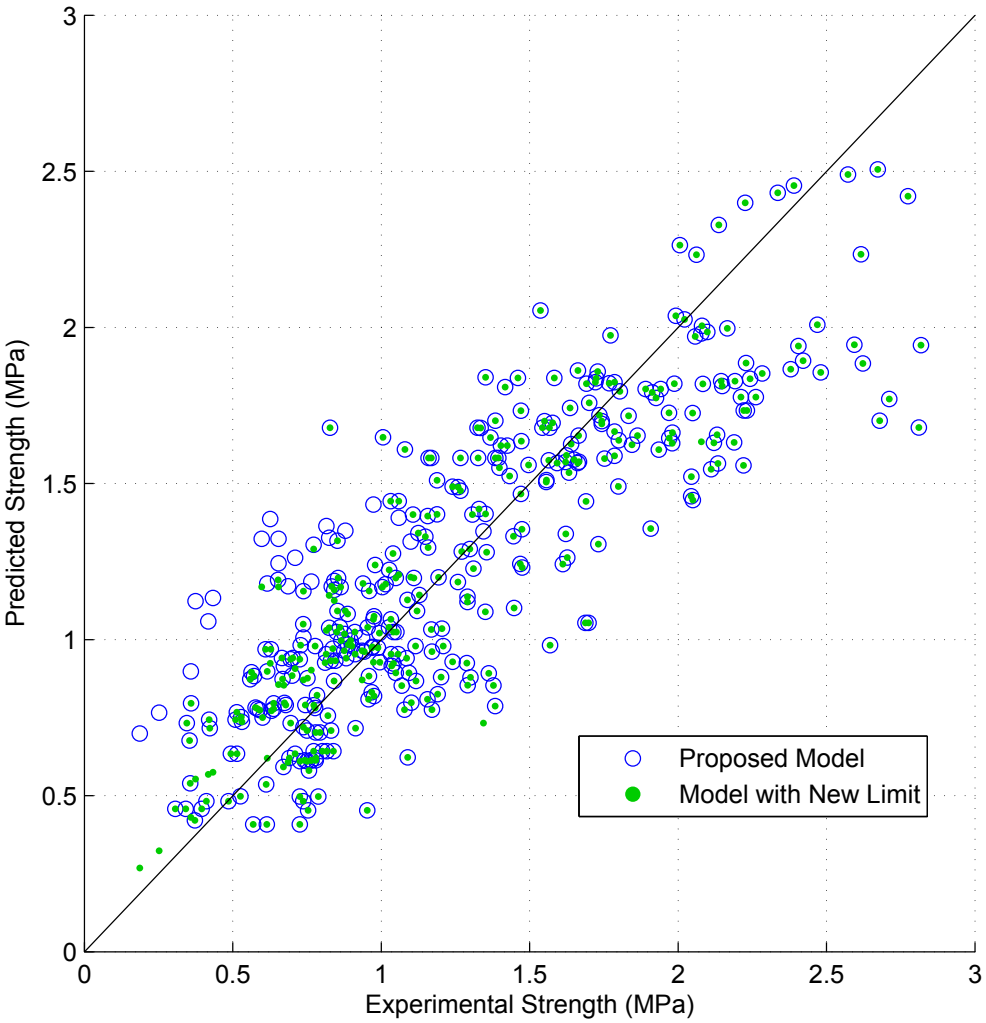

Figure 15.5: New model predictions with flexure limit

CHAPTER 16. DISCUSSION OF MODEL PERFORMANCE

16.1 Performance of Shear Strength Models

The performance of each of the existing models and the new, proposed model were evaluated using the new dataset developed in Part II of this dissertation. Each model is presented in a common format to ease comparison of the individual models. Each model was formatted such that the notation was updated to that used herein and each equation was transformed into units of stress assuming the input and output variables to be in SI units. Each model was also segregated into its component parts to further facilitate comparison and identification of which components are included in each model.

The performance of each model was investigated by calculating the goodness-of-fit statistics for the full dataset and for the fully- and partially-grouted subsets. The root mean square error shows the quadratic mean deviation of the predicted values from the experimental values and the coefficient of determination R^2 shows how well each model accounts for the variation in the experimental values (Chatterjee and Hadi, 2006). The mean of the residuals are given to show how conservative (for positive means) or unconservative (for negative means) the models are for each grouting subset compared to each other and for the whole dataset. The standard deviation of the residuals is a gauge of the variance of the model for each of the subsets and for the data as a whole.

The predicted values for each model were also plotted against the experimental values to visualize how each model fit the dataset. A line of unity slope was included on each plot to denote the perfect fit between predicted and experimental values. As the predicted strength was plotted on the ordinate, any plotted strength appearing above the unity slope line is over-predicted (i.e., unconservative) and any strength below the line is under-predicted (i.e., conservative). Since the experimental strength was constant for all models, it was plotted on the abscissa so that the domain would be consistent between all plots.

The fit for the models for each group is more variable than for the dataset as a whole. While it is inevitable that some models would fit certain data groups better than others, the principal aim of this investigation is to explore which model performs consistently well across all feasible designs. For further inspection and comparison of the performance for each model, plots of the predicted values and experimental values for each group are included in Appendix F.

16.1.1 Matsumura

The Matsumura (1987) equation is given by

$$\begin{aligned} v_n &= v_m + v_p + v_s \\ &= 0.875 k_u k_p \left(\frac{0.76}{\frac{M}{Vd}+0.7} + 0.012 \right) \sqrt{f'_m} \; + \; 0.175\sigma_0 \\ &\quad + 0.1575\gamma\delta\sqrt{\rho_h f_{yh} f'_m} \end{aligned} \tag{16.1}$$

The goodness-of-fit statistics in Table 16.1 show a large disparity in the mean error between the fully- and partially-grouted walls. Since the partially-grouted wall typically experienced a lower failure stress than the fully-grouted walls, this disparity suggests that the model may display some heteroscedasticity. This suspicion is confirmed by the distinct cone shape of the data values plotted in Figure 16.1. One potential cause of the heteroscedasticity is that the equation is based on gross wall area, as opposed to net wall area. The shear strengths are divided by the gross area rather than by the net area, the respective shear stresses for the partially-grouted walls are smaller than they would be otherwise—since the gross area is always larger than the net area. The R^2 values reveal that the Matsumura model is better at predicting the strengths of partially-grouted walls than those of fully-grouted walls. Part of this may be because the Matsumura model was developed predominantly using partially-grouted specimens.

Table 16.1: Goodness-of-Fit Statistics for Matsumura Model

Grouting	RMSE (MPa)	R^2	Residuals (MPa)	
			Mean	Std Dev
Both	0.6021	0.8081	0.4350	0.6056
Full	0.7769	0.7928	0.6343	0.4377
Partial	0.3893	0.8497	0.2467	0.2988

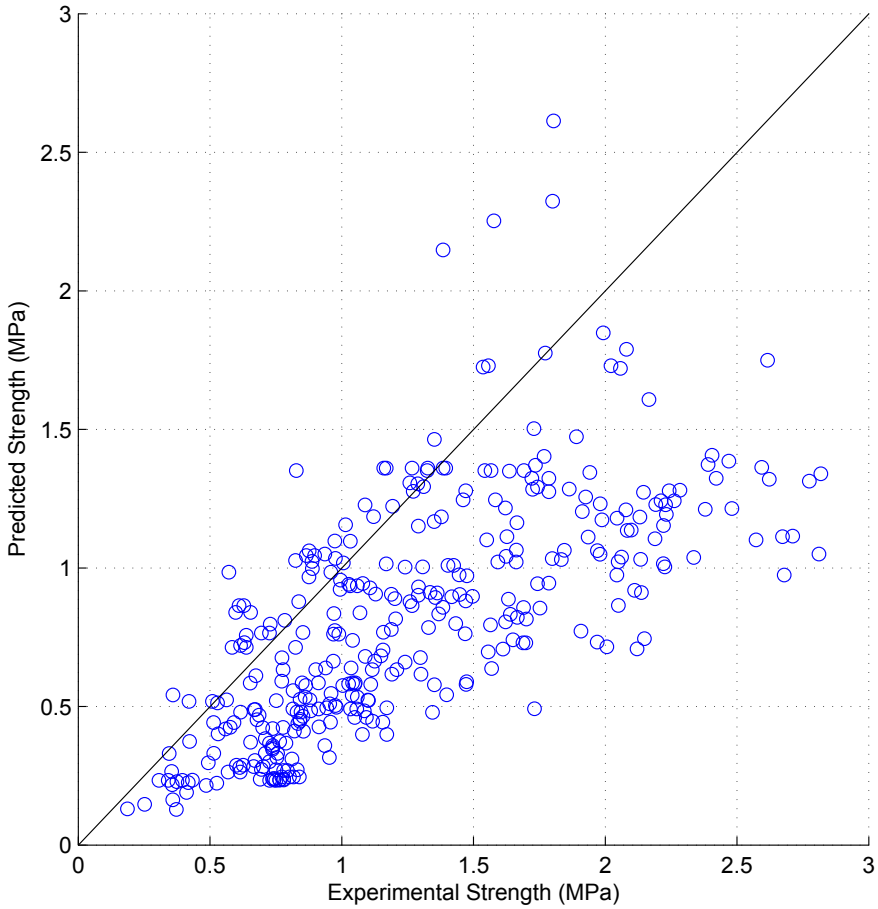

Figure 16.1: Matsumura model predictions

The Matsumura model is notably conservative in that it only over-predicted the strength for about 10 percent of the specimens. This proportion is more typical of the results that would be expected after applying the strength reduction factor to the equation. For this reason, the Matsumura model appears to be very conservative.

16.1.2 Architectural Institute of Japan

The Architectural Institute of Japan code model (Okamoto et al., 1987) is given by

$$\begin{aligned} v_n &= v_m + v_p + v_s \\ &= 0.0464\rho_t^{0.23}\frac{f'_m + 17.7}{\frac{M}{Vl_w} + 0.12} + 0.0875\sigma_0 + 0.740\sqrt{\rho_h f_{yh}} \end{aligned} \tag{16.2}$$

The goodness-of-fit statistics in Table 16.2 show that the AIJ model is a far better fit for the fully-grouted data than for the partially-grouted data. The data plotted in Figure 16.2 show a definite sign of heteroscedasticity due to its wide, cone-shaped pattern. The wide shape is reflected in the relatively large values for the standard deviation. Unlike the Matsumura equation, the AIJ model is fairly representative of the mean strength for the lower two-thirds of the experimental strength range, which is the reason for the small residual mean value for the full dataset. The model is conservative for the upper third of the range of experimental strengths.

Table 16.2: Goodness-of-Fit Statistics for AIJ Model

Grouting	RMSE (MPa)	R^2	Residuals (MPa)	
			Mean	Std Dev
Both	0.5994	0.8098	0.004786	0.6028
Full	0.5395	0.9001	0.3195	0.4318
Partial	0.6632	0.5637	-0.2926	0.5936

It is particularly notable that three of the four statistics for the AIJ model are nearly the same as those for the Matsumura model when considering the full dataset. The difference in statistics between the two model is that the AIJ model has a mean strength of 0.005 MPa (0.7 psi) and the Matsumura model has a mean of approximately 0.44 MPa (63 psi). However, when comparing the statistics between the two models for each of the subsets, the results are very different. One approach to improve the fit for the Japanese model would be to use the Matsumura model for partially-grouted walls and to use the AIJ model for fully-grouted walls.

16.1.3 Blondet et al.

The model developed by Blondet et al. (1989) is given by

$$\begin{aligned} v_n &= v_m + v_s \\ &= \left(\beta_g - 1.75\frac{M}{Vd}\right)\sqrt{f'_m} + \tfrac{1}{2}v_s \end{aligned} \tag{16.3}$$

The goodness-of-fit statistics in Table 16.3 reveal that the Blondet model had a fairly consistent fit between the fully- and partially-grouted subsets. The model is moderately conservative by about

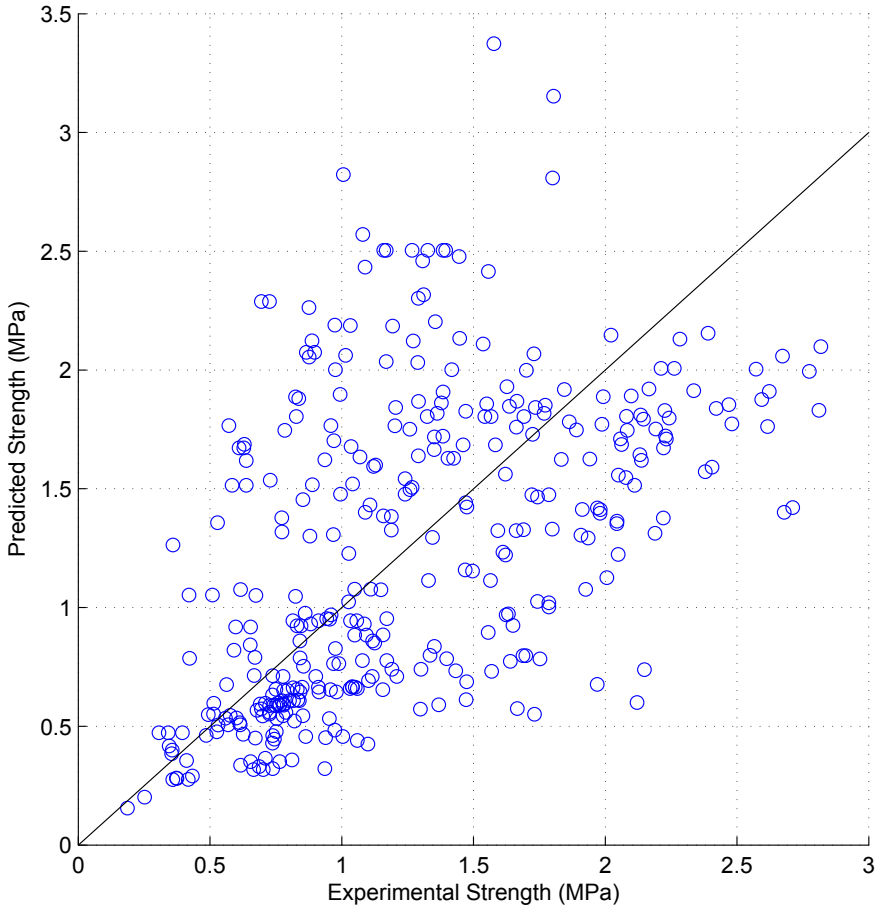

Figure 16.2: AIJ model predictions

0.16 MPa (23 psi) for the fully-grouted data and by about 0.16 MPa (23 psi) for the partially-grouted data. In computing the predicted strengths for the Blondet model, it was necessary to impose a constraint on the shear span ratio such that $\frac{M}{Vd} \leq 1$, otherwise the model would predict some specimens as having negative strength. The imposition of this constraint served to form a lower limit on the predicted strength at about 0.5 MPa, giving the predictions in Figure 16.3 the appearance of being heteroscedastic; otherwise, the data would have followed a more homoscedastic pattern. This constraint also served to inflate the predicted strengths for many of the partially grouted specimens, causing the mean strength for the partially-grouted data to be over-predicted.

Table 16.3: Goodness-of-Fit Statistics for Blondet Model

Grouting	RMSE (MPa)	R^2	Residuals (MPa)	
			Mean	Std Dev
Both	0.4468	0.8943	-0.005911	0.4487
Full	0.5003	0.9136	0.1593	0.4738
Partial	0.3980	0.8419	-0.1620	0.3630

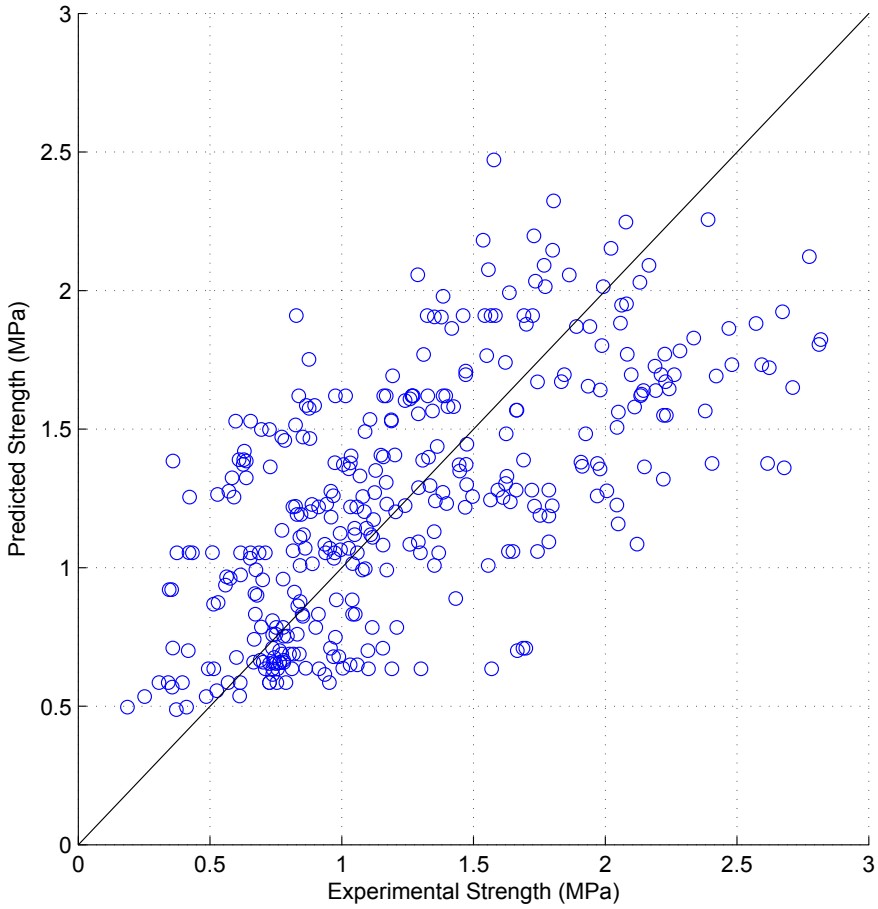

Figure 16.3: Blondet model predictions

16.1.4 Shing et al.

The model developed by Shing et al. (1990) is given by

$$\begin{aligned} v_n &= v_m + v_p + v_s \\ &= \left(0.166 + 0.0217\rho_c f_{yc}\right)\sqrt{f'_m} + 0.0217\sigma_0\sqrt{f'_m} \\ &\quad + \left(\tfrac{l_w - 2d'}{s_h} - 1\right)\rho_h f_y \end{aligned} \tag{16.4}$$

The goodness-of-fit statistics in Table 16.4 reveal that this model had a better fit for the partially-grouted data than for the fully-grouted data. The model was also more accurate at predicting the nominal strength of the partially-grouted specimens as opposed to the fully-grouted specimens. The mean predicted strength of the partially-grouted walls was accurate but was very conservative for the fully-grouted specimens by 0.40 MPa (58 psi). This behavior was unexpected because the masonry shear wall research program at the University of Colorado-Boulder, for which this model was developed, included only fully-grouted specimens.

The data plot in Figure 16.4 shows that the reason for the superior fit for the partially-grouted data is that the data appear to follow a different trendline. Due to this, the predicted values become increasingly conservative with increasing failure stress. Possible reasons for this behavior are that the model is missing parameters and/or the model uses the incorrect coefficient values. The model shows some degree of heteroscedasticity, but nowhere as large as that of the AIJ and Matsumura models.

Table 16.4: Goodness-of-Fit Statistics for Shing Model

Grouting	RMSE (MPa)	R^2	Residuals (MPa)	
			Mean	Std Dev
Both	0.4815	0.8772	0.1929	0.4843
Full	0.6266	0.8652	0.4008	0.4776
Partial	0.3012	0.9100	-0.003438	0.3012

16.1.5 Anderson and Priestley

The Anderson and Priestley (1992) model is given by

$$\begin{aligned} v_n &= v_m + v_p + v_s \\ &= b_1\sqrt{f'_m} + 0.25\sigma_0 + 0.5\rho_h f_y \end{aligned} \tag{16.5}$$

The goodness-of-fit statistics in Table 16.5 show that the model as a whole is fairly accurate, with a mean predicted strength less than 0.07 MPa (10 psi). However, the accuracy of the model varies between the two grouting type, from being conservative by 0.15 MPa (22 psi) for fully-grouted

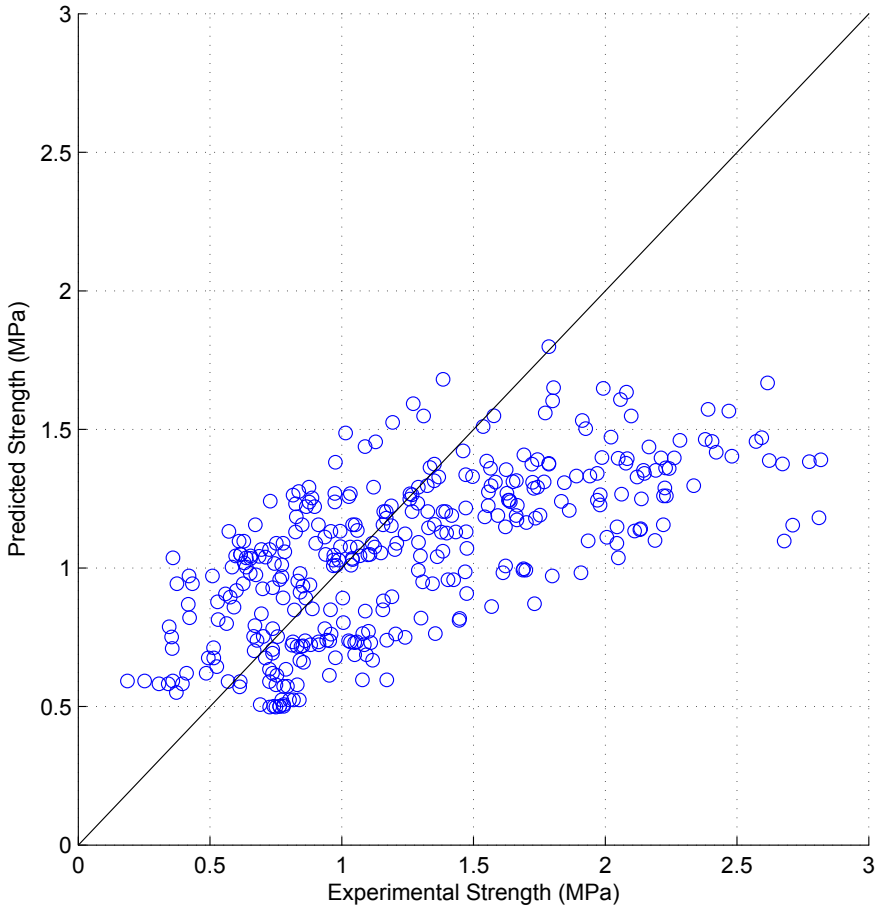

Figure 16.4: Shing model predictions

wall to being unconservative by 0.28 MPa (40 psi) for partially-grouted walls. Inspection of the RMSE and standard deviation values and the data plot in Figure 16.5 reveal that the Anderson and Priestley model has a very low level of precision. The parallelogrammatic shape of the strength plot makes it difficult to ascertain whether the residuals are heteroscedastic—with both increasing and decreasing variance—or homoscedastic with a rotated mean line. In either case, the results suggest that the Anderson and Priestley model is mis-parameterized.

Table 16.5: Goodness-of-Fit Statistics for Anderson and Priestley Model

Grouting	RMSE (MPa)	R^2	Residuals (MPa)	
			Mean	Std Dev
Both	0.5440	0.8434	-0.07048	0.5463
Full	0.5581	0.8924	0.1489	0.5375
Partial	0.5396	0.7096	-0.2778	0.4612

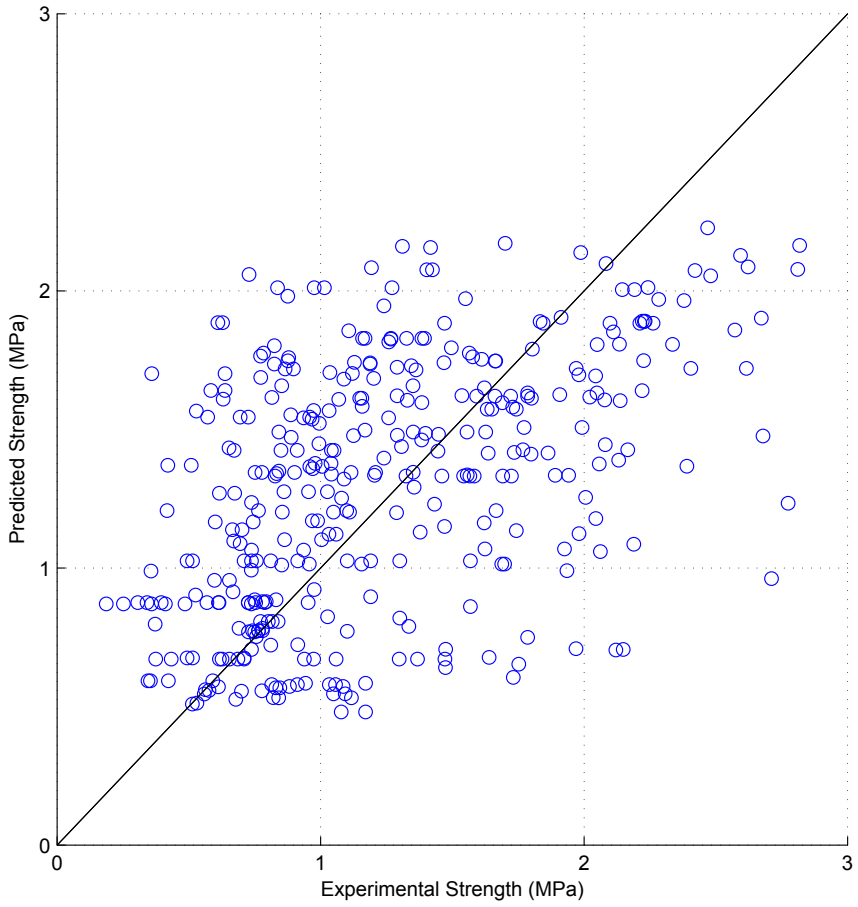

Figure 16.5: Anderson and Priestley model predictions

16.1.6 Fattal

The Fattal (1993) model is given by

$$\begin{aligned} v_n &= v_m + v_p + v_s \\ &= k_0 k_u \left(\frac{0.5}{\frac{M}{Vd}+0.8} + 0.18 \right) \sqrt{f'_m f_{yc}} \rho_c^{0.7} \; + \; 0.012 f'_m + 0.20\sigma_0 \\ &\quad + 0.011 \gamma \delta \rho_h^{0.31} f_{yh} \end{aligned} \tag{16.6}$$

The goodness-of-fit statistics in Table 16.6 show a fairly consistent fit of the model between the two grouting types. The model produces conservative results, with the model being about 50 percent more conservative for the fully-grouted data than for the partially-grouted data. Inspection of the strength plot in Figure 16.6 reveal the residuals to be slightly cone-shaped. The slightly improved

fit and lower standard deviation value for the partially-grouted data are likely because the model was built based on partially-grouted specimen data from three studies: Matsumura (1987), Chen et al. (1978), and Yancey and Scribner (1989).

Table 16.6: Goodness-of-Fit Statistics for Fattal Model

Grouting	RMSE (MPa)	R^2	Residuals (MPa)	
			Mean	Std Dev
Both	0.4641	0.8860	0.2952	0.4682
Full	0.5471	0.8985	0.3521	0.4133
Partial	0.3887	0.8518	0.2415	0.3013

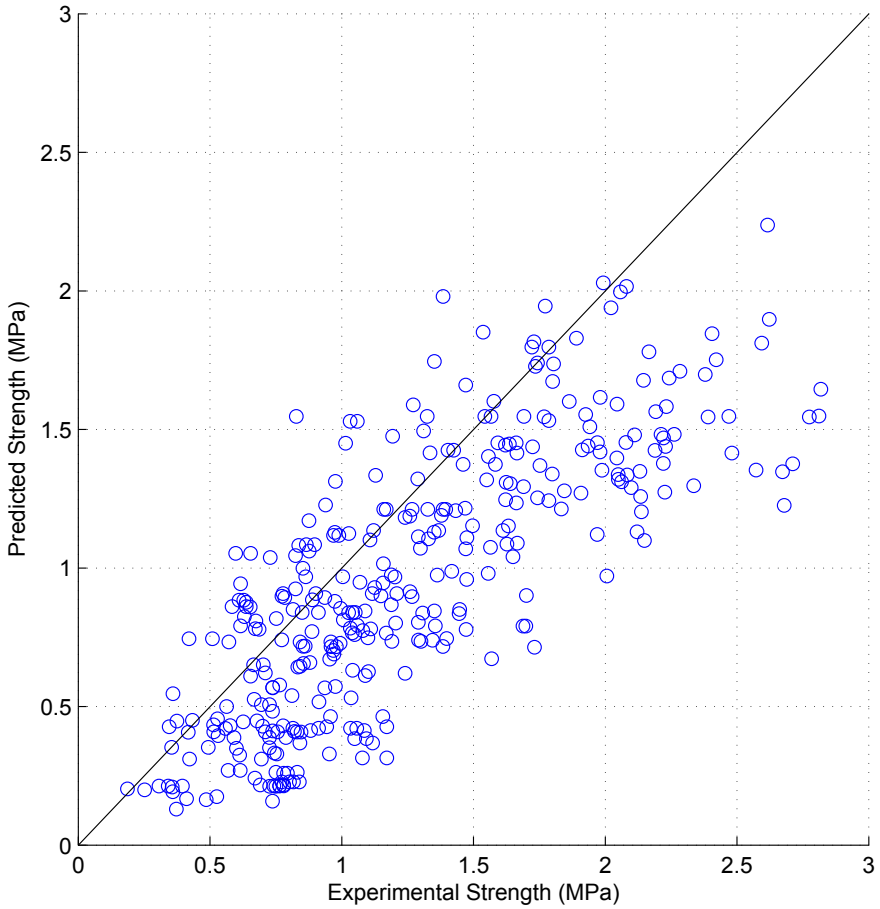

Figure 16.6: Fattal model predictions

16.1.7 TCCMaR

The TCCMaR (NEHRP, 1997) model is given by

$$\begin{aligned} v_n &= v_m + v_p + v_s \\ &= 0.083\left(4 - 1.75\frac{M}{Vl_w}\right)\sqrt{f'_m} \; + \; 0.25\sigma_0 \; + \; 0.5\rho_h f_{yh} \end{aligned} \tag{16.7}$$

The goodness-of-fit statistics in Table 16.7 show that the model is consistently unconservative for all wall types and has a better fit for the fully-grouted data. The strength plot in Figure 16.7 shows that the TCCMaR model offers an improved fit to the data as compared with the Blondet et al. (1989) and Anderson and Priestley (1992) models from which is was built. The TCCMaR model shows a degree of heteroscedasticity in the lower strength range and appears to be fairly homoscedastic for experimental shear failure stresses above 1.5 MPa (220 psi). The predicted strengths appear to follow a slope of unity, but the values are consistently too higher and suggest that some or all of the parameter coefficients used in the model are higher than they should be.

Table 16.7: Goodness-of-Fit Statistics for TCCMaR Model

Grouting	RMSE (MPa)	R^2	Residuals (MPa)	
			Mean	Std Dev
Both	0.7005	0.7402	-0.3095	0.7035
Full	0.8740	0.7362	-0.2651	0.8321
Partial	0.4995	0.7511	-0.3514	0.3521

16.1.8 UBC

The UBC (1997) model is given by

$$\begin{aligned} v_n &= v_m + v_s \\ &= 0.083 C_d \sqrt{f'_m} \; + \; \rho_h f_{yh} \frac{l_w}{s_h} \end{aligned} \tag{16.8}$$

Figure 16.7: TCCMaR model predictions

where

$$C_d = \begin{cases} 2.4 & \text{for} \quad \frac{M}{Vl_w} \leq 0.25 \\ 2.8 - 1.6\frac{M}{Vl_w} & \text{for} \quad 0.25 < \frac{M}{Vl_w} < 1.0 \\ 1.2\sqrt{f'_m} & \text{for} \quad \frac{M}{Vl_w} \geq 1.0 \end{cases}$$

The UBC model was not intended for predicting shear strength, but served as a bound on the shear capacity of masonry walls (NEHRP, 1997). The model was included in this analysis because the model form was later adapted for use as an upper bound for the shear strength in the MSJC (2013)

code. The goodness-of-fit statistics in Table 16.8 show a poor fit between the model and the experimental data. The reason for the poor fit is revealed in Figure 16.8 which shows a large variance in the predicted values, with several values being over-predicted by as much as a factor of 2.5. The results of the UBC model show that the predicted strength cannot be effectively accomplished solely using the shear span ratio and the characteristic strength of the masonry.

Table 16.8: Goodness-of-Fit Statistics for UBC Model

Grouting	RMSE (MPa)	R^2	Residuals (MPa) Mean	Std Dev
Both	0.9177	0.5541	-0.2058	0.9217
Full	1.093	0.5872	-0.2745	1.058
Partial	0.7329	0.4641	-0.1409	0.7190

16.1.9 New Zealand Standard

The Standard Association of New Zealand (NZS) (2004) model for shear walls is given by

$$\begin{aligned} v_n &= v_m + v_p + v_s \\ &= 0.083034\,(C_1 + C_2)\sqrt{f'_m} \;+\; 0.9\sigma_0 \frac{V\,(l_w - a)}{2M} \;+\; C_3 \rho_h f_{yh} \frac{d}{s_h} \\ &\leq 0.45\sqrt{f'_m} \end{aligned} \tag{16.9}$$

where

$$\begin{aligned} C_1 &= 33\rho_f \frac{f_y}{300} \\ C_2 &= \begin{cases} 1.5 & \text{for} \quad \frac{M}{Vl_w} < 0.25 \\ 0.42\left(4 - 1.75\frac{M}{Vl_w}\right) & \text{for} \quad 0.25 \leq \frac{M}{Vl_w} \leq 1.0 \\ 1.0 & \text{for} \quad \frac{M}{Vl_w} > 1.0 \end{cases} \\ C_3 &= 0.8 \end{aligned}$$

The goodness-of-fit statistics in Table 16.9 show the Standard Association of New Zealand (NZS) model to be conservative by 0.11 MPa (16 psi) for partially-grouted walls and slightly conservative by 0.05 MPa (7 psi) for fully-grouted walls. Inspection of the results plotted in Figure 16.9 show

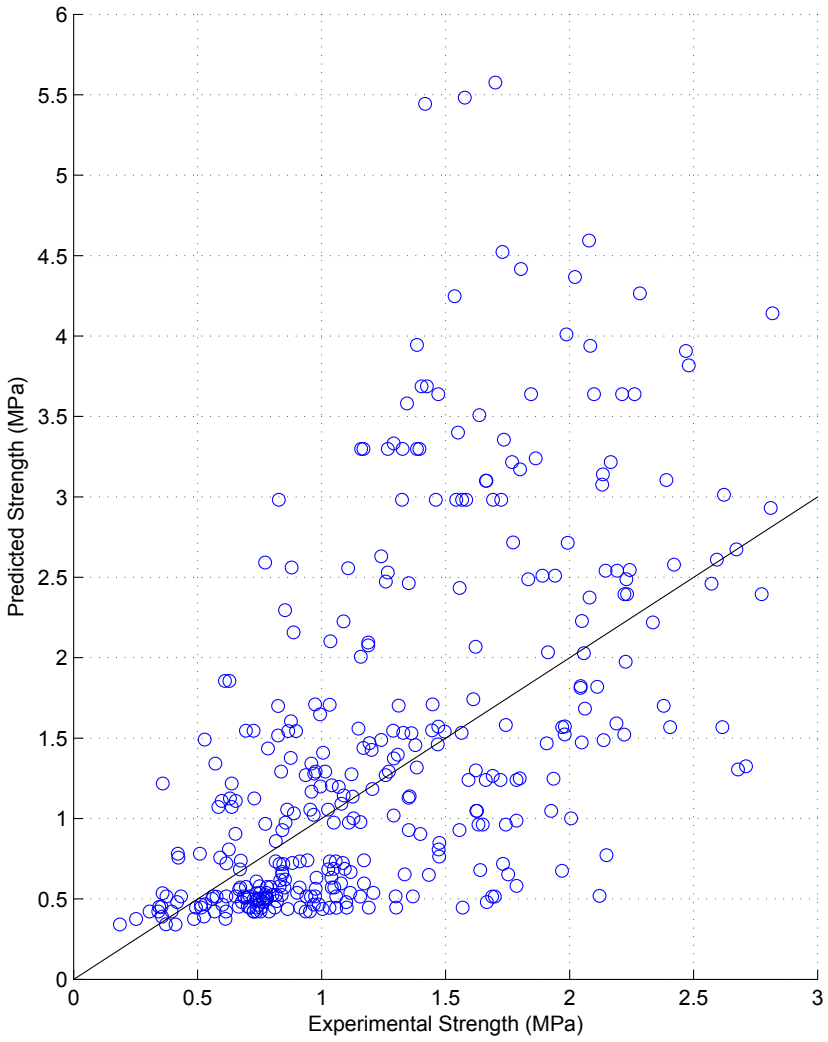

Figure 16.8: UBC model predictions

that the predictions appear to be homoscedastic, at least for experimental values below 2 MPa (300 psi). Above 2 MPa the model under-predicts the data due to the imposition of the $v_n \leq 0.45\sqrt{f'_m}$ constraint, which appears to effectively limit the effective strength to values below 2 MPa.

Table 16.9: Goodness-of-Fit Statistics for NZS Model

Grouting	RMSE (MPa)	R^2	Residuals (MPa)	
			Mean	Std Dev
Both	0.3869	0.9208	0.07881	0.3896
Full	0.4294	0.9371	0.04842	0.4266
Partial	0.3542	0.8763	0.1075	0.3370

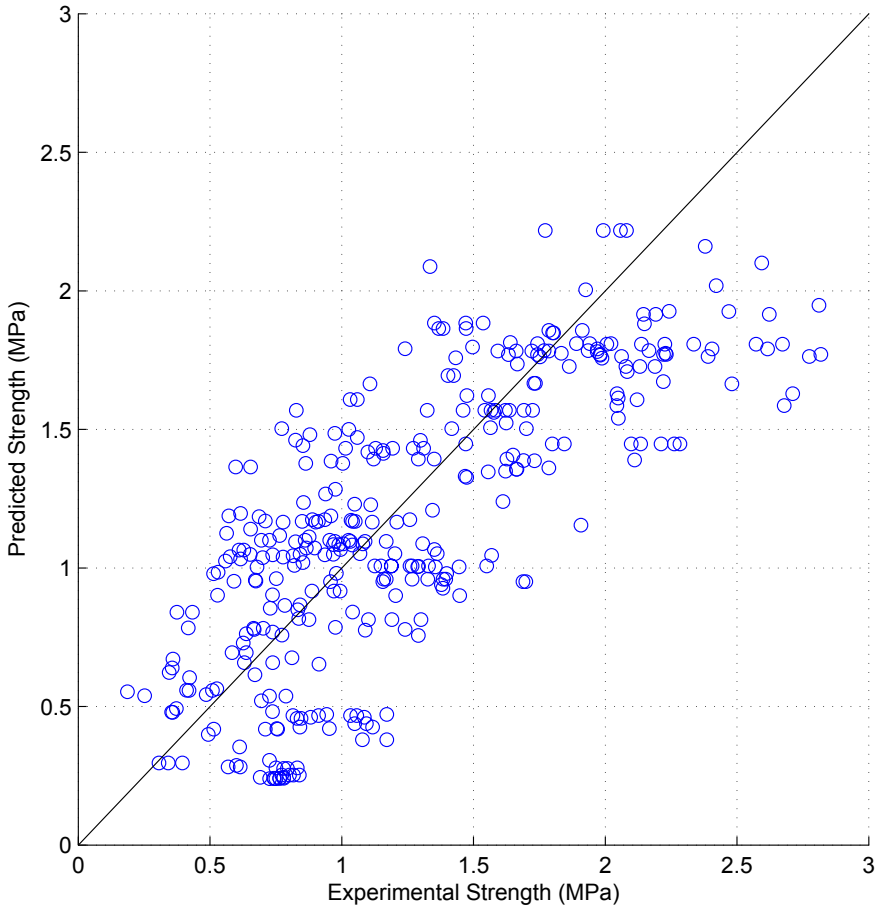

Figure 16.9: NZS model predictions

16.1.10 Voon

The Voon (2007) model is given by

$$\begin{aligned} v_n &= v_m + v_p + v_s \\ &= k\left[0.022\rho_c f_{yc} + 0.083\left(4 - 1.75\frac{M}{Vl_w}\right)\right]\sqrt{f'_m} + 0.9N^* \tan\alpha \\ &\quad + \rho_h f_{yh}\frac{d_{eff}}{s_h} \\ &\leq 0.33\sqrt{f'_m} \end{aligned} \tag{16.10}$$

The k factor is used to account for the strength degradation that occurs with increasing ductility displacement of the wall. Since the displacement ductility was not available for all of the specimens, the Voon model was investigated for $k = 0.8$ and $k = 0$. These values were selected to be

the same as those used by Voon in his analysis. The goodness-of-fit statistics for $k = 0.8$ in Table 16.10 show that the Voon model has a particularly large disparity in model fit between the two grouting types. The poor fit is shown in Figure 16.11 which exposes the influence of the constraint $v_n \leq 0.33\sqrt{f'_m}$ more than the performance of the model itself. For further clarification, the model plot was reproduced with the upper bound removed in Figure 16.12, which shows the model to significantly over-predict the shear strength values. The Voon model is analogous to the TCCMaR model with a reformatted axial contribution parameter and double the contribution of the horizontal reinforcement. It was previously shown than the TCCMaR model over-predicts strength values and that the 0.5 coefficient for the horizontal reinforcement parameter was too high. It only follows that adding the influence of the confinement reinforcement to the TCCMaR model and doubling the influence of the horizontal reinforcement—which was already too high—without decreasing the masonry strength contribution would create a model that over-predicts shear strength significantly more than the TCCMaR model.

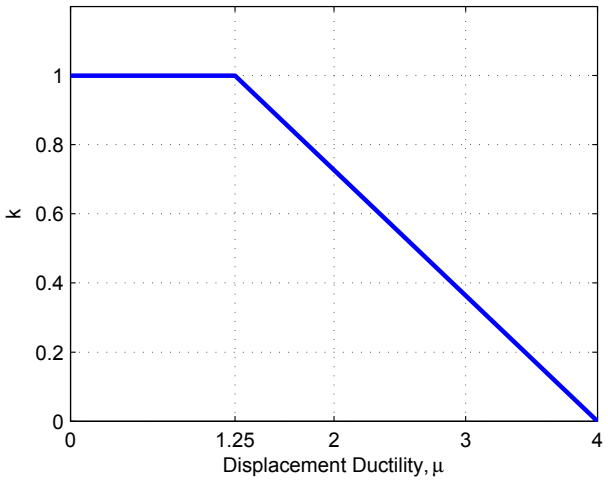

Figure 16.10: Shear resisting mechanism versus masonry ductility (adapted from Voon 2007)

The Voon model was also investigated for the other case where $k = 0$. The goodness-of-fit statistics for $k = 0$ in Table 16.11 show that the Voon model has a smaller disparity in fit between the fully- and partially-grouted data. The difference in model values was evident in the data plots in Figure 16.13, which displays notably lower predicted strengths than those shown in Figure 16.11. The values for this latter case are, for most specimens, too conservative—particularly for the walls

Table 16.10: Goodness-of-Fit Statistics for Voon Model with $k = 0.8$

Grouting	RMSE (MPa)	R^2	Residuals (MPa)	
			Mean	Std Dev
Both	0.6312	0.7891	-0.2861	0.6358
Full	0.5818	0.8845	-0.01183	0.5817
Partial	0.6911	0.5289	-0.5453	0.4145

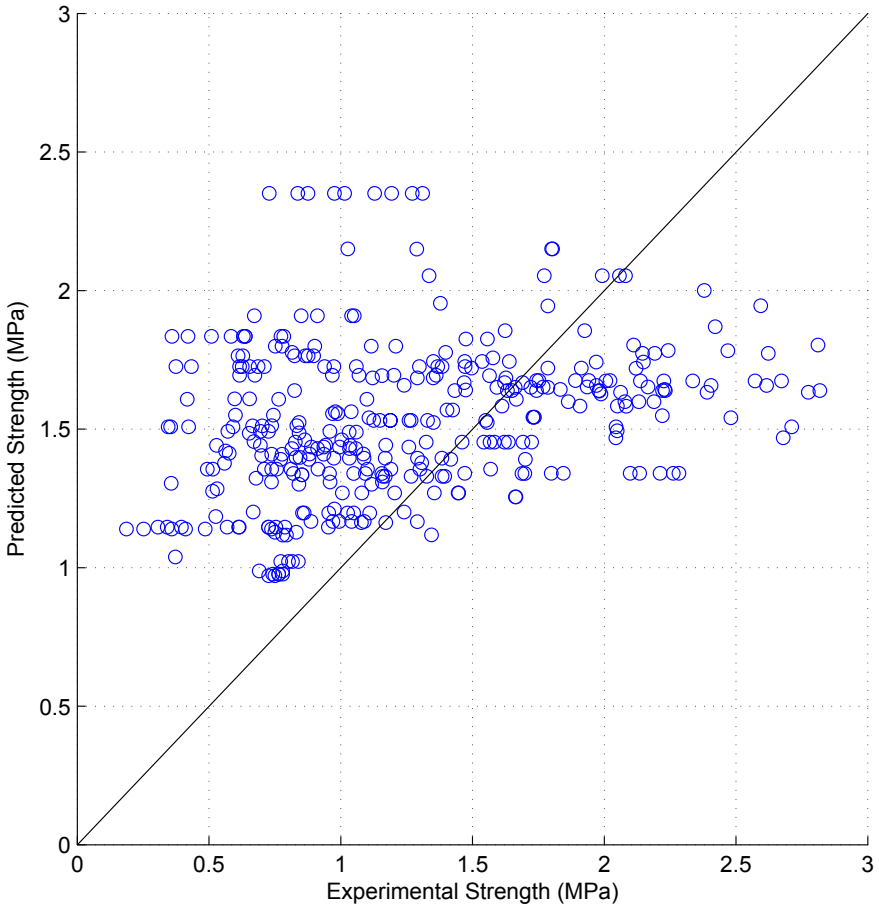

Figure 16.11: Voon model predictions with $k = 0.8$

without horizontal reinforcement or axial load which show a predicted strength of zero. It appears that the optimum fit of the Voon model is for intermediary values of k, which would vary from specimen to specimen.

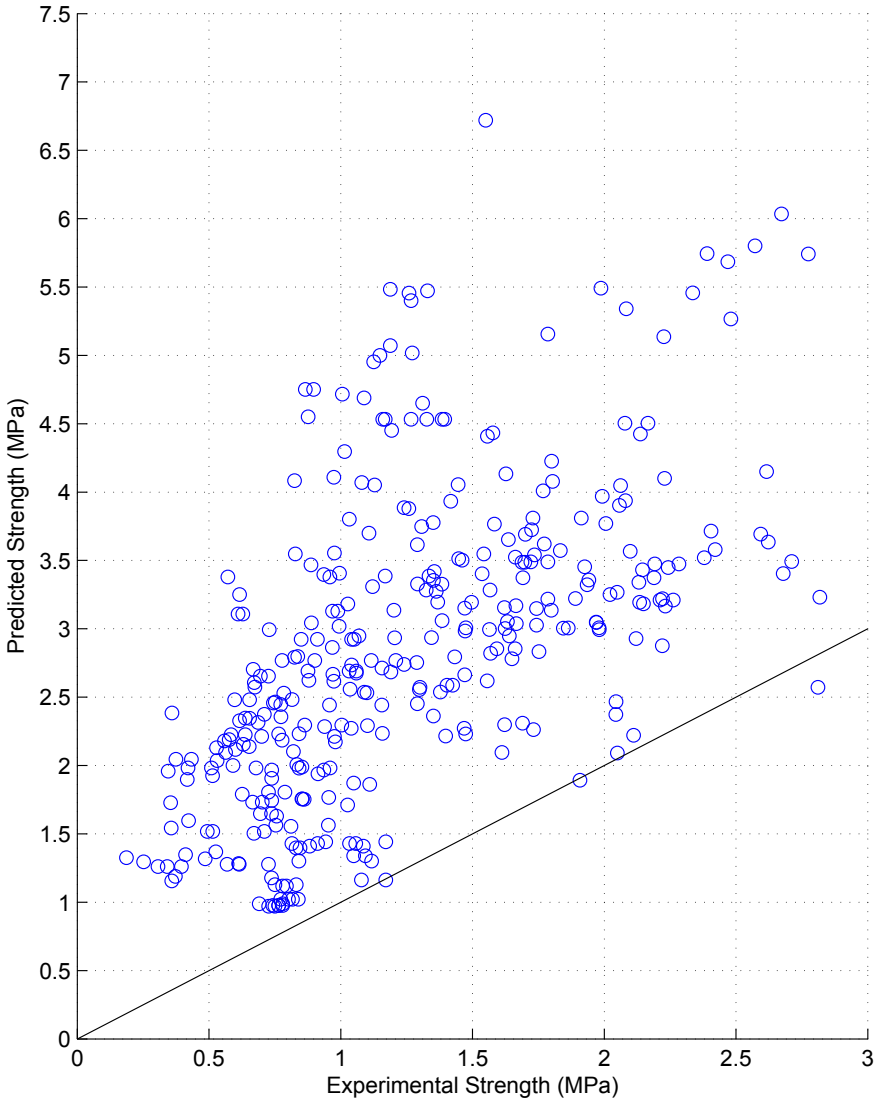

Figure 16.12: Voon model predictions with $k = 0.8$, without upper bound

Table 16.11: Goodness-of-Fit Statistics for Voon Model with $k = 0$

Grouting	RMSE (MPa)	R^2	Residuals (MPa)	
			Mean	Std Dev
Both	0.6228	0.7946	0.3764	0.6273
Full	0.7148	0.8257	0.5669	0.4241
Partial	0.5422	0.7100	0.1964	0.5043

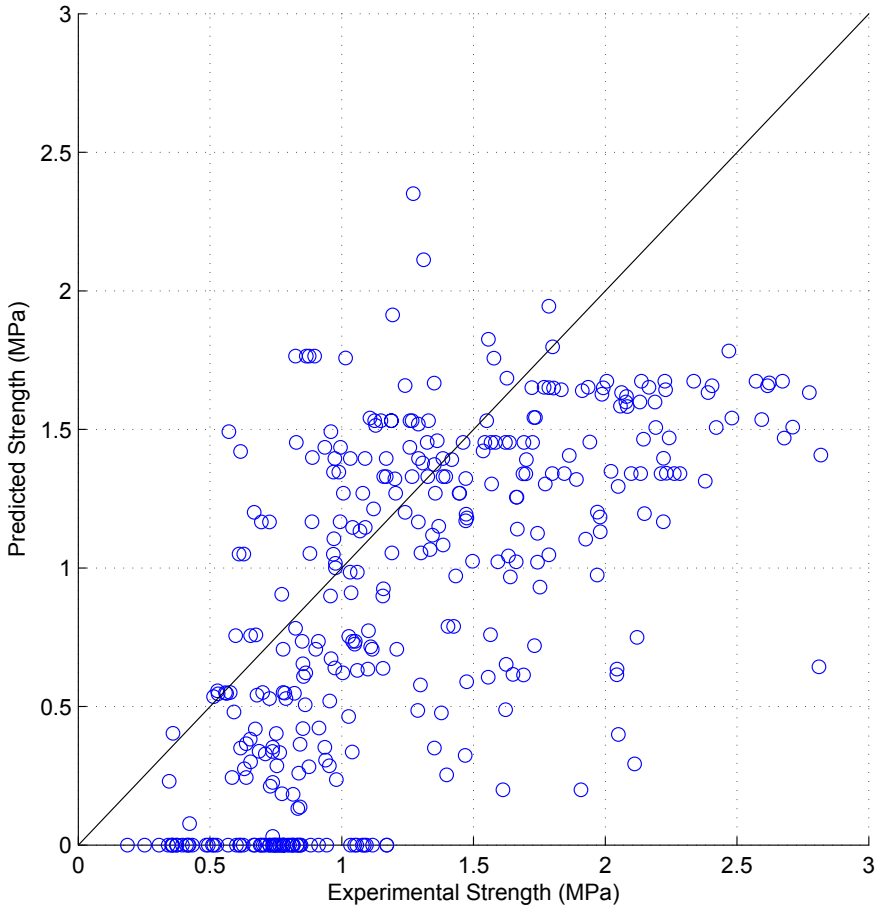

Figure 16.13: Voon model predictions with $k = 0$

16.1.11 Australian Standard

The AS 3700 (2011) model for in-plane shear strength is given by

$$\begin{aligned} v_n &= v_m + v_s \\ &= f_{vr} + 0.8\rho_h f_{yh} \end{aligned} \tag{16.11}$$

where

$$f_{vr} = \left(1.5 - 0.5\frac{h}{l_w}\right) \qquad \text{(MPa)}$$

The goodness-of-fit statistics in Table 16.12 shows that the model is fairly consistent in both fit and

(un)conservativeness between both fully- and partially-grouted walls. The main body of points in Figure 16.14 appear to have only a slight degree of heteroscedasticity but there are about a dozen points which lie above the main trunk of data which could possibly be considered outliers but for the quantity and pattern they show. The reason for the outlying values is revealed in Figure 16.15 where the negative residual values (predicted minus experimental strength) are plotted against the horizontal reinforcement parameter value. The plot reveals that the AS model becomes increasingly unconservative for higher reinforcement strengths because the model over-emphasized the strength of the horizontal reinforcement. The model would be more precise if it used a lower reinforcement coefficient.

The AS model differed from the other models in that it wasn't dependent on the masonry characteristic strength f'_m. The omission of the f'_m variable of the model affected the precision of the model predictions but did not have a large influence on the accuracy of the predictions, with the exception of the outlying predictions. The model's use of the aspect ratio in lieu of the shear span ratio likely also contributed to the increased variance of the model.

Table 16.12: Goodness-of-Fit Statistics for AS Model

Grouting	RMSE (MPa)	R^2	Residuals (MPa)	
			Mean	Std Dev
Both	0.7005	0.7402	-0.3095	0.7035
Full	0.8740	0.7362	-0.2651	0.8321
Partial	0.4995	0.7511	-0.3514	0.3521

16.1.12 Canadian Standards Association

The CSA S304.1 (2004) model is given by

$$\begin{aligned} v_n &= v_m + v_p + v_s \\ &= 0.16\gamma_g \left(2.0 - \tfrac{M}{Vl_w}\right) \sqrt{f'_m} + 0.25\ \gamma_g \sigma_0 + 0.6\rho_h f_{yh} \\ &\leq \begin{cases} 0.4\gamma_g \sqrt{f'_m} & \text{for} \quad \tfrac{h}{Vl_w} > 1 \\ 0.4\gamma_g \left(2.0 - \tfrac{h}{Vl_w}\right) \sqrt{f'_m} & \text{for} \quad \tfrac{h}{Vl_w} \leq 1 \end{cases} \end{aligned} \tag{16.12}$$

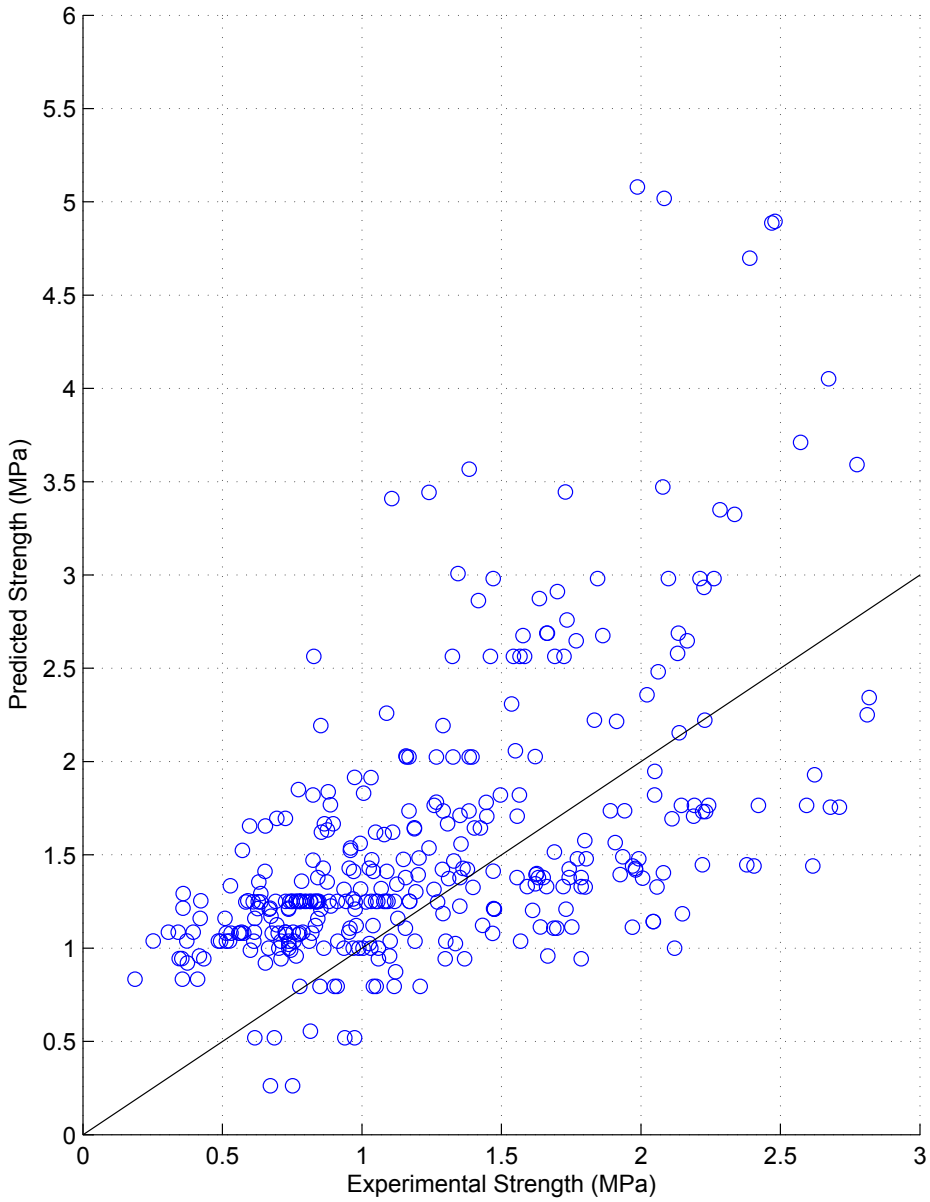

Figure 16.14: AS model predictions

The goodness-of-fit statistics in Table 16.13 show that the CSA S304.1 model is as accurate for the partially-grouted data as for the fully-grouted data, with a mean residual strengths of 0.06 MPa (9 psi) and 0.08 MPa (11 psi), respectively. The accuracy of the CSA model can be seen in Figure 16.16 in which the trend line of the data appears to be collinear with the line of unity slope. The model predictions appear to be heteroscedastic in the lower data range—the part populated principally with partially-grouted specimens—and appears fairly homoscedastic in the upper ech-

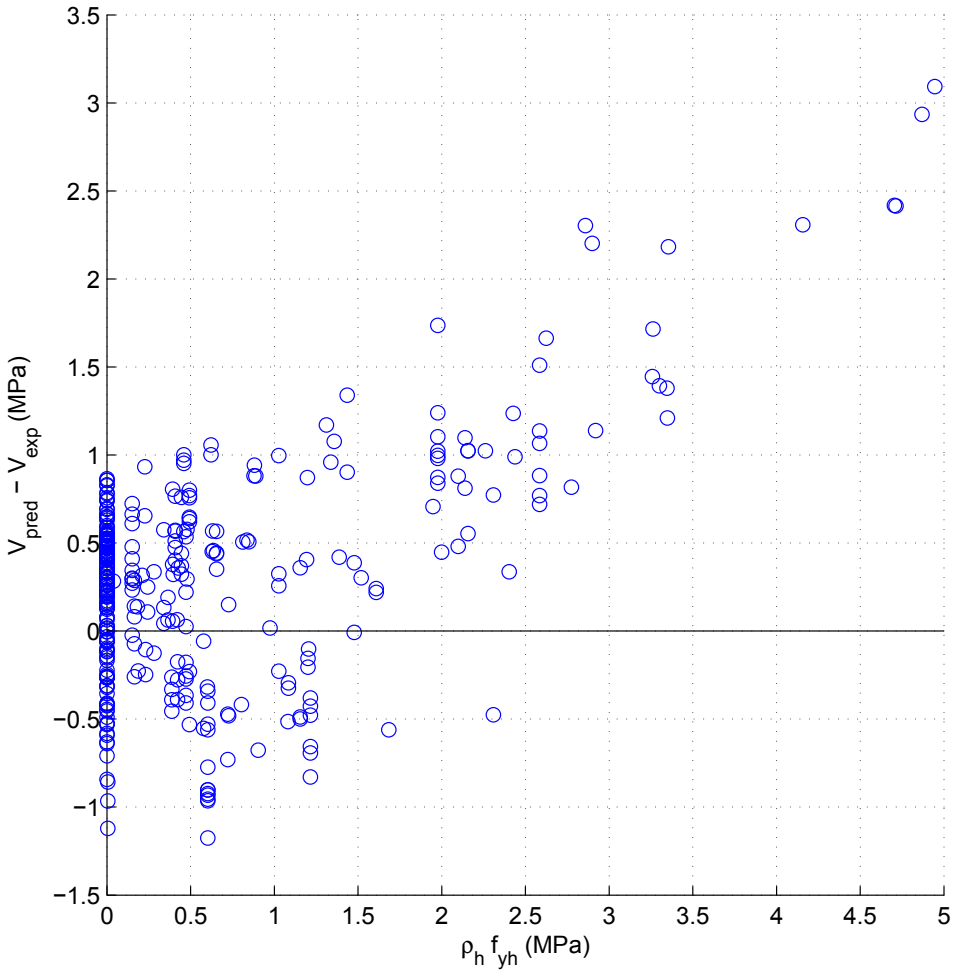

Figure 16.15: AS model residuals

elons of the range. This change in variance is part of the cause of the lower R^2 value for the partially-grouted data than for the fully-grouted data.

Table 16.13: Goodness-of-Fit Statistics for CSA Model

Grouting	RMSE (MPa)	R^2	Residuals (MPa)	
			Mean	Std Dev
Both	0.3649	0.9295	-0.06777	0.3670
Full	0.4137	0.9412	-0.07524	0.4067
Partial	0.3213	0.8976	-0.06071	0.3154

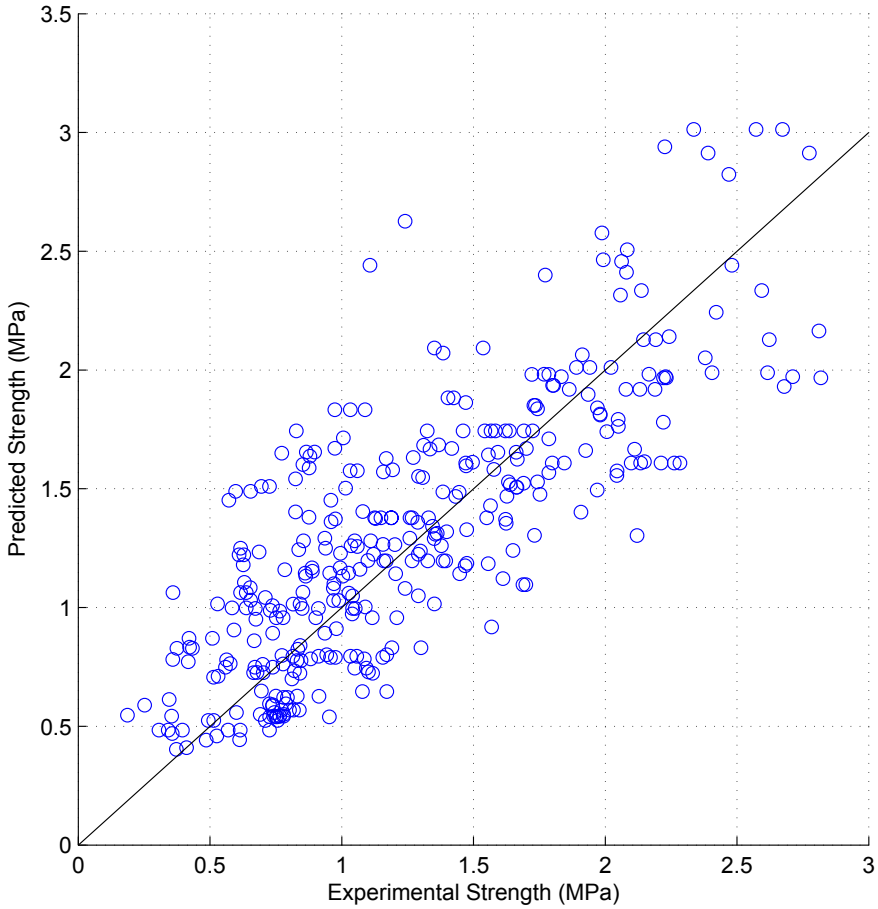

Figure 16.16: CSA model predictions

16.1.13 Masonry Standards Joint Committee

The MSJC (2013) model is given by

$$
\begin{aligned}
v_n &= v_m + v_p + v_s \\
&= 0.083\gamma_g \left(4 - 1.75\tfrac{M}{Vl_w}\right)\sqrt{f'_m} \;+\; 0.25\gamma_g\sigma_0 \;+\; 0.5\gamma_g\rho_h f_{yh} \\
&\leq \begin{cases} 0.50\gamma_g\sqrt{f'_m} & \text{for} \quad \tfrac{M}{Vl_w} \leq 0.25 \\ \left(0.56 - 0.22\tfrac{M}{Vl_w}\right)\sqrt{f'_m} & \text{for} \quad 0.25 < \tfrac{M}{Vl_w} < 1.0 \\ 0.33\gamma_g\sqrt{f'_m} & \text{for} \quad \tfrac{M}{Vl_w} \geq 1.0 \end{cases}
\end{aligned}
\tag{16.13}
$$

The most recent version of the MSJC (2013) introduced the grouted wall factor γ_g to account for the strength disparity for partially grouted walls. This analysis incorporated values for the γ_g factor specified by the MSJC code, which are 1.0 for fully-grouted walls and 0.75 for partially grouted

walls. The goodness-of-fit statistics in Table 16.14 show that the MSJC (2013) model has the best fit for the dataset among the existing shear equations. It has the best fit for the fully-grouted data and is superseded only marginally in fit for the partially-grouted data. The plot of the predicted strengths in Figure 16.17 show the model to be fairly homoscedastic except for some experimental strengths below 1 MPa (150 psi). This bump stems from the differences in model performance of the model for the fully- and partially-grouted data subsets.

The plot of the predictions for fully-grouted data in Figure 16.18 show that the predictions for the fully-grouted data are not collinear with the line of unity slope. In the case of fully-grouted walls, the MSJC model over-predicts the strength for lower failure stresses and under-predicts the strength for higher failure stresses. However, the model appears to be homoscedastic for the fully-grouted data. The behavior for the partially-grouted data, shown in Figure 16.19, is quite the opposite. The mean strength predictions for the partially-grouted data appear to be collinear with the line of unity slope, but the strengths show some degree of heteroscedasticity.

Table 16.14: Goodness-of-Fit Statistics for MSJC Model

Grouting	RMSE (MPa)	R^2	Residuals (MPa)	
			Mean	Std Dev
Both	0.3729	0.9311	0.04658	0.375
Full	0.4147	0.941	0.08575	0.4055
Partial	0.3321	0.9037	0.004389	0.3321

The plot of the predictions for fully-grouted data in Figure 16.18 show that the predictions for the fully-grouted data are not collinear with the line of unity slope. In the case of fully-grouted walls, the MSJC model over-predicts the strength for lower failure stresses and under-predicts the strength for higher failure stresses. However, the model appears to be homoscedastic for the fully-grouted data. The behavior for the partially-grouted data, shown in Figure 16.19, is quite the opposite. The mean strength predictions for the partially-grouted data appear to be collinear with the line of unity slope and show a fair degree of homoscedasticity.

The MSJC (2013) and CSA S304.1 (2004) models have the same form but have different coefficients. The similarity between the two models can be seen by comparing the values from Figures 16.16 and 16.17, particularly for experimental values below 1 MPa (150 psi). Above this

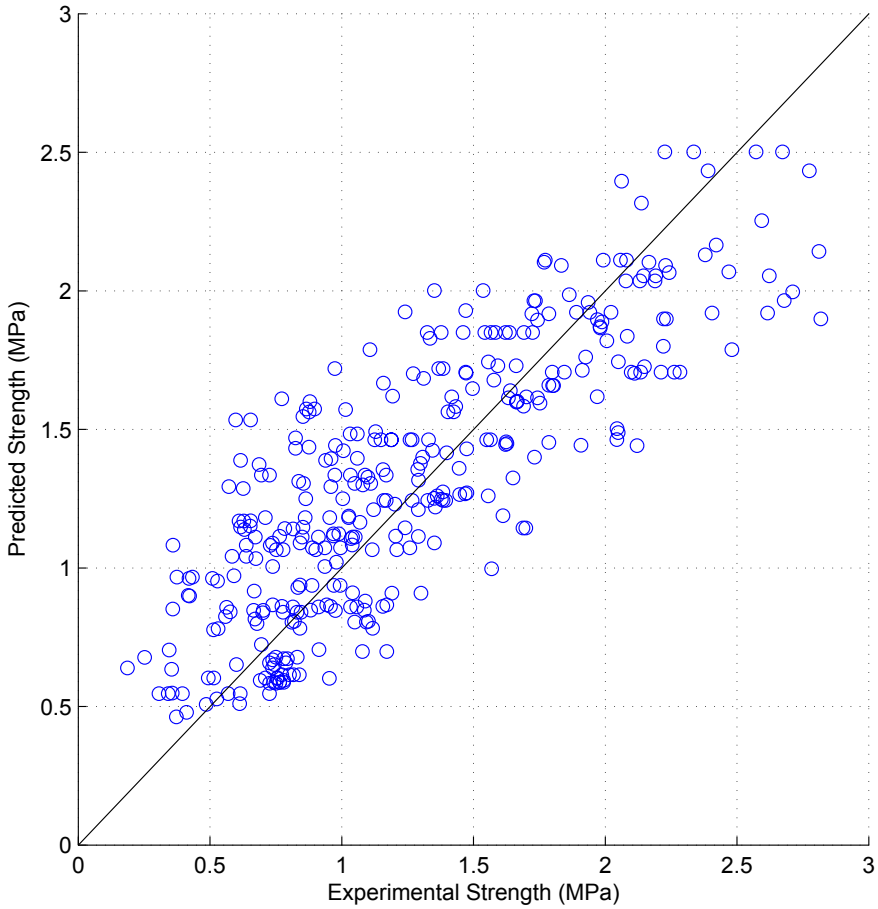

Figure 16.17: MSJC model predictions

value the similarity isn't as apparent because the upper bound on the MSJC (2013) model affects the distribution of the predicted values.

16.1.14 Proposed Model

The new model developed in this study is given by

$$
\begin{aligned}
V_n &= V_m + V_p + V_s \\
&= \begin{cases} \left(1.8 + 0.7\dfrac{V\,l_w}{M}\right)\sqrt{f'_m} & \text{for fully-grouted} \\ \left(1.1 + 0.9\dfrac{V\,s_{gh}}{M}\right)\sqrt{f'_m} & \text{for partially-grouted} \end{cases} \\
&\quad +0.15\sigma_0 \;+\; 0.12\left[\rho_c f_{yc} + \rho_h f_{yh}\right]
\end{aligned}
\tag{16.14}
$$

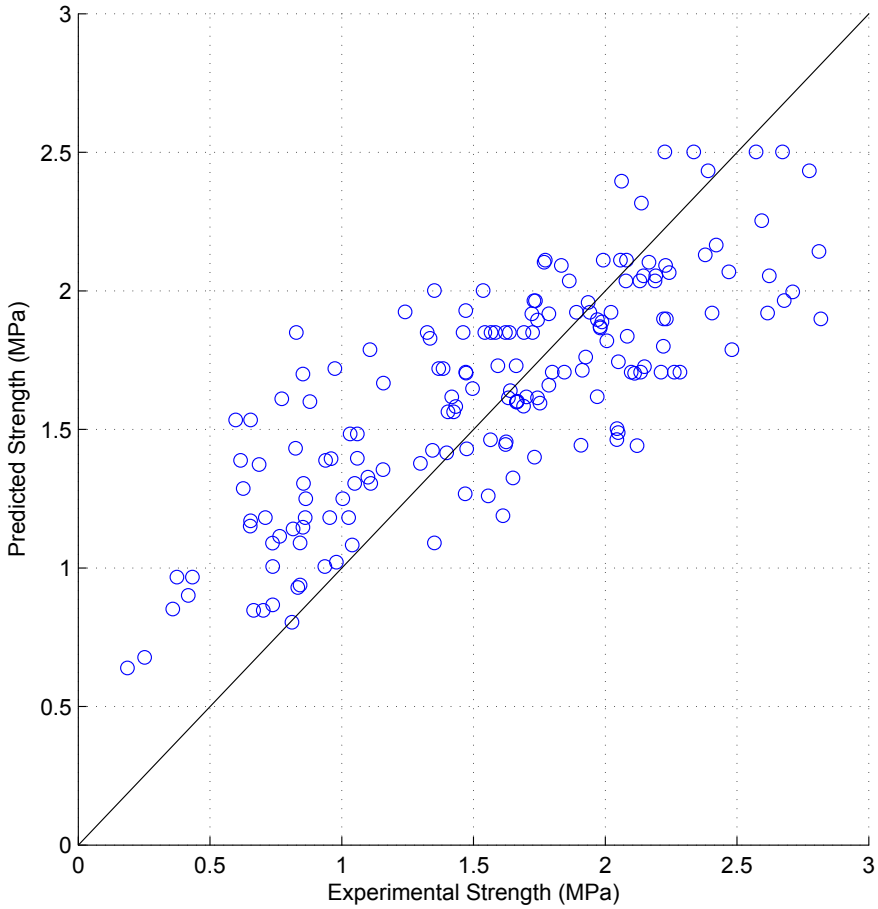

Figure 16.18: MSJC model predictions for fully-grouted data

The goodness-of-fit statistics in Table 16.15 show that the proposed model has a better overall fit to the whole dataset and to each subset. As explained in Chapter 15, the model is not the best possible fit to the experimental data because the coefficients were adjusted so that they would be round numbers and so that the model would have some certain properties. One of the properties of the proposed model is that it is accurate for both fully- and partially-grouted walls. The model also shows a fair degree of consistency between the RMSE and standard deviation values for the whole dataset and each subset. The strength plot in Figure 16.20 shows the model predictions to be homoscedastic with a few outliers. The performance of the model without the effect from the upper strength bound is shown in Table 16.16 and Figure 16.21.

The performance of the model for the fully- and partially-grouted subsets is shown in Figures 16.22b and 16.23b, respectively. The model appears to demonstrate consistent accuracy and precision between both types of grouting. In both grouting cases, the model appears to predict

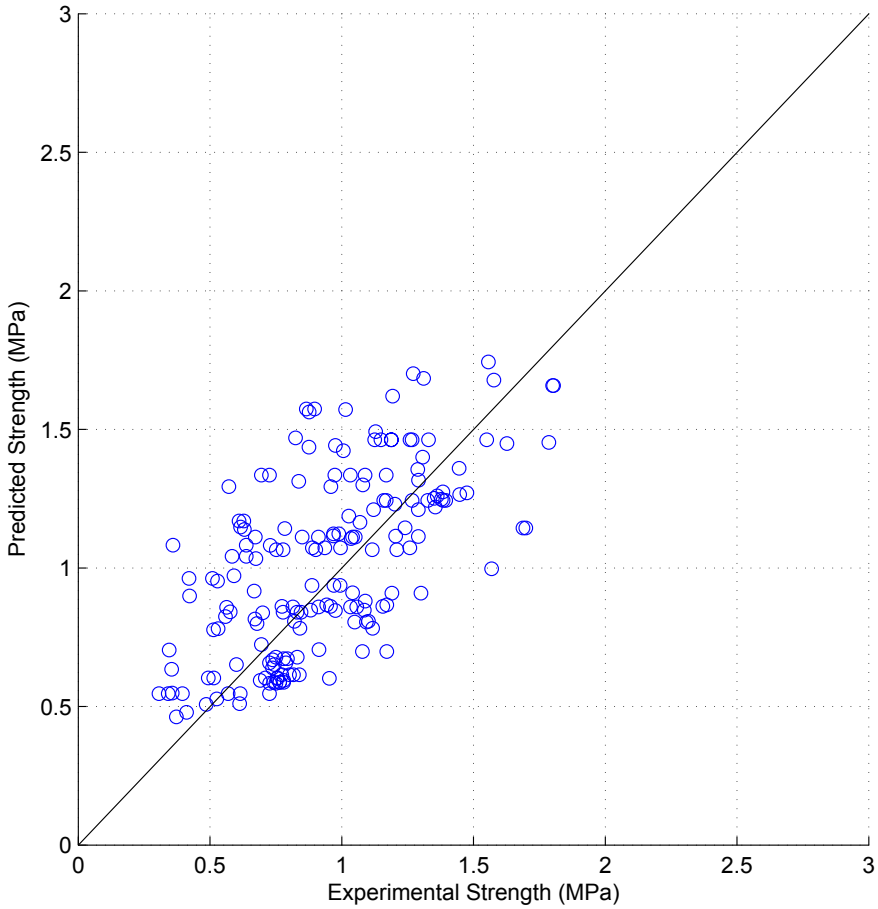

Figure 16.19: MSJC model predictions for partially-grouted data

Table 16.15: Goodness-of-Fit Statistics for Proposed Model

Grouting	RMSE (MPa)	R^2	Residuals (MPa)	
			Mean	Std Dev
Both	0.2906	0.9553	0.0249	0.2936
Full	0.3486	0.9590	0.04132	0.3440
Partial	0.2373	0.9451	0.009391	0.2358

increasingly conservative values in the upper range of experimental values. For the vast majority of the range for each subset, the trend line of the model appears to follow closely the line of unity slope.

Table 16.16: Goodness-of-Fit Statistics for Proposed Model without Upper Bound

Grouting	RMSE (MPa)	R^2	Residuals (MPa)	
			Mean	Std Dev
Both	0.3133	0.9480	-0.000176	0.3165
Full	0.3883	0.9492	-0.009945	0.3858
Partial	0.2377	0.9449	0.009053	0.2361

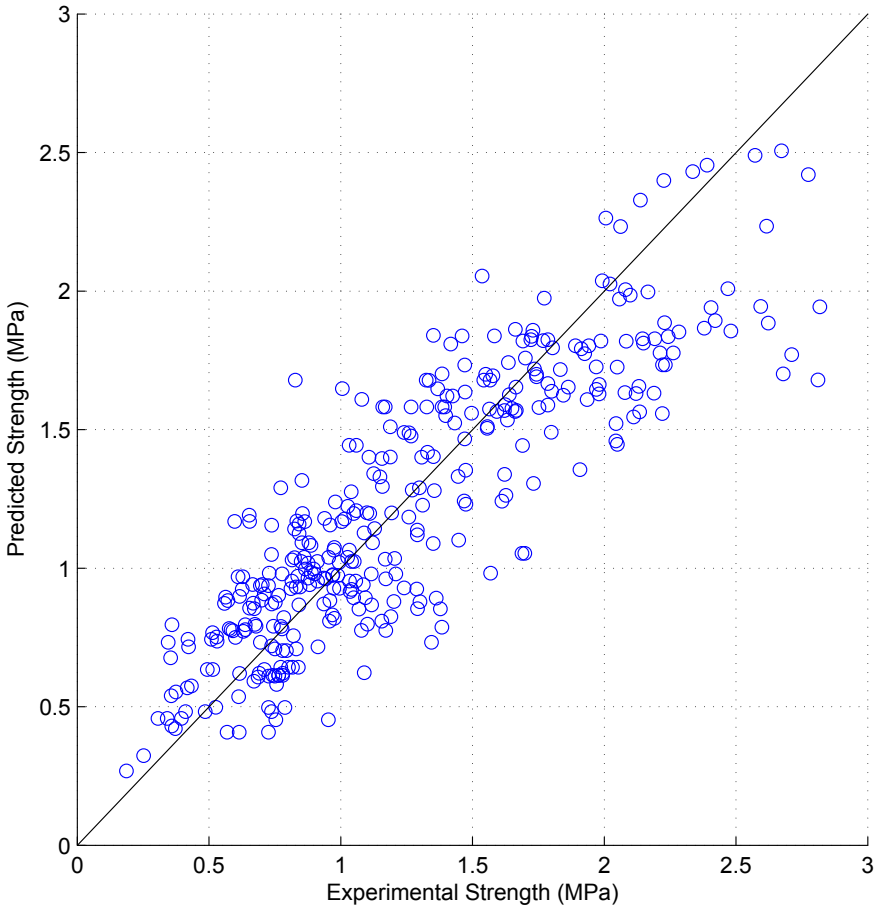

Figure 16.20: Proposed model predictions

16.2 Model Variation

The analysis of the fourteen models showed that the proposed model had the best fit for the dataset. The principal reason is due to the fact that the proposed model was developed using the same dataset which included all compatible data rather than a small subset. It can generally be concluded that each model will provide the best fit to the data that were used in its development.

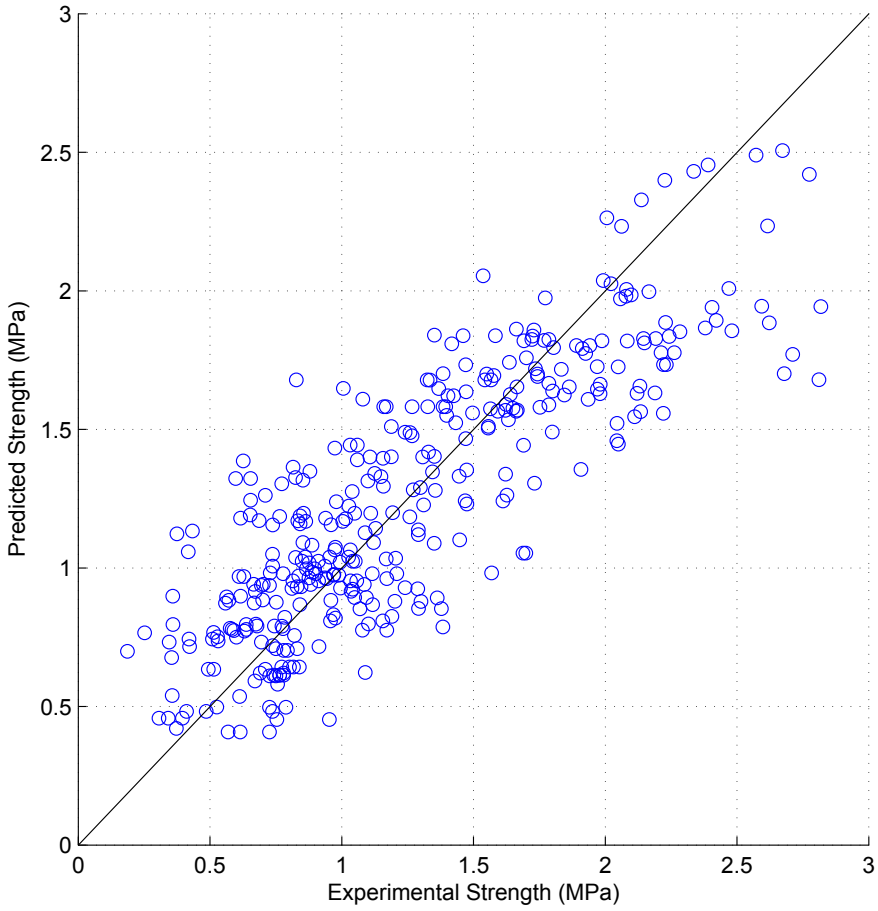

Figure 16.21: Proposed model predictions without upper bound

However, as was shown in Chapter 14, a model may not be the best fit for its constituent dataset if the model does not include the proper parameters, is not built using the optimum methodology, or is based on incorrect assumptions. Any model with a good fit to a smaller dataset does not necessarily translate to being a robust model for other datasets or for all of the data combined. This shows the importance of validating models with a wide assortment of data from multiple and varying sources to examine how robust a model is to different combinations of design variables.

To better understand how each model performed for each data group, the goodness-of-fit parameters and model predictions were calculated for each individual group and included in Appendix F. Despite the difference in the qualifying data from the data originally used to build each model, the overall accuracy of many of the models did not change dramatically when used with the new, expanded dataset. The consistency of model performance between the old and new datasets shows the validity of the new dataset as a tool for building and comparing linear models.

Analysis of the performance of each of the models in the previous section revealed that the MSJC (2013) model out-performed all but the proposed model. In this section, the model comparison is limited to the MSJC (2013) and proposed models because they were the models that best fit the experimental data. The purpose of this section is to investigate how the performance of each model differs from each other and to identify which of the two models is better to use for predicting masonry shear strength.

Comparison of the fully-grouted data plots in Figure 16.22 show the improved fit for the proposed model over the MSJC model. The trend of the predictions for the proposed model is closer to collinear with the line of unity slope than that of the MSJC predictions. The proposed model contains predicted data points that are nearer to the perfect-fit-line than does the MSJC model.

Comparison of the partially-grouted data plots in Figure 16.22 show the improved fit for the proposed model over the MSJC model using the grouted wall factor. The proposed model shows an improvement in the variance of the predictions, with nearly every prediction laying closer the the perfect-fit-line than the MSJC predictions. It is possible that further investigation and refinement of the upper bound model in Part V will further improve the model fit for these predictions.

Regarding the form of the equations, the benefit of the proposed models is that it contains coefficients that were specifically developed for use with partially-grouted shear walls. The grouted wall factor γ_g was originally intended as a temporary fix for the MSJC model and was not intended to be used on a permanent basis. The parameters and coefficients in the proposed model better represent how each aspect of the walls affects their overall behavior because they were developed from the experimental data. This property makes the proposed model better for helping researchers and designers understand how masonry shear walls behave.

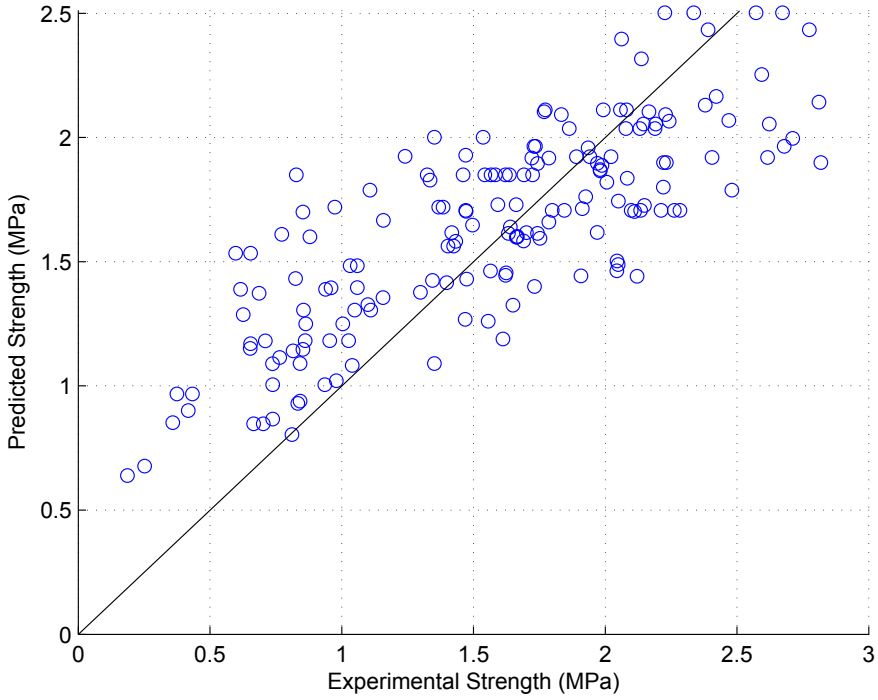

(a) MSJC model

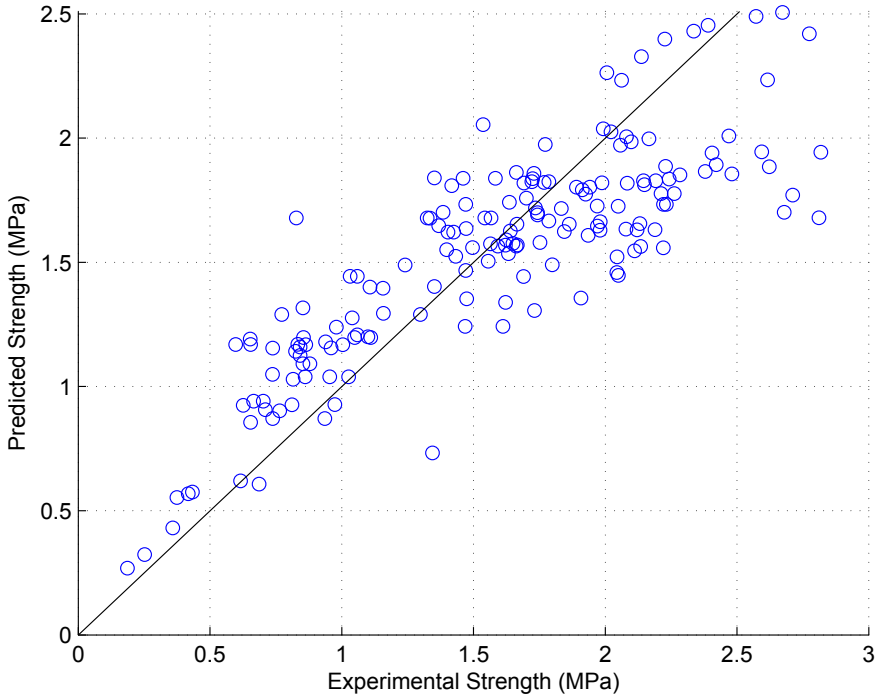

(b) Proposed model

Figure 16.22: Predicted strengths for fully-grouted data

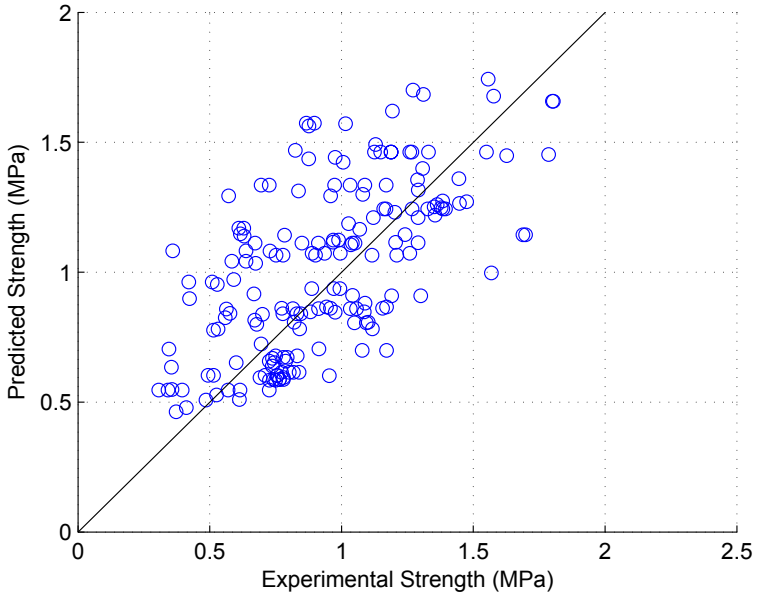

(a) MSJC model

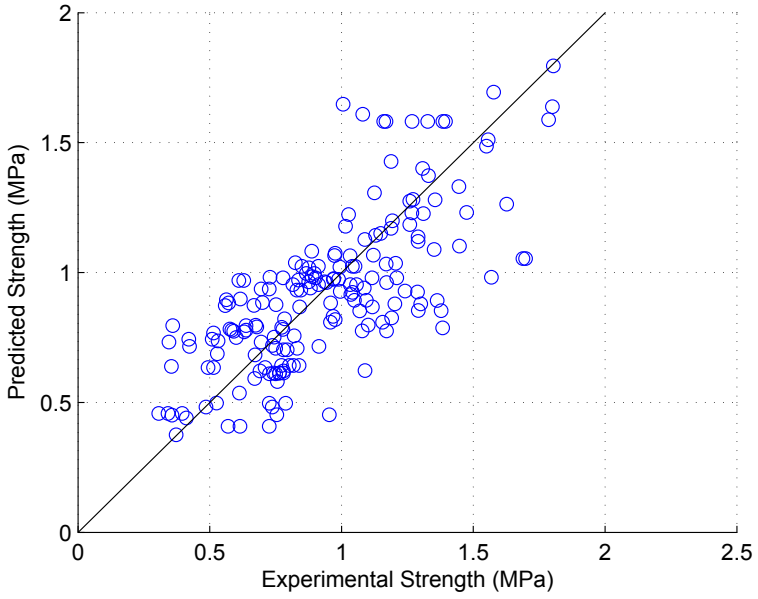

(b) With upper bound

Figure 16.23: Predicted strengths for partially-grouted data

Part V

Strut-and-Tie Modeling

This part details the third and last approach which was the development of the strut-and-tie modeling procedures for masonry shear walls. Chapter 17 introduces and explains strut-and-tie modeling theory and provides a review of uses of the method for masonry from the literature. Chapter 18 continues with an outline of the methodology used in developing the strut-and-tie modeling procedures for masonry shear walls. Chapter 19 details the creation of strut-and-tie models for masonry and development of the modeling procedures for masonry. Chapter 20 presents a comparison of the performance of the practice with the existing and proposed shear equations and a discussion of the method's use in design practice.

This analysis was the first to applied the complete strut-and-tie methodology used for reinforced concrete to masonry. It was determined that the strut and nodal efficiency factors specified in the ACI 318 code can be directly applied to masonry modeling. An inclination factor was developed and proposed to account for the decrease in effective compressive strength in partially-grouted walls when not load normal to the bed joints. Predicted values from strut-and-tie models were compared with those from the shear equations and equivalent truss modeling procedure. It was observed that strut-and-tie models produce predicted values that are more precise than all other methods currently in use.

CHAPTER 17. LITERATURE REVIEW: MASONRY MODELING

17.1 Introduction

Masonry shear wall behavior can be modeled using numerous methodologies and techniques which can be classified as being empirical, mechanical, numerical, or combinations thereof. The current MSJC (2013) code design equation can be viewed as a combination of mechanical and empirical models since the overall format and some of the coefficients were based of mechanical theory and the remaining coefficients were derived empirically. There is a large and varied collection of masonry models due to the highly complex and heterogeneous nature of masonry as a structural material. While the individual masonry components can be considered isotropic at the material level, masonry assemblages—with their regularly repeating pattern of joints and voids—is anisotropic at the structural level. These properties of masonry make it difficult to develop models which accurately and easy describe the material behavior for all design scenarios (Ganz and Thürlimann, 1983).

17.1.1 Numerical Methods

There are generally three approaches used in numerical modeling of masonry: micro, meso, and macro models. Micro modeling is typically implemented using the finite element method in which the masonry units, mortar joints, grout, and reinforcement are each modeled using continuum elements and the interfaces between the element types are modeled using interface elements. Meso modeling is generally implemented using the finite element method, but while the masonry units are modeled using continuum elements, the mortar joints and unit-joint interfaces are modeled together as discontinuous elements. In the literature, meso models are limited to unreinforced and ungrouted masonry assemblages. Macro models represent masonry panels as a continuum in which the material parameters for the assemblage are "smeared" across the entire continuum.

Macro models can be implemented using the finite element method or can be implemented using other analysis tools (Mojsilović, 2011).

Numerical methods in masonry analysis is difficult to implement, let alone to obtain accurate values. Numerical modeling of masonry requires the use of anisotropic constitutive laws which are further complicated by differing behaviors in tension and compression. These constitutive models are governed by several parameters, the number of which increases as the modeling approach moves from macro to meso and from meso to micro (Addessi et al., 2014). The necessary material parameters are not always available for the materials to be analyzed and they are frequently difficult to determine. These drawback make the use of numerical modeling for masonry structural analysis prohibitive for general design situations (Mojsilović, 2011).

17.1.2 Theorem of Limit Analysis

Mechanical models can provide a good combination of efficiency, reliability, and practicality for the majority of masonry design scenarios. One mechanical analysis tool that has been shown to be efficient and reliable is the use of stress fields. Stress fields are based on the lower-bound theorem of the theory of plasticity and provide a safe estimate of the ultimate strength of the material (Mojsilović et al., 2013). The lower-bound theorem states that as long as the stress fields satisfy the boundary conditions, are in equilibrium, and do not violate the yield criterion of the material, then the predicted strength is a lower bound for the ultimate strength of the material (Bower, 2011). The lower-bound theorem was originally intended to apply to elasto-plastic materials, but the theorem is applicable to concrete and masonry because they demonstrate elasto-plastic compression behavior (Foraboschi and Vanin, 2013). These stress fields have been combined with the truss analogy to produce what is known as the strut-and-tie modeling procedure (Marti, 1985; Mueller, 1978; Collins and Mi, 1988; Schlaich et al., 1987).

17.2 Strut-and-Tie Modeling

Strut-and-tie modeling is more predominantly used in analyzing and designing reinforced concrete sections where beam theory does not apply. One of the greatest strengths of strut-and-tie modeling is that it allows designers to consider axial, moment, shear, and torsion forces all within

the same model. The method makes it easy to visualize otherwise complicated stress path through the member and enables designers of reinforced quasi-brittle materials to know where to best place reinforcement and how much reinforcement to use (ASCE-ACI, 1998).

Strut-and-tie modeling is an analysis and design technique that reduces complicated structural members to an equivalent truss assemblage, such as that shown in Figure 17.1. In the model, members are represented as compression struts, tension ties, and nodes. Struts (shown as shaded strips in Figure 17.1) comprise sections of concrete or masonry within the member and carry compressive forces. Ties (shown as dashed lines in Figure 17.1) represent the steel reinforcement in the member and are placed within the member such that the mechanical stability of the member is maintained. Nodes are regions within the member where struts and ties meet so that forces can be transferred between them. The remaining regions within the member are assumed not to act in resisting any load within the member (ACI 318, 2011; ASCE-ACI, 1998).

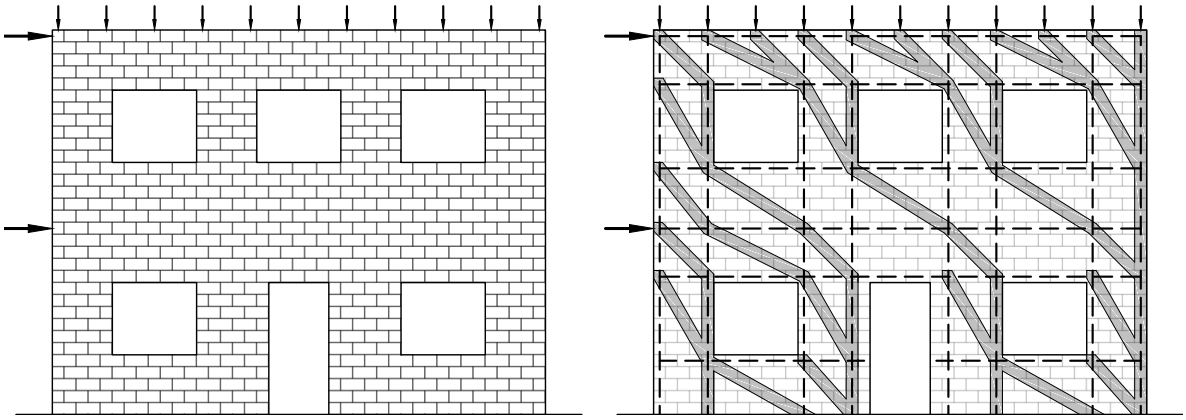

Figure 17.1: Strut-and-tie representation of loads

Each strut must be sized such that its cross section is sufficient to resist the compressive loads to be transmitted. The flow of compressive forces can be idealized as three difference shapes: prismatic, fan-shaped, or prismatic, as shown in Figure 17.2. Ties must be sized and placed within the member to resist the internal tensile forces imposed by the compressive struts. Nodal regions must be sized to 1) resist the combination of compressive forces from applied loads and the junction of struts and 2) provide sufficient anchorage for the reinforcing steel making up the tension tie (ACI 318, 2011; ASCE-ACI, 1998).

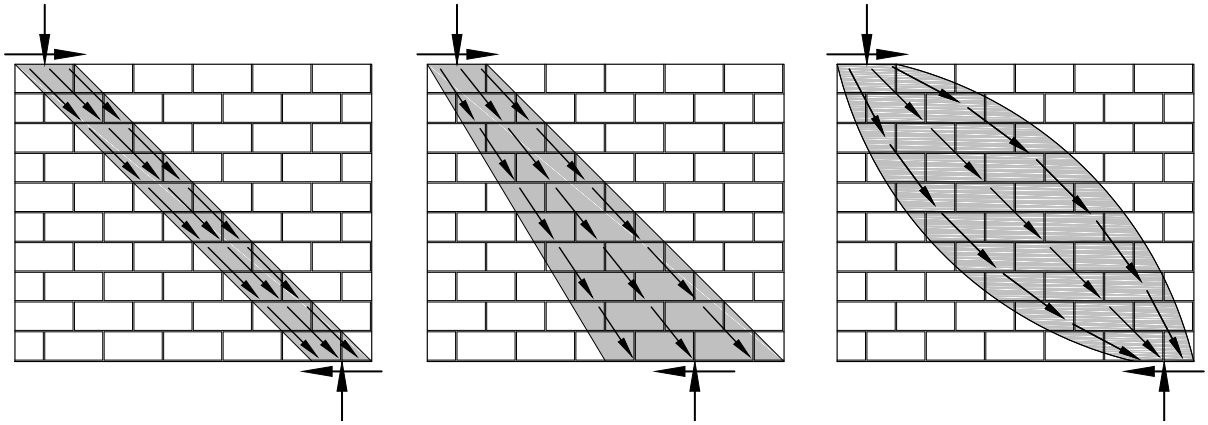

(a) Prismatic strut (b) Fan-shaped strut (c) Bottle-shaped strut

Figure 17.2: Strut shapes

Structural elements representing shear, moments, and axial loads can be divided into two types of regions. Bernoulli, Beam, or (simply) "B" regions, are subsections of an element where the flow of compressive forces is uniform. Within B regions the assumption that plane sections remain plane remains valid (Schlaich et al., 1987). The use of strut-and-tie modeling within B regions is not necessary because the other provisions of the code are more easily applied to these cases (ACI 318, 2011).

Discontinuity, disturbance, detail, or (simply) "D" regions, are subsections where the internal flow of stresses within the member are complex. Within these region, the member may be designed using linear elastic methods (i.e., Hook's Law) as long as the section remains uncracked. Once the material within the D region has cracked, it is inappropriate to assume that the shear stress is uniformly distributed or that plane sections remain plane. D regions are typically found adjacent to concentrated point loads, within deep beam segments, or at geometric discontinuities within the member (Schlaich et al., 1987; ASCE-ACI, 1998). According to Saint-Venant's principle, D regions extend from the location of concentrated load or discontinuity to a distance equal to the width or height of the member at that point. The region beyond the D region, the volume is considered to be a B region and may be designed using traditional design methods. The greatest benefit of strut-and-tie modeling is found in designing or analyzing D regions (ACI 318, 2011).

The results of the strut-and-tie method depend greatly on how the designers choose to model the design region. For any member there are several possible strut-and-tie models that could

model the stress paths within the member. The most appropriate strut-and-tie model is generally considered to be that which requires the least amount of reinforcement. This is due to the fact that the internal forces within the member will seek at path that minimizes the strain energy U within the member such that

$$U = \frac{1}{2}\sum F_{si}\, l_{si}\, \bar{\epsilon}_{si} + \frac{1}{2}\sum F_{tj}\, l_{tj}\, \bar{\epsilon}_{tj} = \text{Minimum} \tag{17.1}$$

where

F_{si} = force in strut i,
l_{si} = length of strut i,
$\bar{\epsilon}_{si}$ = mean strain in strut i,
F_{ti} = force in tie j,
l_{ti} = length of tie j, and
$\bar{\epsilon}_{ti}$ = mean strain in tie j.

Since the reinforcement is much more deformable than the concrete or masonry, the $\sum F_{si}\, l_{si}\, \bar{\epsilon}_{si}$ portion of Equation (17.1) can be assumed to be zero. This indicates that the strut-and-tie model which minimizes the area and length (i.e., total volume) of the reinforcement is the best model (Kupfer, 1964; Schlaich et al., 1987). Since the optimal design is not always immediately apparent, implementation of the strut-and-tie method is commonly an iterative process (AASHTO, 2012; ASCE-ACI, 1998; Liang et al., 2002).

17.3 Strut-and-Tie Research

The formulation of the strut-and-tie modeling method grew out of research into the truss analogy for representing reinforced concrete elements. The thought was first introduced at the turn of the twentieth century by German researchers Wilhelm Ritter (1899) and Emil Mörsch (1908). Marti (1985) and Mueller (1978) used the lower-bound theorem within the theory of plasticity to show that strut-and-tie models represent a lower bound for ultimate member strength. Significant work was conducted with the truss analogy by Collins and Mi (1988) who were able to apply the truss analogy in developing strut-and-tie methods for shear and torsion in reinforced

concrete members. Several researchers have showed that strut-and-tie models could be effectively used for designing deep beams and corbels (Schlaich et al., 1987) while others have applied the methodology to masonry elements.

17.3.1 Schlaich and Schäfer

Jörg Schlaich and Kurt Schäfer were the first to formulate a unified design methodology for using strut-and-tie models in designing an entire reinforced concrete structure applicable to all design scenarios (Schlaich et al., 1987; Schlaich and Schäfer, 1991). They describe the strut-and-tie model as a generalized truss model in which all tension, compression, and nodal members are designed with regard to safety and serviceability using uniform design criteria and that truss models are actually a subset of strut-and-tie models. One of the strengths of their methodology is the ability to use the same model for both the serviceability and ultimate limits states. Another strength is that the method is able to consistently model both B and D regions with similar levels of accuracy.

Schlaich et al. (1987) provide a detailed description of the procedures for applying the strut-and-tie modeling method to designing D regions of reinforced concrete members. One difference between their methodology and other strut-and-tie modeling methodologies is that theirs cannot be solely idealized as a truss with lines and nodes. Their method requires that struts and nodes have sufficient cross-sectional area to resist the applied loads and that the geometry of the struts and nodes are limited by the overall size of the member.

17.3.2 Ganz and Thürlimann

Ganz and Thürlimann (1983, 1984) tested 12 biaxially-loaded masonry panels and seven masonry shear wall specimens to develop a load carrying model for masonry shear walls. All masonry panels and walls were constructed from perforated clay bricks. Ganz and Thürlimann used the lower- and upper-bound theorems of the theory of plasticity to develop the four load carrying models for masonry shear walls shown in Figure 17.3. The first two models, based on the lower-bound theorem, introduced the concept of stress fields within the masonry panel. They

determined that the shear capacity of an unreinforced masonry shear wall is given by

$$V_n = \frac{1}{2} f'_m A_g \tan\left(\frac{\gamma}{2}\right) \tag{17.2}$$

subject to the condition that the axial load has to be at least

$$P \geq f'_m A_g \cos^2\left(\frac{\gamma}{2}\right) \tag{17.3}$$

where

$$\gamma = 2\alpha_s = \arctan\left(\frac{l_w}{h}\right).$$

Ganz and Thürlimann observed a fair agreement between the theoretically predicted strengths and the experimental results.

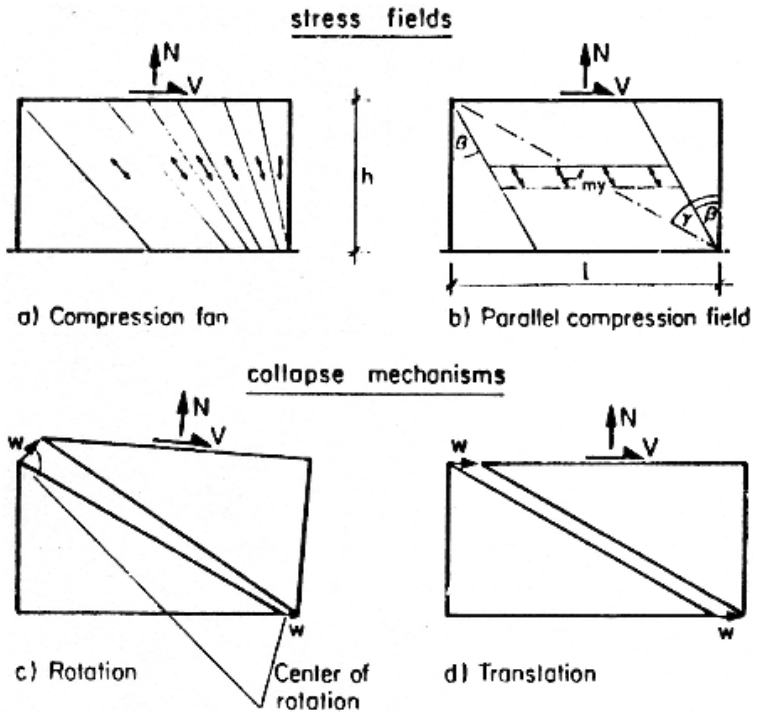

Figure 17.3: Load carrying models from Ganz and Thürlimann (1983)

17.3.3 Roca

Roca (2004, 2006); Roca et al. (2010, 2011) used strut-and-tie theory to predict the ultimate shear capacity of unreinforced masonry walls. Roca et al. (2011) describes that there are limitations to using strut-and-tie modeling theory with unreinforced masonry walls because the theory of plasticity does not apply to walls which do not contain tension-carrying components showing plastic behavior (i.e., reinforcing bars). Roca et al. (2011) overcame this limitation by developing a system of "equilibrium" models which are best described as strut-and-tie models without ties. The models are kept in equilibrium by the exterior forces applied to the masonry panels. The forces paths travel through the masonry as struts with a shape (prismatic, fan, or bottle) determined by where the forces are applied to the panel.

Equilibrium models may contain tensile forces in the case where the transverse strut forces attempt to form diagonal cracks along the center line of a bottle-shaped struts. Roca et al. (2011) explains that due to the brittle behavior associated with diagonal cracking of unreinforced masonry panels, the use of equilibrium models in predicting the ultimate shear capacity is limited to cases where the tensile capacity of the masonry is not the limiting factor. These cases are those where the failure is fully due to plastic behavior, such as frictional sliding, rocking, and toe crushing. Equilibrium models can also be used to calculate the residual shear capacity after diagonal cracking has occurred.

In equilibrium models, the slope of the struts are limited by the frictional response of the bed joint. The Mohr-Coulomb criterion is assumed to describe the minimum angle at which the struts can traverse the bed joints. The maximum strut inclination angle α_s (measured normal to the bed joint) is given by

$$\tan \alpha_s \;=\; \tan \varphi \;+\; \frac{c}{\sigma_0} \tag{17.4}$$

where φ is the friction angle of the unit-mortar interface, c is the cohesion at the unit-mortar interface, and σ_0 is the applied vertical axial stress. Equilibrium models also require that the compression strut be sized such that there is sufficient cross-sectional area to support the axial force applied to the strut. Roca et al. determined that the equilibrium modeling approach are

theoretically supported by the lower-bound theorem within the theory of plasticity, similar to the strut-and-tie modeling approach.

Roca et al. (2011) tested the application of the equilibrium modeling theory to several experimental and numerical cases. The experimental test data was gathered from tests performed by Oliveira (2003), Ganz and Thürlimann (1983, 1984), Martinez (2003), Raijmakers and Vermeltfoort (1992), and Charry (2010). The numerical test data used was produced by Lobato (2009). Since only some of the experimental researchers measured the cohesion along the unit-mortar interface, Roca et al. assumed that the cohesion in the ultimate state was given by

$$c = \frac{V}{t\, f'_m}\,. \tag{17.5}$$

Roca et al. (2011) observed that the predictions from equilibrium models showed satisfactory agreement with the experiment or numerical results for a wide range of loading conditions except in the case of highly perforated brick. They concluded that the equilibrium modeling approach should be limited to solid brick masonry walls until further research could be undertaken for perforated bricks.

17.3.4 Lourenço et al.

Lourenço et al. (2006) developed a simplified design models for use in predicting the capacity of masonry in-fill panels based on strut-and-tie models. They observed that the principal failure modes for the in-fill masonry panels was diagonal cracking and corner crushing. They determined that the traditional single, prismatic strut models did not adequately describe the failure modes and proposed that a more complex strut-and-tie model be used. Since the masonry panels analyzed were unreinforced, the ties consisted of unilateral tension fields within the masonry itself. Their method of analysis is similar to the equilibrium modeling approach proposed by Roca (2004) except that equilibrium is imposed by the surrounding frame and not by axial load. The limitations of the equilibrium method for tensile cracking do not hold for masonry in-fill panels because equilibrium is not lost after the panel cracks.

Lourenço et al. (2006) hypothesized that diagonal cracking in the panel occurs when the transverse splitting stress in the bottle-shaped struts exceeds the tensile strength of the masonry.

They proposed that a single, bottle-shaped strut be represented by four bent struts and a connecting tie. They assumed that the angle between the struts and the center line of the wall diagonal α_d was given by

$$\alpha_d = \arctan\left(l_c \frac{\sqrt{2}}{2} \cdot \frac{\cos\theta}{l_w}\right) \tag{17.6}$$

where l_c is the assumed contact length between the panel and the frame and θ is the angle between the panel diagonal and the bed joints. Using this analogy, they were able to predict the panel shear capacity for the cracking limit state using

$$V_{\text{crack}} = \frac{f_t\, A_g}{2 \tan\theta} \tag{17.7}$$

where f_t is the tensile strength of the unit-mortar interface.

Lourenço et al. (2006) assumed that only the corners of the masonry panel need be considered in checking for masonry crushing of the strut. They noted that the effective strength of the masonry in the corners is affected by the imposition of a biaxial state of stress and a non-uniform stress distribution. They computed the panel shear capacity for the crushing limit state to be

$$V_{\text{crush}} = \frac{1}{2} f'_{m(\text{eff})}\, l_c\, t\, \min\left\{\begin{array}{c} 1 \\ \cot\theta \end{array}\right. \tag{17.8}$$

where t is the panel thickness.

Lourenço et al. validated their strut-and-tie model constructed using numerical finite element analysis. The numerical models were previously validated using data from four experimental tests on masonry in-fill frames. They determined that the average error between their proposed strut-and-tie model and the numerical results to be 14 percent for the diagonal cracking strengths and 12 percent for the corner crushing strengths. They further validated their simplified model using experimental data from twelve tests performed by Braguim (1989) where they again obyained good agreement between the experimental and predicted results. They concluded that their simplified design model is a good tool for predicting the shear capacity of masonry in-fill panels.

17.3.5 Voon and Ingham

Voon and Ingham (2008) conducted experimental tests on ten continuous wall panels and ten walls panels with openings. The purpose of the former group was to understand masonry shear wall behavior and that of the latter group was to validate the strut-and-tie modeling procedures for partially-grouted walls with openings. Voon and Ingham (2008) constructed two sets of strut-and-tie models; the first set of models assumed that the lateral shear force was applied at a single point on the trailing edge and the second set of models placed the load at the top edge and assumed components of it to travel laterally to the tops of the struts. The second set of strut-and-tie models from their study are shown in Figure 17.4.

Since the walls were reinforced, the modeling procedures used were similar to those set forth by Schlaich et al. (1987) in that the ties consisted of reinforcement bars. It appears that Voon and Ingham did not follow fully the methodology developed by Schlaich et al. for at least two points. First, their strut-and-tie models idealized all struts and ties as lines and show the start and end points of the strut center lines to coincide with the center lines of the reinforcement. They did not appear to consider the thickness of the struts or reinforcement development requirements in determining the path and angle of the struts. Second, they made no mention of considering how the shapes of the struts would affect the effective strut strengths. Overall, their methodology might, more-appropriately, be called an idealized truss model. Voon and Ingham (2008) confirmed that the strut-and-tie models provided a lower limit for the ultimate strengths of the tested walls. The latter group of strut-and-tie models performed better than the former group and, overall, performed better at predicting the shear capacity than the Standard Association of New Zealand (NZS) (2004) code equation. They observed that the strut-and-tie models become increasingly conservative when the number of openings in the walls increased from one to two.

17.3.6 Nolph and Elmapruk

Nolph (2010) and Elmapruk (2010) each tested six reinforced masonry shear walls to investigate the validity of the MSJC design Equation and of the strut-and-tie modeling procedures outlined in Appendix A of the ACI 318 (2011) code. Similar to the arrangement used by Voon (2007), Nolph (2010) and Elmapruk (2010) arranged all of the struts such that their center lines

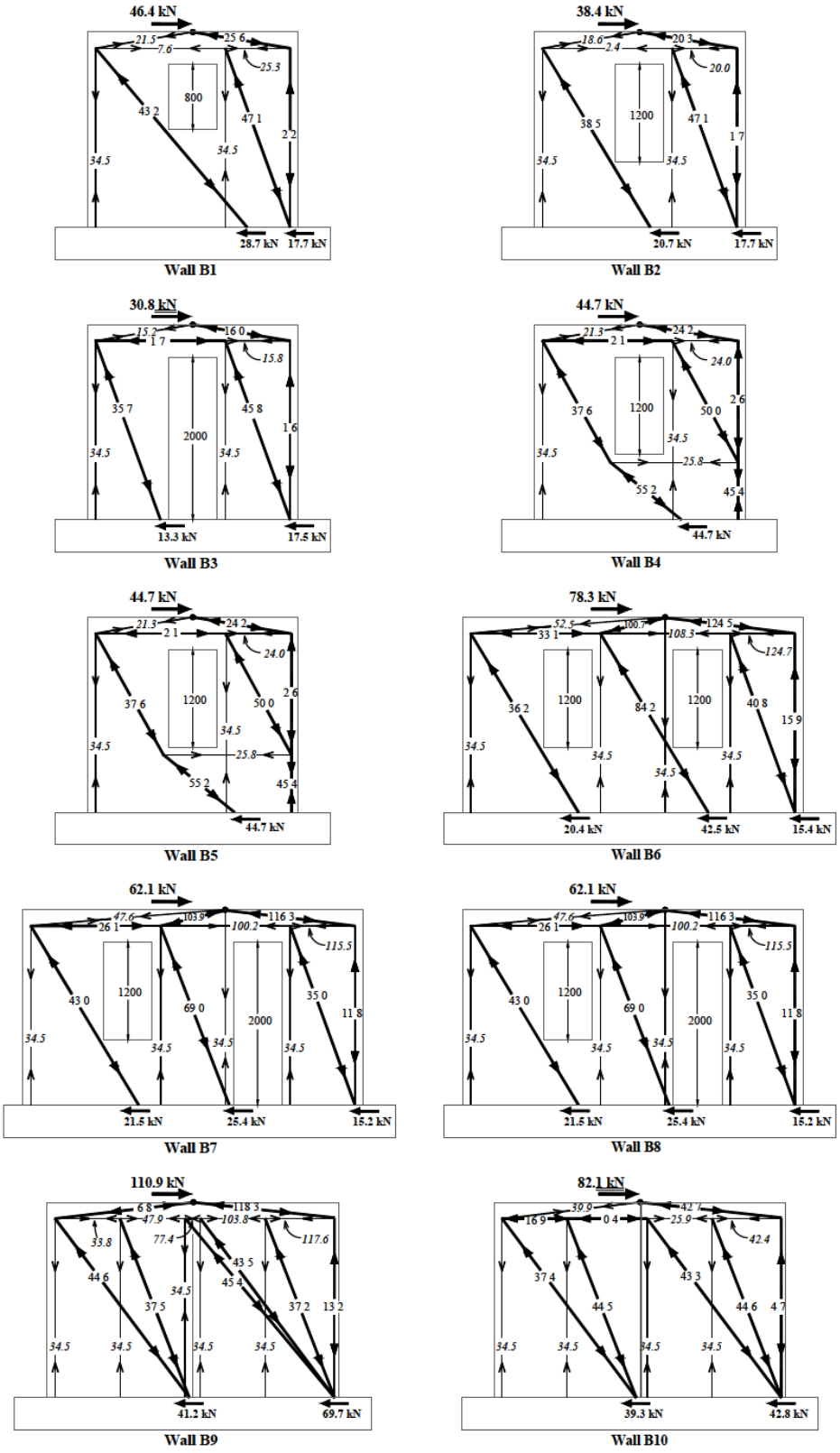

Figure 17.4: Strut-and-tie models from Voon (2007)

began and ended at the intersections of the reinforcement bars, which is more analogous to an idealized truss model. Nolph considered multiple arrangements of strut-and-tie models for two of his six specimens while Elmapruk constructed other model arrangements for all of his specimens. In both cases these researchers reported the results from the most conservative model for each specimen, which does not follow the principle of minimum strain energy.

The principle of minimum strain energy states that—for design scenarios—the model with the minimum strain energy for a given strength demand is the most correct model. This has been shown earlier to mean the model with the minimum volume of reinforcement for a given strength demand. The analysis scenario differs from the design scenario because the amount of reinforcement in each specimen was specified and fixed previously and that the shear strength is the unknown variable. Generalizing the rationale from the design scenario for both, the objective of the strut-and-tie modeling procedure is to minimize the ratio of reinforcement to strength. Since in the amount of reinforcement in the Nolph models was fixed, the models which predicted the highest predicted shear strength (i.e., least-conservative) would have minimized the ratio of reinforcement to strength and would have been the most correct models.

Nolph performed his modeling calculations using the program Visual Analysis. He calculated shear strengths within 14 percent of the experimental strength for the partially-grouted walls but observed that the model for the fully-grouted wall severely over-predicted the strength (by 78 percent), which is far outside the margin of error for the experiment. Since the lower-bound theorem states that the models will always produce safe (i.e., conservative) estimates, the severity of the error can either be attributable to errors in application of the ACI 318 procedures or to discrepancies between the procedures and masonry. Elmapruk calculated shear strengths within 21 percent of the experimental strength for all of this specimen, which does not account for the fact that he used the lowest predicted values. Both studies showed that an idealized truss model can be used to model masonry shear walls but the accuracy and precision are uncertain due to questions about the application and validity of the ACI provisions with masonry.

17.3.7 Varshney

Varshney (2010) conducted numerical simulations using meso models to determine the slope at which the struts diverge from the friction slope in the equilibrium modeling procedure de-

veloped by Roca et al. (2010). The models were constructed with continuum elements representing the bricks and interface elements representing the bed and head joints. The bricks were modeled with four-node quadrilateral isoparametric plane stress elements using a smeared cracking material model—which used a combination of tension cut-off, tension softening, and shear retention. Both joint types were modeled using an interface element between two lines in a two-dimensional configuration. The bed joints elements used a combination cracking/shearing/crushing model—a plasticity-based multi-surface interface model—and the head joint elements used a Coulomb friction model. The modeling parameters investigated in his analysis were the length of the loaded area and the applied axial stress.

Varshney (2010) found that for a loading length less than or equal to 20 percent of the wall height, the angular departure of the struts is approximately one-third of the friction slope. For longer loading lengths, the strut deviations tend to deviate and the assumed value of one-third of the friction slope is only valid for a certain values of friction angle. He also observed that masonry panels with lower friction angles are better able to develop regions of parallel struts compared to walls with higher friction angles.

17.3.8 Foraboschi and Vanin

Foraboschi and Vanin (2013) presented an evolutive strut-and-tie modeling process which was intended to reproduce the in-plane masonry shear behavior and modes of failure in the uncracked, cracked, and softening states. The evolutive procedure accomplishes this through modifying its conformation throughout the various stages of the loading process. Their procedure is similar to that of Roca et al. (2011) in that it relies solely on the masonry to resist the diagonal tensile stresses, but differs in several other aspects from other strut-and-tie modeling methodologies. First, the masonry tensile strength is also used to resist the over-turning tensile forces and does not rely exclusively on exteral forces to maintain equilibrium. Second, the masonry tensile strength in both cases is represented by discrete ties rather than by tension fields as used by Lourenço et al. (2006). Lastly, unlike the methodology of Schlaich et al. (1987) and others which ignores the material displacements and solely considers the forces, the evolutive strut-and-tie modeling process use the principle of virtual work to calculate the lateral forces in the struts and ties.

Foraboschi and Vanin use an idealized truss to represent the arrangements of the struts and ties, ignoring the strength and stiffness contributions of the nodes. The total lateral force resistance of the panels is given by

$$V_n = \frac{\sum_{i=1}^{n} \epsilon_i^2 E_m A_i l_i}{\delta} \tag{17.9}$$

where

n = total number of uncracked truss members,
ϵ_i = elastic strain due to δ in the i^{th} truss member,
E_m = elastic modulus of the masonry,
A_i = cross-sectional area of the i^{th} truss member at $\delta = 0$, and
l_i = length of the i^{th} truss member.

In the initial uncracked condition ($\delta = 0$), the summation includes contributions from all of the truss members. As cracks begin to form, denoted by truss members reaching their ultimate tension strain, cracked members are eliminated. Some potential applications of the evolutive strut-and-tie procedure are to predict whether an unreinforced wall will fail first in tension or in shear and to determine both the ultimate strength and backbone curve for an unreinforced masonry specimen. The evolutive strut-and-tie modeling procedure is more analogous to a numerical macro model than to a mechanical model due to its iterative and computational demands. While it appears to be less computationally intense than applications of the finite element method, the evolutive strut-and-tie modeling procedure is far too rigorous for general design work.

17.3.9 Hamedzadeh

Hamedzadeh (2013) tested 21 masonry shear walls of various dimensions to investigate the behavior of wide-spaced reinforced partially-grouted shear walls. Part of his investigation examined the practicality of strut-and-tie modeling with these wall types. The strut-and-tie models were constructed and analyzed using the finite element software package ABAQUS. It is uncertain why he constructed and analyzed his strut-and-tie models using ABAQUS since one of the justifica-

tions for the use of strut-and-tie modeling is that they are simple to analyze and, in simple cases such as shear walls, can be analyzed by hand. Hamedzadeh concluded that strut-and-tie models can predict the shear capacity of wide-spaced partially-grouted shear walls within an acceptable range. His findings were somewhat limited in scope because he did not investigate the possibility of reinforcement failure.

17.3.10 Morrison

Morrison (2013) collected data from 200 shear wall tests conducted over the past three decades to investigate the validity of the strut-and-tie methodology for the design of masonry shear walls. The modeling procedures used were influenced by those listed in Appendix A of the ACI 318 and AASHTO codes. He created 58 strut-and-tie models to represent 35 fully- and 23 partially-grouted walls taken from his larger dataset.

He analyzed his models using the program Visual Analysis, similar to Nolph. He loaded each model until it became statically unstable, one of the masonry struts crushed, or the deflection exceeded 5 percent of the largest structural dimension. The reinforcement was modeled assuming a bilinear force-deformation curve with a constant force after the yield point. Similar to previous research by Voon (2007), Nolph (2010), and Elmapruk (2010), Morrison placed the center of each node at the intersection of reinforcement bars, essentially generating an equivalent truss model. This assumption is necessary for the model to be analyzed using a structural analysis program.

Equivalent truss models may be considered as a subset of strut-and-tie models, but there exists several differences between equivalent truss models and models constructed using the methodology of Schlaich et al. (1987) and the ACI 318 (2011) code. Equivalent truss models have the limitation in that they do not consider

1. Reinforcement development length requirements in determining the center points of nodes or the paths of struts.

2. That struts can cross ties without forming a node

3. That struts terminating into a rigid member (i.e., reinforced concrete foundation) can be anchored by the body itself and do not need to enter at the intersection of a vertical reinforcement bar

4. The width of the struts or nodes to ensure that they do not extend outside of the masonry panel (especially in partially-grouted walls)

He surmounted some of the limitations of equivalent truss procedure by requiring that the vertical reinforcement be fully developed at the top point of intersection with the horizontal bars and by assuming that the maximum strut width to be

$$w_s = \frac{w_t}{\cos \alpha_s} \tag{17.10}$$

where

w_s = maximum width of diagonal strut,
w_t = minimum of reinforcement diameter plus twice the clear cover and the wall thickness, and
α_s = inclination of a strut (measured from the vertical).

Morrison determined the ratio of predicted to experimental strengths to be 0.67 for partially-grouted walls and 0.61 for fully-grouted walls. He observed that all but seven of the 23 partially-grouted models and all but 15 of the 35 fully-grouted wall failed by strut crushing. He also observed that struts tended to form at 45 degree angles regardless of the aspect ratio of the wall. Morrison concluded that strut-and-tie modeling is a sound and all-encompassing method for calculating the in-plane shear strength for both fully- and partially-grouted masonry shear walls.

17.3.11 Summary

Several researchers have studied the use of various strut-and-tie methodologies in predicting the shear capacity of masonry shear walls. In every research study reviewed, the strut-and-tie modeling procedures have introduced some simplifying assumptions which altered the method from that originally prescribed by Schlaich et al. (1987). To date, no research has been performed with masonry shear walls using the exact methodology prescribed by Schlaich et al., which introduces the possibility that the models presented may not be the optimum models for use in design.

17.4 Code Provisions for Reinforced Concrete

17.4.1 ACI Design Provisions

Strut-and-tie modeling is currently used for reinforced concrete structures and is governed by the provisions in Appendix A of ACI 318 (2011). The ACI strut-and-tie provisions specify guiding principles for designers to follow while using the strut-and-tie modeling procedure. The code provisions for strut-and-tie design follows the same strength design approach used in the main body of the code. The code requires that struts, ties, and nodal zones be designed such that

$$\phi F_n \geq F_u \tag{17.11}$$

or that factored forces acting on the member be less than the design strength of the same (ACI 318, 2011).

The nominal strength of struts is based on the effective compressive strength of the concrete multiplied by the smallest cross-section of the strut. The code provides factors for reducing the effective compressive strength of struts for several reasons. No reduction is required for struts that are prismatic, but the code uses a strut efficiency factor β_s to reduce the strength of fan-shaped or bottle-shaped struts. Factors are also given to reduce the effective strength of struts that are located in tensile regions of members (e.g., tension flanges) or in areas where they are likely to be traversed diagonally by cracks (e.g., beam webs). In all cases the code permits less-stringent reductions to be used for areas meeting minimum reinforcement requirements.

The nominal strength of nodal zones is similar to that of compression struts. Nodal zones typically have three faces, one for each member that meets in the node. If more than three struts or ties intersect in a nodal zone, then the resultant forces and faces are determined by combining some of the forces together. Each face of the nodal zone is measured normal to the axis of the strut or tie, and the critical area used in design is the smallest of the three faces. The effective compressive strength of the nodal zone is reduced by the factor β_n for nodal zones that contain ties. The code also restricts the feasible inclined angle θ, the angle at which struts and ties intersect at nodal zones, to be between 25 and 65 degrees (ACI 318, 2011).

The nominal strength of tension ties is the sum product of the tensile strength and cross section of the reinforcement bars in the tie. The tension ties include parallel reinforcement bars that are close enough together to act as a unit and the concrete between and immediately around the bars. The concrete between and around the reinforcement does not contribute any tensile strength to the tie, but it is included because it is necessary for transferring the forces between the tie and the adjacent concrete. The tension force for each tie is assumed to act through the centroid of the cross section of the reinforcement. The code requires adequate development length for tension ties beginning at the point where the axis of the tie first crosses into the intersecting strut to the end of the nodal zone (ACI 318, 2011).

17.4.2 AASHTO Design Provisions

Strut-and-tie modeling is also used in the design of reinforced concrete bridges and is governed by several provisions of chapter 5 of the AASHTO (2012) LRDF Bridge Design Specifications. The focus of the AASHTO strut-and-tie procedures is particularly on deep beams and, for this reason, are narrower in scope and not as developed as the procedures in the ACI 318 (2011) procedures. The AASHTO provisions follow the same theory and guidelines as the ACI 318 provisions but contain some differences in the specifications for the strut inclination and strut effective strength.

The AASHTO procedures do not specify a limit for the angle at which struts and ties intersect but decrease the effective strut strength for increasing strains in the reinforcement. In the AASHTO provisions the effective strut strength f_{cu}, in units of kips, is given by

$$f_{cu} = \frac{f'_c}{0.8 + 170\epsilon_1} \leq 0.85\, f'_c \tag{17.12}$$

where

ϵ_1 = $\epsilon_s + (\epsilon_s + 0.002)\cot^2 \alpha_s$,
α_s = the smallest angle between the compressive strut and adjoining tension ties,
ϵ_s = the tensile strain in the concrete in the direction of the tension tie, and
f'_c = specified concrete compressive strength (kips).

Equation (17.12) can be seen as a penalty factor for the strut strength to account for the increased strain in the concrete induced by the elongation and yielding of tension ties joining struts at shallow angles. Unlike the ACI provisions, the AASHTO provisions do not reduce the effective strut strength to account for bottle-shaped struts depending on the amount of crack control reinforcement. The AASHTO provisions require that all members meet the minimum specified amount of crack control reinforcement so a strength reduction for bottle-shaped struts is not necessary.

17.5 Adapting the Provisions for Masonry

Several researchers (Roca et al., 2011; Varshney, 2010; Voon and Ingham, 2006, 2008; Mojsilović, 2011; Nolph, 2010) have concluded that strut-and-tie modeling is a practical tool for designing masonry shear walls. There are, however, no recommended practices or guiding principles for implementing the strut-and-tie method in masonry design. This section will outline some of the possible issues that will need to be surmounted to develop strut-and-tie modeling guidelines for reinforced masonry structures. Similar to how other aspects of the MSJC (2013) code where developed, the ACI 318 (2011) provisions for strut-and-tie modeling may be used as a beginning point for developing provisions for use with masonry. This section will also present and comment on the current ACI 318 provisions in light of the current masonry knowledge to identify areas of analysis and research such that the provisions can be adapted for use with masonry design.

The ACI principles cannot be applied directly to masonry design because of the great number of differences between the two materials. Concrete is typically considered to be an isotropic material because it consists of a random assortment and arrangement of aggregates within a cement matrix. Concrete members are typically cast monolithically and usually do not contain constructions joints within the disturbed regions. The assumptions of isotropy, monolithic construction, and continuity for concrete allow designers to use the same compressive strength for any orientation of the struts or nodes within the member.

Masonry is an anisotropic and non-monolithic material due to the presence of regularly occurring joints and the use of different constituent materials within the material. The joints within masonry assemblages create planes of weakness with different compressive strength depending of the orientation of the axial stress. Research has shown (Bennett et al., 1997; Liu et al., 2006) that masonry in compression follows the Mohr-Coulomb failure criteria because of the friction

that occurs along the joints. The greatest compressive strength in masonry is obtained when it is axially loaded normal to the bed joints, which is typically determined from prism compression tests. The lowest compressive strength occurs when the load is between 45 and 90 degrees of the vector normal to the bed joint, depending on the friction angle of the unit-mortar interface φ (Guo, 1991; Liu et al., 2006). Unlike concrete, it will be necessary to decrease the compressive strength of the struts depending on the orientation of the strut relative to the bed joint plane.

Masonry typically contains significant voids within the assemblage. The most notable sources of large voids is from the presence of hollow (i.e., ungrouted) masonry cells within the assemblage. Even when cells are fully-grouted, the shrinkage that occurs in the grout during curing is exacerbated by the wicking of moisture from the grout into the surrounding masonry units. The grout shrinkage can create areas of non-contact between the grout and the masonry such that compressive forces do not transfer well between the masonry units and the grouted cores and flues. This intransmissibility of stress is more-commonly evident in the direction parallel to the bed joints. Even though the MSJC specification requires that the grouted cores be vibrated a second time after the grout has had an opportunity to shrink, this non-total contact may be an issue.

Head joints are another potential area of large voids within the masonry assemblage, particularly for walls using wide and hollow masonry units. During construction, it is common for the head joints to be buttered only along the exterior edges, leaving the interior hollow. Even if the wall is to be fully-grouted, the grout will most likely not fill the voids in the head joints, leaving voids in the cross section of the wall. Research has shown (Bennett et al., 1997) that head joints typically demonstrate lower compressive strength than bed joints because of the lack of vertical confinement during curing which decreases the bonded area between joint and masonry unit. Due to these reasons, the equivalent cross sectional thickness of the masonry available for resisting compressive stresses parallel to the bed joint is less than that for loading normal to the bed joint. The exception to this issue may be the case of thin, solid masonry walls, such as traditional brick walls, where the head joints are fully buttered and solid between the two faces.

In masonry walls constructed with hollow masonry units, the assumption of plane stress conditions does not hold because at some locations within the wall there exists regions were the stress flow component normal to the plane of the wall is not zero. This is the case regardless of the grouting pattern, though the location and frequency will vary depending on the frequency of

grouting used. Force components normal to the plane of the wall induce tensile splitting forces within the masonry units. If this force component exceeds the tensile strength of the masonry webs, then the masonry will fail by vertical tensile splitting of the unit before the strut can develop its full capacity.

In the case of partially-grouted shear walls, the compressive stresses will travel principally through the shells near the exterior faces of the wall and the tensile forces will travel through the reinforcement bars located along the center of the wall, as shown in Figure 17.5. As compressive and tensile forces are transferred between the compressive struts and the tension ties at nodes, the forces must travel from the exterior shells to the center of the wall, resulting in a force vector component normal to the plane of the wall. If this lateral force component exceeds the lateral tension capacity of the surrounding webs, then the forces will cause the tensile splitting of the masonry units surrounding the node before the strut can reach its ultimate capacity.

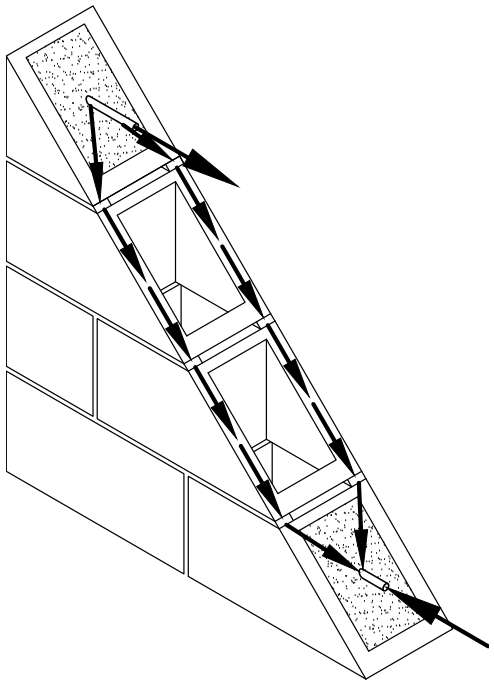

Figure 17.5: Path of stress from shells to reinforcement

In the case of fully-grouted walls, the compressive stresses must traverse a bottleneck as they travel through the head joint between one fully-grouted masonry unit and another, as shown in Figure 17.6. The influence of this behavior changes with the orientation of the stress path relative to

the bed joint plane, varying from non-effectual when loaded normal to the bed joint plane to fully effectual when loaded parallel to the bed joint plane. This concentration of compressive stress is somewhat assuaged for masonry laid in running bond where some of the compressive stress may travel around the head joint through the fully-grouted units immediately above or below the bottleneck.

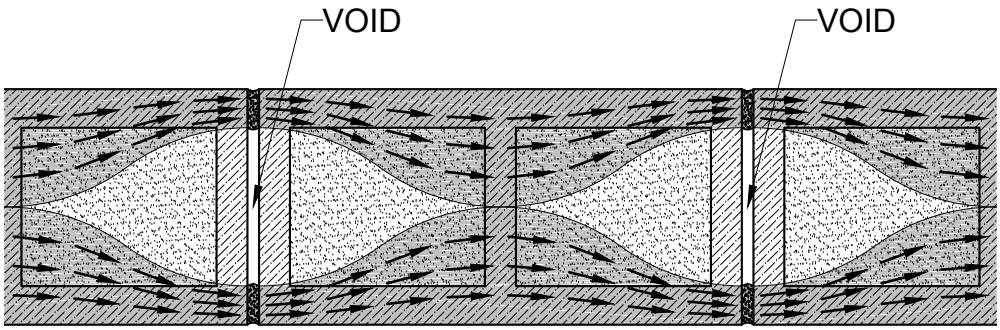

Figure 17.6: Path of stress around head joint voids

Liu et al. (2006) observed that the ratio between biaxial compressive strength and uniaxial compressive strength is greater for masonry than for concrete. They concluded that the existence of area of weakness near the interfaces of different material types decreases the uniaxial compressive strength of masonry. Since the uniaxial compressive strength is used as the reference strength for the material, this suggests that the biaxial compressive strength for masonry might be higher than assumed by following the same strength proportions used for concrete. This means that in nodal regions, points of intersection between struts and ties where the masonry is multidirectionally stressed, the actual strength may be notably stronger than the f'_m value determined from prism tests or from the unit strength method.

17.5.1 Parameters Needing Investigation

The development of strut-and-tie modeling procedures will best be accomplished by building off the work previously performed in developing the strut-and-tie guidelines for reinforced concrete available in Appendix A of ACI 318 (2011) and the AASHTO (2012) LRFD Bridge Design Specification. Due to the differences between reinforced concrete and reinforced masonry,

many of the guidelines, limits, and factors will need to be revised for the reinforced masonry case. Furthermore, some new guidelines may need to be added to the procedures to meet the unique needs of masonry construction. This section provides an outline of revisions and additions that may need to be made to adapt the existing provisions for use with masonry construction.

Strut Efficiency Factor

The strut efficiency factor β_s is an empirical factor used to account for reductions in effective strut compressive strength from the effects of internal strut geometry, reinforcement ratio, and member type (ACI 318, 2011). In masonry, the grouting type and reinforcement placement will also affect the effective strength of the strut because they introduce tensile splitting forces into the masonry units. Since the tensile strength is functionally related to the compressive strength of the masonry, using a factor is preferred to using a formula due to its simplicity. Further analytical and/or experimental research will need to be performed to determine the empirical factors to be used to account for these reductions in strength capacity.

Special Reinforcement Requirements

Section A.3.3 of the ACI 318 (2011) code lists requirements for reinforcement that resists the tensile forces from lateral spreading in bottle-shaped struts. These special reinforcement requirements for concrete will need to revised for masonry because multiple, perpendicular layers of closely-spaced reinforcement are not feasible within masonry walls. In partially-grouted walls, the transverse strut reinforcement would consist of joint reinforcement placed in every joint or mesh reinforcement bonded to the outside faces of the wall, which likely would not be received by the construction community. For fully-grouted walls, smaller reinforcement bars could be placed within the cells not occupied by the main vertical reinforcement in addition to the methods listed for partially-grouted walls.

Strut Inclination Factor

The nominal compressive strength of struts must be decreased for loading that is not normal to the bed joint plane (Liu et al., 2006). This can be accomplished by introducing a strut inclination

factor β_α for masonry which is represented by a two-part linear function of the inclination angle α_s. The inclination angle of the strut center line is measured normal of the bed joint plane. The minimum compressive strength typically varies between 45 and 90 degrees, depending on the friction angle of the unit-mortar interface. Since the friction angle varies between different types of masonry, mortar, and construction, the strut inclination factor would likely be the most appropriate approach.

The inclination factor would vary linearly from unity at 0 degrees to a predetermined value at a specified inclination angle. Above this specified angle, the strut inclination factor would remain constant, as shown in Figure 17.7. The value of the inclination angle for the plateau needs to be determined from analysis of angled uniaxial prism tests.

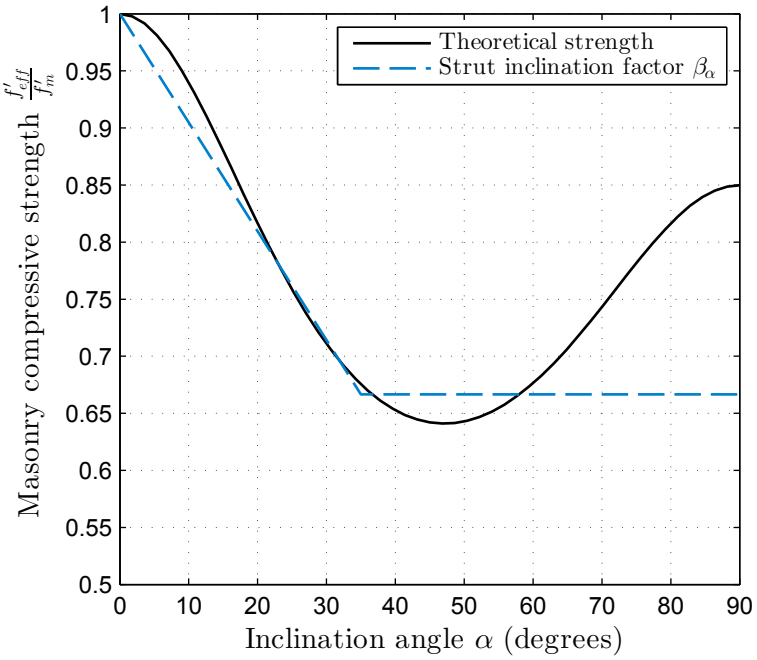

Figure 17.7: Hypothesized strut inclination factor values

Feasible Inclined Angle

ACI 318 (2011) places limits on the feasible angle at which struts and ties can meet at any node to prevent cracking and strain incompatibilities. At excessively low values, the shortening

of the strut and elongation of the tie will cause the member to fail before reaching its ultimate strength, which is analogous to the snap-through-buckling scenario. It will be necessary to determine whether the feasible inclined angle limits in ACI 318 (2011) are applicable to masonry structures or whether new limits should be imposed.

Nodal Efficiency Factor

The nodal efficiency factor β_n is an empirical factor used to account for the effect of the anchorage of ties on the effective compressive strength of a nodal zone (ACI 318, 2011). The forces applied to a nodal zone are assumed to create a biaxial stress condition for the material within the nodal zone. In nodes where three struts meet, the two principal stresses are equal and the nodal material is said to be in a near-hydrostatic state where there are no in-plane shear stresses. When one or two ties are anchored within a nodal zone, in-plane shear stresses are introduced within the nodal region and effective compressive strength is reduced.

Research has shown (Liu et al., 2006) that the difference between uniaxial and biaxial compressive strength is more exaggerated for masonry than for concrete. It is possible that the strength reduction for masonry may not need to be as great because the biaxial strength for masonry is so much higher than its uniaxial strength. However, the tensile splitting forces in masonry nodes (see Figure 17.5) may negate any or all of the increased biaxial compressive strength. Analysis is needed to quantify the effect of tie anchorage and tensile splitting forces on the compressive strength of nodal zones.

17.6 Conclusions

Strut-and-tie modeling has been shown to be a valid tool for use in masonry structural design. Guidelines need to be developed such that the use of strut-and-tie modeling for masonry design can be standardized. The existing guidelines in Appendix A of ACI 318 and in AASHTO Bridge Design Provisions appear to be a good starting point for developing strut-and-tie modeling guidelines for masonry. There are numerous differences between reinforced concrete and reinforced masonry such that the existing provisions should not be used for masonry without modification. The development of strut-and-tie modeling standards for reinforced masonry will require

changes and additions to the existing guidelines to make them suitable for use. Further analysis in specific areas of masonry research relating to strut-and-tie modeling is requisite for the formulation of the new guidelines to proceed.

CHAPTER 18. STRUT-AND-TIE MODELING METHODOLOGY

18.1 Introduction

This chapter explains the methodology undertaken in developing and using the strut-and-tie modeling methodology to model the shear strength capacity of masonry shear walls. The end goal of this work is to create and validate a set of preliminary modeling guidelines for constructing strut-and-tie models for masonry shear walls. Existing guidelines are already developed for use with reinforced concrete and are publishing in Appendix A of ACI 318 (2011) and in the AASHTO (2012) LRFD Bridge Design Specifications. This work will be conducted by constructing multiple models for each specimen to investigate which guidelines can be adopted. The development of modeling guidelines will necessitate the consideration of the differences between masonry and concrete, as described in Section 17.5 of this dissertation. These considerations will be investigated using data from the full-size assemblies in the dataset from this investigation. This analysis will outline further investigations that will need to be performed on individual components in which the effect of a single guideline can be investigated independent of the others.

18.2 Objective Criterion

The analysis of existing masonry shear walls is different from the general use of strut-and-tie models. Strut-and-tie models are typically used to determine the required reinforcement amount and placement within a member to resist the ultimate load demands placed on the member. This means that in a typical scenario, the loads are known and reinforcement is unknown. In an analysis case, the reinforcement size and spacing are known and the object of the analysis is to determine the member capacity. This difference in modeling approach requires a generalization of the objective criterion for evaluating strut-and-tie models that works for both scenarios.

For design scenarios, the principle of minimum strain energy states that the model with the minimum strain energy for a given strength demand is the most correct model. This has been shown using equation (17.1) to mean the model with the minimum volume of reinforcement for a given strength demand. Generalizing the rationale from the design scenario for both design and analysis scenarios, the objective of the strut-and-tie modeling procedure is to minimize the ratio of reinforcement to strength capacity. For the case of analyzing existing shear walls, the objective can be stated as the strut-and-tie model which produces the highest predicted capacity and meets all of the modeling guidelines is the most correct model.

18.3 Specimens

Selected specimens were selected from the dataset to model using strut-and-tie modeling to compare the modeling results with the experimental results. Modeling all masonry shear wall specimens from the dataset was outside of the scope of this study, so specimens were selected to correlate with the equivalent-truss models constructed previously by Voon (2007), Nolph (2010), Elmapruk (2010), and Morrison (2013). The former three studies constructed strut-and-tie models solely for specimens that those researchers tested themselves while Morrison selected a few specimens from several studies from the literature for analysis. The current study constructed strut-and-tie models for all of the specimens that were modeled previously as well as the remaining specimens in the studies from which Morrison selected only a few. Models were constructed for 69 fully-grouted walls and 47 partially-grouted walls (10 of which contained openings).

18.4 Procedure

Each specimen was initially modeled using the strut-and-tie methodology prescribed in Appendix A of the ACI 318 (2011) code. The base compression strength f'_m of the masonry struts and nodal regions was assumed to be the strength obtained by the researchers through prism tests. This base strength was multiplied by the respective factors to obtain the effective strengths of the members. The reinforcement yield strength was taken directly from the studies from which the specimen data came. The distributed applied axial load was resolved into equivalent point loads

acting at the nodes across the top of each wall. The experimental strength used in the comparison was the average of the peak strengths from each of the two loading directions.

The performance of the models was examined using the mean and coefficient of variation of the ratios of experimental to predicted strength, similar to the approach used in Chapter 10. The two statistics were calculated separately for the fully- and partially-grouted groups as well as for the group of walls with openings. Performing a group-wise comparison of experimental and predicted results was judged to be a superior approach than comparing the strengths wall-by-wall since the experimental results and measured data parameters both contained several potential sources of variation. While the mean was useful in judging the overall accuracy of the modeling procedures, the coefficient of variation was deemed to be the best for comparing the performance of the modeling procedures because they showed how precise the method is in accounting for the variations in wall strength.

As the number of models for each wall type were developed, the errors between the results and the experimental strengths were inspected to identify patterns which could identify the source of each error. As potential sources of error were identified, variations from the ACI 318 modeling procedures were made to observe how they affected the modeling results in comparison with the experimental results. The modeling variations were taken from the AASHTO (2012) bridge specifications and/or developed based on masonry knowledge gleaned from the literature. They were applied in a systematic way for all masonry walls to assure that they did not worsen the errors in the models for other masonry specimens. The adaptations which proved to consistently ameliorate the modeling results were adopted in the final modeling methodology.

18.5 Analysis

The models were analyzed using a custom computer program coded and ran using MatLab (2014). The program consisted of functions which computed the parameters for each type of strut, a program which computed the strength for the entire model assembly, and a unique input file created for each specimen. Both the functions and the main program used an iterative process to reach each solution because there is no direct approach for solving all but the most rudimentary strut-and-tie models. The program was meant to be a means of performing the highly repetitive

and iterative sequence of calculations involved in analyzing strut-and-tie models caused by the highly-interconnected nature of all the member parameters.

During the preliminary planning stages of this analysis several types of strut geometries were identified to be common in masonry strut-and-tie models. These strut types were labeled according to the location of the known constraint locations at the top and bottom connections of the struts. Struts were classified as being in one of the following categories:

- Center to edge
- Center to stirrup
- Edge to edge
- Stirrup to edge

Illustrations of the four common strut types are shown in Figure 18.1. The first two strut types were sub-classified by whether or not their top anchorage extended into the header beam. This extension was depended based on the rigidity of the header beam in comparison with the masonry panel. A function was created for each strut type which calculated the size and resultant forces based on the given geometry, constraints, and applied force.

The main program used parameters from the input file to determine the geometry, constraints, and applied forces for each strut and passed those values to the appropriate strut-type function. The input parameters included the locations of the reinforcement, the grid points to which each strut was connected, the type of each strut, values for the various strut and node factors, and material properties. The program kept track of the stresses in the reinforcement bars and struts and adjusted the forces applied to the struts to ensure that the capacity of every member was not exceeded and that the model was in equilibrium. The main program summed the lateral contribution of all struts terminating in the base of the wall and output that value as the shear strength of the wall.

The layout and optimization of the models was performed manually by making changes to the input file for each specimen. This manual approach helped the analyst to observe how different perturbations to the models affected the resulting strengths. The program was updated throughout the study to accommodate the various adaptations that were developed specifically for the modeling

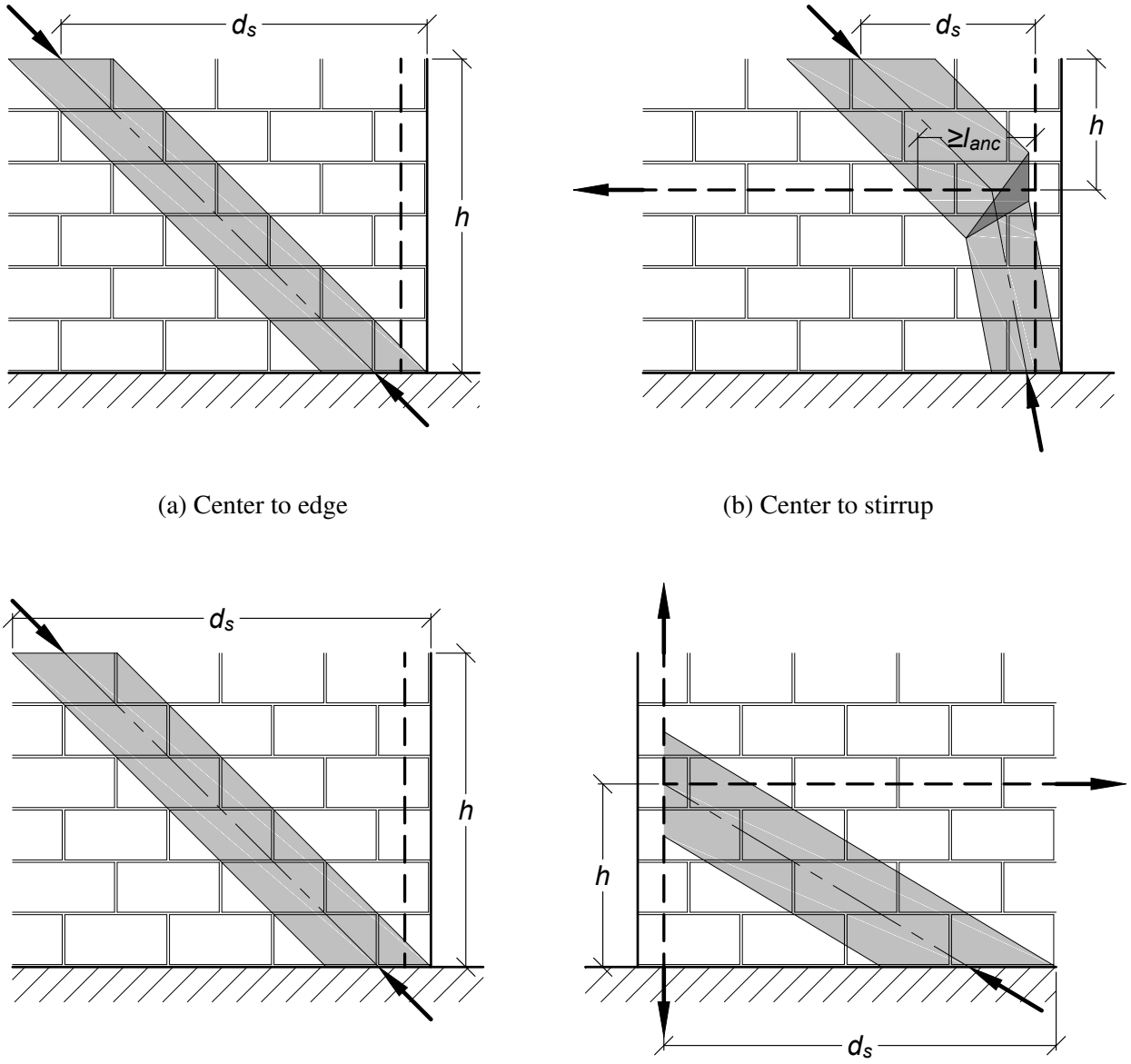

(a) Center to edge

(b) Center to stirrup

(c) Edge to edge

(d) Stirrup to edge

Figure 18.1: Four types of common struts

of masonry shear walls. Further development and refinement of the computer program for general use was outside of the scope of this study.

CHAPTER 19. STRUT-AND-TIE MODELING ANALYSIS

19.1 Compression Struts

The effective compressive strength used in constructing the masonry struts was assumed to be

$$f'_s = 0.8\beta_s \beta_\alpha f'_m \tag{19.1}$$

where

β_s = the strut efficiency factor,
β_α = the strut inclination factor, and
f'_m = the masonry characteristic strength.

Equation (19.1) is similar to that specified in ACI 318 (2011) except that the 0.85 factor for concrete was changed to 0.8 to maintain compatibility with other masonry strength equations and the strut inclination factor is introduced to account for the anisotropic behavior of masonry. The determination of values for each of the factors is detailed in the following sections.

19.1.1 Strut Efficiency Factor

The strut efficiency factor β_s values from the ACI 318 code were initially chosen as a baseline for the development of strut-and-tie models for the masonry specimens analyzed in this study. Struts which traveled in a near vertical direction near the edge of the wall were assumed to have a β_s value of 1.0 because the propinquity of the strut to the edge would prevent the stress fields from bulging. The remaining struts which traversed the wall panels diagonally were assigned a β_s value of 0.75 for those which crossed at least one horizontal or vertical reinforcement bar or assigned a value of 0.60 if they did not cross a reinforcement bar. During the course of the analysis

the values of β_s from ACI 318 appeared to also work for the masonry models and at no time was there sufficient cause found to change the factor values from those initially chosen. A more detailed investigation of strut efficiency factors was prevented by a lack of suitable data in the dataset for the purpose. Further investigation and validation of the β_s values from ACI 318 for use with masonry will require a text matrix of specimen groups each with similar strut layouts but varying levels of reinforcement and material strengths. Until further validation of strut efficiency factors can be performed with isolated specimens, the current values from the ACI 318 (2011) code have been observed to be the best choice for use with masonry.

19.1.2 Special Reinforcement Requirements

The ACI 318 provisions specify that reinforcement that traverses the struts may be considered to resist the transverse tensile splitting forces within the strut if they exceed a specified reinforcement ratio. Many masonry specimens included one or more diagonal struts which included the necessary transverse reinforcement ratio but were crossed by a single horizontal or vertical reinforcing bar. The provisions specify no maximum spacing requirement for the transverse reinforcement so long as the provided reinforcement ratio exceeds that required in the provisions. It was assumed that a single reinforcing bar (providing the necessary transverse reinforcement area) was sufficient to justify the use of a β_s value of 0.75 rather than that of 0.60. During the analysis there was not sufficient cause found to reject this assumption.

19.1.3 Strut Inclination Factor

The strut inclination factor β_α values used in this analysis were initially chosen based on the theoretical strength curve

$$\begin{aligned}\left(-37.78\sin^4(\alpha_s) + 42.99\sin^2(\alpha_s) + 17.86\right) f_m'^2 \\ - \left(1.57\sin^2(\alpha_s) + 16.86\right) f_m' \quad = \quad 1\end{aligned} \tag{19.2}$$

which was developed by Liu et al. (2006) for uniaxial masonry strength. The values for β_α were assumed to follow a bilinear approximation of the theoretical curve in Equation (19.2) which gradually decreased from a value of 1.0 at a strut inclination of 0 degrees to a value of 2/3 at an angle

of 37.5 degrees, after which the value was fixed at 2/3. A graphical comparison of the theoretical and approximated values is shown in Figure 19.1.

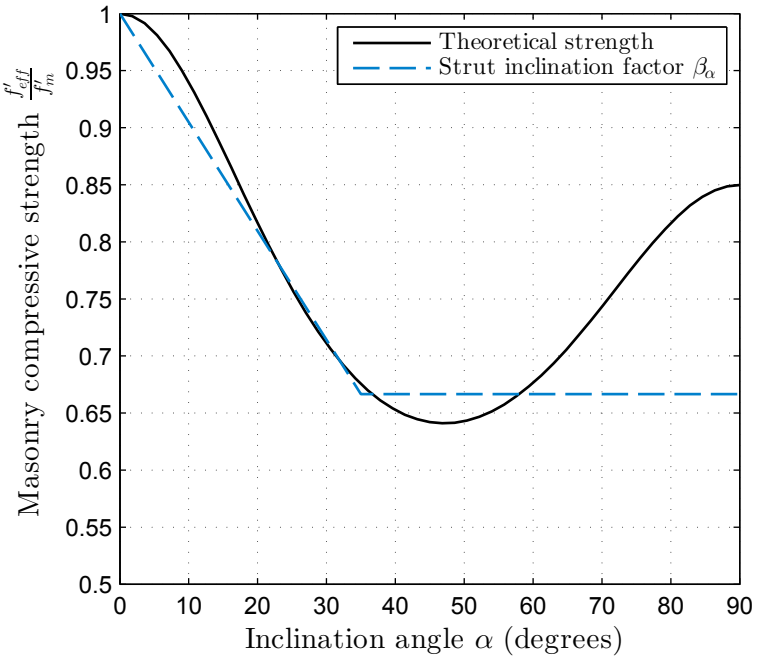

Figure 19.1: Strut inclination factor values used in this study (adapted from Liu et al. 2006)

The applicability of the strut inclination factor was studied separately for fully- and partially-grouted walls. It was observed that the strut-and-tie models for the fully-grouted specimens produced predicted strengths that where closer to the experimental strengths and had lower variation when the strut inclination factor was omitted from the model. A comparison between the models with and without the strut inclination factor is presented in Table 19.1. Conversely, it was observed that the strut-and-time models for the partially-grouted specimens produced better predicted strengths when the strut inclination factor was included in the model, as shown in Table 19.2. The reason for this disparity is likely explained by Drysdale and Hamid (1980) who observed that the grouted cores decreased the level of anisotropy introduced by the bed joints by facilitating the transfer of shear stresses between the different courses of masonry.

Table 19.1: Evaluation of Strut Inclination Factor for Fully-Grouted Walls

Study	Specimen	Ultimate Shear Load (kN)			Strut-and-Tie Models			
					Including β_α		Excluding β_α	
		Min	Max	Avg	V_n (kN)	$\frac{V_{exp}}{V_n}$	V_n (kN)	$\frac{V_{exp}}{V_n}$
Hidalgo et al. (1978)	HCBR-21-2	238	328	283	245	1.16	279	1.01
	HCBR-21-4	328	424	376	354	1.06	415	0.91
	HCBR-21-6	401	473	437	365	1.20	439	1.00
	HCBR-21-8	407	477	442	364	1.21	437	1.01
	HCBR-21-9	366	480	423	363	1.17	434	0.97
Chen et al. (1978)	HCBL-11-3	194	218	174	164	1.06	205	0.85
	HCBL-11-4	257	279	227	227	1.00	264	0.86
	HCBL-11-6	489	545	274	319	0.86	362	0.76
	HCBL-11-7	792	293	202	180	1.12	270	0.75
	HCBL-11-9	223	253	202	340	0.59	405	0.50
	HCBL-11-11	362	390	318	231	1.38	353	0.90
	HCBR-11-3	400	440	420	214	1.96	256	1.64
	HCBR-11-4	507	555	531	347	1.53	430	1.23
	HCBR-11-6	489	545	517	314	1.65	358	1.44
	HCBR-11-7	401	441	421	415	1.01	557	0.76
	HCBR-11-8	335	381	358	262	1.37	354	1.01
	HCBR-11-10	438	466	452	407	1.11	460	0.98
	HCBR-11-12	408	432	420	417	1.01	559	0.75
	HCBR-11-13	491	517	504	434	1.16	589	0.86
Sveinsson et al. (1985)	HCBL-11-13	–	–	461	335	1.38	392	1.18
	HCBL-11-15	–	–	561	362	1.55	466	1.20
	HCBL-11-17	–	–	309	241	1.28	333	0.93
	HCBL-11-18	–	–	308	196	1.57	280	1.10
	HCBL-11-19	–	–	396	271	1.46	349	1.13
	HCBL-11-20	–	–	410	267	1.54	369	1.11
	HCBL-11-21	–	–	389	196	1.98	280	1.39
	HCBL-11-22	–	–	273	261	1.05	306	0.89
	HCBL-11-23	–	–	334	190	1.76	284	1.18
	HCBL-11-24	–	–	424	267	1.59	369	1.15
	HCBL-11-25	–	–	342	271	1.26	350	0.98
	HCBL-11-26	–	–	420	267	1.57	369	1.14
	HCBR-11-15	–	–	525	388	1.35	486	1.08
	HCBR-11-17	–	–	429	349	1.23	403	1.06
	HCBR-11-19	–	–	321	276	1.16	331	0.97
	HCBR-11-20	–	–	334	345	0.97	440	0.76

Table 19.1: Evaluation of Strut Inclination Factor for Fully-Grouted Walls (Continued)

Study	Specimen	Ultimate Shear Load (kN)			Strut-and-Tie Models			
					Including β_α		Excluding β_α	
		Min	Max	Avg	V_n (kN)	$\frac{V_{exp}}{V_n}$	V_n (kN)	$\frac{V_{exp}}{V_n}$
Sveinsson et al. (1985)	HCBR-11-21	–	–	410	291	1.41	378	1.08
	HCBR-11-22	–	–	418	312	1.34	414	1.01
	HCBR-11-23	–	–	354	292	1.21	388	0.91
	HCBR-11-24	–	–	384	293	1.31	388	0.99
	HCBR-11-25	–	–	380	276	1.38	331	1.15
	HCBR-11-26	–	–	374	345	1.08	440	0.85
	HCBR-11-27	–	–	393	276	1.42	331	1.19
	HCBR-11-28	–	–	397	348	1.14	447	0.89
	HCBR-11-30	–	–	469	380	1.23	486	0.97
Shing et al. (1990)	3	445	467	456	331	1.38	426	1.07
	4	320	387	354	291	1.22	343	1.03
	5	396	418	407	300	1.36	376	1.08
	6	209	231	220	175	1.26	187	1.18
	7	432	432	432	331	1.30	398	1.08
	8	209	222	216	180	1.20	191	1.13
	9	427	427	427	286	1.49	337	1.27
	10	298	307	302	235	1.29	256	1.18
	11	396	423	409	321	1.27	365	1.12
	13	485	516	500	357	1.40	407	1.23
	14	436	498	467	333	1.40	398	1.17
	15	365	418	391	287	1.36	321	1.22
	16	534	538	536	338	1.59	435	1.23
	21	480	485	483	358	1.35	415	1.16
	22	383	432	407	299	1.36	328	1.24
Voon (2007)	A1	205	215	210	183	1.15	194	1.08
	A2	177	195	186	187	0.99	205	0.91
	A4	201	233	217	203	1.07	215	1.01
	A7	261	263	262	229	1.14	245	1.07
	A8	244	250	247	212	1.17	225	1.10
	A9	204	207	206	156	1.32	172	1.19
	A10	572	598	585	578	1.01	622	0.94
Minaie (2009)	FMC 2	–	–	329	426	0.77	447	0.74
	FPLC 2	–	–	360	426	0.85	447	0.81
Nolph (2010)	FG085-48	311	355	333	365	0.91	381	0.87
					Mean	1.27	Mean	1.04
					COV	0.25	COV	0.18

Table 19.2: Evaluation of Strut Inclination Factor for Partially-Grouted Walls

Study	Specimen	Ultimate Shear Load			Strut-and-Tie Model Predicted Strength							
					Including β_α						Excluding β_α	
		Min	Max	Avg	$\gamma_x = 0$		$\gamma_x = 0.5$		$\gamma_x = 1$		$\gamma_x = 0.5$	
		(kN)	(kN)	(kN)	(kN)	$\frac{V_{exp}}{V_{pred}}$	(kN)	$\frac{V_{exp}}{V_{pred}}$	(kN)	$\frac{V_{exp}}{V_{pred}}$	(kN)	$\frac{V_{exp}}{V_{pred}}$
Hidalgo et al. (1978)	HCBR-21-3	104	138	121	116	1.04	137	0.88	177	0.68	163	0.74
	HCBR-21-5	194	230	212	215	0.99	268	0.79	319	0.66	320	0.66
	HCBR-21-7	191	231	211	215	0.98	267	0.79	318	0.66	318	0.66
Chen et al. (1978)	HCBL-11-5	195	221	208	117	1.78	152	1.37	188	1.11	209	1.00
	HCBL-11-8	159	169	164	76.6	2.14	111	1.48	147	1.12	165	0.99
	HCBL-11-10	201	223	212	133	1.59	174	1.22	210	1.01	278	0.76
	HCBR-11-5	171	223	197	176	1.12	217	0.91	259	0.76	289	0.68
	HCBR-11-9	164	218	191	102	1.87	135	1.41	168	1.14	192	0.99
	HCBR-11-11	179	231	205	253	0.81	291	0.70	327	0.63	370	0.55
Yancey and Scribner (1989)	R2	129	159	144	118	1.22	187	0.77	246	0.59	231	0.62
	R4	142	149	146	117	1.24	173	0.84	224	0.65	207	0.70
	R5	113	189	151	118	1.28	188	0.80	259	0.58	249	0.61
	R6	145	156	151	118	1.28	176	0.86	227	0.66	210	0.72
	R7	157	164	161	118	1.36	181	0.89	235	0.68	219	0.73
	R9	161	177	169	118	1.43	188	0.90	254	0.67	241	0.70
	R10	182	201	192	118	1.62	188	1.02	259	0.74	258	0.74
	R11	148	172	160	118	1.36	185	0.86	242	0.66	226	0.71
Schultz et al. (1998)	2	–	–	261	278	0.94	312	0.84	342	0.76	468	0.56
	4	–	–	254	188	1.35	232	1.09	272	0.93	348	0.73
	6	–	–	176	111	1.59	159	1.11	205	0.86	235	0.75

Table 19.2: Evaluation of Strut Inclination Factor for Partially-Grouted Walls (Continued)

Study	Specimen	Ultimate Shear Load			Strut-and-Tie Model Predicted Strength							
					Including β_α						Excluding β_α	
		Min	Max	Avg	$\gamma_x = 0$		$\gamma_x = 0.5$		$\gamma_x = 1$		$\gamma_x = 0.5$	
		(kN)	(kN)	(kN)	(kN)	$\frac{V_{exp}}{V_{pred}}$	(kN)	$\frac{V_{exp}}{V_{pred}}$	(kN)	$\frac{V_{exp}}{V_{pred}}$	(kN)	$\frac{V_{exp}}{V_{pred}}$
Schultz et al. (1998)	8	–	–	243	278	0.87	312	0.78	342	0.71	468	0.52
	10	–	–	270	188	1.44	232	1.16	272	0.99	348	0.78
	12	–	–	211	111	1.90	159	1.33	205	1.03	236	0.89
Voon (2007)	A5	134	143	139	125	1.11	151	0.92	175	0.79	188	0.74
	A6	93	93	93	108	0.86	121	0.77	133	0.70	132	0.70
Minaie (2009)	PCL 1	–	–	318	297	1.07	327	0.97	357	0.89	381	0.83
Nolph (2010)	PG085-24	290	302	296	215	1.38	241	1.23	269	1.10	289	1.02
	PG085-32	258	262	260	209	1.24	234	1.11	256	1.02	285	0.91
	PG085-48	211	234	223	176	1.26	202	1.10	226	0.98	235	0.95
	PG120-48	227	230	229	176	1.30	202	1.13	226	1.01	235	0.97
	PG169-48	193	215	204	176	1.16	200	1.02	223	0.91	234	0.87
Elmapruk (2010)	PG127-24	–	400	376*	272	1.38	302	1.25	329	1.14	393	0.96
	PG127-32	–	344	323*	268	1.21	297	1.09	320	1.01	371	0.87
	PG127-48	–	238	224*	242	0.93	271	0.83	298	0.75	322	0.70
	PG127-48I	–	252	237*	242	0.98	271	0.87	298	0.80	322	0.74
	PG180-48	–	266	250*	242	1.03	271	0.92	298	0.84	322	0.78
	PG254-48	–	286	269*	242	1.11	271	0.99	298	0.90	322	0.84
*Corrected values (see section 6.4 for more details)					Mean	1.28	Mean	1.00	Mean	0.84	Mean	0.78
					COV	0.24	COV	0.20	COV	0.21	COV	0.17

19.1.4 Toe Extension Length

It was observed that the partially-grouted models were consistently under-predicting the shear strength of the walls more than the fully-grouted models. The strut inclination factor was eliminated as the cause because its exclusion cause the models to severely over-predict the specimen strength. It was hypothesized that since the end cells were always grouted and the effective thickness of the wall for the final half-block length was much greater than that of the ungrouted wall panels, it was possible that the stress fields in the grouted jamb were able to take a steeper descent to the wall toe. This would have the effect of lengthening the wall, increasing the strut angle for any struts constrained by the wall length, and increasing the struts' lateral force components and the overall strength capacity of the model. This was analyzed by assuming the effective toe of the wall to extend past the edge of the wall a distance given by

$$l_x = \gamma_x \frac{l_b}{2} \frac{t - t_s}{t_s} \tag{19.3}$$

where

γ_x = toe extension factor,
l_b = length of a whole masonry block or brick unit,
t = outside thickness of the wall, and
t_s = total (face) shell thickness of the wall.

The toe extension factor γ_x was investigated for three values $\{0, \frac{1}{2}, 1\}$ to determine which value produced the best-fitting models.

Analysis of the toe extension hypothesis revealed that $\gamma_x = \frac{1}{2}$ produced model predictions that were were the best fit to the experimental data, as shown in Table 20.2. This factor value corresponds to a toe extension length that is proportional to the grouted shear area for a quarter length of a masonry unit or to the masonry shear area between the flexural reinforcement and the nearest wall edge, as shown in Figure I.2. The toe extension length can be represented by

$$l_x = \frac{l_b}{4} \frac{t - t_s}{t_s} \equiv d' \frac{t - t_s}{t_s} \tag{19.4}$$

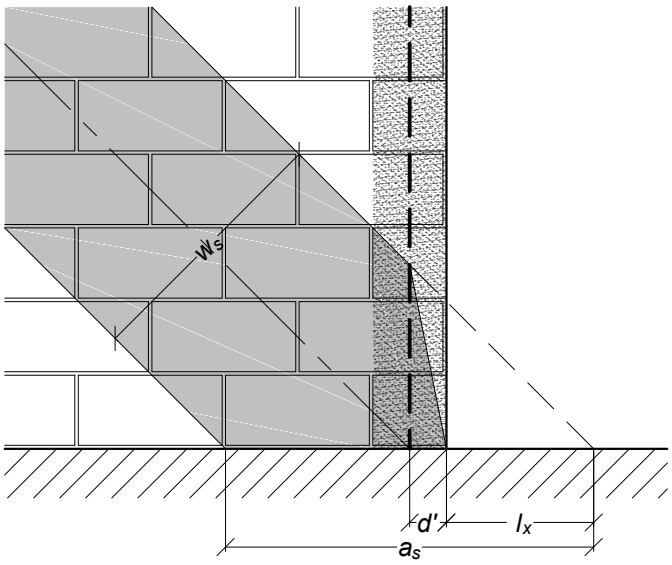

Figure 19.2: Toe extension in partially-grouted walls

where d' is the distance between the centroid of the flexural reinforcement and the nearest wall edge. This phenomenon can be visualized by a diagonal strut whose top edge angled down toward the wall toe when it crosses the flexural reinforcement bar at the end of the wall, as shown in Figure I.2.

19.1.5 Feasible Inclined Angle

The limits on the feasible inclination angle between compression struts and tension ties from the ACI 318 code were investigated to determine if they could be used with masonry strut-and-tie models. The inclusion of inclination angle limits had varying effect on the different strut-and-tie models analyzed in this study. In most models the angle of the struts did not approach the inclination limits and the inclusion or exclusion of the limits had no effect on the model shear capacity. In the remaining models which contained at least one strut exceeding the ACI 318 limits, the inclusion of the limits required the omission of one or more struts from the model and resulted in models which under-predicted the shear strength, generally by a large margin. In a few models, there was only one strut and its omission resulted in a predicted capacity of zero. It appears that the ACI 318 limits placed on reinforced concrete strut-and-tie models are not compatible with

modeling masonry shear walls. Additional research should be performed to either validate this observation or to propose new limits.

19.2 Nodal Zones

The effective strength of nodal regions was assumed to be given by

$$f'_n = 0.8\,\beta_n\,f'_m \tag{19.5}$$

where β_n is the node efficiency factor. The node efficiency factor was initially assumed to follow the provisions in ACI 318 (2011) which prescribe a value of 0.80 for nodal zones anchoring one tie and a value of 0.60 for nodal zones anchoring two ties. During the course of the analysis, no reason was found to justify any adjustment to the values initially chosen from the ACI 318 provisions.

19.2.1 Rigid Boundary Members

The shear wall specimens were all affixed to a reinforced concrete beam at their bases and to some sort of header beam at their tops. The header beams were either separate members affixed to the top with mortar and reinforcement—consisting of either reinforced concrete or a steel shape—or was a section of heavily-reinforced, fully-grouted masonry integrated into the construction of the masonry wall. During the construction of the strut-and-tie models, it was assumed that the base and header beam were rigid bodies into which the struts could extend and in which the struts were anchored sufficiently. It was also assumed that the compressive and shear strengths along the wall-base and wall-header interfaces were at least as strong as the strengths of the bed joints within the wall panel. These two assumptions enabled the struts to transfer forces into the base or header at diagonal angles (in addition to vertically), negating the need for nodal zones within the masonry panel at the ends of some of the struts to redirect the forces in a vertical direction, as shown in Figure 19.3. The omission of nodal zones at the corners of the wall panel, along with their anchorage requirements, permitted the path of the strut from the wall panel directly into the header or base to extend clear to the edge of the wall panel, increasing the horizontal length and

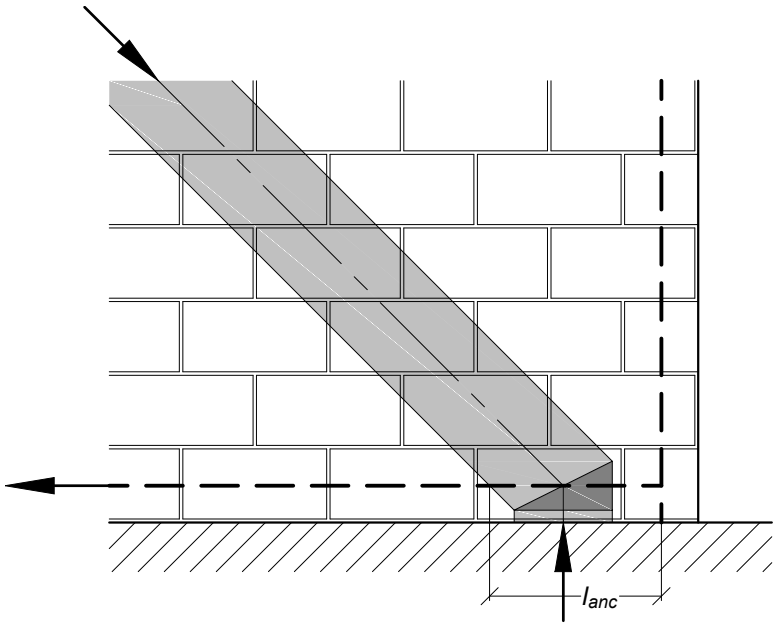

(a) Deformable base assumption

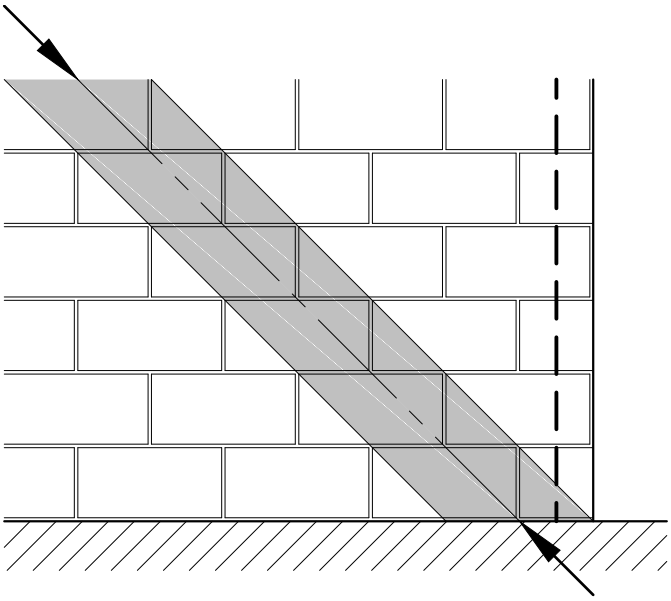

(b) Rigid base assumption

Figure 19.3: Comparison of different boundary member assumptions

force contribution of the strut. It was observed, during the analysis, that these two assumptions appeared to be valid in the case of masonry shear walls.

19.2.2 Reinforcement Anchorage

The reinforcement anchorage requirements used in constructing the masonry strut-and-tie models were assumed to follow those in ACI 318 (2011) except that the equation for development length was taken instead from the MSJC (2013) code. There were three types of anchorage identified amongst the many types of shear wall geometries. The first type of anchorage was located at the tops of the walls and involved a vertical reinforcement bar and the top of a diagonal strut. The second type of anchorage was located where the bottom of a diagonal strut intersected with one of the horizontal bars (or stirrups). The third type of anchorage was located at the intersection of a stirrup with the active flexural bar.

The first anchorage type was located within the header beam and the vertical bar could generally be assumed to be fully developed. Two exceptions to this assumption were the two studied performed at Washington State University by Nolph (2010) and Elmapruk (2010) which included bundled pairs of large reinforcing bars in some of the walls. While performing the analysis, it was observed that several of the walls from these two studies were failing at considerably lower strengths that what was being predicted by the strut-and-tie models. In the course of investigating the cause, it was discovered that the height of the grouted header beam at the tops of these walls was not sufficiently high to permit the full development of the vertical bars.

The MSJC code does not specify procedures for calculating the development length of bundled bars because it does not permit the use of bundled bars in masonry walls. It appears that Nolph (2010) and Elmapruk (2010) assumed that the development length for the bundled pair was the same as that for a single bar which—if true—would have meant that sufficient development length was provided. The ACI 318 code requires that the development length of bundled bars be calculated assuming the diameter of a single theoretical bar having the same area as the bundled bars together. This principle was used to adjust the effective tensile strengths of the bars to account for the inadequate anchorage. When the effective tensile strength was used in the strut-and-tie models the predicted strengths approximated those of the experimental values.

In the second anchorage type, the lateral location of the nodal zone was governed by the width of the compressive struts and the development length of the stirrup, as shown in Figure 19.4a. Since the stirrup was always either bent at a 90 degree angle or hooked around the flexural reinforcement bar with a 180 degree hook, the MSJC specifies that the development length is equal

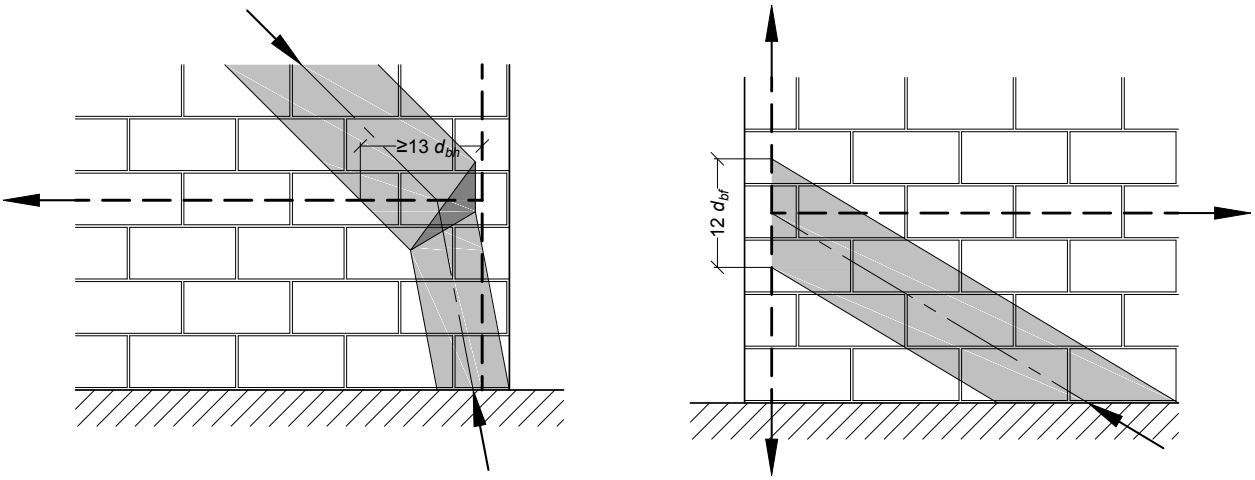

(a) Second anchorage type

(b) Third anchorage type

Figure 19.4: Stirrup anchorage types

to 13 (stirrup) bar diameters. The majority of the lateral force component from the diagonal strut was transferred to the stirrup while all of the vertical force component was transferred downward to the second, vertical strut. The strength of the stirrup was sometimes the limiting factor for the size of the diagonal strut.

The last anchorage type differed from the second because it consisted to two ties and a single strut, as shown in Figure 19.4b. The AASHTO (2012) provisions permit struts to extend up to six flexural bar diameters to either side of the stirrup when the stirrup is anchored to the flexural bar. In this scenario the AASHTO code permits the flexural bar to provide full anchorage to the stirrup and strut and development lengths do not need to be calculated. The strut width permitted by this provision was generally sufficiently large to transfer the full capacity of the stirrup if needed. The few cases where the strut area was not sufficient to carry the full capacity were limited to partially-grouted walls with large horizontal reinforcement ratios.

CHAPTER 20. STRUT-AND-TIE MODELING DISCUSSION

20.1 Comparison with Shear Equations

20.1.1 Fully-Grouted Walls

The results of the strut-and-tie models for the analyzed fully-grouted specimens were compared with the predicted strengths using the MSJC (2013) and proposed shear equations and the results are summarized in Table 20.1. The fit of the strut-and-tie model predictions showed a lower coefficient of variation than both of the shear equations, suggesting that strut-and-tie models are better at accounting for the variation in the wall behavior. The MSJC equation results showed a lower coefficient of variation for this group of specimens than the proposed equation and also showed to be considerably unconservative. These results disagree with the results from the full dataset in Chapter 16 which showed that the proposed equation has a lower coefficient of variation overall than the MSJC equation and that the mean MSJC strength agreed fairly well with the experimental results. This disparity in results is due to the analysis being performed on a smaller sample from the whole dataset. The predicted strengths from the strut-and-tie models was marginally more conservative than the proposed shear equation for fully-grouted walls.

20.1.2 Partially-Grouted Walls

The results of the strut-and-tie models for the analyzed fully-grouted specimens were compared with the predicted strengths using the MSJC (2013) and proposed shear equations and the results are summarized in Table 20.2. The performance of the strut-and-tie models for the analyzed partially-grouted walls was more-noticeably improved over the two shear equations than for the fully-grouted walls. The results from the MSJC equation were again more unconservative than the results for the whole dataset given in Chapter 16 the the reasons previously mentioned.

Table 20.1: Strut-and-Tie Models and Shear Equations for Fully-Grouted Walls

Study	Specimen	Ultimate Shear Load (kN)			Strut-and-Tie Models		Shear Equations			
					Excluding β_α		MSJC		Proposed	
		Min	Max	Avg	V_n (kN)	$\frac{V_{exp}}{V_n}$	V_n (kN)	$\frac{V_{exp}}{V_n}$	V_n (kN)	$\frac{V_{exp}}{V_n}$
Hidalgo et al. (1978)	HCBR-21-2	238	328	283	279	1.01	366	0.77	335	0.84
	HCBR-21-4	328	424	376	415	0.91	490	0.77	394	0.95
	HCBR-21-6	401	473	437	439	1.00	480	0.91	393	1.11
	HCBR-21-8	407	477	442	437	1.01	496	0.89	400	1.11
	HCBR-21-9	366	480	423	434	0.97	511	0.83	406	1.04
Chen et al. (1978)	HCBL-11-3	194	218	174	205	0.85	258	0.67	248	0.70
	HCBL-11-4	257	279	227	264	0.86	330	0.69	273	0.83
	HCBL-11-6	489	545	274	362	0.76	430	0.64	306	0.90
	HCBL-11-7	792	293	202	270	0.75	272	0.74	258	0.78
	HCBL-11-9	223	253	202	405	0.50	366	0.55	288	0.70
	HCBL-11-11	362	390	318	353	0.90	563	0.56	173	1.84
	HCBR-11-3	400	440	420	256	1.64	320	1.31	298	1.41
	HCBR-11-4	507	555	531	430	1.23	481	1.10	372	1.43
	HCBR-11-6	489	545	517	358	1.44	568	0.91	377	1.37
	HCBR-11-7	401	441	421	557	0.76	614	0.69	392	1.07
	HCBR-11-8	335	381	358	354	1.01	327	1.09	309	1.16
	HCBR-11-10	438	466	452	460	0.98	453	1.00	343	1.32
	HCBR-11-12	408	432	420	559	0.75	728	0.58	424	0.99
	HCBR-11-13	491	517	504	589	0.86	770	0.65	452	1.12
Sveinsson et al. (1985)	HCBL-11-13	–	–	461	392	1.18	575	0.80	406	1.14
	HCBL-11-15	–	–	561	466	1.20	642	0.87	446	1.26
	HCBL-11-17	–	–	309	333	0.93	471	0.66	288	1.07
	HCBL-11-18	–	–	308	280	1.10	471	0.65	325	0.95

Table 20.1: Strut-and-Tie Models and Shear Equations for Fully-Grouted Walls (Continued)

Study	Specimen	Ultimate Shear Load (kN)			Strut-and-Tie Models		Shear Equations			
					Excluding β_α		MSJC		Proposed	
		Min	Max	Avg	V_n (kN)	$\frac{V_{exp}}{V_n}$	V_n (kN)	$\frac{V_{exp}}{V_n}$	V_n (kN)	$\frac{V_{exp}}{V_n}$
Sveinsson et al. (1985)	HCBL-11-19	–	–	396	349	1.13	437	0.91	273	1.45
	HCBL-11-20	–	–	410	369	1.11	407	1.01	278	1.47
	HCBL-11-21	–	–	389	280	1.39	407	0.96	315	1.23
	HCBL-11-22	–	–	273	306	0.89	316	0.86	224	1.22
	HCBL-11-23	–	–	334	284	1.18	341	0.98	260	1.28
	HCBL-11-24	–	–	424	369	1.15	453	0.94	291	1.46
	HCBL-11-25	–	–	342	350	0.98	362	0.94	252	1.36
	HCBL-11-26	–	–	420	369	1.14	407	1.03	278	1.51
	HCBR-11-15	–	–	525	486	1.08	697	0.75	455	1.15
	HCBR-11-17	–	–	429	403	1.06	631	0.68	415	1.03
	HCBR-11-19	–	–	321	331	0.97	592	0.54	383	0.84
	HCBR-11-20	–	–	334	440	0.76	592	0.56	383	0.87
	HCBR-11-21	–	–	410	378	1.08	592	0.69	419	0.98
	HCBR-11-22	–	–	418	414	1.01	592	0.71	419	1.00
	HCBR-11-23	–	–	354	388	0.91	592	0.60	419	0.84
	HCBR-11-24	–	–	384	388	0.99	592	0.65	419	0.92
	HCBR-11-25	–	–	380	331	1.15	592	0.64	383	0.99
	HCBR-11-26	–	–	374	440	0.85	592	0.63	383	0.98
	HCBR-11-27	–	–	393	331	1.19	502	0.78	358	1.10
	HCBR-11-28	–	–	397	447	0.89	643	0.62	397	1.00
	HCBR-11-30	–	–	469	486	0.97	447	1.05	367	1.28
Shing et al. (1990)	3	445	467	456	426	1.07	423	1.08	445	1.02
	4	320	387	354	343	1.03	286	1.24	367	0.96
	5	396	418	407	376	1.08	330	1.23	394	1.03
	6	209	231	220	187	1.18	286	0.77	294	0.75

Table 20.1: Strut-and-Tie Models and Shear Equations for Fully-Grouted Walls (Continued)

Study	Specimen	Ultimate Shear Load (kN)			Strut-and-Tie Models		Shear Equations			
					Excluding β_α		MSJC		Proposed	
		Min	Max	Avg	V_n (kN)	$\frac{V_{exp}}{V_n}$	V_n (kN)	$\frac{V_{exp}}{V_n}$	V_n (kN)	$\frac{V_{exp}}{V_n}$
Shing et al. (1990)	7	432	432	432	398	1.08	347	1.24	412	1.05
	8	209	222	216	191	1.13	375	0.58	299	0.72
	9	427	427	427	337	1.27	423	1.01	401	1.06
	10	298	307	302	256	1.18	355	0.85	365	0.83
	11	396	423	409	365	1.12	383	1.07	412	0.99
	13	485	516	500	407	1.23	572	0.87	469	1.07
	14	436	498	467	398	1.17	435	1.07	436	1.07
	15	365	418	391	321	1.22	432	0.91	408	0.96
	16	534	538	536	435	1.23	474	1.13	451	1.19
	21	480	485	483	415	1.16	442	1.09	445	1.08
	22	383	432	407	328	1.24	365	1.12	398	1.02
Voon (2007)	A1	205	215	210	194	1.08	235	0.89	295	0.71
	A2	177	195	186	205	0.91	219	0.85	291	0.64
	A4	201	233	217	215	1.01	237	0.92	292	0.74
	A7	261	263	262	245	1.07	274	0.96	322	0.81
	A8	244	250	247	225	1.10	258	0.96	312	0.79
	A9	204	207	206	172	1.19	288	0.71	259	0.79
	A10	572	598	585	622	0.94	596	0.98	651	0.90
Minaie (2009)	FMC 2	–	–	329	447	0.74	846	0.39	644	0.51
	FPLC 2	–	–	360	447	0.81	846	0.43	644	0.56
Nolph (2010)	FG085-48	311	355	333	381	0.87	589	0.57	608	0.55
					Mean	1.04	Mean	0.84	Mean	1.03
					COV	0.18	COV	0.21	COV	0.25

Table 20.2: Strut-and-Tie Models and Shear Equations for Partially-Grouted Walls

Study	Specimen	Ultimate Shear Load (kN)			Strut-and-Tie Models		Shear Equations			
					Including β_α		MSJC		Proposed	
		Min	Max	Avg	$\gamma_x = 0.5$		V_n (kN)	$\frac{V_{exp}}{V_n}$	V_n (kN)	$\frac{V_{exp}}{V_n}$
Hidalgo et al. (1978)	HCBR-21-3	104	138	121	137	0.88	131	0.92	135	0.90
	HCBR-21-5	194	230	212	268	0.79	230	0.92	198	1.07
	HCBR-21-7	191	231	211	267	0.79	202	1.04	181	1.17
Chen et al. (1978)	HCBL-11-5	195	221	208	152	1.37	163	1.28	132	1.58
	HCBL-11-8	159	169	164	111	1.48	120	1.37	116	1.41
	HCBL-11-10	201	223	212	174	1.22	182	1.16	138	1.54
	HCBR-11-5	171	223	197	217	0.91	231	0.85	184	1.07
	HCBR-11-9	164	218	191	135	1.41	155	1.23	150	1.27
	HCBR-11-11	179	231	205	291	0.70	233	0.88	172	1.19
Yancey and Scribner (1989)	R2	129	159	144	187	0.77	186	0.77	170	0.85
	R4	142	149	146	173	0.84	194	0.75	169	0.86
	R5	113	189	151	188	0.80	233	0.65	192	0.79
	R6	145	156	151	176	0.86	217	0.69	178	0.85
	R7	157	164	161	181	0.89	238	0.67	188	0.85
	R9	161	177	169	188	0.90	207	0.82	180	0.94
	R10	182	201	192	188	1.02	293	0.65	216	0.89
	R11	148	172	160	185	0.86	239	0.67	189	0.85
Schultz et al. (1998)	2	–	–	261	312	0.84	315	0.83	389	0.67
	4	–	–	254	232	1.09	229	1.11	239	1.06
	6	–	–	176	159	1.11	163	1.08	151	1.17

Table 20.2: Strut-and-Tie Models and Shear Equations for Partially-Grouted Walls (Continued)

Study	Specimen	Ultimate Shear Load (kN)			Strut-and-Tie Models		Shear Equations			
					Including β_α		MSJC		Proposed	
		Min	Max	Avg	$\gamma_x = 0.5$		V_n (kN)	$\frac{V_{exp}}{V_n}$	V_n (kN)	$\frac{V_{exp}}{V_n}$
Schultz et al. (1998)	8	–	–	243	312	0.78	373	0.65	399	0.61
	10	–	–	270	232	1.16	270	1.00	249	1.08
	12	–	–	211	159	1.33	192	1.10	161	1.31
Voon (2007)	A5	134	143	139	151	0.92	122	1.14	147	0.94
	A6	93	93	93	121	0.77	101	0.92	116	0.80
Minaie (2009)	PCL 1	–	–	318	327	0.97	430	0.74	293	1.09
Nolph (2010)	PG085-24	290	302	296	241	1.23	240	1.23	169	1.75
	PG085-32	258	262	260	234	1.11	228	1.14	231	1.13
	PG085-48	211	234	223	202	1.10	218	1.02	224	0.99
	PG120-48	227	230	229	202	1.13	253	0.90	234	0.98
	PG169-48	193	215	204	200	1.02	302	0.68	248	0.82
Elmapruk (2010)	PG127-24	–	400	376*	302	1.25	347	1.08	214	1.76
	PG127-32	–	344	323*	297	1.09	330	0.98	214	1.51
	PG127-48	–	238	224*	271	0.83	357	0.63	245	0.91
	PG127-48I	–	252	237*	271	0.87	357	0.66	245	0.97
	PG180-48	–	266	250*	271	0.92	440	0.57	259	0.97
	PG254-48	–	286	269*	271	0.99	314	0.86	237	1.14
*Corrected values (see section 6.4 for more details)					Mean	1.00	Mean	0.91	Mean	1.07
					COV	0.20	COV	0.24	COV	0.26

20.1.3 Summary

The predictions for the strut-and-tie models analyzed in this study outperformed those of both the MSJC and proposed shear equations. In some cases, the strut-and-tie model predicted a value that was far from the experimental results for a specimen. Comparison of the experimental-to-predicted strength ratios for these specimens revealed that the lack of accuracy was consistent across all three predictions and that the specimens could possibly be labeled as outliers because they did not perform as would be expected. The disparities between the experimental and predicted values in these cases could be a result of premature failure of the specimen or errors in the measured material or other wall parameters reported in the literature. It appears that the ability of the strut-and-tie models to consider the subtle differences in reinforcement placement and wall geometry is more precise at describing and predicting the shear behavior of masonry walls that the shear equations. The improved precision of the strut-and-tie modeling method comes at a cost of requiring more effort and understanding on the part of the designer.

20.2 Comparison with Other "Strut-and-Tie" Models

The previous section showed that the strut-and-tie modeling procedures developed in this research study produced more-precise predictions of masonry shear wall strength than the two best masonry shear prediction equations. The strut-and-tie modeling procedures were also compared with other recent studies by Voon (2007), Nolph (2010), Elmapruk (2010), and Morrison (2013) which employed "strut-and-tie" modeling procedure to develop similar mechanical models. As was mentioned in Chapter 17, the modeling process undertaken in these other studies did not follow the full theoretical rationale presented by Schlaich et al. (1987) and might more appropriately be labeled as "equivalent truss" models. Semantics aside, it was important to compare the proposed strut-and-tie modeling methodology against other mechanical modeling techniques to determine the quantitative differences between the two.

20.2.1 Washington State University

Nolph (2010) and Elmapruk (2010) each tested six masonry shear walls and created and analyzed models for each wall. All but one of the total of twelve walls were partially-grouted and

the other wall was fully-grouted. Their model analyses were conducted by idealizing all struts and ties as 1-dimensional truss elements and by using a structural analysis program to perform a linear push-over analysis for each wall. The ultimate predicted strength from each of their models is compared with the predicted strengths from the current analysis in Table 20.3. Both modeling techniques showed a slight tendency to under-predict the strengths for the Nolph specimens and over-predict the strengths for the Elmapruk specimens—which had a lower aspect ratio. The comparison shows that the proposed methodology produced more accurate and more precise estimates than the equivalent truss modeling methodology for the specimens from both tests.

20.2.2 Morrison

Morrison (2013) created and analyzed models for selected specimens from a number of past masonry research studies collected from the literature. His analyses were conducted using the same methodology and tools as those used by Nolph (2010) and Elmapruk (2010)—namely, using idealized-truss models and performing the analysis using a structural analysis computer program. The ultimate predicted strength from each of his models is compared with the predicted strengths from the current analysis to compare the results from the two techniques. The comparison of the fully-grouted specimen results are presented in Table 20.4 and those of the partially-grouted specimens are shown in Table 20.5. The results for both grouting types showed that, overall, the proposed methodology is more conservative than the "equivalent truss" methodology. The reason for this conservativeness is likely due to the inclusion of anchorage and transverse reinforcement requirements in the current study which were both absent from the idealized-truss approach. The models from the current studies were more precise than those created by Morrison, particularly for the partially-grouted specimens, suggesting that the proposed methodology is slightly better at representing the masonry shear behavior.

20.2.3 Partially-Grouted Walls with Openings

Voon (2007) built, tested, and created idealized truss models for ten partially-grouted shear walls with openings. Three of the ten walls were constructed with asymmetric geometry and/or reinforcement placement, resulting in different strengths for the push and pull directions. The

Table 20.3: Strut-and-Tie Model Comparison with Nolph and Elmapruk

Study	Specimen	Grouting	Ultimate Shear Load (kN)			Strut-and-Tie Models			
						Current Study		Original Study	
			Min	Max	Avg	V_n (kN)	$\frac{V_{exp}}{V_n}$	V_n (kN)	$\frac{V_{exp}}{V_n}$
Nolph (2010)	FG085-48	Full	311	355	333	381	0.87	623	0.53
	PG085-24	Partial	290	302	296	241	1.23	280	1.06
	PG085-32	Partial	258	262	260	234	1.11	280	0.93
	PG085-48	Partial	211	234	223	202	1.10	192	1.16
	PG120-48	Partial	227	230	229	202	1.13	192	1.19
	PG169-48	Partial	193	215	204	200	1.02	192	1.06
Elmapruk (2010)	PG127-24	Partial	–	400	376*	302	1.25	427	0.88
	PG127-32	Partial	–	344	323*	297	1.09	284	1.14
	PG127-48	Partial	–	238	224*	271	0.83	278	0.81
	PG127-48I	Partial	–	252	237*	271	0.87	278	0.85
	PG180-48	Partial	–	266	250*	271	0.92	294	0.85
	PG254-48	Partial	–	286	269*	271	0.99	294	0.91
*Corrected values (see section 6.4 for more details)						Mean	1.03	Mean	0.95
						COV	0.13	COV	0.20

Table 20.4: Fully-Grouted Strut-and-Tie Model Comparison with Morrison (2013)

Study	Specimen	Ultimate Shear Load (kN)			Strut-and-Tie Models			
					Current Study		Morrison (2013)	
		Min	Max	Avg	V_n (kN)	$\frac{V_{exp}}{V_n}$	V_n (kN)	$\frac{V_{exp}}{V_n}$
Hidalgo et al. (1978)	HCBR-21-2	238	328	283	279	1.01	293	0.97
	HCBR-21-6	401	473	437	439	1.00	352	1.24
Chen et al. (1978)	HCBL-11-3	194	218	174	205	0.85	179	0.97
	HCBL-11-4	257	279	227	264	0.86	214	1.06
	HCBL-11-9	223	253	202	405	0.50	390	0.52
	HCBR-11-3	400	440	420	256	1.64	255	1.65
	HCBR-11-6	489	545	517	358	1.44	558	0.93
Sveinsson et al. (1985)	HCBL-11-13	–	–	461	392	1.18	365	1.26
	HCBL-11-18	–	–	308	280	1.10	334	0.92
	HCBL-11-21	–	–	389	280	1.39	298	1.31
	HCBR-11-21	–	–	410	378	1.08	391	1.05
	HCBR-11-23	–	–	354	388	0.91	359	0.99
Shing et al. (1990)	4	320	387	354	343	1.03	393	0.90
	9	427	427	427	337	1.27	324	1.32
	13	485	516	500	407	1.23	565	0.89
	16	534	538	536	435	1.23	558	0.96
Voon (2007)	A4	201	233	217	215	1.01	248	0.88
	A9	204	207	206	172	1.19	149	1.38
	A10	572	598	585	622	0.94	672	0.87
					Mean	1.10	Mean	1.06
					COV	0.23	COV	0.24

strength values predicted by Voon using idealized truss models were compared to the strut-and-tie model predictions from the current study and are shown in Table 20.6. The accuracy of the current methodology was better for several specimens in the current models than for those of Voon because they accounted for the transfer of vertical shear force through the coupling beam across an opening to the strut on the other side. The transfer of shear stresses across the openings increased the load on the strut, increased the lateral strength of the wall, and resulted in more accurate predictions of the wall strength. The precision of the proposed methodology was significantly greater than the idealized truss models (by over 500 percent), showing that the proposed methodology is superior in accuracy and precision than the idealized-truss approach and that the proposed methodology is equally applicable to simple and complex shear wall configurations.

Table 20.5: Partially-Grouted Strut-and-Tie Model Comparison with Morrison (2013)

Study	Specimen	Ultimate Shear Load (kN)			Strut-and-Tie Models			
					Current Study		Morrison (2013)	
		Min	Max	Avg	V_n (kN)	$\frac{V_{exp}}{V_n}$	V_n (kN)	$\frac{V_{exp}}{V_n}$
Hidalgo et al. (1978)	HCBR-21-3	104	138	121	137	0.88	167	0.72
	HCBR-21-5	194	230	212	268	0.79	200	1.06
Chen et al. (1978)	HCBL-11-5	195	221	208	152	1.37	145	1.43
	HCBL-11-8	159	169	164	111	1.48	145	1.13
	HCBL-11-10	201	223	212	174	1.22	143	1.48
	HCBR-11-5	171	223	197	217	0.91	217	0.91
	HCBR-11-9	164	218	191	135	1.41	217	0.88
Yancey and Scribner (1989)	R2	129	159	144	187	0.77	138	1.04
	R5	113	189	151	188	0.80	134	1.13
Schultz et al. (1998)	2	–	–	261	312	0.84	448	0.58
	4	–	–	254	232	1.09	303	0.84
Voon (2007)	A5	134	143	139	151	0.92	128	1.08
	A6	93	93	93	121	0.77	128	0.73
Minaie (2009)	PCL 1	–	–	318	327	0.97	469	0.68
Nolph (2010)	PG085-24	290	302	296	241	1.23	303	0.98
	PG085-48	211	234	223	202	1.10	300	0.74
	PG120-48	227	230	229	202	1.13	300	0.76
					Mean	1.04	Mean	0.95
					COV	0.23	COV	0.27

Table 20.6: Strut-and-Tie Model Comparison for Walls with Openings

Specimen	Ultimate Shear Load (kN)		Strut-and-Tie Models					
			Current Study			Voon (2007)		
	Push (kN)	Pull (kN)	Push (kN)	Pull (kN)	$\frac{V_{exp}}{V_n}$	Push (kN)	Pull (kN)	$\frac{V_{exp}}{V_n}$
B1	50.2	49.0	49.4	49.4	1.00	44.7	44.7	1.11
B2	41.2	38.7	38.7	38.7	1.03	35.9	35.9	1.38
B3	33.3	34.4	35.0	35.0	0.97	28.0	28.0	1.77
B4	47.4	48.8	50.9	50.9	0.94	41.0	41.0	1.21
B5	52.4	50.4	45.7	43.6	1.15	41.0	35.9	1.29
B6	94.3	94.6	89.2	89.2	1.06	58.0	58.0	0.86
B7	82.8	82.5	78.0	71.7	1.11	50.0	50.0	0.99
B8	82.7	93.2	78.0	86.5	1.07	50.0	55.0	0.95
B9	125	115	113	113	1.06	80.2	80.2	0.62
B10	89.0	84.6	85.0	85.0	1.02	80.2	80.2	0.62
				Mean	1.04		Mean	1.08
				COV	0.06		COV	0.33

20.3 Foundational Principles

The construction of strut-and-tie models for simple masonry shears walls showed that the process is straightforward and can be mastered quickly with some practice due to the regularly appearing geometry of masonry shear walls. The principles can be applied to more complex shear walls with openings by envisioning the walls as a series of individual wall panels connected together, as shown in Figure 20.1. The methodology is the same for walls loaded as cantilevers or in reverse-bending, though there are some differences in implementation which are presented below. The most important principles of creating strut-and-tie models are that all forces and reactions are in equilibrium, the design strength of all members meet or exceed the ultimate factored load applied to them, and that the geometry of all members is considered in determining their layout, loading, and strength. Apart from these foundational principles, the other provisions are adaptable to the specific material being modeled.

All loads and reactions applied to the masonry shear wall must be in equilibrium so as to prevent rigid-body translation or rotation of the model. Loads and reactions have to be applied to the model at nodes, including distributed loads which must be resolved into equivalent point loads based on the principles of tributary area and static equilibrium. Without these last two principles there would be nothing to prevent the designer from assuming that the entire distributed load acts at the point which would produce the greatest lateral force component. Models must have a path for the entire axial load to traverse the wall from the top to bottom; so it is generally best to first model the struts to indicate the path of the axial load to the ground. Once the model has been laid out for the axial load component, the strut widths can be increased to account for the additional vertical forces contributed by the vertical reinforcement.

The design strength of all members must meet or exceed the ultimate factored load applied to them in order to preclude failure of the member. Plasticity theory assumes that stresses have already been redistributed to other members within the wall due to yielding and cracking, meaning that strut-and-tie models already account for much of the redundancy from the indeterminate geometry of the wall. Due to the relatively small number of members in a strut-and-tie model and the weakest link theory, failure of any single member in a strut-and-tie model would typically result in a reduction in peak strength capacity for the entire wall. The corollary to this requirement is that

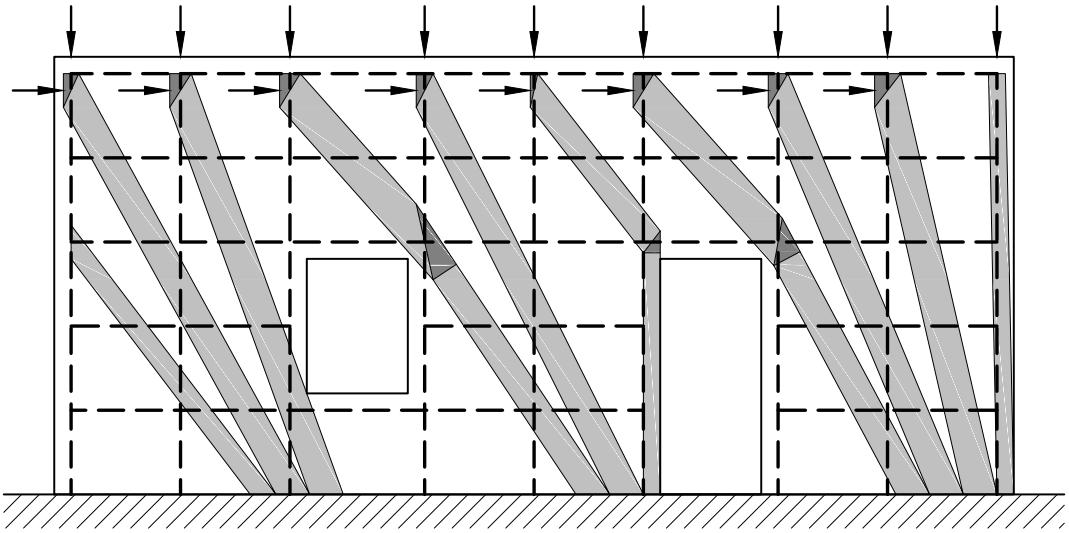

(a) Example of a complex shear wall

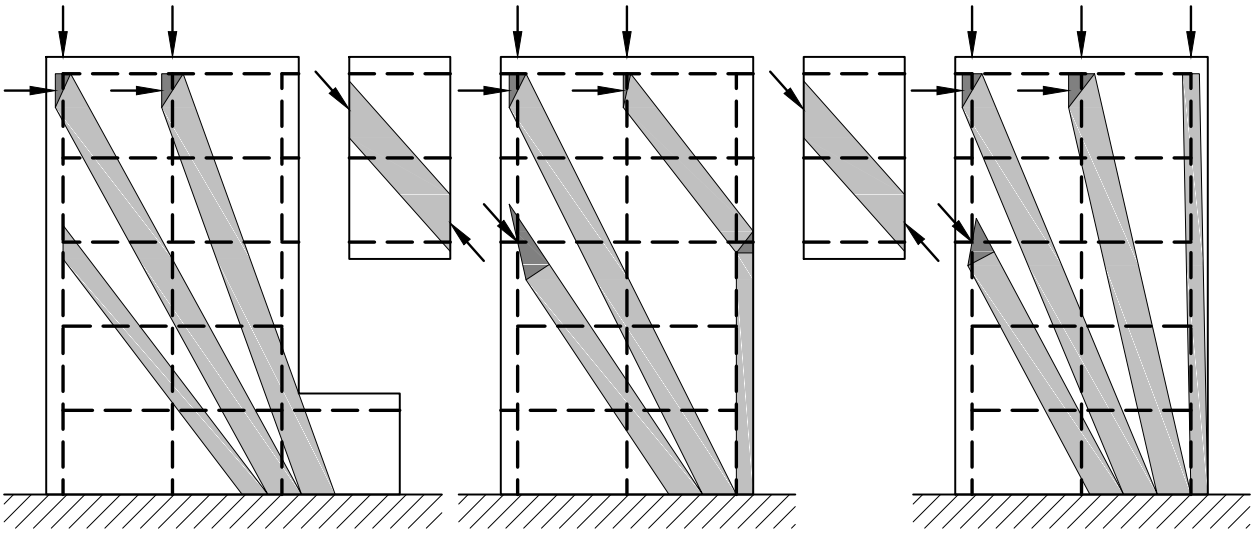

(b) Components

Figure 20.1: Segmentation of a complex shear wall into simple components

the members—particularly the reinforcement and nodes—do not have to be fully stressed to their capacity in the final model.

It was observed during the analysis that in most cases, attempting to use the full strength of the reinforcement bars resulted in a model with a less-than-optimum strength capacity or an infeasible model. This is due to the fact that the struts traversing the wall diagonally contributed the most to the lateral capacity of the wall. The inclination of the diagonal struts was determined to be heavily influenced by the less-inclined strut which terminated in the toe between the diagonal

strut and the edge. As the width of the less-inclined strut increased it pushed the terminus of the diagonal strut farther from the leading edge, reducing the diagonal strut's inclination and its lateral force component. The increase in the lateral strength component of the less-inclined strut was frequently less than the loss in strength by the diagonal strut, resulting in an overall decrease in the wall shear capacity. This explains the observation that the leading flexural bar never contributes to the shear capacity of the shear wall, except for anchoring the horizontal reinforcement bars or if the shear load is reversed.

The geometry of the struts, ties, and nodes must be considered in determining they layout of the model, the loading applied to each member, and the strength capacity of each member. This principle is the foremost difference between the full strut-and-tie modeling procedure and the equivalent-truss modeling procedure used by previous researchers for reinforced masonry shear walls. The greatest impact to the layout of the struts is caused by the requirement for sufficient reinforcement anchorage and the ordering of struts in the compression toe of the wall. The effect of the anchorage requirements is typically encountered at the leading end of a horizontal reinforcement bar where the center line of the intersecting struts must be moved away from the intersection of the horizontal and vertical bars, as shown in Figure 20.2. Since the back face of the node cannot extend past the end of the horizontal bar, the center line of the struts will always be pushed farther back into the wall, reducing the lateral strength component of the top strut and increasing the vertical component and width of the bottom strut. As discussed previously, the increase in strength of the bottom strut typically results in a greater decrease in the lateral capacity of the diagonal strut further back in the wall.

Equivalent-truss models idealize the intersection of struts in the compression toe of the wall to all coincide with the intersection of the flexural reinforcement bar with the base, as shown in Figure 20.3a. Since the full strut-and-tie modeling methodology requires that struts cannot overlap, the struts terminating in the compression toe each enter the base adjacent but separately from one another, as shown in Figure 20.3b. The leading-most struts enter the base nearest the edge of the wall and the subsequent struts each enter the base behind the previous strut. This arrangement generally leads to lower shear strength since the resultant of the combined struts in the wall toe is predominantly farther back than the interface of the flexural bar with the base, leading to lower strut inclination angles and lateral force components.

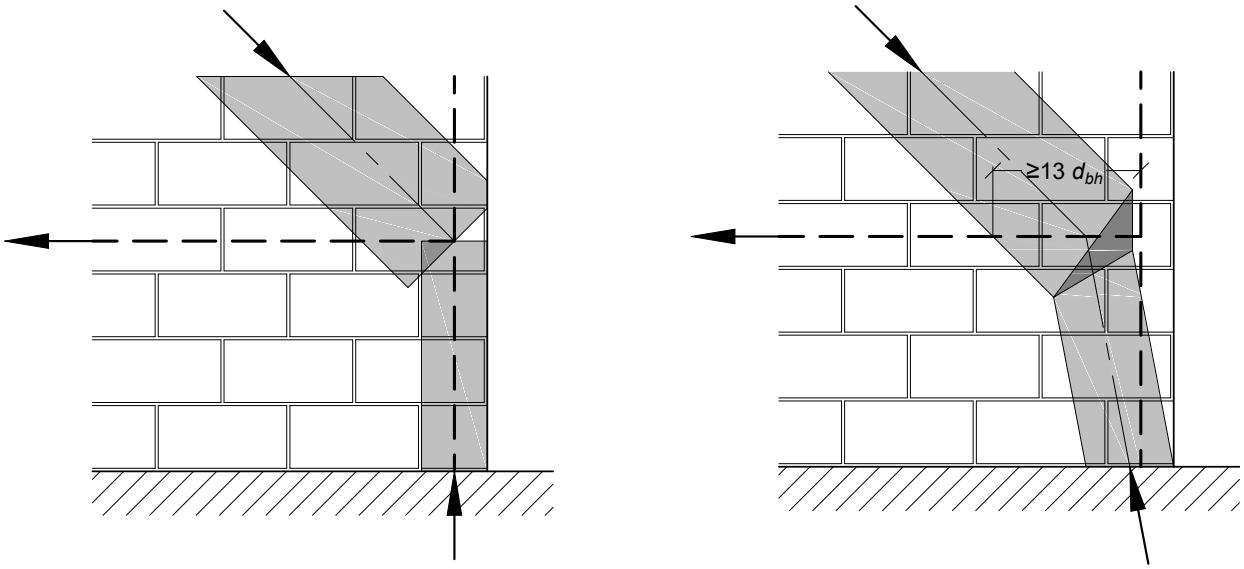

(a) Idealized-truss model

(b) Strut-and-tie model

Figure 20.2: Tie and strut anchorage types for the two modeling approaches

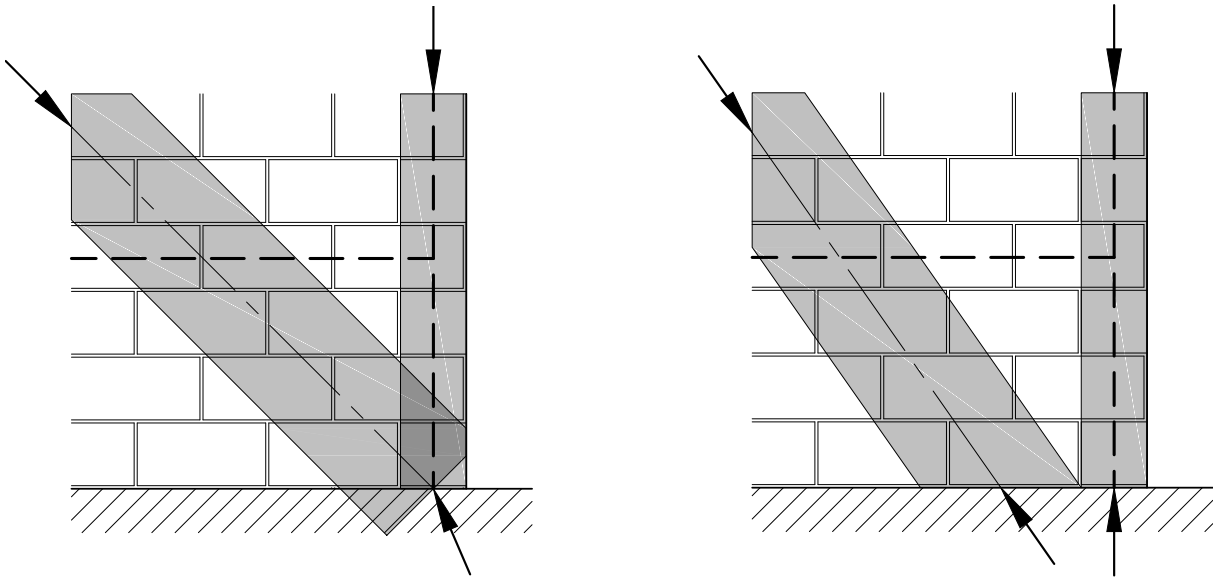

(a) Idealized-truss model

(b) Strut-and-tie model

Figure 20.3: Strut layouts in the compression toe for the two modeling methodologies

20.4 Model Optimization

The process of strut-and-tie modeling is implemented using an iterative approach in which multiple models are created and analyzed to determine which model produces the highest predicted strengths. Though the process of creating strut-and-tie models has some element of engineering judgment associated with it, several modeling principles were observed that influence whether a model iteration produced a higher strength capacity than other models. The principle which had the largest determination on the strength of a model was the portion of the vertical reinforcement capacity that was permitted to be transferred to each strut. Another principle which had an influence on model strength was whether horizontal reinforcement bars were permitted to directly participate in the model. The understanding of how these principles affect the model strength should eliminate much of the subjectivity that is associated with strut-and-tie modeling.

20.4.1 Vertical Reinforcement

The principle of equilibrium requires that strut-and-tie models provide paths for the fully axial load to travel from the top of the wall to the base because they are externally applied to the wall. The vertical forces induced by the vertical reinforcement into the wall are member forces and, therefore, are variable within the range $0 \leq F_s \leq F_y$ where F_y is the yield strength of the bar and F_s is the force induced by the bar. Diagonal struts connected to the vertical bars closest to the trailing edge of the wall have the greatest shear strength contribution to the wall because they have a greater angle of inclination. The struts closer to the leading edge provide some lateral force contribution, but since they are nearer to the leading edge their widths push the toes of the diagonal struts farther into the wall, decreasing their inclination angles and force contributions. As the width of the leading struts continues to increase, the increase in their lateral force component becomes smaller than the decrease in the lateral force component in the diagonal strut, resulting in a net decrease in wall shear strength. This phenomenon was observed to be more pronounced in partially-grouted walls because of the decreased wall thickness due to the wider struts and the use of the inclination factor β_α.

For many wall layouts it was observed that the optimal layout did not include the contribution by the leading flexural bar, a full contribution by the trailing flexural bar, and varying

contributions by the confinement bars, depending on the wall parameters. The construction of strut-and-tie models is best accomplished by first laying out the struts to handle the applied axial load forces by spanning from the points of intersection of the vertical reinforcement with the top of the wall to the compression toe of the wall. The layout of struts for a partially grouted wall and the corresponding lateral force components for each strut are shown in Figure 20.4a. After the struts have been laid out, determining the optimal contributions for all of the vertical bars is most easily accomplished by incrementally increasing the contribution of each bar from null to F_y, one bar at a time, starting with the trailing-most bar and working forward until the calculated wall strength reaches a maximum value, as shown in Figure 20.4b. Figure 20.4c shows that the model with full contribution of all vertical reinforcement bars produces a strength that is 5 percent lower than the optimum model where the contribution of only the two trailing vertical reinforcement bars is considered.

20.4.2 Horizontal Reinforcement

It was observed that the principal benefit of the horizontal reinforcement was to resist the transverse tensile forces induced within the struts by the tendency to assume a bottle shape. This resistance permitted the use of a higher strut efficiency factor than would otherwise have been permitted if the horizontal reinforcement was not present. In some walls the optimum model included horizontal reinforcement bars which directly participated in the lateral load resisting system while in other models the horizontal bars did not directly participate. The participation of the horizontal bars was generally limited to cases where the inclination of a hypothetical strut from the top of the leading vertical confinement bar would change notably by terminating in the horizontal bar rather than the wall toe. The true determination of whether the horizontal reinforcement bar directly increased the shear capacity is an optimization problem with several input variables and constraints.

The horizontal reinforcement participation is illustrated in Figure 20.5. The horizontal reinforcement bars participate directly in the lateral load resisting layout by transferring most of the lateral force component from a leading strut ① to the trailing side of the wall where the width of the strut descending from its trailing end ④ will not influence the path of the principal diagonal struts. This behavior is possible because the tension tie is permitted to cross the diagonal strut ② without transferring any forces between the two members. The amount of lateral force imparted

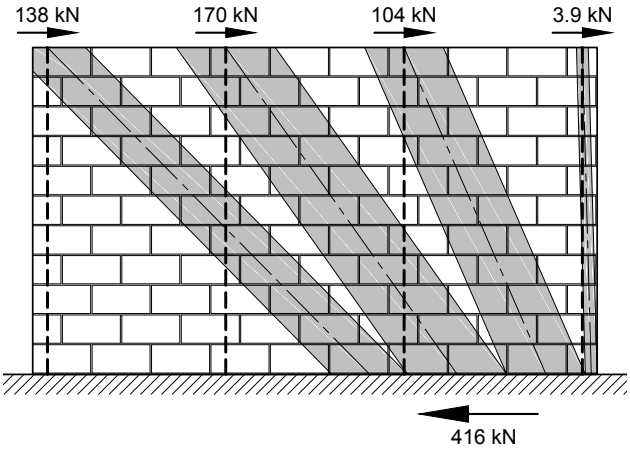

(a) No reinforcement contribution

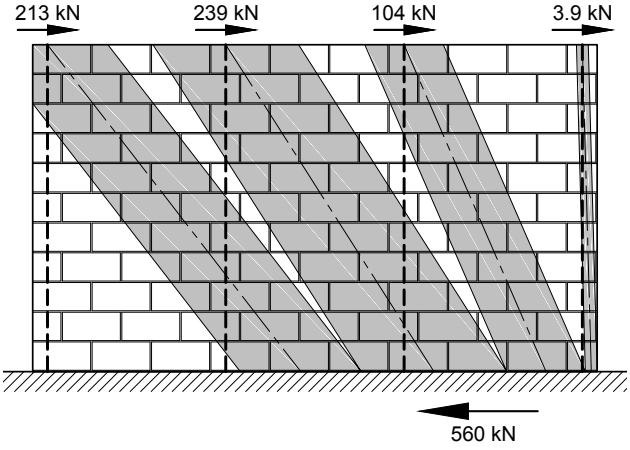

(b) Optimum reinforcement contribution

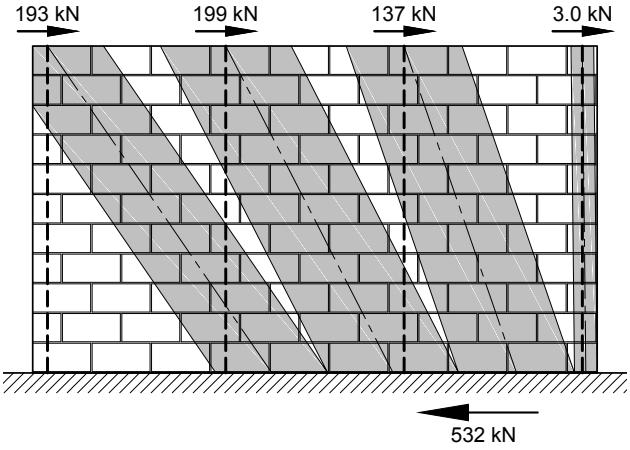

(c) Full reinforcement contribution

Figure 20.4: Models with different reinforcement contributions

from the upper leading strut ① to the horizontal reinforcement bar is dependent on the difference in inclination angles between the upper leading strut and the lower leading strut ③ which transfers the residual forces from the node at the leading edge of the bar to the wall toe. This force in the horizontal bar is transferred to the trailing strut ④ generating a vertical force component which must be resisted by the flexural reinforcement bar. This decreases the bar capacity that is available to the diagonal strut ②, decreasing the size and lateral force component of the diagonal strut. In many cases the decrease in the lateral force component of the diagonal strut ② from the null case is greater than the increase in lateral strut in the other struts introduced by the horizontal reinforcement bar such that

$$F_{2x(a)} + F_{3x} + F_{4x} < F_{1x(b)} + F_{2x(b)},$$

resulting in a net decrease in wall capacity.

In practice, the amount of force that can be transferred to a horizontal bar is limited by the strength and anchorage of the bar, the strength of the adjoining struts, and the location of the node. All of these parameters are affected by the development length of the horizontal bar. In some cases, particularly among partially-grouted walls, the anchorage of the horizontal bar was the governing factor in wall strength because the $12d_{bf}$ limit placed on the width of the trailing descending strut ④ produced a strength that was smaller than the yield strength of the horizontal bar. This $12d_{bf}$ strut width limit leads to the following two modeling constraints. First, the diameter of a vertical reinforcing bar around which a horizontal bar is anchored must not be smaller than one-twelfth the shear thickness of the wall ($12d_{bf} \geq t_s$), otherwise the thickness of the trailing descending strut ④ cannot be assumed to be t_s. Second, the diameter of the horizontal bars should be limited by

$$d_{bh} \leq 3.5\sqrt{\frac{f'_m}{f_{yh}}\, t_s\, d_{bf}} \tag{20.1}$$

to ensure that the performance of horizontal bars is governed by steel yielding and not strut crushing.

It was observed that the horizontal bars in roughly the upper and lower quarters of the wall height did not participate in increasing the shear capacity of the models. Due to their proximity

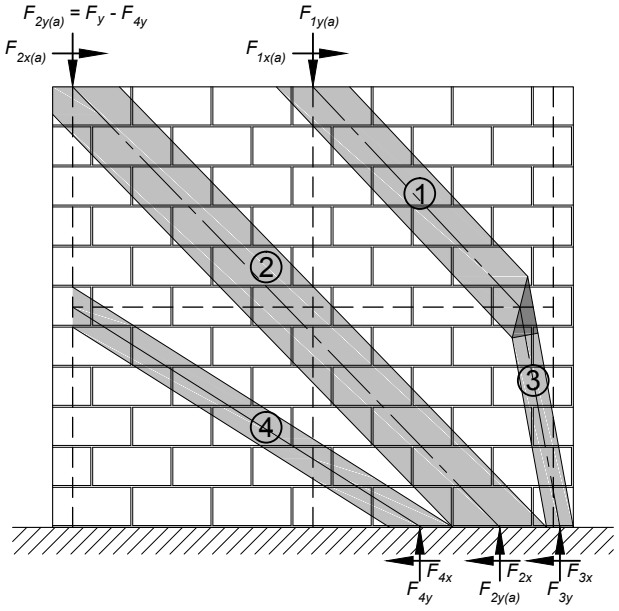

(a) Participating

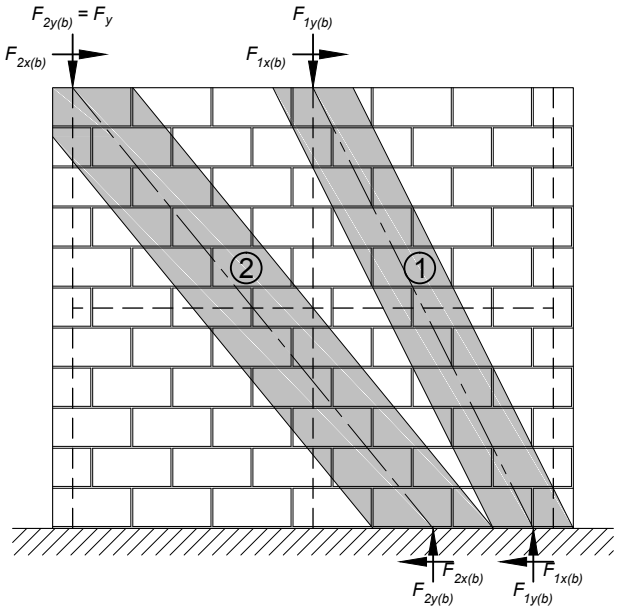

(b) Not participating

Figure 20.5: Wall strengths with and without horizontal bar participation

to the top corners of the wall their anchorage locations tended to overlap with one of the diagonal struts, preventing them from being effective. Since the transverse splitting stresses were greater in the middle of the struts, the horizontal reinforcement near the strut ends was ineffectual in resisting

these splitting stresses. This observation partially confirms the hypothesis from Blondet et al. (1989) that only the reinforcement in the middle half of the wall was effectual in resisting shear loads. However, the prevailing theory in how the horizontal reinforcement contributes to shear strength is very different from that observed in this analysis.

20.4.3 Coupling Beams

It was observed that several of the initial models for the Voon (2007) walls with openings under-predicted the strength by a noticeably large margin. It was observed that the margin of error increased as the bottom of the opening got lower, producing a taller opening and a steeper strut behind the opening. The phenomenon can be explained by considering the stiffnesses of the coupling beam versus that of the wall panel. In the specimens with a shorter opening (such as that shown in Figure 20.6a), the shear stiffness of the wall panels to either side of the opening are significantly stiffer than that of the coupling beam which spans the opening. As the height of the opening increases (as shown in Figure 20.6b), the aspect ratios of the panels to either side increase, which decreases their shear stiffnesses in comparison to that of the coupling beam. The decrease in panel stiffness result in larger angular deformations at their tops, since they can be considered to be loaded as cantilevers, applying a double-curvature load the coupling beam. The loading on the coupling beam produces a shear reaction in the coupling beam which pulls up on the left panel and pushes down on the right panel.

Strut-and-tie models do not consider member stiffness because the members are considered to have yielded, so a different theory is needed to explain how to determine when the shear strength of the coupling beam is being engaged. The hypothesis proposed is that as the toe of the strut retreated back closer to the jamb bar, the jamb bar started to pull down on the trailing end of the coupling beam over the opening, as shown in Figure 20.6b. Due to the presence of vertical shear stirrups in the coupling beam, this downward vertical force was transferred across the opening to the top of the leading strut on the other side, as shown in Figure 20.7. The increase in force applied to the leading strut increased its lateral force component and, hence, the total shear capacity of the wall. The trailing strut in the former wall passes below the short opening and ends near the toe of the leading strut, as shown in Figure 20.6a. The forces in the trailing strut cannot transfer into the jamb steel at the lower-left corner of the opening because the decrease the vertical component of

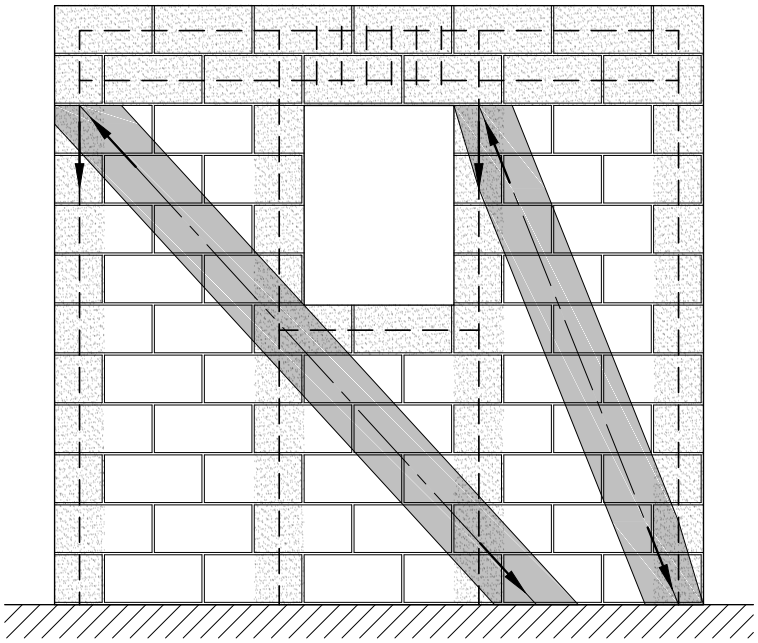

(a) Wall with short opening

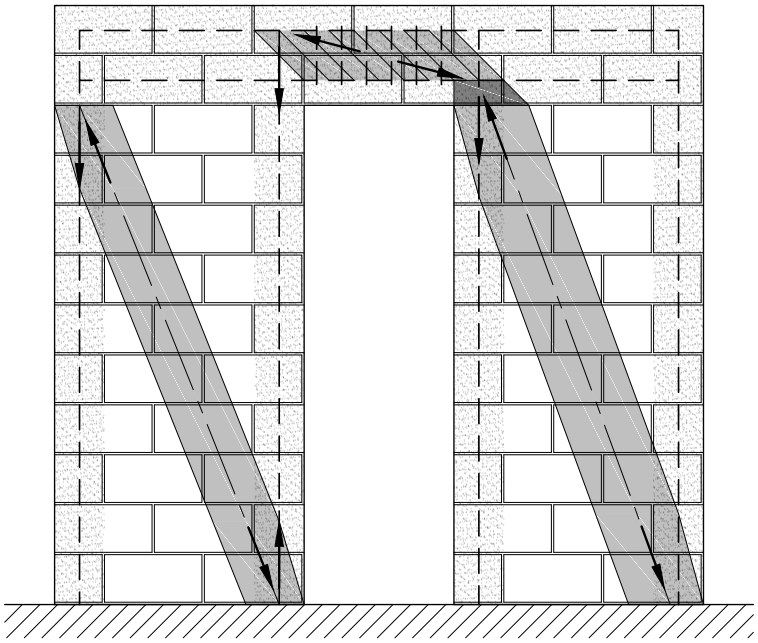

(b) Wall with tall opening

Figure 20.6: Walls with openings of different height

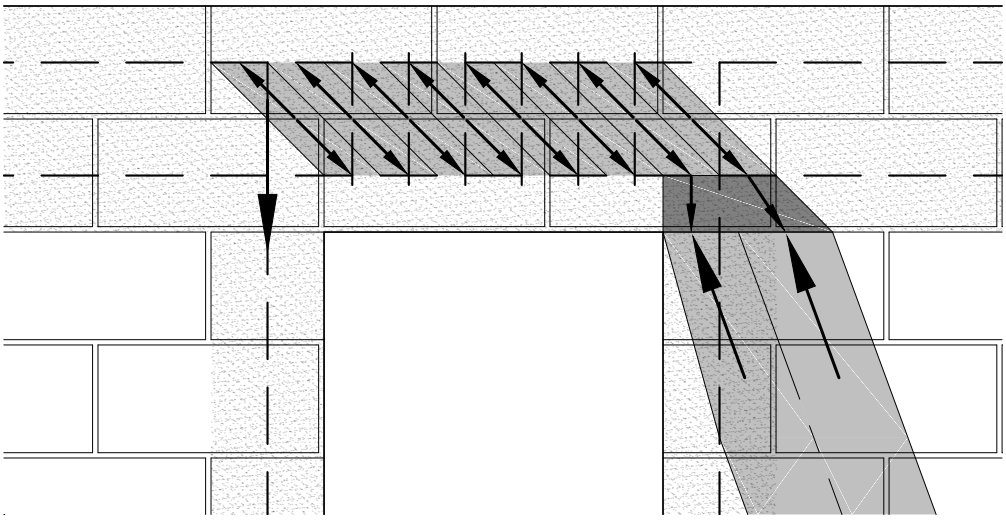

Figure 20.7: Transfer of vertical shear stresses across opening

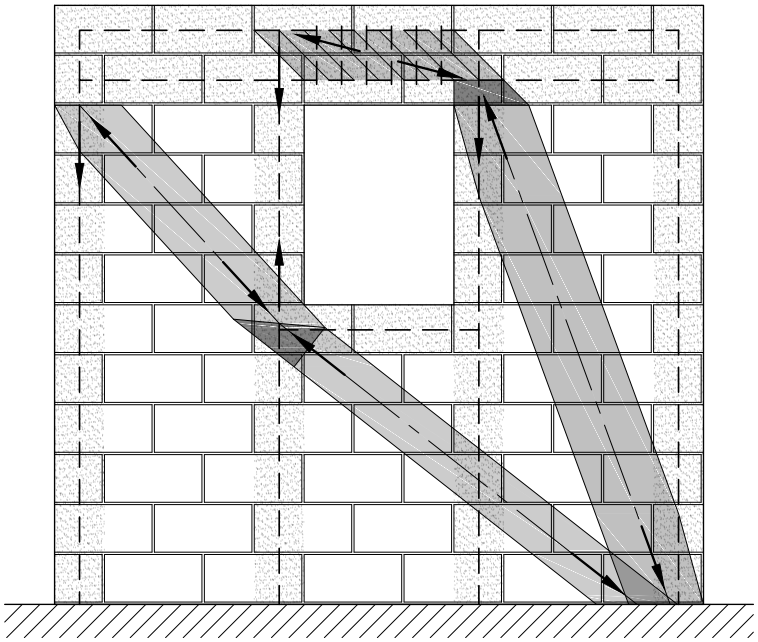

Figure 20.8: Incorrect model of wall with opening

the strut under the opening, causing it to bend upward and run into the toe of the leading strut, as shown in Figure 20.8.

Another consideration in whether to include the coupling beam in the model is whether the increase in shear capacity of the wall by including the coupling beam is greater than the increase in total strain energy in the wall. By including the coupling beam in the model, the reinforcement bar

to the left of the opening and the shear stirrups in the coupling beam become engaged, increasing the total volume of strained reinforcement in the wall and the total strain energy. If the increase in shear capacity cannot be proportionally greater than the increase in strain energy, then the principle of minimum strain energy states that the model will not be correct and the contribution of the coupling beam should be neglected. These latter two methods can be used to objectively determine whether the contribution of a coupling beam should be included in a strut-and-tie model. In computing the shear strength of the coupling beam, the geometry and size of the stirrups should be considered so that the capacity of the beam is not exceeded.

20.5 Procedure

The analysis of masonry shear walls using strut-and-tie models varied slightly between walls loaded as cantilevers and those loaded in reverse-curvature. During the process of creating and analyzing strut-and-tie models for both walls types, it was observed that the modeling of walls in reverse-curvature could be simplified if the geometry and reinforcement layout was doubly symmetrical about the center of the wall. If this condition was satisfied, then only the bottom half of wall needed to be analyzed and the process would be the same as that used in modeling a cantilever wall. The procedures for constructing strut-and-tie models for masonry shear walls is given in this section for both loading types.

20.5.1 Cantilever Walls

1. Resolve the distributed axial load into point loads acting along the center lines of the nodes located at the tops of the vertical reinforcement bars. If needed, the load may also be applied to additional nodes created between vertical reinforcement bars. Divide the distributed load according to the tributary area of each node assuming that the shear thickness is constant for the entire length of the wall.

2. Determine the necessary anchorage length for the horizontal reinforcement bars. Choose the horizontal bar layout to be considered in the model analysis.

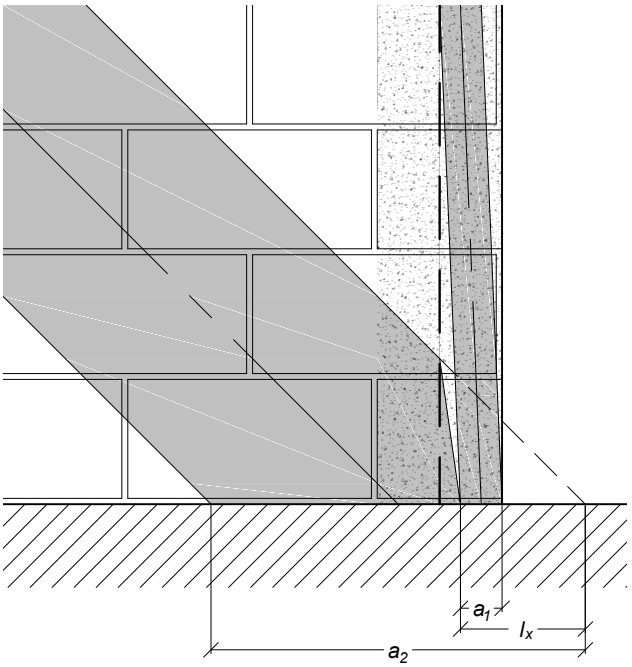

Figure 20.9: Toe extension of second strut in a partially-grouted wall

3. Layout struts from the nodes to the compression toe of the wall, incorporating the usage of horizontal reinforcement bars as necessary. Each strut should enter the toe sequentially and be placed such that no two struts cross or overlap. The thickness of each strut should be calculated beginning with the leading-most strut and working backwards toward the trailing strut. Once the thickness of a strut has been determined, the toes of the struts behind it are moved such that they touch but do not intersect.

4. In the case of partially-grouted walls, the thickness of the first strut should be calculated assuming the grouted thickness t and the thicknesses of the remaining struts should be calculated assuming the shear thickness t_s. For partially-grouted walls, the thickness and placement of the second strut should be determined assuming the toe of the wall extends a distance l_x past the edge of the wall and accounting for the thickness of the first strut, as shown in Figure 20.9. The leading edge of the second strut is then assumed to bend down from the point where it crosses the vertical bar to the point where the inside edge of the first strut exits the wall.

5. After the model is in equilibrium for the exterior applied forces, add in the contribution of the vertical reinforcement beginning with the trailing-most vertical bar and working toward the leading-most bar. As the contribution increases the applied force to the corresponding strut, the strut width must be increased so that the strut strength is equal to the force applied to it. As the strut widths change, the strut paths must be adjusted accordingly so that they do not encroach into one another.

6. When the trailing end of a horizontal reinforcement bar is anchored to a vertical bar, then the vertical component of the descending strut must be subtracted from the peak contribution of the bar at its top.

7. The model is complete when the forces are in equilibrium, the strength of all materials are less than the applied forces, the anchorage requirements are met, no two struts cross or overlap, and the model strength is maximum. It this point, other variations of the model may be investigated (e.g., by changing the amount and placement of vertical and/or horizontal reinforcement) to find the optimal model for the design scenario.

20.5.2 Reverse-Curvature Walls

The procedure for cantilever walls may be used for shear wall panels with fixed-fixed boundary conditions if the wall geometry and reinforcement placement is doubly symmetric about the wall center. In this case the bottom half of the wall is analyzed as a cantilever wall and the forces and members are assumed to be the same as those in the top half of the wall. Note that the dividing line between the top and bottom halves does not need to be straight or horizontal; it is only required to pass through the center point of the wall panel, as shown in Figure 20.10. The purpose of this requirement is so that the contribution of reinforcement bars about the mid-height of the wall can be more easily considered in the design.

The process of constructing strut-and-tie models of walls in reverse-curvature is the same as that for cantilever walls except for the following points. First, all of the applied axial load is assumed to act at the center point of the wall, or at the top middle of the lower wall half being modeled. Second, the forces in the horizontal reinforcement bars must be symmetric about the

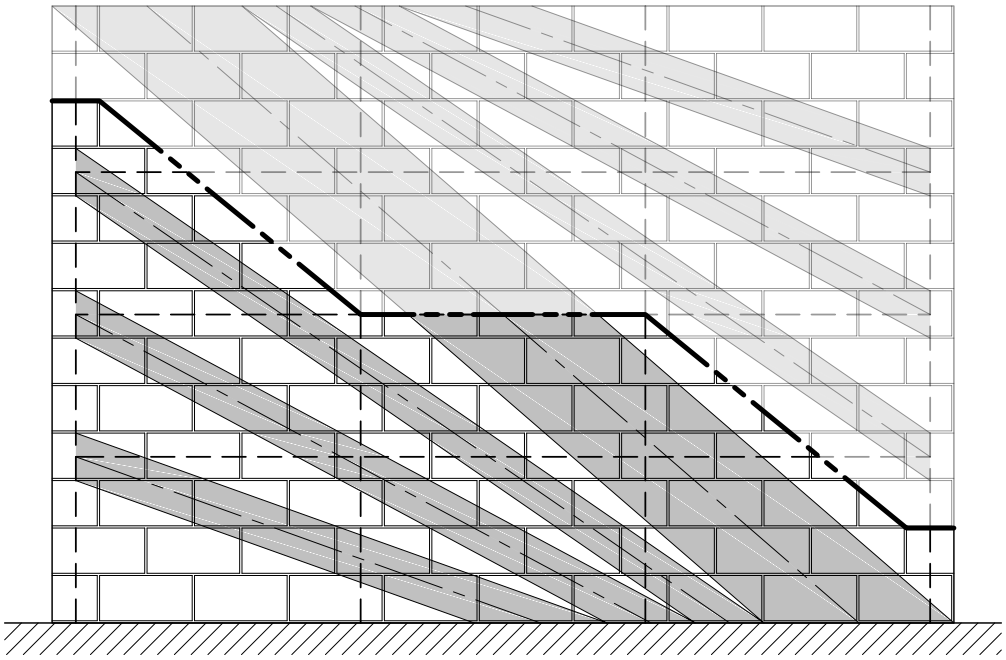

Figure 20.10: Division of walls in reverse-curvature models

mid-height of the wall, or that the force in one bar must be the same as its counterpart in the other half of the wall. Both points are illustrated in Figure 20.11.

20.6 Summary

While the proposed methodology is preliminary and still imperfect, the results of this analysis have shown that strut-and-tie model guidelines based on the methodology originally proposed by Schlaich et al. (1987) for reinforced concrete are valid for masonry design with minor adaptations. The shear strength predictions from the proposed strut-and-tie modeling methodology were shown to consistently out-perform those of the two best masonry shear strength equations and models built using the idealized truss analogy. It has been observed that the vertical reinforcement nearest the trailing edge of the wall and the horizontal reinforcement in the middle half of the wall are most effective in contributing to the shear capacity of masonry shear walls. The proposed methodology from this study should be further refined and validated in preparation for inclusion in future editions of the MSJC and other masonry design standards.

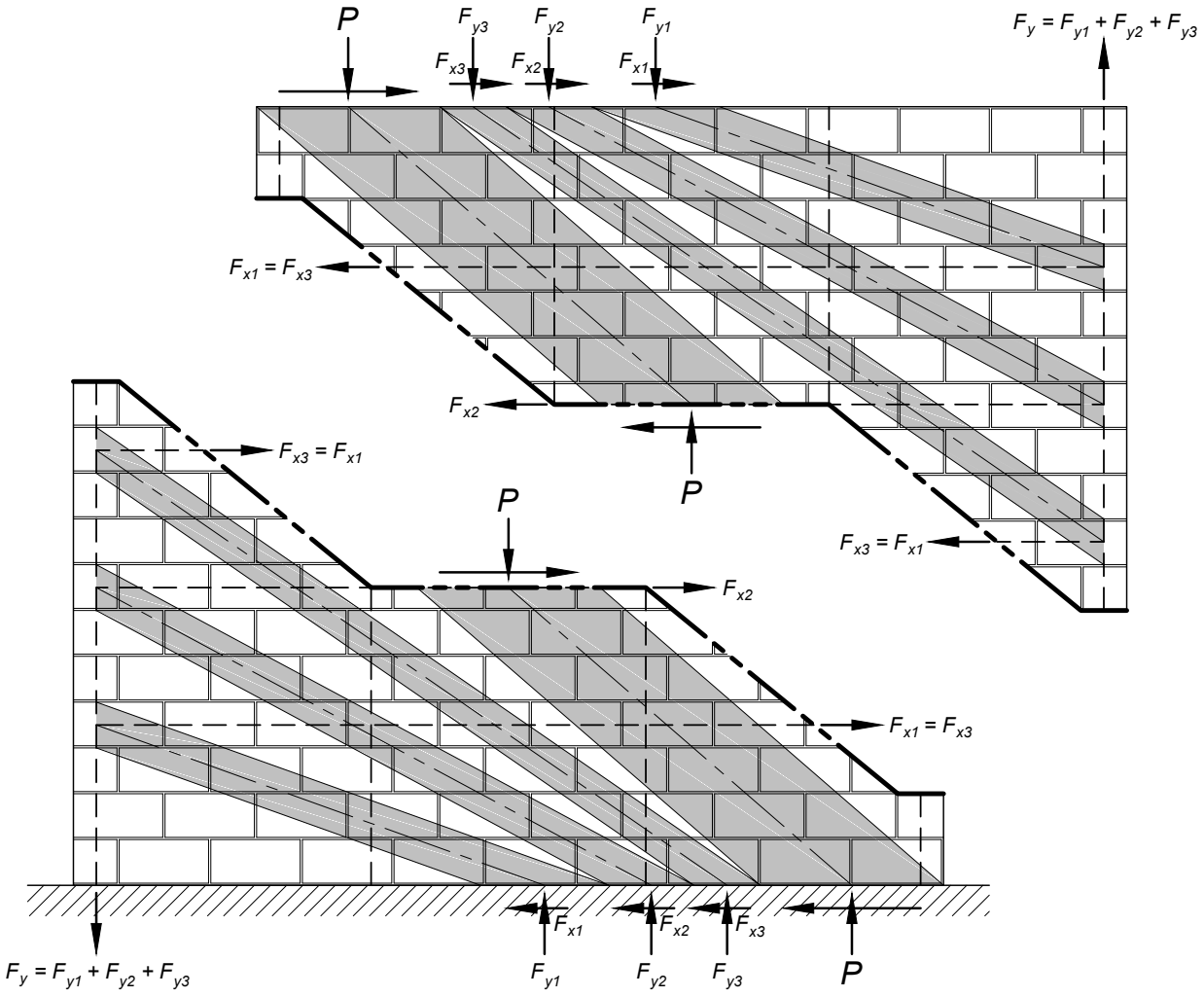

Figure 20.11: Symmetry of geometry and loads in a reverse-curvature model

Part VI

General Discussion and Conclusions

This part provides general discussion and conclusions for the entire research study. Chapter 22 discusses the performance of masonry shear walls as an assemblage and details the behavior leading to the two principal failure modes. Chapter 21 discusses how each design parameter influences the masonry shear capacity, performance, and failure mode. Chapter 23 presents the overall conclusions and recommendations from this study.

CHAPTER 21. INFLUENCE OF MASONRY ATTRIBUTES

21.1 Introduction

This chapter will discuss the discoveries made during the course of this study into the influence of the masonry wall parameters on the wall shear strength. The discussion of parameter influences will be made both qualitatively and quantitatively. Analysis on an example shear wall is conducted as a means of developing plots to explain the qualitative relationships in this and the next chapter. The example wall used in this explanation is shown in Figure 21.1 and the panel properties are shown in Table 21.1. The panel is loaded as a cantilever because the condition can be easily applied to the reverse-curvature loading condition.

Table 21.1: Model Parameters Used in Example

Parameter	Value
l_w	2600 mm
h_e	2000 mm
t	194 mm
f'_m	15.0 MPa
A_t	200 mm^2
f_{yt}	400 MPa
A_c	200 mm^2
f_{yc}	400 MPa
σ_0	varies

21.2 Stress Analysis

Each wall parameter influences the magnitudes and distributions of the shear and normal stress within the wall panel. The shear stresses in an uncracked masonry panel can be expressed

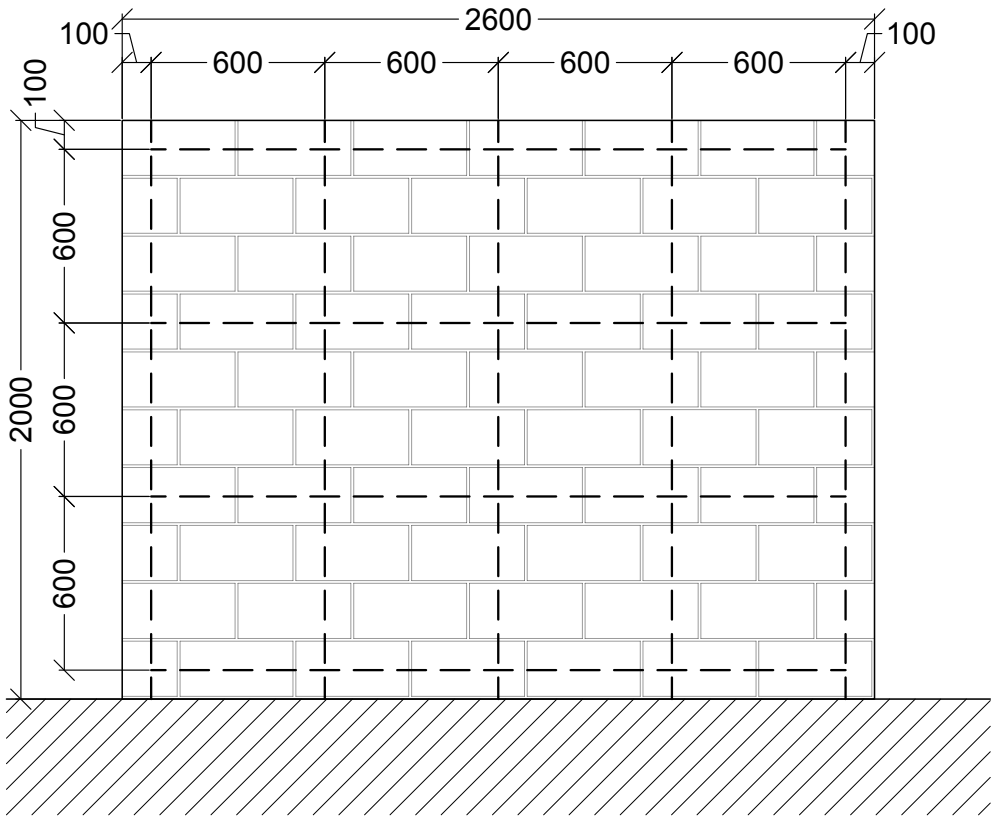

Figure 21.1: Diagram of model used in example

using the shear stress equation

$$\tau = \frac{VQ}{I_g t} \tag{21.1}$$

where

V = the shear force,

Q = the first moment of area,

I_g = moment of inertia of the gross, uncracked section, and

t = width of the member.

Equation (21.1) is not applicable to sections with non-linear stress distributions, concentrated forces, or axial load. A second method for determining the shear stress at any point in a shear wall is conducted by dividing a shear wall into small vertical strips, as illustrated in Figure 21.2. The

relationship in Mohr's Circle states that shear stresses are the same between two orientations that are 90 degrees apart, so the shear stress in the vertical direction is equal to the shear stress in the horizontal direction. As the width of the strips is decreased toward zero, the limit produces the distribution of the shear strength along the length of the wall. Applying the method in Figure 21.2 is analogous to using plots of loads on a beam to determine the shear and moment diagrams.

The masonry constitutive model in Section 22.2.1 was used in lieu of the Whitney stress block approach in determining the stress distributions for the example wall because it provides a more correct representation. The principal tensile stress σ_1 distribution in the wall panel is a function of the shear stress τ and the vertical axial stress σ_0 given by

$$\sigma_1 = \frac{\sigma_0}{2} + \sqrt{\tau^2 + \left(\frac{\sigma_0}{2}\right)^2} \tag{21.2}$$

which is a functional representation of Mohr's Circle. The magnitude and location of the shear and principal tensile stresses determine the cracking pattern, performance characteristics, and failure model of the wall.

21.3 Compressive Strength

The results of the analysis confirmed the earlier observation by several researchers (Matsumura, 1987; Meli et al., 1968; Shing et al., 1990) that the shear strength of masonry walls is better related to the square root of the masonry compressive strength. No reasoning behind this relationship has been given and the relationship has typically been assumed to be empirical. The strut-and-tie modeling theory provides a good theoretical background behind the behavior of this observed relationship.

The phenomenon can be explained by considering a reinforced masonry wall panel with a vertical reinforcement bar in each jamb, with an applied axial load, and without horizontal reinforcement. The horizontal reinforcement is omitted to compare the theory to the masonry component of the shear equation without the influence of the horizontal reinforcement. The masonry panel is assumed to be loaded in reverse-curvature so that a single masonry strut is present in the panel between the two corners. The width of the compression strut is governed by the strength

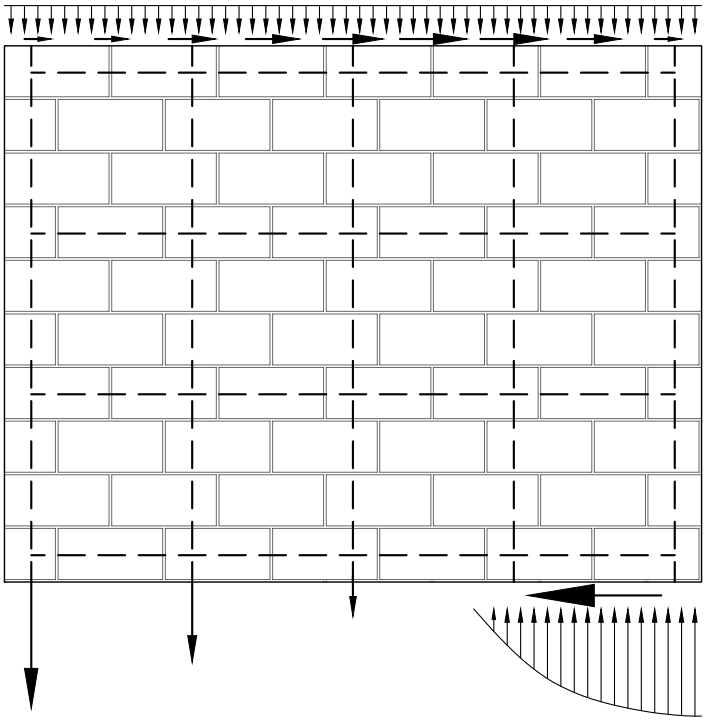

(a) Loaded masonry shear wall

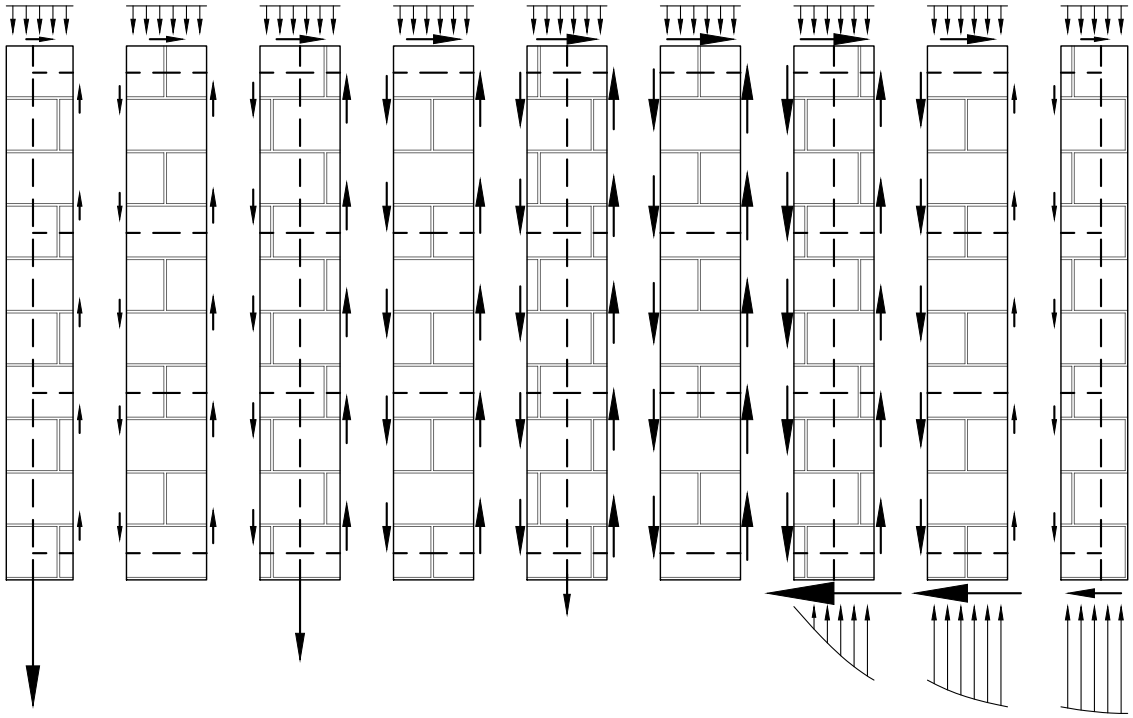

(b) Shear wall divided into vertical sections

Figure 21.2: Method for computing shear stress distribution

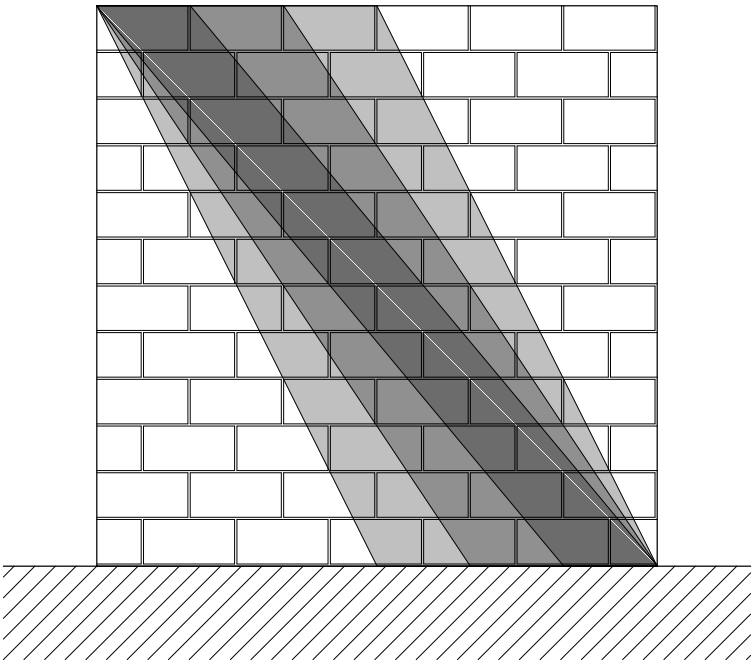

Figure 21.3: Variation in strut width and inclination

of the masonry and the inclination of the strut is governed by the width of the strut, as shown in Figure 21.3.

As the masonry strength increases, the width of the compression strut decreases. As the compression strut decreases in width, the inclination of the strut increases asymptotically to the constant value corresponding to a strut of infinitesimal strength and zero width spanning from one corner to the other. The relationship of the panel shear strength to the masonry compressive strength compared to those determined using the MSJC (2013) and proposed shear equations are shown in Figure 21.4. As the figure shows, the relationship between the shear capacity and the compressive strength is not linear but the square root term used in the shear equations is not exactly the best match for the relationship.

The overall fit of the shear equations to the strut-and-tie model results will vary depending on the other model parameters such as axial load and spear span ratio. Overall, the term used in the shear equations will have a tendency to over-predict the masonry strength component for extremely high or extremely low values of f'_m. However, since these extreme strength values are uncharacteristic for masonry, the square root relationship used in the shear equations is likely to be sufficiently accurate for model design scenarios.

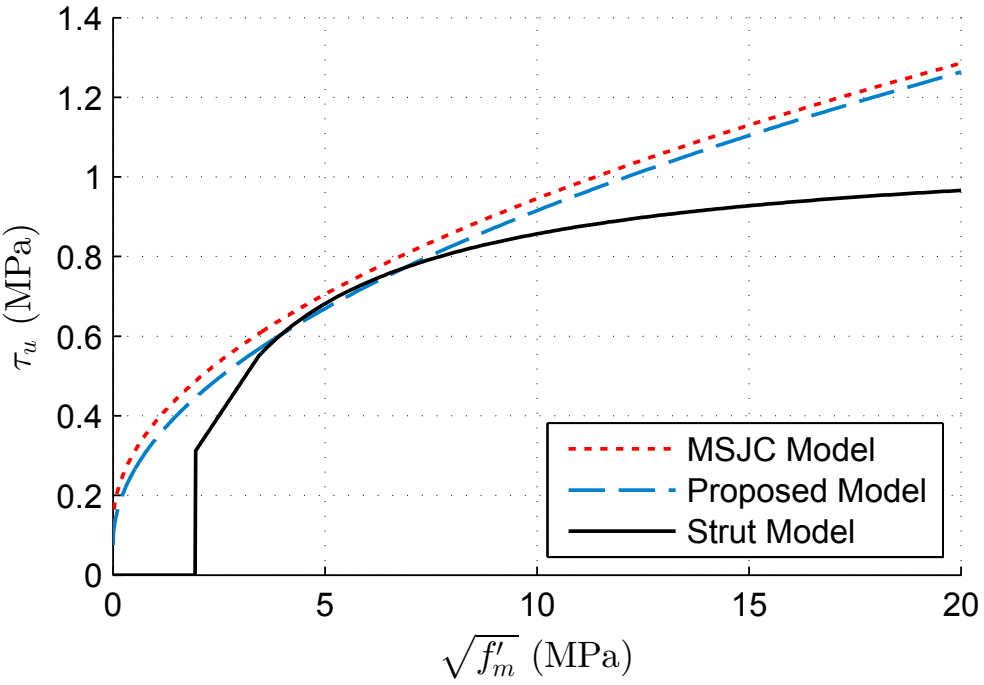

Figure 21.4: Relation between compressive strength and shear capacity

21.4 Axial Load

The results of the analysis confirmed the earlier observation by several researchers (Matsumura, 1987; Shing et al., 1990; Schultz, 1996a; Voon, 2007; Haach et al., 2010a) that the axial load influences the ultimate shear strength of a reinforced masonry wall. The MSJC and proposed shear equations assume that the relationship between the axial load and the ultimate shear strength is linear. The relationship between the axial load and the shear capacity for the two shear equations is compared to that predicted using the strut-and-tie modeling theory in Figure 21.5 for three difference values of f'_m. The strut-and-tie model theory shows that the relationship is nonlinear and that the nonlinearity accentuates as the strength of the masonry decreases. Further comparison was made of the ratio of applied axial load to the compressive strength of the concrete in Figure 21.6, showing that both shear equations perform satisfactory for low ratios but become increasingly conservative as the ratio increases.

The axial load also influences shear wall performance by determining whether it will be dominated by flexural or shear behavior. In cases where little to no axial load is applied to the wall, the wall will have a greater propensity to fail in the flexural mode. As the applied axial

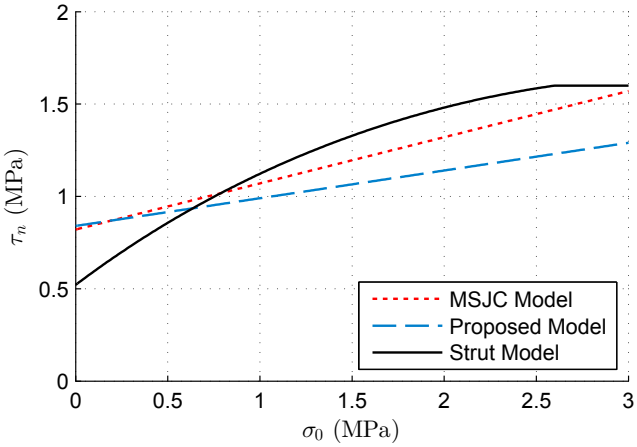

(a) For f'_m = 10 MPa

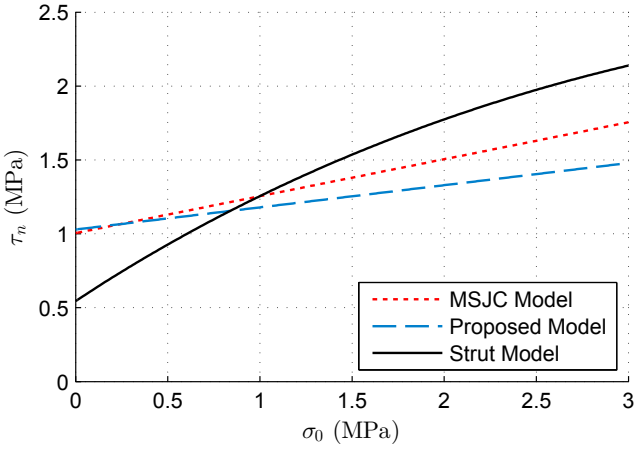

(b) For f'_m = 15 MPa

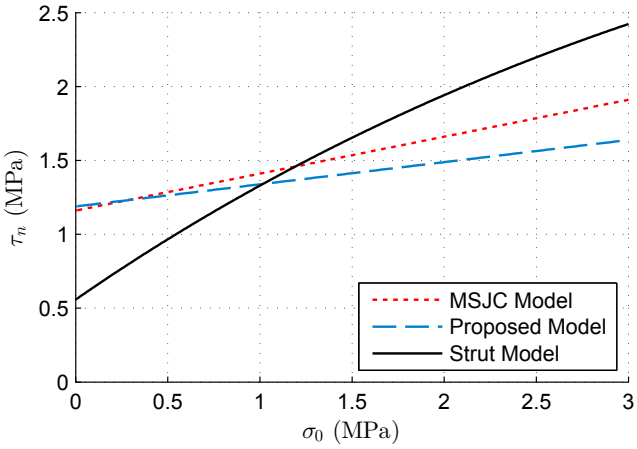

(c) For f'_m = 20 MPa

Figure 21.5: Relationship between axial load and shear strength

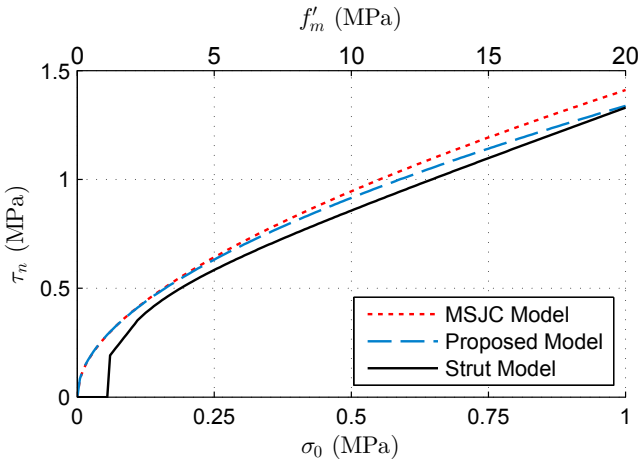

(a) For $\frac{\sigma_0}{f'_m} = 0.05$

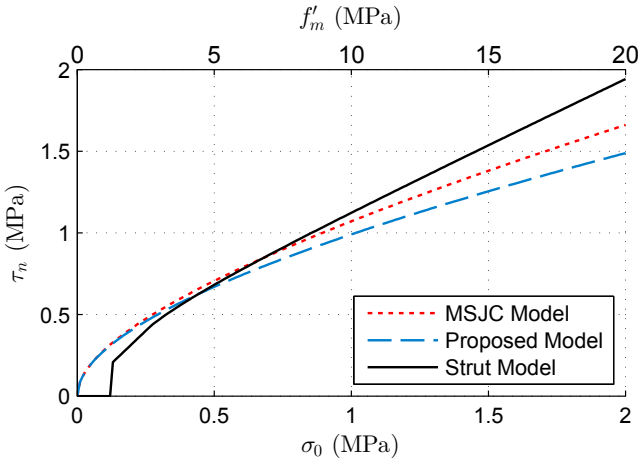

(b) For $\frac{\sigma_0}{f'_m} = 0.1$

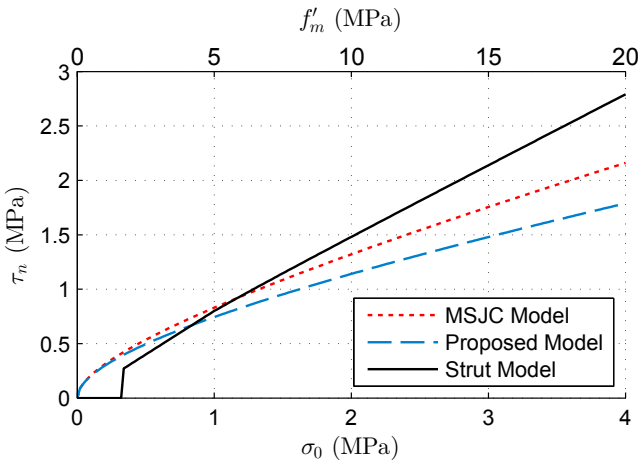

(c) For $\frac{\sigma_0}{f'_m} = 0.2$

Figure 21.6: Relationship between axial load ratio and shear strength

load increases the tensile stress in the center of the wall panel will become greater than that at the extreme tensile fiber of the wall (as shown in Figure 21.7) and the wall will crack diagonally before it cracks horizontally. The shear force values in Figure 21.7 also show that the axial load also increases the shear strength capacity of a wall

In walls dominated by flexural cracking, increasing the axial load causes an increase in the peak shear stress in the panel (as shown in Figure 21.8) increasing the likelihood that the wall will transition to shear-dominated behavior before failing in flexure. In walls governed by shear behavior, increasing the axial load increases the load in each compression strut, decreasing the amount of strain and stress in the reinforcement bars for any given lateral load. The peak lateral load will occur at smaller lateral drifts and with less yielding of the vertical reinforcement, resulting in a behavior which dissipates less energy and is less ductile. Ghanem et al. (1993) concluded that the axial load should not exceed 5 percent of the compressive strength of the masonry to prevent the wall from experiencing a brittle shear failure. This limit appears to produce a satisfactory agreement between the shear equations and the strut-and-tie models. A higher limit on the ratio of axial load to masonry compressive strength could be feasible if the size of the vertical reinforcement was decreased to permit it to yield before reaching the ultimate shear capacity, but more research is necessary to determine what an appropriate limit should be.

21.5 Shear Span Ratio

Researchers (Schneider, 1969; Matsumura, 1987; Voon, 2007) have observed that the ultimate shear strength of masonry shear walls is inversely proportional to the shear span ratio. The relationships obtained by Schneider and Matsumura are shown in Figures 21.9 and 21.10, respectively. For reasons that were not explained in the literature, the shear equations developed later on by Blondet et al. (1989) and the TCCMaR committee (NEHRP, 1997) used a linear relationship for the influence of the shear span ratio. It was observed during the development of the proposed shear equation in Chapter 15 that the linear model provided a better fit to the experimental data when the inverse of the shear span ratio was used. The proposed approach has the added benefit of eliminating the requirement that the shear span ratio not be taken greater than one, providing a small simplification over the MSJC equation.

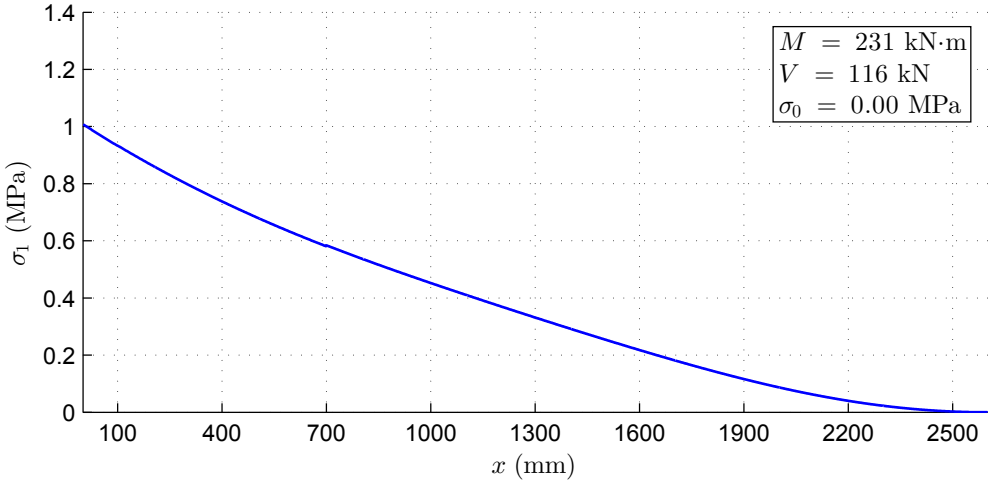

(a) For $\sigma_0 = 0.0$

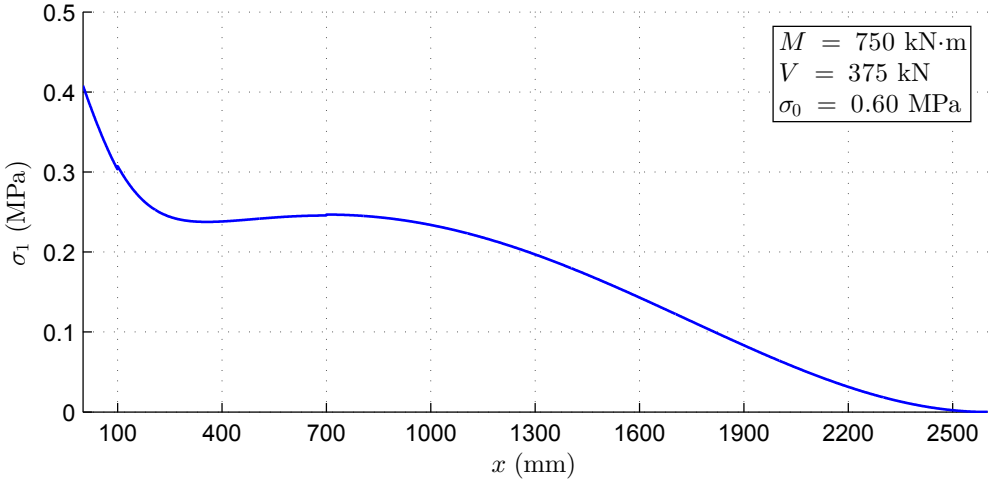

(b) For $\sigma_0 = 0.6$

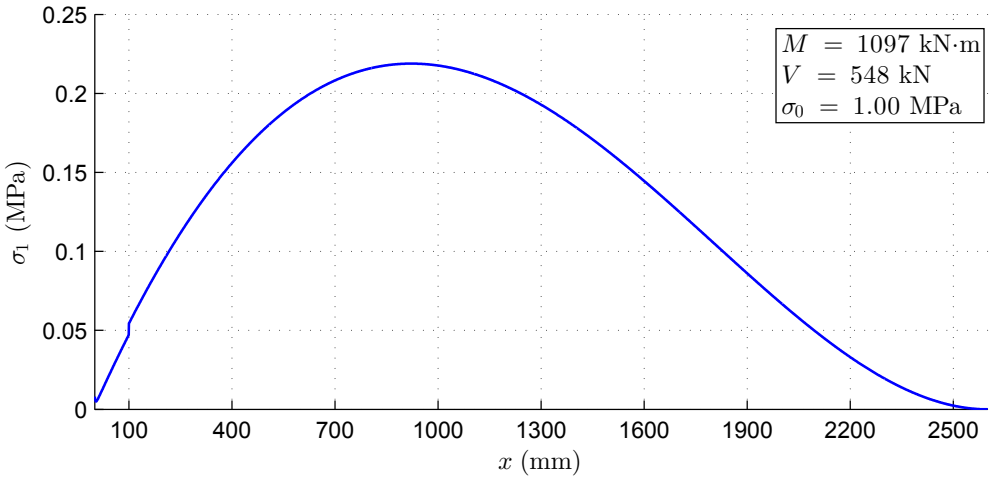

(c) For $\sigma_0 = 1.0$

Figure 21.7: Influence of axial load on flexural or diagonal cracking

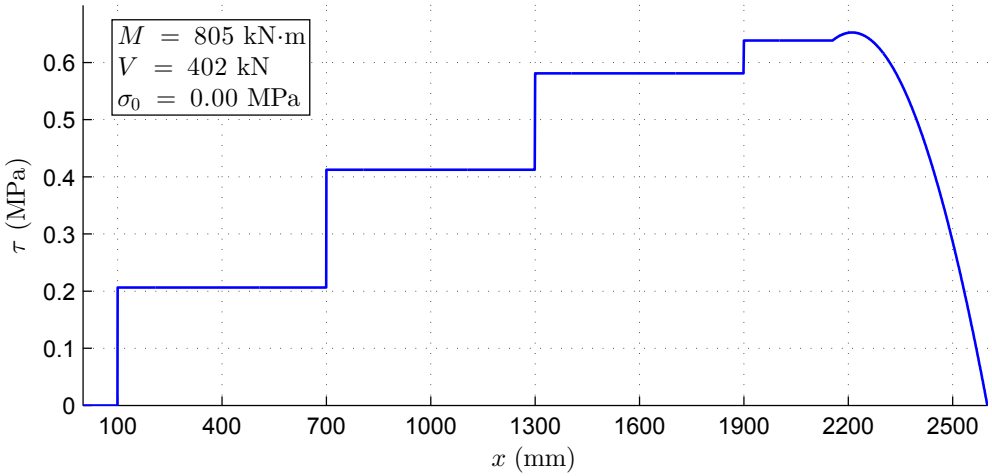

(a) Excluding axial load

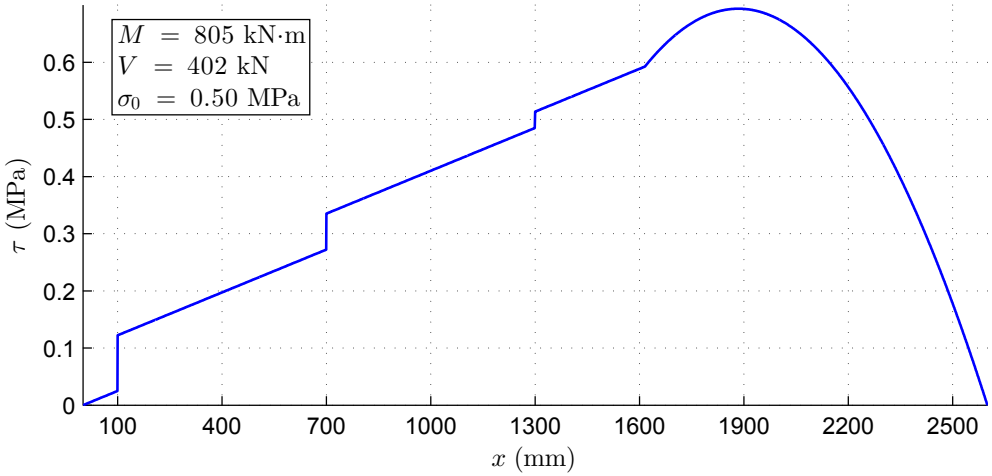

(b) Including axial load

Figure 21.8: Relationship between axial load and shear strength

The relationship between shear span ratio and the shear capacity for the two shear equations is compared to that predicted using the strut-and-tie modeling theory in Figure 21.11 for three different values of f'_m. The three plots show the proposed shear model to better fit the strut-and-tie model than the MSJC equation. Both shear equations over-predict the strength for shear span ratios greater than about 1.0 whereas the MSJC equation under-predicts the strength for shear span ratios less than about 0.5. These bounds would change for different combinations of f'_m, σ_0, and ρ_f values.

The shear span ratio also influences shear wall performance by determining whether it will be dominated by flexural or shear behavior. For a given induced moment force, walls with

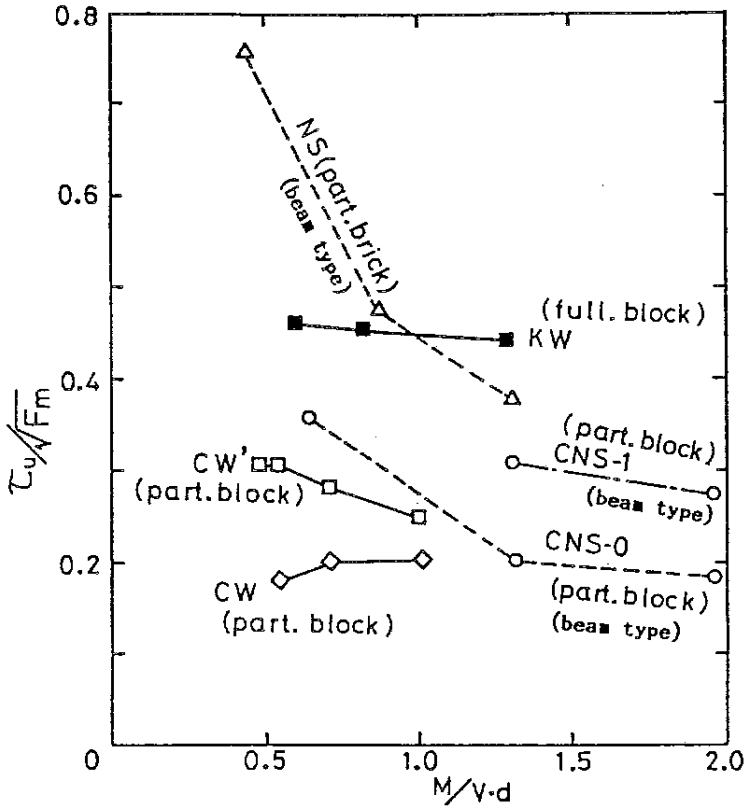

Figure 21.9: Influence of shear span (from Matsumura 1987)

higher shear span ratios have a greater height and vertical shear area to resist the masonry shear forces, resulting in a lower peak shear stress. Increasing the shear span ratio increases the induced moment force for a given lateral shear load, partially canceling the effect of the height on peak shear stress and resulting in a net decrease in peak shear stress, as shown in Figure 21.12. The plateaus on the contour plot represent the shear load at which the wall begins experience large rotational deflections due to overturning.

The principal tensile stress at the neutral axial decreases with increasing spear span ratio because it is functionally related to the peak shear stress. The principal tensile stress at the extreme tension fiber increases with increasing shear span ratio due to the greater moment arm of the lateral shear load. As the shear span ratio increases the stress in the extreme tension fiber governs, leading to tensile cracking and flexural behavior of the panel. As the shear span decreases the stress at the neutral axis governs, leading to diagonal cracking and shear behavior of the panel.

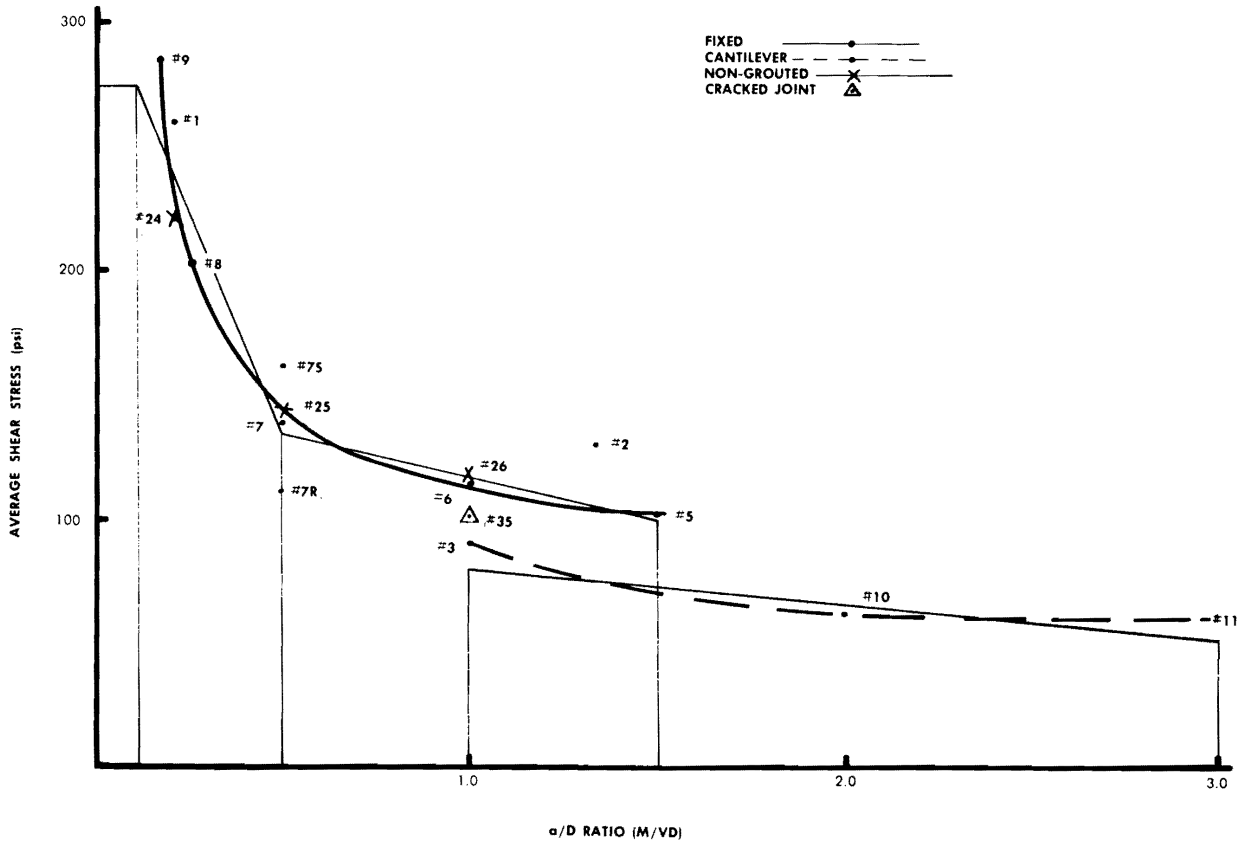

Figure 21.10: Influence of shear span (from Schneider 1969)

21.6 Vertical Reinforcement

The vertical reinforcement has a similar effect on wall strength and behavior as the axial loading, but with some distinct differences. The vertical contribution of each bar is variable from zero to the yield strength whereas the axial load is constant. It was shown in Section 20.4.1 that in some cases the optimum shear capacity is obtained when not all of the vertical reinforcement bars are fully contributing. As the wall approaches and exceeds this optimum strength, overturning of the wall segments will be accompanied by further stressing and yielding of the reinforcement. Energy is dissipated by the plastic yielding and strain hardening of the reinforcement bars, resulting in a ductile failure. Since the axial load is constant the overturning of the wall panels with little to no vertical reinforcement results in a loss of equilibrium and a brittle failure.

The force in each reinforcement bar increases the peak shear stress in the wall panel. The shear stress in the wall panel is greater at a given lateral shear load for reinforcement concentrated at the ends than when the reinforcement is distributed throughout the wall, as shown in Figure

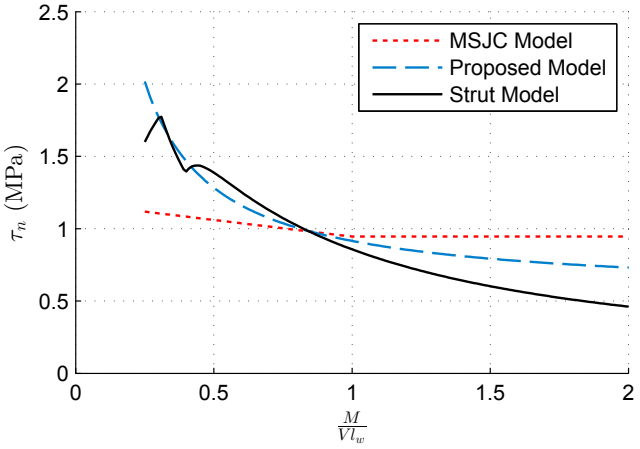

(a) For $f'_m = 10$ MPa

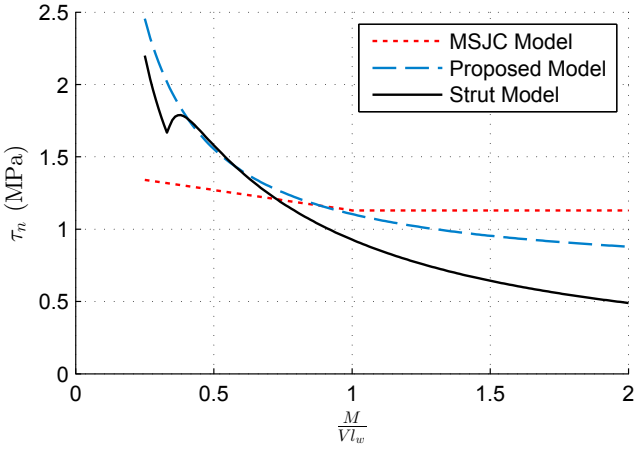

(b) For $f'_m = 15$ MPa

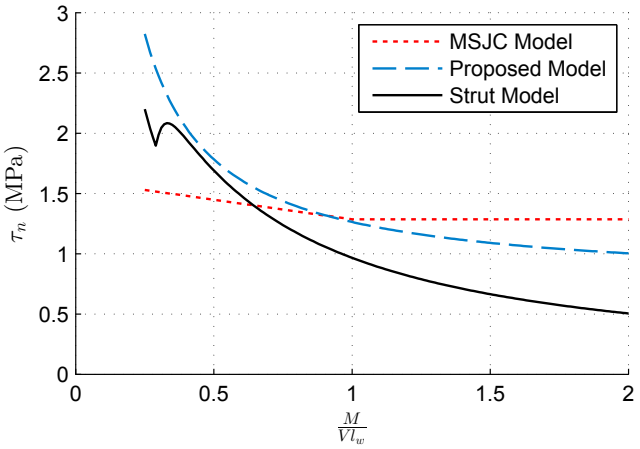

(c) For $f'_m = 20$ MPa

Figure 21.11: Relationship between shear span ratio and shear strength

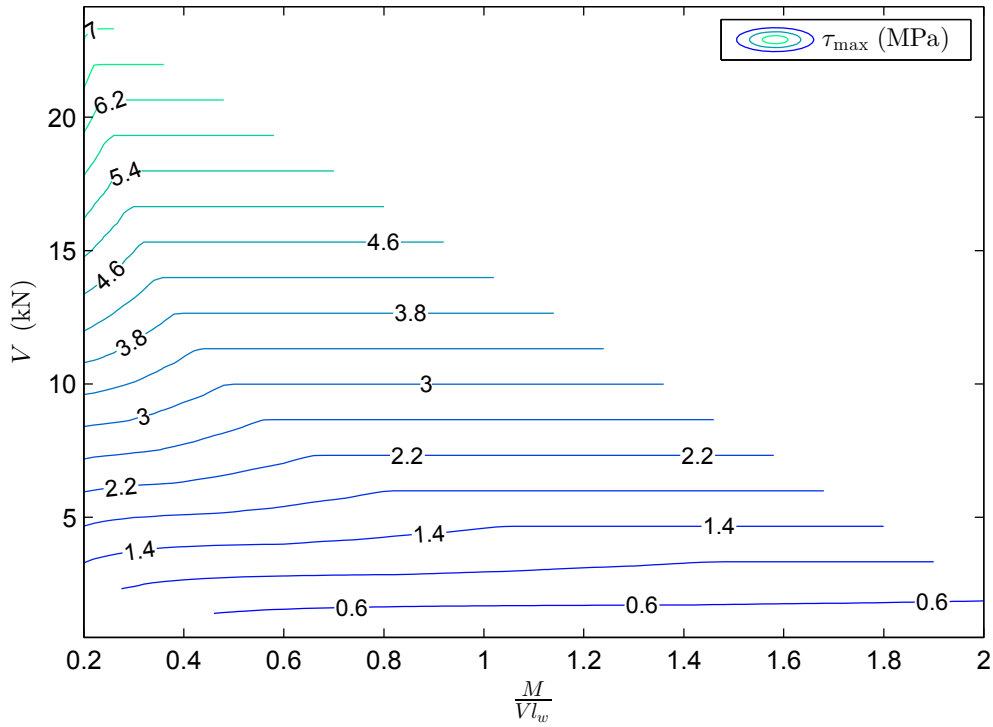

Figure 21.12: Peak shear stress for given shear loads and shear span ratios

21.13. This increase in peak shear stress reduces the lateral load at which shear cracks will form, causing the wall to be more brittle. The concentration of the reinforcement at the end also increases the required development length and the width of the diagonal strut. Since the masonry area available for strut anchorage between the flexural bar and edge of the panel is small, concentration of the reinforcement increases the possibility of anchorage failure and decreases the overall shear capacity.

Distributing the vertical reinforcement throughout the wall panel results in varying moment arm lengths for each bar. As the wall is loaded such that the reinforcement begins to yield, the pushover curve for distributed reinforcement is more plastic and ductile than walls with concentrated reinforcement, as shown in Figure 21.14 These observations agree with the observation of Ghanem et al. (1992) that even distribution of reinforcement produces increased shear strength and those of Nolph (2010) and Elmapruk (2010) who both observed that the shear strength is inversely proportional to the horizontal grout spacing. In Chapter 15 of this study it was presented that the wall strength of partially-grouted wall was inversely proportional to the ratio of horizontal grout spacing and wall length.

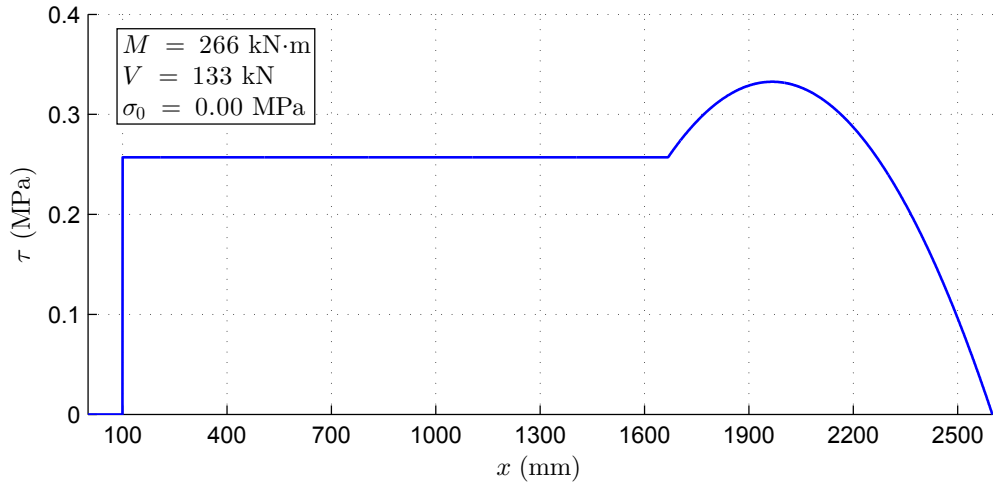

(a) Concentrated reinforcement

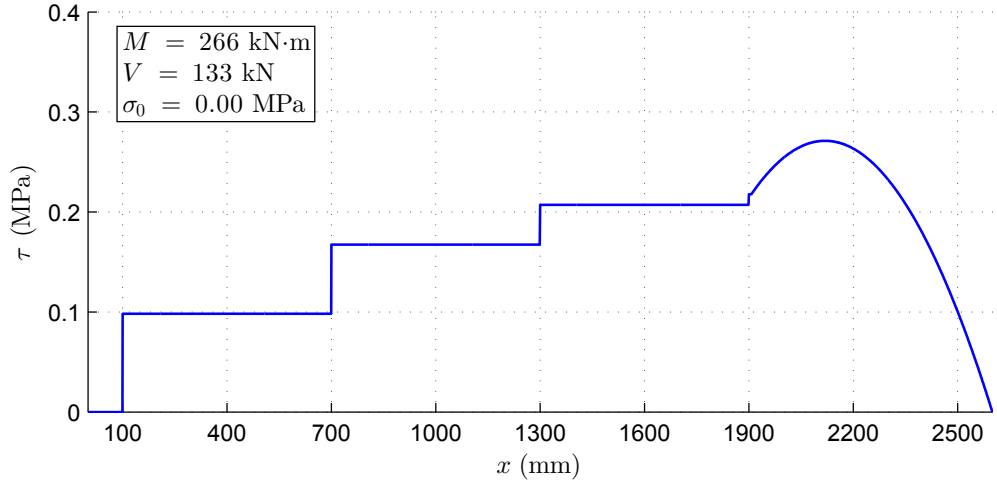

(b) Distributed reinforcement

Figure 21.13: Effect of vertical reinforcement distribution on wall ductility

21.7 Horizontal Reinforcement

The meta-regression performed in Chapter 15 revealed that the contribution of the horizontal reinforcement is not as great as originally supposed by Blondet et al. (1989), Shing et al. (1990), Anderson and Priestley (1992), and the TCCMaR committee (NEHRP, 1997). While these studies assumed that the direct strength contribution of the horizontal reinforcement to the shear strength was limited to the reinforcement in the middle half of the vertical section, the regression showed that the direct contribution was approximately 12 percent of the strength capacity. The observed

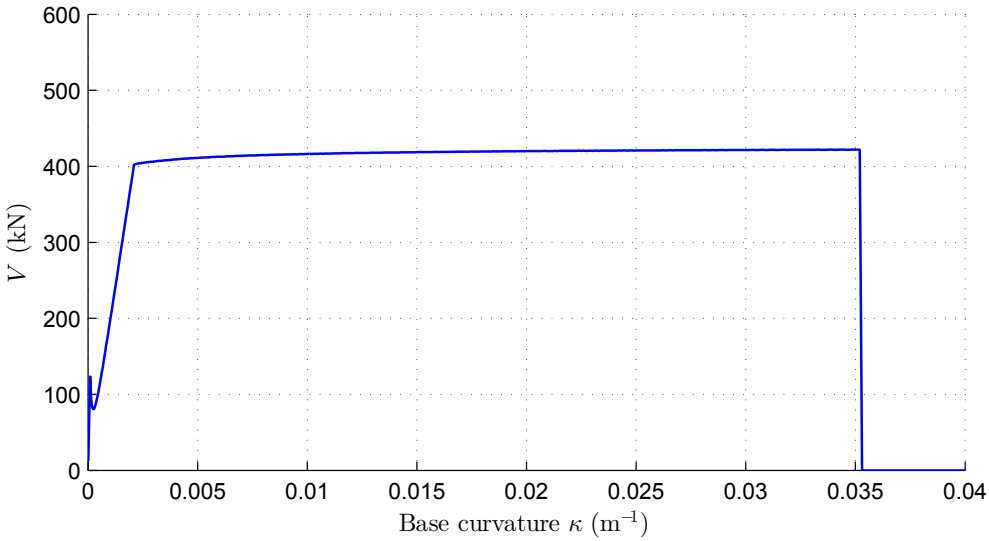

(a) Concentrated reinforcement

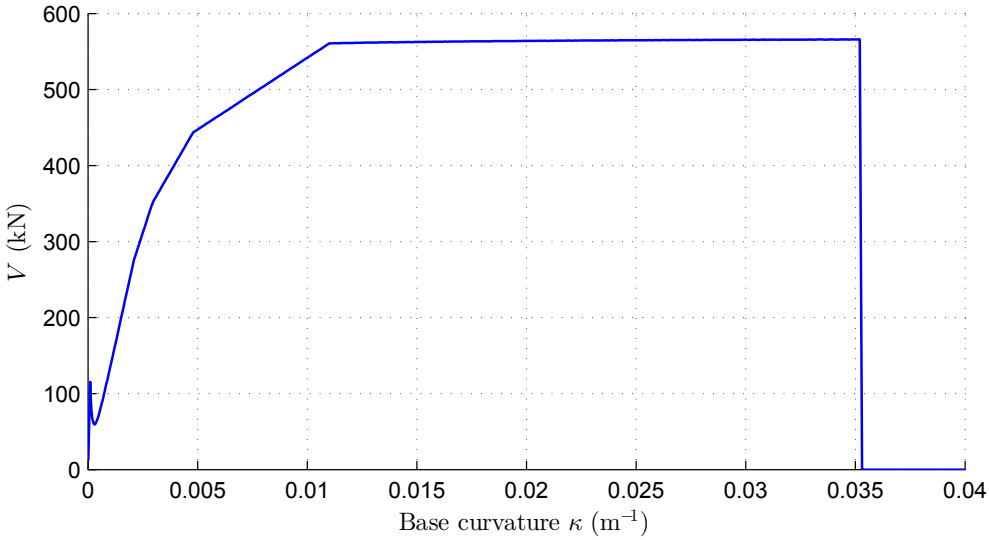

(b) Distributed reinforcement

Figure 21.14: Effect of vertical reinforcement distribution on wall ductility

difference in strength contribution between the experimental data and the theoretical results can be explained through strut-and-tie modeling theory.

The generation of strut-and-tie models revealed that the horizontal reinforcement principally acts by confining the transverse spreading and splitting forces in the inclined compression struts. In the cases where the horizontal reinforcement is directly engaged in resisting the lateral load, the bars in roughly the top and bottom quarters of the wall do not contribute because the other

struts interfere with the anchorage of the bars. This behavior agrees with the hypothesis of Blondet et al. and Shing et al. that only the reinforcement in the middle half of the wall contributes because there is not sufficient development length for the bars at the bottom and top to be fully engaged. While their hypothesis agrees with the amount of reinforcement that contributes, the method in which the bars contribute is different from what has been assumed.

The horizontal bars are only engaged after diagonal cracks form in the wall. In the extreme load state the cracks can be assumed to travel between the struts, separating the panel into segments, as shown in Figure 21.15a. The struts and masonry within each segment can be assumed to act as a unit in which plane sections remain plane. Since the toe of the strut is restrained laterally by the lateral component of the compression force, the horizontal bars spanning the cracks between segments will act more like longitudinal reinforcement in a beam by preventing the segment from rotating, as shown in Figure 21.15b.

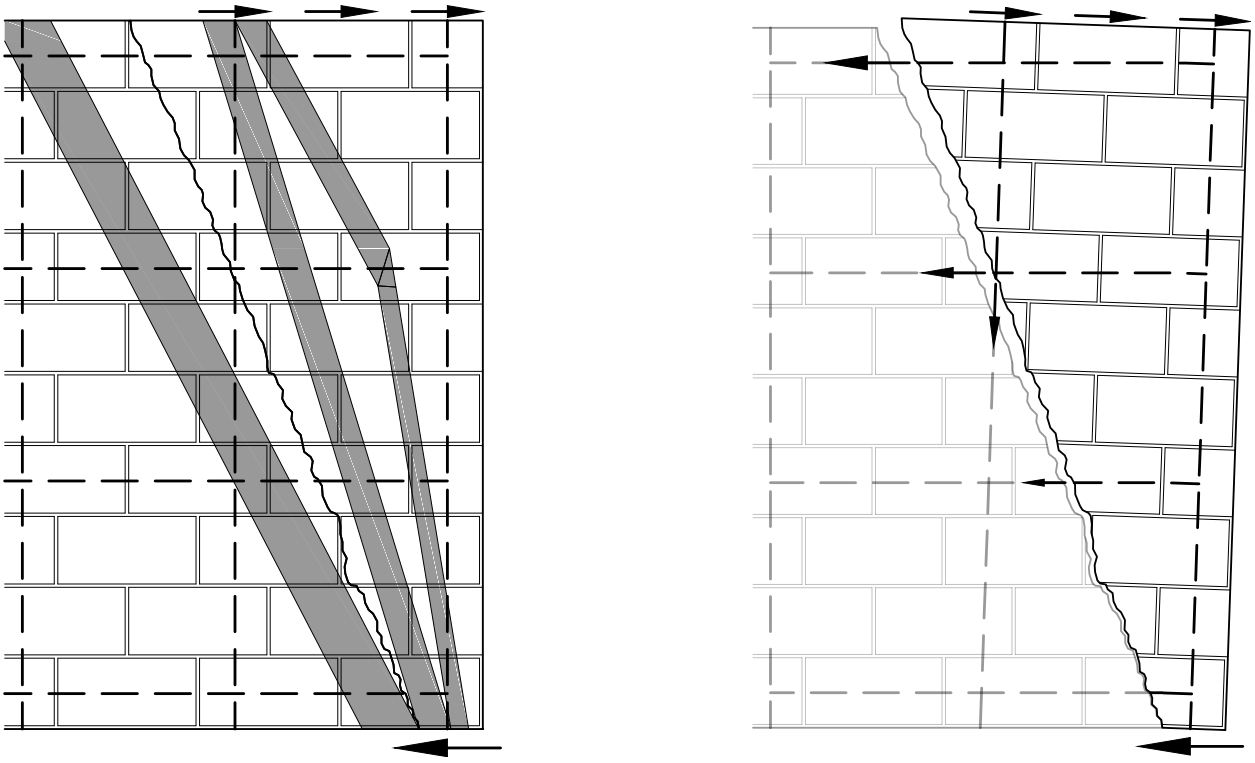

(a) Path of shear crack

(b) Force distribution in stirrups

Figure 21.15: Behavior of stirrups in a shear wall

The length of the vertical reinforcement bars anchored in the base of the wall and the strain in each bar is proportional to the absolute rotation of the attached wall segment. The horizontal bars traverse the masonry segments and so the strain in each horizontal bar is proportional to the relative rotations of the panels and to the distance of the bar from the base of the wall. The vertical reinforcement is generally not smaller than the horizontal reinforcement bars. The difference in strains and bar areas between the two reinforcement directions result in the vertical reinforcement being the principal mechanism resiting the rotation in each segment. The principal role of the horizontal reinforcement is to distribution the lateral forces between the wall segments and to prevent the segments from separating from each other.

Sveinsson et al. (1985) observed that sufficient anchorage of horizontal stirrups was necessary to prevent the sudden brittle behavior associated with sudden anchorage failure. They observed that to be sufficiently anchored the horizontal stirrups must be anchored around a vertical reinforcement bar with a 180 degree hook or welded to a plate. Since the grade of steel used in reinforcement is typically not suitable for welding, all horizontal bars should be hooked around a vertical bar at both ends.

It is also necessary that the vertical bar be sized to provide the necessary anchorage for the strut and stirrup. The AASHTO (2012) provision permit the strut anchored by a stirrup and vertical bar to extend 6 vertical bar diameters from the intersection of the two bars in both the vertical and out-of-plane directions. If the diameter of the vertical bar is less than one-twelfth of the masonry thickness, then the thickness of the strut cannot be assumed to be the same as the wall thickness. The reason is that without sufficient area for the masonry strut to bear against the vertical bar, it is possible that the force in the stirrup could cause the vertical bar to be pulled through the masonry, causing lateral splitting of the masonry.

Researchers Matsumura (1985), Sveinsson et al. (1985), Yancey and Scribner (1989), Nolph (2010), and Elmapruk (2010) observed that the relationship between the horizontal reinforcement and the increase in wall shear strength is not linear. Sveinsson et al., Nolph, and Elmapruk further observed that there is an upper limit above which any increase in the amount of horizontal reinforcement does not increase the shear strength of the wall. Sveinsson et al. determined that the maximum effective horizontal reinforcement ratio was on the order of 0.07% whereas Nolph found

that the maximum ratio was in the range of 0.085% to 0.100%. One probable explanation for this observed phenomenon is given by the strut-and-tie modeling theory.

When a horizontal stirrup is anchored around a vertical bar, the lateral force in the stirrup is transferred from the stirrup through the vertical bar into the adjoining compression strut. The force transfer between the vertical bar and strut is accomplished through bearing of the strut against the bar and is effective for a distance of 6 vertical bar diameters from the center of the anchorage. When the stirrup is small, the cross sectional area of the strut is more than sufficient to resist the lateral force and the strength of the anchorage is governed by yielding of the stirrup. As the stirrup size increases, the force in the strut increases to match the force in the stirrup. When the strength capacity of the stirrup exceeds that of the strut the strength is governed by crushing and lateral splitting of the masonry around the anchorage. As yielding of the stirrup is preferable to a sudden brittle failure of the strut, Equation (20.1) was proposed to preclude failure of stirrup anchorages.

The limit imposed by Equation (20.1) is applied to each stirrup anchorage independently as long as they are spaced more that 12 vertical bar diameters apart; otherwise, they are combined into a single anchorage with multiple stirrups. As the horizontal reinforcement ratio is related to the spacing of the stirrups and the Equation (20.1) limit is not, the two cannot be directly related to each other. Since masonry shear walls are constructed with varying heights and reinforcement spacings, there no single limit on horizontal reinforcement ratio that can be applied universally to all walls. The difference in maximum effective horizontal reinforcement ratios observed between Sveinsson et al. (1985) and Nolph (2010) were caused by the difference in reinforcement spacing between the two studies.

Take for example the scenario of two walls constructed with identical horizontal reinforcement ratios; the first wall has all reinforcement concentrated at a single location at the mid-height of the wall and the second has the reinforcement distributed throughout its height. The former wall has a significantly higher chance of suffering a stirrup anchorage failure because all of the horizontal stirrup forced is concentrated into a single strut, as shown in Figure 21.16a. The latter wall will show greater strength and ductility because the horizontal stirrup force is spread between multiple struts, as shown in Figure 21.16b. This principal is in agreement with Thurston and Hutchison (1982) and Porter and Baenziger (2007) who concluded that smaller bars distributed over the wall height produced better inelastic wall performance than larger, concentrated bars.

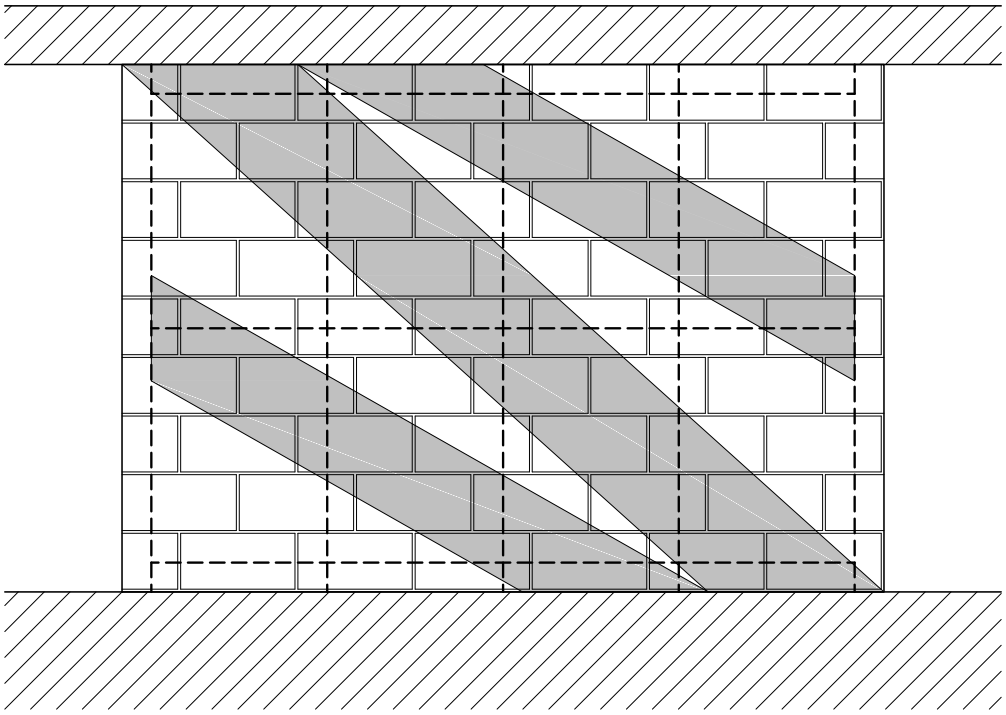

(a) Concentrated reinforcement

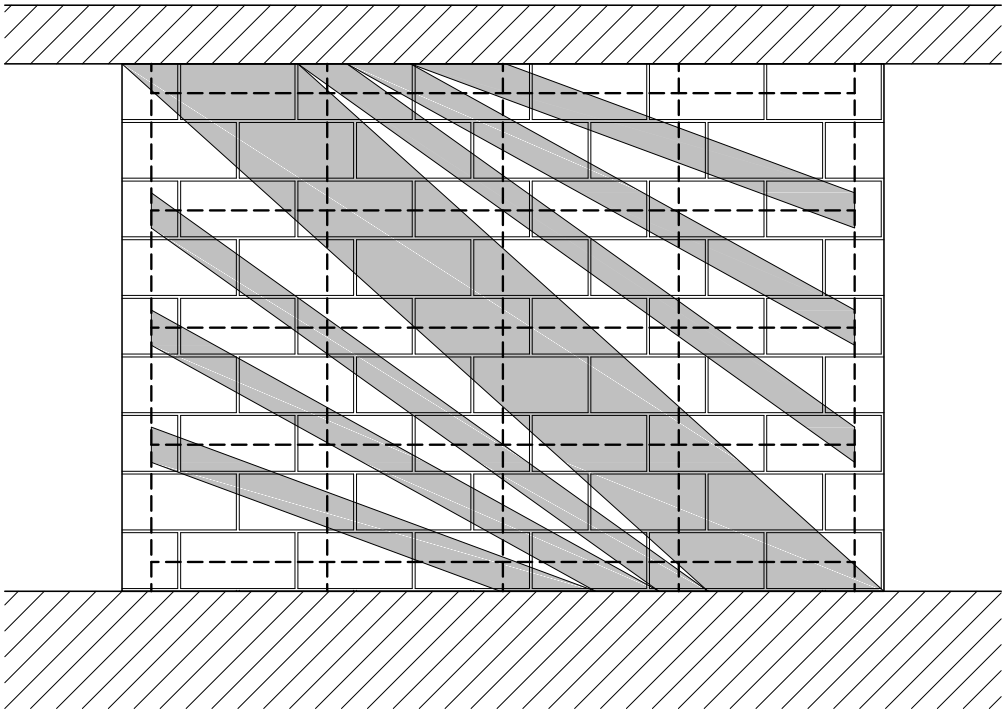

(b) Distributed Reinforcement

Figure 21.16: Effect of horizontal reinforcement distribution on strut width

CHAPTER 22. SHEAR WALL BEHAVIOR

22.1 Introduction

This chapter will expand the discussion of the discoveries made during the course of this study to the behavior and performance of masonry shear walls panels. Analysis on the example shear wall described in Chapter 21 is presented to explain the qualitative relationships in this chapter.

22.2 Components of Plasticity

Strut-and-tie models were observed to provide the best predictions for the ultimate shear capacity of reinforcement masonry walls. The accuracy of the models is attributable to their consideration of the plastic behavior of masonry shear walls under extreme strains. The plasticity of reinforced masonry shear walls can be attributed to at least three factors: the non-linear behavior of masonry, the bi-linear behavior of the reinforcement, and the redistribution of stresses through masonry cracking.

22.2.1 Masonry Non-linearity

Masonry exhibits non-linear behavior for all but the smallest strains and is similar to the behavior of concrete. To simplify the analysis process, the properties of the masonry panel are typically smeared across the entire continuum. The constitutive model for the compressive behavior of masonry is typically assumed to be parabolic from the origin through the ultimate stress and into the beginning phases of strain softening and to follow a inverse exponential function for the strain softening tail. The model for the tensile behavior is linear up to the rupture strain after which the model experiences a sharp decline in strength, which is commonly modeled using an inverse exponential function (Lotfi and Shing, 1991; Al-Chaar and Mehrabi, 2008; Minaie, 2009).

The crushing strains for masonry are taken as 0.0025 for concrete masonry and 0.0035 for clay masonry (MSJC, 2013). Values for the masonry tensile rupture strain varied in the literature with two values being 0.0001 (Al-Chaar and Mehrabi, 2008) or 0.000156 (Wu and Hao, 2008).

When computing the flexural capacity of reinforced masonry members, the non-linear distribution of compression stresses are typically idealized using the Whitney stress block approach. The equivalent stress block is assumed to extend 80 percent of the way from the extreme compression fiber to the neutral axis. The resultant force of the stress block is assumed to be equal to $0.8f'_m$ multiplied by the compression area of the block. These parameters and the crushing strains from the MSJC provisions can be used to determine the coefficients for the parabolic function for the compressive behavior. To make the determination, it must be assumed that the compression strains vary linearly from zero at the neutral axis to the rupture strain at the extreme compression fiber and that the slope of the stress-strain curve is zero at the crushing strain.

Using this approach the constitutive model for masonry in compression can be expressed as

$$\frac{\sigma}{f'_m} = 1.68\frac{\epsilon}{\epsilon_{mu}} + 0.36\left(\frac{\epsilon}{\epsilon_{mu}}\right)^2 - 0.32\left(\frac{\epsilon}{\epsilon_{mu}}\right)^3 \tag{22.1}$$

where

σ = normal stress in the masonry,
f'_m = uniaxial compressive strength of masonry,
ϵ = normal strain in the masonry, and
ϵ_{mu} = crushing strain of the masonry.

A cubic polynomial is necessary to satisfy the third assumption that the slope of the stress-strain curve is zero at the crushing strain. A plot of Equation (22.1) and the equivalent stress block is shown in Figure 22.1. Using the integral to locate the strain corresponding to half the area under the curve, it was determined that the resultant of the stress block was located slightly farther than the center of the block from the neutral axis. This results in the the stress block representation being slighting conservative when compared to the constitutive model.

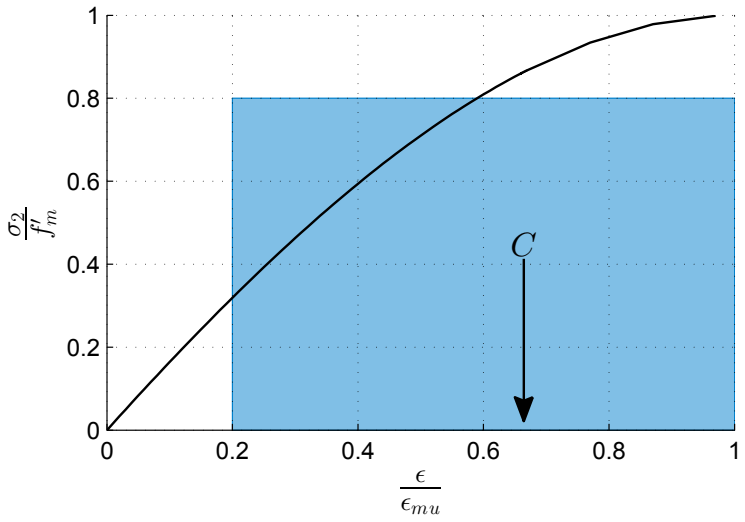

Figure 22.1: Consitutive model and stress block

To produce a curve with a resultant at the center of the stress block would require the use of a fourth-order polynomial (as shown in Figure 22.2a) or to eliminate the assumption that the curve slope is zero at the crushing strain (as shown in Figure 22.2b). Comparison of both plots with those in the literature revealed that neither plot matched those developed from testing as well as that for Equation (22.1). The fourth-order approximation in Figure 22.2a is not continually increasing up to the peak strength. The non-zero slope at crushing strain in Figure 22.2b results in too much strain softening at the crushing strain. The strain-softening branch of the curve typically changes to positive curvature (or concavity) and an inverse exponential function at approximately half of the ultimate stress (Lotfi and Shing, 1991).

Taking the derivative of Equation (22.1) produces the tangential elastic modulus for masonry given by

$$E_m \;=\; 1.68\frac{f'_m}{\epsilon_{mu}}\,. \tag{22.2}$$

The above definition of tangential elastic modulus produces values of $672 f'_m$ for concrete masonry and $480 f'_m$ for clay masonry. Both values are lower than the MSJC code specified values of $900 f'_m$ for concrete masonry and $700 f'_m$ for clay masonry. The tensile constitutive model for masonry is assumed to increase with a slope of E_m until the rupture strain, after which point the strength drops off. For the purpose of this discussion, it is assumed that the tensile stress is zero after the

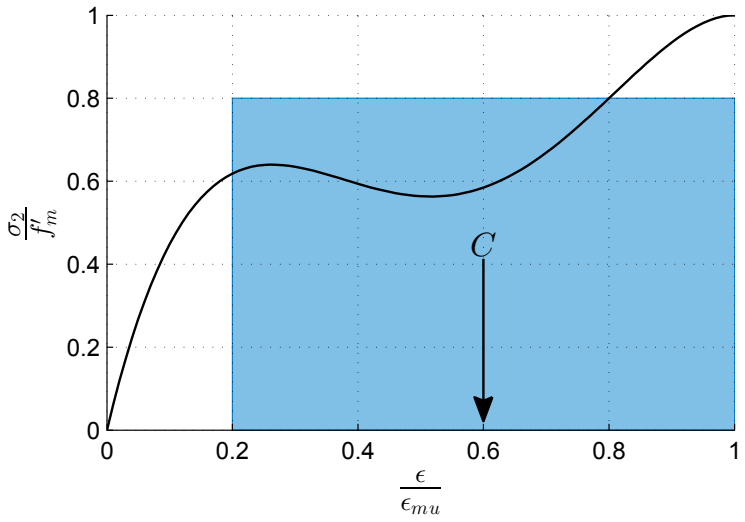

(a) Fourth-order polynomial representation

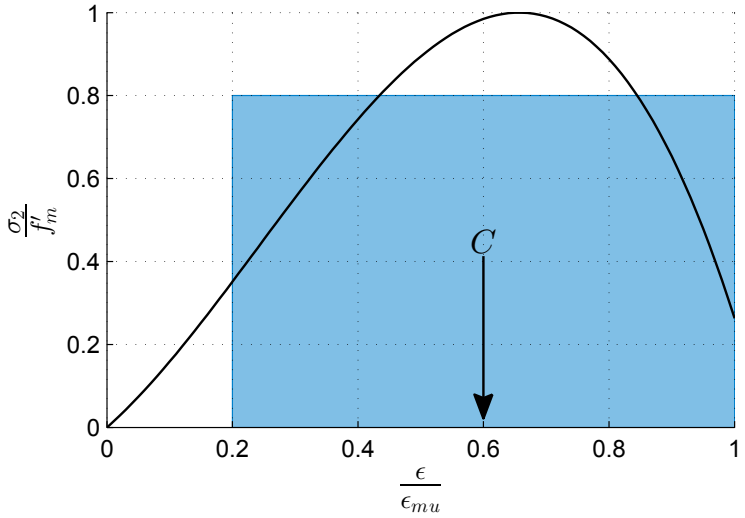

(b) Non-zero slope at crushing strain

Figure 22.2: Constitutive models with resultant centered in stress block

rupture strain is exceeded. This assumption ignores the effect of tensile strain softening but is more accurate than the common design assumption for reinforced masonry that the tensile strength does not participate at all.

22.2.2 Reinforcement Yielding

The steel grades used for reinforcement bars are commonly assumed to demonstrate bi-linear behavior for the strains typically used in design. The yielding of the vertical reinforcement closest to the trailing edge of the wall permits the strains in the other bars to increase with increasing load until each of them in turn also yields. This behavior results in a non-linear push-over curve for masonry shear walls as each subsequent vertical bar yields, providing a large degree of ductility and energy dissipation for cases where the wall does not fail in shear.

22.2.3 Masonry Cracking

Cracking in the masonry panel occurs in the elements where the normal tensile stress exceeds the rupture strength of the masonry. In unreinforced masonry, the onset of cracking typically leads to failure of the member because of the weakest link theorem states that there is not enough residual strength left in the material to dissipate the energy released by the initiation of cracking. Reinforced masonry members are assumed to crack before the reinforcement can be fully engaged. The reinforcement is able to absorb the energy released with the formation of new cracks and help redistribute the path of stresses around the cracks to other portions of the member. As shear cracks form, the Euler-Bernoulli assumption that plane sections remain plane is no longer applicable to the member and the strains in the interior vertical bars are able to increase more than what is determined through flexural theory.

22.3 Masonry Shear Wall Theory

At the beginning stages of lateral loading, the masonry panel is uncracked and the entire length of the masonry is effective in resisting the overturning moment force. Due to strain compatibility, the trailing-most reinforcement bars have some tensile contribution, but the contribution is small compared to the tensile contribution of the masonry, as shown by the small vertical jumps at $x = 100$ and 700 in Figure 22.3.

As the lateral shear load applied to the masonry panel increases, the normal tensile stress in the extreme tensile fiber and the maximum shear stress in the center of the wall panel both increase. The shear stress in the center of the wall is inversely related to the effective height of the

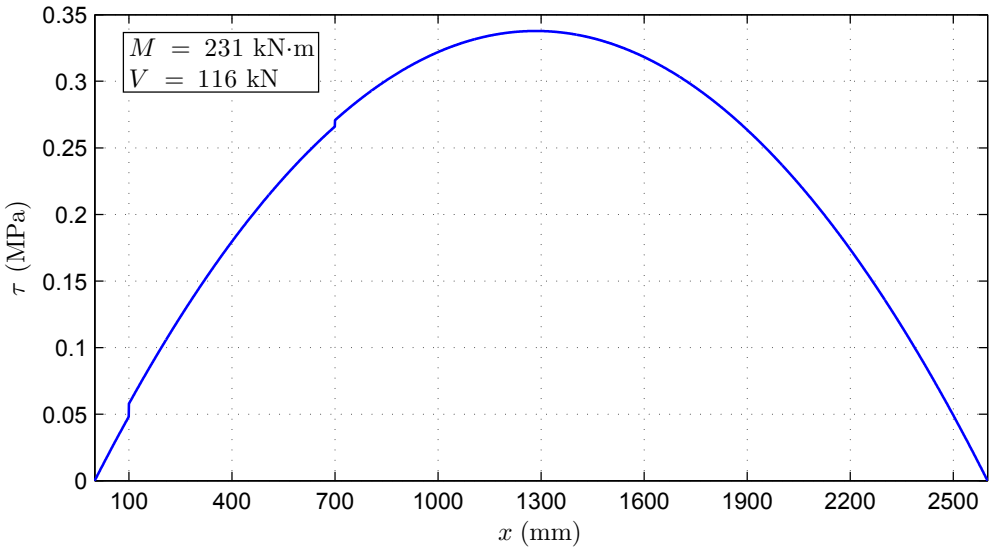

Figure 22.3: Shear stress in uncracked shear wall

wall panel. For walls with lower axial stress and higher shear span ratios, the normal tensile stress at the extreme tensile fiber will be the first to exceed the rupture stress and cracking will initiate as horizontal cracks at the extreme tensile fiber, as shown in Figure 22.4. For walls with higher axial stress and lower shear span ratios, the normal tensile stress at the wall center will be the first to exceed the rupture stress (as shown in Figure 22.5a) and cracking will initiate as diagonal cracks in the center of the wall panel (as shown in Figure 22.5b). In the former case the next stage of wall performance will be dominated by flexural behavior and in the latter case it will be dominated by shear behavior.

22.3.1 Flexural Behavior

When the tensile strain in the extreme tensile fiber of the masonry exceeds the rupture strain, a horizontal crack propagates from the edge of the wall towards the other edge. As the crack opens, the wall panel rotates further until the reinforcement is engaged sufficiently until static equilibrium is regained. The effect of flexural rupturing of the masonry panel can be seen in Figure 22.6 which shows the increase in strain at the wall base that must occur before the uncracked shear capacity is regained. After tensile cracking initiates, the distribution of shear stress in the wall shown in Figure 22.4a is notably difference from the uncracked stress pattern shown in Figure 22.3. The horizontal tensile crack can be seen to propagate more than half-way through the panel,

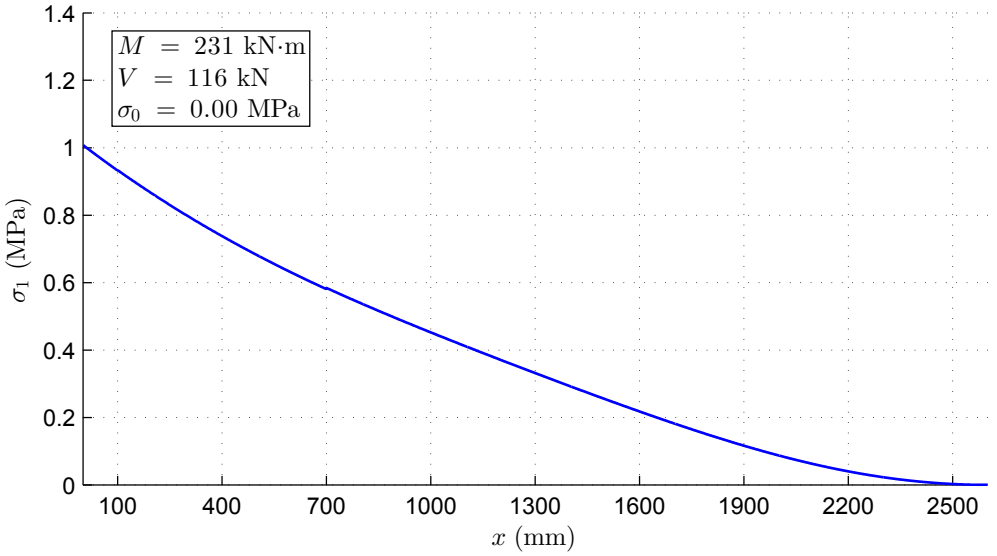

(a) Plot of principal tensile stress σ_1

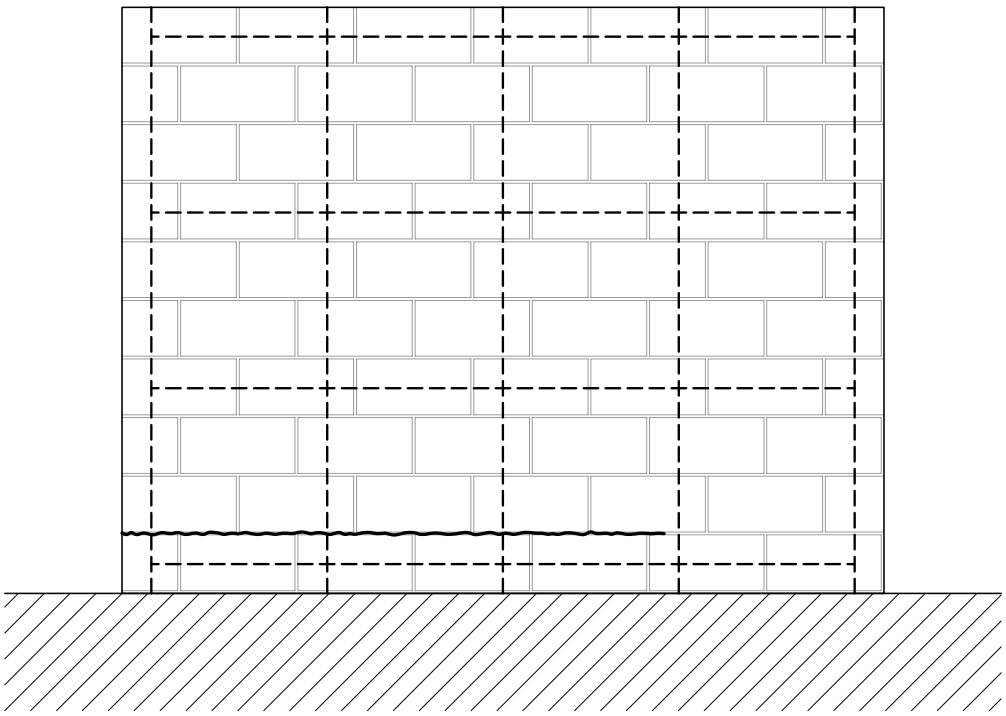

(b) Initial horizontal crack

Figure 22.4: Initiation of tension cracking

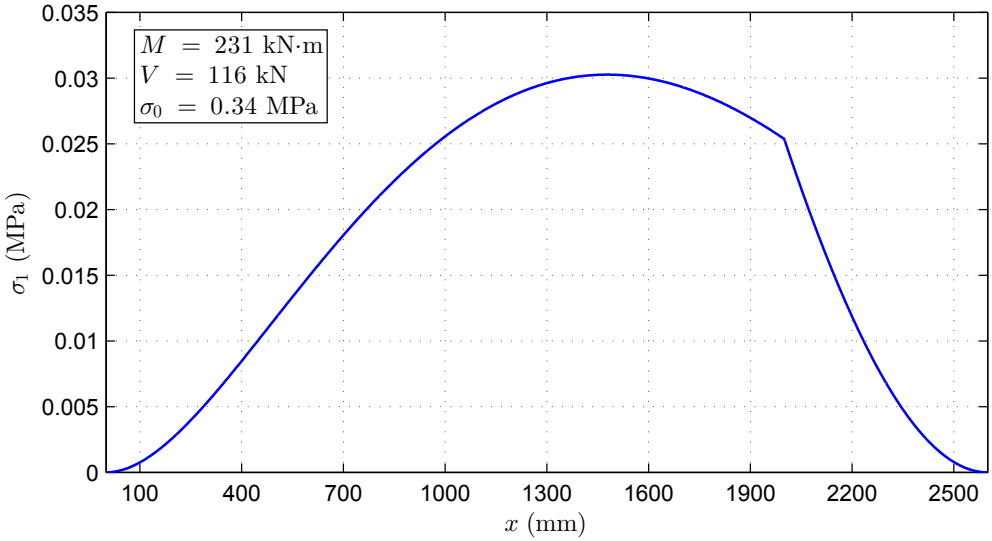

(a) Plot of principal tensile stress σ_1

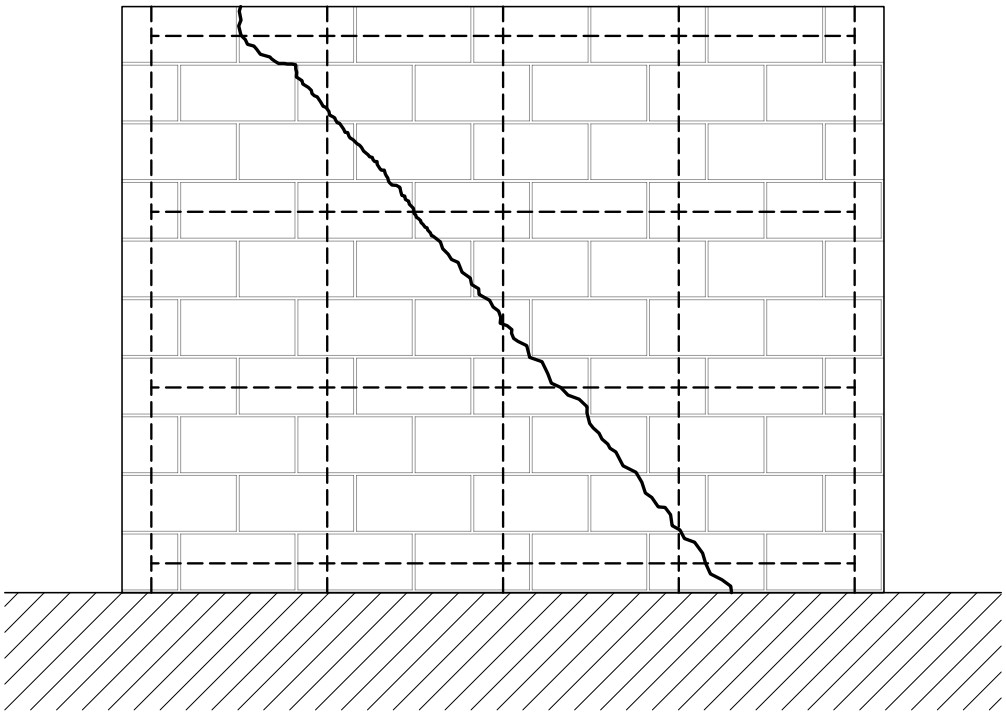

(b) Initial diagonal crack

Figure 22.5: Initiation of diagonal cracking

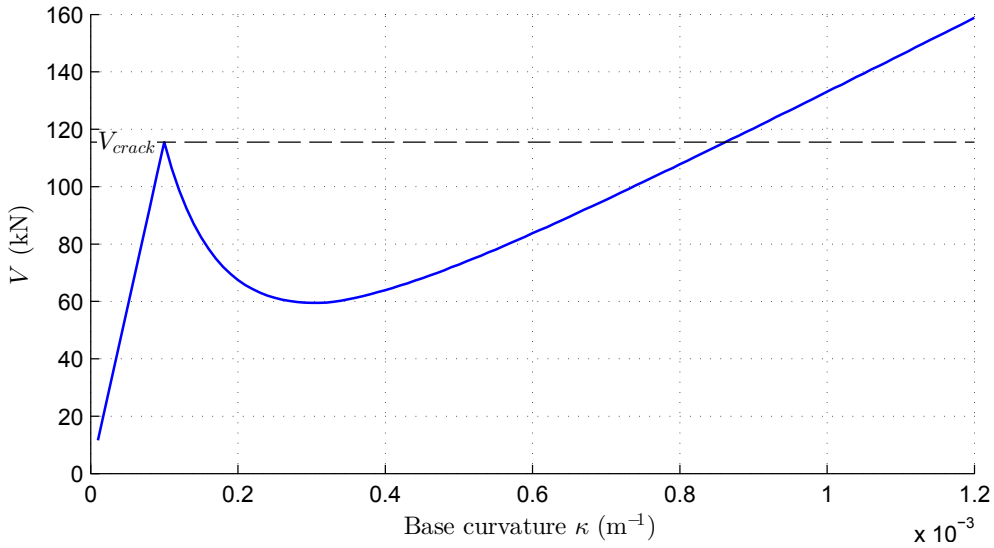

Figure 22.6: Shear load for pre- and post-cracking ($\sigma_0 = 0$)

as shown in Figure 22.4b. This release in masonry tensile strain strain results in a large release of energy which could be sufficient to rupture the flexural reinforcement bar if it is not sufficiently large.

As the lateral load continues to increase, the stress increases in the vertical reinforcement bars until each one reaches its yield stress. Each time a vertical bar begins to yield the slope of the pushover curve decreases, as shown in Figure 22.7. The force of each reinforcement bar increases the peak shear stress within the wall panel. The peak shear stress in the wall panel continues to increase with increasing lateral load until one of three events happens: toe crushing, overturning, sliding, and transition to shear behavior.

Toe crushing occurs when the compressive strain in the extreme compression fiber exceeds the crushing strain of the masonry, typically characterized by tensile splitting and spalling of the face shells. Panel overturning occurs when all of the vertical reinforcement bars have yielded, eliminating the external equilibrium forces that prevent the wall from experiencing large rotational deformations. Both failures are characterized as being flexural failure. In reality, the possibility of the latter failure mode is not typical because either the vertical reinforcement will strain harden until the toe experiences crushing or the horizontal crack will proliferate through the entire panel causing a sharp decrease in shear capacity and resulting in a sliding failure. If the normal tensile stress at the point of maximum shear exceeds the tensile rupture stress of the masonry before one

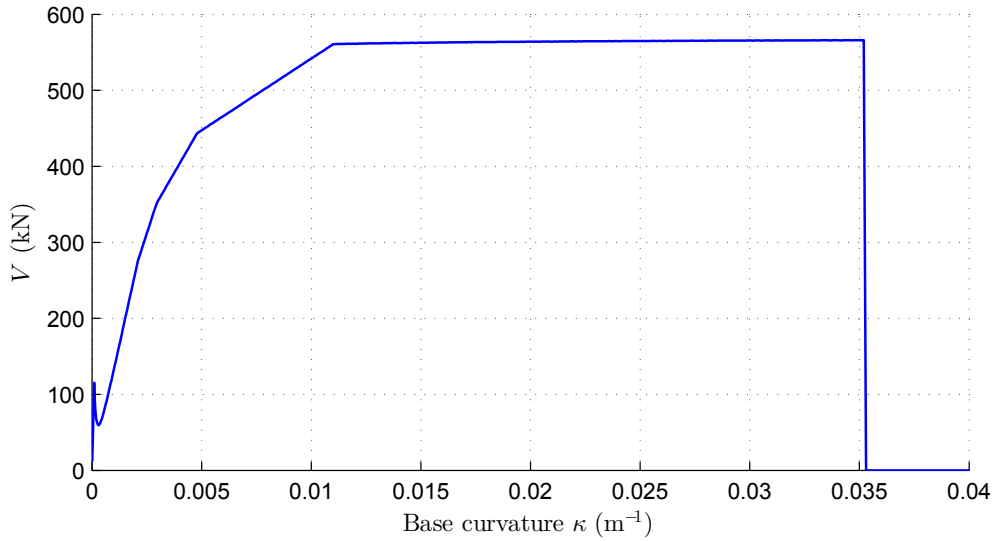

Figure 22.7: Pushover curve for shear wall model ($\sigma_0 = 0$)

of the flexural failure models occurs, then diagonal cracking will initiate at the point of maximum shear and transitioning the behavior of the panel to become shear dominated.

22.3.2 Shear Behavior

The peak shear stress in the shear wall is located along the neutral axis. When the normal tensile strain at the point of peak shear stress exceeds the rupture stress of the masonry, a diagonal crack forms within the wall panel. This separation causes a release of energy in the wall panel as the diagonal crack propagates and the vertical reinforcement crossing the crack to become engaged. Since the diagonal cracks cross the horizontal planar sections of the wall, the Euler-Bernoulli beam assumption is violated because the planar sections are no longer continuous. The segments of the wall on either side of the crack can be assumed to experience different rotational deformations, as shown in Figure 22.5b.

Diagonal cracking changes the shear stress distribution in both segments on either side of the crack, reducing the peak shear stress in the wall panel. Both segments are subsequently analyzed separately for each other and each has a distinct shear stress distribution, as shown in Figure 22.8. Since the shear contributions from the reinforcement and axial loads are no longer cumulative over the entire length of the wall, the peak shear stress in each segment is lower than before the diagonal crack formed.

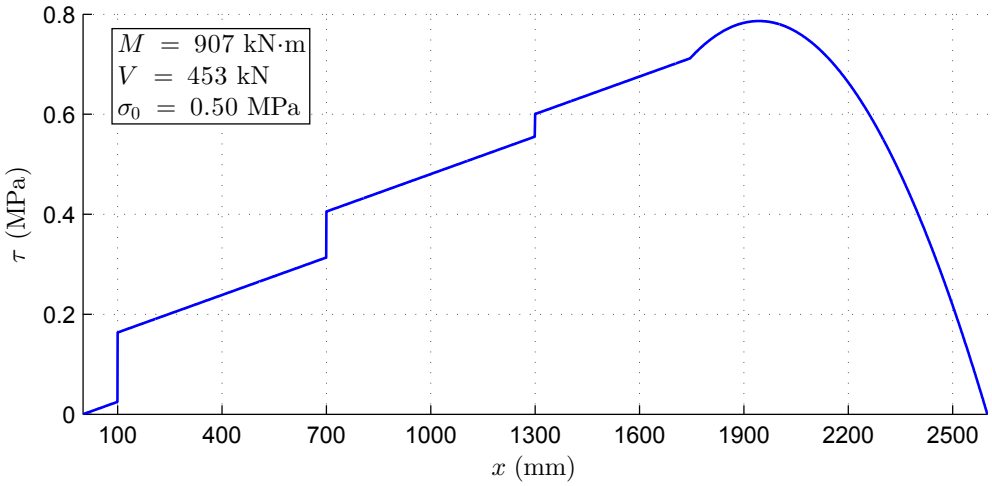

(a) Shear stress before diagonal crack formation

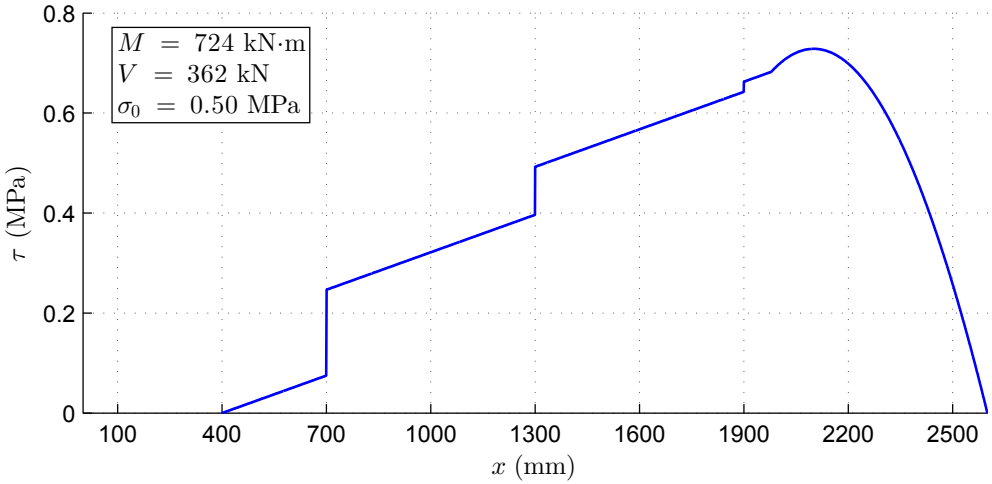

(b) Redistribution in top segment

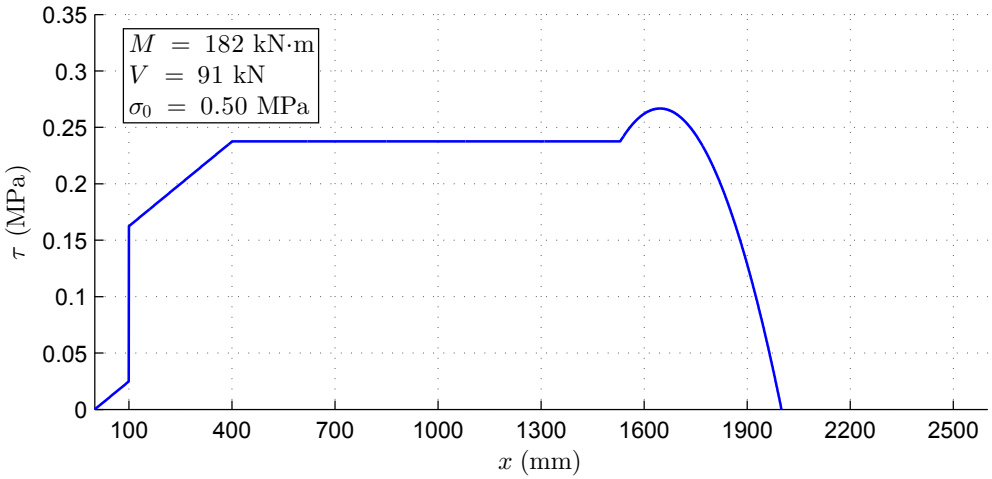

(c) Redistribution in bottom segment

Figure 22.8: Shear stress redistribution due to diagonal cracking

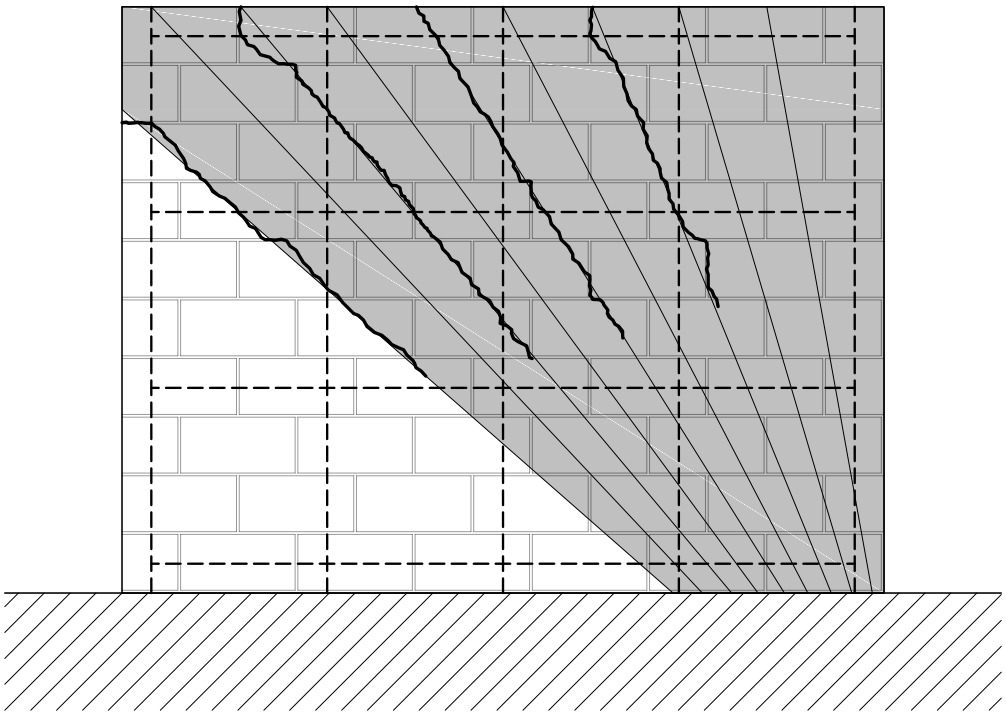

Figure 22.9: Commencement of cracking in fan-shaped strut

Within each segment the stress paths in the wall can be represented by a single fan-shaped strut extending from the top of the segment to the compression toe. The divergent compression stress fields traveling from the bottom to the top of each strut induce transverse tensile forces within the strut. As the transverse tensile stresses in the struts increases with increasing strut compression load, diagonal cracks will form separating the strut into multiple segments, as shown in Figure 22.9. Diagonal cracks will continue to form with increasing lateral load creating one strut for each vertical reinforcement bar in tension, forming the strut-and-tie model shown in Figure 22.10. At this point the tensile strain in each bar is independent of the strains in the other bars.

The shear cracking enables the interior vertical reinforcement bars to experience higher tensile strains for a given wall drift than an uncracked wall with a similar cross section. In the uncracked plane sections, the strain in the reinforcement bars increases linearly from the neutral axis to the extreme tension fiber. When the plane sections assumption is violated, the strains in the interior bars are no longer governed by their distance from the neutral axis but are governed by the principle of minimum strain energy. As a result, the flexural reinforcement at the edge of the wall does not experience the same magnitude of yielding and energy dissipation in order for the

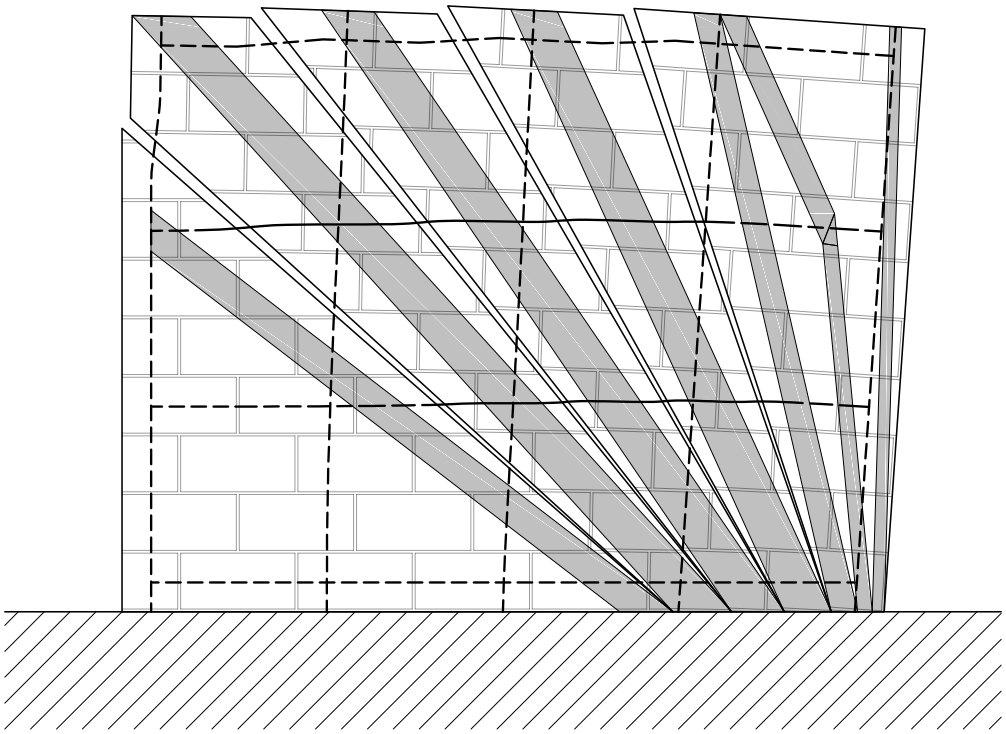

Figure 22.10: Final strut-and-tie model

interior bars to begin yielding. This is, in large measure, why walls failing in shear experience less ductility than walls failing in flexure.

Failure of walls dominated by shear behavior is caused by strut crushing, overturning, or anchorage failure. Strut crushing occurs when the strength of one of the struts is exceeded and typically occurs at the wall toe where multiple struts converge. Overturning occurs when the vertical bars in tension all reach their yield strengths and is characterized by opening of the diagonal cracks between struts. Similar to the case of flexural reinforcement, the vertical bars will begin to strain harden until the panel toe experiences crushing. Anchorage failure occurs when one of the reinforcement anchorages fails causing a loss of capacity for one strut and triggering cascading failures of the remaining struts.

22.4 Conclusions

Use of the strut-and-tie modeling procedure reveals a more detailed and correct explanation into the behavior of reinforced masonry shear walls. The observed decrease in wall ductility is due to the wall cracking which enable the interior reinforcement to become effective at lower wall drifts

and decreases the amount of yielding in the flexural reinforcement before the interior bars can be fully stressed.

CHAPTER 23. CONCLUSIONS

23.1 MSJC Shear Factor Modification

The analysis of the modification approach results led to the following conclusions:

1. Both weighted data groups appear to more-closely follow the normal distribution than the lognormal.

2. The mean performance of current MSJC shear strength equation is approximately 0.97 for predicting the strengths of fully-grouted walls, which is close enough to unity that no change to γ_g is warranted for fully-grouted walls.

3. The mean for the partially-grouted data is 0.73, which is close enough to the assumed value of 0.75 currently used for partially-grouted walls to warrant no change to γ_g for partially-grouted walls.

4. The current factors listed in the MSJC code produce a probability of failure that is 21 percent higher for partially-grouted masonry shear walls than for fully-grouted masonry shear walls. The increase in failure probability for partially-grouted walls is due to the greater variance for partially-grouted walls than for fully-grouted walls and needed to be accounted for in the design strength so that the probabilities of failure for the two grouting type are similar.

5. The value of the resistance factor ϕ_v for partially-grouted masonry shear walls was determined to be 0.73 using tolerance intervals and 0.76 using LRFD theory. Both methods produced values that were in good agreement with each other and show that the resistance factor should be taken as 0.75 for partially-grouted shear walls.

23.2 Linear Regression Modeling

The development of a new proposed shear strength model led to the following conclusions:

1. The development of the equation coefficients from Blondet et al. (1989) and Anderson and Priestley (1992) could not be replicated using the data used in the original analyses. It appears that theirs and other shear prediction models were not developed using multivariate least-squares regressions. Researchers may have used bivariate regression after assuming values for the other coefficients based on theory and engineering judgment. The coefficient values chosen by the original researchers were not the optimum values which would have minimized the error and the variance of each model.

2. The conclusion by the TCCMaR committee that the vertical reinforcement did not contribute to shear strength did not agree with the linear regression analysis results. Using the original dataset, it was detemined that the vertical reinforcement reinforcement had a statistically significant contribution to the shear strength. The significance of the vertical reinforcement strength contribution was close to that of the horizontal reinforcement. The proposed equation is given by

$$
\begin{aligned}
V_n &= V_m + V_p + V_s \\
&= \begin{cases} \left(1.8 + 0.7\dfrac{V\,l_w}{M}\right) A_{nv}\sqrt{f'_m} & \text{for fully-grouted} \\ \left(1.1 + 0.9\dfrac{V\,s_{gh}}{M}\right) A_{nv}\sqrt{f'_m} & \text{for partially-grouted} \end{cases} \\
&\quad + 0.15P \\
&\quad + 0.12\left[\frac{A_c f_{yc}}{s_c}\,l_w + \left(\frac{A_h f_{yh}}{s_h} + \frac{A_j f_{yj}}{s_j}\right) h_g\right] .
\end{aligned}
\tag{23.1}
$$

3. The regression results showed that wall shear strength is more closely correlated with the square root of the masonry compressive strength than to the compressive strength.

4. The shear strength of walls is better correlated to the reciprocal of the shear span ratio than with the shear span ratio. This relationship has been shown in previous studies but was not incorporated into the MSJC equation. The shear strength of fully-grouted walls is related to

the shear length multiplied by the shear span ratio reciprocal. The shear strength of partially-grouted walls is better correlated with the horizontal grout spacing multiplied by the shear span ratio reciprocal.

5. The results from the stepwise regression analyses showed that the parameters $\sqrt{f'_m}$ and σ_0 were common to both grouting types.

6. The masonry has the greatest contribution to the shear strength of a wall.

7. The theory that the horizontal reinforcement is directly involved in resisting the lateral shear force was determined to be invalid. The new hypothesis is that the horizontal reinforcement works by keeping the diagonal cracks in the masonry closed and enabling the masonry to transfer stresses via strut action and crack friction, similar to the role of the vertical reinforcement. Since diagonal cracking typically forms at a 45 °angle, the horizontal and vertical reinforcement are equally effective in restricting the diagonal cracks from opening and have the same coefficient.

8. The MSJC limit equation worked fairly well for because the MSJC equation tended to over-predict the strength for stronger walls. The MSJC limit equation does not provide a useful upper bound for the proposed model. A new limit was developed to use with the proposed shear equation to better match the performance of the model and represent the behavior of the components of the shear wall.

9. Comparison of the shear equations show a better fit for the proposed model over the MSJC shear strength equation. The proposed model shows an improvement in the variance of the predictions, with nearly every prediction laying closer the the perfect-fit-line than the MSJC predictions.

10. The benefit of the proposed models is that it contains coefficients that were specifically developed for use with partially-grouted shear walls. The parameters and coefficients in the proposed model better represent how each aspect of the walls affects their overall behavior than the grouted wall factor approach because they were developed directly from the experimental data.

23.3 Strut-and-Tie Modeling

The development of the strut-and-tie modeling methodology provided the greatest insight into how masonry shear walls perform. The analysis led to the following conclusions.

1. The values of β_s from ACI 318 appeared to also work for masonry models. Further investigation and validation of the β_s values from ACI 318 for use with masonry requires a text matrix of specimen groups each with similar strut layouts but varying levels of reinforcement and material strengths.

2. Strut-and-tie models for the fully-grouted specimens predict strengths that are closer to the experimental strengths and have lower variation when the strut inclination factor is omitted. Conversely, strut-and-time models for the partially-grouted specimens produce better predicted strengths when the strut inclination factor is included. The reason for this disparity is likely explained by Drysdale and Hamid (1980) who observed that the grouted cores decreased the level of anisotropy introduced by the bed joints by facilitating the transfer of shear stresses between the different courses of masonry.

3. The end cells of partially grouted walls were always grouted and the effective thickness of the wall for the final half-unit length was much greater than that of the ungrouted wall panels. The stress fields in the grouted jamb are able to take a steeper descent to the wall toe because of the greater shear area available in the jamb. A toe extension factor l_x was found to account for the observed difference between predicted and observed wall strengths.

4. The ACI 318 limits placed on reinforced concrete strut-and-tie models are not compatible with modeling masonry shear walls. Additional research should be conducted to either determined whether new limits should be imposed.

5. Strut-and-tie models provide more accurate and precise shear strength predictions than either the MSJC or the proposed shear equation. This is associated with the ability of the strut-and-tie modeling procedure to account for the geometric particularities of each wall. The robustness of the strut-and-tie modeling procedure was shown to apply also to shear walls with openings.

6. Researchers up to this point have used an "equivalent truss model" for performing strut-and-tie analysis. The full strut-and-tie modeling methodology is more accurate and precise than "equivalent truss models" because it can be more easily generalized to all arrangements of reinforced masonry shear walls.

7. Strut-and-tie modeling provides a more correct representation of the behavior of masonry shear walls and provides insights into previously unexplained phenomena. These includes a mechanical explanation of why the shear strength appears to be better correlated to the square root of the compressive strength, how the horizontal and vertical reinforcement contribute to shear strength, and why sections do not remain plane.

8. Strut-and-tie modeling is a valid tool for masonry shear wall analysis and design. The criterion for selecting the optimum strut-and-tie model is that the model which minimizes the ratio of reinforcement area to shear strength.

REFERENCES

AASHTO (2012). *LRFD Bridge Design Specifications*. American Association of State Highway and Transportation Officials (AASHTO), Washington.

Abaqus (2014). *Abaqus 6.14-AP*. Dassault Systemes Simulia Corp., Providence, RI.

Abrams, D. P. (1988). "Dynamic and static testing of reinforced concrete masonry structures." *Proceedings of the Ninth World Conference on Earthquake Engineering*, vol. 6, 18–22. Tokyo-Kyoto.

Abrams, D. P. and Kreger, M. E. (1982). "Modelling of reinforced concrete members at small scales." *Proceedings of the Seventh World Conference on Earthquake Engineering*, 585–592. Istanbul.

Abrams, D. P. and Tangkijngamvong, S. (1984). "Dynamic response of reduced-scale models and reinforced concrete structures." *Proceedings of the Eighth World Conference on Earthquake Engineering*, 371–378. San Francisco.

ACI 318 (2011). *Building Code Requirements for Structural Concrete (ACI 318-02) and Commentary (ACI 318R-02)*. American Concrete Institute (ACI), Farmington Hills, MI.

ACI-ASCE (1988). "Building code requirements for masonry structures (aci 530–88, and asce 5–88)."

Addessi, D., Mastrandrea, A., and Sacco, E. (2014). "An equilibrated macro-element for nonlinear analysis of masonry structures." *Engineering Structures*, 70, 82–93.

AISC (1986). *Specification for Structural Steel Buildings–Load and Resistance Factor Design*. American Institute of Steel Construction (AISC), Chicago.

Al-Chaar, G. K. and Mehrabi, A. (2008). "Constitutive models for nonlinear finite element analysis of masonry prisms and infill walls." *Tech. Rep. ERDC/CERL TR-08-19*, Construction Engineering Research Laboratory, US Army Corps of Engineers, Washington.

Anderson, D. L. and Priestley, M. J. N. (1992). "In plane shear strength of masonry walls." *Proceedings of the 6th Canadian Masonry Symposium*, vol. 1, 223–234. Saskatoon, SK, Canada.

ANSI Standard A58.1 (1982). *Minimum Design Loads for Buildings and Other Structures*. American National Standards Institute (ANSI), New York.

AS 3700 (2011). *Code of practice for the use of masonry–Part 2: Structural use of reinforced and prestressed masonry*. Standards Australia Ltd, Sydney.

ASCE 7 (2010). *Minimum Design Loads for Buildings and Other Structures*. American Society of Civil Engineers (ASCE), Reston, VA.

ASCE-ACI (1998). "Recent approaches to shear design of structural concrete." *Journal of Structural Engineering*, 124(12), 1375–1417.

Astbury, N. F. and West, H. W. H. (1969). *Tests on Storey-Height Brickwork Panels and Development of Site Control Test for Brickwork*, 216–225. Gulf Publishing, Co., Houston.

ASTM C1314 (2014). "Standard test method for compressive strength of masonry prisms." *Book of Standards Volume: 04.05*. ASTM International, West Conshohocken, PA.

ASTM C270 (2014). "Standard specification for mortar for unit masonry." *Book of Standards Volume: 04.05*. ASTM International, West Conshohocken, PA.

ASTM C34 (2014). "Standard specification for structural clay load-bearing wall tile." *Book of Standards Volume: 04.05*. ASTM International, West Conshohocken, PA.

ASTM C652 (2014). "Standard specification for hollow brick (hollow masonry units made from clay or shale)." *Book of Standards Volume: 04.05*. ASTM International, West Conshohocken, PA.

ASTM C90 (2014). "Standard specification for loadbearing concrete masonry units." *Book of Standards Volume: 04.05*. ASTM International, West Conshohocken, PA.

ASTM:C1072 (2014). "Standard test methods for measurement of masonry flexural bond strength." *Book of Standards Volume: 04.05*. ASTM International, West Conshohocken, PA.

Bažant, Z. P. (1997). "Scaling of quasibrittle fracture: asymptotic analysis." *International Journal of Fracture*, 83(1), 9–40.

Bažant, Z. P. (2009). "Universal size effect law and effect of crack depth on quasi-brittle structure strength." *Journal of Engineering Mechanics*, 135(2), 78–84.

Bažant, Z. P. and Yu, Q. (2006). "Reliability, brittleness, covert understrength factors, and fringe formulas in concrete design codes." *Journal of Structural Engineering*, 132(1), 3–12.

Bagenal, P. (1980). *The illustrated atlas of the world's great buildings: a history of world architecture from the classical perfection of the Parthenon to the breathtaking grandeur of the skyscraper*. Leisure Books, London.

Bennett, R. M., Boyd, K. A., and Flanagan, R. D. (1997). "Compressive properties of structural clay tile prisms." *Journal of Structural Engineering*, 123(7), 920–926.

Bernoulli, J. (1713). *Ars Conjectandi*. Thurnisius, Basilea.

BIA (1969). *Building Code Requirements for Engineered Brick Masonry*. Brick Institute of America (BIA), McLean, VA.

Bienaymé, I. (1852). "Sur la probabilité des erreurs d'après la méthod des moindres carrés." *Journal de Mathématiques Pures et Appliquées,*, 171, 33–78.

Bienaymé, I. (1853). "Sur les differences qui distinguent l'interpolation de m. cauchy de la méthod des moindres carrés, et qui assurent la supériorité de cette méthode." *Journal de Mathématiques Pures et Appliquées,*, 181, 299–308.

Bischoff, P. H. and Perry, S. H. (1991). "Compressive behaviour of concrete at high strain rates." *Materials and Structures*, 24(6), 425–450.

Blondet, J. M., Mayes, R. L., Kelly, T., Villablanca, R., and Klinger, R. E. (1989). "Performance of engineered masonry in the Chilean earthquake of March 3, 1985: implications for U.S. design practice." *Tech. Rep. 89-2*, University of Texas at Austin, Austin, TX.

Blume, J. A. and Proulx, J. (1968). "Shear in grouted brick masonry wall elements." *Tech. rep.*, Western States Clay Products Association, San Francisco.

Borenstein, M. and Hedges, L. V. (2009). *Introduction to Meta-Analysis*. John Wiley & Sons, Hoboken, NJ.

Boscovich, R. J. (1760). "Notes of b stay." *Philosophiae Recentioris, II*. (French translation in Boscovich and Maire 1770).

Boscovich, R. J. and Maire, C. (1755). *De Litteraria Expeditione per Pontificam ditionem ad dimentiendas duas Meridiani gradus*. Palladis, Rome. (French translation in Boscovich and Maire 1770).

Boult, B. F. (1979). "Concrete masonry prism testing." *American Concrete Institute Journal, Proceedings*, 76(4), 513–536.

Bowditch, N. (1809). "Observations of the comet of 1807." *Memoirs of the American Academy of Arts and Sciences*, 3(1), 1–17.

Bowditch, N. (1815). "Elements of the orbit of the comet of 1811." *Memoirs of the American Academy of Arts and Sciences*, 32(2), 313–325.

Bower, A. F. (2011). *Applied mechanics of solids*. CRC Press, Boca Raton, FL. (Available online at: http://solidmechanics.org/).

Braguim, J. R. (1989). *Contributions to the study of stiffening in steel structures for high rise buildings*. Master's thesis, Polytechnic School, University of São Paulo, São Paulo. (in Portuguese).

Brammer, D. R. (1995). *The lateral force-deflection behaviour of nominally reinforced concrete masonry walls*. Master's thesis, University of Auckland, Auckland.

Brunner, J. D. (1996). *Shear Strength of Reinforced Masonry Walls*. Master's thesis, University of Colorado, Boulder, Boulder, CO.

Brunner, J. D. and Shing, P. B. (1996). "Shear strength of reinforced masonry walls." *TMS Journal*, 14(1), 65–77.

BS 5628-2 (2000). *Code of practice for the use of masonry–Part 2: Structural use of reinforced and prestressed masonry*. British Standards Institution, London.

Carroll, R. J. and Ruppert, D. (1988). *Transformation and Weighting in Regression*. Chapman and Hall, New York.

Cauchy, A. (1835). "Mémoire sur l'interpolation." *Reprinted in Journal de Mathématiques Pures et Appliquées*, 2, 193–205.

Cauchy, A. (1853a). "Mémoire sur l'évaluation d'inconnues déterminées par un grand nombre d'équations approximatives du premier degré." *Comptes rendues hebdomadaires des scéances de l'Académie des sciences*, 36, 1114–1122.

Cauchy, A. (1853b). "Sur la probabilité des erreurs qui affectent des résultats moyens d'observations de même nature." *Comptes rendues hebdomadaires des scéances de l'Académie des sciences*, 37, 264–272.

Cauchy, A.-L. (1853c). "Mémoire sur les résultats moyens d'un très grand nombre observations." *Comptes rendues hebdomadaires des scéances de l'Académie des sciences*, 37, 381–385.

CEB (1988). "Concrete structures under impact and impulsive loading." *Tech. Rep. Synthesis Report/Bulletin d'Information No. 178*, Comité Euro-International du Béton (CEB), Geneva.

Charry, J. (2010). *Experimental study on the response of brick masonry walls subjected to shear forces*. Ph.D. thesis, Universitat Politècnica de Catalunya, Barcelona.

Chatterjee, S. and Hadi, A. S. (2006). *Regression Analysis by Example*. John Wiley & Sons, Hoboken, NJ.

Chebyshev, P. L. (1859). "Sur l'interpolation par la méthode des moindres carrés." *Mémoires de l'Académie de Science de St Pétersbourg*, 115, 1–24.

Chebyshev, P. L. (1864). "Sur l'interpolation." *Mémoires de l'Académie impériale de science de St Pétersbourg*, 4(5).

Chebyshev, P. L. (1875). "Sur l'interpolation des valeurs équidistantes." *Mémoires de l'Académie impériale de science de St Pétersbourg*, 25(5).

Chebyshev, P. L. (1887). "Sur deux théorèmes relatifs aux probabilités." *Bulletin physio–mathématique de l'Académie impériale de Science de St Pétersbourg*, 115, 1–24.

Chen, S. W., Hidalgo, H. A., Mayes, L. R., Clough, R. W., and McNiven, H. M. (1978). "Cyclic loading of masonry single piers, vol 2–height to width ratio of 1." *Tech. Rep. UCB/EERC–78/28*, University of California, Berkeley, CA.

Cohen, J. (1988). *Statistical Power Analysis for the Behavioral Sciences, 2nd ed*. Erlbaum Associates, Hillsdale, NJ.

Collins, M. P. and Mi (1988). "Shear and torsion design of prestressed and non-prestressed concrete beams." *Journal of the Prestressed Concrete Institute*, 25(5), 32–100.

Commission, C. S. S. (2009). "The field act and its relative effectiveness in reducing earthquake damage in california public schools." *Tech. Rep. CSSC 09-02*, State of California Seismic Safety Commission, Sacramento, CA.

Cotes, R. (1722). *Aestimatio Errorum in Mixtia Mathesi, per Variationes Partium Trianguli Plani et Sphaerici*. Lemgoviae.

CSA S304.1 (2004). *Design of Masonry Structures*. Canadian Standards Association, Mississauga.

Curtin, W. G. and Hendry, A. W. (1969). *Design and Construction of Slender Wall Brickwork Buildings*, 329–335. Gulf Publishing, Co., Houston.

Da Porto, F., Mosele, F., and Modena, C. (2011). "In–plane cyclic behaviour of a new reinforced masonry system: Experimental results." *Engineering Structures*, 33(9), 2584–2596.

Davis, C. L. (2008). *Evaluation of Design Provisions for In–Plane Shear in Masonry Walls*. Master's thesis, Washington State University, Pullman, WA.

Dhanasekar, M. (2011). "Shear in reinforced and unreinforced masonry: Response, design and construction." *Procedia Engineering*, 14, 2069–2076.

Dillon, P. B. and Fonseca, F. S. (2014a). "Analysing masonry research data in matrix form." *Proceedings of the 9th International Masonry Conference*, 1592. Guimarães, Portugal.

Dillon, P. B. and Fonseca, F. S. (2014b). "Preliminary study into the standardisation of masonry shear wall reporting methods." *Proceedings of the 9th International Masonry Conference*, 1593. Guimarães, Portugal.

Drysdale, R. G. and Hamid, A. A. (1980). "Concrete masonry under combined shear and compression along the mortar joints." *Journal of the American Concrete Institute*, 77(5), 314–320.

Drysdale, R. G. and Hamid, A. A. (2008). *Masonry Structures: Behavior and Design, 3e*. The Masonry Society, Boulder, CO.

Eisenhart, C. (1961). *Roger Joseph Boscovich and the combination of observations*. Allen & Unwin, London.

Ellingwood, B. (2000). "Lrfd: Implementing structural reliability in professional practice." *Engineering Structures*, 22, 106–115.

Ellingwood, B. and Galambos, T. V. (1982). "Probability-based criteria for structural design." *Structural Safety*, 1, 15–26.

Ellingwood, B., Galambos, T. V., MacGregor, J. G., and Cornell, C. A. (1980). "Development of a probability based load criterion for american national standard a58." *Tech. Rep. NBS Special Publication 557*, National Bureau of Standards, Gaithersburg, MD.

Ellis, R. L. (1844). "On the method of least squares." *Transactions, Cambridge Philosophical Society*, 8, 204–219.

Elmapruk, J. H. (2010). *Shear Strength of Partially Grouted Squat Masonry Shear Walls*. Master's thesis, Washington State University, Pullman, WA.

Escrig, F. (2006). *The great structures in Architecture: Antiquity to Baroque*. WIT Press, Boston.

Esteva, L. (1966). "Behavior under alternating loads of masonry diaphragms framed by reinforced concrete members." *Symposium on the effects of repeated loading on material and structural elements*. Mexico City.

Euler, L. (1749). *Recherches sur la question des inégalités du movement de Saturne et de Jupiter, sujt propose pour le prix de l'année 1748, par l'Académie royale des sciences de Paris*, vol. 25, 45–157. Basel, Turcini, Romania.

Fattal, S. G. (1993). "Strength of partially grouted masonry walls under lateral loads." *Tech. Rep. NISTIR 5147*, National Institute of Standards and Technology, Gaithersburg, MD.

Fattal, S. G. and Cattaneo, L. (1976). *Structural Performance of Masonry Walls Under Compression and Flexure*. National Bureau of Standards, Washington.

Fattal, S. G. and Cattaneo, L. (1977). *Evaluation of Structural Properties of Masonry in Existing Buildings*. National Bureau of Standards, Washington.

Fattal, S. G. and Todd, D. R. (1991). "Ultimate strength of masonry shear walls: Predictions vs test results." *Tech. Rep. NISTIR 4633*, National Institute of Standards and Technology, Gaithersburg, MD.

Fieller, E. C. (1932). "The distribution of the index in a normal bivariate population." *Biometrika*, 24(3/4), 428–440.

Fisher, R. A., Sir (1912). "On an absolute criterion for fitting frequency curves." *Messenger of Mathematics*, 41, 155–160.

Fisher, R. A., Sir (1915). "Frequency distribution of the values of the correlation coefficient in samples from an indefinitely large population." *Biometrika*, 10, 507–521.

Fisher, R. A., Sir (1921). "On the 'probable error' of a coefficient of correlation deduced from a small sample." *Metron International Journal of Statistics*, 1, 3–32.

Fisher, R. A., Sir (1922). "On the mathematical foundations of theoretical statistics." *Philosophical Transactions of the Royal Society of London*, 222, 309–368.

Fisher, R. A., Sir (1925). "Applications of 'student's' distribution." *Metron International Journal of Statistics*, 5(3), 90–104.

Fisher, R. A., Sir (1928). "On a distribution yielding the error functions of several well know statistics." *Proceedings of the International Congress of Mathematicians Vol. 2*, 805–803. Toronto.

Fletcher, B., Sir (1996). *Sir Banister Fletcher's a history of architecture*. C Scribner's Sons, New York.

Foraboschi, P. and Vanin, A. (2013). "Non-linear static analysis of masonry buildings based on a strut-and-tie modeling." *Soil Dynamics and Earthquake Engineering*, 55, 44–58.

Francis, A. J., Horman, C. B., and Jerrems, L. E. (1970). "The effect of joint thickness and other factors on the compressive strength of brickwork." *Proceedings of the Second International Brick Masonry Conference*, 31–37. British Ceramic Research Association, Stoke-on-Trent, England.

Fujisawa, M. (1985). "Effect of shear span ratio." *Proceedings of the 1st Joint Technical Coordinating Committee on Masonry Research*. Tokyo.

Galambos, T. V. and Ravindra, M. K. (1978). "Properties of steel for use in lrfd." *Journal of the Structural Division, Proceedings of the American Society of Civil Engineers*, 104(9), 1459–1468.

Galton, F., Sir (1875). "Statics by intercomparison, with remarks on the law of frequency of error." *Philosophical Magazine*, 49(4), 33–46.

Galton, F., Sir (1877). "Typical laws of heredity." *Nature*, 15, 492–495, 512–514, 532–533.

Galton, F., Sir (1879). "The geometric mean, in vital and social statistics." *Proceedings, Royal Society of London,*, 29, 365–367.

Galton, F., Sir (1889a). "Co–relations and their measurement, chiefly from anthropometric data." *Proceedings, Royal Society of London*, 45, 135–145.

Galton, F., Sir (1889b). *Natural Inheritance*. Macmillan, London.

Galton, F., Sir (1899). "A geometric determination of the median value of a system of normal variants, from two of its entities." *Nature*, 61, 102–104.

Ganz, H. R. and Thürlimann, B. (1983). "Strength of brick walls under normal and shear forces." *Proceedings of the 8th International Symposium on Load-Bearing Brickwork*, 27–29. London.

Ganz, H. R. and Thürlimann, B. (1984). "Tests on masonry walls subjected to normal and shear forces." *Tech. Rep. 7502–4*, Institut für Baustatik und Konstruktion ETH, Zürich. (in German).

Gauss, C. F. (1809). *Theoria motus corporum coelestium in sectionibus conicis solem ambientium*. Perthes et Besser, Hamburg.

Gauss, C. F. (1823). "Theoria combinationis observationum erroribus minimis obnoxiae pars prior, et pars posterior." *Königliche Gesellschaft der Wissenschaften zu Göttingen*, 5, 33–90.

Geary, R. C. (1930). "The frequency distribution of the quotient of two normal variates." *Journal of the Royal Statistical Society*, 93(3), 442–446.

Ghanem, G. M., Essawy, A. S., and Hamid, A. A. (1992). "Effect of steel distribution on the behavior of partially reinforced masonry walls." *Proceedings of the 6th Canadian Masonry Symposium*, vol. 1, 365–376. Saskatoon, SK, Canada.

Ghanem, G. M., Salama, A. E., Elmagd, S. A., and Hamid, A. A. (1993). "Effect of axial compression on the behavior of partially reinforced masonry shear walls." *Proceedings of the 6th North American Masonry Conference*, 1145–1157. Philadelphia.

Glaisher, J. W. L. (1872). "On the law of facility of errors of observations and on the method of least squares." *Memoires of the Royal Astronomical Society*, 39, 75–124.

Gram, J. P. (1879). *Om Rœkkeudviklinger, bestemte ved hjælp af de mindste Kvadraters Methode*. Høst, Copenhagen.

Grimm, C. T. (2002). "Quality control of concrete masonry compressive strength." *TMS Journal*, 20(1), 81–84.

Guo, P. (1991). *Investigation and Modelling of the Mechanical Properties of Masonry*. Ph.D. thesis, McMaster Univeristy, Hamilton, Ontario.

Haach, V. G., Vasconcelos, G., and Lourenço, P. B. (2007). "Cyclic behaviour of truss type reinforced concrete masonry walls." *7o Congresso de Sismologia e Engenharia Sísmica*. Universidade do Porto, Faculdade de Engenharia, Porto, Portugal.

Haach, V. G., Vasconcelos, G., and Lourenço, P. B. (2010a). "Experimental analysis of reinforced concrete block masonry walls subjected to in–plane cyclic loading." *Journal of Structural Engineering*, 136(4), 452–462.

Haach, V. G., Vasconcelos, G., Lourenço, P. B., and Mohamad, G. (2010b). "Influence of the mortar on the compressive behavior of concrete masonry prisms." *Mecânica Experimental*, 18, 79–84.

Haider, W. (2007). *Inplane Response of Wide Spaced Reinforced Masonry Shear Walls*. Ph.D. thesis, Central Queensland University, North Rockhampton, QLD, Australia.

Haider, W. and Dhanasekar, M. (2004). "Experimental study of monotonically loaded wide spaced reinforced masonry shear walls." *Australian Journal of Structural Engineering*, 52, 101–118.

Hald, A. (1998). *A History of Mathematical Statistics From 1750 to 1930*. Wiley, New York.

Hald, A. (2007). *A History of Parametric Statistical Inference from Bernoulli to Fisher 1713–1935*. Springer, New York.

Hall, I. J. and Sampson, C. B. (1973). "Tolerance limits for the distribution of the product and quotient of normal variates." *Biometrics*, 29(1), 109–119.

Hamedzadeh, A. (2013). *On the Shear Strength of Partially Grouted Concrete Masonry*. Master's thesis, University of Calgary, Calgary.

Hamid, A. A., Chaderakeerthy, S. R., and Elnawawy, O. A. (1992). "Flexural tensile strength of partially grouted concrete masonry." *Journal of Structural Engineering*, 118(12), 3377–3392.

Hamid, A. H., Drysdale, R. G., and Heidebrecht, A. C. (1978). "Effect of grouting on the strength characteristics of concrete block masonry." Noland, J. L. and Amrhein, J. E., eds., *Proceedings of the North American Masonry Conference*, 11, 11–1–11–17. University of Colorado, The Masonry Society, Boulder, CO.

Hao, B., H Tarasov (2008). "Experimental study of dynamic material properties of clay brick and mortar at different strain rates." *Australian Journal of Structural Engineering*, 8(2), 117–131.

Hayya, J., Armstrong, D., and Gressis, N. (1975). "A note on the ratio of two normally distributed variables*." *Management Science*, 21(11), 1338–1341.

Hedstrom, R. O. (1961). "Load tests of patterned concrete masonry walls." *ACI Journal*, 32(10), 12965–1286.

Hegemier, G. A., Krishnamoorthy, G., Nunn, R. O., and Moorthy, T. (2003). *Lea's Chemistry of Cement and Concrete*. Butterworth–Heinemann, Oxford.

Hegemier, G. A., Krishnamoorthy, G., Nunn, R. O., and Moorthy, T. V. (1978). "Prism tests for the compressive strength of concrete masonry." *Proceedings of the North American Masonry Conference*, 18, 18–1–18–17. Boulder, CO.

Hess, R. L. (1979). "The shakeout scenario supplemental study: Unreinforced masonry (urm) buildings." *Tech. Rep. U.S. Geological Survey Circular 1324, California Geological Survey*

Special Report 207 version 1.0, U.S. Geological Survey and California Geological Survey, Pasadena, CA and Sacramento, CA.

Hidalgo, P. A., Mayes, R. L., McNiven, H. D., and Clough, R. W. (1978). "Cyclic loading tests of masonry single piers, vol. 1–height to width ratio of 2." *Tech. Rep. UCB/EERC–78/27*, University of California, Berkeley, CA.

Hidalgo, P. A., Mayes, R. L., McNiven, H. D., and Clough, R. W. (1979). "Cyclic loading tests of masonry single piers, vol. 3–height to width ratio of 0.5." *Tech. Rep. UCB/EERC–79/12*, University of California, Berkeley, CA.

Hilsforf, H. K. (1969). "An investigation into the failure mechanism of brick masonry under axial compression in designing." *Designing, engineering, and constructing with masonry products*, 31–41. Gulf Publishing, Houston.

Hinkley, D. V. (1969). "On the ratio of two correlated normal random variables." *Biometrika*, 56(3), 635–639.

Igarashi, I. and Matsumura, A. (1984). "Effects of height–to–length ratio on shear strength of reinforced hollow concrete block loadbearing walls." *Transactions, Architectural Institute of Japan*, 59(10), 1783–1784. (in Japanese).

Igarashi, I., Matsumura, A., and Shigenobu, K. (1988). "Effectiveness of shear reinforcement in fully grouted clay brick masonry walls." *Transactions, Architectural Institute of Japan*, 63(10), 1229–1290. (in Japanese).

Ingham, J. M., Davidson, B. J., Brammer, D. R., and Voon, K. C. (2001). "Testing and codification of partially grout–filled nominally–reinforced concrete masonry subjected to in–plane cyclic loads." *TMS Journal*, 191, 83–96.

Irwin, J. O. and Rest, E. D. V. (1961). "Edgar charles fieller, 1907-1960." *Journal of the Royal Statistical Society: Series A (General)*, 124(2), 275–277.

Isoishi, H., Teshigawara, M., Nakaoka, A., and Terada, T. (1988). "Experimental study on seismic performance of reinforced masonry beams." *Proceedings of the Ninth World Conference on Earthquake Engineering*, vol. 6, 151–156. Tokyo-Kyoto.

Johal, L. S. P. and Anderson, E. D. (1988). *Shear Strength of Masonry Piers Under Cyclic Loading*, 18–32.

Jorquera G, L. (1963). "Estudio experimental sobre la resistencia de muros de albañileria sometidos a cargas horizontales." *Primeras Jornadas Chilenas de Sismologia e Ingenieria Antisismica*, 3, 1–30.

Kaminosono, T., Teshigawa, M., Hiraishi, H., Fujisawa, M., and Nakaoka, A. (1988). "Experimental study on seismic performance of reinforced masonry walls." *Proceedings of the Ninth World Conference on Earthquake Engineering, Vol. VI*. Tokyo-Kyoto.

Kasparik, T. (2009). *Behaviour of Partially Grouted Nominally Reinforced Masonry Shear Walls under Dynamic Loading*. Master's thesis, McMaster University, Hamilton, ON, Canada.

Korany, Y. and Glanville, J. (2005). "Comparing masonry compressive strength in various codes." *Concrete International*, 27(7), 35–39.

Krishnamoorthy, K. and Mathew, T., eds. (2009). *Statistical Tolerance Regions: theory, application, and computation*. John Wiley & Sons, Hoboken, NJ.

Kupfer, H. (1964). "Erweiterung der mohrsch'schen fachwerkanalogie mit hilfe des prinzips vom minimum der formanderungsarbeit (expansion of morsch's truss analogy by application of the principle of minimum strain energy)." *CEB Bulletin*, 40.

Lambert, J. H. (1765). "Theorie der zuverlässigkeit der beobachtungen and versuche." *Beyträge*, 1, 424–448.

Laplace, P. S. (1774). "Mémoire sur la probabilité des causes par les énènements." *Mémoires de l'Académie Royale de Science de Paris (Savants Etrangers)*, 6, 621–656.

Laplace, P. S. (1786). "Mémoire sur les approximations des formules qui sont fonctions de très grand nombres." *Mémoires de l'Académie Royale des Sciences de Paris*, 1–88.

Laplace, P. S. (1793). "Sur quelques points du système du monde." *Mémoires de l'Académie Royale des Sciences de Paris*, 1–87.

Laplace, P. S. (1799). *Mécanique céleste*, vol. 2. Duprat, Paris.

Laplace, P. S. (1810). "Mémoire sur les approximations des formules qui sont fonctions de très grands nombres et sur leur application aux probabilités." *Mémoires de l'Académie Royale des Sciences de Paris*, 353–415.

Laplace, P. S. (1812). *Théorie analytique des probabilities*. Courcier, Paris.

Lee, J. and Fenves, G. L. (1998). "Plastic-damage model for cyclic loading of concrete structures." *Journal of Engineering Mechanics*, 124(8), 892–900.

Legendre, A. M. (1798). *Méthode pour déterminer la longueur exacte du quart du Méridien, d'après les observations faites pour la mesure de l'arc compris entre Denkerque et Barcelonne*.

Legendre, A. M. (1805). *Nouvelles méthodes pour la détermination des orbites des comètes*. Courcier, Paris.

Levin, J. R. (1998). "What if there were no more bickering about statistical significance tests?" *Research in the Schools*, 5(2), 43–53.

Liang, Q. Q., Uy, B., and Steven, G. P. (2002). "Performance-based optimization for strut-tie modeling of structural concrete." *Journal of Structural Engineering*, 128(6), 815–823.

Liapounov, A. M. (1901). "Nouvelle forme du théorème sur la limite de probabilité." *Mémoires de l'Académie Impériale de Science de St Pétersbourg*, 12(8), 1–24.

Liu, L., Tang, D., and Zhai, X. (2006). "Failure criteria for grouted concrete block masonry under biaxial compression." *Advances in Structural Engineering*, 9(2), 229–239.

Lobato, M. E. (2009). *Simple method for the analysis of hollow masonry walls subjected to in plane loading*. Ph.D. thesis, Universitat Politècnica de Catalunya, Barcelona. (in Spanish).

Lotfi, H. R. and Shing, P. B. (1991). "An appraisal of smeared crack models for masonry shear wall analysis." *Computers & Structures*, 41(3), 413–425.

Lourenço, P. B., Alvarenga, R. C., and Silva, R. M. (2006). "Validation of a simplified model for the design of masonry infilled frames." *Masonry International*, 19.

Lubliner, J., Oliver, J., Oller, S., and Onate, E. (1989). "A plastic-damage model for concrete." *International Journal of Solids and Structures*, 25(3), 299–326.

Lévy, P. (1925). *Calcul des Probabilités*. Gaunthier–Villars, Paris.

MacGregor, J. G. (1983). "Load and resistance factors for concrete design." *ACI Journal Proveedings*, 80(4), 279–287.

Maleki, M. (2008). *Behaviour of Partially Grouted Reinforced Masonry Shear Walls under Cyclic Reversed Loading*. Ph.D. thesis, McMaster University, Hamilton, ON, Canada.

Malhotra, V. M. and Mehta, P. K. (1996). *Pozzolanic and Cementitious Materials*. Taylor & Francis, Oxford.

Malvar, L. J. and Crawford, J. E. (1998). "Dynamic increase factors for concrete." *Twenty-Eighth DDESB Seminar*.

Markov, A. A. (1900). *Ischislenie veroyatnostej*. St Petersburg.

Marti, P. (1985). "Basic tools of reinforced concrete beam design." *ACI Journal, Proceedings*, 821, 45–56.

Martinez, J. L. (2003). *Theoretical and experimental determination of stress interaction diagrams in masonry structures and application to the analysis of historical construction*. Ph.D. thesis, Universidad Politécnica de Madrid, Madrid. (in Spanish).

MatLab (2014). *MatLab R2014a*. MathWorks, Natick, MA.

Matsumura, A. (1985). "Effect of shear reinforcement in concrete masonry wall." *Proceedings of the 1st Joint Technical Coordinating Committee on Masonry Research*. Tokyo.

Matsumura, A. (1987). "Shear strength of reinforced hollow unit masonry walls—differences between partially grouted walls and fully grouted walls." *Proceedings of the 4th North American Masonry Conference*. Los Angeles.

Matsumura, A. (1988). "Shear strength of reinforced masonry walls." *Proceedings of the 9th World Conference on Earthquake Engineering, Vol VI*, 121–126. Tokyo.

Matsumura, A. and Igarashi, I. (1983). "Effects of height–to–length ratio on shear strength of filled cell concrete masonry loadbearing walls." *Transactions, Architectural Institute of Japan*, 58(9), 2367–2368. (in Japanese).

Matsumura, A. and Igarashi, I. (1991). "Influence of flexural reinforcement on shear strength of hollow unit concrete masonry." *Transactions, Architectural Institute of Japan*, (9), 1771–1772. (in Japanese).

Mayer, T. (1750). "Abhandlung über die umwalzung des monds um seine axe und die scheinbare bewegung der mondsflecten." *Kosmographische Nachrichten und Sammungen auf das Jahr 1748*, 1, 52–183.

Mayes, R. L., Omote, Y., Chen, S., and Clough, R. W. (1976a). "Expected performance of uniform building code designed masonry structures." *Tech. Rep. UCB/EERC–76/7*, University of California, Berkeley, CA.

Mayes, R. L., Omote, Y., and Clough, R. W. (1976b). "Cyclic shear tests of masonry piers, vol 1–test results." *Tech. Rep. UCB/EERC–76/8*, University of California, Berkeley, CA.

Mayes, R. L., Omote, Y., and Clough, R. W. (1976c). "Cyclic shear tests of masonry piers, vol 2–analysis of test results." *Tech. Rep. UCB/EERC–76/16*, University of California, Berkeley, CA.

Meli, R. and Salgado, G. (1969). "Comportamiento de muros de mampostería sujetos a carga lateral, segundo informe." *Tech. rep.*, Insituto de Ingeniera, Universidad Nacional Autónoma de México, Mexico City.

Meli, R., Wolf, A. Z., and Esteva, L. (1968). "Comportamiento de muros de mampostería hueca ante carga lateral alternada." *Revista Ingeniera*, 38(3), 371–390.

Minaie, E. (2009). *Behavior and Vulnerability of Reinforced Masonry Shear Walls*. Ph.D. thesis, Drexel University, Philadelphia.

Mises, R. v. (1919). "Fundamentalsätze der wahrscheinlicnkeitsrechnung." *Mathematische Zeitschrift*, 4, 1–97.

Moivre, A. d. (1733). *Approximato ad Summam Terminorum Binomii (a + b)n in Seriem expansi*. Printed for private circulation.

Mojsilović, N. (2011). "Strength of masonry subjected to in-plane loading: A contribution." *International Journal of Solids and Structures*, 48, 865–873.

Mojsilović, N., Kostić, N., and Schwartz, J. (2013). "Modelling of the behaviour of seismically strengthened masonry walls subjected to cyclic in-plane shear." *Engineering Structures*, 56, 1117–1129.

Monk, C. (1969). "Compressive, transverse, and shear strength tests of six- and eight-inch single-wythe walls built with solid and heavy-duty hollow clay masonry units." *Tech. Rep. 16*, Structural Clay Products Institute, McLean, VA.

Montmort, P. (1713). *Essay d'Analyse sur les Jeux de Hazard, 2nd Ed., revûe et augmentée de plusieurs Lettres*. Quillau, Paris.

Morrison, S. C. (2013). *In-Plane Shear Investigation on Masonry Walls*. Ph.D. thesis, University of Tennessee, Knoxville, TN.

Mörsch, E. (1908). *Der Eisenbetonbau, seine Theorie und Anwendung (Reinforced Concrete, Theory and Application)*. Verlag Konrad Wittwer, Stuttgart.

MSJC (2013). *Building Code Requirements for Masonry Structures (TMS 402–13, ACI 530–13, and ASCE 5–13)*. The Masonry Society, American Concrete Institute, and ASCE, Boulder, CO; Farmington Hills, MI; and Reston, VA.

Mueller, P. (1978). "Plastische berechnung von stahlbetonscheiben und balken' (plastic analysis of reinforced concrete deep beams and beams)." *Tech. Rep. 83*, ETH Zürich,, Zürich. (in German).

NCMA (1977). *Specification for the Design and Construction of Load-Bearing Concrete Masonry*. National Concrete Masonry Association (NCMA), McLean, VA.

NEHRP (1997). *NEHRP recommended provisions (FEMA 302) and commentary (FEMA 303) for seismic regulations for new buildings and other structures*. Federal Emergency Management Agency (FEMA), Washington, DC.

Nielsen, M. P. and Hoang, L. C. (2011). *Limit Analysis and Concrete Plasticity, 3e*. CRC Press, Boca Raton, FL.

Nolph, S. M. (2010). *In–Plane Shear Performance of Partially Grouted Masonry Shear Walls*. Master's thesis, Washington State University, Pullman, WA.

Nolph, S. M. and ElGawady, M. A. (2012). "Static cyclic response of partially grouted masonry shear walls." *Journal of Structural Engineering*, 138(7), 864– 879.

OED (2013). *Oxford English Dictionary Third Edition*. Oxford University Press, Oxford.

Ohta, K., Matsumura, A., and Igarashi, I. (2000). "Strength and behaviors of fully grouted concrete masonry members used thin joints (shear strength in bearing walls)." *Transactions, Architectural Institute of Japan*, (9), 1039–1040. (in Japanese).

Okamoto, S., Yamazaki, Y., Kaminosono, T., Teshigawara, M., and Hirashi, H. (1987). "Seismic capacity of reinforced masonry walls and beams in wind and seismic effects." Raufaste, N. J., ed., *Proceedings of the 18th joint Meeting, U.S.-Japan Panel on Wind and Seismic Effects*, NBSIR 97-3540. National Institute of Standards and Technology, Gaithersburg, MD.

Oliveira, D. V. (2003). *Experimental and numerical analysis of blocky masonry structures under cyclic loading*. Ph.D. thesis, Universidade do Minho, Guimarães, Portugal.

Paulay, T. and Priestley, M. J. N. (1992). *Seismic Design of Reinforced Concrete and Masonry Buildings*. John Wiley & Sons, New York.

Paulson, T. J. and Abrams, D. P. (1990). "Correlation between static and dynamic response of model masonry structures." *Earthquake Spectra*, 6(3), 376–591.

Pearson, K. (1893). "Asymmetrical frequency curves." *Nature*, 48, 615–616.

Pearson, K. (1894). "Contribution to the mathematical theory of evolution." *Philosophical Transactions, Royal Society of London, Series A: Mathematical, Physical and Engineering Sciences*, 185, 71–110.

Pearson, K. (1895). "Contributions to the mathematical theory of evolution. ii skew variation in homogeneous material." *Philosophical Transactions, Royal Society of London, Series A: Mathematical, Physical and Engineering Sciences*, 186, 343–414.

Pearson, K. (1900). "On the criterion that a given system of deviations from the probable in the case of a correlated system of variables is such that it can be reasonably supposed to have arisen from random sampling." *Philosophical Magazine*, 50(5), 157–175.

Pearson, K. (1917). "On the general theory of multiple contingency with special reference to partial contingency." *Biometrika*, 11, 145–158.

Pearson, K. (1921). "Notes on the history of correlation." *Biometrika*, 13, 25–45.

Placket, R. L. (1958). "The principle of the arithmetic mean"." *Biometrika*, 45, 130–135.

Pólya, G. (1920). "Über den zentralen grenzwertsatz der wahrscheinlichkeitsrechung und das momentproblem." *Mathematische Zeitschrift*, 8, 171–181.

Poisson, S. (1824). "Sur la probabilité des résultats moyens des observations." *Connaissance des temps pour l'année 1827*, 273–302.

Poisson, S. (1829). "Suite du mémoire sur la probabilité du résultat moyen des observations." *Connaissance des temps pour l'année 1832*, 3–22.

Porter, M. L. (1987). "Sequential phased displacement procedure for tccmar testing." *Proceedings of the Third Meeting of the Joint Technical Coordinating Committee on Masonry Research*. Tomamu, Japan.

Porter, M. L. and Baenziger, G. (2007). "Joint reinforcement as shear reinforcement for masonry shear walls." *Proceedings of the 10th North American Masonry Conference*, 860–871. St. Louis, MO.

Priestley, M. J. N. (1977). "Seismic resistance of reinforced concrete-masonry shear walls with high steel percentages." *Bulletin of the New Zealand Society for Earthquake Engineering*, 10(1), 1–16.

Priestley, M. J. N. and Bridgeman, D. O. (1974). "Seismic resistance of brick masonry walls." *Bulletin of the New Zealand Society for Earthquake Engineering*, 7(4), 167–187.

Priestley, M. J. N. and Elders, D. M. (1982). "Seismic behavior of slender concrete masonry shear walls." *Tech. Rep. 82.4*, University of Canterbury, Christchurch.

Prony, R. (1804). *Recherches physio–mathématiques sur la théorie des eaux courantes*. Imprimerie Impériale, Paris.

Puissant, L. (1807). *Traité de topographie, d'arpentage et de nivellement*. Courcier, Paris.

Raijmakers, T. M. J. and Vermeltfoort, A. T. (1992). "Deformation controlled tests in masonry shear walls." *Tech. Rep. B-92-1156*, Delft, The Netherlands. (in Dutch).

Ravindra, M. K. and Galambos, T. V. (1994). "Load and resistance factor design for steel." *Journal of the Structural Division, Proceedings of the American Society of Civil Engineers*, 104(9), 1337–1353.

Read, J. B. and Clements, S. W. (1972). "The strength of concrete block walls under uniaxial loading." *Tech. Rep. 42.473*, Cement and Concrete Association, London.

Rencher, A. C. and Schaalje, G. B. (2008). *Linear Models in Statistics, 2nd Ed.* John Wiley & Sons, Hoboken, NJ.

Ritter, W. (1899). "Die bauweise hennebique (the hennebique system)." *Schweizerische Bauzeitung*, 33(7).

Robinson, D. H. and Levin, J. R. (1997). "Reflections on statistical and substantive significance, with a slice of replication." *Educational Researcher*, 26(5), 21–26.

Roca, P. (2004). "Simplified methods for assessment of masonry shear walls." *Proceedings of 6th Congresso Nacional de Sismologia e Engenharia Sísmica*, 101–117. Guimarães, Portugal.

Roca, P. (2006). "Assessment of masonry shear-walls by simple equilibrium models." *Construction and Building Materials*, 20, 229–238.

Roca, P., Lobato, M., Viviescas, ., and Villalba, V. (2010). "Limit analysis of shear walls by simple equilibrium models." *Proceedings of 8th International Masonry Conference*. Dresden.

Roca, P., Viviescas, A., Lobato, M., Diaz, C., and Serra, I. (2011). "Capacity of shear walls by simple equilibrium models." *International Journal of Architectural Heritage*, 5(4-5), 229–238.

Rossi, P., Van Mier, J. G. M., Toutlemonde, R., Le Maou, F., and Boulay, C. (1994). "Effect of loading rate on the strength of concrete subjected to uniaxial tension." *Materials and Structures*, 27(5), 260–264.

Saiedi, H. (2011). *In-Plane Shake Table Testing of Heavily-Reinforced Concrete Masonry Shear Walls*. Master's thesis, University of Calgary, Calgary.

Schlaich, J. and Schäfer, K. (1991). "Design and detailing of structural concrete using strut–and–tie models." *The Structural Engineer*, 69(6), 113–125.

Schlaich, J., Schäfer, K., and Jennewein, M. (1987). "Toward a consistent design of structural concrete." *Journal of the Prestressed Concrete Institute*, 32(3), 74–150.

Schmidt, E. (1907). "Zur theorie der linearen und nichtlinearen integralgleichungen. i teil: Entwicklung willkurlicher funktionen nach systemen vorgeschriebener." *Mathematische Annalen*, 63, 433–476.

Schmidt, F. L. and Hunter, J. E. (1997). "Eight common but false objections to the discontinuation of significance testing in the analysis of research data." *What if there were no significance tests?*, 37–64. Lawrence Erlbaum Associates Publishers, Hillsdale, NJ.

Schneider, R. R. (1969). "Shear in concrete masonry piers." *Tech. rep.*, Masonry Research of Los Angeles, Los Angeles.

Schneider, R. R. and Dickey, W. (1994). *Reinforced Masonry Design, 3rd Ed.* Prentice Hall, Englewood Cliffs, NJ.

Schultz, A. E. (1994). "Nist research program on the seismic resistance of partially-grouted masonry shear walls." *Tech. Rep. NISTIR 5481*, National Institute of Standards and Technology, Gaithersburg, MD.

Schultz, A. E. (1996a). "Seismic resistance of partially–grouted masonry shear walls." *Worldwide Advances in Structural Concrete and Masonry*, 211–222. American Society of Civil Engineers (ASCE).

Schultz, A. E. (1996b). "Seismic resistance of partially–grouted masonry shear walls." *Proceedings of the 11th World Conference on Earthquake Engineering*, 1221. Acapulco, Mexico.

Schultz, A. E., Hutchinson, R. S., and Cheok, G. C. (1998). "Seismic performance of masonry walls with bed joint reinforcement." *Structural Engineers World Congress Proceedings*, T119-4. San Francisco.

Scrivener, J. C. (1966). "Concrete masonry wall panel tests-static racking tests with predominant flexural effect." *New Zealand Concrete Construction*, 10, 119–125.

Scrivener, J. C. (1969). "Static racking tests on concrete masonry walls proceedings." *International Conference on Masonry Structural Systems*, 185–191. University of Texas, Austin, TX.

Scrivener, J. C. and Williams, D. (1971). "Behaviour of reinforced masonry shear walls under cyclic loading." *Bulletin of the New Zealand Society for Earthquake Engineering*, 4(2), 316–330.

Shigenobu, K., Matsumura, A., and Igarashi, I. (1987). "Comparison of shear strength and behavior of fully grouted reinforced concrete masonry walls between those made with different type concrete block units." *Transactions, Architectural Institute of Japan*, 62(10), 773–774. (in Japanese).

Shing, P. B., Klamerus, E., Spaeh, H., and Noland, J. L. (1988). "Seismic performance of reinforced masonry shear walls." *Proceedings of the Ninth World Conference on Earthquake Engineering*, vol. 6, 103–108. Tokyo-Kyoto.

Shing, P. B., Noland, J. L., Klamerus, E., and Spaeh, H. (1989). "Inelastic behavior of concrete masonry walls." *Journal of Structural Engineering*, 15(9), 2204–2225.

Shing, P. B., Schuller, M., and Hoskere, V. S. (1990). "In–plane resistance of reinforced masonry shear walls." *Journal of Structural Engineering*, 116(3), 619–639.

Simms, L. G. (1965). "The strength of walls built in the laboratory in some types of clay bricks and blocks." *Transactions of the British Ceramic Society*, 81–92.

Simpson, T. (1756). "A letter to the right honorable george earl of macclesfield, president of the royal society, on the advantage of taking the mean of a number of observations, in practical astronomy." *Philosophical Transactions of the Royal Society of London*, 49, 82–93.

Soper, H. E., Young, A. W., Cave, B. M., and Pearson, K. (1917). "On the distribution of the correlation coefficient in small samples. appendix ii to the papers of 'student' and r a fisher a cooperative study." *Biometrika*, 11, 328–413.

Standard Association of New Zealand (NZS) (2004). *Code of practice for the design of masonry structures (NZS 4230:2004)*. Wellington, New Zealand.

Stigler, S. M. (1986). *The History of Statistics: The Measure of Uncertainty before 1900*. The Belknap Press of Harvard University Press, Cambridge, MA.

'Student' (1908a). "Probable error of a correlation coefficient." *Biometrika*, 6, 302–310.

'Student' (1908b). "The probable error of a mean." *Biometrika*, 6, 1–25.

Sveinsson, B. I., McNiven, H. D., and Sucuoglu, H. (1985). "Cyclic loading tests of masonry single piers, vol 4–additional tests width height to width ratio of 1." *Tech. Rep. UCB/EERC–85/15*, University of California, Berkeley, CA.

Thurston, S. J. and Hutchison, D. L. (1982). "Reinforced masonry shear walls: cyclic loading tests in contraflexure." *Bulletin of the New Zealand Society for Earthquake Engineering*, 15(1), 27–45.

Tomaževič, M. (2000). "Some aspects of experimental testing of seismic behavior of masonry walls and models of masonry buildings." *ISET Journal of Earthquake Technology*, 37(4), 101–117.

Tomaževič, M. and Lutman, M. (1988). "Seismic resistance of reinforced masonry walls." *Proceedings of the Ninth World Conference on Earthquake Engineering*, vol. 6, 97–102. Tokyo-Kyoto.

Tomaževič, M., Lutman, M., and Petković, L. (1996). "Seismic behavior of masonry walls: Experimental simulation." *Journal of Structural Engineering*, 122(9), 1040–1047.

Tomaževič, M. and Velechovsky, T. (1992). "Some aspects of testing small-scale masonry building models on simple earthquake simulators." *Earthquake Engineering & Structural Dynamics*, 21(11), 945–963.

UBC (1997). *Uniform building code*. International Conference of Building Officials (ICBO), Whittier, CA.

Vardeman, S. B. (1992). "What about the other intervals?" *The American Statistician*, 46(3), 193–197.

Varshney, A. (2010). *Simplified Analysis of Strength of Masonry Shear Walls*. Master's thesis, Universitat Politècnica de Catalunya, Barcelona.

Voon, K. C. (2007). *In–Plane Seismic Design of Concrete Masonry Structures*. Ph.D. thesis, University of Auckland, Auckland.

Voon, K. C. and Ingham, J. M. (2006). "Experimental in-plane shear strength investigation of reinforced concrete masonry walls." *Journal of Structural Engineering*, 132(3), 400–408.

Voon, K. C. and Ingham, J. M. (2008). "Experimental in-plane investigation of reinforced concrete masonry walls with openings." *Journal of Structural Engineering*, 134(5), 758–768.

Wald, A. (1943). "An extension of wilks' method for setting tolerance limits." *The Annals of Mathematical Statistics*, 14(1), 45–55.

Wald, A. and Wolfowitz, J. (1946). "Tolerance limits for a normal distribution." *The Annals of Mathematical Statistics*, 17(2), 208–215.

Wei, X. and Hao, H. (2009). "Numerical derivation of homogenized dynamic masonry material properties with strain rate effects." *International Journal of Impact Engineering*, 36(3), 522–536.

Wilks, S. S. (1941). "Determination of sample sizes for setting tolerance limits." *The Annals of Mathematical Statistics*, 12(1), 91–96.

Wilks, S. S. (1942). "Prediction with special reference to the problem of tolerance limits." *The Annals of Mathematical Statistics*, 13(4), 400–409.

Williams, D. (1971). *Seismic Behaviour of Reinforced Masonry Shear Walls*. Ph.D. thesis, University of Canterbury, Christchurch.

Williams, D. and Scrivener, J. C. (1974). "Response of reinforced masonry shear walls to static and dynamic cyclic loading." *Proceedings of the 5th World Conference on Earthquake Engineering*, 1491–1494. Rome.

Woodward, K. and Rankin, F. (1985). "Shear resistance of unreinforced hollow concrete block masonry walls." *Proceedings from the Third North American Masonry Conference*, 38. Arlington, TX.

Wu, C. and Hao, H. (2008). "Numerical derivation of averaged material properties of hollow concrete block masonry." *Engineering Structures*, 30, 870–883.

Yamazaki, Y., Hiraishi, H., and Teshigawa, M. (1983). "Seismic capacity of reinforced masonry walls and beams, part 1, test plan." *Transactions, Architectural Institute of Japan*, 60(10), 1083–1084. (in Japanese).

Yancey, C. W. C. and Scribner, C. F. (1989). "Influence of horizontal reinforcement on shear resistance of concrete block masonry walls." *Tech. Rep. NISTIR 4202*, National Institute of Standards and Technology, Gaithersburg, MD.

Yokel, F. Y., Mathey, R. G., and D, D. R. (1970). *Compressive Strength of Slender Concrete Masonry Walls*. National Bureau of Standards, Washington.

Yokel, F. Y., Mathey, R. G., and D, D. R. (1971). *Strengths of Masonry Walls Under Compressive and Transverse Load*. National Bureau of Standards, Washington.

Zhang, L., Mathew, T., and Yang, H. (2009). "Tolerance limits for a ratio of normal random variables." *Journal of biopharmaceutical statistics*, 20(1), 172–184.

APPENDIX A. EQUIVALENT METRIC REINFORCEMENT AREAS USED IN THIS STUDY

Table A.1: American Reinforcement

Size	Bar Area (mm^2)
#3	71.0
#4	129
#5	200
#6	284
#7	387
#8	510
#9	645
#10	819
#11	1006
9-ga	11.1
5-ga	21.7
3/16”	17.8

Table A.2: Australian Reinforcement

Size	Bar Area (mm^2)
N12	110
N16	200
N20	310
N24	450
N28	620
N32	800
N36	1020
N40	1260
R6.5	30
R10	80

Table A.3: Canadian Reinforcement

Size	Bar Area (mm^2)
M10	100
M15	200
M20	300
M25	500
M30	700
M35	1000
M45	1500
M55	2500
D3	19.4
D4	25.8
D7	45.0

Table A.4: Japanese Reinforcement

Size	Bar Area (mm^2)
D10	71
D13	129
D16	200
D19	284
D22	387
D25	510
D29	645
D32	819
D38	1006

Table A.5: Mexican Reinforcement

Size	Bar Area (mm^2)
#2.5	49
#3	71
#4	127
#5	199
#6	287
#8	507
#10	794
#12	1140

Table A.6: New Zealander Reinforcement

Size	Bar Area (mm^2)
R6	28.3
D8	50.3
D10	78.5
D12	113
D16	201
D20	314
D22	380
D24	542
D25	491

Table A.7: Other Reinforcement

Ø (mm)	Bar Area (mm^2)
2.5	4.91
3.1	7.55
3.33	8.71
3.66	10.5
4	12.6
4.2	13.9
4.76	17.8
5	19.6
6	28.3
9	63.6
10	78.5
13	133
16	201

APPENDIX B. ANALYZING RESEARCH DATA IN MATRIX FORM

B.1 Introduction

The development of linear regression is considered to be the foundation of the field of statistics. Regression was originally developed by scientists and geodesists as a tool for interpreting observational data. Scientists and mathematicians expanded our understanding and acceptance of this tool by incorporating principles of probability and mathematics to prove its validity and usefulness. It was not until the beginning of the twentieth century that the topic of statistics began to emerge as a distinct field from science. During the past near century, contemporary engineers have lost sight of the fact that regression analysis was originally developed as a tool for scientists. Many believe, erringly, that all but the most basic statistical analyses should be reserved for statisticians, to the detriment of our field and science.

Statistics provides many tools within the area of linear modeling that could be useful to engineers, but while—presumably for the reasons given above—many engineers have been taught these tools they do not use them in their experimental analyses. The mathematics involved in using these tools fits within the education of one with an advanced engineering education. This paper will describe how the use of linear modeling and analysis of variance can be used to quantify and understand the effects of input parameters used in engineering experiments.

Statistical tests can be used to make quantitative decisions and make objective conclusions about the results in a study. This paper will further expound the benefits and uses of these tools by considering the subject as it relates to masonry shear wall research.

B.2 Background

An epistemological review of masonry shear wall research has revealed that many masonry research studies have been essentially comparative in nature. Researchers, in attempting to un-

derstand the influence of certain input parameters on wall behavior, have focused primarily on the relative effects of these parameters on the shear strength of masonry walls. These studies have been noteworthy and laudable for their contribution to the conglomeration of masonry knowledge. The state of the art of masonry understanding is at the point where further advancement in the field will require more quantitative measures of the effects of design parameters.

The current state of the art in masonry research has been somewhat disjointed. On one side of the epistemological spectrum, researchers have conducted studies to explore the effect that different design (or input) parameters (e.g., quantity of shear reinforcement, amount of axial load, type of grouting) have on masonry shear wall performance. On the far end of the spectrum, researchers have attempted to fit existing constitutive models to masonry shear walls for modeling the nonlinear performance of masonry shear walls within structural analysis software. Most of these constitutive models have been based on those originally developed for concrete. A few researchers have focused their attention at the center of the spectrum by attempting to understand and model the mechanics of masonry shear walls using non-finite-element analytical methods. The sole example that the authors have found in their review of the research has been the strut-and-tie modeling procedure. The other modeling methods currently in use are principally empirical in nature and have vague mechanical representation.

Much information has been gathered at both ends of the spectrum which will aid researchers as they try to chip away at the problem from both sides and fill the knowledge gap in the center. As stated earlier, many researchers have overlooked some statistical tools while analyzing their data. By using some of these tools on existing data sets, additional insight can be gleaned from these previous studies. A further benefit is that these tools provide a way to estimate the effect size on shear strength for the design variables. Understanding of the effect size of the design variables will help in developing and proving theories about the contribution of each design parameter to the shear strength of the wall.

This appdendix will review the use of basic linear regression modeling and analysis of variance (ANOVA) for finding point estimates and confidence intervals for the effect size of design parameters and for performing hypothesis testing on the parameters.

B.3 Linear Model Construction

Linear regression provides researchers means to quantify the contribution of individual design parameters and ANOVA helps to examine how significant the contribution of each one of these parameters is to the overall findings. Both tools (linear regression and ANOVA) can be used together on existing data to develop new empirical models to describe the behavior of the subject matter or to investigate areas of research need.

B.3.1 Data Types

There are two types of variables that are used within experimental designs, quantitative and qualitative. Quantitative variables are represented by a numerical value and may be continuous or discrete. Examples of quantitative variables include shear reinforcement ratio, shear span ratio, shear area, and axial load. Qualitative variables are those in which their values are taken from a list of categories. Examples of qualitative variables are partial versus full grouting, concrete versus clay masonry, and monotonic versus cyclic testing procedures.

B.3.2 Data Matrix

The first and most intensive part of performing linear regression and ANOVA is the construction of the data matrix. The data matrix contains the input data organized such that each row represents an individual test specimen and each column represents an input parameter the researcher wishes to study. In linear modeling, the regression coefficients come into the model linearly. Each input parameter may include a single, unchanged input variable from the original experimental data or may be formed by reparameterizing one or more input variables. The data matrix must be full rank for the least squares regression method to produce a unique solution.

B.3.3 Parameter Selection

The number of parameters (i.e., columns) that can be included in the data matrix is governed by the design of the experiment. Quantitative variables are the simplest to use in building a data matrix because they only require a single column to represent the data used in the experiment.

Experiments that contain only quantitative data typically produce data matrices that are full rank. The case where a purely quantitative experiment produces a non-full-rank matrix is due to an improper experimental design and can be easily avoided.

The introduction of qualitative variables into experimental designs produces the situation where the data matrix is not full rank. In the case of qualitative variables, each category requires a unique column. This means that each qualitative variable requires multiple columns to fully represent the data. Since each category in the study increases the number of columns in the data matrix without increasing its rank, the matrix becomes non-full rank. The situations where the design produces a non-full rank matrix can be rectified by redefining parameters and reparameterizing the model.

Full Rank Case

To illustrate the full rank case, we will use a small example from Schultz et al. (1998) who tested three different aspect ratios and two different sizes of shear reinforcement within six specimens. One possible model that represents their experiment is

$$V_i = \mu + \beta_1 \left(\frac{M_u}{V_u d_v}\right)_i + \beta_2 \left(\frac{A_v}{s}\right)_i + \varepsilon_i \tag{B.1}$$

where

V_i = the experimental shear strength for specimen i,
μ = the intercept and represents the mean shear strength for masonry,
$\left(\frac{M_u}{V_u d_v}\right)_i$ = the shear span ratio for specimen i,
$\left(\frac{A_v}{s}\right)_i$ = the shear reinforcement level for specimen i,
ε_i = the error term for specimen i, and
β_j = the regression coefficient for model term j.

The model given by Equation (B.1) is the simplest representation that can be constructed from their data. While it is numerically correct, the parameters do not exhibit consistent units.

Though this does not present a problem to the regression analysis, it does create a difficultly in interpreting the results. This issue is easily rectified by reparameterizing the variables in the model. The new, more-familiar-looking model is given by

$$V_i = \beta_0 \left(A_{nv}\sqrt{f'_m}\right)_i + \beta_1 \left(\frac{M_u}{V_u d_v} A_{nv}\sqrt{f'_m}\right)_i + \beta_2 \left(\frac{d_v}{s} A_v f_y\right)_i + \varepsilon_i \tag{B.2}$$

where

A_{nv} = the net shear area of the wall,
f'_m = the masonry compressive strengths, and
d_v = the shear length of each wall specimen.

This updated model in (B.2) produces regression coefficients that are unit-less and the model as a whole is more meaningful to engineers. It should be noted that though the shear area changes from specimen to specimen, hence making the first term not constant, this does not present a problem because the overall form of the model is still linear. This can be observed more clearly by looking at a reparameterized form of the model given by

$$\left(\frac{V}{A_{nv}}\right)_i = \beta_0 \left(\sqrt{f'_m}\right)_i + \beta_1 \left(\frac{M_u}{V_u d_v}\sqrt{f'_m}\right)_i + \beta_2 \left(\frac{d_v}{A_{nv} s} A_v f_y\right)_i + \varepsilon_i \,. \tag{B.3}$$

The reparameterized model (B.3)shows that the first term still represents the average masonry shear strength neglecting the effects of aspect ratio and shear reinforcement.

A final note to mention is that neither of the latter two models represents the contribution of the axial load on the shear strength of the wall. Schultz et al. (1998) varied the axial load between specimens so as to maintain a constant axial stress in their specimens. Since the axial load in the study was wholly correlated to the shear area, including it on right side of the equation would break the necessary assumption that the parameters be independent. However, for purposes of coefficient calculation and analysis, the axial load component of the strength can be subtracted from the left side of the equation, as shown in

$$(V - 0.25P_u)_i = \beta_0 \left(A_{nv}\sqrt{f'_m}\right)_i + \beta_1 \left(\frac{M_u}{V_u d_v} A_{nv}\sqrt{f'_m}\right)_i + \beta_2 \left(\frac{d_v}{A_{nv} s} A_v f_y\right)_i + \varepsilon_i \,. \tag{B.4}$$

After the regression coefficients have been computed and analyzed, the $0.25P_u$ term could be moved to the right side to facilitate comparison with the existing MSJC (2013) shear strength equation. In this example, the coefficient 0.25 for the axial load was assumed to match that currently used in the MSJC code, but another may have equally been chosen from another code for comparison with that standard. For the case of our latest model, the matrix representation is given by

$$\begin{pmatrix} 43.9 \\ 46.6 \\ 32.2 \\ 39.8 \\ 50.2 \\ 40.0 \end{pmatrix} = \begin{bmatrix} 22.8 & 11.4 & 36.1 \\ 17.1 & 5.98 & 25.8 \\ 12.8 & 6.39 & 18.1 \\ 22.8 & 5.71 & 70.7 \\ 17.1 & 5.98 & 50.5 \\ 12.8 & 6.39 & 32.3 \end{bmatrix} \begin{pmatrix} \beta_0 \\ \beta_1 \\ \beta_2 \end{pmatrix} + \boldsymbol{\varepsilon} \,. \tag{B.5}$$

Non-Full-Rank Case

When qualitative variables are included in the experimental design, the number of columns in the matrix exceeds the rank of the matrix. Without any modification the problem cannot be solved because a unique solution does not exist. However, modifying the data matrix is a simple process and with some practice it is fairly intuitive.

To illustrate the process of data matrix modification, we will refer to the data from Tomaževič et al. (1996) who tested 16 pairs of specimens subject to one of two axial loads, two loading rates (static and dynamic), and four displacement-based loading histories. The loading histories used were monotonic loading, incrementally increasing cyclic, sequential-phased displacement cyclic procedure, and simulated seismic—referred to as loading types A, B, C, and D, respectively. While the first variable in the study was quantitative, the other two variables were clearly qualitative in nature. The study results could be represented by the model

$$V_i = \mu + \beta_\sigma A_{nv}\sigma_i + \beta_s\zeta_{si} + \beta_d\zeta_{di} + \beta_A\zeta_{Ai} + \beta_B\zeta_{Bi} + \beta_C\zeta_{Ci} + \beta_D\zeta_{Di} + \varepsilon_i \tag{B.6}$$

where

V_i = the experimental shear strength for specimen i,

μ = the intercept and represents the mean shear strength for masonry,

A_{nv} = the net shear area of the masonry,

σ_i = the axial stress applied to the specimen,

ζ_{si} = 1 if specimen i was statically loaded and 0 otherwise,

ζ_{di} = 1 if specimen i was dynamically loaded and 0 otherwise,

ζ_{Ai} = 1 if specimen i was subjected to loading history A and 0 otherwise,

ζ_{Bi} = 1 if specimen i was subjected to loading history B and 0 otherwise,

ζ_{Ci} = 1 if specimen i was subjected to loading history C and 0 otherwise,

ζ_{Di} = 1 if specimen i was subjected to loading history D and 0 otherwise,

ε_i = the error term for specimen i,

and the betas represent the respective regression coefficient for each term.

At this point, it will be more helpful to represent the data in its matrix form

$$\boldsymbol{v} = \begin{bmatrix} 1 & 60 & 1 & 0 & 1 & 0 & 0 & 0 \\ 1 & 60 & 1 & 0 & 0 & 1 & 0 & 0 \\ 1 & 60 & 1 & 0 & 0 & 0 & 1 & 0 \\ 1 & 60 & 1 & 0 & 0 & 0 & 0 & 1 \\ 1 & 60 & 0 & 1 & 1 & 0 & 0 & 0 \\ 1 & 60 & 0 & 1 & 0 & 1 & 0 & 0 \\ 1 & 60 & 0 & 1 & 0 & 0 & 1 & 0 \\ 1 & 60 & 0 & 1 & 0 & 0 & 0 & 1 \\ 1 & 120 & 1 & 0 & 1 & 0 & 0 & 0 \\ 1 & 120 & 1 & 0 & 0 & 1 & 0 & 0 \\ 1 & 120 & 1 & 0 & 0 & 0 & 1 & 0 \\ 1 & 120 & 1 & 0 & 0 & 0 & 0 & 1 \\ 1 & 120 & 0 & 1 & 1 & 0 & 0 & 0 \\ 1 & 120 & 0 & 1 & 0 & 1 & 0 & 0 \\ 1 & 120 & 0 & 1 & 0 & 0 & 1 & 0 \\ 1 & 120 & 0 & 1 & 0 & 0 & 0 & 1 \end{bmatrix} \begin{pmatrix} \mu \\ \beta_\sigma \\ \beta_s \\ \beta_d \\ \beta_A \\ \beta_B \\ \beta_C \\ \beta_D \end{pmatrix} kN + \boldsymbol{\varepsilon} \tag{B.7}$$

where $\boldsymbol{v}$ is a vector of experimental shear strengths and $\boldsymbol{\varepsilon}$ is a vector of errors. In the above matrix there are only six linearly independent columns, giving the matrix a rank of six. Since two of the columns are linear combinations of the others the system of equations has no unique solution.

As will be shown shortly, in addition to having no solution the form of (B.7) isn't practical when viewed in light of what the terms represent in reality.

By respecifying the parameters in (B.7) we can develop a form that is both full rank and representative of masonry. To identify how to change the equation we will first look at how its parameters are defined. As mentioned previously, μ represents the mean masonry strength minus the effects of the other parameters. To represent the beta parameters, we will look more specifically at β_s and β_d. The parameters β_s and β_d represent the contribution to masonry strength of the static and dynamic loading rates. Including both terms is not realistic since both categories are mutually exclusive and collectively exhaustive. The average strength μ could not exist without being loaded at one rate or another. The same scenario is true of the loading history variables in this study. It should now be apparent how redefining the parameters is not only necessary to find a solution but also for the solution to represent realistic conditions.

To correct the problem it will be necessary to redefine the μ parameter since it currently has no symbolic meaning. To do so will necessitate selecting a base testing scenario for the two sets of parameters. The first set presents little difficultly because there are only two options and hence a single degree of freedom between them. It presents a simple choice of whether we prefer that the mean shear strength be tied to the static or to the dynamic loading rate. In this case, we believe that it is better to tie the average value to the static loading rate because static loading rates have a relatively constant effect whereas dynamic loading rates are approximately double-logarithmically related to the strength gain Schultz et al. (1998).

Selecting from among the loading history parameters, however, is subjective because there are three degrees of freedom and because the choice will affect the analyses of variance on the data and how they are interpreted. The effect on the analysis will be covered more in-depth later in this paper. For now, we will select the loading type B as the history which we will tie to the mean shear strength. Having selected the two bases for our analysis, we redefine μ as μ_{sB} which is the average masonry shear strength under static loading and subjected to load history B. The change in definition permits us to eliminate the third and sixth columns in the data matrix. This produces

the full-rank matrix

$$\begin{pmatrix} 47.05 \\ 41.22 \\ 32.64 \\ 40.57 \\ 51.33 \\ 42.85 \\ 43.69 \\ 42.79 \\ 61.52 \\ 45.05 \\ 49.23 \\ 53.78 \\ 62.12 \\ 50.45 \\ 57.26 \\ 60.19 \end{pmatrix} kN = \begin{bmatrix} 1 & 60 & 1 & 1 & 0 & 0 & 0 \\ 1 & 60 & 1 & 0 & 1 & 0 & 0 \\ 1 & 60 & 1 & 0 & 0 & 1 & 0 \\ 1 & 60 & 1 & 0 & 0 & 0 & 1 \\ 1 & 60 & 0 & 1 & 0 & 0 & 0 \\ 1 & 60 & 0 & 0 & 1 & 0 & 0 \\ 1 & 60 & 0 & 0 & 0 & 1 & 0 \\ 1 & 60 & 0 & 0 & 0 & 0 & 1 \\ 1 & 120 & 1 & 1 & 0 & 0 & 0 \\ 1 & 120 & 1 & 0 & 1 & 0 & 0 \\ 1 & 120 & 1 & 0 & 0 & 1 & 0 \\ 1 & 120 & 1 & 0 & 0 & 0 & 1 \\ 1 & 120 & 0 & 1 & 0 & 0 & 0 \\ 1 & 120 & 0 & 0 & 1 & 0 & 0 \\ 1 & 120 & 0 & 0 & 0 & 1 & 0 \\ 1 & 120 & 0 & 0 & 0 & 0 & 1 \end{bmatrix} \begin{pmatrix} \mu_{sB} \\ \beta_\sigma \\ \beta_s \\ \beta_d \\ \beta_{A/B} \\ \beta_{C/B} \\ \beta_{D/B} \end{pmatrix} kN + \boldsymbol{\varepsilon} \tag{B.8}$$

where $\beta_{A/B}$, $\beta_{C/B}$, and $\beta_{D/B}$ represent the relative increase in shear strength for loading histories A, C, and D—respectively—compared to that of loading history B.

B.3.4 Quantifying Parameter Influence

Having reviewed the necessary steps for parameter selection and data matrix construction, we can determine the influence that each parameter has on the response of the wall. Linear regression modeling assumes that the data are related by the equation

$$\boldsymbol{y} = \boldsymbol{X}\boldsymbol{\beta} + \boldsymbol{\varepsilon} \tag{B.9}$$

where $\boldsymbol{y}$ is the response vector, $\boldsymbol{X}$ is the data matrix, $\boldsymbol{\beta}$ is the vector of regression coefficients, and $\boldsymbol{\varepsilon}$ is the vector of residuals.

Since we do not know the true values of the regression coefficients, we will estimate them using least squares regression. The estimated coefficients are represented by $\hat{\boldsymbol{\beta}}$ where the hat represents the fact that the coefficients are estimates of the unknown true values. Least squares regression is a powerful tool because no stochastic or scedastic assumptions are required to find

the unbiased estimators with minimum variance Rencher and Schaalje (2008). Essentially, least squares regression will always find a solution no matter how well or poorly the equation fits the data or how the data are distributed.

As the name implies, least squares regressions is based on minimizing the squares of the errors, $\boldsymbol{\varepsilon}'\boldsymbol{\varepsilon}$. Through a relatively easy-to-follow processes that is readily found in most advanced statistics texts (e.g., Rencher and Schaalje 2008), the $\boldsymbol{\varepsilon}'\boldsymbol{\varepsilon}$ term can be rearranged and differentiated to produce the estimates of the regression coefficients given by

$$\hat{\boldsymbol{\beta}} = (\boldsymbol{X}'\boldsymbol{X})^{-1}\boldsymbol{X}'\boldsymbol{y}. \tag{B.10}$$

Equation 10 shows, mathematically, the reason the data matrix must be full rank; otherwise, $\boldsymbol{X}'\boldsymbol{X}$ is singular and has no inverse. Having obtained estimates for the regression coefficients, we can now revisit the previous two examples to learn how to use and interpret the results.

Schultz et al.

In the case of the first example, representing the data from Schultz et al. (1998) in matrix form—Equation (B.5)—and performing least squares regression produces estimates for the regression coefficients given by

$$\hat{\boldsymbol{\beta}} = \begin{pmatrix} \hat{\beta}_0 \\ \hat{\beta}_1 \\ \hat{\beta}_2 \end{pmatrix} = \begin{pmatrix} 1.15 \\ 1.99 \\ 0.164 \end{pmatrix}. \tag{B.11}$$

These coefficients can now be interpreted and compared to the existing body of knowledge. For example, from the $\hat{\beta}_2$ term we observe a correlation of 0.164 between the level of shear reinforcement and shear capacity of the wall. The data suggest that each unit increase in shear reinforcement results in a net increase of 0.164 units in the ultimate shear capacity of the wall. This value is quite low compared to the contribution cited by most code equations. However, there is also a possibility that the reinforcement had no contribution to the shear capacity in this study and that the 0.164 value is due to random variation in the data. We will check for this soon hereafter.

Tomaževič et al.

In the case of the second example, the data from the Tomaževič et al. (1996) can be similarly analyzed using least squares regression, producing the regression estimates given by

$$\hat{\boldsymbol{\beta}} = \begin{pmatrix} \hat{\mu}_{sB} \\ \hat{\beta}_{\sigma} \\ \hat{\beta}_{d} \\ \hat{\beta}_{A/B} \\ \hat{\beta}_{C/B} \\ \hat{\beta}_{D/B} \end{pmatrix} = \begin{pmatrix} 24.14 \\ 0.2030 \\ 4.953 \\ 10.61 \\ 0.8125 \\ 4.440 \end{pmatrix}. \tag{B.12}$$

Interpretation of the coefficients for the quantitative parameters is identical to that from the previous study. The data show that the mean masonry shear strength for the walls was 24.14 kN assuming the walls are statically loaded using history B. The data suggest that a 1.0 kN increase in the axial load increases the shear capacity by approximately 0.20 kN, which is not too different from the coefficients used in many masonry standards.

Interpreting the coefficients for the qualitative parameters is also a straightforward process. The $\hat{\beta}_d$ coefficient suggests that a mean increase of roughly 5 kN was realised in the dynamic tested walls compared to the statically tested ones. The procedure can be equally applied to the coefficient for the monotonic loading, which suggests a mean increase of 10.6 kN in wall strength compared to the step-wise increasing cyclic procedure. The simulated seismic procedure also produced a notable increase in shear capacity, but this value, like the others, must first be substantiated before attempting to draw conclusions.

B.3.5 Quantification of Significance

Having quantified the influence of each parameter, we will now determine whether the influence is statistically significant. Understanding how significant a parameter is helps researchers to know how strong of conclusions can be drawn from the data and whether to include or exclude some parameters from the model Schmidt and Hunter (1997). The method that we will use in this article is similar to that used for hypothesis testing, but rather than selecting a threshold probability value a priori we will calculate the probability so that the researcher can gauge the significance

in view of the experimental data. Unlike least squares regression, the effectiveness of significance testing is based on the assumption that $\boldsymbol{y}$ is normally distributed with mean $\boldsymbol{X\beta}$ and variance σ^2.

The first step is to rearrange, if necessary, the $\boldsymbol{X}$ matrix such that the parameters to be analyzed are located in the last columns and the corresponding coefficients in the $\boldsymbol{\beta}$ vector are in the last rows. Next, the $\boldsymbol{X}$ matrix and $\boldsymbol{\beta}$ vector are partitioned so that the parameters in question can be removed from the analysis, forming a reduced model. The columns of $\boldsymbol{X}$ excluding the selected parameter are labeled as the submatrix $\boldsymbol{X}_1$ and the columns for the parameters are labeled as the submatrix $\boldsymbol{X}_2$. The rows in $\boldsymbol{\beta}$ are similarly partitioned as $\boldsymbol{\beta}_1$ and $\boldsymbol{\beta}_2$ vectors, respectively. To simply notation, we will define$\boldsymbol{H}$ and $\boldsymbol{H}_1$ such that

$$\boldsymbol{H} = \boldsymbol{X}\left(\boldsymbol{X}'\boldsymbol{X}\right)^{-1}\boldsymbol{X}' \tag{B.13}$$

and

$$\boldsymbol{H}_1 = \boldsymbol{X}_1\left(\boldsymbol{X}_1'\boldsymbol{X}_1\right)^{-1}\boldsymbol{X}_1'. \tag{B.14}$$

To analyze the parameters, we calculate the F statistic using the equation

$$\boldsymbol{F} = \frac{\boldsymbol{y}\prime\left(\boldsymbol{H}-\boldsymbol{H}_1\right)\boldsymbol{y}/h}{\boldsymbol{y}'\left(\boldsymbol{I}-\boldsymbol{H}\right)\boldsymbol{y}/\left(n-k\right)} \tag{B.15}$$

where

h = the number of columns in $\boldsymbol{X}_2$,
k = the number of columns in $\boldsymbol{X}$, and
n = the number of specimens (i.e., rows in $\boldsymbol{X}$).

The p-value is found from area of the upper tail (i.e., right tail) of the F-distribution with h and $(n-k)$ degrees of freedom bounded on the left by the F statistic calculated above. A function to calculate the upper-tail area of an F-distribution is included in most data analysis programs (e.g., F.INV.RT in MS Excel and pcdf in MatLab).

The p-value calculated from the above procedure represents the probability that the reduced model $\boldsymbol{X}_1\boldsymbol{\beta}_1$, which ignores the selected parameters, better represents the data than the full model $\boldsymbol{X\beta}$ with the selected parameters included. Lower p-values suggest that the parameters' influence

Table B.1: Full-Model Parameters for Schultz et al. (1998)

Parameter	Value	p
$\hat{\beta}_0$	1.15	0.625
$\hat{\beta}_1$	1.99	0.58
$\hat{\beta}_2$	0.164	0.745

on the final shear strength is significant and that the observed effect is not due to chance. Higher p-values suggest that the findings from this study are inconclusive because the contribution to the effect due to chance cannot be excluded.

The p-value is useful to researchers by giving them an objective means of judging if findings are conclusive. It should be remembered that smaller studies contain fewer degrees of freedom and will typically have higher p-values. Researchers should consider the study size, observed sources of error and variation during tests, masonry mechanics, and prior studies when interpreting the p-values from their studies. Researchers should not be hesitant to make conclusions based on low-significance observations for fear of their conclusions being misapplied. Results from individual studies ought to be considered as tentative and preliminary since only a meta-analysis of multiple studies has the power to form dependable scientific conclusions Vardeman (1992).

Schultz et al.

Returning to the example from Schultz et al. (1998) and following the above steps to analyze the significance of the parameter representing the shear reinforcement contribution produces the p-values shown in Table B.1. Considering the small sample size used in that study, the p-value for $\hat{\boldsymbol{\beta}}_2$ is still very high, suggesting that the 0.164 value obtained in Equation (B.11) was likely either caused by variation in the data (and not by the reinforcement) or that the estimated form of the model does not reflect its true form. With this understanding, we will likely choose to omit the reinforcement parameter from the analysis and focus on the remaining variable from that study, the aspect ratio. In choosing to eliminate the reinforcement parameter from the model, the $\boldsymbol{X}_1$ from the latest model becomes the data matrix $\boldsymbol{X}$ for the new model. Least squares regression is performed on this new model to obtain the new coefficient estimates and respective p-value shown in Table B.2.

Table B.2: Full-Model Parameters for Schultz et al. (1998)

Parameter	Value	p
$\hat{\beta}_0$	1.84	0.088
$\hat{\beta}_1$	1.19	0.606

It can be seen that eliminating the last parameter drastically increased the significance of the $\hat{\beta}_0$ term, suggesting that dropping the reinforcement parameter was the correct choice. It is interesting to note that for the original model, the p-value for the $\hat{\beta}_1$ term was originally 0.580, meaning that eliminating the reinforcement parameter from the model introduced more variance into the aspect ratio parameter. A large reason for the poor fit with the aspect ratio parameter is likely because we tried to fit a straight line to the data when some non-linear function (e.g., a square root or a negative inverse relationship) would fit the data better. This would have likely been discovered and corrected in the original parameterization process described earlier by looking at plots of the data. If not, the analysis of variance process provides a way to identify poor correlations to the data and to evaluate different models to select the best one.

By following the above steps, a better model to describe the data from Schultz et al. is given by

$$(V - 0.25P_u)_i = 2.82\left(A_{nv}\sqrt{f'_m}\right)_i - 0.46\left(\frac{V_u d_v}{M_u}A_{nv}\sqrt{f'_m}\right)_i + 0.33\left(\frac{d_v}{s}A_v f_y\right)_i + \varepsilon_i \tag{B.16}$$

where p-values for the individual coefficients are 0.027, 0.319, and 0.496, respectively. As can be seen, reparameterizing the model improves the p-values for all three of the coefficients. The above equation can be rewritten in standard form as

$$V_i = \left(\left(2.82 - 0.46\frac{V_u d_v}{M_u}\right)A_{nv}\sqrt{f'_m}\right)_i + 0.25P_{ui} + 0.33\left(\frac{d_v}{s}A_v f_y\right)_i + \varepsilon_i \tag{B.17}$$

The model fits the data better by using the reciprocal of the shear span ratio $\frac{V_u d_v}{M_u}$ in place of the shear span ratio $\frac{M_u}{V_u d_v}$ which is typically found in the shear strength prediction equation in most masonry standards.

Table B.3: Full-Model Parameters for
Tomaževič et al. (1996)

Parameter	Value	p
$\hat{\mu}_{sB}$	24.14	0.00043
$\hat{\beta}_{\sigma}$	0.203	0.0007
$\hat{\beta}_{d}$	4.953	0.18248
$\hat{\beta}_{A/B}$	10.61	0.02309
$\hat{\beta}_{C/B}$	0.8125	0.9996
$\hat{\beta}_{D/B}$	4.44	0.59773

Tomaževič et al.

The example from Tomaževič et al. (1996) will further show how this method can be used to draw conclusions about the contribution of specific input parameters on the shear capacity of a wall. The regression coefficients and corresponding p-values for Equation (B.8) are given in Table B.3. It can be seen that the contribution of the $\hat{\beta}_{C-B}$ coefficient is very insignificant, leading to the conclusion that there is little, if any, difference between the incrementally increasing cyclic loading procedure and the sequential-phased displacement cyclic procedure. Apart from the loading type C, the analysis also shows that there is low significance in the difference between the simulated seismic loading (type D) and loading type B.

The next step in the analysis is to modify the model by eliminating insignificant parameters and to reanalyze the data to determine any difference. In this case, we will eliminate the parameter for loading type C since we have seen that there is very little reason to maintain it in the model. We have sufficient justification to remove the parameter for loading type D as well, but we will only remove one parameter to demonstrate how the model changes with the removal of a single parameter. In the process of reparameterizing the model, we refine the $\hat{\mu}_{sB}$ term to also encompass walls tested using loading type C. The data table for the reduced model are given in Table B.4.

In the reduced model each of the parameters increased in significance. A large part of this increase came from eliminating an insignificant parameter from the model. Eliminating a parameter adds a degree of freedom to the analysis and can potentially decrease the variance for some of the parameters. At this point, we see that the significance for the loading D case increased, but not sufficiently for us to retain it in the model. We will, thus, eliminate the loading D parameter

Table B.4: Reduced-Model Parameters for Tomaževič et al. (1996)

Parameter	Value	p
$\hat{\mu}_{sBC}$	24.55	0.00004
$\hat{\beta}_{\sigma}$	0.203	0.00017
$\hat{\beta}_{d}$	4.953	0.09694
$\hat{\beta}_{A/BC}$	10.61	0.00405
$\hat{\beta}_{D/BC}$	4.033	0.3889

Table B.5: Further Reduced-Model Parameters for Tomaževič et al. (1996)

Parameter	Value	p
$\hat{\mu}_{sBCD}$	25.89	0.00002
$\hat{\beta}_{\sigma}$	0.203	0.00017
$\hat{\beta}_{d}$	4.953	0.09674
$\hat{\beta}_{A/BCD}$	8.862	0.00797

from the model and redefine the mean to also encompass those tests using the simulated seismic loading history. The latest reduced model is shown in Table B.5.

In the latest reduced model, it can be seen that eliminating the extraneous parameter for seismic loading had little effect on the other parameters' significance. Furthermore, all of the terms are significant at the 10 percent level or better. This suggests that the latest reduced model best represents the data from their study. Equipped with a model with all-significant parameters, we can objectively draw conclusions based on the data.

From the Tomaževič et al. study, it is apparent that axial load, dynamic loading, and loading history influence the shear capacity of a masonry shear wall. The data show a very significant increase in shear strength for monotonically loaded wall compared to periodically and harmonically loaded walls. This is likely because subsequent loadings at smaller displacements induce multiple areas of masonry damage that decrease the shear capacity at higher displacements. The data also suggest that there is no significant difference in shear strengths for walls tested using either incrementally increasing cyclic, sequential-phased displacement cyclic, or simulated seismic loading procedures. This conclusion is notably beneficial to those wanting to compare tests in the

TCCMAR series to other tests because it appears that the two load procedures produce similar results Dillon and Fonseca (2014a)

Some final notes should be made about this example. Since the data matrix was originally non-full rank, the mean shear strength parameter was redefined to include the base assumption that the data were tested statically using the loading type B procedure. This choice of basic assumptions affects what conclusions can be obtained from the analysis. During the analysis we discovered that the loading types C and D were not significantly different from type B. However, if loading type A were selected as the base load history, the analysis would have determined that the parameters for loading types B, C, and D were significantly different from type A, but it would not have identified that there is little significant difference between types B, C, and D.

In linear regression modeling, the individual parameters entering the equation must be additive. However, through reparameterization of the model and the use of logarithmic functions, coefficients for multiplicative parameters can be found. For example, if we believed that the parameters for the dynamic and monotonic procedures should be multiplicative in nature—and they likely are—then we can use algebraic manipulation to find a form of the problem that can be solved. This produces the equation

$$V_i = \gamma_{dyn}\gamma_{mt}\mu_{sBCD} + \beta_\sigma\sigma_i + \varepsilon_i \,. \tag{B.18}$$

where

γ_{dyn} = 1.33 is an adjustment coefficient for dynamically tested walls,
γ_{mt} = 1.19 is a strength adjustment coefficient for monotonically tested walls,
μ_{sBCD} = 25.65 kN, and
β_σ = 0.203 m^2 which was assumed from the previous analysis.

Equation (B.18) suggests that monotonic testing inflates the strength of a wall by about 19 percent. The dynamic tests in their study averaged 33 percent higher strength, but this value is not universally applicable due to variations produced by strain rate effects.

Tomaževič et al. actually tested 32 individual masonry specimens during the course of their study; however, in the literature they report the average of each pair of identical specimens.

It would be more ideal to analyze the entire data set with each specimen listed on a separate row so that the full effects of the variance within each pair is included within the analysis of variance. However, using the average from each pair made no difference in the estimated value of each coefficient. Furthermore, since they designed their study as a balanced model (i.e., equal numbers of specimens within each group and subgroup), the p-values determined in the analysis are relatively correct as long as the variance is similar between the pairs.

B.4 Conclusions

In this article we have shown that experimental data on masonry can be represented in matrix form to facilitate least squares regression and analysis of variance. This was demonstrated using two examples from prior studies on the in-plane shear strength of masonry walls, Schultz et al. (1998) and Tomaževič et al. (1996). The former study contained only quantitative data and the latter contained both quantitative and qualitative data. Both studies were analyzed using least squared regression and analysis of variance to draw conclusions from the data. Analysis of the data from Schultz et al. (1998) led the following conclusions:

- It appears that the shear reinforcement did not contribute to the shear strength of the wall.
- The wall shear strength is better correlated with the reciprocal of the shear span ratio.

Analysis of the data from Tomaževič et al. (1996) led to the following conclusions:

- There appears to be no significant difference in shear strengths for walls tested using either incrementally increasing cyclic, sequential-phased displacement cyclic, or simulated seismic loading procedures. Data from tests using any one of these three histories can be effectively compared without need for correction.
- Monotonic loaded specimens demonstrate an increase in apparent shear strength over specimens tested using incrementally increasing cyclic load histories.
- Axial load has a positive correlation with wall shear capacity.

In both cases, the results from the statistical analysis revealed new insights from the data that were not previously noted. These tools can be equally used with data from new research as

well as from prior studies. By using these procedures to reanalyze data from existing studies, new facts can be uncovered that were not previously revealed by the data, adding to the existing body of knowledge.

Though not covered in this article, the advanced application of these procedures can be used to compile and compare data from more than one research study.

APPENDIX C. SHEAR TEST REPORTING METHODOLOGY STANDARDIZATION

C.1 Introduction

Our understanding of masonry has undergone a significant and substantial increase over the past half century—greater than that from all the previous millennia combined. Much of this increase in knowledge has been facilitated by the transition of masonry practice from traditional construction methods to an engineered-design approach. As part of the transition to engineering design masonry materials have been standardized and experimental studies have been performed to better understand masonry as a building material. Standardization of the components and assembly methods for masonry have created a consistency such that designers can be confident that the structures that are constructed will meet or exceed the standards assumed during the design process. To date, this same level of standardization has not been present in all aspects of the design and execution of masonry research studies.

The growth in masonry knowledge over the last half century has been significant in helping engineers understand masonry performance during seismic excitations. Researchers have had to surmount the hurdles of anisotropy and modeling difficulties that are inherent in a material assembled from so many different constituent materials. The effectuality of this growth has arisen from the quantity of experimental studies that have taken place. These masonry studies have been conducted on a very wide array of topics using diverse experimental methods. The breadth and quality of the research have enabled engineers to quickly grasp and understand many of the qualities (both positive and negative) that are unique to masonry as a building material.

Viewed in an epistemological light, the end goal of all masonry research is to develop constitutive models that can accurately represent the strength and behavior of masonry elements. These models are particularly necessary when trying to understand masonry performance under seismic excitations because of the substantial variability present in these scenarios. Since single research studies do not contain sufficient information to build or validate such models Schmidt and

Hunter (1997), model construction and validation are performed through meta-analysis on a large set of data amalgamated from multiple research studies. The data used in meta-analysis must be compatible so that variations between research practices don't artificially inflate the experimental variance of the data.

One subfield of masonry research that is a key focus within the area of earthquake engineering has been the testing of masonry shear walls and the development of predictive equations for shear strength. Many new studies have been added to the repertoire of masonry shear wall research since the current equations were originally developed. The development of new, updated equations will necessitate the meta-analysis of many studies within the body of shear wall studies. Within this conglomerate of data, researchers have used a wide array of procedures in designing, performing, and reporting their experiments.

The varying implementation practices of masonry research have created uncertainty in how data from one study relate to those of another and how they all relate to masonry in the field. For example, uncertainties and biases that are present within shear wall test data result from disparities in boundary conditions; neglecting strain rate effects; the use of varying loading patterns; and from ignoring size effects. These uncertainties must be remedied to successfully synthesize the data together.

The first and most important step of data synthesization is to choose a standard method to report data for each source of uncertainty. This choice of standard is crucial because it will function as the baseline for comparing data between past, present, and future research studies. The significance of standard selection necessitates that it not be made arbitrarily, but with a clearly stated methodology and reasoning. Standard methods, objectively chosen and accepted, will provide a means by which research data may be properly correlated with those from other studies. They also broaden the scope of the combined research and make the results of the data synthesis more widely applicable to the greater population of masonry structures

An important disclaimer that must be made is that the standards function solely as a baseline measure and do not restrict researchers from performing specific types of tests, nor do they necessitate that specific methods be employed in gathering experimental data. Each standard merely requires that any data collected also be reported in a standardized form. However, for a standard to be fully efficacious, correlations between the standard and other common measures must be

quantified such that the standardization of data is possible. This field of masonry research has been little-tread by researchers and the understanding of the varying correlation effects is poorly understood, especially at a quantifiable level.

C.2 Purpose

This article will present a review of some of the experimental data practices used by researchers in performing in-plane masonry shear wall research. In addition, it will present a methodical procedure for developing appropriate standards to be used in systematically synthesizing data from multiple masonry shear wall studies. The authors will discuss each source of uncertainty listed previously and will recommend a method to be used in standardizing both past and future research data. The authors will also address limitations in current understanding and list areas of future research.

C.3 Methodology

The creation and selection of standards should be done as objectively and transparently as possible. This ensures that the results of meta-analyses are acceptable within the professional community and that such results can be replicated and expanded as additional masonry research data become available. As described earlier, the use of disparate methods in gathering and reporting data do not pollute the analysis, but enrich and broaden it. However, the varying methods in use impose a situation in which a choice must be made between one or more methods as to which one will become the standard for reporting data. To make the choice as unbiased and objective as possible, the authors will first set out the methodologies to be used in selecting the standards to be proposed in this article.

C.3.1 Plurality

The authors feel that the first criterion to be investigated while performing a systematic review of the research literature ought to be to observe and note which procedures are used most by researchers in our field. In addition to providing a de facto consensus about which method to

choose, the preferential selection of one method over another by erudite researchers suggests that there may be a rational basis to their preference.

C.3.2 Representation

The next criterion used in judging procedures will be to investigate which ones most accurately agree with observed performance of masonry walls. It should be noted that this criterion is liable, somewhat, to subjectivity because of the poor replicability of conditions under lateral loading and because the results of tests may be somewhat biased by the testing procedures used. The true behavior of masonry under seismic excitations is still somewhat uncertain and is evidenced by the non-standard methods of testing used by researchers. At the very least, the authors will provide and epistemic study of current procedures in light of the understood behavior of masonry shear walls.

C.4 Analysis

C.4.1 Boundary Conditions

The actual boundary conditions for masonry shear walls are variable depending on the configuration and stiffnesses of the wall and connecting elements. Researchers have attempted various in-plane loading methods for testing masonry shear walls. While the individual test setups have varied widely, the individual tests can be grouped into three types of boundary conditions, namely: cantilever conditions, racking conditions, and fixed-fixed conditions. The use of each type of end condition for 492 masonry shear wall tests are listed in Table 1. The table shows three distinct trends in when each type was used, the number of studies using each one, and the number of specimens in each individual study.

Racking tests were the predominant end condition in the first series of masonry shear wall research. In racking tests the lateral load is applied to a top corner of the wall using a hydraulic actuator. Lateral movement of the specimen is restrained at the opposite, lower corner of the specimen and the overturning moment is resisted vertically by a frame connected at the same upper corner as the actuator. The racking tests are quite similar in loading to diagonal compression

tests, but enable the testing of full-size specimens and facilitate the application of axial load during the test. Racking tests were quickly supplanted by other testing modes, first by cantilever tests and eventually by fixed-fixed tests.

The first cantilever masonry test found was a single specimen tested in 1963. Cantilever tests have the advantage in that they are simple to set up, require less-specialized equipment to perform than fixed-fixed tests, and are more cost effective for smaller studies. This is evidenced by the fact that studies using a cantilever test set-up only averaged about nine specimens per study. For these reasons, it is the method used by the greatest number of researchers. In cantilever studies the load is commonly applied to a beam affixed to the top of the masonry panel, causing the inflection point (i.e., the height at which the lateral load is applied) to be located higher than the height of the masonry wall. This is significant because it will affect the analytical results if a researcher assumes the moment arm to be equal to the height of the masonry.

The first set of masonry walls tested under fixed-fixed conditions occurred in 1976. These tests consisted of double-pier specimens in which the whole assemblage was tested as a cantilever but each individual pier was subjected to fixed-fixed conditions. The first true fixed-fixed test occurred in 1978. This method of testing is more complicated and expensive than the other two, making it only economical for studies with larger quantities of specimens and advanced research facilities. This is evidenced by the fact that studies using fixed-fixed conditions were performed by fewer researchers but averaged over sixteen specimens each. The quantity of masonry walls tested in this mode made this the most-used method in the research literature. With this method of testing, the inflection point is generally considered to be located at the mid-height of the wall.

Since real-life conditions vary from wall to wall, there is not one method of testing that is more representative than the others. However, there must be a way that data from the three types of tests can be correlated together. Researchers have traditionally used the height to length ratio of a masonry panel for the purpose of comparing the performance of walls panels with relatively differing geometries. This term is called the aspect ratio. The aspect ratio has limited use within masonry shear wall research and is only useful for comparing shear wall strengths for walls that are tested under identical boundary conditions.

Since aspect ratio is insufficient at providing a means of comparing tests from studies which use different boundary conditions, there must be a better parameter that overcome the limitations

Table C.1: Summary of Boundary Conditions for Masonry Shear Wall Studies

Boundary Conditions	Research Study	Specimens	Study Count	Specimen Count
Racking	Jorquera G (1963)	9	4	33
	Scrivener (1966)	4		
	Meli and Salgado (1969)	8		
	Scrivener (1969)	12		
Cantilever	Jorquera G (1963)	1	21	192
	Meli et al. (1968)	10		
	Williams (1971)	21		
	Priestley and Bridgeman (1974)	4		
	Priestley (1977)	6		
	Priestley and Elders (1982)	3		
	Tomaževič and Lutman (1988)	16		
	Shing et al. (1990)	22		
	Ghanem et al. (1992)	6		
	Brammer (1995)	12		
	Tomaževič et al. (1996)	16		
	Haider and Dhanasekar (2004)	14		
	Voon (2007)	10		
	Maleki (2008)	5		
	Kasparik (2009)	5		
	Minaie (2009)	6		
	Haach et al. (2010a)	8		
	Nolph (2010)	6		
	Elmapruk (2010)	6		
	Da Porto et al. (2011)	14		
	Saiedi (2011)	1		
Fixed	Mayes et al. (1976b)	17	16	267
	Hidalgo et al. (1978)	9		
	Chen et al. (1978)	24		
	Hidalgo et al. (1979)	12		
	Thurston and Hutchison (1982)	8		
	Sveinsson et al. (1985)	26		
	Woodward and Rankin (1985)	7		
	Matsumura (1985)	75		
	Matsumura (1987)	6		
	Igarashi et al. (1988)	9		
	Kaminosono et al. (1988)	19		
	Johal and Anderson (1988)	32		
	Yancey and Scribner (1989)	9		
	Schultz (1996a)	6		
	Schultz et al. (1998)	6		
	Minaie (2009)	2		

of the aspect ratio. An absolute means of comparing wall geometries for all boundary conditions has been developed through the research and is currently used in the code shear strength equation for several codes. This ratio is called the shear span ratio. The shear span ratio has historically been represented by a/D but more recently has been represented in its code form

$$\frac{a}{D} \equiv \frac{M_u}{V_u l_w} \tag{C.1}$$

where

a = is the vertical distance from the inflection point to point of maximum moment,
M_u = the ultimate moment demand at a along the height of the wall panel,
V_u = the ultimate shear demand at the same height along the wall panel, and
$D = l_w$ = the shear length of the wall panel.

The shear span ratio is defined as the ratio of the effective height between the points of maximum and zero moment and the shear length of the wall (see (C.1)).

Recommendation

Researchers should use the shear span ratio over the aspect ratio when describing masonry shear wall geometry. The shear span ratio is already in use in the shear strength equations from several masonry standards. The shear span ratio is more favorable to use because it more directly correlates to masonry shear strength than does the aspect ratio and permits research results to be compared independent of the boundary conditions. It appears from the literature that some treat the two terms as though they were synonymous. Though there is one situation where the two ratios are equal, their definitions are distinct. The shear span ratio should be calculated by dividing the vertical distance between the points of inflection and maximum moment by the shear length of the wall or by using equation (C.1).

C.4.2 Strain Rate Effects

Most materials exhibit an increase in strength that is proportional to the increase in the strain rate on the material. To date, little quantitative research has been performed on strain rate effects in masonry structural elements or materials. All the studies performed on shear walls found in the literature show only qualitative type testing in which specimens are divided between static and dynamic categories. Many of the properties for strain rate effects are inferred from research about the strain rate effect in concrete. Many researchers (Abrams, 1988; Paulson and Abrams, 1990; Tomaževič and Velechovsky, 1992; Tomaževič, 2000; Tomaževič et al., 1996; Williams and Scrivener, 1974) have observed strain rate effects in masonry. In all cases they have measured higher shear strengths in dynamic than in static experiments. This increase in strength appears to be limited solely to the strength of the specimens. It has been observed that the drift values for characteristic points in the hysteresis envelopes (e.g., diagonal cracking) do not change with differing strain rates Paulson and Abrams (1990); Tomaževič (2000).

Paulson and Abrams (1990) found that the strain rate can have an appreciable effect on crack propagation within shear walls. They observed that cracking was more severe in the case of statically tested specimens than for dynamically tested ones. In the case of the static specimens, they observed cracks that slowly propagated over the course of several minutes as alternate stress paths developed within the masonry panel. They hypothesized that one reason for the apparent increase in strength for the dynamic specimens is that the wall is strained at a high enough rate that crack dispersion is not able to occur.

It is probable that many, if not most, of the mechanics involved in the strain rate effects for masonry are similar to those for concrete. Researchers have found that strain rate effects in compression are more pronounced for concrete with weaker strength. Rossi et al. (1994) hypothesized that this is due to the presence of free water in the concrete. Since lower strength concretes typically have a higher water/cement ratio, they would be more pronouncedly affected by increasing strain rates. The potential impact of this phenomenon on masonry is uncertain.

In the case of brick masonry, very little free water remains in the units after the firing process, but free water would be present in the mortar and grout of a clay masonry assemblage. In the case of concrete masonry, the net strength of the units typically corresponds more closely to the strengths of weaker concretes, but the units are made from a very low-slump (typically zero)

concrete mix with a low water/cement ratio. Since these two properties seems to contradict each other, it is uncertain whether the strain rate effects in concrete masonry would more closely match those of stronger or weaker concretes.

Research conducted by Bischoff and Perry (1991); Malvar and Crawford (1998) has shown that materials have a threshold strain rate below which the strength of the material is independent of the strain rate. Below the threshold the strain rates are considered to be quasi-static (or often simply referred to as static). Above the threshold the strain rates are considered dynamic. In the dynamic rage the dynamic increase factor (DIF)—the ratio of strength to quasi-static strength—increases as a logarithmic function of the strain rate. The threshold between the quasi-static and dynamic ranges of loading is known as the reference static strain rate. The Comité Euro-International du Béton (CEB, 1988) defines the transition strain rate as $\dot{\varepsilon}_s = 30 \times 10^{-6}\, s^{-1}$. Malvar and Crawford (1998) have shown that strain rate effects in concrete are different in the tension and compression directions.

Hao (2008) conducted uniaxial compressive tests to study the strain rate effects on brick and mortar. They found a reference static strain rate of $\dot{\varepsilon}_s = 20 \times 10^{-6}\, s^{-1}$ for mortar—a relatively insignificant variation from the CEB value—and $\dot{\varepsilon}_s = 2 \times 10^{-6} s^{-1}$ for brick. Wei and Hao (2009) numerically synthesized these parameters together and derived a reference static strain rate of $\dot{\varepsilon}_s = 1 \times 10^{-3}\, s^{-1}$ for a clay brick/mortar assemblage. They made no explanation as to why the reference strain rate for the assembly is several orders of magnitude greater than the constituent materials. Part of the reason may have been the lack of research into the strain rate effects for the material under tension and their assuming the same coefficients for tension and compression.

The vast majority of masonry shear wall tests fall within the quasi-static range. This is due to the specialized equipment and additional cost that dynamic testing requires. A large part of all the masonry walls tests were carried out before the necessary equipment was developed. In practice, masonry shear walls may be designed to resist static loads (e.g., earth pressure loads), dynamic loads (e.g., seismic and wind loads), or both. In current design practice, there is no distinction in the shear strength prediction equations for static or dynamic shear capacity.

Since masonry wall are a conglomeration of multiple different materials, their response to strain rate effects is difficult to postulate. Hao (2008) found that clay brick is not as sensitive to strain rate effects as is mortar. Since clay brick typically exhibits a greater strength than mortar, is

it possible that at sufficiently high rates of strain that the strength of the mortar could exceed the strength of the brick. Though there is likely a greater compatibility between mortar and concrete block, the greater amount of free water within mortar could likely cause it to exceed the strength of the concrete masonry units under sufficiently high rates of strain. A similar scenario could occur in the case of grout and reinforcement. The case of reinforcement is more poignant.

The ultimate strength of steel is less sensitive to strain rate effects than its yield strength and both are less sensitive than the strength of concrete and fired clay. Paulay and Priestley (1992) point out that as the rate of strain increases for a reinforced masonry shear wall, the ultimate force exerted on the reinforcement increases faster than the apparent strength of the steel. Under high enough rates of strain it is theoretically possible for the reinforcement to instantaneously rupture at the onset of cracking in the masonry panel. This is significant as a shear wall that fails in a ductile manner at quasi-static loads could theoretically fail in a brittle manner under sufficiently high rates of strain.

Recommendation

In order to correlate data between research studies, it is necessary to have a standard procedure for reporting data that is independent of strain rate effects. The two options available are for researchers to report the equivalent static or equivalent dynamic strength. Looking at the available research it appears that it would be best for all to report the equivalent static strength.

More test data are available for static testing conditions than for dynamic conditions. The effect of strain rate is still not well understood in masonry, especially under shear situations. Many studies performing dynamic tests also included static tests for correlating the data. In these cases, the data from the experiment can be used to determine the correlation between static and dynamic tests. This correlation can then be used to adjust the data from the dynamically tested specimens to provide their equivalent static shear strength.

In studies that solely use dynamic loadings there are currently no methods in place to adjust the data. Until more research is performed on the strain rate effects for masonry assemblages, the only possible means of correlating data for a dynamic-only study is to find one or more similar studies in which both categories were tested and to use the correlation determined from those

studies. This last method is encumbered by the fact that many researchers do not report any time rate data from their studies.

Static loads can be considered to involve less uncertainty than dynamic loads. Static loads can generally be determined analytically with a fairly good level of confidence. Dynamic loads are dependent on a greater number of variables, many of which are uncertain or are determined probabilistically. Dynamic loads occur randomly and generally have a lower probability of occurrence. The uncertainty for static loading and strength conditions is much lower than that for dynamic scenarios. Using representative strengths for static loads is justified because the phenomena are fairly-well understood whereas the conservatism in the case of dynamic loads accounts for some of the uncertainty.

Below the reference strain rate, the DIF is constant and equal to unity. This means that there exists a wide range of quasi-static strain rates that are equivalent and are naturally correlated to each other. Within the dynamic range of strain rates, all strengths are correlated to the rate of strain used. To choose dynamic testing as the standard procedure would also require the selection of a standardized strain rate. Selecting such a rate would be a highly subjective process since all dynamic loads are highly variable functions of location, environment, and structure. No single strain rate would effectively represent all possible situations. Additionally, any dynamic-equivalent strength would be unconservative for static loads and would have to be reduced to find the static capacity.

Using a dynamic strain rate standard would either require all future masonry researchers to use dynamic strain rates in their tests or to have to adjust their static data to the dynamic equivalent. In the first case, dynamic tests require more complicated test equipment and additional considerations in setting up the test. The additional equipment, labor, and costs would make dynamic testing prohibitive for many researchers with an interest in masonry research. In the second case, much research would need to be conducted to determine the correlation between the static and hypothetically-chosen dynamic loading rates before past research data could be effectively adjusted and compared to dynamically tested data. Even if this were to happen, all data adjusted from static tests would be dependent on the results of these initial correlation studies, eliminating some of the independence between research studies.

In summary, the solely justifiable decision is to use the static-equivalent strength as the standard for reporting masonry research data. By reporting the static-equivalent strength for their study data, researchers will be able to correlate and compare their data to those from other researchers and to masonry design equations already in place.

C.4.3 Loading History

Seismically induced loads on masonry walls are highly variable and unpredictable. There have been multiple loading histories proposed and used in testing masonry shear walls. The masonry literature shows five procedures that have been used in testing masonry walls. This article will refer to the differing loading procedures found in the literature as: Monotonic; Reversed monotonic; Incrementally-increasing cyclic; Sequential-phased displacement, and Simulated seismic. Each loading pattern may include different input parameters, but the overall motion is the same. A summary of the loading histories used in the various masonry shear wall research studies is provided in Table 2.

The monotonic method is the easiest to perform because it only requires a single-action actuator. In the monotonic procedure, the specimen is loaded at a constant strain or stress rate until failure. The reversed monotonic procedure is similar in how it begins, but after some level of strength or damage the load is reversed and measurements are taken in the other direction. The load may be reversed multiple times during the course of the test. Load reversal is accomplished through either a dual-action actuator or by unmounting the actuator and affixing it to the other side of the specimen. The primary differences between the reversed monotonic procedure and the incrementally-increasing cyclic procedure are that the initial amplitudes of the reversed monotonic are generally greater than the yield displacement of the wall, that the amplitudes increase very little, and a lower number of load reversals is used.

In the incrementally-increasing cyclic procedure, the wall is subjected to cyclic lateral loads of increasing amplitude. Two or three successive cycles are used at each displacement level before increasing the amplitude. The initial set of cycles at designed to occur at or below the calculated yield strength of the wall. The displacements for each subsequent group is chosen arbitrarily or to correspond to calculated ductility ratios. The cycles can either be sinusoidal or saw-tooth shaped.

The incrementally increasing cyclic procedure is the most-commonly used procedure in masonry shear wall tests.

The sequential-phased displacement procedure was originally developed and proposed by Porter (1987). It organizes drift cycles into undulated sets in which the drift amplitude of each succeeding cycle gradually increases up to a peak then decreases to null. Each subsequent undulated set has a higher peak wave amplitude. When the first major event (FME) occurs, the drift amplitude during the event is recorded for that specimen. The peak amplitude for each subsequent set is then determined as function of the drift at the FME. Reducing the amplitude to null between each set helps to better define the hysteretic behavior by providing a stabilized hysteretic curve.

The simulated seismic procedures use either recorded or synthesized earthquake motions to develop a loading history to apply to a masonry wall specimen. The history can either be applied directly to the top of the wall or applied intertially through a shake table. Due to the limitations of test equipment, the motions must be put through a band pass filter to eliminate those frequencies that cannot be reproduced. Some researchers use a single earthquake motion while others use several motions either separately or amalgamated together to form a new history. The sheer number of variables and disparities between researchers make seismic-based procedures very difficult to standardise.

Analysis performed by Dillon and Fonseca (2014a, see also Appendix B) on the data from Tomaževič et al. (1996) found that there is no statistical significance between walls tested using the incrementally-increasing cyclic and sequential-phased displacement procedures. They also found that there was little statistical significance between those two procedures and the simulated seismic history. On the other hand, Dillon and Fonseca found a very statistically significant difference between the monotonic history and the periodic or harmonic histories. Their analysis of the data showed a 19 percent increase in shear strength for walls that were tested monotonically as opposed to those tested periodically or harmonically.

As part of this current study, a similar statistical analysis was performed on data from Woodward and Rankin (1985) and Haider (2007). The authors found no statistically significant difference between the reversed monotonic and incrementally-increasing cyclic loadings. This suggests that the reversed monotonic loading may be included with data from the other periodic loading patterns.

Table C.2: Masonry Shear Wall Studies Using Monotonic Loading

Research Study	Specimens	Studies	Specimens
Scrivener (1966)	4	7	60
Scrivener (1969)	12		
Meli and Salgado (1969)	8		
Woodward and Rankin (1985)	3		
Matsumura (1987)	23		
Ghanem et al. (1992, 1993)	6		
Tomaževič et al. (1996)	4		

Table C.3: Masonry Shear Wall Studies Using Reversed-Monotonic Loading

Research Study	Specimens	Studies	Specimens
Jorquera G (1963)	10	3	24
Woodward and Rankin (1985)	4		
Haider (2007)	10		

Recommendation

It is proposed that researchers report the strength of masonry shear wall data equivalent to periodically and harmonically tested specimens. Data from wall tested under monotonic loading would need to be adjusted to provide the strength equivalent to the other histories. Since monotonic testing has not been used on masonry shear walls for nearly two decades, this practice would affect few researchers.

Using the cyclic-equivalent strength to report masonry shear wall data is conservative for design cases with monotonic loads since walls demonstrate a greater shear capacity under this loading. Any uncertainty between the various periodic or harmonic loading patterns does not add unnecessarily to the variance of the pool of shear wall data. The variation in loading patterns from seismic loads is likely greater since they occur outside of laboratory conditions and have a much more complicated frequency content. On the contrary, the variations in cyclic load testing help make the data pool more representative of the random perturbations encountered in real-life scenarios.

Table C.4: Masonry Shear Wall Studies Using Phased-Sequential Displacement Loading

Research Study	Specimens	Studies	Specimens
Meli et al. (1968)	10	32	398
Williams (1971)	21		
Priestley and Bridgeman (1974)	4		
Priestley (1977)	6		
Mayes et al. (1976a)	17		
Hidalgo et al. (1978)	9		
Chen et al. (1978)	24		
Hidalgo et al. (1979)	12		
Thurston and Hutchison (1982)	8		
Priestley and Elders (1982)	3		
Sveinsson et al. (1985)	26		
Matsumura (1985)	52		
Matsumura (1987)	6		
Igarashi et al. (1988)	9		
Kaminosono et al. (1988)	19		
Johal and Anderson (1988)	32		
Tomaževič and Lutman (1988)	16		
Brammer (1995)	12		
Tomaževič et al. (1996)	4		
Haider (2007)	40		
Voon (2007)	10		
Maleki (2008)	5		
Minaie (2009)	8		
Haach et al. (2010a)	8		
Nolph (2010)	6		
Elmapruk (2010)	6		
Da Porto et al. (2011)	14		
Yancey and Scribner (1989)	9		
Shing et al. (1990)	22		
Schultz (1996a)	6		
Tomaževič et al. (1996)	4		
Schultz et al. (1998)	6		

Table C.5: Masonry Shear Wall Studies Using Simulated Seismic Loading

Research Study	Specimens	Studies	Specimens
Tomaževič et al. (1996)	4	3	10
Kasparik (2009)	5		
Saiedi (2011)	1		

C.5 Size Effects

Due to cost, lab space, or other constraints, many researchers choose to test reduced-scale models in their studies. When reduced-scale specimens are tested, different test parameters must be scaled differently in order to provide for consistency of units. The vast majority of structural researchers using small-small specimens favor the Simple Model Scaling over the Complete Model Scaling due to the difficultly in scaling the modulus of elasticity of the material Hamedzadeh (2013). In the Simple Model, the parameters of strength, stress, strain, Young'modulus, and velocity are maintained without scaling. The only notable parameter adjustment for the Simple Model is that of time. However, since strain rate is not scaled in the Simple Model, no adjustment of strain rate is necessary.

Size effects have been extensively studied and reviewed in the literature Tomaževič and Velechovsky (1992); Tomaževič (2000); Abrams and Kreger (1982); Abrams and Tangkijngamvong (1984); Bažant (1997, 2009). There appears to be an overall consensus as to validity of reduced-scale testing, but there have been some limitations that have been noted. Abrams and Kreger (1982) noted that reduced-scale models perform well in modeling energy dissipation, modeling strength and stiffness degradation with increasing loading cycles, and in modeling hysteretic behavior. Abrams and Tangkijngamvong (1984) found that response and displacements were similar between the models and prototypes, but that the cracking patterns were not the same. Tomaževič (2000) summarized the applicability of scaling by noting that it can generally model the overall behavior of the structural system and its global failure mechanisms, but the degree of accuracy in modelling structural elements limits the reduction in model size.

Bažant 1997; 2009 has done much experimentally and analytically to understand the effect that size has on quasi-brittle materials, e.g., concrete and masonry. Many of his tests have focused on concrete specimens, but he suggests a likely correlation of his findings with masonry. He found that the scaling factor (i.e., the ratio of strengths between models of differing scales) is a function of the scale and the largest aggregate size. He notes that for materials with microscopically sized aggregates (i.e., clay brick), the size effect is roughly unity within the typical scale limits for masonry tests. For large aggregate sizes relative to the size of the structural elements the scale effect is more pronounced, but it is still close to one at the scales used in masonry testing. The findings of Bažant have two effects on reduced-scale masonry tests. First, the relatively small

scale factors used in research aren't significantly large enough to produce notable scale effects in the studies. Second, since scale effects are a function of the ratio between element and aggregate sizes, any size effects would be accounted for through the testing of reduced-scale masonry prisms.

Recommendation

There are two means whereby researchers can report the results of scaled masonry research. The first is to report the reduced-scale data as measured from the experimental model. The second is to report the equivalently adjusted full-scale data for the prototype. The second method is more useful when interpreting results because they are more similar to the values to which designers are accustomed. When comparing and compiling data from multiple research studies, it is not advantageous for the parameters of one study to be outside of the typical range used for masonry design. When analyzing data, the presence of outlying independent variables can unduly influence the analysis due to their distance from the main body of data.

As discussed above, it has been shown that there are limits to the scale by which a masonry model may be effectively reduced. Within these relatively small limits it has been found that size effects are ineffectual, and any effect would be considered within the strength of masonry prisms constructed of the same reduced-scale materials. It has been further shown that data is more advantageous when represented in its equivalent full-scale form. This article proposes that that standard method of reporting reduced-scale masonry test data is to report the full-scale data for the equivalent prototype.

C.5.1 Shear Strength Reporting

Researchers used three methods were used two methods to report the experimental shear strength of masonry shear walls. The first was that researchers reported the peak strengths in each of the two directions (i.e., pushing and pulling). The second method was to report average of the peak strength in each direction. The third method was to report the ultimate experimental shear strength of the shear walls regardless of direction. Wall strengths found using monotonic testing were naturally reported using this last method.

The shear strength from the two directions are theoretically independent. After each load reversal the diagonal shear cracks from the opposite direction close due to diagonal compression forces. After these cracks close the diagonal compressive strength is unaffected. The shear capacity for the new direction is unaffected by the strength degradation of the opposite direction. The theory of strength independence is partially limited by horizontal shear cracking and yielding of the shear reinforcement, which are not directionally independent. Some evidence of this strength independence is the fact that the ultimate peak strength for different specimens is distributed between both directions.

The variance between the two peak strengths provides an indication of the variance in material strength within the wall panel.

Recommendation

Ideally, all three methods should be report together with the coefficient of variation for the specimen. If only one method can be used then the first reporting method is preferable because the ultimate, average, and coefficient variance of the wall can be determined from the data. The average peak strength is more representative of the wall strength as a whole and is the most reported value. The ultimate peak strength represents the upper limit of the specimen strength. Using this value in regression analysis would result in an equation that is unconservative.

C.5.2 Prism Geometry

The effect of prism aspect ratio has been considered by several researchers. Hamid et al. (1978) tested 146 concrete block masonry prisms and concluded that two block high prisms do not accurately represent the strength and failure mode of walls. They found that three block high prisms better represented the strength of the masonry walls for the block type used. They noted that blocks of differing geometries may require more courses to overcome the influence of the lateral confinement from the platens.

Boult (1979) tested several different types of masonry blocks using prism aspect ratios between two and five. Their tests showed that the compressive prism strength decreased with increasing aspect ratio. Boult observed that the decrease in compressive strength became negligible

for heights between five and twelve courses. Hegemier et al. (1978) performed similar masonry prism tests and concluded that it is the number of courses and that primarily influenced the prisms strength and not the prisms aspect ratio.

Hilsforf (1969) performed analytical analysis of clay masonry prisms neglecting lateral confinement. Hilsforf found from his analysis that mortar joint thickness also has an influence on prism strength. The influence of joint thickness on prism strength was experimentally studied by Francis et al. (1970) who tested a series of four-course brick prisms with varying joint thickness. They found that joint thickness was significantly influential in the strength of the masonry prisms. As joint thickness increased, the normalized prism strength (i.e., the ratio to prism strength to masonry unit strength) decreased. They observed that the data trend lines followed the shapes predicted by Hilsdorf, but their plot of the predicted values and trend lines in Figure C.1 shows differences in vertical scaling between the two.

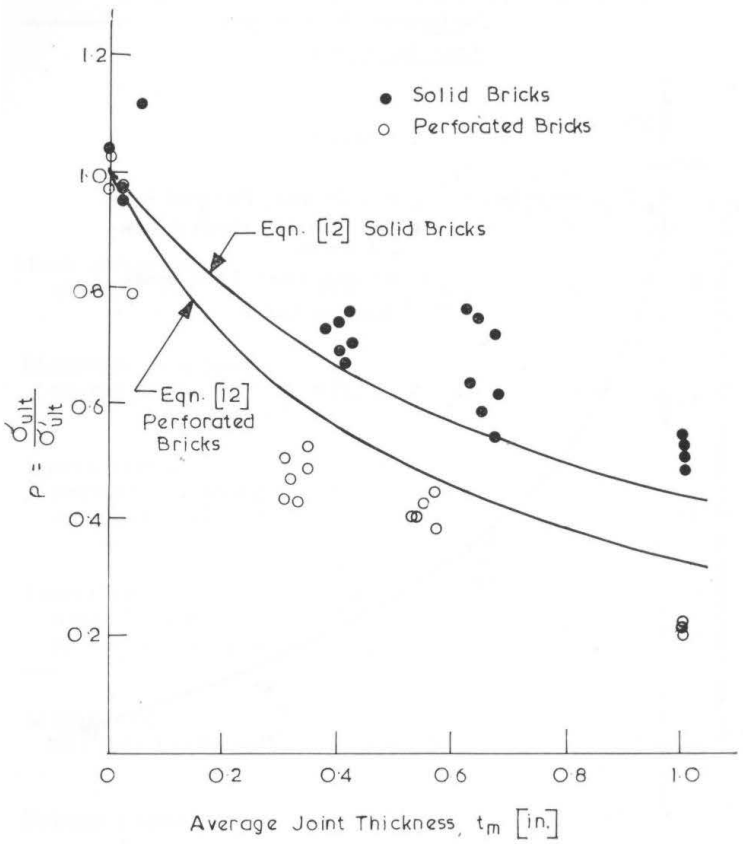

Figure C.1: Joint thickness versus normalized prism thickness (Francis et al., 1970)

From a theoretically standpoint, the effect of prism height on prism strength can be explained by three causes, lateral confinement, Weakest Link Theory, and measurement error. Lateral confinement has a pronounced effect for lower aspect ratios but diminishes quickly for ratios greater than two. The Weakest Link Theory has an effect for all prisms heights but is likely overshadowed by lateral confinement effects at lower prism heights. Accidental eccentricity has an increasing effect at greater prism aspect ratios due to secondary moment effects.

The principle failure mechanism of masonry prisms is the lateral tension induced in the masonry units by the laterally expanding mortar. Hamid et al. (1978) found that in grouted prisms, the lateral expansion of the grout also contributed to the lateral tensile failure of the masonry units. In all prism tests, the ends of the prism are laterally confined due to friction between the ends and the much stiff platens of the testing machine.

For prisms constructed from only two courses there is a gradient lateral confinement that decreases from the ends to the mid-joint. The lateral tensile stress is maximum in the masonry only at the points adjacent to the joint. These prisms demonstrate artificially high compressive strength. In the case of prisms constructed of at least three courses, there is at least one course where the lateral tensile stress is approximately constant over the whole height of the course. This means that there is significantly more masonry volume that is available to initiate a failure. In summary, it appears that the effect of lateral confinement becomes negligible for prisms with an aspect ratio of 2 or more and constructed of at least three courses.

Masonry is classified as a quasi-brittle material along with concrete Bažant and Yu (2006) and failure can be approximated by the Weakest Link Theorem. The Weakest Link Theorem assumes that failure within a single element within the masonry initiates failure of the whole specimen analogous to how a chain fails when a single link ruptures. Since the failure stresses of individual elements within the masonry are randomly distributed, increasing the volume of the stressed material increases the probability that the applied stress exceeds the ultimate stress of one of the elements and initiates failure of the entire material.

As the number of courses increases the probability of failure increases, but at a diminishing rate. The probability of failure P_f for the whole material can be approximated by the equation

$$P_f = 1 - [1 - P_1(\sigma_k)]^N \tag{C.2}$$

where N is the number of representative volume elements (RVE) in the material and $P_1(\sigma_k)$ is the probability of failure of one RVE under stress σ Bažant and Yu (2006). From (C.2) it can deduced that the probability of failure is a function of the maximum lateral tensile stress and the volume of masonry that is stressed to this level. The maximum aggregate size can be considered as the characteristic length of one RVE.

The lateral tensile stress in the masonry is a function of the material and geometric properties of the prism. The stress increases as the ratio of stiffnesses between the masonry and mortar decreases. The opposite is true in the cases of Poisson's ratio; the stress increases as the ratio between Poisson's ratios for the masonry and mortar increases. In terms of geometry, the lateral tensile stress in the masonry increases as the ratio of masonry unit height to joint thickness decreases. As the maximum lateral tensile stress increases the probability of failure increases and the prism fails at a lower compressive load.

The number of RVEs in the prism is proportional to the height of the prism. Considering the number of RVEs in vertical cross section of a masonry prism, the increases in the probability of failure becomes negligible with the increase in the height of unconstrained masonry. It is likely this effect that was observed in the study by Boult (1979) that led him to conclude that the difference between prisms with five to twelve courses is negligible. In the case of clay masonry the characteristic length is microscopic and the number of RVEs is very high. In clay masonry prisms the change in strength likely becomes negligible more quickly than for concrete masonry prisms.

Accidental eccentricity is a probable yet unstudied source of influence on prism strength. The obvious source of eccentricity is eliminated through centering the specimen properly on the bottom platen and by using a spherical-seated platen on top. Accidental eccentricity is caused by lateral variations in material stiffnesses within the prism itself. Since the materials are not uniformly stiff throughout the horizontal cross section, the center of rigidity of each specimen layer is not necessarily coaxial with the center of mass or with the other layers. As the high of the prism increases the effects of accidental eccentricity become more pronounced. Strength reduction to account for the effects of accidental eccentricity would be difficult to predict based on mechanics of materials because they are difficult to separate from the other causes of prism strength degradation. The effects of accidental eccentricity are likely best approximated together with the other influences on prism strength using empirical relationships.

The previous research and underlying theories suggest that prism strength is a function of the number of courses and not of the aspect ratio, assuming that a minimum aspect ratio is provided. Despite this knowledge, it appears that masonry standards throughout the world rely solely on prism aspect ratio for correlating prism strengths. The American standards found in ASTM C1314 use a prism aspect ratio of 2 for the base prisms height. The other masonry standards investigated, Canadian Standards Association (CSA) S304.1, British Standards (BS) 5628-2, and Australian Standards (AS) 3700, use a prism aspect ratio of 5 for the base prism height. Prisms tested in using the US standards will always reflect a higher f'_m value.

The Canadian standard is the most detailed of the four in the area of prism strength. CSA prescribes different conditions for solid and hollow masonry. It appears that this is because CSA calculates aspect ratio based on the net dimensions of the prism and not the gross dimensions. Since the ratio of height to face shell thickness in ungrouted, hollow concrete prisms is always significantly higher than 5, CSA prescribes an adjustment factor of unity if the prism is constructed of at least three courses. If a two-course prism is tested then a correction factor is applied. CSA prescribes separate correction factors for hollow clay brick prisms and solid prisms based on aspect ratio. The remaining three standards base their respective correction factors on gross dimensions only and do not differentiate between solid or hollow and concrete or clay prisms. They contain not correction the artificial strength inflation caused by using two-course prisms.

The Canadian justification of using the ratio of height to shell thickness does not appear to agree with the underlying theory of prism failure. Hollow prisms typically fail as a result of lateral tensile stresses that are coplanar with the shell plane and not normal to it. This is because the smaller thickness of the mortar normal to the shell plane does not produce sufficient cumulative lateral expansion for the shell to fail in this direction. Additionally, there is significantly more vertical shell area along the shell plane to resist the lateral tensile stress as opposed to the vertical shell area perpendicular to the shell plane. It appears that the use of gross prism dimensions is a better method for calculating prism aspect ratio for hollow prisms. The penalty in the CSA standard for prisms with only two courses agrees well with the findings of prism research.

Between the standards there are differing requirements for the quantity of prism specimens to be tested. The American and Australian standards require that only three prisms be tested whereas the Canadian and British standards require a minimum of five be tested. The British

standard is unique is that uses an additional correction factor based on the number of prisms tests. Another disparity between codes comes in how the f'_m value is calculated. In the American and Australian standards the mean strength of the three prisms is used but the Canadian and British standards used the lower bound of a statistical confidence interval based on the mean and standard deviation of the data. The CSA uses a 95 percent confidence level and assumes that the data are normally distributed. The BS uses a confidence interval that decreases as the number of tested specimens increases from five to ten and assumes a log-normal distribution.

From a statistical view the Canadian and British standards produce better approximations for prism strength because they use a higher sample size for testing and because they account for the random variation in the prism data. The Australian standard follows the recommendations of the research by requiring prisms to contain at least three courses. The other three standards generally meet or exceed this requirement for clay bricks but permit block prisms with as few as two courses.

Recommendation

There still remains much uncertainty over whether the prism aspect ratio or the number of courses has more influence over the prism strength. It seems likely that prism strength is a function of both parameters.There are also other factors, such as joint thickness, that have also been shown to influence the strength but are completely ignored by modern standards. It is also uncertain whether the relationships are the same for concrete masonry and clay masonry.

Until further research can be performed onto the area of masonry prism strength the best course is to continue with using prism aspect ratio to correlate strength between difference prism geometries. The ASTM practice of using a base masonry aspect ratio of 2 appears to be a carryover from UBC Standard 21-17. As noted earlier, prisms tested under the American standard produce strengths that are artificially high, especially if compared with the Canadian and British codes which base the strength on a confidence interval lower bound. This likely produces shear strength predictions that are unconservative since the equation was developed from older masonry research which used prism aspect ratios greater than two.

Apart from the American practice there is a good consensus between masonry standards and prism research that a prism aspect ratio of 5 is the preferable standard for reporting masonry

strength. It is recommended that masonry prisms with aspect ratios of 5 or greater be tested. If other aspect ratios are used then the prism strength should be corrected to correspond to the equivalent strength for a prism aspect ratio of 5. The allowance in the masonry standards for testing block masonry prisms constructed of two courses should be discontinued and replaced with a minimum requirement of 3 courses.

The Canadian and British practices of using a confidence interval to compute the prism strength is the statistically favorable approach. This approach is unsuited for comparing older masonry studies because many of them only reported the mean strength of the tested prisms or did not report masonry strength at all. When comparing older and contemporary studies it is necessary to compare the mean strengths of the prisms.

C.5.3 Net Shear Area

There are multiple definitions for the shear area to be used in shear strength calculations for partially grouted walls. These include the gross area, the net area, and the net shear area of a horizontal cross section of the wall. Prior to a recent edition of the MSJC the definition to be used by designers was ambiguous. In its 2011 code edition the MSJC settled on the net shear area which is defined as the sum of the areas of the face shells, the grouted cores, and the webs adjacent to the grouted cores. In the case of ungrouted, hollow masonry walls the net shear area is the area of the face shells only.

The definition for net shear area assumes that the webs that do not contain grout are ineffectual in resisting the in-plane shear load. Part of this is because of their narrow dimension in the direction of shear is not well suited for carrying shear forces. These webs are also neglected because they are commonly not bedded so there is no mortar to transfer the shear stresses between adjacent webs.

Recommendation

The MSJC practice of using the net shear area for in-plane shear strength calculation is the best method for representing the equivalent area that resists the shear mechanisms.

C.5.4 Grouted, Solid, and Hollow Prism Strength

The MSJC defines solid masonry as those units whose net to gross volume is at least 75 percent. Units that do not meet this minimum threshold are considered to be hollow. Fully grouted masonry are treated to be solid. When defining masonry strength the corresponding solid, grouted, or hollow masonry prism strength are used in the strength calculations. The MSJC is ambiguous of whether the grouted prism strength, hollow prism strength, or a weight average of the two should be used for partially grouted masonry walls.

Recommendation

Nolph (2010) recommended that the hollow prism strength be used for partially grouted wall, though he did not explain why. This is because the primary load resisting mechanism is the masonry itself and the grout serves primarily as a medium to transfer stresses and strains between the masonry and the reinforcement.

C.5.5 Shear Length

The length of the wall panel considered to participate in the lateral shear resistance varies between codes. The definition of shear length considered in the codes are the total wall length L_w, the effective length d, or some multiple of one of the values. The effective length is defined as the distance from the extreme compression fiber in the masonry to centroid of the extreme tensile reinforcement. This definition for effective length is the same as that employee by ACI for reinforced concrete.

The use of the total wall length has merit from the standpoint that all reinforced masonry shear walls are assumed to be cracked. Near the ultimate strength the shear cracks propagate both horizontally and vertically through the masonry panel from one end to the other. In this state the masonry shear strength component of the shear equation represents the strength from masonry aggregate interlock. Since shear is resisted along cracks that extend through the entire length of the panel, it is justifiable to assume that the masonry shear strength is a function of the entire wall length.

The use of the effective wall length has merit by the assumption that the masonry outside of the tensile reinforcement is not vertically confined. Aggregate interlock requires vertical confinement to keep the aggregates on either side a shear crack interlocked. Without vertical confinement the aggregates would slide past each other and mechanical mode of shear resistance would be replaced by friction. The vertical confinement of the shear cracks is provided by the vertical reinforcement and the vertical axial load. Since it is uncertain whether the influence of the vertical reinforcement extends beyond the extreme-most vertical reinforcement bar, it is justifiable to neglect the masonry in that region by using the effect wall length.

Recommendation

To date there has been no research found that has investigated the two shear length definitions to determine which is best suited for use in predicting masonry shear strength. Until this question can be settle definitively it is recommended that researchers report both values to facilitate the comparison of test results. It has been observed that this data is available in all masonry shear wall research that has been reported.

C.6 Conclusions

This section has discusses the causes of uncertainty in masonry shear wall data reporting from four disparities in testing methodology. The four sources of discrepancies discussed were boundary conditions, strain rate effects, loading patterns, size effects. The testing methodologies from each source have been reviewed by the extent of their use by researchers and by their relation to actual masonry performance. This article recommended a standard method of reporting data for each category. The recommended practices given in this article are summarized as follows.

The influence of different boundary conditions between specimens can be eliminated by reporting the shear span ratio for each specimen. The shear span ratio should be calculated by dividing the vertical distance between the point of inflection and maximum moment by the shear length of the wall. For the purpose of this standard the shear length should be taken as the full length of the shear wall.

All test data should be adjusted to correspond to the statically tested strength. For studies using dynamic loading, the best method is to test both static and dynamic specimens so that a study-specific correlation coefficient can be determined. Statically tested specimens should be tested such that no part of the wall experiences a compression strain rate greater than $\dot{\varepsilon}_s = 20 \times 10^{-6} s^{-1}$, which corresponds to the tested reference strain rate for mortar.

It is proposed that researchers report the strength of masonry shear wall data equivalent to periodic or harmonic patterns. Data from wall tested under monotonic loading would need to be adjusted to provide the cyclic-equivalent strength.

This article proposes that that standard method of reporting reduced-scale masonry test data is to report the full-scale data for the equivalent prototype. It has been shown that there are limits to the scale by which a masonry model may be effectively reduced. Within these relatively small limits it has been found that size effects are ineffectual, and any effect would be considered in the strength of masonry prisms constructed of the same reduced-scale materials. It has been further shown that data is more advantageous when represented in its equivalent full-scale form.

One of the possible concerns about standardization is the loss of research freedom. Research is conducted with the hope that the finding will advance the knowledge in that field of study. The proposed standardization in reporting results do not govern what and how future masonry tests are conducted, they are merely a standardized means for researchers to share their data with the masonry community. The choice is totally left up to the individual researcher whether to use these standards to supplant or to supplement their existing means of reporting data. Using standardized reporting methods will aid in making individual findings more useful, applicable, and relevant to the collective masonry community.

APPENDIX D. MASONRY PRISM STRENGTH PREDICTION

D.1 Introduction

Several studies were candidates for inclusion in the data set in which the prism strength was not reported but which, instead, listed the strengths of the constituent materials. Currently, the underlying principles of masonry prism behavior are fairly well understood at a qualitative level but the high variability of prism data have made it difficult for researchers to formulate accurate predictive equations for prism strength based in the strengths of the constituent materials. In order for these candidate studies to be included within the data set, equations were formulated to estimate prism strength from the constituent material strengths provided in the respective studies. The studies included are listed in Tables D.1 and D.2.

The estimation of prism strength is likely to introduce measurement error into the analysis due to the high variability of masonry prism strengths. Including a greater number of specimens means that a larger domain of testing parameters would be included in the analysis. A larger domain of specimen parameters would make the results more representative of a larger portion of the masonry shear wall population. Since the results of this analysis are intended to cover the entire masonry shear wall population, it was judged more valuable to the analysis to analyze a greater number of specimens by including those with estimated f'_m values than to reduce possible measurement error by excluding them.

Masonry prism tests typically demonstrate high variability, with a coefficient of variation of 6.3 percent observed to be the average for several groups (Grimm, 2002). Some of this variability can be attributed to defects introduced during the assembly and handling of the prisms. The unknown measurement error introduced by estimating f'_m values for specimens is assumed to be less than that of prisms because constituent material tests typically have less variability. As better models are developed in the future to quantify the behavior of masonry assemblages it may become

more accurate and economical to estimate f'_m from a function of the constituent material properties than from testing masonry prisms.

Any measurement error in the f'_m value has a reduced impact on the error of the whole shear prediction equation. Part of this reduction comes from the use of the square root of the f'_m value. The root function has the effect of reducing any error from the term, especially at the higher values typically used for f'_m. The other part of the reduction is due to the fact that the f'_m value is only used in the masonry component of the shear equation. The predicted shear strengths of the axial load and shear reinforcement components of the shear equation are unaffected by an error in the f'_m value.

D.2 Data Analysis

Two linear models were developed to predict the masonry prism compressive strength, one for hollow and another for grouted prisms. The models were developed using linear regression on a data set of masonry prisms and constituent material strengths and geometry. For each prism type multiple models were developed and compared using adjusted R^2 values. The data set contained 63 specimens that were missing values for the ungrouted prism strength and 20 specimens missing values for the grouted prism strength Weighted linear regression was used to develop two models to use in estimating values for these parameters These models were then used to estimate values for the missing prism strength data.

The masonry research literature was reviewed for masonry prism test data with the necessary parameters reported that could be used in building the linear regression models Since the procedures for masonry prism testing are standardized and the results are related to a wide array of masonry properties, the search for prism test data extended beyond the pool of masonry shear wall research These parameters included unit strength, mortar strength, grout strength, joint thickness, prism height, prism width, net to gross area ratio (v), ungrouted prism strength, grouted prism strength, and specimen count These data types were reported by the researchers with missing prism strength data and could be used to estimate the missing prism data The majority of the prism data found represented the average of multiple tests on identical specimen samples.

The data were organized into two data sets, one for building the ungrouted model and one for building the grouted model Those data that included the ungrouted prism strengths were

included in the former data set and those that included the grout and grouted prism strengths were included in the latter data set Some data reported all three and were included in both data sets The ungrouted data set included 200 data points and represented 432 individual prism tests The grouted data set included 164 data point and represented 593 individual prism tests.

The data sets included prisms of varying heights and aspect ratios In order for the masonry data to be compatible the grouted and ungrouted prism strengths were adjusted to correspond to a standardized aspect ratio of 5 The reasoning behind the standardized aspect ratio of 5 is presented in Appendix C of this paper

The data were analyzed using weighted least squares regression The weight chosen for each data point was the number of trials tested for that point This was chosen so that the total of the weights within each data set would be equal to the total number of specimens tested The weights gave stronger influence to those data points that were averages of a greater number of specimens These data points have lower variance and weighting them accordingly should have reduced the variance of the two linear models.

D.3 Ungrouted Prism Model

Prior to attempting to fit a model to the data, partial regression plots were graphed of the prism strength versus the various parameters The plots showed that there was too little variation in the joint thickness data to include it as a parameter in the regression analysis Two initial models were fit to the ungrouted data, a traditional arithmetical linear model and a logarithmic linear model These models were initially built using the parameters of net to gross area ratio, unit strength, and mortar strength for the predictor variables and ungrouted prism strength as the response variable.

The output of the regressions showed that the logarithmic model had a higher R^2 value than the corresponding arithmetical model, hinting that the logarithmic model better correlated with the data Inspection of the output for the logarithmic model revealed that the p-value for the estimate of the intercept was very high, signaling that the intercept contributed very little to the overall model The new logarithmic model had a slightly improved correlation over the previous model, showing that the intercept can be dropped from the model.

The residuals for the arithmetical model and the improved logarithmic model were compared using normal probability plots The logarithmic model showed better fit to a normal distribu-

tion than did the arithmetic model, which suggests that the prism data are log-normally distributed This is likely since the variance of masonry prism data tends to increase proportionally with the prism strength.

D.4 Grouted Prism Model

Prior to attempting to fit a model to the data, partial regression plots were graphed of the prism strength versus the various parameters Two initial models were fit to the ungrouted data, a traditional arithmetical linear model and a logarithmic linear model These models were initially built using the parameters of joint thickness, net to gross area ratio, unit strength, mortar strength, and grout strength for the predictor variables and ungrouted prism strength as the response variable.

The output of the regression showed that the arithmetical model had a notably higher R^2 value than the corresponding arithmetical model The R^2 values for both grouted models was notably lower than the models for the ungrouted prism data, demonstrating the higher variability in the grouted data from the addition of the grout in the prism The residuals for the two models were compared using normal probability plots The logarithmic model showed better fit to a normal distribution than did the arithmetic model, which suggests that the prism data are log-normally distributed.

A second arithmetic model was created to gauge the highest correlation possible with a large number of parameters The second arithmetic model was built using forward selection, second-order stepwise linear regression with adjusted R^2 value used as the selection criterion The predictor variables, squared roots of the predictor variables, and inverse of the predictor variables were used as possible input parameters The resulting model contained 21 coefficients Three of the coefficients with larger p-values were removed from the model one-by-one until all of the 18 remaining coefficients with small p-values remained Removal of the three coefficients negligibly affected the R^2 value

The second arithmetical model had an R^2 value of 0.841 which still lagged behind those for the ungrouted data models This model showed that it was very improbable to find a model with a very good fit to the data The normal residual plot for this model showed an more significant departure from normality in the upper and lower tails It was decided to next attempt to find logarithmic linear models with higher R^2 values It was found during the building of the last arithmetic linear

model that the narrowest width of the masonry prism was also correlated with the strength This width parameter was also included in the building of the next models.

The first model included the joint thickness, net-to-gross area ratio, and the grout strength as parameters The latter model included the prism width and grouted-to-gross area ratio as parameters Both models also included the masonry unit strength, the sum of joint and unit strengths, and the sum of grout and unit strengths The intercept was omitted from both models because it was found to be non-influential The two models had nearly equal R^2 values that exceeded the R^2 values for the first two grouted prism models The normal probability plots of the residuals for both models were similar and showed a good match with normality. The latter model was chosen for the grouted data because it had a root mean squared error nearly half that of the former and had one less coefficient.

D.5 Conclusions

Two linear models were produced to predict the masonry prism strengths for ungrouted and grouted prisms The analyses for both ungrouted and grouted masonry data showed that the prism data are log-normally distributed The models were used to predict the 83 missing prism strengths from the data set shown in Tables D.1 and D.2.

Table D.1: Predicted Strengths for Ungrouted Prisms

Study	Specimen	ν	f'_b		f'_j		$f'_{m(gro)}$	
			psi	MPa	psi	MPa	psi	MPa
Scrivener 1969	C1	46%	2050	(14.1)	2880	(19.9)	1440	(9.9)
	D2	46%	2700	(18.6)	3180	(21.9)	1796	(12.4)
	C7	46%	2050	(14.1)	2880	(19.9)	1440	(9.9)
	C8	46%	2050	(14.1)	2880	(19.9)	1440	(9.9)
	C9	46%	2050	(14.1)	2880	(19.9)	1440	(9.9)
	D11	46%	2700	(18.6)	3180	(21.9)	1796	(12.4)
	C3	46%	2050	(14.1)	2880	(19.9)	1440	(9.9)
	D12	46%	2700	(18.6)	3180	(21.9)	1796	(12.4)
	D13	46%	2700	(18.6)	3180	(21.9)	1796	(12.4)
	D14	46%	2700	(18.6)	3180	(21.9)	1796	(12.4)
Williams 1971	4	64%	7500	(51.7)	2300	(15.9)	4037	(27.8)
Hidalgo et al. 1978	HCBR-21-3	55%	8550	(58.9)	4380	(30.2)	4929	(34.0)
	HCBR-21-4	55%	8550	(58.9)	4380	(30.2)	4929	(34.0)
	HCBR-21-5	55%	8550	(58.9)	4380	(30.2)	4929	(34.0)
	HCBR-21-7	55%	8550	(58.9)	4380	(30.2)	4929	(34.0)
Chen et al. 1978	HCBL-11-1	60%	1800	(12.4)	2754	(19.0)	1538	(10.6)
	HCBL-11-2	60%	1800	(12.4)	2754	(19.0)	1538	(10.6)
	HCBL-11-3	60%	1800	(12.4)	2965	(20.4)	1575	(10.9)
	HCBL-11-4	60%	1800	(12.4)	2965	(20.4)	1575	(10.9)
	HCBL-11-5	60%	1800	(12.4)	2754	(19.0)	1538	(10.6)
	HCBL-11-6	60%	1800	(12.4)	2965	(20.4)	1575	(10.9)
	HCBL-11-7	60%	1800	(12.4)	2322	(16.0)	1458	(10.0)
	HCBL-11-8	60%	1800	(12.4)	2942	(20.3)	1571	(10.8)
	HCBL-11-9	60%	1800	(12.4)	2942	(20.3)	1571	(10.8)
	HCBL-11-10	60%	1800	(12.4)	2322	(16.0)	1458	(10.0)
	HCBL-11-11	60%	1800	(12.4)	2322	(16.0)	1458	(10.0)
	HCBR-11-1	53%	5816	(40.1)	3840	(26.5)	3551	(24.5)
	HCBR-11-2	53%	5816	(40.1)	3840	(26.5)	3551	(24.5)
	HCBR-11-3	53%	5816	(40.1)	3840	(26.5)	3551	(24.5)
	HCBR-11-4	53%	5816	(40.1)	3044	(21.0)	3299	(22.7)
	HCBR-11-5	53%	5816	(40.1)	3840	(26.5)	3551	(24.5)
	HCBR-11-6	53%	5816	(40.1)	4316	(29.8)	3685	(25.4)
	HCBR-11-7	53%	5816	(40.1)	1870	(12.9)	2828	(19.5)
	HCBR-11-8	53%	5816	(40.1)	3080	(21.2)	3312	(22.8)
	HCBR-11-9	53%	5816	(40.1)	3840	(26.5)	3551	(24.5)
	HCBR-11-10	53%	5816	(40.1)	3044	(21.0)	3299	(22.7)
	HCBR-11-11	53%	5816	(40.1)	3044	(21.0)	3299	(22.7)
	HCBR-11-12	53%	5816	(40.1)	1870	(12.9)	2828	(19.5)
	HCBR-11-13	53%	5816	(40.1)	3044	(21.0)	3299	(22.7)

Table D.1: Predicted Strengths for Ungrouted Prisms (Continued)

Study	Specimen	ν	f'_b		f'_j		$f'_{m(ung)}$	
			psi	MPa	psi	MPa	psi	MPa
Tomaževič and Lutman (1988)	CN-0	60%	2524	(17.4)	1349	(9.3)	1542	(10.6)
	CN-14	60%	2524	(17.4)	1349	(9.3)	1541	(10.6)
	CN-28	60%	2524	(17.4)	1349	(9.3)	1541	(10.6)
	CN-50	60%	2524	(17.4)	1349	(9.3)	1541	(10.6)
	CV-0	60%	2524	(17.4)	1349	(9.3)	1541	(10.6)
	DN-0	60%	2248	(15.5)	1015	(7.0)	1301	(9.0)
	DN-14	60%	2248	(15.5)	1015	(7.0)	1301	(9.0)
	DN-28	60%	2248	(15.5)	1015	(7.0)	1301	(9.0)
	DN-50	60%	2248	(15.5)	1015	(7.0)	1301	(9.0)
	DV-0	60%	2248	(15.5)	1015	(7.0)	1301	(9.0)
Haach et al. (2007) Haach et al. (2010a)	WSRM #1	54%	5800	(40.0)	1200	(8.3)	2471	(17.0)
	WSRM #2	54%	5800	(40.0)	1350	(9.3)	2565	(17.7)
	WSRM #3	54%	5800	(40.0)	1410	(9.7)	2601	(17.9)
	WSRM #4	54%	5800	(40.0)	1380	(9.5)	2583	(17.8)
	WSRM #5	54%	5800	(40.0)	770	(5.3)	2148	(14.8)
	WSRM #6	54%	5800	(40.0)	1000	(6.9)	2333	(16.1)
	WSRM #7	54%	5800	(40.0)	730	(5.0)	2112	(14.6)
	WSRM #8	54%	5800	(40.0)	930	(6.4)	2280	(15.7)
	ECRM #9	54%	5800	(40.0)	1450	(10.0)	2624	(18.1)
	URM #10	54%	5800	(40.0)	740	(5.1)	2121	(14.6)
	#11	54%	5800	(40.0)	990	(6.8)	2325	(16.0)
	#12	54%	5800	(40.0)	990	(6.8)	2325	(16.0)
	#13	54%	5800	(40.0)	990	(6.8)	2325	(16.0)
	#14	54%	5800	(40.0)	990	(6.8)	2325	(16.0)

Table D.2: Predicted Strengths for Grouted Prisms

Study	Specimen	ν	w		f'_b		f'_j		f'_g		$f'_{m(gro)}$	
			in	mm	psi	MPa	psi	MPa	psi	MPa	psi	MPa
Williams (1971) Scrivener and Williams (1971) Williams and Scrivener (1974)	1	64%	4.25	(108)	7500	(51.7)	2300	(15.9)	2800	(19.3)	3170	(21.9)
	2	64%	4.25	(108)	7500	(51.7)	2300	(15.9)	2800	(19.3)	3170	(21.9)
	3	64%	4.25	(108)	7500	(51.7)	2300	(15.9)	2800	(19.3)	3170	(21.9)
	5	64%	4.25	(108)	7500	(51.7)	2300	(15.9)	2800	(19.3)	3170	(21.9)
	CB 1	64%	3.63	(92)	5400	(37.2)	2300	(15.9)	2800	(19.3)	2756	(19.0)
	CB 2	64%	3.63	(92)	5400	(37.2)	2300	(15.9)	2800	(19.3)	2756	(19.0)
	CB 3	64%	3.63	(92)	5400	(37.2)	2300	(15.9)	2800	(19.3)	2756	(19.0)
	CB 4	64%	3.63	(92)	5400	(37.2)	2300	(15.9)	2800	(19.3)	2756	(19.0)
	A1	64%	4.25	(108)	7500	(51.7)	2300	(15.9)	2800	(19.3)	3170	(21.9)
	A2	64%	4.25	(108)	7500	(51.7)	2300	(15.9)	2800	(19.3)	3170	(21.9)
	B1	64%	4.25	(108)	7500	(51.7)	2300	(15.9)	2800	(19.3)	3170	(21.9)
	B2	64%	4.25	(108)	7500	(51.7)	2300	(15.9)	2800	(19.3)	3170	(21.9)
	B4	64%	4.25	(108)	7500	(51.7)	2300	(15.9)	2800	(19.3)	3170	(21.9)
	D1	64%	4.25	(108)	7500	(51.7)	2300	(15.9)	2800	(19.3)	3170	(21.9)
	D2	64%	4.25	(108)	7500	(51.7)	2300	(15.9)	2800	(19.3)	3170	(21.9)
	Dyn 1	64%	4.25	(108)	7500	(51.7)	2300	(15.9)	2800	(19.3)	3170	(21.9)
	Dyn 2	64%	4.25	(108)	7500	(51.7)	2300	(15.9)	2800	(19.3)	3170	(21.9)
	Dyn B1	64%	4.25	(108)	7500	(51.7)	2300	(15.9)	2800	(19.3)	3170	(21.9)
Priestley and Bridgeman (1974)	CBU3	64%	5.51	(140)	7630	(52.6)	2000	(13.8)	3740	(25.8)	3011	(20.8)
	CBU4	64%	5.51	(140)	7630	(52.6)	1960	(13.5)	4510	(31.1)	3060	(21.1)

APPENDIX E. FULL DATASET

This Appendix contains tables of the full dataset used in this study. The dataset was assembled and formatted using the principles of data collection, scrutinization, and synthesization detailed in Part II of this paper. A key to the symbols used within the tables is shown in Table E.1. The dataset is grouped into four tables by specimen attribute. The four attribute groupings are geometric properties (Table E.2), reinforcement details (Table E.3), material strengths (Table E.4), and loadings (Table E.5). A key to the nomenclature used in this paper is provided in the front matter.

Table E.1: Key to Symbols Used in Data Tables

* Values that were not found in the paper and were assumed based on the context and outside sources
† Values that were not explicitly stated in the paper but were calculated based on other provided data
‡ Values calculated using estimated functional relationships (see Appendix D)

Table E.2: Geometric Properties of Specimens

Serial	Block	Grout	Scale	Height		Length		Thickness		Shear Area		$\frac{h_g}{l_w}$	$\frac{M}{Vl_w}$	Boundary
				h_g (mm)	h_e (mm)	l_w (mm)	d (mm)	t (mm)	t_s (mm)	A_g (mm^2)	A_{nv} (mm^2)			
1968-MX-ME-09	CMU	PG	1	2650	2650	3200	3000†	150	50*	480000	330322	0.83	0.83	Cantilever
1968-MX-ME-10	CMU	PG	1	2650	2650	3200	3000†	150	50*	480000	330322	0.83	0.83	Cantilever
1968-MX-ME-11	CMU	PG	1	2650	2650	3200	3000†	150	50*	480000	330322	0.83	0.83	Cantilever
1968-MX-ME-12	CMU	PG	1	2650	2650	3200	3000†	150	50*	480000	297419	0.83	0.83	Cantilever
1968-MX-ME-13	CMU	PG	1	2650	2650	3200	3000†	150	50*	480000	297419	0.83	0.83	Cantilever
1968-MX-ME-14	CMU	PG	1	2650	2650	3200	3000†	150	50*	480000	330322	0.83	0.83	Cantilever
1968-MX-ME-15	CMU	PG	1	2650	2650	3200	3000†	150	50*	480000	297419	0.83	0.83	Cantilever
1968-MX-ME-16	CMU	PG	1	2650	2650	3200	3000†	150	50*	480000	330322	0.83	0.83	Cantilever
1968-MX-ME-17	CMU	PG	1	2650	2650	3200	2800†	150	50*	480000	330322	0.83	0.83	Cantilever
1968-MX-ME-18	CMU	PG	1	2650	2650	3200	3000†	150	50*	480000	330322	0.83	0.83	Cantilever
1969-MX-ME-11	CMU	PG	1	2000	1850	2000	1800†	150	50*	300000	180000	1.00	1.00	Cantilever
1969-MX-ME-14	CMU	PG	1	2000	1850	2000	1900†	150	50*	300000	140000	1.00	1.00	Cantilever
1969-MX-ME-15	CMU	PG	1	2000	1850	2000	1800†	150	50*	300000	180000	1.00	1.00	Cantilever
1969-MX-ME-16	CMU	PG	1	2000	1850	2000	1800†	150	50*	300000	180000	1.00	1.00	Cantilever
1969-MX-ME-17	CMU	PG	1	2000	1850	2000	1800†	150	50*	300000	180000	1.00	1.00	Cantilever
1969-MX-ME-18	CMU	PG	1	2000	1850	2000	1800†	150	50*	300000	180000	1.00	1.00	Cantilever
1969-MX-ME-19	CMU	PG	1	2000	1850	2000	1800†	150	50*	300000	180000	1.00	1.00	Cantilever
1969-MX-ME-20	CMU	PG	1	2000	1850	2000	1800†	150	50*	300000	180000	1.00	1.00	Cantilever
1969-MX-ME-21	CMU	PG	1	2000	1850	2000	1800†	150	50*	300000	180000	1.00	1.00	Cantilever
1969-MX-ME-24	CMU	PG	1	2000	1850	2000	1900†	150	50*	300000	140000	1.00	1.00	Cantilever
1969-MX-ME-25	CMU	FG	1	2000	1850	2000	1800†	150	150*	300000	300000	1.00	1.00	Cantilever
1969-MX-ME-29	CMU	PG	1	2000	1850	2000	1800†	150	50*	300000	180000	1.00	1.00	Cantilever
1971-NZ-WI-01	Clay	FG	1	1143	1245	1118	1061†	108	108	120744	120744	1.02	1.11	Cantilever
1971-NZ-WI-02	Clay	FG	1	1143	1245	1118	1061†	108	108	120744	120744	1.02	1.11	Cantilever
1971-NZ-WI-03	Clay	FG	1	1143	1245	1118	1061†	108	108	120744	120744	1.02	1.11	Cantilever
1971-NZ-WI-04	Clay	PG	1	1143	1245	1118	1061†	108	44.5	120744	76774	1.02	1.11	Cantilever
1971-NZ-WI-05	Clay	FG	1	1143	1245	1118	1061†	108	108	120744	120744	1.02	1.11	Cantilever
1971-NZ-WI-06	CMU	FG	1	1219	1321	1219	1143†	92	92	112148	112148	1.00	1.08	Cantilever

Table E.2: Geometric Properties of Dataset (Continued)

Serial	Block	Grout	Scale	Height		Length		Thickness		Shear Area		$\frac{h_g}{l_w}$	$\frac{M}{Vl_w}$	Boundary
				h_g (mm)	h_e (mm)	l_w (mm)	d (mm)	t (mm)	t_s (mm)	A_g (mm^2)	A_{nv} (mm^2)			
1971-NZ-WI-07	CMU	FG	1	1219	1321	1219	1143†	92	92	112148	112148	1.00	1.08	Cantilever
1971-NZ-WI-08	CMU	FG	1	1219	1321	1219	1143†	92	92	112148	112148	1.00	1.08	Cantilever
1971-NZ-WI-09	CMU	FG	1	1219	1321	1219	1143†	92	92	112148	112148	1.00	1.08	Cantilever
1971-NZ-WI-10	Clay	FG	1	1143	1245	1118	1061†	108	108	120744	120744	1.02	1.11	Cantilever
1971-NZ-WI-11	Clay	FG	1	1143	1245	1118	1061†	108	108	120744	120744	1.02	1.11	Cantilever
1971-NZ-WI-12	Clay	FG	1	1194	1295	660	603†	108	108	71280	71280	1.81	1.96	Cantilever
1971-NZ-WI-13	Clay	FG	1	1194	1295	660	603†	108	108	71280	71280	1.81	1.96	Cantilever
1971-NZ-WI-15	Clay	FG	1	1194	1295	660	603†	108	108	71280	71280	1.81	1.96	Cantilever
1971-NZ-WI-16	Clay	FG	1	965	1067	1854	1797†	108	108	200232	200232	0.52	0.58	Cantilever
1971-NZ-WI-17	Clay	FG	1	965	1067	1854	1797†	108	108	200232	200232	0.52	0.58	Cantilever
1971-NZ-WI-18	Clay	FG	1	1194	1295	660	603†	108	108	71280	71280	1.81	1.96	Cantilever
1971-NZ-WI-19	Clay	FG	1	1194	1295	1118	1061†	108	108	120744	120744	1.07	1.16	Cantilever
1971-NZ-WI-20	Clay	FG	1	1194	1295	1118	1061†	108	108	120744	120744	1.07	1.16	Cantilever
1976-US-MA-01	CMU	FG	1	1626	813	813	607†	143	143	116259	116259	2.00	1.00	Fixed
1976-US-MA-02	CMU	FG	1	1626	813	813	607†	143	143	116259	116259	2.00	1.00	Fixed
1976-US-MA-03	CMU	FG	1	1626	813	813	607†	143	143	116259	116259	2.00	1.00	Fixed
1976-US-MA-04	CMU	FG	1	1626	813	813	607†	143	143	116259	116259	2.00	1.00	Fixed
1976-US-MA-05	CMU	FG	1	1626	813	813	607†	143	143	116259	116259	2.00	1.00	Fixed
1976-US-MA-06	CMU	FG	1	1626	813	813	607†	143	143	116259	116259	2.00	1.00	Fixed
1976-US-MA-07	CMU	FG	1	1626	813	813	607†	143	143	116259	116259	2.00	1.00	Fixed
1976-US-MA-08	CMU	FG	1	1626	813	813	607†	143	143	116259	116259	2.00	1.00	Fixed
1976-US-MA-09	CMU	FG	1	1626	813	813	607†	143	143	116259	116259	2.00	1.00	Fixed
1976-US-MA-10	CMU	FG	1	1626	813	813	607†	143	143	116259	116259	2.00	1.00	Fixed
1976-US-MA-11	CMU	PG	1	1626	813	813	607†	143	63.5	116259	80000	2.00	1.00	Fixed
1976-US-MA-12	CMU	PG	1	1626	813	813	607†	143	63.5	116259	80000	2.00	1.00	Fixed
1977-NZ-PR-05	CMU	FG	1	1651	1829	2428	2226†	143	143	347204	347204	0.68	0.75	Cantilever
1977-NZ-PR-06	CMU	FG	1	1651	1829	2428	2226†	143	143	347204	347204	0.68	0.75	Cantilever
1977-NZ-PR-07	CMU	FG	1	1651	1829	2428	2226†	143	143	347204	347204	0.68	0.75	Cantilever

Table E.2: Geometric Properties of Dataset (Continued)

Serial	Block	Grout	Scale	Height		Length		Thickness		Shear Area		$\frac{h_g}{l_w}$	$\frac{M}{Vl_w}$	Boundary
				h_g (mm)	h_e (mm)	l_w (mm)	d (mm)	t (mm)	t_s (mm)	A_g (mm^2)	A_{nv} (mm^2)			
1977-NZ-PR-08	CMU	FG	1	1651	1829	2428	2226†	143	143	347204	347204	0.68	0.75	Cantilever
1977-NZ-PR-09	CMU	FG	1	1651	1829	2428	2226†	143	143	347204	347204	0.68	0.75	Cantilever
1977-NZ-PR-10	CMU	FG	1	1651	1829	2428	2226†	143	143	347204	347204	0.68	0.75	Cantilever
1978-US-CH-02	CMU	PG	1	1422	711	1219	1067	194	69.9	236486	141935	1.17	0.58	Fixed
1978-US-CH-03	CMU	FG	1	1422	711	1219	1067	194	194	236486	236486	1.17	0.58	Fixed
1978-US-CH-04	CMU	FG	1	1422	711	1219	1067	194	194	236486	236486	1.17	0.58	Fixed
1978-US-CH-05	CMU	PG	1	1422	711	1219	1067	194	69.9	236486	141935	1.17	0.58	Fixed
1978-US-CH-06	CMU	FG	1	1422	711	1219	1067	194	194	236486	236486	1.17	0.58	Fixed
1978-US-CH-07	CMU	FG	1	1422	711	1219	1067	194	194	236486	236486	1.17	0.58	Fixed
1978-US-CH-08	CMU	PG	1	1422	711	1219	1067	194	69.9	236486	141935	1.17	0.58	Fixed
1978-US-CH-09	CMU	FG	1	1422	711	1219	1067	194	194	236486	236486	1.17	0.58	Fixed
1978-US-CH-10	CMU	PG	1	1422	711	1219	1067	194	69.9	236486	141935	1.17	0.58	Fixed
1978-US-CH-11	CMU	FG	1	1422	711	1219	1067	194	194	236486	236486	1.17	0.58	Fixed
1978-US-CH-14	Clay	FG	1	1422	711	1219	1067	187	187	227953	227953	1.17	0.58	Fixed
1978-US-CH-15	Clay	FG	1	1422	711	1219	1067	187	187	227953	227953	1.17	0.58	Fixed
1978-US-CH-16	Clay	PG	1	1422	711	1219	1067	187	82.3	227953	121935	1.17	0.58	Fixed
1978-US-CH-17	Clay	FG	1	1422	711	1219	1067	187	187	227953	227953	1.17	0.58	Fixed
1978-US-CH-18	Clay	FG	1	1422	711	1219	1067	187	187	227953	227953	1.17	0.58	Fixed
1978-US-CH-19	Clay	FG	1	1422	711	1219	1067	187	187	227953	227953	1.17	0.58	Fixed
1978-US-CH-20	Clay	PG	1	1422	711	1219	1067	187	82.3	227953	121935	1.17	0.58	Fixed
1978-US-CH-21	Clay	FG	1	1422	711	1219	1067	187	187	227953	227953	1.17	0.58	Fixed
1978-US-CH-22	Clay	PG	1	1422	711	1219	1067	187	82.3	227953	121935	1.17	0.58	Fixed
1978-US-CH-23	Clay	FG	1	1422	711	1219	1067	187	187	227953	227953	1.17	0.58	Fixed
1978-US-CH-24	Clay	FG	1	1422	711	1219	1067	187	187	227953	227953	1.17	0.58	Fixed
1978-US-HI-01	Clay	SU	1	2032	1016	1067	991†	187	187	199529	199529	1.90	0.95	Fixed
1978-US-HI-02	Clay	FG	1	2032	1016	1067	991†	187	187	199529	199529	1.90	0.95	Fixed
1978-US-HI-03	Clay	PG	1	2032	1016	1067	991†	187	82.3	199529	110322	1.90	0.95	Fixed

Table E.2: Geometric Properties of Dataset (Continued)

Serial	Block	Grout	Scale	Height		Length		Thickness		Shear Area		$\frac{h_g}{l_w}$	$\frac{M}{Vl_w}$	Boundary
				h_g (mm)	h_e (mm)	l_w (mm)	d (mm)	t (mm)	t_s (mm)	A_g (mm^2)	A_{nv} (mm^2)			
1978-US-HI-04	Clay	FG	1	2032	1016	1067	991†	187	187	199529	199529	1.90	0.95	Fixed
1978-US-HI-05	Clay	PG	1	2032	1016	1067	991†	187	82.3	199529	110322	1.90	0.95	Fixed
1978-US-HI-06	Clay	FG	1	2032	1016	1067	991†	187	187	199529	199529	1.90	0.95	Fixed
1978-US-HI-07	Clay	PG	1	2032	1016	1067	991†	187	82.3	199529	110322	1.90	0.95	Fixed
1978-US-HI-08	Clay	FG	1	2032	1016	1067	991†	187	187	199529	199529	1.90	0.95	Fixed
1978-US-HI-09	Clay	FG	1	2032	1016	1067	991†	187	187	199529	199529	1.90	0.95	Fixed
1979-US-HI-01	CMU	FG	1	1016	508	2032	1829	194	194	394208	394208	0.50	0.25	Fixed
1979-US-HI-02	CMU	FG	1	1016	508	2032	1829	194	194	394208	394208	0.50	0.25	Fixed
1979-US-HI-03	CMU	FG	1	1016	508	2032	1829	194	194	394208	394208	0.50	0.25	Fixed
1979-US-HI-04	CMU	FG	1	1016	508	2032	1829	194	194	394208	394208	0.50	0.25	Fixed
1979-US-HI-05	CMU	FG	1	1016	508	2032	1829	194	194	394208	394208	0.50	0.25	Fixed
1979-US-HI-06	CMU	FG	1	1016	508	2032	1829	194	194	394208	394208	0.50	0.25	Fixed
1979-US-HI-08	Clay	FG	1	1016	508	1981	1829	187	187	370447	370447	0.51	0.26	Fixed
1979-US-HI-09	Clay	FG	1	1016	508	1981	1829	187	187	370447	370447	0.51	0.26	Fixed
1979-US-HI-10	Clay	FG	1	1016	508	1981	1829	187	187	370447	370447	0.51	0.26	Fixed
1982-NZ-TH-01	CMU	PG	1	2400	1200	1600	1500	140	70†	224000	143934	1.50	0.75	Fixed
1982-NZ-TH-02	CMU	FG	1	2400	1200	1600	1500	140	140†	224000	224000	1.50	0.75	Fixed
1982-NZ-TH-03	CMU	PG	1	2400	1200	1600	1500	140	70†	224000	143871	1.50	0.75	Fixed
1982-NZ-TH-04	CMU	PG	1	2400	1200	1600	1500	140	70†	224000	143871	1.50	0.75	Fixed
1982-NZ-TH-05	CMU	FG	1	2400	1200	1600	1500	140	140†	224000	224000	1.50	0.75	Fixed
1982-NZ-TH-06	CMU	FG	1	2400	1200	1600	1500	140	140†	224000	224000	1.50	0.75	Fixed
1982-NZ-TH-08	CMU	FG	1	2400	1200	1600	1500	140	140†	224000	224000	1.50	0.75	Fixed
1983-JP-MA-01	CMU	FG	1	1800	900	1590	1500	150	150†	238500	238500	1.13	0.57	Fixed
1983-JP-MA-03	CMU	FG	1	1800	900	1190	1100	150	150†	178500	178500	1.51	0.76	Fixed
1983-JP-MA-04	CMU	FG	1	1800	900	790	700	150	150†	118500	118500	2.28	1.14	Fixed
1984-JP-IG-01	CMU	PG	1	1800	900	1970	1880	150	60†	295500	210064	0.91	0.46	Fixed
1984-JP-IG-02	CMU	PG	1	1800	900	1970	1880	150	60†	295500	210064	0.91	0.46	Fixed

Table E.2: Geometric Properties of Dataset (Continued)

Serial	Block	Grout	Scale	Height		Length		Thickness		Shear Area		$\frac{h_g}{l_w}$	$\frac{M}{Vl_w}$	Boundary
				h_g (mm)	h_e (mm)	l_w (mm)	d (mm)	t (mm)	t_s (mm)	A_g (mm^2)	A_{nv} (mm^2)			
1984-JP-IG-03	CMU	PG	1	1800	900	1770	1680	150	60†	265500	182000	1.02	0.51	Fixed
1984-JP-IG-04	CMU	PG	1	1800	900	1370	1280	150	60†	205500	143096	1.31	0.66	Fixed
1984-JP-IG-05	CMU	PG	1	1800	900	970	880	150	60†	145500	104193	1.86	0.93	Fixed
1984-JP-IG-06	CMU	PG	1	1800	900	970	880	150	60†	145500	104193	1.86	0.93	Fixed
1985-JP-FU-01	CMU	FG	1	1800	900	1990	1895†	190	190	378100	378100	0.90	0.45	Fixed
1985-JP-FU-02	Clay	FG	1	1800	900	1990	1895†	190	190	378100	378100	0.90	0.45	Fixed
1985-JP-FU-03	CMU	FG	1	1800	900	1190	1095†	190	190	226100	226100	1.51	0.76	Fixed
1985-JP-FU-04	Clay	FG	1	1700	850	1090	995†	190	190	207100	207100	1.56	0.78	Fixed
1985-JP-FU-05	CMU	FG	1	1800	900	790	695†	190	190	150100	150100	2.28	1.14	Fixed
1985-JP-FU-06	Clay	FG	1	1800	900	790	695†	190	190	150100	150100	2.28	1.14	Fixed
1985-JP-MA-01	CMU	FG	1	1800	900	1190	1095	190	190	226100	226100	1.51	0.76	Fixed
1985-JP-MA-02	CMU	FG	1	1800	900	1190	1095	190	190	226100	226100	1.51	0.76	Fixed
1985-JP-MA-03	CMU	FG	1	1800	900	1190	1095	190	190	226100	226100	1.51	0.76	Fixed
1985-JP-MA-05	CMU	FG	1	1800	900	1190	1095	190	190	226100	226100	1.51	0.76	Fixed
1985-JP-MA-06	CMU	FG	1	1800	900	1190	1095	190	190	226100	226100	1.51	0.76	Fixed
1985-JP-YA-05	CMU	FG	1	1200	600	950	850†	190	190	180500	180500	1.26	0.63	Fixed
1985-JP-YA-06	CMU	FG	1	1200	600	950	850†	190	190	180500	180500	1.26	0.63	Fixed
1985-JP-YA-07	CMU	FG	1	2000	1000	950	850†	190	190	180500	180500	2.11	1.05	Fixed
1985-JP-YA-08	CMU	FG	1	1200	600	950	850†	190	190	180500	180500	1.26	0.63	Fixed
1985-JP-YA-09	CMU	FG	1	1200	600	950	850†	190	190	180500	180500	1.26	0.63	Fixed
1985-US-SV-01	CMU	FG	1	1422	711	1219	1143†	194	194	236486	236486	1.17	0.58	Fixed
1985-US-SV-02	CMU	FG	1	1422	711	1219	1143†	194	194	236486	236486	1.17	0.58	Fixed
1985-US-SV-03	CMU	FG	1	1422	711	1219	1143†	143	143	174317	174317	1.17	0.58	Fixed
1985-US-SV-04	CMU	FG	1	1422	711	1219	1143†	143	143	174317	174317	1.17	0.58	Fixed
1985-US-SV-05	CMU	FG	1	1422	711	1219	1143†	143	143	174317	174317	1.17	0.58	Fixed
1985-US-SV-06	CMU	FG	1	1422	711	1219	1143†	143	143	174317	174317	1.17	0.58	Fixed
1985-US-SV-07	CMU	FG	1	1422	711	1219	1143†	143	143	174317	174317	1.17	0.58	Fixed

Table E.2: Geometric Properties of Dataset (Continued)

Serial	Block	Grout	Scale	Height		Length		Thickness		Shear Area		$\frac{h_g}{l_w}$	$\frac{M}{Vl_w}$	Boundary
				h_g (mm)	h_e (mm)	l_w (mm)	d (mm)	t (mm)	t_s (mm)	A_g (mm^2)	A_{nv} (mm^2)			
1985-US-SV-08	CMU	FG	1	1422	711	1219	1143†	143	143	174317	174317	1.17	0.58	Fixed
1985-US-SV-09	CMU	FG	1	1422	711	1219	1143†	143	143	174317	174317	1.17	0.58	Fixed
1985-US-SV-10	CMU	FG	1	1422	711	1219	1143†	143	143	174317	174317	1.17	0.58	Fixed
1985-US-SV-11	CMU	FG	1	1422	711	1219	1143†	143	143	174317	174317	1.17	0.58	Fixed
1985-US-SV-12	CMU	FG	1	1422	711	1219	1143†	143	143	174317	174317	1.17	0.58	Fixed
1985-US-SV-13	Clay	FG	1	1422	711	1219	1143†	187	187	227953	227953	1.17	0.58	Fixed
1985-US-SV-15	Clay	FG	1	1422	711	1219	1143†	187	187	227953	227953	1.17	0.58	Fixed
1985-US-SV-16	Clay	FG	1	1422	711	1219	1143†	187	187	227953	227953	1.17	0.58	Fixed
1985-US-SV-17	Clay	FG	1	1422	711	1219	1143†	187	187	227953	227953	1.17	0.58	Fixed
1985-US-SV-18	Clay	FG	1	1422	711	1219	1143†	187	187	227953	227953	1.17	0.58	Fixed
1985-US-SV-19	Clay	FG	1	1422	711	1219	1143†	187	187	227953	227953	1.17	0.58	Fixed
1985-US-SV-20	Clay	FG	1	1422	711	1219	1143†	187	187	227953	227953	1.17	0.58	Fixed
1985-US-SV-21	Clay	FG	1	1422	711	1219	1143†	187	187	227953	227953	1.17	0.58	Fixed
1985-US-SV-22	Clay	FG	1	1422	711	1219	1143†	187	187	227953	227953	1.17	0.58	Fixed
1985-US-SV-23	Clay	FG	1	1422	711	1219	1143†	187	187	227953	227953	1.17	0.58	Fixed
1985-US-SV-24	Clay	FG	1	1422	711	1219	1143†	187	187	227953	227953	1.17	0.58	Fixed
1985-US-SV-25	Clay	FG	1	1422	711	1219	1143†	187	187	227953	227953	1.17	0.58	Fixed
1985-US-SV-26	Clay	FG	1	1422	711	1219	1143†	187	187	227953	227953	1.17	0.58	Fixed
1986-JP-IG-01	Clay	FG	1	1700	850	1100	1005	190	190	209000	209000	1.55	0.77	Fixed
1986-JP-IG-02	Clay	FG	1	1700	850	1100	1005	190	190	209000	209000	1.55	0.77	Fixed
1986-JP-IG-03	Clay	FG	1	1700	850	1100	1005	190	190	209000	209000	1.55	0.77	Fixed
1986-JP-IG-04	Clay	FG	1	1700	850	1100	1005	190	190	209000	209000	1.55	0.77	Fixed
1986-JP-MA-15	CMU	PG	1	1800	900	920	855	150	60	138000	101548	1.96	0.98	Fixed
1986-JP-MA-16	CMU	PG	1	1800	900	920	855	150	60	138000	101548	1.96	0.98	Fixed
1986-JP-MA-17	CMU	PG	1	1800	900	1320	1255	150	60	198000	140387	1.36	0.68	Fixed
1986-JP-MA-18	CMU	PG	1	1800	900	1320	1255	150	60	198000	140387	1.36	0.68	Fixed
1986-JP-MA-19	CMU	PG	1	1800	900	1370	1293	150	60	205500	143096	1.31	0.66	Fixed

Table E.2: Geometric Properties of Dataset (Continued)

Serial	Block	Grout	Scale	Height		Length		Thickness		Shear Area		$\frac{h_g}{l_w}$	$\frac{M}{Vl_w}$	Boundary
				h_g (mm)	h_e (mm)	l_w (mm)	d (mm)	t (mm)	t_s (mm)	A_g (mm^2)	A_{nv} (mm^2)			
1986-JP-MA-20	CMU	PG	1	1800	900	1320	1255	150	60	198000	140387	1.36	0.68	Fixed
1986-JP-MA-21	CMU	PG	1	1800	900	1320	1255	150	60	198000	140387	1.36	0.68	Fixed
1986-JP-MA-22	CMU	PG	1	1800	900	1320	1255	150	60	198000	140387	1.36	0.68	Fixed
1986-JP-MA-23	CMU	PG	1	1800	900	1320	1255	150	60	198000	140387	1.36	0.68	Fixed
1986-JP-MA-24	CMU	PG	1	1800	900	1320	1255	150	60	198000	140387	1.36	0.68	Fixed
1986-JP-MA-25	CMU	PG	1	1800	900	1320	1255	150	60	198000	140387	1.36	0.68	Fixed
1986-JP-MA-26	CMU	PG	1	1800	900	1320	1255	150	60	198000	140387	1.36	0.68	Fixed
1986-JP-MA-27	CMU	PG	1	1800	900	1320	1255	150	60	198000	140387	1.36	0.68	Fixed
1986-JP-MA-28	CMU	PG	1	1800	900	1320	1255	150	60	198000	140387	1.36	0.68	Fixed
1986-JP-MA-29	CMU	PG	1	1800	900	1370	1293	150	60	205500	143096	1.31	0.66	Fixed
1986-JP-MA-30	CMU	PG	1	1800	900	1320	1255	150	60	198000	140387	1.36	0.68	Fixed
1986-JP-MA-31	CMU	PG	1	1800	900	1320	1255	150	60	198000	140387	1.36	0.68	Fixed
1986-JP-MA-32	CMU	PG	1	1800	900	1370	1293	150	60	205500	143096	1.31	0.66	Fixed
1986-JP-MA-33	CMU	PG	1	1800	900	1320	1255	150	60	198000	140387	1.36	0.68	Fixed
1986-JP-MA-34	CMU	PG	1	1800	900	1370	1293	150	60	205500	143096	1.31	0.66	Fixed
1986-JP-MA-35	CMU	PG	1	1800	900	1720	1655	150	60	258000	179290	1.05	0.52	Fixed
1986-JP-MA-36	CMU	PG	1	1800	900	1720	1655	150	60	258000	179290	1.05	0.52	Fixed
1986-JP-MA-37	CMU	PG	1	1800	900	1320	1255	150	60	198000	140387	1.36	0.68	Fixed
1986-JP-MA-38	CMU	PG	1	1800	900	1370	1293	150	60	205500	143096	1.31	0.66	Fixed
1986-JP-MA-53	Clay	PG	1	1600	800	1320	1255	150	70*	198000	144387	1.21	0.61	Fixed
1986-JP-MA-54	Clay	PG	1	1600	800	1320	1255	150	70*	198000	144387	1.21	0.61	Fixed
1986-JP-SH-01	CMU	FG	1	1800	900	1190	1095	190	190	226100	226100	1.51	0.76	Fixed
1986-JP-SH-02	CMU	FG	1	1800	900	1190	1095	190	190	226100	226100	1.51	0.76	Fixed
1986-JP-SH-03	CMU	FG	1	1800	900	1190	1095	190	190	226100	226100	1.51	0.76	Fixed
1986-JP-SH-04	CMU	FG	1	1800	900	1190	1095	190	190	226100	226100	1.51	0.76	Fixed
1986-JP-SH-05	CMU	FG	1	1800	900	1190	1095	190	190	226100	226100	1.51	0.76	Fixed
1986-JP-SH-06	CMU	FG	1	1800	900	1190	1095	190	190	226100	226100	1.51	0.76	Fixed

Table E.2: Geometric Properties of Dataset (Continued)

Serial	Block	Grout	Scale	Height		Length		Thickness		Shear Area		$\frac{h_g}{l_w}$	$\frac{M}{Vl_w}$	Boundary
				h_g (mm)	h_e (mm)	l_w (mm)	d (mm)	t (mm)	t_s (mm)	A_g (mm^2)	A_{nv} (mm^2)			
1987-JP-OK-01	CMU	FG	1	1800	900	1190	1095†	190	190	226100	226100	1.51	0.76	Fixed
1987-JP-OK-02	CMU	FG	1	1800	900	1190	1095†	190	190	226100	226100	1.51	0.76	Fixed
1987-JP-OK-10	CMU	FG	1	1800	900	1200	1105†	190	190	228000	228000	1.50	0.75	Fixed
1987-JP-OK-11	CMU	FG	1	1800	900	1200	1105†	190	190	228000	228000	1.50	0.75	Fixed
1988-JP-IG-05	Clay	FG	1	1700	850	1100	1005	190	190	209000	209000	1.55	0.77	Fixed
1988-JP-IG-06	Clay	FG	1	1700	850	1100	1005	190	190	209000	209000	1.55	0.77	Fixed
1988-JP-IG-07	Clay	FG	1	1700	850	1100	1005	190	190	209000	209000	1.55	0.77	Fixed
1988-JP-IG-08	Clay	FG	1	1700	850	1100	1005	190	190	209000	209000	1.55	0.77	Fixed
1988-JP-IG-09	Clay	FG	1	1700	850	1100	1005	190	190	209000	209000	1.55	0.77	Fixed
1988-SL-TO-01	CMU	PG	0.5	759	860	610	560†	100	40†	61000	36387	1.24	1.41	Cantilever
1988-SL-TO-02	CMU	PG	0.5	759	860	610	560†	100	40†	61000	36387	1.24	1.41	Cantilever
1988-SL-TO-03	CMU	PG	0.5	759	860	610	560†	100	40†	61000	36387	1.24	1.41	Cantilever
1988-SL-TO-04	CMU	PG	0.5	759	860	610	560†	100	40†	61000	36387	1.24	1.41	Cantilever
1988-SL-TO-05	CMU	PG	0.5	1410	1510	610	560†	100	40†	61000	36387	2.31	3.12	Cantilever
1988-SL-TO-09	CMU	PG	0.5	759	860	610	560†	100	40†	61000	36387	1.24	1.41	Cantilever
1988-SL-TO-10	CMU	PG	0.5	759	860	610	560†	100	40†	61000	36387	1.24	1.41	Cantilever
1988-SL-TO-11	CMU	PG	0.5	759	860	610	560†	100	40†	61000	36387	1.24	1.41	Cantilever
1988-SL-TO-12	CMU	PG	0.5	759	860	610	560†	100	40†	61000	36387	1.24	1.41	Cantilever
1988-SL-TO-13	CMU	PG	0.5	1410	1510	610	560†	100	40†	61000	36387	2.31	3.12	Cantilever
1988-US-JO-01	Clay	PG	1	914	457	914	838†	194	82.3*	177316	102580	1.00	0.50	Fixed
1988-US-JO-02	Clay	PG	1	914	457	914	838†	194	82.3*	177316	102580	1.00	0.50	Fixed
1988-US-JO-03	Clay	PG	1	914	457	914	838†	194	82.3*	177316	102580	1.00	0.50	Fixed
1988-US-JO-04	Clay	PG	1	914	457	914	838†	194	82.3*	177316	102580	1.00	0.50	Fixed
1988-US-JO-05	Clay	PG	1	914	457	914	838†	194	82.3*	177316	102580	1.00	0.50	Fixed
1988-US-JO-06	Clay	PG	1	914	457	914	838†	194	82.3*	177316	102580	1.00	0.50	Fixed
1988-US-JO-07	Clay	PG	1	914	457	914	838†	194	82.3*	177316	102580	1.00	0.50	Fixed
1988-US-JO-08	Clay	PG	1	914	457	914	838†	194	82.3*	177316	102580	1.00	0.50	Fixed

Table E.2: Geometric Properties of Dataset (Continued)

Serial	Block	Grout	Scale	Height		Length		Thickness		Shear Area		$\frac{h_g}{l_w}$	$\frac{M}{Vl_w}$	Boundary
				h_g (mm)	h_e (mm)	l_w (mm)	d (mm)	t (mm)	t_s (mm)	A_g (mm^2)	A_{nv} (mm^2)			
1988-US-JO-09	Clay	PG	1	914	457	914	838†	194	82.3*	177316	102580	1.00	0.50	Fixed
1988-US-JO-10	Clay	PG	1	914	457	914	838†	194	82.3*	177316	102580	1.00	0.50	Fixed
1988-US-JO-11	Clay	PG	1	914	457	914	838†	194	82.3*	177316	102580	1.00	0.50	Fixed
1988-US-JO-12	Clay	PG	1	914	457	914	838†	194	82.3*	177316	102580	1.00	0.50	Fixed
1988-US-JO-13	Clay	PG	1	914	457	914	838†	194	82.3*	177316	102580	1.00	0.50	Fixed
1988-US-JO-14	Clay	PG	1	914	457	914	838†	194	82.3*	177316	102580	1.00	0.50	Fixed
1988-US-JO-15	Clay	PG	1	914	457	914	838†	194	82.3*	177316	102580	1.00	0.50	Fixed
1988-US-JO-16	Clay	PG	1	914	457	914	838†	194	82.3*	177316	102580	1.00	0.50	Fixed
1988-US-JO-17	CMU	PG	1	813	406	813	711†	194	69.9*	157722	104516	1.00	0.50	Fixed
1988-US-JO-18	CMU	PG	1	813	406	813	711†	194	69.9*	157722	104516	1.00	0.50	Fixed
1988-US-JO-19	CMU	PG	1	813	406	813	711†	194	69.9*	157722	104516	1.00	0.50	Fixed
1988-US-JO-20	CMU	PG	1	813	406	813	711†	194	69.9*	157722	104516	1.00	0.50	Fixed
1988-US-JO-21	CMU	PG	1	813	406	813	711†	194	69.9*	157722	104516	1.00	0.50	Fixed
1988-US-JO-22	CMU	PG	1	813	406	813	711†	194	69.9*	157722	104516	1.00	0.50	Fixed
1988-US-JO-23	CMU	PG	1	813	406	813	711†	194	69.9*	157722	104516	1.00	0.50	Fixed
1988-US-JO-24	CMU	PG	1	813	406	813	711†	194	69.9*	157722	104516	1.00	0.50	Fixed
1988-US-JO-25	CMU	PG	1	813	406	813	711†	194	69.9*	157722	104516	1.00	0.50	Fixed
1988-US-JO-26	CMU	PG	1	813	406	813	711†	194	69.9*	157722	104516	1.00	0.50	Fixed
1988-US-JO-27	CMU	PG	1	813	406	813	711†	194	69.9*	157722	104516	1.00	0.50	Fixed
1988-US-JO-28	CMU	PG	1	813	406	813	711†	194	69.9*	157722	104516	1.00	0.50	Fixed
1988-US-JO-29	CMU	PG	1	813	406	813	711†	194	69.9*	157722	104516	1.00	0.50	Fixed
1988-US-JO-30	CMU	PG	1	813	406	813	711†	194	69.9*	157722	104516	1.00	0.50	Fixed
1988-US-JO-31	CMU	PG	1	813	406	813	711†	194	69.9*	157722	104516	1.00	0.50	Fixed
1988-US-JO-32	CMU	PG	1	813	406	813	711†	194	69.9*	157722	104516	1.00	0.50	Fixed
1988-US-SH-03	CMU	FG	1	1829	1829	1829	1727†	143	143	261547	261547	1.00	1.00	Cantilever
1988-US-SH-04	CMU	FG	1	1829	1829	1829	1727†	143	143	261547	261547	1.00	1.00	Cantilever
1988-US-SH-05	CMU	FG	1	1829	1829	1829	1727†	143	143	261547	261547	1.00	1.00	Cantilever

Table E.2: Geometric Properties of Dataset (Continued)

Serial	Block	Grout	Scale	Height		Length		Thickness		Shear Area		$\frac{h_g}{l_w}$	$\frac{M}{Vl_w}$	Boundary
				h_g (mm)	h_e (mm)	l_w (mm)	d (mm)	t (mm)	t_s (mm)	A_g (mm^2)	A_{nv} (mm^2)			
1988-US-SH-06	CMU	FG	1	1829	1829	1829	1727†	143	143	261547	261547	1.00	1.00	Cantilever
1988-US-SH-07	CMU	FG	1	1829	1829	1829	1727†	143	143	261547	261547	1.00	1.00	Cantilever
1988-US-SH-08	CMU	FG	1	1829	1829	1829	1727†	143	143	261547	261547	1.00	1.00	Cantilever
1988-US-SH-09	CMU	FG	1	1829	1829	1829	1727†	143	143	261547	261547	1.00	1.00	Cantilever
1988-US-SH-10	CMU	FG	1	1829	1829	1829	1727†	143	143	261547	261547	1.00	1.00	Cantilever
1988-US-SH-11	CMU	FG	1	1829	1829	1829	1727†	143	143	261547	261547	1.00	1.00	Cantilever
1988-US-SH-13	CMU	FG	1	1829	1829	1829	1727†	143	143	261547	261547	1.00	1.00	Cantilever
1988-US-SH-14	CMU	FG	1	1829	1829	1829	1727†	143	143	261547	261547	1.00	1.00	Cantilever
1988-US-SH-15	CMU	FG	1	1829	1829	1829	1727†	143	143	261547	261547	1.00	1.00	Cantilever
1988-US-SH-16	CMU	FG	1	1829	1829	1829	1727†	143	143	261547	261547	1.00	1.00	Cantilever
1989-US-YA-02	CMU	PG	1	1422	711	1219	1119†	194	63.5*	236486	127097	1.17	0.58	Fixed
1989-US-YA-03	CMU	PG	1	1422	711	1219	1119†	194	63.5*	236486	127097	1.17	0.58	Fixed
1989-US-YA-04	CMU	PG	1	1422	711	1219	1119†	194	63.5*	236486	127097	1.17	0.58	Fixed
1989-US-YA-05	CMU	PG	1	1422	711	1219	1119†	194	63.5*	236486	127097	1.17	0.58	Fixed
1989-US-YA-06	CMU	PG	1	1422	711	1219	1119†	194	63.5*	236486	127097	1.17	0.58	Fixed
1989-US-YA-08	CMU	PG	1	1422	711	1219	1119†	194	63.5*	236486	127097	1.17	0.58	Fixed
1989-US-YA-09	CMU	PG	1	1422	711	1219	1119†	194	63.5*	236486	127097	1.17	0.58	Fixed
1989-US-YA-10	CMU	PG	1	1422	711	1219	1119†	194	63.5*	236486	127097	1.17	0.58	Fixed
1990-US-SH-21	Clay	FG	1	1829	1829	1829	1727†	137	137	250573	250573	1.00	1.00	Cantilever
1990-US-SH-22	Clay	FG	1	1829	1829	1829	1727†	137	137	250573	250573	1.00	1.00	Cantilever
1991-JP-MA-01	CMU	FG	1	1800	900	1390	1290†	190	190	264100	264100	1.29	0.65	Fixed
1991-JP-MA-02	CMU	FG	1	1800	900	1390	1290†	190	190	264100	264100	1.29	0.65	Fixed
1991-JP-MA-03	CMU	FG	1	1800	900	1390	1290†	190	190	264100	264100	1.29	0.65	Fixed
1991-JP-MA-04	CMU	FG	1	1800	900	2190	1290†	190	190	416100	416100	0.82	0.41	Fixed
1991-JP-MA-05	CMU	FG	1	1800	900	2190	2090†	190	190	416100	416100	0.82	0.41	Fixed
1991-JP-MA-06	CMU	FG	1	1800	900	2190	2090†	190	190	416100	416100	0.82	0.41	Fixed
1992-US-GH-01	CMU	PG	0.333	940	940	940	906†	48	17*	45120	21097	1.00	1.00	Cantilever

Table E.2: Geometric Properties of Dataset (Continued)

Serial	Block	Grout	Scale	Height		Length		Thickness		Shear Area		$\frac{h_g}{l_w}$	$\frac{M}{Vl_w}$	Boundary
				h_g (mm)	h_e (mm)	l_w (mm)	d (mm)	t (mm)	t_s (mm)	A_g (mm^2)	A_{nv} (mm^2)			
1992-US-GH-02	CMU	PG	0.333	940	940	940	906†	48	17*	45120	23226	1.00	1.00	Cantilever
1993-US-GH-05	CMU	PG	0.333	940	940	940	906†	48	17*	45120	21097	1.00	1.00	Cantilever
1993-US-GH-06	CMU	PG	0.333	940	940	940	906†	48	17*	45120	21097	1.00	1.00	Cantilever
1994-US-BR-01	Clay	FG	1	1321	1435	1422	1320†	137	137	194814	194814	0.93†	1.01	Cantilever
1994-US-BR-02	Clay	FG	1	1321	1435	1829	1727†	137	137	250573	250573	0.72†	0.78	Cantilever
1994-US-BR-03	Clay	FG	1	1321	1435	2235	2133†	137	137	306195	306195	0.59†	0.64	Cantilever
1995-NZ-BR-01	CMU	FG	1	2000	2400	1800	1700†	90	90	162000	162000	1.11	1.22	Cantilever
1995-NZ-BR-02	CMU	PG	1	2000	2400	2600	2500†	90	60	234000	155912	0.77	0.85	Cantilever
1995-NZ-BR-03	CMU	FG	1	2000	2400	2600	2500†	90	90	234000	234000	0.77	0.85	Cantilever
1995-NZ-BR-04	CMU	FG	1	2000	2400	4200	4100†	90	90	378000	378000	0.48	0.52	Cantilever
1995-NZ-BR-06	CMU	PG	1	2000	2400	1800	1700†	140	60	252000	107951	1.11	1.22	Cantilever
1995-NZ-BR-07	CMU	PG	1	2000	2400	2600	2500†	140	60	364000	155912	0.77	0.85	Cantilever
1995-NZ-BR-08	CMU	PG	1	2000	2400	4200	4100†	140	60	588000	251834	0.48	0.52	Cantilever
1995-NZ-BR-10	CMU	PG	1	2000	2400	1800	1700†	140	60	252000	107951	1.11	1.22	Cantilever
1995-NZ-BR-11	CMU	PG	1	2000	2400	2600	2500†	140	60	364000	155912	0.77	0.85	Cantilever
1995-NZ-BR-12	CMU	PG	1	2000	2400	4200	4100†	140	60	588000	251834	0.48	0.52	Cantilever
1996-SL-TO-06	CMU	PG	0.5	759	380	610	560†	100	40*	61000	36516	1.24	1.36	Cantilever
1996-SL-TO-08	CMU	PG	0.5	759	380	610	560†	100	40*	61000	36516	1.24	1.36	Cantilever
1996-SL-TO-10	CMU	PG	0.5	759	380	610	560†	100	40*	61000	36516	1.24	1.36	Cantilever
1996-SL-TO-12	CMU	PG	0.5	759	380	610	560†	100	40*	61000	36516	1.24	1.36	Cantilever
1996-SL-TO-14	CMU	PG	0.5	759	380	610	560†	100	40*	61000	36516	1.24	1.36	Cantilever
1996-SL-TO-16	CMU	PG	0.5	759	380	610	560†	100	40*	61000	36516	1.24	1.36	Cantilever
1996-US-SH-02	CMU	PG	1	1422	711	2032	1930†	194	67.4	394208	#REF!	0.70	0.35	Fixed
1998-US-SH-01	CMU	PG	1	1422	711	2845	2743†	194	67.4	551930	241887	0.50	0.25	Fixed
1998-US-SH-02	CMU	PG	1	1422	711	2032	1930†	194	67.4	394208	187090	0.70	0.35	Fixed
1998-US-SH-03	CMU	PG	1	1422	711	1422	1320†	194	67.4	275868	145976	1.00	0.50	Fixed
1998-US-SH-04	CMU	PG	1	1422	711	2845	2743†	194	67.4	551930	241887	0.50	0.25	Fixed

Table E.2: Geometric Properties of Dataset (Continued)

Serial	Block	Grout	Scale	Height		Length		Thickness		Shear Area		$\frac{h_g}{l_w}$	$\frac{M}{Vl_w}$	Boundary
				h_g (mm)	h_e (mm)	l_w (mm)	d (mm)	t (mm)	t_s (mm)	A_g (mm^2)	A_{nv} (mm^2)			
1998-US-SH-05	CMU	PG	1	1422	711	2032	1930†	194	67.4	394208	187090	0.70	0.35	Fixed
1998-US-SH-06	CMU	PG	1	1422	711	1422	1320†	194	67.4	275868	145976	1.00	0.50	Fixed
2000-JP-OH-01	CMU	FG	1	1800	900	1197	1144†	197	197	235809	235809	1.50	0.75	Fixed
2000-JP-OH-02	CMU	FG	1	1800	900	1197	1144†	197	197	235809	235809	1.50	0.75	Fixed
2000-JP-OH-03	CMU	FG	1	1800	900	1197	1144†	197	197	235809	235809	1.50	0.75	Fixed
2000-JP-OH-04	CMU	FG	1	1800	900	1197	1144†	197	197	235809	235809	1.50	0.75	Fixed
2007-AU-HA-01	Clay	PG	1	2245	2408	2870	2785	150	70	430500	232900	0.78	0.84	Cantilever
2007-AU-HA-02	Clay	PG	1	2245	2408	2870	2785	150	70	430500	232900	0.78	0.84	Cantilever
2007-AU-HA-03	Clay	PG	1	2245	2408	2870	2785	150	70	430500	232900	0.78	0.84	Cantilever
2007-AU-HA-04	Clay	PG	1	2245	2408	2870	2785	150	70	430500	232900	0.78	0.84	Cantilever
2007-AU-HA-05	Clay	PG	1	2245	2408	2870	2785	150	70	430500	232900	0.78	0.84	Cantilever
2007-AU-HA-06	Clay	PG	1	2245	2408	2870	2785	150	70	430500	232900	0.78	0.84	Cantilever
2007-AU-HA-07	Clay	PG	1	2245	2408	2870	2610	150	70	430500	232900	0.78	0.84	Cantilever
2007-AU-HA-08	Clay	PG	1	2245	2408	2870	2610	150	70	430500	232900	0.78	0.84	Cantilever
2007-AU-HA-09	Clay	PG	1	2245	2408	2870	2785	150	70	430500	216900	0.78	0.84	Cantilever
2007-AU-HA-11	Clay	PG	1	1412	1412	2870	2785	150	70	430500	232900	0.49	0.49	Cantilever
2007-AU-HA-12	Clay	PG	1	1412	1412	2870	2785	150	70	430500	232900	0.49	0.49	Cantilever
2007-AU-HA-13	Clay	PG	1	1412	1412	1270	1185	150	70	190500	142580	1.11	1.11	Cantilever
2007-AU-HA-14	Clay	PG	1	1412	1412	1270	1185	150	70	190500	142580	1.11	1.11	Cantilever
2007-NZ-VO-01	CMU	FG	1	1800	1838	1800	1700†	140	140	252000	252000	1.00	1.02	Cantilever
2007-NZ-VO-02	CMU	FG	1	1800	1838	1800	1700†	140	140	252000	252000	1.00	1.02	Cantilever
2007-NZ-VO-04	CMU	FG	1	1800	1838	1800	1700†	140	140	252000	252000	1.00	1.02	Cantilever
2007-NZ-VO-05	CMU	PG	1	1800	1838	1800	1700†	140	30	252000	185806	1.00	1.02	Cantilever
2007-NZ-VO-06	CMU	PG	1	1800	1838	1800	1700†	140	30	252000	154838	1.00	1.02	Cantilever
2007-NZ-VO-07	CMU	FG	1	1800	1838	1800	1700†	140	140	252000	252000	1.00	1.02	Cantilever
2007-NZ-VO-08	CMU	FG	1	1800	1838	1800	1700†	140	140	252000	252000	1.00	1.02	Cantilever
2007-NZ-VO-09	CMU	FG	1	3600	3638	1800	1700†	140	140	252000	252000	2.00	2.02	Cantilever

Table E.2: Geometric Properties of Dataset (Continued)

Serial	Block	Grout	Scale	Height		Length		Thickness		Shear Area		$\frac{h_g}{l_w}$	$\frac{M}{Vl_w}$	Boundary
				h_g (mm)	h_e (mm)	l_w (mm)	d (mm)	t (mm)	t_s (mm)	A_g (mm^2)	A_{nv} (mm^2)			
2007-NZ-VO-10	CMU	FG	1	1800	1838	3000	2900†	140	140	420000	420000	0.60	0.61	Cantilever
2007-PO-HA-02	CMU	PG	0.5	808	948	1206	1103†	100	30†	112158	55080	0.66	0.66	Cantilever
2007-PO-HA-03	CMU	PG	0.5	808	948	1206	1103†	100	30†	112158	55080	0.66	0.66	Cantilever
2007-PO-HA-04	CMU	PG	0.5	808	948	1206	1103†	100	30†	112158	55080	0.66	0.66	Cantilever
2007-PO-HA-05	CMU	PG	0.5	808	948	1206	1103†	100	30†	112158	55080	0.66	0.66	Cantilever
2008-CA-MA-01	CMU	PG	0.5	1800	1800	1800	1755	90	31	162000	72903	1.00	1.00	Cantilever
2008-CA-MA-02	CMU	PG	0.5	1800	1800	1800	1755	90	31	162000	72903	1.00	1.00	Cantilever
2008-CA-MA-04	CMU	PG	0.5	900	900	1800	1755	90	31	162000	72903	0.50	0.50	Cantilever
2008-CA-MA-05	CMU	PG	0.5	2700	2700	1800	1755	90	31	162000	72903	1.50	1.50	Cantilever
2009-US-MI-01	CMU	PG	1	2642	2642	3851	3754†	194	63.5*	747094	331612	0.69	0.69	Cantilever
2009-US-MI-02	CMU	PG	1	2642	2642	3851	3754†	194	63.5*	747094	331612	0.69	0.69	Cantilever
2009-US-MI-03	CMU	PG	1	2642	1321	3851	3754†	194	63.5*	747094	331612	0.69	0.34	Fixed
2009-US-MI-04	CMU	PG	1	2642	1321	3851	3754†	194	63.5*	747094	331612	0.69	0.34	Fixed
2009-US-MI-07	Clay	FG	1	2642	2642	3851	3754†	143	143	550693	550693	0.69	0.69	Cantilever
2009-US-MI-08	Clay	FG	1	2642	2642	3851	3754†	143	143	550693	550693	0.69	0.69	Cantilever
2010-US-EL-01	CMU	PG	1	1422	1524	2631	2535†	194	63.5*	510414	229677	0.58	0.58	Cantilever
2010-US-EL-02	CMU	PG	1	1422	1524	2631	2535†	194	63.5*	510414	229677	0.58	0.58	Cantilever
2010-US-EL-03	CMU	PG	1	1422	1524	2631	2535†	194	63.5*	510414	229677	0.58	0.58	Cantilever
2010-US-EL-04	CMU	PG	1	1422	1524	2631	2535†	194	63.5*	510414	229677	0.58	0.58	Cantilever
2010-US-EL-05	CMU	PG	1	1422	1524	2631	2535†	194	63.5*	510414	250322	0.58	0.58	Cantilever
2010-US-EL-06	CMU	PG	1	1422	1524	2631	2535†	194	63.5*	510414	271612	0.58	0.58	Cantilever
2010-US-NO-01	CMU	PG	1	2337	2337	2631	2535†	194	63.5*	510414	229677	0.89	0.89	Cantilever
2010-US-NO-02	CMU	PG	1	2337	2337	2631	2535†	194	63.5*	510414	229677	0.89	0.89	Cantilever
2010-US-NO-03	CMU	PG	1	2337	2337	2631	2535†	194	63.5*	510414	229677	0.89	0.89	Cantilever
2010-US-NO-04	CMU	PG	1	2337	2337	2631	2535†	194	63.5*	510414	250322	0.89	0.89	Cantilever
2010-US-NO-05	CMU	PG	1	2337	2337	2631	2535†	194	63.5*	510414	271612	0.89	0.89	Cantilever
2010-US-NO-06	CMU	FG	1	2337	2337	2631	2535†	194	194	510414	510414	0.89	0.89	Cantilever

Table E.3: Reinforcement Details of Specimens

Serial	Reinforcement				Reinforcement Area				Reinforcement Spacing			Grout Spacing	
	Flexural	Vertical	Shear	Joint	A_t (mm^2)	A_c (mm^2)	A_h (mm^2)	A_j (mm^2)	s_c (mm)	s_h (mm)	s_j (mm)	s_{gh} (mm)	s_{gv} (mm)
1968-MX-ME-09	(2)2#4	(3)#3	–	Ø2.5mm	1229	71	–	4.91	650†	–	400	650	2650
1968-MX-ME-10	(2)2#4	(3)#3	–	Ø2.5mm	1229	71	–	4.91	650†	–	400	650	2650
1968-MX-ME-11	(2)2#4	(3)#3	–	Ø2.5mm	1229	71	–	4.91	650†	–	400	650	2650
1968-MX-ME-12	(2)#4	#3	–	Ø2.5mm	579	71	–	4.91	1300†	–	400	1300	2650
1968-MX-ME-13	(2)#4	#3	–	Ø2.5mm	579	71	–	4.91	1300†	–	400	1300	2650
1968-MX-ME-14	(2)2#4	(3)#3	–	–	1229	71	–	–	650†	–	–	650	2650
1968-MX-ME-15	(2)#4	#3	–	–	579	71	–	–	1300†	–	–	1300	2650
1968-MX-ME-16	(2)2#4	(3)#3	–	Ø2.5mm	1229	71	–	4.91	650†	–	400	650	2650
1968-MX-ME-17	(2)4#4	(3)#3	–	Ø2.5mm	2245	71	–	4.91	650†	–	400	650	2650
1968-MX-ME-18	(2)2#4	(3)#3	–	Ø2.5mm	1229	71	–	4.91	650†	–	400	650	2650
1969-MX-ME-11	(2)2#5	–	–	–	796	–	–	–	–	–	–	1600	2000
1969-MX-ME-14	2#5	–	–	–	398	–	–	–	–	–	–	1800	2000
1969-MX-ME-15	(2)2#5	–	–	–	796	–	–	–	–	–	–	1600	2000
1969-MX-ME-16	(2)2#5	–	–	–	796	–	–	–	–	–	–	1600	2000
1969-MX-ME-17	(2)2#5	–	–	–	796	–	–	–	–	–	–	1600	2000
1969-MX-ME-18	(2)2#5	(2)#4	–	–	796	127	–	–	633†	–	–	633	2000
1969-MX-ME-19	(2)2#4	–	–	–	554	–	–	–	–	–	–	1600	2000
1969-MX-ME-20	(2)2#5	(2)#4	–	–	796	127	–	–	633†	–	–	633	2000
1969-MX-ME-21	(2)2#5	–	–	–	796	–	–	–	–	–	–	1600	2000
1969-MX-ME-24	2#3	–	–	–	153	–	–	–	–	–	–	1800	2000
1969-MX-ME-25	(2)2#5	(2)#4	–	–	796	127	–	–	633†	–	–	0	0
1969-MX-ME-29	(2)2#5	–	–	–	796	–	–	–	–	–	–	1600	2000
1971-NZ-WI-01	#3	(2)#3	–	–	71	71	–	–	304.8†	–	–	0	0
1971-NZ-WI-02	#3	(2)#3	–	–	71	71	–	–	304.8†	–	–	0	0
1971-NZ-WI-03	#3	(2)#3	–	–	71	71	–	–	304.8†	–	–	0	0
1971-NZ-WI-04	#3	(2)#3	–	–	71	71	–	–	304.8†	–	–	305	1143
1971-NZ-WI-05	#3	(2)#3	–	–	71	71	–	–	304.8†	–	–	0	0
1971-NZ-WI-06	#3	(2)#3	–	–	71	71	–	–	406.4†	–	–	0	0

Table E.3: Reinforcement Details of Dataset (Continued)

Serial	Reinforcement				Reinforcement Area				Reinforcement Spacing			Grout Spacing	
	Flexural	Vertical	Shear	Joint	A_t (mm^2)	A_c (mm^2)	A_h (mm^2)	A_j (mm^2)	s_c (mm)	s_h (mm)	s_j (mm)	s_{gh} (mm)	s_{gv} (mm)
1971-NZ-WI-07	#3	(2)#3	–	–	71	71	–	–	406.4†	–	–	0	0
1971-NZ-WI-08	#3	(2)#3	–	–	71	71	–	–	406.4†	–	–	0	0
1971-NZ-WI-09	#3	(2)#3	–	–	71	71	–	–	406.4†	–	–	0	0
1971-NZ-WI-10	#7	–	–	–	387	–	–	–	406.4†	–	–	0	0
1971-NZ-WI-11	#7	–	2#5	–	387	–	400	–	406.4†	381†	–	0	0
1971-NZ-WI-12	#3	–	–	–	71	–	–	–	–	–	–	0	0
1971-NZ-WI-13	#3	–	–	–	71	–	–	–	–	–	–	0	0
1971-NZ-WI-15	(2)#6	–	–	–	568	–	–	–	–	–	–	0	0
1971-NZ-WI-16	#3	(4)#3	–	–	71	71	–	–	304.8†	–	–	0	0
1971-NZ-WI-17	#3	(4)#3	–	–	71	71	–	–	304.8†	–	–	0	0
1971-NZ-WI-18	#3	–	–	–	71	–	–	–	–	–	–	0	0
1971-NZ-WI-19	#3	(2)#3	–	–	71	71	–	–	304.8†	–	–	0	0
1971-NZ-WI-20	#3	(2)#3	–	–	71	71	–	–	304.8†	–	–	0	0
1976-US-MA-01	#6	–	–	–	284	–	–	–	–	–	–	0	0
1976-US-MA-02	#6	–	–	–	284	–	–	–	–	–	–	0	0
1976-US-MA-03	#4	–	–	–	129	–	–	–	–	–	–	0	0
1976-US-MA-04	#4	–	–	–	129	–	–	–	–	–	–	0	0
1976-US-MA-05	#6	–	–	–	284	–	–	–	–	–	–	0	0
1976-US-MA-06	#6	–	–	–	284	–	–	–	–	–	–	0	0
1976-US-MA-07	#6	–	(3)#5	–	284	–	200	–	–	406†	–	0	0
1976-US-MA-08	#6	–	(3)#5	–	284	–	200	–	–	406†	–	0	0
1976-US-MA-09	#8	–	–	–	510	–	–	–	–	–	–	0	0
1976-US-MA-10	#8	–	–	–	510	–	–	–	–	–	–	0	0
1976-US-MA-11	#8	–	–	–	510	–	–	–	–	–	–	401	1626
1976-US-MA-12	#8	–	–	–	510	–	–	–	–	–	–	401	1626
1977-NZ-PR-05	(2)#6	(4)#6	(8)#6	–	568	284	284	–	364†	206†	–	0	0
1977-NZ-PR-06	(2)#6	(2)#5	(8)#5	–	568	200	200	–	607†	206†	–	0	0
1977-NZ-PR-07	(2)#6	(4)#6	(8)#6	–	568	284	284	–	364†	206†	–	0	0

Table E.3: Reinforcement Details of Dataset (Continued)

Serial	Reinforcement				Reinforcement Area				Reinforcement Spacing			Grout Spacing	
	Flexural	Vertical	Shear	Joint	A_t (mm^2)	A_c (mm^2)	A_h (mm^2)	A_j (mm^2)	s_c (mm)	s_h (mm)	s_j (mm)	s_{gh} (mm)	s_{gv} (mm)
1977-NZ-PR-08	(2)#6	(2)#5	(8)#5	–	568	200	200	–	607†	206†	–	0	0
1977-NZ-PR-09	(2)#6	(4)#6	(8)#6	–	568	284	284	–	364†	206†	–	0	0
1977-NZ-PR-10	(2)#6	(4)#6	(8)#6	–	568	284	284	–	364†	206†	–	0	0
1978-US-CH-02	#5	–	–	–	200	–	–	–	–	–	–	915	1422
1978-US-CH-03	#5	–	–	–	200	–	–	–	–	–	–	0	0
1978-US-CH-04	#5	–	#5	–	200	–	200	–	–	711†	–	0	0
1978-US-CH-05	#5	–	#5	–	200	–	200	–	–	711†	–	915	711
1978-US-CH-06	#8	–	(4)#5	–	510	–	200	–	–	284†	–	0	0
1978-US-CH-07	#8	–	–	–	510	–	–	–	–	–	–	0	0
1978-US-CH-08	#8	–	–	–	510	–	–	–	–	–	–	915	1422
1978-US-CH-09	#8	–	2#5	–	510	–	200	–	–	474†	–	0	0
1978-US-CH-10	#8	–	(2)#5	–	510	–	200	–	–	474†	–	915	474
1978-US-CH-11	–	–	(4)#6	–	–	–	284	–	–	284†	–	0	0
1978-US-CH-14	#5	–	–	–	200	–	–	–	–	–	–	0	0
1978-US-CH-15	#5	–	#5	–	200	–	200	–	–	711†	–	0	0
1978-US-CH-16	#5	–	#5	–	200	–	200	–	–	711†	–	915	711
1978-US-CH-17	#5	–	(5)#5	–	200	–	200	–	–	237†	–	0	0
1978-US-CH-18	#8	–	(5)#5	–	510	–	200	–	–	237†	–	0	0
1978-US-CH-19	#8	–	–	–	510	–	–	–	–	–	–	0	0
1978-US-CH-20	#8	–	–	–	510	–	–	–	–	–	–	915	1422
1978-US-CH-21	#8	–	#5	–	510	–	200	–	–	474†	–	0	0
1978-US-CH-22	#8	–	(2)#5	–	510	–	200	–	–	474†	–	915	474
1978-US-CH-23	#8	–	(5)#6	–	510	–	284	–	–	237†	–	0	0
1978-US-CH-24	#8	–	(5)#6	–	510	–	284	–	–	237†	–	0	0
1978-US-HI-01	–	–	–	–	–	–	–	–	–	–	–	0	0
1978-US-HI-02	#8	–	–	–	510	–	–	–	–	–	–	0	0
1978-US-HI-03	#8	–	–	–	510	–	–	–	–	–	–	915	2032

Table E.3: Reinforcement Details of Dataset (Continued)

Serial	Reinforcement				Reinforcement Area				Reinforcement Spacing			Grout Spacing	
	Flexural	Vertical	Shear	Joint	A_t (mm^2)	A_c (mm^2)	A_h (mm^2)	A_j (mm^2)	s_c (mm)	s_h (mm)	s_j (mm)	s_{gh} (mm)	s_{gv} (mm)
1978-US-HI-04	#8	–	2#5	–	510	–	400	–	–	677†	–	0	0
1978-US-HI-05	#8	–	2#5	–	510	–	400	–	–	677†	–	915	677
1978-US-HI-06	#8	–	(3)#5	–	510	–	200	–	–	508†	–	0	0
1978-US-HI-07	#8	–	(3)#5	–	510	–	200	–	–	508†	–	915	508
1978-US-HI-08	#8	–	(4)#5	–	510	–	200	–	–	406†	–	0	0
1978-US-HI-09	#8	–	(5)#5	–	510	–	200	–	–	339†	–	0	0
1979-US-HI-01	#7	#7	–	–	387	387	–	–	914†	–	–	0	0
1979-US-HI-02	#7	#7	#5	–	387	387	200	–	914†	508†	–	0	0
1979-US-HI-03	#7	#7	2#5	–	387	387	400	–	914†	339†	–	0	0
1979-US-HI-04	#7	#7	(3)#5	–	387	387	200	–	914†	254†	–	0	0
1979-US-HI-05	#7	#7	(4)#5	–	387	387	200	–	914†	203†	–	0	0
1979-US-HI-06	#7	#7	(4)#6	–	387	387	284	–	914†	203†	–	0	0
1979-US-HI-08	#7	#7	#6	–	387	387	284	–	914	508†	–	0	0
1979-US-HI-09	#7	#7	2#6	–	387	387	568	–	914	339†	–	0	0
1979-US-HI-10	#7	#7	(3)#6	–	387	387	284	–	914	254†	–	0	0
1982-NZ-TH-01	D12	D10	(2)D12	–	113	78.5	113	–	700	800†	–	700	800
1982-NZ-TH-02	D10	(6)D10	(12)D10	–	78.5	78.5	78.5	–	200	200†	–	0	0
1982-NZ-TH-03	D16	D16	–	–	201	201	–	–	700	–	–	700	2400
1982-NZ-TH-04	D16	D16	(4)D12	–	201	201	113	–	700	480†	–	700	480
1982-NZ-TH-05	D16	(2)D16	(12)D16	–	201	201	201	–	467	200†	–	0	0
1982-NZ-TH-06	D16	D16	(4)D16	–	201	201	201	–	700	480†	–	0	0
1982-NZ-TH-08	D20	(2)D20 & (2)D16	(12)D20	–	314	157	216	–	280	200†	–	0	0
1983-JP-MA-01	2D25	(3)D10	D10	–	1020	71	71	–	400	400	–	0	0
1983-JP-MA-03	2D22	(2)D10	D10	–	774	78.5	71	–	400	400	–	0	0
1983-JP-MA-04	D29	D10	D10	–	645	71	71	–	400	400	–	0	0
1984-JP-IG-01	2D22	(4)Ø9	(2)Ø13	–	774	63.6	129	–	390	600	–	390	600
1984-JP-IG-02	2D22	(4)Ø9	(2)Ø13	–	774	63.6	129	–	390	600	–	390	600

Table E.3: Reinforcement Details of Dataset (Continued)

Serial	Reinforcement				Reinforcement Area				Reinforcement Spacing			Grout Spacing	
	Flexural	Vertical	Shear	Joint	A_t (mm^2)	A_c (mm^2)	A_h (mm^2)	A_j (mm^2)	s_c (mm)	s_h (mm)	s_j (mm)	s_{gh} (mm)	s_{gv} (mm)
1984-JP-IG-03	D29	(3)Ø9	(2)Ø13	–	645	63.6	129	–	390	600	–	390	600
1984-JP-IG-04	D25	(2)Ø9	(2)Ø13	–	510	63.6	129	–	390	600	–	390	600
1984-JP-IG-05	D22	Ø9	(2)Ø13	–	387	63.6	129	–	390	600	–	390	600
1984-JP-IG-06	D22	Ø9	(2)Ø13	–	387	63.6	129	–	390	600	–	390	600
1985-JP-FU-01	2D19	(6)D16	(5)D13	–	768	200	129	–	400	400	–	0	0
1985-JP-FU-02	2D19	(6)D16	(5)D13	–	768	200	129	–	300	400	–	0	0
1985-JP-FU-03	2D19	(4)D16	(5)D13	–	768	200	129	–	400	400	–	0	0
1985-JP-FU-04	2D19	(4)D16	(5)D13	–	768	200	129	–	300	400	–	0	0
1985-JP-FU-05	2D19	(2)D16	(5)D13	–	768	200	129	–	400	400	–	0	0
1985-JP-FU-06	2D19	(2)D16	(5)D13	–	768	200	129	–	300	400	–	0	0
1985-JP-MA-01	2D19	(2)D16	–	–	768	200	–	–	400	–	–	0	0
1985-JP-MA-02	2D19	(2)D16	(5)D13	–	768	200	129	–	400	400	–	0	0
1985-JP-MA-03	2D19	(2)D16	(9)D13	–	768	200	129	–	400	200	–	0	0
1985-JP-MA-05	2D25	(2)D16	(9)D13	–	1020	200	129	–	400	200	–	0	0
1985-JP-MA-06	2D25	(2)D16	(9)2D13	–	1020	200	258	–	400	200	–	0	0
1985-JP-YA-05	2D25	D16	(3)D13	–	1020	200	129	–	400	400	–	0	0
1985-JP-YA-06	2D25	D16	(6)D13	–	1020	200	129	–	400	200	–	0	0
1985-JP-YA-07	2D25	D16	(5)D13	–	1020	200	129	–	400	400	–	0	0
1985-JP-YA-08	2D25	D16	(4)D13	–	1020	200	129	–	400	300	–	0	0
1985-JP-YA-09	2D25	D16	(8)D13	–	1020	200	129	–	400	150	–	0	0
1985-US-SV-01	#5	–	(4)#5	–	200	–	200	–	–	284†	–	0	0
1985-US-SV-02	#5	–	(4)#5	–	200	–	200	–	–	284†	–	0	0
1985-US-SV-03	#7	–	(4)#5	–	387	–	200	–	–	284†	–	0	0
1985-US-SV-04	#4	(4)#4	(4)#5	–	129	129	200	–	213	284†	–	0	0
1985-US-SV-05	#7	–	(4)#5	–	387	–	200	–	–	284†	–	0	0
1985-US-SV-06	#7	–	2#5	–	387	–	200	–	–	474†	–	0	0
1985-US-SV-07	#4	(4)#4	2#5	–	129	129	200	–	213	474†	–	0	0

Table E.3: Reinforcement Details of Dataset (Continued)

Serial	Reinforcement				Reinforcement Area				Reinforcement Spacing			Grout Spacing	
	Flexural	Vertical	Shear	Joint	A_t (mm^2)	A_c (mm^2)	A_h (mm^2)	A_j (mm^2)	s_c (mm)	s_h (mm)	s_j (mm)	s_{gh} (mm)	s_{gv} (mm)
1985-US-SV-08	#7	–	2#5	–	387	–	200	–	–	474†	–	0	0
1985-US-SV-09	#7	–	–	(8)3/16" truss	387	–	–	35.6	–	–	203†	0	0
1985-US-SV-10	#7	–	2#5	(8)3/16" truss	387	–	200	35.6	–	474†	203†	0	0
1985-US-SV-11	#7	–	2#5	–	387	–	200	–	–	474†	–	0	0
1985-US-SV-12	#7	–	2#5	–	387	–	200	–	–	474†	–	0	0
1985-US-SV-13	#5	–	(5)#5	–	200	–	200	–	–	237†	–	0	0
1985-US-SV-15	#5	–	(5)#5	–	200	–	200	–	–	237†	–	0	0
1985-US-SV-16	#7	–	2#5	–	387	–	400	–	–	474†	–	0	0
1985-US-SV-17	#7	–	(5)#5	–	387	–	200	–	–	237†	–	0	0
1985-US-SV-18	#7	(2)#5	2#5	–	387	200	400	–	356	474†	–	0	0
1985-US-SV-19	#5	(2)#5	(5)#5	–	200	200	200	–	356	237†	–	0	0
1985-US-SV-20	#4	(4)#4	2#5	–	129	129	400	–	213	474†	–	0	0
1985-US-SV-21	#4	(4)#4	(5)#5	–	129	129	200	–	213	237†	–	0	0
1985-US-SV-22	#7	–	2#5	–	387	–	400	–	–	474†	–	0	0
1985-US-SV-23	#7	–	(5)#5	–	387	–	200	–	–	237†	–	0	0
1985-US-SV-24	#7	–	(2)2#4	–	387	–	258	–	–	474†	–	0	0
1985-US-SV-25	#5	–	(5)2#4	–	387	–	258	–	–	237†	–	0	0
1985-US-SV-26	#7	–	–	(8) 3/16" truss	387	–	–	35.6	–	–	203†	0	0
1986-JP-IG-01	2D19	(2)D16	–	–	768	200	–	–	300	–	–	0	0
1986-JP-IG-02	2D19	(2)D16	(4)D13	–	768	200	129	–	300	400	–	0	0
1986-JP-IG-03	2D19	(2)D16	(8)D13	–	768	200	129	–	300	200	–	0	0
1986-JP-IG-04	2D19	(2)D16	(8)2D13	–	768	200	258	–	300	200	–	0	0
1986-JP-MA-15	2D22†	Ø9†	Ø9†	–	774	63.6	63.6	–	400	900	–	400	900
1986-JP-MA-16	D25†	Ø9†	Ø9†	–	510	63.6	63.6	–	400	900	–	400	900
1986-JP-MA-17	2D22†	(2)Ø9†	–	–	774	63.6	–	–	400	–	–	400	1800
1986-JP-MA-18	2D22†	(2)Ø9†	–	–	774	63.6	–	–	400	–	–	400	1800
1986-JP-MA-19	2D22†	(2)Ø9†	–	–	774	63.6	–	–	400	–	–	400	1800

Table E.3: Reinforcement Details of Dataset (Continued)

Serial	Reinforcement				Reinforcement Area				Reinforcement Spacing			Grout Spacing	
	Flexural	Vertical	Shear	Joint	A_t (mm^2)	A_c (mm^2)	A_h (mm^2)	A_j (mm^2)	s_c (mm)	s_h (mm)	s_j (mm)	s_{gh} (mm)	s_{gv} (mm)
1986-JP-MA-20	2D22†	(2)Ø9†	–	–	774	63.6	–	–	400	–	–	400	1800
1986-JP-MA-21	2D22†	(2)Ø9†	–	–	774	63.6	–	–	400	–	–	400	1800
1986-JP-MA-22	2D22†	(2)Ø9†	Ø9†	–	774	63.6	63.6	–	400	900	–	400	900
1986-JP-MA-23	2D22†	(2)Ø9†	Ø9†	–	774	63.6	63.6	–	400	900	–	400	900
1986-JP-MA-24	D29†	(2)Ø9†	Ø9†	–	645	63.6	63.6	–	400	900	–	400	900
1986-JP-MA-25	2D22†	(2)Ø9†	Ø9†	–	774	63.6	63.6	–	400	900	–	400	900
1986-JP-MA-26	2D22†	(2)Ø9†	Ø9†	–	774	63.6	63.6	–	400	900	–	400	900
1986-JP-MA-27	2D22†	(2)Ø9†	Ø9†	–	774	63.6	63.6	–	400	900	–	400	900
1986-JP-MA-28	2D22†	(2)Ø9†	(2)Ø9†	–	774	63.6	63.6	–	400	600	–	400	600
1986-JP-MA-29	2D22†	(2)Ø9†	(2)Ø9†	–	774	63.6	63.6	–	400	600	–	400	600
1986-JP-MA-30	2D22†	(2)Ø9†	(2)Ø9†	–	774	63.6	63.6	–	400	600	–	400	600
1986-JP-MA-31	2D22†	(2)Ø9†	(3)Ø9†	–	774	63.6	63.6	–	400	400	–	400	400
1986-JP-MA-32	2D22†	(2)Ø9†	(3)Ø9†	–	774	63.6	63.6	–	400	400	–	400	400
1986-JP-MA-33	2D22†	(2)Ø9†	(3)Ø9†	–	774	63.6	63.6	–	400	400	–	400	400
1986-JP-MA-34	2D22†	(2)Ø9†	(4)Ø9†	–	774	63.6	36.6	–	400	200	–	400	200
1986-JP-MA-35	2D22†	(3)Ø9†	Ø9†	–	774	63.6	63.6	–	400	900	–	400	900
1986-JP-MA-36	D25 & D22†	(3)Ø9†	Ø9†	–	897	63.6	63.6	–	400	900	–	400	900
1986-JP-MA-37	D13†	(2)Ø9†	Ø9†	–	129	63.6	63.6	–	400	600	–	400	600
1986-JP-MA-38	D19†	(2)Ø9†	Ø9†	–	284	63.6	63.6	–	400	900	–	400	900
1986-JP-MA-53	2D22†	(3)Ø9†	Ø9†	–	774	63.6	63.6	–	333*	400	–	333	400
1986-JP-MA-54	2D22†	(3)Ø9†	Ø9†	–	774	63.6	63.6	–	333*	400	–	333	400
1986-JP-SH-01	2D25	(2)D16	(8)D13	–	1020	200	129	–	400	200	–	0	0
1986-JP-SH-02	2D25	(2)D16	(8)D13	–	1020	200	129	–	400	200	–	0	0
1986-JP-SH-03	2D25	(2)D16	(8)D13	4mm ladder	1020	200	129	25.1	400	200	200	0	0
1986-JP-SH-04	2D19	(2)D16	(8)D13	–	768	200	129	–	400	200	–	0	0
1986-JP-SH-05	2D25	(2)D16	(8)D13	–	1020	200	129	–	400	200	–	0	0
1986-JP-SH-06	2D25	(2)D16	(8)D13	–	1020	200	129	–	400	200	–	0	0

Table E.3: Reinforcement Details of Dataset (Continued)

Serial	Reinforcement				Reinforcement Area				Reinforcement Spacing			Grout Spacing	
	Flexural	Vertical	Shear	Joint	A_t (mm^2)	A_c (mm^2)	A_h (mm^2)	A_j (mm^2)	s_c (mm)	s_h (mm)	s_j (mm)	s_{gh} (mm)	s_{gv} (mm)
1987-JP-OK-01	2D19	(4)D16	(5)D13	–	768	200	129	–	400	400	–	0	0
1987-JP-OK-02	2D19	(4)D16	(5)D13	–	768	200	129	–	400	400	–	0	0
1987-JP-OK-10	2D19	(2)D16	(5)D13	–	768	200	129	–	400	400	–	0	0
1987-JP-OK-11	2D19	(2)D16	(5)D13	–	768	200	129	–	400	400	–	0	0
1988-JP-IG-05	2D25	(2)D16	–	–	1020	200	–	–	300	–	–	0	0
1988-JP-IG-06	2D25	(2)D16	(4)D13	–	1020	200	129	–	300	400	–	0	0
1988-JP-IG-07	2D25	(2)D16	(8)D13	–	1020	200	129	–	300	200	–	0	0
1988-JP-IG-08	2D25	(2)D16	(8)2D13	–	1020	200	258	–	300	200	–	0	0
1988-JP-IG-09	D22	(2)D16	(8)D13	–	387	200	129	–	300	200	–	0	0
1988-SL-TO-01	Ø10mm	–	–	–	78.5	–	–	–	–	–	–	510	759
1988-SL-TO-02	Ø10mm	–	–	2Ø3.1mm	78.5	–	–	15.1	–	–	110	510	759
1988-SL-TO-03	Ø10mm	–	–	2Ø4.2mm	78.5	–	–	27.7	–	–	110	510	759
1988-SL-TO-04	Ø10mm	–	–	2Ø6mm	78.5	–	–	56.5	–	–	110	510	759
1988-SL-TO-05	Ø10mm	–	–	–	78.5	–	–	–	–	–	–	510	1410
1988-SL-TO-09	2Ø10mm	–	–	–	157	–	–	–	–	–	–	510	759
1988-SL-TO-10	2Ø10mm	–	–	2Ø3.1mm	157	–	–	15.1	–	–	110	510	759
1988-SL-TO-11	2Ø10mm	–	–	2Ø4.2mm	157	–	–	27.7	–	–	110	510	759
1988-SL-TO-12	2Ø10mm	–	–	2Ø6mm	157	–	–	56.5	–	–	110	510	759
1988-SL-TO-13	2Ø10mm	–	–	–	157	–	–	–	–	–	–	510	1410
1988-US-JO-01	#5	–	–	–	200	–	–	–	–	–	–	762	914
1988-US-JO-02	#5	–	–	–	200	–	–	–	–	–	–	762	914
1988-US-JO-03	#5	–	–	–	200	–	–	–	–	–	–	762	914
1988-US-JO-04	#5	–	–	–	200	–	–	–	–	–	–	762	914
1988-US-JO-05	#5	–	–	–	200	–	–	–	–	–	–	762	914
1988-US-JO-06	#5	–	–	–	200	–	–	–	–	–	–	762	914
1988-US-JO-07	#5	–	–	–	200	–	–	–	–	–	–	762	914
1988-US-JO-08	#5	–	–	–	200	–	–	–	–	–	–	762	914

Table E.3: Reinforcement Details of Dataset (Continued)

Serial	Reinforcement				Reinforcement Area				Reinforcement Spacing			Grout Spacing	
	Flexural	Vertical	Shear	Joint	A_t (mm^2)	A_c (mm^2)	A_h (mm^2)	A_j (mm^2)	s_c (mm)	s_h (mm)	s_j (mm)	s_{gh} (mm)	s_{gv} (mm)
1988-US-JO-09	#5	–	–	–	200	–	–	–	–	–	–	762	914
1988-US-JO-10	#5	–	–	–	200	–	–	–	–	–	–	762	914
1988-US-JO-11	#5	–	–	–	200	–	–	–	–	–	–	762	914
1988-US-JO-12	#5	–	–	–	200	–	–	–	–	–	–	762	914
1988-US-JO-13	#5	–	–	–	200	–	–	–	–	–	–	762	914
1988-US-JO-14	#5	–	–	–	200	–	–	–	–	–	–	762	914
1988-US-JO-15	#5	–	–	–	200	–	–	–	–	–	–	762	914
1988-US-JO-16	#5	–	–	–	200	–	–	–	–	–	–	762	914
1988-US-JO-17	#5	–	–	–	200	–	–	–	–	–	–	609	813
1988-US-JO-18	#5	–	–	–	200	–	–	–	–	–	–	609	813
1988-US-JO-19	#5	–	–	–	200	–	–	–	–	–	–	609	813
1988-US-JO-20	#5	–	–	–	200	–	–	–	–	–	–	609	813
1988-US-JO-21	#5	–	–	–	200	–	–	–	–	–	–	609	813
1988-US-JO-22	#5	–	–	–	200	–	–	–	–	–	–	609	813
1988-US-JO-23	#5	–	–	–	200	–	–	–	–	–	–	609	813
1988-US-JO-24	#5	–	–	–	200	–	–	–	–	–	–	609	813
1988-US-JO-25	#5	–	–	–	200	–	–	–	–	–	–	609	813
1988-US-JO-26	#5	–	–	–	200	–	–	–	–	–	–	609	813
1988-US-JO-27	#5	–	–	–	200	–	–	–	–	–	–	609	813
1988-US-JO-28	#5	–	–	–	200	–	–	–	–	–	–	609	813
1988-US-JO-29	#5	–	–	–	200	–	–	–	–	–	–	609	813
1988-US-JO-30	#5	–	–	–	200	–	–	–	–	–	–	609	813
1988-US-JO-31	#5	–	–	–	200	–	–	–	–	–	–	609	813
1988-US-JO-32	#5	–	–	–	200	–	–	–	–	–	–	609	813
1988-US-SH-03	#7	(3)#7	(5)#3	–	387	387	71	–	406	406	–	0	0
1988-US-SH-04	#7	(3)#7	(5)#3	–	387	387	71	–	406	406	–	0	0
1988-US-SH-05	#7	(3)#7	(5)#3	–	387	387	71	–	406	406	–	0	0

Table E.3: Reinforcement Details of Dataset (Continued)

Serial	Reinforcement				Reinforcement Area				Reinforcement Spacing			Grout Spacing	
	Flexural	Vertical	Shear	Joint	A_t (mm^2)	A_c (mm^2)	A_h (mm^2)	A_j (mm^2)	s_c (mm)	s_h (mm)	s_j (mm)	s_{gh} (mm)	s_{gv} (mm)
1988-US-SH-06	#5	(3)#5	(5)#3	–	200	200	71	–	406	406	–	0	0
1988-US-SH-07	#7	(3)#7	(5)#3	–	387	387	71	–	406	406	–	0	0
1988-US-SH-08	#5	(3)#5	(5)#4	–	200	200	129	–	406	406	–	0	0
1988-US-SH-09	#5	(3)#5	(5)#3	–	200	200	71	–	406	406	–	0	0
1988-US-SH-10	#5	(3)#5	(5)#3	–	200	200	71	–	406	406	–	0	0
1988-US-SH-11	#7	(3)#7	(5)#4	–	387	387	129	–	406	406	–	0	0
1988-US-SH-13	#6	(3)#6	(5)#5	–	284	284	200	–	406	406	–	0	0
1988-US-SH-14	#6	(3)#6	(5)#3	–	284	284	71	–	406	406	–	0	0
1988-US-SH-15	#6	(3)#6	(5)#4	–	284	284	129	–	406	406	–	0	0
1988-US-SH-16	#7	(3)#7	(5)#4	–	387	387	129	–	406	406	–	0	0
1989-US-YA-02	–	–	–	9-ga. ladder	–	–	–	22.2	–	–	406	1019	1422
1989-US-YA-03	–	–	–	9-ga. ladder	–	–	–	22.2	–	–	203	1019	1422
1989-US-YA-04	–	–	2#4	–	–	–	258	–	–	711	–	1019	711
1989-US-YA-05	–	–	(3)#5	–	–	–	200	–	–	711	–	1019	711
1989-US-YA-06	–	–	(2)#5	–	–	–	200	–	–	474	–	1019	474
1989-US-YA-08	–	–	#3	9-ga. ladder	–	–	71	22.2	–	711	406	1019	711
1989-US-YA-09	–	–	2#4 & 1#5	9-ga. ladder	–	–	329	22.2	–	711	203	1019	711
1989-US-YA-10	–	–	(2)#5	–	–	–	200	–	–	474	–	1019	474
1990-US-SH-21	#6	(3)#6	(5)#3	–	284	284	71	–	406	406	–	0	0
1990-US-SH-22	#6	(3)#6	(5)#3	–	284	284	71	–	406	406	–	0	0
1991-JP-MA-01	D22	(2)D10	(2)D13	–	387	78.5	129	–	400	600	–	0	0
1991-JP-MA-02	D25	(2)D10	(2)D13	–	510	78.5	129	–	400	600	–	0	0
1991-JP-MA-03	D32	(2)D10	(2)D13	–	819	78.5	129	–	400	600	–	0	0
1991-JP-MA-04	D25	(4)D10	(2)D13	–	510	71	129	–	400	600	–	0	0
1991-JP-MA-05	D32	(4)D10	(2)D13	–	819	71	129	–	400	600	–	0	0
1991-JP-MA-06	D38	(4)D10	(2)D13	–	819	71	129	–	400	600	–	0	0
1992-US-GH-01	2#4/3	–	(2)2#4/3	–	26.6	–	26.6	–	872	871	–	872	871

Table E.3: Reinforcement Details of Dataset (Continued)

Serial	Reinforcement				Reinforcement Area				Reinforcement Spacing			Grout Spacing	
	Flexural	Vertical	Shear	Joint	A_t (mm^2)	A_c (mm^2)	A_h (mm^2)	A_j (mm^2)	s_c (mm)	s_h (mm)	s_j (mm)	s_{gh} (mm)	s_{gv} (mm)
1992-US-GH-02	#5/3	#5/3	(3)#5/3	–	18.6	18.6	18.6	–	436	437	–	436	437
1993-US-GH-05	#5/3	#5/3	(3)#5/3	–	18.6	18.6	18.6	–	436	437	–	436	437
1993-US-GH-06	#5/3	#5/3	(3)#5/3	–	18.6	18.6	18.6	–	436	437	–	436	437
1994-US-BR-01	#6	(2)#6	(4)#3	–	284	284	0.71	–	406	406	–	0	0
1994-US-BR-02	#6	(3)#6	(4)#3	–	284	284	0.71	–	406	406	–	0	0
1994-US-BR-03	#6	(4)#6	(4)#3	–	284	284	0.71	–	406	406	–	0	0
1995-NZ-BR-01	D10	D10	–	–	78.5	78.5	–	–	800	–	–	0	0
1995-NZ-BR-02	D10	(2)D10	–	–	78.5	78.5	–	–	800	–	–	800	2000
1995-NZ-BR-03	D10	(2)D10	–	–	78.5	78.5	–	–	800	–	–	0	0
1995-NZ-BR-04	D10	(4)D10	–	–	78.5	78.5	–	–	800	–	–	0	0
1995-NZ-BR-06	D12	D12	–	–	113	113	–	–	800	–	–	800	2000
1995-NZ-BR-07	D12	(2)D12	–	–	113	113	–	–	800	–	–	800	2000
1995-NZ-BR-08	D12	(4)D12	–	–	113	113	–	–	800	–	–	800	2000
1995-NZ-BR-10	D12	D12	–	–	113	113	–	–	800	–	–	800	2000
1995-NZ-BR-11	D12	(2)D12	–	–	113	113	–	–	800	–	–	800	2000
1995-NZ-BR-12	D12	(4)D12	–	–	113	113	–	–	800	–	–	800	2000
1996-SL-TO-06	#10	–	–	6mm ladder	78.5	–	–	56.5	–	–	110	510	759
1996-SL-TO-08	#10	–	–	6mm ladder	78.5	–	–	56.5	–	–	110	510	759
1996-SL-TO-10	#10	–	–	6mm ladder	78.5	–	–	56.5	–	–	110	510	759
1996-SL-TO-12	#10	–	–	6mm ladder	78.5	–	–	56.5	–	–	110	510	759
1996-SL-TO-14	#10	–	–	6mm ladder	78.5	–	–	56.5	–	–	110	510	759
1996-SL-TO-16	#10	–	–	6mm ladder	78.5	–	–	56.5	–	–	110	510	759
1996-US-SH-02	2#6	–	2#3	–	568	–	142	–	–	711	–	1828	711
1998-US-SH-01	2#6	–	–	9-ga ladder	568	–	–	22.2	–	–	203	2641	1422
1998-US-SH-02	2#6	–	–	9-ga ladder	568	–	–	22.2	–	–	203	1828	1422
1998-US-SH-03	2#6	–	–	9-ga ladder	568	–	–	22.2	–	–	203	1218	1422
1998-US-SH-04	2#6	–	–	5-ga ladder	568	–	–	43.4	–	–	203	2641	1422

Table E.3: Reinforcement Details of Dataset (Continued)

Serial	Reinforcement				Reinforcement Area				Reinforcement Spacing			Grout Spacing	
	Flexural	Vertical	Shear	Joint	A_t (mm^2)	A_c (mm^2)	A_h (mm^2)	A_j (mm^2)	s_c (mm)	s_h (mm)	s_j (mm)	s_{gh} (mm)	s_{gv} (mm)
1998-US-SH-05	2#6	–	–	5-ga ladder	568	–	–	43.4	–	–	203	1828	1422
1998-US-SH-06	2#6	–	–	5-ga ladder	568	–	–	43.4	–	–	203	1218	1422
2000-JP-OH-01	2D25	(2)D16	(2)D13	–	1020	200	129	–	400	600	–	0	0
2000-JP-OH-02	2D25	(2)D16	(2)D13	–	1020	200	129	–	400	600	–	0	0
2000-JP-OH-03	2D25	(2)D16	(2)D13	–	1020	200	129	–	400	600	–	0	0
2000-JP-OH-04	2D25	(2)D16	(2)D13	–	1020	200	129	–	400	600	–	0	0
2007-AU-HA-01	N12	2N16	–	–	110	400	–	–	1350	–	–	1350	2245
2007-AU-HA-02	N12	2N16	–	–	110	400	–	–	1350	–	–	1350	2245
2007-AU-HA-03	N12	(2)N16	–	–	110	200	–	–	900	–	–	900	2245
2007-AU-HA-04	N12	(2)N16	–	–	110	200	–	–	900	–	–	900	2245
2007-AU-HA-05	N12	(2)N16	–	–	110	200	–	–	900	–	–	900	2245
2007-AU-HA-06	N12	(2)N16	–	–	110	200	–	–	900	–	–	900	2245
2007-AU-HA-07	(2)N12	–	–	–	220	–	–	–	–	–	–	2350	2245
2007-AU-HA-08	(2)N12	–	–	–	220	–	–	–	–	–	–	2350	2245
2007-AU-HA-09	(2)N12	–	–	–	220	–	–	–	–	–	–	2700	2245
2007-AU-HA-11	N12	(2)N12	–	–	110	110	–	–	900	–	–	900	1412
2007-AU-HA-12	N12	(2)N12	–	–	110	110	–	–	900	–	–	900	1412
2007-AU-HA-13	(2)N12	–	–	–	220	–	–	–	0	–	–	1100	1412
2007-AU-HA-14	(2)N12	–	–	–	220	–	–	–	0	–	–	1100	1412
2007-NZ-VO-01	D20	(3)D20	(5)R6	–	314	314	28.3	–	400	400	–	0	0
2007-NZ-VO-02	D20	(3)D20	(1)R6	–	314	314	28.3	–	400	1700	–	0	0
2007-NZ-VO-04	D20	(3)D20	2D10	–	314	314	157	–	400	1700	–	0	0
2007-NZ-VO-05	D20	(3)D20	–	–	314	314	–	–	400	–	–	400	1800
2007-NZ-VO-06	D20	D20	–	–	314	314	–	–	800	–	–	800	1800
2007-NZ-VO-07	D20	(3)D20	(5)R6	–	314	314	28.3	–	400	400	–	0	0
2007-NZ-VO-08	D20	(3)D20	(5)R6	–	314	314	28.3	–	400	400	–	0	0
2007-NZ-VO-09	DH25	(3)DH25	(9)R6	–	491	491	28.3	–	400	400	–	0	0

Table E.3: Reinforcement Details of Dataset (Continued)

Serial	Reinforcement				Reinforcement Area				Reinforcement Spacing			Grout Spacing	
	Flexural	Vertical	Shear	Joint	A_t (mm^2)	A_c (mm^2)	A_h (mm^2)	A_j (mm^2)	s_c (mm)	s_h (mm)	s_j (mm)	s_{gh} (mm)	s_{gv} (mm)
2007-NZ-VO-10	D20	(6)D20	(5)R6	–	314	314	28.3	–	400	400	–	0	0
2007-PO-HA-02	Ø5mm tr.	Ø5mm tr.	–	Ø4mm tr.	39.3	39.3	–	25.1	500	–	300	500	800
2007-PO-HA-03	Ø5mm tr.	Ø5mm tr.	–	Ø4mm tr.	39.3	39.3	–	25.1	500	–	300	500	800
2007-PO-HA-04	Ø5mm tr.	Ø5mm tr.	–	Ø4mm tr.	39.3	39.3	–	25.1	500	–	300	500	800
2007-PO-HA-05	Ø5mm tr.	Ø5mm tr.	–	Ø4mm tr.	39.3	39.3	–	25.1	500	–	300	500	800
2008-CA-MA-01	M10	M10	(3)D4	–	100	100	25.8	–	855	855	–	855	855
2008-CA-MA-02	#3	(2)#3	(3)D3	–	71	71	19.4	–	570	570	–	570	570
2008-CA-MA-04	M10	M10	(2)D3	–	100	100	19.4	–	855	855	–	855	855
2008-CA-MA-05	M10	M10	(4)D4	–	100	100	25.8	–	855	855	–	855	855
2009-US-MI-01	#6	(2)#6	(3)#6	–	284	284	284	–	1219	1321	–	1219	1321
2009-US-MI-02	#6	(2)#6	(3)#6	–	284	284	284	–	1219	1321	–	1219	1321
2009-US-MI-03	#6	(2)#6	(3)#6	–	284	284	284	–	1219	1321	–	1219	1321
2009-US-MI-04	#6	(2)#6	(3)#6	–	284	284	284	–	1219	1321	–	1219	1321
2009-US-MI-07	#6	(2)#6	(3)#6	–	284	284	284	–	1219	1321	–	0	0
2009-US-MI-08	#6	(2)#6	(3)#6	–	284	284	284	–	1219	1321	–	0	0
2010-US-EL-01	2#6	2#6	#5	–	568	568	200	–	1219	711	–	1219	711
2010-US-EL-02	2#6	2#6	#6	–	568	568	284	–	1219	711	–	1219	711
2010-US-EL-03	2#6	2#6	2#5	–	568	568	400	–	1219	711	–	1219	711
2010-US-EL-04	2#6	2#6	#5	–	568	568	200	–	1219	711	–	1219	711
2010-US-EL-05	2#6	(2)#6	#5	–	568	284	200	–	813	711	–	813	711
2010-US-EL-06	2#6	(3)#5	#5	–	568	200	200	–	610	711	–	610	711
2010-US-NO-01	2#7	2#7	#5	–	774	774	200	–	1219	1016	–	1219	1016
2010-US-NO-02	2#7	2#7	#6	–	774	774	284	–	1219	1016	–	1219	1016
2010-US-NO-03	2#7	2#7	2#5	–	774	774	400	–	1219	1016	–	1219	1016
2010-US-NO-04	2#6	(2)2#6	#5	–	568	568	200	–	813	1016	–	813	1016
2010-US-NO-05	2#6	(3)2#5	#5	–	568	142	200	–	610	1016	–	610	1016
2010-US-NO-06	2#7	2#7	#5	–	774	774	200	–	1219	1016	–	0	0

Table E.4: Material Strength of Specimens

Serial	Reinforcement Yield Strengths				Masonry Strengths			Prism Strength					
	f_{yt} (MPa)	f_{yc} (MPa)	f_{yh} (MPa)	f_{yj} (MPa)	f'_b (MPa)	f'_j (MPa)	f'_g (MPa)	f'_{pu} (MPa)	f'_{pg} (MPa)	Courses	$\frac{h}{t}$	k	$f'_{m\text{cor}}$ (MPa)
1968-MX-ME-09	245	245	245	–	12.3	–	–	10.3	–	3*	3.93	0.938	9.7
1968-MX-ME-10	245	245	245	–	12.3	–	–	10.3	–	3*	3.93	0.938	9.7
1968-MX-ME-11	245	245	245	–	12.3	–	–	10.3	–	3*	3.93	0.938	9.7
1968-MX-ME-12	245	245	245	–	12.3	–	–	10.3	–	3*	3.93	0.938	9.7
1968-MX-ME-13	245	245	245	–	12.3	–	–	10.3	–	3*	3.93	0.938	9.7
1968-MX-ME-14	245	245	–	–	12.3	–	–	10.3	–	3*	3.93	0.938	9.7
1968-MX-ME-15	245	245	–	–	12.3	–	–	10.3	–	3*	3.93	0.938	9.7
1968-MX-ME-16	245	245	245	–	12.3	–	–	10.3	–	3*	3.93	0.938	9.7
1968-MX-ME-17	245	245	245	–	12.3	–	–	10.3	–	3*	3.93	0.938	9.7
1968-MX-ME-18	245	245	245	–	12.3	–	–	10.3	–	3*	3.93	0.938	9.7
1969-MX-ME-11	392	–	–	–	–	15.2	29.3	10.3	–	3*	3.93	0.938	9.7
1969-MX-ME-14	392	–	–	–	–	20.4	33.0	14.4	–	3*	3.93	0.938	13.5
1969-MX-ME-15	392	–	–	–	–	25.7	13.3	14.4	–	3*	3.93	0.938	13.5
1969-MX-ME-16	392	–	–	–	–	23.0	15.9	14.4	–	3*	3.93	0.938	13.5
1969-MX-ME-17	392	–	–	–	–	24.8	18.8	14.4	–	3*	3.93	0.938	13.5
1969-MX-ME-18	392	392	–	–	–	20.4	10.6	14.4	–	3*	3.93	0.938	13.5
1969-MX-ME-19	392	–	–	–	–	17.6	8.1	14.4	–	3*	3.93	0.938	13.5
1969-MX-ME-20	392	392	–	–	–	17.5	11.9	14.4	–	3*	3.93	0.938	13.5
1969-MX-ME-21	392	–	–	–	–	17.6	14.5	14.4	–	3*	3.93	0.938	13.5
1969-MX-ME-24	392	–	–	–	–	24.1	23.1	14.4	–	3*	3.93	0.938	13.5
1969-MX-ME-25	392	392	–	–	–	17.7	11.7	14.4	14.4*	3*	3.93	0.938	13.5
1969-MX-ME-29	392	–	–	–	–	11.6	12.3	14.4	–	3*	3.93	0.938	13.5
1971-NZ-WI-01	345	345	–	–	51.7	15.9	19.3	–	21.9‡	3	5.56	1	21.9
1971-NZ-WI-02	345	345	–	–	51.7	15.9	19.3	–	21.9‡	3	5.56	1	21.9
1971-NZ-WI-03	345	345	–	–	51.7	15.9	19.3	–	21.9‡	3	5.56	1	21.9
1971-NZ-WI-04	345	345	–	–	51.7	15.9	19.3	27.8‡	–	3	5.56	1	27.8
1971-NZ-WI-05	345	345	–	–	51.7	15.9	19.3	–	21.9‡	3	5.56	1	21.9
1971-NZ-WI-06	345	345	–	–	37.2	15.9	19.3	–	19.0‡	3	6.52	1	19.0

Table E.4: Material Strength of Dataset (Continued)

Serial	Reinforcement Yield Strengths				Masonry Strengths			Prism Strength					
	f_{yt} (MPa)	f_{yc} (MPa)	f_{yh} (MPa)	f_{yj} (MPa)	f'_b (MPa)	f'_j (MPa)	f'_g (MPa)	f'_{pu} (MPa)	f'_{pg} (MPa)	Courses	$\frac{h}{t}$	k	f'_{mcor} (MPa)
1971-NZ-WI-07	345	345	–	–	37.2	15.9	19.3	–	19.0‡	3	6.52	1	19.0
1971-NZ-WI-08	345	345	–	–	37.2	15.9	19.3	–	19.0‡	3	6.52	1	19.0
1971-NZ-WI-09	345	345	–	–	37.2	15.9	19.3	–	19.0‡	3	6.52	1	19.0
1971-NZ-WI-10	345	–	–	–	51.7	15.9	19.3	–	21.9‡	3	5.56	1	21.9
1971-NZ-WI-11	345	–	345*	–	51.7	15.9	19.3	–	21.9‡	3	5.56	1	21.9
1971-NZ-WI-12	345	–	–	–	51.7	15.9	19.3	–	21.9‡	3	5.56	1	21.9
1971-NZ-WI-13	345	–	–	–	51.7	15.9	19.3	–	21.9‡	3	5.56	1	21.9
1971-NZ-WI-15	345	–	–	–	51.7	15.9	19.3	–	21.9‡	3	5.56	1	21.9
1971-NZ-WI-16	345	345	–	–	51.7	15.9	19.3	–	21.9‡	3	5.56	1	21.9
1971-NZ-WI-17	345	345	–	–	51.7	15.9	19.3	–	21.9‡	3	5.56	1	21.9
1971-NZ-WI-18	345	–	–	–	51.7	15.9	19.3	–	21.9‡	3	5.56	1	21.9
1971-NZ-WI-19	345	345	–	–	51.7	15.9	19.3	–	21.9‡	3	5.56	1	21.9
1971-NZ-WI-20	345	345	–	–	51.7	15.9	19.3	–	21.9‡	3	5.56	1	21.9
1976-US-MA-01	545	–	–	–	20.3	15.9	14.0	–	15.7	5	7.04	1	15.7
1976-US-MA-02	545	–	–	–	20.3	15.9	14.0	–	15.7	5	7.04	1	15.7
1976-US-MA-03	373	–	–	–	20.3	15.9	14.0	–	14.6	5	7.04	1	14.6
1976-US-MA-04	373	–	–	–	20.3	15.9	14.0	–	14.6	5	7.04	1	14.6
1976-US-MA-05	538	–	–	–	20.3	15.9	14.0	–	16.8	5	7.04	1	16.8
1976-US-MA-06	538	–	–	–	20.3	15.9	14.0	–	16.8	5	7.04	1	16.8
1976-US-MA-07	538	–	467	–	20.3	15.9	14.0	–	18.1	5	7.04	1	18.1
1976-US-MA-08	538	–	467	–	20.3	15.9	14.0	–	18.1	5	7.04	1	18.1
1976-US-MA-09	541	–	–	–	20.3	15.9	14.0	–	16.3	5	7.04	1	16.3
1976-US-MA-10	541	–	–	–	20.3	15.9	14.0	–	16.3	5	7.04	1	16.3
1976-US-MA-11	516	–	–	–	20.3	15.9	14.0	17.8	15.5	5	7.04	1	17.8
1976-US-MA-12	516	–	–	–	20.3	15.9	14.0	17.8	15.5	5	7.04	1	17.8
1977-NZ-PR-05	528	528	505	–	30.7	37.9	24.8	–	19.3	3	4.20	0.954	18.4
1977-NZ-PR-06	432	432	421	–	30.7	42.9	24.8	–	18.3	3	4.20	0.954	17.5
1977-NZ-PR-07	474	474	513	–	30.7	32.4	24.8	–	20.4	3	4.20	0.954	19.5

Table E.4: Material Strength of Dataset (Continued)

Serial	Reinforcement Yield Strengths				Masonry Strengths			Prism Strength					
	f_{yt} (MPa)	f_{yc} (MPa)	f_{yh} (MPa)	f_{yj} (MPa)	f'_b (MPa)	f'_j (MPa)	f'_g (MPa)	f'_{pu} (MPa)	f'_{pg} (MPa)	Courses	$\frac{h}{t}$	k	$f'_{m\text{cor}}$ (MPa)
1977-NZ-PR-08	454	454	427	–	30.7	32.5	24.8	–	21.2	3	4.20	0.954	20.2
1977-NZ-PR-09	488	488	489	–	30.7	33.5	24.8	–	18.3	3	4.20	0.954	17.5
1977-NZ-PR-10	472	472	488	–	30.7	38.7	24.8	–	24.5	3	4.20	0.954	23.4
1978-US-CH-02	488	–	–	–	12.4	19.0	26.3	10.6‡	9.2	5	5.19	1	10.6
1978-US-CH-03	488	–	–	–	12.4	20.4	27.7	10.9‡	12.6	5	5.19	1	12.6
1978-US-CH-04	488	–	330	–	12.4	20.4	27.7	10.9‡	12.6	5	5.19	1	12.6
1978-US-CH-05	488	–	330	–	12.4	19.0	26.3	10.6‡	9.2	5	5.19	1	10.6
1978-US-CH-06	488	–	330	–	12.4	20.4	27.7	10.9‡	12.6	5	5.19	1	12.6
1978-US-CH-07	488	–	–	–	12.4	16.0	47.5	10.0‡	13.1	5	5.19	1	13.1
1978-US-CH-08	477	–	–	–	12.4	20.3	47.3	10.8‡	13.1	5	5.19	1	10.8
1978-US-CH-09	477	–	330	–	12.4	20.3	47.3	10.8‡	13.1	5	5.19	1	13.1
1978-US-CH-10	477	–	330	–	12.4	16.0	47.5	10.0‡	9.2	5	5.19	1	10.0
1978-US-CH-11	477	–	509	–	12.4	16.0	47.5	10.0‡	9.2	5	5.19	1	9.2
1978-US-CH-14	517	–	–	–	40.1	26.5	29.1	24.5‡	17.5	10	5.38	1	17.5
1978-US-CH-15	492	–	483	–	40.1	21.0	29.8	22.7‡	18.8	10	5.38	1	18.8
1978-US-CH-16	492	–	483	–	40.1	26.5	39.9	24.5‡	17.5	10	5.38	1	24.5
1978-US-CH-17	492	–	443	–	40.1	29.8	33.5	25.4‡	18.8	10	5.38	1	18.8
1978-US-CH-18	517	–	501	–	40.1	12.9	29.1	19.5‡	17.5	10	5.38	1	17.5
1978-US-CH-19	477	–	–	–	40.1	21.2	29.0	22.8‡	19.8	10	5.38	1	19.8
1978-US-CH-20	477	–	–	–	40.1	26.5	39.9	24.5‡	17.5	10	5.38	1	24.5
1978-US-CH-21	502	–	474	–	40.1	21.0	29.8	22.7‡	18.8	10	5.38	1	18.8
1978-US-CH-22	502	–	474	–	40.1	21.0	29.8	22.7‡	18.8	10	5.38	1	22.7
1978-US-CH-23	524	–	509	–	40.1	12.9	29.1	19.5‡	17.5	10	5.38	1	17.5
1978-US-CH-24	502	–	515	–	40.1	21.0	29.8	22.7‡	18.8	10	5.38	1	18.8
1978-US-HI-01	–	–	–	–	58.9	30.2	35.7	–	31	10	5.38	1	31.0
1978-US-HI-02	326	–	343	–	58.9	30.2	35.7	–	31	10	5.38	1	31.0
1978-US-HI-03	326	–	343	–	58.9	30.2	35.7	34.0†	31	10	5.38	1	34.0

Table E.4: Material Strength of Dataset (Continued)

Serial	Reinforcement Yield Strengths				Masonry Strengths			Prism Strength					
	f_{yt} (MPa)	f_{yc} (MPa)	f_{yh} (MPa)	f_{yj} (MPa)	f'_b (MPa)	f'_j (MPa)	f'_g (MPa)	f'_{pu} (MPa)	f'_{pg} (MPa)	Courses	$\frac{h}{t}$	k	$f'_{m\text{cor}}$ (MPa)
1978-US-HI-04	326	–	343	–	58.9	30.2	35.7	–	31	10	5.38	1	31.0
1978-US-HI-05	326	–	343	–	58.9	30.2	35.7	34.0†	31	10	5.38	1	34.0
1978-US-HI-06	326	–	343	–	58.9	30.2	35.7	–	31	10	5.38	1	31.0
1978-US-HI-07	326	–	343	–	58.9	30.2	35.7	34.0†	31	10	5.38	1	34.0
1978-US-HI-08	326	–	343	–	58.9	30.2	35.7	–	31	10	5.38	1	31.0
1978-US-HI-09	326	–	343	–	58.9	30.2	35.7	–	31	10	5.38	1	31.0
1979-US-HI-01	554	554	–	–	12.9	38.1	26.8	–	20.6	5	5.19	1	20.6
1979-US-HI-02	554	554	480	–	12.9	38.1	26.8	–	20.6	5	5.19	1	20.6
1979-US-HI-03	554	554	480	–	12.9	38.1	26.8	–	20.6	5	5.19	1	20.6
1979-US-HI-04	554	554	480	–	12.9	38.1	26.8	–	20.6	5	5.19	1	20.6
1979-US-HI-05	554	554	480	–	12.9	38.1	26.8	–	20.6	5	5.19	1	20.6
1979-US-HI-06	554	554	464	–	12.9	38.1	26.8	–	20.6	5	5.19	1	20.6
1979-US-HI-08	554	554	464	–	40.1	23.9	26.8	–	19.6	10	5.38	1	19.6
1979-US-HI-09	554	554	464	–	40.1	23.9	26.8	–	19.6	10	5.38	1	19.6
1979-US-HI-10	554	554	464	–	40.1	23.9	26.8	–	19.6	10	5.38	1	19.6
1982-NZ-TH-01	389	389	389	–	–	–	26.0	16.0	14.9	3	4.21	0.955	15.3
1982-NZ-TH-02	477	477	477	–	–	–	26.0	16.0	14.9	3	4.21	0.955	14.2
1982-NZ-TH-03	389	389	–	–	–	–	26.0	16.0	14.9	3	4.21	0.955	15.3
1982-NZ-TH-04	389	389	389	–	–	–	26.0	16.0	14.9	3	4.21	0.955	15.3
1982-NZ-TH-05	454	454	454	–	–	–	26.0	16.0	14.9	3	4.21	0.955	14.2
1982-NZ-TH-06	454	454	454	–	–	–	26.0	16.0	14.9	3	4.21	0.955	14.2
1982-NZ-TH-08	434	434	434	–	–	–	26.0	16.0	14.9	3	4.21	0.955	14.2
1983-JP-MA-01	373*	357	357	–	–	–	–	–	21.8	3	3.93	0.938	20.5
1983-JP-MA-03	389*	357	357	–	–	–	–	–	21.8	3	3.93	0.938	20.5
1983-JP-MA-04	355*	357	357	–	–	–	–	–	21.8	3	3.93	0.938	20.5
1984-JP-IG-01	389	321	344	–	–	–	–	24.4	–	3	3.93	0.938	22.9
1984-JP-IG-02	389	321	344	–	–	–	–	24.4	–	3	3.93	0.938	22.9

Table E.4: Material Strength of Dataset (Continued)

Serial	Reinforcement Yield Strengths				Masonry Strengths			Prism Strength					
	f_{yt} (MPa)	f_{yc} (MPa)	f_{yh} (MPa)	f_{yj} (MPa)	f'_b (MPa)	f'_j (MPa)	f'_g (MPa)	f'_{pu} (MPa)	f'_{pg} (MPa)	Courses	$\frac{h}{t}$	k	$f'_{m\text{cor}}$ (MPa)
1984-JP-IG-03	355	321	344	–	–	–	–	24.4	–	3	3.93	0.938	22.9
1984-JP-IG-04	373	321	344	–	–	–	–	24.4	–	3	3.93	0.938	22.9
1984-JP-IG-05	389	321	344	–	–	–	–	24.4	–	3	3.93	0.938	22.9
1984-JP-IG-06	389	321	344	–	–	–	–	24.4	–	3	3.93	0.938	22.9
1985-JP-FU-01	387	371	355	–	–	–	–	–	17.9	3	3.11	0.886	15.9
1985-JP-FU-02	387	364	355	–	–	–	–	–	21.4	3	1.53	0.782	16.7
1985-JP-FU-03	387	371	355	–	–	–	–	–	22.8	3	3.11	0.886	20.2
1985-JP-FU-04	387	371	355	–	–	–	–	–	25.2	3	1.53	0.782	19.7
1985-JP-FU-05	387	371	355	–	–	–	–	–	17.9	3	3.11	0.886	15.9
1985-JP-FU-06	387	371	355	–	–	–	–	–	21.4	3	1.53	0.782	16.7
1985-JP-MA-01	370	372	–	–	–	–	–	–	22.3	3	3.11	0.886	19.8
1985-JP-MA-02	370	372	340	–	–	–	–	–	22.3	3	3.11	0.886	19.8
1985-JP-MA-03	370	372	340	–	–	–	–	–	22.3	3	3.11	0.886	19.8
1985-JP-MA-05	367	372	340	–	–	–	–	–	22.3	3	3.11	0.886	19.8
1985-JP-MA-06	367	372	340	–	–	–	–	–	22.3	3	3.11	0.886	19.8
1985-JP-YA-05	376	372	355	–	–	–	–	–	20.8	3	3.11	0.886	18.4
1985-JP-YA-06	376	372	355	–	–	–	–	–	20.8	3	3.11	0.886	18.4
1985-JP-YA-07	376	372	355	–	–	–	–	–	20.8	3	3.11	0.886	18.4
1985-JP-YA-08	376	372	355	–	–	–	–	–	27.0	3	3.11	0.886	23.9
1985-JP-YA-09	376	372	372	–	–	–	–	–	27.0	3	3.11	0.886	23.9
1985-US-SV-01	465	–	407	–	–	–	–	–	22.5	5	3.04	0.882	19.9
1985-US-SV-02	465	–	407	–	–	–	–	–	22.5	5	3.04	0.882	19.9
1985-US-SV-03	391	–	438	–	–	–	–	–	12.2	5	4.13	0.95	11.6
1985-US-SV-04	410	410	438	–	–	–	–	–	12.2	5	4.13	0.95	11.6
1985-US-SV-05	391	–	438	–	–	–	–	–	13.9	5	4.13	0.95	13.2
1985-US-SV-06	391	–	438	–	–	–	–	–	13.9	5	4.13	0.95	13.2
1985-US-SV-07	410	410	438	–	–	–	–	–	13.9	5	4.13	0.95	13.2

Table E.4: Material Strength of Dataset (Continued)

Serial	Reinforcement Yield Strengths				Masonry Strengths			Prism Strength					
	f_{yt} (MPa)	f_{yc} (MPa)	f_{yh} (MPa)	f_{yj} (MPa)	f'_b (MPa)	f'_j (MPa)	f'_g (MPa)	f'_{pu} (MPa)	f'_{pg} (MPa)	Courses	$\frac{h}{t}$	k	$f'_{m\text{cor}}$ (MPa)
1985-US-SV-08	391	–	438	–	–	–	–	–	13.9	5	4.13	0.95	13.2
1985-US-SV-09	391	–	438	438	–	–	–	–	13.9	5	4.13	0.95	13.2
1985-US-SV-10	391	–	438	438	–	–	–	–	13.9	5	4.13	0.95	13.2
1985-US-SV-11	391	–	438	–	–	–	–	–	13.9	5	4.13	0.95	13.2
1985-US-SV-12	391	–	438	–	–	–	–	–	13.9	5	4.13	0.95	13.2
1985-US-SV-13	465	–	465	–	–	–	–	–	25.6	5	1.55	0.784	20.1
1985-US-SV-15	465	–	465	–	–	–	–	–	25.6	5	1.55	0.784	20.1
1985-US-SV-16	391	–	438	–	–	–	–	–	19.8	5	1.55	0.784	15.5
1985-US-SV-17	391	–	438	–	–	–	–	–	19.8	5	1.55	0.784	15.5
1985-US-SV-18	391	438	438	–	–	–	–	–	19.8	5	1.55	0.784	15.5
1985-US-SV-19	438	438	438	–	–	–	–	–	19.8	5	1.55	0.784	15.5
1985-US-SV-20	410	410	438	–	–	–	–	–	19.8	5	1.55	0.784	15.5
1985-US-SV-21	410	410	438	–	–	–	–	–	19.8	5	1.55	0.784	15.5
1985-US-SV-22	391	–	438	–	–	–	–	–	19.8	5	1.55	0.784	15.5
1985-US-SV-23	391	–	438	–	–	–	–	–	19.8	5	1.55	0.784	15.5
1985-US-SV-24	391	–	410	–	–	–	–	–	19.8	5	1.55	0.784	15.5
1985-US-SV-25	410	–	417	–	–	–	–	–	19.8	5	1.55	0.784	15.5
1985-US-SV-26	391	–	–	438	–	–	–	–	25.6	5	1.55	0.784	20.1
1986-JP-IG-01	370	372	–	–	–	–	–	–	28.6	3	1.53	0.782	22.4
1986-JP-IG-02	370	372	340	–	–	–	–	–	28.6	3	1.53	0.782	22.4
1986-JP-IG-03	370	372	340	–	–	–	–	–	28.6	3	1.53	0.782	22.4
1986-JP-IG-04	370	372	340	–	–	–	–	–	28.6	3	1.53	0.782	22.4
1986-JP-MA-15	389*	321*	321*	–	–	–	–	26.4	–	3	3.93	0.938	24.8
1986-JP-MA-16	346*	321*	321*	–	–	–	–	43.3	–	3	3.93	0.938	40.6
1986-JP-MA-17	389*	321*	–	–	–	–	–	26.4	–	3	3.93	0.938	24.8
1986-JP-MA-18	389*	321*	–	–	–	–	–	26.4	–	3	3.93	0.938	24.8
1986-JP-MA-19	389*	321*	–	–	–	–	–	22.5	–	3	3.93	0.938	21.1

Table E.4: Material Strength of Dataset (Continued)

Serial	Reinforcement Yield Strengths				Masonry Strengths			Prism Strength					
	f_{yt} (MPa)	f_{yc} (MPa)	f_{yh} (MPa)	f_{yj} (MPa)	f'_b (MPa)	f'_j (MPa)	f'_g (MPa)	f'_{pu} (MPa)	f'_{pg} (MPa)	Courses	$\frac{h}{t}$	k	$f'_{m\text{cor}}$ (MPa)
1986-JP-MA-20	389*	321*	–	–	–	–	–	22.5	–	3	3.93	0.938	21.1
1986-JP-MA-21	389*	321*	–	–	–	–	–	43.3	–	3	3.93	0.938	40.6
1986-JP-MA-22	389*	321*	321*	–	–	–	–	26.4	–	3	3.93	0.938	24.8
1986-JP-MA-23	389*	321*	321*	–	–	–	–	26.4	–	3	3.93	0.938	24.8
1986-JP-MA-24	355*	321*	321*	–	–	–	–	43.3	–	3	3.93	0.938	40.6
1986-JP-MA-25	389*	321*	321*	–	–	–	–	43.3	–	3	3.93	0.938	40.6
1986-JP-MA-26	389*	321*	321*	–	–	–	–	43.3	–	3	3.93	0.938	40.6
1986-JP-MA-27	389*	321*	321*	–	–	–	–	43.3	–	3	3.93	0.938	40.6
1986-JP-MA-28	389*	321*	321*	–	–	–	–	26.4	–	3	3.93	0.938	24.8
1986-JP-MA-29	389*	321*	321*	–	–	–	–	22.5	–	3	3.93	0.938	21.1
1986-JP-MA-30	389*	321*	321*	–	–	–	–	43.3	–	3	3.93	0.938	40.6
1986-JP-MA-31	389*	321*	321*	–	–	–	–	26.4	–	3	3.93	0.938	24.8
1986-JP-MA-32	389*	321*	321*	–	–	–	–	22.5	–	3	3.93	0.938	21.1
1986-JP-MA-33	389*	321*	321*	–	–	–	–	43.3	–	3	3.93	0.938	40.6
1986-JP-MA-34	389*	321*	321*	–	–	–	–	22.5	–	3	3.93	0.938	21.1
1986-JP-MA-35	389*	321*	321*	–	–	–	–	26.4	–	3	3.93	0.938	24.8
1986-JP-MA-36	365*	321*	321*	–	–	–	–	43.3	–	3	3.93	0.938	40.6
1986-JP-MA-37	358*	321*	321*	–	–	–	–	26.4	–	3	3.93	0.938	24.8
1986-JP-MA-38	355*	321*	321*	–	–	–	–	22.5	–	3	3.93	0.938	21.1
1986-JP-MA-53	389*	321*	321*	–	–	–	–	34.7	–	3	1.93	0.809	28.1
1986-JP-MA-54	389*	321*	321*	–	–	–	–	42.0	–	3	1.93	0.809	34.0
1986-JP-SH-01	346	348	358	–	–	–	–	–	29.0	3	3.11	0.886	25.7
1986-JP-SH-02	346	348	358	–	–	–	–	–	26.1	3	3.11	0.886	23.1
1986-JP-SH-03	346	348	358	472	–	–	–	–	26.1	3	3.11	0.886	23.1
1986-JP-SH-04	355	348	358	–	–	–	–	–	26.1	3	3.11	0.886	23.1
1986-JP-SH-05	346	348	358	–	–	–	–	–	26.4	3	3.11	0.886	23.4
1986-JP-SH-06	346	348	358	–	–	–	–	–	31.4	3	3.11	0.886	27.8

Table E.4: Material Strength of Dataset (Continued)

Serial	Reinforcement Yield Strengths				Masonry Strengths			Prism Strength					
	f_{yt} (MPa)	f_{yc} (MPa)	f_{yh} (MPa)	f_{yj} (MPa)	f'_b (MPa)	f'_j (MPa)	f'_g (MPa)	f'_{pu} (MPa)	f'_{pg} (MPa)	Courses	$\frac{h}{t}$	k	$f'_{m\text{cor}}$ (MPa)
1987-JP-OK-01	387	371	355	–	–	–	–	–	22.8	3	3.11	0.886	20.2
1987-JP-OK-02	387	371	355	–	–	–	–	–	22.8	3	3.11	0.886	20.2
1987-JP-OK-10	387	322	355	–	–	–	–	–	19.9	3	3.11	0.886	17.6
1987-JP-OK-11	387	322	355	–	–	–	–	–	33.2	3	3.11	0.886	29.4
1988-JP-IG-05	360	372	–	–	–	–	–	–	26.4	3	1.53	0.782	20.6
1988-JP-IG-06	360	372	354	–	–	–	–	–	26.4	3	1.53	0.782	20.6
1988-JP-IG-07	360	372	354	–	–	–	–	–	26.4	3	1.53	0.782	20.6
1988-JP-IG-08	360	372	354	–	–	–	–	–	26.4	3	1.53	0.782	20.6
1988-JP-IG-09	389	372	354	–	–	–	–	–	26.4	3	1.53	0.782	20.6
1988-SL-TO-01	522	–	–	–	17.4	9.3	9.3	26.8	–	–	–	1	26.8
1988-SL-TO-02	522	–	323	–	17.4	9.3	9.3	26.8	–	–	–	1	26.8
1988-SL-TO-03	522	–	391	–	17.4	9.3	9.3	26.8	–	–	–	1	26.8
1988-SL-TO-04	522	–	253	–	17.4	9.3	9.3	26.8	–	–	–	1	26.8
1988-SL-TO-05	522	–	–	–	17.4	9.3	9.3	26.8	–	–	–	1	26.8
1988-SL-TO-09	522	–	–	–	15.5	7.0	7.0	23.8	–	–	–	1	23.8
1988-SL-TO-10	522	–	323	–	15.5	7.0	7.0	23.8	–	–	–	1	23.8
1988-SL-TO-11	522	–	391	–	15.5	7.0	7.0	23.8	–	–	–	1	23.8
1988-SL-TO-12	522	–	253	–	15.5	7.0	7.0	23.8	–	–	–	1	23.8
1988-SL-TO-13	522	–	–	–	15.5	7.0	7.0	23.8	–	–	–	1	23.8
1988-US-JO-01	345	–	–	–	32.7	20.3	–	17.5	–	3	3.09	0.885	15.5
1988-US-JO-02	345	–	–	–	32.7	20.3	–	17.5	–	3	3.09	0.885	15.5
1988-US-JO-03	345	–	–	–	32.7	14.1	–	15.8	–	3	3.09	0.885	14.0
1988-US-JO-04	345	–	–	–	32.7	14.2	–	15.8	–	3	3.09	0.885	14.0
1988-US-JO-05	345	–	–	–	32.7	15.7	–	11.9	–	3	3.09	0.885	10.5
1988-US-JO-06	345	–	–	–	32.7	15.7	–	11.9	–	3	3.09	0.885	10.5
1988-US-JO-07	345	–	–	–	32.7	18.3	–	18.0	–	3	3.09	0.885	15.9
1988-US-JO-08	345	–	–	–	32.7	18.3	–	18.0	–	3	3.09	0.885	15.9

Table E.4: Material Strength of Dataset (Continued)

Serial	Reinforcement Yield Strengths				Masonry Strengths			Prism Strength					
	f_{yt} (MPa)	f_{yc} (MPa)	f_{yh} (MPa)	f_{yj} (MPa)	f'_b (MPa)	f'_j (MPa)	f'_g (MPa)	f'_{pu} (MPa)	f'_{pg} (MPa)	Courses	$\frac{h}{t}$	k	$f'_{m\text{cor}}$ (MPa)
1988-US-JO-09	345	–	–	–	32.7	15.2	–	18.3	–	3	3.09	0.885	16.2
1988-US-JO-10	345	–	–	–	32.7	15.2	–	18.3	–	3	3.09	0.885	16.2
1988-US-JO-11	345	–	–	–	32.7	15.5	–	18.0	–	3	3.09	0.885	15.9
1988-US-JO-12	345	–	–	–	32.7	15.5	–	18.0	–	3	3.09	0.885	15.9
1988-US-JO-13	345	–	–	–	32.7	15.0	–	17.2	–	3	3.09	0.885	15.2
1988-US-JO-14	345	–	–	–	32.7	15.0	–	17.2	–	3	3.09	0.885	15.2
1988-US-JO-15	345	–	–	–	32.7	15.4	–	14.9	–	3	3.09	0.885	13.2
1988-US-JO-16	345	–	–	–	32.7	15.4	–	14.9	–	3	3.09	0.885	13.2
1988-US-JO-17	345	–	–	–	19.3	15.8	–	8.6	–	3	3.09	0.885	7.6
1988-US-JO-18	345	–	–	–	19.3	15.8	–	8.6	–	3	3.09	0.885	7.6
1988-US-JO-19	345	–	–	–	19.3	17.2	–	9.2	–	3	3.09	0.885	8.1
1988-US-JO-20	345	–	–	–	19.3	17.2	–	9.2	–	3	3.09	0.885	8.1
1988-US-JO-21	345	–	–	–	19.3	19.6	–	8.4	–	3	3.09	0.885	7.4
1988-US-JO-22	345	–	–	–	19.3	19.6	–	8.4	–	3	3.09	0.885	7.4
1988-US-JO-23	345	–	–	–	19.3	22.3	–	11.2	–	3	3.09	0.885	9.9
1988-US-JO-24	345	–	–	–	19.3	22.3	–	11.2	–	3	3.09	0.885	9.9
1988-US-JO-25	345	–	–	–	19.3	17.3	–	9.2	–	3	3.09	0.885	8.1
1988-US-JO-26	345	–	–	–	19.3	17.3	–	9.2	–	3	3.09	0.885	8.1
1988-US-JO-27	345	–	–	–	19.3	18.1	–	11.0	–	3	3.09	0.885	9.7
1988-US-JO-28	345	–	–	–	19.3	18.1	–	11.0	–	3	3.09	0.885	9.7
1988-US-JO-29	345	–	–	–	19.3	19.6	–	8.4	–	3	3.09	0.885	7.4
1988-US-JO-30	345	–	–	–	19.3	19.6	–	8.4	–	3	3.09	0.885	7.4
1988-US-JO-31	345	–	–	–	19.3	17.9	–	8.3	–	3	3.09	0.885	7.4
1988-US-JO-32	345	–	–	–	19.3	17.9	–	8.3	–	3	3.09	0.885	7.4
1988-US-SH-03	434	434	386	–	16.5	27.6	30.3	–	20.7	3	4.20	0.954	19.8
1988-US-SH-04	496	496	386	–	16.5	20.7	20.7	–	17.9	3	4.20	0.954	17.1
1988-US-SH-05	496	496	386	–	16.5	20.7	20.7	–	17.9	3	4.20	0.954	17.1

Table E.4: Material Strength of Dataset (Continued)

Serial	Reinforcement Yield Strengths				Masonry Strengths			Prism Strength					
	f_{yt} (MPa)	f_{yc} (MPa)	f_{yh} (MPa)	f_{yj} (MPa)	f'_b (MPa)	f'_j (MPa)	f'_g (MPa)	f'_{pu} (MPa)	f'_{pg} (MPa)	Courses	$\frac{h}{t}$	k	f'_{mcor} (MPa)
1988-US-SH-06	441	441	386	–	16.5	20.7	20.7	–	17.9	3	4.20	0.954	17.1
1988-US-SH-07	496	496	386	–	16.5	20.7	27.6	–	20.7	3	4.20	0.954	19.8
1988-US-SH-08	441	441	462	–	16.5	20.7	27.6	–	20.7	3	4.20	0.954	19.8
1988-US-SH-09	441	441	386	–	16.5	20.7	27.6	–	20.7	3	4.20	0.954	19.8
1988-US-SH-10	441	441	386	–	17.9	18.6	20.0	–	22.1	3	4.20	0.954	21.1
1988-US-SH-11	496	496	462	–	17.9	18.6	20.0	–	22.1	3	4.20	0.954	21.1
1988-US-SH-13	448	448	441	–	17.9	20.7	26.2	–	22.8	3	4.20	0.954	21.8
1988-US-SH-14	448	448	386	–	17.9	20.7	26.2	–	22.8	3	4.20	0.954	21.8
1988-US-SH-15	448	448	462	–	17.9	20.7	26.2	–	22.8	3	4.20	0.954	21.8
1988-US-SH-16	496	496	462	–	17.9	18.6	40.7	–	17.2	3	4.20	0.954	16.4
1989-US-YA-02	0	–	–	693	27.2	–	–	21.1	8.5	2*	2.05	0.817	17.2
1989-US-YA-03	0	–	–	693	27.2	–	–	21.1	7.7	2*	2.05	0.817	17.2
1989-US-YA-04	0	–	336	–	27.2	–	–	21.1	8.4	2*	2.05	0.817	17.2
1989-US-YA-05	0	–	439	–	27.2	–	–	21.1	8.7	2*	2.05	0.817	17.2
1989-US-YA-06	0	–	385	–	27.2	–	–	21.1	7.5	2*	2.05	0.817	17.2
1989-US-YA-08	0	–	355*	693	27.2	–	–	21.1	7.5	2*	2.05	0.817	17.2
1989-US-YA-09	0	–	355	693	27.2	–	–	21.1	5.9	2*	2.05	0.817	17.2
1989-US-YA-10	0	–	373	–	27.2	–	–	21.1	7.4	2*	2.05	0.817	17.2
1990-US-SH-21	448	448	386	–	45.5	22.8	26.9	–	26.2	6	4.38	0.966	25.3
1990-US-SH-22	448	448	386	–	45.5	22.8	26.9	–	26.2	6	4.38	0.966	25.3
1991-JP-MA-01	373	347	361	–	–	–	–	–	11.9	3	3.11	0.886	10.5
1991-JP-MA-02	369	347	361	–	–	–	–	–	11.9	3	3.11	0.886	10.5
1991-JP-MA-03	393	347	361	–	–	–	–	–	11.9	3	3.11	0.886	10.5
1991-JP-MA-04	369	347	361	–	–	–	–	–	11.9	3	3.11	0.886	10.5
1991-JP-MA-05	393	347	361	–	–	–	–	–	11.9	3	3.11	0.886	10.5
1991-JP-MA-06	442	347	361	–	–	–	–	–	11.9	3	3.11	0.886	10.5
1992-US-GH-01	443	443	443	–	19.3	15.5	31.0	15.9	20.0	3	4.17	0.953	15.2

Table E.4: Material Strength of Dataset (Continued)

Serial	Reinforcement Yield Strengths				Masonry Strengths			Prism Strength					
	f_{yt} (MPa)	f_{yc} (MPa)	f_{yh} (MPa)	f_{yj} (MPa)	f'_b (MPa)	f'_j (MPa)	f'_g (MPa)	f'_{pu} (MPa)	f'_{pg} (MPa)	Courses	$\frac{h}{t}$	k	f'_{mcor} (MPa)
1992-US-GH-02	447	447	447	–	19.3	15.5	31.0	15.9	20.0	3	4.17	0.953	15.2
1993-US-GH-05	443	443	443	–	19.3	15.5	31.0	15.9	20.0	3	4.17	0.953	15.2
1993-US-GH-06	443	443	443	–	19.3	15.5	31.0	15.9	20.0	3	4.17	0.953	15.2
1994-US-BR-01	452	452	427	–	–	–	–	–	22.5	6*	4.38	0.966	21.7
1994-US-BR-02	445	445	445	–	–	–	–	–	23.1	6*	4.38	0.966	22.3
1994-US-BR-03	445	445	445	–	–	–	–	–	23.1	6*	4.38	0.966	22.3
1995-NZ-BR-01	300	300	–	–	–	–	–	–	10.0†	3*	4.21	0.955	9.6
1995-NZ-BR-02	300	300	–	–	–	–	–	8.3†	–	3*	4.21	0.955	7.9
1995-NZ-BR-03	300	300	–	–	–	–	–	–	10.0†	3*	4.21	0.955	9.6
1995-NZ-BR-04	300	300	–	–	–	–	–	–	10.0†	3*	4.21	0.955	9.6
1995-NZ-BR-06	300	300	–	–	–	–	–	13.1†	–	3*	4.21	0.955	12.5
1995-NZ-BR-07	300	300	–	–	–	–	–	10.0†	–	3*	4.21	0.955	9.6
1995-NZ-BR-08	300	300	–	–	–	–	–	16.3†	–	3*	4.21	0.955	15.6
1995-NZ-BR-10	300	300	–	–	–	–	–	10.0†	–	3*	4.21	0.955	9.6
1995-NZ-BR-11	300	300	–	–	–	–	–	10.8†	–	3*	4.21	0.955	10.3
1995-NZ-BR-12	300	300	–	–	–	–	–	10.0†	–	3*	4.21	0.955	9.6
1996-SL-TO-06	522	–	–	253	–	–	–	13.0†	–	–	–	1*	13.0
1996-SL-TO-08	522	–	–	253	–	–	–	13.0†	–	–	–	1*	13.0
1996-SL-TO-10	522	–	–	253	–	–	–	13.0†	–	–	–	1*	13.0
1996-SL-TO-12	522	–	–	253	–	–	–	13.0†	–	–	–	1*	13.0
1996-SL-TO-14	522	–	–	253	–	–	–	13.0†	–	–	–	1*	13.0
1996-SL-TO-16	522	–	–	253	–	–	–	13.0†	–	–	–	1*	13.0
1996-US-SH-02	414	–	414	–	–	21.6	29.6	17.1	17.6	2	2.05	0.817	14.0
1998-US-SH-01	414	–	–	517	23.3	22.2	28.2	14.5	16.5	2	2.05	0.817	11.9
1998-US-SH-02	414	–	–	517	23.3	22.2	28.2	14.5	16.5	2	2.05	0.817	11.9
1998-US-SH-03	414	–	–	517	23.3	22.2	28.2	14.5	16.5	2	2.05	0.817	11.9
1998-US-SH-04	414	–	–	517	23.3	22.2	28.2	14.5	16.5	2	2.05	0.817	11.9

Table E.4: Material Strength of Dataset (Continued)

Serial	Reinforcement Yield Strengths				Masonry Strengths			Prism Strength					
	f_{yt} (MPa)	f_{yc} (MPa)	f_{yh} (MPa)	f_{yj} (MPa)	f'_b (MPa)	f'_j (MPa)	f'_g (MPa)	f'_{pu} (MPa)	f'_{pg} (MPa)	Courses	$\frac{h}{t}$	k	$f'_{m\text{cor}}$ (MPa)
1998-US-SH-05	414	–	–	517	23.3	22.2	28.2	14.5	16.5	2	2.05	0.817	11.9
1998-US-SH-06	414	–	–	517	23.3	22.2	28.2	14.5	16.5	2	2.05	0.817	11.9
2000-JP-OH-01	360*	372*	355*	–	–	–	–	–	22.8	3	3.00	0.879	20.0
2000-JP-OH-02	360*	372*	355*	–	–	–	–	–	22.8	3	3.00	0.879	20.0
2000-JP-OH-03	360*	372*	355*	–	–	–	–	–	22.8	3	3.00	0.879	20.0
2000-JP-OH-04	360*	372*	355*	–	–	–	–	–	22.8	3	3.00	0.879	20.0
2007-AU-HA-01	420	420	–	–	40.0	8.3	28.4	17.0‡	12.5	4	2.10	0.82	13.9
2007-AU-HA-02	420	420	–	–	40.0	9.3	23.6	17.7‡	11.9	4	2.10	0.82	14.5
2007-AU-HA-03	420	420	–	–	40.0	9.7	29.5	17.9‡	13.7	4	2.10	0.82	14.7
2007-AU-HA-04	420	420	–	–	40.0	9.5	31.5	17.8‡	14.4	4	2.10	0.82	14.6
2007-AU-HA-05	420	420	–	–	40.0	5.3	34.8	14.8‡	15.5	4	2.10	0.82	12.1
2007-AU-HA-06	420	420	–	–	40.0	6.9	39.7	16.1‡	15.7	4	2.10	0.82	13.2
2007-AU-HA-07	420	–	–	–	40.0	5.0	36.5	14.6‡	18.4	4	2.10	0.82	12.0
2007-AU-HA-08	420	–	–	–	40.0	6.4	34.7	15.7‡	18.1	4	2.10	0.82	12.9
2007-AU-HA-09	420	–	–	–	40.0	10.0	39.7	18.1‡	20.1	4	2.10	0.82	14.8
2007-AU-HA-11	420	420	–	–	40.0	6.8	28.2	20.4‡	20.3	4	2.10	0.82	16.7
2007-AU-HA-12	420	420	–	–	40.0	6.8	28.2	20.4‡	20.3	4	2.10	0.82	16.7
2007-AU-HA-13	420	–	–	–	40.0	6.8	28.2	20.4‡	20.3	4	2.10	0.82	16.7
2007-AU-HA-14	420	–	–	–	40.0	6.8	28.2	20.4‡	20.3	4	2.10	0.82	16.7
2007-NZ-VO-01	318	318	325	–	–	–	–	–	17.6	3	4.21	0.955	16.8
2007-NZ-VO-02	318	318	325	–	–	–	–	–	17.6	3	4.21	0.955	16.8
2007-NZ-VO-04	318	318	320	–	–	–	–	–	17.0	3	4.21	0.955	16.2
2007-NZ-VO-05	318	318	–	–	–	–	–	18.5*	18.5*	3	4.21	0.955	17.7
2007-NZ-VO-06	318	318	–	–	–	–	–	18.5*	18.5*	3	4.21	0.955	17.7
2007-NZ-VO-07	318	318	325	–	–	–	–	–	18.8	3	4.21	0.955	18.0
2007-NZ-VO-08	318	318	325	–	–	–	–	–	18.8	3	4.21	0.955	18.0
2007-NZ-VO-09	320	320	325	–	–	–	–	–	24.3	3	4.21	0.955	23.2

Table E.4: Material Strength of Dataset (Continued)

Serial	Reinforcement Yield Strengths				Masonry Strengths			Prism Strength					
	f_{yt} (MPa)	f_{yc} (MPa)	f_{yh} (MPa)	f_{yj} (MPa)	f'_b (MPa)	f'_j (MPa)	f'_g (MPa)	f'_{pu} (MPa)	f'_{pg} (MPa)	Courses	$\frac{h}{t}$	k	$f'_{m\text{cor}}$ (MPa)
2007-NZ-VO-10	318	318	325	–	–	–	–	–	24.3	3	4.21	0.955	23.2
2007-PO-HA-02	580	580	580	–	12.1	3.8	3.8	14.8†	–	3	3.20	0.892	13.2
2007-PO-HA-03	580	580	580	–	12.1	7.1	7.1	14.8†	–	3	3.20	0.892	13.2
2007-PO-HA-04	580	580	580	–	12.1	8.6	8.6	14.8†	–	3	3.20	0.892	13.2
2007-PO-HA-05	580	580	580	–	12.1	7.7	7.7	14.8†	–	3	3.20	0.892	13.2
2008-CA-MA-01	492	492	691	–	–	21.4	37.6	21.6	12.4	4	4.39	0.966	20.9
2008-CA-MA-02	503	503	744	–	–	21.4	37.6	21.6	12.4	4	4.39	0.966	20.9
2008-CA-MA-04	492	492	744	–	–	21.4	37.6	21.6	12.4	4	4.39	0.966	20.9
2008-CA-MA-05	492	492	691	–	–	21.4	37.6	21.6	12.4	4	4.39	0.966	20.9
2009-US-MI-01	414*	414*	414*	–	14.0	13.8	22.0	17.2	–	4*	4.14	0.951	16.4
2009-US-MI-02	414*	414*	414*	–	14.0	12.6	22.0	17.2	–	4*	4.14	0.951	16.4
2009-US-MI-03	414*	414*	414*	–	14.0	13.8	22.0	17.2	–	4*	4.14	0.951	16.4
2009-US-MI-04	414*	414*	414*	–	14.0	12.6	22.0	17.2	–	4*	4.14	0.951	16.4
2009-US-MI-07	414*	414*	414*	–	–	13.8	22.0	–	22.0†	4*	2.78	0.865	19.0
2009-US-MI-08	414*	414*	414*	–	–	12.6	22.0	–	22.0†	4*	2.78	0.865	19.0
2010-US-EL-01	427	427	608	–	–	14.9	18.2	17.5	24.5	2	2.05	0.817	14.3
2010-US-EL-02	427	427	427	–	–	14.9	18.2	17.5	24.5	2	2.05	0.817	14.3
2010-US-EL-03	427	427	452	–	–	14.9	18.2	17.5	24.5	2	2.05	0.817	14.3
2010-US-EL-04	427	427	452	–	–	14.9	18.2	17.5	24.5	2	2.05	0.817	14.3
2010-US-EL-05	427	427	452	–	–	14.9	18.2	17.5	24.5	2	2.05	0.817	14.3
2010-US-EL-06	427	452	452	–	–	14.9	18.2	17.5	24.5	2	2.05	0.817	14.3
2010-US-NO-01	439	439	439	–	18.1	–	29.2	11.3	–	3	3.10	0.886	10.0
2010-US-NO-02	439	439	439	–	18.1	–	29.2	11.3	–	3	3.10	0.886	10.0
2010-US-NO-03	439	439	439	–	18.1	–	29.2	11.3	–	3	3.10	0.886	10.0
2010-US-NO-04	439	439	439	–	18.1	–	29.2	11.3	–	3	3.10	0.886	10.0
2010-US-NO-05	439	439	439	–	18.1	–	29.2	11.3	–	3	3.10	0.886	10.0
2010-US-NO-06	439	439	439	–	18.1	–	29.2	–	18.3	3	3.10	0.886	16.2

Table E.5: Load Properties of Specimens

Serial	Axial	Peak Shear Load			Corrected Shear Strength				Loading		Failure
	P (kN)	V_{min} (kN)	V_{max} (kN)	V_{avg} (kN)	k_{avg}	k_{mono}	k_{rate}	V_{cor} (kN)	Pattern	Rate	Mode
1968-MX-ME-09	0	–	200	200	0.94	1	1	188	Cyclic	Quasi-Static*	Shear
1968-MX-ME-10	196	–	255	255	0.94	1	1	240	Cyclic	Quasi-Static*	Shear
1968-MX-ME-11	98.1	–	335	335	0.94	1	1	315	Cyclic	Quasi-Static*	Shear
1968-MX-ME-12	0	–	108	108	0.94	1	1	102	Cyclic	Quasi-Static*	Shear
1968-MX-ME-13	0	–	125	125	0.94	1	1	118	Cyclic	Quasi-Static*	Shear
1968-MX-ME-14	98.1	–	265	265	0.94	1	1	249	Cyclic	Quasi-Static*	Shear
1968-MX-ME-15	0	–	97	97	0.94	1	1	91	Cyclic	Quasi-Static*	Shear
1968-MX-ME-16	196	–	277	277	0.94	1	1	260	Cyclic	Quasi-Static*	Shear
1968-MX-ME-17	0	–	255	255	0.94	1	1	240	Cyclic	Quasi-Static*	Shear
1968-MX-ME-18	0	–	216	216	0.94	1	1	203	Cyclic	Quasi-Static*	Shear
1969-MX-ME-11	0	–	144	144	0.94	0.814	1	110	Monotonic	Quasi-Static*	Shear
1969-MX-ME-14	49	–	135	135	0.94	0.814	1	103	Monotonic	Quasi-Static*	Shear
1969-MX-ME-15	98	–	215	215	0.94	0.814	1	165	Monotonic	Quasi-Static*	Shear
1969-MX-ME-16	196	–	259	259	0.94	0.814	1	198	Monotonic	Quasi-Static*	Shear
1969-MX-ME-17	0	–	121	121	0.94	0.814	1	93	Monotonic	Quasi-Static*	Shear
1969-MX-ME-18	0	–	178	178	0.94	0.814	1	136	Monotonic	Quasi-Static*	Shear
1969-MX-ME-19	0	–	116	116	0.94	0.814	1	89	Monotonic	Quasi-Static*	Shear
1969-MX-ME-20	294	–	280	280	0.94	0.814	1	214	Monotonic	Quasi-Static*	Shear
1969-MX-ME-21	294	–	306	306	0.94	0.814	1	234	Monotonic	Quasi-Static*	Shear
1969-MX-ME-24	294	–	287	287	0.94	0.814	1	220	Monotonic	Quasi-Static*	Shear/Flexure
1969-MX-ME-25	0	–	318	318	0.94	0.814	1	243	Monotonic	Quasi-Static*	Shear
1969-MX-ME-29	0	–	167	167	0.94	0.814	1	128	Monotonic	Quasi-Static*	Shear
1971-NZ-WI-01	0	–	56	56	0.94	1	1	52	Cyclic	Quasi-Static	Shear/Flexure
1971-NZ-WI-02	103	–	91	91	0.94	1	1	86	Cyclic	Quasi-Static	Shear/Flexure
1971-NZ-WI-03	207	–	136	136	0.94	1	1	128	Cyclic	Quasi-Static	Shear
1971-NZ-WI-04	414	–	146	146	0.94	1	1	137	Cyclic	Quasi-Static	Shear
1971-NZ-WI-05	414	–	176	176	0.94	1	1	165	Cyclic	Quasi-Static	Shear
1971-NZ-WI-06	0	–	50	50	0.94	1	1	47	Cyclic	Quasi-Static	Shear/Flexure

Table E.5: Load Properties of Dataset (Continued)

Serial	Axial	Peak Shear Load			Corrected Shear Strength				Loading		Failure
	P (kN)	V_{min} (kN)	V_{max} (kN)	V_{avg} (kN)	k_{avg}	k_{mono}	k_{rate}	V_{cor} (kN)	Pattern	Rate	Mode
1971-NZ-WI-07	95.6	–	91	91	0.94	1	1	86	Cyclic	Quasi-Static	Shear/Flexure
1971-NZ-WI-08	191	–	131	131	0.94	1	1	123	Cyclic	Quasi-Static	Shear
1971-NZ-WI-09	383	–	199	199	0.94	1	1	187	Cyclic	Quasi-Static	Shear
1971-NZ-WI-10	198	–	167	167	0.94	1	1	157	Cyclic	Quasi-Static	Shear
1971-NZ-WI-11	198	–	178	178	0.94	1	1	167	Cyclic	Quasi-Static	Shear
1971-NZ-WI-12	120	–	47	47	0.94	1	1	44	Cyclic	Quasi-Static	Shear/Flexure
1971-NZ-WI-13	240	–	74	74	0.94	1	1	69	Cyclic	Quasi-Static	Shear
1971-NZ-WI-15	120	–	71	71	0.94	1	1	67	Cyclic	Quasi-Static	Shear
1971-NZ-WI-16	0	–	133	133	0.94	1	1	125	Cyclic	Quasi-Static	Shear
1971-NZ-WI-17	334	–	314	314	0.94	1	1	295	Cyclic	Quasi-Static	Shear
1971-NZ-WI-18	116	–	58	58	0.94	1	0.9	49	Cyclic	Dynamic	Shear/Flexure
1971-NZ-WI-19	0	–	53	53	0.94	1	0.9	45	Cyclic	Dynamic	Shear/Flexure
1971-NZ-WI-20	97.9	–	93	93	0.94	1	0.9	79	Cyclic	Dynamic	Shear/Flexure
1976-US-MA-01	200	–	116	107	0.94	1	1	100	Cyclic	Quasi-Static	Shear
1976-US-MA-02	200	–	148	138	0.94	1	0.9	117	Cyclic	Dynamic	Shear
1976-US-MA-03	100	–	121	116	0.94	1	1	109	Cyclic	Quasi-Static	Shear/Flexure
1976-US-MA-04	100	–	116	101	0.94	1	0.9	86	Cyclic	Dynamic	Shear/Flexure
1976-US-MA-05	0	–	91	82	0.94	1	1	77	Cyclic	Quasi-Static	Shear
1976-US-MA-06	0	–	113	97	0.94	1	0.9	82	Cyclic	Dynamic	Shear
1976-US-MA-07	200	–	181	174	0.94	1	1	163	Cyclic	Quasi-Static	Shear
1976-US-MA-08	200	–	215	196	0.94	1	0.9	166	Cyclic	Dynamic	Shear
1976-US-MA-09	400	–	131	128	0.94	1	1	120	Cyclic	Quasi-Static	Shear
1976-US-MA-10	400	–	152	146	0.94	1	0.9	123	Cyclic	Dynamic	Shear
1976-US-MA-11	200	–	89	84	0.94	1	1	79	Cyclic	Quasi-Static	Shear
1976-US-MA-12	200	–	97	92	0.94	1	0.9	78	Cyclic	Dynamic	Shear
1977-NZ-PR-05	0	–	770	770	0.94	1	1	723	Cyclic	Quasi-Static	Sliding
1977-NZ-PR-06	0	–	409	409	0.94	1	1	384	Cyclic	Quasi-Static	Sliding
1977-NZ-PR-07	0	–	734	734	0.94	1	1	690	Cyclic	Quasi-Static	Sliding

Table E.5: Load Properties of Dataset (Continued)

Serial	Axial	Peak Shear Load			Corrected Shear Strength				Loading		Failure
	P (kN)	V_{min} (kN)	V_{max} (kN)	V_{avg} (kN)	k_{avg}	k_{mono}	k_{rate}	V_{cor} (kN)	Pattern	Rate	Mode
1977-NZ-PR-08	0	–	458	458	0.94	1	1	431	Cyclic	Quasi-Static	Sliding
1977-NZ-PR-09	240	–	916	916	0.94	1	1	861	Cyclic	Quasi-Static	Sliding
1977-NZ-PR-10	240	–	912	912	0.94	1	1	857	Cyclic	Quasi-Static	Sliding
1978-US-CH-02	188	–	117	112	0.94	1	0.9	95	Cyclic	Dynamic	Shear
1978-US-CH-03	112	–	218	206	0.94	1	0.9	174	Cyclic	Dynamic	Shear
1978-US-CH-04	174	–	279	268	0.94	1	0.9	227	Cyclic	Dynamic	Shear
1978-US-CH-05	134	–	221	208	0.94	1	0.9	176	Cyclic	Dynamic	Shear
1978-US-CH-06	234	–	368	324	0.94	1	0.9	274	Cyclic	Dynamic	Shear/Flexure
1978-US-CH-07	148	–	293	238	0.94	1	0.9	202	Cyclic	Dynamic	Shear
1978-US-CH-08	130	–	169	164	0.94	1	0.9	139	Cyclic	Dynamic	Shear
1978-US-CH-09	186	–	253	238	0.94	1	0.9	202	Cyclic	Dynamic	Shear
1978-US-CH-10	139	–	223	217	0.94	1	0.9	183	Cyclic	Dynamic	Shear
1978-US-CH-11	226	–	390	376	0.94	1	0.9	318	Cyclic	Dynamic	Shear
1978-US-CH-14	233	–	440	420	0.94	1	1	395	Cyclic	Quasi-Static	Shear/Flexure
1978-US-CH-15	508	–	555	531	0.94	1	1	499	Cyclic	Quasi-Static	Shear/Flexure
1978-US-CH-16	239	–	233	202	0.94	1	1	190	Cyclic	Quasi-Static	Shear
1978-US-CH-17	275	–	545	517	0.94	1	1	486	Cyclic	Quasi-Static	Shear/Flexure
1978-US-CH-18	379	–	441	421	0.94	1	1	396	Cyclic	Quasi-Static	Shear/Flexure
1978-US-CH-19	193	–	381	358	0.94	1	1	336	Cyclic	Quasi-Static	Shear
1978-US-CH-20	166	–	218	191	0.94	1	1	180	Cyclic	Quasi-Static	Shear
1978-US-CH-21	241	–	466	452	0.94	1	1	425	Cyclic	Quasi-Static	Shear
1978-US-CH-22	119	–	231	205	0.94	1	1	192	Cyclic	Quasi-Static	Shear
1978-US-CH-23	378	–	432	420	0.94	1	1	394	Cyclic	Quasi-Static	Shear
1978-US-CH-24	492	–	517	504	0.94	1	1	474	Cyclic	Quasi-Static	Shear
1978-US-HI-01	799	–	412	335	0.94	1	1	315	Cyclic	Quasi-Static	Shear
1978-US-HI-02	507	–	328	283	0.94	1	1	266	Cyclic	Quasi-Static	Shear/Flexure
1978-US-HI-03	147	–	138	121	0.94	1	1	113	Cyclic	Quasi-Static	Shear

Table E.5: Load Properties of Dataset (Continued)

Serial	Axial	Peak Shear Load			Corrected Shear Strength				Loading		Failure
	P (kN)	V_{min} (kN)	V_{max} (kN)	V_{avg} (kN)	k_{avg}	k_{mono}	k_{rate}	V_{cor} (kN)	Pattern	Rate	Mode
1978-US-HI-04	572	–	424	376	0.94	1	1	354	Cyclic	Quasi-Static	Shear/Flexure
1978-US-HI-05	238	–	230	212	0.94	1	1	199	Cyclic	Quasi-Static	Shear
1978-US-HI-06	678	–	473	437	0.94	1	1	411	Cyclic	Quasi-Static	Shear/Flexure
1978-US-HI-07	233	–	231	211	0.94	1	1	199	Cyclic	Quasi-Static	Shear
1978-US-HI-08	668	–	477	442	0.94	1	1	415	Cyclic	Quasi-Static	Shear/Flexure
1978-US-HI-09	656	–	480	423	0.94	1	1	398	Cyclic	Quasi-Static	Shear/Flexure
1979-US-HI-01	527	–	891	841	0.94	1	1	791	Cyclic	Quasi-Static	Shear
1979-US-HI-02	543	–	942	896	0.94	1	1	843	Cyclic	Quasi-Static	Shear
1979-US-HI-03	661	–	1118	1079	0.94	1	1	1014	Cyclic	Quasi-Static	Shear
1979-US-HI-04	576	–	972	934	0.94	1	1	878	Cyclic	Quasi-Static	Shear/Sliding
1979-US-HI-05	582	–	1018	980	0.94	1	1	921	Cyclic	Quasi-Static	Shear/Sliding
1979-US-HI-06	636	–	1165	1121	0.94	1	1	1054	Cyclic	Quasi-Static	Shear
1979-US-HI-08	383	–	850	813	0.94	1	1	764	Cyclic	Quasi-Static	Shear
1979-US-HI-09	508	–	1009	942	0.94	1	1	886	Cyclic	Quasi-Static	Shear
1979-US-HI-10	633	–	1139	1093	0.94	1	1	1028	Cyclic	Quasi-Static	Shear
1982-NZ-TH-01	0	74.6	77.5	76.1	1	1	1	76	Cyclic	Quasi-Static*	Sliding
1982-NZ-TH-02	0	190	204	197	1	1	1	197	Cyclic	Quasi-Static*	Sliding
1982-NZ-TH-03	0	94	106	100	1	1	1	100	Cyclic	Quasi-Static*	Shear
1982-NZ-TH-04	0	146	152	149	1	1	1	149	Cyclic	Quasi-Static*	Shear/Flexure
1982-NZ-TH-05	160	307	328	318	1	1	1	318	Cyclic	Quasi-Static*	Shear/Flexure
1982-NZ-TH-06	0	164	182	173	1	1	1	173	Cyclic	Quasi-Static*	Sliding
1982-NZ-TH-08	0	354	408	381	1	1	1	381	Cyclic	Quasi-Static*	Shear/Sliding
1983-JP-MA-01	117	382	424	403	1	1	1	403	Cyclic	Quasi-Static	Shear
1983-JP-MA-03	87.2	246	333	290	1	1	1	290	Cyclic	Quasi-Static	Shear
1983-JP-MA-04	57.8	157	191	174	1	1	1	174	Cyclic	Quasi-Static	Shear
1984-JP-IG-01	290	225	238	232	1	0.814	1	188	Reversed Monotonic	Quasi-Static	Shear
1984-JP-IG-02	290	218	229	224	1	0.814	1	182	Reversed Monotonic	Quasi-Static	Shear

Table E.5: Load Properties of Dataset (Continued)

Serial	Axial	Peak Shear Load			Corrected Shear Strength				Loading		Failure
	P (kN)	V_{min} (kN)	V_{max} (kN)	V_{avg} (kN)	k_{avg}	k_{mono}	k_{rate}	V_{cor} (kN)	Pattern	Rate	Mode
1984-JP-IG-03	260	181	211	196	1	0.814	1	160	Reversed Monotonic	Quasi-Static	Shear
1984-JP-IG-04	202	143	147	145	1	0.814	1	118	Reversed Monotonic	Quasi-Static	Shear
1984-JP-IG-05	71.2	69	87	78	1	0.814	1	64	Reversed Monotonic	Quasi-Static	Shear
1984-JP-IG-06	71.2	69	92	81	1	0.814	1	66	Reversed Monotonic	Quasi-Static	Shear
1985-JP-FU-01	741	887	1139	1013	1	1	1	1013	Cyclic	Quasi-Static	Shear
1985-JP-FU-02	741	912	1138	1025	1	1	1	1025	Cyclic	Quasi-Static	Shear
1985-JP-FU-03	443	430	461	445	1	1	1	445	Cyclic	Quasi-Static	Shear
1985-JP-FU-04	406	396	424	410	1	1	1	410	Cyclic	Quasi-Static	Shear
1985-JP-FU-05	294	298	316	307	1	1	1	307	Cyclic	Quasi-Static	Shear
1985-JP-FU-06	294	297	316	307	1	1	1	307	Cyclic	Quasi-Static	Shear
1985-JP-MA-01	443	265	383	324	1	1	1	324	Cyclic	Quasi-Static	Shear
1985-JP-MA-02	443	429	467	448	1	1	1	448	Cyclic	Quasi-Static	Shear
1985-JP-MA-03	443	489	515	502	1	1	1	502	Cyclic	Quasi-Static	Shear
1985-JP-MA-05	443	491	518	505	1	1	1	505	Cyclic	Quasi-Static	Shear
1985-JP-MA-06	443	613	662	637	1	1	1	637	Cyclic	Quasi-Static	Shear
1985-JP-YA-05	0	300	389	344	1	1	1	344	Cyclic	Quasi-Static	Shear
1985-JP-YA-06	0	359	381	370	1	1	1	370	Cyclic	Quasi-Static	Shear
1985-JP-YA-07	0	268	314	291	1	1	1	291	Cyclic	Quasi-Static	Shear
1985-JP-YA-08	0	309	453	381	1	1	1	381	Cyclic	Quasi-Static	Shear
1985-JP-YA-09	0	493	522	507	1	1	1	507	Cyclic	Quasi-Static	Shear
1985-US-SV-01	445	–	461	461	0.94	1	1	434	Cyclic	Quasi-Static	Shear
1985-US-SV-02	712	–	561	561	0.94	1	1	527	Cyclic	Quasi-Static	Shear
1985-US-SV-03	480	–	309	309	0.94	1	1	290	Cyclic	Quasi-Static	Shear
1985-US-SV-04	480	–	308	308	0.94	1	1	290	Cyclic	Quasi-Static	Shear
1985-US-SV-05	303	–	396	396	0.94	1	1	372	Cyclic	Quasi-Static	Shear
1985-US-SV-06	480	–	410	410	0.94	1	1	386	Cyclic	Quasi-Static	Shear
1985-US-SV-07	480	–	389	389	0.94	1	1	366	Cyclic	Quasi-Static	Shear

Table E.5: Load Properties of Dataset (Continued)

Serial	Axial	Peak Shear Load			Corrected Shear Strength				Loading		Failure
	P (kN)	V_{min} (kN)	V_{max} (kN)	V_{avg} (kN)	k_{avg}	k_{mono}	k_{rate}	V_{cor} (kN)	Pattern	Rate	Mode
1985-US-SV-08	120	–	273	273	0.94	1	1	256	Cyclic	Quasi-Static	Shear/Flexure
1985-US-SV-09	480	–	334	334	0.94	1	1	314	Cyclic	Quasi-Static	Shear
1985-US-SV-10	480	–	424	424	0.94	1	1	398	Cyclic	Quasi-Static	Shear
1985-US-SV-11	303	–	342	342	0.94	1	1	322	Cyclic	Quasi-Static	Shear
1985-US-SV-12	480	–	420	420	0.94	1	1	394	Cyclic	Quasi-Static	Shear
1985-US-SV-13	712	–	525	525	0.94	1	1	494	Cyclic	Quasi-Static	Sliding
1985-US-SV-15	445	–	429	429	0.94	1	1	403	Cyclic	Quasi-Static	Sliding
1985-US-SV-16	480	–	321	321	0.94	1	1	302	Cyclic	Quasi-Static	Shear
1985-US-SV-17	480	–	334	334	0.94	1	1	314	Cyclic	Quasi-Static	Shear/Sliding
1985-US-SV-18	480	–	410	410	0.94	1	1	386	Cyclic	Quasi-Static	Shear
1985-US-SV-19	480	–	418	418	0.94	1	1	393	Cyclic	Quasi-Static	Shear/Sliding
1985-US-SV-20	480	–	354	354	0.94	1	1	333	Cyclic	Quasi-Static	Shear
1985-US-SV-21	480	–	384	384	0.94	1	1	361	Cyclic	Quasi-Static	Shear/Sliding
1985-US-SV-22	480	–	380	380	0.94	1	1	357	Cyclic	Quasi-Static	Shear
1985-US-SV-23	480	–	374	374	0.94	1	1	352	Cyclic	Quasi-Static	Shear/Sliding
1985-US-SV-24	480	–	393	393	0.94	1	1	370	Cyclic	Quasi-Static	Shear
1985-US-SV-25	480	–	397	397	0.94	1	1	373	Cyclic	Quasi-Static	Shear/Sliding
1985-US-SV-26	480	–	469	469	0.94	1	1	441	Cyclic	Quasi-Static	Shear
1986-JP-IG-01	409	383	459	421	1	0.814	1	343	Reversed Monotonic	Quasi-Static	Shear
1986-JP-IG-02	409	343	412	378	1	0.814	1	307	Reversed Monotonic	Quasi-Static	Shear
1986-JP-IG-03	409	333	361	347	1	0.814	1	283	Reversed Monotonic	Quasi-Static	Shear
1986-JP-IG-04	409	359	430	395	1	0.814	1	321	Reversed Monotonic	Quasi-Static	Shear
1986-JP-MA-15	0	73	84	79	1	1	1	79	Cyclic	Quasi-Static	Shear
1986-JP-MA-16	0	74	74	74	1	1	1	74	Cyclic	Quasi-Static	Shear
1986-JP-MA-17	0	58	60	59	1	1	1	59	Cyclic	Quasi-Static	Shear
1986-JP-MA-18	0	65	78	72	1	1	1	72	Cyclic	Quasi-Static	Shear
1986-JP-MA-19	101	84	109	97	1	1	1	97	Cyclic	Quasi-Static	Shear

Table E.5: Load Properties of Dataset (Continued)

Serial	Axial	Peak Shear Load			Corrected Shear Strength				Loading		Failure
	P (kN)	V_{min} (kN)	V_{max} (kN)	V_{avg} (kN)	k_{avg}	k_{mono}	k_{rate}	V_{cor} (kN)	Pattern	Rate	Mode
1986-JP-MA-20	194	78	95	87	1	1	1	87	Cyclic	Quasi-Static	Shear
1986-JP-MA-21	194	137	180	159	1	1	1	159	Cyclic	Quasi-Static	Shear
1986-JP-MA-22	0	64	100	82	1	1	1	82	Cyclic	Quasi-Static	Shear
1986-JP-MA-23	0	87	92	90	1	1	1	90	Cyclic	Quasi-Static	Shear
1986-JP-MA-24	0	93	142	118	1	1	1	118	Cyclic	Quasi-Static	Shear
1986-JP-MA-25	97.0	102	172	137	1	1	1	137	Cyclic	Quasi-Static	Shear
1986-JP-MA-26	194	137	148	143	1	1	1	143	Cyclic	Quasi-Static	Shear
1986-JP-MA-27	291	166	191	179	1	1	1	179	Cyclic	Quasi-Static	Shear
1986-JP-MA-28	0	74	105	90	1	1	1	90	Cyclic	Quasi-Static	Shear
1986-JP-MA-29	101	151	155	153	1	1	1	153	Cyclic	Quasi-Static	Shear
1986-JP-MA-30	194	139	196	168	1	1	1	168	Cyclic	Quasi-Static	Shear
1986-JP-MA-31	0	88	132	110	1	1	1	110	Cyclic	Quasi-Static	Shear
1986-JP-MA-32	101	160	184	172	1	1	1	172	Cyclic	Quasi-Static	Shear
1986-JP-MA-33	194	152	216	184	1	1	1	184	Cyclic	Quasi-Static	Shear
1986-JP-MA-34	101	141	249	195	1	1	1	195	Cyclic	Quasi-Static	Shear
1986-JP-MA-35	0	108	118	113	1	1	1	113	Cyclic	Quasi-Static	Shear
1986-JP-MA-36	0	157	157	157	1	1	1	157	Cyclic	Quasi-Static	Shear
1986-JP-MA-37	0	44	57	51	1	1	1	51	Cyclic	Quasi-Static	Shear
1986-JP-MA-38	101	130	147	139	1	1	1	139	Cyclic	Quasi-Static	Shear
1986-JP-MA-53	0	184	214	199	1	1	1	199	Cyclic	Quasi-Static	Shear
1986-JP-MA-54	0	167	205	186	1	1	1	186	Cyclic	Quasi-Static	Shear
1986-JP-SH-01	443	511	584	548	1	1	1	548	Cyclic	Quasi-Static	Shear
1986-JP-SH-02	443	465	505	485	1	1	1	485	Cyclic	Quasi-Static	Shear
1986-JP-SH-03	443	591	595	593	1	1	1	593	Cyclic	Quasi-Static	Shear
1986-JP-SH-04	443	470	521	496	1	1	1	496	Cyclic	Quasi-Static	Shear/Flexure
1986-JP-SH-05	443	492	522	507	1	1	1	507	Cyclic	Quasi-Static	Shear
1986-JP-SH-06	443	585	588	587	1	1	1	587	Cyclic	Quasi-Static	Shear

Table E.5: Load Properties of Dataset (Continued)

Serial	Axial	Peak Shear Load			Corrected Shear Strength				Loading		Failure
	P (kN)	V_{min} (kN)	V_{max} (kN)	V_{avg} (kN)	k_{avg}	k_{mono}	k_{rate}	V_{cor} (kN)	Pattern	Rate	Mode
1987-JP-OK-01	887	512	575	544	1	1	1	544	Cyclic	Quasi-Static	Shear
1987-JP-OK-02	1330	583	600	592	1	1	1	592	Cyclic	Quasi-Static	Shear
1987-JP-OK-10	447	491	522	506	1	1	1	506	Cyclic	Quasi-Static	Shear
1987-JP-OK-11	447	536	549	543	1	1	1	543	Cyclic	Quasi-Static	Shear
1988-JP-IG-05	409	442	458	450	1	0.814	1	366	Reversed Monotonic	Quasi-Static	Shear
1988-JP-IG-06	409	392	503	448	1	0.814	1	364	Reversed Monotonic	Quasi-Static	Shear
1988-JP-IG-07	409	467	504	486	1	0.814	1	395	Reversed Monotonic	Quasi-Static	Shear
1988-JP-IG-08	409	471	567	519	1	0.814	1	423	Reversed Monotonic	Quasi-Static	Shear
1988-JP-IG-09	409	493	504	499	1	0.814	1	406	Reversed Monotonic	Quasi-Static	Shear/Flexure
1988-SL-TO-01	60.0	–	–	33	0.94	1	1	124	Cyclic	Quasi-Static	Shear
1988-SL-TO-02	60.0	–	–	41	0.94	1	1	153	Cyclic	Quasi-Static	Shear
1988-SL-TO-03	60.0	–	–	35	0.94	1	1	133	Cyclic	Quasi-Static	Shear
1988-SL-TO-04	60.0	–	–	40	0.94	1	1	152	Cyclic	Quasi-Static	Shear
1988-SL-TO-05	60.0	–	–	26	0.94	1	1	98	Cyclic	Quasi-Static	Shear
1988-SL-TO-09	60.0	–	–	30	0.94	1	1	113	Cyclic	Quasi-Static	Shear
1988-SL-TO-10	60.0	–	–	35	0.94	1	1	131	Cyclic	Quasi-Static	Shear
1988-SL-TO-11	60.0	–	–	43	0.94	1	1	162	Cyclic	Quasi-Static	Shear
1988-SL-TO-12	60.0	–	–	47	0.94	1	1	176	Cyclic	Quasi-Static	Shear
1988-SL-TO-13	60.0	–	–	29	0.94	1	1	109	Cyclic	Quasi-Static	Shear
1988-US-JO-01	0	–	96	96	0.94	1	1	91	Cyclic	Quasi-Static	Shear
1988-US-JO-02	0	–	119	119	0.94	1	1	111	Cyclic	Quasi-Static	Shear
1988-US-JO-03	0	–	115	115	0.94	1	1	108	Cyclic	Quasi-Static	Shear
1988-US-JO-04	0	–	119	119	0.94	1	1	112	Cyclic	Quasi-Static	Shear
1988-US-JO-05	0	–	128	128	0.94	1	1	120	Cyclic	Quasi-Static	Shear
1988-US-JO-06	0	–	118	118	0.94	1	1	111	Cyclic	Quasi-Static	Shear
1988-US-JO-07	0	–	113	113	0.94	1	1	106	Cyclic	Quasi-Static	Shear
1988-US-JO-08	0	–	115	115	0.94	1	1	108	Cyclic	Quasi-Static	Shear

Table E.5: Load Properties of Dataset (Continued)

Serial	Axial	Peak Shear Load			Corrected Shear Strength				Loading		Failure
	P (kN)	V_{min} (kN)	V_{max} (kN)	V_{avg} (kN)	k_{avg}	k_{mono}	k_{rate}	V_{cor} (kN)	Pattern	Rate	Mode
1988-US-JO-09	0	–	128	128	0.94	1	1	120	Cyclic	Quasi-Static	Shear
1988-US-JO-10	0	–	103	103	0.94	1	1	97	Cyclic	Quasi-Static	Shear
1988-US-JO-11	0	–	100	100	0.94	1	1	94	Cyclic	Quasi-Static	Shear
1988-US-JO-12	0	–	89	89	0.94	1	1	84	Cyclic	Quasi-Static	Shear
1988-US-JO-13	0	–	91	91	0.94	1	1	85	Cyclic	Quasi-Static	Shear
1988-US-JO-14	0	–	92	92	0.94	1	1	87	Cyclic	Quasi-Static	Shear
1988-US-JO-15	0	–	92	92	0.94	1	1	86	Cyclic	Quasi-Static	Shear
1988-US-JO-16	0	–	122	122	0.94	1	1	115	Cyclic	Quasi-Static	Shear
1988-US-JO-17	0	–	77	77	0.94	1	1	72	Cyclic	Quasi-Static	Shear
1988-US-JO-18	0	–	87	87	0.94	1	1	82	Cyclic	Quasi-Static	Shear
1988-US-JO-19	0	–	93	93	0.94	1	1	88	Cyclic	Quasi-Static	Shear
1988-US-JO-20	0	–	89	89	0.94	1	1	84	Cyclic	Quasi-Static	Shear
1988-US-JO-21	0	–	83	83	0.94	1	1	78	Cyclic	Quasi-Static	Shear
1988-US-JO-22	0	–	85	85	0.94	1	1	80	Cyclic	Quasi-Static	Shear
1988-US-JO-23	0	–	92	92	0.94	1	1	87	Cyclic	Quasi-Static	Shear
1988-US-JO-24	0	–	83	83	0.94	1	1	78	Cyclic	Quasi-Static	Shear
1988-US-JO-25	0	–	91	91	0.94	1	1	85	Cyclic	Quasi-Static	Shear
1988-US-JO-26	0	–	86	86	0.94	1	1	81	Cyclic	Quasi-Static	Shear
1988-US-JO-27	0	–	88	88	0.94	1	1	83	Cyclic	Quasi-Static	Shear
1988-US-JO-28	0	–	87	87	0.94	1	1	82	Cyclic	Quasi-Static	Shear
1988-US-JO-29	0	–	87	87	0.94	1	1	82	Cyclic	Quasi-Static	Shear
1988-US-JO-30	0	–	85	85	0.94	1	1	80	Cyclic	Quasi-Static	Shear
1988-US-JO-31	0	–	83	83	0.94	1	1	78	Cyclic	Quasi-Static	Shear
1988-US-JO-32	0	–	81	81	0.94	1	1	76	Cyclic	Quasi-Static	Shear
1988-US-SH-03	480	445	467	456	1	1	1	456	Phased-Sequential	Quasi-Static	Shear
1988-US-SH-04	0	320	387	354	1	1	1	354	Phased-Sequential	Quasi-Static	Shear
1988-US-SH-05	178	396	418	407	1	1	1	407	Phased-Sequential	Quasi-Static	Shear

Table E.5: Load Properties of Dataset (Continued)

Serial	Axial	Peak Shear Load			Corrected Shear Strength				Loading		Failure
	P (kN)	V_{min} (kN)	V_{max} (kN)	V_{avg} (kN)	k_{avg}	k_{mono}	k_{rate}	V_{cor} (kN)	Pattern	Rate	Mode
1988-US-SH-06	0	209	231	220	1	1	1	220	Phased-Sequential	Quasi-Static	Shear/F/Sliding
1988-US-SH-07	178	432	432	432	1	1	1	432	Phased-Sequential	Quasi-Static	Shear
1988-US-SH-08	0	209	222	216	1	1	1	216	Phased-Sequential	Quasi-Static	Shear/Fliding
1988-US-SH-09	480	427	427	427	1	1	1	427	Phased-Sequential	Quasi-Static	Shear
1988-US-SH-10	178	298	307	303	1	1	1	303	Phased-Sequential	Quasi-Static	Shear/Flexure
1988-US-SH-11	0	396	423	409	1	1	1	409	Phased-Sequential	Quasi-Static	Shear/Sliding
1988-US-SH-13	480	485	516	500	1	1	1	500	Phased-Sequential	Quasi-Static	Shear
1988-US-SH-14	480	436	498	467	1	1	1	467	Phased-Sequential	Quasi-Static	Shear
1988-US-SH-15	178	365	418	391	1	1	1	391	Phased-Sequential	Quasi-Static	Shear/Flexure
1988-US-SH-16	480	534	538	536	1	1	1	536	Phased-Sequential	Quasi-Static	Shear
1989-US-YA-02	321	129	156	143	1	1	1	143	Phased-Sequential	Quasi-Static*	Shear
1989-US-YA-03	268	142	149	146	1	1	1	146	Phased-Sequential	Quasi-Static*	Shear
1989-US-YA-04	368	113	189	151	1	1	1	151	Phased-Sequential	Quasi-Static*	Shear
1989-US-YA-05	275	145	156	151	1	1	1	151	Phased-Sequential	Quasi-Static*	Shear
1989-US-YA-06	294	157	164	161	1	1	1	161	Phased-Sequential	Quasi-Static*	Shear
1989-US-YA-08	346	161	177	169	1	1	1	169	Phased-Sequential	Quasi-Static*	Shear
1989-US-YA-09	395	192	201	197	1	1	1	197	Phased-Sequential	Quasi-Static*	Shear
1989-US-YA-10	310	148	172	160	1	1	1	160	Phased-Sequential	Quasi-Static*	Shear
1990-US-SH-21	476	480	485	483	1	1	1	483	Phased-Sequential	Quasi-Static	Shear
1990-US-SH-22	169	383	432	407	1	1	1	407	Phased-Sequential	Quasi-Static	Shear
1991-JP-MA-01	129	247	257	252	1	1	1	252	Cyclic	Quasi-Static	Shear
1991-JP-MA-02	129	226	229	228	1	1	1	228	Cyclic	Quasi-Static	Shear
1991-JP-MA-03	129	270	273	271	1	1	1	271	Cyclic	Quasi-Static	Shear
1991-JP-MA-04	204	351	360	356	1	1	1	356	Cyclic	Quasi-Static	Shear
1991-JP-MA-05	204	402	472	437	1	1	1	437	Cyclic	Quasi-Static	Shear
1991-JP-MA-06	204	449	475	462	1	1	1	462	Cyclic	Quasi-Static	Shear
1992-US-GH-01	30.9	–	25	25	0.94	0.814	1	169	Monotonic	Quasi-Static	Shear

Table E.5: Load Properties of Dataset (Continued)

Serial	Axial	Peak Shear Load			Corrected Shear Strength				Loading		Failure
	P (kN)	V_{min} (kN)	V_{max} (kN)	V_{avg} (kN)	k_{avg}	k_{mono}	k_{rate}	V_{cor} (kN)	Pattern	Rate	Mode
1992-US-GH-02	30.9	–	30	30	0.94	0.814	1	208	Monotonic	Quasi-Static	Shear/Flexure
1993-US-GH-05	30.9	–	26	26	0.94	0.814	1	178	Monotonic	Quasi-Static	Shear/Flexure
1993-US-GH-06	61.9	–	35	35	0.94	0.814	1	239	Monotonic	Quasi-Static	Shear
1994-US-BR-01	370	–	–	540	0.94	0.814	1	413	Monotonic	Quasi-Static*	Shear/Flexure
1994-US-BR-02	476	–	–	645	0.94	0.814	1	494	Reversed Monotonic	Quasi-Static*	Shear
1994-US-BR-03	582	–	–	860	0.94	0.814	1	658	Monotonic	Quasi-Static*	Shear
1995-NZ-BR-01	0	–	32	32	0.94	1	1	30	Cyclic	Quasi-Static	Sliding
1995-NZ-BR-02	0	–	62	62	0.94	1	1	58	Cyclic	Quasi-Static	Shear
1995-NZ-BR-03	0	–	63	63	0.94	1	1	59	Cyclic	Quasi-Static	Sliding
1995-NZ-BR-04	0	–	144	144	0.94	1	1	136	Cyclic	Quasi-Static	Shear
1995-NZ-BR-06	0	–	41	41	0.94	1	1	39	Cyclic	Quasi-Static	Shear
1995-NZ-BR-07	0	–	81	81	0.94	1	1	76	Cyclic	Quasi-Static	Shear
1995-NZ-BR-08	0	–	180	180	0.94	1	1	169	Cyclic	Quasi-Static	Shear
1995-NZ-BR-10	0	–	47	47	0.94	1	1	44	Cyclic	Quasi-Static	Shear
1995-NZ-BR-11	0	–	87	87	0.94	1	1	82	Cyclic	Quasi-Static	Shear
1995-NZ-BR-12	0	–	198	198	0.94	1	1	186	Cyclic	Quasi-Static	Shear
1996-SL-TO-06	120	–	45	45	0.94	1	1	169	Cyclic	Quasi-Static	Shear
1996-SL-TO-08	120	–	50	50	0.94	1	0.9	171	Cyclic	Dynamic	Shear
1996-SL-TO-10	120	–	49	49	0.94	1	1	185	Phased-Sequential	Quasi-Static	Shear
1996-SL-TO-12	120	–	57	57	0.94	1	0.9	194	Phased-Sequential	Dynamic	Shear
1996-SL-TO-14	120	–	54	54	0.94	1	1	202	Simulated Seismic	Quasi-Static	Shear
1996-SL-TO-16	120	–	60	60	0.94	1	0.9	204	Simulated Seismic	Dynamic	Shear
1996-US-SH-02	191	–	245	245	1	1	1	245	Phased-Sequential	Quasi-Static	Shear
1998-US-SH-01	265	–	261	261	1	1	1	261	Phased-Sequential	Quasi-Static*	Shear
1998-US-SH-02	185	–	254	254	1	1	1	254	Phased-Sequential	Quasi-Static*	Shear
1998-US-SH-03	130	–	176	176	1	1	1	176	Phased-Sequential	Quasi-Static*	Shear
1998-US-SH-04	266	–	243	243	1	1	1	243	Phased-Sequential	Quasi-Static*	Shear

Table E.5: Load Properties of Dataset (Continued)

Serial	Axial	Peak Shear Load			Corrected Shear Strength				Loading		Failure
	P (kN)	V_{min} (kN)	V_{max} (kN)	V_{avg} (kN)	k_{avg}	k_{mono}	k_{rate}	V_{cor} (kN)	Pattern	Rate	Mode
1998-US-SH-05	188	–	270	270	1	1	1	270	Phased-Sequential	Quasi-Static*	Shear
1998-US-SH-06	133	–	211	211	1	1	1	211	Phased-Sequential	Quasi-Static*	Shear
2000-JP-OH-01	815	499	535	517	1	0.814	1	421	Reversed Monotonic	Quasi-Static	Shear
2000-JP-OH-02	408	443	480	461	1	0.814	1	376	Reversed Monotonic	Quasi-Static	Shear
2000-JP-OH-03	815	487	510	499	1	0.814	1	406	Reversed Monotonic	Quasi-Static	Shear
2000-JP-OH-04	408	407	556	482	1	0.814	1	392	Reversed Monotonic	Quasi-Static	Shear
2007-AU-HA-01	215	141	179	160	1	0.814	1	130	Reversed Monotonic	Quasi-Static*	Shear
2007-AU-HA-02	215	161	165	163	1	1	1	163	Cyclic	Quasi-Static*	Shear
2007-AU-HA-03	215	150	180	165	1	0.814	1	134	Reversed Monotonic	Quasi-Static*	Shear
2007-AU-HA-04	215	171	191	181	1	1	1	181	Cyclic	Quasi-Static*	Shear
2007-AU-HA-05	215	148	156	152	1	0.814	1	124	Reversed Monotonic	Quasi-Static*	Shear
2007-AU-HA-06	215	191	191	191	1	1	1	191	Cyclic	Quasi-Static*	Shear
2007-AU-HA-07	215	129	165	147	1	0.814	1	120	Reversed Monotonic	Quasi-Static*	Shear
2007-AU-HA-08	215	153	165	158	1	1	1	158	Cyclic	Quasi-Static*	Shear
2007-AU-HA-09	215	144	156	150	1	0.814	1	122	Reversed Monotonic	Quasi-Static*	Shear
2007-AU-HA-11	108	159	179	169	1	0.814	1	138	Reversed Monotonic	Quasi-Static*	Shear
2007-AU-HA-12	17.2	118	124	121	1	0.814	1	99	Reversed Monotonic	Quasi-Static*	Shear
2007-AU-HA-13	53.0	60	61	61	1	0.814	1	49	Reversed Monotonic	Quasi-Static*	Shear
2007-AU-HA-14	0	56	68	62	1	0.814	1	51	Reversed Monotonic	Quasi-Static*	Shear
2007-NZ-VO-01	0	205	215	210	1	1	1	210	Cyclic	Quasi-Static*	Shear/Flexure
2007-NZ-VO-02	0	177	195	186	1	1	1	186	Cyclic	Quasi-Static*	Shear
2007-NZ-VO-04	0	201	223	212	1	1	1	212	Cyclic	Quasi-Static*	Shear
2007-NZ-VO-05	0	134	143	138	1	1	1	138	Cyclic	Quasi-Static*	Shear
2007-NZ-VO-06	0	93	93	93	1	1	1	93	Cyclic	Quasi-Static*	Shear
2007-NZ-VO-07	126	261	263	262	1	1	1	262	Cyclic	Quasi-Static*	Shear
2007-NZ-VO-08	63.2	244	250	247	1	1	1	247	Cyclic	Quasi-Static*	Shear
2007-NZ-VO-09	63.2	204	207	206	1	1	1	206	Cyclic	Quasi-Static*	Shear

Table E.5: Load Properties of Dataset (Continued)

Serial	Axial	Peak Shear Load			Corrected Shear Strength				Loading		Failure
	P (kN)	V_{min} (kN)	V_{max} (kN)	V_{avg} (kN)	k_{avg}	k_{mono}	k_{rate}	V_{cor} (kN)	Pattern	Rate	Mode
2007-NZ-VO-10	63.2	574	596	587	1	1	1	587	Cyclic	Quasi-Static*	Shear
2007-PO-HA-02	60.0	53	53	53	1	1	1	211	Cyclic	Quasi-Static	Shear
2007-PO-HA-03	60.0	62	65	64	1	1	1	255	Cyclic	Quasi-Static	Shear
2007-PO-HA-04	150	93	93	93	1	1	1	372	Cyclic	Quasi-Static	Shear
2007-PO-HA-05	150	93	94	94	1	1	1	374	Cyclic	Quasi-Static	Shear
2008-CA-MA-01	120	91	97	94	1	1	1	376	Cyclic	Quasi-Static*	Shear/Flexure
2008-CA-MA-02	120	93	104	99	1	1	1	394	Cyclic	Quasi-Static*	Shear/Flexure
2008-CA-MA-04	120	114	123	119	1	1	1	474	Cyclic	Quasi-Static*	Shear
2008-CA-MA-05	120	79	84	82	1	1	1	327	Cyclic	Quasi-Static*	Shear/Flexure
2009-US-MI-01	222	–	0	318	1	1	1	318	Cyclic	Quasi-Static	Shear
2009-US-MI-02	222	–	0	190	1	1	1	190	Cyclic	Quasi-Static	Shear
2009-US-MI-03	0	–	0	241	1	1	1	241	Cyclic	Quasi-Static	Shear
2009-US-MI-04	0	–	0	230	1	1	1	230	Cyclic	Quasi-Static	Shear
2009-US-MI-07	222	–	360	360	1	1	1	360	Cyclic	Quasi-Static	Shear/Flexure
2009-US-MI-08	222	–	329	329	1	1	1	329	Cyclic	Quasi-Static	Shear/Flexure
2010-US-EL-01	49.4	–	238	238	0.94	1	1	224	Cyclic	Quasi-Static	Shear
2010-US-EL-02	49.4	–	252	252	0.94	1	1	237	Cyclic	Quasi-Static	Shear
2010-US-EL-03	49.4	–	266	266	0.94	1	1	250	Cyclic	Quasi-Static	Shear
2010-US-EL-04	49.4	–	286	286	0.94	1	1	269	Cyclic	Quasi-Static	Shear
2010-US-EL-05	49.4	–	344	344	0.94	1	1	323	Cyclic	Quasi-Static	Shear
2010-US-EL-06	49.4	–	400	400	0.94	1	1	376	Cyclic	Quasi-Static	Shear
2010-US-NO-01	49.3	211	234	223	1	1	1	223	Cyclic	Quasi-Static	Shear
2010-US-NO-02	49.3	227	230	228	1	1	1	228	Cyclic	Quasi-Static	Shear
2010-US-NO-03	49.3	193	215	204	1	1	1	204	Cyclic	Quasi-Static	Shear
2010-US-NO-04	49.3	258	262	261	1	1	1	261	Cyclic	Quasi-Static	Shear
2010-US-NO-05	49.3	290	302	296	1	1	1	296	Cyclic	Quasi-Static	Shear
2010-US-NO-06	49.3	311	355	333	1	1	1	333	Cyclic	Quasi-Static	Shear

APPENDIX F. COMPARISON OF MODEL PREDICTIONS BY GROUP

This Appendix provides graphical comparison of the performance of the different prediction models. Figures F.1, F.2, F.3 present the goodness-of-fit statistics for each model segregated by specimen group. The remaining figures present scatter plots of the predicted versus experimental strengths for the specimens in each group, segregated by model.

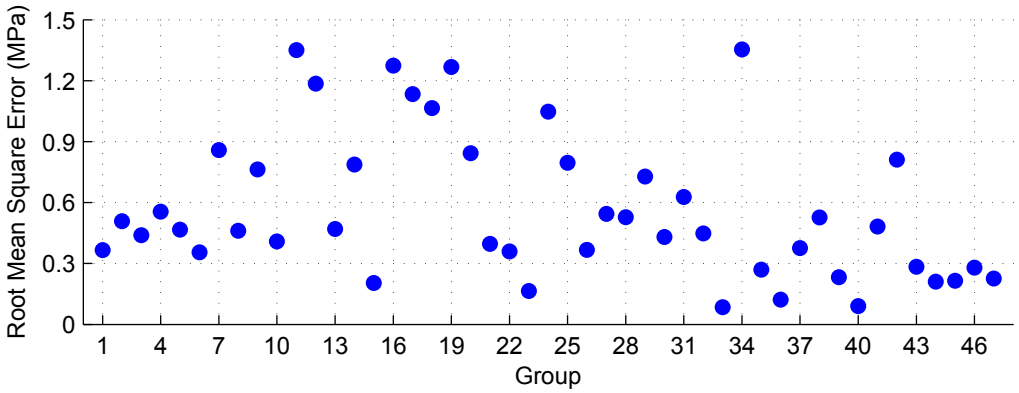

(a) Matsumura Model

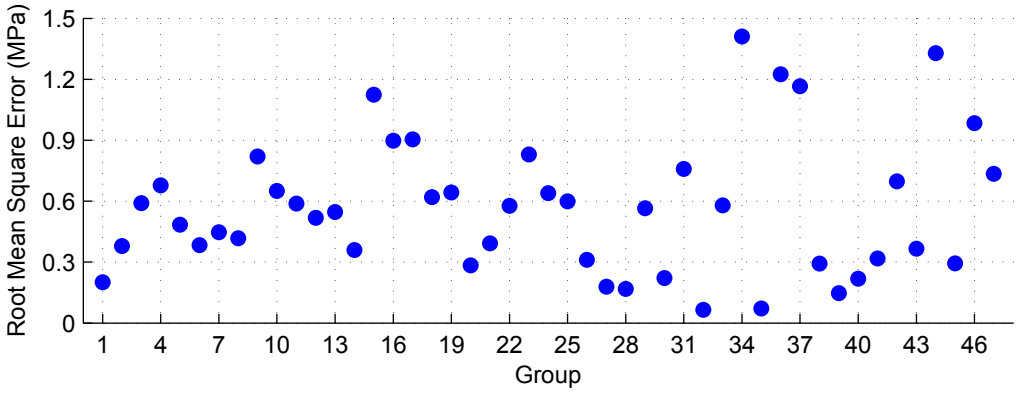

(b) AIJ Model

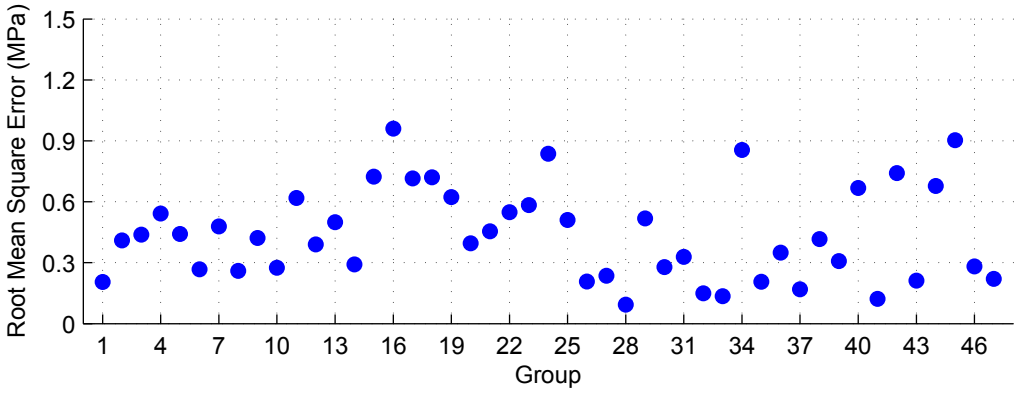

(c) Blondet Model

Figure F.1: Root mean square error by model and group

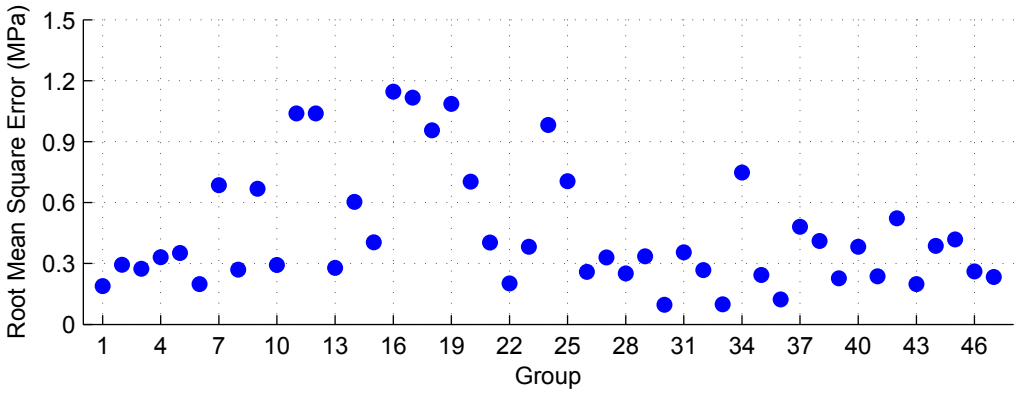

(d) Shing Model

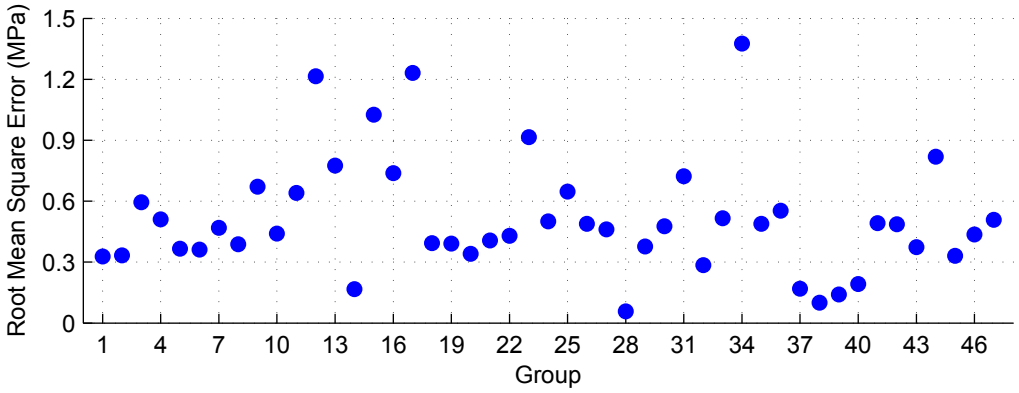

(e) Anderson Model

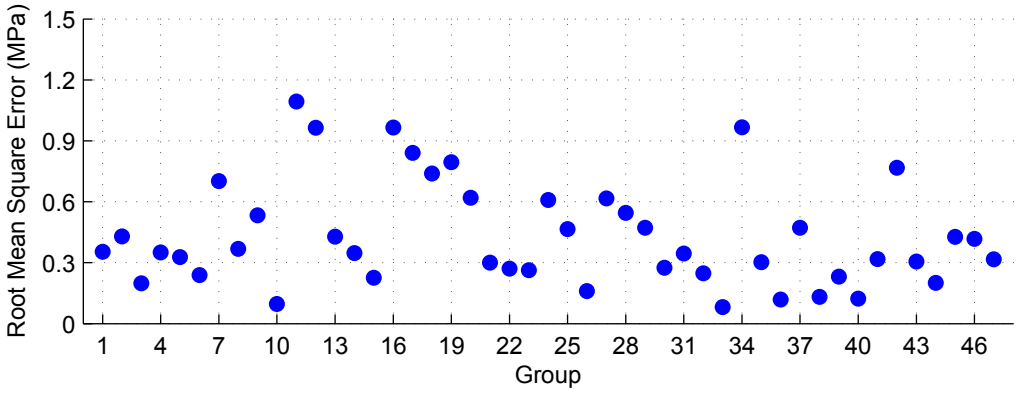

(f) Fattal Model

Root mean square error by model and group (Continued)

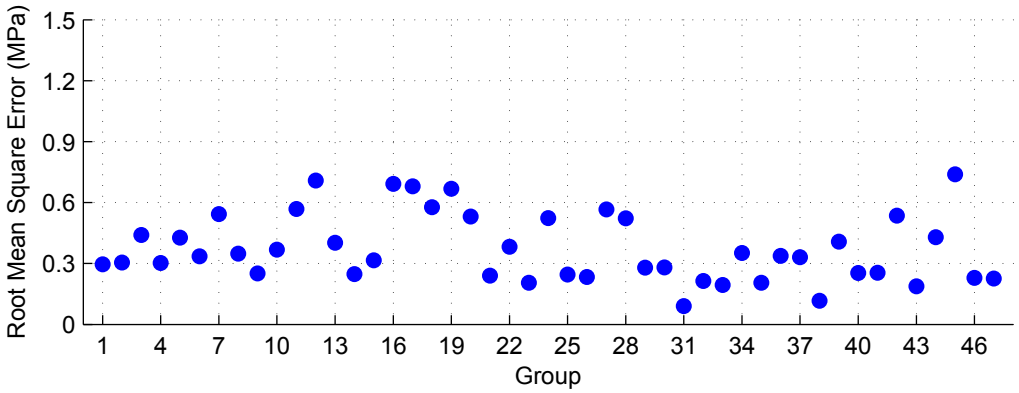

(g) NZS Model

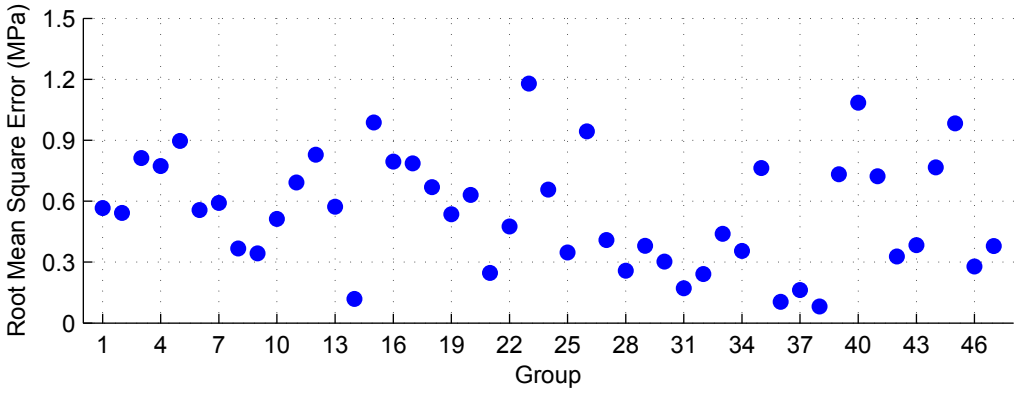

(h) Voon Model

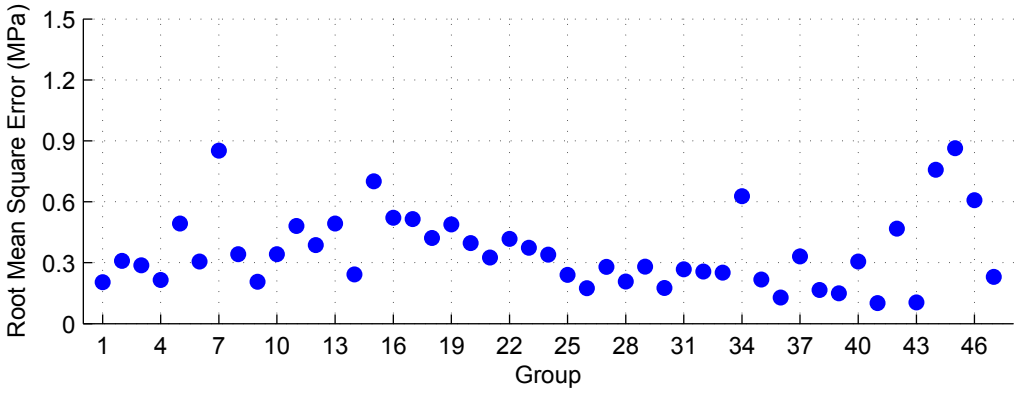

(i) CSA Model

Root mean square error by model and group (Continued)

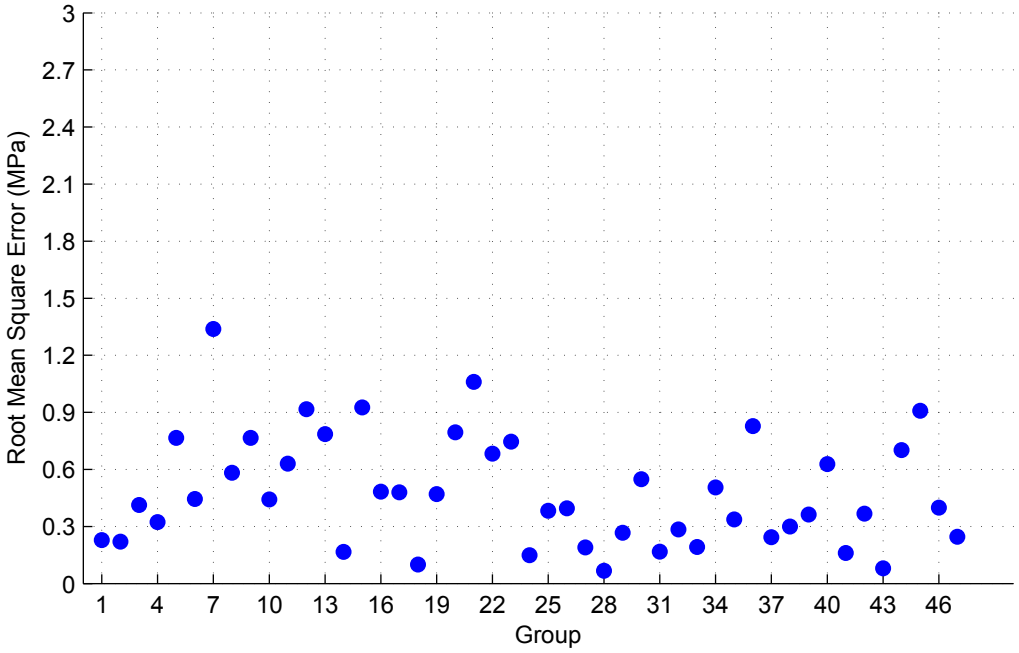

(j) TCCMaR Model

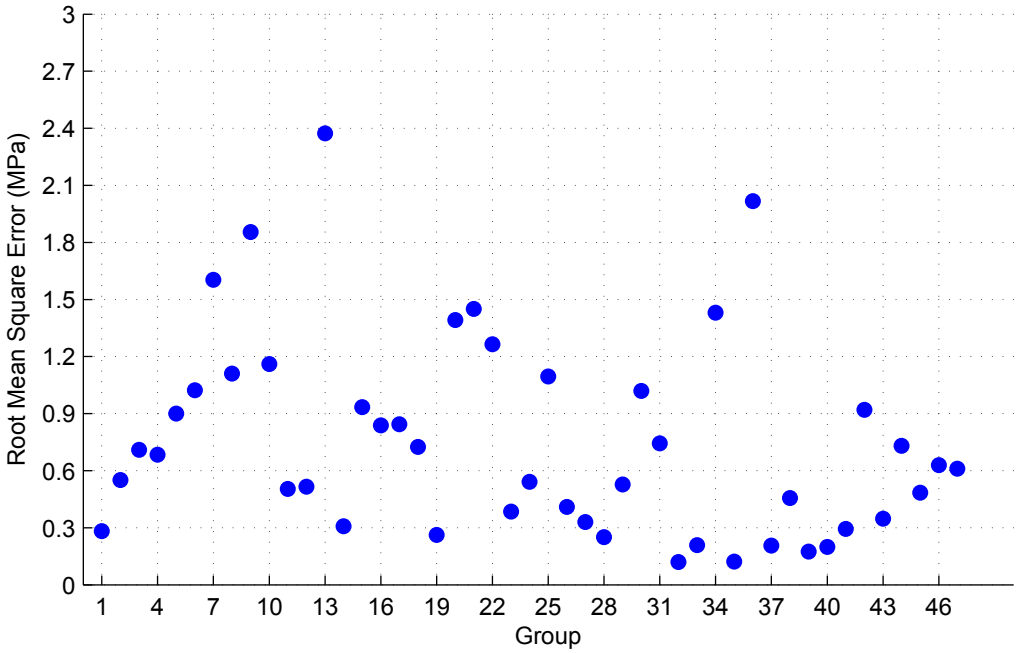

(k) UBC Model

Root mean square error by model and group (Continued)

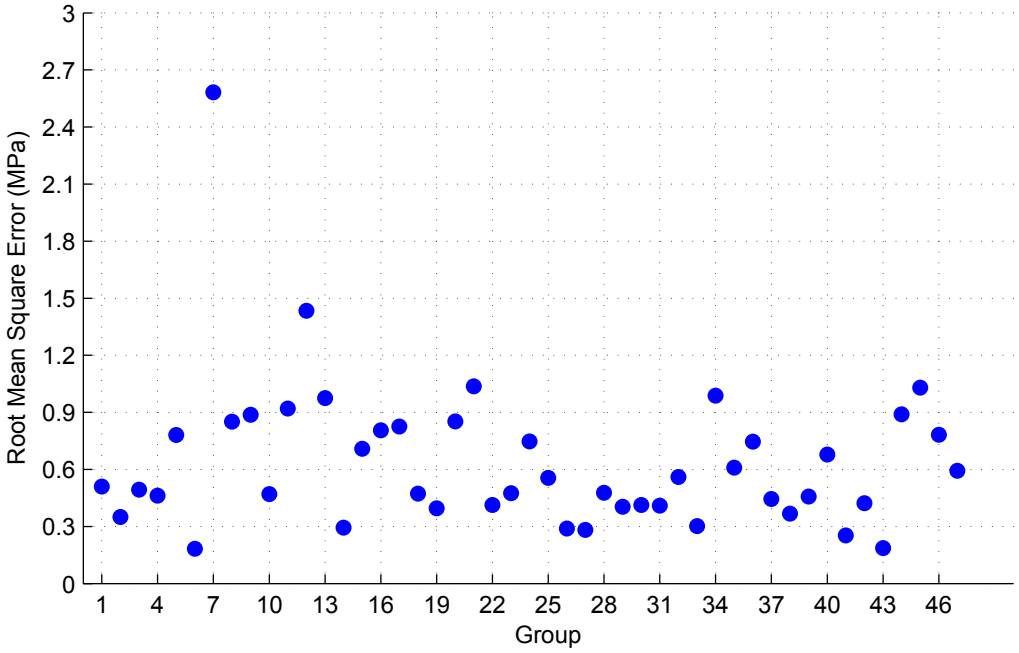

(l) AS Model

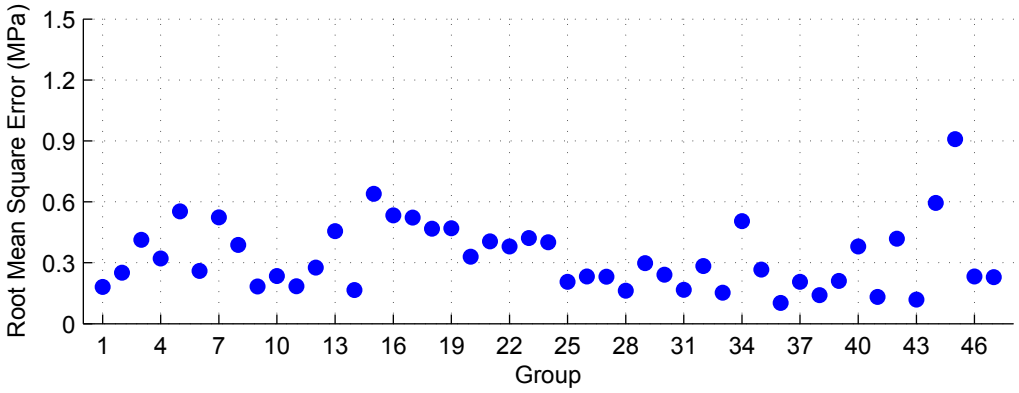

(m) MSJC Model

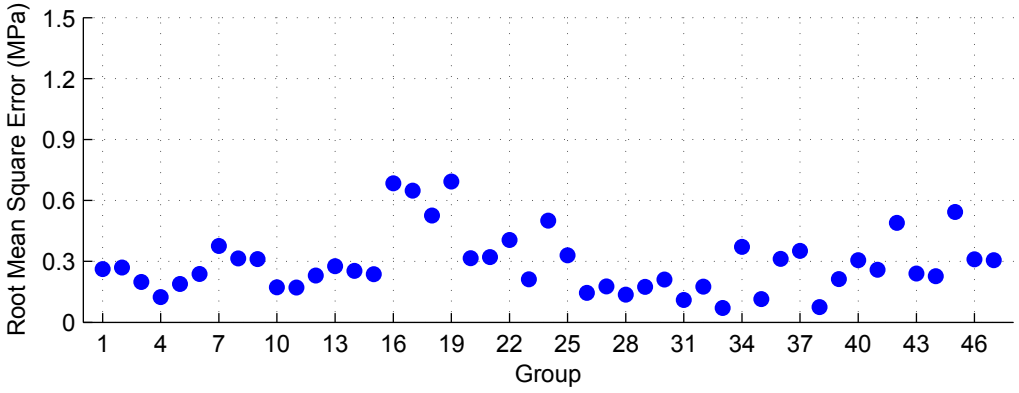

(n) Proposed Model

Root mean square error by model and group (Continued)

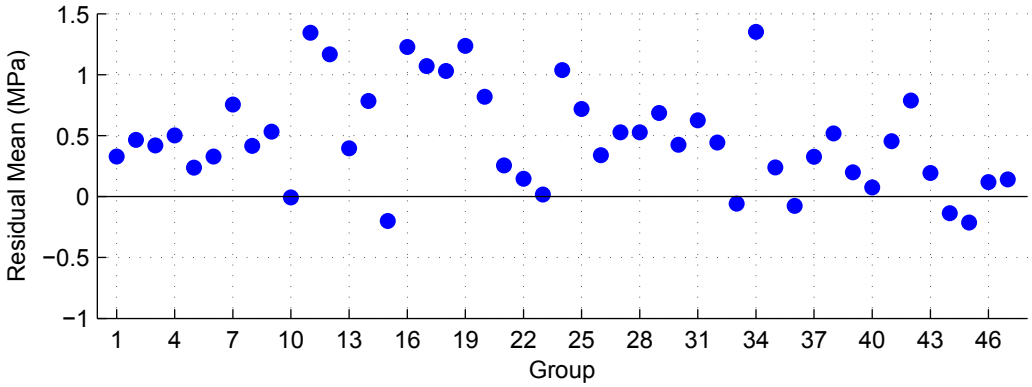

(a) Matsumura Model

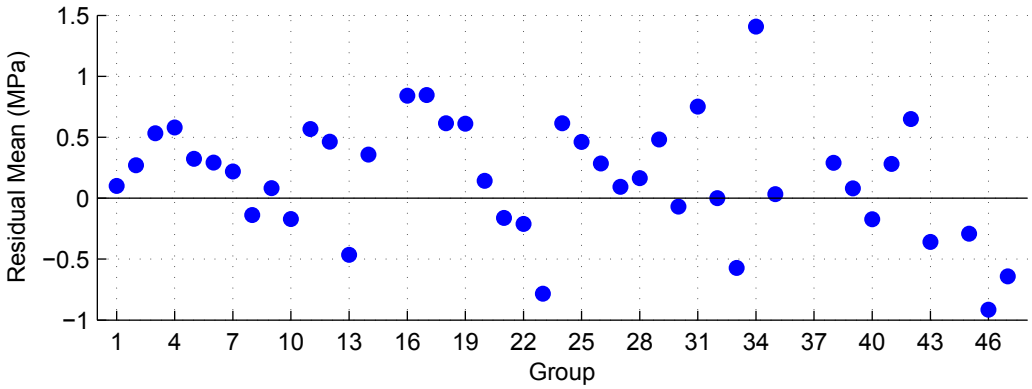

(b) AIJ Model

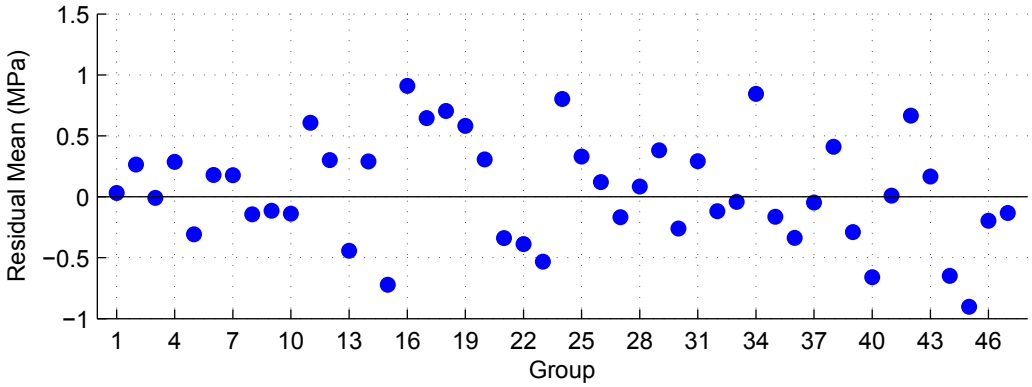

(c) Blondet Model

Figure F.2: Residual mean by model and group

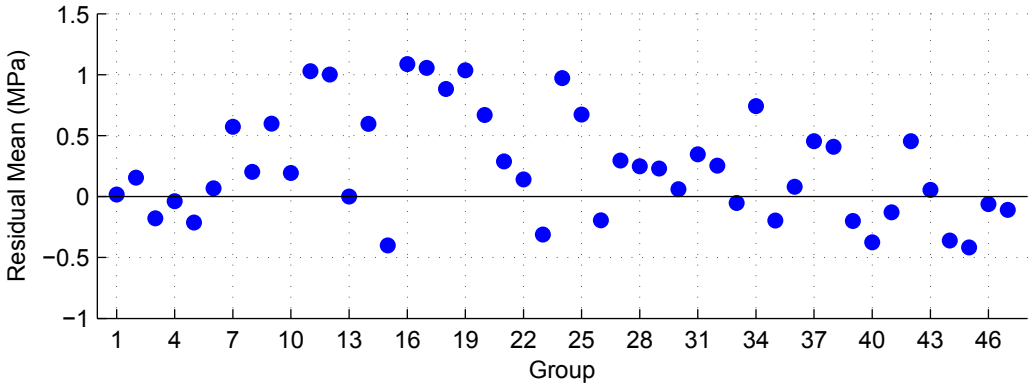

(d) Shing Model

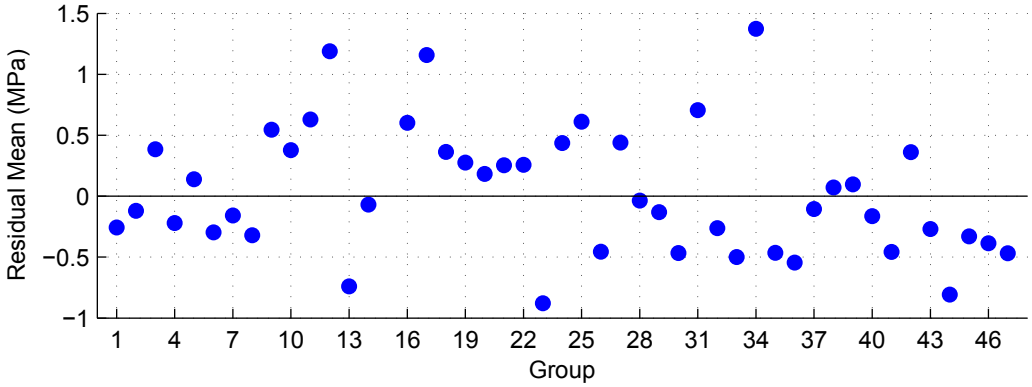

(e) Anderson Model

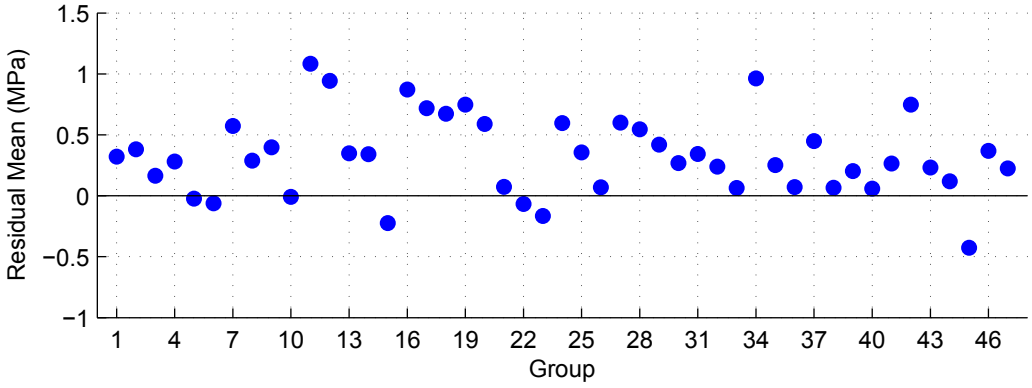

(f) Fattal Model

Residual mean by model and group (Continued)

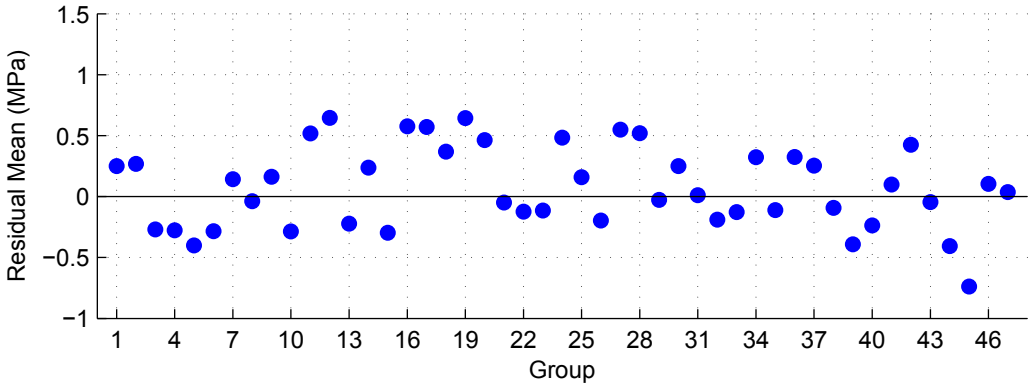

(g) NZS Model

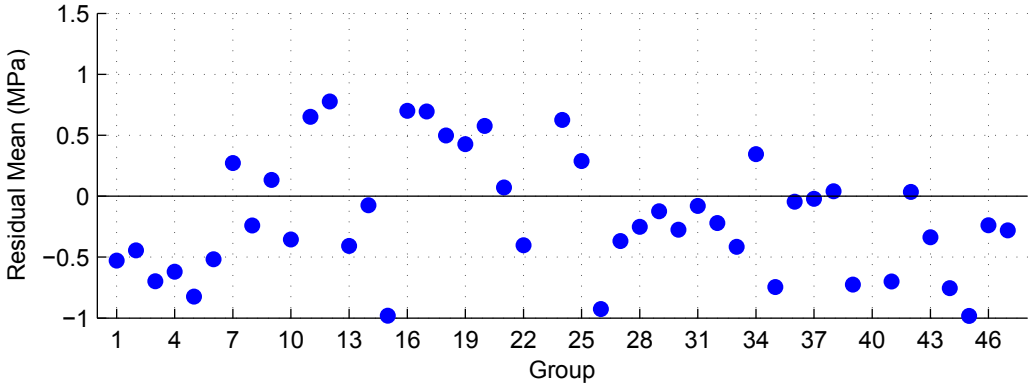

(h) Voon Model

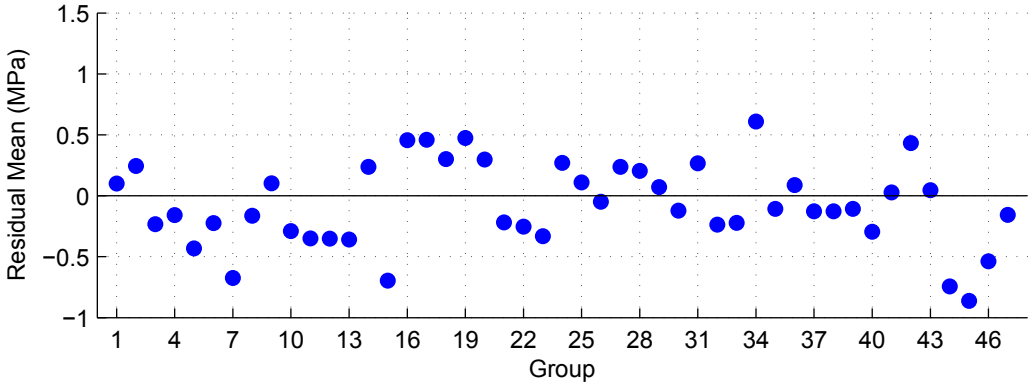

(i) CSA Model

Residual mean by model and group (Continued)

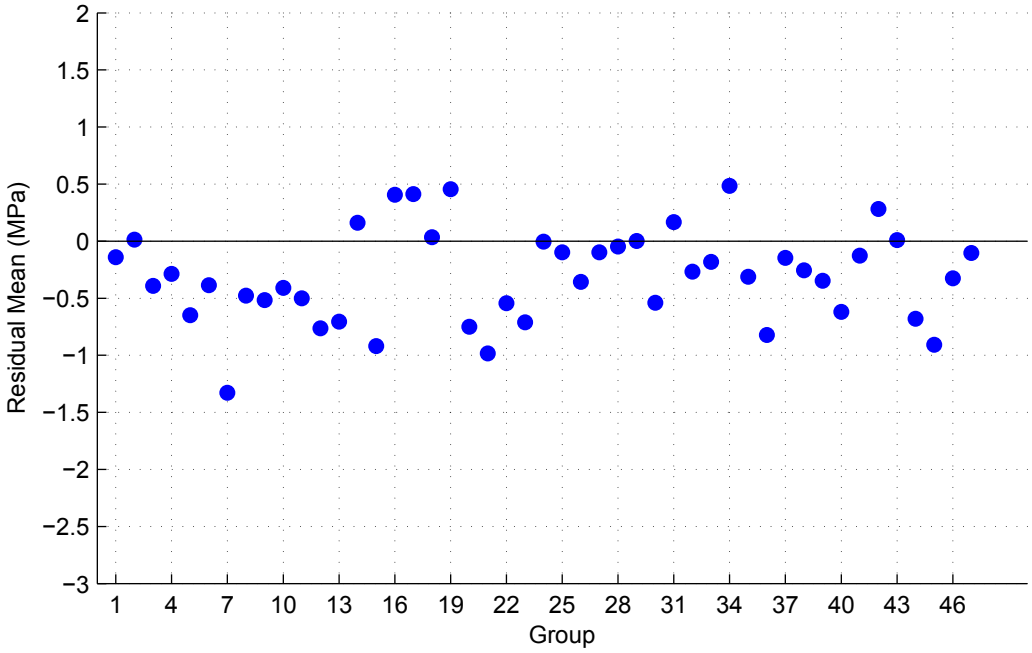

(j) TCCMaR Model

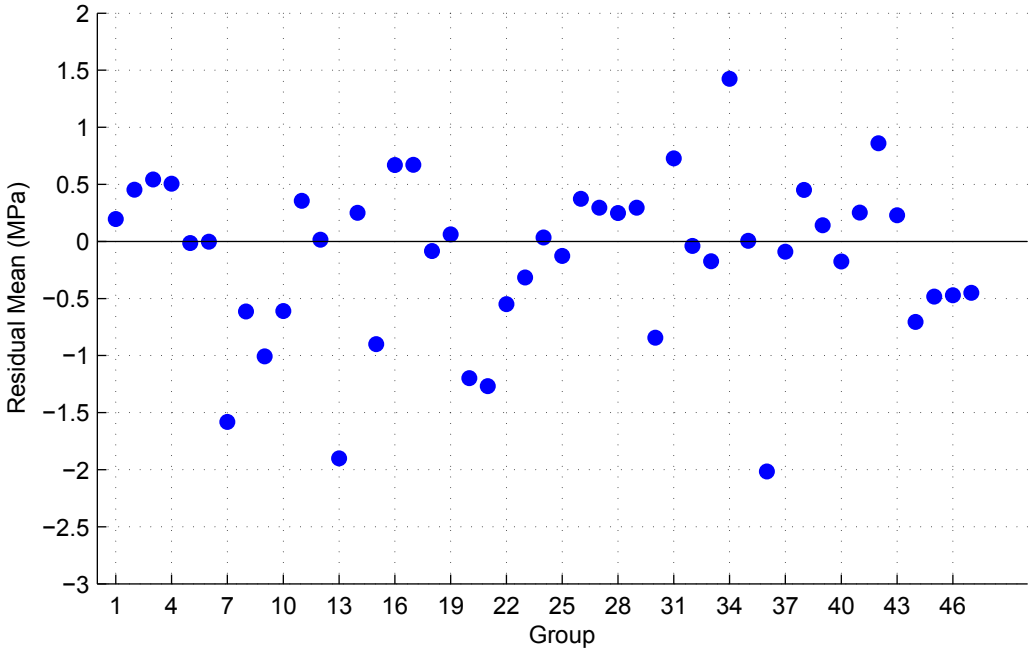

(k) UBC Model

Residual mean by model and group (Continued)

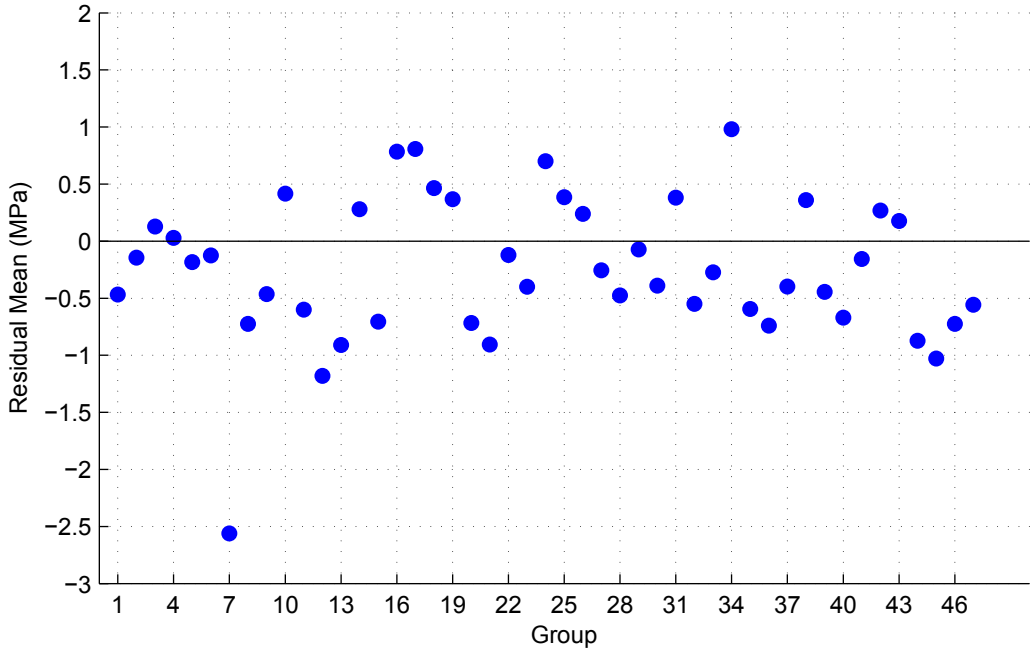

(l) AS Model

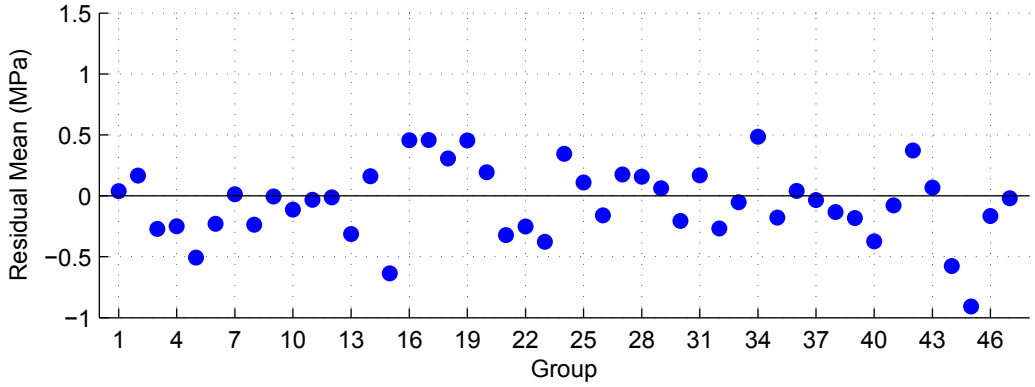

(m) MSJC Model

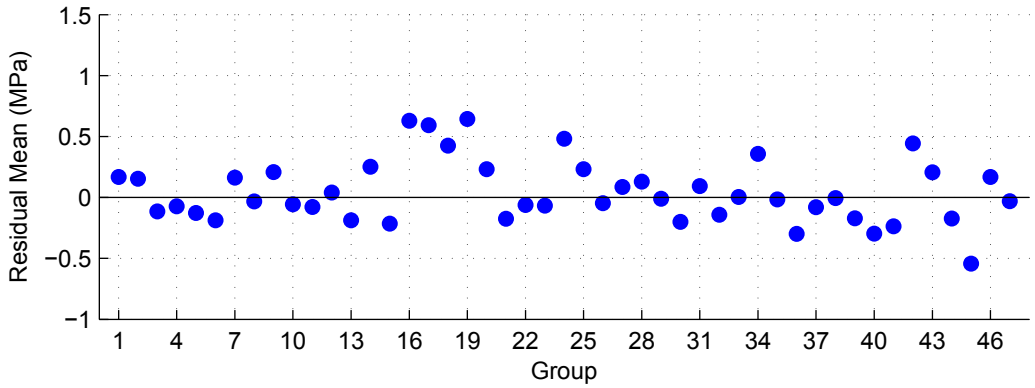

(n) Proposed Model

Residual mean by model and group (Continued)

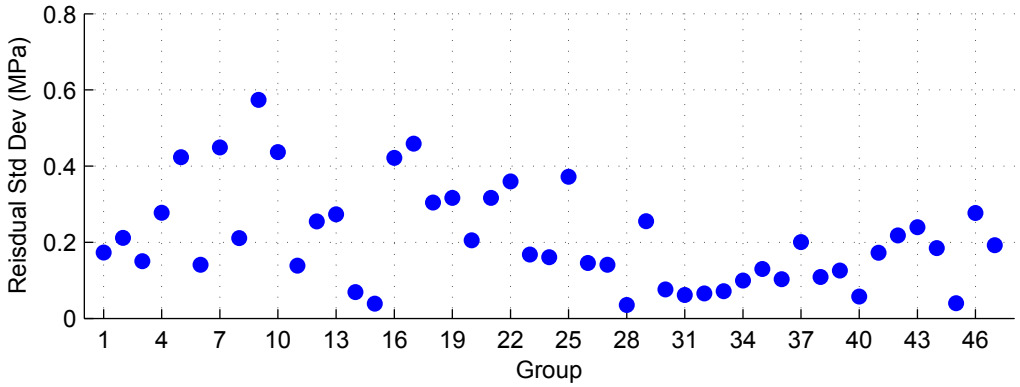

(a) Matsumura Model

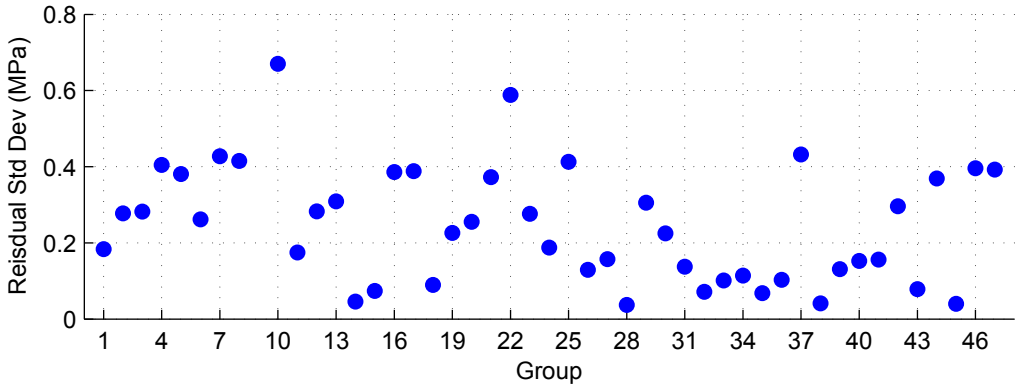

(b) AIJ Model

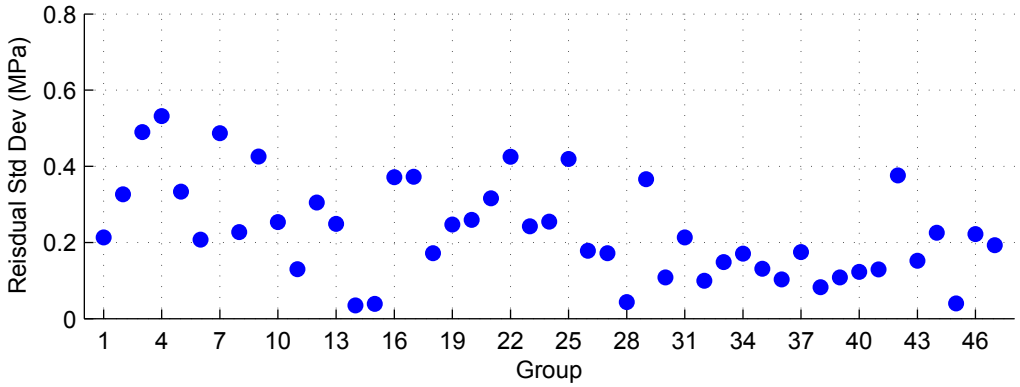

(c) Blondet Model

Figure F.3: Residual standard deviation by model and group

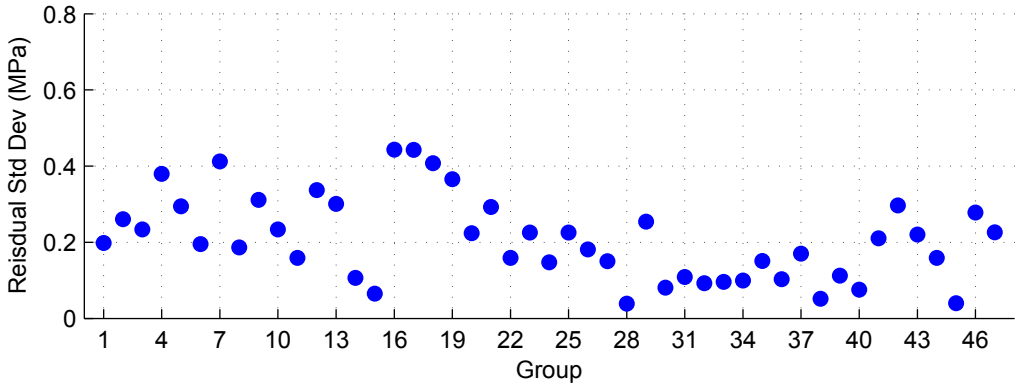

(d) Shing Model

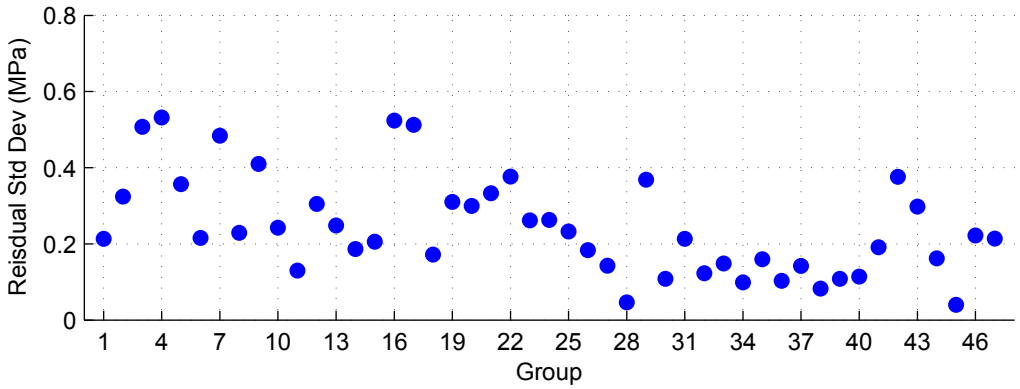

(e) Anderson Model

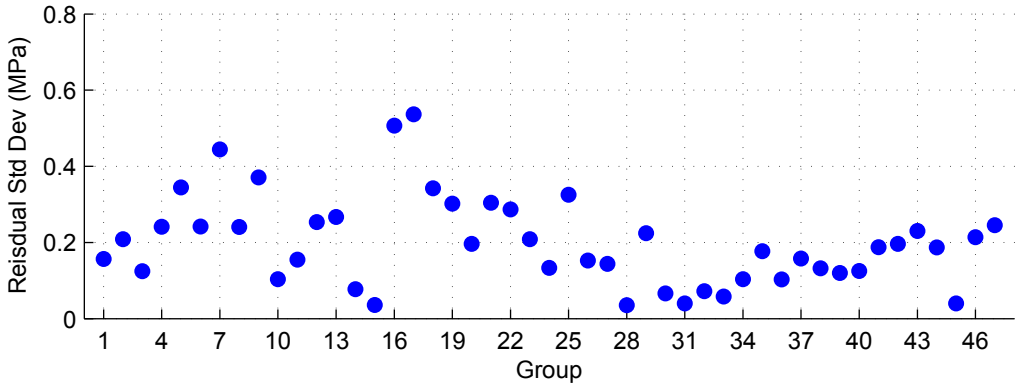

(f) Fattal Model

Residual standard deviation by model and group (Continued)

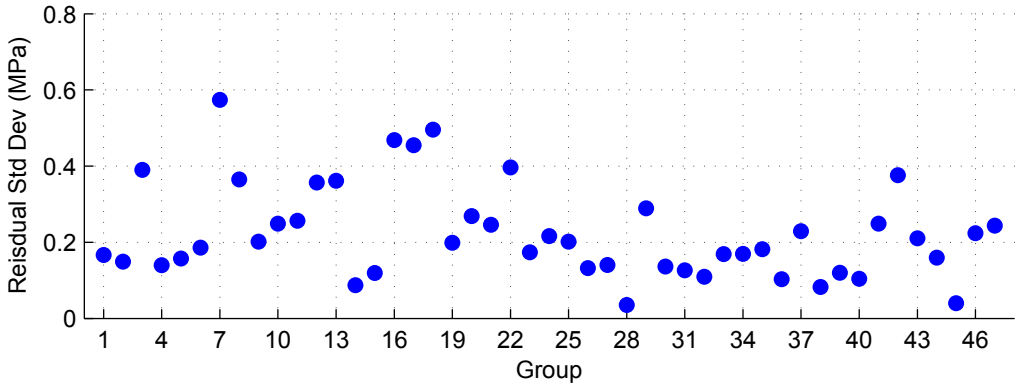

(g) NZS Model

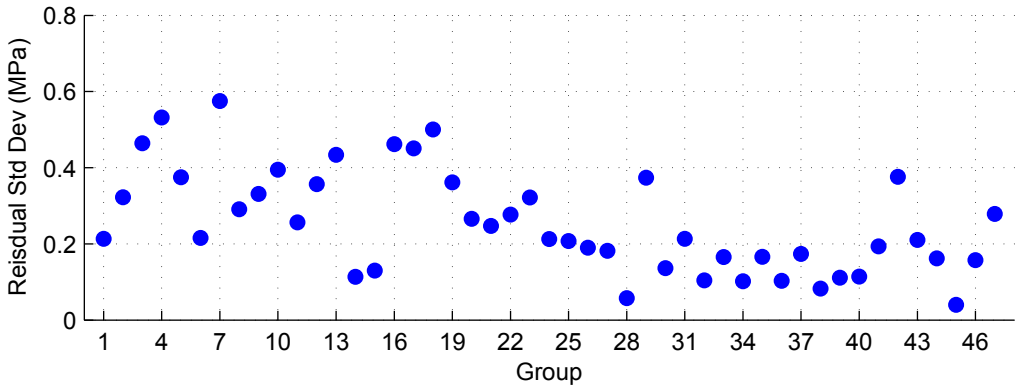

(h) Voon Model

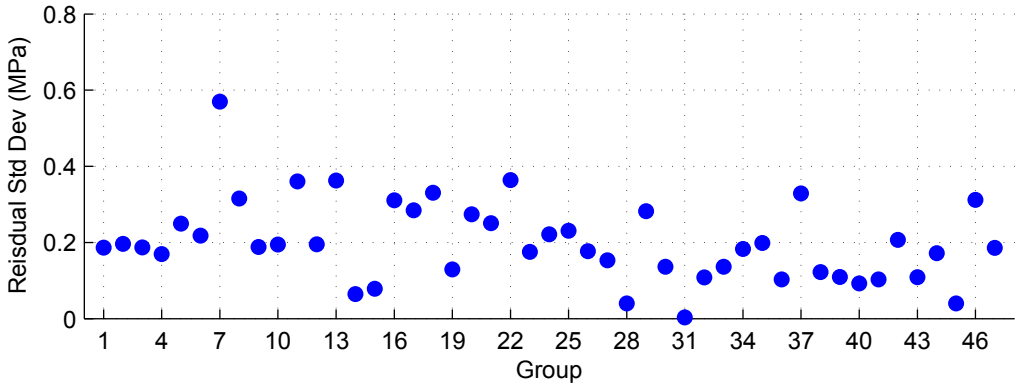

(i) CSA Model

Residual standard deviation by model and group (Continued)

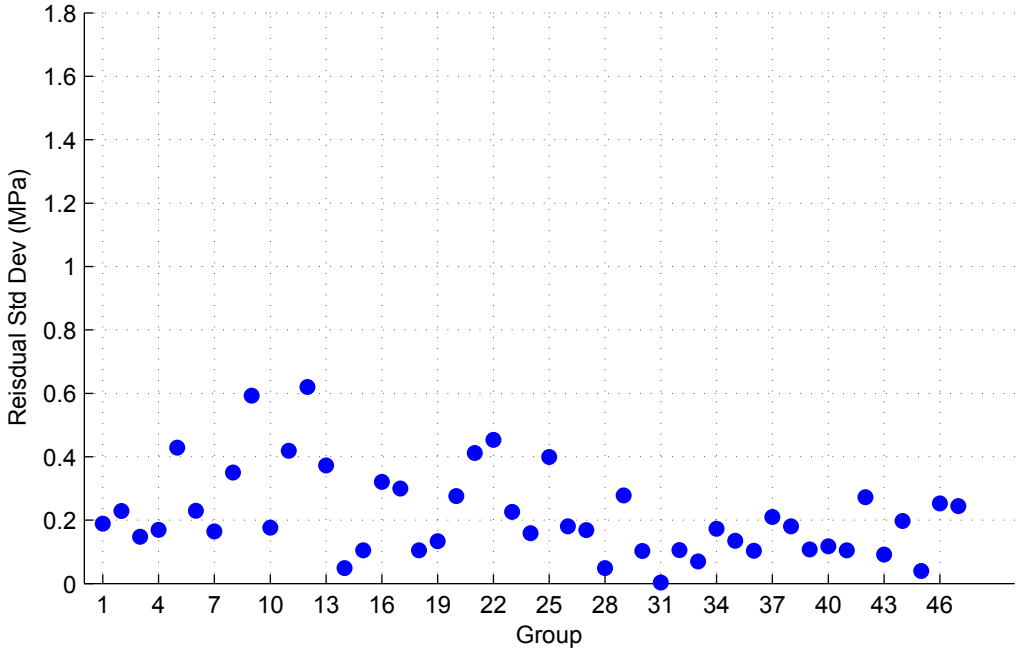

(j) TCCMaR Model

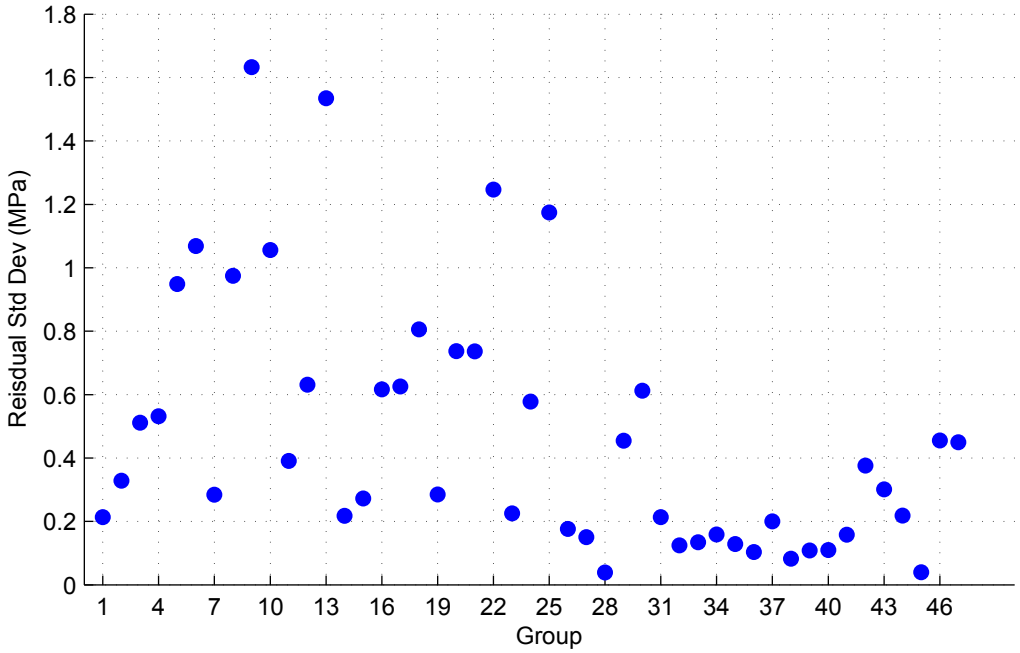

(k) UBC Model

Residual standard deviation by model and group (Continued)

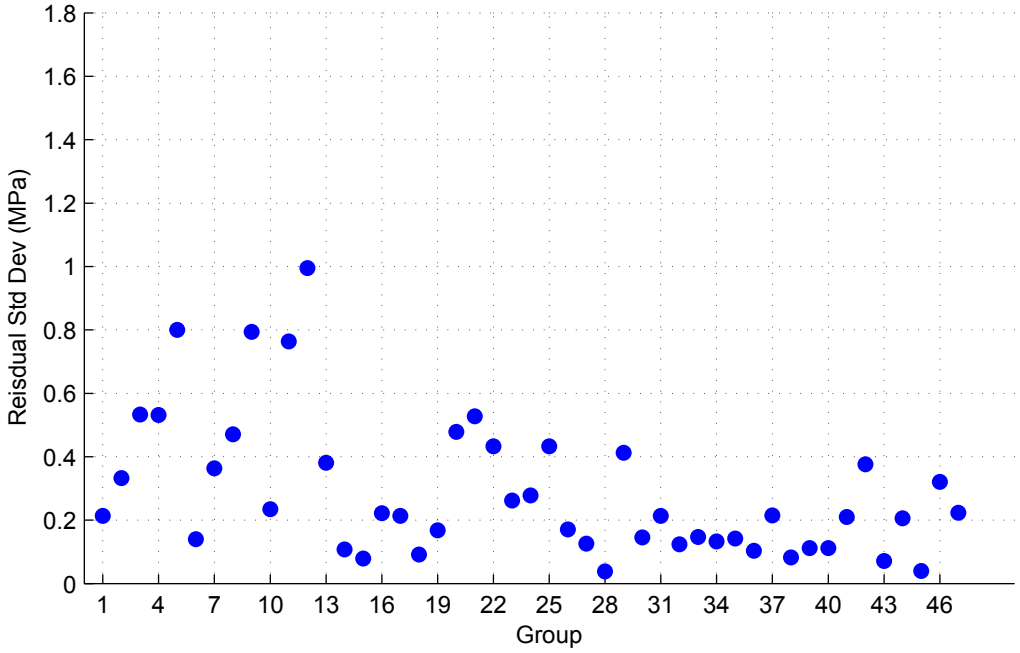

(l) AS Model

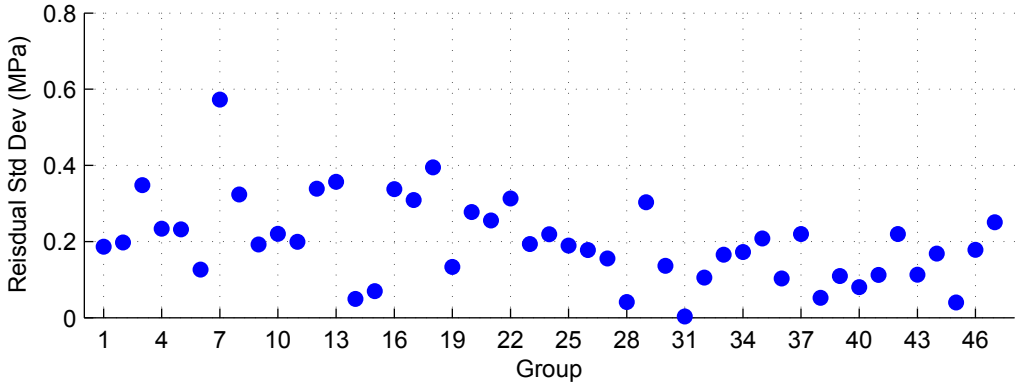

(m) MSJC Model

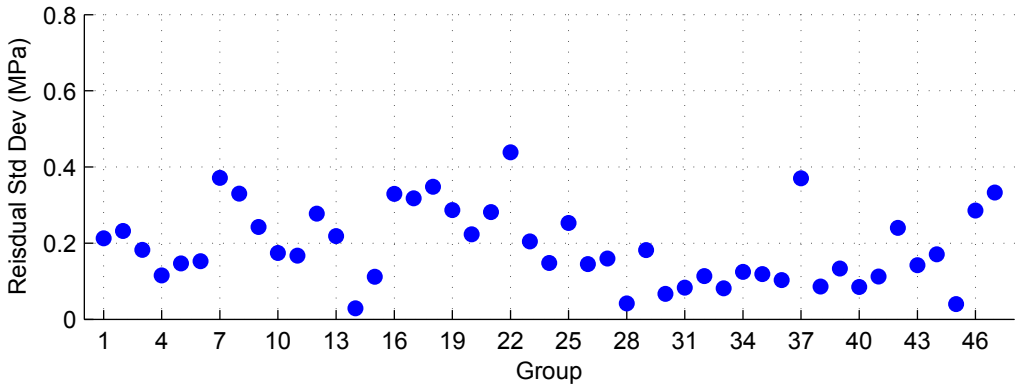

(n) Proposed Model

Residual standard deviation by model and group (Continued)

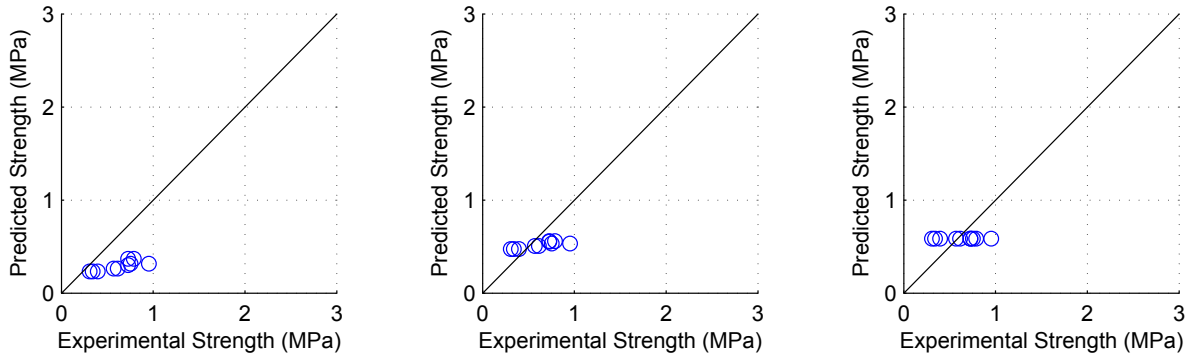

(a) Matsumura Model (b) AIJ Model (c) Blondet Model

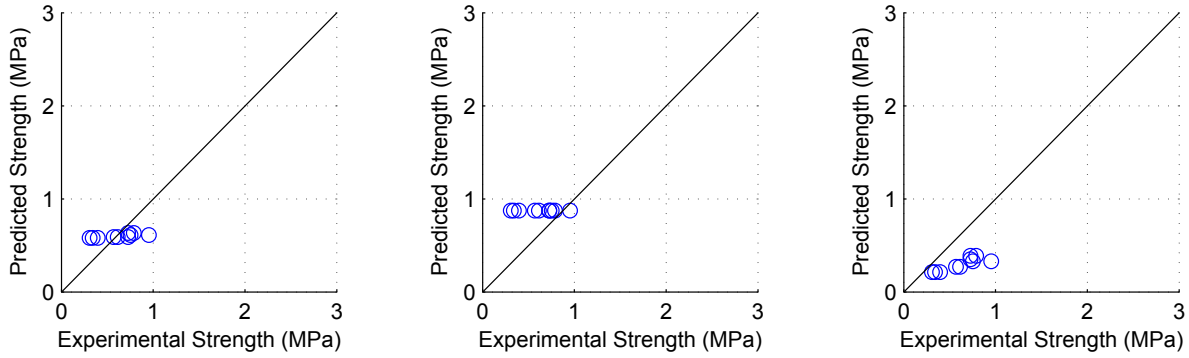

(d) Shing Model (e) Anderson Model (f) Fattal Model

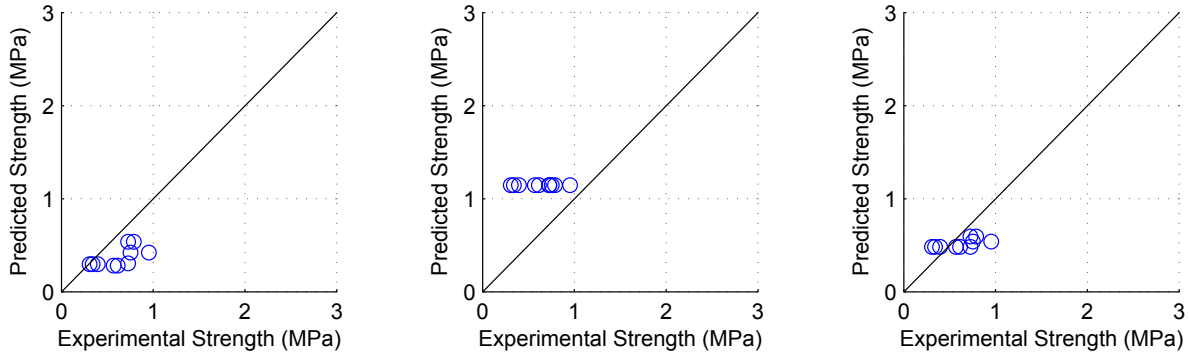

(g) NZS Model (h) Voon Model (i) CSA Model

Figure F.4: Model predictions for group 1

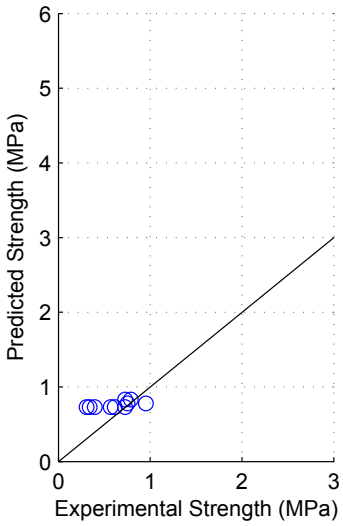

(j) TCCMaR Model

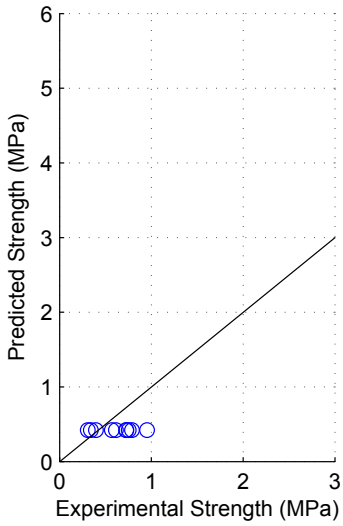

(k) UBC Model

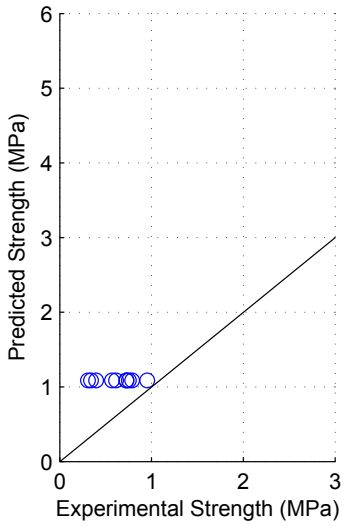

(l) AS Model

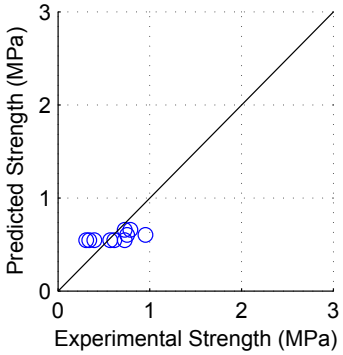

(m) MSJC Model

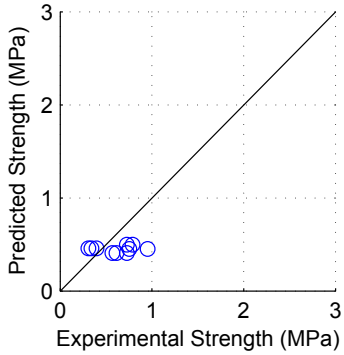

(n) BYU Model

Model predictions for group 1 (Continued)

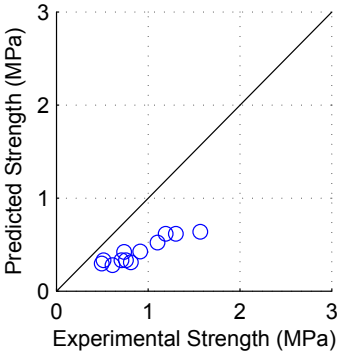

(a) Matsumura Model

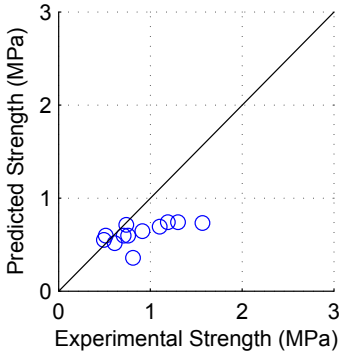

(b) AIJ Model

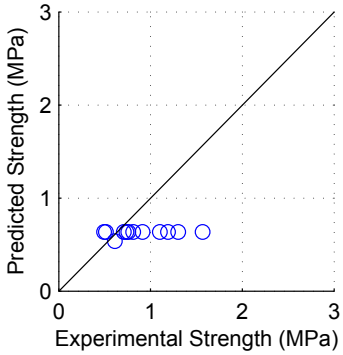

(c) Blondet Model

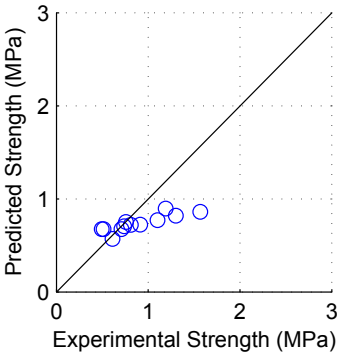

(d) Shing Model

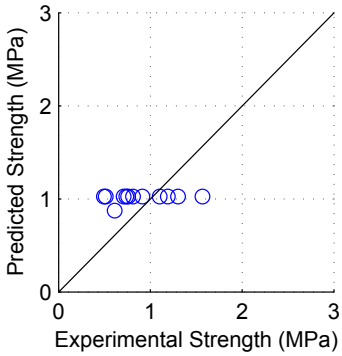

(e) Anderson Model

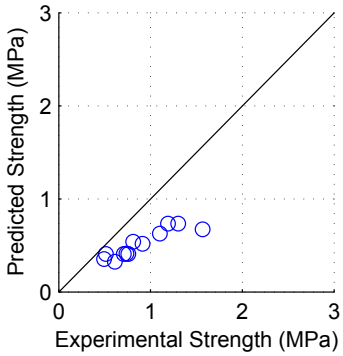

(f) Fattal Model

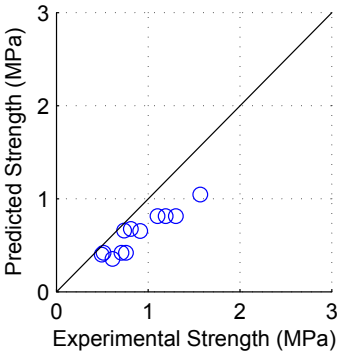

(g) NZS Model

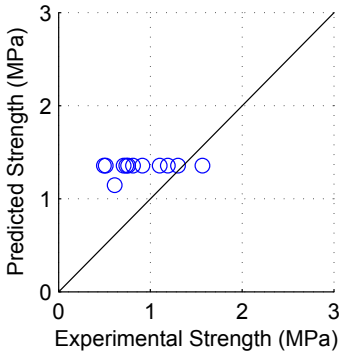

(h) Voon Model

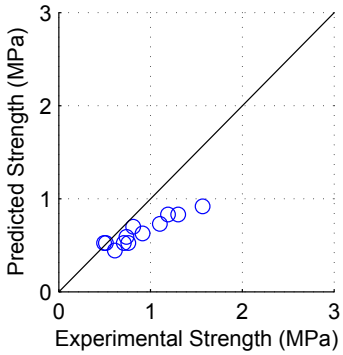

(i) CSA Model

Figure F.5: Model predictions for group 2

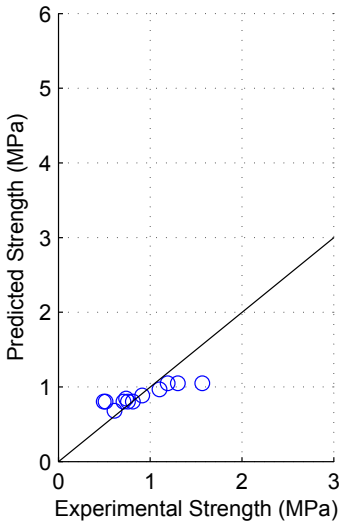

(j) TCCMaR Model

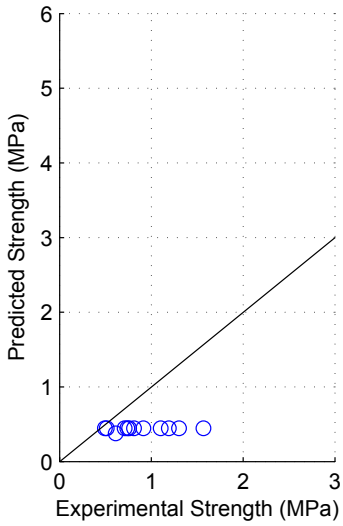

(k) UBC Model

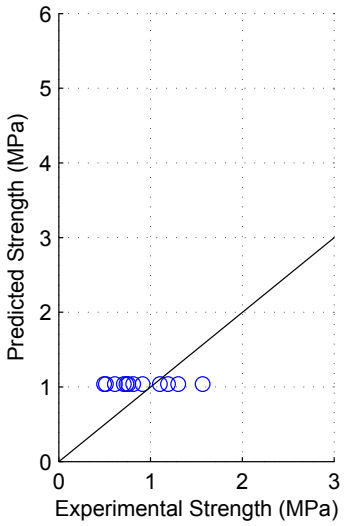

(l) AS Model

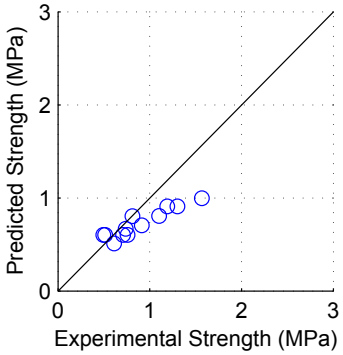

(m) MSJC Model

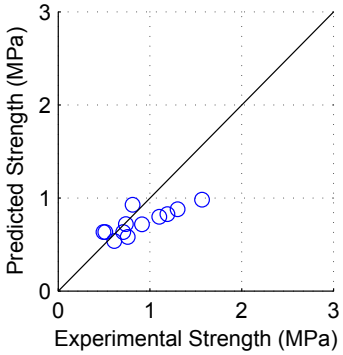

(n) BYU Model

Model predictions for group 2 (Continued)

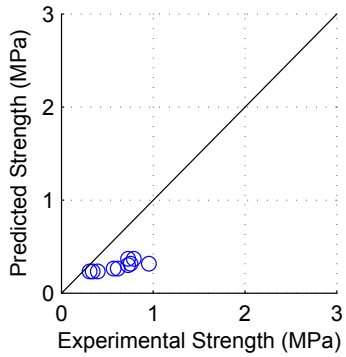

(a) Matsumura Model

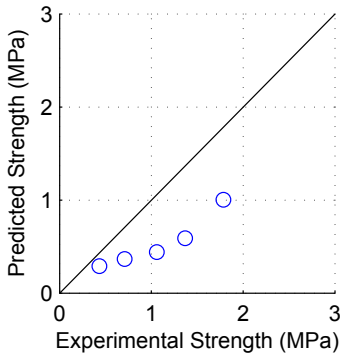

(b) AIJ Model

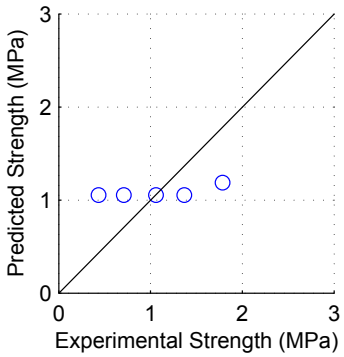

(c) Blondet Model

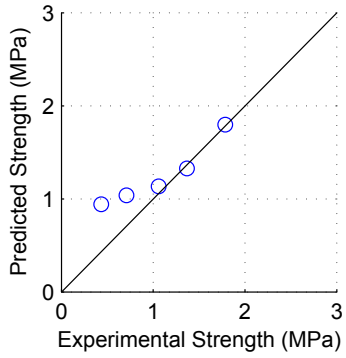

(d) Shing Model

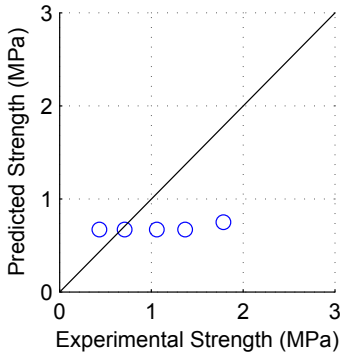

(e) Anderson Model

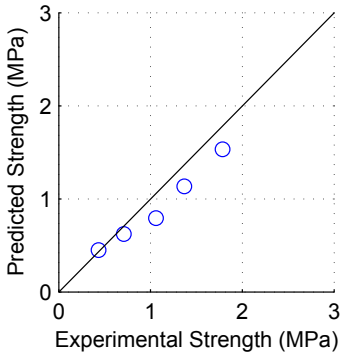

(f) Fattal Model

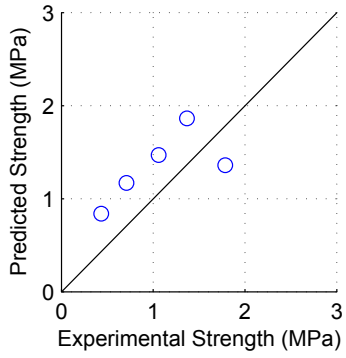

(g) NZS Model

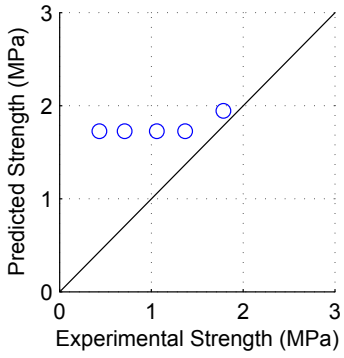

(h) Voon Model

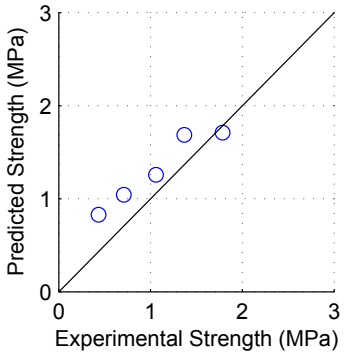

(i) CSA Model

Figure F.6: Model predictions for group 3

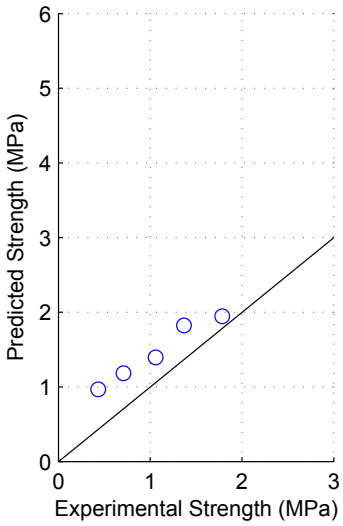

(j) TCCMaR Model

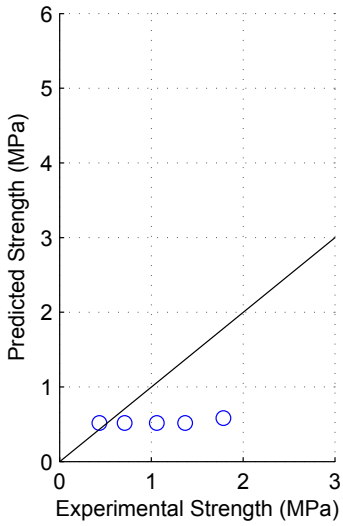

(k) UBC Model

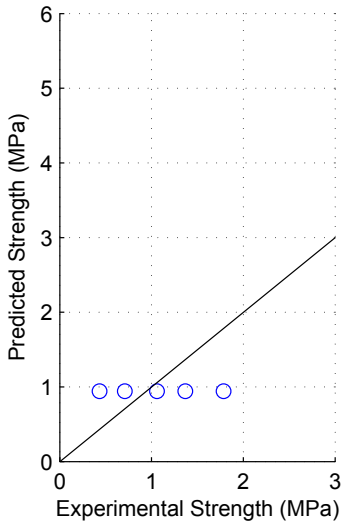

(l) AS Model

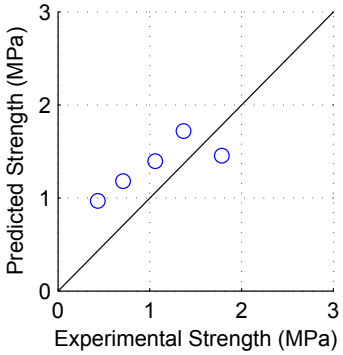

(m) MSJC Model

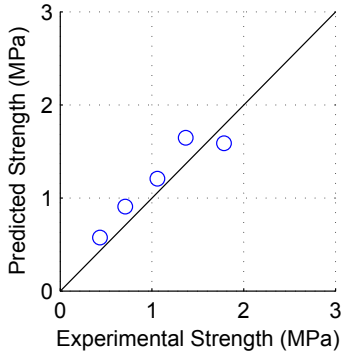

(n) BYU Model

Model predictions for group 3 (Continued)

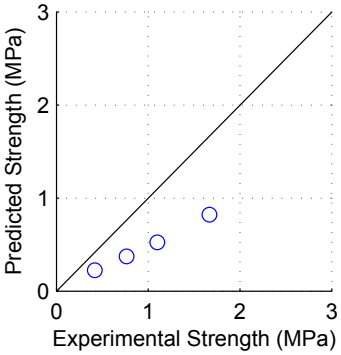

(a) Matsumura Model

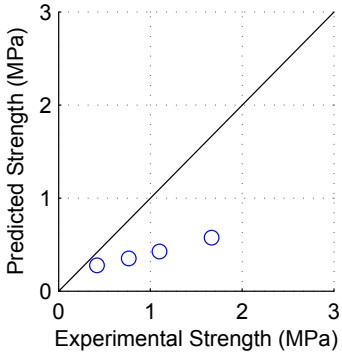

(b) AIJ Model

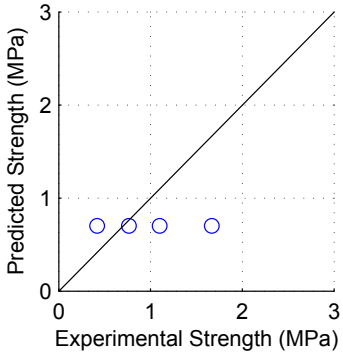

(c) Blondet Model

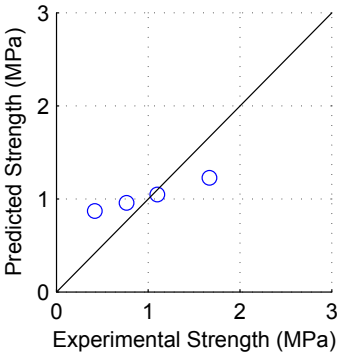

(d) Shing Model

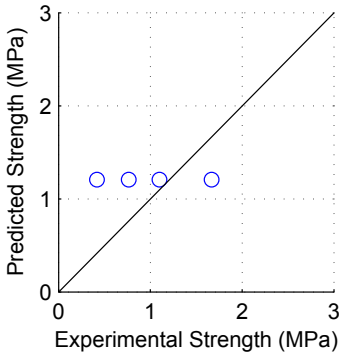

(e) Anderson Model

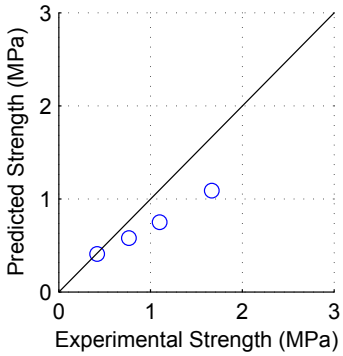

(f) Fattal Model

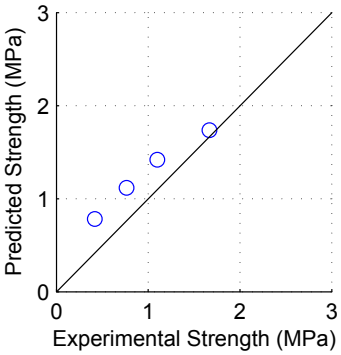

(g) NZS Model

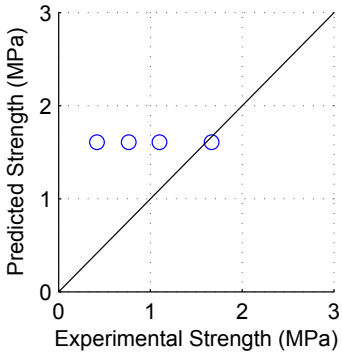

(h) Voon Model

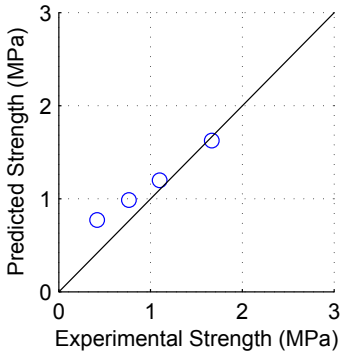

(i) CSA Model

Figure F.7: Model predictions for group 4

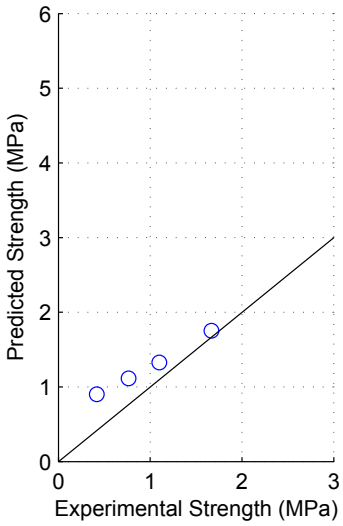

(j) TCCMaR Model

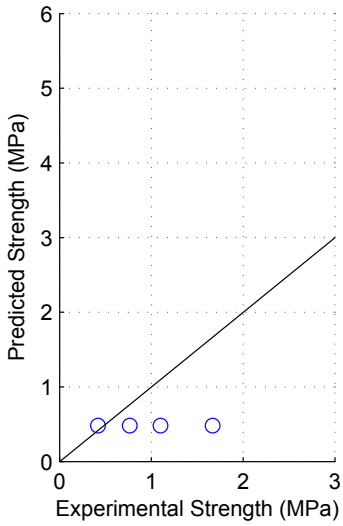

(k) UBC Model

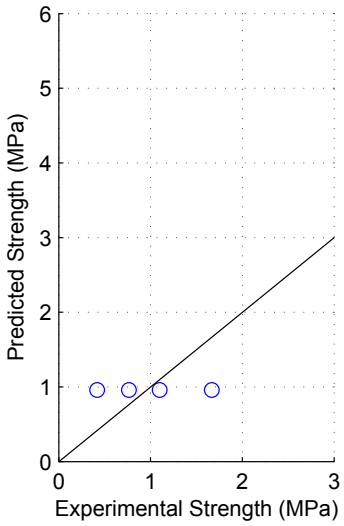

(l) AS Model

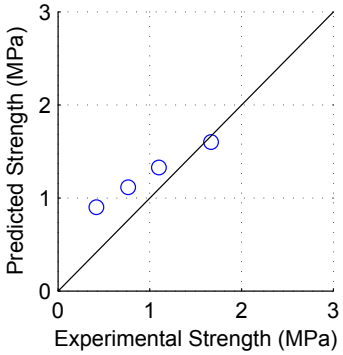

(m) MSJC Model

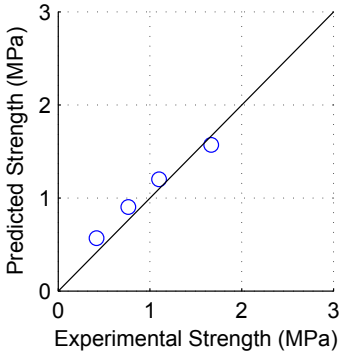

(n) BYU Model

Model predictions for group 4 (Continued)

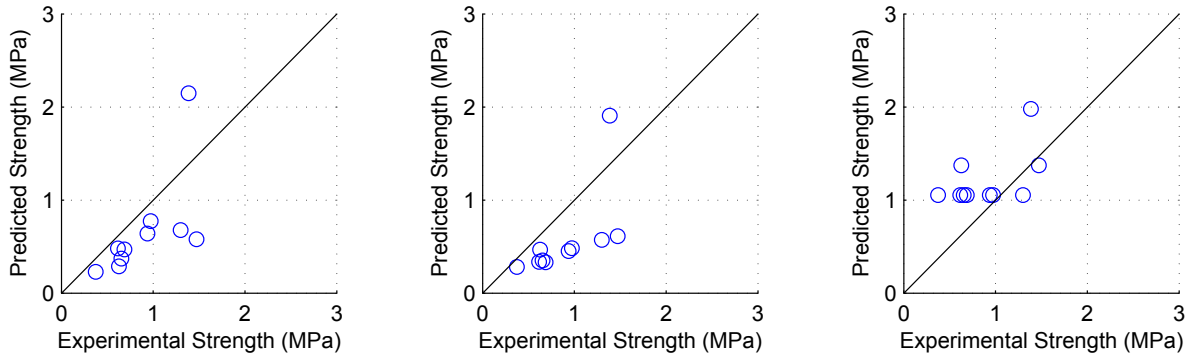

(a) Matsumura Model (b) AIJ Model (c) Blondet Model

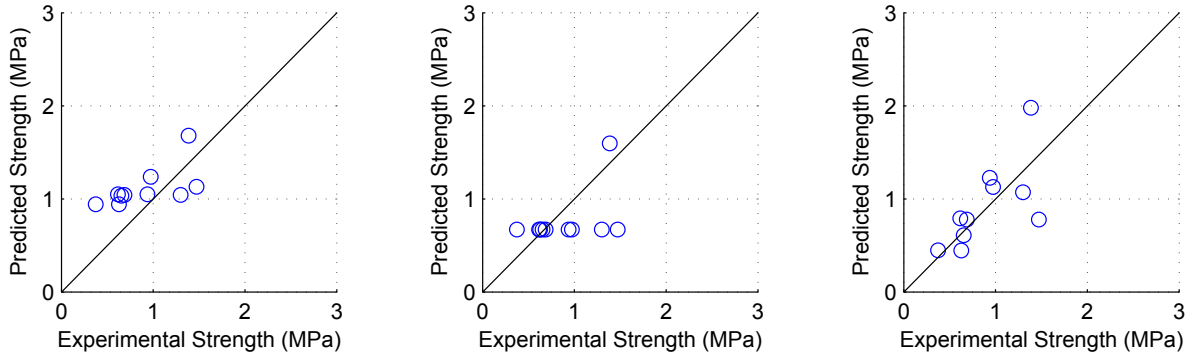

(d) Shing Model (e) Anderson Model (f) Fattal Model

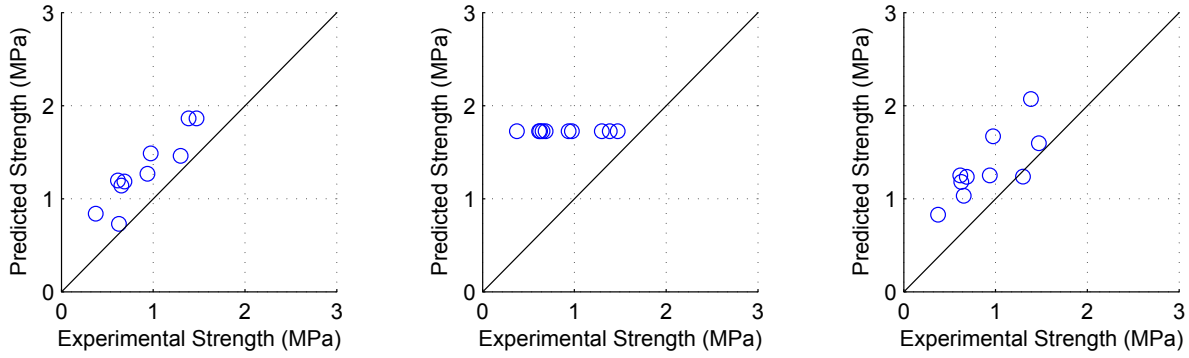

(g) NZS Model (h) Voon Model (i) CSA Model

Figure F.8: Model predictions for group 5

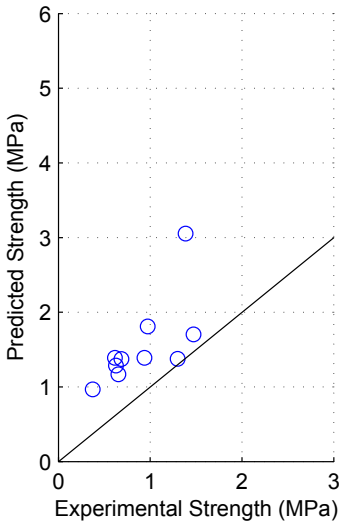

(j) TCCMaR Model

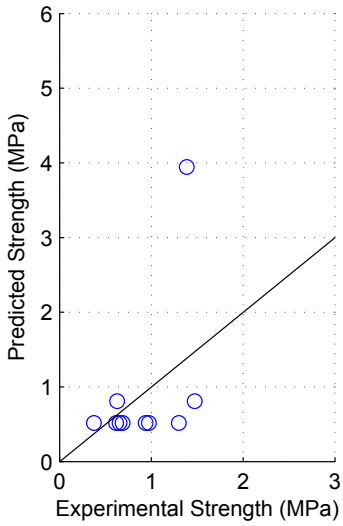

(k) UBC Model

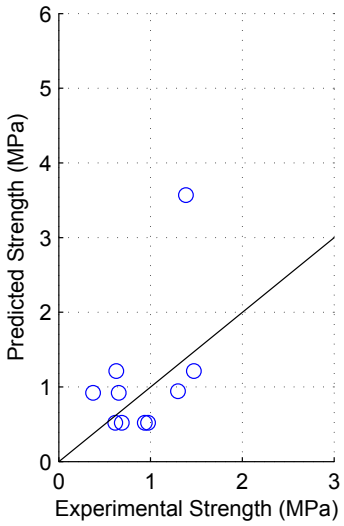

(l) AS Model

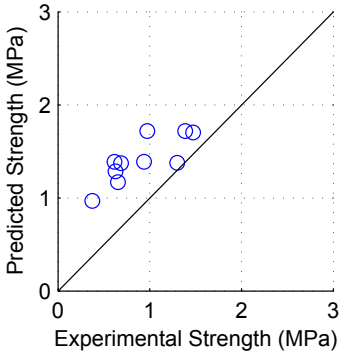

(m) MSJC Model

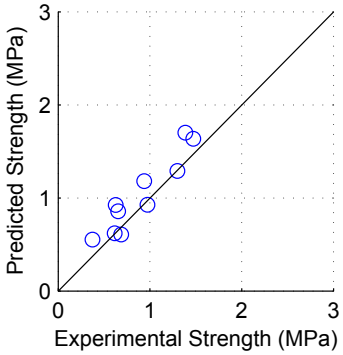

(n) BYU Model

Model predictions for group 5 (Continued)

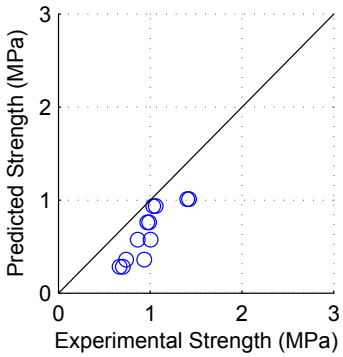

(a) Matsumura Model

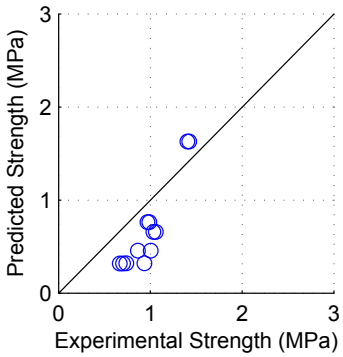

(b) AIJ Model

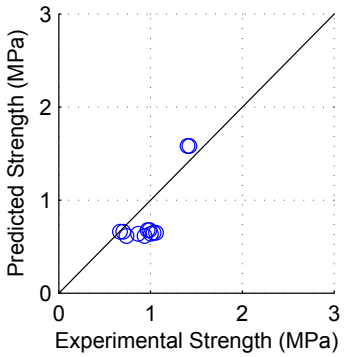

(c) Blondet Model

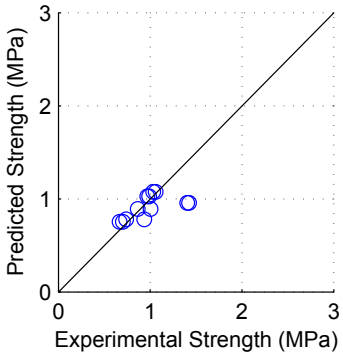

(d) Shing Model

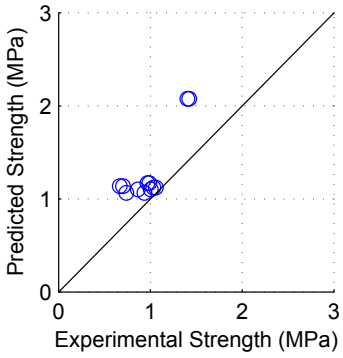

(e) Anderson Model

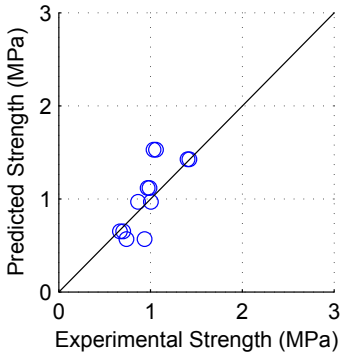

(f) Fattal Model

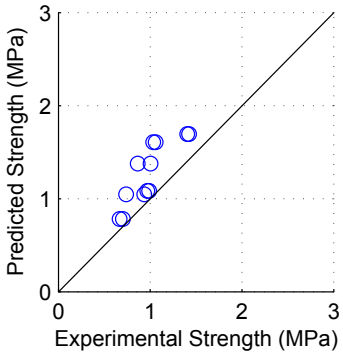

(g) NZS Model

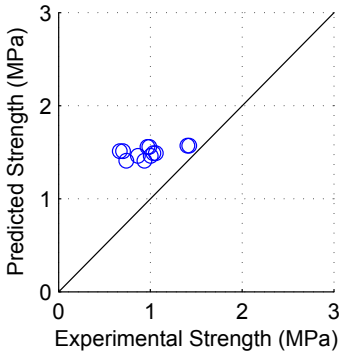

(h) Voon Model

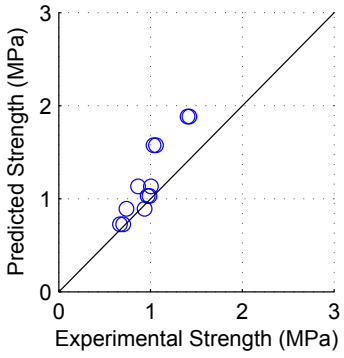

(i) CSA Model

Figure F.9: Model predictions for group 6

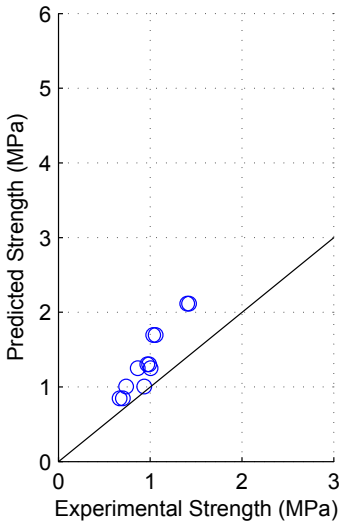

(j) TCCMaR Model

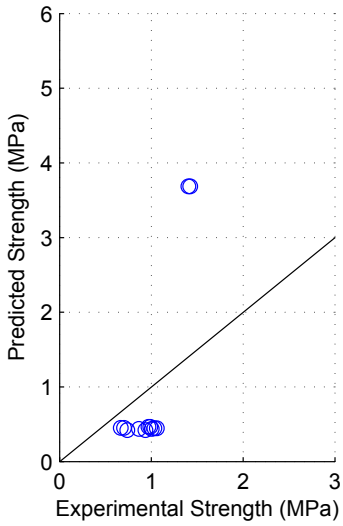

(k) UBC Model

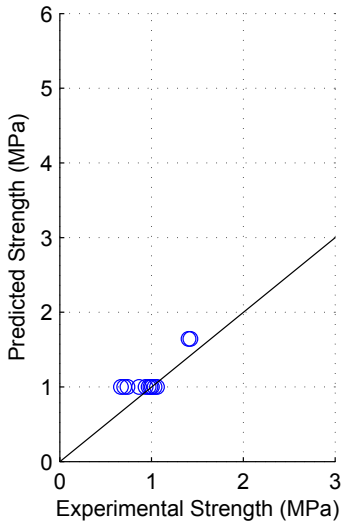

(l) AS Model

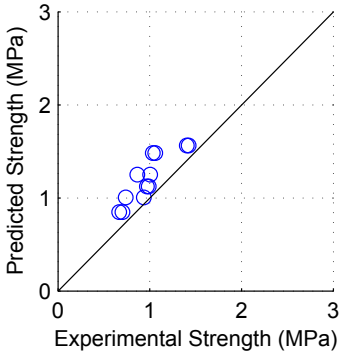

(m) MSJC Model

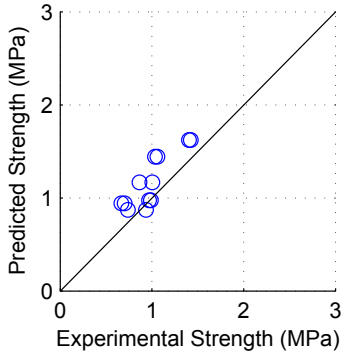

(n) BYU Model

Model predictions for group 6 (Continued)

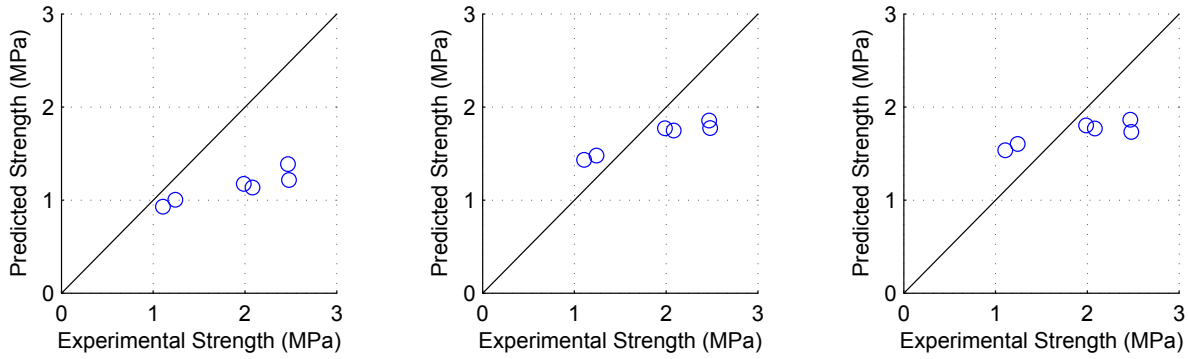

(a) Matsumura Model (b) AIJ Model (c) Blondet Model

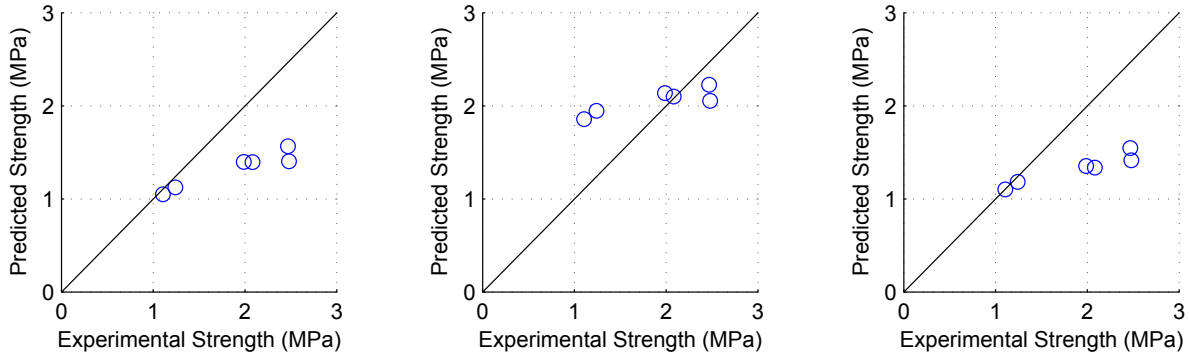

(d) Shing Model (e) Anderson Model (f) Fattal Model

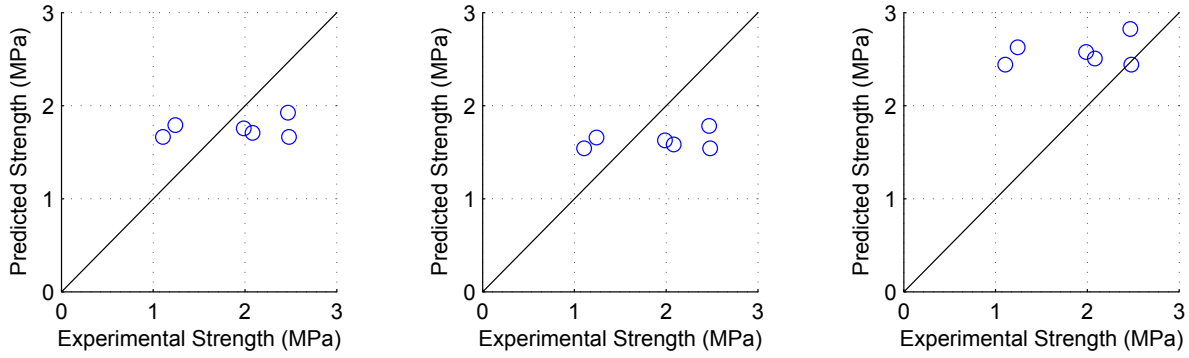

(g) NZS Model (h) Voon Model (i) CSA Model

Figure F.10: Model predictions for group 7

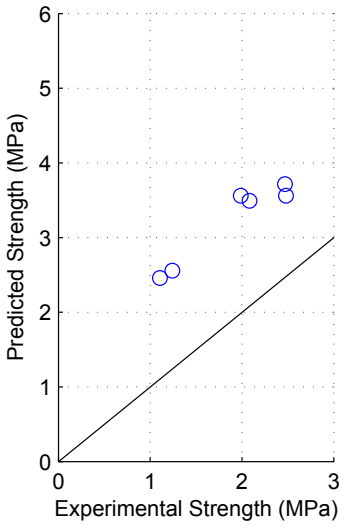

(j) TCCMaR Model

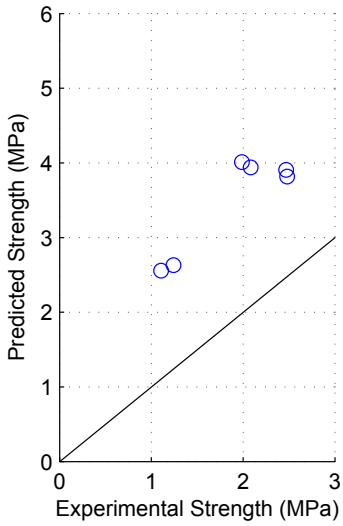

(k) UBC Model

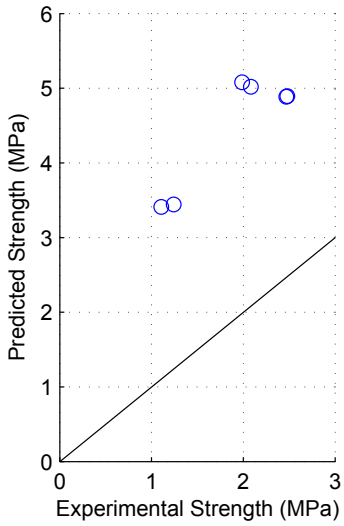

(l) AS Model

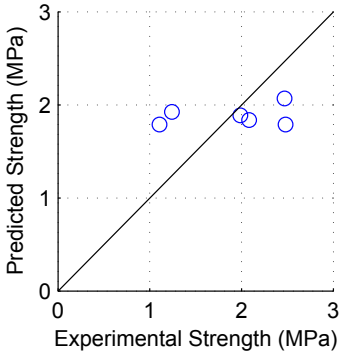

(m) MSJC Model

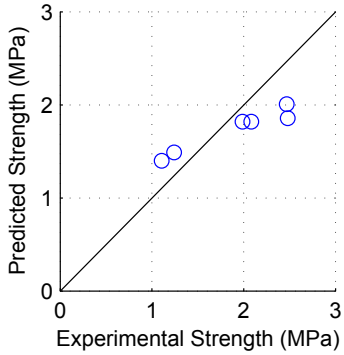

(n) BYU Model

Model predictions for group 7 (Continued)

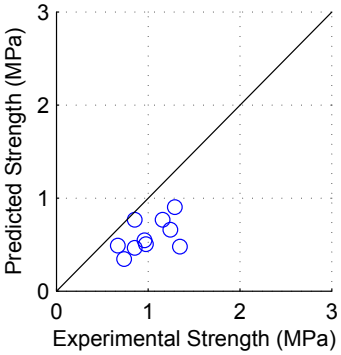

(a) Matsumura Model

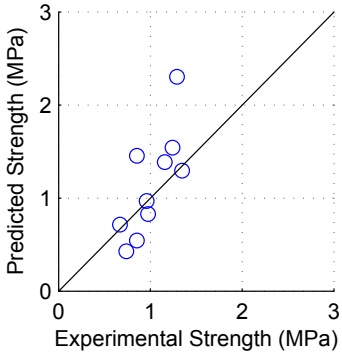

(b) AIJ Model

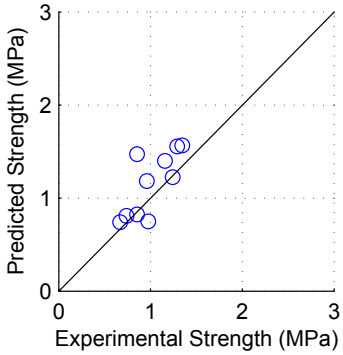

(c) Blondet Model

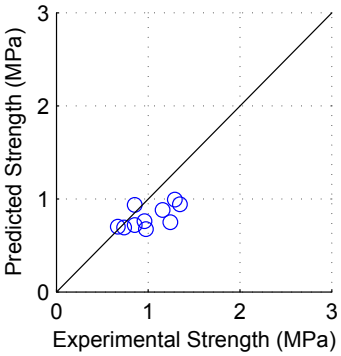

(d) Shing Model

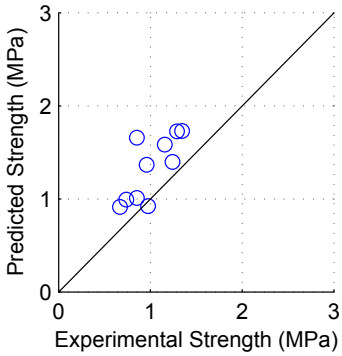

(e) Anderson Model

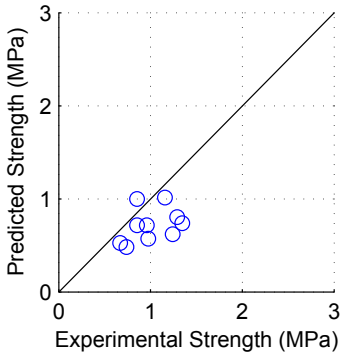

(f) Fattal Model

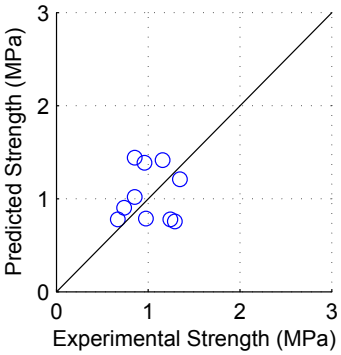

(g) NZS Model

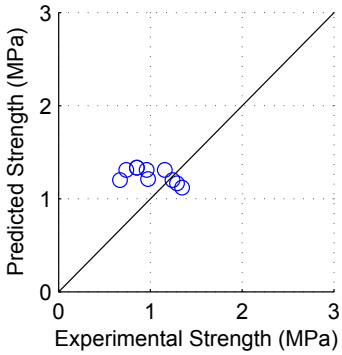

(h) Voon Model

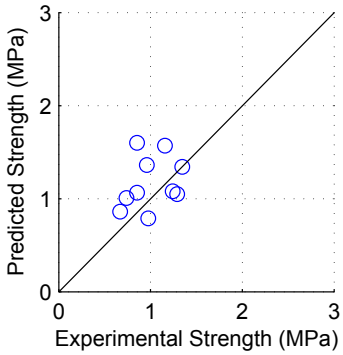

(i) CSA Model

Figure F.11: Model predictions for group 8

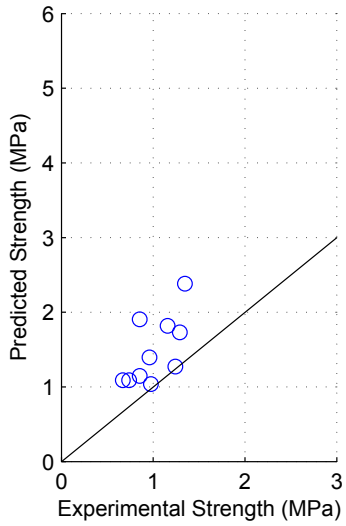

(j) TCCMaR Model

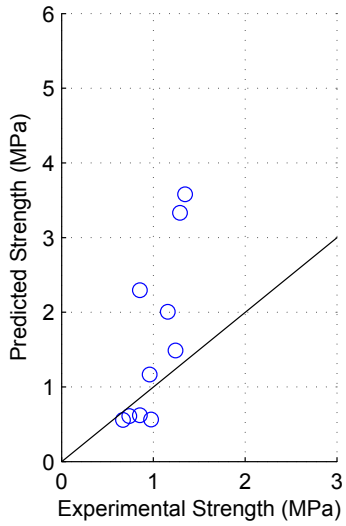

(k) UBC Model

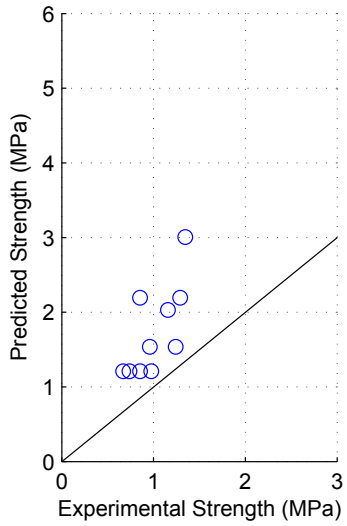

(l) AS Model

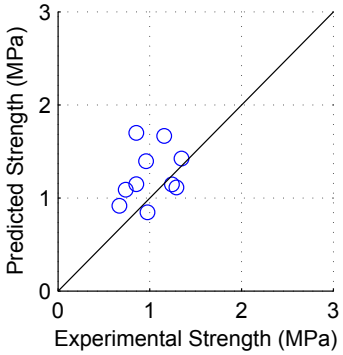

(m) MSJC Model

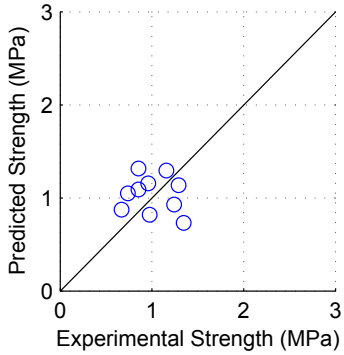

(n) BYU Model

Model predictions for group 8 (Continued)

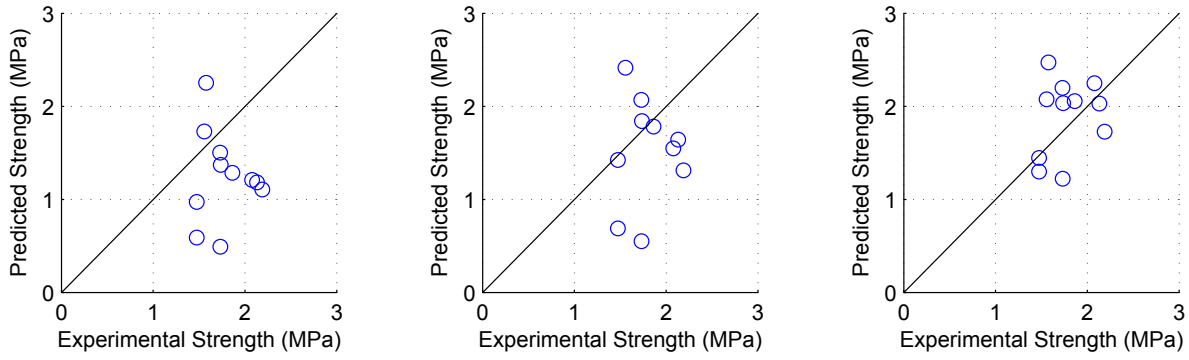

(a) Matsumura Model (b) AIJ Model (c) Blondet Model

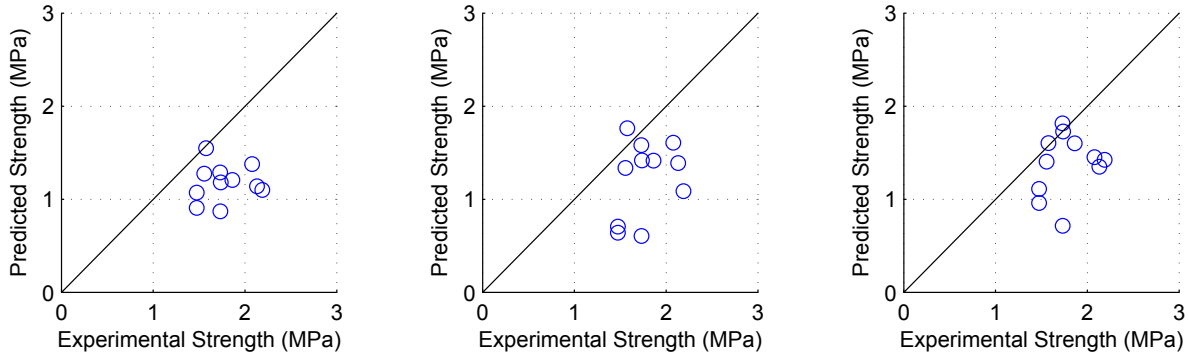

(d) Shing Model (e) Anderson Model (f) Fattal Model

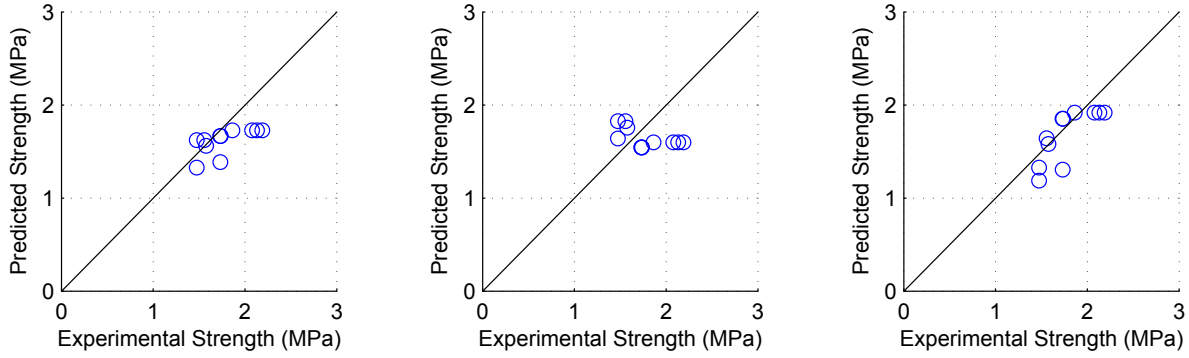

(g) NZS Model (h) Voon Model (i) CSA Model

Figure F.12: Model predictions for group 9

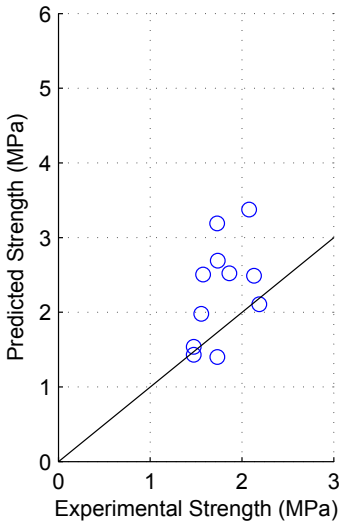

(j) TCCMaR Model

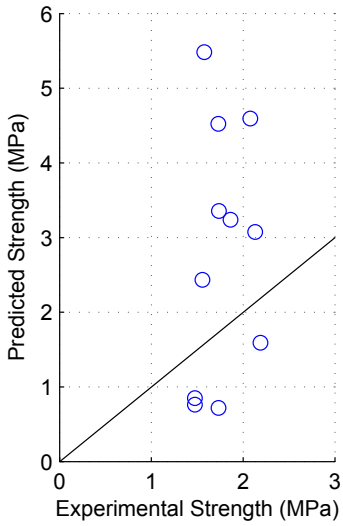

(k) UBC Model

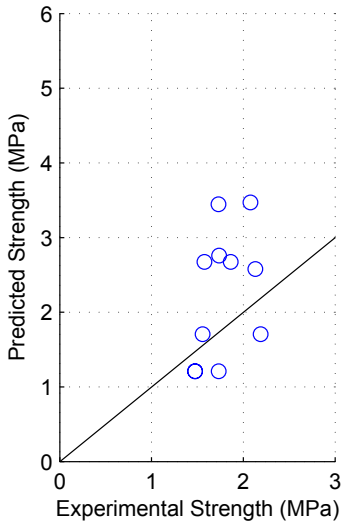

(l) AS Model

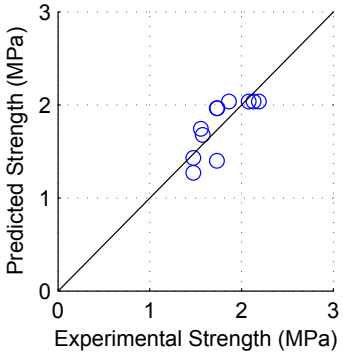

(m) MSJC Model

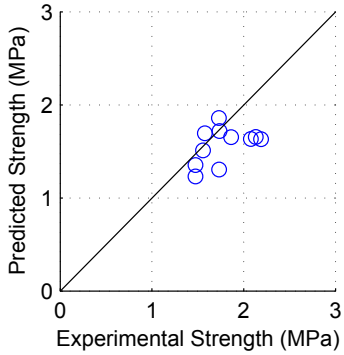

(n) BYU Model

Model predictions for group 9 (Continued)

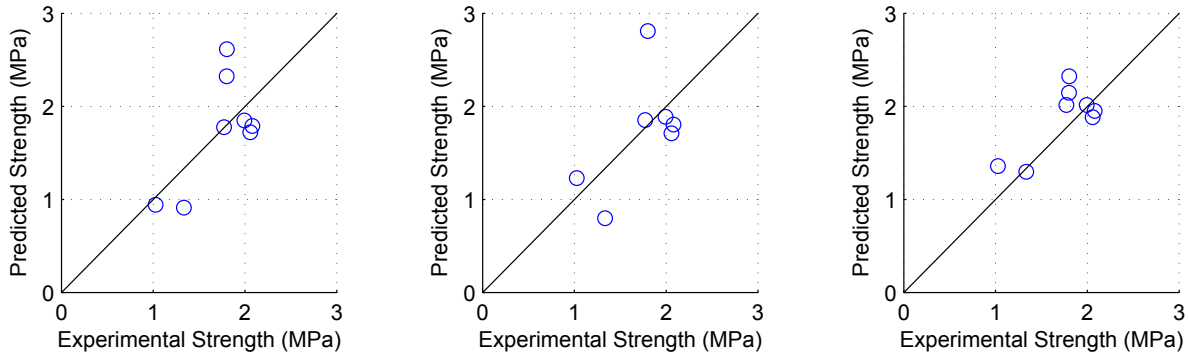

(a) Matsumura Model (b) AIJ Model (c) Blondet Model

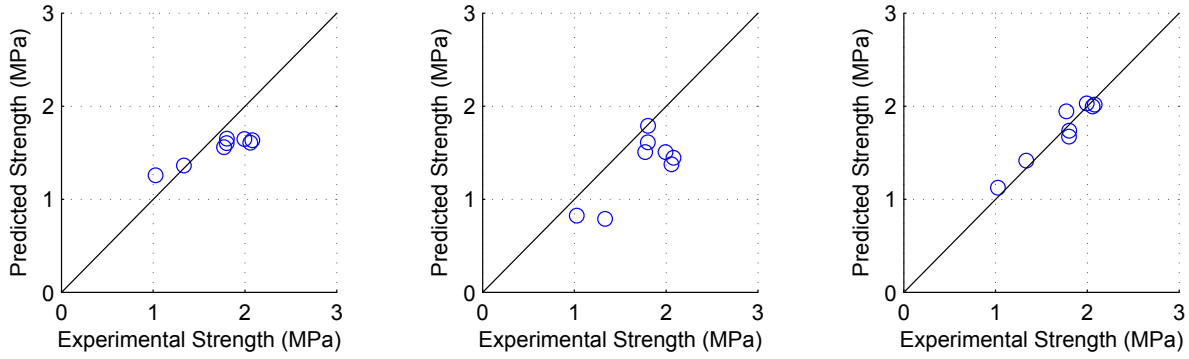

(d) Shing Model (e) Anderson Model (f) Fattal Model

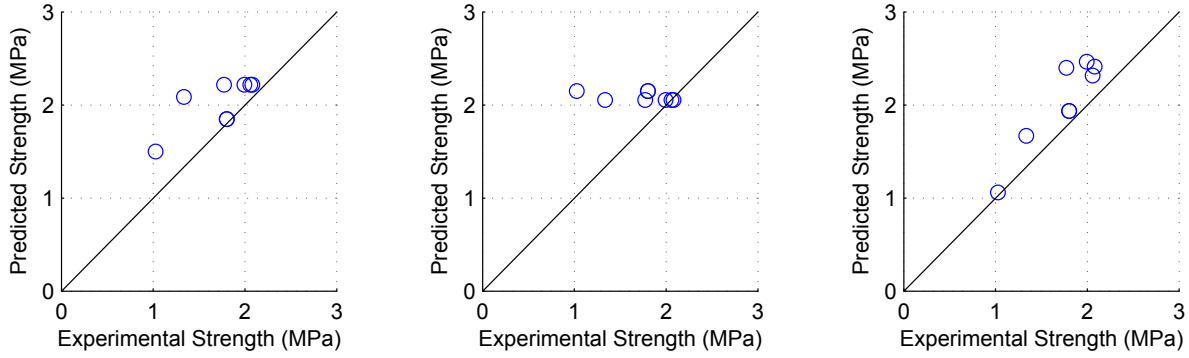

(g) NZS Model (h) Voon Model (i) CSA Model

Figure F.13: Model predictions for group 10

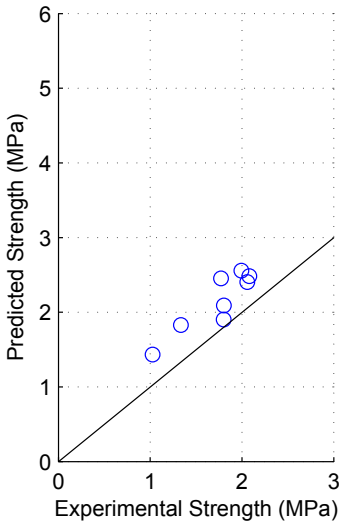

(j) TCCMaR Model

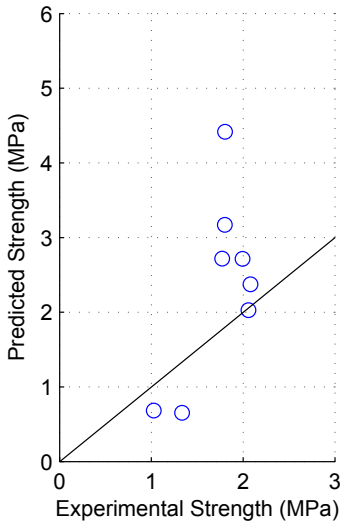

(k) UBC Model

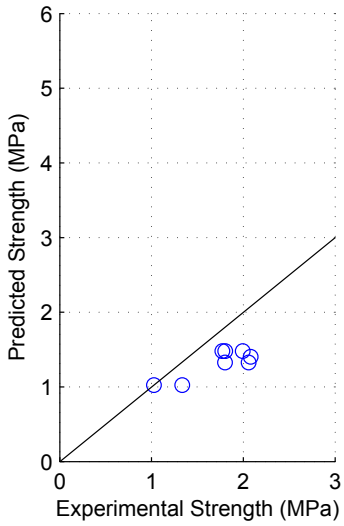

(l) AS Model

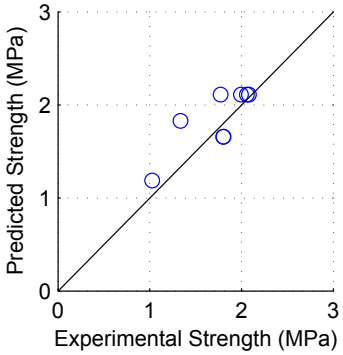

(m) MSJC Model

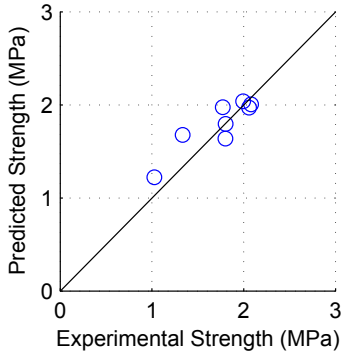

(n) BYU Model

Model predictions for group 10 (Continued)

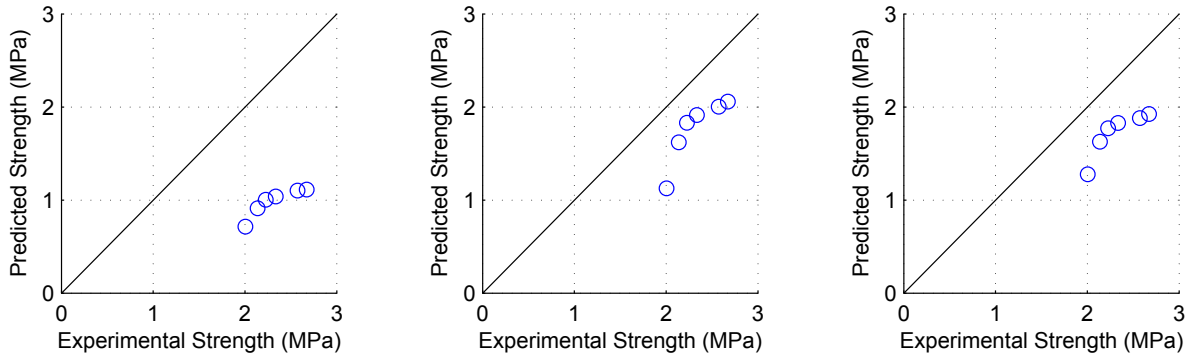

(a) Matsumura Model (b) AIJ Model (c) Blondet Model

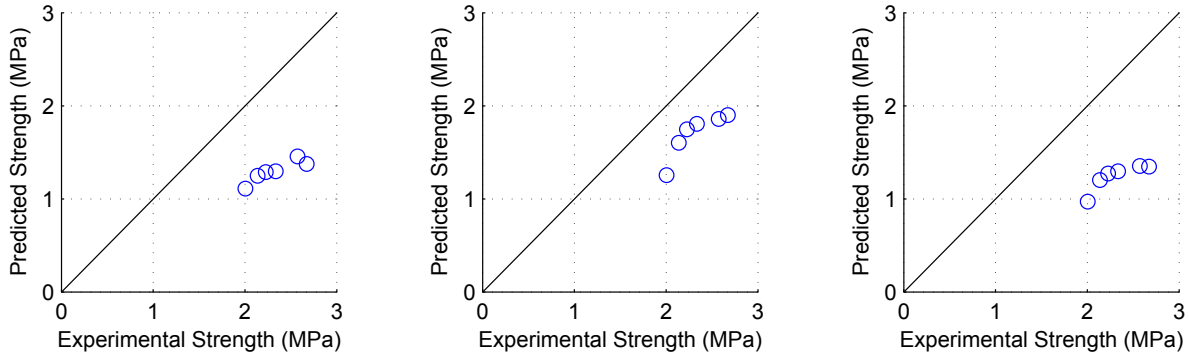

(d) Shing Model (e) Anderson Model (f) Fattal Model

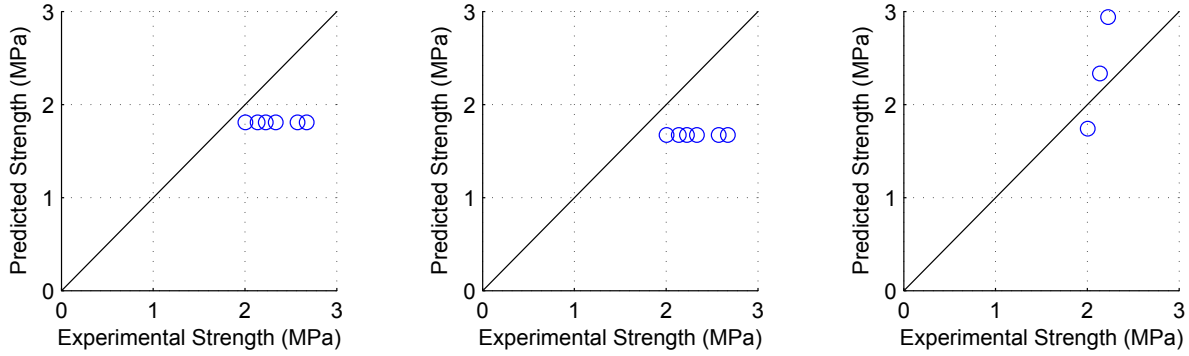

(g) NZS Model (h) Voon Model (i) CSA Model

Figure F.14: Model predictions for group 11

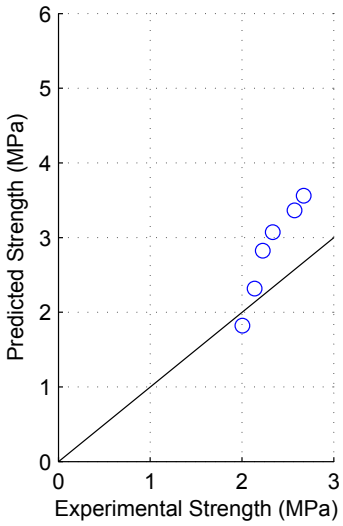

(j) TCCMaR Model

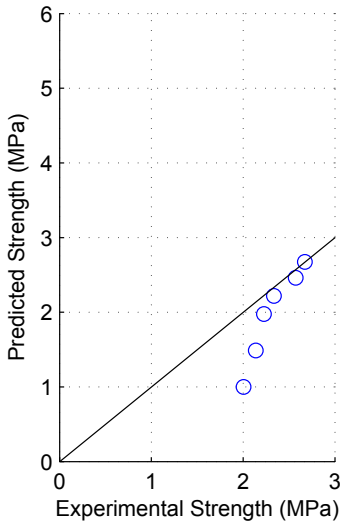

(k) UBC Model

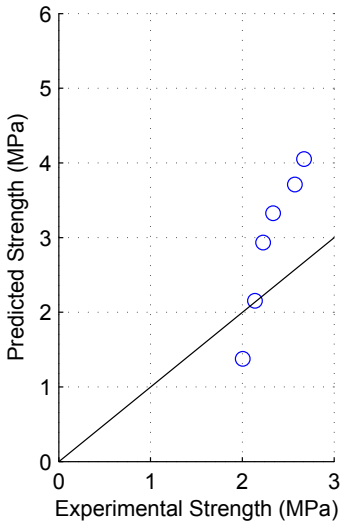

(l) AS Model

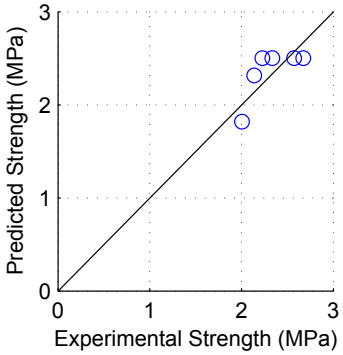

(m) MSJC Model

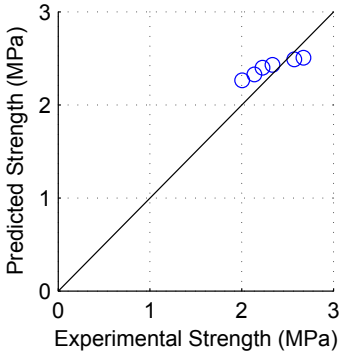

(n) BYU Model

Model predictions for group 11 (Continued)

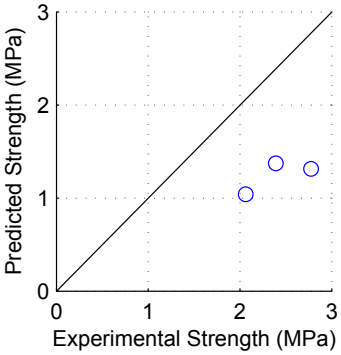

(a) Matsumura Model

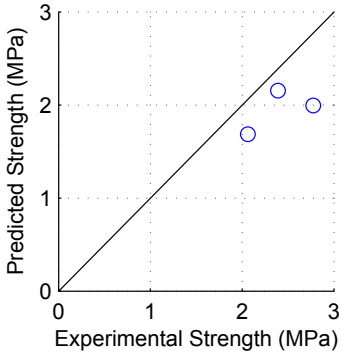

(b) AIJ Model

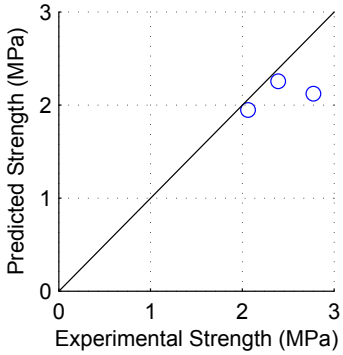

(c) Blondet Model

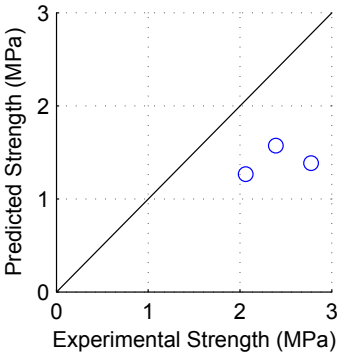

(d) Shing Model

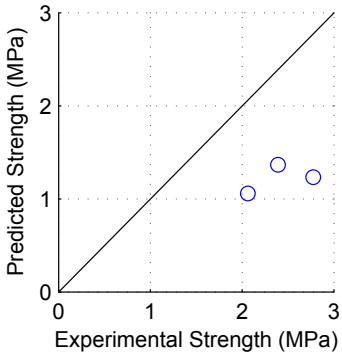

(e) Anderson Model

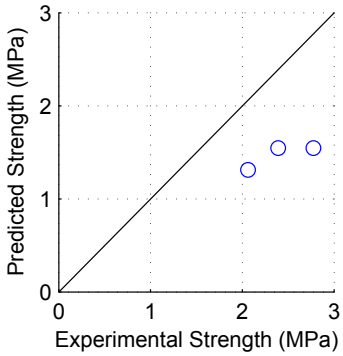

(f) Fattal Model

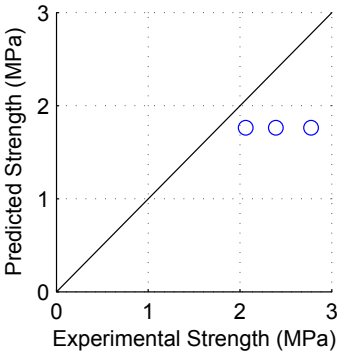

(g) NZS Model

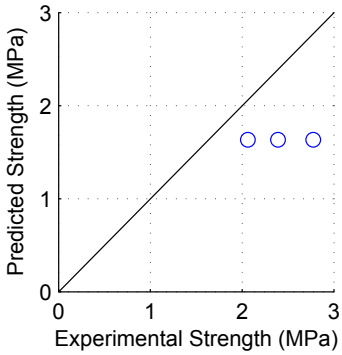

(h) Voon Model

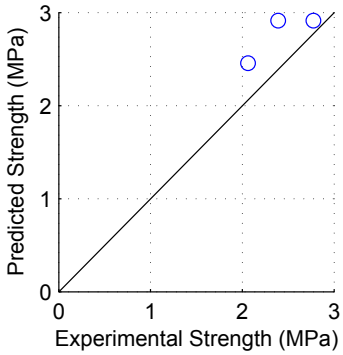

(i) CSA Model

Figure F.15: Model predictions for group 12

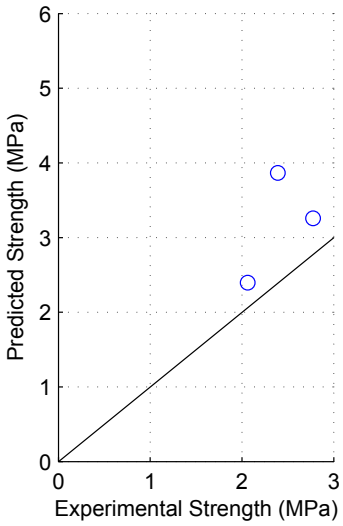

(j) TCCMaR Model

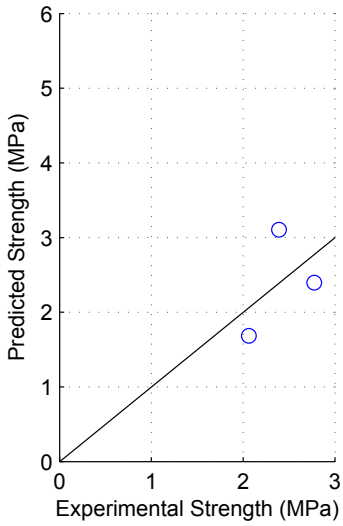

(k) UBC Model

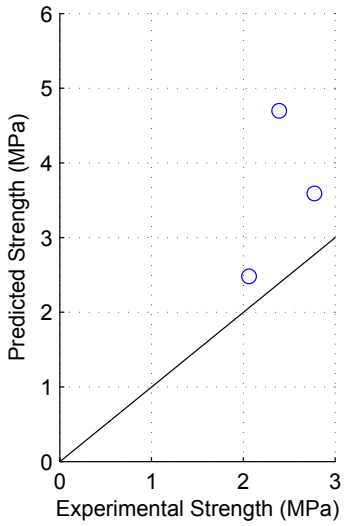

(l) AS Model

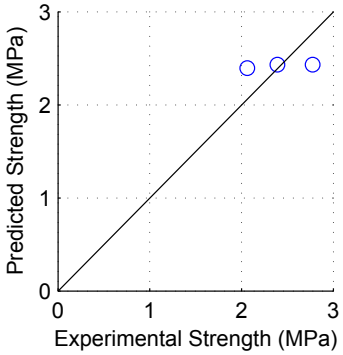

(m) MSJC Model

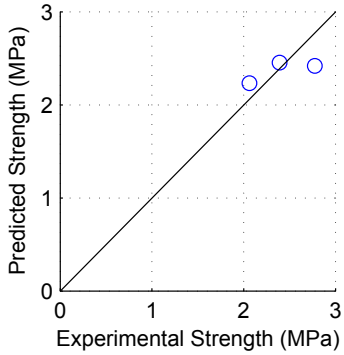

(n) BYU Model

Model predictions for group 12 (Continued)

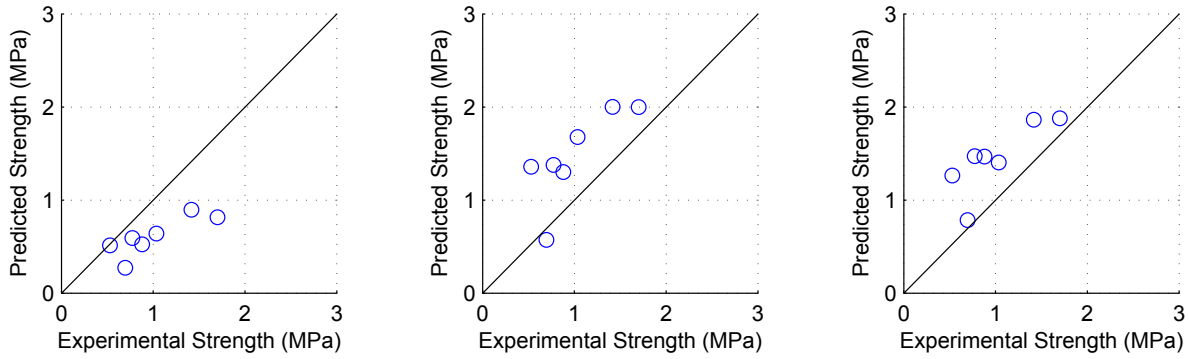

(a) Matsumura Model

(b) AIJ Model

(c) Blondet Model

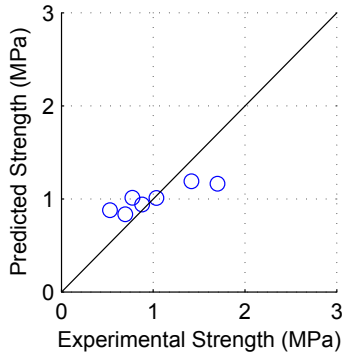

(d) Shing Model

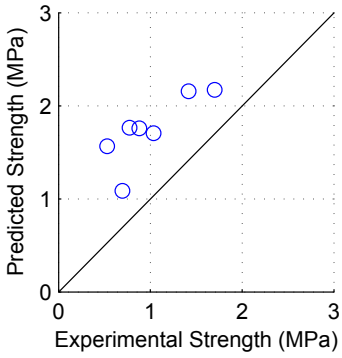

(e) Anderson Model

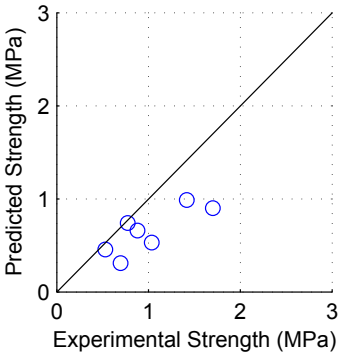

(f) Fattal Model

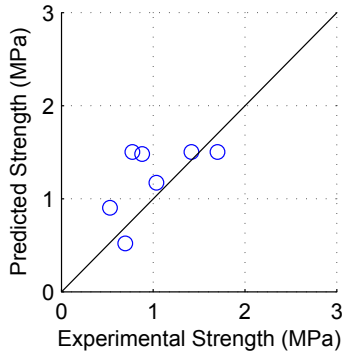

(g) NZS Model

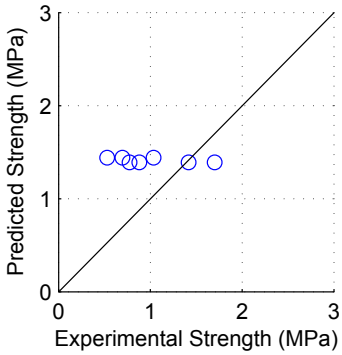

(h) Voon Model

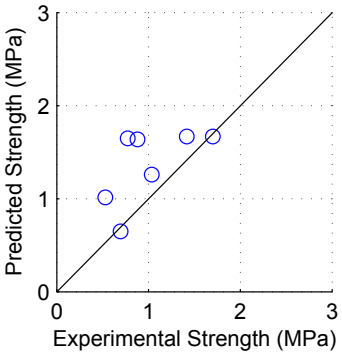

(i) CSA Model

Figure F.16: Model predictions for group 13

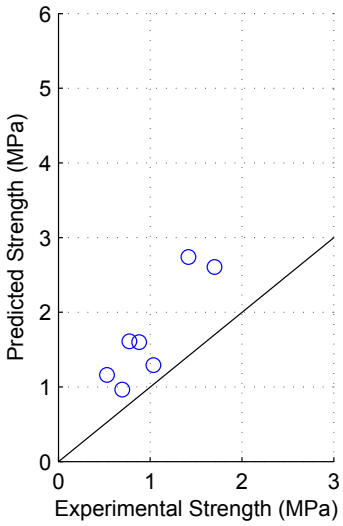

(j) TCCMaR Model

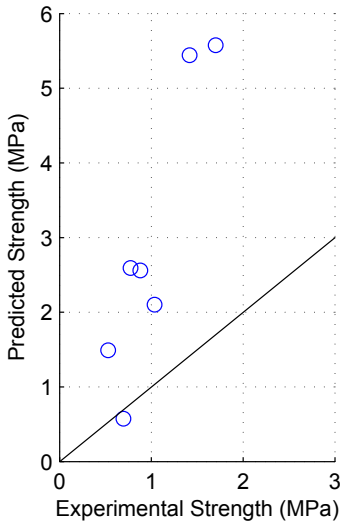

(k) UBC Model

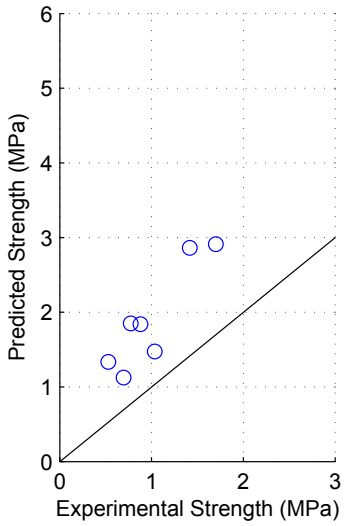

(l) AS Model

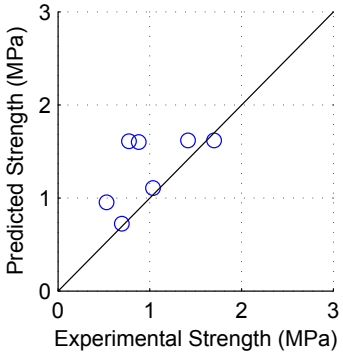

(m) MSJC Model

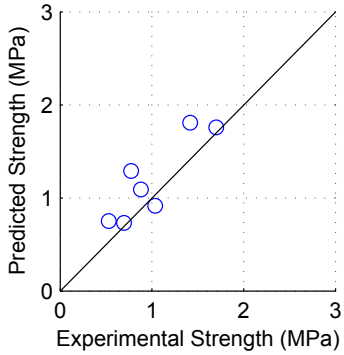

(n) BYU Model

Model predictions for group 13 (Continued)

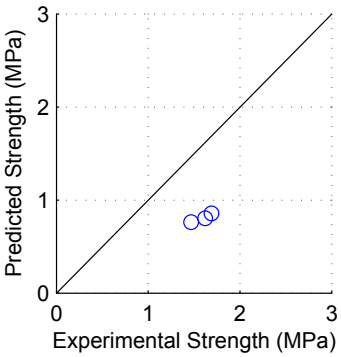

(a) Matsumura Model

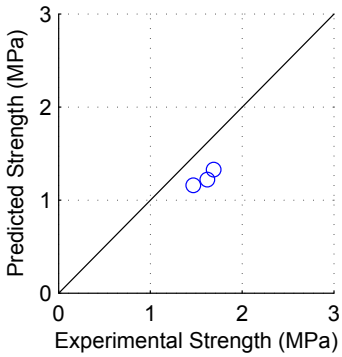

(b) AIJ Model

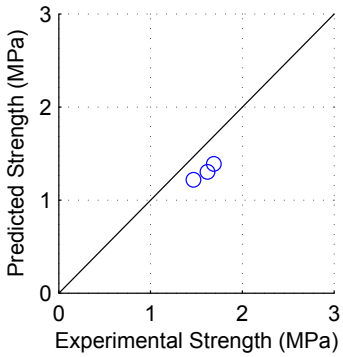

(c) Blondet Model

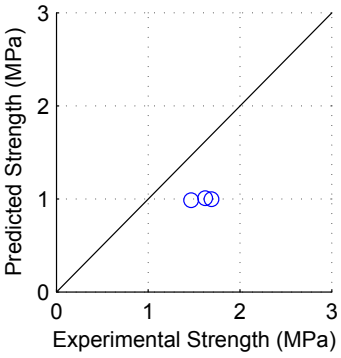

(d) Shing Model

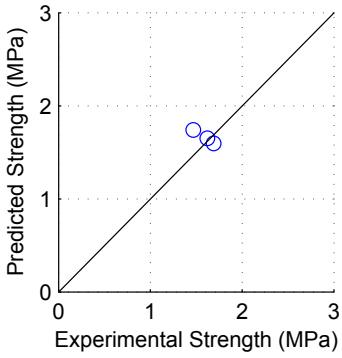

(e) Anderson Model

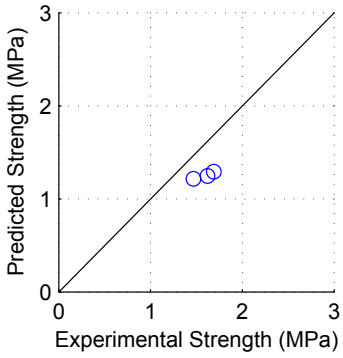

(f) Fattal Model

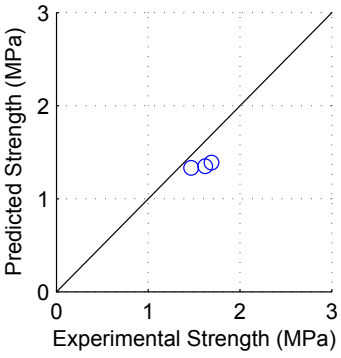

(g) NZS Model

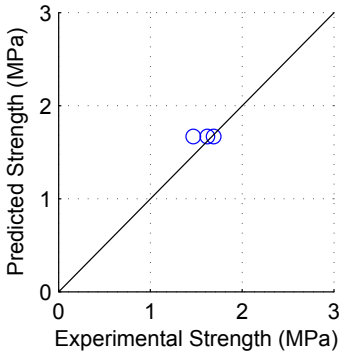

(h) Voon Model

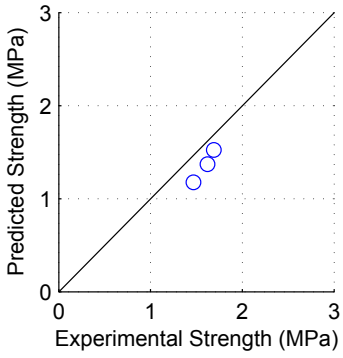

(i) CSA Model

Figure F.17: Model predictions for group 14

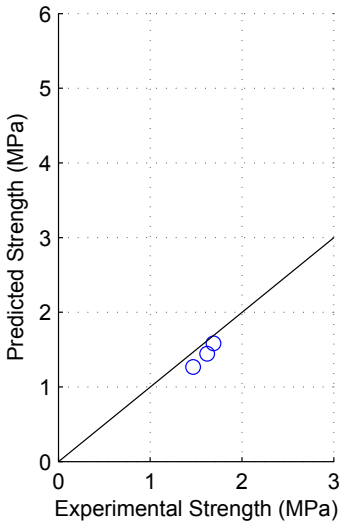

(j) TCCMaR Model

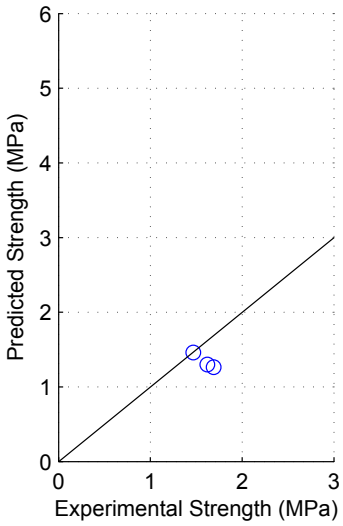

(k) UBC Model

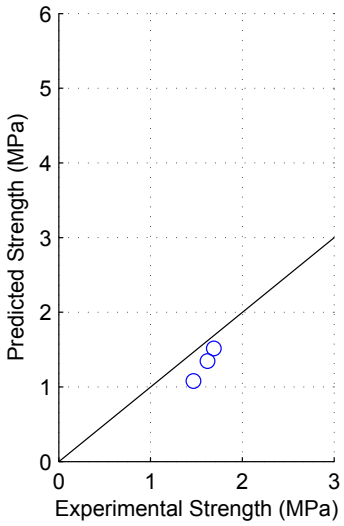

(l) AS Model

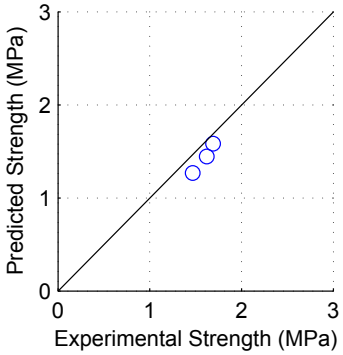

(m) MSJC Model

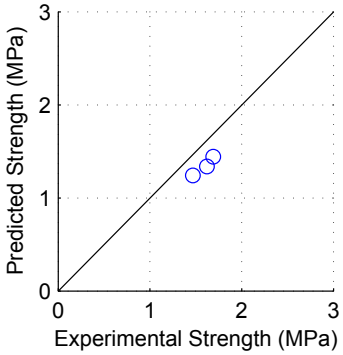

(n) BYU Model

Model predictions for group 14 (Continued)

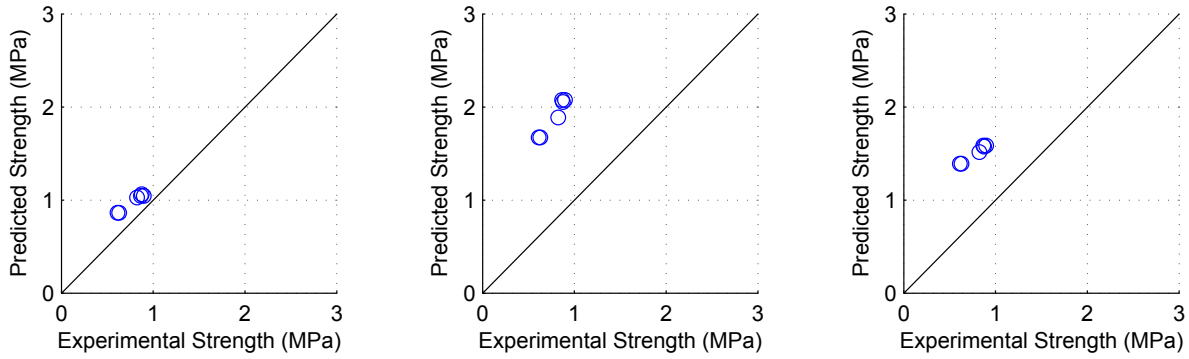

(a) Matsumura Model (b) AIJ Model (c) Blondet Model

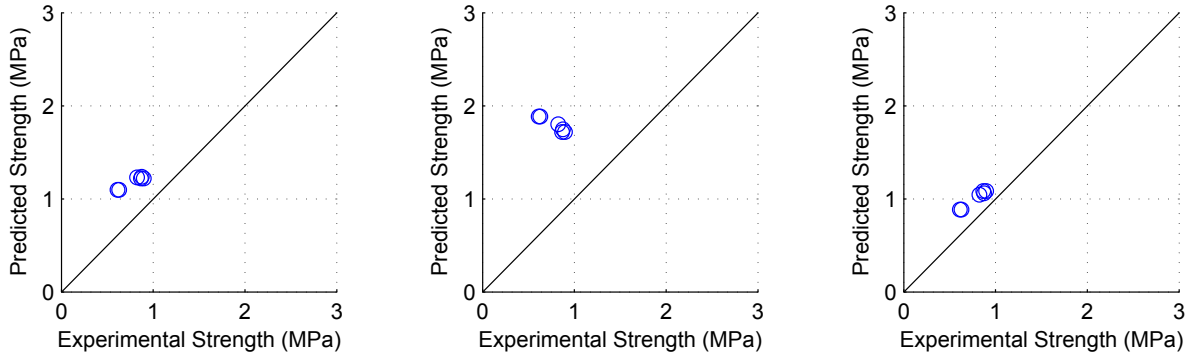

(d) Shing Model (e) Anderson Model (f) Fattal Model

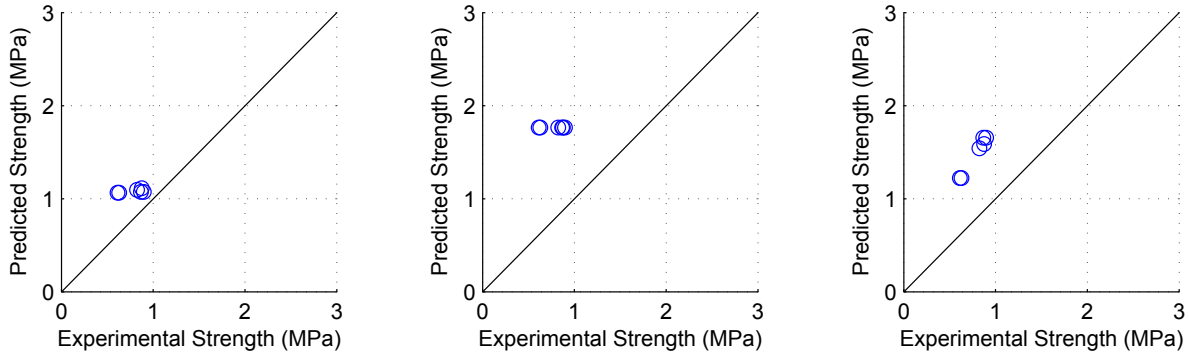

(g) NZS Model (h) Voon Model (i) CSA Model

Figure F.18: Model predictions for group 15

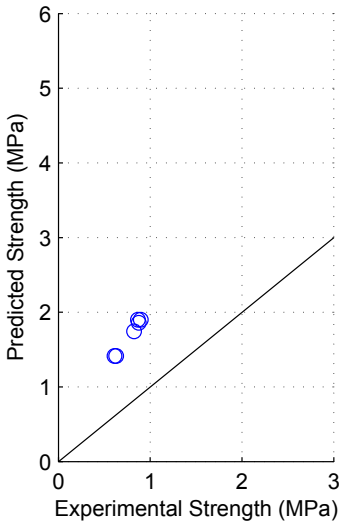

(j) TCCMaR Model

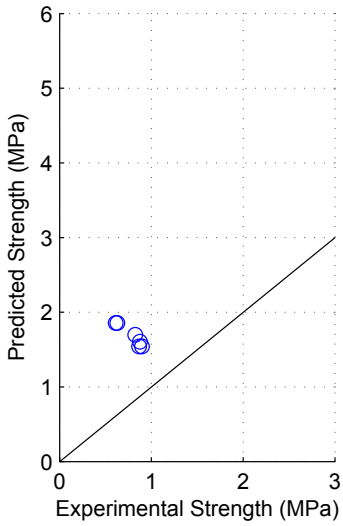

(k) UBC Model

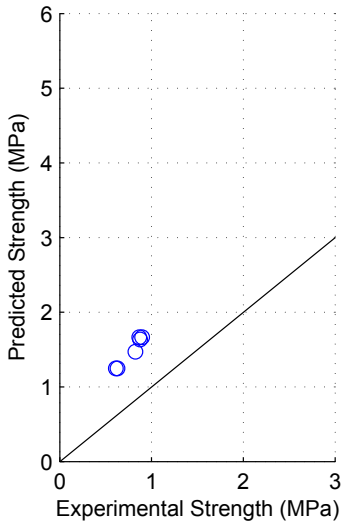

(l) AS Model

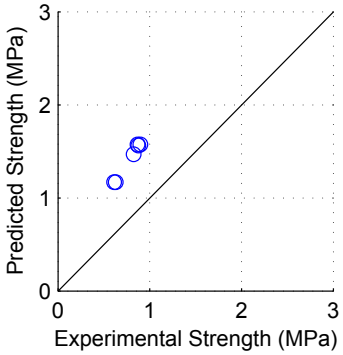

(m) MSJC Model

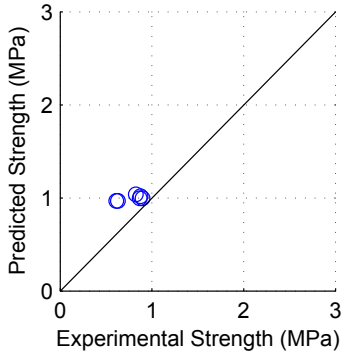

(n) BYU Model

Model predictions for group 15 (Continued)

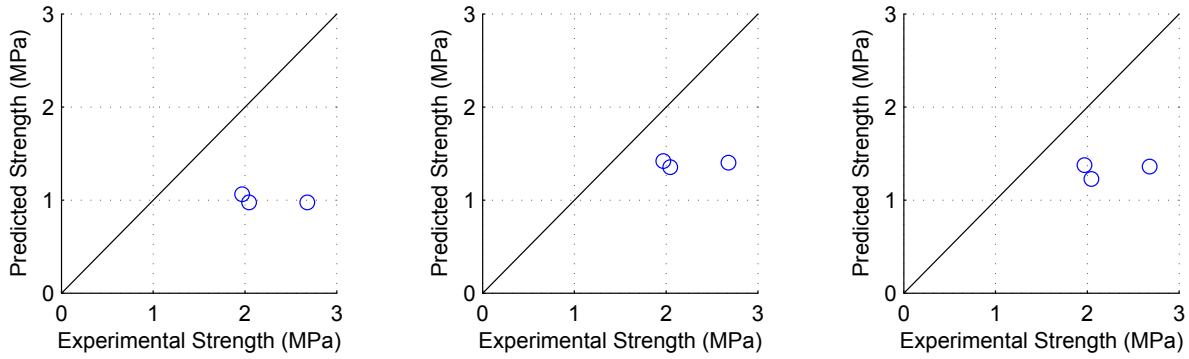

(a) Matsumura Model (b) AIJ Model (c) Blondet Model

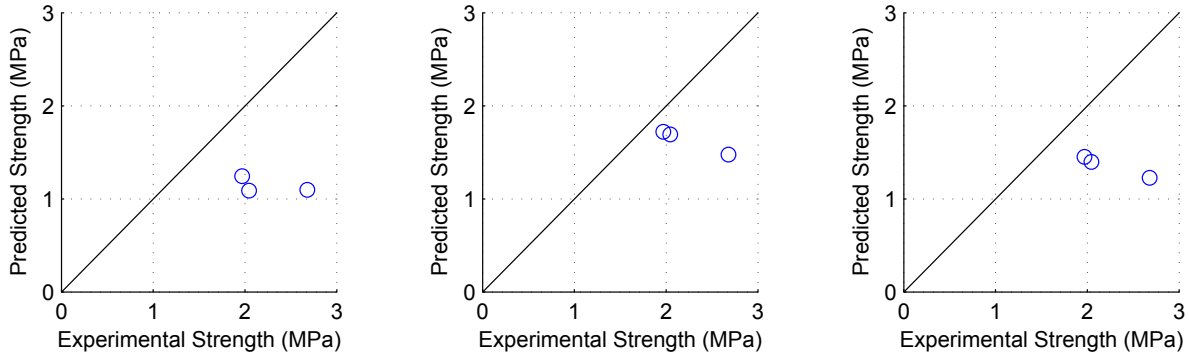

(d) Shing Model (e) Anderson Model (f) Fattal Model

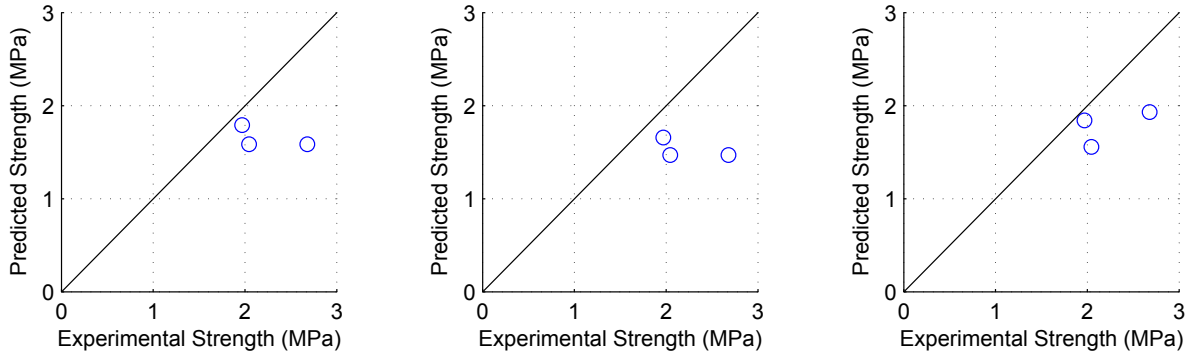

(g) NZS Model (h) Voon Model (i) CSA Model

Figure F.19: Model predictions for group 16

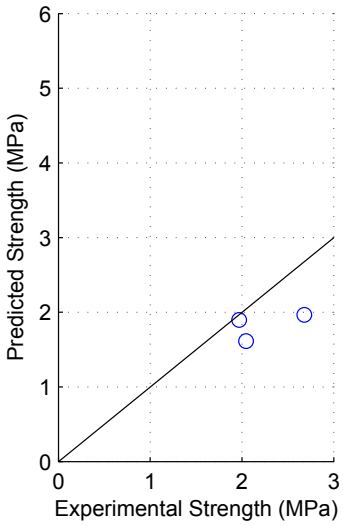

(j) TCCMaR Model

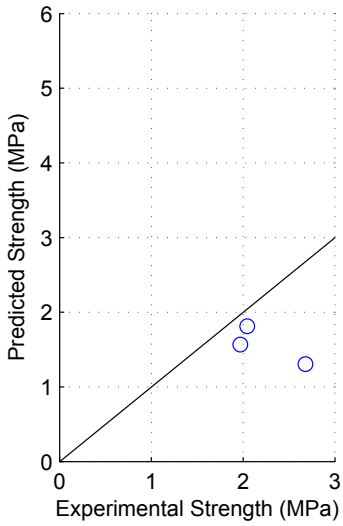

(k) UBC Model

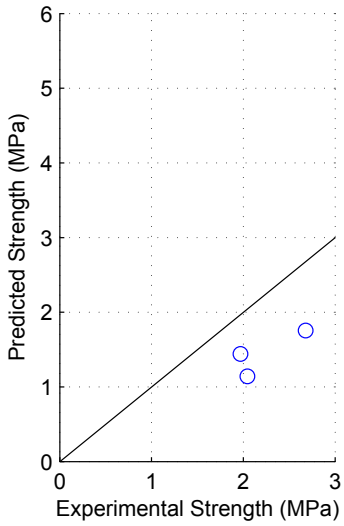

(l) AS Model

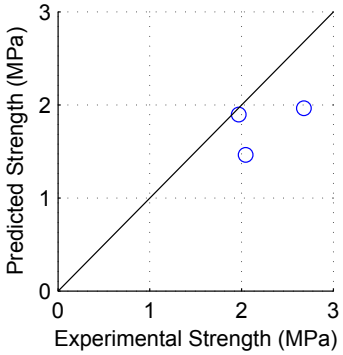

(m) MSJC Model

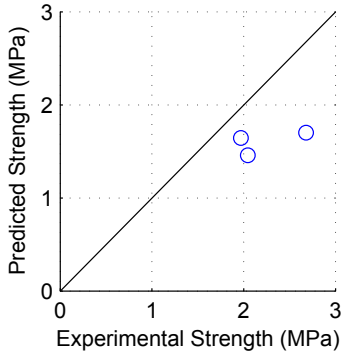

(n) BYU Model

Model predictions for group 16 (Continued)

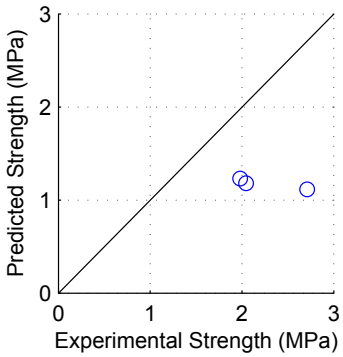

(a) Matsumura Model

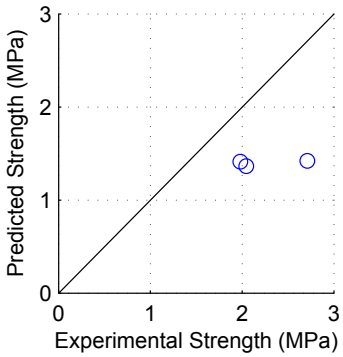

(b) AIJ Model

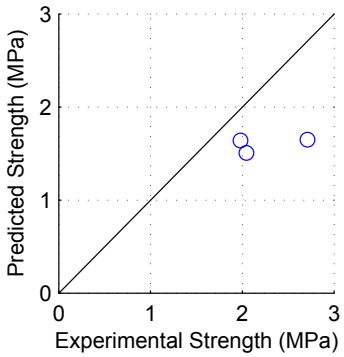

(c) Blondet Model

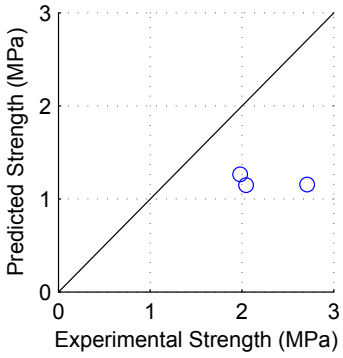

(d) Shing Model

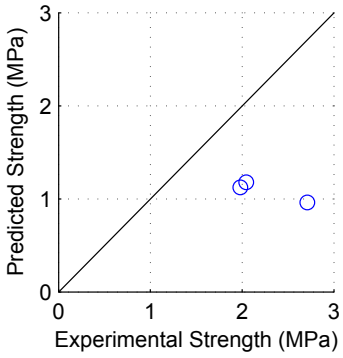

(e) Anderson Model

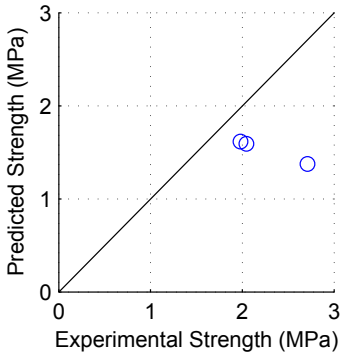

(f) Fattal Model

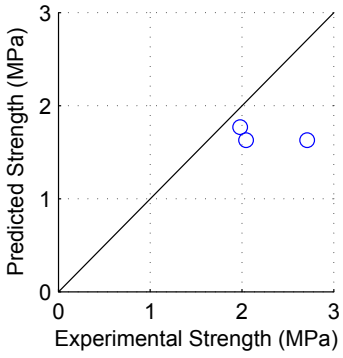

(g) NZS Model

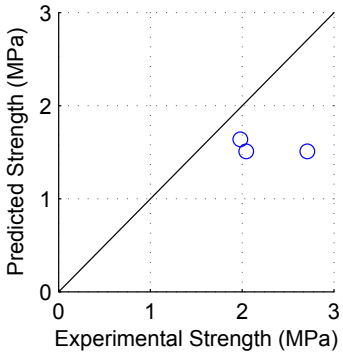

(h) Voon Model

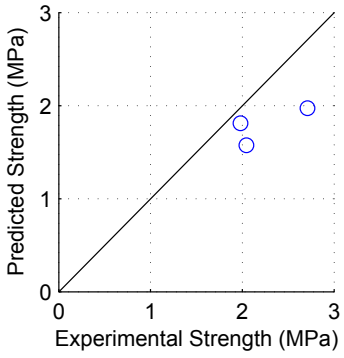

(i) CSA Model

Figure F.20: Model predictions for group 17

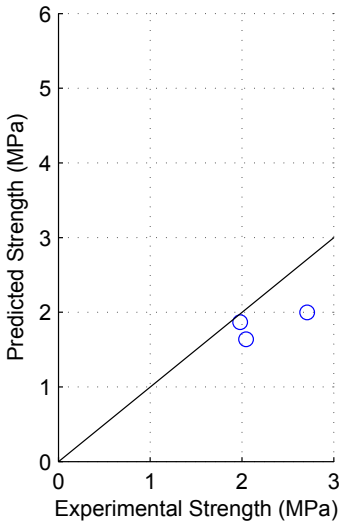

(j) TCCMaR Model

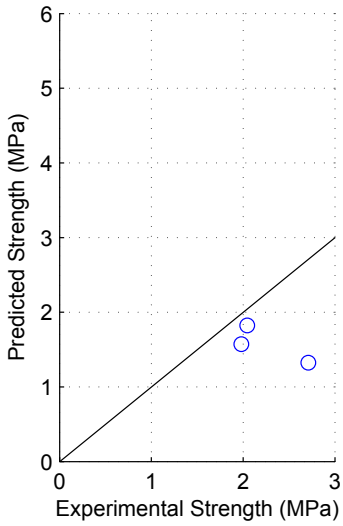

(k) UBC Model

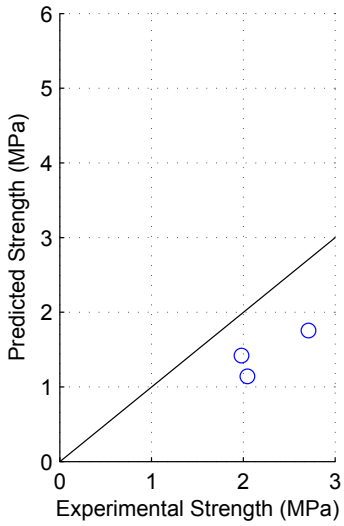

(l) AS Model

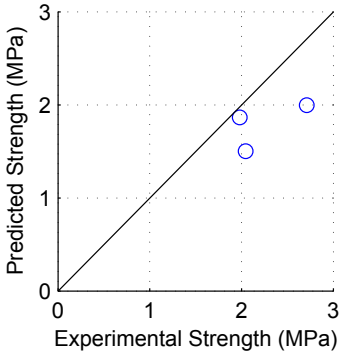

(m) MSJC Model

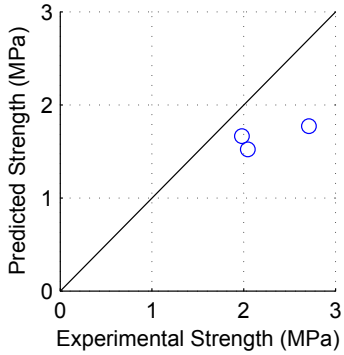

(n) BYU Model

Model predictions for group 17 (Continued)

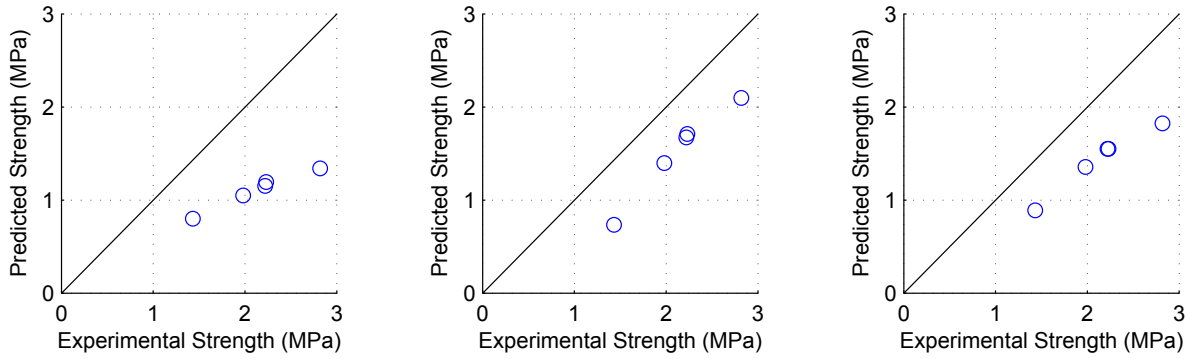

(a) Matsumura Model (b) AIJ Model (c) Blondet Model

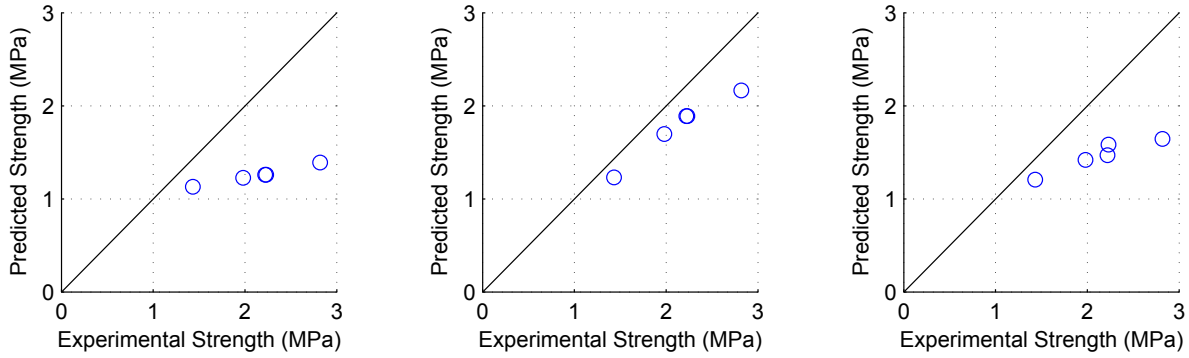

(d) Shing Model (e) Anderson Model (f) Fattal Model

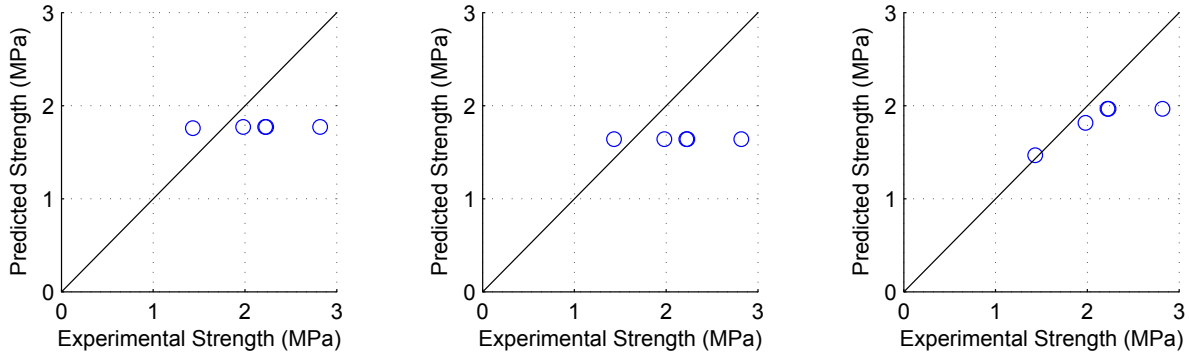

(g) NZS Model (h) Voon Model (i) CSA Model

Figure F.21: Model predictions for group 18

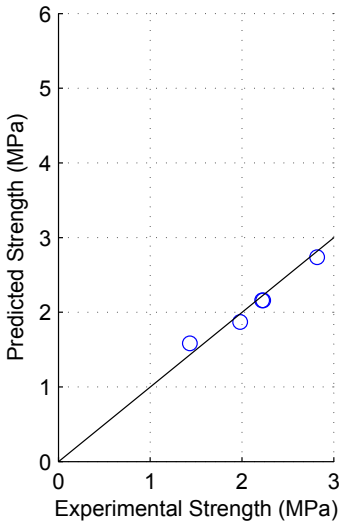

(j) TCCMaR Model

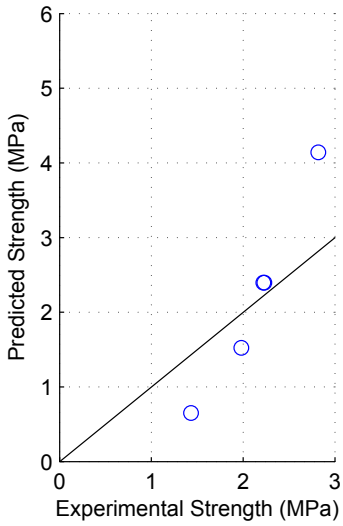

(k) UBC Model

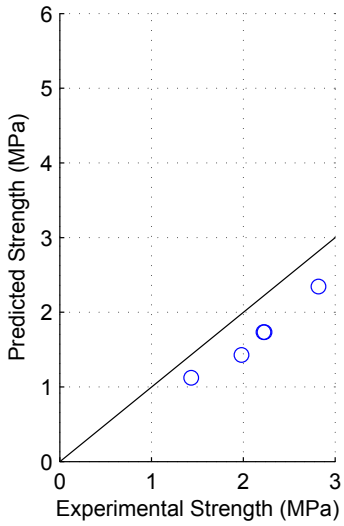

(l) AS Model

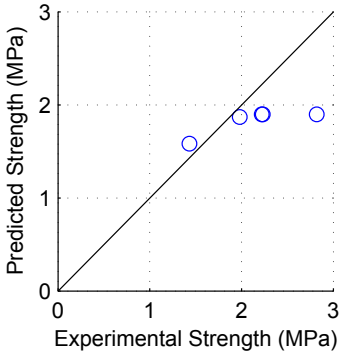

(m) MSJC Model

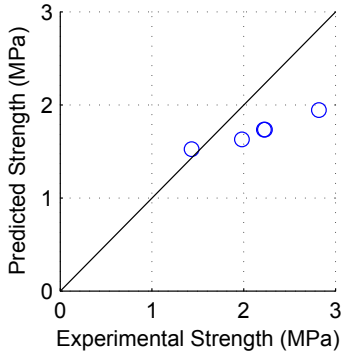

(n) BYU Model

Model predictions for group 18 (Continued)

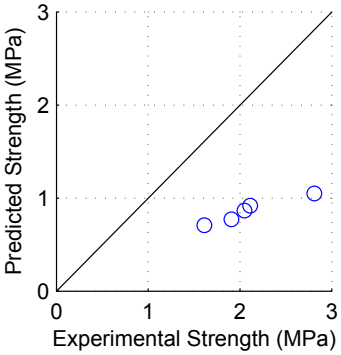

(a) Matsumura Model

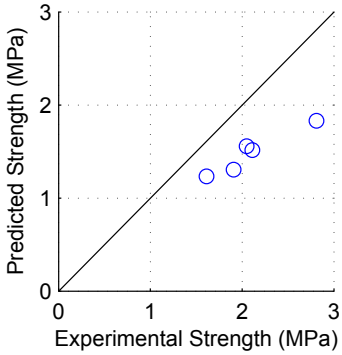

(b) AIJ Model

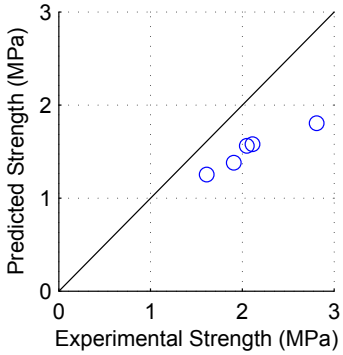

(c) Blondet Model

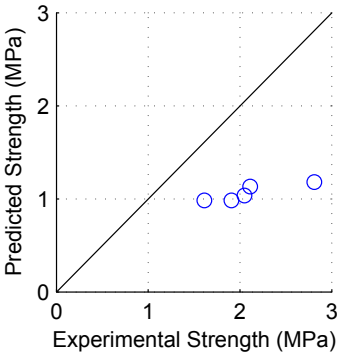

(d) Shing Model

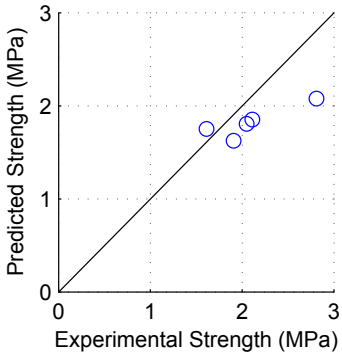

(e) Anderson Model

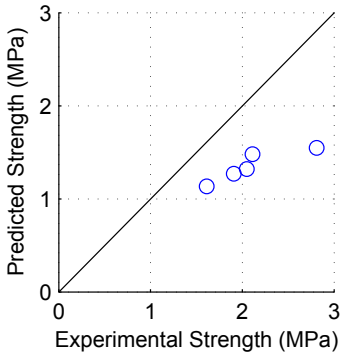

(f) Fattal Model

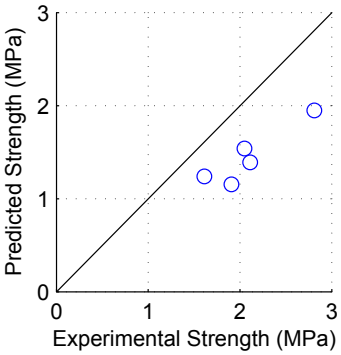

(g) NZS Model

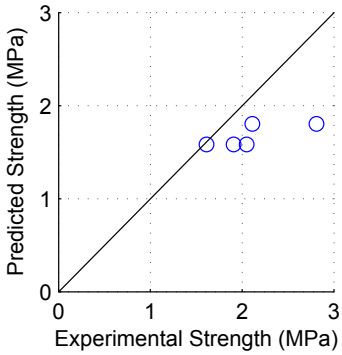

(h) Voon Model

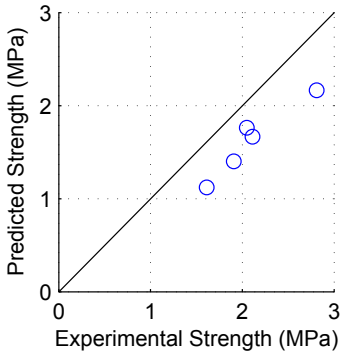

(i) CSA Model

Figure F.22: Model predictions for group 19

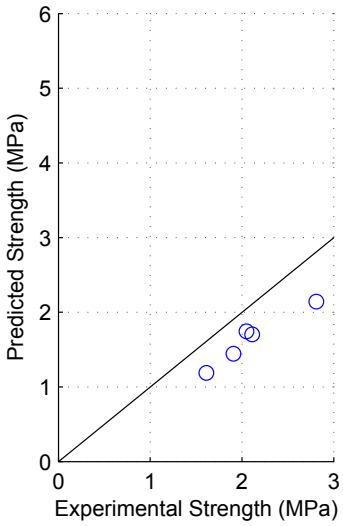

(j) TCCMaR Model

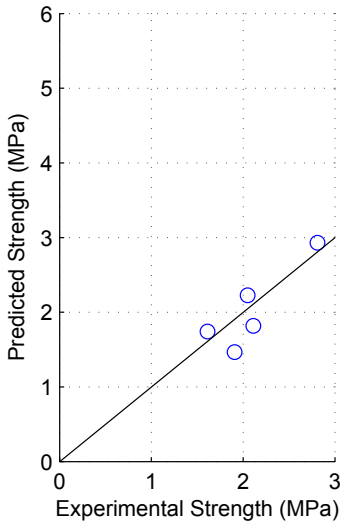

(k) UBC Model

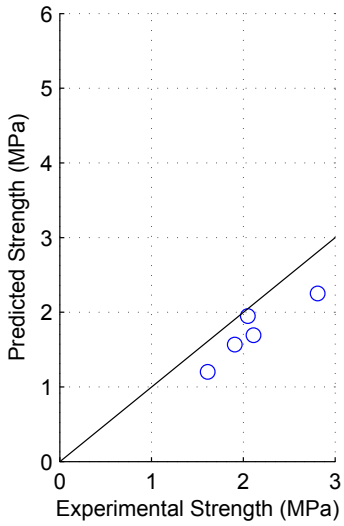

(l) AS Model

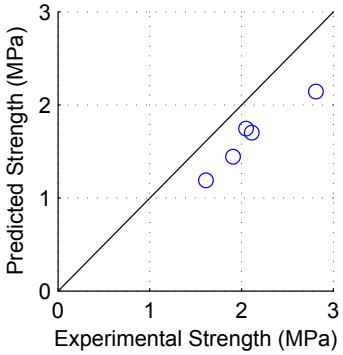

(m) MSJC Model

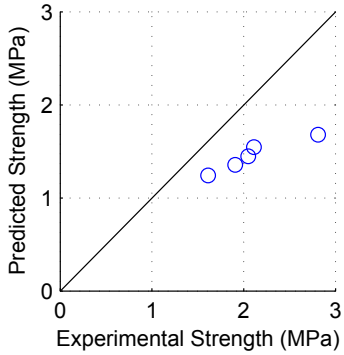

(n) BYU Model

Model predictions for group 19 (Continued)

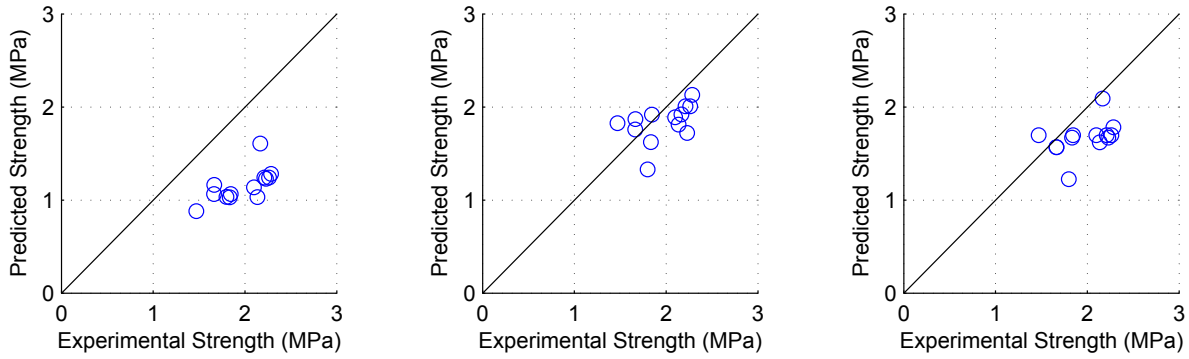

(a) Matsumura Model (b) AIJ Model (c) Blondet Model

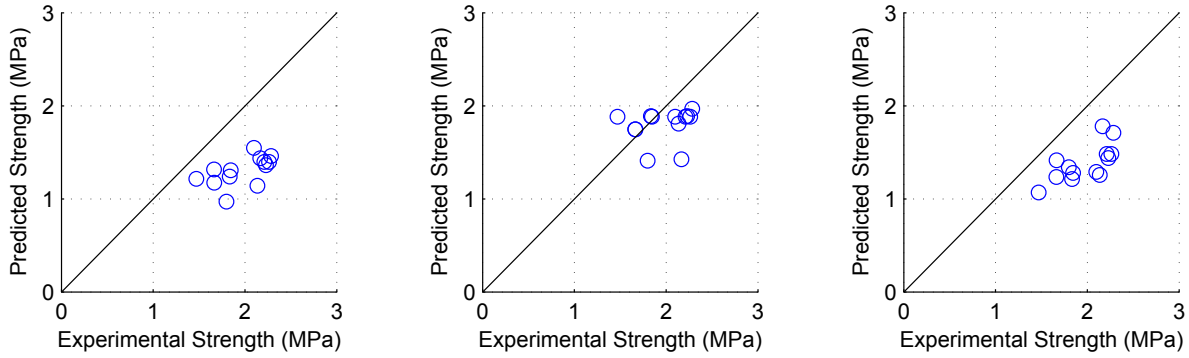

(d) Shing Model (e) Anderson Model (f) Fattal Model

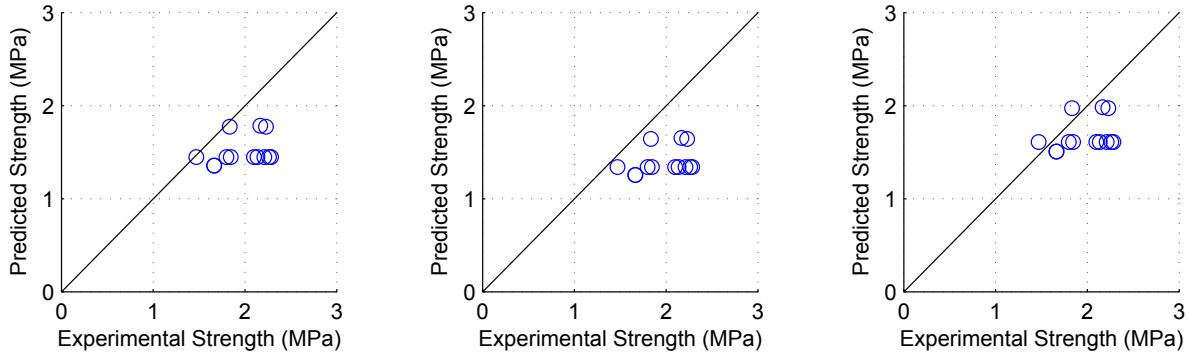

(g) NZS Model (h) Voon Model (i) CSA Model

Figure F.23: Model predictions for group 20

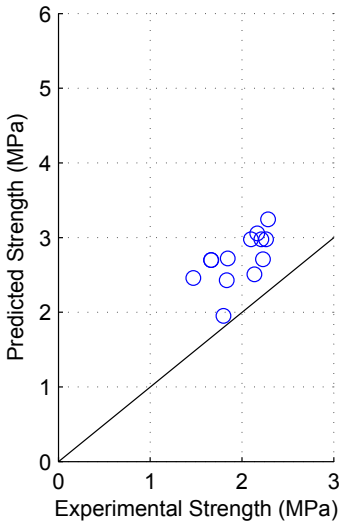

(j) TCCMaR Model

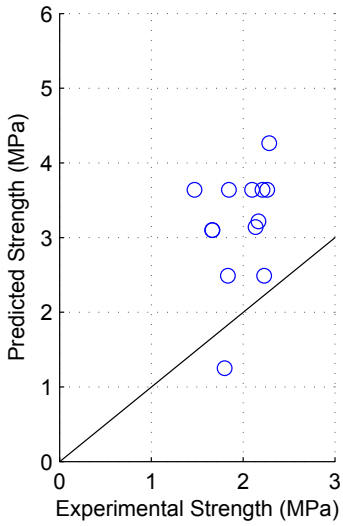

(k) UBC Model

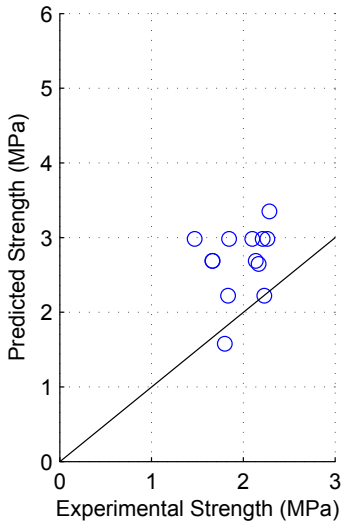

(l) AS Model

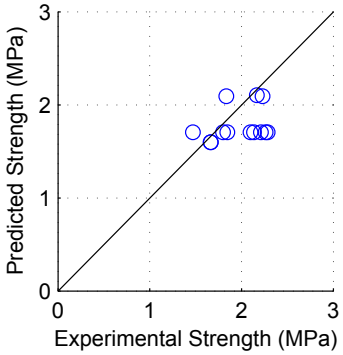

(m) MSJC Model

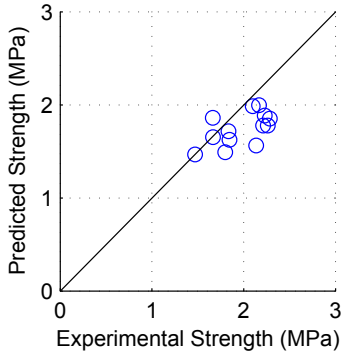

(n) BYU Model

Model predictions for group 20 (Continued)

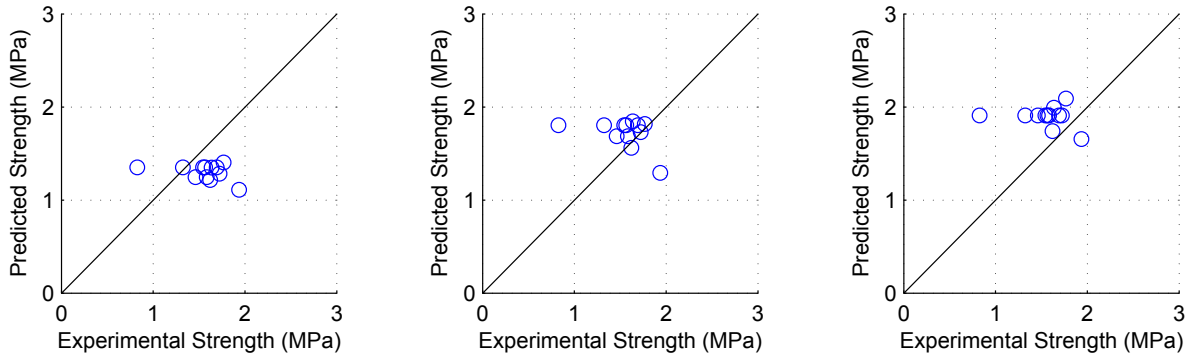

(a) Matsumura Model (b) AIJ Model (c) Blondet Model

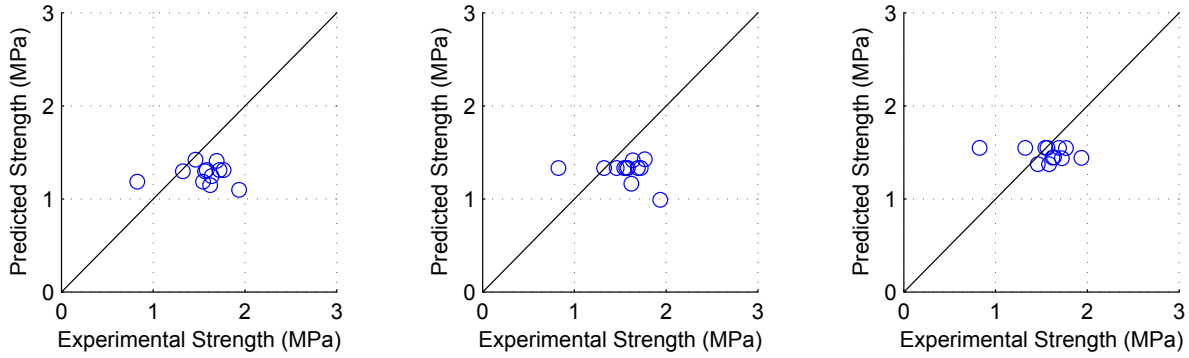

(d) Shing Model (e) Anderson Model (f) Fattal Model

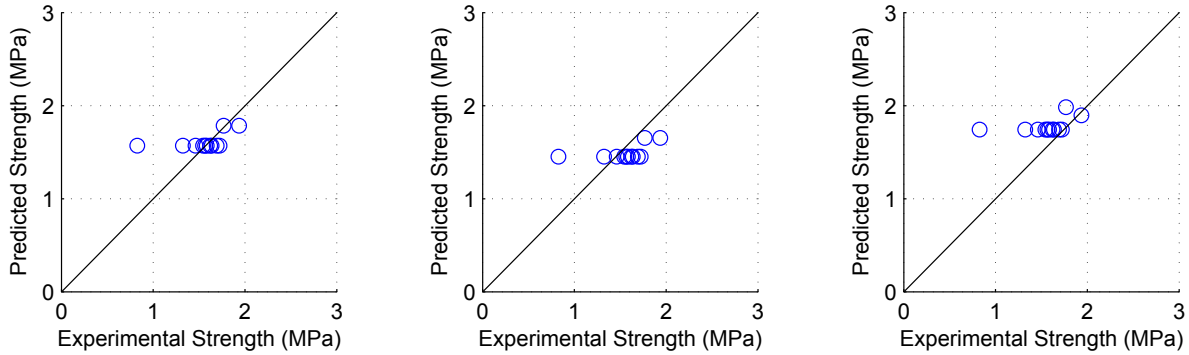

(g) NZS Model (h) Voon Model (i) CSA Model

Figure F.24: Model predictions for group 21

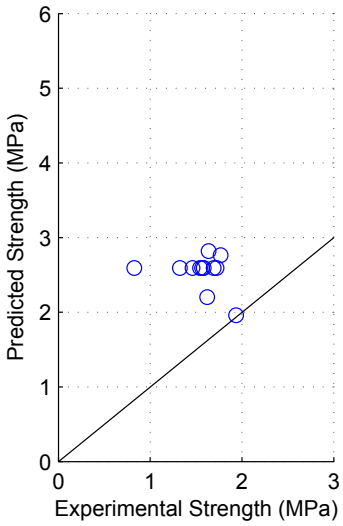

(j) TCCMaR Model

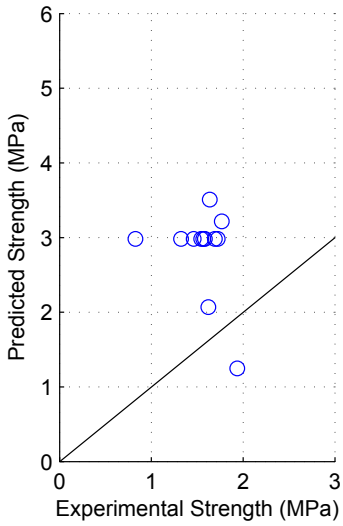

(k) UBC Model

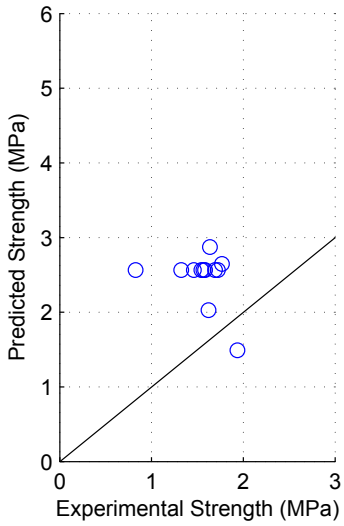

(l) AS Model

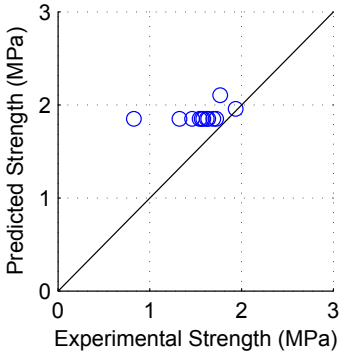

(m) MSJC Model

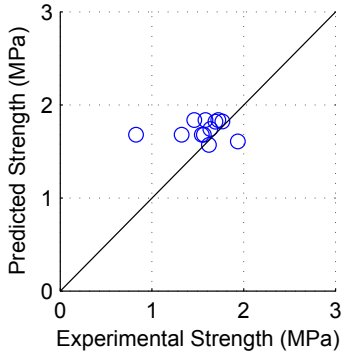

(n) BYU Model

Model predictions for group 21 (Continued)

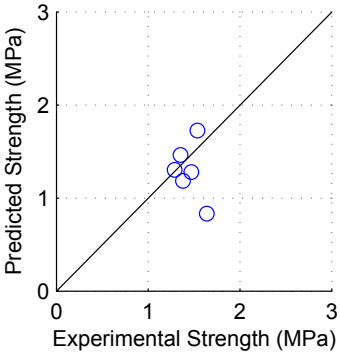

(a) Matsumura Model

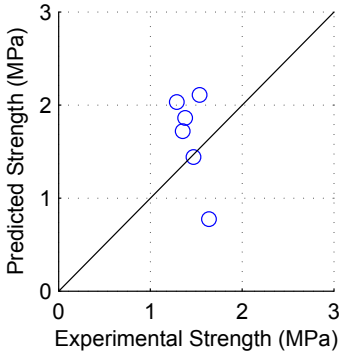

(b) AIJ Model

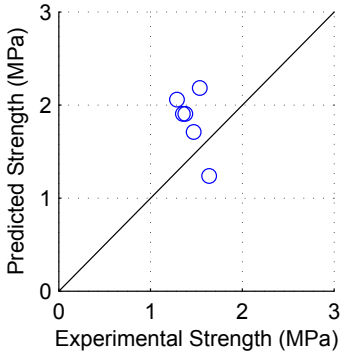

(c) Blondet Model

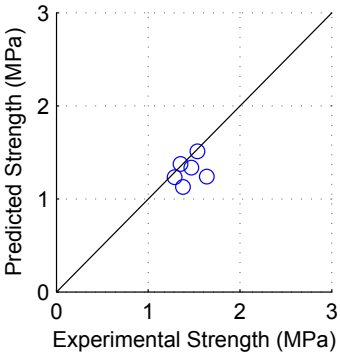

(d) Shing Model

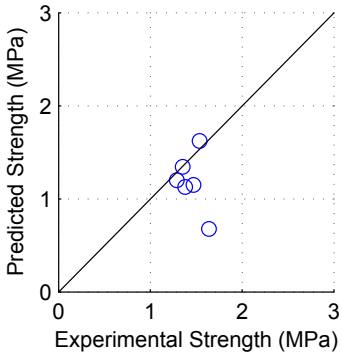

(e) Anderson Model

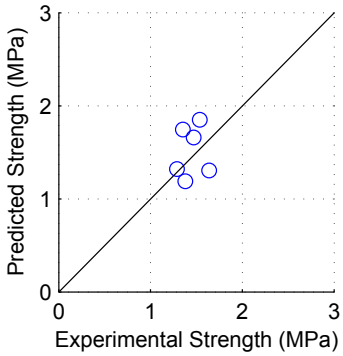

(f) Fattal Model

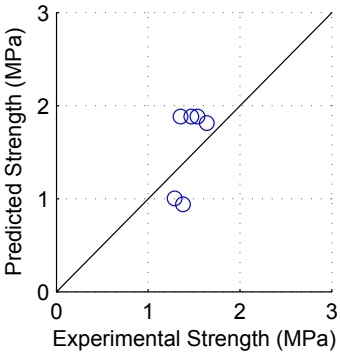

(g) NZS Model

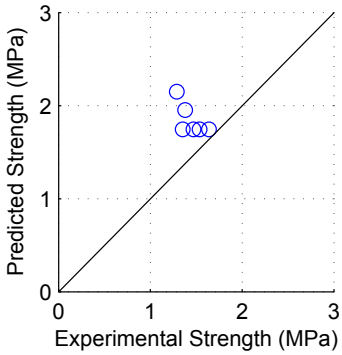

(h) Voon Model

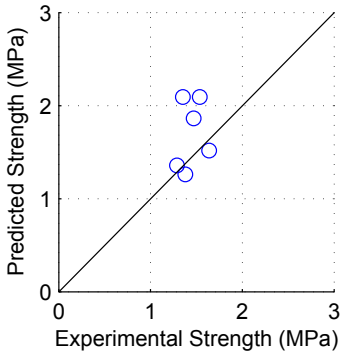

(i) CSA Model

Figure F.25: Model predictions for group 22

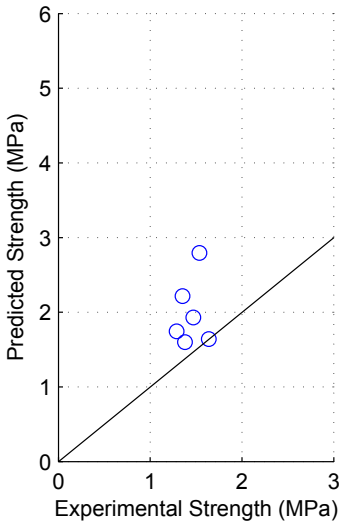

(j) TCCMaR Model

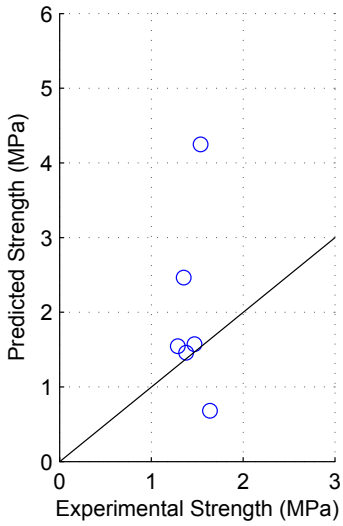

(k) UBC Model

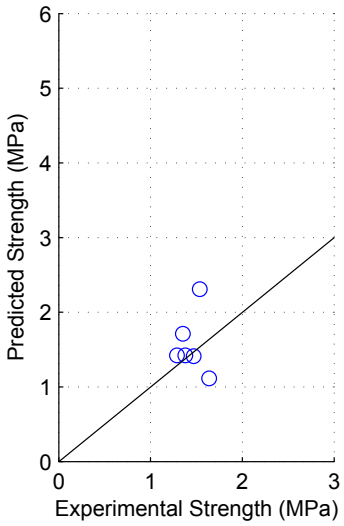

(l) AS Model

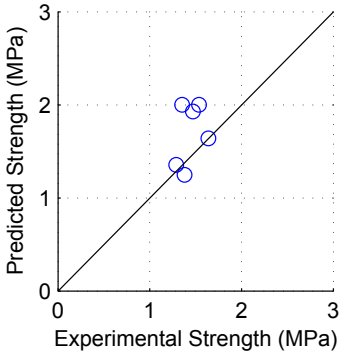

(m) MSJC Model

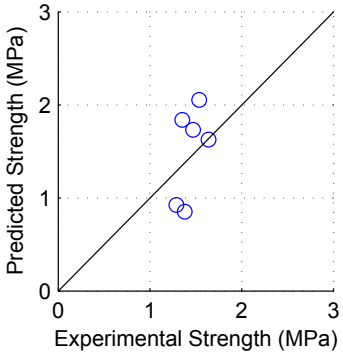

(n) BYU Model

Model predictions for group 22 (Continued)

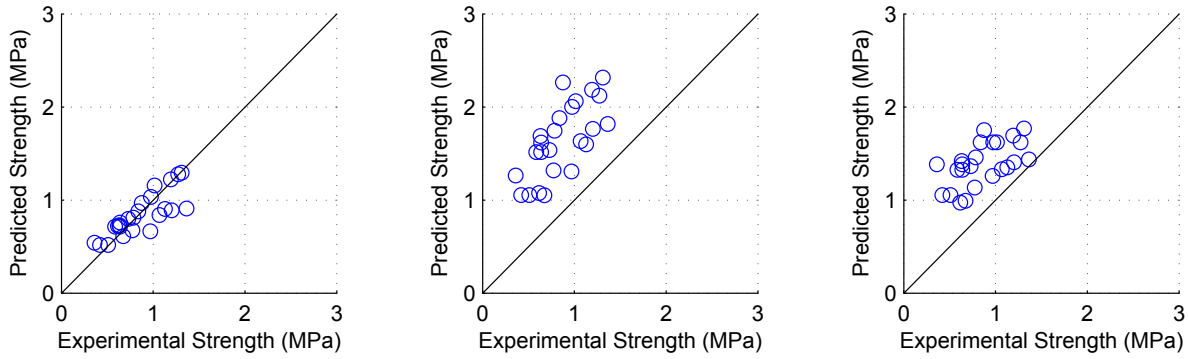

(a) Matsumura Model (b) AIJ Model (c) Blondet Model

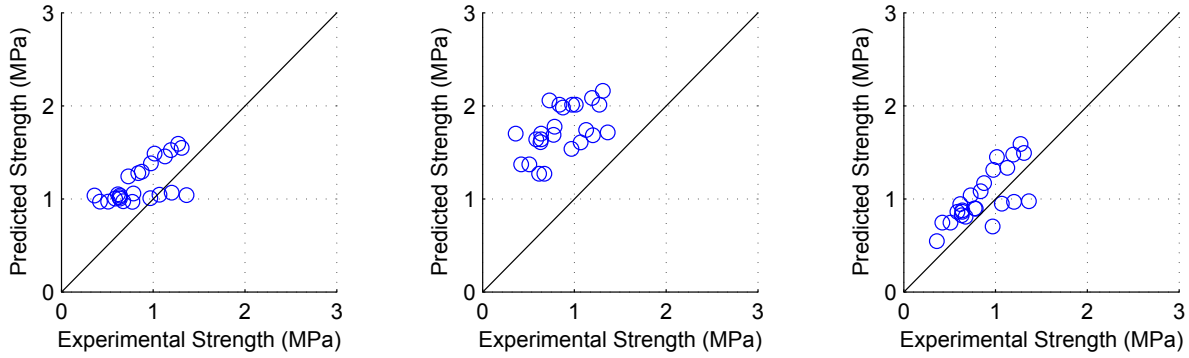

(d) Shing Model (e) Anderson Model (f) Fattal Model

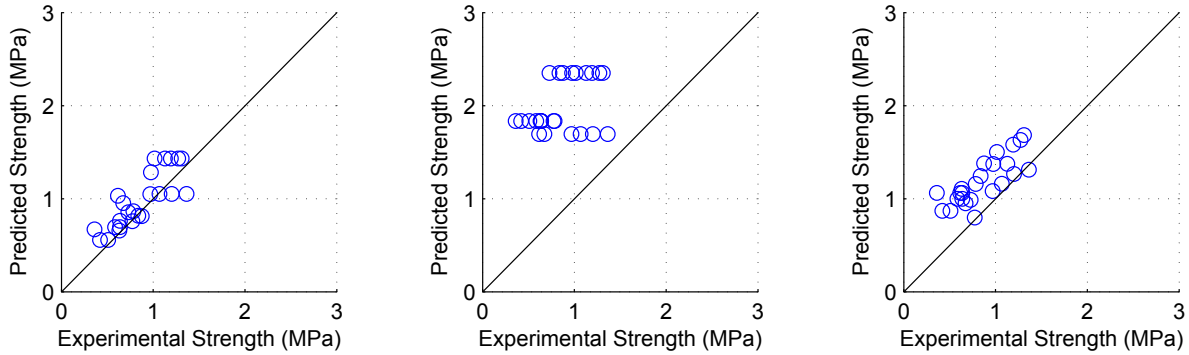

(g) NZS Model (h) Voon Model (i) CSA Model

Figure F.26: Model predictions for group 23

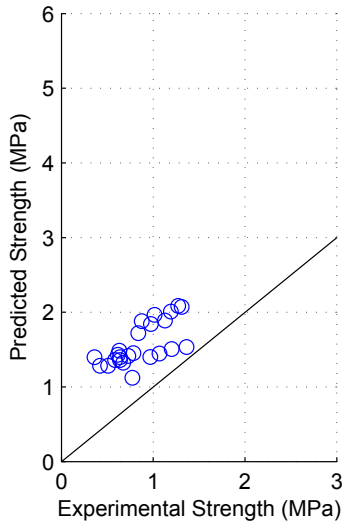

(j) TCCMaR Model

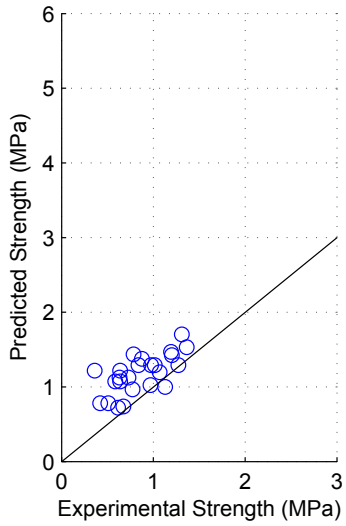

(k) UBC Model

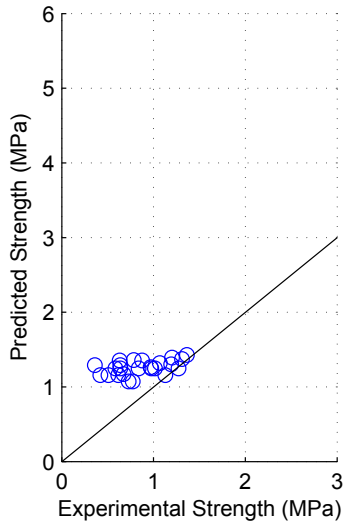

(l) AS Model

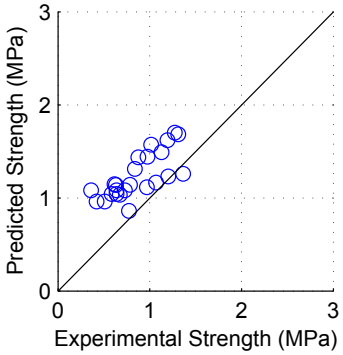

(m) MSJC Model

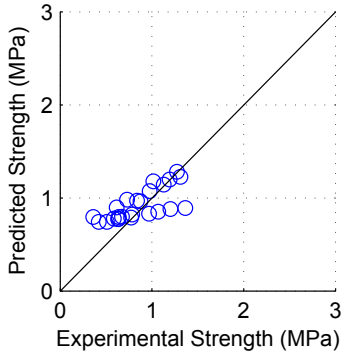

(n) BYU Model

Model predictions for group 23 (Continued)

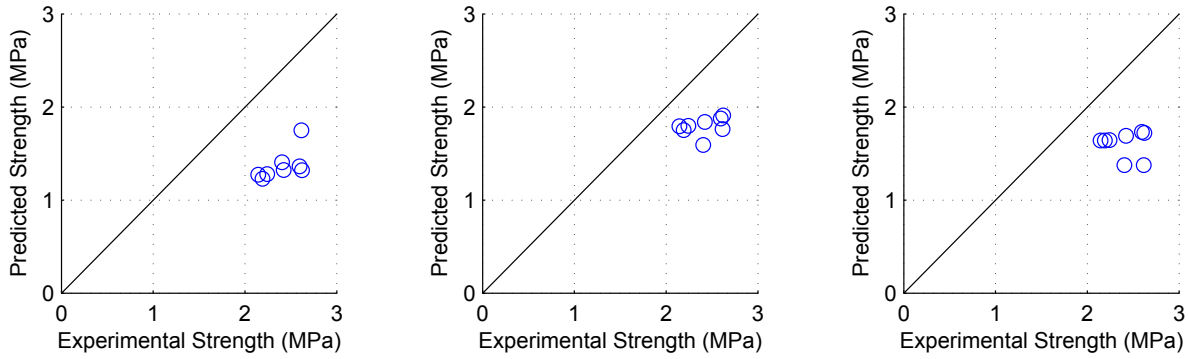

(a) Matsumura Model (b) AIJ Model (c) Blondet Model

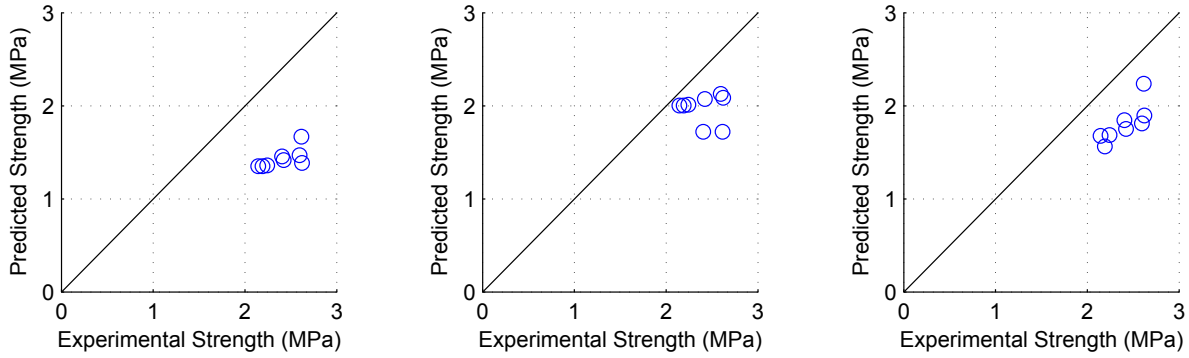

(d) Shing Model (e) Anderson Model (f) Fattal Model

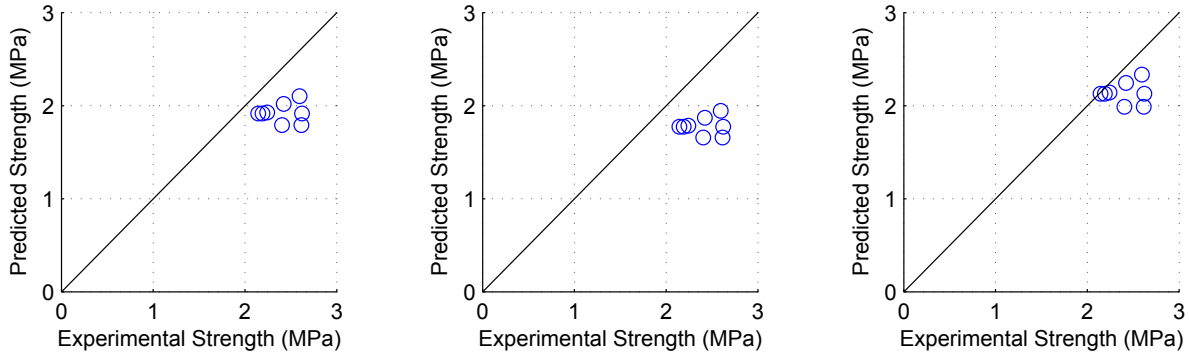

(g) NZS Model (h) Voon Model (i) CSA Model

Figure F.27: Model predictions for group 24

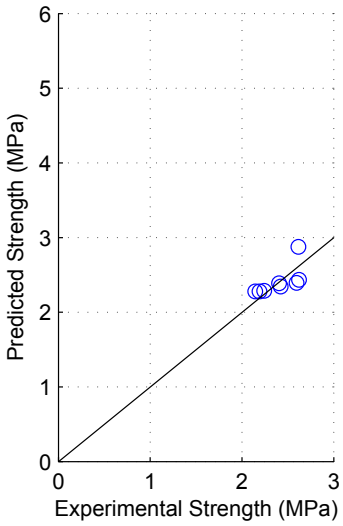

(j) TCCMaR Model

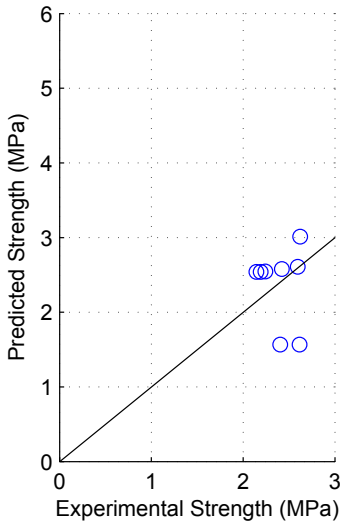

(k) UBC Model

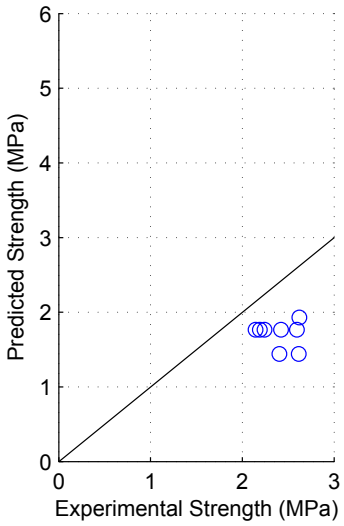

(l) AS Model

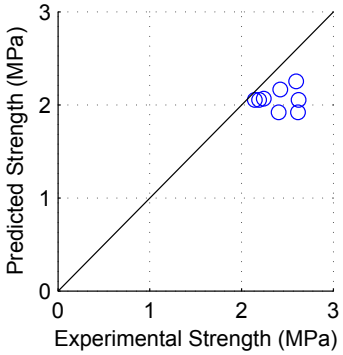

(m) MSJC Model

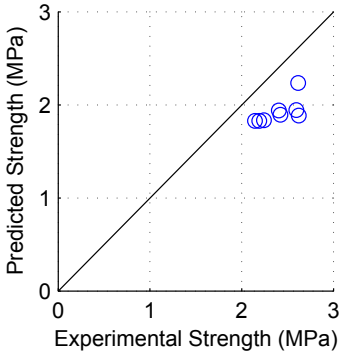

(n) BYU Model

Model predictions for group 24 (Continued)

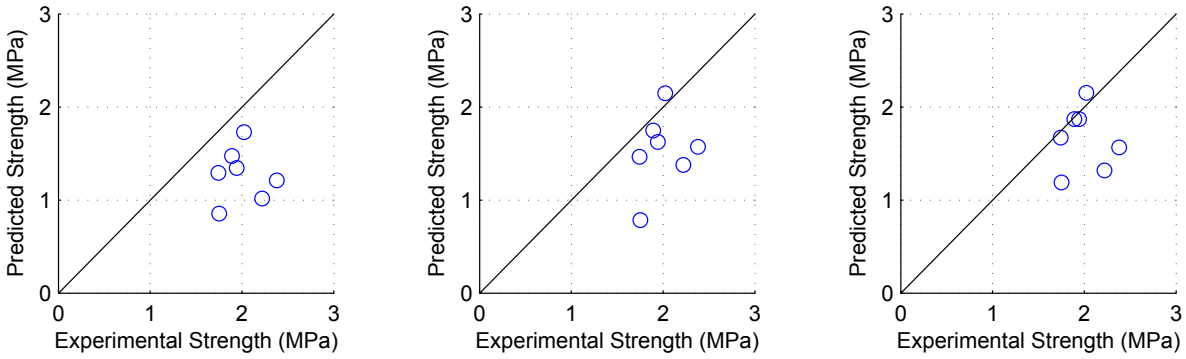

(a) Matsumura Model (b) AIJ Model (c) Blondet Model

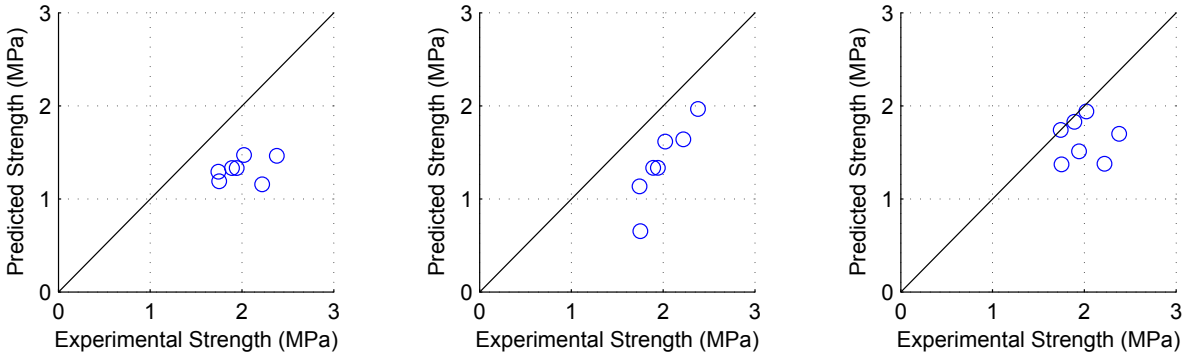

(d) Shing Model (e) Anderson Model (f) Fattal Model

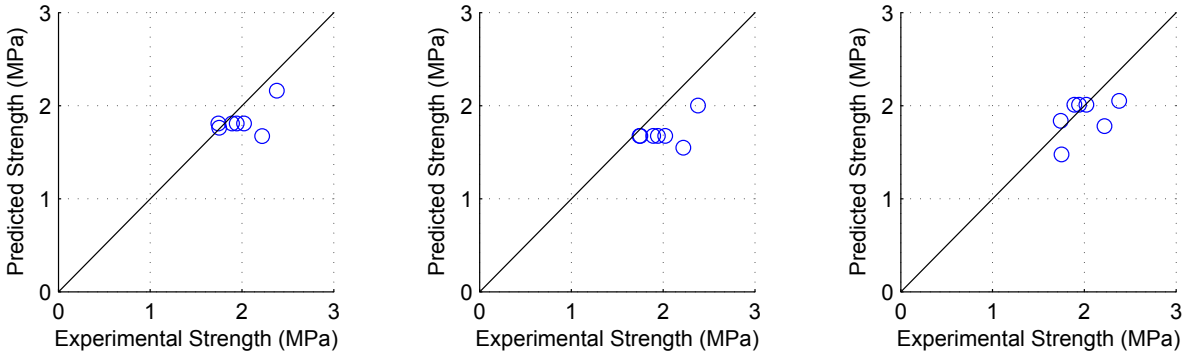

(g) NZS Model (h) Voon Model (i) CSA Model

Figure F.28: Model predictions for group 25

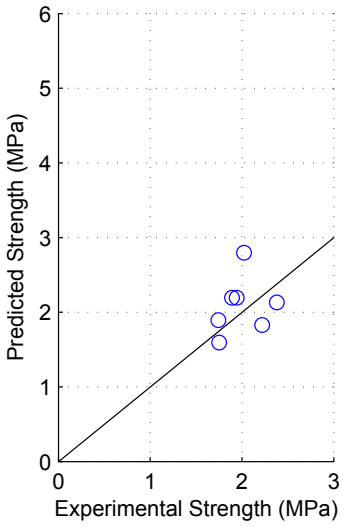

(j) TCCMaR Model

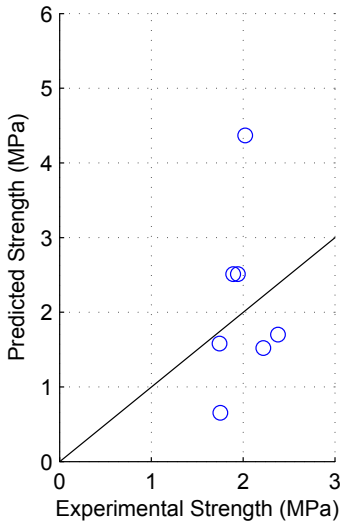

(k) UBC Model

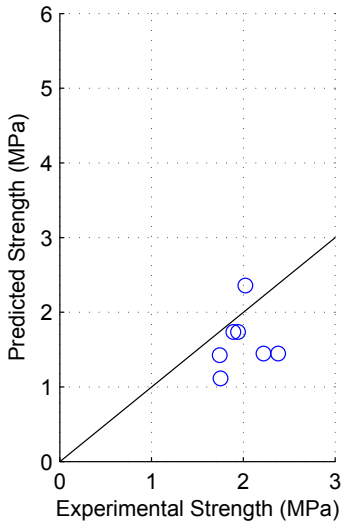

(l) AS Model

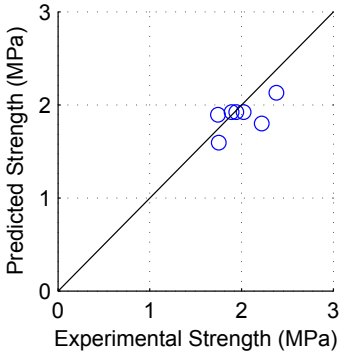

(m) MSJC Model

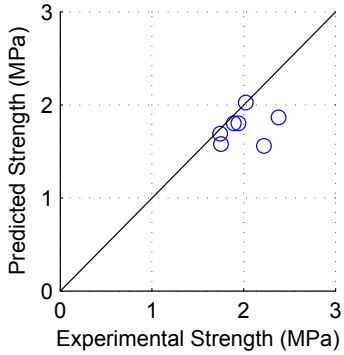

(n) BYU Model

Model predictions for group 25 (Continued)

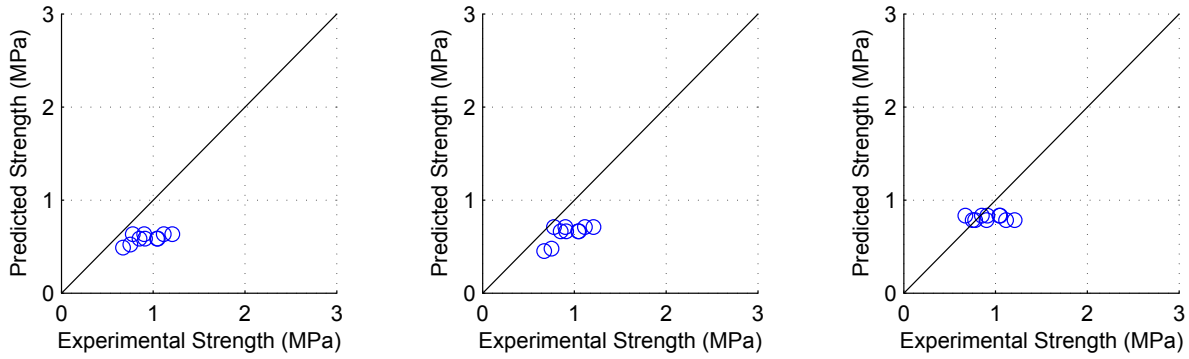

(a) Matsumura Model

(b) AIJ Model

(c) Blondet Model

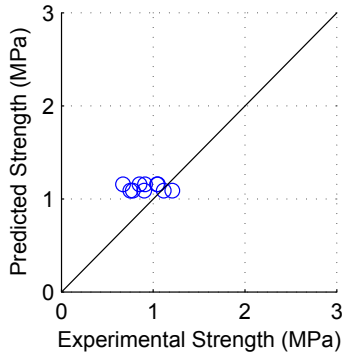

(d) Shing Model

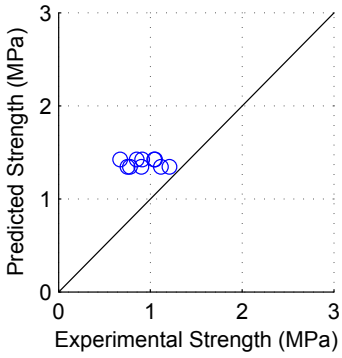

(e) Anderson Model

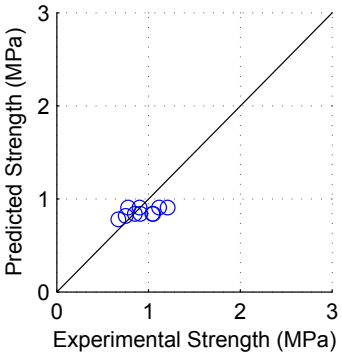

(f) Fattal Model

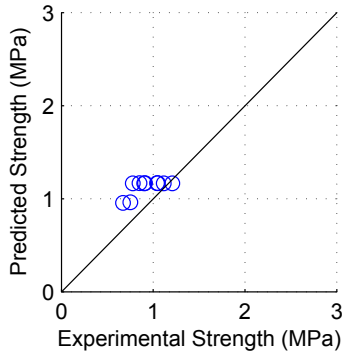

(g) NZS Model

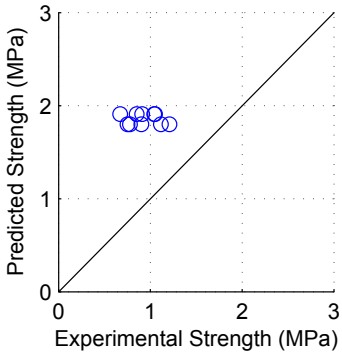

(h) Voon Model

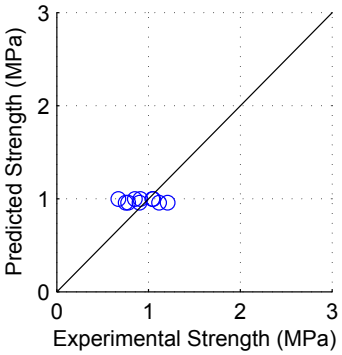

(i) CSA Model

Figure F.29: Model predictions for group 26

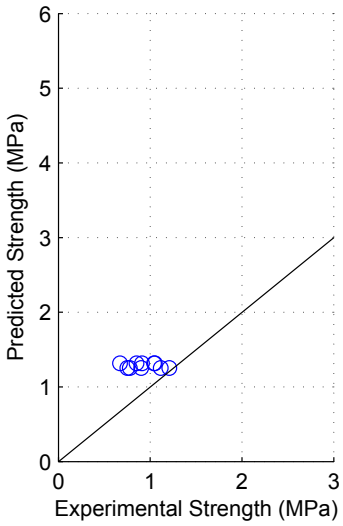

(j) TCCMaR Model

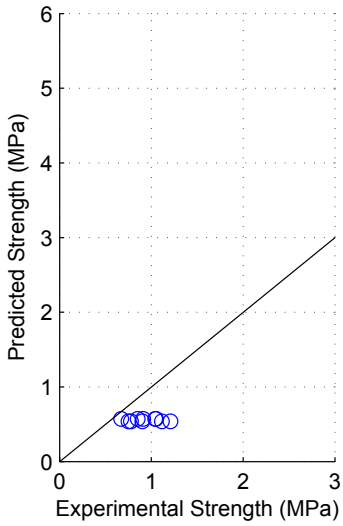

(k) UBC Model

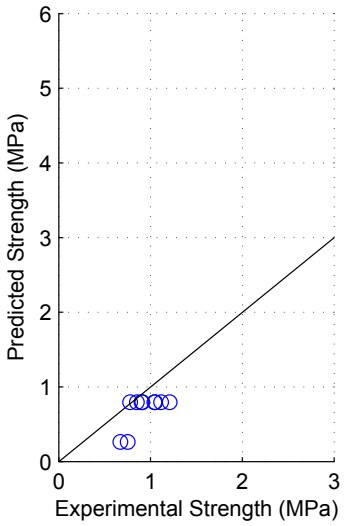

(l) AS Model

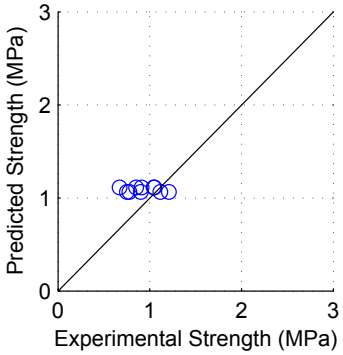

(m) MSJC Model

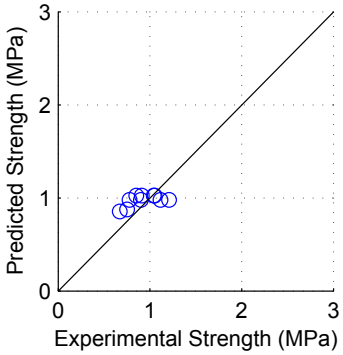

(n) BYU Model

Model predictions for group 26 (Continued)

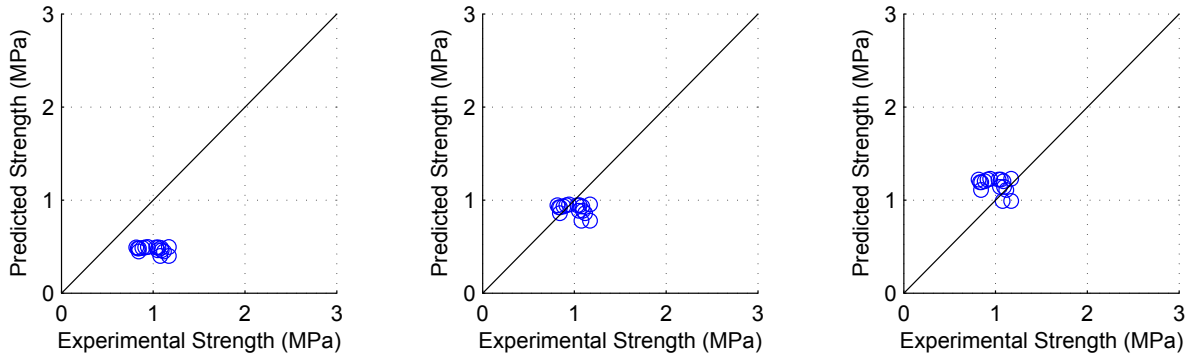

(a) Matsumura Model (b) AIJ Model (c) Blondet Model

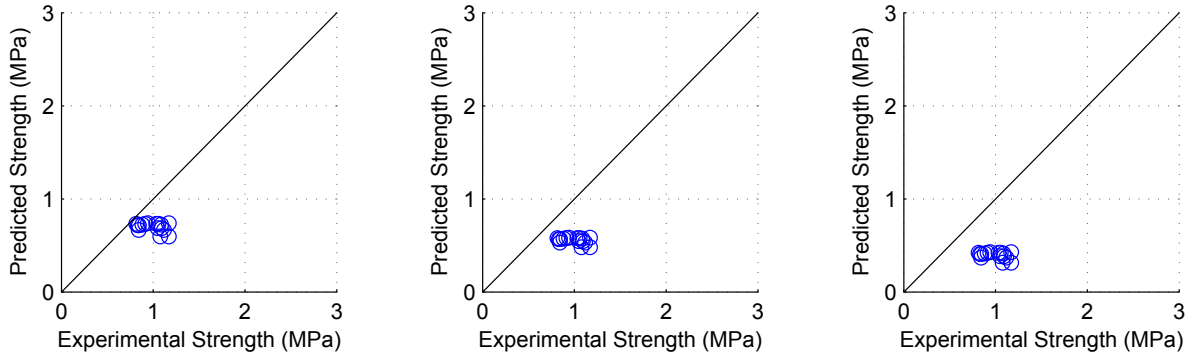

(d) Shing Model (e) Anderson Model (f) Fattal Model

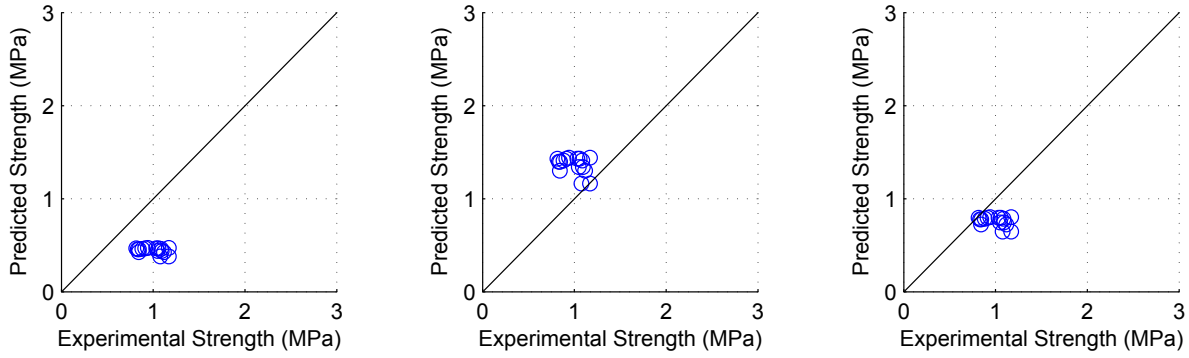

(g) NZS Model (h) Voon Model (i) CSA Model

Figure F.30: Model predictions for group 27

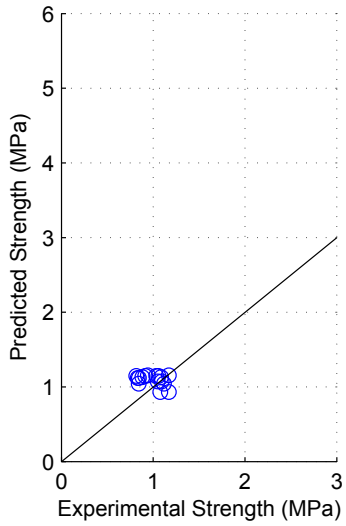

(j) TCCMaR Model

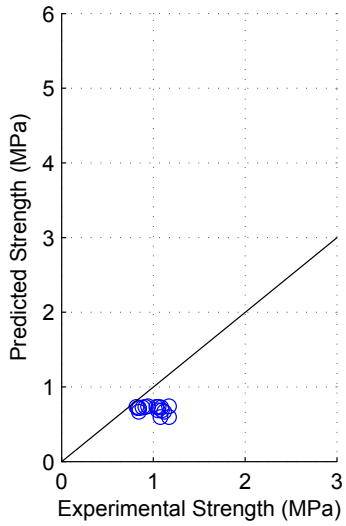

(k) UBC Model

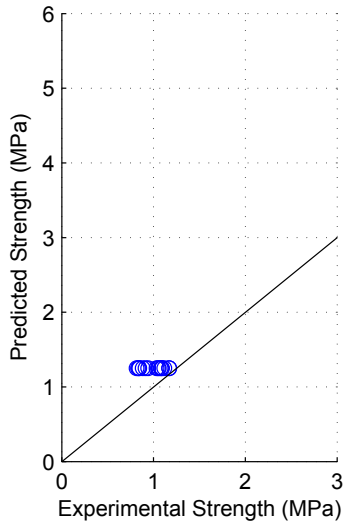

(l) AS Model

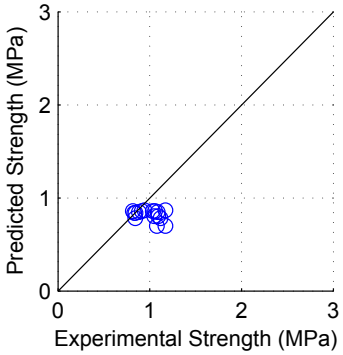

(m) MSJC Model

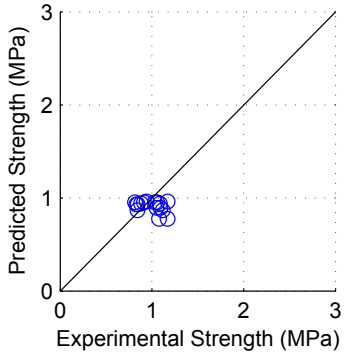

(n) BYU Model

Model predictions for group 27 (Continued)

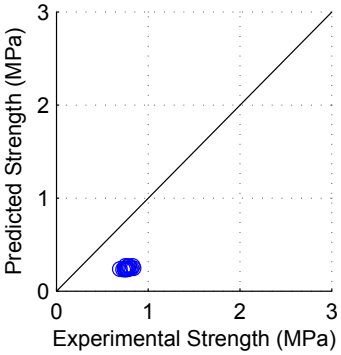

(a) Matsumura Model

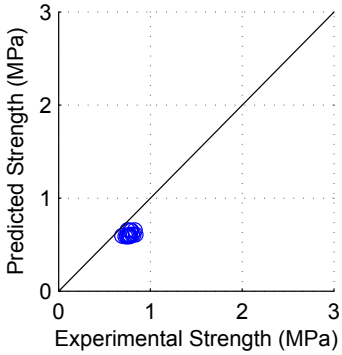

(b) AIJ Model

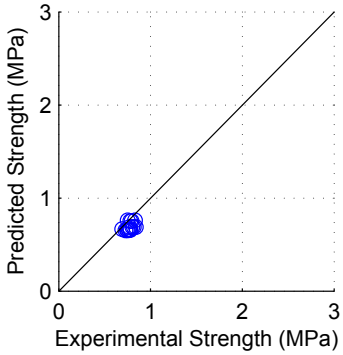

(c) Blondet Model

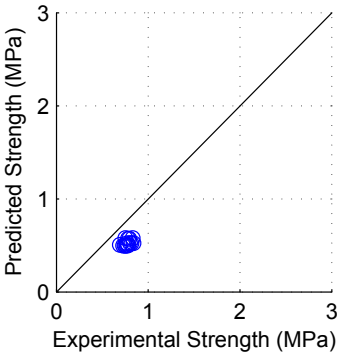

(d) Shing Model

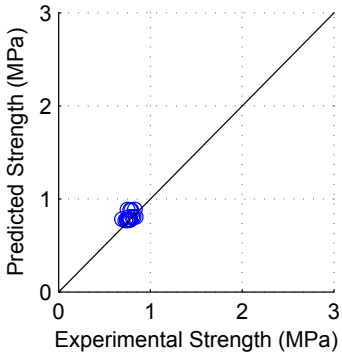

(e) Anderson Model

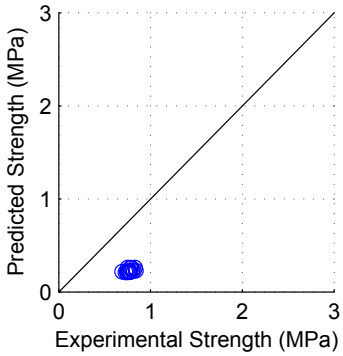

(f) Fattal Model

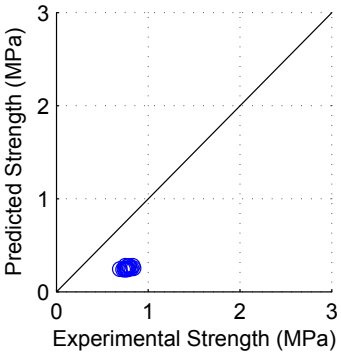

(g) NZS Model

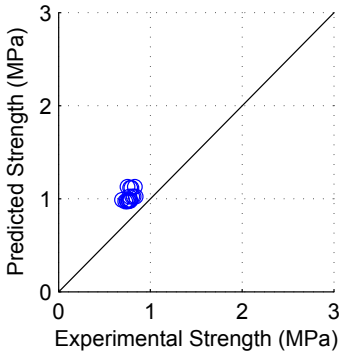

(h) Voon Model

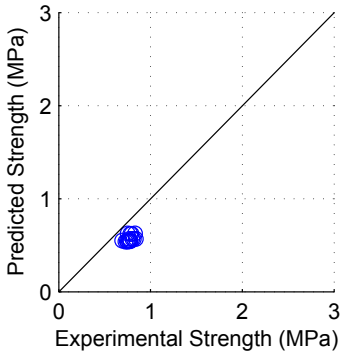

(i) CSA Model

Figure F.31: Model predictions for group 28

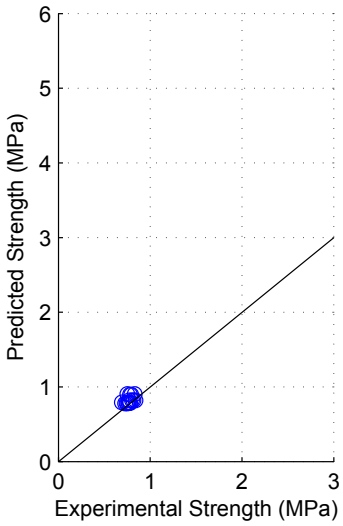

(j) TCCMaR Model

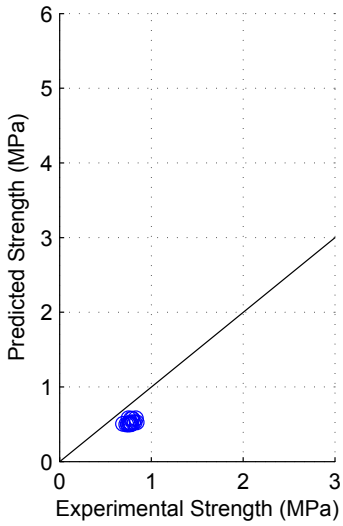

(k) UBC Model

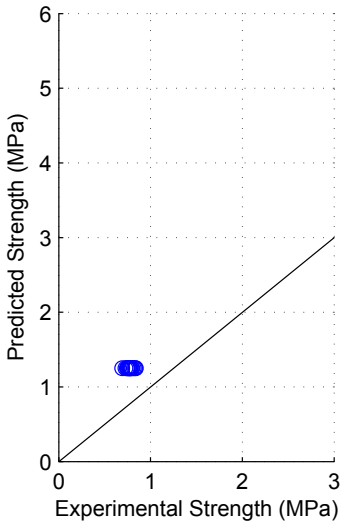

(l) AS Model

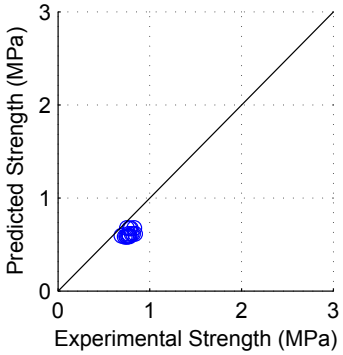

(m) MSJC Model

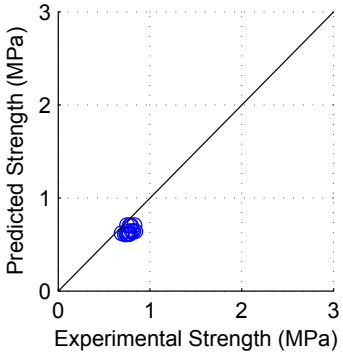

(n) BYU Model

Model predictions for group 28 (Continued)

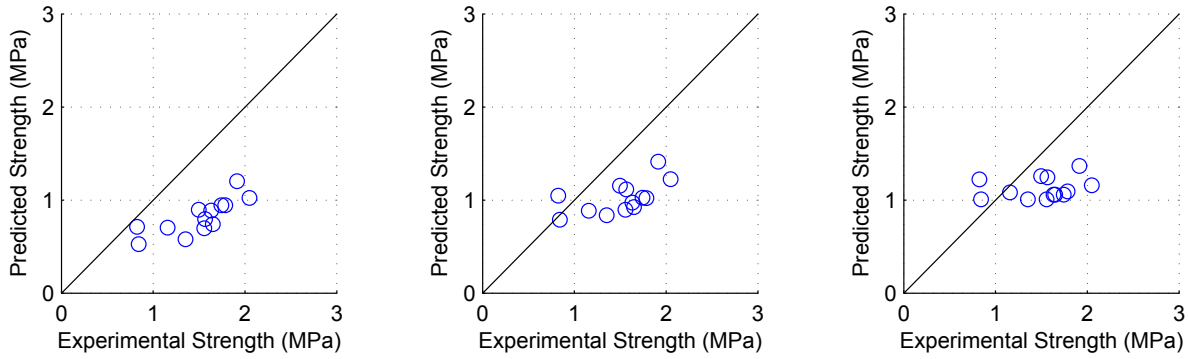

(a) Matsumura Model (b) AIJ Model (c) Blondet Model

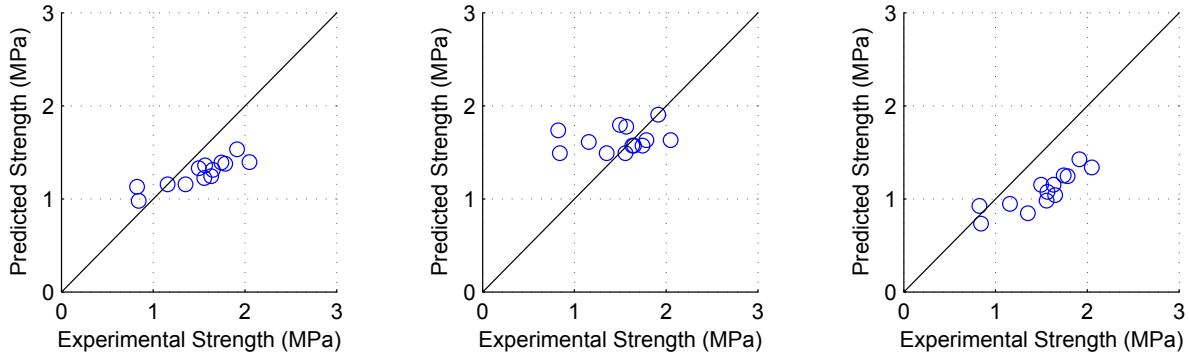

(d) Shing Model (e) Anderson Model (f) Fattal Model

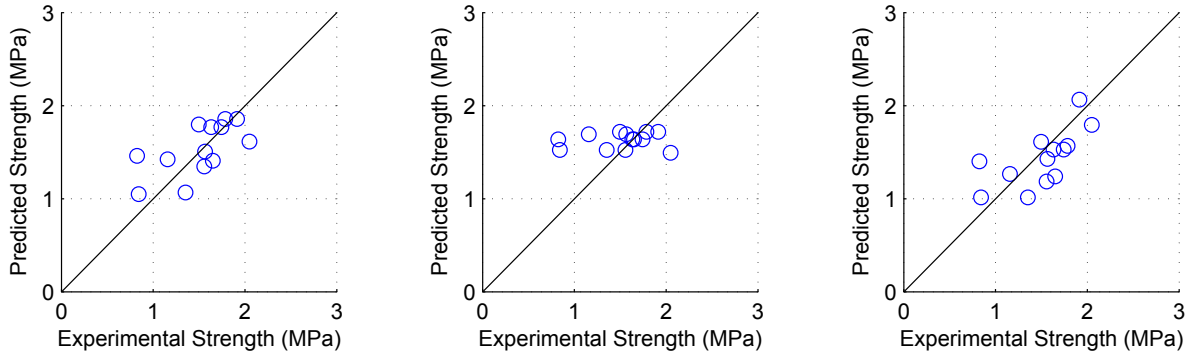

(g) NZS Model (h) Voon Model (i) CSA Model

Figure F.32: Model predictions for group 29

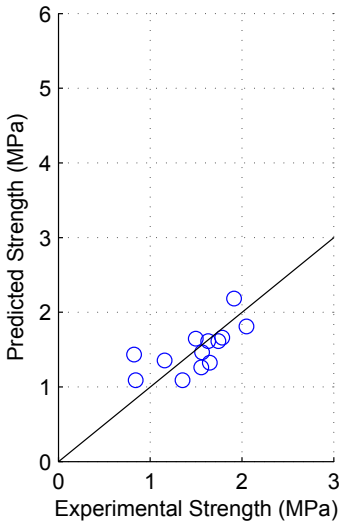

(j) TCCMaR Model

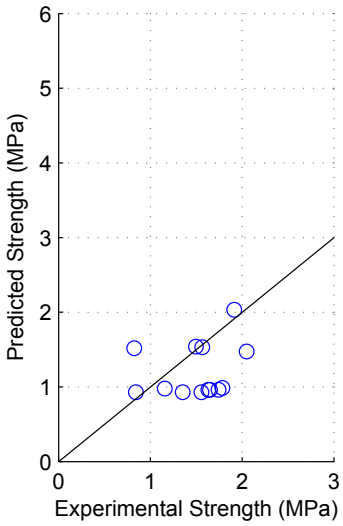

(k) UBC Model

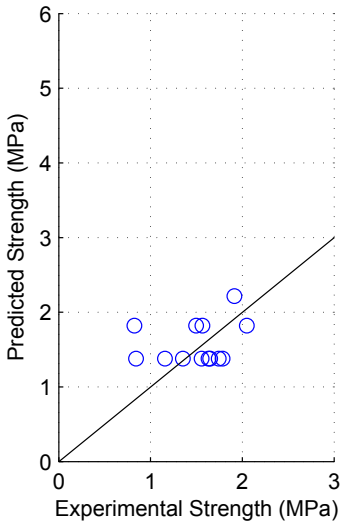

(l) AS Model

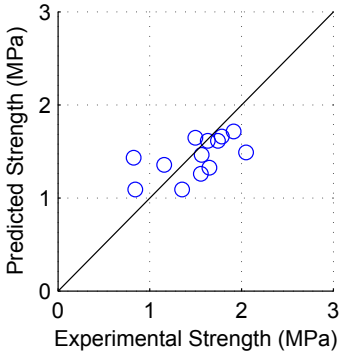

(m) MSJC Model

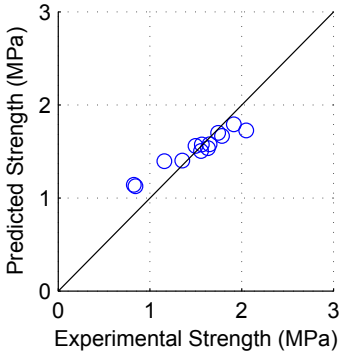

(n) BYU Model

Model predictions for group 29 (Continued)

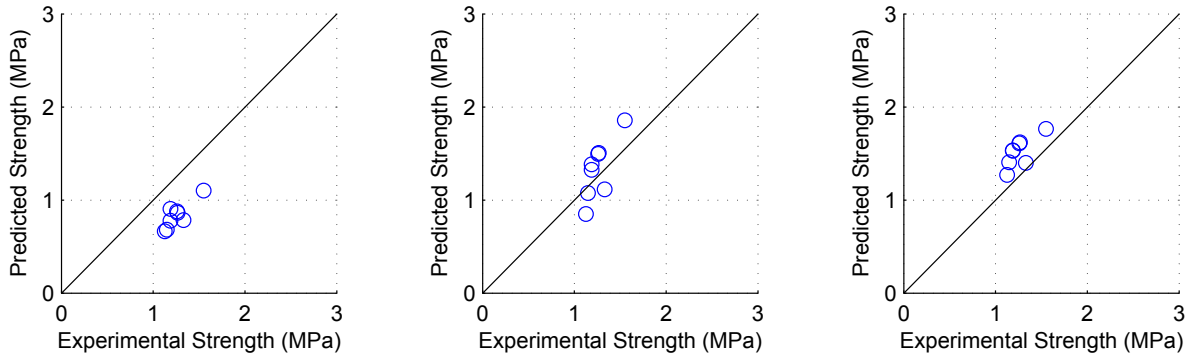

(a) Matsumura Model (b) AIJ Model (c) Blondet Model

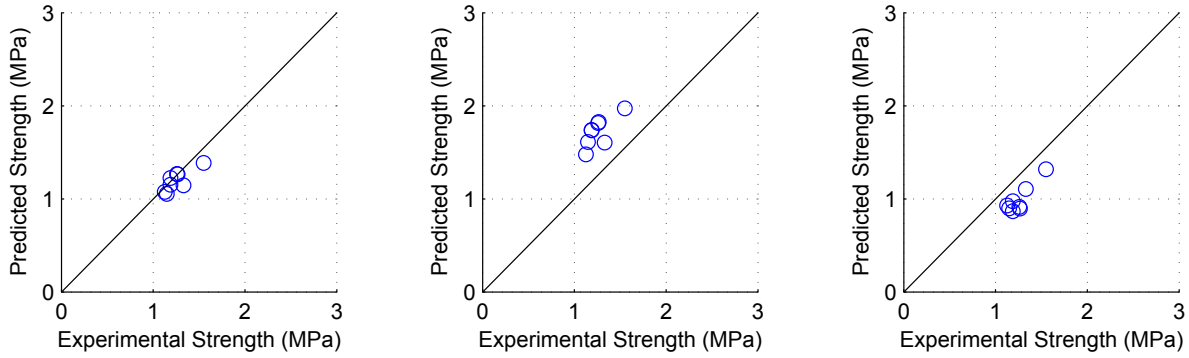

(d) Shing Model (e) Anderson Model (f) Fattal Model

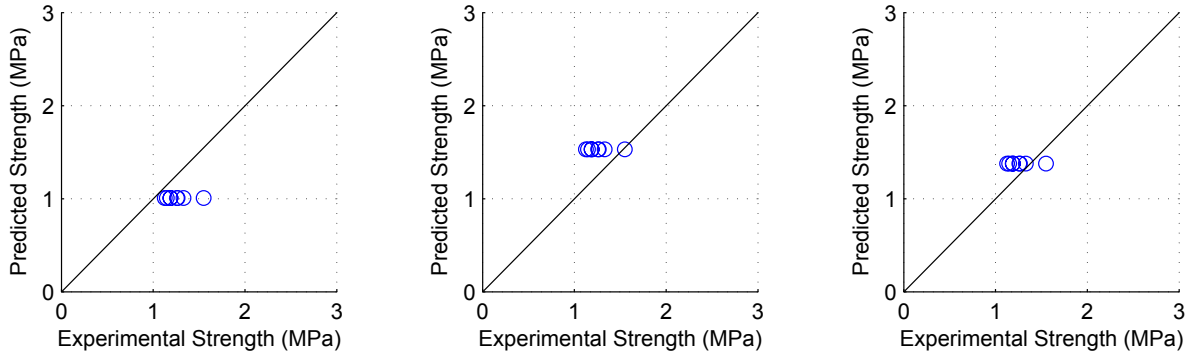

(g) NZS Model (h) Voon Model (i) CSA Model

Figure F.33: Model predictions for group 30

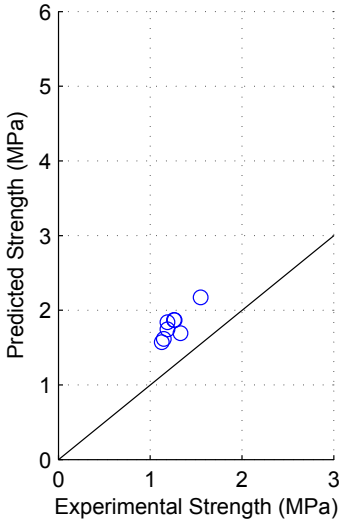

(j) TCCMaR Model

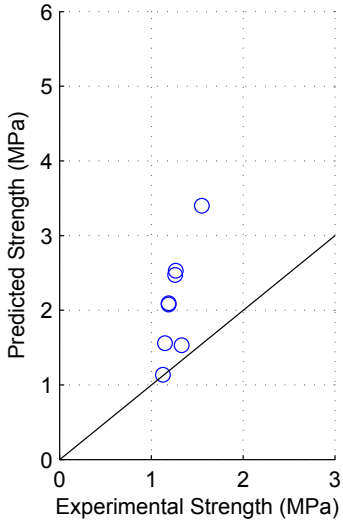

(k) UBC Model

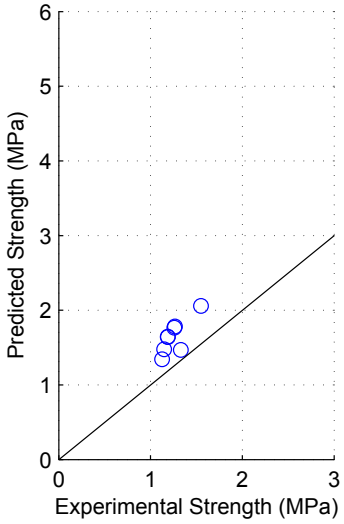

(l) AS Model

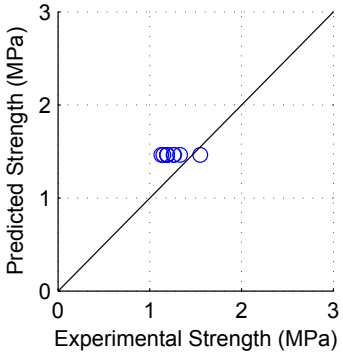

(m) MSJC Model

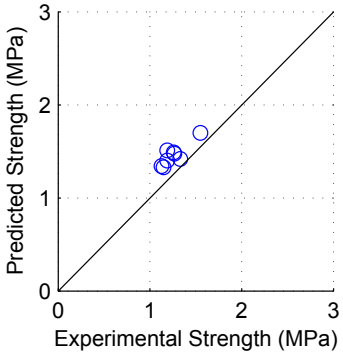

(n) BYU Model

Model predictions for group 30 (Continued)

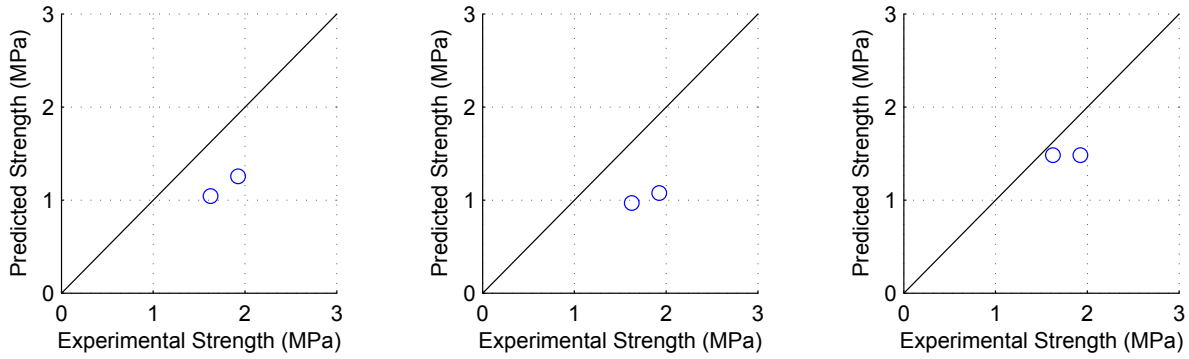

(a) Matsumura Model (b) AIJ Model (c) Blondet Model

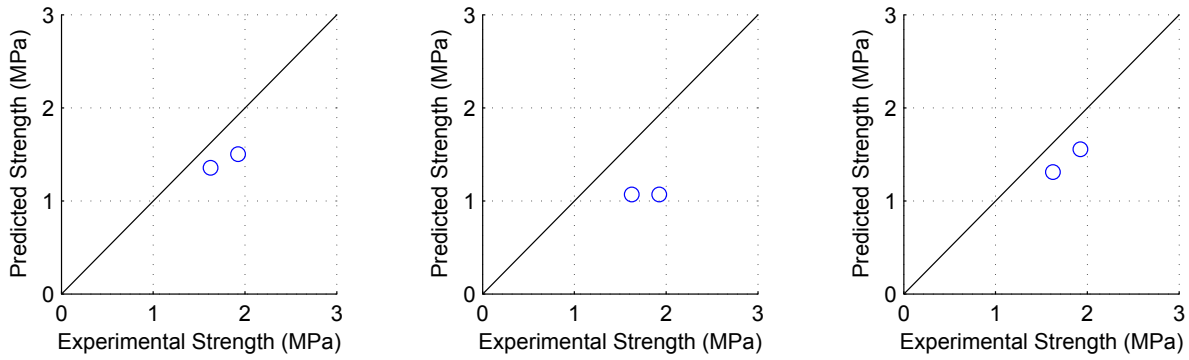

(d) Shing Model (e) Anderson Model (f) Fattal Model

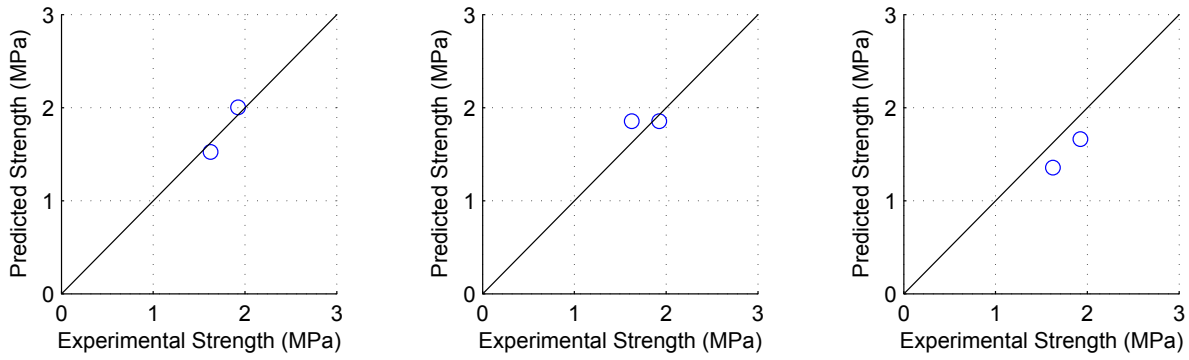

(g) NZS Model (h) Voon Model (i) CSA Model

Figure F.34: Model predictions for group 31

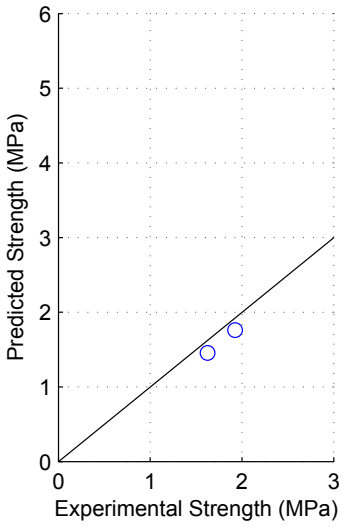

(j) TCCMaR Model

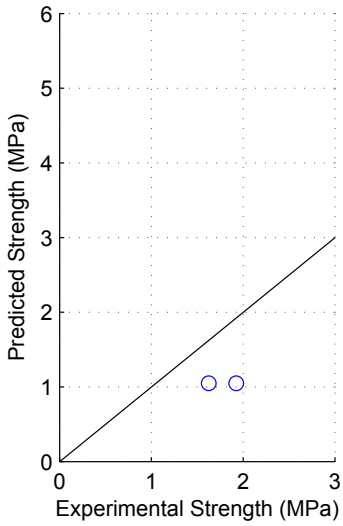

(k) UBC Model

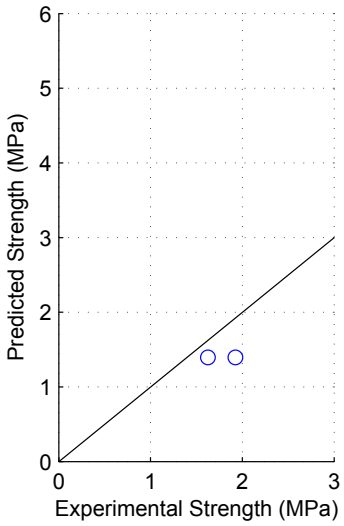

(l) AS Model

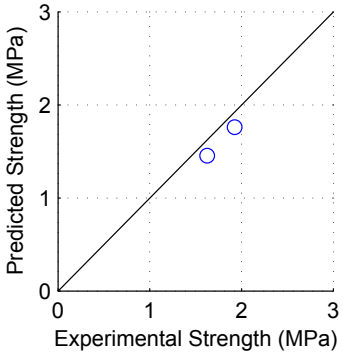

(m) MSJC Model

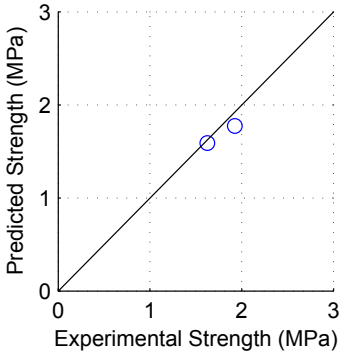

(n) BYU Model

Model predictions for group 31 (Continued)

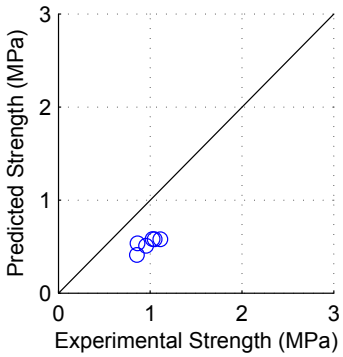

(a) Matsumura Model

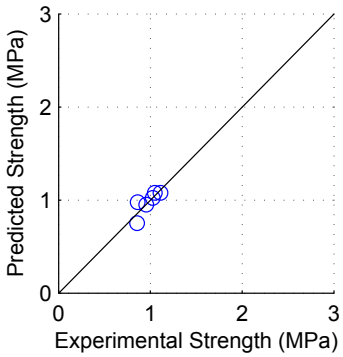

(b) AIJ Model

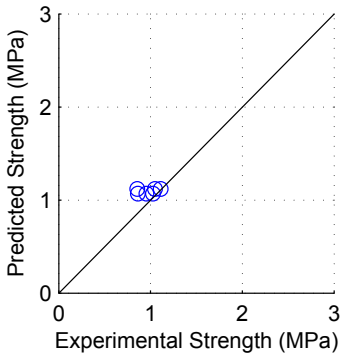

(c) Blondet Model

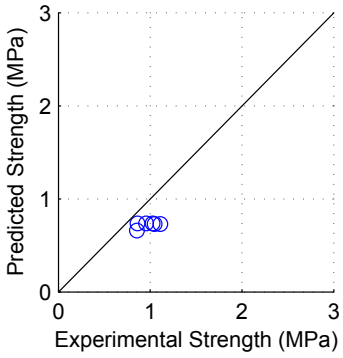

(d) Shing Model

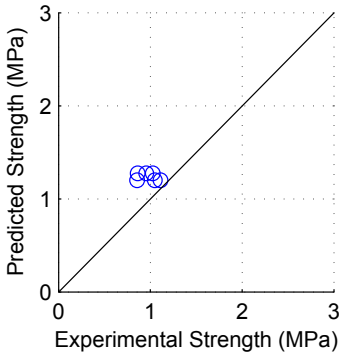

(e) Anderson Model

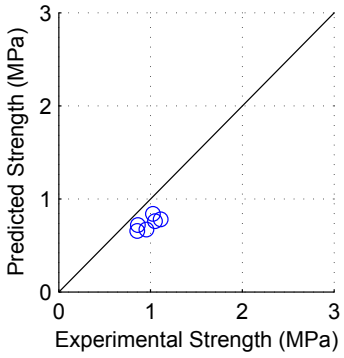

(f) Fattal Model

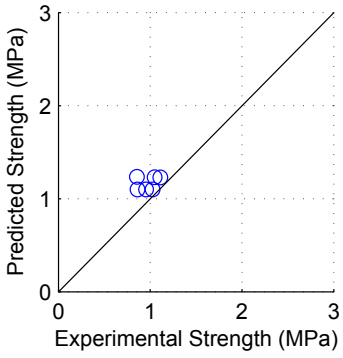

(g) NZS Model

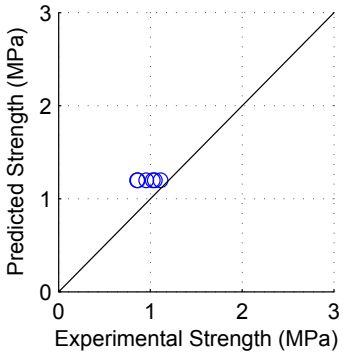

(h) Voon Model

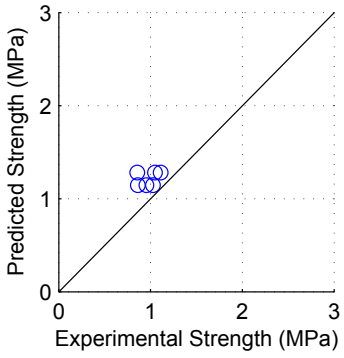

(i) CSA Model

Figure F.35: Model predictions for group 32

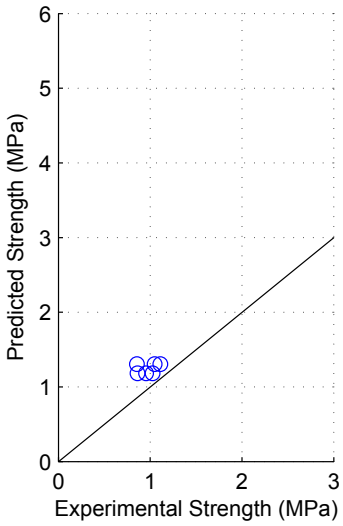

(j) TCCMaR Model

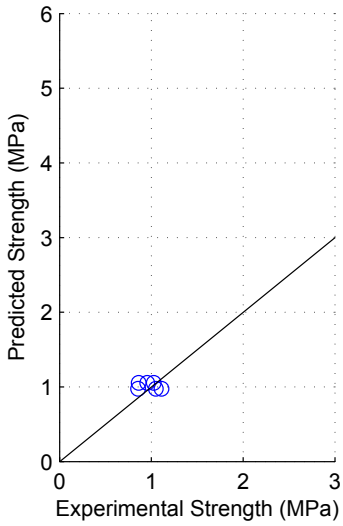

(k) UBC Model

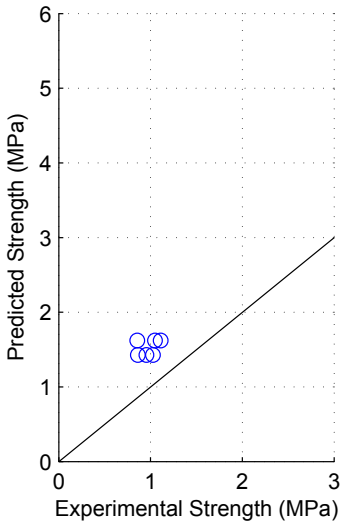

(l) AS Model

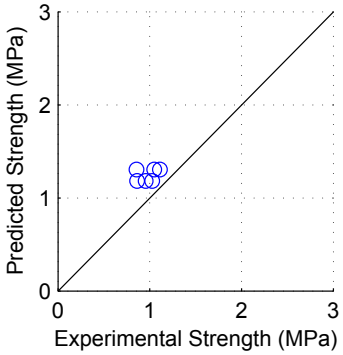

(m) MSJC Model

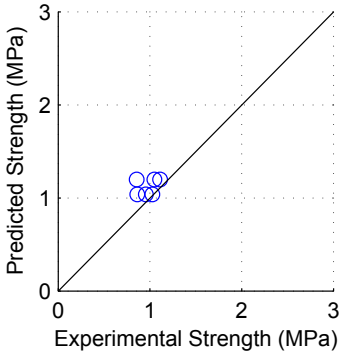

(n) BYU Model

Model predictions for group 32 (Continued)

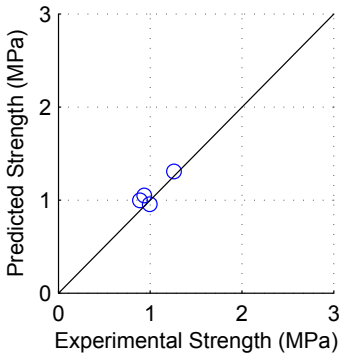

(a) Matsumura Model

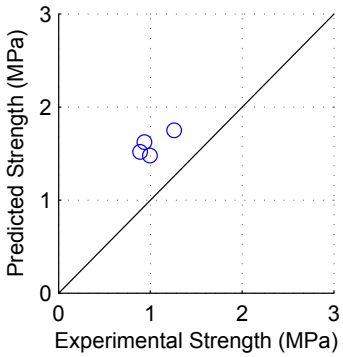

(b) AIJ Model

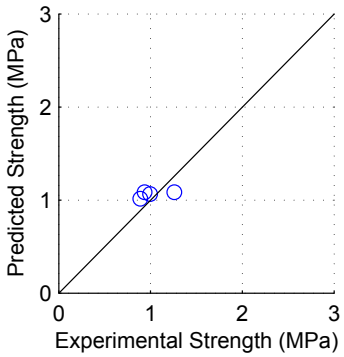

(c) Blondet Model

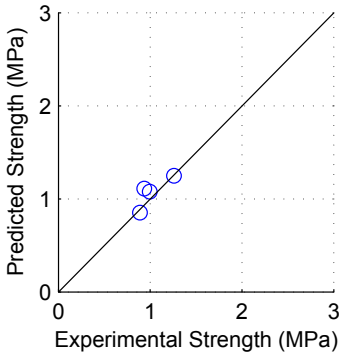

(d) Shing Model

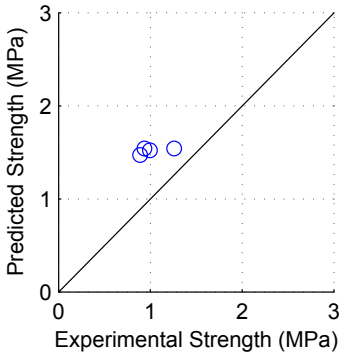

(e) Anderson Model

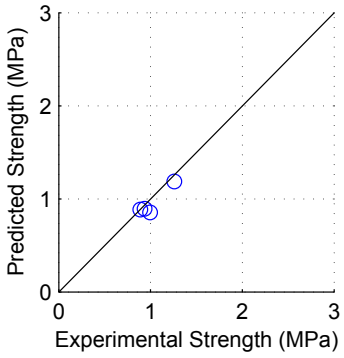

(f) Fattal Model

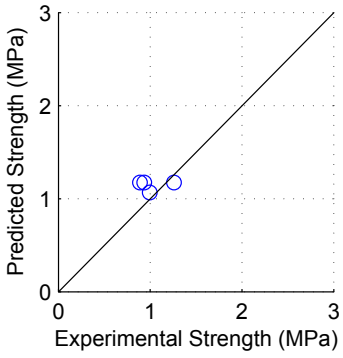

(g) NZS Model

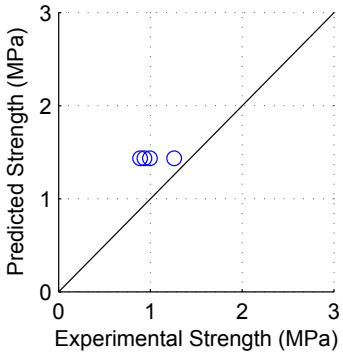

(h) Voon Model

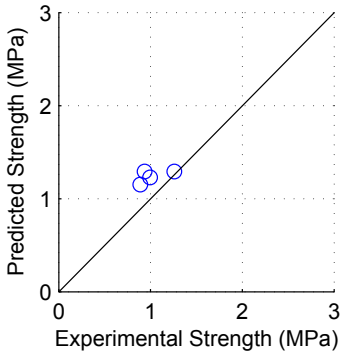

(i) CSA Model

Figure F.36: Model predictions for group 33

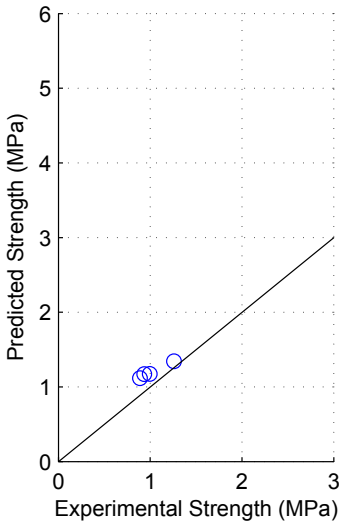

(j) TCCMaR Model

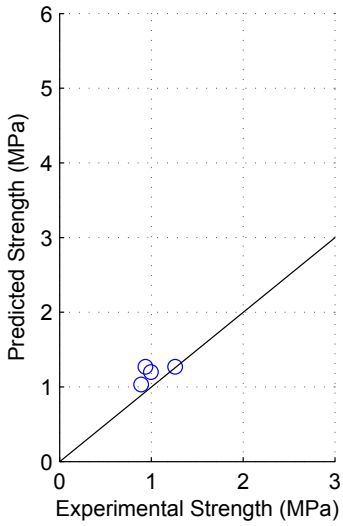

(k) UBC Model

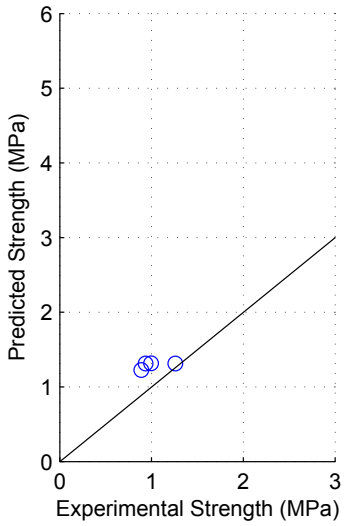

(l) AS Model

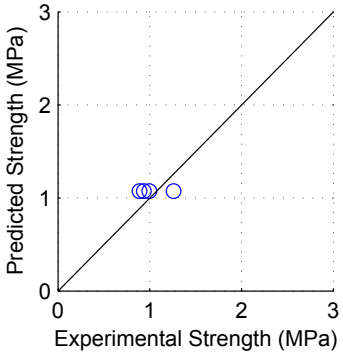

(m) MSJC Model

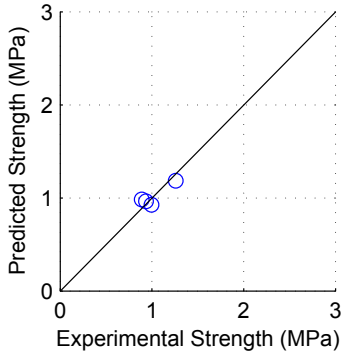

(n) BYU Model

Model predictions for group 33 (Continued)

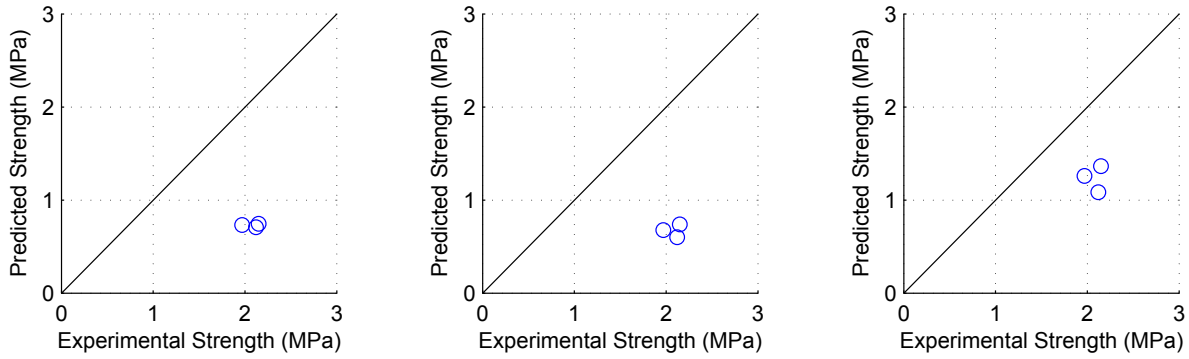

(a) Matsumura Model (b) AIJ Model (c) Blondet Model

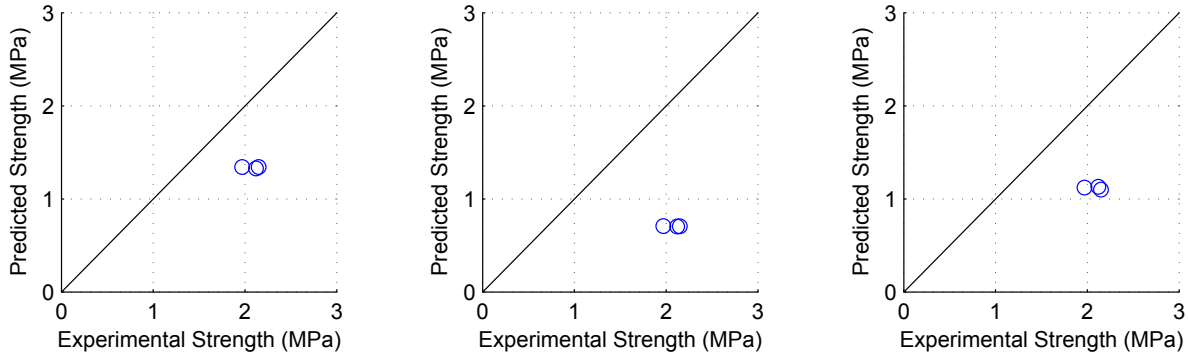

(d) Shing Model (e) Anderson Model (f) Fattal Model

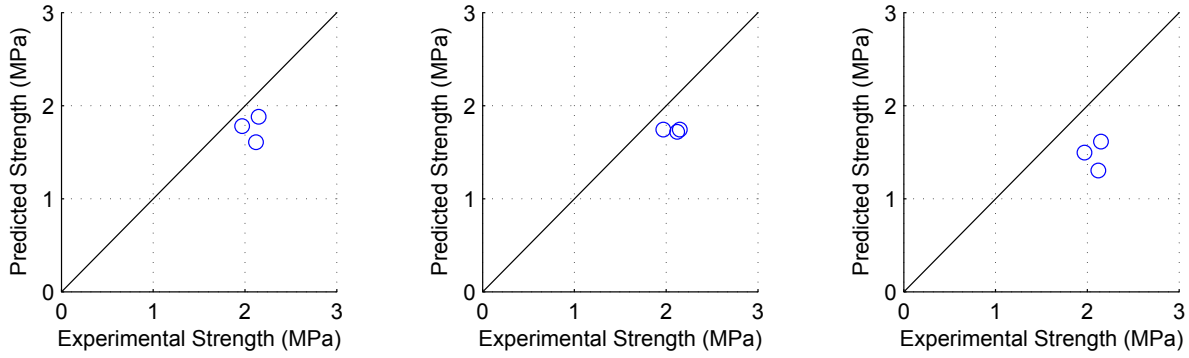

(g) NZS Model (h) Voon Model (i) CSA Model

Figure F.37: Model predictions for group 34

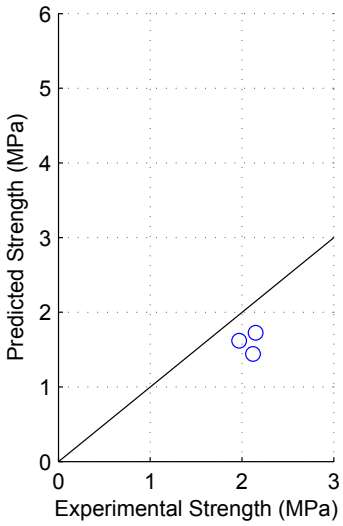

(j) TCCMaR Model

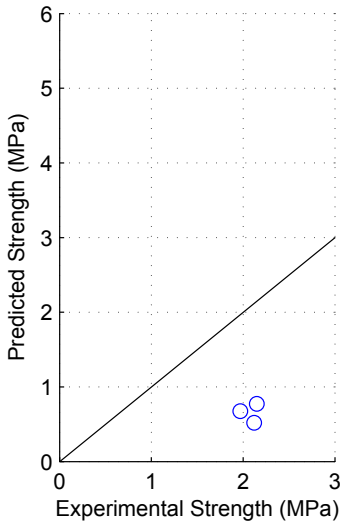

(k) UBC Model

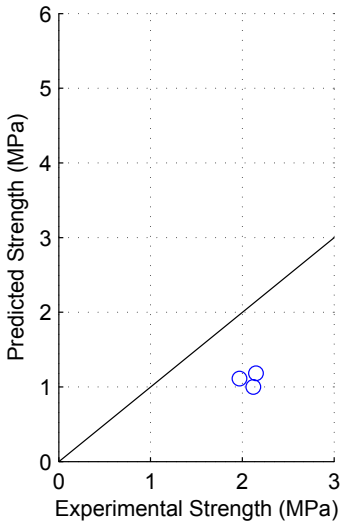

(l) AS Model

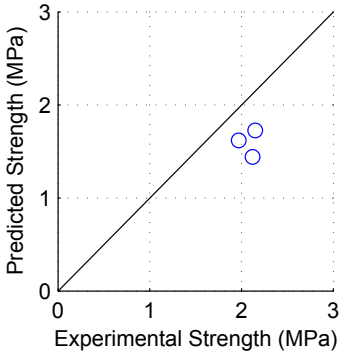

(m) MSJC Model

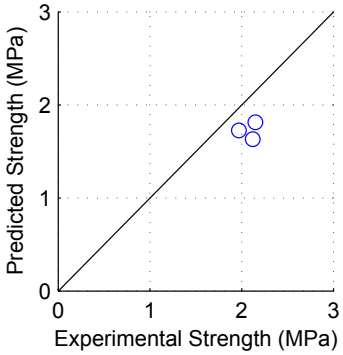

(n) BYU Model

Model predictions for group 34 (Continued)

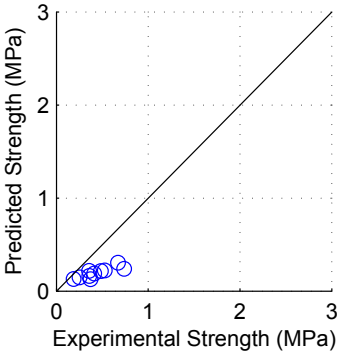

(a) Matsumura Model

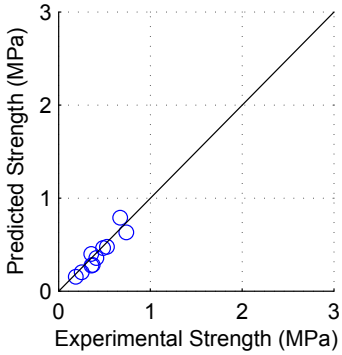

(b) AIJ Model

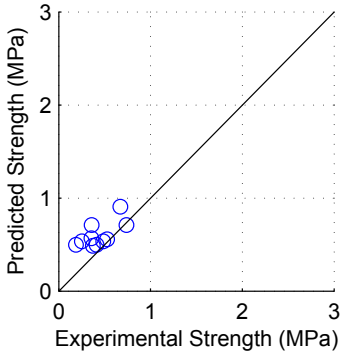

(c) Blondet Model

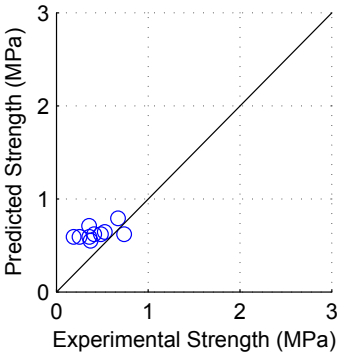

(d) Shing Model

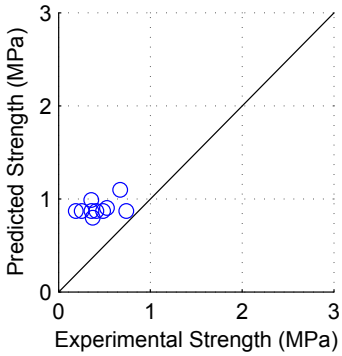

(e) Anderson Model

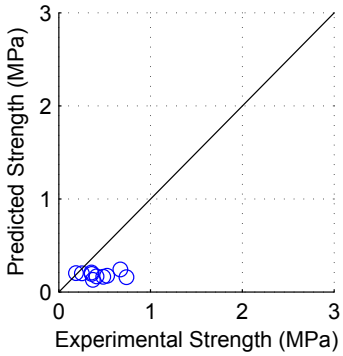

(f) Fattal Model

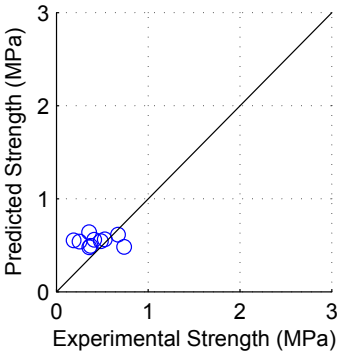

(g) NZS Model

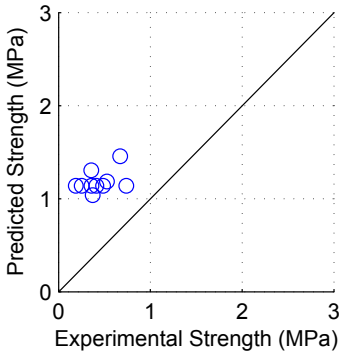

(h) Voon Model

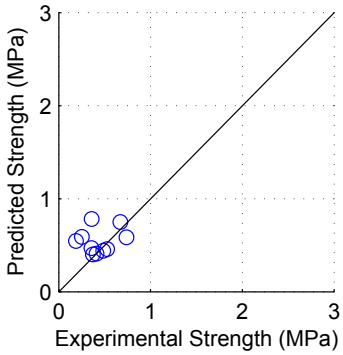

(i) CSA Model

Figure F.38: Model predictions for group 35

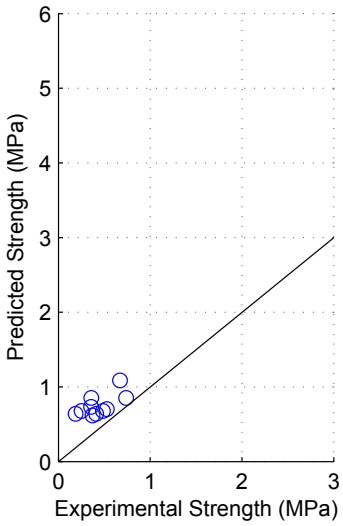

(j) TCCMaR Model

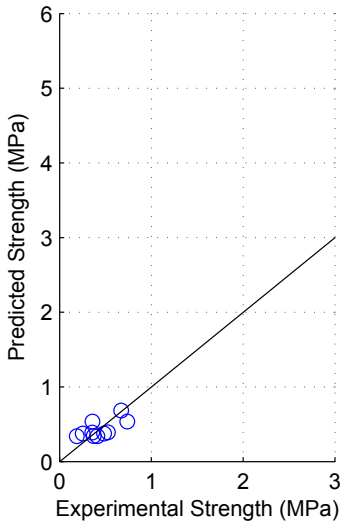

(k) UBC Model

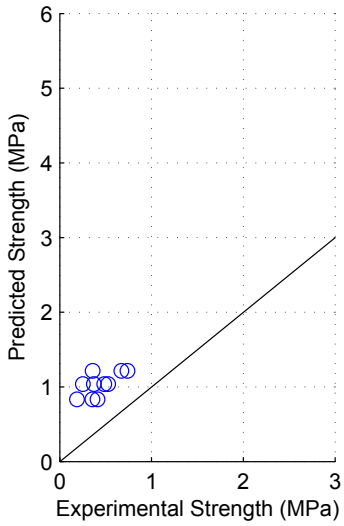

(l) AS Model

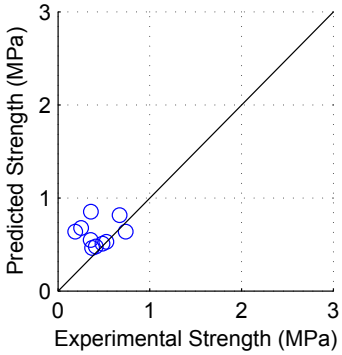

(m) MSJC Model

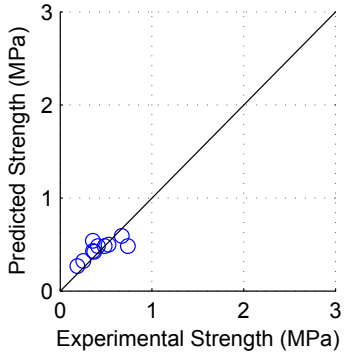

(n) BYU Model

Model predictions for group 35 (Continued)

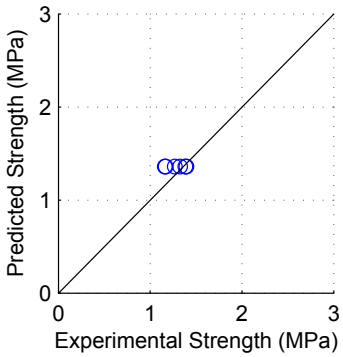

(a) Matsumura Model

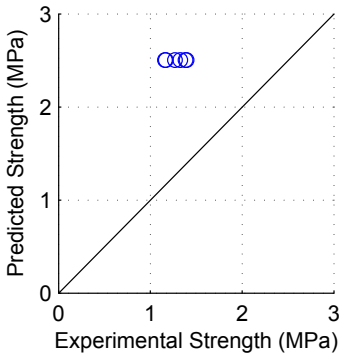

(b) AIJ Model

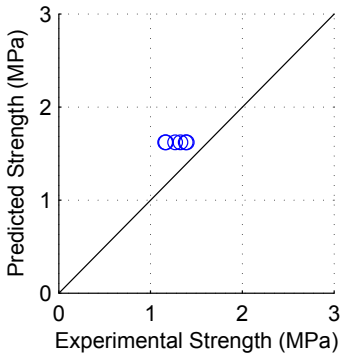

(c) Blondet Model

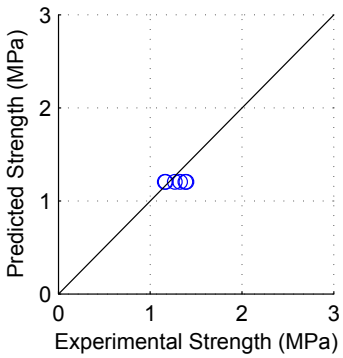

(d) Shing Model

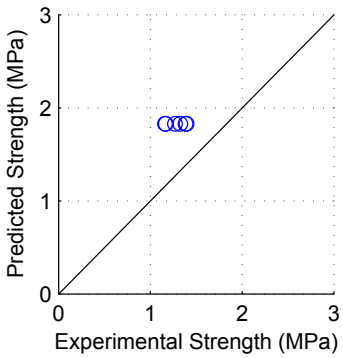

(e) Anderson Model

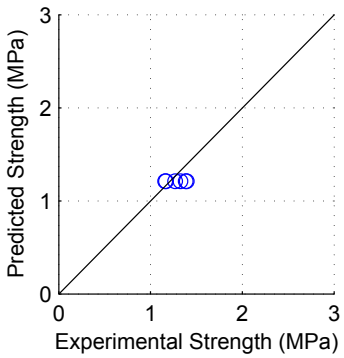

(f) Fattal Model

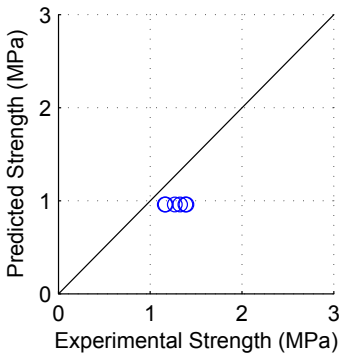

(g) NZS Model

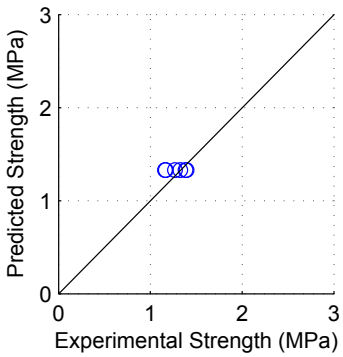

(h) Voon Model

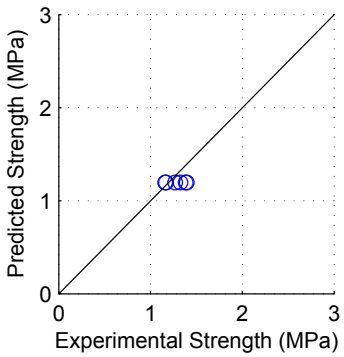

(i) CSA Model

Figure F.39: Model predictions for group 36

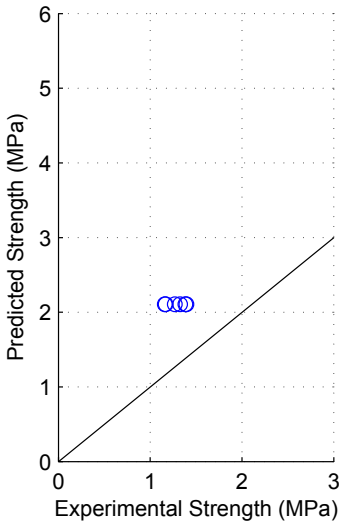

(j) TCCMaR Model

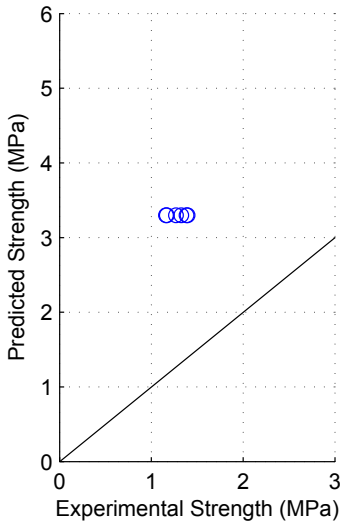

(k) UBC Model

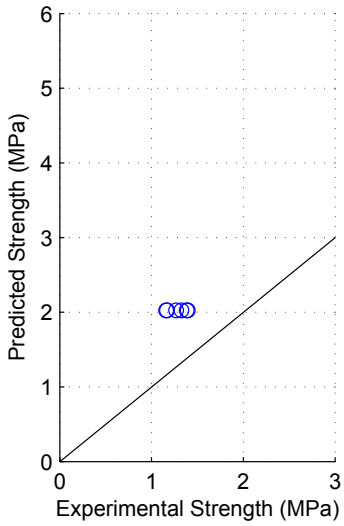

(l) AS Model

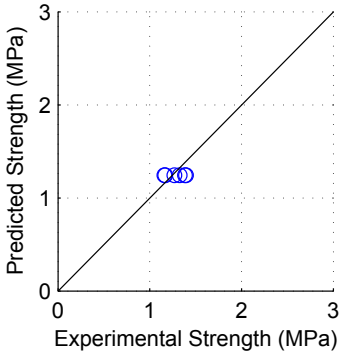

(m) MSJC Model

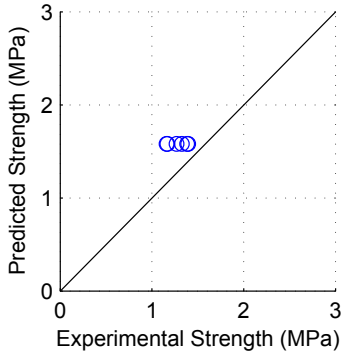

(n) BYU Model

Model predictions for group 36 (Continued)

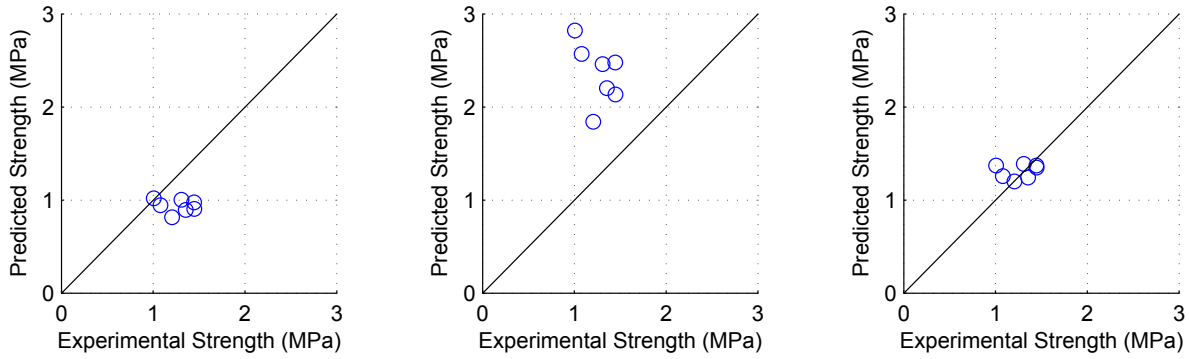

(a) Matsumura Model (b) AIJ Model (c) Blondet Model

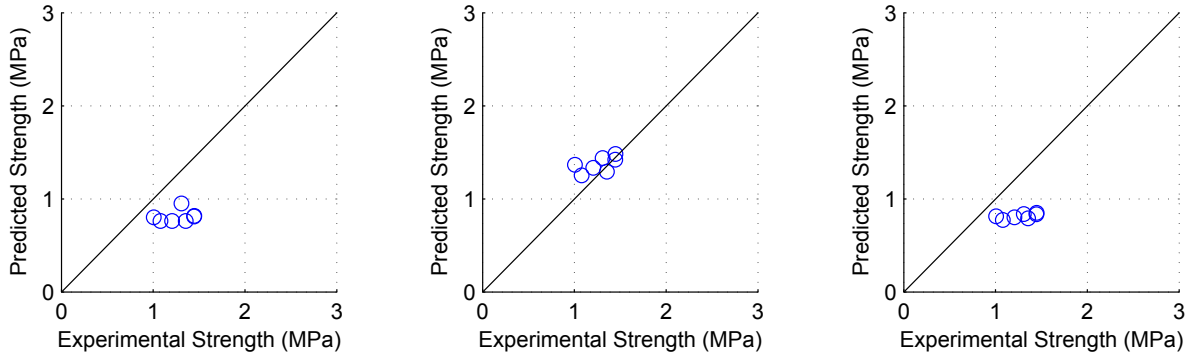

(d) Shing Model (e) Anderson Model (f) Fattal Model

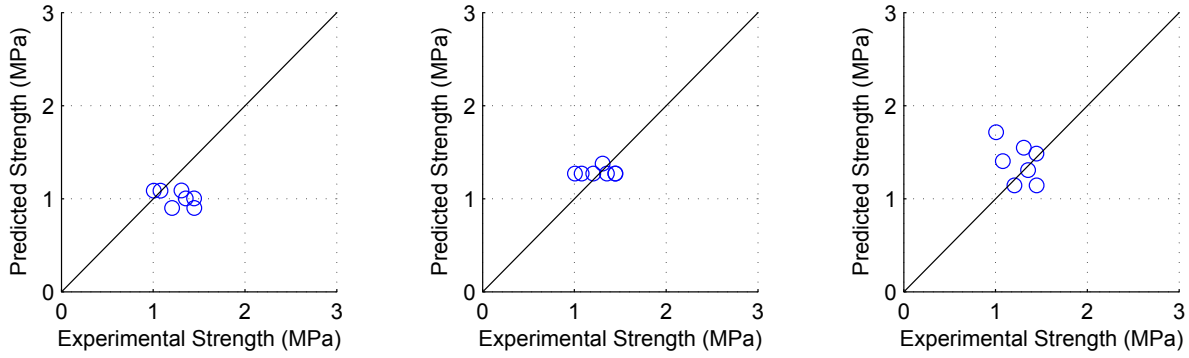

(g) NZS Model (h) Voon Model (i) CSA Model

Figure F.40: Model predictions for group 37

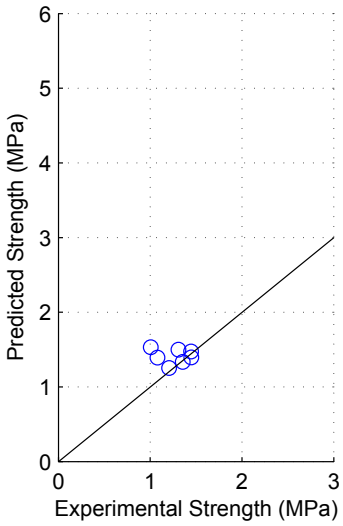

(j) TCCMaR Model

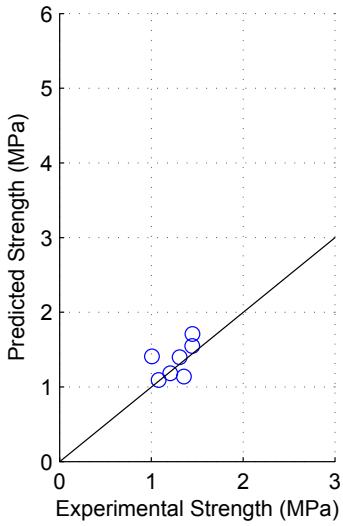

(k) UBC Model

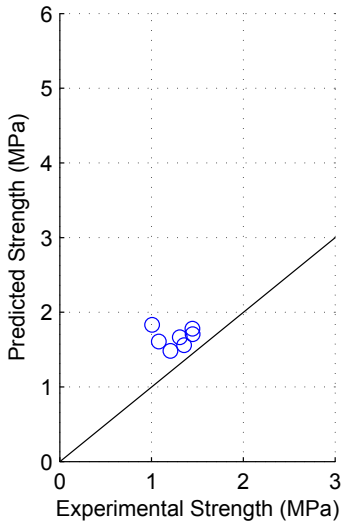

(l) AS Model

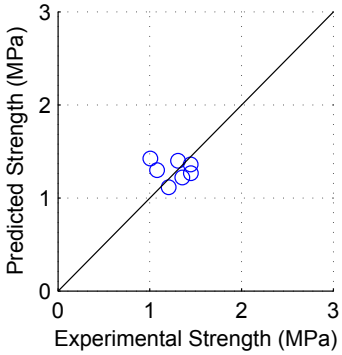

(m) MSJC Model

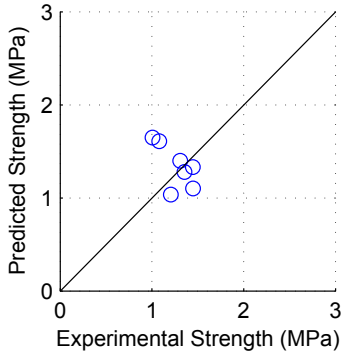

(n) BYU Model

Model predictions for group 37 (Continued)

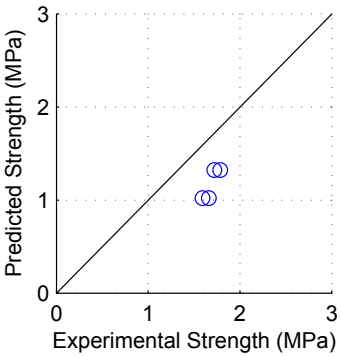

(a) Matsumura Model

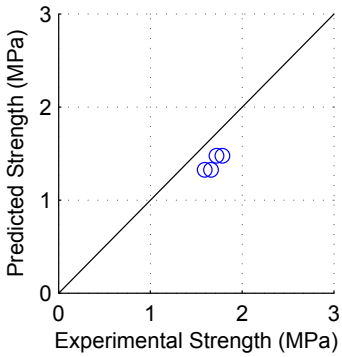

(b) AIJ Model

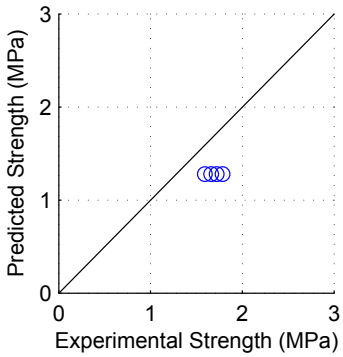

(c) Blondet Model

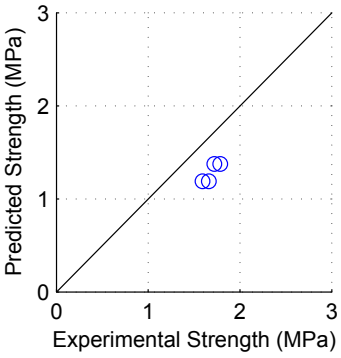

(d) Shing Model

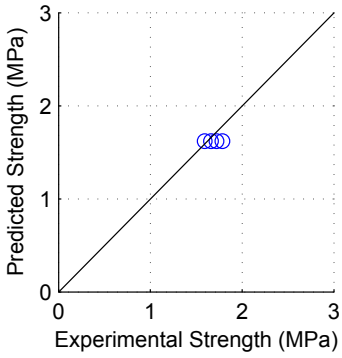

(e) Anderson Model

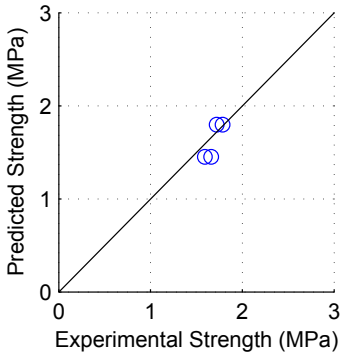

(f) Fattal Model

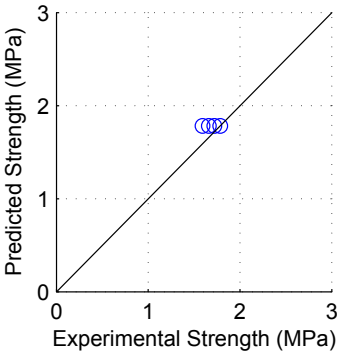

(g) NZS Model

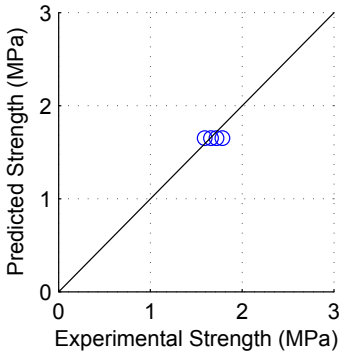

(h) Voon Model

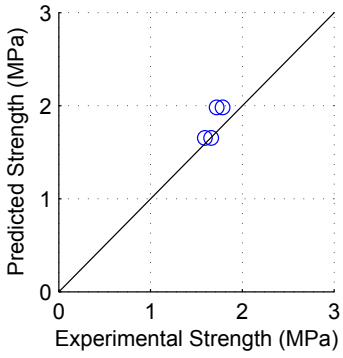

(i) CSA Model

Figure F.41: Model predictions for group 38

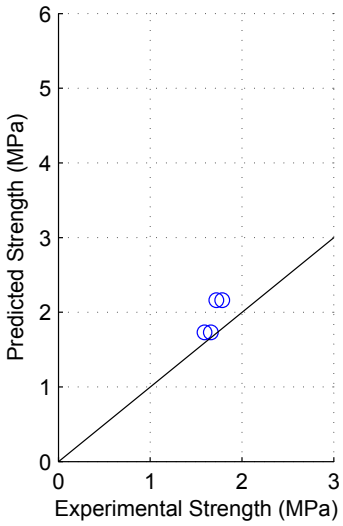

(j) TCCMaR Model

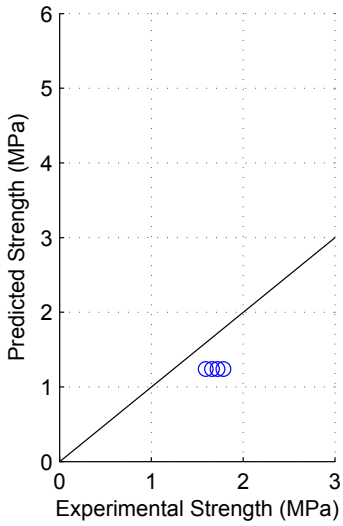

(k) UBC Model

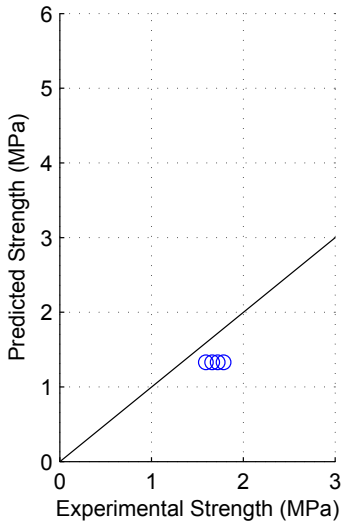

(l) AS Model

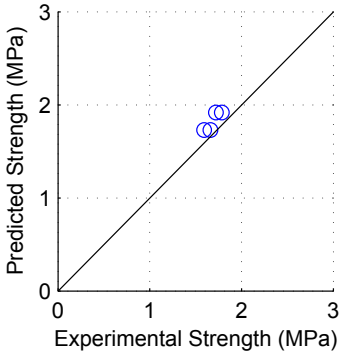

(m) MSJC Model

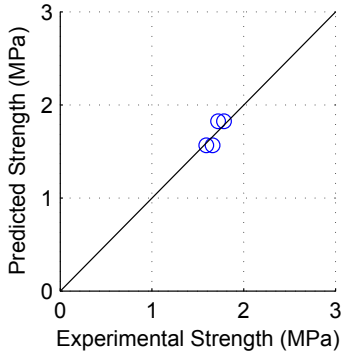

(n) BYU Model

Model predictions for group 38 (Continued)

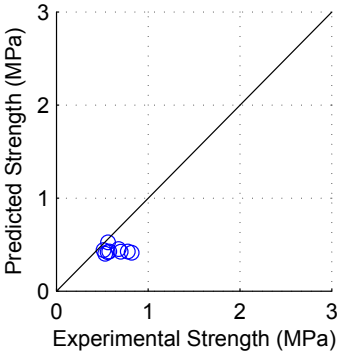

(a) Matsumura Model

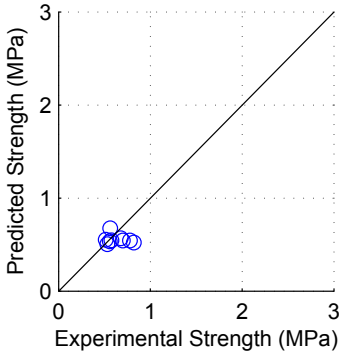

(b) AIJ Model

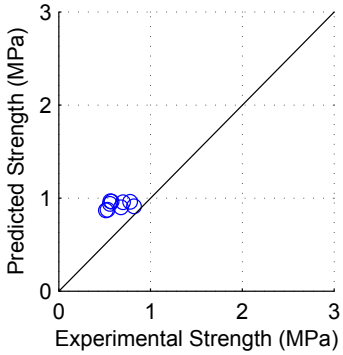

(c) Blondet Model

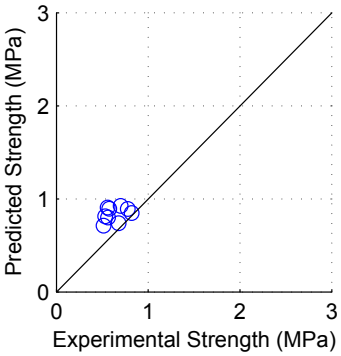

(d) Shing Model

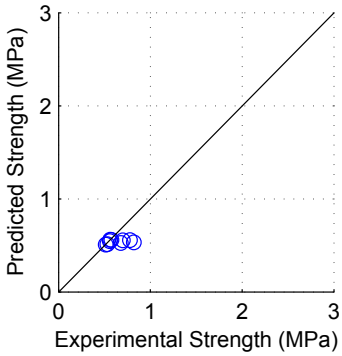

(e) Anderson Model

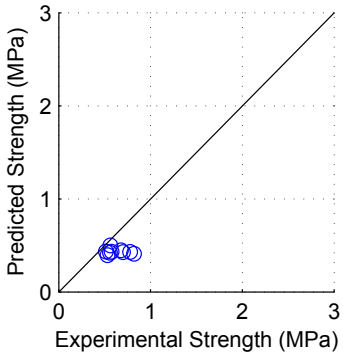

(f) Fattal Model

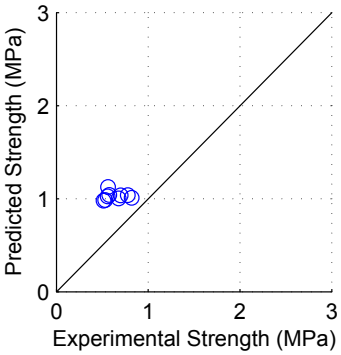

(g) NZS Model

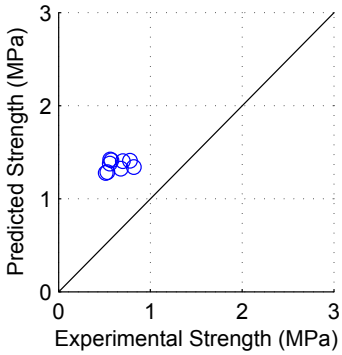

(h) Voon Model

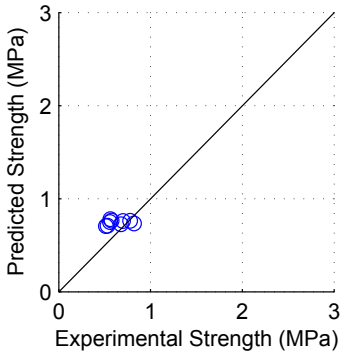

(i) CSA Model

Figure F.42: Model predictions for group 39

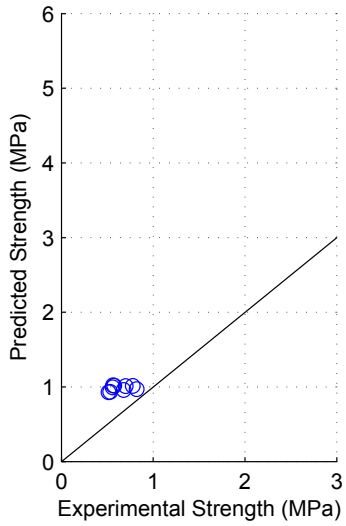

(j) TCCMaR Model

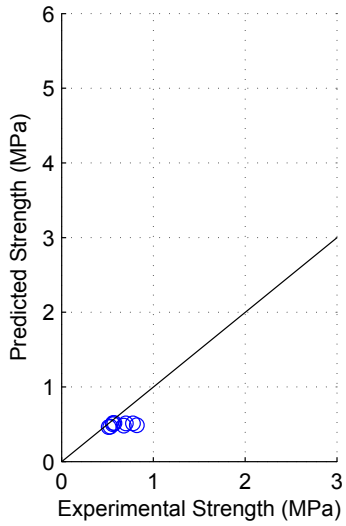

(k) UBC Model

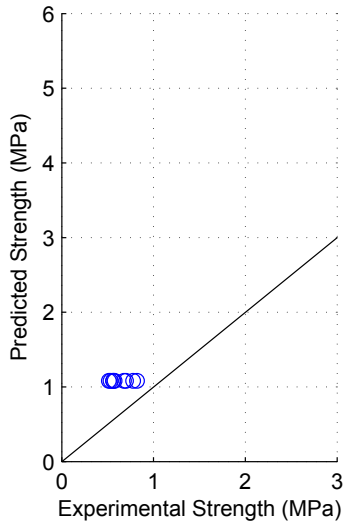

(l) AS Model

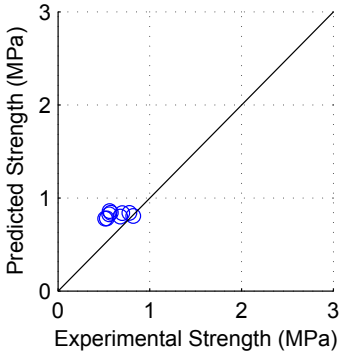

(m) MSJC Model

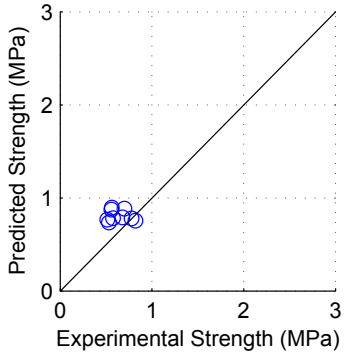

(n) BYU Model

Model predictions for group 39 (Continued)

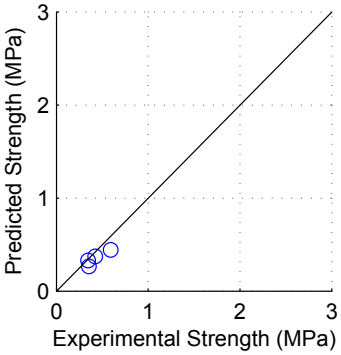

(a) Matsumura Model

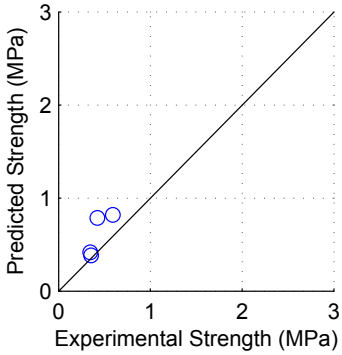

(b) AIJ Model

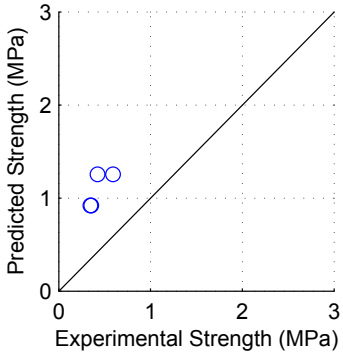

(c) Blondet Model

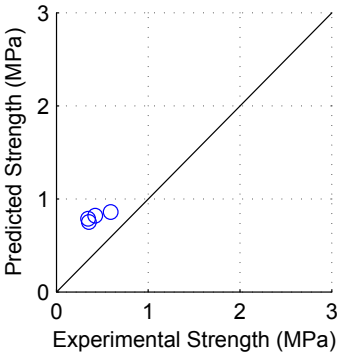

(d) Shing Model

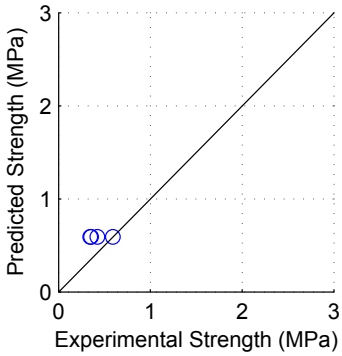

(e) Anderson Model

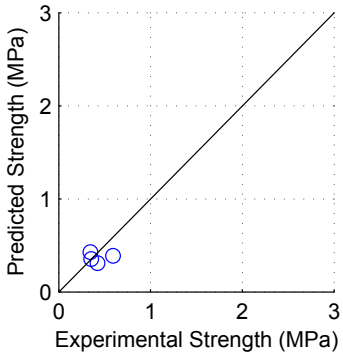

(f) Fattal Model

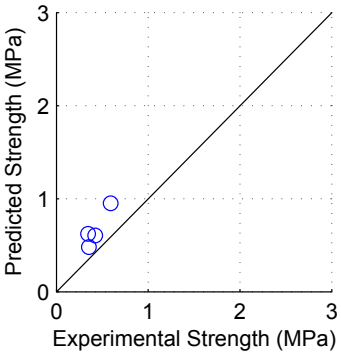

(g) NZS Model

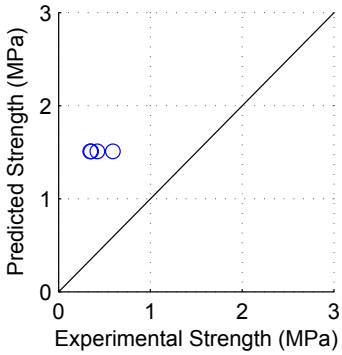

(h) Voon Model

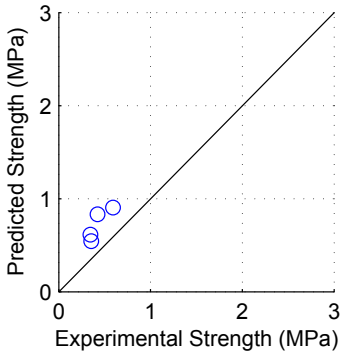

(i) CSA Model

Figure F.43: Model predictions for group 40

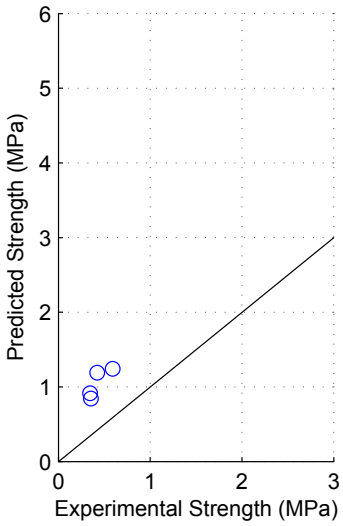

(j) TCCMaR Model

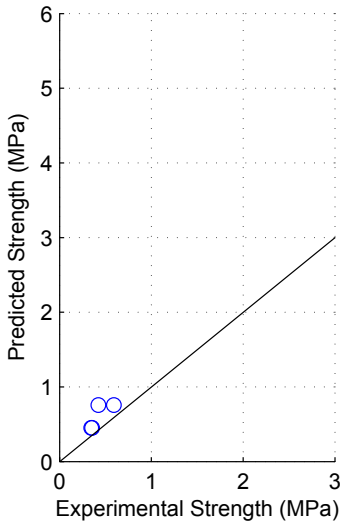

(k) UBC Model

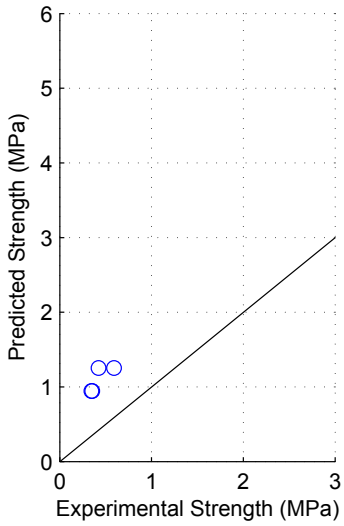

(l) AS Model

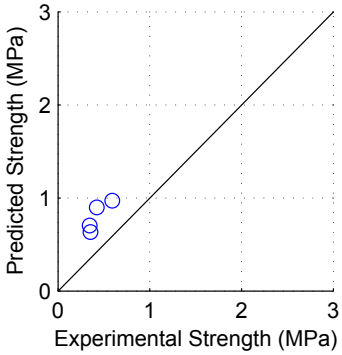

(m) MSJC Model

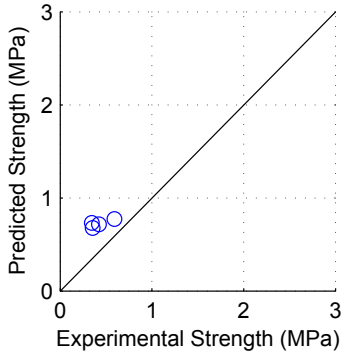

(n) BYU Model

Model predictions for group 40 (Continued)

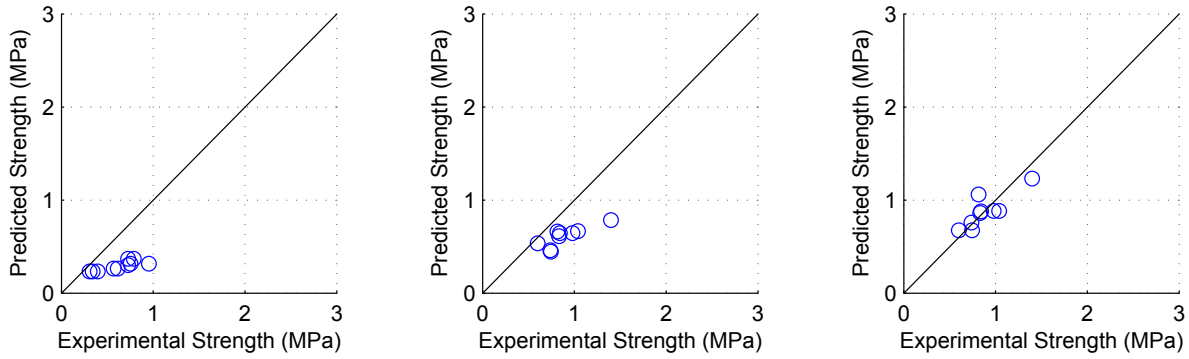

(a) Matsumura Model (b) AIJ Model (c) Blondet Model

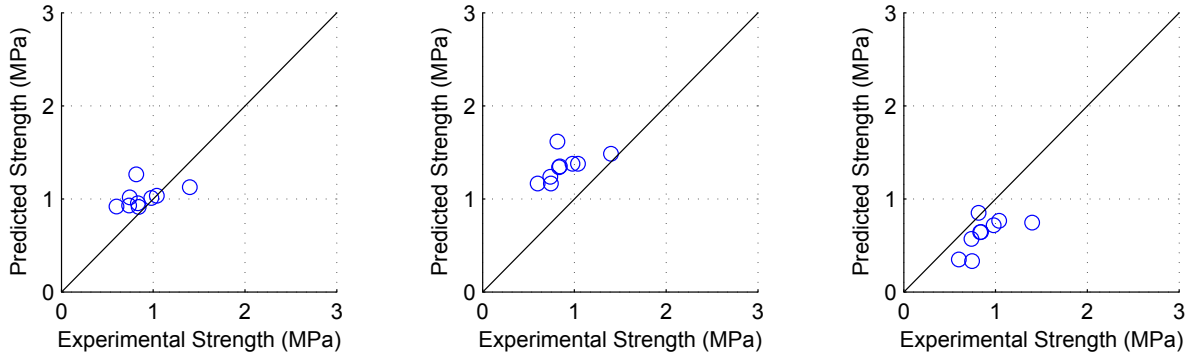

(d) Shing Model (e) Anderson Model (f) Fattal Model

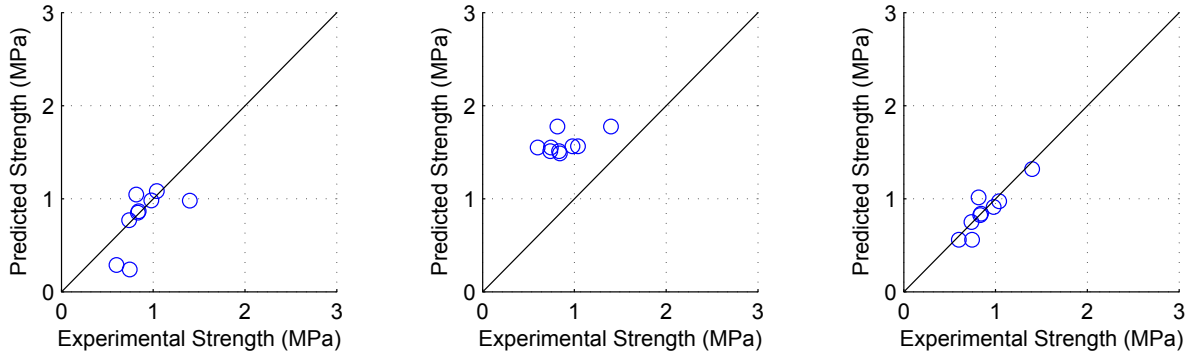

(g) NZS Model (h) Voon Model (i) CSA Model

Figure F.44: Model predictions for group 41

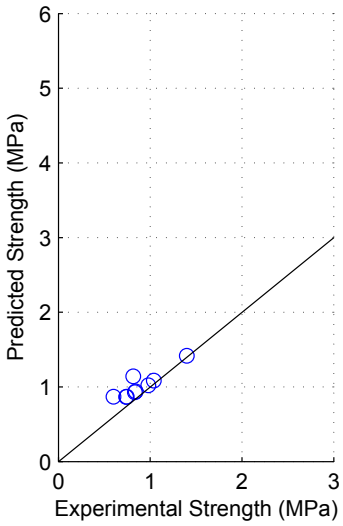

(j) TCCMaR Model

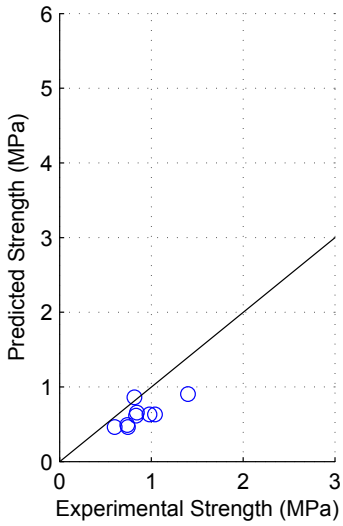

(k) UBC Model

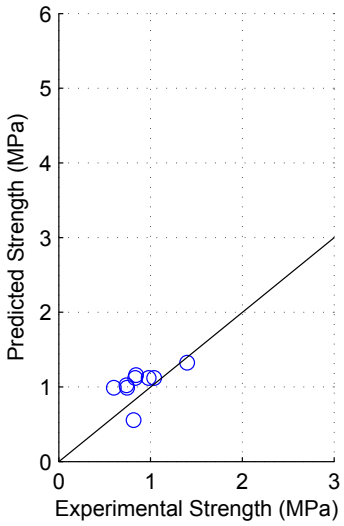

(l) AS Model

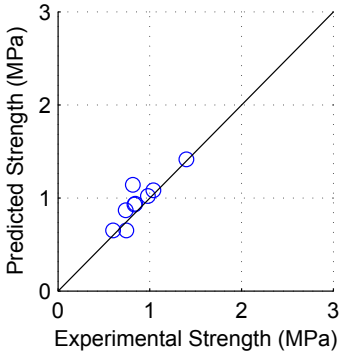

(m) MSJC Model

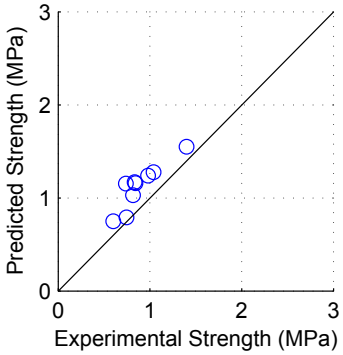

(n) BYU Model

Model predictions for group 41 (Continued)

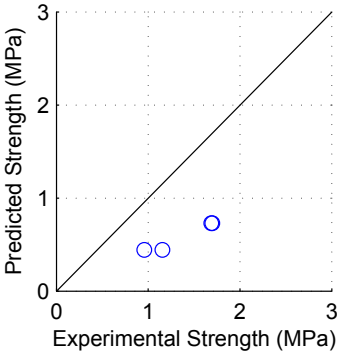

(a) Matsumura Model

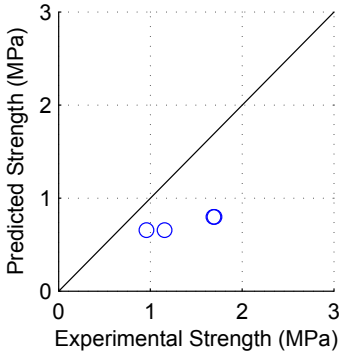

(b) AIJ Model

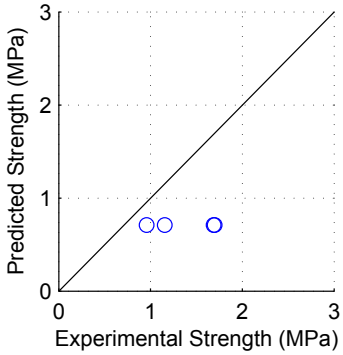

(c) Blondet Model

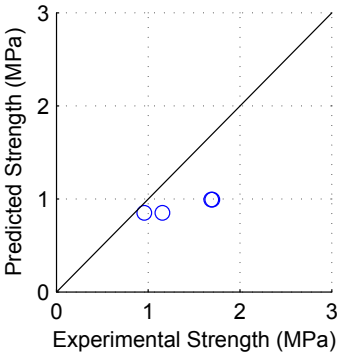

(d) Shing Model

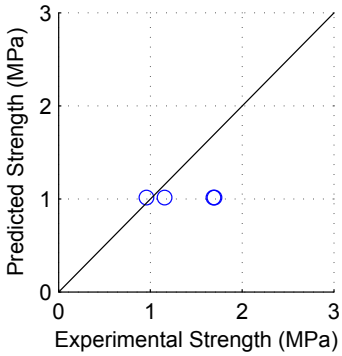

(e) Anderson Model

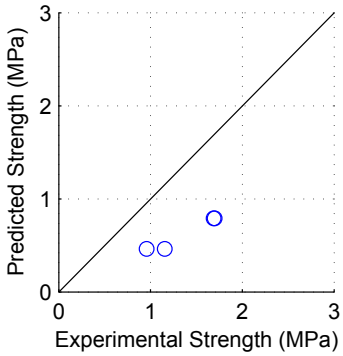

(f) Fattal Model

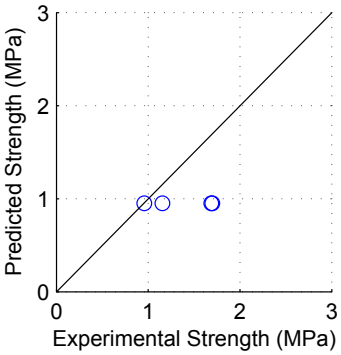

(g) NZS Model

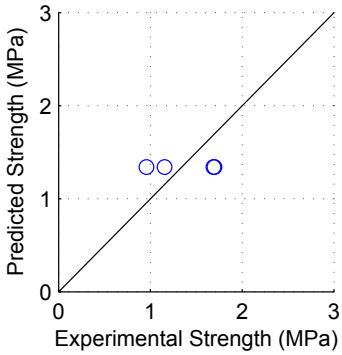

(h) Voon Model

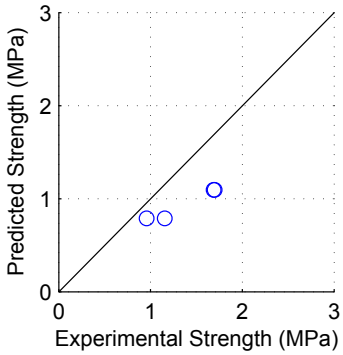

(i) CSA Model

Figure F.45: Model predictions for group 42

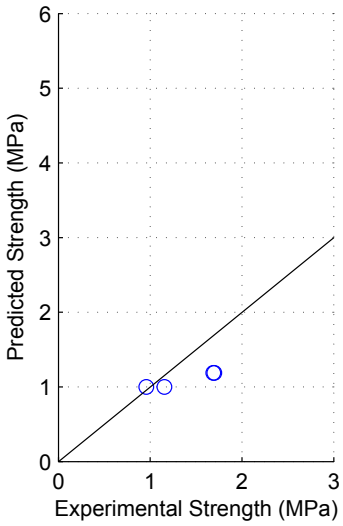

(j) TCCMaR Model

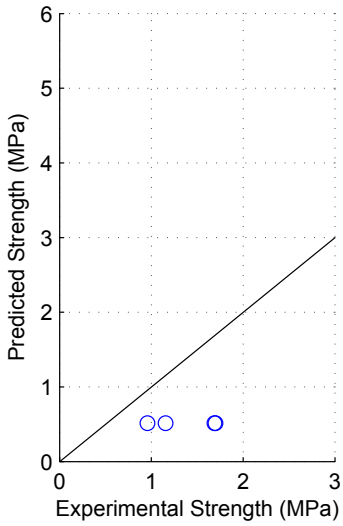

(k) UBC Model

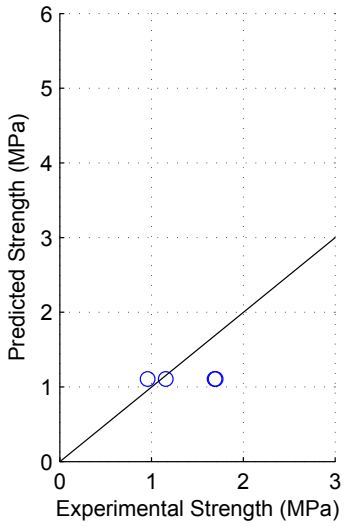

(l) AS Model

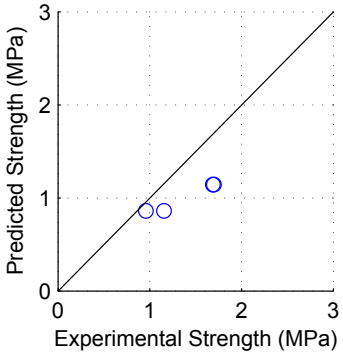

(m) MSJC Model

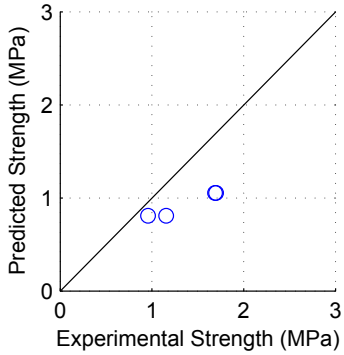

(n) BYU Model

Model predictions for group 42 (Continued)

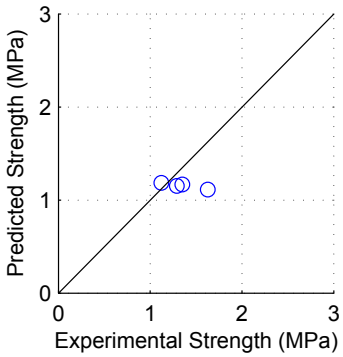

(a) Matsumura Model

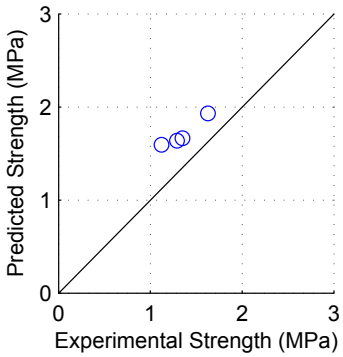

(b) AIJ Model

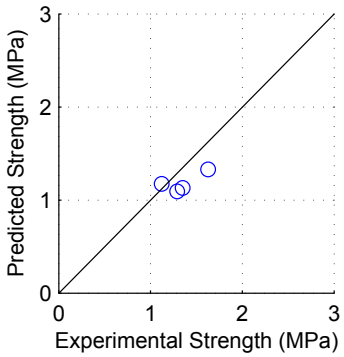

(c) Blondet Model

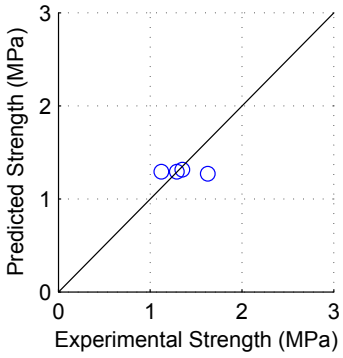

(d) Shing Model

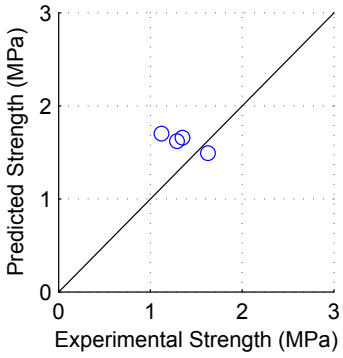

(e) Anderson Model

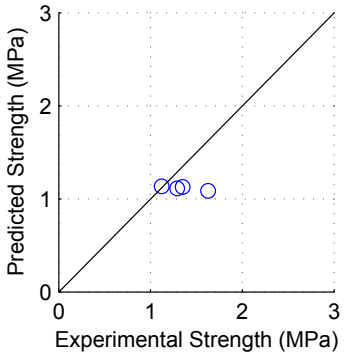

(f) Fattal Model

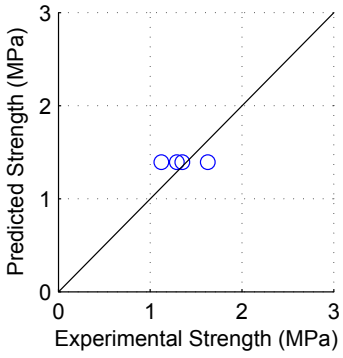

(g) NZS Model

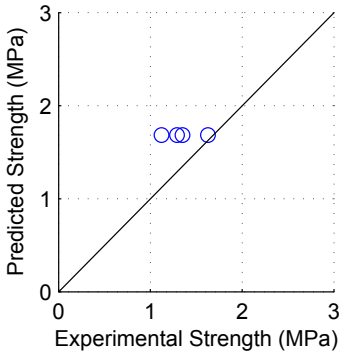

(h) Voon Model

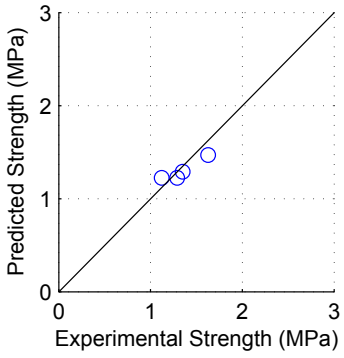

(i) CSA Model

Figure F.46: Model predictions for group 43

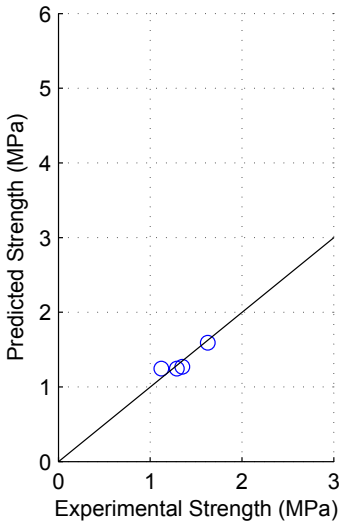

(j) TCCMaR Model

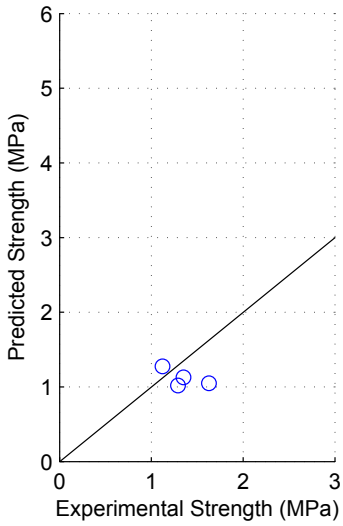

(k) UBC Model

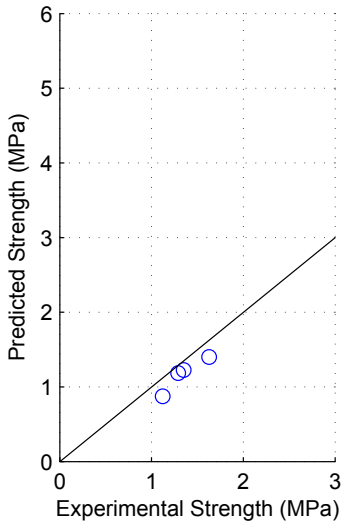

(l) AS Model

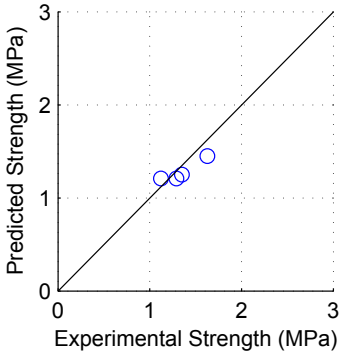

(m) MSJC Model

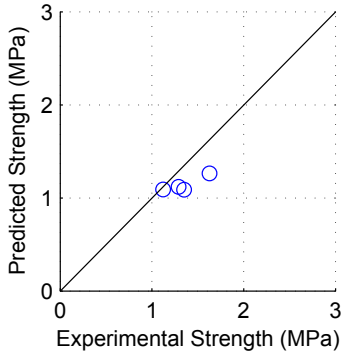

(n) BYU Model

Model predictions for group 43 (Continued)

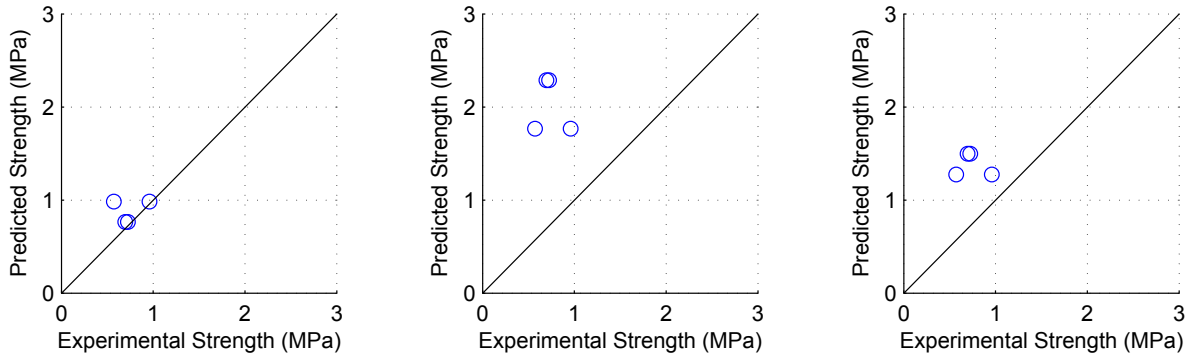

(a) Matsumura Model (b) AIJ Model (c) Blondet Model

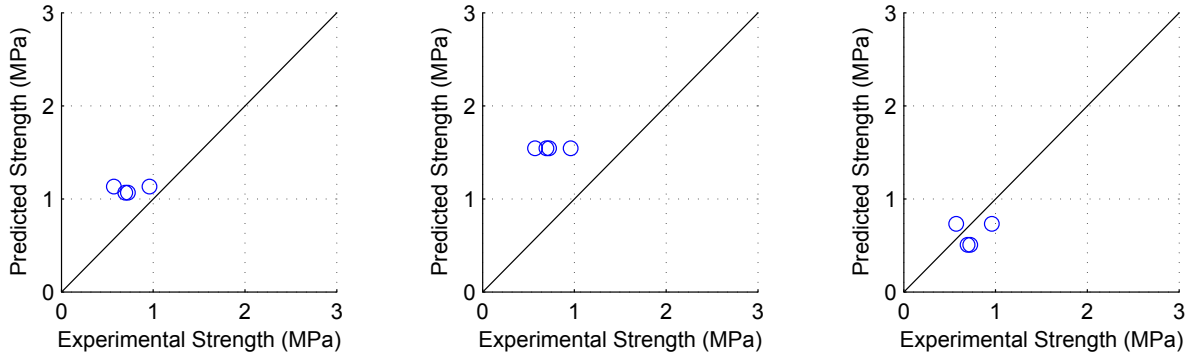

(d) Shing Model (e) Anderson Model (f) Fattal Model

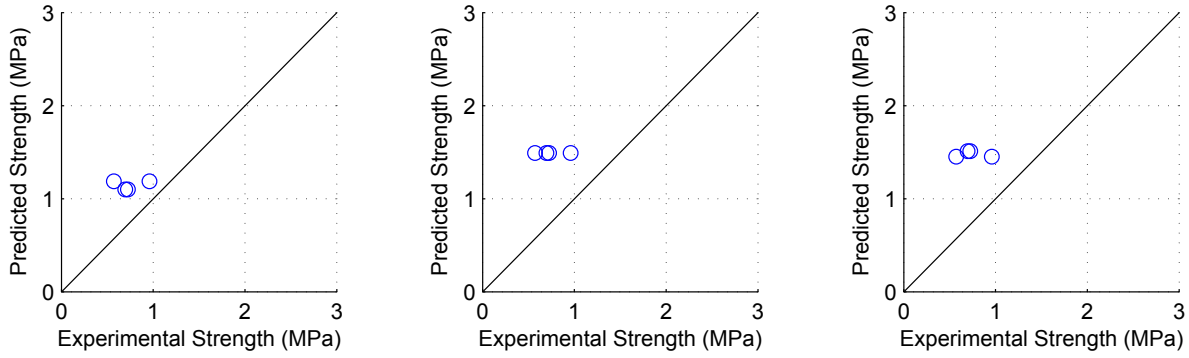

(g) NZS Model (h) Voon Model (i) CSA Model

Figure F.47: Model predictions for group 44

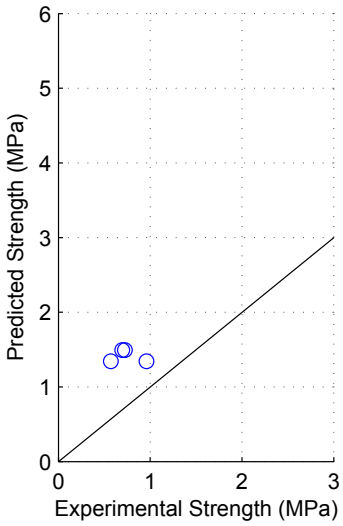

(j) TCCMaR Model

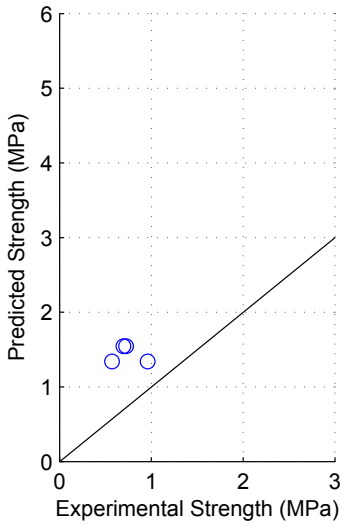

(k) UBC Model

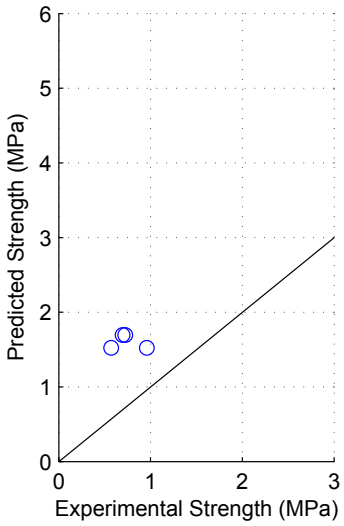

(l) AS Model

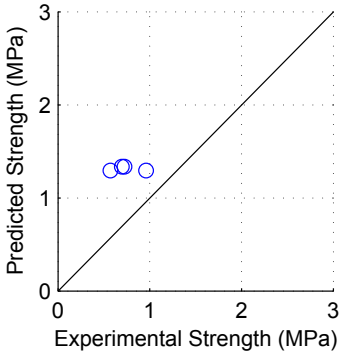

(m) MSJC Model

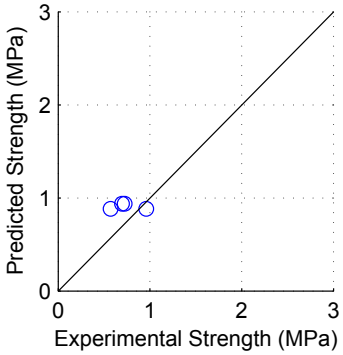

(n) BYU Model

Model predictions for group 44 (Continued)

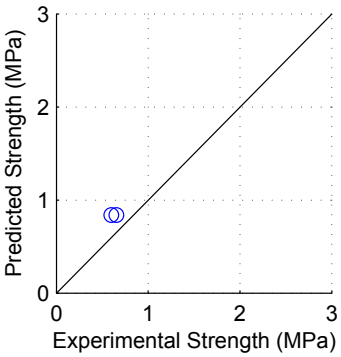

(a) Matsumura Model

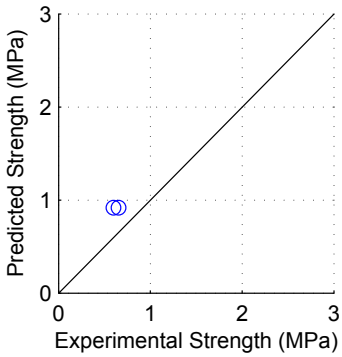

(b) AIJ Model

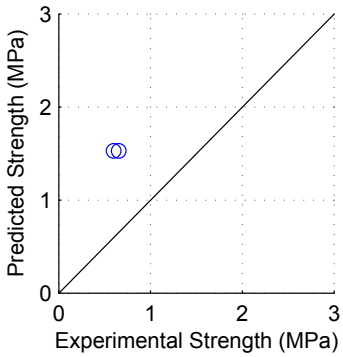

(c) Blondet Model

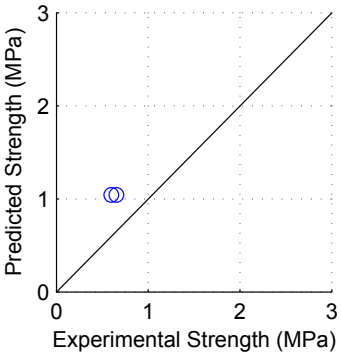

(d) Shing Model

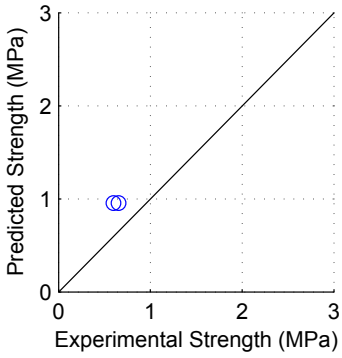

(e) Anderson Model

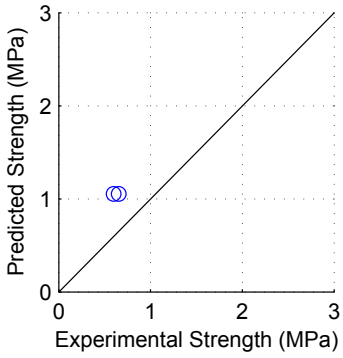

(f) Fattal Model

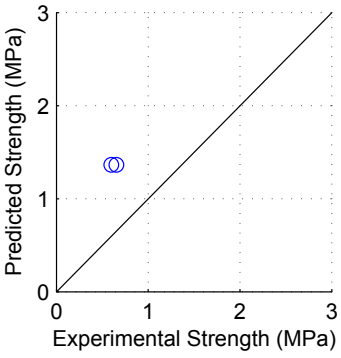

(g) NZS Model

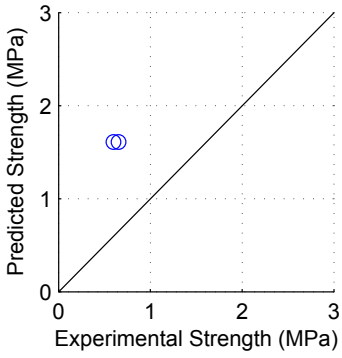

(h) Voon Model

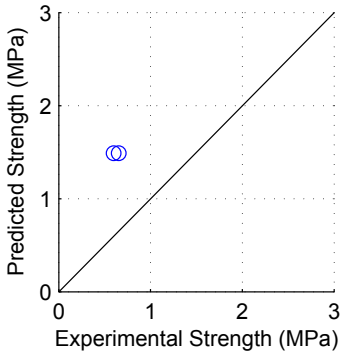

(i) CSA Model

Figure F.48: Model predictions for group 45

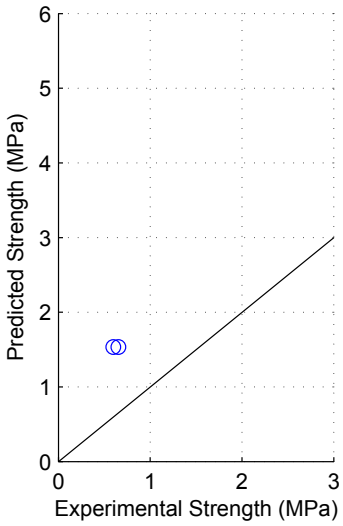

(j) TCCMaR Model

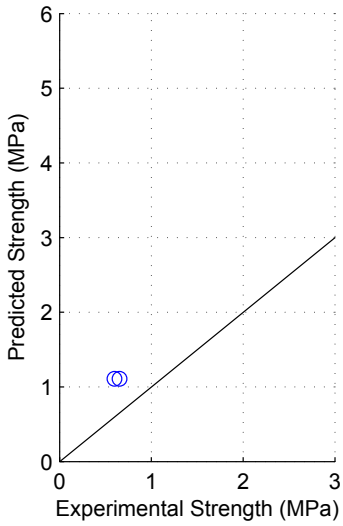

(k) UBC Model

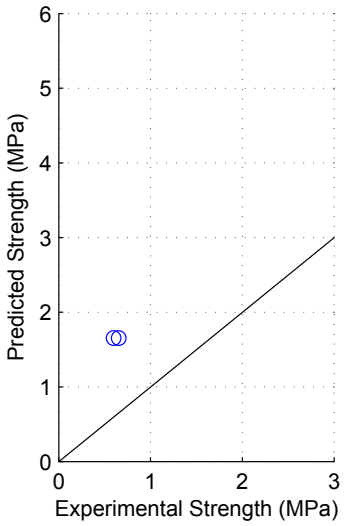

(l) AS Model

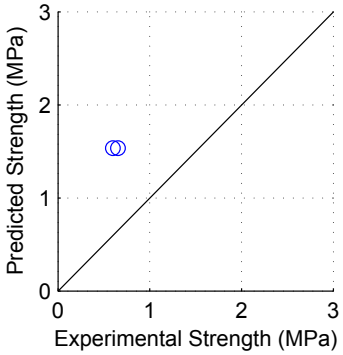

(m) MSJC Model

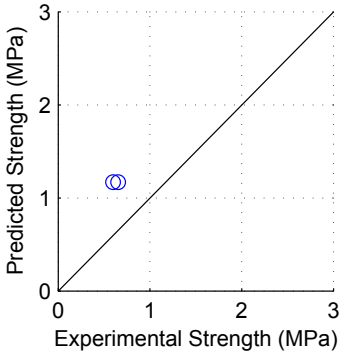

(n) BYU Model

Model predictions for group 45 (Continued)

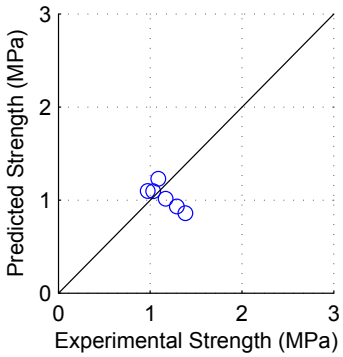

(a) Matsumura Model

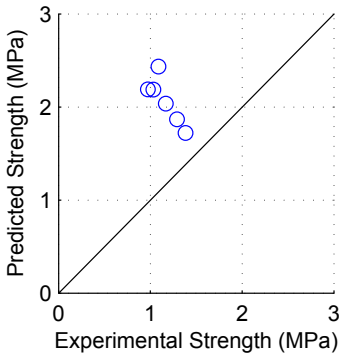

(b) AIJ Model

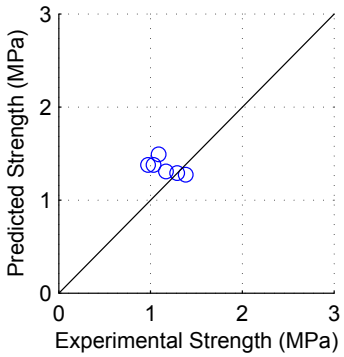

(c) Blondet Model

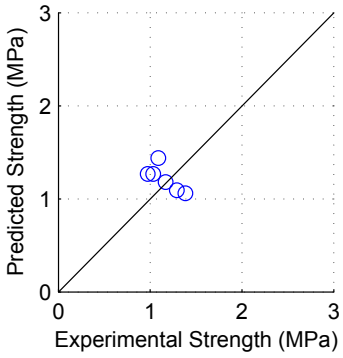

(d) Shing Model

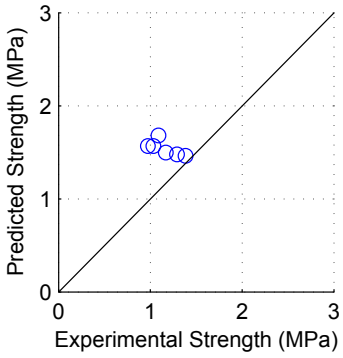

(e) Anderson Model

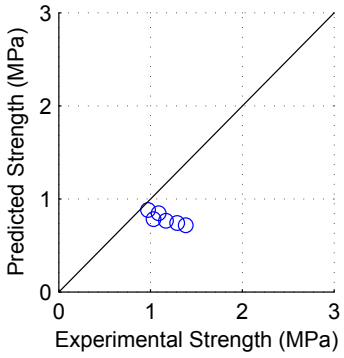

(f) Fattal Model

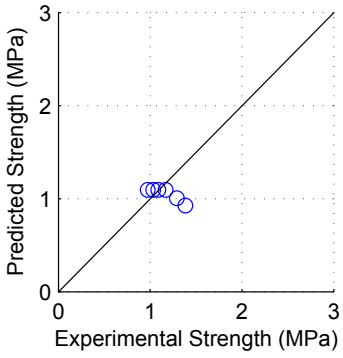

(g) NZS Model

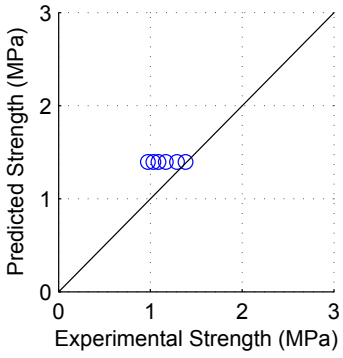

(h) Voon Model

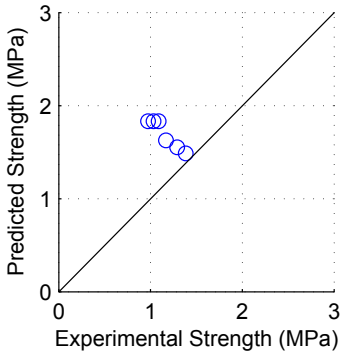

(i) CSA Model

Figure F.49: Model predictions for group 46

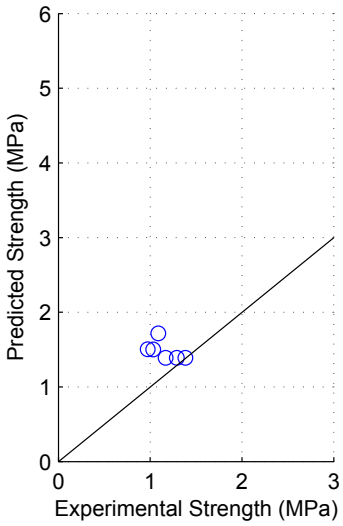

(j) TCCMaR Model

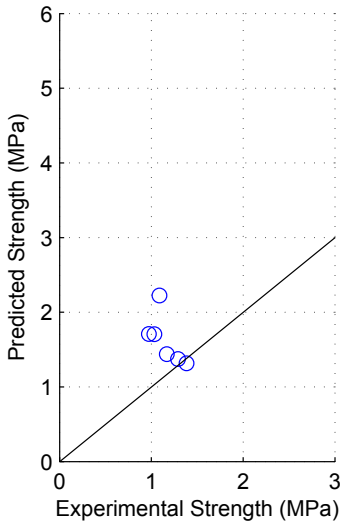

(k) UBC Model

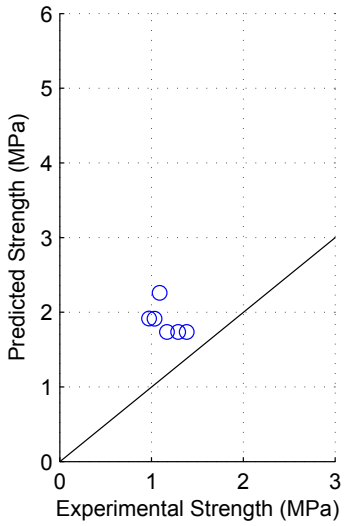

(l) AS Model

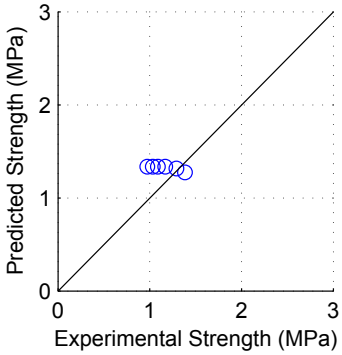

(m) MSJC Model

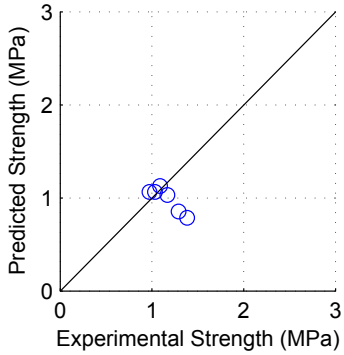

(n) BYU Model

Model predictions for group 46 (Continued)

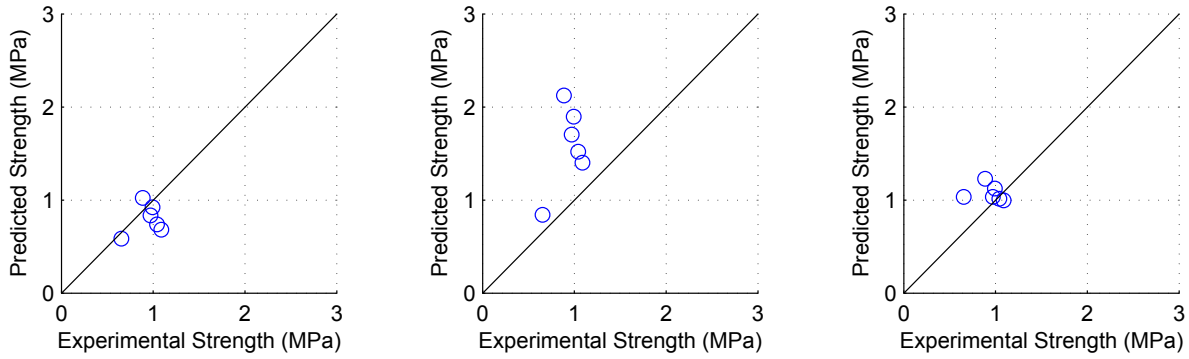

(a) Matsumura Model

(b) AIJ Model

(c) Blondet Model

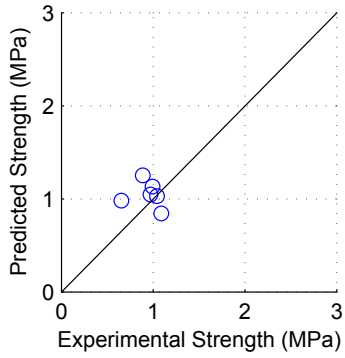

(d) Shing Model

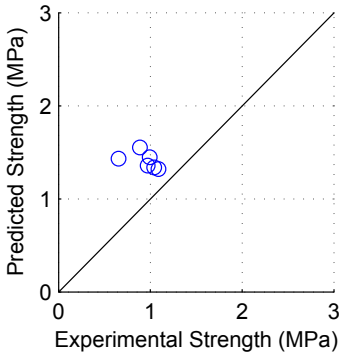

(e) Anderson Model

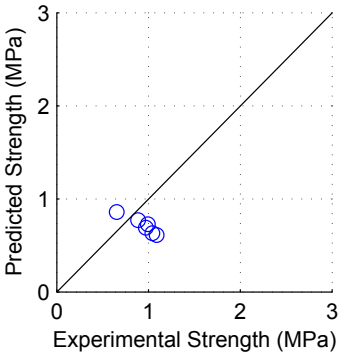

(f) Fattal Model

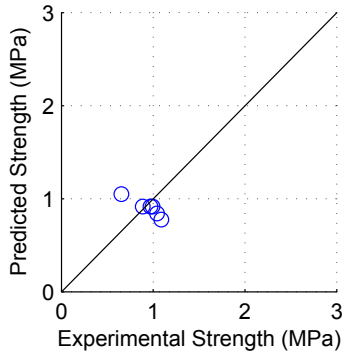

(g) NZS Model

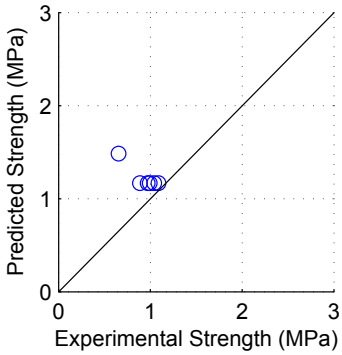

(h) Voon Model

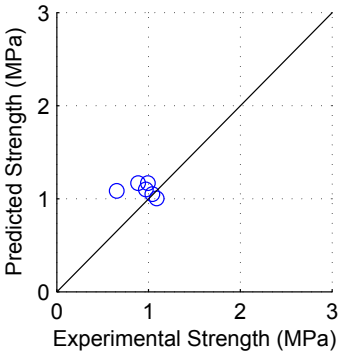

(i) CSA Model

Figure F.50: Model predictions for group 47

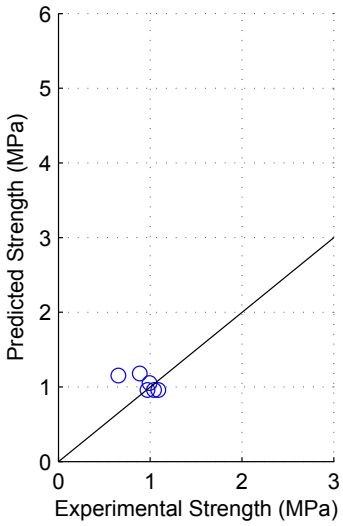

(j) TCCMaR Model

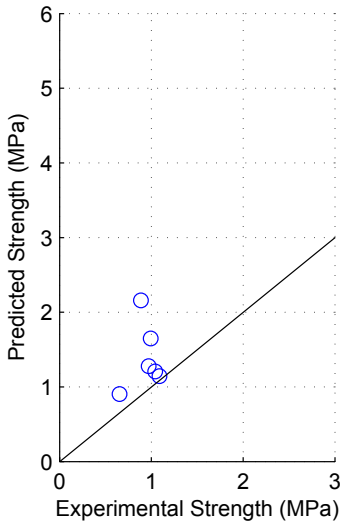

(k) UBC Model

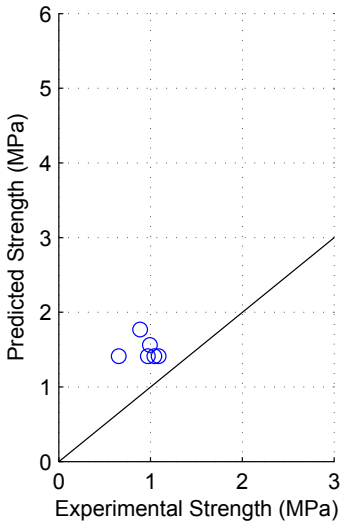

(l) AS Model

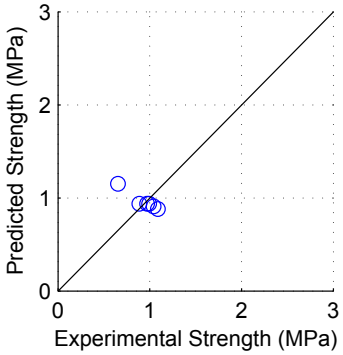

(m) MSJC Model

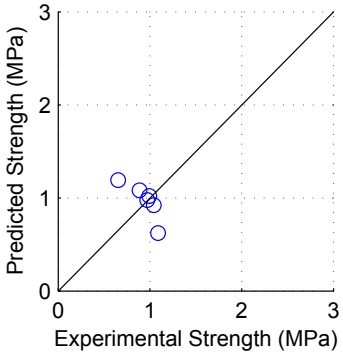

(n) BYU Model

Model predictions for group 47 (Continued)

APPENDIX G. MODIFICATION OF EXISTING MSJC EQUATION

The values used in these suggested revisions represent the values determined through the analysis in Part III of this study. The formatting used in this Appendix has been adjusted to match that used in the MSJC (2013) code.

CODE	COMMENTARY
9.1.4.5 *Shear in fully-grouted and solid masonry* — The value of ϕ shall be taken as 0.80 for fully-grouted masonry subjected to shear.	**9.1.4.5** *Shear in fully-grouted and solid masonry* — The strength-reduction factor for calculating the design shear strength of fully-grouted and solid masonry recognizes the greater uncertainty in calculating nominal shear strength than in calculating nominal flexural strength.
9.1.4.6 *Shear in partially-grouted masonry* — The value of ϕ shall be taken as 0.75 for partially-grouted and hollow masonry subjected to shear.	**9.1.4.6** *Shear in partially-grouted masonry* — The amount of uncertainty for partially-grouted masonry is larger than that for fully-grouted and solid masonry. A different shear strength-reduction factor is specified for partially-grouted masonry to maintain consistency in the probabilities of failure between the two different grouting types.
9.1.4.7 *Shear in unreinforced masonry* — The value of ϕ shall be taken as 0.80 for masonry subjected to shear not otherwise governed by the provisions in 9.1.4.5 or 9.1.4.6.	**9.1.4.7** *Shear in unreinforced masonry* — The strength-reduction factor for calculating the design shear strength of unreinforced masonry recognizes the greater uncertainty in calculating nominal shear strength than in calculating nominal flexural strength.
9.3.4.1.2 *Nominal shear strength* — Nominal shear strength, V_n, shall be calculated using Equation 9-21, and shall not be taken greater than the limits given by 9.3.4.1.2 (a) through (c).	**9.3.4.1.2** *Nominal shear strength* — The shear strength equations in Section 9.3.4.1.2 are derived from research (Shing et al, 1990a; Shing et al, 1990b). the equations have been compared with results from 353 tests of masonry walls failing in in-plane shear (current study). The test data encompassed both concrete masonry walls and clay masonry walls, including both fully- and partially-grouted walls. The average ratio of the test strength to the calculated strength for fully grouted walls was

$$V_n = (V_{nm} + V_{ns})\,\gamma_g \qquad \text{(Equation 9-21)}$$

(a) Where $M_u/(V_u d_v) \le 0.25$:

$$V_n \le \left(6A_{nv}\sqrt{f'_m}\right)\gamma_g \qquad \text{(Equation 9-22)}$$

(b) Where $M_u/(V_u d_v) \ge 1.0$:

$$V_n \ge \left(4A_{nv}\sqrt{f'_m}\right)\gamma_g \qquad \text{(Equation 9-23)}$$

$\gamma_g = 0.75$ for partially grouted shear walls and 1.0 otherwise.

(c) The maximum value of V_n for $M_u/(V_u d_v)$ between 0.25 and 1.0 shall be permitted to be linearly interpolated.

9.3.4.1.2.1 *Nominal masonry shear strength* — Shear strength provided by the masonry, V_{nm}, shall be calculated using Equation 9-24:

$$V_{nm} = \left[4.0 - 1.75\left(\frac{M_u}{V_u d_v}\right)\right] A_{nv}\sqrt{f'_m} + 0.25P_u \qquad \text{(Equation 9-24)}$$

$M_u/(V_u d_v)$ shall be taken as a positive number and need not be taken greater than 1.0.

9.3.4.1.2.2 *Nominal shear strength provided by reinforcement* — Nominal shear strength provided by shear reinforcement, V_{ns}, shall be calculated as follows:

$$V_{ns} = 0.5\left(\frac{A_v}{s}\right) f_y\, d_v \qquad \text{(Equation 9-25)}$$

0.97 with a coefficient of variation of 0.24. The average ratio of the test strength to the calculated strength for partially grouted walls was 0.73 with a coefficient of variation of 0.30.

. . .

. . .

Partially grouted walls have been shown to produce lower strengths than predicted by the shear strength equations using just the reduction of net area (current study; Minaie et al, 2010; Nolph and ElGawady, 2011; Schultz, 1996b; Schultz, 1996c; Schultz and Hutchinson, 2001b). The grouted shear wall factor is used to compensate for this reduction in nominal shear strength and has been validated by a comparison of nominal shear strengths for 172 fully grouted and 181 partially grouted shear wall tests.

9.3.4.1.2.1 *Nominal masonry shear strength* — Portions of Equation 9-24 were originally derived based on theoretical and empirical analysis on fully grouted masonry test data (Blondet et al, 1989; Anderson and Priestley, 1992). The current form of the equation was assembled by members of the TCC-MaR committee (NEHRP, 1994).

9.3.4.1.2.2 *Nominal shear strength provided by reinforcement* — Equation 9-25 was chosen assuming that only the reinforcement in the middle half of the wall height is effective in resisting the shear strength (Blondet et al, 1989, Shing et al, 1990a; Shing et al, 1990b). This assumption is based on the observation that the anchorages of shear reinforcement near the tops and bottoms of walls become interrupted by diagonal cracking and are, therefore, not able to develop their full theoretical strength contributions.

APPENDIX H. IMPROVEMENT OF EXISTING MSJC EQUATION

The values used in these suggested revisions represent the proposed equation developed through the analysis in Part IV of this study. The formatting used in this Appendix has been adjusted to match that used in the MSJC (2013) code.

CODE

2.1 — Notation

. . .

A_c = area of nonprestressed longitudinal confinement reinforcement, in^2. (mm^2)

. . .

s_{gh} = horizontal grout spacing of partially grouted walls, in. (mm)

. . .

t_s = shear thickness of member, taken as the total face shell thickness for partially grouted members and as t_{sp} otherwise, in. (mm)

. . .

V_{np} = nominal shear strength provided by axial load, lb (N)

. . .

9.3.4.1.2 *Nominal shear strength* — Nominal shear strength, V_n, shall be calculated using Equation 9-21, and shall not be taken greater than the limits given by 9.3.4.1.2.4.

$$V_n = V_{nm} + V_{np} + V_{ns} \qquad \text{(Equation 9-21)}$$

COMMENTARY

9.3.4.1.2 *Nominal shear strength* — The shear strength equations in Section 9.3.4.1.2 are derived from research (Shing et al, 1990a; Shing et al, 1990b). the equations have been compared with results from 353 tests of masonry walls failing in in-plane shear (current study). The test data encompassed both concrete masonry walls and clay masonry walls, including both fully- and partially-grouted walls. The average ratio of the test strength to the calculated strength for fully grouted walls was 0.97 with a coefficient of variation of 0.24. The average ratio of the test strength to the calculated strength for partially grouted walls was 0.73 with a coefficient of variation of 0.30.

. . .

9.3.4.1.2.1 *Nominal masonry shear strength* — Shear strength provided by the masonry, V_{nm}, shall be calculated using Equation 9-22 or Equation 9-23, as appropriate:

(a) For masonry which is partially grouted:

$$V_{nm} = \left[1.1 + 0.9\left(\frac{V_u\, s_{gh}}{M_u}\right)\right] A_{nv}\sqrt{f'_m} \quad \text{(Equation 9-22)}$$

(b) For masonry which is solid or fully grouted:

$$V_{nm} = \left[1.8 + 0.7\left(\frac{V_u\, d_v}{M_u}\right)\right] A_{nv}\sqrt{f'_m} \quad \text{(Equation 9-23)}$$

$(V_u d_v)/M_u$ and $(V_u s_{gh})/M_u$ shall both be taken as a positive number.

9.3.4.1.2.2 *Nominal shear strength provided by axial load* — Nominal shear strength provided by axial load, V_{np}, shall be calculated as follows:

$$V_{np} = 0.15P_u \quad \text{(Equation 9-24)}$$

9.3.4.1.2.3 *Nominal shear strength provided by reinforcement* — Nominal shear strength provided by reinforcement, V_{ns}, shall be calculated as follows:

$$V_{ns} = 0.12\left[\left(\frac{A_c f_y}{s_c}\right) d_v + \left(\frac{A_v f_y}{s_v}\right) h\right] \quad \text{(Equation 9-25)}$$

. . .

Partially grouted walls have been shown to produce lower strengths than predicted by the shear strength equations using just the reduction of net area (current study; Minaie et al, 2010; Nolph and ElGawady, 2011; Schultz, 1996b; Schultz, 1996c; Schultz and Hutchinson, 2001b). The grouted shear wall factor is used to compensate for this reduction in nominal shear strength and has been validated by a comparison of nominal shear strengths for 172 fully grouted and 181 partially grouted shear wall tests.

9.3.4.1.2.1 *Nominal masonry shear strength* — Equations 9-22 and 9-23 are empirically derived from linear regression on 353 reinforced masonry shear walls (current study). The regression results showed that partially grouted shear wall strength does not correlate as well with the shear span ratio as do fully grouted walls. The ratio of the horizontal grout spacing s_{gh} to the shear height M_U/V_u was found to provide a better correlation to the partially grouted wall test data. The different coefficients for fully and partially grouted walls represent a better fit for each subset of data and eliminate the need for a grouted wall factor.

9.3.4.1.2.2 *Nominal shear strength provided by axial load* — Equation 9-24 is empirically derived from linear regression on 353 reinforced masonry shear walls (current study).

9.3.4.1.2.3 *Nominal shear strength provided by reinforcement* — Equation 9-25 is empirically derived from linear regression on 353 reinforced masonry shear walls (current study). It was found that the shear reinforcement did not contribute in as great a degree as had originally been assumed based on theory. It was also found that longitudinal reinforcement did have a statistically significant contribution to wall shear strength. It has been found that both types of reinforcement contribute by restraining the diagonal tensile forces that develop perpendicular to the shear stress fields in a member and by helping to redistribute stresses within a cracked masonry member.

9.3.4.1.2.4 *Limit to nominal shear strength* — Nominal shear strength, V_n, calculated in Equation 9-21 shall not be taken greater than the the force necessary for the member to violate the conditions of in-plane rotational equilibrium. When calculating the rotational equilibrium capacity, all longitudinal reinforcement may be considered to contribute up to their respective yield strengths. Any unfactored axial load may also be considered to contribute. The equilibrium limit is give by Equations 9-26 and Equation 9-27:

(a) For computing the rotational equilibrium limit, the depth of the equivalent compression block shall by taken as:

$$a_v = \frac{P + \left(\frac{A_c f_y}{s_c}\right) d_v}{0.8 f'_m t_s} \qquad \text{(Equation 9-26)}$$

(b) The rotational equilibrium limit shall be taken as:

$$V_n \leq \left[P + \left(\frac{A_c f_y}{s_c}\right) d_v\right] \frac{(d_v - a_v)}{2} \frac{V_u}{M_u} \qquad \text{(Equation 9-27)}$$

9.3.4.1.2.3 *Limit to nominal shear strength* — Is is possible for a masonry member to be stronger than the externally applied forces and for the member to fail via large rotational deformations. Equation 9-27 represents the force required for a rigid masonry member to overcome the external equilibrium forces. Equation 9-27 is based on a diagonal strut which travels from the inflection point of the member to the compression block. The axial forces applied at the inflection point are equal to the sum of the axial load and the yield strengths of the longitudinal reinforcement in tension. The limit is equal to the shear force required to cause the vertical component of the diagonal strut to exceed the applied loads and rotate about the centroid of the compression block. This model ignores the tensile strength of the masonry.

The nominal shear strength limits given in previous version of the code were found to not be effective with the new shear strength equation. The new shear strength equation was found to provide adequate protection from critical (brittle) shear-related failures without additional strength limits being imposed.

APPENDIX I. STRUT-AND-TIE MODELING OF SHEAR WALLS

CODE

I.1 Definitions

Nodal Zone — The volume of masonry around a nodal in which forces are transferred between struts, ties, and/or other nodal zones.

Node — A point at which forces from struts, ties, applied loads, and reactions within a strut-and-tie model intersect.

Strut — A compression member in a strut-and-tie model.

COMMENTARY

Nodal zones are represented as a triangular region of masonry with three faces. When more than three forces intersect at a node the region around the node is segmented into smaller nodal zones with three faces each which bear against each other. Nodal zones may be considered to occur within the slabs or the foundation above or below the wall.

A node exists when at least three forces intersect. All forces acting on a node must be in static equilibrium.

Struts travel principally in the diagonal direction through the masonry panel. In partially-grouted walls the struts travel principally through the face shells and mortar joints of the panel. In fully-grouted walls the struts travel through the masonry units, mortar joints, and grouted cores of the panel. In masonry shear walls the compression capacity of the reinforcement is typically ignored.

There are three types of struts—prismatic, fan-shaped, and bottle-shaped—as shown in Figure I.1. Within masonry shear walls, bottle-shaped struts are the most frequent strut type used because the masonry panel typically allow sufficient space between struts for the stress fields to diverge. Prismatic struts are typically limited to the end jamb of the wall. Fan-shaped struts are also possible within masonry shear walls but stresses within a fan-shaped strut are typically idealized as several smaller struts all converging together at the wall toe.

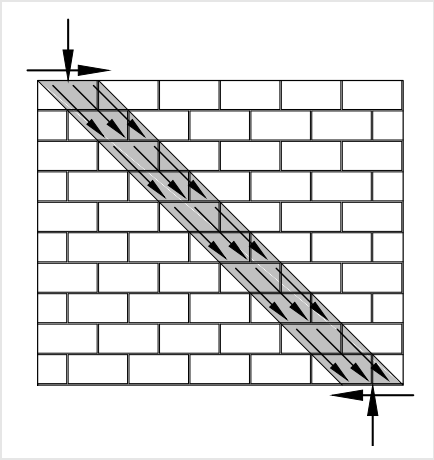

(a) Prismatic strut

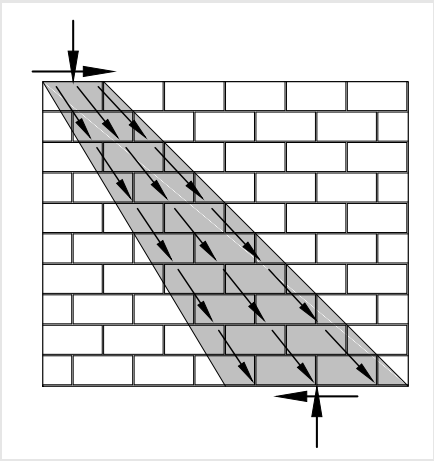

(b) Fan-shaped strut

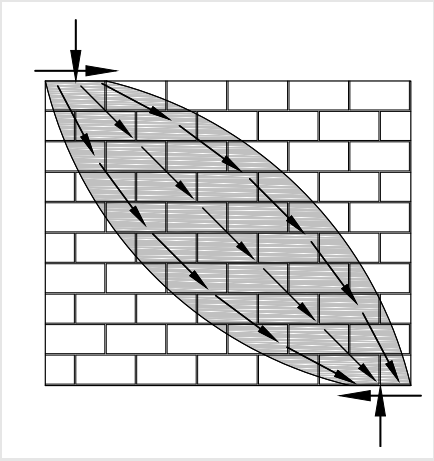

(c) Bottle-shaped strut

Figure I.1: Strut types

Strut-and-tie model — A model of a masonry member based on a truss analogy in which the compressive forces are represented as strut elements and tensile forces are represented by ties. The struts and ties connect at nodes forming a truss in which all members are assumed to carry only axial loads.

Strut-and-tie models are more complex than other, simple truss models in which nodes are located at the intersections of reinforcement bars. Within strut-and-tie models the nodes must be moved and the strut sizes adjusted to account for the geometry of the model elements and provide the necessary anchorage for the ends of the elements.

Strut Inclination Angle — The angle between the axis of the strut and direction normal to the bed joint plane (typically the vertical direction).

The definition of the strut inclination angle was selected such that the angle of 0 degree corresponds to the loading used in masonry prism tests. This angle represents what is considered to be the masonry compressive strength. The angle also corresponds to the equilibrium state of struts within an axially-loaded shear wall without any laterally-applied load.

Tie — A tension member in a strut-and-tie model.

Tie consist of reinforcement bars embedded in grout within the masonry panel and a prismatic section of the grout and masonry immediately between and adjacent to the reinforcement.

I.2 General

Strut-and-tie models may be used for design and analysis of masonry shear walls with or without openings.

Strut-and-tie models for masonry shear walls shall follow the provisions in I.1 through I.5.

The performance of strut-and-tie models constructed for 155 masonry shear wall specimens was compared against the experimental strengths. It was observed that strut-and-tie models produced accurate predictions when the models were developed satisfying the requirements of I.1 through I.5 (current study).

I.2.1 *Strength Reduction Factor* — The strength reduction factor ϕ for strut-and-tie models shall be taken as 0.90.

Strut-and-tie have been observed to demonstrate less uncertainty and to consistently produce lower coefficients of variation than equation-based prediction approaches. The reduction in uncertainty is attributed to the models' improved ability to account for the complex interactions between geometric and material strength properties. Equation-based methods are linear models in which the influence of each parameter is assumed to be linearly related to the wall shear strength. This assumption of linear correlation is a simplification of the observed behavior which are necessitated to produce an equation simple enough for regular use.

The application of strut-and-tie models to masonry design is based on the theory of plasticity.

The lower-bound theorem of the theory of plasticity states that strut-and-tie models should always produce a lower bound to the ultimate strength of the member. This property is due in part to the models neglecting the strength contributions of ancillary mechanisms such as crack friction, dowel action, etc. Another way of stating the lower-bound theorem is by saying that strut-and-tie models should never under-predict the wall strength, or that they are conservative.

Mechanical modeling has shown that when the provisions for strut-and-tie modeling in I.1 through I.5 are properly applied, then the initiation of failure will be through yielding of the reinforcement. Given the lower level of uncertainty compared to equation-based predictions, the gravitation to producing conservative predictions, and the tendency toward ductile failure mode, it was judged that strut-and-tie model design strength would be best represented using a strength reduction factor similar to that of beams.

I.2.2 *Equilibrium* — The forces and reactions applied to the strut-and-tie model shall be in equilibrium. External forces shall be applied to the model at nodes.

Strut-and-tie models are based on a truss analogy in which the truss elements are considered to resist only axial loads. As a result, all forces and resultants must be applies at the ends of struts and/or ties at nodes.

I.2.2.1 *Distributed Loads* — Distributed loads shall be idealized as concentrated loads acting at nodes. The magnitude of the idealized loads shall be based on the principle of tributary length for the node.

The influence of each strut on the overall shear capacity of the wall is a function of the load applied to the strut and the strut's inclination. This requirement is intended to prevent the designer from resolving all of the distributed load onto the strut(s) which would produce the greatest lateral force component, therefore artificially inflating the strength.

I.2.3 *Continuity* — Struts and ties shall be continuous between nodes. Forces may be transferred into or from struts or ties only at nodes.

This requirement is necessary for the truss analogy to hold.

I.2.4 *Geometry* — The geometry and layout of the struts, ties, and nodal zones shall be considered in constructing the strut-and-tie model.

Geometrical considerations in strut-and-tie models are a distinguishing characteristic from other truss analogies. In strut-and-tie models, the masonry not included in struts or nodes and the reinforcement not included within ties is assumed to not contribute to the wall strength. These excluded materials could

be removed from the wall without a loss in equilibrium or in predicted strength. As a result, the materials within the struts, ties, and nodes must be sufficient to meet all of the strength and anchorage requirements. The provision against the overlapping of struts is necessary to prevent the crushing of the masonry within that area.

I.2.4.1 *Crossing of Elements* — Ties shall be permitted to cross struts or other ties without transferring forces between the two element. Struts shall not overlap and shall only intersect or meet at nodes.

I.2.4.2 *Toe Extension* — For struts which traverse grouted and ungrouted portions of a wall, the leading edge of struts ending within a grouted column adjacent to a wall edge shall be permitted to extend past the edge of the wall at the strut end by a distance given by the toe extension length, l_x. The toe extension length shall be determined assuming that the compression bearing area of the strut on the leading side of the strut axis included the grouted cell and adjacent webs.

Through modeling of partially-grouted specimens it was observed that limiting the thickness of all struts to include only the face shell area produced predictions which were overly conservative. The compressive stresses were allowed to spread to the grouted cell over several different lengths, effectively decreasing the horizontal length of the toe and increasing the strut inclination angle, α_s, as shown in Figure I.2. It was determined that the centroid of the compression area was the limit for which the grouted core could be included in the compression area of the strut. The toe extension length, l_x, can be determined depending on whether the axis of the strut ends within or behind of the grouted length, l_g.

(a) For cases where the axis ends within the grouted length:

$$l_x = \frac{a}{2}\left(1 - \frac{t_s}{t_g}\right)$$

(b) For cases where the axis ends behind the grouted length:

$$l_x = l_g\left(\frac{t_g}{t_s} - 1\right)$$

In many cases, a strut ending within the grouted end cell of the wall is preceded by a near-vertical strut traveling wholly within the strut. In such cases the grouted length shall be measure from the trailing edge of the near-vertical strut to the end of the grouted zone, as shown in Figure I.3.

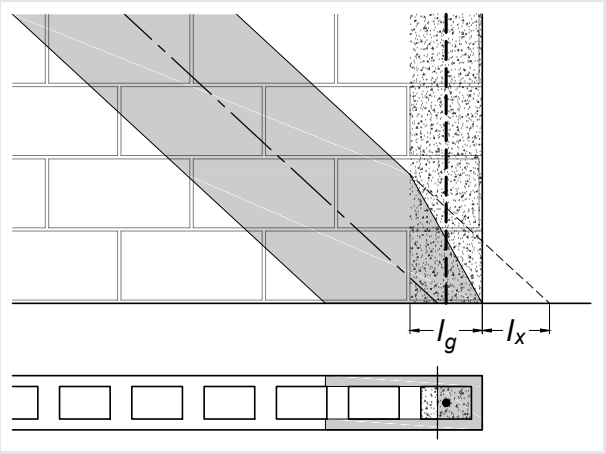

(a) Axis ending within the grouted length

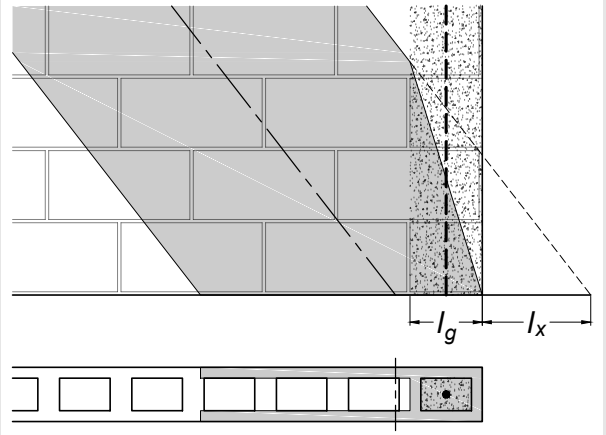

(b) Axis ending behind the grouted length

Figure I.2: Toe extension length

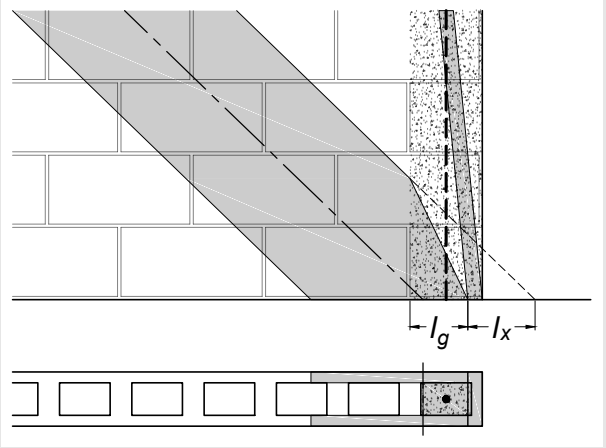

Figure I.3: Toe extension for second strut

I.2.5 *Transfer of Forces* — Nodal zones shall shall have three faces and transfer forces between three model elements, including struts, ties, and other nodal zones. In the case where more than three forces act on a node, the nodal region shall be subdivided into smaller nodal zones such that each resulting nodal zone has only three faces.

A nodal zone is formed where a force path changes direction, resulting in a third force being applied to the node. Additional forces may enter a node but the analysis is simplified when the nodal region is divided such that each nodal zone has three forces acting on it, resulting in three faces, as shown in Figure I.4.

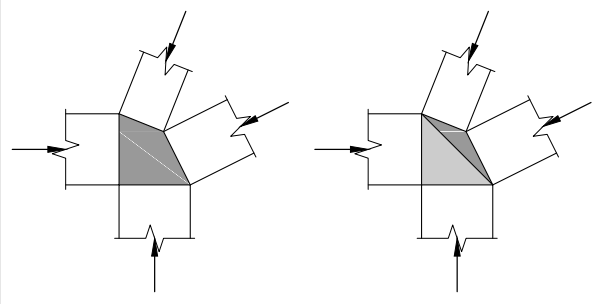

Figure I.4: Subdivision of nodal region

I.2.6 *Strength Design* — Struts, ties, and nodal zones shall be designed such that the design strength of each member is greater than or equal to the ultimate factored force denoted by

$$\phi F_n \geq F_u \qquad \text{(I.1)}$$

where F_n is the nominal strength given in I.3 through I.5. The ultimate factored load F_u shall act on the cross section of a strut or tie or on one face of a nodal zone.

Strut-and-tie models are constructed using the strength design methodology. The factored loads applied to the strut-and-tie model should be computed using the applicable loading cases. As strut-and-tie models are highly indeterminate, a model should be constructed and analyzed for each of the relevant loading cases. For each model, the value of the force applies to each strut, tie, or node, F_u is determined based on the applied loads and geometry of the elements.

I.3 Strength of Struts

I.3.1 *Nominal Strut Compressive Strength* — The nominal compressive strength of a strut, F_{ns}, shall be calculated using Equation I.2.

$$F_{ns} = f_{me} A_{ms} \qquad \text{(I.2)}$$

The compressive strength of each strut is a function of the cross-sectional area and the effective strength. The effective compressive strength of the masonry within struts has been observed to vary from the measured uniaxial compressive strength.

I.3.2 *Strut area* — The effective cross sectional area of a strut shall be the smaller of cross sectional areas measured at each end of the strut perpendicular to the strut axis.

The strut area is the product of the smallest strut width and the shear thickness of the masonry, t_s. For fully-grouted masonry walls, the shear thick-

ness of the masonry shall be taken as the gross wall thickness. For partially-grouted masonry walls, the shear thickness, t_s, shall be taken as the total thickness of the shells only.

I.3.3 *Effective Masonry Strength* — The effective strength of masonry, f_{me}, within a strut shall be calculated using Equation I.3 and shall not exceed the nodal strength given by I.7.

$$f_{me} = 0.8\beta_s\beta_\alpha f'_m \qquad \text{(I.3)}$$

The strength coefficient, $0.8f'_m$, in Equation I.3 represents the effective masonry compressive strength under sustained compression, similar to that used for bearing strength.

I.3.3.1 *Strut Efficiency Factor* — The strut efficiency factor, β_s, shall satisfy the requirements in I.3.3.1 (a) through (c).

(a) For struts which are prismatic:

$\beta_s = 1.0$

(b) For non-prismatic struts satisfying the requirements in I.3.4.1:

$\beta_s = 0.75$

(c) For non-prismatic struts not satisfying the requirements in I.3.4.1:

$\beta_s = 0.60$

The strut efficiency factor accounts for the reduction in effective compressive strength which results from the transverse force components of the stress paths in fan- and bottle-shaped strut. These transverse forces can cause the strut to split longitudinally decreasing the effective strength of the strut. When sufficient transverse reinforcement is provided as specified in I.3.4, the reinforcement resists the transverse splitting force and restrains the crack width, permitting the strut to resist a greater amount of axial load. All struts should be considered to be either fan- or bottle-shaped unless their proximity to the edge of the wall would prevent the stress from diverging from a prismatic path.

I.3.3.2 *Strut Inclination Factor* — The strut inclination factor, β_α, shall be satisfy the requirements in I.3.3.2 (a) through (d).

(a) For fully-grouted masonry:

$\beta_\alpha = 1.0$

(b) For partially-grouted masonry with an inclination angle, α_s, of zero:

$\beta_\alpha = 1.0$

(c) For partially-grouted masonry with an inclination angle, α_s, greater than 35 degrees:

$\beta_\alpha = 2/3$

(d) The value of β_α for α_s between 0.0 and 35 degrees shall be permitted to be linearly interpolated.

The strut inclination factor account for the reduction in effective compressive strength in partially-grouted masonry. When partially-grouted masonry is loaded in uniaxial compression normal to the bed joints, only compressive forces are present across the joint. As the inclination of the compressive force increases, shear stresses are introduced across the bed joint as the compression force travels from one course to another. These shear stresses limit the effective force that can be applied at an angle across the bed joint. This phenomenon has not be observed for fully-grouted masonry and is attributed to the shear stresses being transferred between courses by the grouted cores (Drysdale and Hamid, 1980).

The values for the inclination factor were developed based on a bi-linear approximation of the theoretical curved developed and compared against experimental data by Liu et al. (2006), as shown in

Figure I.5. The inclination factor values were used in constructing 46 strut-and-tie models and comparing them against the respective experimental strengths. It was observed that the selected values for the inclination factor provided a good fit to the experimental data.

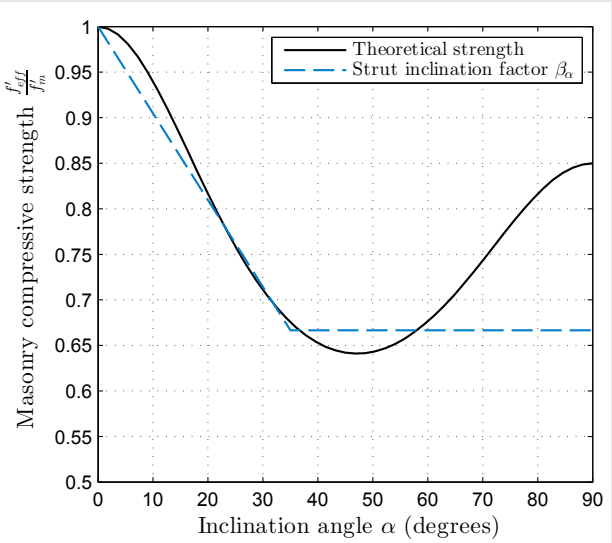

Figure I.5: Strut inclination factor

I.3.4 *Transverse Reinforcement* — If the value of β_s specified in I.3.3.1(b) is used, then the strut shall be crossed by sufficient reinforcement to resist the transverse tensile splitting force within the strut.

I.3.4.1 *Transverse Reinforcement Provided* — The total reinforcement crossing the strut shall satisfy the requirement in Equation I.4.

$$\sum \frac{A_{si} f_y}{s_i t_s} \sin \alpha_i \geq \frac{f_{me}}{15} \qquad \text{(I.4)}$$

I.3.4.2 *Transverse Reinforcement Placement* — The reinforcement in I.3.4.1 shall consist of traverse reinforcement placed in one direction at an angle α to the strut axis or in two orthogonal directions at angles α_1 and α_2 to the strut axis. If a strut is crossed by reinforcement in only one

The reinforcement required by I.3.4 is necessary to resist the transverse tensile forces within a strut caused by the spreading of the strut. The axial force within the strut may be assumed to spread at a 2:1 slope, for a length equal to one-sixth of the strut length, as shown in Figure I.6. As a result, the width of the strut at its mid-length, w_{eff}, is given by

$$w_{eff} = w_s + \frac{l_s}{6}$$

The contribution of the transverse reinforcement in resisting the splitting force can be assumed to act over the entire length of the strut, encouraging the use of smaller distributed bars rather than concentrating bars at the third points along the length of the strut, as idealized by dashed lined in Figure I.6.

Unlike the approach taken in reinforced concrete in specifying a single value for the right side of Equation I.4, it was felt that the wider range of pos-

direction, then the angle α shall not be less than 40 degrees.

I.3.4.3 *Transverse Reinforcement Testing* — If documented by experimental tests and analysis, it shall be permitted to reduce the amount of transverse reinforcement required by Equation I.4.

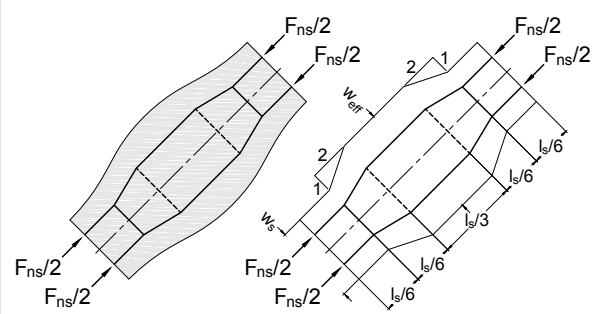

Figure I.6: Representation of forces in bottle-shaped strut

sible masonry strength values would be better served if the limit in Equation I.4 were a function of the masonry strength. This change was intended to eliminate the requirement of excessive amounts of transverse reinforcement for walls with lower masonry strength. The coefficient of $\frac{1}{15}$ on the right side of Equation I.4 is applicable for strut length-to-width ratios, $\frac{l_s}{w_s}$, of up to 24:1. For higher length-to-width ratios, the correct coefficient may be determined by

$$\frac{1}{12}\left(1 - \frac{1}{1 - \frac{1}{6}\frac{l_s}{w_s}}\right)$$

I.4 Strength of Ties

I.4.1 *Nominal Tie Tensile Strength* — The nominal strength of a tie, F_{nt}, shall be calculated using Equation I.5. Ties shall be permitted to carry less force than they are sized.

$$F_{nt} = A_s f_y \qquad \text{(I.5)}$$

I.4.2 *Tie Axis* — The axis of the tie shall coincide with the centroid of the reinforcement.

The effective width of ties includes the grouted masonry immediately between and around the reinforcement bars. The masonry around the tie is not effective in resisting the tensile forces in the tie, but the masonry within the tie acts in transferring stresses from the tie to the masonry. The minimum effective width of the tie is bounded by twice the cover to the surface of the bars plus the equivalent diameter of

the bars. The upper limit of the tie width is limited by the width corresponding to the width of a nodal zone under biaxial loading, calculated as

$$w_t = \frac{F_{nt}}{f_{me}\, t_g}$$

where f_{me} is calculated using Equation I.8.

I.4.3 *Horizontal Reinforcement* — The diameter of all horizontal reinforcement shall be limited such that the yield strength of the bar is equal or less than the strength of the adjoining strut. The diameter of horizontal reinforcement bars shall satisfy the limit in Equation I.6.

$$d_{bh} \leq 3.5\sqrt{\frac{f'_m}{f_{yh}}\, t_s\, d_{bf}} \qquad \text{(I.6)}$$

Research has observed there is a point at which increasing the amount of horizontal reinforcement ceases to increase the wall shear capacity (Nolph, 2010). Brittle failure can be induced by the horizontal bar pulling the vertical reinforcement bar to which it is anchored through the masonry, effectively disturbing the anchorage of the bar and reducing the horizontal confinement provided by the horizontal bar. The purpose of the limit in Equation I.6 is to limit the strength of the horizontal reinforcement area in each horizontal tie such that the tie will yield prior to the flexural bar crushing and pulling through the masonry.

I.4.4 *Vertical Reinforcement* — All continuous reinforcement bars around which at least one other bar is anchored shall be have a diameter, d_{bf}, that equals or exceeds one-twelfth of the gross masonry thickness.

I.4.5 *Tie Anchorage* — The tie reinforcement shall be fully anchored by bar development as required in I.4.5.1 through I.4.5.6.

I.4.5.1 *Horizontal Bar Anchorage* — Horizontal shear reinforcement shall be anchored around a vertical reinforcement satisfying the requirement in I.4.4 with a 180 degree hook.

I.4.5.2 *Tie Strength Development* — Nodal zones shall develop the difference in the tie forces between one side of the nodal zone and the other side.

I.4.5.3 *Tie Development Location* — At nodal zones anchoring one tie, the force shall be developed at the point where the axis of the tie leaves the extended nodal zone.

A special requirement of strut-and-tie models is that all reinforcement bars be fully developed before leaving the extended nodal zone. This point is defined as the intersection of the axis of the tie and the extension of the outline of the strut, as shown in Figure I.7. As needed, additional anchorage may be provided by moving the centroid of the nodal zone away from the end of the tie, effectively increasing the development length provided.

In cases where a strut and a tie are both anchored by another continuous tie, the effective bearing area of the strut is limited by the equivalent diameter of the bars in the continuous tie. The limit is equal to six bar diameters from the intersection of the two ties measured both along the axis of the continuous tie and normal to the plane of the wall. The minimum bar size specified in I.4.4 ensures that the thickness of the bearing area is not smaller than the gross thickness of the wall and the limit in I.4.5.5 only needs to consider the dimension along the axis of the continuous bar, as shown in Figure I.8.

I.4.5.4 *Anchorage of One Tie* — At nodal zones anchoring one tie, the force shall be developed at the point where the axis of the tie leaves the extended nodal zone.

I.4.5.5 *Anchorage of Stirrups* — At nodal zones anchoring two orthogonal ties such that the vertical tie passes through the nodal zone and is anchored within another nodal zone, the strut shall be permitted to be anchored by the vertical reinforcement. The effective width area may be considered to extend up to six vertical bar diameters along the axis of the vertical tie from the anchored horizontal bar.

I.4.5.6 *Anchorage of Two Ties* — At nodal zones anchoring two orthogonal ties not satisfying the requirements in I.4.5.5, the force in each tie shall be developed at the point where the axis of each tie leaves the extended nodal zone.

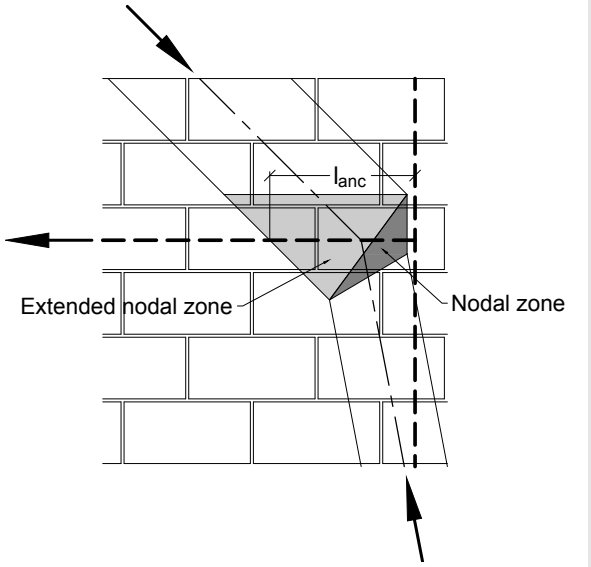

Figure I.7: Extended nodal zone for one ties

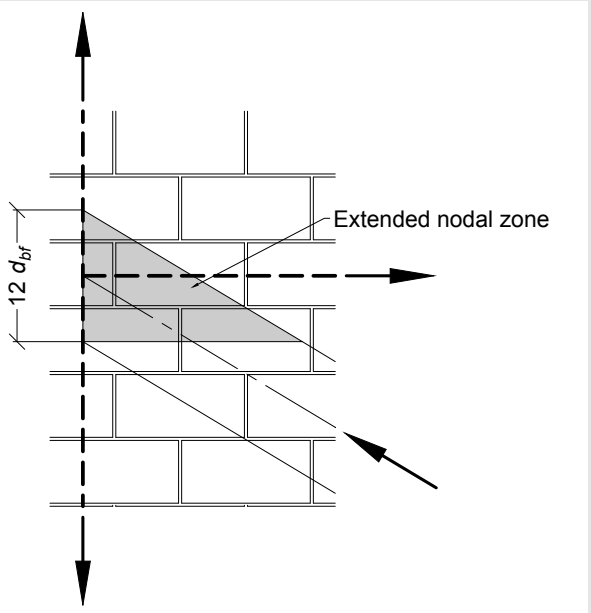

Figure I.8: Anchorage to a continuous tie

I.5 Strength of Nodal Zones

I.5.1 *Nominal Nodal Zone Compressive Strength* — The nominal compressive strength of a nodal zone, F_{nn}, shall be calculated using Equation I.7.

$$F_{nn} = f_{me} A_{nz} \qquad \text{(I.7)}$$

I.5.2 *Nodal Zone Face Area* — The effective face area of a nodal zone, A_{nz}, on which F_u acts shall be taken perpendicular to the axis on which F_u acts.

I.5.3 *Effective Masonry Strength* — The effective strength of masonry, f_{me}, for a face of a nodal zone shall be calculated using Equation I.3.

$$f_{me} = 0.8\beta_n f'_m \qquad \text{(I.8)}$$

I.5.3.1 *Nodal Efficiency Factor* — The nodal efficiency factor, β_n, shall satisfy the requirements in I.3.3.1 (a) through (c).

(a) For nodal zones bounded by struts, bearing areas, other nodal zones, or combinations thereof:
$\beta_n = 1.0$

(b) For nodal zones anchoring one tie:
$\beta_n = 0.80$

(c) For nodal zones anchoring two or more ties:
$\beta_n = 0.60$

The nodal efficiency factor accounts for the effective masonry compressive strength that is present within zonal zones. When a nodal zone is bounded solely by compressive forces, the material within the nodal zone is in a bi-directional state of stress. Research has shown that masonry under biaxial compression stresses demonstrates a higher effective strength than under uniaxial compression loading (Liu et al., 2006). The inclusion of ties introduces shear stresses within the nodal zone, which decreases the effective compressive strength of the masonry within the nodal zone due to incompatibilities between the tensile strains.